CRANFIELD UNIVERSITY

TEODÓRA POLYÁK

INVESTIGATION OF EARLY MEDIEVAL POTTERY PRODUCTION IN LOWER AUSTRIA: AN ARCHAEOLOGICAL SCIENCE APPROACH

CRANFIELD DEFENCE AND SECURITY

PhD in Archaeology

PhD

Academic Year: 2017 – 2021

Supervisor: Prof Andrew Shortland

Associate Supervisors: Dr Dennis Braekmans and Dr Hajnalka Herold

June 2021

CRANFIELD UNIVERSITY

CRANFIELD DEFENCE AND SECURITY
PhD in Archaeology

PhD

Academic Year 2017 – 2021

TEODÓRA POLYÁK

Investigation of early medieval pottery production in Lower Austria: an archaeological science approach

Supervisor: Prof Andrew Shortland
Associate Supervisors: Dr Dennis Braekmans and Dr Hajnalka Herold
June 2021

© Cranfield University 2021. All rights reserved. No part of this publication may be reproduced without the written permission of the copyright owner.

ABSTRACT

This thesis aims to contribute to a better understanding of early medieval pottery production in Lower Austria by the scientific analysis of ceramics. The investigation is based on 135 potsherds, including graphite-containing ceramics, which originate from the Erlauf Valley and other sites of Lower Austria and Vienna. The ceramics are dated to the 1st–12th centuries AD, with a majority of samples (n=123) from the 6th–11th centuries AD. The potsherds are studied, in addition to macroscopic analysis, by four scientific methods: petrographic thin section analysis, scanning electron microscopy (SEM), inductively coupled plasma optical emission spectrometry (ICP-OES) and X-ray diffraction (XRD).

These methods are used to identify and characterise the origin and manufacturing technology of the ceramics in order to gain insight into wider aspects of pottery production such as the organisation of production, technological choices, traditions and innovation. The compositions of the studied ceramics are consistent with different parts of one geological unit, the Bohemian Massif. This information, together with the distribution of the pots, provides details about connectivity and suggests the presence of local, regional and supra-regional trade/exchange networks within the study area. Traces of the applied production techniques indicate a relatively low level of standardisation for most of the ceramics; observations in this regard along with scale, degree of control and specialisation are used to discuss organisation of production. Through the reconstruction of the ceramic making process, technological choices are examined, such as the use of a new raw material, graphite, from the 8th/9th centuries. The analysis of the manufacturing steps also sheds light on practices of different periods and reveals, for example, differences in raw material preparation between the 1st–7th and 8th–9th centuries, which suggest a more sophisticated technology of pottery production in the former than in the latter period in the Erlauf Valley.

Keywords:

Ceramic archaeometry, Erlauf Valley, graphite-containing ceramics, ceramic petrography, petrographic thin section analysis, SEM, ICP-OES, XRD

ACKNOWLEDGEMENTS

I am most grateful to my supervisors Prof Andrew Shortland and Dr Dennis Braekmans from Cranfield University and Dr Hajnalka Herold from the University of Exeter for supervising my work, for their valuable guidance, suggestions and support, which helped me to do my best throughout the whole research project.

I would like to thank Dr Herold for making the studied ceramic samples available to me. I would also like to thank all of those who kindly provided samples for analysis including Mag. Franz Sauer (Austrian Federal Office for the Protection of Monuments) providing potsherds from the 8th–9th-century cemetery of Purgstall (S1–S30) and Andreas W. Rausch providing ceramics from his own and Franz Ressl's collection (S31–S90). I am also grateful for the samples from the Museum für Ur- und Frühgeschichte in Wieselburg (S91–S98), Dr Karin Kühtreiber (S99–S107), Prof Sabine Felgenhauer-Schmiedt (S108–S110), Department Lower Austria of the Austrian Federal Office for the Protection of Monuments (S111–S127), Dr Martin Krenn (S128–S132) and Vienna City Archaeology (S133–S135).

Special thanks to the Katholieke Universiteit Leuven in Belgium for making thin sections for S1–S98 and S103 and carrying out ICP-OES analysis for this research project. I would like to thank Dr Braekmans for his help in arranging sample preparation, chemical analysis and the transportation of samples between the UK and Belgium. The thin sections for S99–S102 and S104–S135 were produced by Andreas Wagner (Eggenburg, Austria) in the framework of a project of the Roman-Germanic Central Museum (Mainz, Germany); I would like to thank Prof Falko Daim (retired General Director of the Roman-Germanic Central Museum) for agreeing to the analysis of these thin sections in this thesis.

I am very grateful to one of my former professors, Dr György Szakmány (Faculty of Science, Eötvös Loránd University, Hungary) for giving his opinion about some of the thin sections as well as for drawing my attention to this PhD project and encouraging me to start it. I really appreciate the insightful comments of Dr Sándor Józsa, Dr Rudolf Dell'mour and Dr Judit Molera on certain topics of this thesis.

I would like to thank all staff members of the Cranfield Forensic Institute who supported me in any way during my research, especially Dr Jonathan Painter (SEM analysis), Prof Keith Rogers (XRD analysis), Prof David Lane (chair of my Progress Review Team) and Roland Wessling (member of my Progress Review Team). I am particularly grateful to Dr Emily Arnold for

helping me with XRD sample preparation and analysis. I would like to acknowledge Helen Lyne and Adrian Mustey, who were always keen to help when I had any problems.

I would like to thank Sarah and Ashley Rolfe for all their help with grammatical corrections and being so welcoming and supportive during my stay in Shrivenham.

I am deeply grateful to Csaba, my family and friends including my fellow PhD students from our daily Crossword Club; without their support and encouragement the completion of this thesis would not have been possible.

This research was funded by the Exeter-Cranfield PhD studentship as part of a collaboration between Cranfield Forensic Institute and the Archaeology Department of the University of Exeter.

TABLE OF CONTENTS

ABSTRACT i
ACKNOWLEDGEMENTS iii
LIST OF FIGURES viii
LIST OF TABLES xvii
1 INTRODUCTION 1
2 LITERATURE REVIEW 5
2.1 History of the study area from the Roman to the Babenberg era 6
2.1.1 The Roman Empire (15 BC – late 4th century AD) 7
2.1.2 Barbarians and the decline of the Roman rule (late 4th century – late 5th century) 8
2.1.3 Langobards (early 6th century – 568) 9
2.1.4 Between the Avar Khaganate and Bavaria (568 – end of the 8th century) 10
2.1.5 The Bavarian Eastland of the Carolingian Empire (9th century) 11
2.1.6 Christianisation and church organisation in the 7th–9th centuries 14
2.1.7 Hungarians (first half of the 10th century) 15
2.1.8 The Babenbergs (late 10th century – 11th century) 15
2.1.9 Summary 17
2.2 Archaeology of the region 18
2.2.1 Romans and Barbarians (1st–5th centuries AD) 18
2.2.2 Langobards (first half of the 6th century) 22
2.2.3 The Avars and the Carolingian period (7th–9th century) 23
2.2.4 The 10th and 11th centuries 28
2.2.5 Summary 29
2.3 The geology of Lower Austria and the Erlauf Valley 30
2.3.1 The geological setting of Lower Austria 30
2.3.2 Geological units in the Erlauf Valley 43
2.3.3 Clay deposits 44
2.3.4 Graphite deposits 46
2.3.5 Summary 48
2.4 Ceramic archaeometry in Lower Austria 49
2.4.1 Graphite-free pottery 49
2.4.2 Graphite-containing ceramics 50
2.4.3 Summary 51
2.5 Theoretical approaches to pottery and borderland archaeology 52
2.5.1 Theoretical concepts in pottery studies 52
2.5.2 Borderland archaeology 73

3 MATERIALS AND METHODS....83
3.1 Materials....83
3.2 Macroscopic analysis....95
3.2.1 Characterisation of macroscopic features and their interpretation....95
3.2.2 Macroscopic study of the ceramics from Lower Austria....99
3.2.3 Summary....101
3.3 Petrographic thin section analysis....102
3.3.1 The method of ceramic petrography....102
3.3.2 Ceramic petrography of the samples from Lower Austria....109
3.3.3 Summary....113
3.4 Scanning electron microscopy....114
3.4.1 The method of SEM....114
3.4.2 SEM of archaeological ceramics....117
3.4.3 SEM of the ceramic samples from Lower Austria....122
3.4.4 Summary....124
3.5 Inductively coupled plasma optical emission spectrometry (ICP-OES)....125
3.5.1 The method of ICP-OES....125
3.5.2 ICP-OES analysis of archaeological ceramics....128
3.5.3 ICP-OES analysis of the ceramic samples from Lower Austria....129
3.5.4 Statistical analyses of chemical data....130
3.5.5 Summary....134
3.6 X-ray diffraction....135
3.6.1 The method of XRD....135
3.6.2 XRD analysis of archaeological ceramics....138
3.6.3 XRD analysis of the ceramic samples from Lower Austria....140
3.6.4 Summary....141
4 RESULTS OF THE ANALYSES....143
4.1 Macroscopic analysis....143
4.1.1 Fabrics....143
4.1.2 Vessel form....150
4.1.3 Traces of the forming technique....155
4.1.4 Decoration....155
4.1.5 Summary....156
4.2 Petrographic thin section analysis....157
4.2.1 Graphite-free samples....157
4.2.2 Graphite-containing ceramics....176
4.2.3 Summary....185

4.3 Scanning electron microscopy 186
4.3.1 Results of vitrification analysis 186
4.3.2 Results of chemical analysis by SEM-EDS 188
4.3.3 Summary 204
4.4 Inductively coupled plasma optical emission spectrometry (ICP-OES) 205
4.4.1 Raw data analysis 205
4.4.2 Statistical analysis 223
4.4.3 Summary 236
4.5 X-ray diffraction 237
4.5.1 Graphite-free ceramics 237
4.5.2 Graphite-containing ceramics 243
4.5.3 Mineral phases and firing temperature 246
4.5.4 Summary 246
5 DISCUSSION 249
5.1 Ceramic groups and chronology 249
5.2 Provenance of the ceramics 255
5.3 Distribution of the ceramics 265
5.4 From clay to ceramics: pottery production technologies 270
5.4.1 Raw material procurement and preparation 270
5.4.2 Shaping: fashioning and finishing 275
5.4.3 Surface treatment and decoration 276
5.4.4 Firing 278
5.4.5 Summary 282
5.5 Organisation of pottery production 285
5.6 Technological continuity and change in pottery production and socio-political processes in early medieval Lower Austria 296
5.6.1 Technological choices, tradition and innovation in pottery production 296
5.6.2 Changing pottery technology – changing society? 304
5.6.3 Summary 309
5.7 Comparison of the studied ceramics with other ceramics from Lower Austria and the Central European region 312
6 CONCLUSIONS 325
REFERENCES 331
APPENDICES 367

LIST OF FIGURES

Figure 1. The location of Lower Austria and the Erlauf Valley (Base map: Google Maps).....5

Figure 2. The area of present-day Lower Austria (marked by red outline) with towns, settlements, archaeological sites and water bodies mentioned in the text (Base map: Google Maps) 6

Figure 3. Late Roman provinces in Central Europe (modified after Wolfram 1995, 25) 8

Figure 4. Peoples and regions in the 8th and 9th centuries in Central Europe (modified after Wolfram 1995, 221) 12

Figure 5. Remains of fort Arelape at Pöchlarn (Hinterwallner and Schmid 2015, 197: Abb. 117) 19

Figure 6. Fibulae from the female grave of Untersiebenbrunn (Friesinger and Vacha 1988, 55) 21

Figure 7. Avar belt fitting depicting a griffin from Mödling (Friesinger and Vacha 1988, 93).....24

Figure 8. Reconstruction of the manor house in the fortified settlement of Thunau am Kamp (Herold 2007, 83: Abb. 3.5.5) 27

Figure 9. The Ottonian church in Wieselburg as a side chapel of the modern parish church (photo by the author).....29

Figure 10. The Bohemian Massif, the Alps and Lower Austria (red area) (modified after Dill et al. 2008, 1343: Fig. 21.1) 31

Figure 11. Lower Austria with its major geological units (modified after Wessely 2006b, 12: Abb. 2).....32

Figure 12. Typical landscape of the Bohemian Massif in the Waldviertel (Wessely 2006c, 15: Abb. 4) 33

Figure 13. Subunits of the Bohemian Massif in Lower Austria (modified after Janoschek and Matura 1980, 17: Fig. 4 and Wessely 2006b, 12: Abb. 2).....34

Figure 14. Subunits of the Alpine-Carpathian Foreland in Lower Austria (modified after Wessely 2006b, 12: Abb. 2, 13: Abb. 3) 37

Figure 15. The so-called Melk Sand of the Molasse Zone (Wessely 2006e, 47: Abb. 65) 37

Figure 16. Subunits of the Eastern Alps in Lower Austria (modified after Wessely 2006b, 12: Abb. 2, 13: Abb. 3) 38

Figure 17. Flow marks in sandstone of the Rhenodanubian Flysch Zone (Wessely 2006g, 85: Abb. 157) 39

Figure 18. The cliff of Konradsheim in the Gresten Klippen Zone (Wessely 2006g, 97: Abb. 184) 40

Figure 19. The units of the Austro-Alpine Zone in Lower Austria (modified after Matura 2006a, 168–169: Abb. 338).....41

Figure 20. Geological units in the Erlauf Valley (modified detail of Wessely 2006f, 78: Abb. 153). Cross-section through line 5 (marked red) is presented in Figure 21. 44

Figure 21. North-south cross-section of the Erlauf Valley drawn along line 5 in Figure 20 (modified detail of Wessely 2006f, 81: Abb. 155). Abbreviations: Z.=Zone, GR. KL.=Gresten Klippen Zone, Y=Ybbsitz Klippen Zone, FN=Frankenfels Nappe, LN=Lunz Nappe, SN=Sulzbach Nappe, RN=Reisalpen Nappe, GÖLLER N.=Göller Nappe. Different colour stripes in the Austro-Alpine Zone mark different formations not detailed here. 44

Figure 22. Clay, loam, kaolin and kaolin-rich clay deposits in Lower Austria (based on Heinrich 2006, 274: Abb. 527, 292: Abb. 536; base map: Wessely 2006b, 12: Abb. 2) 45

Figure 23. Graphite deposits in Central Europe and in Lower Austria (red area) (modified after Scharrer-Liška 2007, 17: Abb. 1) 47

Figure 24. Occurrences of graphite in the Moldanubicum (Bohemian Massif) (based on Schrauder et al. 1993, 176: Fig. 1 and the map annex of Holzer 1964; base map: Wessely 2006b, 12: Abb. 2) 48

Figure 25. Location of the archaeological sites in the Erlauf Valley (bottom left corner) and in other parts of Lower Austria and Vienna (right-hand side map). The sites corresponding to the numbers are listed in Table 4 above. 85

Figure 26. Recorded data of the ceramic sherds 99

Figure 27. Characteristics forming the basis of fabric identification 99

Figure 28. Labels used for the description of feel 100

Figure 29. Labels used for the description of fracture 100

Figure 30. Labels used for the description of sizes ranges 100

Figure 31. Labels used for the description of the amount of inclusions 100

Figure 32. Terms used for the definition of vessel parts. (Drawing of the vessel of Sample 9 from the excavation documentation of the 8th-9th-century cemetery of Purgstall provided by excavator Franz Sauer.) 101

Figure 33. Decoration elements 101

Figure 34. System of the investigated data of the thin sections 110

Figure 35. Terms used for the description of homogeneity/heterogeneity 110

Figure 36. Labels used for the description of alignment 110

Figure 37. Void types and prefixes for void size 111

Figure 38. Colour labels used for the definition of colour 111

Figure 39. Terms used for the description of optical activity 112

Figure 40. Labels used for the definition of grain-size distribution 112

Figure 41. Labels used for the definition of the degree of sorting 112

Figure 42. Labels used for the description of grain shape 112

Figure 43. Labels used for the description of roundness/angularity of grains 112

Figure 44. Frequency labels used for the definition of the amount of inclusions 113

Figure 45. Labels used for the description of argillaceous inclusions 113

Figure 46. Micaceous fabrics: GMA (S98), GMB (S60) and WM (S5) (photo by the author) 145

Figure 47. Feldspar and quartz-rich fabrics: FQA (S81) and FQB (S83) (photo by the author) 147

Figure 48. Carbonate rock-containing fabrics: CRA (S58) and CRB (S89) (photo by the author) 148

Figure 49. Graphite fabrics: GA (S128) and GB (S53) (photo by Hajnalka Herold and the author) 149

Figure 50. Vessels from the 8th–9th-century cemetery of Purgstall (excavation documentation; drawing provided by excavator Franz Sauer) 152

Figure 51. Vessels from the 8th–9th-century cemetery of Purgstall (excavation documentation; drawing provided by excavator Franz Sauer) 153

Figure 52. Vessels from the 8th–9th-century cemetery of Purgstall (excavation documentation; drawing provided by excavator Franz Sauer) 154

Figure 53. Vessels from the 8th–9th-century cemetery of Mühling (Friesinger 1971–1974, Tf. 12, Tf. 14) 154

Figure 54. Subgroup 'Granitoid A1' containing abundant feldspar (S4, PPL and XP) 161

Figure 55. Subgroup 'Granitoid A2' with abundant and very fine-grained fine fraction (S69, PPL and XP) 161

Figure 56. Subgroup 'Granitoid A3' containing few inclusions (S42, PPL and XP) 162

Figure 57. Grog (?) grains in S51 (upper left and lower right corner of the photomicrographs) (PPL and XP) 162

Figure 58. The outer and inner surface of rim fragment S51. Reddish grog (?) grains are visible in the inner surface (e.g. in the upper left edge of the sherd) (photo by the author) 162

Figure 59. Subgroup 'Granitoid B1' with moderate sorting of grains (S80, PPL and XP) 163

Figure 60. Subgroup 'Granitoid B2' with very poor sorting of grains (S7, PPL and XP) 164

Figure 61. Subgroup 'Granitoid B3' containing few inclusions (S45, PPL and XP) 164

Figure 62. Subgroup 'Granitoid C' with abundant biotite and potassium feldspar exhibiting microcline structure (S22, PPL and XP) 165

Figure 63. Subgroup 'Granitoid D' with abundant coarse-grained muscovite (S5, PPL and XP) 165

Figure 64. Amphibole group with abundant amphibole crystals and granitoid fragments containing feldspar with a yellowish initial alteration (S61, PPL and XP) 167

Figure 65. Composition of S91 including granitoid fragments of the Amphibole group with initial alteration of feldspar (e.g. top right-hand quarter of the photomicrograph) and colourless amphibole-aggregate (bottom right-hand quarter of the picture) which is characteristic of subgroup 'Diorite A' (PPL and XP) 168

Figure 66. Subgroup 'Diorite A' containing diorite fragments with zoned feldspars (e.g. bottom right-hand corner) and colourless amphibole-aggregates (bottom left-hand quarter) (S75, PPL and XP) 170

Figure 67. Subgroup 'Diorite B' with diorite fragments including diopside (bottom left-hand corner) (S67, PPL and XP) 170

Figure 68. Graphic texture of the rock fragments of 'Diorite B' (S97, PPL and XP) 171

Figure 69. Subgroup 'Carbonate A' containing calcite/dolomite and diopside crystals in a matrix rich in very fine-grained quartz (S58, PPL and XP) 172

Figure 70. Subgroup 'Carbonate B' containing calcite/dolomite and diopside crystals in an inclusion-poor matrix (S59, PPL and XP) 172

Figure 71. S15 containing abundant quartz, some rutile (centre of the picture) and garnet grains (inside rock fragment, bottom edge of the photomicrograph) (PPL and XP) 173

Figure 72. S17 with calcite/dolomite fragments (PPL and XP) 174

Figure 73. S23 including abundant biotite and some green amphibole crystals (e.g. top left-hand corner of the picture) (PPL and XP) 175

Figure 74. Vitreous matrix of S48 showing optical inactivity in XP (PPL and XP) 175

Figure 75. S131 containing kyanite-bearing mica schist (PPL and XP) 176

Figure 76. Subgroup 'Graphite A1' containing graphite gneiss (upper part of the picture) and sillimanite-bearing graphite gneiss (bottom left-hand corner) fragments (S101, PPL and XP) 178

Figure 77. Subgroup 'Graphite A2' with rock fragments including quartz and feldspar grains with triple junctions as a sign of equilibrium crystallisation (S104, PPL and XP) 179

Figure 78. Subgroup 'Graphite A3' containing garnet (right edge of the photomicrograph) (S32, PPL and XP) 179

Figure 79. Clay pellets in S107 (e.g. bottom left-hand corner of the picture) (PPL and XP) 180

Figure 80. Subgroup 'Graphite A4' with kyanite (top right-hand corner) (S31, PPL and XP) 180

Figure 81. Microstructure of subgroup 'Graphite A5' (S113, PPL and XP) 180

Figure 82. Glaze/deposition layer on the inner side of S113. On the top of this layer, another carbonate-rich layer can be observed (PPL and XP) 181

Figure 83. The outer and inner side of S113 (photo by the Austrian Federal Office for the Protection of Monuments) 181

Figure 84. Altered feldspars with a reddish-brown colour in S125 (PPL and XP) 182

Figure 85. Subgroup ‘Graphite B’ containing graphitic mica schist fragments (S133, PPL and XP) 182

Figure 86. Subgroup ‘Graphite C1’ containing graphite marble fragments (bottom left-hand quarter of the picture) (S119, PPL and XP).....183

Figure 87. Subgroup ‘Graphite C2’ containing micrite fragments (middle of the right edge of the photomicrograph) (S124, PPL and XP) 184

Figure 88. Chert fragments in S62 (lower half of the photomicrograph) (PPL and XP) 185

Figure 89. Argillaceous rock fragments in S54 (e.g. top left-hand quarter of the picture) (PPL and XP) 185

Figure 90. Examples for unvitrified microstructure (a. S8, b. S10, c. S97, d. S130) 187

Figure 91. Initial vitrification structure of S90 188

Figure 92. Legend for the graphs and diagrams used throughout the thesis 188

Figure 93. Matrix compositions plotted on the ternary diagram of SiO_2, Al_2O_3 and fluxes (K_2O, Fe_2O_3, CaO, MgO, TiO_2) following Maniatis and Tite (1978, 485: Fig. 1).....189

Figure 94. Matrix compositions plotted on the ternary diagram of Fe_2O_3+MgO, Al_2O_3 and K_2O+Na_2O+CaO following Philpotts and Wilson (1994, 615: Fig. 8) 189

Figure 95. Matrix compositions plotted on the ternary diagram of Si, Al+Fe+Mg+Ti and K+Na+Ca with the position of the three main types of clay minerals (smectites, illites and kaolinite) following Tite et al. (1982, 112: Fig. 5) 190

Figure 96. Si/Al ratios of the matrices. The fields of kaolinite, illite and montmorillonite are based on the values published by Velde and Druc (1999, 249) 191

Figure 97. Matrix compositions plotted on the ternary diagram of SiO_2, CaO and Al_2O_3 following Artioli (2010, 233) 191

Figure 98. Feldspar compositions plotted on the ternary diagram of anorthite (An, $CaAlSi_2O_8$), albite (Ab, $NaAlSi_3O_8$) and orthoclase (Or, $KAlSi_3O_8$). (The diagram includes the data of 226 feldspar grains from 47 samples.).....193

Figure 99. Zircon compositions plotted on the ternary diagram of ZrO_2, Al_2O_3 and Fe_2O_3. The values of ZrO_2 are divided by 10 for a better presentation of the data. (The diagram includes the data of 55 zircon grains from 30 samples.).....194

Figure 100. Al_2O_3 and Fe_2O_3 content of rutile grains. (The diagram includes the data of 36 rutile grains from 21 samples.).....195

Figure 101. Titanite compositions plotted on the ternary diagram of Fe_2O_3, CaO and TiO_2. Fe_2O_3 values are multiplied by 10. (The diagram includes the data of 8 titanite grains from 6 samples.) 195

Figure 102. Compositions of iron-rich phases plotted on the ternary diagram of SiO_2, Fe_2O_3 and Al_2O_3. (The diagram includes the data of 103 iron-rich phases from 31 samples.).....196

Figure 103. Na_2O and CaO content of amphibole grains of the Amphibole and Diorite groups. (The diagram includes the data of 25 amphibole grains from 7 samples.) 197

Figure 104. Na_2O and Fe_2O_3 content of amphibole grains of the Amphibole and Diorite groups. (The diagram includes the data of 25 amphibole grains from 7 samples.) 197

Figure 105. MgO and Al_2O_3 content of amphibole grains of the Amphibole and Diorite groups. (The diagram includes the data of 25 amphibole grains from 7 samples.) 198

Figure 106. Q-J diagram of pyroxenes of the Carbonate group and subgroup 'Diorite B' following Morimoto et al. (1988, 1127: Fig. 2). (The diagram includes the data of 19 pyroxene grains from 5 samples.) 199

Figure 107. Q-J diagram for pyroxenes with the 13 endmembers (Morimoto et al. 1988, 1127: Fig. 2) 199

Figure 108. Nomenclature of Ca-Mg-Fe clinopyroxenes by Morimoto et al. (1988, 1129: Fig 4) 200

Figure 109. Pyroxene compositions of the Carbonate group and subgroup 'Diorite B' plotted on the ternary diagram of wollastonite (Wo, $Ca_2Si_2O_6$), enstatite (En, $Mg_2Si_2O_6$) and ferrosilite (Fs, $Fe_2Si_2O_6$) following Morimoto et al. (1988, 1128, 1129: Fig. 4). (The diagram includes the data of 19 pyroxene grains from 5 samples.) 200

Figure 110. Mica compositions plotted on the ternary diagram of Fe_2O_3+MgO, Al_2O_3 and K_2O+Na_2O+CaO following Shriner and Dorais (1999, 40: Fig. 7). The upper group of measurements represents biotite, the lower group of measurements represents muscovite. (The diagram includes the data of 38 mica flakes from 13 samples.) 202

Figure 111. Fe_2O_3+MgO and TiO_2 content of mica flakes. The upper group of measurements represent biotite, the lower group of measurements represent muscovite. (The diagram includes the data of 38 mica flakes from 13 samples.) 202

Figure 112. Garnet compositions of the Graphite group and S15 plotted on the ternary diagram of pyrope (Prp, $Mg_3Al_2Si_3O_{12}$), almandine (Alm, $Fe^{2+}{}_3Al_2Si_3O_{12}$) and spessartine (Sps, $Mn_3Al_2Si_3O_{12}$). (The diagram includes the data of 19 garnet grains from 5 samples.) 203

Figure 113. Surface layer on the inner side of S113 204

Figure 114. Concentration of major element oxides (wt%) in the samples by petrographic groups. The last sample (S15) is an outlier based on petrography. 206

Figure 115. Box plot of Al_2O_3 (wt%) by petrographic groups 208

Figure 116. Box plot of CaO (wt%) by petrographic groups 208

Figure 117. Box plot of Fe_2O_3 (wt%) by petrographic groups 209

Figure 118. Box plot of K_2O (wt%) by petrographic groups 209

Figure 119. Box plot of MgO (wt%) by petrographic groups 210

Figure 120. Box plot of Na_2O (wt%) by petrographic groups 210

Figure 121. Box plot of P_2O_5 (wt%) by petrographic groups 210

Figure 122. Box plot of SiO_2 (wt%) by petrographic groups 210

Figure 123. Box plot of TiO_2 (wt%) by petrographic groups 211

Figure 124. Concentration of trace elements (ppm) in the samples by petrographic groups. The last sample (S15) is an outlier based on petrography. Those trace elements which have values below the limit of quantification (Mn, Pb, Sn, Zn) are not presented in this diagram. 212

Figure 125. Box plot of Ba (ppm) by petrographic groups 213

Figure 126. Box plot of Cr (ppm) by petrographic groups 213

Figure 127. Box plot of Cu (ppm) by petrographic groups 214

Figure 128. Box plot of Ni (ppm) by petrographic groups 214

Figure 129. Box plot of Rb (ppm) by petrographic groups 215

Figure 130. Box plot of Sc (ppm) by petrographic groups 215

Figure 131. Box plot of Sr (ppm) by petrographic groups 216

Figure 132. Box plot of V (ppm) by petrographic groups 216

Figure 133. Box plot of Y (ppm) by petrographic groups 216

Figure 134. Box plot of Zr (ppm) by petrographic groups 216

Figure 135. Ternary diagram of Al_2O_3, Fe_2O_3 and TiO_2. The values of TiO_2 are multiplied by 10 for a better presentation of the data. 217

Figure 136. Ternary diagram of Al_2O_3, K_2O and Na_2O (Al_2O_3 values are divided by 5) 219

Figure 137. Ternary diagram of Fe_2O_3, TiO_2 and Mn (Mn values are multiplied by 100). Only those samples are presented on this graph which contain Mn above the limit of quantification. 219

Figure 138. Ternary diagram of K_2O, Na_2O and Rb (Rb values are multiplied by 100) 220

Figure 139. Ternary diagram of MgO, CaO and Sr (Sr values are multiplied by 100). S54 is not present in the graph as its CaO content is below the limit of quantification. 220

Figure 140. Scatterplot of Ba and Sr showing slight correlation 222

Figure 141. Ternary diagram of V, Cr and Zr 222

Figure 142. Scatterplot of the first two principal components (PC1 and PC2) based on all (major and trace) elements without sample numbers (upper graph) and with sample numbers (lower graph) 224

Figure 143. Projection of the variables for PC1 and PC2 based on all (major and trace) elements 225

Figure 144. Scatterplot of the first and third principal components (PC1 and PC3) based on all (major and trace) elements without sample numbers (upper graph) and with sample numbers (lower graph) 226

Figure 145. Projection of the variables for PC1 and PC3 based on all (major and trace) elements 227

Figure 146. Scatterplot of the first two principal components (PC1 and PC2) based on the major elements without sample numbers (upper graph) and with sample numbers (lower graph) 228

Figure 147. Projection of the variables for PC1 and PC2 based on the major elements 229

Figure 148. Scatterplot of the first two principal components (PC1 and PC2) based on the trace elements without sample numbers (upper graph) and with sample numbers (lower graph) 230

Figure 149. Projection of the variables for PC1 and PC2 based on the trace elements 231

Figure 150. Cluster analysis of all 17 elements of graphite-free pottery using complete linkage and Euclidean distances. Petrographic groups/subgroups are indicated below the sample numbers: Granitoid group = red subgroups, Amphibole group = green triangles, Diorite group = yellow subgroups, Carbonate group = blue subgroups, and S15 as an individual sample = pink square. 233

Figure 151. Cluster analysis of all 17 elements of graphite-free pottery using Ward's method and Euclidean distances. Petrographic groups/subgroups are indicated below the sample numbers as explained in the caption of Figure 150. 233

Figure 152. Cluster analysis of the major elements of graphite-free pottery using weighted pair-group average and Euclidean distances. Petrographic groups/subgroups are indicated below the sample numbers as explained in the caption of Figure 150. 234

Figure 153. Cluster analysis of the trace elements of graphite-free pottery using Ward's method and Euclidean distances. Petrographic groups/subgroups are indicated below the sample numbers as explained in the caption of Figure 150. 234

Figure 154. Cluster analysis of all 17 elements of graphite-containing pottery using complete linkage and Euclidean distances. Subgroups within the Graphite group are indicated below the sample numbers. 235

Figure 155. Cluster analysis of the trace elements of graphite-containing pottery using complete linkage and Euclidean distances. Subgroups within the Graphite group are indicated below the sample numbers. 235

Figure 156. Diffractograms of the samples of the Granitoid group (data are normalised) with the indication of the most significant peaks of important phases. Abbreviations of phases as follows based on Siivola and Schmid 2007. Ab = albite, Bt = biotite, Hbl = hornblende, Ill = illite, Lab = labradorite, Mc = microcline, Ms = muscovite, Or = orthoclase, Qtz = quartz, Vrm = vermiculite. 241

Figure 157. Diffractograms of the samples of the Amphibole, Diorite and Carbonate groups and the individual sample (data are normalised) with the indication of the most significant peaks of important phases. Abbreviations of phases as follows based on Siivola and Schmid 2007. Ab = albite, Alm = almandine, Aug = augite, Bt = biotite, Cal = calcite, Di = diopside, Hbl = hornblende, Ill = illite, Lab = labradorite, Ms = muscovite, Or = orthoclase, Qtz = quartz, Rt = rutile, Tr = tremolite, Vrm = vermiculite. 242

Figure 158. Diffractograms of the samples of the Graphite group (data are normalised) with the indication of the most significant peaks of important phases. Abbreviations of phases as follows based on Siivola and Schmid 2007. Ab = albite, Bt = biotite, Cal = calcite, Gr = graphite, Grt = garnet, Hbl = hornblende, Hem = hematite, Ill = illite, Kln = kaolinite, Ms = muscovite, Or = orthoclase, Qtz = quartz, Rt = rutile, Sil = sillimanite, Vrm = vermiculite. 245

Figure 159. Geological map of the Erlauf Valley and its vicinity with potential sources of the inclusions of graphite-free ceramic samples (modified detail of the geological map compiled by the Geologische Bundesanstalt (2002)) 256

Figure 160. Potential sources of the inclusions of graphite-containing ceramic samples in the Bohemian Massif (modified detail of the geological map compiled by the Geologische Bundesanstalt (2002)) 262

Figure 161. Archaeological sites in the Erlauf Valley with the indication of the petrographic groups and subgroups of the ceramics investigated in this thesis (Base map: Google Maps). The usual symbols are used for the petrographic groups as shown in Figure 92 (page 188). Individual samples were found at archaeological sites numbered 1 and 3 on this map.....265

Figure 162. Archaeological sites and subgroups of graphite-containing ceramics from outside of the Erlauf Valley (Base map: Google Maps). The boundaries of Lower Austria and Vienna are marked with a red outline. One individual sample originates from Sachsendorf. 267

Figure 163. Depiction of a potter and his turntable from the 13th century (Fresco from the 'Bischofskapelle' in the west gallery of the Gurk Cathedral, Carinthia, Austria) 276

Figure 164. The location of the sites in Lower Austria studied in this thesis (orange markers, 1–20) and the sites included in the comparison (blue markers, 21–48) (Base map: Google Maps) 312

Figure 165. Comparison of the chemical compositions of the samples from Lower Austria with samples from Hungary and Czechia. The scatterplot shows the result of PCA (including PC1 and PC2) of the major and trace elements measured by ICP-OES in the samples from Lower Austria and by XRF in the samples from Hungary and Czechia. The Lower Austria samples are marked by the usual symbols in colour (see Figure 92 on page 188) and the other samples are marked by black filled an unfilled shapes as shown in Table 28. 322

Figure 166. Projection of the variables for Figure 165.....322

Figure 167. Comparison of the chemical compositions of the samples from Lower Austria with samples from Hungary and Czechia. The scatterplot shows the result of PCA (including PC1 and PC2) of the major elements. For legend, see caption of Figure 165. 323

Figure 168. Projection of the variables for Figure 167.....323

Figure 169. Comparison of the chemical compositions of the samples from Lower Austria with samples from Hungary and Czechia. The scatterplot shows the result of PCA (including PC1 and PC2) of the trace elements. For legend, see caption of Figure 165. 324

Figure 170. Projection of the variables for Figure 169.....324

LIST OF TABLES

Table 1. Geologic time scale from the Devonian with eras, periods and epochs relevant to the text (based on the International Chronostratigraphic Chart, Version 2020/03) 30

Table 2. Summary of the main units, subunits and rock types of the Bohemian Massif in Lower Austria 35

Table 3. Summary of the main units, subunits and rock types of the Eastern Alps in Lower Austria 39

Table 4. Archaeological sites of the ceramic samples. Site numbers in the first column are used to mark the location of the sites on the map below. 84

Table 5. Characteristics of ceramic samples observed by ceramic petrography following Whitbread (1995, 379–88) and Quinn (2013, 80–102) 104

Table 6. Vitrification stages and the corresponding firing temperature ranges in oxidising (O) and reducing (R) atmosphere after Maniatis and Tite (1981, 61, 65, 68: Table 1). The upper boundary of the last stage (continuous vitrification) represents the temperature by which continuous vitrification is totally developed. 118

Table 7. Relative standard deviation and relative error calculations for data quality assessment (precision and accuracy) of SEM-EDS analysis 124

Table 8. Relative standard deviation and relative error calculations for data quality assessment (precision and accuracy) of ICP-OES analysis 131

Table 9. Mineral phases in ceramics indicative of firing temperatures. Clay composition or types of inclusions which influence the formation of some phases are indicated in brackets. 139

Table 10. Graphite-free fabrics and samples 144

Table 11. Gold mica (GMA and GMB) and white mica (WM) fabrics 144

Table 12. Feldspar and quartz-rich fabrics 146

Table 13. Carbonate rock-containing fabrics 147

Table 14. Graphite fabrics and samples 148

Table 15. Graphite fabrics 149

Table 16. Parameters of pots found in Lower Austria 151

Table 17. Petrographic groups of graphite-free ceramics 158

Table 18. Subgroups of the Graphite group 177

Table 19. Samples investigated by SEM, ICP-OES and XRD with their petrographic groups 186

Table 20. Minimum values, maximum values, means and standard deviations of the compositional data of all samples and the different petrographic groups. Major elements

are expressed in weight percentages as oxides and trace elements are expressed in ppm. 207

Table 21. Mineral phases in the Granitoid group detected by XRD. Abbreviations as follows based on Siivola and Schmid 2007. Ab = albite, Bt = biotite, Cal = calcite, Hbl = hornblende, Ill = illite, Lab = labradorite, Mc = microcline, Ms = muscovite, Or = orthoclase, Phl = phlogopite, Ttn = titanite, Vrm = vermiculite. 238

Table 22. Mineral phases in the Amphibole, Diorite and Carbonate groups and the individual sample detected by XRD. Abbreviations as follows based on Siivola and Schmid 2007. Ab = albite, Alm = almandine, Ann = annite, Aug = augite, Bt = biotite, Cal = calcite, Di = diopside, Hbl = hornblende, Ill = illite, Lab = labradorite, Ms = muscovite, Or = orthoclase, Phl = phlogopite, Rt = rutile, Tr = tremolite, Vrm = vermiculite. 240

Table 23. Mineral phases in the Graphite group detected by XRD. Abbreviations as follows based on Siivola and Schmid 2007. Ab = albite, Alm = almandine, An = anorthite, Ann = annite, Ant = anatase, Bt = biotite, Grs = grossular, Hbl = hornblende, Hem = hematite, Ill = illite, Kln = kaolinite, Ms = muscovite, Or = orthoclase, Phl = phlogopite, Prp = pyrope, Rt = rutile, Sil = sillimanite, Tr = tremolite, Ttn = titanite, Vrm = vermiculite. 243

Table 24. An overview of the chronology of the petrographic groups and subgroups 250

Table 25. Table summarising the site, dating and petrographic group of the samples. Subgroups are indicated with the symbol of the main petrographic group (Figure 92) and the group code of the subgroup; e.g. ✚A1 = 'Granitoid A1', ◆B = 'Carbonate B'. Individual samples are abbreviated as 'Indiv. s.' 253

Table 26. Methods used for the interpretation of the different steps of the ceramic chaîne opératoire in this thesis 270

Table 27. Estimated maximum firing temperatures of the samples by petrographic subgroups based on the results of SEM, XRD and thin section analysis 280

Table 28. Details of the ceramics from Hungary and Czechia included in the comparison 320

1 INTRODUCTION

This thesis aims to investigate early medieval pottery production in the north-eastern part of Austria using a range of analytical techniques. Central to the research is the valley of the river Erlauf, a tributary of the Danube in Lower Austria, from where the majority (98 samples) of the studied ceramics originate. The main focus is on pottery from the 6th–11th centuries AD, and additionally some potsherds from an earlier period (1st–5th centuries AD) are also included in the analysis as comparative material. A small part of the assemblage from the Erlauf Valley represents a special pottery type containing graphite, which appears from the 9th century onwards in the Valley. In relation to this, other graphite-containing ceramic samples are examined from other sites of Lower Austria and Vienna (37 samples), which are dated from the 9th to the 11th/12th centuries. Thus, a total of 135 ceramic samples are investigated in this thesis originating from a long time span between the 1st to the 12th centuries AD.

Studies involving the scientific analysis of archaeological ceramics, also called ceramic archaeometry, are scarce concerning the early Middle Ages in Lower Austria (Section 2.3). Consequently, there is little detailed information available about early medieval pottery making practices and raw material sources. This thesis intends to contribute to this knowledge by examining potsherds from the Erlauf Valley and graphite-containing ceramics from other parts of Lower Austria and Vienna.

There are several reasons which make the Erlauf Valley an ideal choice for a study area. Being unexplored by studies of pottery analysis, it provides new data to discover. The importance of the Valley throughout its history is shown by the remains of a Roman fort at the confluence of the Erlauf and the Danube and a beautiful still-standing Ottonian church in Wieselburg from the end of the 10th century. There is a multitude of archaeological ceramics available from the Valley from the whole duration of the early Middle Ages thanks to cemetery excavations and field surveys as well as the participation and support of local people in these activities. This thesis is also part of a large-scale research project aiming at the investigation of landscape transformations between the late Roman period and the high Middle Ages in the Erlauf Valley conducted by my supervisor, Dr Hajnalka Herold.

The inclusion of graphite-containing pottery in the analysis originating from other parts of Lower Austria and Vienna provides opportunity to compare them with the Erlauf Valley samples. Besides, there are very few studies dealing with the scientific analysis of early

medieval graphite-containing ceramics in Lower Austria and most of them incorporate one or two methods only (Section 2.4.2). The multi-analytical examination carried out in this thesis seeks to develop a better understanding of early medieval graphite-containing pottery.

This thesis addresses the central question of what information can be obtained about early medieval pottery production and raw material sources in the Erlauf Valley and Lower Austria by the analysis of ceramics. Within this main research question, the investigation has the following objectives:

- to characterise the material of the investigated samples, assess similarities and differences, establish ceramic groups;
- to identify potential sources of raw materials;
- to evaluate if the studied ceramics are local or imported;
- to reconstruct the different steps of the ceramic making process from raw material preparation to firing;
- to analyse technological choices made at each stage of the manufacturing sequence;
- to examine the organisation of production, including possible number and location of production units;
- to compare ceramics within and across specific time periods, examine different traditions and assess continuity/discontinuity of ceramic technologies over time including the appearance of early medieval graphite-containing ceramics in Lower Austria;
- and to explore how changes in pottery technology and other changes in history are related.

These topics are investigated through the use of four scientific methods in addition to macroscopic observation: petrographic thin section analysis, scanning electron microscopy (SEM), inductively coupled plasma optical emission spectrometry (ICP-OES) and X-ray diffraction (XRD).

The structure of the thesis follows the traditional division of theses and other scientific studies. The literature review is provided in Chapter 2, which gives insight into the history, archaeology and geology of the Erlauf Valley and Lower Austria, summarises the publications about ceramic archaeometry from the region and provides an overview about theoretical approaches to pottery and borderland archaeology. This is followed by the Materials and Methods chapter

(Chapter 3), which presents the studied ceramic material and the archaeological sites where they were found, as well as the different methods used for its analysis and the reason of using these methods on archaeological ceramics. Then the results (Chapter 4) are detailed by analysis techniques. The data of the different analyses are summarised and interpreted in the next chapter (Chapter 5), which concentrates on questions related to provenance and distribution, technology, organisation of production, technological choices, continuity of technologies, innovation of graphite-containing ceramics, changes in technology and society and comparison of the investigated ceramic assemblage with other ceramics from the region. Finally, the main outcomes and closing thoughts are presented (Chapter 6). The thesis includes multiple appendices detailing the archaeological information of the samples and the data from the five analysis methods.

2 LITERATURE REVIEW

This chapter gives an overview about the history, archaeology and geology of Lower Austria and the Erlauf Valley. It also summarises the publications about scientific analyses of archaeological ceramics from the region. Furthermore, the last part of this chapter deals with how ceramic assemblages can be approached theoretically and how borderland archaeology can contribute to the understanding of processes affecting political, social, cultural and economic changes. All these pieces of information help putting the investigated ceramic material into context and will be essential when interpreting the results.

The study area, Lower Austria, is the north-eastern state of Austria (*Figure 1*). It is bordered by three other Austrian states: Upper Austria to the west, Styria to the south and Burgenland to the southeast, and two countries: Slovakia to the east and Czechia to the north. The capital of Austria, Vienna, is located within Lower Austria, but forms a separate state. Lower Austria consists of four regions ('quarters'): Waldviertel, Weinviertel, Mostviertel and Industrieviertel. The northern and southern regions are separated by the Danube, which runs across the state. One of its tributaries, the River Erlauf, is located in the Mostviertel.

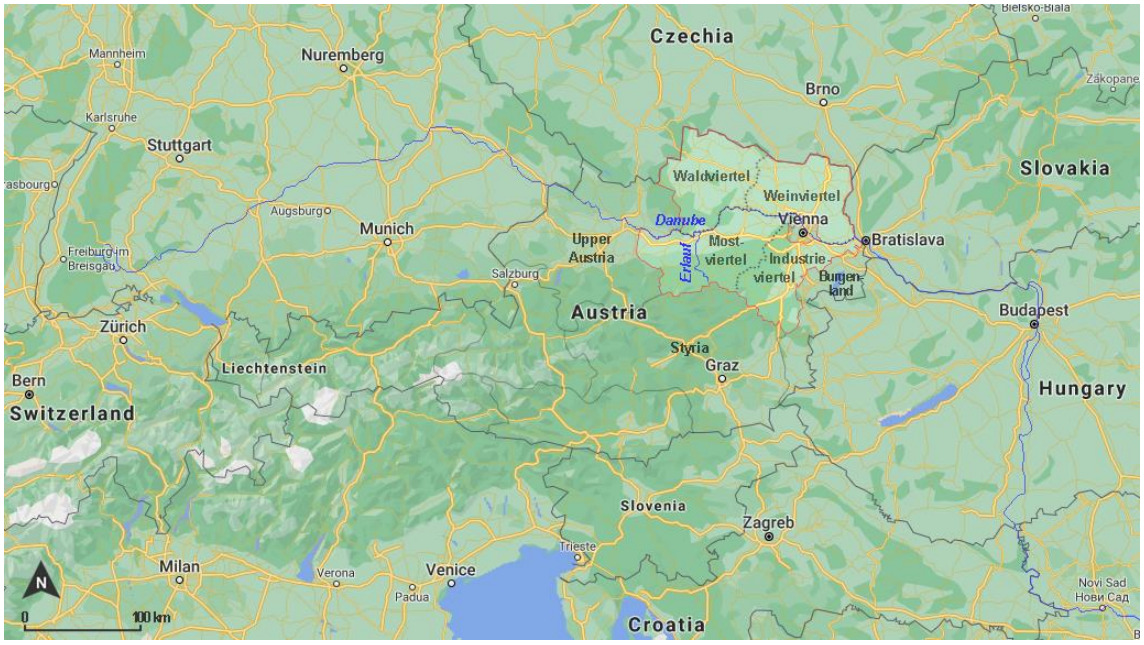


Figure 1. The location of Lower Austria and the Erlauf Valley (Base map: Google Maps)

2.1 History of the study area from the Roman to the Babenberg era

This subchapter outlines the key points in the history of the area of present-day Lower Austria between the 1st and the 11th centuries. The establishment of the Roman rule in the southern part of the region and its decline as well as the 'Barbarian' peoples of the Migration Period present in this area are detailed. This is followed by the description of the appearance of the Avars and Slavs and their contest with the Bavarians over the control of the region. Then the area as part of the Carolingian Empire and the Christian missionary activities are discussed. Following the summary of the Hungarian invasion, the subchapter ends with the Babenberg family coming to power in the region as part of Bavaria and the East Frankish Kingdom.

The map of Lower Austria below includes some important geological features, towns and settlements, which facilitates the comprehension of the history as well as the archaeology of the region (*Figure 2*).



Figure 2. The area of present-day Lower Austria (marked by red outline) with towns, settlements, archaeological sites and water bodies mentioned in the text (Base map: Google Maps)

2.1.1 The Roman Empire (15 BC – late 4th century AD)

The Celtic kingdom of Noricum, including the area of present-day Lower Austria, was annexed peacefully to the Roman Empire in 15 BC (Zöllner 1970, 25; Hameter 2015, 21). By the middle of the 1st century AD the western part of the kingdom became Noricum province while its eastern part (east of the Alps, especially the Vienna Basin) was joined to Pannonia province (Zöllner 1970, 25–26; Hameter 2015, 22–23). The militarily controlled border of the Roman Empire, the *limes*, was running along the southern bank of the Danube and was strengthened by watchtowers and forts as well as camps including Vindobona/Vienna, Carnuntum (no present-day equivalent, see *Figure 2*) and, after the Marcomannic wars (166–180 AD), Lauriacum/Enns (Zöllner 1970, 26, 31; Alföldy 1974, 150; Hameter 2015, 23–24).

Over time Roman towns developed from Celtic settlements and from settlements belonging to the Roman camps and forts (Zöllner 1970, 27). The system of Roman roads provided platform for military logistics and trade activities (Zöllner 1970, 28). Oil, vine, ceramics (including *terra sigillata*) and glass were imported from other parts of the Roman Empire and leather, fur, honey, wax, wild animals from the Barbarians (Zöllner 1970, 29). In turn, Noricum provided salt, iron, copper, lead, wool and cattle (Zöllner 1970, 29).

North of the Danube beyond the *limes*, Barbarian, mostly Germanic tribes were settled such as the Marcomanni and Quadi, which often intruded into the Empire and caused disturbance. With the end of the Marcomannic wars (166–180 AD), the Romans managed to pacify the Marcomanni, but soon (from 213 AD) they had to deal with the Alemannic invasion in Raetia, the province west of Noricum (Zöllner 1970, 31–32).

Following the reform of Diocletian (284–305) including the reorganisation of provinces and the army as well as the separation of military and civilian administration, the area of Lower Austria became the part of Noricum Ripense (the northern part of the former Noricum) and Pannonia Prima (*Figure 3*; Wolfram 1995, 24; Gerberding 2005, 17–21). As a result of the imperial reform, the Roman army was open to the Barbarians to a greater extent than previously (Wolfram 1995, 22). With the edict of Constantine the Great (306–337), Christianity gained legal status and started to spread around the Empire; sources report about small bishoprics covering the area of a town (*civitas*) already in the 5th century such as Lauriacum/Enns (Zöllner 1970, 34–35; Wolfram 1995, 41, 22). After the division of the Roman Empire to eastern and

western empires in 364, and permanently in 395 AD, Noricum Ripense and Pannonia Prima belonged to the Western Roman Empire (Wolfram 1995, 26; Gerberding 2005, 19).

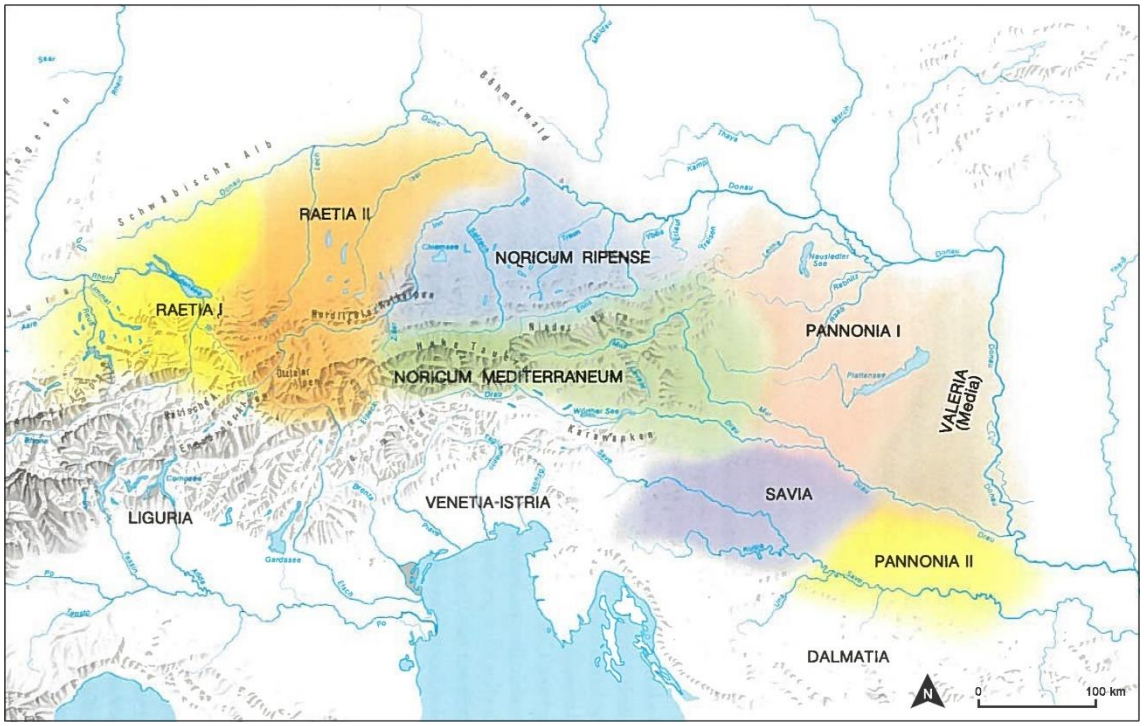


Figure 3. Late Roman provinces in Central Europe (modified after Wolfram 1995, 25)

2.1.2 Barbarians and the decline of the Roman rule (late 4th century – late 5th century)

The appearance of the nomadic Huns at the River Don in 375 induced several peoples to migrate westward and the period that historiography calls 'Migration Period' (German: Völkerwanderungszeit) had began (Vocelka 2010, 10). The pressure on the Roman borders was increasing due to repeated Barbarian onslaughts (Wolfram 1995, 26). The Roman approach included the settling of the invading Barbarians as *foederati* (allies) inside the borders such as the Marcomanni in Noricum Ripense in 397 (Zöllner 1970, 36; Wolfram 1995, 30; Gerberding 2005, 24). Pannonia Prima was ceded to the Huns sometime before 433 and after their defeats in 451 and 454/455, the Ostrogoths settled there as *foederati* until their departure for Gaul in 473 (Wolfram 1995, 33–35, 38). The Ostrogoths probably also occupied parts of eastern Noricum Ripense (Alföldy 1974, 220). At the same time (454/455), the east Germanic tribe of the Rugii, probably as a Roman federate, established its kingdom north of the *limes*, in the north-eastern part of present-day Lower Austria (Wolfram 1995, 53).

The Barbarian onslaughts gradually lead to the collapse of the *limes* and the Roman Empire, and at the same time, the weakening of the Roman rule allowed and induced the Barbarian invasions and the consolidation of the Barbarian kingdoms (Alföldy 1974, 213–214; Halsall 2005). With the Germanic chieftain Odoacer (476–493) coming to power in 476 in Italy, the Western Roman Empire is considered to be 'officially' ended (Wolfram 1995, 46; Gerberding 2005, 25). Odoacer could not protect Noricum form the attacks of the surrounding Barbarians, thus ordered the Romans to leave for Italy in 488 (Alföldy 1974, 224–226). The Vita Sancti Severini, written in 511, reports about the destruction and poverty of the 460s – 470s caused by the attacks of the Rugii and Alemanni and how Severinus, the monk and missionary, tried to secure the living conditions of the Roman population by concluding contracts and maintaining good relationship with the Barbarians (Eugippius 1–46; Alföldy 1974, 223; Wolfram 1995, 46–53). Nevertheless, life was still going on as the Vita also refers to trade/exchange activity such as the weekly market of the Rugii held north of the Danube, close to Favianis/Mautern, which was frequently visited by the Romans (Eugippius 9; Wolfram 1995, 49). The kingdom of the Rugii, however, was not long-lived: it ended with two lost battles against Odoacer in 487/488 and the Rugii left Noricum and joined the Ostrogoth army moving towards the west (Wolfram 1995, 55).

After three and a half years of war and the murder of Odoacer, Theodoric the Great (493–526) took over the power in Italy in 493, but the territory of Lower Austria probably was not part of his Ostrogothic Kingdom (Wolfram 1995, 58, 64; Moorhead 2005, 143–148).

2.1.3 Langobards (early 6th century – 568)

Soon after 488, the former land of the Rugii was occupied by the Germanic Langobards, who were the subjects of the Germanic Herules (or Heruli; Wolfram 1995, 58). The kingdom of the Herules, formed after 454/455, was located north and east of the Rugii and with the departure of the Rugii for Gaul its western borders became unprotected (Wolfram 1995, 58). The Langobards were settled there to secure the Herulian territory against the neighbouring peoples (Wolfram 1995, 58). Probably around 505, the Langobards crossed the Danube and occupied areas south of the river close to Tulln (Wolfram 1995, 58, 60). After the Heruli suffered defeat by the Langobards in *c.* 507, they lost their dominant position, king and unity, and the Langobards became the heirs of the Herulian kingdom (Wolfram 1995, 61, 66; Curta 2001, 191). The Langobards started to expand their rule over eastern Austria and western Hungary, and they occupied Pannonia in 526 (Wolfram 1995, 66). They had alliances both with

the Eastern Roman Empire (Byzantine Empire) to the east and the emerging Kingdom of the Franks to the west (Wolfram 1995, 66–67). Participating in a decisive battle of the Byzantine-Gothic wars (535–553) in 552 as allies of the Byzantine emperor Justinian I (527–565), they largely contributed to the end of the Ostrogothic Kingdom in Italy (Wolfram 1995, 68–69; Moorhead 2005, 149). They also defeated the Gepids in 567 with the help of the newcomer nomadic Avars (Wolfram 1995, 69). In exchange for the Avar help, the Langobards left for Italy in 568, handing over their Pannonian territories to the Avars and Slavic tribes (Wolfram 1995, 69–70; Moorhead 2005, 151–155). The arrival of the Avars is often considered as the end of the Migration Period and the start of the Middle Ages in central and eastern Europe (Curta 2001, 204).

2.1.4 Between the Avar Khaganate and Bavaria (568 – end of the 8th century)

The Avars fleeing from central Asia due to the expansion of the Turks appeared at the Black Sea in the mid-6th century, soon settled in the Carpathian Basin and established the Avar Khaganate lead by the khagan (Wolfram 1995, 306–307; Kobyliński 2005, 536; Pohl 2018, 19, 33–38). They conquered the people living there, amongst them probably Gepids and late antique communities (Pohl 2018, 100–109).

In the last decades of the 6th century, the territory of present-day Lower Austria was situated between the Avars and the Frankish vassal Bavarians (Wolfram 1995, 71); it is, however, unclear to what extent either of these powers had control over the territory. The Bavarians were ruled by the Agilolfing dynasty from the middle of the 6th century until the end of the 8th century, members of which attempted to gain independence from the Franks, but they never managed to achieve that aim in terms of church organisation, legislation and major politics (Wolfram 1995, 71, 76).

By the beginning of the 7th century, after several battles, the border zone between the Frankish-Bavarian and Avar-Slavic territories had probably developed along the north-south section of the River Enns at its confluence with the Danube (Wolfram 1995, 79; Beller 2006, 12). The area of present-day Lower Austria was likely under Avar control and was possibly inhabited by Slavic people. It is unclear when the Slavs arrived in this area, it might have been in the 6th century (Curta 2001, 99; Kobyliński 2005, 532; Vocelka 2010, 10), but there is no obvious mention of local Slavs in the historical sources before 777 (MGH Dipl. Kar. 1. 169, 226–

228; Wolfram 1995, 134). The first archaeological traces that can be connected to the Slavs are dated from the 7th century (Breibert 2005, 418; Section 2.2.3).

The Chronicle of Fredegar mentions a Slavic polity founded by Samo, a Frankish merchant in the 620s (Fredegar 4.48). The exact location, size, and importance of this polity is highly debated; nevertheless, it is often thought that its influence extended over the Lower Austrian region and the Alpine Slavic Carantans (Wolfram 1995, 80, 301; Kobyliński 2005, 540; Pohl 2018, 310).

The Carantans were likely a group of multi-ethnic origin including predominantly Slavs, but also remaining 'Roman' inhabitants and Germanic people, who eventually had Slavic rulers and established their early medieval polity during the 8th century (Wolfram 1995, 301; Kobyliński 2005, 538, 544). They were settled in the Eastern Alps mainly in the southern and western part of modern Austria (including the southern part of Lower Austria) and in Slovenia (Wolfram 1995, 301). The Carantans managed to keep independence and could preserve their territories from the Avars; in contrast, Samo's polity ended with the death of its founder in 669, which was followed by the restoration of the Avar rule (Wolfram 1995, 302; Beller 2006, 12).

2.1.5 The Bavarian Eastland of the Carolingian Empire (9th century)

With the end of the Agilolfing rule in 794, the Bavarian territories came under direct Frankish control as part of the expanding Frankish Empire of Charlemagne (768–814), which by then had already included the Langobard Italy from 773/774 (Wolfram 1995, 89, 93). Charlemagne carried out several campaigns against the Avars between 788 and 811, which – including the repeated looting and devastation of the Avar centre, the so-called 'ring' in 795 and 796 – very likely contributed to the collapse of the Khaganate (Wolfram 1995, 233–241; Pohl 2018, 376–389).

From the end of the 8th century, Bavaria – similarly to the other parts of the Carolingian Empire – was divided into administrative districts, called *pagi* or Gaue, which were governed by *grafiones* (counts), who were the representatives of the king and appointed by the king (Wolfram 1995, 213, 216). Some *pagi* were possibly also established outside of Bavaria such as Grunzwitigau east of the Enns in today's Lower Austria and a smaller county southeast of it (mentioned in 844) with the centre of *Savaria* (Szombathely, Hungary), although the existence and exact location/extent of these are debated (*Figure 4*; Wolfram 1995, 213, 250). The control of the borders was secured through the system of large border areas called marches

headed by prefects, who were appointed by the king and were personally responsible to him (Wolfram 1995, 217). After the subjugation of the Avars, a march was established east of the Enns covering the Avar-Slavic Pannonia and the Alpine Slavic state of Carantania (Wolfram 1995, 219). In a source from 870, this area was called *plaga orientalis*, meaning 'eastern region' which is often referred to as the Bavarian Eastland in publications (*Conversio* 10; Wolfram 1995, 219–220; Wolfram 1999, 294).



Figure 4. Peoples and regions in the 8th and 9th centuries in Central Europe (modified after Wolfram 1995, 221)

Under the direction of the prefects (called margraves from the end of the 9th century in the Bavarian Eastland) there were Frankish counts, but also leaders (*duces*) of peoples living in the border zone (Wolfram 1995, 217). Just as the Roman Empire had federal empires outside its borders, the Carolingian Empire was surrounded by dependent principalities such as the Avar Principality, the principality of Joseph, initially Carantania and the Pannonian principality of Moosburg (Wolfram 1995, 217, 220, 311). The Avar Principality is supposed to have been founded in 805, when one of the Avar leaders, Khapkan Theodorus received permission from Charlemagne to rule the territories 'between Carnuntum and Savaria' because his people were displaced by Slavs from their previous settlement areas (*Annales regni Francorum* a. 805; Wolfram 1995, 240). This was possibly dissolved during the reorganisation of 828, when several tribal leaders were replaced by Bavarian counts and came under direct Frankish-Bavarian administration (Wolfram 1995, 248). Another principality, referred to as the principality of Joseph, is hypothesised in the area of today's northern Lower Austria. Joseph is

mentioned in the early 900s by historical sources (Trad. Hoch. Freising I. 1037, 781–782), but it is possible that the principality already existed in the mid-9th century (Wolfram 1995, 441: note 190). The centre of Joseph's principality is assumed to have been at the archaeological site of Thunau am Kamp (see Section 2.2.3; Wolfram 1995, 311).

In his imperial decree (*Ordinatio imperii*; MGH Capit. 1. 136, 270–273) of 817, Charlemagne's son and successor, Louis the Pious (814–840), made his youngest son, Louis (the German, 817–(843)–876), the king of Bavaria and allocated the "Bavarians, Carantans, Bohemians, Avars and Slavs, who live east of Bavaria" to him (Wolfram 1995, 160; Fried 1995, 142). By 833 at the latest, a prefect called Ratpot was appointed to rule the Bavarian Eastland, who had a royal treasury in Tulln according to the historical sources (MGH Dipl. reg. Germ. 1. 96, 138–139; Wolfram 1995, 248–249). By this time, the Slavic Moravians were about to form their polity consisting of dependent ducal seats north of the Danube (its core being roughly in the area of present-day eastern Czechia and western Slovakia), which possibly extended its influence on the north-eastern part of Lower Austria as well (Wolfram 1995, 248, 319–320; Pohl 2018, 393). Simultaneously with the consolidation of the Moravian power, a former prince called Pribina was exiled from Nitra (in present-day Slovakia) and went to Ratpot, where Pribina was baptised (*Conversio* 10; Wolfram 1995, 248). The Franks recognized the possibility of using Pribina for the consolidation of central Pannonia and Louis the German granted him an area in Pannonia with the centre at Moosburg (near today's Zalavár, Hungary; *Conversio* 11, 13; Wolfram 1995, 249; Smith 1995, 183).

Following the division of the Carolingian Empire in 843, Louis the German became the king of the East Frankish kingdom, also called East Francia (Fried 1995, 146; Wolfram 1995, 162). In 856, he entrusted his eldest son, Carloman (king of Bavaria: 876–879/880) with the administration of the Bavarian Eastland (Fried 1995, 153; Wolfram 1995, 162). Louis the German wanted him to attack and subjugate the increasingly dangerous Moravians, but Carloman did not follow his father's will and made peace with them instead (Fried 1995, 153; Wolfram 1995, 251). In the early 870s, however, the Moravians with their prince Zwentibald I (871–894) turned against Carloman and annihilated the Bavarian army (Wolfram 1995, 255–256).

In 876, Carloman handed the Bavarian Eastland over to his son Arnulf (of Carinthia, king of East Francia: 887–899; Fried 1995, 162; Wolfram 1995, 164). Carloman was followed by his brother Louis the Younger in Bavaria (879/880–882), who acknowledged Arnulf in his Carantanian-

Pannonian territories (Wolfram 1995, 164). In 884, the successor of Louis the German, Charles III (876–887) concluded a peace treaty with Zwentibald I at Tulln and a couple of years later, in 892, Arnulf devastated Moravia with the help of the Hungarians (Fried 1995, 162; Wolfram 1995, 257, 269). After the death of Arnulf, his seven-year-old son, Louis (the Child, 900–911) was made king of East Francia in 900 (Fried 1995, 166; Wolfram 1995, 169). One of his most influential magnates was Margrave Luitpold who pursued his own policy and took over the border control against the consolidating state of Bohemia (in the area of modern Czechia), Moravia and the increasingly dangerous Hungarians completely independently from the child-king (Wolfram 1995, 169; Wolfram 1999, 295; Strzelczyk 1999, 516–519). In 907, however, he lost a battle and his life against the Hungarians near Pressburg (today: Bratislava, Slovakia), when the Carolingian rule came to an end in the Lower Austrian region few years before Louis the Child's death in 911 (Fried 1995, 165; Wolfram 1995, 169; Wolfram 1999, 295). The territories east of the Enns were lost to the Hungarians: the river formed the eastern border of Bavaria again (Wolfram 1995, 272).

2.1.6 Christianisation and church organisation in the 7th–9th centuries

The Christianity of the Roman era had survived at several places of Bavaria such as Iuvavum/Salzburg and Lauriacum/Enns (Wolfram 1995, 96). An ecclesiastical restoration started here in the 7th century, which led to the development of an advanced church organisation (Wolfram 1995, 96). Bavarian missions began east of the Enns among the Slavs including the Carantans (Wolfram 1995, 96, 105). Salzburg, as a bishopric from 739 and archbishopric from 798, became the centre of missionary activity from the 8th century (Beller 2006, 14–15; Vocelka 2010, 11).

Following the Frankish victory over the Avars in 796, Pepin summoned a synod for the conversion of the Avars, who showed willingness to accept the Christian faith (MGH Conc. 2.1. 20, 172–176; Wolfram 1995, 224). The synod was chaired by Patriarch Paulinus of Aquileia, who was entrusted to take care of the Avar mission (Wolfram 1995, 224–225). The ecclesiastical jurisdiction and the right to mission in the conquered areas, however, caused dispute between Salzburg and Aquileia as the territories east of the Enns had already been subjected to the Bavarian mission of Salzburg (Smith 1995, 188; Wolfram 1995, 225–226). In 811, Charlemagne settled the dispute by confirming the Drava as the border: the territories north of the Drava belonged to Salzburg and those south of the river to Aquileia (*Annales regni Francorum* a. 811; Wolfram 1995, 226). With the charter of Louis the German in 828/830, the

areas north of the River Raba were taken over by Passau (MGH Dipl. reg. Germ. 1. 173, 244–245; Wolfram 1995, 227).

Missionaries of the Byzantine Empire also took part in the Christianisation activity in the area. The brothers Cyril and Methodius came to Moravia in 863 bringing the Glagolitic alphabet with them, which provided the basis for the introduction of the Slavonic liturgy (Shepard 1995, 241–243; Wolfram 1995, 261). They were also welcomed in the Pannonian Moosburg, which provoked disapproval of the archbishop of Salzburg as it belonged to the Salzburg diocese (Wolfram 1995, 261–262). For Moosburg, however, this meant independence from Salzburg and the Bavarian church for a short time (Wolfram 1995, 262).

2.1.7 Hungarians (first half of the 10th century)

In 862, previously unknown nomadic troops devastated the empire of Louis the German according to Frankish annals (*Annales Bertiniani* a. 862; Wolfram 1995, 325; Bakay 1999, 536). The Hungarians, or Magyars as they called themselves, were referred to as Huns and Avars in contemporary Byzantine and Frankish sources (Bakay 1999, 536–537). They were pushed by the Turkic Pechenegs to move westward from the steppe, while they were joined by groups of people such as Kabars (Wolfram 1995, 325–326). Following their smaller invasions, they appeared in large groups around 895/896, settled in the Carpathian Basin and soon started their campaign of raids to the west and south (Zöllner 1970, 59-60; Bakay 1999, 539; Beller 2006, 13). Before the Hungarians crossed the Enns for the first time in 900, they fought battles in the area of Lower Austria: in 881 there was a fight with them near Vienna and a second encounter with their Kabar allies probably near Pöchlarn (Wolfram 1995, 271, 325). They destroyed Moravia by 906, and a year later, they defeated the Bavarian army at Pressburg resulting in the collapse of the eastern Carolingian marches (Wolfram 1995, 272; Wolfram 1999, 297; Beller 2006, 13). With their raiding campaigns in the area of modern Italy, Austria, Germany, France, Switzerland, Luxembourg and even Spain, the Hungarians posed a great danger for Europe until their defeat of 955 near Augsburg by the army of the east Frankish king Otto I (936–(962)–973), which put an end to their western campaigns (Wolfram 1995, 273; Bakay 1999, 541–544; Beller 2006, 13).

2.1.8 The Babenbergs (late 10th century – 11th century)

In 962, Otto I became emperor following his coronation in Rome (Müller-Mertens 1999, 250; Beller 2006, 13). He started the gradual recovery of the lost territories in east Bavaria and east

of the Enns and set up a new march covering the core of modern Austria (Wolfram 1995, 273; Wolfram 1999, 305; Beller 2006, 13). South of today's Lower Austria, the march of Styria developed from Carantania (Beller 2006, 14; Vocelka 2010, 15). The rest of the former Carantania, including the southeast part of Lower Austria, became the Dutchy of Carinthia in 976, when it was separated from the Dutchy of Bavaria (Wolfram 1999, 305; Vocelka 2010, 16).

The Austrian March was governed by Margrave Leopold I (976–994) from 976, who was the first member of the Babenberg dynasty, which was ruling the area of Lower Austria (later also that of present-day Upper Austria and Styria) until 1246 (Zöllner 1970, 63; Wolfram 1999, 305; Vocelka 2010, 12). The march belonged to the Duchy of Bavaria and the Babenbergs were under the Bavarian duke until 1156 (Beller 2006, 15–16). Leopold I initially governed a small part of the Danube Valley with his centre in Melk and during his rule he managed to extend the march up to Vienna (Zöllner 1970, 62; Vocelka 2010, 12). In a donation certificate of 996 (MGH Dipl. reg. imp. Germ. 2.2. 232, 647), the name Ostarrichi was mentioned for the first time, the medieval equivalent of the German name Österreich for Austria, which was ruled then by Henry (994–1018), the son of Margrave Leopold I (Beller 2006, 14; Vocelka 2010, 12).

The recovery of eastern territories and eastward expansion of the Austrian March came to an end when Hungary became a Christian state under the rule of the first Hungarian king, Stephen I (997–1000/1001–1038; Bakay 1999, 548–551; Vocelka 2010, 13). Nevertheless, during the rule of Henry and his successors Adalbert (1018–1055) and Ernest (1055–1075), there were some conflicts regarding the location of the border between Bavaria (thus the East Frankish Kingdom) and Hungary, which was finally fixed around the River Leitha (Zöllner 1970, 64–67; Wolfram 1999, 306).

The Babenbergs were not the only landowners in the Austrian March and it was not obvious that they could keep their leading position among other powerful families. By the time of Ernest coming to rule, however, eventually almost all other influential families died out, and they were able to consolidate and gradually extend their power (Zöllner 1970, 66; Vocelka 2010, 12).

When the investiture controversy broke out in 1075 between the pope, Gregory VII (1073–1085), and the German king, Henry IV (1054–(1084)–1105), concerning the right of selection and installation of bishops, the Babenbergs had to decide which side they stand (Zöllner 1970,

67; Beller 2006, 18). Probably the most prominent member of the family was Leopold III (1095–1136), who clearly turned to the imperial side in the investiture dispute after his predecessor (Leopold II, 1075–1095) had fluctuated (Zöllner 1970, 67; Vocelka 2010, 13). He also managed to relate the Babenberg family to the most powerful families, the Salian and the Hohenstaufen dynasties, which were providing the East Frankish Kingdom (later Holy Roman Empire) with emperors (Vocelka 2010, 13).

The Babenberg rule resulted in the consolidation and stabilisation of the Austrian March. During the 11th and 12th centuries, the settlements were expanding, which can be inferred from place names (Vocelka 2010, 13). Church life was flourishing as shown by the foundation of several monasteries in the area of Lower Austria such as Göttweig, Melk, Herzogenburg, Seitenstetten, Heiligenkreuz, Klosterneuburg, Zwettl, Altenburg, Geras and Lilienfeld (Vocelka 2010, 13).

2.1.9 Summary

The history of Lower Austria between the 1st and the 11th centuries was a dynamic period filled with constant changes. Peoples followed one another in this region, which had seen the forming and decline of several kingdoms and empires. Probably the only common feature of these centuries is that Lower Austria had always been a border area. With the Danube and the Roman *limes* running across it, the southern part of Lower Austria was the northern border of the Roman Empire. Following the Bavarian-Avar conflict, the region became a western borderland of the Avar Khaganate. After the conquest of the Avars by the Franks, the territory of Lower Austria was part of the easternmost march of the Carolingian Empire. Apart from the short intervention of the Hungarians, it remained a western border region in the 10th and 11th centuries, that of Bavaria and the East Frankish Kingdom.

2.2 Archaeology of the region

This section provides an overview of the archaeological features and findings characteristic to the different periods between the 1st and the 11th century AD in Lower Austria. Special emphasis is placed on the Erlauf Valley as most of the ceramic sherds studied in this thesis originate from this area.

For the location of the main archaeological sites mentioned in the text see the map of Lower Austria (*Figure 2*) in Section 2.1.

2.2.1 Romans and Barbarians (1st–5th centuries AD)

Roman camps, forts and watchtowers were built during the Roman period along the Danube *limes*. The *limes* itself eventually was fortified with palisades, stone or earth walls and trenches (Fischer 2015, 26). The camps and their smaller versions, the forts, provided living space for legions and auxiliary troops, respectively (Fischer 2015, 26). On the Lower Austrian *limes* section legionary camps were built at Albing (relocated to the neighbouring Enns/Lauriacum between AD 185 and 205), Vienna/Vindobona and Carnuntum (Gassner and Pülz 2015, 333: Abb. 189; Harreither 2015, 165). Forts were documented by historical and archaeological evidence at many places in Lower Austria (Wallsee, Mauer an der Url, Mautern/Favianis, Traismauer/Augustiana, Zwentendorf/Asturis, Tulln/Comagenis, Zeiselmauer, Klosterneuburg, Schwechat/Ala Nova, Höflein) including Pöchlarn/Arelape in the Erlauf Valley (Gassner and Pülz 2015, 333: Abb. 189). The fortifications initially were built in timber and earth, and for the construction of the interior buildings clay and wood were used; these were gradually replaced by stone walls and buildings in the 1st and 2nd centuries AD at locations where these raw materials were available (Fischer 2015, 27–30). Inside the camps and forts various buildings emerged including the *principia* (large building complex enclosing a courtyard), *praetorium* (providing superior living comfort for legion legates), tribune houses (for the military tribune), elongated barrack buildings, baths, granaries, hospital buildings and workshops (Fischer 2015, 30–33).

Between the camps and forts, numerous watchtowers (*burgi*) were located. The remains of the masonry watchtowers found along the Austrian *limes* are dated from the end of the 2nd century (Fischer 2015, 34). The closest watchtowers to the Erlauf Valley were built at Ybbs, Sarling and Neumarkt an der Ybbs to the west and at Melk to the east (Gassner and Pülz 2015, 333: Abb. 189). The inscription of the watchtower at Ybbs, found in the early 1500s and lost

since, allowed the exact dating of the building to AD 370, which might have been one of the last attempts to secure the *limes* here (Denk 1962, 83–84).

Near the camps and forts, civil towns and settlements (*canabae legionis* and *vicus*, respectively) were founded, which were subordinate to the military administration and provided home for the families of the soldiers as well as craftsmen and traders (Fischer 2015, 33). Such civil settlements were excavated near the above-mentioned camps as well as forts at Mautern/Favianis, Zwentendorf/Asturis and Tulln/Comagenis (Scherrer 2015, 53). Autonomous civil towns (*municipium*, *colonia*) were also established near the fortifications and further from the *limes* such as that of St Pölten/Aelium Cetium in the first half of the 2nd century AD (Scherrer 2015, 49, 57). The forum, baths, sanctuaries and amphitheatres were all important features of both dependent and autonomous civil towns (Fischer 2015, 34, Scherrer 2015, 65–67).

One of the main sites of the Roman period in the Erlauf Valley was the fort of Arelape, remains of which were uncovered in the town centre of present-day Pöchlarn (*Figure 5*; Hinterwallner and Schmid 2015). It may be possible that the fort, which is now situated south of the Danube, was located on an island of the Danube in Roman times (Hinterwallner and Schmid 2015, 194). The excavated features suggest the dating of the fort from the 2nd century AD (Hinterwallner and Schmid 2015, 196). Near the fort, the adjoining *vicus* including a bath and a cemetery were also found. The cemetery was still in use in the first half of the 5th century (Hinterwallner and Schmid 2015, 197).



Figure 5. Remains of fort Arelape at Pöchlarn (Hinterwallner and Schmid 2015, 197: Abb. 117)

In the countryside, villas were built consisting of a main residential building, administrator's house, bath, stables, barns, storage buildings, occasionally sanctuaries, etc. (Scherrer 2015, 54). Their function was initially mostly agricultural, which by the end of the Roman period gradually faded in favour of the representative country house character (Scherrer 2015, 55). The remains of similar building complexes were also found in the Erlauf Valley north and south of Purgstall including floor heating systems (hypocausts; Denk 1962, 114–115, 121–129) and east of Purgstall near Gries (Rausch 1992 and 1993).

Roman cemeteries were attached to each camp and fort with burials arranged in groups or rows, or both ways such as in Pöchlarn/Arelape (Kremer 2015, 89). Both cremation and inhumation were used to bury the dead with cremation being the predominant type of burial in the 1st–2nd centuries AD and inhumation becoming more popular from the 3rd century AD (Kremer 2015, 90). The urns could be of different materials including ceramics, glass or stone (Kremer 2015, 90). In the case of inhumation, the body was commonly wrapped in a cloth and put in the grave pit; occasionally the use of a wooden board or coffin could also be proven (Kremer 2015, 90). In some cases, bricks, tiles and stones were used to line and cover the grave pits and stone or lead sarcophagi were also present in Roman cemeteries (Kremer 2015, 90–91). The grave goods such as food, lamps, dishes, glasses, jewellery, boxes, mirrors, keys, tools and weapons were frequent until the late 2nd century AD from when a general decline in the amount of grave goods is noticeable (Kremer 2015, 91–92). Many of the graves were marked by a stelae or grave monument, which were often reused in the subsequent centuries and thus found in secondary find contexts (Kremer 2015, 92–94).

This was the case with many gravestones that are built into church walls and other buildings in the Erlauf Valley (e.g. Pyhrafeld, Wieselburg, Ockert, Oberndorf an der Melk; Denk 1962, 88, 95–97, 107–108). Burial mounds with cremations were found north of Purgstall from the beginning of the Roman occupation including most likely the graves of the indigenous Celtic population that had been partly Romanised (Denk 1962, 109–114). Early rock tombs with holes carved in the rock floor for urns were also found east of Wieselburg, near Koth. Based on the inscriptions, the site is dated to the 1st century AD (Denk 1962, 91–95). The remains of a Roman cemetery were excavated near Mühling at Gumprechtsfelden, which originates from the 4th century AD (Denk 1962, 99–107).

Barbarian settlements and cemeteries dated to the Roman period were also excavated in Lower Austria. The Roman cemeteries west of Lake Neusiedl, south and southwest of Vienna

contained finds of Germanic origin and Germanic names appeared on the tombstones (Stuppner 2015, 112–113). This indicates the appearance of Barbarians south of the Danube, possibly that of the Quadi led by Vannius, who were admitted to the Empire following their defeat in AD 51 by rival Germanic groups (Stuppner 2015, 112).

Most of the sites with Germanic finds, however, were located outside of the province of Noricum and Pannonia, north of the Danube. Based on the Germanic settlement remains including wooden structures and sunken-featured buildings, the northern part of Lower Austria was gradually populated by Germanic people from the middle of the 1st century AD (Adler 1977a, 50–52, Stuppner 2015, 114). Residences of probably the Germanic elite from the end of the Roman period (late 4th century – 5th century AD) were also excavated in north-eastern Lower Austria (Niederleis, Oberleiserberg) and Slovakia with an architecture similar to that of Roman villas (Stuppner 2015, 119–123).



Figure 6. Fibulae from the female grave of Untersiebenbrunn (Friesinger and Vacha 1988, 55)

A mixture of Germanic, Roman and Nomadic influences can be detected in some burials such as the well-equipped graves of a woman and a child excavated in the Lower Austrian Untersiebenbrunn (*Figure 6*). The deceased of the Untersiebenbrunn graves were most probably members of the Barbarian elite in the first half of the 5th century AD (Stuppner 2015, 124–125). Some burials of the 5th century in the eastern part of Lower Austria and in Vienna show the appearance of eastern weapons (bows and arrowheads) as well as the adoption of

artificial skull deformation among the Germanic people, which was brought by the Huns into Europe (Friesinger 1977, 62–63).

In addition to settlements and burials, the Romans had an impact on the Barbarian ceramic production as well. The Germanic tribes produced hand modelled pottery until the end of the 3rd century, when they also adopted the potter's wheel under the influence of Roman ceramic technology (Adler 1977a, 53–54, Stuppner 2015, 124). Wheel-thrown vessels are detectable until the 5th century both within and outside the *limes* in the study area (Adler 1977a, 54; Herold 2014, 665). A decline in pottery quality, the abandonment of the potter's wheel and a return to hand modelled and slow wheel turned ceramics could also be detected at other parts of the late antique world following the collapse of the Roman rule (Arthur 2007, 165–173).

2.2.2 Langobards (first half of the 6th century)

In spite of their relatively short stay between the beginning of the 6th century and 568, the Langobards left archaeological traces in the territory of Lower Austria. Their settlements have been hardly detectable, but based on the concentration of cemeteries and finds, they probably settled close to the remains of the Roman legion camps, forts and civil settlements (Adler 1977b, 76).

The excavated Langobard cemeteries, however, are abundant and were found both north and south of the Danube (e.g. Maria Ponsee, Schwechat, Unterrohrendorf, Poysdorf, Hauskirchen, Baumgarten an der March) including many disturbed graves (Adler 1977b, 75–76). The dislocation of body parts in some graves suggest that the disturbance happened relatively soon after burial (Adler 1977b, 81; Aspöck 2003, 251). The systematic disturbance of the graves is often termed as 'robbing' in older publications, and although there is no evidence of the identity of the people reopening the graves, they are often associated with members of Herulian or Slavic tribes or even the Langobards themselves (Adler 1977b, 81; Bóna et al. 1993, 124–125; Wolfram 1995, 61; Stadler et al. 2003). The idea of grave reopening as a symbolic or ritual act by the same community that buried the dead was also highlighted recently (Aspöck 2003; Aspöck 2011, 313).

The Langobard graves were relatively deep (usually 2–3 m, but even up to 7 metres in the case of elite graves), west–east orientated rectangular pits, within which the dead was laid out facing east (Adler 1977b, 76–77; Bóna et al. 1993, 122). Coffins were detected occasionally, and the design of some pits might suggest the presence of wooden boards in the graves (Adler

1977b, 77). The construction of a small wooden 'mortuary house' in the grave is a characteristic of some rich Langobard burials (Bóna et al. 1993, 122).

Women were typically buried with four brooches (fibulae) as parts of their clothing accessories: two of them were smaller and located on the chest (e.g. S-shaped fibulae ending in bird heads, disc fibulae), while the other two were bigger (gilded silver or bronze fibulae) and found in the pelvic area (Adler 1977b, 77). The role of the big fibulae might be interpreted as aesthetical rather than functional; they were hanging from the belt on ribbons or straps (*cingulum*), which could be decorated with silver or bronze fittings (Bóna et al. 1993, 128). A knife and pendants could also be attached to the end of the *cingulum* (Adler 1977b, 77; Bóna et al. 1993, 128). Some women wore a necklace which could include colourful glass beads, multicoloured millefiori beads, amber beads or even gold bracteates as Barbarian imitations of Roman coins (Adler 1977b, 77).

In male graves, belt buckles were often found as an indication of a fabric or leather belt (Adler 1977b, 77). Men were usually buried with weapons such as double-edged longswords, spears, shields and bows with arrows (Adler 1977b, 77–78). Both men and women could have a small bag hanging from their belts, which could contain a fire making set (consisting of a fire striker, flint and tinder), tweezers and scissors in the case of men and a key, a needle, an iron knife and broken glass in the case of women (Adler 1977b, 77). Occasionally small buckles and metal strap ends were found around the legs or feet in both male and female burials, which were used for tying up leather shoes (Adler 1977b, 77).

Ceramic vessels are frequent grave goods in both Langobard male and female graves and sometimes wooden vessels with metal fittings, metal vessels (such as the so-called Perlrandbecken) and glassware were also detected (Adler 1977b, 78). The Langobard pottery found in the graves is mostly hand modelled, but from around the 530s wheel-turned vessels are also present (Adler 1977b, 78–79; Bóna et al. 1993, 141). A kiln used for firing pottery, dated to the first half of the 6th century, was excavated at Ternitz (Friesinger and Kerchler 1981, 193–196, 232–243).

2.2.3 The Avars and the Carolingian period (7th–9th century)

After the migration of the Langobards to Italy, their territories were occupied by the nomadic Avars, who gradually changed to a sedentary lifestyle (Daim 1977, 91; Daim 2003, 518). The main settlement area of the Avars was located in the territory of present-day Hungary. It can

be seen from finds in the Carpathian Basin that the material culture of the Avars was influenced by Byzantine, late antique and Germanic elements, which were integrated into their eastern tradition (Daim 2003, 518–519).

A number of Avar period cemeteries (such as Vienna-Liesing, Mödling, Leobersdorf and Mistelbach) were excavated, through which the presence of the Avars can be assumed in the eastern part of Lower Austria from about the middle of the 7th century (Daim 1977, 93). Based on the finds of the male graves, men were buried with their weapons including bows, quivers, arrows with three-winged arrowheads, sabres and spears (Daim 1977, 92–93; Daim 2003, 465–468, 488). A knife and a small bag were usually hanging from their belts including a fire striker, flint and tinder (Daim 1977, 92). The belts were frequently decorated with metal fittings (*Figure 7*; Daim 1977, 92; Daim 2003, 497–499, 501–504). Women often wore earrings, bracelets and necklaces; knifes, spindle whorls and needles can also be found in their graves (Daim 1977, 92).



Figure 7. Avar belt fitting depicting a griffin from Mödling (Friesinger and Vacha 1988, 93)

Only few Avar period settlements were excavated in the eastern part of Lower Austria, which were usually characterised by sunken-featured buildings, postholes indicating ground-level buildings and a large variety of pits (Herold 2013, 132; Daim 2003, 484–486). They were often built on former Roman sites (Herold 2013, 136).

As for the other parts of Lower Austria, finds (especially grave finds) dated to the 7th and 8th centuries are very few, while there are a relatively large number of cemeteries dated to the 9th century (Friesinger 1971–1974, 112). This can be explained in different ways. One of the suggestions is that this area between the Enns and Vienna Woods (west of Vienna) was an

extensive border area of the Avar Khaganate in the 8th century with no or very low population for strategic reasons (Daim 1977, 93–94; Friesinger and Friesinger 1977, 104; Szőke 2004, 181). With the downfall of the Khaganate at the end of the 8th century, the Slavic groups living under Avar rule east of Vienna became free and, together with other Slavic incomers from the north and northeast and Germanic groups from the Frankish Empire, they settled in the previously uninhabited areas (Friesinger 1971–1974, 112–113; Friesinger and Friesinger 1977, 104).

According to another view, the depopulation of this area is not probable, and the chronology of some archaeological sites can be extended into the 8th century (Szameit 1991; Szameit 2000). The existence of surviving population groups of the Roman period can be hypothesised which along with immigrating Slavs and Avars formed a mixed population with late antique, Slavic, Frankish-Bavarian and Avar archaeological attributes by the 8th century (Szameit 1991; Szameit 2000; Breibert 2005, 420, 425). Because of the mixed characteristics, the ethnicity of this population can no longer be determined (Szameit 2000; Breibert 2005, 420–422).

Another explanation can be a research gap, that the excavations carried out in Lower Austria somehow have not included 7th–8th-century sites and finds. This option seemed unlikely about 50 years ago already based on the intensive construction activity of the 1960s – 1970s in the Danube region (Friesinger 1971–1974, 113). It is possible however, that the Slavic population used cremation in the 7th and 8th centuries as few cremation burials suggest, which is less easily detectable archaeologically than inhumation burials (Breibert 2005, 418–422). The change to inhumation at the beginning of the 9th century might have been induced by the people surrounding the Slavic groups (late antique population, Avars and Germanic people), which all used inhumation (Breibert 2005, 418–422).

A number of cemeteries (e.g. Pottenbrunn, Tulln, Pitten, Erlach) can be connected to the mixed ‘non-Avar’ population in Lower Austria (Friesinger 1971–1974; Friesinger and Friesinger 1977, 104–105; Herold 2015a). Many of them were published by researchers supporting the theory of the unpopulated border area and thus dated to the 9th century and connected to the Slavic population. These burials often showed Frankish-Bavarian influence (jewellery, weapons) and links to the Carpathian Basin, Moravia and the so-called Köttlach culture of the eastern Alpine region (Giesler 1980) could also be identified (Friesinger 1971–1974, 91–108; Friesinger and Friesinger 1977, 105–106, 111). Remains of such ‘non-Avar’ cemeteries were found in the Erlauf Valley at Ornding, Wieselburg, Mühling and Purgstall (Denk 1962, 154–163;

Friesinger 1971–1974, 56–68; Sauer and Czubak 1997; for Mühling and Purgstall see Section 3.1).

The graves are usually arranged in rows frequently with west-east orientation (Friesinger 1971–1974, 80–82). Wooden coffins were recorded at several places (Friesinger 1971–1974, 82–83). Accessories are abundant in female graves including earrings, temple rings and finger rings (Friesinger 1971–1974, 87–88, 99–104). Women could wear necklaces made of different beads with often various objects attached to them such as pendants and glass buttons with iron eyelets as well as bells in the case of children burials (Friesinger 1971–1974, 87–88, 104–105). In some female graves ceramic or stone spindle whorls were found, usually at the feet (Friesinger 1971–1974, 87). The belts of the men are seldom indicated by metal buckles, but indirectly the objects attached to the belt prove its existence, such as a piece of flint, occasionally a fire striker (both probably put in a small bag) or a knife (Friesinger 1971–1974, 89–93). Rarely, weapons are also found in male graves including spears, arrowheads and axes (Friesinger 1971–1974, 90–91, 94–95). Typical Avar finds may be present in these 'non-Avar' cemeteries such as belt sets of the so-called 'griffin and tendril' type, which were also recovered in the Erlauf Valley in the cemetery of Purgstall (Sauer n.d.) and a fitting of this type were found as a stray find near Zelking (Winter 1997, 194–195).

The practice of burying food with the deceased was very popular. Remains of chicken and sheep/goat are frequently found in the graves along with chicken eggshell. The food was placed into ceramic pots or wooden vessels which latter are recognised from their metal parts (Friesinger 1971–1974, 86, 105–108). The placement of skulls of sheep and goats or partial cattle skull with horn roots in the grave was another characteristic burial custom in numerous cemeteries (Friesinger 1971–1974, 85).

Many of the above-mentioned 'non-Avar' cemeteries closed around the middle of the 9th century (Friesinger 1971–1974, 110). In other 'non-Avar' cemeteries people started to bury their dead without food addition around the same time (although food was still present in some graves until the end of the 9th century north of the Danube; Friesinger 1971–1974, 110–111). These changes might be interpreted in relation to Christianisation, which brought the establishment of new cemeteries around churches and the abandonment of the pagan custom of giving food to the dead (Friesinger and Friesinger 1977, 107).

A distinct group of burials was found in the north-western part of Lower Austria: these graves were covered by burial mounds (tumuli; Breibert 2005, 415–418). This burial form is very similar to the Slavic tumuli in today's Czechia and Slovakia and might suggest Slavic immigration from the north and northeast (Friesinger and Friesinger 1977, 104; Breibert 2005, 415–418). Several tumuli were also uncovered very close to the Erlauf Valley just on the opposite (northern) side of the Danube at Wimm (Breibert 2005).

The known settlements of the 7th–9th centuries (e.g. Sommerein, Michelstetten, Pellendorf, Michelhausen, Thunau am Kamp) are few and usually only partially excavated (Herold 2011a, 526–527). Sunken-featured buildings were frequent and ground-level buildings with wooden structures also occurred. Ovens inside and outside of buildings as well as numerous pits were found in these settlements (Herold 2007, 77–81; Herold 2011a, 526–527).

Archaeological investigations also uncovered fortified settlements from the 9th–10th centuries located mainly in the northern part of Lower Austria (Herold 2011a, 526). One of them is Thunau am Kamp, the supposed centre of Joseph's principality (Section 2.1.5), where remains of a manor farm, a cemetery and numerous settlement features were excavated within the fortification rampart, which was made of wood, earth and stones (*Figure 8*; Herold 2011a).



Figure 8. Reconstruction of the manor house in the fortified settlement of Thunau am Kamp (Herold 2007, 83: Abb. 3.5.5)

Mautern and Tulln were central administrative points of the Frankish Empire based on the historical sources (Friesinger 1971–1974, 118). The occupation of these past Roman sites during the 9th and 10th centuries was also detected by archaeology (Herold 2007, 81; Herold 2011a, 527; Kühtreiber and Obenaus 2017, 180; see also Section 3.1).

2.2.4 The 10th and 11th centuries

The Hungarians, conquering the Carpathian Basin at the end of the 9th century, kept the territory of today's Lower Austria under military surveillance and based on the sporadic Hungarian-related finds, they probably did not settle there in large numbers (Fodor 1996, 437). Some cemeteries (e.g. Bruck an der Leitha, Bad Deutsch-Altenburg) and single burials (Lanzenkirchen, Gnadendorf) show strong Hungarian characteristics in terms of weapons (reflex bow) and costume elements (e.g. snakehead bracelets), which suggest the presence of Hungarians in the easternmost part of Lower Austria (Obenaus 2014, 167–168).

Other cemeteries of the 10th and early 11th centuries exhibit late Carolingian and Ottonian influences (the so-called 'Horizont Köttlach II'; Giesler 1980; Eichert 2013) such as Zwentendorf containing headdress rings and disc brooches with enamel inlay (Obenaus 2014, 166). There are also cemeteries with mixed finds having a connection both to the western and eastern cultural sphere (e.g. Köttlach, Thunau am Kamp, Langenschönbichl, Oberleiserberg; Obenaus 2014, 169–171).

Settlements of the period in question are difficult to detect similarly to the previous centuries. There are only few finds and features which can be connected to settlements of the 10th and 11th centuries (Obenaus 2014, 183). An exception is the so-called 'Talsiedlung' located in the immediate vicinity of the fortified settlement of Thunau am Kamp, which shows the traces of strong economic use; however, it cannot be considered as a typical rural settlement because of its relation to the fortified settlement (Obenaus 2014, 183–185).

Significantly more information is available on fortifications and fortified settlements. Some fortified settlements established in the 9th century (e.g. Thunau am Kamp, Stein an der Donau) continued to exist in this period and new fortifications were also built throughout the 10th–11th centuries (e.g. Sand near Oberpfaffendorf, Sachsendorf, Wieselburg, Raabs an der Thaya; Kühtreiber and Obenaus 2017, 174–188). From the finds and features, the Lower Austrian area was in the middle of overlapping cultural influences adopting elements from the Moravian, Bohemian, Hungarian and Ottonian regions (Kühtreiber and Obenaus 2017, 36–44). A development can be seen from large establishments bordered by timber and earth ramparts of the 9th century to smaller castles built in stone from the late 10th and 11th century (Kühtreiber and Obenaus 2017, 207–209). The form of the fortifications was very different as was their

supposed function including temporary refuge, protection of a settlement, residence of the nobility, etc. (Herold 2007, 87–89; Kühtreiber and Obenaus 2017, 207–209).

The Erlauf Valley is home of a rampart fortification in Wieselburg, which, in addition to archaeological evidence, is also documented by exceptional historical sources confirming that it was built in the late 10th century (Ladenbauer-Orel 1972; Kühtreiber and Obenaus 2017, 117–123; NÖUB I. 17, 205–207, 212–213). The fortified area contains an octagonal Ottonian church from the end of the 10th century, a large part of which is still preserved and visible in the present-day parish church (*Figure 9*; Ladenbauer-Orel 1972; Benesch 2003; on the church and the fortification see Section 3.1).



Figure 9. The Ottonian church in Wieselburg as a side chapel of the modern parish church (photo by the author)

2.2.5 Summary

The archaeological remains found in Lower Austria illustrate the diversity of the peoples living there between the 1st and 11th centuries. As a constant border region, a mixture of influences of the neighbouring areas had always been present in the material culture of the different periods. Several finds and features show that the Erlauf Valley provided a popular living environment throughout the centuries.

2.3 The geology of Lower Austria and the Erlauf Valley

The investigation of raw materials and provenance of ceramics requires a comprehensive assessment and understanding of the geology of the study area. Therefore, the aim of this subchapter is to provide information about the geological background of the Erlauf Valley and Lower Austria. Emphasis is placed especially on rock types and formations as these are the most important when defining possible sources of pottery raw materials.

The first part of this section gives information about the geological units and zones of Lower Austria including the description of the Bohemian Massif, the Alpine foreland, the different rock formations of the Eastern Alps and the Vienna Basin. This is followed by a geological overview of the Erlauf Valley. Finally, clay and graphite deposits are discussed as important raw materials of ceramics. These sections contain references to different geological eras, periods and epochs, which are summarised in *Table 1* below.

Table 1. Geologic time scale from the Devonian with eras, periods and epochs relevant to the text (based on the International Chronostratigraphic Chart, Version 2020/03[1])

Era	Period	Epoch	Age (Ma)
			present
Cenozoic	Quaternary	Holocene	0.0117
		Pleistocene	2.58
	Neogene	Pliocene	5.333
		Miocene	23.03
	Paleogene	Oligocene	33.9
		Eocene	56.0
		Paleocene	66.0
Mesozoic	Cretaceous	Upper	100.5
		Lower	~ 145.0
	Jurassic	Upper	163.5 ±1.0
		Middle	174.1 ±1.0
		Lower	201.3 ±0.2
	Triassic	Upper	~ 237
		Middle	247.2
		Lower	251.902 ±0.024
Paleozoic	Permian		298.9 ±0.15
	Carboniferous		358.9 ±0.4
	Devonian		419.2 ±3.2

2.3.1 The geological setting of Lower Austria

The territory of Lower Austria is dominated by two big geological units, the Bohemian Massif to the north and the Eastern Alps to the south (*Figures 10* and *11*). The Bohemian Massif is situated mostly in Czechia and also extends to the eastern part of Germany (Bavaria) and the

[1] https://stratigraphy.org/icschart/ChronostratChart2020-03.jpg (accessed on 17/09/2020)

northern edge of Austria (Janoschek and Matura 1980, 15). This unit is part of the Variscan belts[2] of Europe along with the Black Forest in Germany and the Vosges and Massif Central in France (Mazur and Kroner 2008, 611). The Bohemian Massif consists of two major zones, the Saxo-Thuringian Zone to the north and the Moldanubian Zone to the south, as well as one smaller zone, the Moravo-Silesian Zone to the east. The Moldanubian Zone can be subdivided into the Teplá-Barradian Unit to the north and the Moldanubicum *sensu stricto* to the south (Linnemann et al. 2008, 60). Among these units, the Moravo-Silesian Zone and the Moldanubicum *sensu stricto* are present in Lower Austria.

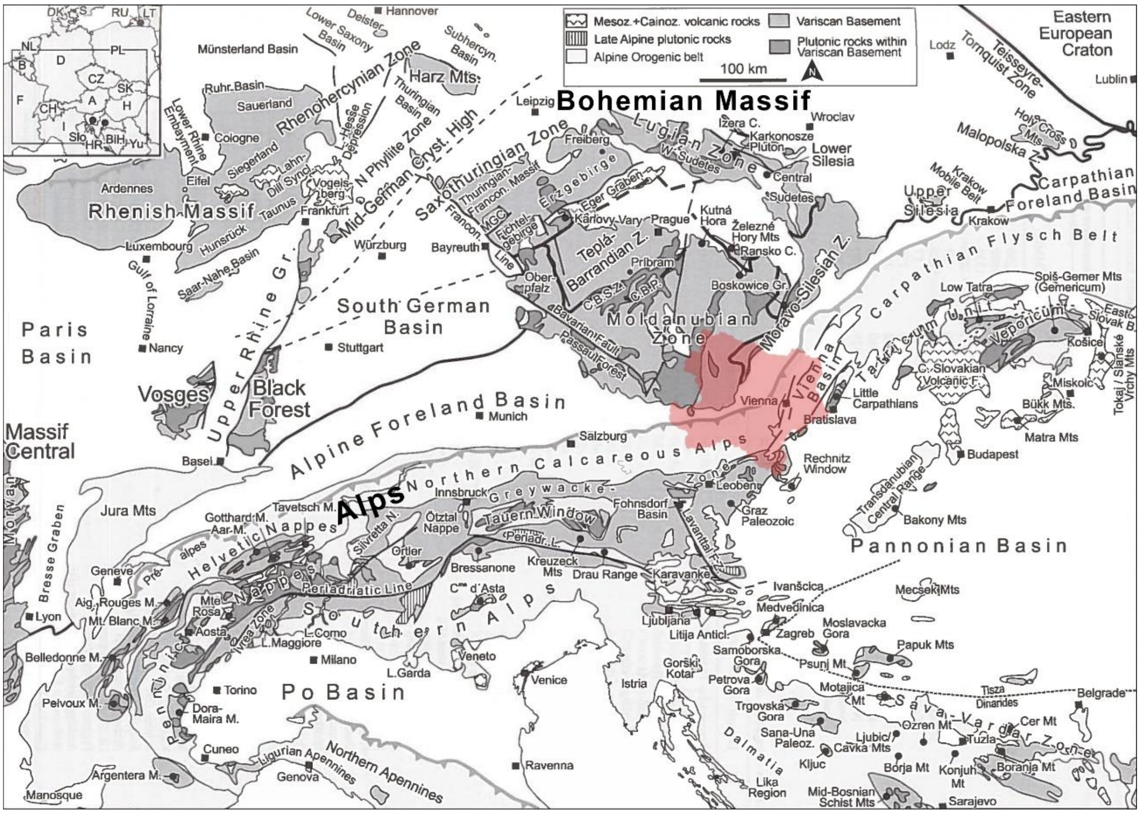


Figure 10. The Bohemian Massif, the Alps and Lower Austria (red area) (modified after Dill et al. 2008, 1343: Fig. 21.1)

The southern part of Austria is occupied by the Eastern Alps, which disappear beneath the Neogene sediments of the Vienna Basin to the east (*Figures 10* and *11;* Janoschek and Matura 1980, 12). The Alps, formed by Jurassic and Tertiary tectonics, are separated geographically into Western, Central, Eastern and Southern Alps, and tectonically into Helvetic, Penninic,

[2] The Variscan Orogeny was an important event in the Middle to Late Palaeozoic (during the Devonian and Carboniferous) when two continents, Gondwana and Laurussia, had their final collision (Kroner et al. 2008, 599; Allaby 2013, 274–275).

Austro-Alpine and South-Alpine zones (Froitzheim and Schuster 2008, 1141, 1143).[3] All tectonic zones, except the South-Alpine Zone, are present in Lower Austria.

Between the Eastern Alps and the Bohemian Massif, the Alpine-Carpathian Foreland is exposed (*Figure 10* and *11*).

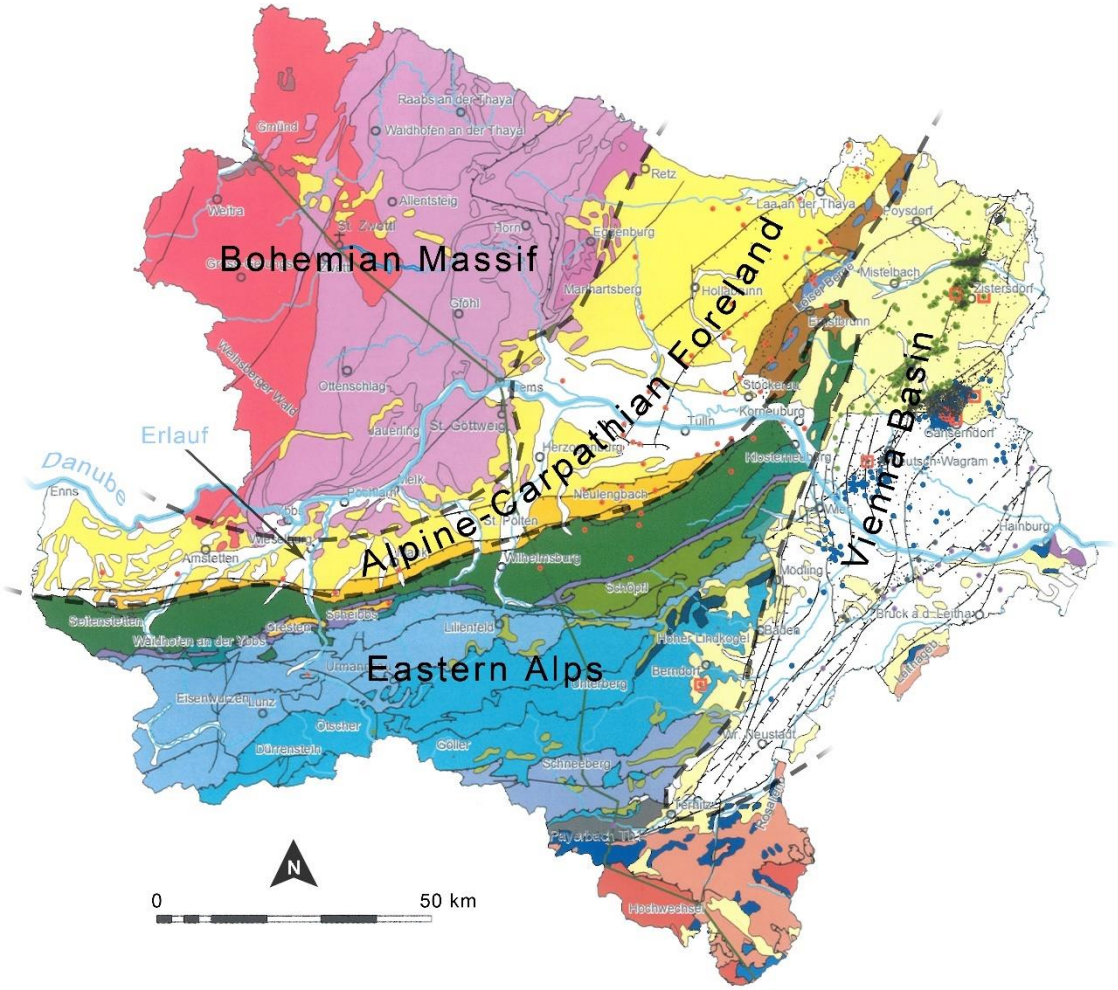


Figure 11. Lower Austria with its major geological units (modified after Wessely 2006b, 12: Abb. 2)

The Bohemian Massif

The Bohemian Massif is an extensive crystalline rock complex of metamorphic and igneous rocks (Matura 2006c, 25). It has gone through intensive erosion cycles and now forms a hilly landscape with average elevations of 500 to 800 metres above sea level (*Figure 12*; Matura 2006c, 25). Its southern and eastern edges dip under the Molasse Zone and the Eastern Alps

[3] These geographical and tectonic divisions do not coincide with each other except in the case of the Southern Alps and the South-Alpine Zone which cover the same areas (Froitzheim and Schuster 2008, 1143).

(Janoschek and Matura 1980, 15). The Lower Austrian part of the Bohemian Massif has three main units called Moravo-Silesian Zone, Moldanubicum *sensu stricto* and the South Bohemian Pluton (*Figure 13, Table 2;* Janoschek and Matura 1980, 15; Matura 2006c, 33).



Figure 12. Typical landscape of the Bohemian Massif in the Waldviertel (Wessely 2006c, 15: Abb. 4)

The Moravo-Silesian Zone

The Moravo-Silesian Zone occupies the south-easternmost part of the Bohemian Massif. Its rocks underwent progressive metamorphism; they show greenschist facies except the western part where amphibolite facies can be observed (Janoschek and Matura 1980, 15). The deepest and easternmost section of the Moravo-Silesian Zone involves the Thaya Pluton of mainly granitic to granodioritic composition with about 5% biotite content and with a generally foliated structure (Janoschek and Matura 1980, 15; Matura 2006c, 28). The Thaya Pluton is followed by the Pleißing Unit westwards, consisting of a series of garnet bearing paragneisses, marbles and carbonate bearing mica schists (Janoschek and Matura 1980, 15; Matura 2006c, 29). To the west of the Pleißing Unit the Bittesch Unit extends. It includes the so-called Bittesch Gneiss at its base (Matura 2006c, 29), which has granitic to granodioritic composition typically with augen of potassium feldspars and its upper section is interbedded with amphibolite layers (Janoschek and Matura 1980, 15). The Bittesch Gneiss shows a great similarity with another part of the Bittesch Unit, the Dobra Gneiss (Matura 2006c, 30), which is an orthogneiss of granitic to granodioritic composition, is intercalated with amphibolites, biotite-amphibolite or biotite schists and is also characterised by augen structure (Janoschek and Matura 1980, 16).

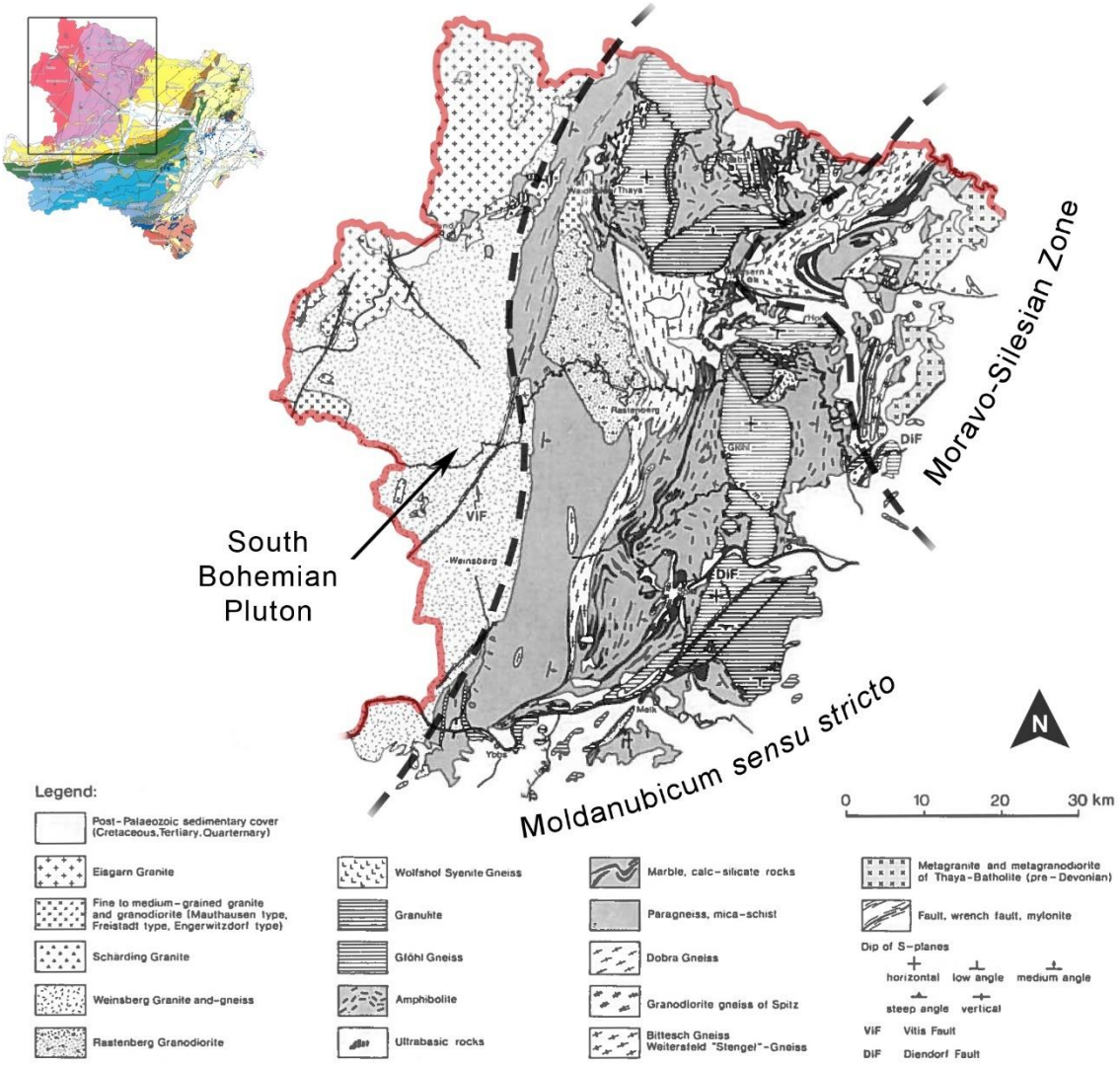


Figure 13. Subunits of the Bohemian Massif in Lower Austria (modified after Janoschek and Matura 1980, 17: Fig. 4 and Wessely 2006b, 12: Abb. 2)

The Moldanubicum

To the west of the Moravo-Silesian Zone extends the Moldanubicum, which represents the central region of the Lower Austrian part of the Bohemian Massif. It consists mainly of medium to high-grade gneisses and intrusions of Carboniferous granites (Mazur and Kroner 2008, 611). Its structurally lowermost subunit, the so-called Monotonous Group consists of biotite-plagioclase-bearing paragneisses and orthogneisses (including garnet and sillimanite) as well as cordierite gneisses (Janoschek and Matura 1980, 16; Mazur and Kroner 2008, 612). The Variegated Group is built up of inhomogeneous biotite-plagioclase gneisses (containing garnet and sillimanite), and is interbedded with quartzites, marbles, graphitic schists, amphibolites and granitic gneisses in its deeper section (Janoschek and Matura 1980, 16; Mazur and Kroner

2008, 612). The third major and uppermost subunit of the Moldanubicum is the Gföhl Unit, which is of high pressure granulites, garnet and spinel peridotites, pyroxenites, amphibolites, orthogneisses and metagabbros (Mazur and Kroner 2008, 612).

Table 2. Summary of the main units, subunits and rock types of the Bohemian Massif in Lower Austria

Main units and subunits		Rock types
Moravo-Silesian Zone	Thaya Pluton	Gneiss with granitic-granodioritic composition
	Pleißing Unit	Garnet-bearing paragneiss, marble, carbonate-bearing mica schist
	Bittesch Unit	'Bittesch gneiss' (granitic-granodioritic composition, augen structure, layers of amphibolite); 'Dobra gneiss' (granitic-granodioritic composition, augen structure, layers of amphibolite, biotite schist)
Moldanubicum *sensu stricto*	Monotonous Group	Biotite-plagioclase-bearing paragneiss and orthogneiss (including garnet and sillimanite), cordierite gneiss
	Variegated Group	Biotite-plagioclase gneiss (containing garnet and sillimanite) with layers of quartzite, marble, graphitic schist, amphibolite, granitic gneiss
	Gföhl Unit	High pressure granulite, garnet and spinel peridotite, pyroxenite, amphibolite, orthogneiss, metagabbro
South Bohemian Pluton		Granitoid rocks (granite, granodiorite)

The South Bohemian Pluton

The Moldanubicum is bounded to the west by the South Bohemian Pluton. This intrusive mass consists of several generations of granitoid rocks which can be divided into the older synorogenic, coarse-grained group (e. g. Weinsberg Granite, Rastenberg Granodiorite, Schrems Granite, Eisgarn Granite) and the younger postorogenic, fine to medium-grained group (e.g. Mauthausen Granite; Matura 2006c, 33). The South Bohemian Pluton is cut by several faults (e.g. Vitis Fault, Rodl Fault) with roughly northeast-southwest direction (Janoschek and Matura 1980, 18).

Post-Variscan sediments

Some parts of the Bohemian Massif are covered by post-Variscan sediments which are partly continental accumulations (predominantly freshwater deposits of rivers or lakes) and partly

marine deposits along the southern and eastern marginal area (Matura 2006c, 38). The Lower Permian sedimentary cover comprises mainly conglomerates, sandstones and arkoses. During the Tertiary, isolated pebbles, boulders and windkanters were deposited. This was also the period when the crystalline basement became deeply weathered, crumbled and locally kaolinized (Janoschek and Matura 1980, 19).

The Alpine-Carpathian Foreland

The Alpine-Carpathian Foreland includes the Molasse Zone (often referred to as the Molasse Basin or the North Alpine Foreland Basin) and the Waschberg Zone north of the Danube (*Figure 14*; Berger 2008, 1054; Janoschek and Matura 1980, 10; Rasser 2008, 1035).

The Molasse Zone represents the sediment filling of the former sea, Paratethys, between the Bohemian Massif and the Eastern Alps (*Figure 15*; Wessely 2006e, 41). The present Molasse Basin is only a thin remnant of the original basin; its width ranges from 5 to 50 km in Austria (Harzhauser and Roetzel 2008, 1056). Its succession lies on the dipping rocks of the Bohemian Massif and southwards extends under the Eastern Alps along with them (Janoschek and Matura 1980, 21). In the south, the Molasse layers were folded and shifted northward due to the tectonic movements of the Alps (Wessely 2006e, 41). Based on the intensity of these movements, the Molasse Zone can be separated into three parts: the undisturbed (autochthonous) Foreland Molasse, the folded Disturbed (allochthonous) Molasse and the strongly folded and imbricated (allochthonous) Sub-Alpine Molasse (Janoschek and Matura 1980, 20).[4]

The sedimentation of the Molasse Basin started in the Upper Eocene and ended in the Upper Miocene. The sediments vary from shallow-water formations of the northern area to deep-water deposits at the foot of the Eastern Alps (Wessely 2006e, 41).

The Waschberg Zone, similarly to the Sub-Alpine Molasse, became strongly folded during the formation of the Eastern Alps (Janoschek and Matura 1980, 28). Its sedimentary succession includes greensands, calcareous sandstones, glauconitic marls, silts, clays, nearshore sandstones, feldspar-bearing wackes and arkoses (Wiese and Čech 2008, 964).

[4] Autochthonous units were formed in their present position, while allochthonous units were displaced from their original site of formation (Allaby 2013, 17, 46–47).

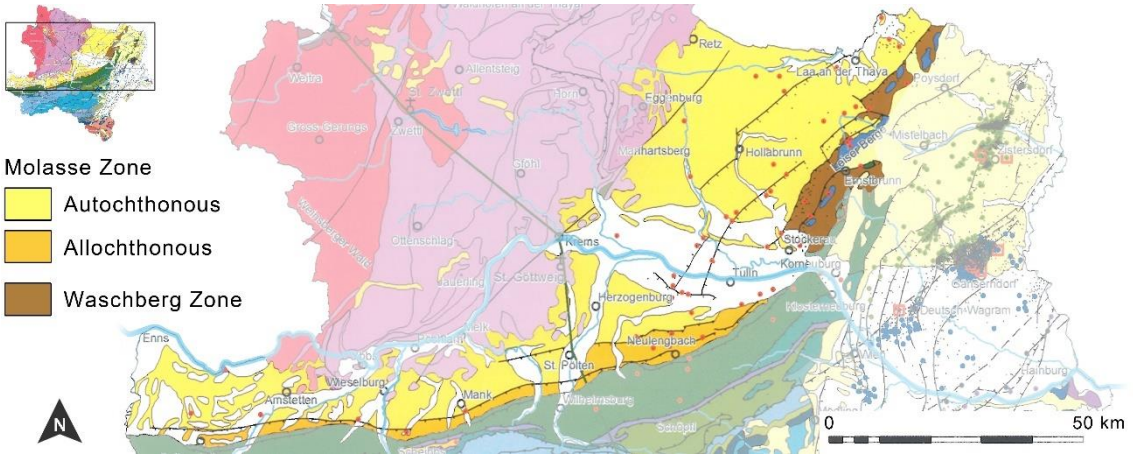


Figure 14. Subunits of the Alpine-Carpathian Foreland in Lower Austria (modified after Wessely 2006b, 12: Abb. 2, 13: Abb. 3)



Figure 15. The so-called Melk Sand of the Molasse Zone (Wessely 2006e, 47: Abb. 65)

The Eastern Alps

The Eastern Alps have a very complex structure and composition, which are also reflected in their numerous units and subunits. In Lower Austria, from the north to the south, the main domains are the Helvetic Zone, the Penninic Zone and the Austro-Alpine Zone (*Figure 16, Table 3*).

The Helvetic Zone

The narrow belt of the Helvetic Zone represents the northernmost nappes of the Eastern Alps. It includes sediment layers from the Lower Jurassic to the Eocene such as limestones, marls and sandstones. It is tectonically superimposed by the nappes of the Rhenodanubian Flysch Zone (of the Penninic Zone) and by those of the Austro-Alpine Zone located south of it (Janoschek and Matura 1980, 28). The units of the Helvetic Zone and the overlying

Rhenodanubian Flysch Zone became imbricated as the result of the thrusting of this two unit complexes northward on the sediment fill of the Molasse Basin (Froitzheim and Schuster 2008, 1150).

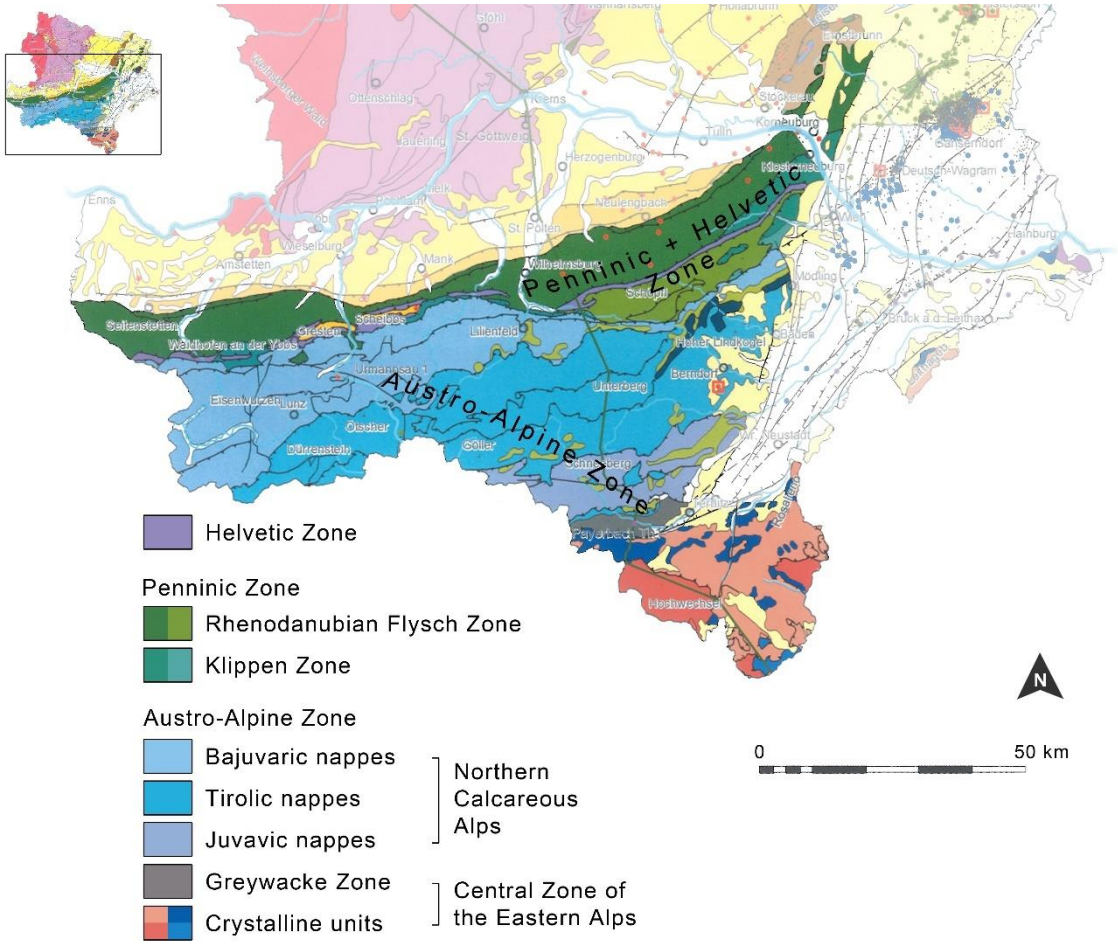


Figure 16. Subunits of the Eastern Alps in Lower Austria (modified after Wessely 2006b, 12: Abb. 2, 13: Abb. 3)

The Penninic Zone

The Penninic Zone comprises the Penninic nappes of the Eastern Alps, the Rhenodanubian Flysch Zone and the Klippen Zone (*Figure 16*).

The Penninic nappes are exposed in tectonic windows of the Eastern Alps such as the Tauern Window in the western part of Austria. In Lower Austria they are present along the eastern margin of the Eastern Alps consisting of ophiolites and metasediments (calcareous mica schists, graphite phyllites, quartz phyllites). They show greenschist-facies metamorphism and at some places blueschist-facies metamorphism could also be observed (Froitzheim and Schuster 2008, 1159).

Table 3. Summary of the main units, subunits and rock types of the Eastern Alps in Lower Austria

Main units and subunits				Rock types
Helvetic Zone				Limestone, marl, sandstone
Penninic Zone	Penninic nappes			Ophiolite, metasediments (calcareous mica schist, graphite phyllite, quartz phyllite)
	Rhenodanubian Flysch Zone			Sandstone, schistose pelite, calcareous marl
	Klippen Zone			Core: arkose, siltstone, limestone, radiolarite; Cover: pelite, sandstone
Austro-Alpine Zone	Upper Austro-Alpine units	Northern Calcareous Alps	Bajuvaric nappes	Limestone, shale, gypsum, dolomite, radiolarite, silty marl
			Tirolic nappes	
			Juvavic nappes	
		Central zone of the Eastern Alps	Greywacke Zone	Metasediments with layers of metamorphosed coal and magnesite, phyllite interbedded with chlorite schist, riebeckite gneiss, paragneiss, mica schist, amphibolite, metavolcanics, quartzite, marble, dolomite
			Crystalline units	'Rechnitz Complex' (calcite phyllite, graphite phyllite, quartzite, marble, serpentinite, mafic rock); 'Wechsel Complex' (gneiss, slate); 'Grobgneis Complex' (phyllitic mica schist, granitic orthogneiss, metagranite); 'Sieggraben Complex' (garnet-biotite gneiss with kyanite)



Figure 17. Flow marks in sandstone of the Rhenodanubian Flysch Zone (Wessely 2006g, 85: Abb. 157)

The Rhenodanubian Flysch Zone along the northern border of the Eastern Alps is formed by deep-marine clastic sediments from the Lower Cretaceous to the Upper Eocene including layers of sandstones, schistose pelites and calcareous marls. The sediments are mostly turbidites (*Figure 17*) which were transported by high-speed turbidity currents; initially coarser and successively finer material was deposited (Wessely 2006g, 86).

The Klippen Zone is represented by remnants of cliffs within and along the southern border of the Rhenodanubian Flysch Zone (*Figure 18*). These cliffs consist of a core of arkose, siltstone, limestone and radiolarites, and a cover of pelites and sandstones (Janoschek and Matura 1980, 30; Wessely 2006g, 85). They were detached from their original basement and displaced to their present location with their covers (Wessely 2006g, 85).



Figure 18. The cliff of Konradsheim in the Gresten Klippen Zone (Wessely 2006g, 97: Abb. 184)

The Klippen Zone is subdivided into Gresten, St Veit, Sulz and Ybbsitz klippen zones.[5] The first three zones are mostly similar in stratigraphic and lithologic characteristics and their sediments lay on a continental shelf. The Ybbsitz Klippen Zone, however, differs from them because its sedimentation began later and rests on the top of an oceanic crust (Wessely 2006g, 96, 101).

[5] All parts of the Klippen Zone are considered to be parts of the Penninic Zone except the Gresten Klippen Zone which represents the Ultrahelvetic Zone in Lower Austria, i.e. the palaeographic area between the Helvetic and the Penninic zones (Wessely 2006g, 95–96).

The Austro-Alpine Zone

The Austro-Alpine Zone includes a series of (meta)sedimentary and magmatic rocks. The nappes can be separated into two major groups: the Lower and the Upper Austro-Alpine units, and both groups consist of several nappe systems (Froitzheim and Schuster 2008, 1160).

The Lower Austro-Alpine units are present mainly in eastern Switzerland, in the western edges of the Austro-Alpine nappes (Froitzheim and Schuster 2008, 1160). However, the Upper Austro-Alpine units appear in Lower Austria and are subdivided into the Northern Calcareous Alps and the central zone of the Eastern Alps. The latter includes the so-called Greywacke Zone and a group of crystalline rock units (*Figures 16* and *19*).

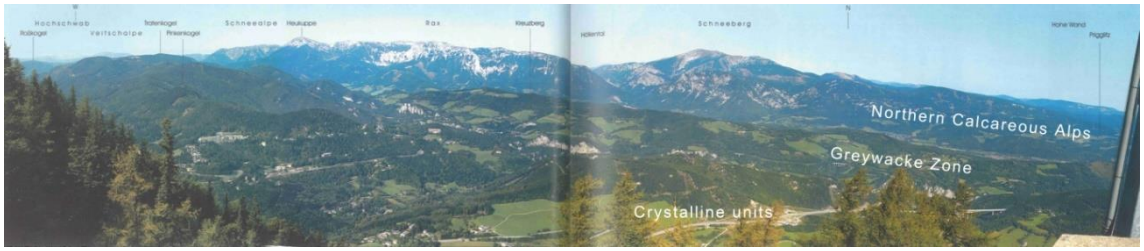


Figure 19. The units of the Austro-Alpine Zone in Lower Austria (modified after Matura 2006a, 168–169: Abb. 338)

The Northern Calcareous Alps consist of three nappe systems, the Bajuvaric, Tirolic and Juvavic systems (*Figure 16*). They are all formed mostly by carbonate sediments from the Permian to the Palaeocene, but they differ in terms of their evolution during the Triassic as well as their Jurassic and Cretaceous sediments (Froitzheim and Schuster 2008, 1160; Wessely 2006a, 105). In the Permian, fluviatile red beds and shallow-marine evaporites were deposited in the shelf which occupied the place of the subsequent nappe systems (Froitzheim and Schuster 2008, 1160).[6] By the end of the Triassic, layers of siliciclastic materials, nodular limestones, shales, pelagic limestones, gypsum, dolomites and dark marly sediments were settled (Froitzheim and Schuster 2008, 1160, 1162).

At the beginning of the Jurassic, strongly condensed nodular limestones with ammonoids and crinoids, marly and cherty limestones, and subsequently radiolarites were deposited in the Austro-Alpine shelf. Due to tectonic events, parts of the Triassic succession of the shelf were mobilised and with other mass-transport complexes deposited again. This mobilised material

[6] The shelf belonged to the so-called Meliata Ocean, which existed between the Middle Triassic and the Jurassic/Cretaceous. It was bounded on the north and west by the Western Carpathian, the Austro-Alpine Zone and the South Alpine domain (Froitzheim and Schuster 2008, 1167).

represents the Juvavic Nappe System which was emplaced on top of the units of the subsequent Tirolic Nappe System. In the Lower Cretaceous (Valanginian), the Tirolic nappes were detached from their basement and along with the Juvavic nappes on top were thrust onto the area of the subsequent Bajuvaric Nappe System (Froitzheim and Schuster 2008, 1162).

The deposition continued during the Cretaceous with layers of silty marls, turbidites, deep-marine conglomerates and detritus including phengites and glaucophanes. In the Turonian, the Northern Calcareous Alps became partly terrestrial and the deposition of mainly fluviatile conglomerates (Lower Gosau Subgroup) began. From the Campanian, deep-water sediments such as marl-rich sediments with slumps and breccias, and terrigenous metamorphic detritus started to deposit (Upper Gosau Subgroup; Froitzheim and Schuster 2008, 1162–1163).

The Greywacke Zone extends south of the Northern Calcareous Alps in the central zone of the Eastern Alps. It consists of several nappes which dip under the Northern Calcareous Alps to the north and rest on the metamorphic rocks of other Austro-Alpine units to the south (Matura 2006a, 167). They comprise metasediments intercalated by metamorphosed coal and magnesite, phyllites interbedded with chlorite schists, riebeckite gneiss, paragneisses, mica schists, amphibolites, acidic and basic metavolcanics, quartzites, marbles and dolomites (Froitzheim and Schuster 2008, 1163). The lower parts of the Greywacke Zone show metamorphism of upper greenschist facies, which decreases towards the upper nappes (Froitzheim and Schuster 2008, 1163).

The Greywacke Zone is bounded by crystalline units to the south in the southernmost part of Lower Austria (Matura 2006b, 173). These metamorphic crystalline units formed before the Alpine orogeny and metamorphosed again with different intensities in later times (Matura 2006b, 174). They include metasediments (such as calcite phyllite, graphite phyllite, quartzite, marble), serpentinites and mafic rocks (Rechnitz Complex); fine to coarse grained gneisses and slates (Wechsel Complex); phyllitic mica schists, granitic orthogneisses and metagranites (Grobgneis Complex); and garnet-biotite gneisses that contain locally kyanite (Sieggraben Complex; Matura 2006b, 176, 180, 181). These crystalline units are covered with Permian-Triassic metasediments of shale, quartzite, and carbonate rocks such as the so-called Semmering Group (Matura 2006b, 174).

The Vienna Basin

The Vienna Basin, situated in the eastern part of Austria (*Figure 11*), is a Neogene basin and its basement is formed by the nappes of the Eastern Alps and its continuation, the Western Carpathians. The basin fill can reach 5500 meters at some places (Harzhauser et al. 2008, 1060). The sediments include coarse deposits of the former coasts and estuaries, fine sediments of the basin interior and calcifications of the shallow water area (Wessely 2006d, 197). The top layers of the thick succession consist of a range of clays, marls and silts interbedded with sands and gravels (Harzhauser et al. 2008, 1062).

2.3.2 Geological units in the Erlauf Valley

The Erlauf Valley is situated in that part of Lower Austria where the surface rocks of the Bohemian Massif and the Eastern Alps are the closest to each other. Many of the above-mentioned zones and units are present in this region (*Figure 20*). The description below is based on the cross-section in *Figure 21*.

In the northern part of the valley, the Bohemian Massif emerges represented by the granulite of Pöchlarn-Wieselburg, which belongs to the Moldanubicum (Menzl 1988, 68).[7] The crystalline rocks of the Bohemian Massif are close to the surface up to Wieselburg, where they start sloping under younger layers and units such as those of the Eastern Alps (Matura 2006c, 36, 37: Abb. 46.)

Southwards the Molasse Zone is layered on the Bohemian Massif with its sedimentary succession. Its northern part is formed by the undisturbed, autochthonous Foreland Molasse and to the south the strongly folded, allochthonous Sub-Alpine Molasse is exposed (Janoschek and Matura 1980, 27).

The Penninic Zone of the Alps is represented by the Rhenodanubian Flysch Zone and the Ybbsitz Klippen Zone which are separated by the Gresten Klippen Zone.[8] The Penninic Zone is bounded to the south by the Northern Calcareous Alps of the Austro-Alpine Zone. The alternating Frankenfels Nappe and Lunz Nappe together with the Sulzbach Nappe are parts of

[7] The granulite of Pöchlarn is composed of quartz, perthitic orthoclase, antiperthitic oligoclase-andesine, garnet with high almandine content and biotite. Disthen, sillimanite and accessory minerals such as rutile, zircon and tourmaline also occur (Menzl 1988, 68).
[8] The Gresten Klippen Zone belongs to the Ultrahelvetic Zone (see footnote 5 on page 36).

the Bajuvaric Nappe System. The Tirolic Nappe System here consists of the so-called Reisalpen, Ötscher and Göller nappes.

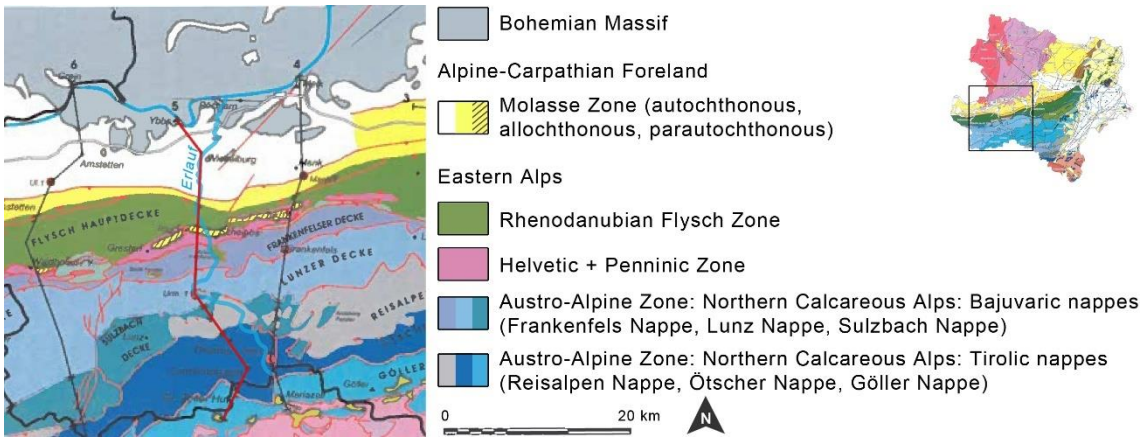


Figure 20. Geological units in the Erlauf Valley (modified detail of Wessely 2006f, 78: Abb. 153). Cross-section through line 5 (marked red) is presented in Figure 21.

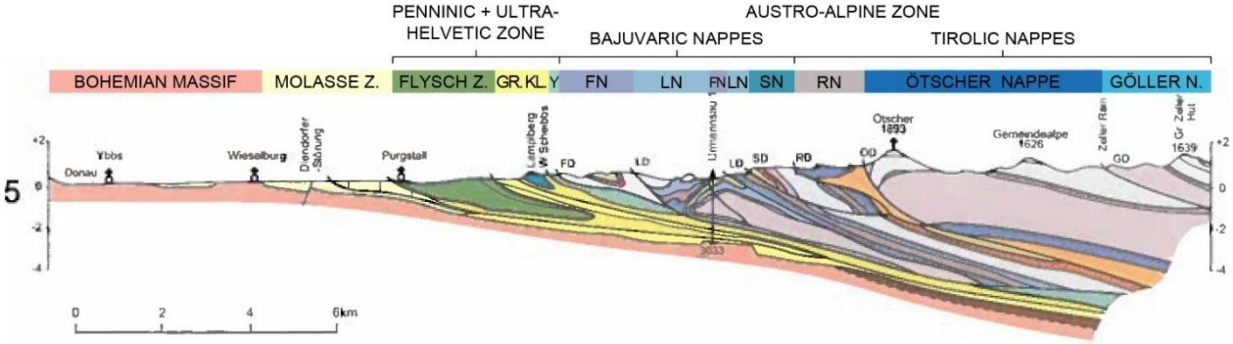


Figure 21. North-south cross-section of the Erlauf Valley drawn along line 5 in Figure 20 (modified detail of Wessely 2006f, 81: Abb. 155). Abbreviations: Z.=Zone, GR. KL.=Gresten Klippen Zone, Y=Ybbsitz Klippen Zone, FN=Frankenfels Nappe, LN=Lunz Nappe, SN=Sulzbach Nappe, RN=Reisalpen Nappe, GÖLLER N.=Göller Nappe. Different colour stripes in the Austro-Alpine Zone mark different formations not detailed here.

2.3.3 Clay deposits

In Lower Austria, clay and kaolin occur as erosion products of feldspar-rich rocks (granites, gneisses, granulites) of the Bohemian Massif (*Figure 22*; Heinrich 2006, 274, 296). Kaolin is a mineral mixture, which mainly consists of kaolinite as well as quartz, feldspar and mica and occurs in primary or secondary deposits (Heinrich 2006, 296–297). Primary deposits are *in situ* formed deposits where the structure of the parent rock is still recognisable. Secondary deposits were transported from their original forming environment and also contain clays and sands. The most important occurrences of primary kaolin are in Grametten (Bittesch Gneiss of

the Bohemian Massif) and Mallersbach (Eisgarn Granite of the Bohemian Massif; Heinrich 2006, 297).

Kaolinite-rich clays (secondary deposits) were accumulated in the Paleogene/Neogene in fluviatile, lacustrine and brackish environment in Lower Austria (Heinrich 2006, 274). Their best-known occurrences are in Paleogene-Neogene basins of the Bohemian Massif as well as along the southern and south-eastern edge of the same crystalline unit, for example at Niederfladnitz, Droß-Priel, Maiersch, Unterwölbling and Karlstetten (Weber 1997b; Heinrich 2006, 276, 297). Clays are also present in the Vienna Basin (e.g. Sooß, Schönau; Heinrich 2006, 277).

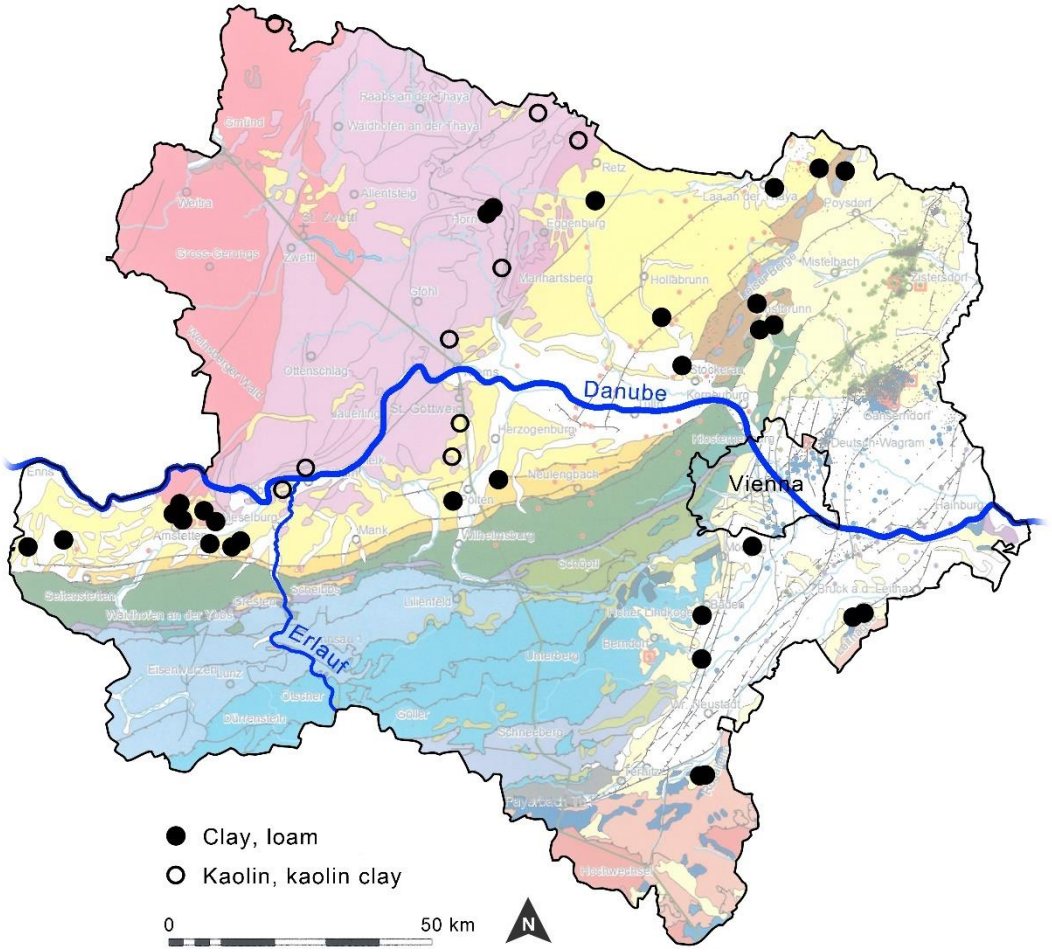


Figure 22. Clay, loam, kaolin and kaolin-rich clay deposits in Lower Austria (based on Heinrich 2006, 274: Abb. 527, 292: Abb. 536; base map: Wessely 2006b, 12: Abb. 2)

Clayey deposits are also frequent in the Erlauf Valley. Kaolinitic clay can be found near Klein-Pöchlarn which is situated opposite to the mouth of the Erlauf, on the northern bank of the Danube. Clay mining activity can be documented here from the 16th century, but the deposit was probably known earlier (Otruba, 1987, Map annex showing 16th-century mining).

Kaolinitic sand was recorded near Krummnußbaum, located west of the mouth of the Erlauf, which appears in small erosive basins of the granulite of Pöchlarn-Wieselburg (Menzl 1988, 67). It occupies the structurally lowest position of the so-called Melk Formation of the Molasse Zone, which lies directly on the crystalline basement of the Bohemian Massif (Menzl 1988, 67; Wessely 2006e, 45). It has sedimentary origin and formed by the chemical weathering of feldspars of the granulite (Menzl 1988, 67).

Clay and kaolin sources are also present near Wieselburg in the Erlauf Valley (Weber 1997a, 6).

Clay-loam occurs at several places under the soil between the Erlauf and the River Enns, which latter bounds Lower Austria to the west (Hönig and Schedl 1984, 45). In these deposits, montmorillonite and illite are the predominant clay minerals, followed by kaolinite (Hönig and Schedl 1984, 47). Furthermore, silt, loam and loamy clay can also be found throughout the Erlauf Valley within a depth of 1 meter under the surface according to the soil map of Austria.[9]

2.3.4 Graphite deposits

In Central Europe, graphite deposits occur in the Bohemian Massif in the area of south-eastern Germany (Bavarian Forest), Czechia and Austria (in the regions of Mühlviertel, Waldviertel and Dunkelsteinerwald) as well as in the Eastern Alps in the area of Austria (in the states of Lower Austria, Styria and Carinthia; *Figure 23*; Scharrer-Liška 2007, 15).

In Lower Austria, more than a hundred graphite occurrences are known in the Bohemian Massif (Drosendorf Unit of the Moldanubicum) and in the Eastern Alps (Veitsch Nappe in the Greywacke Zone; Heinrich 2006, 298; Holzer 1964, 164).

The graphite of the Bohemian Massif is coarse and medium-grained, is rich in sulphide (pyrite) and tourmaline, is characterised locally by non-ferrous metal mineralisation and occurs in host rocks such as paragneisses, quartzites, amphibolites, calcsilicate rocks and marbles (Weber and Götzinger 1997; Heinrich 2006, 298: Tabelle 22). The intergrowth of graphite and minerals such as diopside, rutile, titanite, tourmaline, apatite and occasionally corundum is typical in this region and also quartz, feldspar (oligoclase), tremolite and mica are closely associated with this type of graphite (Holzer 1964, 165). The sedimentation of these graphite-bearing rocks was probably in pre-Palaeozoic times in the form of marine sapropelites, which were

[9] https://bodenkarte.at/ (accessed on 02/03/2021)

subsequently overprinted by submarine volcanism (Holzer 1964, 164; Schrauder et al. 1993; Weber and Götzinger 1997). The graphite deposits of the Bohemian Massif frequently have surface outcrops (Kappel 1969, 25; Scharrer-Liška 2007, 15). Graphite-containing clays can also be found on the surface as weathering products of graphite-bearing rocks (Scharrer-Liška 2007, 15).

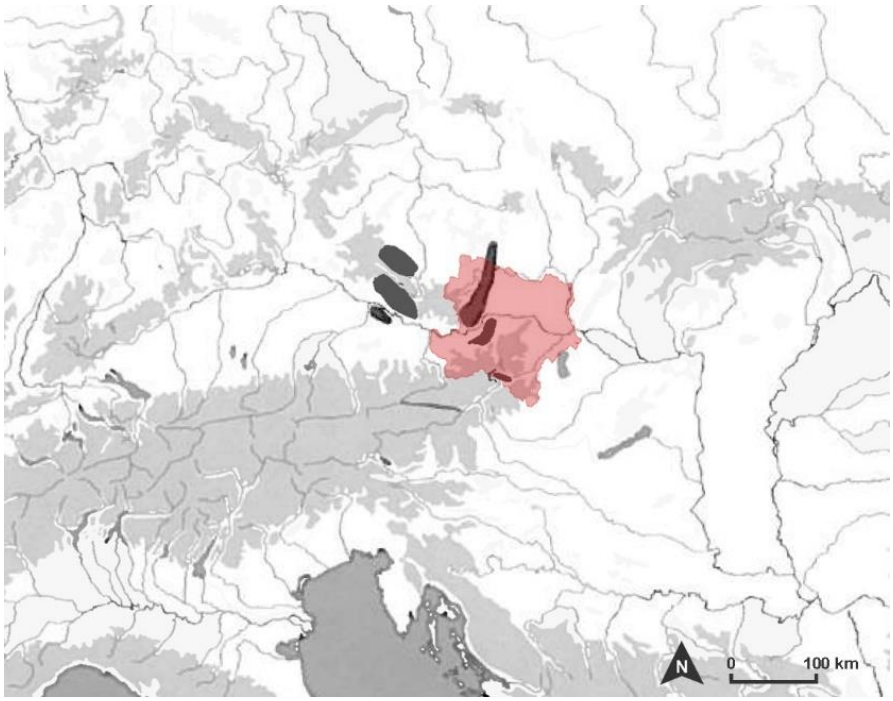


Figure 23. Graphite deposits in Central Europe and in Lower Austria (red area) (modified after Scharrer-Liška 2007, 17: Abb. 1)

The graphite of the Eastern Alps is fine-grained, characterised by 40–90% carbon and low sulphur content, and is found in phyllites or quartzites. This type of graphite was altered from coal seams by metamorphosis (Heinrich 2006, 298: Tabelle 22; Weber 1997c). Surface outcrops of graphite or graphitic clays are not known in the in the Greywacke Zone (Scharrer-Liška 2007, 16).

The Drosendorf Unit of the Bohemian Massif (consisting of the Monotonous and Variegated Groups, see *Table 2*) contains numerous graphite sources, some of which are very close to the Erlauf Valley (*Figure 24*). The Unit is located mainly north of the Danube in the Waldviertel, but a small part of it is exposed south of the Danube as well in the Dunkelsteinerwald (Weber 1987, 374).

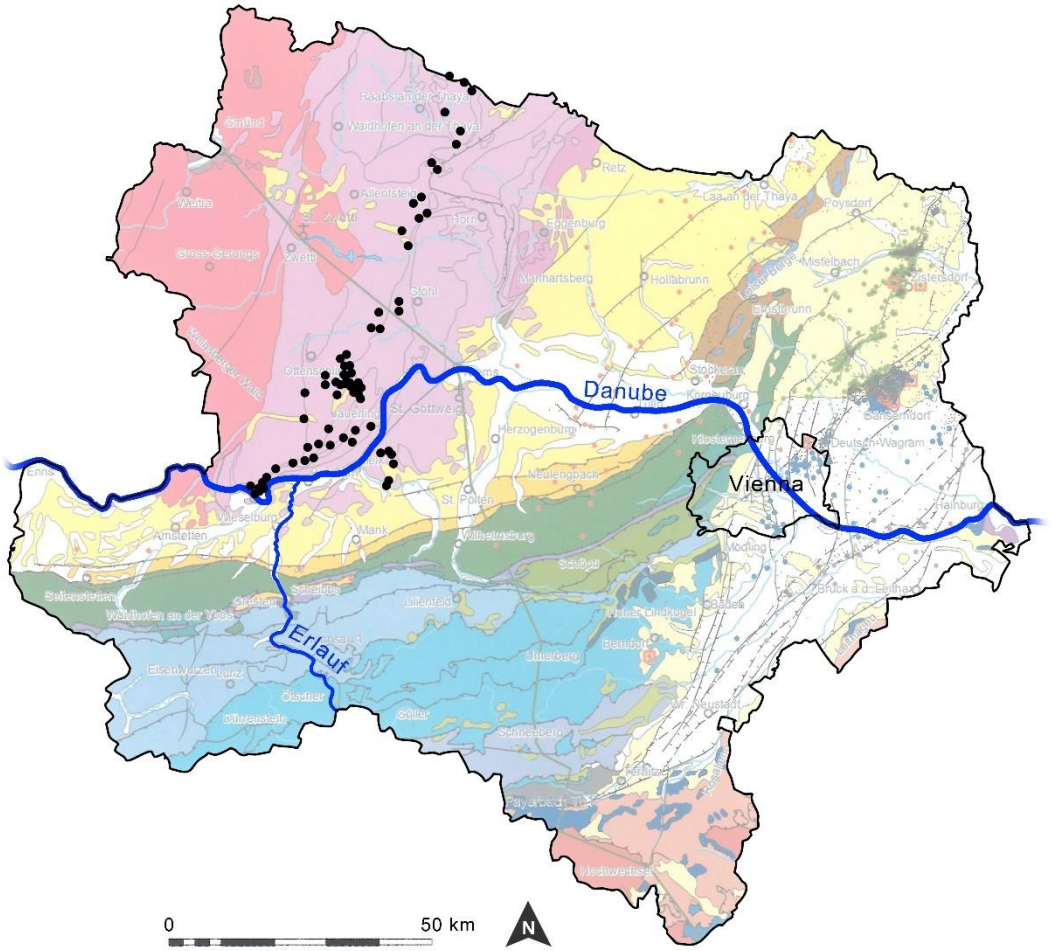


Figure 24. Occurrences of graphite in the Moldanubicum (Bohemian Massif) (based on Schrauder et al. 1993, 176: Fig. 1 and the map annex of Holzer 1964; base map: Wessely 2006b, 12: Abb. 2)[10]

2.3.5 Summary

Sitting on the boundaries of different geological formations, Lower Austria has an extremely diverse and complex geology compared to its relatively small territory. The Erlauf Valley, situated between two distinct units, the Bohemian Massif and the Eastern Alps, is characterised by similar geological diversity. Lower Austria is rich in raw materials used in pottery making such as clay and graphite, which are also present in the Erlauf Valley or in its close vicinity.

[10] The map does not mark all graphite deposits; there are references in the literature to graphite sources in the south-eastern part of the Dunkelsteinerwald (Felgenhauer-Schmiedt 1998, 199) and graphite can be found on the surface around Feuersbrunn as well (Dr Hajnalka Herold, personal communication, February 2021).

2.4 Ceramic archaeometry in Lower Austria

This subchapter reviews the publications about scientific analysis of pottery found in Lower Austria. There are not many such works; essentially, three researchers published on this topic: Rudolf Dell'mour, Roman Sauer and Hajnalka Herold. Because of the small number of publications related to the area, publications containing pottery archaeometry of other (neighbouring) regions and other periods are also mentioned. The literature detailing ceramics with and without graphite content is reviewed separately.

2.4.1 Graphite-free pottery

The results of ceramic petrography from one of the well-known sites of the 9th–10th century in Lower Austria, the fortified hilltop settlement of Thunau am Kamp, was published by Dell'mour in 2001 (Dell'mour 2001). A large number of sherds (178 samples) were analysed and categorised into three main groups: coarse-grained ceramics containing crystalline rock fragments, fine-grained ceramics and graphite-containing ceramics. The analysis of clay samples from the vicinity of the site was also included in the investigation. Identification of the origin of the raw materials and the reconstruction of some elements of the production technology were attempted in this paper.

Pottery of the Avar period was analysed from a settlement near Brunn am Gebirge (Sauer 2002 and Hammer 2002, both in Herold 2002a). Combined methods (thin section analysis, heavy mineral analysis and XRD) were applied to seven samples resulting in the establishment of four archaeometric fabrics including a quartzite, mica schist and gneiss-containing group, a carbonate-rich group, a fine-grained group and a grog-tempered group.

The petrographic analysis of 50 pottery samples was carried out from three 8th–9th-century cemeteries (Frohsdorf, Pitten and Erlach) in the Valley of the River Leitha (Herold 2009a; Herold 2009b; Herold 2015a; Herold 2015b). In addition to the pots, spindle whorls and raw clays were also sampled. The cemeteries belonged to two cultural milieus ('Avar' and 'non-Avar') represented by different material culture, but they also displayed similar characteristics regarding the production technology of the ceramics.

One last site should be mentioned in Lower Austria, a settlement near Michelstetten, from where 30 hand modelled and slow wheel-turned ceramics were investigated, which were dated to the Roman period and the early Middle Ages (Herold 2016). The thin section analysis

resulted in the definition of four fabrics containing carbonate, rock fragments, 'white' mica (muscovite) or 'gold' mica (biotite). The raw materials used in Roman and early medieval times were of similar types, but technological differences could be pointed out.

Ceramics were also examined from some sites located just outside of the boundaries of today's Lower Austria. These sites include the Roman cemetery excavated at Halbturn from where pottery and clay samples were investigated by polarising microscopy (Herold 2014), the Avar settlement and cemetery of Zillingtal with abundant ceramic material analysed by thin section analysis and XRD (Herold 2002b; Herold and Petschick 2003; Herold 2004; Herold 2010a; Herold 2011b) and the 8th–10th-century fortified settlement at Mikulčice (Czechia) from where ceramics were studied by petrographic (Dvorská and Poláček 1995; Herold 2008a) and chemical analysis (Dvorská et al. 1998).

2.4.2 Graphite-containing ceramics

Publications investigating medieval ceramics that include graphite in their paste from Lower Austria are even more scarce than those dealing with graphite-free ceramics. The Dell'mour article from 2001 has already been mentioned (Dell'mour 2011), which also contains thin section analysis results of graphite-containing pottery from Thunau am Kamp.

The analysis of 54 medieval graphite-containing ceramics as well as raw materials (graphite and clay) was carried out by Sauer from the 10th-century fortification of Sand near Oberpfaffendorf and Castle Raabs (built in the 11th century). The manuscript summarising the results of the thin section and heavy mineral analyses has not been published (Sauer n.d.). The assemblages of Sand and Raabs include very similar fabrics (sillimanite-rich, rutile-rich, tourmaline-rich fabrics), which is not surprising seeing the close location of the two sites (*c.* 1.5 km).

Pieces of 49 medieval vessels from two Lower Austrian sites (Muggendorf, St. Pölten) and two Upper Austrian sites (Auhof, Ratzlburg) were investigated by petrography and heavy mineral analysis (Sauer 2007). Identification of local or imported ware as well as potential graphite sources were given in the publication if it was possible. Striking is the variability of compositions of the Lower Austrian samples.

Although its early medieval version can be seen as an innovation, graphite-containing pottery was produced in the Iron Age as well. Ceramics of five Lower Austrian Iron Age sites

(Braunsberg, Göttweig, Purgstall-Schauboden, Schwarzenbach, Vienna-Leopoldsberg) were investigated as a part of a larger project including the analysis of samples from Bavaria, Lower Austria, Vienna, Slovakia and Hungary (Sauer 1994). Analysis results of further samples from the fortified settlement of Schwarzenbach were published a couple of years later (Herold 2008b).

In the wider region, there are publications on the analysis of graphite-containing ceramics from 9th–11th-century sites in north-western Hungary (Little Hungarian Plain; Szakmány and Bendő 2016) as well as from the 11th–12th-century settlement of Nitra-Šindolka (Fusek and Spišiak 2005) and the 12th–13th-century settlement of Beluša (Spišiak 2007), both in Slovakia.

2.4.3 Summary

Although the scientific analysis of ceramics is still at its beginnings in Lower Austria, the above-mentioned publications provide basis for comparison to the samples studied in this thesis. Almost all of the works include the results and interpretation of thin section analysis, and in case of some assemblages, other methods (heavy mineral analysis, XRD, chemical analysis) were also used in addition to this technique.

2.5 Theoretical approaches to pottery and borderland archaeology

In this subchapter, two different topics are explored, both connected to archaeological theory and both important in terms of the interpretation of the ceramic assemblage investigated in this thesis. In the first part of this subchapter, different theories relating to material culture and especially pottery technology are presented with a special attention to how these concepts can be applied to ceramic sherds analysed by scientific techniques. This is followed by the discussion of the concept of borderland archaeology and what is known about archaeological borderlands in Lower Austria.

2.5.1 Theoretical concepts in pottery studies

By investigating an assemblage with archaeological or scientific techniques, valuable data can be provided about the provenance and production techniques of the different artefacts. These data, however, might be far from socio-economic interpretations of past communities. Archaeologists use theoretical approaches to bridge this gap and gain a better understanding of the people behind the objects. Useful concepts in pottery interpretation include the *chaîne opératoire* approach investigating the manufacturing sequence, the examination of technological choices made at each stage of the sequence, technological traditions, change communities of practice, innovation and organisation of production. In this section, these approaches are explored.

Objects have always been parts of human life. They represent one of the main sources for archaeology to characterise different periods, areas and communities. Archaeology invokes the help of material culture studies and ethnography to understand what could be the relation between people and objects and what conclusions can be drawn about the past based on the study of objects.

Several aspects of society can be better understood through the investigation of its material culture as it is embedded in the society (Tilley et al. 2006, 1). It is evident that people shape and influence the world of objects. Things too, although without intentionality, have a power to act (agency), to shape and change human lives (Latour 2005, 63–86; Gell 1998, 17–21). People and things are interrelated: people produce things, but things in turn affect people's lives and make them action in certain ways (Tilley et al. 2006, 4; Gosden 2005, 429). Thus, people make things and things make people (Skibo and Schiffer 2008, 8; Hodder 2012, 13; Ingold 2013). This strong relationship and interdependence between objects and people is

evident, whether it is approached and described as a network (Latour 1988; Law 1992; Latour 2005) or an entanglement (Hodder 2012).

The *chaîne opératoire* approach

The *chaîne opératoire* is an approach that proposes investigating technology as a series of actions. It originates from French anthropology and was first defined by André Leroi-Gourhan as the operational sequence through which raw materials are transformed into products (Leroi-Gourhan 1964, 164; for the beginnings of this theory see also Cresswell 1976, 2010 and Lemonnier 1976). The main stages of a sequence can also be considered as individual *chaîne opératoires* since they consist of several smaller actions (Roux 2017, 103; Roux 2019, 2; Gosselain 2018, Fig. 2).

Each *chaîne opératoire* is characterised by raw materials, tools, knowledge, skills, gestures and energy sources that are needed to produce an artefact (Martinón-Torres 2002, 33; Lemonnier 2012). The different actions of the sequence can be functionally and/or socially motivated (Schlanger 2005, 28; Gosselain 2018). The aim of this concept is to find the people behind the objects, their behaviours, interactions and ideologies and this way to link material culture to society (Roux 2019, 2).

Although this approach is best suited to ethnographical studies, where not only the products and tools, but also the gestures and the whole production process can be observed, it also provides useful aspects for the analysis of items of material culture from archaeological contexts, including pottery. Ceramic production can be investigated in detail by concentrating on the different elements of the operational sequence. The main actions of the *chaîne opératoire* of pottery production include the procurement and processing of the raw materials, shaping and finishing of the ceramic body, application of surface treatment and decoration as well as the firing of the vessel (Roux 2017, 103; Roux 2019, 15–127).[11]

In addition to the reconstruction of pottery technology by carefully examining the different stages of the manufacturing process, the *chaîne opératoire* approach allows the investigation of the variability of techniques used for the production of an object and the comparison of these techniques over space and time, as well as the assessment of technological choices and

[11] Other main elements of the *chaîne opératoire* can be drying as well as prefiring and postfiring (if applicable) according to Gosselain (2018).

traditions (Lemonnier 1993, 3; Sillar and Tite 2000, 4). Furthermore, the chronological ('vertical') comparison of production sequences permits to identify technological continuity or change within communities (Roux 2019, 294–302). A 'horizontal' comparison of the different *chaînes opératoires* may help outline spatial distribution and boundaries (Gosselain 2018).

As techniques are social productions and each community has their own practices and traditions, social and cultural dimensions of technology can also be studied through the framework of the *chaîne opératoire* (Lemonnier 1993, 2–6; Roux 2019, 2, 5). As a result of this strong relationship between technology and society, this approach may also give a basis to differentiate between social groups or communities of practice (see below) using different techniques (Roux 2019, 5–6).

When investigating fragmented ceramic materials using the *chaîne opératoire* approach, information on many of the used production techniques can be gathered from sherds by examining them at a macroscopic scale, such as raw material processing (e.g. tempering), forming methods, decoration and firing (atmosphere). To achieve the best interpretation, however, macroscopic observation is normally accompanied by scientific analyses to explore 'invisible' traces of technology. Materials science techniques also provide reliable data and less subjective results to build on when examining pottery production (Martinón-Torres 2002, 38). Recent examples of these archaeometric studies applying *chaîne opératoire* approach to ceramics were able to contribute successfully to the above-mentioned topics of pottery technology at different places and times, such as the reconstruction of the *chaîne opératoire* (e.g. Burke et al. 2020; Kreiter et al. 2021; Peña et. al 2021), organisation of production (e.g. Borgers et al. 2019), technological continuity (e.g. Mentesana et al. 2016; D'Ercole et al. 2017), transmission of technologies (e.g. Lewis et al. 2020) and group identity (e.g. Ross et al. 2018; Lara and Iliopoulos 2020).

Although the concept of *chaîne opératoire* focuses on production technology, re-use and re-shaping of object should not be neglected (Martinón-Torres 2002, 33; Lewis and Arntz 2020, 7). A similar approach to the *chaîne opératoire*, originating from processual archaeology, is examining objects as products of behavioural chains. Behavioural chains refer to a series of interactions and performances that occur in the life history of an object from its birth to its burial, including performances such as material characteristics that are needed for the object to serve its function or the skills of the artisan (Schiffer 1975, 106–112; Skibo and Schiffer 2008, 9). Cultural factors affecting the behavioural chains such as ideologies and rituals are

also emphasised in this concept (Skibo and Schiffer 2008, 29) as in the case of the *chaîne opératoire*. In several recent works, these two approaches are not handled as two entirely separate concepts, in fact, these studies include elements of both theories (Lewis and Arntz 2020, 10 and papers in the same volume).

Technological choices and influences on technology

When examining and comparing *chaînes opératoires*, one may find different solutions for the production of the same artefact. Thus, it is apparent that each action in the manufacturing process is the result of the choices of the producer (Lemonnier 1993, 6). Similarly to the *chaîne opératoire*, the concept of technological choices also has roots in French anthropology and was introduced by Pierre Lemonnier (1993).[12]

In principle, there are multiple ways to create an artefact, but it is likely, that producers were only aware and chose between a couple of possibilities (Mahias 1993; Sillar and Tite 2000, 10). However, only some technological choices are made consciously, and most of them are inherent and transmitted through tradition when learning the craft (Lemonnier 1993, 6–7). Each community has an idea about the proper way of doing things and the proper raw materials to use based on which they adopt some techniques and reject others (Lemonnier 1993, 6, 14). Thus, each community has their own technological style, which includes all the choices made at different stages of the *chaîne opératoire* (Lechtman 1977; Stark 1998, 211; Gosselain 2011, 244).

Because of their inherent nature, most 'choices' are deeply embedded in the society and as such, provide an avenue to study social identity (Lemonnier 1993, 3, 18–21; Mahias 1993; Gosselain 2000; Livingstone Smith 2000; Gosselain 2011). As part of the technical system that encompasses all technologies of a society (Lemonnier 1986), choices made within a certain technology should not be investigated as an isolated phenomenon, but together with other related technologies within the social organisation (van der Leeuw 1993, 240; Sillar 2000, 58).

Technological choices are made concerning five main constituents of the production process: raw materials, tools, energy sources, techniques and the production sequence itself (the latter

[12] A similar term, 'technical choice', used by the americanist tradition, has a slightly narrower meaning than that of 'technological choice' referring only to the choices made during the procurement of raw materials and the manufacturing process as opposed to 'technological choice', which includes other processes as well such as adoption (Skibo and Schiffer 2008, 11; Stark 1998).

including the order, frequency and location of the different stages of the *chaîne opératoire*; Sillar and Tite 2000, 4). The choices, and by extension technologies, are influenced by material/technical and symbolic/cultural aspects.

Among technical influences affecting technological choices, direct and indirect influences can be distinguished. Turning to technological choices in pottery production specifically, direct influences include the geological environment (e.g. availability of clay and temper resources), the political-economic system (e.g. control over deposits) and the knowledge and experience of the potter about the technological process (Schiffer and Skibo 1997, 33–39; Sillar and Tite 2000, 5, 7). Indirect influences on choices can be generated by the organisation of pottery production (e.g. degree of specialisation), transportation and use (Sillar and Tite 2000, 7). Transportation and use may require certain mechanical, thermal and visual performance characteristics for the vessels to fulfil their function (Schiffer and Skibo 1997, 33–39; Sillar and Tite 2000, 8; Tite et al. 2001). These performance characteristics are, for example, impact resistance, stackability, heating effectiveness, thermal shock resistance, permeability to water and abrasion resistance (e.g. when cleaning; Schiffer and Skibo 1997, 33–39).

At the same time, cultural factors such as politics, religion and symbolism may have as much impact on technological behaviour as functional factors do (Lemonnier 1993, 3–4). It is important that symbolic aspects of technological choices are given equal emphasis to functional ones as often "not nature but culture is the main constraint of technique" (van der Leeuw 1993, 241; see also Livingstone Smith 2000). Nevertheless, often these two aspects are interrelated and cannot be separated: practical characteristics may also serve cultural purposes, or *vice versa* (Sillar and Tite 2000, 8; Sillar 2000, 58). Furthermore, these categories are somewhat arbitrary representing the ideology of today's researcher, while past people may have not distinguished between practical and cultural functions (Mahias 1993, 163).

The social and symbolic aspect of technological choices are especially tangible if one encounters seemingly illogical choices (from the perspective of today's researcher), which, however, were perfectly appropriate in their social context (Lemonnier 1993, 4). There are certain material constraints, which need to be met to produce a usable product ('strategic tasks') and there are elements of the manufacturing process, which can be changed ('technical variants'; Lemonnier 1992, 21–24; Gosselain 2018). These latter elements of the production sequence are deeply influenced by social factors (Lemonnier 1993, 19–20).

Choices often made by a group, but there are also individual ways of doing things. In archaeology, one can usually investigate collective, cultural choices, but in special cases, it is possible to grasp individual choices in the form of an invention (Sillar and Tite 2000, 10; and see below).

Because of its close relationship with the framework of the *chaîne opératoire*, it is evident that the approach of technological choices is also very useful when interpreting ceramic sherds based on both visual examination and scientific data. Many studies examining pottery from this perspective include methods of experimental archaeology as well (Whitbread 2001). Archaeometric studies of technological choices have been dealing with choices made at different stages of the pottery production sequence, such as selection of clays and temper (e.g. Martineau et al. 2007; Sahlén 2013; Falabella et al. 2013, Frahm 2018; Sorresso and Quinn 2020) and application techniques and recipes of surface coatings and glazes (e.g. Tite 2009; Kreiter et al. 2014). The change of practices can be pointed out over time (e.g. Poblome et al. 2002; Grave et al. 2013) or space (e.g. Albero Santacreu and Cau Ontiveros 2017) and potential reasons for the change may be discussed. Sometimes the expression of cultural identity and group affiliations (e.g. Quinn and Burton 2009) or connections between seemingly separate population groups (e.g. Herold 2015a) may be suspected by the investigation of technological choices.

Technological tradition, change, communities of practice and innovation

The repetition of the same technological choices synchronically or diachronically forms technological traditions, "that is, shared ways of doing that stem from a shared set of knowledge" (Gosselain 2018, 152; see also Roux 2019, 6). Technological traditions are characterised by learning systems through which the craft is reproduced and technological continuity is maintained. Different influences, however, may induce a change of traditions, which sometimes is reflected in innovations.

Communities of practice – the transmission and reproduction of technology

An important moment in the formation of technological traditions is, when the knowledge of a generation is passed on to the next generation. The arenas where these transmissions happen can be defined as communities of practice. The communities of practice are places of collective learning where people interact with other members of the group. The three main elements of communities of practice are: people in the community are connected by their collective

understanding about their community ('joint enterprise'), there is interaction between them which maintains and develops the community ('mutual engagement'), and members use a 'shared repertoire' of resources (Wenger 1998, 72–85; Wenger 2000, 229).

The transfer of knowledge and cultural preferences in the past may have happened through apprenticeship within a community of practice. Apprenticeship could take place in one-to-one interactions or in a group, aiming at the "development of dexterity, skill, endurance, memory, consideration, and properness, while gaining knowledge, inspiration, and/or motivation" (Wendrich 2012a, 3). One of the most important functions of apprenticeship is learning 'properness' (appropriate attitude), in order for the pupil to get ready to join the group of practitioners and become one of them (Wendrich 2012a, 3). Learning a craft thus has not only economic aspects in terms of the future livelihood of the pupil, but it is also a process of enculturation and admission into the society (Gosselain 2008, 176; Wendrich 2012a, 15). Learning in adulthood can often be associated with postmarital resocialisation in patrilocal societies, referring to the integration of new wives into their husband's community where they are taught craft production usually by their mother-in-law (Herbich and Dietler 2008).

Concerning pottery production, it is possible that apprentices first took part in the procurement and preparation of the raw materials and were mostly observing the actual production process, and this stage of learning could last for years (Wendrich 2012a, 9–10). After this, they might have assisted the potter and done smaller tasks in the main production stage and been incorporated more and more into the whole *chaîne opératoire* until being able to produce vessels by themselves (Wendrich 2012a, 10).

However, archaeologists are usually not able to observe the process of learning, but have to deal with its material results instead (Minar and Crown 2001, 374–375; Herbich and Dietler 2008, 224). In archaeology, the concept of communities of practice may be used to recognise cultural identity, interactions between communities and social organisation by the thorough examination of artefacts (Minar and Crown 2001, 369; Wendrich 2012b, 256; Roux 2019, 311; e.g. Sassaman and Rudolphi 2001). In some cases, objects of 'poor quality' have been determined as apprentices' work, but this identification is rather problematic as it is also likely that these objects were not kept, but instead they were reused, remade or corrected (Wendrich 2012b, 255, 258). In the special case of having enough fingerprints on pottery to measure, the works of children may be identified (e.g. Kamp 2001).

When investigating well-documented finds regarding both chronology and stratigraphy, a good practice to follow is focusing on variability at a micro scale within the assemblage, which may give information about different communities of practice and knowledge transfer (Wendrich 2012b, 258–259). Variability can be measured, for example, by examining the results of automatic movements, also called motor habits, such as forming techniques in pottery production (Arnold 1985, 233–234; Gosselain 1998; Minar and Crown 2001, 375; Roux 2019, 311). In the case of motor learning, pupils first pay much attention to copy their masters and they work slowly to understand every detail of the process, but after numerous repetitions their movements become unconscious, quick, smooth and automatic (Minar and Crown 2001, 373). Because changing these automatic motions is hard (requires effort and concentration), there is potential to distinguish between individuals or communities of practice when automaticity is recognised in the material culture (Minar and Crown 2001, 373, 375; e.g. Minar 2001). Further possible ways of investigating learning processes in communities of practice include the investigation of depictions or written evidence related to apprenticeship and grave finds related to crafts (Minar and Crown 2001, 375; e.g. Hasaki 2012).

The inclusion of materials science techniques to investigate communities of practice in pottery archaeology adds a different perspective to the macroscopic observation of the objects, through which other traces of technological variability can be identified. This way, scientific analysis approaches used in the study of a seemingly uniform ceramic material may allow for distinguishing between different communities of practice, investigating the relationship between them and identifying potential immigrants (Eckert et al. 2015). Group identity, interaction between communities of practice, as well as shared and differing elements of their technological traditions can be explored by investigating clay recipes and forming methods (e.g. Amicone et al. 2020; Jordan et al. 2020; Espinosa et al. 2021; Casale et al. 2022.). Based on the identification of communities of practice, technological and social change (e.g. Živković et al. 2021) and social integration (e.g. Echenique et al. 2021) may be studied.

Technological change and innovation

In some cases, technological traditions may have taken other routes than what they had followed previously, which were often represented by the appearance of inventions and innovation. Invention may be defined as a novel object or technology (and the process how it comes into being), while innovation may be used for a wider process (and its subject) including

the moment of invention as well as the spread and adoption of invention (see Erb-Satullo 2020, 38, summarising also other definitions of the two terms).

Innovation may be investigated from several perspectives including the reasons for innovation, adoption and spread of new objects or practices (as well as their non-adoption), and the effects of innovation on social and technical systems of the innovating community (Rogers 1983).

The causes of innovation could be numerous spanning from inner intentions of the producer to external demand of consumers (Roux 2019, 304; Erb-Satullo 2020, 46). Invention may have been motivated by social factors, such as peer competition, expectations deriving from social role, formation of new social groups and reproduction of social hierarchy (Schiffer 2011, 43–54). Invention could be initiated if there was no appropriate technology to solve a problem (project-stimulated invention), if new raw materials or tools became available, or its appearance could be stimulated by other inventions (Shortland 2004, 3; Schiffer 2011, 57–85).

Innovation could also happen unexpectedly as an accident (Schiffer 2011, 67–69). Some of the reasons of unintentional innovation might be the mistaken imitation of an object (O'Brien and Bentley 2011, 318; Gandon et al. 2014), an error made during the manufacture of another artefact or an accidental event independent of production processes (Shortland 2004, 3).

Inventions are usually adopted by a community, if they are compatible or can be altered to fit in the existing technological, social and cultural systems of the group (Pfaffenberger 1992, 500; Lemonnier 1993, 12–16; Bernbeck and Burmeister 2017; Erb-Satullo 2020, 39). However, it should not be assumed that the appearance of certain technologies follows a developmental sequence, because this would lead to generalisations and may not be the case in certain areas and periods (Erb-Satullo 2020, 41–42).

Some inventions were adopted rapidly, while others spread slowly (Rogers 1983, 7). The spreading of technological traditions in archaeology may be defined as the diffusion process (Rogers 1983, 5; Roux 2019, 306; Erb-Satullo 2020, 40).[13] It may consist of five main stages through which the invention has to pass through to be successfully adopted, including knowledge (people learn about the invention), persuasion (decision maker forms an opinion

[13] Diffusion, however, is a wider term in 'diffusion research' and includes adoption, modification, reinvention and other processes induced by the invention in the recipient community (Rogers 1983, 5–7; Erb-Satullo 2020, 40).

about the invention), decision (adopting or rejecting innovation), implementation (using innovation) and confirmation (reinforcement of the decision, potential discontinuance; Rogers 1983, 163–191).

The adoption of an invention depended on the consumers: whether they could afford the object, what their household size was, how mobile they were, etc. (Schiffer 2011, 141–144). The adoption process may have been successful if the novel artefact enhanced certain activities, if the adoption process required the acquisition of another invention (ensemble adoption), if newly introduced activities could not be performed without the invention (activity-entailed adoption), if it was imposed by social power, or if the invention was connected to a social process (e.g. gifting, rituals, ceremonies; Schiffer 2011, 144–150). A need for a replacement of an object, competition, or uniqueness might have also influenced the adoption process (Schiffer 2011, 150–163). Furthermore, adoption could be fostered or held back by economic, political, social and demographic dynamics (Erb-Satullo 2019, 580–583).

Not all innovations were adopted; there were examples when people did not follow the new technological trends of their neighbours (Schiffer 2011, 17–18; Erb-Satullo 2020, 44; e.g. Sørensen 1989; de Groot and Bloxam 2022). It is also possible that adoption took place, but it was followed by a decline and abandonment of the adopted practice or artefact (Erb-Satullo 2020, 44; e.g. Thornton and Rehren 2009; Erb-Satullo 2021). The reasons for discontinuance of technological traditions are probably related to social factors in most cases, and additionally population changes and the depletion of resources can be mentioned as potential causes for abandonment (Erb-Satullo 2021, 2–3).

When examining a certain archaeological assemblage, one of the main questions is whether innovation was developed locally or had been adopted and if adopted, to what extent it contains endogenous and exogeneous elements (Erb-Satullo 2020, 41). The answer, however, is more complicated than deciding between invention with local roots and adopted invention as adoption was often not unidirectional, and the adopted and modified invention could also have an impact on and shape the ‘original’ invention (Erb-Satullo 2020, 45–46; e.g. Watson 2014; Shortland et al. 2018).

Scientific analyses of archaeological assemblages may identify innovation, locate its first examples (by confirming intentionality and consistency of production), outline its distribution, identify end products of experimentation or accidental innovations and distinguish between

imported artefacts and their local imitations (Erb-Satullo 2020, 43–46, with further references). By investigating the distribution of adoption patterns, different technological traditions and their boundaries can be outlined, as well as interactions between them can be studied (Erb-Satullo 2020, 43, 45–46). As for ceramic research, topics related to possible clay recipe and glaze innovation (e.g. de Groot et al. 2017; Burlot et al. 2020), adoption and rejection of the potter's wheel (e.g. Baldi and Roux 2016; Thér et al. 2017; Thér and Mangel 2021; de Groot and Bloxam 2022), innovation and continuity of ceramic technologies (e.g. D'Ercole et al. 2017; Charalambidou et al. 2018) as well as local traditions and population stability (e.g. Donner et al. 2019) have been discussed, among others.

Technological traditions and society

Technological traditions, through the shared ways of doing things, are the representations of social groups, and as such, they may reflect social boundaries (Costin 1998; Roux 2019, 6, 295, 311). When examining social identity, some traits of an artefact, which are less liable to change, are more meaningful than others, which can be altered easily (Gosselain 1998, 82; Roux 2019, 6, 294–295).

In the case of pottery production, some techniques during the manufacturing process result in visible features of the end product, such as certain types of tempering (e.g. grog), certain forming (preforming, secondary forming), decorative and firing methods in the case of ceramic technology (Gosselain 2000, 191). These visible characteristics might be influenced by economic, aesthetic or symbolic factors and relatively easily imitated or changed (Gosselain 2000, 191). There are also techniques, such as collection and processing of clays as well as firing, which leave no traces for the naked eye, but still can easily be altered (Gosselain 2000, 192). Because only a limited number of people (usually specialist) are interested in and therefore influence these actions, these techniques likely spread only locally or regionally (Gosselain 2000, 192).

The most specific element of the *chaîne opératoire* is fashioning (or primary forming), when the rough shape of the vessel is created (Rye 1981, 62; Gosselain 2000, 192). This technique is characteristic to the potter as it consists of 'motor habits' that are the result of years of experience (Gosselain 2000, 192). They gradually became inherent qualities and a part of the potter's *habitus*, which refers to the system of long-term dispositions developed by a person of ways of living and doing things that generates practices (Bourdieu 1977, 17, 72, 78; Dietler and

Herbich 1998, 246). Because of these motor habits, fashioning can hardly be changed or modified, thus it is strongly related to social identity (Arnold 1985, 235–237; Gosselain 1998, 92–93; Gosselain 2000, 192–193; Roux 2019, 311). However, the result of this initial stage of the forming process cannot always be traced on the finished product as it may be masked by subsequent forming stages. Nevertheless, it is important to conclude from this that not all elements of the production process and characteristics of the finished products have the same potential to outline deeper levels of social identity.

The tracing of technological traditions thus sheds light on social identities and group affiliations, for which materials science can be very useful by pointing out macroscopically invisible features (e.g. Quinn and Burton 2009; Day et al. 2010; Quinn and Burton 2016; Cootes and Quinn 2018; Nam et al. 2020; Prado et al. 2020; Echenique et al. 2021). A case study investigating early medieval ceramics from the south-eastern part of Lower Austria also presented this use of archaeometric techniques (Herold 2015a).

To sum up, technological traditions are characterised by continuity and change. Technological continuity is maintained and reproduced by the transmission of knowledge in communities of practice, which also contribute to the reproduction of society (Day et al. 2006). Similarly, technological change has a social dimension as well, regardless of the technological or the cultural change occurring first (Shennan 2000, 813; Arnold 2008; Roux 2015; Roux 2019, 301; Erb-Satullo 2020, 42–43; Frieman 2021). Scientific analyses of ancient ceramic materials and technology have a great potential to contribute to the investigation of the relationship between technological and cultural change (Fragnoli and Palmieri 2017; Hein and Stilborg 2019; Živković et al. 2021).

Organisation of production

An interesting field within archaeological pottery research is related to how ceramic production was organised. Vessels may have been manufactured in different units ranging from small households to large workshops. The organisation of production is most commonly approached through the investigation of different variables such as scale, degree of control, level of standardisation and level of specialisation. Based on these parameters, different modes of production can be identified, which is one way of reconstructing past production organisation besides other strategies such as the recently suggested relational approach.

Pottery production, as other craft production activities, was an integral part of past societies as it was strongly related to and influenced by distribution and consumption, and because the producers themselves were members of the society with their identities and roles (Costin 1991, 2–3; Costin 2005, 1035; Duistermaat 2017, 115). Thus when studying organisation of production, its embedded nature into society should also be considered.

In archaeology, there is direct and indirect evidence that can be used to investigate the organisation of pottery production. Direct evidence includes concentration of raw materials (e.g. clay, pigments), wasters, remains of tools (e.g. moulds) and production facilities (e.g. kilns, firing pits), based on which, among others, the place of production and its spatial arrangement can be identified (Costin 1991, 18–19; Costin 2005, 1056–1058). In the case of indirect evidence, only the product is available to be analysed. Examining standardisation, skilfulness, efficiency and distribution of regional variations of an artefact may help in getting information about past production organisations (Costin 1991, 32). Scientific analyses may contribute to studies using direct evidence, but they are almost inevitable when it comes to examining production organisation based on indirect evidence (see examples below).

Scale

The scale of production has been explained different ways. According to Prudence Rice (1987, 170, 180), it refers to the level of labour and resources input and the amount of pottery produced. Philip Arnold (1991, 364) adds the "physical size" of the production unit to Rice's parameters. Cathy Costin (1991, 15) understands the size of production units (households or workshops) and labour recruitment under scale. Her definition of size includes the number of people working in a production unit and labour recruitment refers to the ways in which people were brought into the production unit such as kinship, skill, availability. She associated small-scale production with kinship-based households and large-scale production with skill-based workshops. However, the interrelation between these two different parameters of Costin's definition (size and labour recruitment) has been disputed since the size of a production unit is not necessarily related to how producers were recruited (Pool and Bey 2007; Arnold 2008, 7–8).

The relationship between the other two terms linked with scale, output and the size of the production unit, is also slightly problematic. Although these parameters are often interlinked, meaning that if more producers are included in a production unit, the output will be higher

(Rice 1987, 180–181), this is not universal as small groups of producers can also achieve large outputs by intensifying production or changing to new technologies (Costin 1991, 30; Costin 2005, 1069). Scale is thus not always directly proportional to organisational complexity of production (e.g. Erb-Satullo et al. 2017, 123–124). Small-scale and large-scale are also relative terms and make sense only when comparing different assemblages. In short, small-scale production may be connected to households, but large-scale production does not necessarily imply the presence of workshops (Costin 1991, 30).

Archaeological features and assemblages offer some opportunities to estimate the scale of production. When direct evidence is available, such as the remains of the place of production, size might be estimated based on its dimensions and its relation to the other parts of the archaeological site (e.g. whether it can be connected to a household or it is outside of the settlement area; Costin 1991, 29–30). When pottery wasters are found, they can give information about the different ceramic types produced, and estimations can be made regarding the output and firing loads based on experimental archaeology (Rice 1987, 181).

Scientific techniques may also be used to obtain information about the scale of production especially when only indirect evidence is available. By identifying potential places of production based on mineralogical or chemical composition, tracing variability in the assemblage (see below) and identifying different paste recipes and production methods, products of different production units may be distinguished and production scale may be estimated (e.g. Falabella et al. 2013; Wright 2016; Druc et al. 2017; Cohen et al. 2018).

Degree of control

Production may have been influenced or determined if there was a social/political group that exercised control over it. Besides production and production organisation, the control may have been extended to raw material access, distribution and use of the products (Costin 2007, 152).

For the description of those production systems where control was detectable, the term ‘attached production’ has been used in the literature, and ‘independent production’ for those

systems where no such control was tangible (Earle 1981, 230).[14] Producers in attached production worked for members of the elite, a patron or governmental institutions, and thus manufactured high-value goods, luxury items or weaponry (Brumfiel and Earle 1987, 6; Costin 1991, 11).[15] The control over attached producers might have been exercised directly by monitoring the production process, but it is also likely that elites chose an easier and less labour-intensive way, such as controlling the distribution of goods instead (Arnold and Munns 1994, 477).

Independent producers experienced no control from political elite, but that did not mean that they were not influenced by the political, economic and social systems that they were a part of (Brumfiel and Earle 1987, 6; Costin 1991, 11). They produced utilitarian goods for ordinary consumers (Brumfiel and Earle 1987, 6; Costin 1991, 11). The control over distribution was probably in the hands of independent producers, which may indicate a more direct contact with consumers than in the case of attached producers (Arnold and Munns 1994, 487).

The distinction between attached and independent production, however, is not straightforward since there is no scheme based on which the artefacts produced by the two types of systems can be separated (Costin 2005, 1070, 1072). This is partly because the boundary between high value goods and utilitarian objects cannot always be identified (Arnold and Munns 1994, 476; Flad and Hruby 2007, 8–12; Duistermaat 2017, 118).

Nevertheless, in some cases, it is possible to demonstrate the presence of control over production or some level of coordination (Erb-Satullo et al. 2017) between production units in archaeological materials. In those specific cases, when production sites are found near residential structures of the elite, it is evident that attached production was physically 'attached' to these elite residences (Costin 1991, 25). It is possible, though, that attached production units were located farther from elite structures (Arnold and Munns 1994, 476), and

[14] As political control used to be linked to specialised production (see below), these terms are referred to as 'attached specialists' and 'independent specialists' in early publications (e.g. Earle 1981; Brumfiel and Earle 1987; Costin 1991).

[15] A somewhat different system was suggested by Carla Sinopoli (1988, 581–582) for the identification of the degree of control over production, which includes three categories. Sinopoli's 'administered production' resembles the category of attached production, but additionally it includes a powerful group or institution that monitors producers under the control of the elite. Furthermore, she distinguishes 'centralised production', which is defined as a "large-scale and spatially segregated production" that may be indirectly (e.g. taxation) influenced by administrative authority. Her third category, 'noncentralised production' is characterised by small-scale production, low output and dispersed location with the least involvement of the administrative authority.

in this case, it is useful to examine whether archaeological features show any signs of restricted access (e.g. fence) or not, which might help identify control over production (Costin 1991, 25). The locations of the production units compared to one another may also indicate that production was monitored; e.g. nucleated arrangement of production sites could permit easier overseeing (Erb-Satullo et al. 2017, 110). At the same time, there might have been other reasons for this arrangement (e.g. interaction between producers) and it could also be that spatially dispersed units were working under the same supervisor (Martinón-Torres 2014, 552; Erb-Satullo et al. 2017, 110).

When only the products of these units are available to study, it is worth going through the *chaîne opératoire* and identifying those segments of the sequence where control could have modified technological choices, and deciding whether indications of control are present or not and to what degree (Erb-Satullo et al. 2017, 110). Including materials analysis in the archaeological investigation may help identify, confirm (e.g. Sanders 2015; Quinn et al. 2017; Quinn et al. 2021) or argue against (e.g. Li et al. 2012; Druc et al. 2018; Druc et al. 2020) the controlled nature of production.

Standardisation

Evaluation of the level of standardisation is another important aspect when characterising production organisation. The widely accepted definition of standardisation originates from Rice (1991, 268), who explains standardisation in terms of ceramics as "the relative degree of homogeneity or reduction in variability in the characteristics of the pottery, or […] the process of achieving that relative homogeneity" (see also Kostonas 2014, 8). Standardisation is thus relative and can be used when comparing one assemblage to another (Rice 1991, 268). The other, sometimes differently defined terms connected to standardisation are variation and variability. According to Antonis Kostonas (2014, 8) "variation can be defined as the relative degree of heterogeneity seen on the attributes of artifacts, whereas variability can be taken to refer (often at an abstract level) to the liability of these attributes to change and become more varied or standardized". Variability thus includes both standardisation and variation, which latter two terms should be seen as the two ends of a continuum instead of as opposing terms (Kostonas 2014, 17).

Standardisation may be present in different characteristics of an assemblage, such as its compositional, morphological and decorative elements (Rice 1996, 268). It is possible that one

attribute of an artefact type shows some degree of standardisation while another feature of the same type reflects variation (Underhill 2003; Berg 2004; Kostonas 2014, 12). Standardisation is usually connected to the production process, but the investigation of variability may be extended to distribution and use as well (Rice 1996, 268).

There are numerous factors that could influence the degree of standardisation such as raw material availability, technological traditions, the artisan's skill and experience, the scale of production and consumer demand (Kostonas 2014, 12). The reasons that promoted the appearance of standardised production might have been varied as well, including easier transportation and stackability, a need for standardised units and measures, easy recognition of different vessel functions/contents, a need for making production more predictable, consumer demand and social or symbolic reasons such as expression of identity (Costin 1991, 33–34; Kostonas 2014, 14–16).

Standardisation used to be associated with mass production and complex organisational systems in older literature, particularly with specialisation (see below; e.g. Rice 1991, 268–272; Costin 1991, 33–36; Blackman et al. 1993; Costin and Hagstrum 1995). Since then, however, studies have demonstrated that such links cannot be assumed automatically. Standardised products might have also been manufactured during part-time work (Arnold 1991), or made by non-specialists (Stark 1995), or been an unintentional result of a technological change or other socio-political factors (Berg 2004).

Standardisation may be observed in different characteristics of archaeological artefacts. In the case of pottery, examining the results of the different steps of the *chaîne opératoire* may help identify the degree (or the lack) of standardisation in composition[16], paste preparation, form, surface treatment and decoration as well as firing characteristics (Rice 1987, 202; Hilditch 2014, 26–27). One of the most popular approaches to identify standardisation is the measurement and comparison of the shape and different dimensions of the vessels by methods such as coefficient variation (Kostonas 2014, 10; Roux 2003; Wang and Marwick 2020; Mączyńska 2021). Other studies investigate the similarity/distinctiveness of decorative elements and motifs (e.g. Clark 2007, 293). Scientific techniques are especially useful for

[16] Based on his ethnoarchaeological research, Dean Arnold (2000) argues that variability of paste compositions might be a result of geological and social factors besides technological modifications, thus compositional data should be carefully used when interpreting production organisation. He finds that paste composition tells more about the organisation of distribution.

investigating the degree of standardisation in terms of chemical or mineralogical paste composition and tempering methods (e.g. Sanjurjo-Sánchez et al. 2016; Bray and Minc 2020; Caso et al. 2022). In rare cases, standardisation of vessels fired together as parts of the same kiln load may be analysed and compared (Blackman et al. 1993). More complex topics can also be discussed based on the analytical investigation of standardisation, such as technological (Hilditch 2014) and socio-economic change (Fragnoli 2018).

Specialisation

The definition of specialisation in production organisation has changed over time (Flad and Hruby 2007, 3–6). Early works emphasise that specialisation can be identified based on the time that specialists spent on production, whether this activity was carried out for subsistence, whether the occupation had a recognised name, and whether the activity included getting payment or renumeration (Tatje and Naroll 1973; Rice 1981, 219; Rice 1987, 188–189; Costin 1991, 3). Since then, the definition has been slightly reduced and now specialisation may be described as an organisation form, where a "specialist produces more of some goods than he or she personally uses" (Costin 2005, 1036). Specialisation is characterised by its degree. If there are, in theory, few producers and many consumers of a product that would indicate a high level of specialisation, while many producers and few consumers would correspond to a low level of specialisation (Costin 1991, 4–5).

Specialisation can occur in different forms. It has been recognised early that it is not necessarily represented spatially, thus producer specialisation and site specialisation are two different things (Muller 1984; Stark 1991, 73). Further types of specialisations include resource specialisation and functional specialisation (Rice 1991, 262).

A parameter that is often investigated in relation to specialised production is the time involved in craft making (often referred to as 'intensity' of production following Costin 1991, 16–18). Usually two types of specialists are distinguished: full-time specialists work all year round, while part-time work is seasonal (Rice 1987, 189; Costin 1991, 16–18). Part-time specialisation could be combined with other activities, such as agricultural work, and craft production could be carried out off-season (Costin 1991, 17).

Another important factor in identifying specialised organisation is the skill level of the producer. Skill is gained by years of experience and a specialist is more likely to be more experienced that a non-specialist, thus specialised production would be likely to show

proficiency, consistency and few errors in the manufactured objects (Costin and Hagstrum 1995, 623; Costin 2005, 1068). Skill is more obvious when an artefact exhibits artistic features or intricate design (Costin and Hagstrum 1995, 623).

Specialisation in production organisation used to be associated with complex societies in early studies (Dow 1985; Rice 1987, 188; Arnold and Munns 1994, 475). It was assumed that specialisation implied the division of labour in terms of the production process (Brumfiel and Earle 1987, 5; Clark and Parry 1990, 292; Costin 1991, 3–4). The emergence of specialisation was linked to attached producers, referred to as 'attached specialists', which also meant the appearance of the first elite groups for whom these specialists were producing (Rice 1981, 223; Arnold and Munns 1994, 475–477). Attached specialists were the 'result' of political processes, in contrast to 'independent specialists' who came into being because of economic reasons as the uneven distribution of resources gave rise to population stress (Brumfiel and Earle 1987, 5–6; Costin 1991, 7; Arnold and Munns 1994, 476). Because of its coevolution with the elite, attached specialisation was suggested to reflect social inequality, and independent specialisation was proposed to be the sign of social solidarity (Costin 2005, 1071).

Many elements of these assumptions, however, have been questioned by Peter Day and others (2010), especially the connection between specialisation and socio-political centralisation as well as the division of labour. Furthermore, the way that the development of independent specialisation is explained (profit governed, cost-cutting strategies, etc.) is rooted in modern capitalist thinking and may not be applicable to ancient scenarios (Day et al. 2010, 209). It was proposed that instead of focusing on the above-mentioned parameters, the investigation of time and skill involvement are more fruitful when studying specialisation (Day et al. 2010, 210). The value of a product, which was determined by consumption and exchange mechanisms besides technological and symbolic properties, should also be evaluated in their specific socio-historical context (Flad and Hruby 2007, 8–12; Day et al. 2010, 210).

An interesting question is how specialised production is recognisable in the archaeological material. It was suggested that the differential distribution of production evidence (such as materials originating from the different steps of the pottery making process) across households or communities could be used to identify specialisation (Costin 1991, 21–24). However, specialisation does not necessary include the division of labour (Day et al. 2010, 208–210), thus there are forms of standardisation which cannot be recognised by differential distributions. It is rarely possible to conclude from archaeological remains whether production

was carried out full-time or part-time, but in the special case, for example, if there is evidence for specialisation in a household and other finds in the household's assemblage refer to agricultural activities, craft making was probably a part-time activity (Costin 1991, 30–32). Another potential way to point out specialisation could be if an assemblage of a period contains a large number of only few variants (Costin 1991, 41).

Materials science techniques are often used to distinguish between different paste recipes, which may help outline provenience and distribution of specialised products (e.g. Vaughn and Neff 2004; Stoner et al. 2008; Heidke 2009; Niziolek 2013; Sahlén 2013; Callaghan et al. 2017). Based on compositional features, exchange patterns may be analysed as well (e.g. Curewitz and Foit 2018). Specialisation might be tangible in the forming techniques (Ross et al. 2018) or in the firing characteristics (e.g. Marghussian et al. 2017) of the vessels. Centralised production and technological continuity may be inferred from standardised compositions (e.g. Li et al. 2022) as well as functional analysis of specialised shapes can be carried out by residue analysis (e.g. Dunne et al. 2020).

Reconstructing production organisation: modes of production and a novel approach

Based on the above-mentioned and other parameters of production, there were attempts to create models with which different levels of production organisation could be described. The most often cited examples of these 'modes of production' originate from Sander van der Leeuw (1977) and David Peacock (1982).

Van der Leeuw identified six modes of production based on his comparison of ethnographic studies about pottery production conducted by researchers at different parts of the world (van der Leeuw 1977, 70: Table 1, 72–74). His first category, 'household production' is characterised by occasional production for the household's needs using local raw materials, very few tools, hand-made techniques and open firing. 'Household industry', is a seasonal activity for some income, but also local raw materials, hand-forming techniques and open firing are used. He describes 'individual industry' as a mode of production related to itinerant specialists working almost all year round for their subsistence, using local raw materials, turntables and sunken mud kilns. A large technological 'jump' characterises the next mode of production compared to the previous ones, 'workshop industry', as it includes mass production by specialists and their assistants through careful clay preparation and using potter's wheel and (semi-)permanent kilns. A similar production form to workshop industry is 'village industry' when

whole villages are specialised to pottery manufacture, which are influenced and controlled by entrepreneurs. Finally, 'large-scale industry' is pottery production with considerate investment in machinery and technology and the use of hired labour.

Peacock distinguished several modes of production in his publication about Roman pottery (Peacock 1982, 6–11). He defines 'household production' as the simplest category, where each household makes ceramics to their own needs. It is likely that turntable or wheel are not available in this type of production. A more organised form of production is what Peacock calls 'household industry'. Making pottery is still a part-time activity, but carried out by professionals for side income. The presence of a turntable is probable and ceramics are open fired or fired in a simple kiln construction. 'Individual workshops' include potters whose main source of profit comes from ceramic making, but can have other supplementary activities such as agricultural work. These workshops are equipped with wheels and kilns. It may be one potter making pottery in his/her workshop, but he/she can also employ assistants. 'Nucleated workshops' encompass groups of individual workshops, which share the same raw material sources, labour or market. Pottery making is the main if not the only source of income for the potters. Building infrastructure permits them to work all year long and cooperation gives them a high financial stability. These workshops are characterised by large-scale production as well as standardised and high-quality products. There are more modes of production identified by Peacock, but these are specifically Roman (estate and military production) or usually not relevant when dealing with archaeological materials (manufactory, factory).

A critique of using modes of production in an archaeological context has been expressed by Kim Duistermaat (2017). In her opinion, because these models are predefined categories, they often fail to characterise what production organisation really looked like in the past – they are too generalised and inflexible. They make researchers fit their results into one of these categories instead of describing the production organisation with a bottom-up approach and building up a theory based on the actual assemblage (Duistermaat 2017, 116, 119).

Central to the relational approach proposed by Duistermaat (2017, 124–137) is the tracing of entanglements[17], interactions and relations between different actants (people and things) during the production process and the following life history of the products. The artefact or assemblage in question may be analysed through four strategies. The first strategy includes

[17] For the idea of entanglement explaining the relationship between people and things see Hodder 2012.

focusing on material properties, how they interact and what they afford to, how they influence technological choices during production and use. Identifying the actants of the *chaîne opératoire* of production (second strategy), such as vessels, tools, potters, assistants, spaces, etc., may help in making interpretations about the potter's skills, task differentiation, the presence of children, seasonality, the time needed for the production of the artefact in question, communities of practice and social identity. The *chaîne opératoire* approach may be extended to the investigation of the life history of the objects after production (third strategy) to gain information about how production was influenced by use-related factors. Also spaces, tools and facilities can be analysed in the same way. The fourth strategy involves the study of spatial aspects of production, distribution and use, such as localising potential raw material sources, investigating the spatial arrangement of the workshop (if known), examining distribution and exchange as well as temporal aspects of production, use, reuse and discard. Although the relational approach offers a fresh view and analysis method by breaking with assumptions and predefined relationships between variables of production, it is very complicated to compare organisations of production described in this way – as Duistermaat (2017, 136) expresses this herself as well.

Summary

As the previous sections have shown, the interpretation of material culture can be approached in several ways. Whether it is done by investigating the *chaîne opératoire* of manufacture, focusing on technological choices, emphasising technological traditions, changes, and innovation, characterising communities of practice or organisational aspects of production, the aim is the same. All of these theories and concepts, especially when combined, can contribute to developing a better understanding of past people and societies who produced the analysed objects. These approaches are interrelated, and represent the multitude of ways of how elements of material culture can be investigated and can help examine social dimensions of technology by analysing results of past human activities.

2.5.2 Borderland archaeology

When examining the history of Lower Austria during the late Roman period and early Middle Ages, it is apparent that this area represents a borderland with several constantly changing borders running across it (Section 2.1). Therefore, in this section, a discussion is given about what borderland means and how the investigation of borderlands has been approached

archaeologically. This is followed by the description and analysis of the different borderlands present in the territory of Lower Austria during the study period.

Archaeological borderlands

Borderlands are special areas where various population groups meet and numerous dynamic processes happen and thus, they represent interesting subjects for archaeological investigation. Borderlands may include different boundaries, borders, and frontiers. Having similar meanings, these terms might be confusing, thus a short explanation is given following the suggestions of Bradley Parker (2002, 372–375; 2006, 78–80).

A 'boundary' is an unspecific divide, a general term used to define the bounds or limits of things, which may refer to both borders and frontiers (Parker 2002, 373; Parker 2006, 79). The term 'border' is more specific and can be explained as a political or administrative boundary, such as border is used in the context of modern nation states (Parker 2002, 373; Parker 2006, 79). Border is usually referred to as static and linear (Parker 2006, 81). A 'frontier' can be defined as a transition zone between different ethnic, cultural or political units, which may imply some degree of blending between these units or, on the contrary, frontiers may be made up of empty areas where no physical contact between these entities is observable (Parker 2002, 373; Parker 2006, 79). Frontiers are seen as fluid compared to borders, and may consist of different overlapping boundaries, such as political, cultural and economic boundaries (Parker 2002, 374; Parker 2006, 80–81).

Borderlands may be defined as "regions around or between political or cultural entities", which are characterised by different borders and frontiers (Parker 2006, 80). In his model referred to as the 'continuum of boundary dynamics', Parker (2002, 374–375; 2006, 80–89) suggests to describe borderlands using a continuum that ranges from 'static', through 'restrictive' and 'porous' to 'fluid', where the first two attributes (static and restrictive) are associated with borders and the latter two attributes (porous and fluid) with frontiers. This continuum can be investigated from many perspectives, including geographic, political, demographic, cultural and economic aspects (Parker 2002, 375; Parker 2006, 81). Borderlands might not be described by the same level of fluidness from these five aspects, e.g. a borderland can be geographically restrictive and demographically porous (Parker 2006, 81). All of these perspectives in fact represent boundary sets, which include further components that can be investigated (Parker 2006, 81).

Among geographic boundaries, topographic features, natural resources, flora and fauna as well as climate can be mentioned, which may restrict or shape the population area (e.g. mountain ranges), but can also provide lines of communication (e.g. rivers; Rodseth and Parker 2005, 13–14; Parker 2006, 82: Table 1, 83). Within the category of political boundaries, administrative and military boundaries can be discussed along with topics such as direct or indirect rule, vassal states and colonisation (Parker 2006, 82: Table 1, 83–85). As borderlands are usually rich in resources including raw materials, land and people, they might have been the stages of conflicts between political entities in terms of the exploitation of resources and control over these areas (Feuer 2016, 55–57). Some borderlands might have been used as a buffer zone to give protection for the core area against outer attacks and invasion (Feuer 2016, 52–54).

When studying demographic boundaries, the evaluation of ethnic distribution, population density as well as the health and gender of the inhabitants are important to identify movements of population groups in or out from borderland regions (Parker 2006, 82: Table 1, 85–87). Borderlands may shape the identity of the people living there, who might define themselves connected more strongly to the borderland than to the core entity (Mullin 2011a, 8; Mullin 2011b, 99). In some cases, borderlands provide a stage for interaction between different ethnic groups, which might lead to the 'birth' of another group with a new identity or even ethnogenesis (Rodseth 2005; Rice and Rice 2005; Parker 2006, 86; Naum 2012, 64–68, 74–75; St. John and Ferris 2019, 46).

Borderlands, sometimes termed as 'contact zones', 'middle grounds' or 'third spaces' in anthropological literature (see Stockhammer and Athanassov 2018 with further references), may provide opportunity for culture contact, which is defined as a "predisposition for groups to interact with "outsiders" […] and to want to control that interaction" (Cusick 2015, 4). Cultural boundaries may be determined by language, religious practices as well as characteristic elements of material culture (Parker 2006, 82: Table 1, 87–88). The investigation of ancient place names and archaeological research play an important role in reconstructing these boundaries (Parker 2006, 87). In colonial situations, although often investigated from the perspective of the coloniser, it is important to note the two-directional ways of cultural changes affecting both the indigenous population and the colonisers (Lightfoot and Martinez 1995, 475–477; Rice 2015, 52). Culture contacts may also enhance the spreading of technologies as well as provide a stimulating environment for innovation (Mullin 2011a, 6; Rice 2015, 52–54).

And finally, economic boundaries within borderlands may be understood, among others, through the investigation of the modes of resource extraction as well as the import and export of raw materials and finished products, and trade mechanisms (Parker 2006, 82: Table 1, 88–89; Feuer 2016, 57–70). This way, topics such as overexploitation, deforestation, effects of colonisation to markets and subsistence activities, and smuggling can be touched on (Parker 2006, 88–89).

All these economic, political, demographic, cultural and geographic boundary sets determine borderland processes. Although they offer different perspectives for studying borderlands, they cannot be separated, they overlap and interact and may be seen as a dynamic web, also referred to as the 'borderland matrix' by Parker (2006, 89–91). The relationships of different boundaries within and between boundary sets are never the same as they constantly change over time (Parker 2006, 90; St. John and Ferris 2019, 46).

Archaeological research can contribute greatly to the investigation of borderlands. In special cases, borders or frontiers may be identified by the remains of a border structures, such as the Roman *limes* or the Chinese Great Wall (Feuer 2016, 4). Military buildings and infrastructure might also define borderlands (Parker 2006, 84). In other cases, settlement patterns, the distribution of elements of material culture or written documentation might help in outlining boundaries (Feuer 2016, 4). Changes in settlement patterns might signal invasive military interventions, population shifts, settling and deportation of groups, migration and population decrease (e.g. because of the appearance of a new disease; Parker 2006, 85–86).

Archaeological finds and features and the way they were made reflect identities whether they were designed to express group affiliation or were only objects and features of everyday life (Lightfoot and Martinez 1995, 485). Burials and grave finds have especially important part in outlining different social groups spatially (Parker 2006, 87). All of these pieces of evidence may identify mixed populations, new identities, or 'conservative' groups in borderlands as boundaries may also reinforce adherence to traditions (Lightfoot and Martinez 1995, 485; Mullin 2011a, 4–5; Wells 2015, 327). By comparing archaeological features and items of material culture in an area before, during and after the formation of borderlands and culture contact, these changes or conservativism become visible (Lightfoot and Martinez 1995, 486).

It is important however, that ancient boundaries are different from modern ones and should not be imagined as lines on a map (Lightfoot and Martinez 1995, 478–482). They are socially

constructed and depend on the specific historical context, which make each borderland a unique case (Boozer 2018, 207; St. John and Ferris 2019, 44–45). Instead of searching past 'outlines', archaeology can focus on social networks to characterise the spatial extent of political entities (Campbell 2021, 39, 45).

A case study investigating the northern borderland of Assyria shows how complex ancient borderlands were and how different boundaries of Assyria appeared gradually in this region (Parker 2002, 375–392; Parker 2003, 528–551; Parker 2006, 91–94). Firstly, military boundaries were established by the beginning of the 9th century BC. The geographic features (mountains) delayed the appearance of political and administrative boundaries until 883 BC, when Assyrian king Ashurnasirpal II started extending these boundaries to this borderland. This was soon followed by a demographic, cultural and economic expansion. Colonisation had begun with forced and voluntary migrations, which caused the collapse of existing settlements as shown by the archaeological record. At the same time, ethnic and linguistic boundaries were extended and a new material culture appeared in the borderland. Finally, economic boundaries were shifted too with the exploitation of resources (especially timber).

Borderlands can be extensively studied in the case of the Roman Empire as abundant pieces of historical evidence are available and many sections of its borders can be followed archaeologically by tracing remains of the *limes*. The territories beyond the *limes* were called *barbaricum* by the Romans, but Roman control could be extended to these areas through alliances with tribes and kingdoms living there (Elton 1996, 36; Boozer 2018, 211). The case studies of two Roman borderlands in Africa (Great Oasis in Egypt and the border with Nubia) show that Roman rule brought changes into these territories after their annexation; the extent of these changes, however, varied (Boozer 2018, 212–231). The landscape may have been altered by the construction of fortresses, the establishment or expansion of settlements and temple buildings (Great Oasis), or may have been free of significant landscape transformations after the Roman invasion (Nubia). There are also indications of the incorporation of local elite to the Roman political structure (Great Oasis). Changes could be identified in local agriculture in both borderlands such as the introduction of cotton and new types of crops, which also implied the export of these goods to other parts of the Empire.

Different treatment of different borderlands of the same empire may also be studied in the case of ancient China (Feuer 2016, 90–95). At the end of the 3rd century BC, the newly established Chinese empire with the lead of the Ch'in state gradually started its expansion by

incorporating territories to the north (towards the Mongolian steppes) and to the south (towards the valley of the River Yangtze) of the empire's core area (valley of the River Wei). The steppes, however, differed very much from Chinese territories in terms of agriculture, as they were not suitable for intensive crop growing, but rather for pasturage. Chinese had also difficulties to incorporate some tribal societies into the empire, thus Chinese expansion to the north eventually stopped and a borderland was created between the empire and nomadic tribes of the steppe defined by the Great Wall. The nomads living north of the Wall imposed threat on the empire which was eliminated through military conflicts or alliances. In contrast, the lands, agriculture and population groups located south of the Chinese empire were more similar to those of the empire which resulted in an easier incorporation of these areas and a more fluid and dynamic borderland.

In the case of Anatolia and the South Caucasus, the often opposing nature of borderlands may be observed between the Late Chalcolithic and the late Iron Age (3500–500 BC; d'Alfonso and Rubinson 2021, 11–15). This area is characterised by plains (Eurasia and Mesopotamia) divided by mountain ranges and plateaus (Pontic Mountains, the Taurus and the Zagros, Central Anatolian Plateau). It may be interpreted as a region that was restricted by geographical features and characterised by isolation, a periphery to ancient Greece and a border between Asia and Europe. The isolated and conservative nature of this borderland was illustrated by items of material culture in the Bronze Age in the Central Anatolian Plateau, showing continuity of pottery traditions. At the same time, this borderland was also a link between Asia and Europe, a corridor characterised by migration, crossing of long-distance trade routes as well as short-distance interactions and socio-economic dynamics. Archaeological evidence for the important role of the highlands is represented by places of cultic gatherings. Furthermore, this borderland had also significant resources, which is shown by traces of obsidian exploitation and metallurgical activities.

Borderlands in Lower Austria in the late Roman period and early Middle Ages

The territory of Lower Austria had been a part of many borderlands between the late Roman period and the early Middle Ages. In the following paragraphs, these constantly shifting boundaries are explored in this area in a chronological order.

In the late Roman period, the border of the Empire is evident from written and archaeological evidence in Lower Austria (see Sections 2.1.1 and 2.2.1). The *limes* was running in east-west

direction along the southern bank of the River Danube; the Erlauf Valley thus was located within Roman territory. The role of the geographical features in shaping borderlands is well observable in this case as the location of the *limes* was defined by the Danube. Political and military boundaries could be traced archaeologically along the *limes* in the form of Roman camps, forts (including one in the Erlauf Valley at Pöchlarn) and watchtowers as well as Roman towns near the Danube and south of it (Fischer 2015, 26–30, 33–36). The *limes*, however, might have been rather a fluid boundary in terms of economic transactions, as the Roman Empire maintained intensive trade connections with the 'Barbarian' groups living outside its territory (Zöllner 1970, 29). Historical sources also point out trade/exchange between people living on the southern and northern part of the Danube in the second half of the 5th century (Wolfram 1995, 49). Influence of the Roman culture among the tribes living north of the *limes* could be illustrated by villa like buildings of the Germanic elite and some elite burials exhibiting Germanic, Hunnic as well as Roman features (Stuppner 2015, 119–125).

The mountain peaks of the Eastern Alps, expanding into the southernmost part of Lower Austria, would indicate a static or restrictive geographical boundary. Interestingly, however, Roman expansion did not stop there, the northern border of the Empire was north of the Eastern Alps along the Danube as mentioned above. Although some evidence indicates that fortifications were built to exercise control over passing the mountain range, the Eastern Alps, located within the *limes* of the Empire, cannot be interpreted as a boundary in the late antique period (Winckler 2012, 148–150).

With the collapse of the Roman rule and abandonment of Noricum in 488 AD, the territory of Lower Austria ceased to be a borderland for more than a century. Various Germanic groups appeared such as Langobards, who came from the north of the study area (present-day Czechia) and settled both north and south of the Danube based on their archaeological traces (Adler 1977b, 75–76). South of the Eastern Alps in Italy, the Ostrogothic Kingdom of Theodoric was formed at the end of the 5th century, which was followed by the kingdom of the Langobards from about 568 (Sections 2.1.2 and 2.1.3). While it is possible that the Ostrogothic sphere of influence extended over the Eastern Alps, the northern boundaries of the Langobard Kingdom were located at the southern foothills of the Eastern Alps, where remains of fortifications suggest that the Langobards made efforts to secure them militarily (Winckler 2012, 150–152).

By the 7th century, the border between the Bavarian west and Avar-Slavic east was probably around the River Enns (on the western border of present-day Lower Austria; *Figure 2*), but there is no direct indication of this in historical or archaeological evidence (Wolfram 1995, 79). Indirect evidence may include the presence of 'Bavarian style' raw cemeteries (German: Reihengräberfelder) in Upper Austria (located west of Lower Austria), while these burials are absent in Lower Austria (Aspöck 2001, 235–240). In general, there are very few finds dated to the 7th and 8th centuries in Lower Austria west of Vienna, which might suggest an unpopulated buffer zone of the Avar Khaganate here as discussed in Section 2.2.3 (Daim 1977, 93–94; Friesinger and Friesinger 1977, 104; Szőke 2004, 181). This idea, however, is debated as this chronological gap might be caused by site and find dating issues (Szameit 1991; Szameit 2000). In any case, from the 8th or 9th centuries, cemeteries showing mixed influences appeared in the Avar borderland including the Erlauf Valley as well. They reflect Frankish-Bavarian, Avar, Moravian and Carantanian characteristics (Friesinger and Friesinger 1977, 105–106; Zehetmayer 2007a, 117). These burials are good examples of how borderlands can provide place for culture contact and give rise to the blending of influences and identities.

The Carolingian expansion after the Avar wars (788–811) likely affected the Erlauf Valley along with territories south of the Danube up to the River Leitha on the east (south-eastern border of present-day Lower Austria; *Figure 2*), but no archaeological finds or features have been found yet in Lower Austria, which could support this hypothesis (Zehetmayer 2007a, 108; Zehetmayer 2007b, 21, 26). There is, however, historical evidence that Carolingian rule extended over western Hungary by the mid-9th century, the potential centre of which was also excavated near Zalavár with several churches and manor houses (Wolfram 1995, 249; Szőke 2021, 314–410). While the southern part of Lower Austria was part of the eastern borderland of the Carolingian Empire, the north-eastern part of Lower Austria (Weinviertel) was possibly the borderland of the Moravian Empire emerging in the first half of the 9th century (Wolfram 1995, 248; Zehetmayer 2007b, 27). Boundaries between these two political powers, however, must have not been static as historical evidence points out intensive trade interactions (e.g. salt trade) between them (Zehetmayer 2007b, 28). Besides the cemeteries with mixed influences mentioned above and the Moravian finds in the north-eastern part of Lower Austria, a range of tumuli in the north-western part of Lower Austria suggest a potentially Slavic group immigrating from the north contributing to the diversity of cultural/demographic boundaries in this area in the Carolingian period (Zehetmayer 2007a, 153; Breibert 2005, 415–418).

The 10th century is characterised by constant shifting of boundaries between the western and eastern edge of present-day Lower Austria. The battle near Bratislava in 907 ending with the defeat of the Bavarian troops and the collapse of the eastern Carolingian marches, changed the *status quo* again and the River Enns became the border between Bavarians and the newcomer Hungarians (Wolfram 1995, 272; Zeller 2007, 45). The Erlauf Valley thus came under Hungarian rule, but Hungarians did not settle in Lower Austria based on their scattered archaeological traces (except maybe for the easternmost part of Lower Austria; Fodor 1996, 437; Obenaus 2014, 167–168). The demographic and settlement structure seems to have remained roughly the same as it had been before the Hungarian rule (Zehetmayer 2007b, 28–29).

Another battle, fought in the area of present-day Germany (Augsburg) in 955, resulted in the withdrawal of the Hungarians and once again the River Leitha was regarded as the boundary between Bavarian and Hungarian territories (Wolfram 1995, 273; Bakay 1999, 544). Although written evidence from 976/979 mentions that the *castellum* of Zuisila (identified as present-day Wieselburg in the Erlauf Valley) was built against the attacks of the Hungarians, this might have been a *topos*, as Hungarians by this time had finished their raids to western territories and were settling in the Carpathian Basin well beyond the River Leitha (Ladenbauer-Orel 1972, 26). The material culture of people living in the territory of Lower Austria continued to be diverse showing western (Carolingian, Ottonian), northern (Moravian, Bohemian) and eastern (Hungarian) traditions (Obenaus 2014, 169–171; Kühtreiber and Obenaus 2017, 36–44).

With the rule of the Babenbergs from 976, the territory of Lower Austria gradually became a centre of power for the first time since many centuries (Wolfram 1999, 305; Vocelka 2010, 12). Although politically it belonged to Bavaria and the East Frankish Kingdom, with the presence of this powerful ruling dynasty it started living its own life and it was soon more than just a borderland, representing the core of what later became Austria.

Summary

Borderlands represent divides, but at the same time meeting points. They both separate and link cultures, population groups and empires (Rodseth and Parker 2005, 16; Mullin 2011a, 7). A borderland perspective helps identifying ancient dynamics and all those processes that are linked to the encounter of different geographic, cultural, demographic, economic and political spheres as well as it puts the ‘peripheries’ in the centre of research, where often new

identities and ideas are created. The territory of Lower Austria had been a multifaceted borderland in the late Roman and early Medieval period, and provides an example of how shifting boundaries can shape history.

3 MATERIALS AND METHODS

The first part of this chapter presents the studied ceramics and gives information about the archaeological sites they originate from. This is followed by the description of the different methods used in this thesis highlighting their use in archaeological ceramic analysis and interpretation. The analysis process, adjustments of the equipment or terminology used for the analysis of the studied ceramic material are also detailed within each methodology chapter.

3.1 Materials

The investigated material consists of 135 archaeological ceramic samples from Austria, which are of two main pottery types: graphite-free ceramics[18] (1st–9th centuries AD) and graphite-containing ceramics (9th–11th/12th centuries AD) that include graphite scattered within their paste in the form of flakes and graphitic rocks fragments (Sections 4.1.1 and 4.2.2). Most of the samples are dated to the early Middle Ages (6th–11th centuries), and some graphite-free ceramics (11 samples) originating from the Roman/late Roman period (1st–5th centuries) are also examined. A couple of graphite-containing sherds (six samples) are dated up to the 12th century.

The ceramics were found at different sites of Lower Austria and Vienna (*Figures 1* and *25*). The majority of them (98 samples, both graphite-free and graphite-containing ceramics) are from 12 sites located in one region, the valley of the River Erlauf. The rest of the samples (37 samples, graphite-containing ceramics) are derived from eight archaeological sites of Lower Austria and Vienna (*Table 4*).

Ceramics from settlements and cemeteries are both present in the studied material. Most of them, 99 samples, were derived from 17 settlements, including five fortified settlements, and 35 samples came from two cemeteries.[19] About half of the ceramics (68 samples) was found by surface collection and the other half (67 samples) was recovered during excavation.

[18] Graphite-free samples may contain few grains of graphite, the amount of which is usually below 5% (area %) of inclusions (but does not exceed 15%), in contrast with samples defined as graphite-containing ceramics, which include 30% or more graphite flakes and graphitic rock fragments among their inclusions (see Section 4.2).

[19] In one case (Weinzierl, Wieselburg Land) the type of the site was undefined.

The archaeological data of each sample can be found in Appendix A. These contain all necessary information for the identification of the samples including the sample number given by the author, name and type of site, method of find collection (excavation/surface collection), context, find/inventory number, any previous sample numbers and the dating of the sample.[20]

The following sections give an overview about the archaeological sites from where the samples originate. The description of the sites in the Erlauf Valley (site numbers 1–12 in *Figure 25*) are followed by the sites located in other parts of Lower Austria and Vienna (site numbers 13–20 in *Figure 25*).

Table 4. Archaeological sites of the ceramic samples. Site numbers in the first column are used to mark the location of the sites on the map below.

Site number	Site	Samples
1	Purgstall, 8th–9th-century cemetery	S1–S30 (30 samples)
2	Wieselburg, Kirchenberg	S31–S36 (6 samples)
3	Purgstall, Site 10	S37–S50 (14 samples)
4	Purgstall, Site 26	S51–S54 (4 samples)
5	Purgstall, Site 47	S55–S61 (7 samples)
6	Zehnbach, Site 16	S62–S63 (2 samples)
7	Hochrieß, site 39	S64–S87 (24 samples)
8	Gries, Site 115	S88–S89 (2 samples)
9	Landfriedstetten, Site 8	S90 (1 sample)
10	Wieselburg, Plot 246/6, 16 Johann Winter Gasse	S91–S92 (2 samples)
11	Weinzierl, Wieselburg Land	S93 (1 sample)
12	Mühling, 8th–9th-century cemetery	S94–S98 (5 samples)
13	Hausstein near Grünbach am Schneeberg	S99–S103 (5 samples)
14	Ternitz, Dunkelstein	S104–S107 (4 samples)
15	Sand	S108–S110 (3 samples)
16	Tulln, Wassergasse	S111–S114 (4 samples)
17	Tulln, Hauptplatz	S115–S118 (4 samples)
18	Mautern, Römerhalle	S119–S127 (9 samples)
19	Sachsendorf	S128–S132 (5 samples)
20	Vienna, Ruprechtsplatz	S133–S135 (3 samples)

[20] The chronology of the samples, where literature is not available (especially those collected by field walking), is based on conversations with my supervisor, Dr Hajnalka Herold (September 2019).

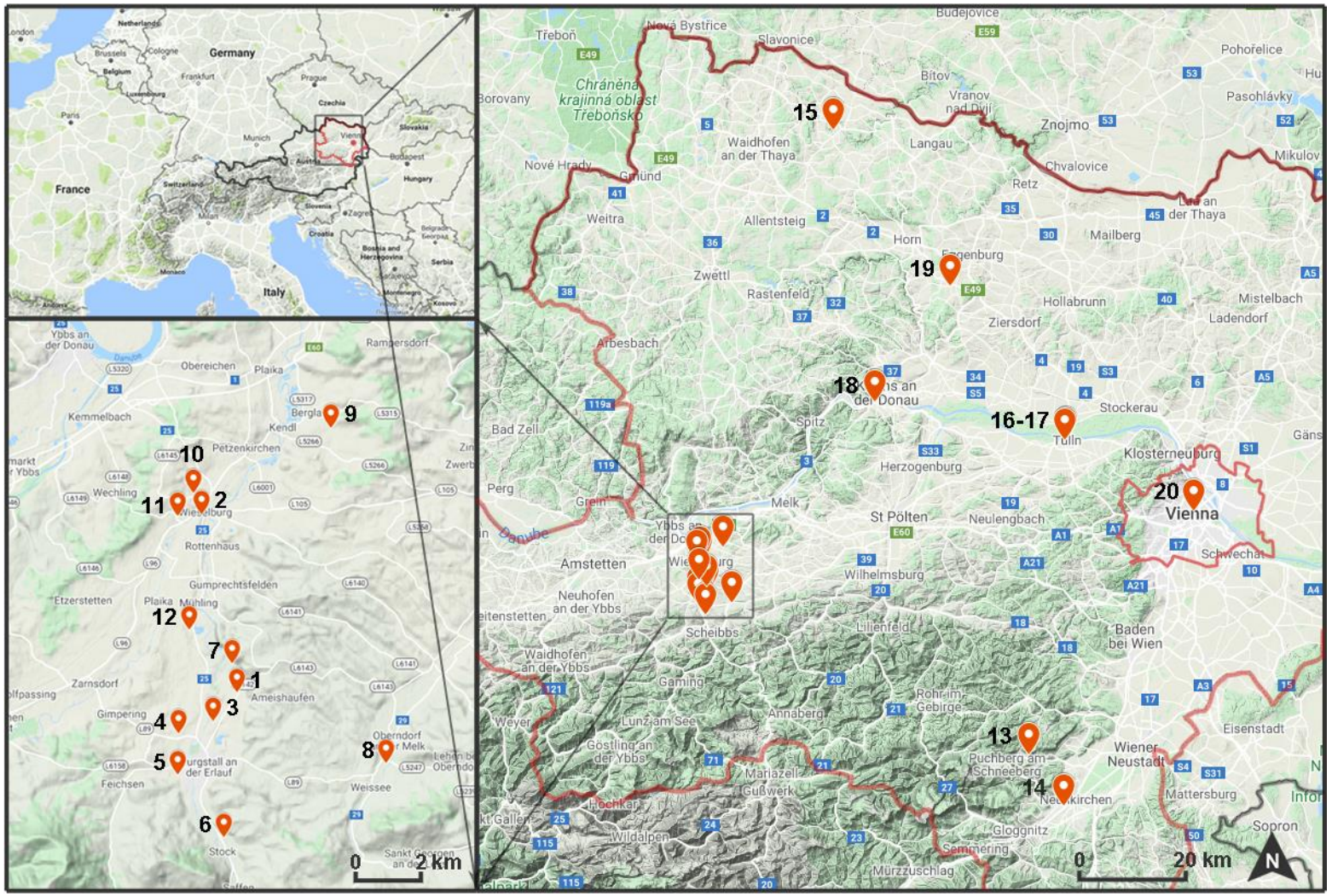


Figure 25. Location of the archaeological sites in the Erlauf Valley (bottom left corner) and in other parts of Lower Austria and Vienna (right-hand side map). The sites corresponding to the numbers are listed in Table 4 above.

Purgstall, 8th–9th-century cemetery

In 1997, during the opening of a gravel pit near Purgstall an der Erlauf, the remains of a cemetery were found including 225 burials. The cemetery was excavated in the same year by Franz Sauer from the Austrian Federal Office for the Protection of Monuments (Bundesdenkmalamt). The results of the excavation have not been published, but a brief report (Sauer and Czubak 1997) and a leaflet for an exhibition (Sauer n.d.) are available containing basic information. Samples of 30 ceramic vessels (S1–S30) from 29 graves are investigated in this thesis (two pots originate from the same grave).

Two phases of the cemetery were distinguished based on the clothing elements and other finds such as weapons and jewellery found in the graves (Sauer n.d.). The early phase occupied the inner zone of the cemetery and could be dated to the second half of the 8th century. It was surrounded by the graves of the later phase, which could be dated to the first half of the 9th century. Burials of the first phase exhibited Bavarian, Frankish, Avar and Slavic characteristics and there were many grave goods (such as food placed in ceramic vessels) as indicators of pre-Christian traditions. The second phase showed a more integrated and unified spectrum of finds with Slavic attributes. The cemetery was probably abandoned during the first half of the 9th century as with the spread of Christianity new cemeteries were established near churches (Sauer n.d.).

Wieselburg, Kirchenberg

The sherds analysed in this thesis (S31–S36), dated to the 10th–11th centuries, were found by surface collection close to the St Ulrich parish church in Wieselburg on the church hill. Other pottery fragments, dated to the 10th–13th centuries or later, were also found during small-scale excavations on the hill conducted by Herta Ladenbauer-Orel between 1952 and 1965 (Ladenbauer-Orel 1972, 48; Kühtreiber and Obenaus 2017, 118).

The church has its roots in the late 10th century: the remains of an Ottonian central-plan church are still preserved as a chapel of the modern building. This old church, based on written evidence, was probably founded by Wolfgang, bishop of Regensburg, and consecrated in 993/994 (Ladenbauer-Orel 1972, 54). The walls were soon (first half of the 11th century) decorated with paintings, which are considered as the oldest monumental wall paintings of the Middle Ages in Austria (Ladenbauer-Orel 1972, 27; Benesch 2003, 2687). The church was

extended twice: around 1500, when it was turned into a late Gothic church, and in 1952, when it got its present-day appearance (Ladenbauer-Orel 1972, 28; Benesch 2003, 2684).

An earthwork fortification was likely also built on this hill before the establishment of the church. A charter from 976/979 gives authorisation to the above-mentioned Bishop Wolfgang to build a *castellum* called Zuisila at the confluence of the two streams of the River Erlauf (Great and Little Erlauf) as a refuge from the Hungarian attacks (Ladenbauer-Orel 1972, 26). In addition to Wieselburg being situated at this confluence, it is apparent that the name of Wieselburg includes the name Zuisila/Zwisila, thus it is assumed that the fortification was located on the present-day church hill (Ladenbauer-Orel 1972, 26).

Remains of a *castellum* in the sense of an actual building complex could not be unambiguously identified, but the presence of a rampart and a ditch was confirmed closing the southern part of the site (Ladenbauer-Orel 1972, 28–31).[21] Three phases of the rampart were distinguished, which can be dated presumably to around 900, to the late 10th century (around 976/979 or 993/994) and to the 11th century or later (Ladenbauer-Orel 1972, 53–56, 60–61; Kühtreiber and Obenaus 2017, 119–120). The second phase rampart was possibly equipped with a palisade and the third one with a stone wall (Kühtreiber and Obenaus 2017, 119–120).[22] The remains of a rectangular tower at the rampart were also excavated, which can probably be dated to the late Middle Ages (Kühtreiber and Obenaus 2017, 120). Apart from the Ottonian church, there were few remains found inside the fortification based on which it has been interpreted as a fortified refuge site, as also indicated by the written sources (Ladenbauer-Orel 1972, 60-61; Kühtreiber and Obenaus 2017, 123).

Purgstall (Sites 10, 26 and 47), Zehnbach (Site 16), Hochrieß (Site 39), Gries (Site 115) and Landfriedstetten (Site 8)

In the Erlauf Valley, very active community-led archaeology has existed from the 1940s up to the present day. Many sherds of the studied material (S37–S90) were found during field walking carried out by local people.

[21] The other sides are naturally protected by the slopes of the church hill, which is in fact the northern end of a terrace between the two streams of the Erlauf (Kühtreiber and Obenaus 2017, 117).

[22] It must be emphasised, however, that the chronology of the different phases of the rampart is hypothetical and based on small-scale excavations; extensive archaeological research has not been carried out on the church hill.

These sites are all unexcavated settlements, and their dating is possible based on finds found on the surface. The samples from Purgstall, Site 10 and Site 26 investigated in this thesis can be dated to the Roman/late Roman period (1st–5th centuries) and the early Middle Ages (6th–11/12th centuries). Sherds from all the other sites originate from different periods of the early Middle Ages: including those from Purgstall, Site 47 and Gries, Site 115[23] dated to the 6th–9th centuries, that from Landfriedstetten, Site 8 dated to the 8th–9th centuries,[24] and those from Zehnbach, Site 16 and Hochrieβ, Site 39 dated to the 8th–11th centuries.

Purgstall, Site 47 is located in the area of an archaeological site called Köttlach-Siedlung. The site has not been excavated, but some archaeological features and finds were found while carrying out earthworks in 1953 (Purgstall, Plot 270/13; Denk 1962, 162). These included pits containing animal bones (cattle, horse, pig, deer, bird), a piece of an iron smelting furnace, iron slag and many pottery sherds. The sherds had incised decoration of parallel wavy lines and parallel lines based on which the site was dated at the time to the 10th century (Denk 1962, 162; however, this dating is no longer seen as valid or exact, see Section 2.2.3).

Wieselburg, Plot 246/6, 16 Johann Winter Gasse

In 16 Johann Winter Gasse, Wieselburg, finds of a settlement were collected during gardening in 1953 and the following years (Denk 1962, 158). The finds included pieces of ceramics that were decorated with incised lines and incised wavy lines and originated from the 8th–9th centuries, two of which are analysed in this thesis (S91 and S92). Remains of a cemetery from the same age were also found *c.* 1 km east of 16 Johann Winter Gasse in the area of the present-day neighbourhood Ötscherland-Kosmos (Denk 1962, 154–158).

Weinzierl, Wieselburg Land

In 1975, during the excavation of a cellar in Weinzierl (Plot 942, house number 78) some ceramic sherds were recovered (Denk 1975). Most of them were undecorated, but a large part of a pot with incised wavy lines, dated to the 8th–9th centuries, was also found (Denk 1975,

[23] Short reports have been published about the Roman finds collected at this site: Rausch 1992 and 1993.
[24] Although this one piece from Landfriedstetten can also originate from the Roman period based on its fine texture (Dr Hajnalka Herold, personal communication, September 2019).

181: Abb. 281), which is analysed as S93 in this thesis. There is no record about other finds and the type of the site is also unknown.[25]

Mühling, 8th–9th-century cemetery

Multiple excavations were carried out near Mühling between 1954 and 1964 after the discovery of two burials by a local researcher in a gravel pit. During the 10 years of archaeological research initiated by the Austrian Federal Office for the Protection of Monuments (Bundesdenkmalamt) remains of 36 graves from the 8th–9th centuries were excavated (Friesinger 1971–1974, 57).

The graves usually contained grave goods including knives, pots, eggshell, chicken bones, arrowheads, fire strikers and spindle whorls (Friesinger 1971–1974, 57–68). Sometimes elements of clothing and jewellery could also be documented such as imprints of fabrics, belt buckle, earrings, rings and beads. In some graves, partial cattle skulls with horn roots were detected, which, often together with food remains or pots, were placed on top of the coffin at the time of the burial.

The ceramic material analysed in this thesis includes pieces of five vessels (S94–S98) from the cemetery of Mühling.[26]

Hausstein near Grünbach am Schneeberg

The rock of Hausstein (845 m), located southwest of Vienna, was most likely the site of a castle in the 11th–12th centuries. The site consists of the plateau of the rock itself with a steep western slope and a saddle to the east (Kühtreiber and Obenaus 2017, 133).

A short (5-day) excavation was carried out on the saddle in 1959 by the Lower Austria Museum (Kühtreiber and Obenaus 2017, 133–134). The archaeological research uncovered the remains of a building possibly with a stone foundation and a wooden structure (Kühtreiber and Obenaus 2017, 134). The rocky outcrop has not been excavated, but based on the abundant

[25] It is possible that the large piece of the pot came from a grave as it is more frequent to find full pots or large parts of pots in cemeteries than in settlements. Human bones, however, were not recorded from this site (Hajnalka Herold and Andreas W. Rausch, personal communication, July 2020).

[26] The drawing and description of the analysed vessels and sherds are published by Friesinger as below. S94 – Friesinger 1971–1974, 65: Grab 31, Tf. 14; S95 – Friesinger 1971–1974, 57: Grab 3, Tf. 10; S96 – Friesinger 1971–1974, 58: Grab 4, Tf. 11; S97 – Friesinger 1971–1974, 65: Grab 32; S98 – Friesinger 1971–1974, 62: Grab: 19, Tf. 12

finds from its western slope and from its plateau it must have been in use in the 11th–12th centuries (Kühtreiber and Obenaus 2017, 134).

Although after 1959, there have not been further excavations at Hausstein, local people contributed to the increase of the archaeological assemblage originating from the site by collecting ceramic and metal finds (Kühtreiber and Obenaus 2017, 134). These finds proved the use of the site in the Neolithic and in the 11th and 12th centuries AD, and some artefacts can also indicate an earlier start regarding the medieval castle: the second half or the end of the 10th century (Kühtreiber and Obenaus 2017, 134–135). The sherds that are investigated in this thesis (S99–S103) can be dated to the 10th–11th centuries.

Ternitz, Dunkelstein

The castle of Dunkelstein, occupied the highest point (410 m) of a ridge near Ternitz (Kühtreiber 2006, 241). It was founded in the second half of the 11th century and was abandoned before the middle of the 13th century (Kühtreiber 2006, 242–243). It covered a relatively small area (15 m x 28 m) containing a tower and a wall at the beginning, which was first supplemented by a long rectangular residential building including the kitchen in one of its rooms, and later (late 12th century) by numerous other buildings (Kühtreiber 2006, 39–105; 207–240). The site got its present-day appearance during the 17th–18th century when it went through substantial changes due to the construction of a calvary and a chapel on top of the castle ruins as well as a church (Peterskirche) to the east of the site (Kühtreiber 2006, 105–121; 243–244).

The archaeological research at Dunkelstein started in 1992 after the discovery of one of the walls of the castle during gardening and continued in the subsequent years until 2002 (Kühtreiber 2006, 35–39). The excavations revealed the buildings and walls of the castle as well as numerous finds such as pottery, keys and locks, knives, weights, elements of horse harnesses and horseshoes (Kühtreiber 2006, 122–198). In addition to the 11th–13th centuries, the finds also confirmed the use of the site in the Neolithic and Late Bronze Age (Kühtreiber 2006, 39–40). The four samples from Ternitz that are analysed in this thesis (S104–S107) came from the early layers of the castle and can be dated to the second half of the 11th century (Befundphase 1; Kühtreiber 2006, 242).

Sand near Oberpfaffendorf

The archaeological remains of Sand *c.* 450 m above sea level east of Raabs an der Thaya in the northern part of Lower Austria can be identified as parts of a fortified hilltop settlement (Felgenhauer-Schmiedt 2008, 329; Saliari and Felgenhauer-Schmiedt 2017, 97). The beginnings of the short-lived stronghold can be estimated *c.* 926–930 based on dendrochronology, and the finds suggest that it was abandoned in the second half of the 10th century possibly because of a Hungarian attack (Felgenhauer-Schmiedt 2008, 330; Saliari and Felgenhauer-Schmiedt 2017, 96).

The excavations between 1993 and 2008 revealed the northern, western, and two southern walls, which included wood-earth-stone structures and dry stone walls (Felgenhauer-Schmiedt 2008, 330; Saliari and Felgenhauer-Schmiedt 2017, 96). The remains of a building made of stone and wood in the central part of the hill, a wooden building attached to the northern wall, and many settlement structures along the west wall were found (Felgenhauer-Schmiedt 2008, 330). The two walls on the south closed off two (an upper and a lower) settlement terraces, both of which included the remains of several buildings (Felgenhauer-Schmiedt 2008, 330).

Practically all ceramic finds excavated at the site are made of graphite-containing material, which are decorated with wavy lines, parallel wavy lines and comb-impressed dots (Felgenhauer-Schmiedt 2008, 330). Three sherds from Sand are analysed in this thesis (S108–S110).

Several different activities can be assumed at the site based on the finds such as pottery making, textile production, metal processing, skin/fur processing, woodworking as well as small-scale trading activity (Felgenhauer-Schmiedt 2008, 330–332; Saliari and Felgenhauer-Schmiedt 2017). The finds related to pottery making include prepared graphite-containing raw material, unfired ceramics and waster pottery (Felgenhauer-Schmiedt 2008, 330), but no further details have been published so far.

Tulln, Wassergasse and Hauptplatz

In the area of the present-day town of Tulln an der Donau, located on the south bank of the Danube to the northwest of Vienna, there was a Roman fort called *Comagenis* between the end of the 1st and 5th centuries AD (Scholz 2015, 15). The medieval use of the site started in the 9th century, which was shown by burials west of the former fort excavated in 4 and 2

Wassergasse in 2007 and 2012, respectively (Scholz 2015, 16, 272). In the next century, sunken-featured buildings appeared in the area of Tulln and it was gradually populated leading to the development of the medieval town (Scholz 2015, 272). An extensive gravel floor was also found during the excavations in Wassergasse, which might indicate a market square that was relocated to the Hauptplatz in the 12th century (Zimmermann 2012, 236). The analysis of four graphite-containing sherds found in Wassergasse, dated to the 10th–11th centuries, is included in this thesis (S111–S114).

Finds from the Hauptplatz (Main square) can be dated from the 11th century onwards (Scholz 2015, 171). The square has been used as a marketplace from the 12th century up to the present day, which was indicated by, among others, medieval scales, weights, coins, storage vessels embedded in the ground, wagon tracks, and ovens for on-site food production (Scholz 2015, 226–261, 334). As a result of the excavations in 2007 and 2008, thirteen phases of the marketplace were distinguished based on site stratigraphy and the chronology of the finds (Scholz 2015, 171, 176–225). In the 12th and early 13th centuries probably mobile and semi-mobile stands were used (Scholz 2015, 334). A more settled market structure is assumed in the 13th century with newly installed paving and wells, which was renewed and reorganised in the 14th century (Scholz 2015, 225, 334–335). The pottery fragments from the Hauptplatz analysed in this thesis are from the early phases (Phases 1 and 2) of the site and are dated to the 11th to mid-12th centuries (S115–S117) or the middle of the 12th century (S118).

Mautern, Römerhalle

The medieval town of Mautern was built on the remains of the Roman fort *Favianis* and its *vicus* areas and cemeteries (Kühtreiber and Obenaus 2017, 160). The first traces of the medieval settlement are known from the late 8th and early 9th centuries when structures of the fort must have been visible as they influenced the arrangement of the fortifications of the medieval town (Kühtreiber and Obenaus 2017, 161).

The rescue excavation at the building called ‘Römerhalle’ in the northwest corner of the fort was carried out in relation to the construction of a restaurant in 2005 (Krenn et al. 2005, 26). In addition to the remains of a Roman horseshoe-shaped tower joining to the northern wall of the fort and late antique structures, 10th-century settlement features (pits and post holes) and remains of a medieval building from the early 13th century were found south of the fort wall

(Krenn et al. 2005, 27). Ceramic finds, including the 9th–11th-century sherds analysed in this thesis (S119–S127), are not mentioned in the brief excavation report.

Sachsendorf

The remains of a castle at the western edge of the village Sachsendorf (Municipality of Burgschleinitz-Kühnring) were still visible before the archaeological investigations between 1987 and 1997 (Krenn 1991, 351; Kühtreiber and Obenaus 2017, 89). The existence of the castle could be followed throughout a long period between the second half of the 10th century and the end of the 15th century based on the numerous finds and features excavated there (Krenn 1991; Krenn and Krenn-Leeb 1993). The earliest features belonged to a 10-century settlement including a sunken-featured and some wooden buildings (Krenn 1991, 354–358). The first stone building (8.70 m x 7.50 m), possibly a tower, was erected in the second half of the 10th century, which was soon eliminated and a small stone building (possibly for residential purpose) and some wooden structures were established in the second half of the 11th century (Krenn 1991, 358–360; Krenn and Krenn-Leeb 1993, 54).

In the 12th century, a Romanesque chapel was built and the stone building was replaced with a new residential building (Krenn 1991, 362; Krenn and Krenn-Leeb 1993, 55). In the middle of the 13th century, a tower (9 m x 9 m) was constructed immediately to the west of the chapel and simultaneously the chapel was partly remodelled (Krenn 1991, 363–365).

The castle was surrounded by a stone wall and a moat from the second half of the 14th century and a multi-storey residential building were built in the northwest area (Krenn and Krenn-Leeb 1993, 57). The chapel was separated with a wall from the rest of the castle and used as a cemetery area (Krenn and Krenn-Leeb 1993, 57). A large number (*c.* 200) of graves, dated to the 14th and early 15th centuries, were excavated around the chapel (Krenn 1991, 365–368; Krenn and Krenn-Leeb 1993, 57).

In the 15th century, the development of the final plan of the castle continued through the construction of more features: a 5 m high rampart with a palisade on its top and bastions protruding from the ramparts (Krenn 1991, 368–370; Krenn and Krenn-Leeb 1993, 57–58). The castle is mentioned as a deserted place in a document from 1482, which was confirmed by the rich find material from its destruction layer (Krenn 1991, 353, 370).

The analysed ceramic material includes five samples (S128–S132) from the earliest phases of the castle of Sachsendorf, which can be dated to the 10th–11th centuries.

Vienna, Ruprechtsplatz

The Ruprechtsplatz is one of the sites where the earliest phases of medieval Vienna have been documented. It is located south of the Danube at the highest point of the former Roman fort *Vindobona* and is the home of the Ruprechtskirche, which is the oldest church still standing in Vienna dating from the early 12th century (Felgenhauer-Schmiedt 1992, 61; Jeitler and Schön 2019, 150). The excavation in 1970, following the demolition of two war-damaged 19th-century houses, recovered some remains indicating settlement features that can possibly be dated to the 9th–10th centuries (Felgenhauer-Schmiedt 1992, 66), but certainly predate the 12th century (Schön et al. 2019, 57).

Many ceramic fragments were found in the medieval layers, which represent different types including ceramics without graphite, graphite-containing pottery and mica-rich wares (Felgenhauer-Schmiedt 1992, 64–66; Gaisbauer 2019). The assessment of the graphite-containing ceramics from the Ruprechtsplatz and other sites resulted in the identification of trends concerning the appearance of the graphite-containing ceramics, which could be linked to approximate periods (Felgenhauer-Schmiedt 1992, 65–66). For example, the raised band as a decoration element became common in the 10th and 11th centuries and the reddish colour of the surface is typical for the 11th and 12th centuries. Three 9th–11th-century graphite-containing sherds originating from Vienna Ruprechtsplatz are analysed in this thesis (S133–S135).[27]

Summary

The investigated 135 samples of ceramic vessels are dated to the period between the 1st and 12th centuries AD (6th–11th centuries mainly). They originate from numerous (20) archaeological sites within the Erlauf Valley and other parts of Lower Austria and Vienna, and were collected by field walking or recovered during excavation. The sites of the samples represent a variety of types such as settlements, fortified settlements, castles and cemeteries.

[27] These sherds are published in Felgenhauer-Schmiedt 1992 and Gaisbauer 2019 as below.
S133 – Felgenhauer-Schmiedt 1992, 73: Taf. 5:3; Gaisbauer 2019, 117: RU 42, 132: Taf. 08_04: RU 42.
S134 – Felgenhauer-Schmiedt 1992, 74: Taf. 6:2; Gaisbauer 2019, 113: RU 51, 129: Taf. 08_01: RU 51.
S135 – Felgenhauer-Schmiedt 1992, 76: Taf. 8:1; Gaisbauer 2019, 118: RU 73, 132: Taf. 08_04: RU 73.

3.2 Macroscopic analysis

The investigation of macroscopic features is an important part of archaeometric studies because some characteristics of pottery can only be detected or can be detected better with the naked eye than using scientific methods. Such characteristics are, for example, the shape, decoration and colour of the vessel as well as traces of the forming technique (Orton and Hughes 2013). Macroscopic investigation is also the basis of sample selection for instrumental analyses (Whitbread 2017, 202–203). Often only a small number of samples can be investigated of an assemblage by archaeometric methods and it is macroscopic analysis that facilitates linking the results to those finds that have not been sampled. In the following sections, the method of macroscopic analysis as well as the method and terminology applied for the ceramics from Lower Austria are detailed.

3.2.1 Characterisation of macroscopic features and their interpretation

An overview of the commonly recorded macroscopic characteristics of ceramics and their contribution to the interpretation of ceramic technology and provenance is provided below. Main characteristics include the fabric, morphology, technological traces (e.g. traces of the forming technique) and surface decoration.

Fabric

The fabric, i.e. “the material of which ceramics are made” (Peacock 1970, 375), is the primary basis of macroscopic classification. Fabric characterisation includes the description of colour, hardness, feel, fracture and inclusions (Whitbread 2017, 203–204). These features are interrelated and depend on many variables such as the composition of the raw materials, manufacturing technology, use and post-depositional alteration.

Colour is one of the characteristics recorded during fabric analysis. To achieve a better comparability between studies, usually a colour description system is used for the definition of colour, the most common being the Munsell colour system (Orton and Hughes 2013, 155–158). Both the surface colour of the ceramics and the colour of a fresh fracture are recorded (Orton and Hughes 2013, 73).

The colour can be an indicator of the firing conditions as well as the presence of organic materials and the amount and distribution of iron in the clay (Rice 1987, 333–336). The firing atmosphere is oxidising if there is an excess of oxygen during firing (which involves free air

circulation) and reducing if there is no free oxygen available (which involves the exclusion of air; Rye 1981, 25; Rice 1987, 81). An oxidising environment produces reddish, brownish, yellowish vessels while ceramics fired in a reducing atmosphere are greyish or blackish (Dell'mour 1989, 30; Orton and Hughes 2013, 88). Firing of clay containing organic material results in dark shades (grey, black) of the pottery (Rice 1987, 334–335). Depending on its state, iron enhances red-brown colours (ferric iron, Fe^{3+}) or grey-black colours (ferrous iron, Fe^{2+}) of the vessels (Rice 1987, 335). Light colours (white, cream) can be obtained if the clay lacks iron and organic material (Rice 1987, 333).

Firing conditions are often mixed due to the uneven distribution of air resulting in multiple shades of the surface of one vessel (Rye 1981, 120). In some cases, the firing atmosphere is (consciously or unconsciously) changed during firing or cooling of the ceramics, which can be deducted from the different colour stripes present on the cross section of the ceramic walls. A black core with red margins, for example, can be the result of a vessel fired in a reducing atmosphere, which was exposed to air (oxygen) during cooling. However, it can also be that an organic material-rich clay was fired in oxidising conditions, but the carbon in the core (left after the organic material) has not burned out (Rye 1981, 116: Fig. 104). The use of the ceramics can also contribute to their colour; for example, a red sherd with a black outer surface may be the result of the vessel having direct contact with the fire during cooking (Rye 1981, 116). These examples demonstrate that the interpretation of colour can be quite complicated and depends on many circumstances, thus colour should not be overrated when establishing fabrics (Whitbread 2017, 203).

The hardness of the fabrics is measured by scratching the surface of the ceramics with an object of a known hardness. Commonly the Mohs' scale is used, which consists of a series of minerals from the softest (talc) to the hardest (diamond) and by using progressively harder minerals the hardness of the ceramics can be estimated (Rice 1987, 355–357). The hardness provides information about the degree of vitrification of one specimen compared to another, which is an indicator of the firing temperature, but it also depends on other features such as composition and post-depositional environment (Orton and Hughes 2013, 158; Whitbread 2017, 204).

The surface roughness of the ceramics, termed as 'feel', and the nature of the fracture may be a discriminator between fabrics. Additionally, feel can provide details about surface treatment. Both characteristics are related to hardness and inclusion size (Orton and Hughes 2013, 74–

75). A surface slip on the pottery can influence the macroscopic perceptions of fabrics, for example it can distort the assessment of the ratio of coarse and fine particles by hiding the larger grains as well as have an effect on feel and hardness. Hence, it is important to examine both the surface and the fracture of a sample.

Inclusions are coarse particles (mostly rock fragments and minerals) in the clay, of which the larger grains can be detected by the naked eye or by using a loupe/hand lens. Several characteristics of inclusions are recorded during macroscopic analysis including their types, frequency, modal (common) grain size, maximum size, sorting and rounding/angularity (Orton and Hughes 2013, 75–76, 158–160; Whitbread 2017, 204). The study of these features aids the identification of fabrics of different compositions, which indicate the use of different raw materials.

Vessel shape and traces of the forming method

The description of shape is often carried out using terms which also express the function of the vessels at some extent (e.g. pot, jar, plate, etc.), although the exact function is often hidden from the eye of the observer (Rice 1987, 211–212, 215–216; Orton and Hughes 2013, 81–82). Other classifications use geometric shapes as the basis of grouping (Rice 1987, 217–222). In the case of whole vessels or large sherds, the dimensions of the ceramics can be recorded such as height, maximum width and the diameter of the rim and base (Orton and Hughes 2013, 85). The identification of vessel form is often difficult when examining sherds, however, a basic distinction can usually be made such as hollow or flat and closed or open wares (Rice 1987, 222–224; Orton and Hughes 2013, 85–86).

Recognising the form of a vessel is important as it can give an idea about its function(s) (e.g. storage, cooking, drinking, etc.) and if it had a different or additional role other than utilitarian (e.g. status symbol, religious use, etc.; Rice 1987, 236–242; Orton and Hughes 2013, 81–82). Together with the decoration and fabric, the studied vessel may be compared to an existing typology (if available), which might help narrowing down its production area or period (Orton and Hughes 2013, 219–220).

The thorough observation of the vessels can reveal traces of the forming method, based on which some aspects of the production technology can be discussed. Potters could use one or more techniques to form ceramics such as hand building (including pinching, drawing, coiling and slab building), moulding as well as techniques requiring the use of a wheel (slow wheel

turning, wheel throwing; Rye 1981, 67–83; Rice 1987, 125–132). Indentations, grooves, the texture of the surfaces and cracks can all be indicators of the used shaping techniques. For example, regular and rhythmic indentation can be the result of pinching and vertical grooves can refer to drawing (Rye 1981, 70, 72). In the case of the coiling technique (placing clay coils on top of each other and smoothing them together), coil joints can be visible or the vessel can crack along the joints often resulting in a smooth and rounded fracture surface (Rice 1987, 128). A spiral groove on the inner surface of the base and typical 'shell pattern' cutting-off marks on the bottom as well as grooves, ridges and fine parallel lines spiralling around the wall can all be the sign of wheel throwing (Rye 1981, 75; Rice 1987, 123).

Often a combination of techniques was used during the different stages of the forming process including the roughing out, preforming and finishing of the vessel (Roux 2017, 104, 105: Fig. 8.1). For example, vessels could be built up of coils and a turntable (also called tournette or slow wheel) could be used to smooth the coils, make the walls even or carry out further forming (Holl 1956; Peacock 1982, 55). This technique is referred to as slow wheel turning or wheel finishing and is differentiated from wheel throwing as pottery cannot be thrown on a turntable because its rotation is intermittent (Rice 1987, 133–134; Orton and Hughes 2013, 127–128, 146). Slow wheel turned vessels could preserve the impression of the turntable (or its cover disk) as vessels are not cut off, but simply lifted from it. This impression is often represented as a protuberant geometric mark on the bottom of the ceramics (Höllrigl 1930; Holl 1956; Herold 2015a, 333).

Various techniques were not only used in different phases of forming, but also different parts of the vessel (e.g. rim, base, body, handle) could be formed by different techniques.

Finishing techniques and decoration

Finishing techniques can have a shaping role as well as a decorative function, thus they can be categorised under both forming techniques (as secondary forming techniques) and decorations. They include beating, scraping, trimming, smoothing, burnishing and polishing (Rye 1981, 84–90; Rice 1987, 136–141). Those finishing techniques that refine the very surface of the vessels (e.g. burnishing and polishing) are also termed as surface treatments along with coating techniques (e.g. slips and glazes), which often have a decorative function in addition to practical aspects (Roux 2017, 104).

A range of different techniques could be applied to decorate the vessels such as incising, combing, impressing, stamping, roller-stamping, attaching appliqués, painting, using slips and glazes and so on (Rye 1981, 53–56, 90–94; Rice 1987, 144–152; Orton and Hughes 2013, 86–90). The investigation of decoration, similarly to that of form, can contribute to the stylistic and typological research of the vessels, which may provide information about possible production areas (workshops) and chronology of the study material as well as contacts between sites and communities (Rice 1987, 249–252). In addition to its aesthetic (or functional) role, decoration can also have a symbolic meaning; it may reflect the beliefs and values of the producers and their communities, thus may reveal information about the past society (Rice 1987, 251).

3.2.2 Macroscopic study of the ceramics from Lower Austria

In this section, the system and terminology of the macroscopic data collection used in this thesis are detailed following the suggestions of Clive Orton and Michael Hughes (2013, 275–285) and Ian Whitbread (2017) as well as the author's personal experience.

The macroscopic analysis of the potsherds from Lower Austria included the recording of their fabric, location in the vessel, form, potential forming technique and decoration (*Figure 26*).



Figure 26. Recorded data of the ceramic sherds

Ceramic fabrics are identified based on colour, hardness, feel, fracture and inclusions (*Figure 27*).

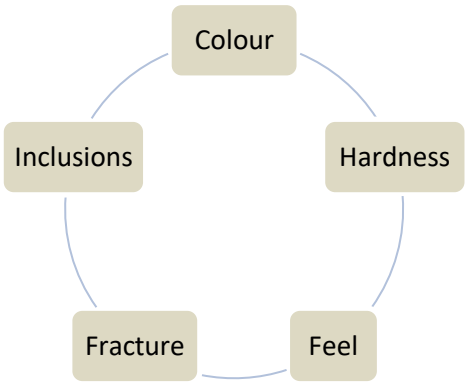


Figure 27. Characteristics forming the basis of fabric identification

The colour of a fabric is recorded verbally (e.g. reddish-brown) and using the Munsell colour charts (Munsell Color Company 2004). Usually a colour range is noted to include the different shades present on the sherds. For defining hardness, the Mohs' scale is used and two numbers

are recorded corresponding to the hardness of the two minerals between which the hardness of the sherd falls.

For the description of feel three categories are distinguished as shown in *Figure 28*. The fracture is defined based on its irregularities using a five-point scale from the coarsest to the finest texture (*Figure 29*).



Figure 28. Labels used for the description of feel



Figure 29. Labels used for the description of fracture

A brief characterisation of the inclusions was carried out.[28] Grain sizes are described with three size labels: sand, granule and pebble size (*Figure 30*) following the Udden-Wentworth scale, which is commonly used in sedimentary petrology (Adams et al. 1984, 3). The frequency of inclusions is estimated using a three-point scale (*Figure 31*).

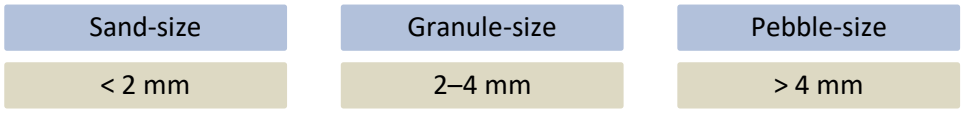


Figure 30. Labels used for the description of sizes ranges



Figure 31. Labels used for the description of the amount of inclusions

The sherd types are identified in terms of the part they occupied in the vessel (*Figure 32*). Three main categories are used (rim, body and base) and if it is possible, a more precise location of the body sherds is given (neck, shoulder).

Many of the ceramics were found during field walking or excavation as a single sherd thus the form of the vessels to which they used to belong is not evident and only a possible identification of the vessel shape can be noted. However, there are also cases where the form is obvious (especially in the case of ceramics from graves) as more pieces of the same vessel were found and the full profile of the vessel can be reconstructed.

[28] There was no need for an exhaustive investigation as each sherd was also analysed by thin section analysis, which gives more accurate and detailed information about the types and characteristics of the inclusions.

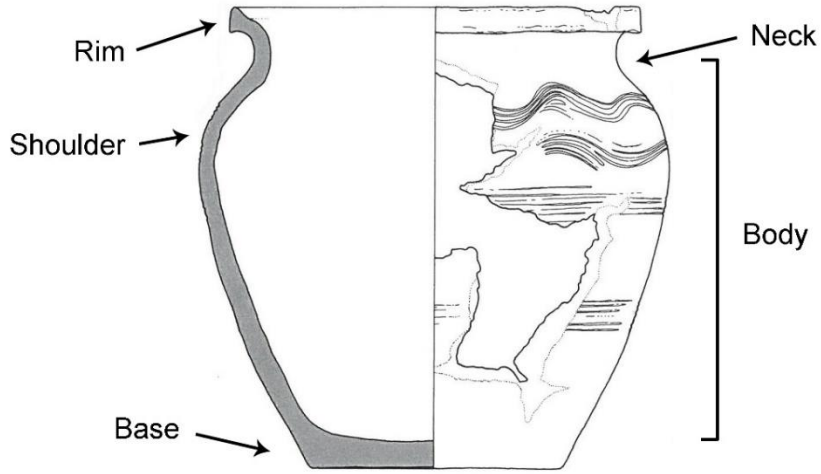


Figure 32. Terms used for the definition of vessel parts. (Drawing of the vessel of Sample 9 from the excavation documentation of the 8th-9th-century cemetery of Purgstall provided by excavator Franz Sauer.)

The forming technique of the vessels is inferred from features such as surface texture, turning marks, cracks and evenness of wall thickness.

The decoration of the ceramics is described using the expressions presented in *Figure 33* below which shows all the decoration elements occurring in the studied ceramic material.

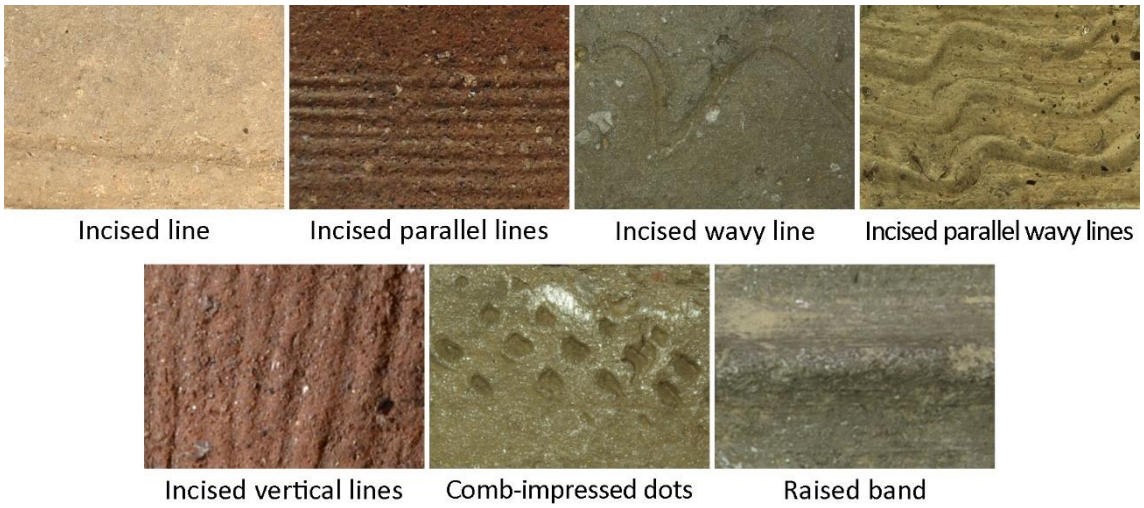


Figure 33. Decoration elements

3.2.3 Summary

Macroscopic analysis is the best way to have a first impression of the ceramics, carry out preliminary grouping, and select samples for further analysis. Macroscopic characterisation includes the description of fabric, vessel shape and decoration, based on which interpretations can be made, among others, about forming techniques, firing atmosphere and vessel function.

3.3 Petrographic thin section analysis

Petrographic thin section analysis, also called polarising microscopy, is a method for studying and classifying geological samples such as minerals, rocks and soils. Ceramics are essentially of the same constituents as rocks as they contain minerals and rock fragments; they can also be termed as 'artificial rocks' (Dell'mour 1989, 19; Szakmány 2013, 735, 754; Heimann and Maggetti 2014, 70). Therefore, thin section analysis can be applied to the characterisation of ceramics as well and it has become one of the most important analytical techniques in archaeological pottery analysis, referred to as ceramic petrography. This subchapter provides an overview about the method of ceramic petrography and its application for the samples from Lower Austria.

3.3.1 The method of ceramic petrography

Ceramic petrography involves the visual investigation of thin ceramic slices using a polarising microscope. The following sections detail the preparation of the thin sections, the main parts and operation of the polarising microscope, the characteristics that are observed and described in a ceramic sample and the use of this method in archaeology.

Sample preparation

Ceramic pieces chosen for sampling are cut or polished to have a flat surface and mounted to a glass slide (with their flat surfaces) using epoxy resin. When they are attached to the slide they are cut and ground to a thickness of 0.03 mm and usually covered with a cover glass for protection (Whitbread 2017, 205).

The polarising microscope

The polarising microscope, also called petrographic microscope, is a transmitted light microscope, which uses light passing through the sample during observation. Similarly to other transmitted light microscopes (used in biology, for example), the main parts of a polarising microscope include a light source with a light adjustment system (condenser system), a sample stage, a rotating nosepiece with objective lenses and (one or) two eyepieces with the ocular lenses (Shelley 1985, 21–23; Nesse 1991, 16–20). It has, however, two major distinctive features which make it suitable for rock and ceramic analyses, most importantly for the identification of minerals. These are the two polarising filters and the rotating sample stage (Shelley 1985, 19–21). In addition, polarising microscopes are also equipped with accessory

plates and lenses (e.g. gypsum plate, mica plate, Bertrand lens; Shelley 1985, 24; Nesse 1991, 19–20).

The sample is placed on the rotating stage which is positioned between the two built-in polarising filters (sheets of polaroid), which are called polariser (below the sample) and analyser (above the sample). The polarising filters polarise the light, which naturally vibrates in all directions, producing light rays vibrating in a single direction (Shelley 1985, 27). The direction of vibration of the polariser and the analyser are perpendicular to each other (Shelley 1985, 28). The analyser can be switched on or off during analysis producing two different views of the same area of the sample. If only the polariser is used (the analyser is not inserted), the sample is seen in plane polarised light (PPL) and 'natural' colours of the minerals and inclusions are seen. If the analyser is inserted, the sample is observed in crossed polarisers (XP) and 'artificial' colours (interference colours) appear in the case of birefringent minerals.[29] This is because these minerals give rise to double reflection by resolving the polarised light into two rays with perpendicular vibration directions to each other (Shelley 1985, 30–31; Nesse 1991, 37). After passing through the analyser and being polarised again, the two light rays interfere with each other. Depending on the phase shift of the two light rays, the interference can be either constructive or destructive and birefringent minerals will exhibit different interference colours (Shelley 1985, 32; Nesse 1991, 38–43).

Collected information

Several features of archaeological ceramics can be studied by ceramic petrography. Thin sections of ceramics consist of three main parts: the matrix, inclusions and voids (Quinn 2013, 39). The matrix is the fine-grained paste with a particle-size below 0.01-0.015 mm[30] including mainly clay minerals such as illite, kaolinite and smectite (Velde and Druc 1999, 39; Whitbread 2001, 450). All the other particles enclosed by the matrix are referred to as inclusions. There are two main types of inclusions: the non-plastic inclusions (non-plastics, aplastic inclusions) such as minerals, rock fragments, organic material (e.g. chaff, bone, remains of fossilized organisms), fragments of former ceramics (also termed as grog or

[29] Minerals can be anisotropic which are birefringent thus produce interference colours, and isotropic, which are non-birefringent thus do not exhibit interference colours (Shelley 1985, 28–29).

[30] Some publications tend to prefer using 0.01 mm for the maximum grain size of the matrix (e.g. Quinn 2013, 42; Whitbread 1995, 381), some authors mention 0.015 mm as the upper limit (e.g. Dell'mour 1989, 20; Maggetti 1982, 123; Szakmány 2013, 735).

chamotte), and plastic inclusions such as clay pellets and iron-rich nodules (Whitbread 1986; Quinn 2013, 47–61; Braekmans and Degryse 2017, 252). Voids are 'empty' (air-filled) spaces in the thin sections (Braekmans and Degryse 2017, 252). Some ceramics also have a thin layer of slip, paint or glaze on their surface as a fourth major part in addition to the matrix, inclusions and voids (Braekmans and Degryse 2017, 234).

Many characteristics of the matrix, inclusions and voids can be analysed under the polarising microscope. Furthermore, microstructural features of the thin sections are also studied. A summary of the pieces of information commonly recorded about ceramic samples is listed in *Table 5*. A more detailed description of the methodology and terminology used in this thesis can be found in the following section (Section 3.3.2).

Table 5. Characteristics of ceramic samples observed by ceramic petrography following Whitbread (1995, 379–88) and Quinn (2013, 80–102)

Matrix	Inclusions	Voids	Microstructure
• Colour (PPL, XP) • Optical activity • Calcareous/ non-calcareous	Texture: • Grain-size distribution • Modal grain size • Maximum grain size • Degree of sorting • Shape • Roundness/ angularity Composition: • Identity • Frequency • Special characteristics	• Shape • Size • Filling	• Ratio of matrix, inclusions and voids • Homogeneity/ heterogeneity • Alignment of elongated grains and voids (preferred orientation)

As thin section analysis was first used in geology, many elements of the descriptive system for ceramics are derived from the methodology developed for geological samples, especially from that used in sedimentary petrography and soil micromorphology (Whitbread 1995, 391). The identification of minerals and rock fragments is aided by geological manuals and textbooks (e.g. MacKenzie and Guilford 1980; MacKenzie et al. 1982; Adams et al. 1984; Shelley 1985; Yardley et al. 1990; Nesse 1991; Deer et al. 1992; Adams and MacKenzie 1998).

The description of thin sections is usually qualitative with an estimation of proportions such as the ratio of the matrix, inclusions and voids and the frequency of the different inclusions and voids present in the sample (Whitbread 2017, 206). For the estimation of quantities several comparator charts are available (e.g. Matthew et al. 1991; Quinn 2013, 82: Fig. 4.9). There are also quantitative methods in ceramic petrography used for textural analysis (grain-size

analysis) and modal analysis (frequency analysis), which involve the systematic counting of inclusions (e.g. point counting, line counting, area counting methods) and digital image analysis (Middleton et al. 1985; Quinn 2013, 102–113; Whitbread 2017, 211–212). The quantitative approach, however, tend to be less popular as it is rather laborious and often there is no need for this level of detail to achieve the aim of the analysis.

In addition to the various uses of ceramic petrography, naturally it has some limitations as well. Thin section analysis is unsuitable for the compositional investigation of the clay matrix and usually poorly applicable for the characterisation of fine-grained pottery as the magnification of the microscope is finite (Dell'mour 1989, 17–18; Quinn 2013, 10). The report of the results can be quite subjective due to the qualitative nature of thin section descriptions and different data recording systems can be used by different researchers, which make the comparison between different sample sets rather complicated (Whitbread 1995, 396). However, there are other methods to complement and enhance the petrographic results such as chemical analysis, X-ray diffraction and scanning electron microscopy. Nevertheless, thin section analysis remains one of the most important analyses in archaeological pottery science.

Archaeological interpretation of petrographic data

The thorough investigation of the different components and the microstructure of the ceramic thin sections allows establishing petrographic groups, also called fabrics (see Section 3.2.1). In addition to the possible confirmation, modification or elaboration of the macroscopic grouping, petrographic data provide valuable information about the origin of the raw materials and pottery production technologies. Based on this information, complex archaeological questions can be answered related to pottery distribution, trade/exchange, organisation of workshops and the level of specialisation of societies.

Provenance

Sourcing of ceramic raw materials may be possible based on the rock fragments and minerals present in the matrix (Maggetti 1994, 26; Quinn 2013, 117–149; Szakmány and Nagy 2017, 252–253). The inclusions are identified and compared to the geological surroundings of the archaeological sites where the samples were found to decide whether the inclusions have a local origin. The search for potential raw material sources is usually done by studying the geology of the region using geological maps and reports (Dell'mour 1989, 31–32; Quinn 2013, 131). Collection and analysis of comparative raw materials can also be carried out (Quinn 2013,

131–137). Archaeological evidence related to the studied samples or other excavations in the region including find context, typology and possible traces of pottery production (kiln, wasters) as well as archaeometric literature and data might be of help in determining provenance (Quinn 2013, 122–129). Occasionally, microfossils are present in the clay, which can be useful to study past geological environments and identifying raw material sources (Quinn and Day 2007, 160–164; Quinn 2008, 280–282; Wilkinson et al. 2017, 275–278).

Technology

Conclusions can be drawn about the technological process from the microstructure and textural features of thin sections. Raw material preparation techniques such as mixing of clays, sieving, levigation and tempering can be assessed based on the homogeneity of the sample, grain sizes and shapes, sorting of the inclusions and grain size-distribution (Whitbread 1995, 392–393). In the case of a heterogeneous sample having, for example, colour stripes in the matrix or inclusions not evenly distributed, one can think of mixing of raw materials and incomplete kneading of the clay paste (Dell'mour 1989, 27–28; Quinn 2013, 168; Braekmans and Degryse 2017, 254). However, clays can naturally include inhomogeneities and this must be considered when interpreting from microstructure (Szakmány and Nagy 2017, 252; Quinn 2013, 168–171; Braekmans and Degryse 2017, 254).

The addition of non-plastic materials (e.g. sand or crushed rocks) to the clay by the potter, known as tempering, is also a possible technique used in paste preparation (Rye 1981, 31–39; Quinn 2013, 156–71). From a technological point of view, inclusions are essential components of the ceramics as they enhance workability of the paste and prevent the formation of cracks during drying and firing of the clay (Rye 1981, 31; Quinn 2013, 156–159; Dell'mour 1989, 20). The difficulty of defining temper arises from the fact that natural clays usually also contain inclusions as clays are the weathering products of rocks. If the weathering is incomplete, rock fragments can still be present (primary or residual clays) as well as clays can be enriched by inclusions during their transportation (secondary or sedimentary clays; Rice 1987, 72; Velde and Druc 1999, 59–61; Quinn 2013, 159). However, there are some textural and compositional features which can suggest the deliberate addition of inclusions to the paste. Bimodal grain-size distribution (i.e. the presence of two separate grain-size ranges) or high angularity of the grains might be the indicator of tempering as natural clays often contain multiple grain-sizes and the grains tend to be less angular or rounded due to weathering or transportation (Quinn 2013, 161–165; Braekmans and Degryse 2017, 255). In some cases, tempering is obvious from

the systematic presence of certain inclusions such as grog, slag, animal bone and chaff, all of which are not typical constituents of natural clay sources (Quinn 2013, 159–161). Tempering can also be inferred from mineralogy if, for example, the inclusions present are not probable to occur together in natural raw material sources (Quinn 2013, 161).

There are also techniques to remove large grains from the clay such as sieving (either in a dried state or as a suspension) or levigation during which the large grains are settled out in water (Rye 1981, 36–37; Quinn 2013, 154–156). It is usually not easy to detect the removal of inclusions, especially if temper was added to the clay after levigation/sieving, but a 'pure' matrix with relatively small grain sizes might suggest that such a refining method was applied (Quinn 2013, 156; Braekmans and Degryse 2017, 255).

The orientation of elongated grains and voids as well as domains of the matrix (observed in XP) can provide details about the forming methods such as pinching, moulding, coiling and wheel throwing (Rye 1981, 62–89; Dell'mour 1989, 30: Abb. 14; Whitbread 1996; Quinn 2013, 174–181; Braekmans and Degryse 2017, 255–256). Concentric orientation of inclusions may refer to the coiling technique as the result of rolling out the coils, while a strongly aligned microstructure can be the indicator of wheel throwing (Quinn 2013, 176–177; Braekmans and Degryse 2017, 256). Thin sections from the same vessel cut at different orientations (horizontal, vertical, tangential) enhance the successful investigation of forming techniques (Whitbread 1989, 133). However, the determination of these techniques from thin sections can be challenging. The main reasons of this include the possibility that more methods were combined to make one vessel as well as the fact that different forming techniques can leave the same traces in thin section. In many cases, macroscopic observation is more informative and reliable thus macroscopic and microscopic features should be considered together when interpreting shaping methods (Szakmány and Nagy 2017, 256; Quinn 2013, 174, 181).

Finishing techniques such as smoothing and burnishing can also be recognised in thin sections as they can cause preferred orientation in the surface region (Quinn 2013, 182; Braekmans and Degryse 2017, 256). Surface treatments including slips (thin layer of fine clay suspension) and glazes are easily detectable due to their grain-sizes, compositions or optical properties being different from those of the matrix (Quinn 2013, 182–185; Braekmans and Degryse 2017, 256–257).

Some features of the ceramic thin sections can reveal pieces of information about firing temperatures (Whitbread 1995, 394). The optical activity of the matrix observed in XP reflects the level of vitrification, i.e. the sintering and melting of the clay paste due to the temperature rise during firing. Generally, the matrix is optically active (birefringent) up until 800–850 °C at around which point ceramics start losing their optical activity as their vitrification progresses (Rice 1987, 431; Quinn 2013, 191).[31] Some minerals can also be an index of the maximum temperature such as calcite, which starts disintegrating at 650–750 °C and is entirely decomposed at 930 °C (Rice 1987, 98; Szakmány and Nagy 2017, 258–259). Recording unusual colour of a mineral may be important in temperature estimation such as that of the hornblende, which changes from green to brown at around 750 °C (McGovern 1989, 65; Gregerová and Procházka 1998, 276; Quinn 2013, 191).[32]

Post-depositional changes

Another use of petrographic analysis includes the detection of the minerals formed during the burial phase due to interactions with the soil and groundwater (Whitbread 1995, 394; Quinn 2013, 204–210). These secondary minerals (e.g. calcite, gypsum) can be deposited in voids and cracks or on the surface of the vessels (Quinn 2013, 204–207). As post-depositional changes should be excluded from the interpretation of pottery provenance and technology, distinguishing between primary and secondary minerals is an important function of the petrographic analysis especially when bulk analysis (XRD, chemical analysis) is also carried out as bulk analyses cannot make this distinction (Szakmány and Nagy 2017, 259).

Next level of interpretation

In addition to the above-mentioned information, which can be inferred directly from the ceramic samples, further interpretation is possible based on the petrographic data.

The determination of potential sources of raw materials gives an idea about the rough location of the sites of pottery production assuming that raw materials were collected close to the production site, which is the case with most ceramics (Arnold 1985, 39–49; Quinn 2013, 119;

[31] For example, the firing experiments of Maggetti et al. 1984 regarding Mexican majolica showed that the sample's light brown calcareous matrix turned to isotropic red at around 800 °C and isotropic black at around 1100 C° (Maggetti et al. 1984, 177: Fig. 13).

[32] It is important to know the origin of the amphibole however, as the colour change might have happened during the metamorphism of the rock of which the amphibole derives.

Braekmans and Degryse 2017, 236). Knowing the area of production and the archaeological site where the samples were found, conclusions can be drawn about the products being import or local wares and about how the vessels were transported to their final destination. A range of possibilities can be considered from the movement of objects (including trade, exchange and distribution) to the mobility of people (e.g. migration), which can shed light on economic and social networks (Rice 1987, 191–200; Quinn 2013, 142−146).

The investigation and comparison of a large number of samples can provide information about different preparation, forming and firing techniques used simultaneously as well as continuity/discontinuity and development of pottery technologies across cultural, geographical and temporal boundaries (Dell'mour 1989, 18; Herold 2008b, 25; Peterson and Betancourt 2009, 2). Based on textural and compositional features of the petrographic groups, the level of standardisation of production as well as the number and complexity of the production units can be discussed (Rice 1987, 180–191, 201–204; Orton and Hughes 2013, 144–149). Conclusions can also be drawn about the past society as the structure and organisation of the producing units reflect the degree of economic specialisation of communities (Rice 1987, 188–191; Peacock 1982, 8–9).

3.3.2 Ceramic petrography of the samples from Lower Austria

The thin section analysis of the samples from Lower Austria were carried out using a Leica DM750P polarising microscope at Cranfield University (Shrivenham campus). This section describes the procedure and terminology used for the analysis and description of the samples. This methodology is based on the descriptive systems of ceramic thin sections by Ian Whitbread (1986; 1995, 379–88) and Patrick Quinn (2013, 80–102).

Among others, the microstructure and groundmass of the studied samples are investigated (*Figure 34*). The analysis of the microstructure includes recording the ratio of inclusions, matrix and voids, the homogeneity of the sample, the alignment of elongated constituents (preferred orientation) and the characteristics of voids. The two components of the groundmass, the matrix and inclusions are observed concerning several aspects such as colour, optical activity and calcareousness of the matrix and the types and textural properties of the inclusions, as detailed below. The boundary between the matrix and inclusions used in the present thesis is 10 μm (0.01 mm).

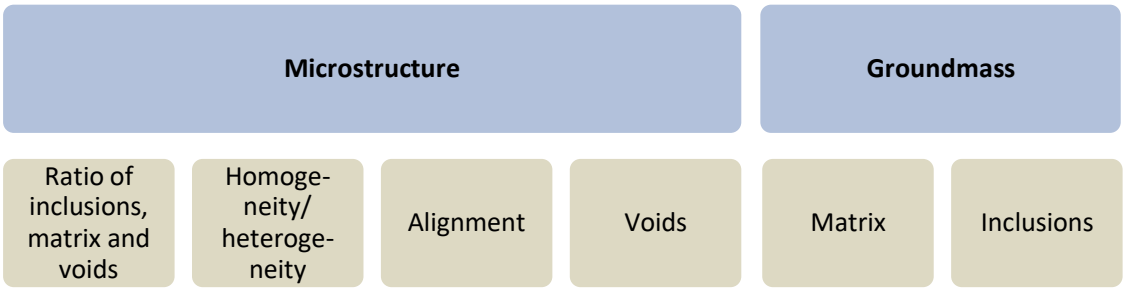


Figure 34. System of the investigated data of the thin sections

The ratio of inclusions, matrix and voids in the thin sections is estimated using comparison charts (Matthew et al. 1991). The degree of homogeneity/heterogeneity includes that of the matrix, differences in the distribution of the inclusions and voids and in the alignment of elongated constituents. *Figure 35* illustrates the four categories used to describe homogeneity following Quinn (2013, 94).



Figure 35. Terms used for the description of homogeneity/heterogeneity

Alignment refers to the degree of parallelism of elongated inclusions and voids to one another and to the walls of the ceramics. The four categories (weak – moderate – strong – very strong) proposed by Quinn (2013, 83) were completed by the author with two transition categories as shown in *Figure 36* below. In the case of a weak alignment, preferred orientation can hardly be observed in the thin section. The microstructure is moderately aligned if elongated grains and voids are more or less parallel to each other and to the walls of the ceramics, but the direction of alignment slightly changes in one sample. Elongated grains and voids are almost parallel to one another and to the walls of the ceramics in the case of a strong alignment.



Figure 36. Labels used for the description of alignment

As for the voids, their types, minimum and maximum sizes and their most common size ranges present in the sample are recorded (*Figure 37*). Void type names and descriptions were defined by Whitbread (1995, 380: Table A3.3) and Quinn (2013, 97); prefixes indicating common sizes are used after Whitbread (1995, 380: Table A3.3).

Vesicle	spherical void with smooth edges	Micro	<0.05 mm
Channel	elongated void with parallel walls and rounded ends	Meso	0.05–0.5 mm
Planar void	narrow, elongated void with pointed ends	Macro	0.5–2 mm
Vugh	shapeless, irregular void	Mega	>2 mm

Figure 37. Void types and prefixes for void size

Characteristics of the matrix are noted including colour (in PPL and XP), optical activity and calcareous/non-calcareous nature of the matrix. The colour of the thin sections often varies within one sample. For example, the core and margins (or one margin) of the ceramics can have different colour. Sometimes the interior and exterior of the sherds have different shades and the sample shows colour transition from one shade to another. The matrix usually has similar colours in PPL and in XP apart from that XP colours are slightly darker and have a more reddish tone in the case of the reddish-brown ceramics. *Figure 38* shows the corresponding Munsell notation (Munsell Color Company 2004) for the different labels used for describing the colour of the thin sections in PPL and XP.

	Very dark reddish-brown	Dark reddish-brown	Light reddish-brown	Very light reddish-brown
PPL	7.5YR 3/2 – 5YR 3/4	7.5YR 4/4 – 5YR 4/6	5YR 5/10 – 7.5YR 5/8	7.5YR 6/10 – 10YR 6/8
XP	10YR 2/2 – 5YR 2/2	10R 3/6 – 10R 4/8	2.5YR 4/8 – 2.5YR 5/10	5YR 6/10 – 7.5YR 6/10

	Very dark yellowish-greyish-brown	Dark yellowish-greyish-brown	Light yellowish-greyish-brown	Very light yellowish-greyish-brown
PPL	-	10YR 4/2 – 2.5Y 4/2	10YR 5/4 – 2.5Y 5/2	10YR 6/4 – 2.5Y 7/2
XP	10YR 3/2 – 2.5Y 3/4	2.5Y 5/2 – 5Y 5/2	2.5Y 6/4 – 5Y 6/2	2.5Y 7/2 – 5Y 7/2

	Black	Very dark grey	Very light yellowish-grey
PPL	N1	-	-
XP	N1	N3	2.5Y 7/2 – 2.5Y 8/4

Figure 38. Colour labels used for the definition of colour

The terms used for the description of optical activity of the matrix are based on suggestions of Whitbread (1995, 382) and Quinn (2013, 94, 97), completed with the categories 'very slightly active' and 'very highly active' by the author (*Figure 39*).



Figure 39. Terms used for the description of optical activity

Textural properties and types of inclusions are also recorded. Textural properties of inclusions include grain-size distribution, modal grain size (of both the fine and coarse fraction of the inclusions if present), maximum grain size, degree of sorting, shape and roundness/angularity of the grains. The labels of *Figure 40* show simplified categories for grain-size distribution after Quinn (2013, 85).

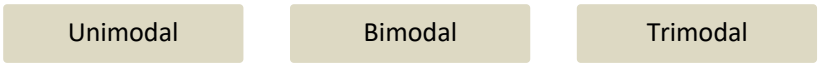


Figure 40. Labels used for the definition of grain-size distribution

The degree of sorting (*Figure 41*), shape (*Figure 42*) and roundness/angularity (*Figure 43*) of the grains were defined with the help of comparison charts (Quinn 2013, 84: Fig. 4.11, 87: Fig. 4.15).



Figure 41. Labels used for the definition of the degree of sorting



Figure 42. Labels used for the description of grain shape



Figure 43. Labels used for the description of roundness/angularity of grains

The description of thin sections also contains the list of inclusions in decreasing order of abundance such as minerals, rock fragments, primary or secondary carbonates, argillaceous and organic inclusions. Relevant characteristics of inclusions (e.g. colour, alteration) are also noted. The frequency of inclusions is recorded using frequency labels (*Figure 44*) after Whitbread (1995, 379: Table A3.1).

Predominant	Dominant	Frequent	Common
>70 vol%	70–50 vol%	50–30 vol%	30–15 vol%
Few	Very few	Rare	Very rare
15–5 vol%	5–2 vol%	2–0.5 vol%	<0.5 vol%

Figure 44. Frequency labels used for the definition of the amount of inclusions

Argillaceous inclusions are listed among inclusions and detailed using the terms below (*Figure 45*) after Whitbread (1986). Colour, shape and roundness/angularity are defined with the same labels as the matrix and textural properties of inclusions as mentioned above.

Type	Argillaceous rock fragment (ARF)	Grog	Clay pellet	Clay temper
Colour (PPL, XP)				
Shape				
Roundness/ angularity				
Maximum size				
Optical density	High	Neutral	Low	
Boundaries	Sharp	Clear	Diffuse	Sharp to merging
Concordance	Concordant	Discordant		
Internal composition	Similar to matrix	Distinctive from matrix		

Figure 45. Labels used for the description of argillaceous inclusions

3.3.3 Summary

Thin section analysis is a useful method to explore compositional and microstructural properties of ceramic samples. These properties provide basis for provenance identifications and interpretations of production technology. Through the investigation of origin and the pottery making process, larger topics can be touched on such as the question of local/import, trade/exchange networks, organisation of production and continuity of technologies.

3.4 Scanning electron microscopy

Scanning electron microscopy (SEM) is used to analyse the structure and composition of samples at a much higher magnification than optical microscopes. The first part of this section includes information about the structure and operation of the scanning electron microscope (SEM)[33] as well as the two main types of data (microstructural and compositional) it produces. This is followed by the description of some possible uses of SEM in archaeological ceramic analysis. At the end of this section, the details of how this method was applied specifically to the samples from Lower Austria are given.

3.4.1 The method of SEM

Main parts of a scanning electron microscope

There are various designs of SEM, but all of them normally include

- an electron gun for generating an electron beam,
- electron lenses for projecting a demagnified image of the beam onto the specimen,
- scanning coils for scanning the beam across the sample,
- detectors for the detection of electrons and other types of signals emitted by the sample, and
- an image-display system for visualisation (Goodhew et al. 2001, 37–38; Reed 2005, 21–40).

Interactions of incident electrons and specimen

The electron beam causes several interactions in the sample resulting in the emission of various particles, which can be detected with different detectors. After entering the specimen, some electrons of the electron beam are deflected without significant energy loss ('elastic scattering') of their initial energy (adjustable, commonly 5–30 keV; Reed 2005, 7–9; Goodhew et al. 2001, 30, 34–35). These electrons, following their deflection and ejection, are referred to as backscattered electrons (BSE). The deflection can happen either at a high-angle (more common for elements with high atomic numbers) or through a series of low-angle scatterings (more common for elements with low atomic numbers; Reed 2005, 9). Backscattered electrons

[33] The acronym SEM is used both for the method (scanning electron microscopy) and the instrument (scanning electron microscope).

deflected in the latter way carry lower (but still high) energies because of the energy loss caused by the multiple scatterings (Reed 2005, 9).

Incident electrons of the electron beam can also 'knock out' previously bound electrons of the sample while small part of their energy is transferred to the bound electrons ('inelastic scattering'; Reed 2005, 7, 11; Goodhew et al. 2001, 31–32). These previously bound and emitted electrons are called secondary electrons (SE). They carry very low energies (few electron volts) compared to the backscattered electrons, and thus only those can escape which are situated close to the surface of the sample (Reed 2005, 11; Egerton 2005, 131). Secondary electrons can also be produced when backscattered electrons leave the specimen (Reed 2005, 11).

When the electron beam reaches the sample, X-rays are generated. They are of two types: the continuous and characteristic X-rays. Continuous ('Bremsstrahlung') X-rays are the result of the interaction between the incident electrons and the atomic nuclei (Reed 2005, 11; Goodhew et al. 2001, 36). Continuous X-rays have an undesirable effect on the results, which make the element-identification less accurate: they create a background noise, which covers the spectrum of characteristic X-ray lines of elements present in small concentrations (Reed 2005, 12).

Characteristic X-rays, however, are of great use in identifying elements. They are produced when electrons residing in the inner electron shells, excited by primary electrons of the electron beam, leave the atom in an ionised state (Reed 2005, 13; Egerton 2005, 21). The inner shell vacancies are then filled by outer-shell electrons while energy is released in the form of X-ray photons (Egerton 2005, 158) as staying in an outer shell (which has lower binding energy) requires more energy than staying in an inner shell (which has higher binding energy; Goodhew et al. 2001, 22). The energies of the X-ray photons generated this way, which equal to the energy difference between the outer and the inner shell, are specific to each element (Egerton 2005, 158; Reed 2005, 13).

Observation conditions

If multiple detectors are present, a detector is chosen and observation conditions (e.g. vacuum, accelerating voltage, working distance) are adjusted depending on the type of the specimen and the aim of the analysis. Bombarding with electron beam causes the charging of non-conductive samples, which can be eliminated by coating them with a thin conductive layer

(e.g. carbon, gold) or using low vacuum (Egerton 2005, 148-149; Artioli 2010, 68). Environmental SEM (ESEM) is a special type of SEM, which uses low vacuum in the specimen chamber enabling the analysis of uncoated specimens as well as fragile and volatile-containing samples such as animal tissue, textile, rubber and ceramics (Egerton 2005, 150; Reed 2005, 53; Artioli 2010, 68).

Imaging – topographic and compositional images

Different types of images can be acquired when detecting secondary and backscattered electrons. The SE image shows topographic differences of the specimen (Reed 2005, 43; Egerton 2005, 131). This image can easily be interpreted as it appears very similar to a 3D image perceived by the human eye when looking at an illuminated object (Reed 2005, 43; Egerton 2005, 133). However, in a SE image the edges always appear bright as a result of the fact that more electrons can escape from the edges than from other areas of the sample (so-called edge-effect; Reed 2005, 44).

The detection of backscattered electrons provides an image showing compositional differences. The amount and energy of backscattered electrons emitted by the specimen depends on atomic number; the higher the atomic number the more high-energy electrons emerge from the sample (Reed 2005, 9, 54). Those areas of the sample which emit more high-energy electrons appear brighter in the greyscale image thus the higher the atomic number of the element the brighter the colour (Reed 2005, 54). In addition to composition, BSE images can also exhibit topographic contrast although with worse spatial resolution than SE images (Reed 2005, 57; Goodhew et al. 2001, 146). This is due to a shadowing effect as a result of the detector being on one side of the specimen and not detecting areas facing away from it (Reed 2005, 44). Therefore, to achieve the best compositional image, the topography must be excluded by using well-polished specimens (Reed 2005, 55; Goodhew et al. 2001, 148).

Chemical analysis with SEM-EDS/WDS

Chemical analysis can be carried out with a SEM if it is equipped with an energy-dispersive (ED) or wavelength-dispersive (WD) spectrometer. ED spectrometers measure the energies of the X-ray photons, which generate pulses when arriving at the detector (Reed 2005, 77; Goodhew et al. 2001, 175–178). These pulses are then amplified and converted into a spectrum (Reed 2005, 82). WD spectrometers contain specific crystals, which reflect and enhance the intensity of the X-rays emitted by the specimen (Reed 2005, 86–87). These crystals also disperse the X-

rays according to their wavelengths and direct them to the detector (Reed 2005, 86; Goodhew et al. 2001, 181). The ED spectrometers are quicker, cheaper and more convenient to use than the WD spectrometers, but WD spectrometers give a better spectral resolution and thus facilitate the interpretation of the results (Reed 2005, 76, 95–96; Egerton 2005, 169-170).

The peaks of the spectra produced by the spectrometer can be identified based on tables of energies (energy-dispersive X-ray spectroscopy, EDS) or wavelengths (wavelength-dispersive X-ray spectroscopy, WDS), but nowadays automatic identification is also available (however, it still needs checking; Reed 2005, 110–111). The chemical analysis gives semi-quantitative results, but these element concentrations can be quantified by carrying out corrections for background and comparing them to standards of known compositions (Reed 2005, 107; Goodhew et al. 2001, 200–203).

Another possible function of EDS/WDS is element mapping which shows the spatial distribution of a chosen element in a selected area (Reed 2005, 97; Goodhew et al. 2001, 187). The spectrometer counts the number of characteristic X-ray photons emitted by each point of the sample and converts it into brightness on the screen (Reed 2005, 97; Goodhew et al. 2001, 189). This is mainly spatial information, but quantification of the results is possible with background corrections (Reed 2005, 100).

3.4.2 SEM of archaeological ceramics

Both imaging and chemical analysis carried out by SEM can be useful when interpreting ceramic materials. The importance of these two uses of SEM in archaeological interpretations of ceramic production are reviewed in the following sections.

Imaging

One of the possible applications of SEM in ceramic analysis is the examination of vitrification structure of the potsherds, which can give information about the ceramic technology in terms of firing temperature. Clay platelets and other minerals are well-distinguished in unfired clays. During the firing process, the body of the ceramics starts ‘melting’ (above a certain temperature) and it becomes more and more vitrified until it is totally molten (Tite 1992, 115).

The observation of the degree of vitrification is normally carried out on freshly fractured surfaces using SE images.[34]

The vitrification process can be divided into stages based on the amount of glass or high temperature crystalline phases present. The commonly used[35] system of vitrification stages established by Yannis Maniatis and Michael Tite (1981) is based on the investigation of Neolithic to Bronze Age pottery of calcareous and non-calcareous clays in both oxidising and reducing atmosphere. They assigned firing temperature ranges to the vitrification stages by observing and comparing the microstructure of the samples in 'as-received' state and after re-firing at different known temperatures (*Table 6*). The use of this system requires prior knowledge about the composition of the clay matrix and the firing atmosphere of the sample.

Table 6. Vitrification stages and the corresponding firing temperature ranges in oxidising (O) and reducing (R) atmosphere after Maniatis and Tite (1981, 61, 65, 68: Table 1). The upper boundary of the last stage (continuous vitrification) represents the temperature by which continuous vitrification is totally developed.

Vitrification stages	Non-calcareous clays (< 6% CaO)	Calcareous clays (> 6% CaO)
No vitrification (clay plates are intact, rounding of the edges cannot be observed)	O: < 800 °C R: < 750 °C	O: < 800 °C R: < 750 °C
Initial vitrification (appearance of isolated smooth areas or glass fibres)	O: 800–850 °C R: 750–800 °C	O: 800–850 °C R: 750–800 °C
Extensive vitrification (progressive development of glass phase or high temperature crystalline phases)	O: 850–950 °C R: 800–900 °C	O: 850–1050 °C R: 850–1050 °C
Continuous vitrification (continuous smooth vitrified surface, unconnected rounded pores)	O: 950–1150 °C R: 850–1050/1150 °C	O: 1050–1150 °C R: 1050–1150 °C

According to their research, vitrification starts at around 800 °C in oxidising atmosphere and at about 750 °C in reducing atmosphere for both non-calcareous and calcareous clays. The appearance of glass remains are more or less isolated during the next 50 °C. At about this point the vitrification stops being local and extend to the whole surface (extensive vitrification). This stage differs in the case of calcareous and non-calcareous clays: the glass phase increases in

[34] Polished surfaces may also be used for vitrification analysis, although polished sections are not as informative as fresh fracture surfaces (Tite et al. 1982, 110; Tite 1992).
[35] E.g. Tite et al. 1982; Kilikoglou 1994; Day and Kilikoglou 2001, 120–124; Floyd 1995; Gilstrap et al. 2016; Tite et al. 2018.

non-calcareous clays while high temperature crystalline phases develop in calcareous clays (Maniatis and Tite 1981, 61, 65). Another important observation of Maniatis and Tite was that in calcareous clays containing enough fine-grained and evenly distributed calcium oxide, the extensive vitrification structure remains unchanged between 850 °C and 1050 °C (Tite and Maniatis 1975, 123; Maniatis and Tite 1981, 66) in contrast with non-calcareous clays where vitrification keeps increasing with increasing temperature (Maniatis and Tite 1981, 72). A continuous vitrified layer (continuous vitrification) develops around 850/950 °C (in reducing/oxidising atmosphere, respectively) in non-calcareous clays, and around 1050 °C in calcareous clays (in both reducing and oxidising atmosphere).

There are, however, some limitations of vitrification analysis as well. The above-mentioned authors emphasised that little is known about ancient firing time and atmosphere, which significantly influence the vitrification structure (Maniatis and Tite 1981, 72; Tite et al. 1982, 112). Furthermore, the temperature can differ in different parts of the kiln/pit (Maniatis and Tite 1981, 73; Tite et al. 1982, 113); the difference can be more than 100 °C or even 300 °C based on Roman period kiln-firing experiments (Mayes 1961, 11: Fig. 3; Byrant 1970, 6: Table 1; Byrant 1971, 8–13: Table 1).

BSE images of polished surfaces can also reveal important information about pottery technology. Due to the high magnification of the SEM, it can be used for the examination of surface decorations such as glaze or slip layers and different types of surface finish, which can be very thin or weathered and thus unobservable with petrographic microscope. Also, for example the differentiation between burnishing and slip may be possible by comparing the microstructure and composition (grey level) of the ceramic body with that of the surface treatment (Tite et al. 1982; Tite 1992, 115; Tite 1999, 187).

Although compositional contrast is exhibited in BSE images, the assignment of a certain shade of grey to a certain mineral is problematic since a mineral can have a range of compositional variations (Reed 2005, 55). However, in some cases, the proportion of coexisting known phases with significantly different mean atomic numbers can be estimated where it is not possible with polarising microscope (e.g. distinguishing different carbonates (Reed 2005, 55), distinguishing between graphite flakes and the dark matrix). The BSE signal is also the basis of selecting areas for chemical analysis with SEM.

Chemical analysis

The advantage of using SEM-EDS/WDS for chemical analysis is that it allows investigating selected spots or areas of the sample. In contrast, bulk chemical analyses such as XRF, INAA, ICP-MS and ICP-OES[36] give information about the composition of the entirety of the ceramic sample including the matrix and the inclusions; individual grains or matrix composition cannot be measured separately.

SEM-EDS/WDS analysis is usually carried out on polished surfaces. Uncovered thin sections can be used for this purpose, which previously were investigated by polarising microscopy thus a knowledge of the components of the sample is already given (Olsen 1988, 3). The results of the chemical analysis can contribute to the characterisation of the place of origin of the raw materials, and can thus sharpen the information given by petrography.

Having the benefit of choosing a spot/area of interest means that the composition of the matrix can be investigated separately from the inclusions. Probably the most important among the components of the clay is the carbonate content. Distinguishing between calcareous and non-calcareous clays is useful for provenance interpretations and also for estimating the firing temperature range based on vitrification structure (as mentioned above). A clay is referred to be calcareous if it contains more than 6 wt% of calcium oxide (Maniatis and Tite 1981, 65).[37]

The ratio of silicon and aluminium content is also used to characterise different clays (Velde and Druc 1999, 247–250). The Si/Al ratio is between 1.53 and 2.62 in the case of illites, 2.58 and 3.47 in the case of montmorillonites and close to 1 in the case of kaolin clays according to Velde and Druc (1999, 249).[38]

Matrix compositions can be presented on a ternary diagram including the three characteristic components mentioned above (SiO_2, Al_2O_3, CaO; Artioli 2010, 232) or the three element groups (Si – Al, Fe, Mg, Ti – Na, K, Ca) within which elements can substitute each other in terms of the chemical formula of the clay minerals (Tite et al. 1982, 112: Fig. 5). Ternary diagrams can

[36] X-ray fluorescence, instrumental neutron activation analysis, inductively coupled plasma mass spectrometry and inductively coupled plasma optical emission spectrometry

[37] Although there are other publications of the authors defining the border between calcareous and non-calcareous clays at 5 wt%: Maniatis and Tite 1978, 484–485; Tite et al. 1982, 111; Tite 1992, 115; Tite et al. 2018, 1078.

[38] The authors refer to Newman 1987, but page numbers are not given and were not possible to identify.

be made containing the two main components of the clay (SiO_2, Al_2O_3) and the fluxes[39] (K_2O, Fe_2O_3, CaO, MgO, TiO_2; Maniatis and Tite 1978, 485: Fig.1) as well as including Al_2O_3, Fe_2O_3+MgO and K_2O+Na_2O+CaO (Philpotts and Wilson 1994, 615: Fig. 8).

The analysis of different inclusions can be useful for elaborating the grouping and narrowing down the source area of the raw materials. The chemical composition of the minerals is determined by the host rock from which they were derived, thus a more precise sourcing can be given (Freestone 1982, 107). Compositions of feldspars can be visualised on ternary graphs based on their sodium ($NaAlSi_3O_8$, albite, Ab), potassium ($KAlSi_3O_8$, orthoclase, Or) and calcium content ($CaAlSi_2O_8$, anorthite, An; Deer et al. 1992, 393). The compositional variations of other minerals such as pyroxenes, amphiboles and heavy minerals can be detected and compared to local compositions in order to get an idea about their closer place of origin (e.g. Freestone 1982; Braekmans et al. 2012; Shriner and Dorais 1999). Knowledge about the composition of individual inclusions can also be useful when interpreting the results of bulk chemical analyses (Braekmans et al. 2012, 186).

Occasionally, petrographic data is not sufficient to identify a mineral. Chemical analysis by SEM-EDS/WDS may help determine mineral species such as in the case of calcite and dolomite, which have the same optical characteristics but differ in composition (Freestone 1982, 107).

As mentioned above, surface treatments, slips and glazes can also be investigated by SEM. In addition to microstructural features, chemical composition can confirm the application of a surface layer by having different (concentration of) elements in the slip and ceramic body (e.g. Tite et al. 1982; Middleton 1987).

The element mapping function of the SEM is useful to investigate different distribution patterns of certain elements. For example, it can enhance grouping and contribute to observations on technology, such as compositional differences of areas of the matrix as result of the inhomogeneity of the clay or clay mixing – although at a high magnification level.

SEM-EDS/WDS also has limitations deriving from the instrument or the nature of the analysed material. When operating in a standardless mode, as a semi-quantitative analysis, the compositional data is not as accurate as it could be with the use of standards. The detection

[39] Fluxes facilitate the hardening of pottery during firing by lowering the melting point of the minerals (Artioli 2010, 234).

limit for EDS is lower than WDS, which might result in elements of small concentrations not showing on the spectrum (Reed 2005, 139). Therefore, SEM-EDS is not appropriate for trace element analysis. As in the case of all chemical analyses of pottery, the results can also be affected by other factors than the equipment itself. The concentration of 'mobile' elements such as calcium, iron and manganese can change in the sample after burial due to interactions with the soil (Peacock 1970, 377; Buxeda i Garrigós 1999; Maritan 2020). This can lead to results about the post-burial alteration of pottery instead of its production/use. Because of these reasons, SEM is normally supplemented by other techniques such as petrography, X-ray diffraction and bulk chemical analysis.[40]

3.4.3 SEM of the ceramic samples from Lower Austria

Vitrification analysis and chemical analysis were performed on uncoated samples from Lower Austria using an environmental SEM (Hitachi SU3500) with an attached EDS system at Cranfield University (Shrivenham campus). The adjustment of the equipment and the methodology used are detailed below.

Vitrification analysis

Vitrification analysis was carried out on freshly fractured surfaces of the ceramic sherds using SE signal. Based on literature including vitrification analysis of pottery and after experimenting with different adjustments, high vacuum mode and 15 kV accelerating voltage were chosen. The samples were examined at three magnification levels: 500x, 1000x and 2000x.

Chemical analysis

Chemical analysis was carried out on uncovered thin sections or on the flat surface of ceramic pieces left after thin sectioning (if uncovered thin sections were not available). The SEM-EDS was operated at 20 kV in standardless analytical mode and each chosen spot/area of the samples was measured for 30 seconds.

The chemical analysis included the matrix, different minerals and a surface layer (glaze/deposition) in one case. At least three points of inclusion-free areas of the matrix were measured and averaged following Velde and Druc (1999, 248–249) to exclude false data in case of hitting a small mineral grain by accident.

[40] E.g. Tite et al. 1982, Middleton 1987; Gilstrap et al. 2016; Tite et al. 2018.

The mineral to be analysed was chosen by polarising microscopy first and the same grain was spotted on the BSE image and X-ray image. Most of the minerals analysed by SEM-EDS were identified by thin section analysis, but some of them were uncertain or unknown and intended to be identified by means of chemical data. The mineral measurements concentrated on feldspars (both potassium feldspar and plagioclase if it was possible), heavy minerals and those minerals which represent characteristic or distinctive constituents of their petrographic groups (e.g. amphibole, pyroxene, garnet).

For the chemical data of the samples, an Excel document was created with different sheets containing the measurements of the matrix and minerals. A sheet including the general chemical formula and cation numbers of the expected minerals was also created for easing the identification of uncertain or unknown minerals.

10 elements (silicon, aluminium, magnesium, sodium, calcium, potassium, iron, manganese, titanium and oxygen) as the main components of ceramic materials were selected to be measured at each case by SEM-EDS, and carbon was excluded from measurement.[41] Results are given as oxide wt% in the thesis following the usual practice (Artioli 2010, 232).

For monitoring machine drift and evaluating the performance of SEM-EDS measurements, archaeological glass standards Corning A and Corning B were used (Brill 1999, 540–541, 544). Accuracy and precision of the analyses were calculated based on the recently updated compositional data of these reference materials (Adlington 2017, 5: Table 3; see also Brill 1999, 544; Vicenzi et al. 2002, 720: Table 1; Wagner et al. 2012, 1675: Table 5). Averages of replicated measurements (n=5) of the standards by SEM-EDS instrument used for the analysis of the studied ceramics were compared to the certified values, and relative standard deviation and error were calculated to identify precision and accuracy, respectively (Stanley and Lawie 2007; Abzalov 2008). Precision of the SEM-EDS analyses could be measured 7% or less for Na_2O, Al_2O_3, SiO_2, K_2O, CaO and CuO, while relative standard deviations were exceeding 14% in the case of MgO, P_2O_5, SO_3, TiO_2, Fe_2O_3 and MnO (*Table 7*). The accuracy of the measurements was acceptable to good (< 10%) in the case of some major elements including Na_2O, MgO, SiO_2 and K_2O, was between 10% and 16% in the case of Al_2O_3, CaO, Fe_2O_3 and MnO, while the detection of P_2O_5, SO_3, TiO_2 and CuO showed relatively poor accuracy (> 16%; *Table 7*).

[41] For what elements are worth being measured regarding chemical analysis of ceramics see Peacock 1970, 377.

Table 7. Relative standard deviation and relative error calculations for data quality assessment (precision and accuracy) of SEM-EDS analysis

	Corning A				Corning B			
	Certified	Measured (n=5)	Relative standard deviation (%)	Relative error (%)	Certified	Measured (n=5)	Relative standard deviation (%)	Relative error (%)
Na_2O (wt%)	14,3	15,2	0,7	6,2	17,0	17,6	4,7	3,7
MgO (wt%)	2,7	2,9	2,4	9,8	1,0	1,0	23,4	-3,9
Al_2O_3 (wt%)	1,0	1,2	6,3	16,0	4,4	4,7	5,3	8,0
SiO_2 (wt%)	66,6	66,1	2,7	-0,7	61,6	60,8	2,5	-1,2
P_2O_5 (wt%)	0,1	0,1	20,9	-25,0	0,8	0,7	20,1	-20,7
SO_3 (wt%)	0,1	0,2	35,0	14,3	0,5	0,4	6,5	-16,3
K_2O (wt%)	2,9	2,8	3,3	-3,5	1,0	1,0	1,7	2,0
CaO (wt%)	5,0	5,7	1,8	13,1	8,6	9,2	3,6	6,9
TiO_2 (wt%)	0,8	0,7	5,5	-12,7	0,1	0,1	14,3	-33,3
Fe_2O_3 (wt%)	1,1	1,0	45,4	-11,0	0,3	0,4	11,0	8,8
MnO (wt%)	1,0	0,9	52,3	-11,0	0,3	0,3	5,8	12,0
CuO (wt%)	1,2	0,9	1,5	-26,5	2,7	2,4	6,1	-9,4

3.4.4 Summary

SEM is used for two main purposes concerning the analysis of archaeological ceramics: for the investigation of the vitrification structure and the chemical composition of the ceramic matrix, minerals and coatings (slips and glazes). The results of vitrification analysis can provide details about past firing temperatures contributing this way to the reconstruction of ceramic technology of the studied samples. Chemical data given by SEM-EDS/WDS may be useful in identifications of geological origin and can enhance and supplement archaeological or petrographic grouping.

3.5 Inductively coupled plasma optical emission spectrometry (ICP-OES)

Chemical analysis is an important part of many ceramic studies as it provides a new insight into the samples' composition, thus raw material-related questions can be discussed in more detail. This subchapter gives an overview about the method of ICP-OES and its use in ceramic archaeology. Sample preparation and the equipment used for the analysis of the investigated ceramics are also detailed. As chemical data is often treated statistically (including this thesis), the most frequent statistical analyses are outlined at the end of this section.

3.5.1 The method of ICP-OES

Inductively coupled plasma optical emission spectrometry (ICP-OES), also called inductively coupled plasma atomic emission spectroscopy (ICP-AES),[42] is a bulk analysis which is used to characterise the chemical composition of gas, fluid or solid samples. It can detect and identify all major elements (SiO_2, Al_2O_3, Fe_2O_3, MgO, CaO, Na_2O, K_2O, TiO_2, MnO and P_2O_5) and most trace elements (e.g. Li, Sr, Ba, Sc, Y, La, Zr, V, Nb, Cr, Co, Ni, Cu and Zn; Thompson and Walsh 2003, 15).

Main types of ICP-OES and evaluation of the method

Two main types of ICP-OES instruments are distinguished. The first type is equipped with a simultaneous spectrometer (polychromator) and carries out simultaneous analysis, which includes the detection of many, previously chosen elements at the same time. The second type has an attached sequential spectrometer (monochromator) for sequential analysis, which includes the detection of all elements of the sample, one by one.

One of the advantages of the ICP-OES is that it has excellent detection limits (Boumans 1987c, 102; Thompson and Walsh 2003, 17). The precision ((un)certainty of measurement, repeatability) and accuracy (closeness of the measured value and the true value) of the ICP-OES are also good (Boumans 1987c, 176; Thompson 1987, 193; Tsolakidou and Kilikoglou 2002, 569; Thompson and Walsh 2003, 17–18, 32–37). Another benefit of this method is that only a relatively small quantity of sample is required (usually well below 1 g), the cost of the analysis is relatively low and the analysis is relatively quick when using a polychromator (Thompson and Walsh 2003, 18–19). However, this method is destructive even if only small amount of

[42] ICP-OES is preferred here as AES is also the acronym of Auger electron spectroscopy (Boumans 1987a, 2).

sample is needed. There are some limitations of the chemical analysis of ceramic materials as well (see below in Section 3.5.2).

Instrumentation and sample analysis

An ICP-OES instrument usually consists of the following main parts:

- a nebulizer system,
- a spray chamber,
- a plasma torch,
- a radiofrequency generator,
- a spectrometer
- and a computer provided with a software.

Sample preparation is relatively easy with some samples while it is more laborious with others. Gas or liquid samples need less preparation than solid samples such as rocks and ceramics, which need to be dissolved for ICP-OES analysis (Thompson and Walsh 2003, 39).

To acquire accurate compositional data, the sample needs to be in an atomised/ionised form, which is achieved by the help of the first four components of the list above. The nebulizer introduces the liquid sample to the system by separating it into small droplets (less than *c.* 10 µm) and thus converting it into an aerosol (Greenfield 1987, 141; Thompson and Walsh 2003, 8). This aerosol consists of gases, particles (i.e. solid or liquid droplets) and usually some solvent vapor in the case of dissolved solid samples (Gustavsson 1987, 410). From the nebulizer the aerosol flows into the spray chamber, which is for the removal of waste, i.e. larger droplets than *c.* 10 µm are sorted out (Broekaert and Boumans 1987, 299; Thompson and Walsh 2003, 77-80).

After passing through the spray chamber the aerosol is introduced into the plasma torch. The torch contains typically argon and consists of three concentric gas flows: the coolant gas (outer flow), the auxiliary gas (middle flow) and the injector gas (inner flow; Thompson and Walsh 2003, 59-66). The aerosol is blown into the inner flow where the sample is excited by the inductively coupled plasma (ICP) to be separated into atoms and ions (Boumans 1987a, 2). The ICP is formed when the plasma (i.e. ionised gas) flows through an oscillating magnetic field generated by the radiofrequency generator, which makes the plasma electrically conductive and induce high-frequency currents in the plasma (Boumans 1987b, 72–73; Thompson and

Walsh 2003, 9, 80). The interaction (inductive coupling) between the plasma flow and the magnetic field produces the ICP flame due to ohmic resistance (Greenfield 1987, 124; Thompson and Walsh 2003, 9–10). The flame has a shape of a prolate spheroid and the tailflame is used as a spectroscopic source (Greenfield 1987, 140–141).

Following the interaction with the high-temperature ICP, the sample consists of free atoms, ions and molecules (Boumans 1987a, 5; de Galan and van der Plas 1987, 530). When an atom is excited by the hot plasma some of its electrons move from an inner electron shell (lower energy state) to an outer electron shell (higher energy state). The excited atoms emit photons as their electrons return their lower energy state (Young and Pollard 2000, 32–33). The wavelength of the photons depends on the energy difference of the electron shells involved and is characteristic to each element (Boumans 1987a, 4; Artioli 2010, 37).

The spectrometer distinguishes the light arriving from the sample by wavelengths with the help of a diffraction grating (Olesik 1987, 467–468). The photoelectrons of a wavelength passing through a slit fall onto a photomultiplier tube where they are multiplied and collected by an anode (Bubert and Hagenah 1987, 539). The number of photomultipliers depends on the type of the spectrometer. In the case of a sequential spectrometer (monochromator), only one photomultiplier is present, however, several photomultipliers are needed in a simultaneous spectrometer (polychromator), one for each element to be determined (Olesik 1987, 512). The two types of spectrometers have their own advantages: polychromators are quicker and more stable than monochromators. However, in the case of monochromators, the number and type of elements to be investigated do not need to be determined, and they are also cheaper than polychromators (Thompson and Walsh 2003, 47, 55; Boumans 1987a, 16).

At the output of the detector, a signal is generated by converting the light into electric voltages which are then amplified and converted into digital values (Bubert and Hagenah 1987, 545, 557). The optical emission spectrum as the result of the ICP-OES analysis consists of different spectral lines produced by photons of different wavelengths (Boumans 1987a, 3–4). A chemical element is present in various forms in the plasma: molecules, atoms and ions with different charges (singly, doubly, triply). They all produce a characteristic spectrum and by choosing one or more lines (the most sensitive lines) the element can be identified (Boumans 1987a, 6). In a sample, which consists of different elements, line coincidences and overlaps in the spectrum are inevitable. These can be overcome partly by enhancing the resolution so that the instrument is able to distinguish between the lines that are close to each other (e.g. rare

earth elements) and partly by selecting other spectral lines of the given element for identification (Boumans 1987a, 12; Thompson 1987, 189).

However, exact coincidences can still occur and there are correction procedures to solve this problem carried out by the ICP-OES software (Strasheim 1987, 113; Thompson 1987, 189). Correction for background is also necessary as the light intensity captured by the detector does not purely consist of the photons emitted by the sample, but also of other photons originating from the plasma (Thompson 1987, 175). Stray light involving the reflections of the photons from the interior surfaces and photons scattered by the imperfections of the instrument can also contribute to the background continuum (Strasheim 1987, 100). The background is subtracted from the total intensity with different procedures (on-peak subtraction, off-peak subtraction) to obtain 'real' concentration data of the sample (Olesik 1987, 506, 509; Thompson 1987, 175).

The quantification of the element concentrations is based on the measurement of relative intensities of the elemental lines present in the sample and the comparison to standards with known concentrations (Boumans 1987a, 6, 18; Young and Pollard 2000, 39). Even if the amount of an element is above the detection limit, some instruments need greater certainty to identify concentrations reliably. Therefore, the limit of quantitative determination (LQD) or limit of quantification (LOQ) is used, which is calculated usually as five times the detection limit (Thompson 1987, 183).

3.5.2 ICP-OES analysis of archaeological ceramics

ICP-OES can be used for the analysis of the chemical composition of ceramic materials as well. About 100–200 mg of sample is enough for the analysis and needs to be dissolved to be suitable for introduction into the plasma (Walton 2003, 232). Ceramic samples are commonly dissolved in a mixture of hydrofluoric acid and perchloric acid ($HF–HClO_4$; Tsolakidou et al. 2002; Thompson and Walsh 2003, 39). Silicon is removed from the sample before analysis during the evaporation procedure (Thompson and Walsh 2003, 39).

ICP-OES analysis of pottery can contribute to the formation of a broad compositional database of pottery types in different areas and periods. It can enhance classification and grouping of the samples and, if enough reference data are available, may help identify the potential clay source by comparing the chemical signature of the samples and that of the surrounding geological environment (Walton 2003, 235). Raw material sourcing by chemical analysis is

based on the assumption that different clay sources provide different chemical fingerprints, and this difference is greater between deposits than within deposits (Rice 1987, 413–414; Hein et al. 2004a; Hein et al. 2004b). In an area well-known by chemical analyses, products may be linked to different workshops based on chemical differences (Orton and Hughes 2013, 153).

However, there are some considerations to be kept in mind when analysing the chemical results and identifying clay sources. Undoubtedly, the use of temper can change the chemical composition of the ceramic. Also, the use of several clay sources at one production site can be confusing and result in the false identification of multiple production sites. Incomplete mixing of raw materials or inhomogeneity of the samples can also cause difficulties. Finally, sample treatment (conservation and restoration) should be taken into account and sampling should be done carefully by avoiding contamination (Baxter and Buck 2000, 687).

3.5.3 ICP-OES analysis of the ceramic samples from Lower Austria

The preparation of the samples from Lower Austria included pinching off a small piece of the ceramic sherd and grinding it in an agate mortar to a fine powder. The sample powders were placed in sealable plastic vials for their transportation to the laboratory. The ICP-OES analysis was carried out at the geology department of Katholieke Universiteit Leuven (Belgium).

The analytical equipment consists of a Varian 720-ES instrumentation which is defined as a simultaneous ICP-OES with axially viewed plasma, supplied with a double-pass glass cyclonic spray chamber and concentric glass nebulizer 'SeaSpray' and a 'high solids' torch. A lithium metaborate ($LiBO_2$) fusion procedure (100% non-fused, CAS-13453-69-5; Flux Nr 100A-Spectroflux) in graphite crucibles was used to achieve the digestion of all silicates. This method involves the rapid dissolution in 0.42M nitric acid (HNO_3) (Suhr and Ingamells 1966). The detection limits of the measurement method are within the range of 10^{-1} and 10^{-4} mg/l.[43]

For the assessment of the quality of ICP-OES measurements three specific certified reference materials were used: GBW7311 (Chinese sediment), SO2 (sediment) and QCM-31 (light sandy soil). Performance was evaluated through calculations of relative standard deviation (precision) and relative error (accuracy) based on certified values and repeated measurements (n=3) of the certified standards by the ICP-OES instrument of the Leuven laboratory (Stanley and Lawie 2007; Abzalov 2008). Precision of the analyses was excellent (< 1%) for the major

[43] Dr Dennis Braekmans, personal communication (by email), October 2019.

elements and some trace elements including Ba, Mn, Sr, Zn and Zr, and was within 5% for Cr, Sc, V and Y. Precision for Cu, Ni, Pb, Rb, Sb and Sn exceeded 15% (*Table 8*).

The accuracy of the measurements was very good (< 5%) in the case of Fe_2O_3, SiO_2 and TiO_2, and was below 10% in the case of K_2O and MgO (*Table 8*). Values of relative error for Al_2O_3 and Na_2O were just above 10%. The rest of the major element oxides (CaO and P_2O_5) exhibited poor accuracy compared to the certified values of one of the three reference materials. Among the trace elements, Ba, Sc, Sr, V and Y were measured with good accuracy (< 10%), while the relative error calculations for the rest of the trace elements (Cr, Cu, Mn, Ni, Pb, Zn and Zr) exceeded 10%. Replicate measurements of the standards by the Leuven ICP-OES instrument consistently underestimated the amount of K_2O, Na_2O, Cr, Mn and Ni, while overestimated the amount of CaO.

3.5.4 Statistical analyses of chemical data

Statistical analysis of chemical data can contribute to the interpretation of results. Chemical data of archaeological ceramics are normally multivariate (or multidimensional), i.e. having three or more variables (that are oxides/elements) and thus difficult to visualise graphically (Baxter and Buck 2000, 684). Statistical analysis reduces the information to a more comprehensible level. However, statistical results still need interpretation and an understanding of data transformation during statistical analysis.

Before turning to statistics, it is worth taking an overview of the data set (Massart and Kaufman 1983, 211; Baxter and Buck 2000, 695). Significant differences and extremities in the data can be recognised at this stage. Histograms, box plots, bivariate and trivariate plots can also be of help in preliminary data analysis as they visualise the values and thus ease perception (Baxter and Buck 2000, 698–700).

Two of the most common statistical analyses carried out on archaeological compositional data are principal component analysis and cluster analysis. A brief theoretical description of these methods can be found below.[44]

[44] For the mathematical background of principal component analysis and cluster analysis the reader is advised consulting the referred literature.

Table 8. Relative standard deviation and relative error calculations for data quality assessment (precision and accuracy) of ICP-OES analysis

	GBW7311						SO2					QCM-31				
	Certified (ppm)	Mea-sured (n=3)	Recalcu-lated (ppm)	Standard deviation	Relative standard deviation (%)	Relative error (%)	Certified	Mea-sured (n=3)	Standard deviation	Relative standard deviation (%)	Relative error (%)	Certified	Mea-sured (n=3)	Standard deviation	Relative standard deviation (%)	Relative error (%)
Al_2O_3 (wt%)	54000	10,50	55566	0,01	0,00	2,90	15,1	14,73	0,06	0,42	-2,43	15,41	13,73	0,05	0,36	-10,90
CaO (wt%)	3360	0,52	3686	0,00	0,00	9,71	2,77	2,78	0,01	0,23	0,26	1,5	2,27	0,01	0,35	51,36
Fe_2O_3 (wt%)	30700	4,52	31617	0,01	0,00	2,99	7,89	7,87	0,03	0,35	-0,22	4,73	4,56	0,02	0,34	-3,62
K_2O (wt%)	27200	3,19	26464	0,01	0,00	-2,70	2,94	2,77	0,02	0,69	-5,66	3,16	2,88	0,02	0,58	-8,99
MgO (wt%)	3740	0,58	3495	0,00	0,00	-6,55	0,89	0,89	0,00	0,22	-0,21	1,27	1,33	0,01	0,49	4,78
Na_20 (wt%)	3400	0,41	3031	0,00	0,00	-10,86	2,48	2,35	0,01	0,45	-5,35	2,35	2,33	0,02	0,98	-0,79
P_2O_5 (wt%)	255	0,04	183	0,01	0,00	-28,18	0,69	0,76	0,01	0,72	10,66	0,34	0,31	0,00	0,66	-9,92
SiO_2 (wt%)	356500	76,67	358369	0,12	0,00	0,52	53,42	52,24	0,14	0,27	-2,20	65,06	64,78	0,25	0,39	-0,43
TiO_2 (wt%)	2100	0,36	2161	0,00	0,00	2,91	1,43	1,37	0,00	0,19	-4,41	0,52	0,51	0,00	0,74	-1,24
Ba (ppm)	260	234,23	234	0,51	0,22	-9,91	966	979,23	3,22	0,33	1,37	970	879,32	2,55	0,29	-9,35
Cr (ppm)	40	38,28	38	0,29	0,76	-4,30	16	11,99	0,29	2,44	-25,08	89,6	85,73	0,00	0,00	-4,32
Cu (ppm)	78,6	79,26	79	1,55	1,95	0,84	7	1,01	0,51	50,00	-85,53	30,8	25,87	1,01	3,92	-16,00
Mn (ppm)	2490	2435,91	2436	4,02	0,16	-2,17	900	696,61	2,28	0,33	-22,60	540	414,80	2,50	0,60	-23,18
Ni (ppm)	14,3	6,24	6	2,88	46,10	-56,37	8	0,68	6,33	937,75	-91,56	31,9	27,06	6,89	25,46	-15,18
Pb (ppm)	-	623,94	624	19,15	3,07	-	21	11,82	2,92	24,74	-43,72	43,8	47,35	5,86	12,37	8,10
Rb (ppm)	-	406,41	406	2,92	0,72	-	78	72,60	11,70	16,11	-6,93	-	128,52	10,56	8,22	-
Sb (ppm)	-	-10,12	-10	30,35	-300,00	-	-	1,69	38,68	2291,29	-	-	15,22	33,27	218,58	-
Sc (ppm)	7,4	6,75	7	0,29	4,33	-8,85	11,3	10,30	0,29	2,84	-8,86	-	7,61	0,00	0,00	-
Sn (ppm)	-	363,24	363	15,99	4,40	-	-	14,35	3,09	21,57	-	-	11,16	14,14	126,70	-
Sr (ppm)	29	28,84	29	0,00	0,00	-0,56	340	338,51	1,27	0,38	-0,44	-	246,89	1,06	0,43	-
V (ppm)	46,8	44,69	45	1,27	2,85	-4,51	57	58,92	0,58	0,99	3,37	58,7	59,02	1,28	2,16	0,54
Y (ppm)	42,7	41,89	42	0,57	1,36	-1,90	40	36,10	0,44	1,21	-9,76	-	17,37	0,33	1,88	-
Zn (ppm)	373	376,90	377	1,52	0,40	1,04	117	247,17	1,52	0,61	111,26	120	107,89	0,29	0,27	-10,10
Zr (ppm)	153	136,42	136	0,77	0,57	-10,83	760	588,72	1,63	0,28	-22,54	-	265,15	0,77	0,29	-

Some of the challenges of the statistical analyses include missing values in a data set as a result of elements being present with an amount below the detection limit. Those samples which miss values are not incorporated in the statistical analysis. To overcome this, the missing value can be replaced by a small amount close to zero. Alternatively, a value equal to the detection limit, or half-way between the detection limit and zero can also be used (Baxter and Buck 2000, 724).

Principal component analysis

Principal component analysis (PCA) makes possible the conversion of multivariate data set into a two-dimensional picture which can help in differentiating between chemical groups of the samples (Baxter 1994, 48). It also provides information about the relationship (correlation) of the variables (oxides/elements) and about which variables are influential for the data structure and how (Baxter 1994, 48–49). PCA reduces dimensions by producing new variables based on the variance in the data (Baxter and Buck 2000, 701). These new uncorrelated variables (principal components, PCs) are linear transformations of the initial correlated variables, which attempt to preserve most of the variability of the original data (Aitchison 1986, 184; Baxter 2003, 73). The first PC has maximum variance followed by the second PC, third PC and so on (Aitchison 1986, 185).

Data treatment is needed before carrying out PCA so that those variables which have higher variance do not dominate, but have the same weight in the analysis as variables with a lower variance (Baxter and Buck 2000, 702). This can either be done through standardisation or log transformation of the data. Standardisation includes the transformation of variables to have mean zero and unit variance and is usually incorporated in the PCA software (Baxter and Buck 2000, 702). Log transformation of data results in the transformation of data to logarithms (base 10; Baxter and Buck 2000, 702). Both data treatments normally have very similar outcome (Baxter and Buck 2000, 703).

PCA, among others, results in two graphs: a scatterplot showing the distribution of the samples based on the principal components (new variables) and a vector plot of the original variables explaining this distribution. When examining these two graphs together, samples plotted close to a vector are rich in that element which is represented by the vector and samples plotted far from a vector are poor in that element which is represented by the vector (Baxter and Buck 2000, 703–704). The vector plot also shows the relationship among variables. Strong positive

correlation, low correlation or strong negative correlation exist between two variables if their vectors show acute angles, approximate right angle or oblique angles, respectively (Baxter 1994, 70; Baxter and Buck 2000, 703). A unit circle can be drawn around the centre of the vector plot and the extent of how close a vector approaches this circle is the measure how well the given element is represented and how much it contributes to the PCA (Baxter 1994, 70; Baxter and Buck 2000, 703).

Cluster analysis

Cluster analysis is a generic term for statistical analyses, which create clusters based on the similarity of the data (Baxter 1994, 104; Baxter and Buck 2000, 705). This can be achieved by using various methods, mostly hierarchic agglomerative methods (Baxter and Buck 2000, 705). This means that the analysis starts with one case (sample), which is merged with the most similar case, and then again this cluster is merged with the most similar case etc., until one large cluster remains (Massart and Kaufman 1983, 78; Baxter 2003, 90). A common representation of the hierarchical agglomerative clustering is the dendrogram (Massart and Kaufman 1983, 75).

Regardless of the applied method, cluster analysis needs the standardisation or log transformation of data beforehand, similarly to PCA (Baxter and Buck 2000, 705). For defining the dissimilarity between cases, commonly Euclidean or squared Euclidean distance are used irrespective of the chosen method (Baxter and Buck 2000, 705).

The hierarchic agglomerative methods are different in terms of the criteria based on which the clusters are merged (Massart and Kaufman 1983, 79). The method of *single linkage* (also called nearest neighbour) merges those two clusters which have the two most similar cases (one from each cluster; Massart and Kaufman 1983, 79; Baxter 1994, 141). In contrast, in *complete linkage* (also called furthest neighbour), the largest distance existing between two cases of two clusters is considered as a grouping/separating criterion (Massart and Kaufman 1983, 79; Baxter and Buck 2000, 705). *Average linkage* uses the average distance between all pairs of cases of two clusters to identify the similarity between clusters, and groups together the most similar clusters (Baxter 1994, 142; Baxter and Buck 2000, 705). Average linkage has two variants: the weighted pair group and unweighted pair group methods (Massart and Kaufman 1983, 90–91). Another popular clustering method used with chemical data of ceramics is the *Ward's method* (or error sum of squares method; Baxter and Buck 2000, 705; Massart and

Kaufman 1983, 80–81), which considers the clusters that can be formed and “decides to retain the one for which the increase of “heterogeneity” is least” (Massart and Kaufman 1983, 81). Among these methods, average linkage and Ward’s method are the most common in ceramic analysis as their results tend to be more easily interpretable than those of the others (Baxter 1994, 143–144; Baxter and Buck 2000, 705).

As much as cluster analysis can add to the interpretation of the chemical data, it must be noted that it can also be misleading as it forces grouping and creates a structure even if the data are random and no real structure exists (Baxter 2003, 93; Baxter and Buck 2000, 707).

3.5.5 Summary

ICP-OES analysis of a ceramic sherd defines its chemical signature, which can facilitate the identification of origin through a comparison with the geological environment. It also provides data about other aspects of ceramic production and often, if large amount of data is available, the differentiation between products of different workshops is possible. Statistical analysis of chemical data can ease interpretation by converting the data into visually more user-friendly graphs and dendrograms.

3.6 X-ray diffraction

X-ray diffraction (XRD) can be used to characterise single crystals as well as to identify, characterise and quantify the crystalline phases in a multiphase material (Jenkins and Snyder 1996, 231). Besides its industrial and geological application for the analysis of materials such as corrosion products, alloys, clays and ores, it can also be used for archaeological pottery analysis (Cullity and Stock 2014, 284). As archaeological ceramics are analysed mainly in powder form, this subchapter focuses on powder analysis by XRD, also called powder X-ray diffraction (PXRD) or X-ray powder diffraction (XRPD). The following sections describe the instrumentation and how the analysis is carried out from sample preparation to data analysis as well as the XRD analysis of archaeological ceramics and the use of this method in archaeology.

3.6.1 The method of XRD

Sample preparation

For phase identification, the samples are required to be in powder form (with a grain-size below 0.1 mm), which can be achieved by grinding (Warren 1969, 51). When placing the powder into the sample holder, care must be taken to ensure that the surface of the powder sample is flat and the grains are randomly orientated as surface roughness and preferred orientation have a significant influence on the results of the analysis (Cullity and Stock 2014, 197–198).

Instrumentation and measurement

XRD instruments usually consist of an X-ray tube with a high-voltage generator, a diffractometer and a detector with counting electronics (Jenkins and Snyder 1996, 178). The instrument is connected to a computer, which controls the measurement and records the data, and where data analysis can be carried out using different pieces of software.

The source of radiation is an X-ray tube, which can be of different types such as a sealed tube or a rotating anode tube (Jenkins and Snyder 1996, 97).[45] The sealed tube includes a tungsten

[45] Instead of tube sources, synchrotron radiation can also be used, which produce X-rays of very high intensity making possible the analysis of certain materials, which cannot be analysed with a conventional XRD or present in a small amount (Cullity and Stock 2014, 25; Maritan 2019, 5089).

filament (cathode) and a target metal (anode), with the latter usually being made of copper (can also be of chromium, iron etc.; Jenkins and Snyder 1996, 108; Cullity and Stock 2014, 19). The transformer provides the tube with high voltage and the filament with a filament current (Jenkins and Snyder 1996, 100). When the current passes through the filament, it emits electrons, which are accelerated towards the target by the high voltage in the tube (Jenkins and Snyder 1996, 106; Cullity and Stock 2014, 21). As a result of the electron bombardment, the target emits X-rays, which escape through the windows of the tube (made usually of beryllium; Cullity and Stock 2014, 21). The rotating anode tube produces X-rays of a higher intensity than the sealed tube as the target is rotated at high speed bringing fresh surface to the flow of electrons, thus a larger surface is irradiated (Jenkins and Snyder 1996, 118, 119; Cullity and Stock 2014, 23).

X-rays are electromagnetic waves with relatively short wavelength and high energy, located between the gamma rays and ultraviolet rays in the electromagnetic spectrum (Jenkins and Snyder 1996, 2; Cullity and Stock 2014, 2). The X-radiation consists of a continuous radiation (bremsstrahlung) and characteristic wavelengths, with the latter being unique for each target material (Jenkins and Snyder 1996, 3).[46] The characteristic wavelengths are sets of lines in the X-ray spectrum (*K, L, M* sets) of which the $K\alpha$ ($K\alpha_1$ if possible) of the *K* lines is used in XRD measurements (Jenkins and Snyder 1996, 266–267; Cullity and Stock 2014, 7, 191).

The diffractometer includes two sets of slits: in for the tube radiation and out for the radiation diffracted from the sample (Warren 1969, 54; Cullity and Stock 2014, 201–202). The sample is placed between the entrance slits (at the X-ray tube) and the receiving slits (at the detector) at equal distances from them and can be rotated in order to allow more crystals to diffract and to reduce the effects of preferred orientation (Warren 1969, 55; Jenkins and Snyder 1996, 255–256). During the measurement, either the detector is rotated about the sample through 2*x* degrees while the sample is rotated through *x* degrees or, in recent instruments, the tube and the detector perform angular motions (through degrees *x* and *x*) to have the appropriate angle for focusing and to cover the required range of diffraction angles (Ermrich and Opper 2013, 31; Cullity and Stock 2014, 193).

[46] The process of how the continuous and characteristic X-rays are produced has been described earlier in this thesis related to the method of SEM-EDS, see Section 3.4.1.

The X-rays arriving from the X-ray tube pass through the entrance slits, reach the sample and diffract from the crystals of the sample (Cullity and Stock 2014, 192–193). The X-rays are diffracted by the crystallographic planes formed by atoms, molecules or ions, which have a regular and repetitive arrangement in every crystalline material (Cullity and Stock 2014, 31). Diffraction is a type of scattering, which only takes place if special conditions are present (defined by the so-called Bragg's law), as X-rays scattered from parallel crystallographic planes (or family of planes) should strengthen each other (constructive interference) to be able to form a diffracted beam (Jenkins and Snyder 1996, 48; Cullity and Stock 2014, 93–94). Each material has a different set of diffraction angles depending on their unique crystal structure, especially on the spacing between the planes (*d*-spacing; Jenkins and Snyder 1996, 151; Cullity and Stock 2014, 305–306).

The diffracted radiation goes through the receiving slits and arrives at the detector. Before detection however, the radiation, consisting of several wavelengths, should be reduced to a single wavelength (process of monochromatisation) in order to eliminate the measurement of unwanted peaks and reduce the background noise (Jenkins and Snyder 1996, 155; Cullity and Stock 2014, 5). This can be done by a filter or a monochromating crystal placed either in the incident beam or more commonly in the diffracted beam (Cullity and Stock 2014, 193).

The detector converts the X-rays into an electric current and the current is converted into voltage pulses (Jenkins and Snyder 1996, 121). The energy of a diffracted X-ray photon (and thus its wavelength) determines the size of the pulse and therefore filtering of unwanted wavelengths can also be done at this stage of the analysis with a pulse height analyser (Jenkins and Snyder 1996, 136). The pulses are counted by the counting electronics: a rate meter or more commonly a scaler (Cullity and Stock 2014, 224, 228). The data are recorded by a computer, a diffractogram is produced including the intensities (number of counts) and diffraction angles (2Θ), and *d*-spacing is calculated (Jenkins and Snyder 1996, 287).

Data analysis

The interpretation of a diffractogram is not always obvious as in addition to the diffraction peaks it can also include unwanted peaks (peaks of other than the required wavelength) and background noise (consisting of scatter from the sample and the instrument as well as fluorescence of the sample; Jenkins and Snyder 1996, 154–155). Therefore, data treatment can

be carried out such as the removal of unwanted wavelengths and the subtraction of the background (Jenkins and Snyder 1996, 291).

Qualitative analysis, i.e. the identification of the phases, is done by comparing the diffractogram to known diffraction patterns. Computer programs can be used for this purpose (Search-Match programs), which list the phases with the closest pattern to the unknown from which the user can choose the appropriate phases (Cullity and Stock 2014, 296).

Quantitative analysis can also be carried out as the peak intensities are proportional to the concentrations of the different phases in the analysed sample (Cullity and Stock 2014, 283). For quantification of the phases of a powder sample usually the so-called Rietveld method is used, but internal or external standards may be used as well (Young 1993; Cullity and Stock 2014, 361–370).

3.6.2 XRD analysis of archaeological ceramics

Ceramic samples are usually prepared in the same way as general powder samples. The analysis process is the same as for other powder materials, and adjustments (step size, 2Θ range etc.) can be made that are appropriate for the analysed ceramic material and the purpose of the XRD analysis.

XRD can be used to detect the mineral phases of which the pottery is composed. Two main groups of minerals can be distinguished in the ceramics: primary minerals, which were present in the clay before the firing process, and secondary minerals, which were formed during firing and during the use and the burial of the pottery (Maggetti 1981, 37). Some minerals such as clay minerals and post-burial phases may not be observed in the polarising microscope because of their small size, which is one of the reasons why XRD is used in pottery analysis (Artioli 2010, 239–240; Szakmány 2013, 738; Quinn and Benzonelli 2018; Maritan 2019, 5088). Another advantage of this method is that it can provide a more precise identification than polarising microscopy by determining the phases of the minerals, as minerals can have a range of compositional variations. XRD of archaeological ceramics may also yield information about the firing atmosphere (Maritan 2019, 5088).

However, the main use of XRD in archaeological ceramic analysis is connected to the estimation of ancient firing temperatures. Since ceramics can be interpreted as artificial metamorphic rocks, the transformation (hardening) of the clay to form pottery can be

considered as high-temperature and low-pressure metamorphism, which takes place during firing and is associated with mineralogical changes (Riccardi et al. 1999, 393–394; Cultrone et al. 2001, 621; Heimann and Maggetti 2014, 70). Some mineral phases are sensitive to the changes in temperature and may form or decompose at certain temperatures. Based on the presence or absence of these phases, an estimation of the firing temperature is possible (Quinn and Benzonelli 2018). Some of these phases are presented in *Table 9* below.

Table 9. Mineral phases in ceramics indicative of firing temperatures. Clay composition or types of inclusions which influence the formation of some phases are indicated in brackets.[47]

Name of phase	Decomposition/formation	Temperature range
Clay minerals		
Smectite	Decomposition	300–550 °C
Kaolinite	Decomposition	500–600 °C
Chlorite	Decomposition	400–700 °C
Montmorillonite	Decomposition	800–950 °C
Illite	Decomposition	800–950 °C
Muscovite	Decomposition	800–1000 °C
Carbonates		
Calcite	Decomposition	700–900 °C
Dolomite	Decomposition	700–800 °C
Hematite	Formation	700–1000 °C
Gehlenite	Formation and decomposition (calcareous clays/ carbonate inclusions)	800–950 °C and 1100 °C
Diopside	Formation (calcareous clays/carbonate inclusions)	800–1000 °C
Wollastonite	Formation (calcareous clays/carbonate inclusions)	850–1000 °C
Spinel	Formation	850–1100 °C
Mullite	Formation (non-calcareous clays)	900–1100 °C
Anorthite	Formation (calcareous clays/carbonate inclusions)	950–1050 °C

When carrying out firing temperature estimations some considerations must, however, be taken into account as not only temperature can define the changes in mineralogy. The composition of the clay (calcareous, non-calcareous) and the types of inclusions present have a great influence on what types of new phases form during firing (Riccardi et al. 1999, 394, 396). Mineralogical changes seem to be more significant if carbonates are present; phases in

[47] Based on Maggetti 1981, 39: Fig. 4; Maggetti 1982, 127: Fig.11, 128: Fig. 15, Fig. 16; Maggetti 1986, 96: Fig. 10, 98: Fig. 13; González-García et al. 1990, 374; Orts et al. 1993, 195–196; Maggetti et al. 1994, 174: Figure 11, 175: Figure 12; Dondi et al. 1995, 304: Figura 3; Duminuco et al. 1998, 189; Jordán et al. 1999, 230–232; Riccardi et al. 1999, 396, 399, 403; Cultrone et al. 2001, 624, 633; Hein et al. 2002, 180; Rodriguez-Navarro et al. 2003, 714: Table 1.; Cultrone et al. 2005, 40: Table 1; Maritan et al. 2006, 6: Fig. 4, 7: Fig. 5; Nodari et al. 2007, 4668: Fig. 2; Jordán et al. 2009, 177: Table 5; Trindade et al. 2009, 348: Fig. 4, 349: Fig. 5; Artioli 2010, 237: Table 3.4; Heimann and Maggetti 2014, 87: Figure 6.13, 89: Figure 6.15; El Ouahabi et al. 2015, 410–411; Daghmehchi et al. 2018, 148; Laita and Bauluz 2018, 287: Fig. 2; Miras et al. 2018, 178: Fig. 2; Viani et al. 2018, 113–114, 113: Table 2–3.

carbonate-free ceramics do not show substantial transformation below 1000 °C (Maggetti 1982, 128; Duminuco et al. 1998, 189; Cultrone et al. 2001, 626–627, 630; Heimann and Maggetti 2014, 88). Additionally, the grain sizes of the inclusions, the firing atmosphere (oxidising, reducing) and the soaking time (the time for which the highest temperature was sustained) may also be important factors and can have an effect on phase formation, transformation or decomposition (Maggetti 1981, 39–41; Maritan et al. 2006; Heimann and Maggetti 2014, 87–89; Quinn and Benzonelli 2018; Viani et al. 2018, 115).

A major advantage of XRD is that it is relatively quick as samples can be analysed in automated batches, so the analysis can be done overnight, for example. The sample preparation is not complicated and only a small amount of sample is needed. The data analysis is relatively quick and easy since the introduction of computer programs; however, some prior knowledge is still required regarding the composition of the sample to choose the appropriate phases from the list provided by the software. XRD analysis is cost-effective and easily accessible, as instruments are commonly owned by different institutions (Maritan 2019, 5088).

Naturally, there are also drawbacks of XRD. It requires powder samples thus it is destructive.[48] Preparation of random samples if the ceramics are not homogeneous (e.g. coarse-grained) can be another difficulty. This analysis is useful for identifying the main components of the sample, but phases present in a small amount (5–10%) are not detected because of the relatively high detection limit (Cultrone et al. 2001, 630; Rodriguez-Navarro et al. 2003, 715). Ceramic petrography or SEM is advised to be carried out in addition to XRD so that primary and secondary phases can be distinguished (e.g. in case of firing temperature estimation, it is important to identify if calcite was present in the pottery before firing or formed during burial; Szakmány and Nagy 2017, 259).

3.6.3 XRD analysis of the ceramic samples from Lower Austria

The preparation of the samples from Lower Austria included the grinding of small pieces of the ceramic sherds in an agate mortar and back-loading the powder samples into the sample holders.

[48] A new XRD technique called micro X-ray diffraction (μXRD) is also available for identifying areas of the ceramics on a microscopic level (e.g. individual mineral grains) *in situ* which is non-destructive (Flemming 2007; Maritan 2019, 5089).

The analysis was carried out at Cranfield University (Shrivenham campus) using a PANalytical X'Pert PRO Multi-Purpose Diffractometer with Cu Kα radiation. The analysis conditions were 40 kV and 40 mA. A diffraction angle range of 5° 2Θ – 80° 2Θ was scanned with a step size 0.013° 2Θ s^{-1} and diffracted X-rays were detected by a PIXcel strip detector. Phases were identified using the Crystallographica Search-Match software.

3.6.4 Summary

XRD analysis permits the identification of mineral phases present in the samples, often those phases that are abundant but too small to be investigated by polarising microscopy (e.g. clay minerals). Based on the presence or absence of certain temperature-sensitive phases, the estimation of firing temperatures of the studied vessels can be carried out, which may help outline past firing practices and contribute to the reconstruction of ancient ceramic technology.

4 RESULTS OF THE ANALYSES

Following the description of the different methods used for ceramic analysis in this thesis, here the results are reported by analysis techniques. Graphite-free and graphite-containing ceramics are often treated separately and usually petrographic groups are used as a basis to present the data. In this chapter, the collective results are discussed, which are based on the data of the individual samples detailed in the appendices.

4.1 Macroscopic analysis

The macroscopic characteristics of all 135 ceramic samples were investigated and are detailed below including fabric, vessel form, traces of the forming technique and decoration. A table presenting the results of the macroscopic analysis of each sample is shown in Appendix B.

4.1.1 Fabrics

Two main assemblages can be distinguished within the studied ceramic material: graphite-free and graphite-containing pottery including 81 and 54 samples, respectively. Various fabrics can be differentiated within both types.

Graphite-free ceramics

Graphite-free ceramics can be split into three groups of fabrics based on composition: micaceous fabrics, feldspar and quartz-rich fabrics and carbonate rock-containing fabrics (*Table 10*). The naming of the groups refers to the inclusions, which are most distinctive or abundant within the groups, i.e. mica, feldspar + quartz and carbonate rock fragments, respectively.

Micaceous fabrics

Micaceous fabrics are the most common among graphite-free ceramics including 54 samples. They are all characterised by reddish-brown to greyish-brown colour often varying within one sample (Munsell notation: 5YR 4/6 – 10YR 3/2), usually a Mohs' scale hardness between 2 and 3,[49] and harsh or rough feel. They are divided into two 'gold mica' fabrics (53 samples) and a 'white mica' fabric represented by one sample only (*Table 11, Figure 46*).

[49] A few (8) samples of gold mica fabric have a hardness under 2 of the Mohs scale. Most of them (7) represent fabric GMA, but one also occurs in GMB.

Table 10. Graphite-free fabrics and samples

MICACEOUS FABRICS (54)	• **Gold mica A** (GMA) – 3, 6, 8, 10, 25, 26, 37, 64, 65, 66, 67, 68, 69, 70, 71, 72, 88, 91, 92, 93, 94, 95, 96, 97, 98 • **Gold mica B** (GMB) – 1, 4, 11, 14, 22, 23, 27, 28, 29, 30, 38, 39, 40, 41, 42, 43, 44, 55, 56, 60, 61, 63, 73, 74, 75, 76, 87, 90 • **White mica** (WM) – 5
FELDSPAR AND QUARTZ-RICH FABRICS (23)	• **Feldspar + quartz A** (FQA) – 9, 12, 15, 18, 19, 20, 45, 51, 77, 78, 79, 80, 81 • **Feldspar + quartz B** (FQB) – 2, 7, 16, 17, 24, 46, 47, 48, 82, 83
CARBONATE ROCK-CONTAINING FABRICS (4)	• **Carbonate rock A** (CRA) – 57, 58, 59 • **Carbonate rock B** (CRB) – 89

Table 11. Gold mica (GMA and GMB) and white mica (WM) fabrics

	Gold mica A (GMA)	**Gold mica B (GMB)**	**White mica (WM)**
Number of samples	25	28	1
Colour	Reddish-brown (5YR 4/6 – 7.5YR 4/4)	Greyish-brown – reddish-brown (10YR 3/2 – 7.5YR 4/4)	Reddish-brown (5YR 4/6 – 7.5YR 4/4)
Mohs' hardness	< 3	2–3	2–3
Feel	Harsh or rough	Rough	Rough
Fracture	Hackly	Irregular	Irregular
Inclusion sizes	Abundant sand-size > moderate granule-size > sparse pebble-size	Abundant sand-size > sparse granule-size	Abundant sand-size > sparse granule-size
Inclusion types	Abundant 'gold mica' (biotite) + abundant white and grey grains (feldspar and quartz)	Abundant 'gold mica' (biotite) + moderate white and grey grains (feldspar and quartz)	Abundant 'white mica' (muscovite) + moderate white and grey grains (feldspar and quartz)

Gold mica fabrics contain biotite, which (together with other similar mica types) is commonly called 'gold mica' from its shiny golden appearance when reflecting the light. The samples of gold mica fabrics are quite similar, but two fabrics can be distinguished based on slight differences in inclusion frequency and fracture characteristics: Gold mica A (GMA) and Gold mica B (GMB). Both GMA and GMB contain abundant gold mica as well as white and grey

inclusions representing feldspar and quartz with different frequencies (GMA: abundant, GMB: moderate). Mostly sand-size grains occur in both fabrics, but larger, granule-size grains consisting of white and grey inclusions are also present in a moderate amount in GMA and sparse amount in GMB. Additionally, GMA includes sparse white and grey grains of pebble-size, which makes the fracture of GMA hackly. In contrast, GMB has no pebble-size inclusions, thus its fracture is slightly less coarse (irregular).

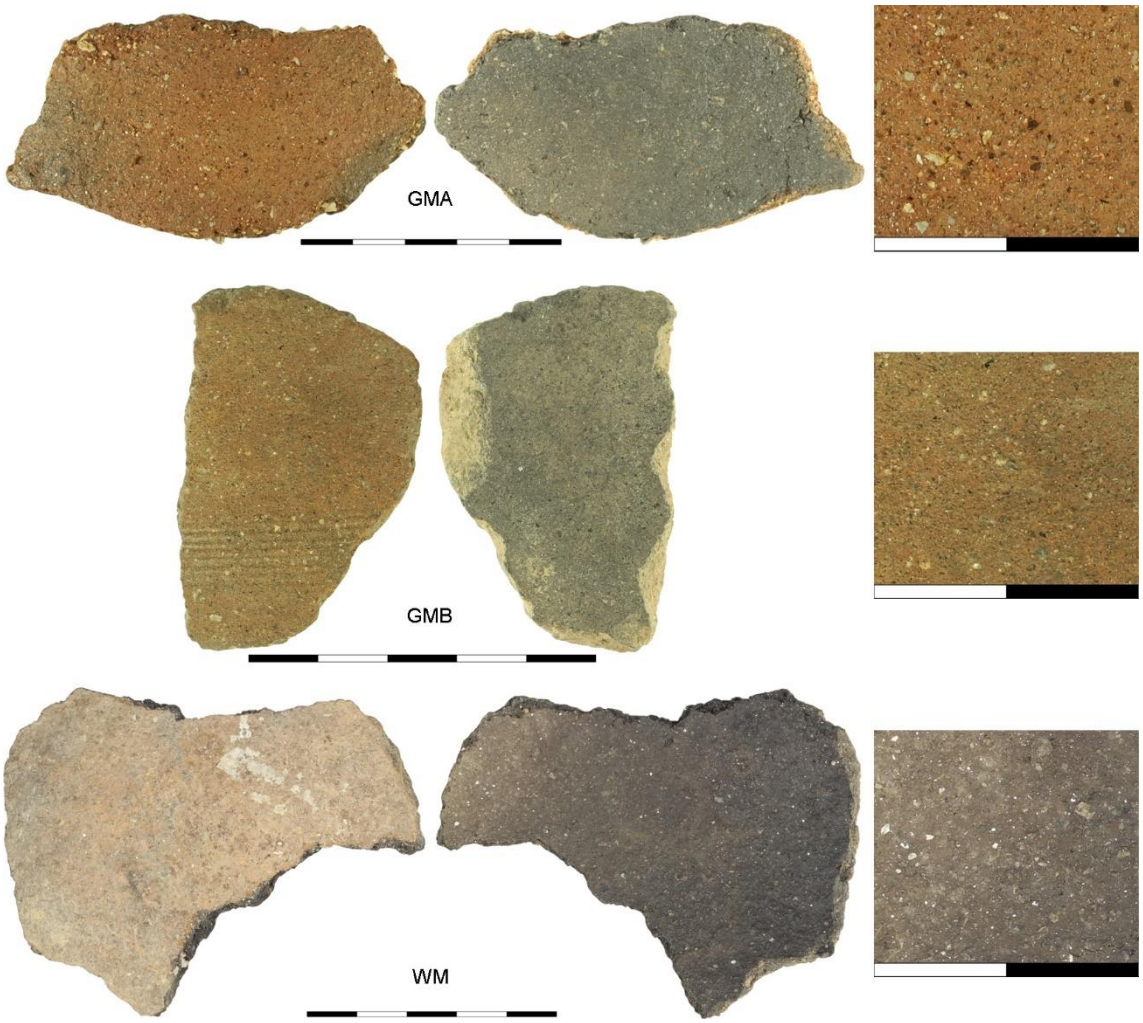


Figure 46. Micaceous fabrics: GMA (S98), GMB (S60) and WM (S5) (photo by the author)

One sample of micaceous fabric has different composition from gold mica fabrics. Instead of gold mica, it contains 'white mica', also called 'silver mica' from its shiny silvery look, which probably represents muscovite. This fabric is characterised by irregular fracture as well as abundant white mica and moderate white and grey particles (feldspar and quartz) present as sand-size (abundant) and granule-size (sparse) grains.

Feldspar and quartz-rich fabrics

Pieces of 23 ceramics have feldspar and quartz-rich fabrics which are dominated by the presence of white and grey grains indicating feldspar and quartz. They can also include few flakes of gold mica, however, the presence of this mineral is minimal in contrast with the gold-mica-rich micaceous groups. All samples of feldspar and quartz-rich fabrics have reddish-brown to greyish-brown shades (Munsell notation: 5YR 4/6 – 10YR 3/2), a hardness between 2 and 3 of the Mohs' scale, harsh or rough feel and abundant sand-size grains. Slight differences are exhibited in the inclusion sizes and frequencies, which divide the ceramics into two fabrics: Feldspar + quartz A (FQA) and Feldspar + quartz B (FQB; *Table 12, Figure 47*).

As for the differences, fabric FQA include moderate amount of granule-size grains and sparse amount of pebble-size particles which latter contribute to the hackly fracture of the ceramics. In contrast, FQB is characterised by sparse granule-size inclusions and irregular fracture. The frequency of white and grey grains is abundant in FQA and moderate in FQB. Thus, the main difference between FQA and FQB is that FQA contains generally more inclusions than FQB and large (pebble-size) grains are present in FQA in contrast with FQB. The boundary between these two feldspar and quartz-rich fabrics, however, is not always clear-cut as the samples share very similar characteristics. They also resemble the gold mica fabrics apart from the lack of gold mica.

Table 12. Feldspar and quartz-rich fabrics

	Feldspar + quartz A (FQA)	**Feldspar + quartz B (FQB)**
Number of samples	13	10
Colour	Reddish-brown (5YR 4/6 – 7.5YR 4/4)	Greyish-brown – reddish-brown (10YR 3/2 – 7.5YR 4/4)
Mohs' hardness	2–3	2–3
Feel	Harsh or rough	Rough
Fracture	Hackly	Irregular
Inclusion sizes	Abundant sand-size > moderate granule-size > sparse pebble-size	Abundant sand-size > sparse granule-size
Inclusion types	Abundant white and grey grains (feldspar and quartz) + sparse or no 'gold mica' (biotite)	Moderate white and grey grains (feldspar and quartz) + sparse or no 'gold mica' (biotite)

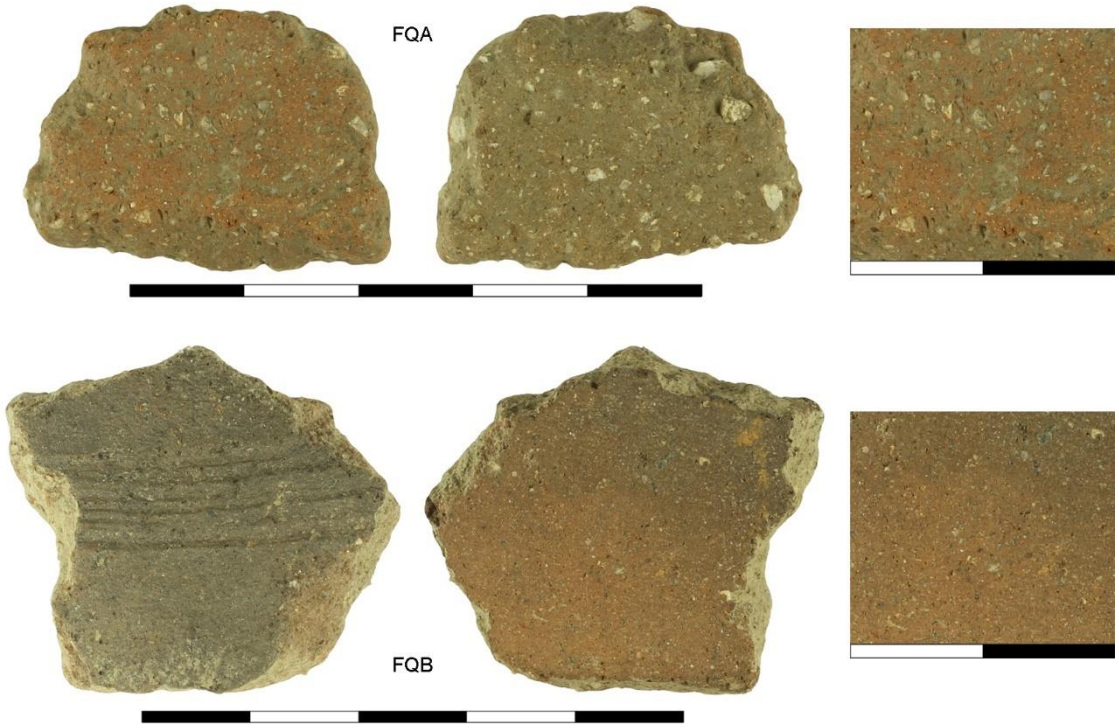


Figure 47. Feldspar and quartz-rich fabrics: FQA (S81) and FQB (S83) (photo by the author)

Carbonate rock-containing fabrics

The carbonate rock-containing fabrics are represented by four sherds including three very similar samples (fabric Carbonate rock A, CRA) and one sample, which slightly differs from the rest (fabric Carbonate rock B, CRB). All four ceramics have a hardness between 2 and 3 of the Mohs' scale, rough feel, a porous surface exhibiting numerous circular or oval voids and irregular fracture (*Table 13, Figure 48*).

Table 13. Carbonate rock-containing fabrics

	Carbonate rock A (CRA)	Carbonate rock B (CRB)
Number of samples	3	1
Colour	Brownish-grey (7.5YR 4/2 – N 4.75)	Reddish-brown (5YR 4/6 – 7.5YR 4/4)
Mohs' hardness	2–3	2–3
Feel	Rough, porous	Rough, porous
Fracture	Irregular	Irregular
Inclusion sizes	Abundant sand-size > sparse granule-size	Abundant sand-size > moderate granule-size
Inclusion types	Moderate bright white grains (calcite?) + moderate 'white mica' (muscovite)	Abundant bright white grains (calcite?)

The colour of the fabrics is slightly different showing greyish-brownish shades (CRA: 7.5YR 4/2 – N 4.75; CRB: 5YR 4/6 – 7.5YR 4/4). Both fabrics contain bright white inclusions, representing most probably calcite grains, but with different frequency, which is abundant in CRB and moderate in CRA. In addition, fabric CRA includes moderate white mica as well. Both fabrics have abundant sand-size grains and sparse (CRA) or moderate (CRB) granule-size inclusions.

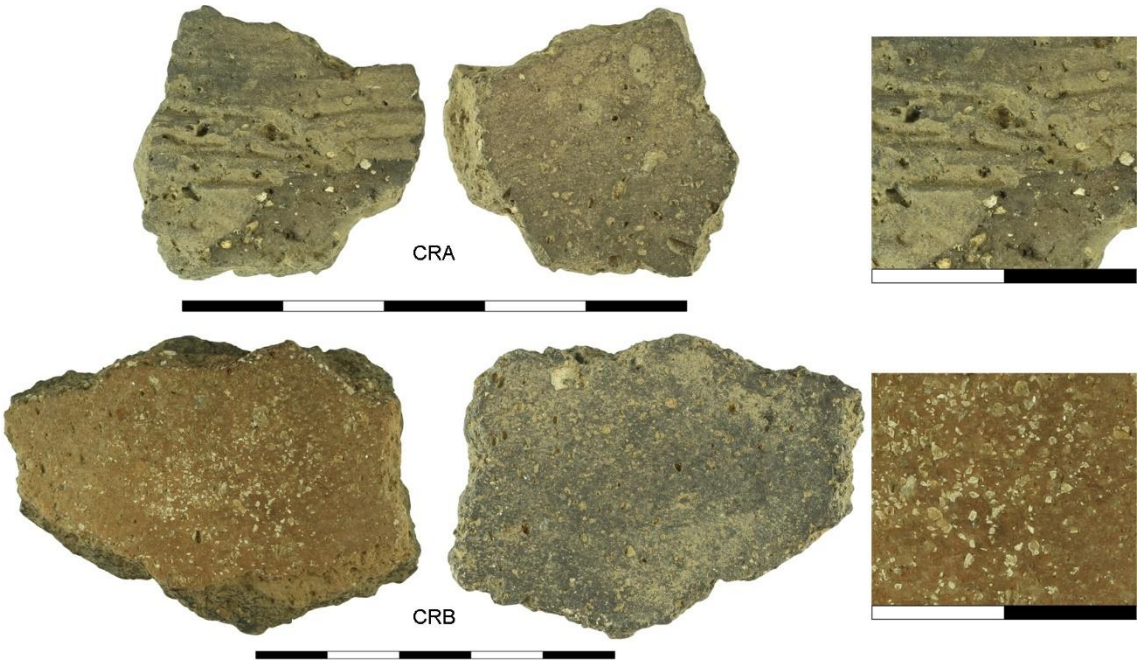


Figure 48. Carbonate rock-containing fabrics: CRA (S58) and CRB (S89) (photo by the author)

Graphite-containing ceramics

Graphite can be detected in 54 ceramics by macroscopic analysis (*Table 14*). Two fabrics of graphite-containing ceramics are distinguished: Graphite A (GA) and Graphite B (GB). Few similarities connect these graphite fabrics in addition to the graphite content; they both have a Mohs' hardness between 2 and 3 and irregular fracture (*Table 15, Figure 49*).

Table 14. Graphite fabrics and samples

GRAPHITE FABRICS (54)	• **Graphite A** (GA) – 31, 32, 33, 34, 35, 36, 84, 85, 86, 99, 100, 101, 102, 103, 104, 105, 106, 107, 108, 109, 110, 111, 112, 113, 114, 115, 116, 117, 118, 119, 120, 121, 122, 123, 124, 125, 126, 127, 128, 129, 132, 133, 134, 135 • **Graphite B** (GB) – 13, 21, 49, 50, 52, 53, 54, 62, 130, 131

However, fabric GA and GB have many differing characteristics. The main difference is compositional and is exhibited by the amount of graphite and other inclusions present in the

fabrics. Fabric GA contains abundant graphite and other inclusions are hardly distinguishable by macroscopic analysis; rarely few white and grey inclusions can be detected. In contrast, fabric GB has less graphite and moderate amount of white and grey grains also occur, occasionally with sparse or moderate amount of mica flakes.

Table 15. Graphite fabrics

	Graphite A (GA)	Graphite B (GB)
Number of samples	44	10
Colour	Dark grey (N3.5 – 5Y 4/1)	Brownish-grey – reddish-brown (10YR 3/2 – 7.5YR 5/4)
Mohs' hardness	2–3	2–3
Feel	Smooth (occasionally rough)	Rough (occasionally smooth)
Fracture	Irregular	Irregular
Inclusion sizes	Abundant sand-size > sparse granule-size	Moderate sand-size > moderate granule-size
Inclusion types	Abundant graphite (other particles are hardly detectable macroscopically)	Moderate graphite + moderate white and grey grains (feldspar and quartz) + occasionally sparse (or moderate) mica

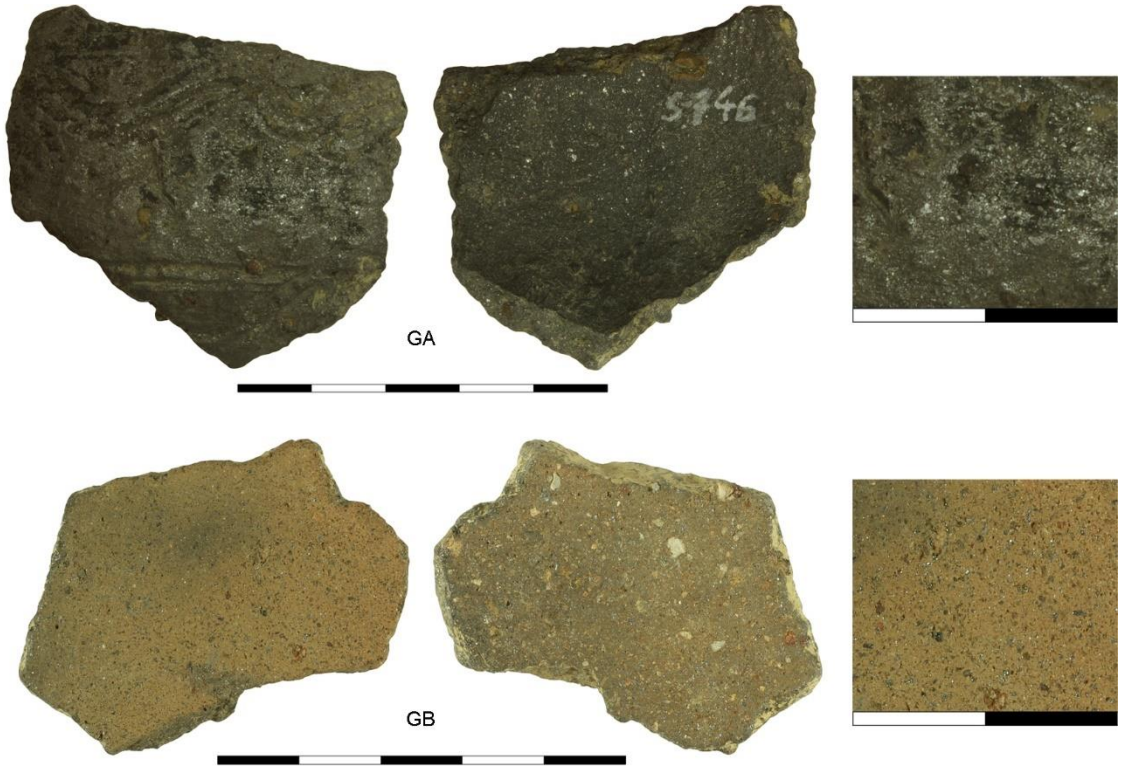


Figure 49. Graphite fabrics: GA (S128) and GB (S53) (photo by Hajnalka Herold and the author)

Ceramics of fabric GA have dark grey colour (Munsell notation: N3.5 – 5Y 4/1) and silvery appearance because of the high graphite content. Their feel is smooth, occasionally slightly rough and the fractures are irregular with rounded grains due to the relatively 'soft' nature of the graphite. The inclusions in GA are mainly of sand-size and sparsely of granule-size.

Fabric GB includes brownish-grey to reddish-brown samples (Munsell notation: 10YR 3/2 – 7.5YR 5/4) with mainly rough and occasionally smooth feel. The occurrence of sand-size and granule-size grains is moderate. From its characteristics, GB seems to be a transition category between GA and the above-mentioned graphite-free fabrics.

4.1.2 Vessel form

Most likely all ceramic sherds represent pieces of pots (jars). In those cases (37 samples), where large sherds, more sherds of the same vessel, or the whole vessels were found, the form of a jar can clearly be identified. Many of the investigated ceramics are small sherds from which the vessel shape is not obvious, but some characteristics (such as decoration, rim form, curvature etc.) suggest that they were also jars. No evidence of other vessel forms can be detected in the studied ceramic material.

The following table presents the vessels and vessel parts of which the vessel parameters could be measured (*Table 16)*. All of the pots that could be entirely reconstructed were found in the 8th–9th-century cemetery of Purgstall (S1–S30) and Mühling (S94, S98), thus the below characterisation of form will mainly concern the assemblages of these two sites. The drawings of the vessels are presented in *Figure 50* to *Figure* 53.

Pots of different sizes are present in the studied material, their height ranging from 8.5 cm to 22 cm. The maximum diameter is usually between 10 cm and 23.5 cm, and it commonly equals to or is slightly larger than the height of the vessel. Few pots (S21, S22, S26 and S29) have smaller maximum diameter than height: they represent 'oblong' forms. There are also 'squat' pots with maximum diameters more than 130% of their heights (S1, S4 and S5). The rest of the vessels can be placed between these two extremes.

The vessels usually show their largest diameter in the upper third of their height, having a well-noticeable shoulder ('shouldered' vessels: S1–S6, S9–S11, S13, S15, S16, S18–S22, S24, S26–S28, S30, S94 and S98). There are also pots having their maximum diameter in the middle zone of their body ('bellied' vessels: S7, S8, S12, S14, S17, S23, S25 and S29).

Table 16. Parameters of pots found in Lower Austria

	Fabric	Rim diameter (cm)	Base diameter (cm)	Maximum diameter (cm)	Height (cm)	Height of maximum diameter (cm)
S1	GMB	14	10.5	16	12	7
S2	FQB	13.5	9	13.5	13.5	9.5
S3	GMA	21.5	10	23	19	14
S4	GMB	12	8.5	13	8.5	5
S5	WM	17	11	19.5	14	9.5
S6	GMA	15.5	9.5	17	13.5	9
S7	FQB	12	8	12.5	10	5
S8	GMA	18.5	10	20	19	11.5
S9	FQA	17	10.5	20	19.5	13
S10	GMA	16	9.5	19.5	17.5	10.5
S11	GMB	10	7	12	11.5	7
S12	FQA	17	-	17.5	-	-
S13	GB	21.5	12.5	23	21.5	16
S14	GMB	19	13.5	23.5	22	13
S15	FQA	13	8	14.5	13.5	9
S16	FQB	14.5	7.5	15.5	14.5	9.5
S17	FQB	11	7.5	13	11	7
S18	FQA	21	13.5	23.5	20	14
S19	FQA	11.5	6.5	11.5	10	6.5
S20	FQA	21.5	12	19.5	17	12
S21	GB	8.5	6	11.5	13	9
S22	GMB	13	9.5	15	17.5	11
S23	GMB	17	13.5	20	20.5	11.5
S24	FQB	9.5	6	10.5	8.5	6
S25	GMA	15.5	13.5	18.5	19	9.5
S26	GMA	16	11.5	20	22	16.5
S27	GMB	14	9	17	16.5	11.5
S28	GMB	18.5	12.5	21.5	21	13
S29	GMB	12	9	14	16	10
S30	GMB	17.5	10.5	20	16	12
S94	GMA	14	11	18	17.5	13
S95	GMA	22.5	-	21.5	-	-
S98	GMA	15.5	11.5	17.5	18	12
S104	GA	17	-	-	-	-
S108	GA	16	-	-	-	-
S110	GA	31	-	-	-	-
S111	GA	20	-	-	-	-
S112	GA	14	-	-	-	-
S115	GA	18	-	-	-	-
S118	GA	20	-	-	-	-
S120	GA	15	-	-	-	-
S121	GA	18	-	22	-	-

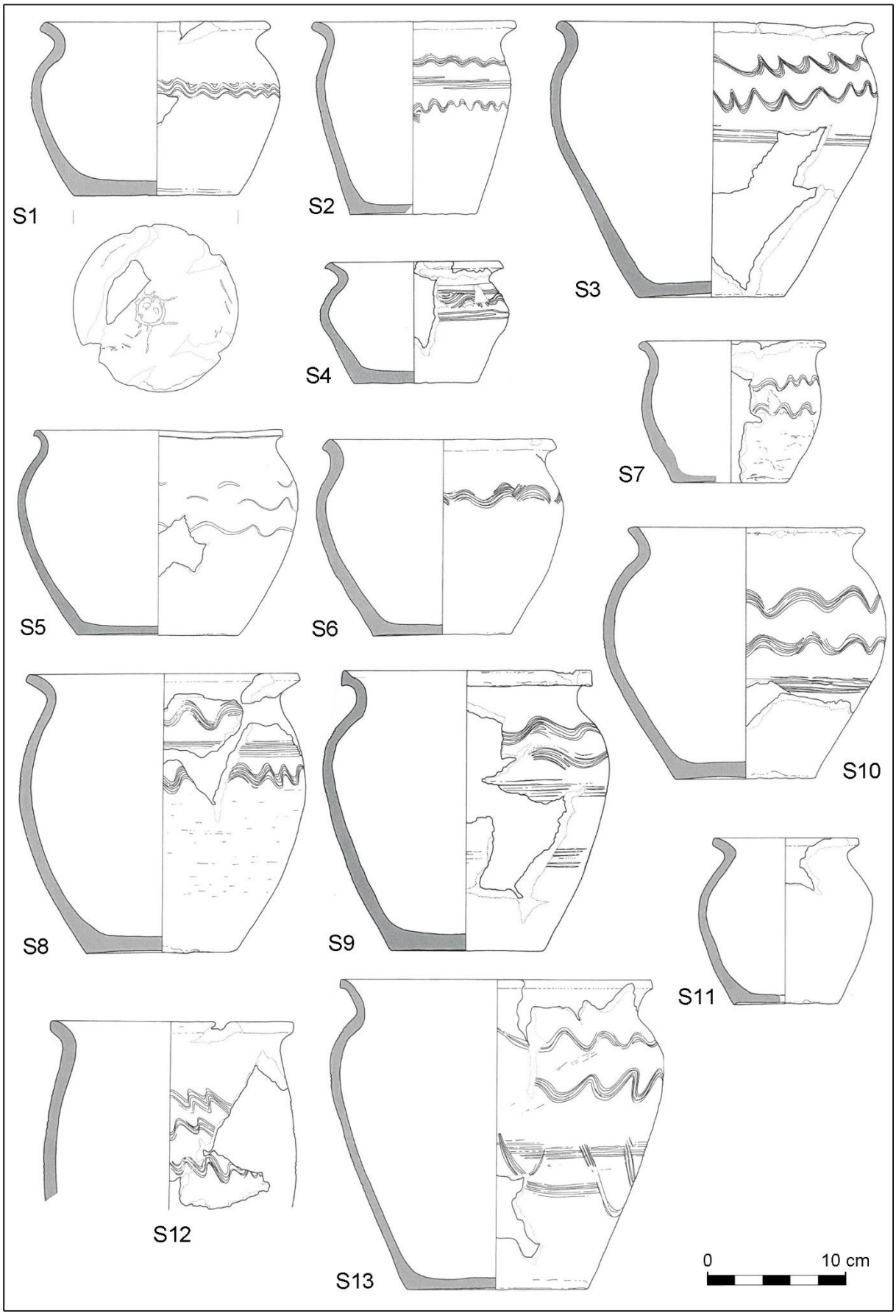


Figure 50. Vessels from the 8th–9th-century cemetery of Purgstall (excavation documentation; drawing provided by excavator Franz Sauer)

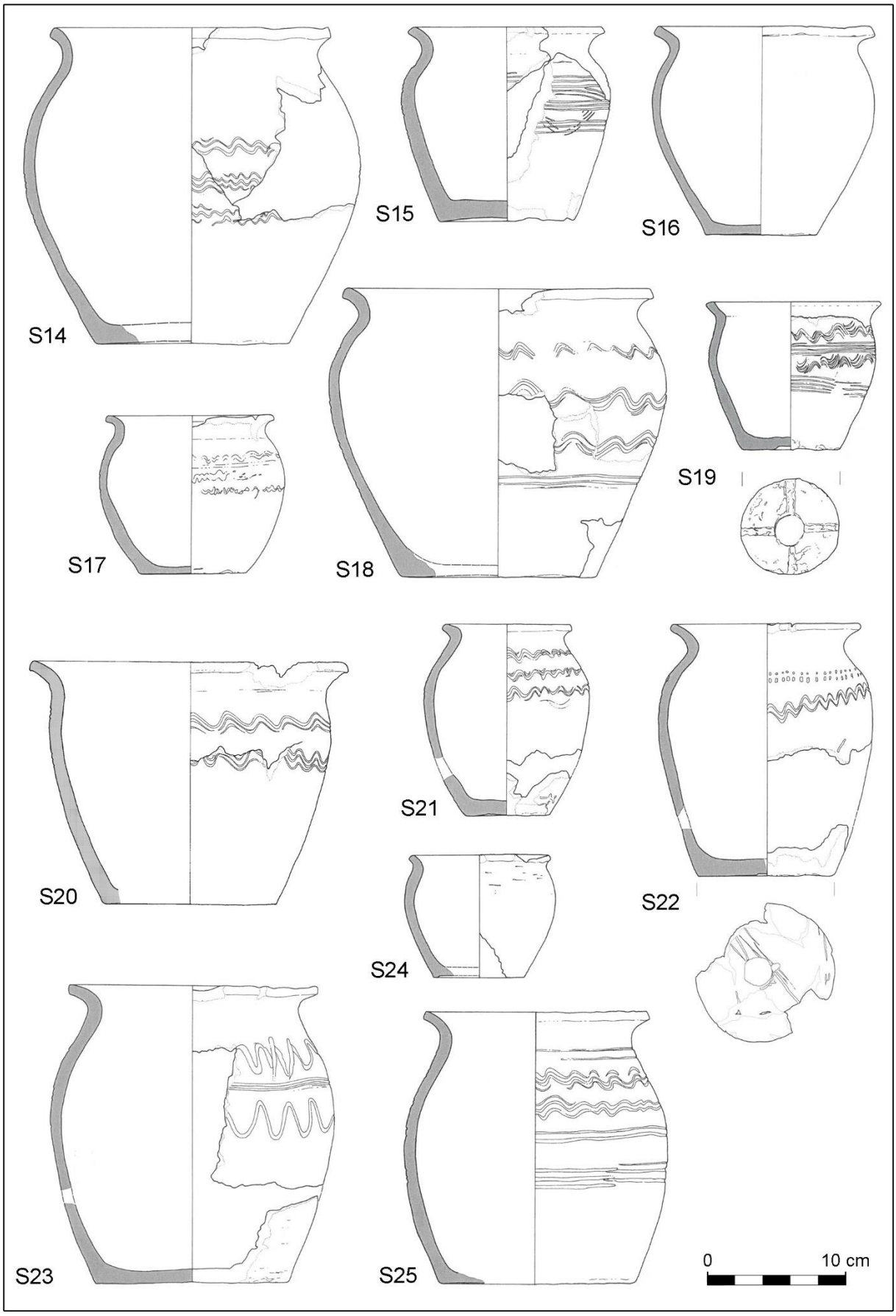


Figure 51. Vessels from the 8th–9th-century cemetery of Purgstall (excavation documentation; drawing provided by excavator Franz Sauer)

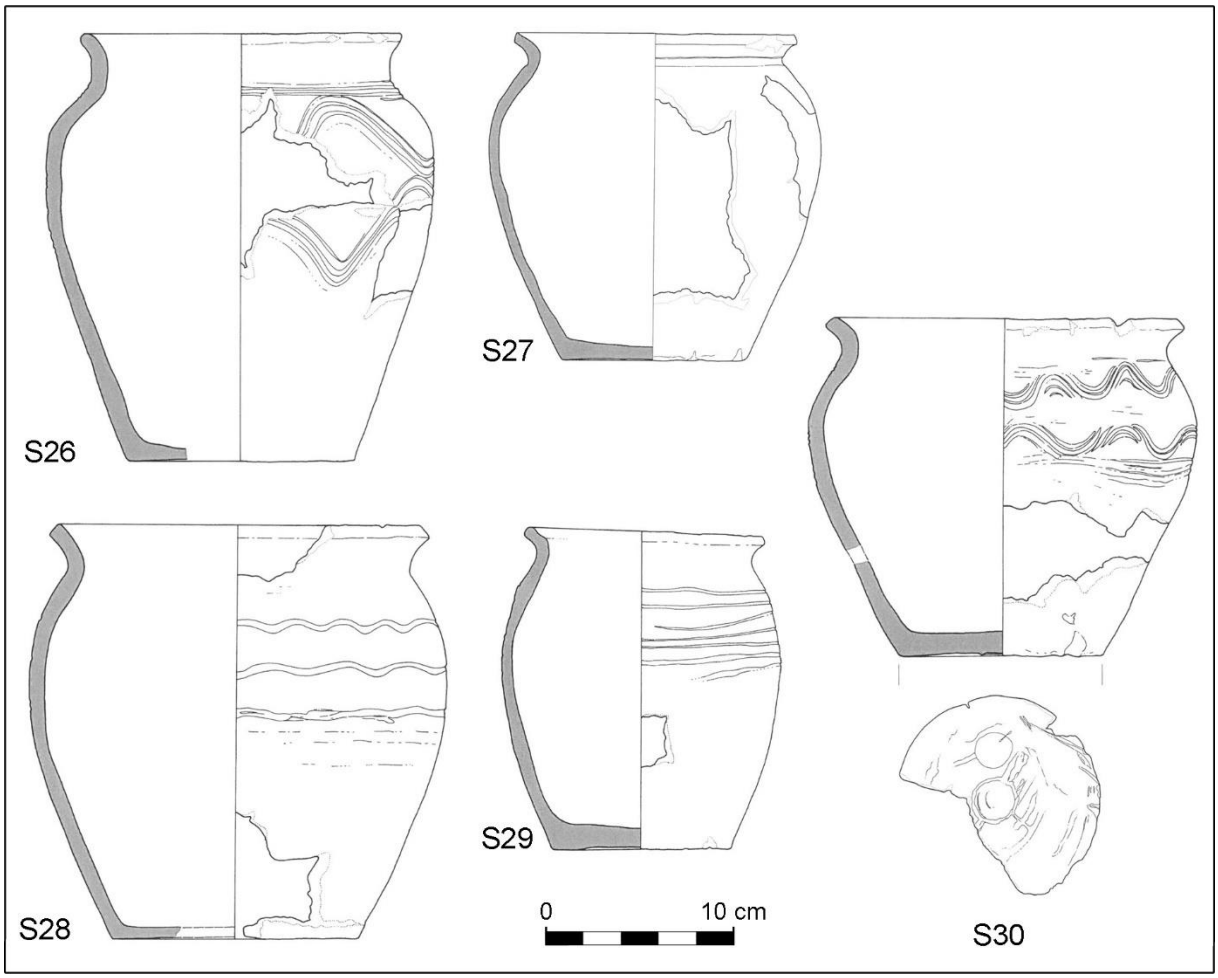


Figure 52. Vessels from the 8th–9th-century cemetery of Purgstall (excavation documentation; drawing provided by excavator Franz Sauer)

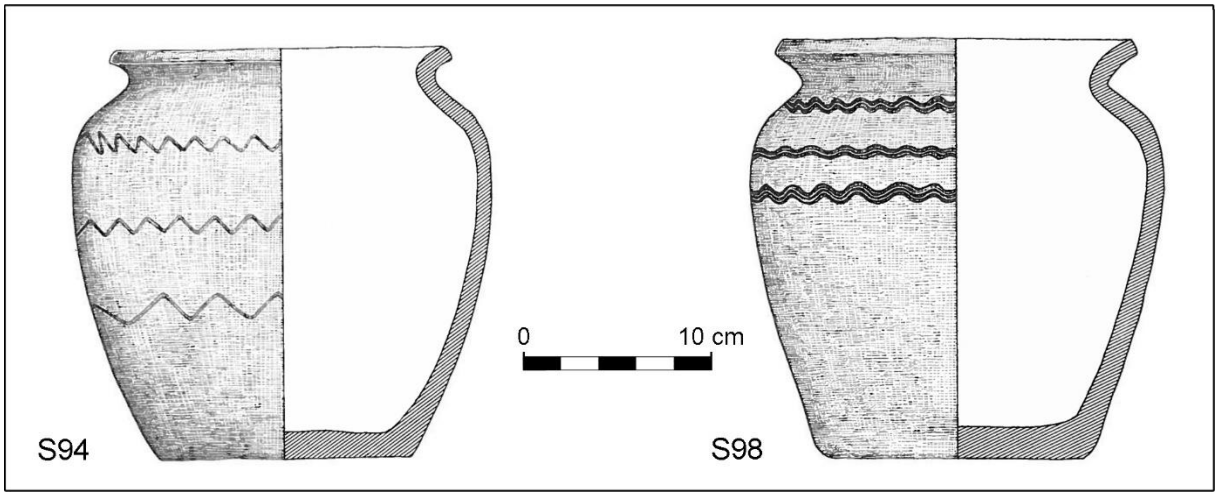


Figure 53. Vessels from the 8th–9th-century cemetery of Mühling (Friesinger 1971–1974, Tf. 12, Tf. 14)

Other important parameters of the pots are the diameter of the rim and base. The rim diameter ranges between 8.5 cm and 22.5 cm, but more than half of the samples from Purgstall and Mühling have a rim diameter between 12 cm to 17 cm. Samples of the graphite-rich fabric GA are 14 cm to 31 cm wide at the rim, the common rim diameter being around 18–20 cm. The base diameter can also be measured in the case of ceramics from graves ranging between 6 cm and 13.5 cm. The base diameter is always smaller than that of the rim representing 50% to 90% of the rim diameter.

4.1.3 Traces of the forming technique

The studied ceramics were most probably made using the same forming technique, which resulted in uneven wall thickness of the potsherds and occasionally few fine parallel lines on the surface. The decoration of the pots (see below) indicates that the vessels were rotated in many cases. All these characteristics suggest slow wheel turning as the finishing forming technique. The bottom of some pots from Purgstall (S1, S19, S22 and S30) also feature the impression of the turntable or turntable cover (*Figures 50–52*). Prior to slow wheel turning, for the building of the body of the vessels a hand forming technique (probably coiling) was used, but the fragmentary nature of the studied material does not allow investigating this technique any further.[50]

On the surface of two vessels of graphite-containing fabrics (S62 and S105) the fine parallel lines are more apparent and present continuously on the whole sherd. These ceramics seem to have a higher level of fineness compared to the other samples, but they still lack the evenness of wall thickness characteristic of wheel-thrown vessels. They might have been made with an apparatus between the turntable and the fast wheel.

4.1.4 Decoration

The most common decoration elements of the studied ceramics are incised parallel wavy lines, which are present on both graphite-free and graphite-containing ceramics either on their own or combined with other decorations. Incised parallel lines are also frequent on graphite-free ceramics (except WM and CRB). Furthermore, vessels of graphite-free fabrics are also

[50] Whole vessels from the cemeteries of Purgstall and Mühling would be ideal for the investigation of the forming techniques, but since the main focus is on material analysis in this thesis, only sherds and drawings were available for examination.

decorated with incised non-parallel wavy lines (GMA, GMB, WM, FQB) and incised non-parallel lines (GMB). Single lines (GMB) and single wavy lines (FQA) are present on some sherds probably as a fragment of a decoration including multiple non-parallel lines or wavy lines. Rarely comb-impressed dots (GMB), incised vertical parallel lines (GMB) and two line-band crossing each other (FQB) also occur on graphite-free ceramics.

Although there are decorative elements in common such as incised parallel wavy lines, incised non-parallel wavy lines and incised parallel lines, slight differences can be detected between the decoration of graphite-containing and graphite-free ceramics. Comb-impressed dots are more frequent on graphite-containing ceramics and there is a decoration element, the raised band, which only appears on the pots of the graphite-rich fabric GA in the studied ceramic material.

Vessels are often decorated with more than one decoration elements as shown by the pots from Purgstall and Mühling (*Figures 50–53*). The decoration usually appears on the upper third or upper half of the body. A common combination of decoration elements includes incised parallel wavy lines + incised parallel lines in the case of graphite-free ceramics and incised parallel wavy lines + comb-impressed dots + raised band in the case of graphite-containing ceramics. There are also pots (e.g. S11, S16, S24 and S27) which have no decoration.

4.1.5 Summary

Macroscopic characteristics reveal similarities and differences among the investigated ceramic samples. A clear distinction is exhibited between the graphite-free and graphite-containing pottery and several fabrics can be identified in both of these big groups. The fewer graphite containing GB may be seen as an intermediate group between the graphite-rich GA (both GA and GB contains graphite) and the graphite-free ceramics (both graphite-free ceramics and GB have a reddish/greyish-brown colour). Large vessel parts show similar forms representing pots (jars), which is most likely the case with the small fragments as well. The sherds have similar traces of forming technique indicating the use of the slow wheel. The decoration of the pots usually includes a combination of decoration elements such as incised lines and wavy lines.

4.2 Petrographic thin section analysis

Petrographic analysis of all 135 samples were carried out. The thin sections are described individually in Appendix C applying the terminology presented in Section 3.3.2. The investigation of the samples allows the identification of several petrographic groups and subgroups. The basis of grouping is primarily the mineralogical composition of the samples and subgroups are established based on microstructure or smaller compositional differences.

The thin sections are divided into two large categories: graphite-free and graphite-containing ceramics including 85 and 50 samples, respectively. Graphite-containing ceramics refer to ceramics with at least 30% graphite-content. Graphite-free ceramics, however, can also contain one or two grains of graphite/opaque mineral up to a 'few' amount (5–15%), but the term 'graphite-free' will be used in this thesis to improve clarity and comprehension. These two types of pottery along with their main groups and subgroups are discussed separately in the following subchapters. All similarities between the subgroups are described under the main groups and all differences are included in the description of the subgroups.

4.2.1 Graphite-free samples

The graphite-free ceramics are divided into four main groups and several subgroups (*Table 17*). There are also five individual samples which do not belong to any of the groups. The description of these petrographic groups and individual samples follows below.

Granitoid group

The Granitoid group is the largest among graphite-free groups including 57 samples (S1, S3–S7, S9, S10, S12, S14, S18–S22, S25, S26, S30, S37–S47, S50–S52, S64–S66, S68–S74, S76–S83, S87, S88, S93–S96 and S98).

These thin sections contain 15% to 35% of inclusions and usually 5% to 10% of voids. (The amount of inclusions can be different in the subgroups, see below.) Meso- and macroplanar voids are usually abundant followed by meso- and macrovughs. The alignment of the elongated grains and voids compared to each other and the walls of the ceramics changes between weak and strong. The matrix of the samples is non-calcareous and has different shades of reddish-brown both in PPL and XP. The colour usually changes within one sample. The optical activity of the thin sections in XP varies between inactive and very highly active following the colour changes. The matrix of the samples is homogeneous apart from few

exceptions (S9, S18, S38, S41, S42, S47 and S51) which contain pure clay nodules or colour stripes.

Table 17. Petrographic groups of graphite-free ceramics

GRANITOID GROUP (57) Granitoid fragments	• **'Granitoid A'** - Feldspar-rich • 'Granitoid A1' - 25–30% inclusions, no special microstructure: 3, 4, 6, 10, 18, 19, 25, 30, 44, 64, 70, 71, 73, 74, 76, 77, 88, 94, 95, 96, 98 • 'Granitoid A2' - Large part of fine fraction is less than 50 µm: 39, 50, 52, 65, 66, 68, 69, 72, 78, 79, 81 • 'Granitoid A3' - Few inclusions (15–20%): 37, 38, 40, 41, 42, 43, 51 • **'Granitoid B'** - Quartz-rich • 'Granitoid B1' - Moderately/poorly sorted grains: 12, 20, 80, 82, 83 • 'Granitoid B2' - Very poorly sorted grains: 7, 9, 14, 26, 93 • 'Granitoid B3' - Few inclusions (20%): 45, 46, 47 • **'Granitoid C'** - Biotite-rich (30–50%): 1, 22, 87 • **'Granitoid D'** - Muscovite-rich (5–30%): 5, 21
AMPHIBOLE GROUP (12) Granitoid fragments + >5% amphibole	• 2, 8, 28, 29, 55, 56, 60, 61, 63, 90, 91, 92
DIORITE GROUP (7) Diorite fragments	• **'Diorite A'** - Aggregates of colourless amphibole, very fine-grained fine fraction: 11, 16, 24, 27, 75 • **'Diorite B'** - Diopside, graphic texture, coarser-grained fine fraction: 67, 97
CARBONATE GROUP (4) Calcite/dolomite + diopside	• **'Carbonate A'** - 45% of inclusions, abundant fine fraction: 57, 58 • **'Carbonate B'** - Few inclusions (15%), almost no fine fraction: 59, 89
INDIVIDUAL SAMPLES (5)	• 15, 17, 23, 48, 131

All samples have bimodal grain-size distribution with varying ratios as well as varying upper and lower boundaries of the fine and coarse fraction, respectively. The average upper boundary of the fine fraction ranges between 150 µm and 500 µm and the average lower boundary of the coarse fraction ranges between 400 µm and 800 µm. The grains are very

poorly sorted (except the samples of the Granitoid B1 group, see below), have elongated or equant shape (usually the first being the more abundant) and have mostly very angular to sub-angular boundaries.

The samples of the Granitoid group contain granitic rock fragments and minerals from the decomposition of the same rock type incorporating mainly quartz and feldspar crystals and usually biotite mica. Both mono- and polycrystalline quartz occur in the samples with undulose extinction and mostly sutured boundaries. (Quartz grains have both sutured and straight boundaries in S22, S25, S30 and S47.[51])

In almost all thin sections feldspars include potassium feldspar and plagioclase (except S5, S21 and S52 containing only potassium feldspar). The amount of the potassium feldspar is larger than that of the plagioclase (except in S7, S47 and S93 which have slightly more plagioclase than potassium feldspar). Feldspars are usually cloudy in PPL because of partial or total alteration to sericite, a reddish-brown alteration product or saussurite. In the majority of the samples some potassium feldspars also have a perthitic texture.

Biotite is present in almost all samples (except S46 and S80) with a varying amount and usually a smaller amount of relatively fine (< 100 μm) muscovite is spread in their matrix (except S37, S38, S40 and S41 which do not contain muscovite). Biotite occurs both in rock fragments and in the matrix, while muscovite is usually present scattered in the matrix.

All samples of the Granitoid group contain few grains of accessory minerals. Graphite or opaque mineral usually occur in the thin sections representing less than 15% of the inclusions. The differentiation between graphite and opaque minerals is hardly possible by polarising microscope in some cases; however, 20 samples (S3, S6, S14, S18–S21, S26, S38, S39, S41–S43, S50, S52, S69, S70, S77, S88 and S96) very likely contain graphite, which can also occur together with other minerals such as quartz and feldspar. Green or greenish-brown amphibole can be recognised in the majority of the thin sections (except S3, S5, S7, S9, S12, S18, S20, S25, S26, S39, S45–S47, S50, S52, S76, S80–S83, S93 and S94) individually in the matrix or within granitoid fragments usually with a proportion less than 5%. The occurrence of one or two grains of zircon is possible in the samples (S10, S22, S66, S68, S71, S72, S81, S88 and S93–S95).

[51] Straight boundaries suggest equilibrium crystallisation including triple junctions of three quartz grains with an angle of *c.* 120°. Sutured boundaries together with undulose extinction refer to distortion of the quartz grains during metamorphism.

Many of the thin sections (S3–S6, S9, S10, S14, S18, S25, S26, S30, S38, S39, S42, S46, S50, S51, S65, S66, S68, S69, S73, S78, S79, S83, S93 and S95) contain argillaceous inclusions (up to 15%), probably clay pellets, which are usually darker and denser than the matrix, have slight/very slight activity in XP, rather elongated shape, rounded and diffuse/sharp to merging boundaries, concordant orientation and similar composition to the matrix. Almost inclusion-free clay pellets and clay concentrations in S9, S18, S41, S42 and S47 probably represent pure clay nodules. In few thin sections (S43, S45, S51 and S96) nodules are present with a rather reddish tone, which can be limonitic concentrations.

The Granitoid group is divided into four subgroups on the basis of the frequency of certain minerals, namely the feldspar-rich, quartz-rich, biotite-rich and muscovite-rich subgroups. Within these subgroups, further grouping is possible based on textural properties of the inclusions.

Feldspar-rich subgroup ('Granitoid A')

The feldspar-rich subgroup 'Granitoid A' includes 39 thin sections (S3, S4, S6, S10, S18, S19, S25, S30, S37–S44, S50–S52, S64–S66, S68–S74, S76–S79, S81, S88, S94–S96 and S98). These samples of the Granitoid-group contain more feldspar than quartz grains. Biotite flakes have usually a significant amount in the samples which can vary between 0.5% and 30%. Less than 2% of muscovite is scattered in the matrix of these thin sections (except S37, S38, S40 and S41, which have no muscovite). Green or greenish-brown amphibole is present in 29 samples (S4, S6, S10, S19, S30, S37, S38, S40–S44, S51, S64–S66, S69–S74, S77–S79, S88, S95, S96 and S98) with a small amount (up to 5%, except S51 which contains 5–15% of green amphibole). The proportion of graphite/opaque mineral is usually less than 5% in 32 samples of which 17 contain most likely graphite (graphite: S3, S4, S6, S18, S19, S38, S39, S41–S43, S50, S52, S69, S70, S77, S88 and S96; opaque mineral/graphite: S10, S25, S30, S51, S65, S66, S68, S71, S72, S76, S79, S81, S94, S95 and S98). Less than 2% zircon is present in 9 samples (S10, S66, S68, S71, S72, S81, S88, S94 and S95).

Subgroup 'Granitoid A' is divided into three further subgroups based on textural properties: 'Granitoid A1', 'Granitoid A2' and 'Granitoid A3'.

Subgroup 'Granitoid A1' (S3, S4, S6, S10, S18, S19, S25, S30, S44, S64, S70, S71, S73, S74, S76, S77, S88, S94, S95, S96 and S98; *Figure 54*) and 'Granitoid A2' (S39, S50, S52, S65, S66, S68, S69, S72, S78, S79 and S81; *Figure 55*) contain about 25–35% of inclusions of bimodal grain-

size distribution. The two subgroups are very similar and only small microstructural differences make the samples of 'Granitoid A2' stand out from the samples of 'Granitoid A1'. The fine fraction of 'Granitoid A2' makes up a relatively large part of the inclusions (45–55%) and about two thirds of the fine fraction consist of very fine grains with a grain-size less than 50 µm. These features together produce a distinctive view under the microscope which is characterised by the presence of larger grains of the coarse fraction surrounded by abundant little 'dots' of the fine fraction. It has to be noted that 'Granitoid A2' has three samples (S39, S50 and S52) which contain a relatively large amount of graphite (5–15%), but except for this, these samples do not differ from the other samples of 'Granitoid A2' neither in terms of composition nor microstructure.

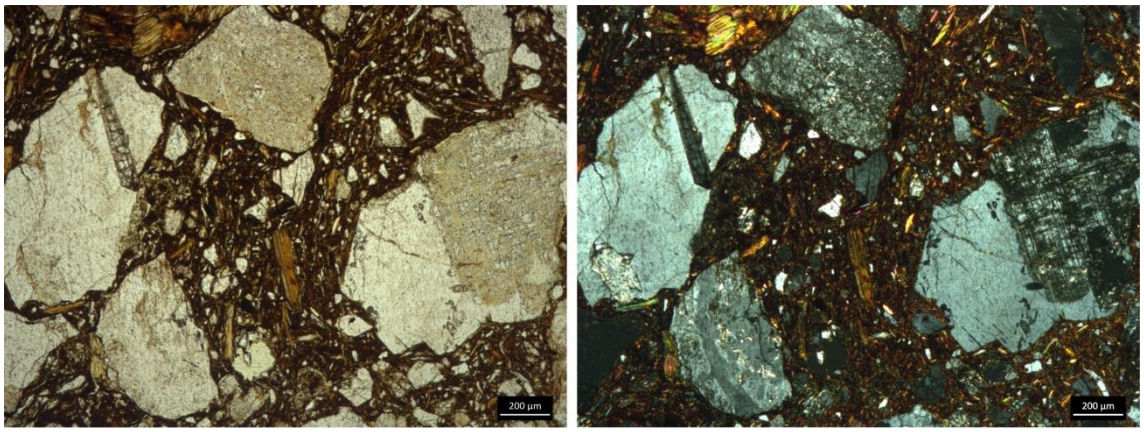


Figure 54. Subgroup 'Granitoid A1' containing abundant feldspar (S4, PPL and XP)

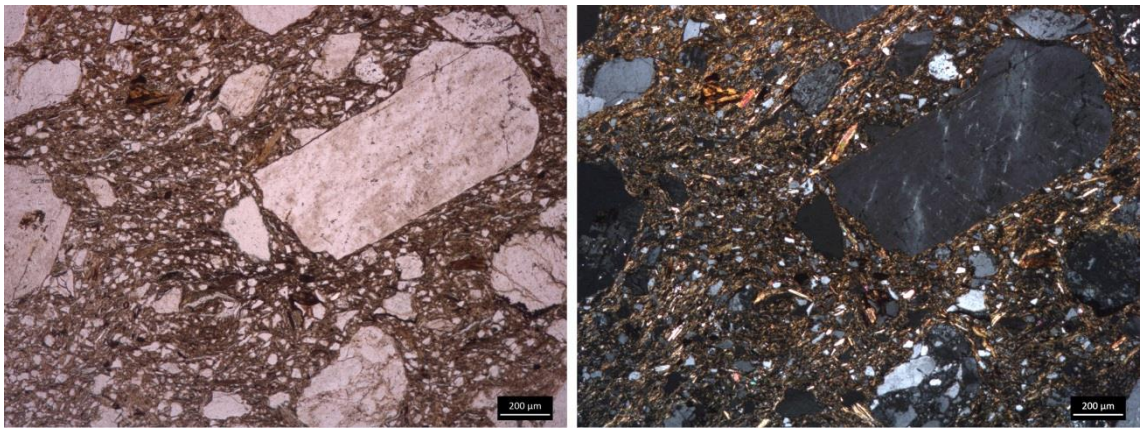


Figure 55. Subgroup 'Granitoid A2' with abundant and very fine-grained fine fraction (S69, PPL and XP)

Samples of subgroup 'Granitoid A3' (S37, S38, S40, S41, S42, S43 and S51; *Figure 56*) are more distinctive from 'Granitoid A1' and 'Granitoid A2'. This is because they contain less inclusion which makes up only 15–20% of the whole thin section. The fine fraction is present with a

small percentage (20–35% of inclusions) thus large areas of clay are visible among inclusions in the thin sections. The colour of these samples is also distinctive as they are usually light or very light reddish-brown in PPL and they turn into a yellowish-greyish shade (light or very light yellowish-greyish-brown) in XP.

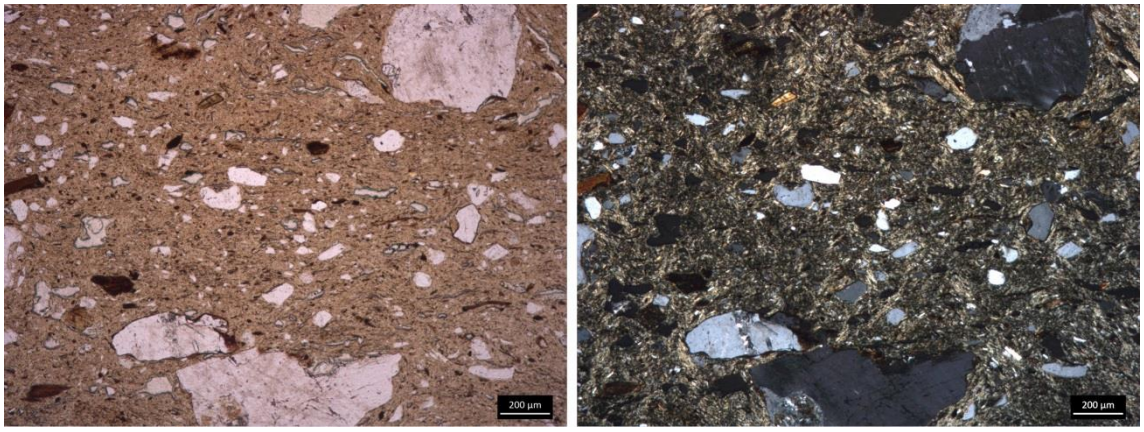


Figure 56. Subgroup 'Granitoid A3' containing few inclusions (S42, PPL and XP)

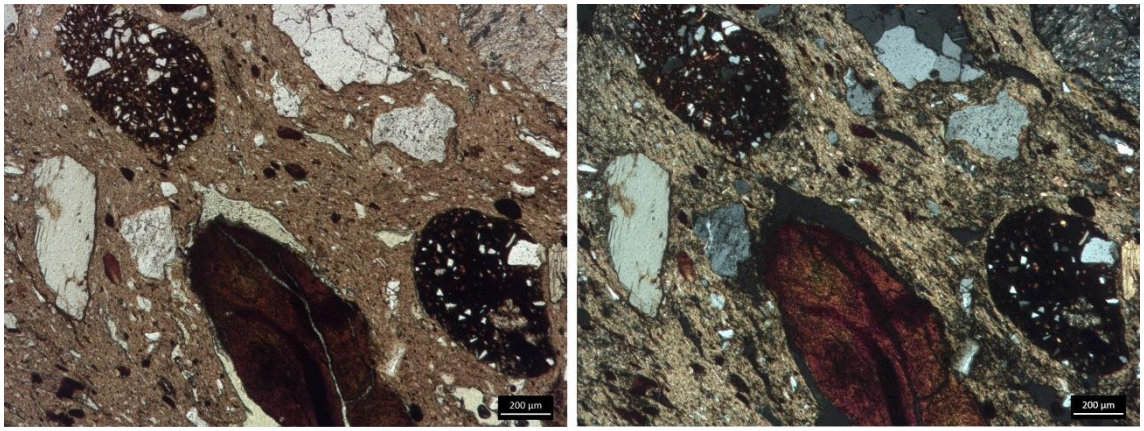


Figure 57. Grog (?) grains in S51 (upper left and lower right corner of the photomicrographs) (PPL and XP)



Figure 58. The outer and inner surface of rim fragment S51. Reddish grog (?) grains are visible in the inner surface (e.g. in the upper left edge of the sherd) (photo by the author)

It is possible that S51 from 'Granitoid A3' contains previously fired ceramic fragments (grog) as some grains have more characteristics supporting this possibility, such us different (much darker) colour to the matrix, sharp boundaries, discordant orientation and distinctive composition from that of the matrix (*Figure 57*). At the same time, these grains have rounded to well-rounded outlines, which are not typical for grog. The macroscopic appearance of the sherd could, however, indicate the presence of grog grains (*Figure 58*). Some other samples of this subgroup (S38, S40 and S42) contain similar argillaceous inclusions.

Quartz-rich subgroup ('Granitoid B')

The quartz-rich subgroup of the Granitoid group, i.e. 'Granitoid B', includes 13 samples (S7, S9, S12, S14, S20, S26, S45, S46, S47, S80, S82, S83 and S93). The amount of quartz exceeds the amount of feldspar in these samples. Most of the thin sections of this subgroup (except S7, S14, S26, S47 and S93) contain less biotite (< 5%) than the feldspar-rich 'Granitoid A' and two samples (S46 and S80) contain no biotite at all. Less than 2% of muscovite is present in the thin sections. Except for S46 and S82, graphite/opaque mineral is common usually up to 5% with definite graphite content in S14, S20 and S26. However, amphibole occurs only in S14 in this subgroup. Four samples (S45, S46, S47 and S93) include garnet with a proportion less than 15% and two thin sections contain one (S12) or few (< 5%, S45) grains of tourmaline.

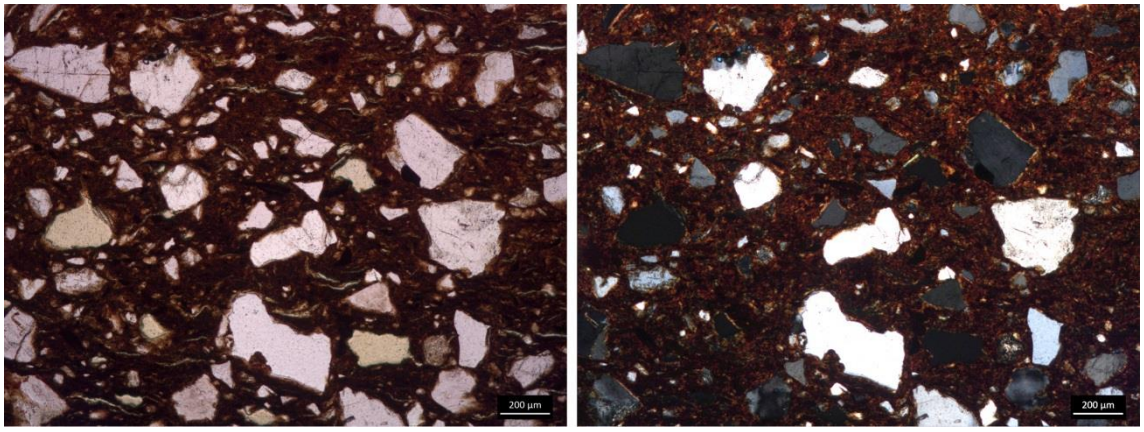


Figure 59. Subgroup 'Granitoid B1' with moderate sorting of grains (S80, PPL and XP)

The quartz-rich thin sections are divided into three subgroups based mainly on microstructure: 'Granitoid B1', 'Granitoid B2' and 'Granitoid B3'. Samples of 'Granitoid B1' (S12, S20, S80, S82 and S83; *Figure 59*) contain *c.* 25% of inclusions and have moderately or poorly sorted grains. 'Granitoid B2' (S7, S9, S14, S26 and S93; *Figure 60*) has 25–30% of inclusions and a very poor sorting of grains. The amount of biotite is usually larger in 'Granitoid B2' (5–30%, except S9) than in 'Granitoid B1' (below 5% or none).

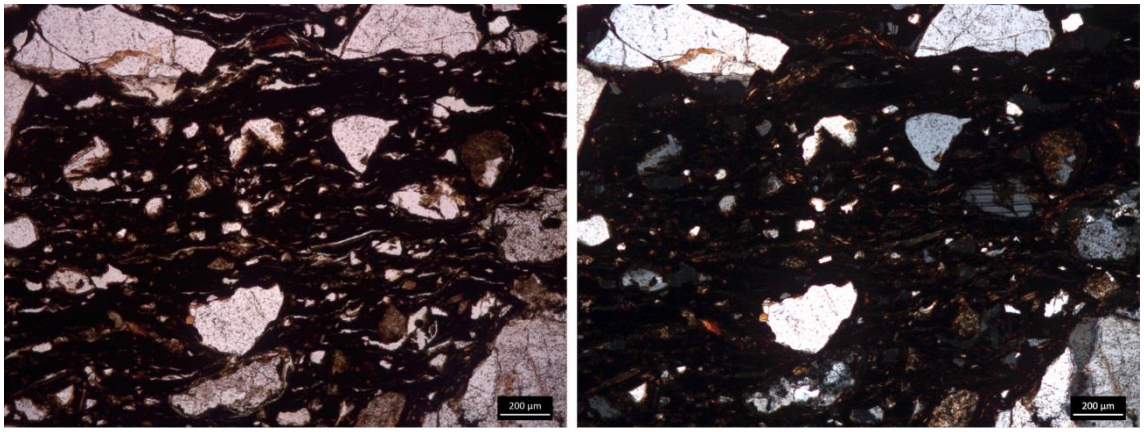


Figure 60. Subgroup 'Granitoid B2' with very poor sorting of grains (S7, PPL and XP)

Subgroup 'Granitoid B3' (S45, S46 and S47; *Figure 61*) contain less inclusions (about 20%) than 'Granitoid B1' and 'Granitoid B2', thus a similar view can be seen under microscope as in the case of the inclusion-poor 'Granitoid A3'. Furthermore, samples of 'Granitoid B3' have sub-angular to rounded grains in contrast to the very angular to sub-angular inclusions of the other two quartz-rich subgroups. An 'unusual' accessory mineral (garnet) is also present in all samples of 'Granitoid B3'.

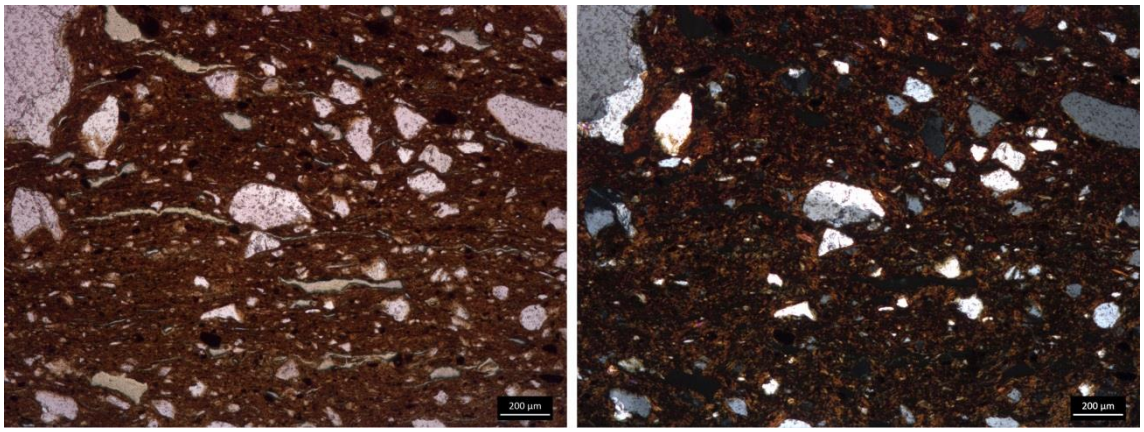


Figure 61. Subgroup 'Granitoid B3' containing few inclusions (S45, PPL and XP)

Two samples of 'Granitoid B2' and one sample of 'Granitoid B3' are slightly unique in the quartz-rich subgroup. S9 contains 5–15% of loess grains, S26 contains a notable amount (5–15%) of graphite and S47 contains some (less than 5%) sedimentary rock fragments. However apart from these differences, they are very similar to the other members of their subgroups.

Biotite-rich subgroup ('Granitoid C')

Three samples (S1, S22 and S87) belong to the third, biotite-rich subgroup ('Granitoid C'; *Figure 62*) of the Granitoid group. All of these samples contain a large amount (30–50%) of

biotite mica. Less than 5% of muscovite and green amphibole is present in all thin sections. As accessory minerals, S1 contains few grains of graphite/opaque mineral and S22 contains one grain of zircon. Additionally, S1 includes 5 to 15% of pseudomorphs which are possibly muscovite or sillimanite pseudomorphs after an undefined mineral.[52] It is important to note that some feldspar crystals exhibit microcline structure in all samples, which cannot be observed in the feldspar-rich and quartz-rich subgroups.

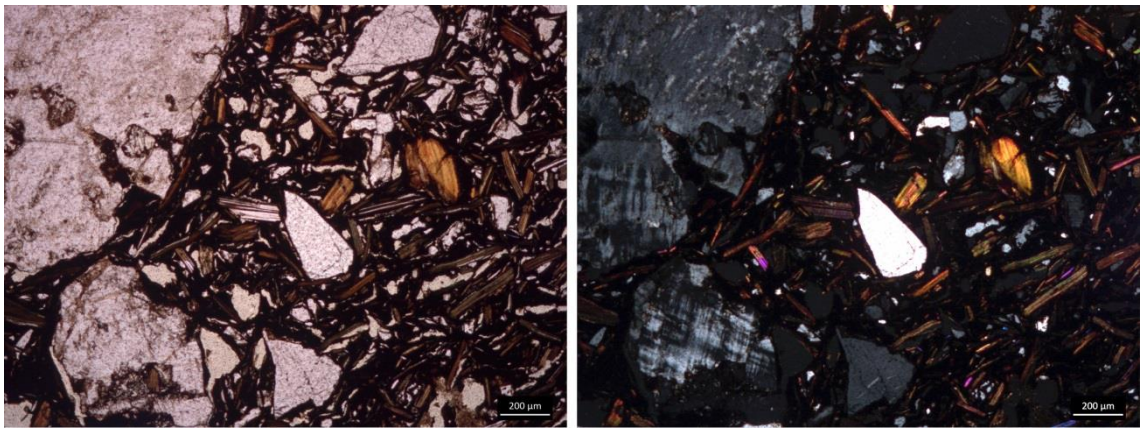


Figure 62. Subgroup 'Granitoid C' with abundant biotite and potassium feldspar exhibiting microcline structure (S22, PPL and XP)

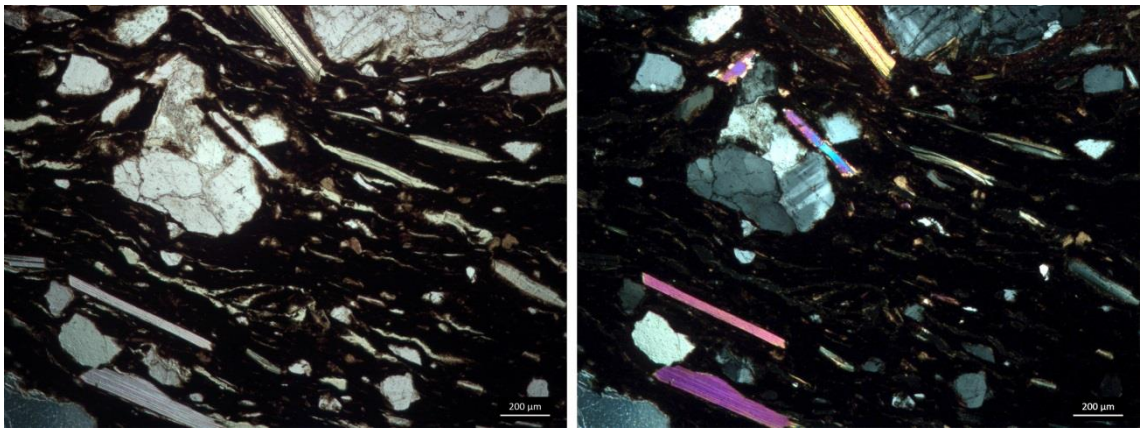


Figure 63. Subgroup 'Granitoid D' with abundant coarse-grained muscovite (S5, PPL and XP)

Muscovite-rich subgroup ('Granitoid D')

S5 and S21 belong to the muscovite-rich subgroup ('Granitoid D'; *Figure 63*) and contain coarse-grained muscovite flakes in a relatively large amount (S5: 15–30%; S21: 5–15%) compared to the other samples of the Granitoid group. These muscovite flakes together with

[52] This mineral might be an aluminium-rich mineral (andalusite?, cordierite?) as suggested by Dr György Szakmány based on photomicrographs (June 2018).

biotite (2–15%) are present both in the matrix and in rock fragments. As feldspar, they both contain potassium feldspar only, which exhibits microcline structure. The two samples are slightly different regarding accessory minerals as S5 contains few grains of graphite/opaque mineral while S21 is quite rich (5–15%) in graphite. In addition, S21 also includes one grain of green amphibole. In terms of microstructure, both are relatively poor in inclusions (*c.* 20%).

Amphibole group

The Amphibole group consists of 12 thin sections (S2, S8, S28, S29, S55, S56, S60, S61, S63, S90, S91 and S92; *Figure 64*). They contain 30% to 45% of inclusions and 5% to 10% of voids being mostly meso- and macrovughs and mesoplanar voids. They have usually moderately aligned microstructure and homogeneous matrix. The matrix is non-calcareous and has a range of reddish-brown colours in PPL and XP changing usually within one sample. The optical activity varies from inactive to highly active changing also within one sample.

The samples have bimodal grain-size distribution with abundant fine fraction (usually 60–70% of inclusions) and a lesser amount (usually 30–40% of inclusions) of the coarse fraction. The average upper boundary of the fine fraction is between 200 µm and 350 µm and the average lower boundary of the coarse fraction is around 500 µm. Usually more elongated than equant grains are present with very angular to sub-angular boundaries and very poor sorting.

The samples of the Amphibole group contain abundant (more than 5%) amphibole crystals and amphibole-rich granitoid fragments.[53] The granitoid fragments are probably gneiss fragments,[54] however there is no clear indication of this structure in the thin sections (except S28, see below). The main constituents of these granitoid fragments are quartz, feldspar, biotite and amphibole in decreasing abundance. Both mono- and polycrystalline quartz occurs with undulose extinction and sutured boundaries. The ratio of the feldspar types varies in the samples: usually they contain more plagioclase than potassium feldspar (S2, S8, S29, S55, S61, S63, S90, S91 and S92), but few thin sections have more potassium feldspar than plagioclase (S28, S56 and S60). Many feldspar crystals have a special appearance in the Amphibole group as they exhibit an initial yellowish-brownish (PPL/XP) alteration along edges and cleavage lines.

[53] It is possible that the individual amphibole grains originate partly from granitoid rock and partly from weathered amphibolite (Rudolf Dell'mour, personal communication (by email), October 2019).
[54] Rudolf Dell'mour, personal communication (by email), October 2019.

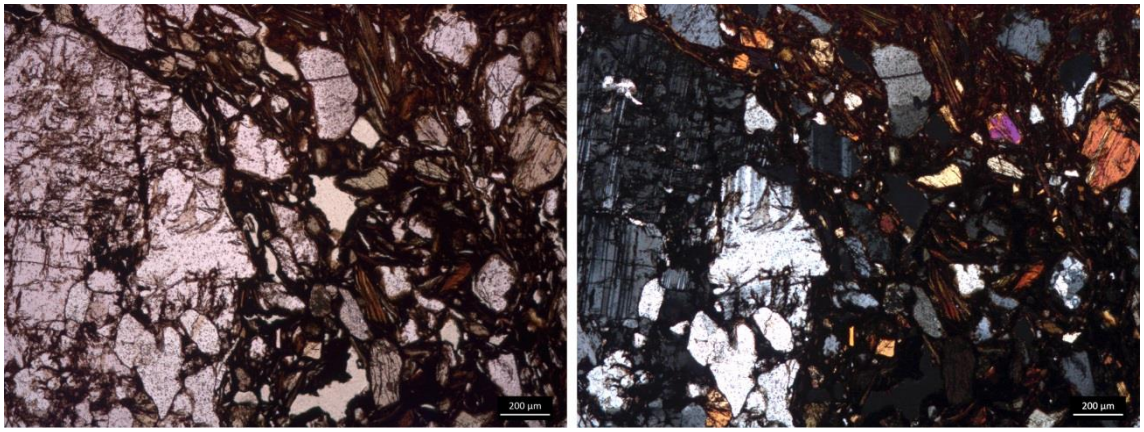


Figure 64. Amphibole group with abundant amphibole crystals and granitoid fragments containing feldspar with a yellowish initial alteration (S61, PPL and XP)

Green amphibole is usually the most abundant mineral (5–50%) present individually in the matrix after quartz and feldspar. It is followed by biotite ranging from 5 to 30%. The occurrence of muscovite is not significant (< 2%): few small (< 100 µm) grains can be observed in the matrix in seven samples (S8, S28, S29, S56, S63, S91 and S92). (Muscovite is also present in rock fragments in S28.) Less than 2% graphite/opaque mineral occurs sporadically in the matrix or in rock fragments in all samples excluding S55, and in seven thin sections (S28, S29, S60, S61, S63, S91 and S92) it is probably graphite. Few samples also contain garnet (S2, S28 and S60) and zircon (S8, S60 and S91) grains.

Six of the samples (S29, S56, S61, S63, S90 and S91) include clay pellets (< 2%) with dark or very dark reddish-brown colour (in PPL and XP), slight or very slight optical activity in XP, usually elongated shape, sub-rounded or rounded and sharp to merging boundaries. Compared to the matrix, they have higher density, concordant orientation and similar composition.

Two samples (S28 and S29) have unique features besides the above-mentioned features characteristic to the Amphibole group. Rock fragments of S28 contain feldspar crystals totally altered to sericite which cannot be observed in the other samples. Few rock fragments of this sample had gone through metamorphism based on their aligned structure and probably are gneiss fragments. S29 is distinctive because some of its biotite flakes within the granitoid fragments and its amphibole crystals have started altering to chlorite.

S91 and S92 are slightly stand out from the other samples in terms of composition (*Figure 65*). These samples represent a transition category between the Amphibole and the Diorite groups (see below). They contain the diagnostic granitoid fragments of the Amphibole group with

initially altered feldspar grains as well as the same diorite fragments (and colourless amphibole-aggregates) as subgroup ‘Diorite A’ in about the same amount. However, they are listed under the Amphibole group because the microstructure of these samples is more similar to that of the Amphibole group than that of the ‘Diorite A’. (The abundant very fine-grained monocrystalline quartz present in subgroup ‘Diorite A’ is missing from these two samples.)

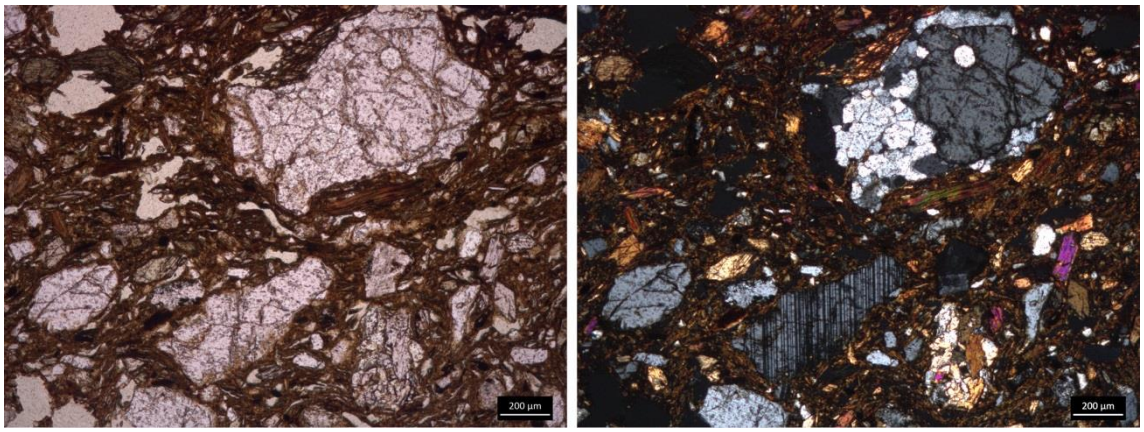


Figure 65. Composition of S91 including granitoid fragments of the Amphibole group with initial alteration of feldspar (e.g. top right-hand quarter of the photomicrograph) and colourless amphibole-aggregate (bottom right-hand quarter of the picture) which is characteristic of subgroup ‘Diorite A’ (PPL and XP)

Diorite group

The Diorite group comprises seven samples (S11, S16, S24, S27, S67, S75 and S97). The ratio of the inclusions varies between 30% and 40%. Mostly mesoplanar voids are present followed by mesovughs and the voids make up 5 to 10% of the samples. The elongated grains and pores are usually moderately aligned. The matrix is non-calcareous, usually homogeneous and has reddish-brown shades in PPL and XP. The optical activity in XP varies within the samples ranging between inactive and very highly active.

The samples have strongly bimodal grain-size distribution with varying ratio of the coarse and fine fraction. The average upper boundary of the fine fraction is between 100 µm and 300 µm and average lower boundary of the coarse fraction is between 300 µm and 700 µm. These boundaries are different in the subgroups; especially the features of the fine fraction are subgroup-specific (see below). The grains are very poorly sorted and very angular to sub-angular. The proportion of the elongated and equant grains varies in the samples.

The thin sections of the Diorite group contain rock fragments including feldspar (plagioclase and few potassium feldspar), quartz, biotite, amphibole and usually graphite. Based on the

composition and structure of the rock fragments and the geological setting of the Erlauf Valley, these rock fragments are probably diorites.[55] The feldspar crystals show zoning as they have a core altered to very fine micas (sericite) and an unaltered outer zone.

Most of the inclusions are diorite fragments, but the components of these rock fragments also occur in the matrix in small amounts. Biotite is present usually with 5–15% (except S97 which has 15–30% of biotite). The muscovite, amphibole and graphite/opaque mineral content are less than 5%. The samples most probably contain graphite with the exception of S16 and S75, which contain graphite or opaque mineral. Garnet is present in S27 (one grain) and S67 (2–5%).

Clay pellets are common in the Diorite group and present up to 5% (except S97 which does not contain clay pellet). They are dark or very dark reddish brown (in PPL and XP) with slight optical activity in XP and a higher density than the matrix. Their shape is mostly elongated with sub-rounded to well-rounded and sharp to merging or diffuse boundaries. They have concordant orientation and similar composition to the matrix.

The Diorite group is divided into two subgroups, 'Diorite A' and 'Diorite B', which have slightly different rock fragments and fine fraction concerning composition and microstructure.

'Diorite A'

As mentioned above, rock fragments of the Diorite group contain amphiboles. In the case of subgroup 'Diorite A' (S11, S16, S24, S27 and S75; *Figure 66*) two types of amphiboles occur in the rock fragments: quite dark, greenish-brown amphiboles and aggregates of smaller grains of colourless amphiboles. These aggregates occasionally contain pyroxene as well.

Subgroup 'Diorite A' contains 35–40% of inclusions which consist of diorite fragments and minerals derived from these fragments as well as a significant amount of very fine-grained (< 100 µm) monocrystalline quartz. Essentially, these small quartz grains make up the fine fraction. Thus, the thin sections have a similar appearance to type 'Granitoid A2' under microscope, which is characterised by large grains of diorite surrounded by small 'dots' of quartz.

[55] This identification along with monzonite was proposed by Dr György Szakmány and Dr Sándor Józsa based on photomicrographs (June 2018). Another option is to identify this rock as gabbro or biotite-rich paragneiss according to Rudolf Dell'mour (based on photomicrographs, October 2019).

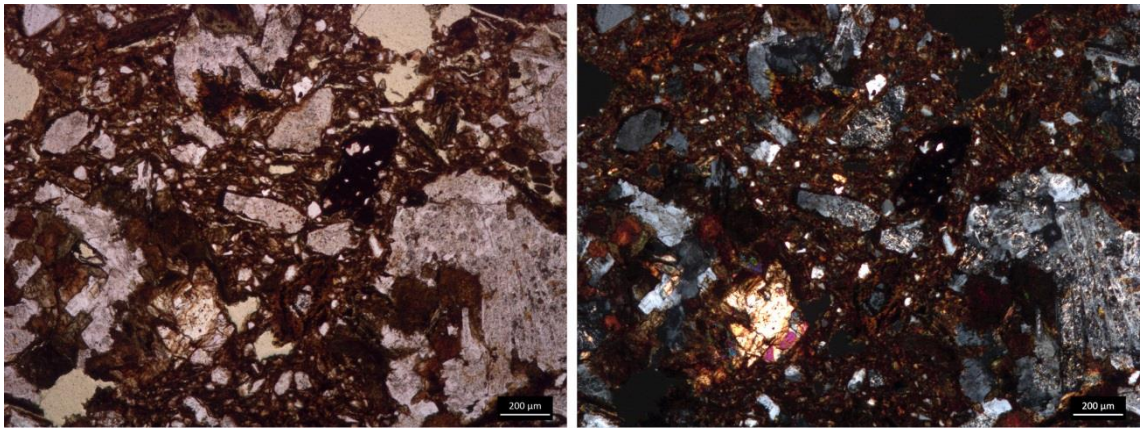


Figure 66. Subgroup 'Diorite A' containing diorite fragments with zoned feldspars (e.g. bottom right-hand corner) and colourless amphibole-aggregates (bottom left-hand quarter) (S75, PPL and XP)

'Diorite B'

There is only one type of amphibole occurring in the two samples of subgroup 'Diorite B' (S67 and S97; *Figure 67*), which is lighter green and 'clearer' compared to the greenish-brown amphibole of 'Diorite A'. In addition, slightly weathered clinopyroxene (augite) grains are present in the rock fragments and the matrix. There is no colourless amphibole in 'Diorite B'. The two samples of 'Diorite B' are also connected by a special texture referred to as micrographic texture observed in some parts of the rock fragments (*Figure 68*), which is the result of oriented intergrowth of quartz and feldspar (MacKenzie et al. 1982, 46–47).

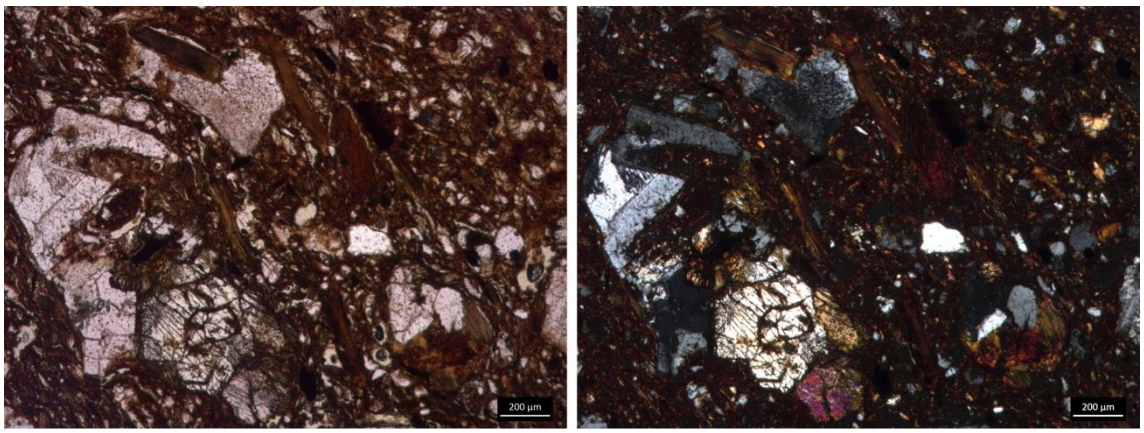


Figure 67. Subgroup 'Diorite B' with diorite fragments including diopside (bottom left-hand corner) (S67, PPL and XP)

'Diorite B' contains 30% of inclusions and the samples have the 'usual' microstructure, i.e. their fine fraction is more coarse-grained (< 300 µm) than that of 'Diorite A' (< 100 µm). Fine-grained quartz is partly present (S67) or missing (S97).

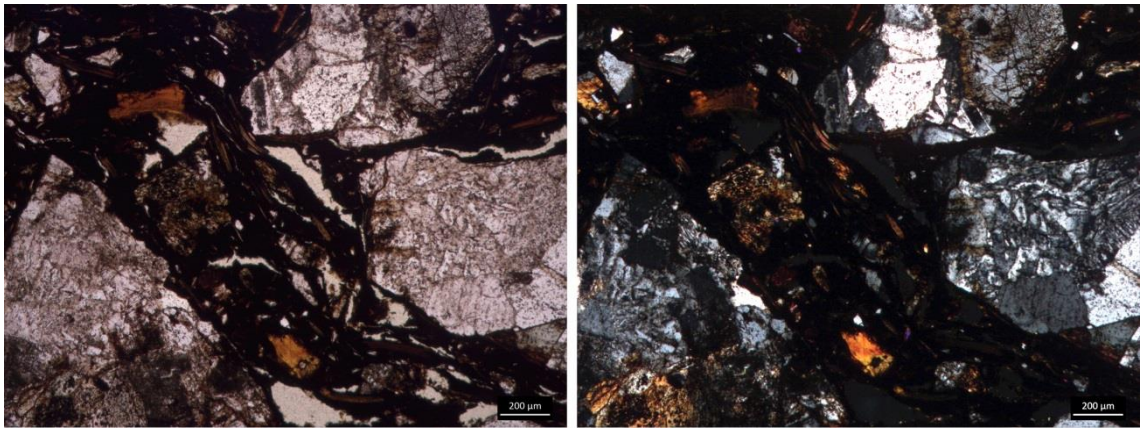


Figure 68. Graphic texture of the rock fragments of 'Diorite B' (S97, PPL and XP)

Carbonate group

The Carbonate group consists of four samples (S57, S58, S59 and S89). Overall, the ratio of inclusions ranges from 15% to 45% in the samples of the Carbonate group, but the subgroups have a more precise ratio (see below). Voids, which are mainly mesovughs, are present with 3% to 7%. The samples have moderate alignment and homogeneous and non-calcareous matrix. The colour of the matrix is mixed within a sample showing reddish-brown shades (PPL, XP) and accordingly inactive to highly active optical activity in XP.

The samples of the Carbonate group have bimodal grain-size distribution with a fine fraction up to 100 µm and a coarse fraction starting from 300–500 µm. The ratio of these fractions is subgroup-specific (see below). Usually more elongated than equant grains occur with very poor sorting and mostly very angular to sub-angular boundaries.

The main inclusions of the Carbonate group are carbonate rock (limestone or dolomite) fragments and fine-grained (< 100 µm) monocrystalline quartz. The carbonate rock fragments include predominantly calcite/dolomite crystals,[56] some diopside grains, muscovite (S57, S59 and S89), faded biotite (S57 and S58), graphite/opaque mineral (S58 and S59) and colourless amphibole (S89). These minerals can be present individually in the matrix as well with different proportions. Clay pellets occur in all samples up to 15%.

The four samples are compositionally consistent, but differ concerning microstructure. Two subgroups can be separated: 'Carbonate A' (S57 and S58) and 'Carbonate B' (S59 and S89).

[56] These minerals cannot be distinguished in the polarising microscope without special treatment of the thin section.

'Carbonate A'

S57 and S58 contain abundant (about 45%) inclusions with a very fine-grained (< 100 µm) fine fraction made mostly up of monocrystalline quartz (*Figure 69*). The fine fraction represents 50–60% of the inclusions.

These two samples have the same very dark reddish-brown (PPL and XP) clay pellets with moderate optical activity to inactivity in XP. They are mostly elongated, sub-rounded and denser than the matrix. They have sharp to merging boundaries, concordant or discordant orientation compared to the matrix and similar composition as the matrix.

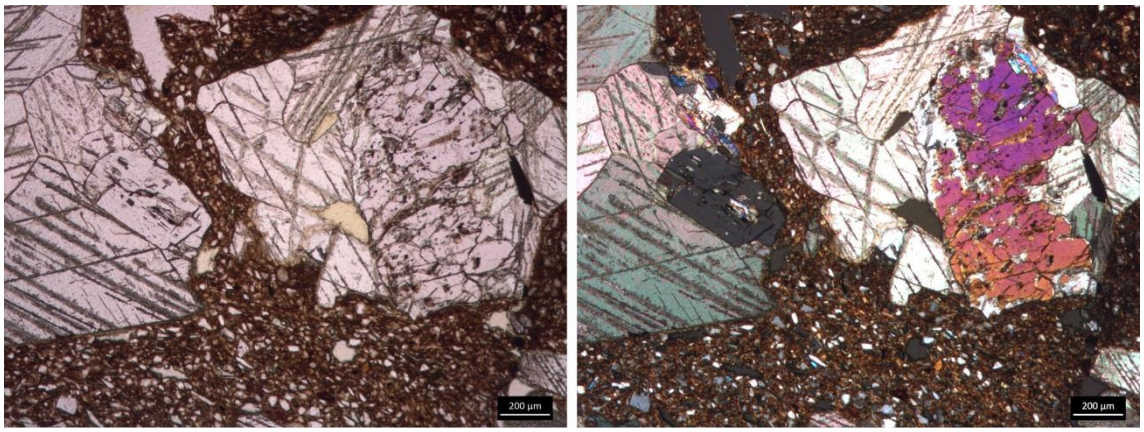


Figure 69. Subgroup 'Carbonate A' containing calcite/dolomite and diopside crystals in a matrix rich in very fine-grained quartz (S58, PPL and XP)

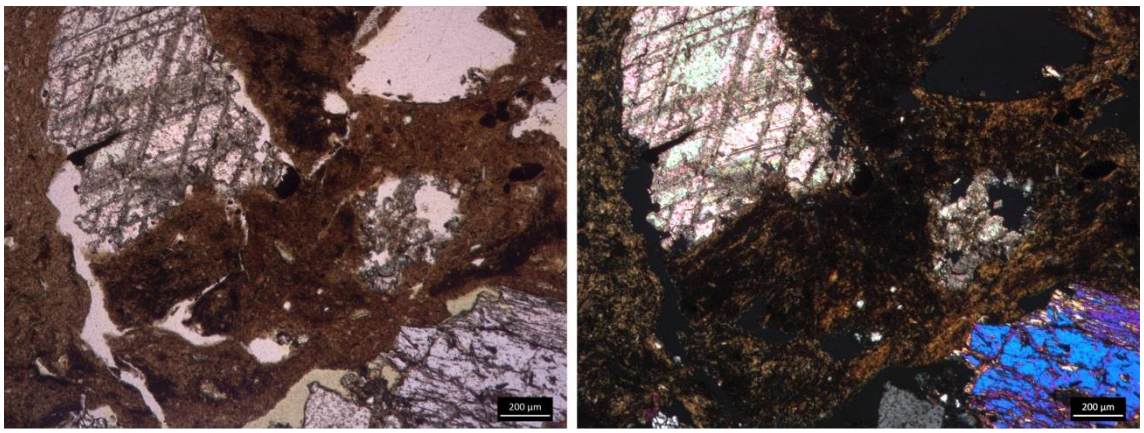


Figure 70. Subgroup 'Carbonate B' containing calcite/dolomite and diopside crystals in an inclusion-poor matrix (S59, PPL and XP)

'Carbonate B'

S59 and S89 contain the same rock fragments as the other two samples, but the difference is exhibited in the amount of inclusions and fine fraction; samples of 'Carbonate B' contain only

15–20% of inclusions and the fine fraction is very few (5–15%). This produces a view featuring larger carbonate rock fragments that are surrounded by almost pure clay under microscope (*Figure 70*).

Individual samples

There are 5 samples (S15, S17, S23, S48 and S131) that differ considerably from the samples of the above-mentioned four groups, and are therefore described separately.

S15 is unique regarding both microstructure and composition (*Figure 71*). It contains abundant inclusions (*c.* 50%) and *c.* 10% of voids being meso- and macrovughs and mesoplanar voids. The sample has weak alignment and a non-calcareous and homogeneous matrix. The matrix is light reddish-brown with dark reddish-brown patches in the core (in PPL and XP) and has moderate optical activity in XP. The sample has bimodal grain-size distribution with an average upper boundary of the fine fraction of about 150 µm and an average lower boundary of the coarse fraction of about 400 µm. More equant than elongated grains occur with poor sorting and very angular to sub-rounded boundaries. The inclusions are mainly equant quartz grains with undulose extinction and sutured or straight boundaries. Some granitoid fragments also occur (5–15%) consisting of quartz, potassium feldspar, plagioclase, garnet, rutile, muscovite/sillimanite, biotite and graphite/opaque mineral. Small amount (< 5%) of biotite, kyanite and muscovite also occur in the matrix. The sample has similarly altered feldspars as the Amphibole group has, but with its quartz-abundance, garnet, rutile and kyanite content S15 differs completely from all the other samples.

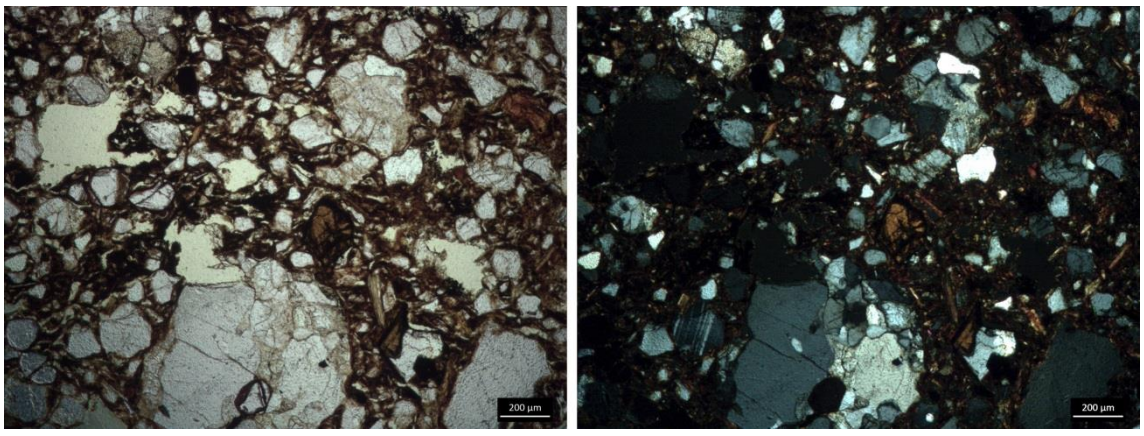


Figure 71. S15 containing abundant quartz, some rutile (centre of the picture) and garnet grains (inside rock fragment, bottom edge of the photomicrograph) (PPL and XP)

S17 is very similar to the quartz-rich samples of the Granitoid group, however it contains calcite/dolomite grains (2–5%; *Figure 72*), which cannot be observed in the Granitoid group. The sample contains *c.* 30% of inclusions and *c.* 15% of voids. The voids are meso- and macroplanar voids and mesovughs. The alignment of elongated grains and voids is moderate-strong. The matrix of the sample is non-calcareous, homogeneous, shows transition from very dark to light reddish-brown (PPL, XP) and have slight to high optical activity in XP. The grain-size distribution is bimodal with grains under 250 µm in the fine fraction and grains above 500 µm in the coarse fraction. The amount of elongated grains exceeds that of the equant grains, they are very poorly sorted and very angular to angular. S17 contains mostly granitoid fragments consisting of quartz, potassium feldspar, plagioclase and biotite in decreasing order of abundance. These minerals occur individually in the matrix as well; the quartz grains have undulose extinction and sutured boundaries. Green amphibole is also present in about the same amount as the calcite/dolomite crystals (2–5%). Calcite/dolomite grains once occur together with clinopyroxene. Few grains (0.5–2%) of graphite/opaque mineral are also spread in the matrix.

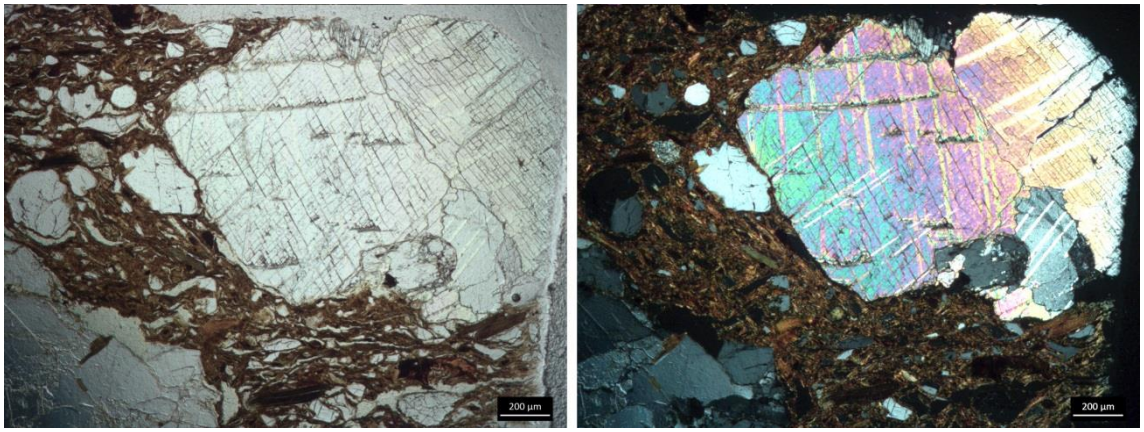


Figure 72. S17 with calcite/dolomite fragments (PPL and XP)

The inclusion-rich (*c.* 75%) S23 comprising abundant biotite, is very different from the other samples (*Figure 73*). It has mainly mesovughs and less mesoplanar voids which make up *c.* 5% of the sample. Elongated grains and voids show strong alignment. The sample has a non-calcareous and homogeneous matrix showing transition from dark to light reddish-brown (in PPL and XP) and accordingly moderate to very high optical activity in XP. The sample has bimodal grain-size distribution with a fine fraction under *c.* 200 µm and a coarse fraction above *c.* 700 µm. The grains are poorly sorted, angular to sub-angular and usually elongated. The main component of S23 is biotite which is present in such a large amount (50–70%) that it seems to make up the matrix at first sight. In this dense mass of biotite flakes, some (15–30%)

plagioclase, potassium feldspar and quartz grains occur. A few grains (< 5%) of green amphibole, amphibole-rich rock fragments (consisting of green amphibole, sericitic potassium feldspar and quartz), graphite/opaque mineral and muscovite are also present in the sample.

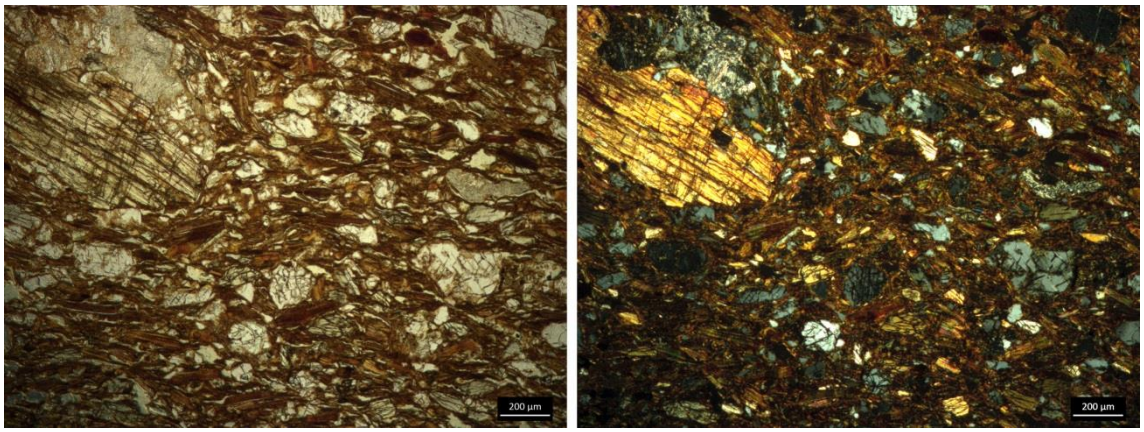


Figure 73. S23 including abundant biotite and some green amphibole crystals (e.g. top left-hand corner of the picture) (PPL and XP)

S48 is compositionally similar to subgroup 'Granitoid A2', but has a very different matrix (*Figure 74*). It contains about 45% of inclusions and 10% of meso- and macrovughs. The elongated constituents of the sample have weak alignment. The matrix is non-calcareous, homogeneous, very light yellowish-greyish brown in PPL and very dark grey and inactive in XP, which suggest a vitreous matrix. The sample has bimodal grain-size distribution with a fine fraction under 100 µm and a coarse fraction above 400 µm. More equant than elongated grains are present with very poor sorting and subangular boundaries. Quartz is the most abundant inclusion occurring mainly as very fine-grained (< 100 µm) monocrystalline quartz followed by granitoid fragments including plagioclase, potassium feldspar, quartz, biotite and zircon. The components of the rock fragments occur also individually in the matrix. Few grains of muscovite are also present (< 2%).

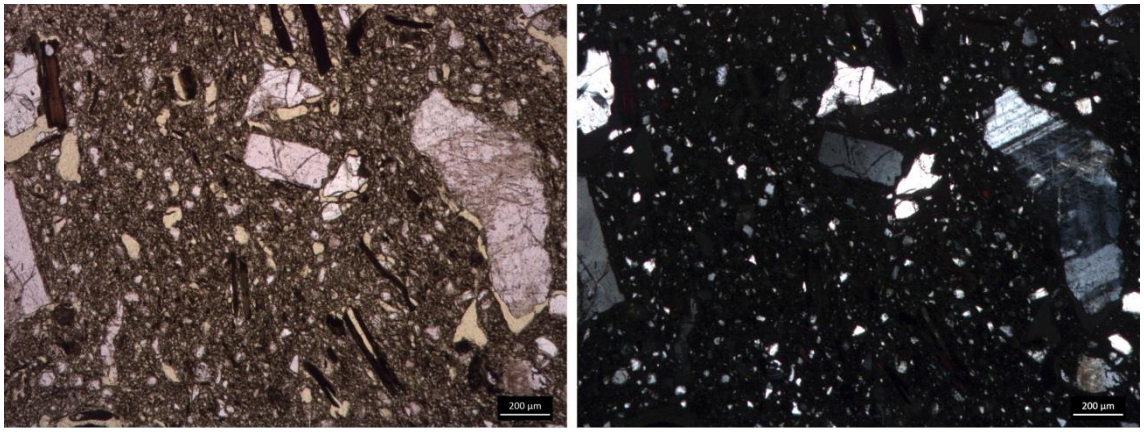


Figure 74. Vitreous matrix of S48 showing optical inactivity in XP (PPL and XP)

S131 is unique in composition as it contains kyanite-bearing mica schist fragments (*Figure 75*). The ratio of inclusions is *c.* 30% in the sample. Meso- and macroplanar voids, meso- and macrochannels and mesovughs occur making up *c.* 7% of the sample. The alignment of elongated grains and voids is moderate. The sample has homogeneous, non-calcareous matrix showing light reddish-brown colour both in PPL and XP with a high optical activity in XP. It has bimodal grain-size distribution with an average upper boundary of the fine fraction of *c.* 500 µm and an average lower boundary of the coarse fraction of *c.* 750 µm. More elongated than equant grains are present with very poor sorting and angular to subangular boundaries. The sample contain 50% to 70% of kyanite-bearing mica schist consisting of quartz, muscovite, biotite, kyanite, graphite, potassium feldspar and rutile. (These minerals also occur in the matrix.) Plagioclase and scapolite are also present with a frequency between 0.5% and 2%.

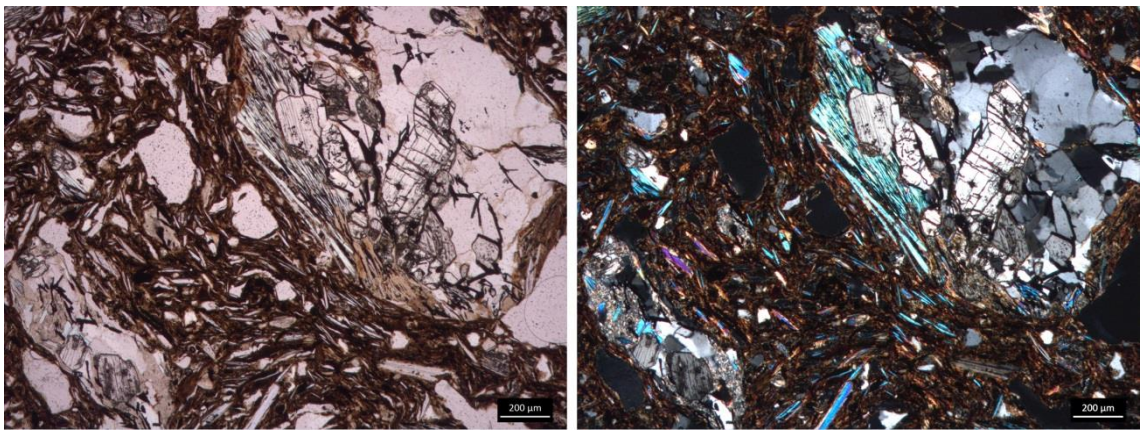


Figure 75. S131 containing kyanite-bearing mica schist (PPL and XP)

4.2.2 Graphite-containing ceramics

The Graphite group represents a varied selection of samples from several sites of Lower Austria (50 samples: S13, S31–S36, S49, S53, S54, S62, S84–S86, S99–S130 and S132–S135). However, they are similar in that all of them include more than 30% graphite-containing rock fragments and graphite flakes.

The graphite-containing samples have different amount of inclusions ranging from 15% to 40%. The ratio of the voids is usually 5% to 10% which are mainly meso- and macrovughs and lesser mesoplanar voids and mesochannels are also present. The alignment of elongated grains and voids compared to each other and the walls of the ceramics is usually moderate. The colour of the matrix is mostly dark reddish-brown, very dark reddish-brown or black in PPL which turn into the same colours or occasionally yellowish-greyish brown in XP. The optical

activity of the matrix is usually inactive or very slightly active apart from two subgroups (see below). The matrix of the samples of the Graphite group is probably non-calcareous, although often it cannot be properly investigated under microscope because of the very dark colour of the matrix.

These samples have bimodal grain-size distribution usually with a higher proportion of fine fraction (50–70%) than that of coarse fraction (30–50%). The average upper boundary of the fine fraction is between 200 µm and 500 µm and average lower boundary of the coarse fraction is between 400 µm and 750 µm varying in different samples. The grains are usually very poorly sorted, have rather elongated than equant shape and very angular to sub-angular boundaries.

Within the Graphite group, four subgroups can be distinguished ('Graphite A', 'Graphite B', 'Graphite C' and 'Graphite D') based on the type of the graphite-containing rock fragments and the amount of graphite present in the samples. Samples of subgroup 'Graphite A', 'Graphite B' and 'Graphite C' contain more than 50% of graphite flakes and graphite-containing rock fragments while subgroup 'Graphite D' contain a fewer amount of those ranging between 30% and 50% (*Table 18*).

Table 18. Subgroups of the Graphite group

GRAPHITE GROUP (50) More than 30% graphite flakes + graphitic rock fragments	• **'Graphite A' -** Graphite gneiss • 'Graphite A1' - Sillimanite gneiss: 99, 101, 102, 103, 110, 111 • 'Graphite A2' - Gneiss structure + equilibrium crystallisation: 100, 104, 105, 117, 120, 126, 134 • 'Graphite A3' - Garnet-rich (2–15%): 32, 34, 36, 84, 85, 86, 107, 112, 118, 135 • 'Graphite A4' - Kyanite-rich (2–15%): 31, 122, 128 • 'Graphite A5' - No special mineral/rock fragment**:** 33, 35, 106, 108, 109, 113, 114, 125, 127 • **'Graphite B'** - Graphitic mica schist: 130, 133 • **'Graphite C' -** Carbonate rock • 'Graphite C1' - Coarse-grained: 115, 116, 119, 121, 132 • 'Graphite C2' - Micritic: 123, 124, 129 • **'Graphite D'** - Low graphite content (30–50%): 13, 49, 53, 54, 62

Graphite gneiss subgroup ('Graphite A')

This subgroup consists of 35 samples (S31–S36, S84–S86, S99–S114, S117, S118, S120, S122, S125–S128, S134 and S135), which contain graphite gneiss fragments and minerals of the

decomposition of the same rock. The gneiss fragments usually consist of graphite, quartz, feldspar (potassium feldspar > plagioclase), biotite, muscovite and rutile. Graphite occurs most commonly in the form of flakes and frequently larger graphite nodules are also present containing inclusions of rutile, scapolite, quartz or feldspar. The gneiss fragments and the graphite flakes are the most abundant in the samples (above 50%) followed usually by individual grains of quartz, feldspar, biotite and muscovite. The mica content is less than 15%. The samples commonly contain green, colourless or brown amphibole (< 15%), scapolite (< 15%), rutile (< 5%) and secondary carbonate (< 2%), occasionally less than 15% of clay pellets, sillimanite, garnet, kyanite and pyroxene.

The Graphite gneiss subgroup can be divided into five smaller subgroups ('Graphite A1', 'Graphite A2', 'Graphite A3', 'Graphite A4' and 'Graphite A5') based on the composition and structure of the graphite gneiss fragments or the presence of certain minerals. Due to the diversity of the samples, the thin sections within a subgroup usually share only one or two characteristics.

The samples of subgroup 'Graphite A1' (S99, S101, S102, S103, S110 and S111) contain few grains of sillimanite-bearing graphite gneiss in addition to the sillimanite-free graphite gneiss fragments described above (*Figure 76*). The sillimanite-bearing graphite gneiss fragments consist mainly of fine-grained sillimanite and a small amount of graphite; quartz or feldspar are rarely present.[57]

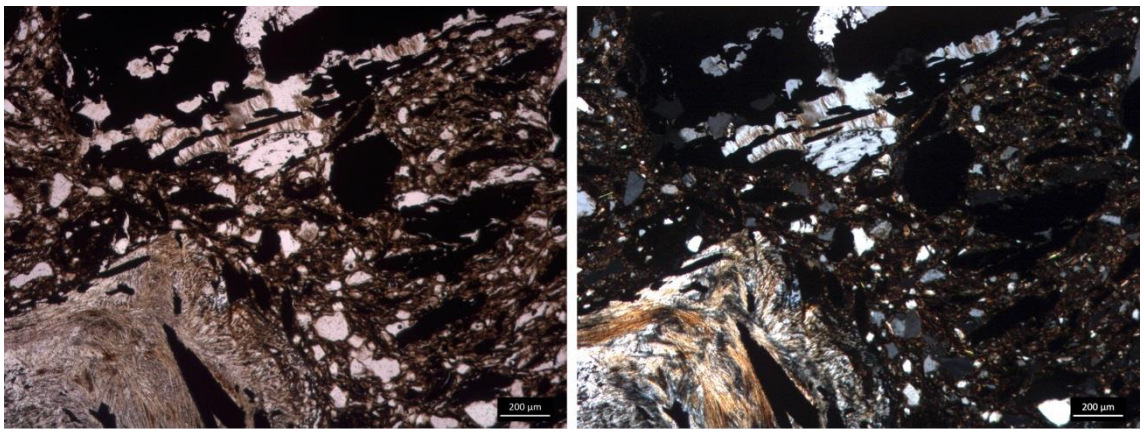


Figure 76. Subgroup 'Graphite A1' containing graphite gneiss (upper part of the picture) and sillimanite-bearing graphite gneiss (bottom left-hand corner) fragments (S101, PPL and XP)

[57] S99, S103 and S111 have fragments of sillimanite gneiss without any attached graphite, but they are most probably sillimanite-bearing graphite gneiss fragments as well.

The rock fragments of subgroup ‘Graphite A2’ (S100, S104, S105, S117, S120, S126 and S134) can be separated into two microstructural types. (Both types are compositionally the same.) Most of them have gneissose structure showing more or less alignment. However, some rock fragments include triple junctions of quartz and feldspar grains, which refer to equilibrium crystallisation (*Figure 77*). These two microstructural types originate from the same rock as shown by their occasional co-occurrence within the same grain.

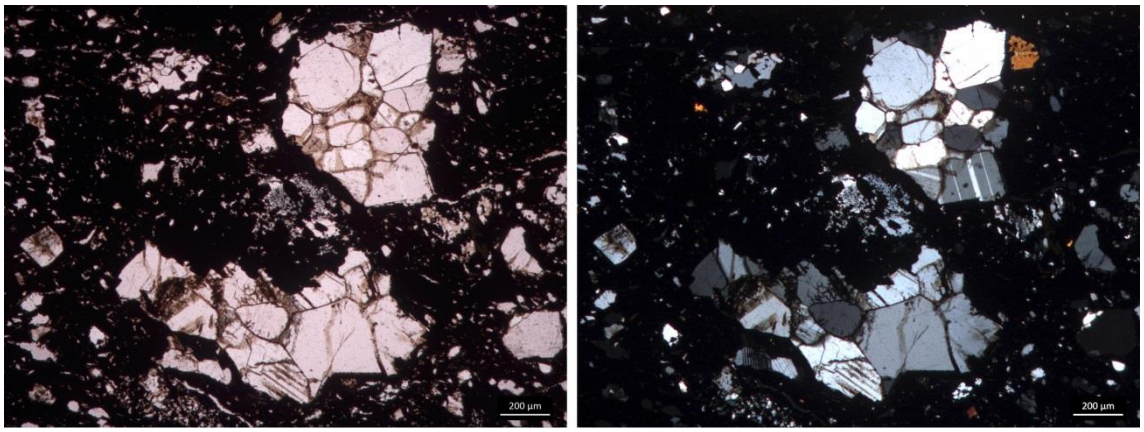


Figure 77. Subgroup ‘Graphite A2’ with rock fragments including quartz and feldspar grains with triple junctions as a sign of equilibrium crystallisation (S104, PPL and XP)

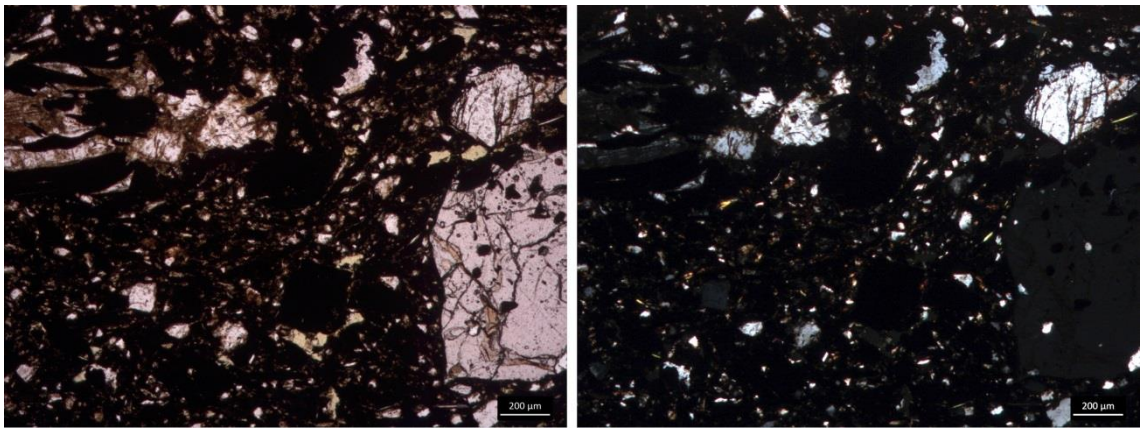


Figure 78. Subgroup ‘Graphite A3’ containing garnet (right edge of the photomicrograph) (S32, PPL and XP)

Subgroup ‘Graphite A3’ (S32, S34, S36, S84, S85, S86, S107, S112, S118 and S135) is characterised by the significant presence (2–15%) of colourless garnet (*Figure 78*). Three samples (S107, S112 and S118) contain less garnet (2–5%) than the other samples in this subgroup and are also linked together by distinctive clay pellets occurring with 5–30% in the matrix (*Figure 79*). These clay pellets are light yellowish-greyish brown in PPL, dark yellowish-greyish brown and optically very slightly or moderately active in XP. They have

elongated/distorted shape with angular to sub-rounded and diffuse boundaries, concordant orientation and similar composition to the matrix.

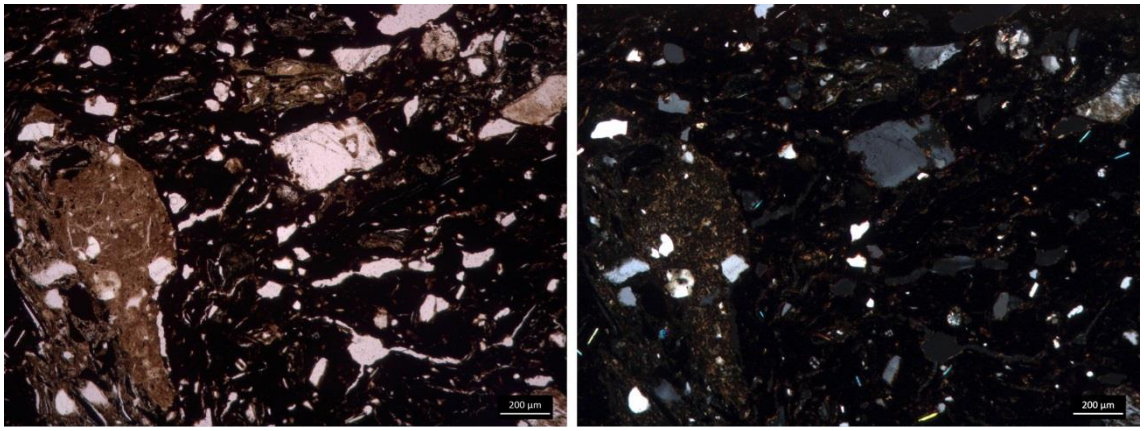


Figure 79. Clay pellets in S107 (e.g. bottom left-hand corner of the picture) (PPL and XP)

The three samples of subgroup 'Graphite A4' (S31, S122 and S128) contain a distinctive amount (2–15%) of kyanite (*Figure 80*). In S122 and S128 kyanite has started decomposing which is manifested in a brown alteration product along the edges and cleavage lines.

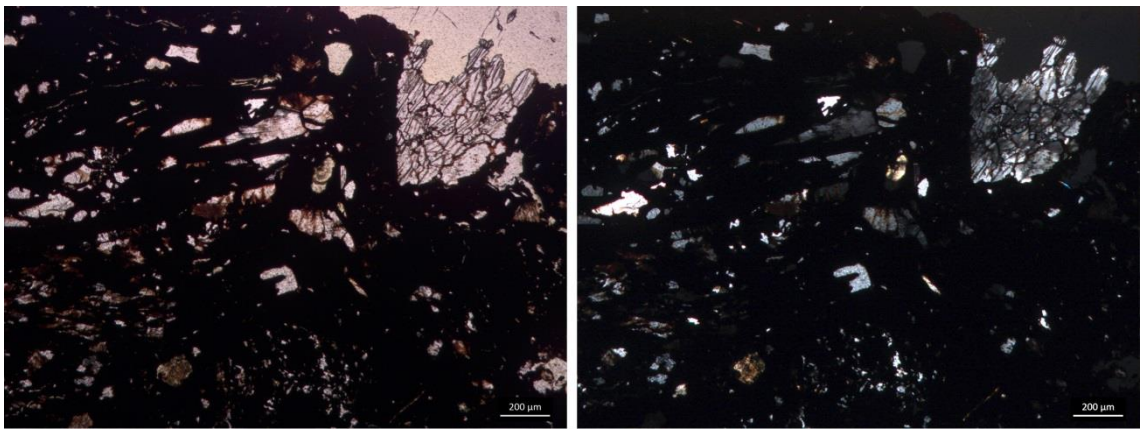


Figure 80. Subgroup 'Graphite A4' with kyanite (top right-hand corner) (S31, PPL and XP)

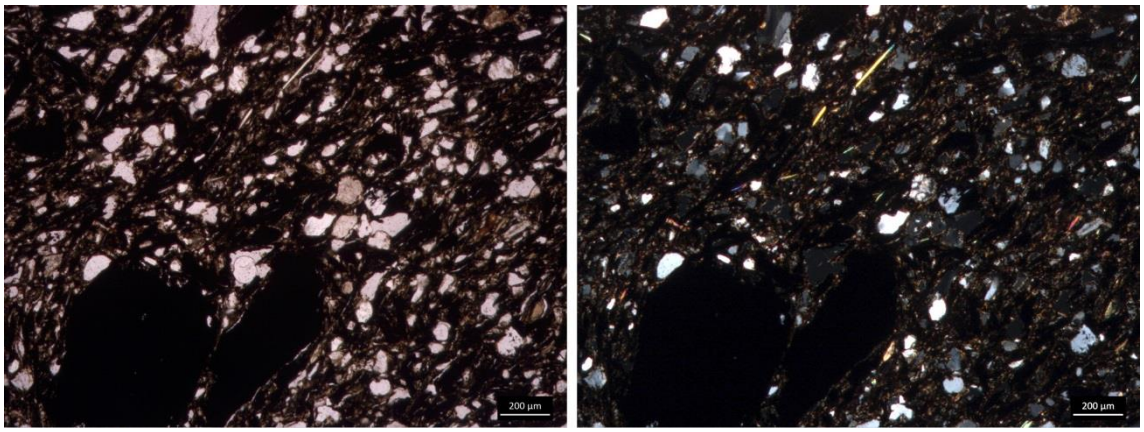


Figure 81. Microstructure of subgroup 'Graphite A5' (S113, PPL and XP)

Finally, subgroup ‘Graphite A5’ involves all those graphite gneiss-containing samples which do not have any special minerals or rock fragments present with a significant amount (S33, S35, S106, S108, S109, S113, S114, S125 and S127; *Figure 81*). Slight difference can be observed regarding the colour of the matrix of these samples which is usually brighter than the other samples of subgroup ‘Graphite A’ and has slight or moderate optical activity in XP.

Two samples have features which differentiate them from the other samples of subgroup ‘Graphite A5’. On the inner side of S113, there is an eroded layer of glaze or surface deposition with a pale yellow/brown colour in PPL (isotropic in XP; *Figure 82*). On the top of this glaze/deposition there is another layer consisting of calcite/dolomite crystals, quartz and muscovite in a calcareous dark yellowish-greyish brown matrix in PPL. (The matrix is very dark grey, optically almost inactive in XP.) The macroscopic appearance of these layers is shown in *Figure 83*.

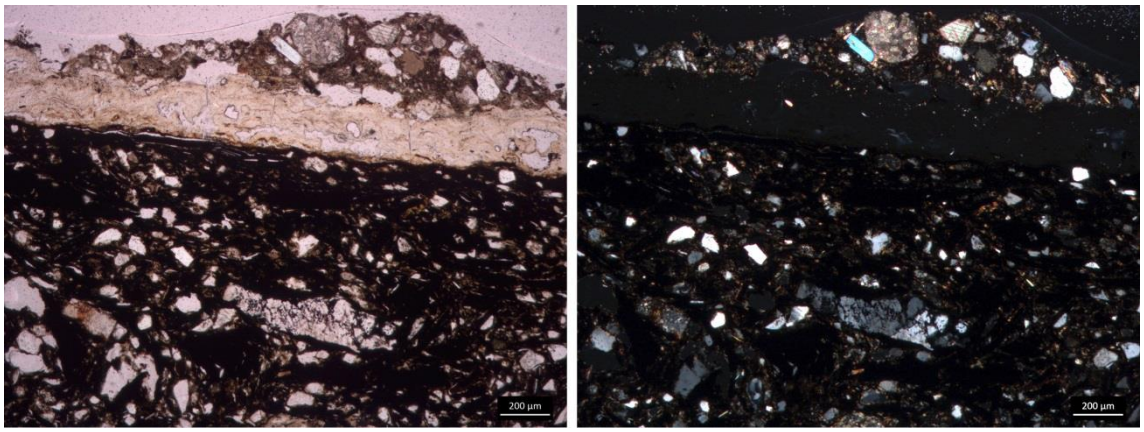


Figure 82. Glaze/deposition layer on the inner side of S113. On the top of this layer, another carbonate-rich layer can be observed (PPL and XP)



Figure 83. The outer and inner side of S113 (photo by the Austrian Federal Office for the Protection of Monuments)

In the other distinctive sample, S125, some feldspar grains have an unusual reddish-brown colour in PPL (*Figure 84*). This can either be a sign of high iron content or some kind of alteration. These reddish-brown feldspar grains include both potassium feldspar and plagioclase and present individually in the matrix or within graphite gneiss fragments.

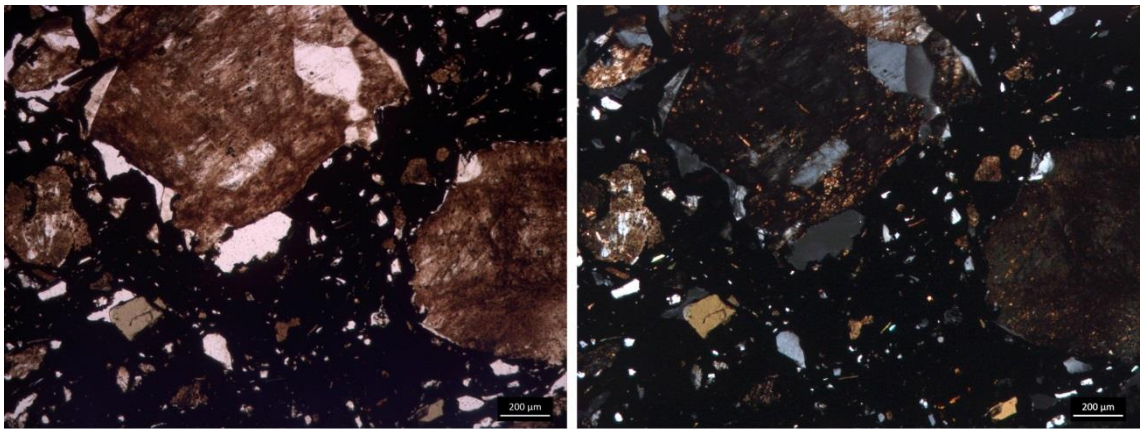


Figure 84. Altered feldspars with a reddish-brown colour in S125 (PPL and XP)

It is important to note that the boundaries of the subgroups of 'Graphite A' are slightly flexible. There are two samples which can be grouped in two different subgroups at the same time. S110 of 'Graphite A1' (sillimanite gneiss) and S128 of 'Graphite A4' (kyanite) also contain rock fragments with equilibrium crystallisation, thus they could be placed in subgroup 'Graphite A2' as well.

Graphitic mica schist subgroup ('Graphite B')

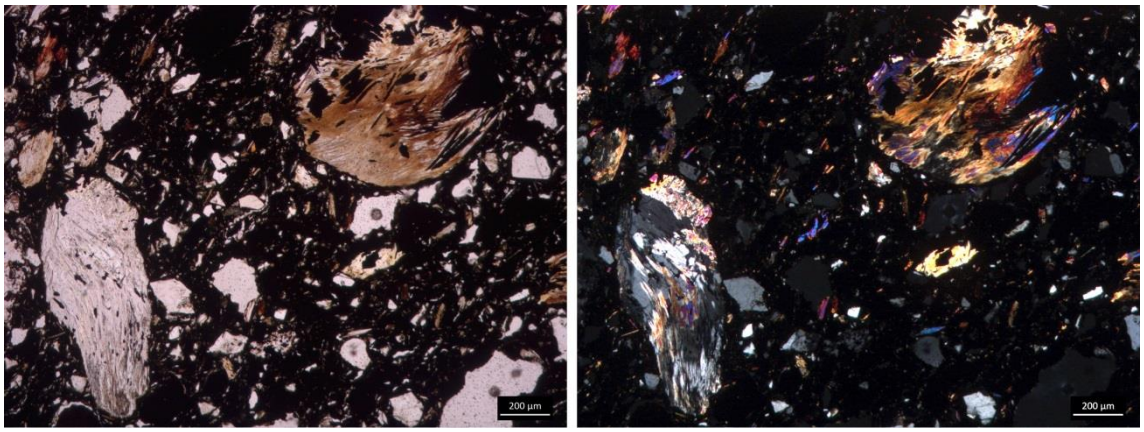


Figure 85. Subgroup 'Graphite B' containing graphitic mica schist fragments (S133, PPL and XP)

This subgroup consists of two samples (S130 and S133) both of which are rich in graphite and fragments of graphite-containing mica schist (above 50%; *Figure 85*). Graphite, mica and quartz are the main components building up the mica schist fragments. The proportion of the

mica types is different in the samples: schist fragments in S130 are rather biotite-rich while in S133 they contain more muscovite than biotite. As fragments of the schist, some individual mica flakes (2–15%), quartz (2–30%) and feldspar (0.5–15%) grains are also present in the matrix. Rutile is the only accessory mineral that occurs in both samples (0.5–2%).

Carbonate rock subgroup ('Graphite C')

This subgroup includes all graphite-containing ceramics with primary carbonate. Primary carbonate occurs in two different forms: five samples (S115, S116, S119, S121 and S132) have coarse-grained carbonate rock fragments and three samples (S123, S124 and S129) have carbonate rock fragments with micritic structure. This difference identifies the two subgroups, 'Graphite C1' and 'Graphite C2'.

Subgroup 'Graphite C1' contains coarse-grained carbonate rock fragments with graphite often referred to as 'graphite marble' (*Figure 86*). In addition to calcite/dolomite and graphite crystals, rock fragments can contain feldspar, quartz, mica (mainly biotite), scapolite and epidote/zoisite/clinozoisite. In the matrix, individual grains of quartz (5–30%), potassium feldspar (2–15%), plagioclase (except S132, 2–5%), biotite (2–30%) and muscovite (0.5–2%) are present in all samples. Calcite/dolomite crystals occur in three samples outside rock fragments with different proportions (S116: 5–15%, S119: <0.5%, S132: 15–30%). The most common accessory minerals are scapolite (0.5–15%; S115, S116, S132), epidote/zoisite/clinozoisite (2–5%; S119, S121) and garnet (<0.5%; S119, S121).

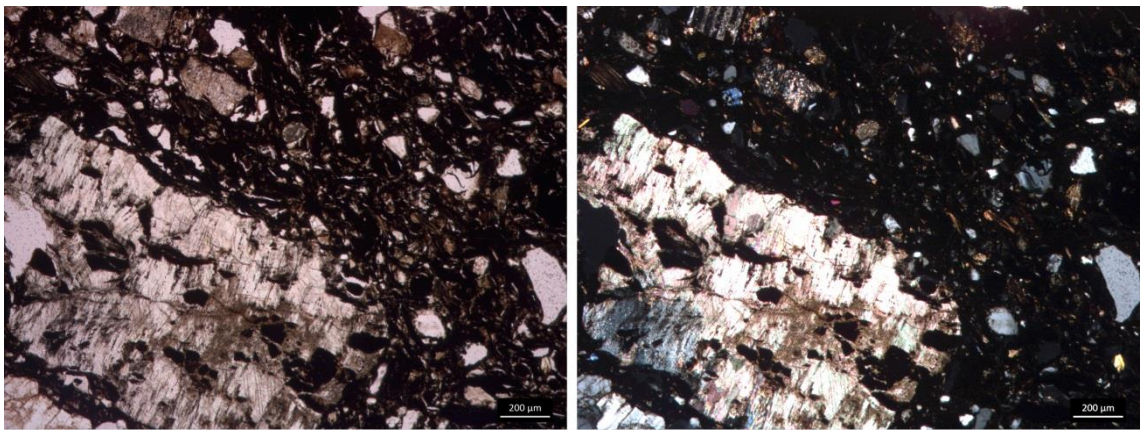


Figure 86. Subgroup 'Graphite C1' containing graphite marble fragments (bottom left-hand quarter of the picture) (S119, PPL and XP)

Subgroup 'Graphite C2' includes graphite gneiss and micrite as rock fragments (*Figure 87*). S123 is slightly different from S124 and S129 as it contains predominantly graphite gneiss

fragments and only two fragments of micrite. In contrast, S124 and S129 involve abundant micrite fragments, which occasionally have inclusions of quartz or graphite/opaque mineral. Graphite gneiss fragments consist of graphite, quartz, feldspar and biotite in all samples and additional rutile and scapolite in S123 and S129. Apart from rock fragments, individual crystals of quartz (5–30%), potassium feldspar (2–15%), plagioclase (except S123, 2–5%), biotite (2–15%) and muscovite (0.5–2%) are present in the matrix. Some grains of scapolite (0.5–5%) and rutile (0.5–2%) occur in S123 and S129, and a small amount of green amphibole (< 5%) is present in S124 and S129.

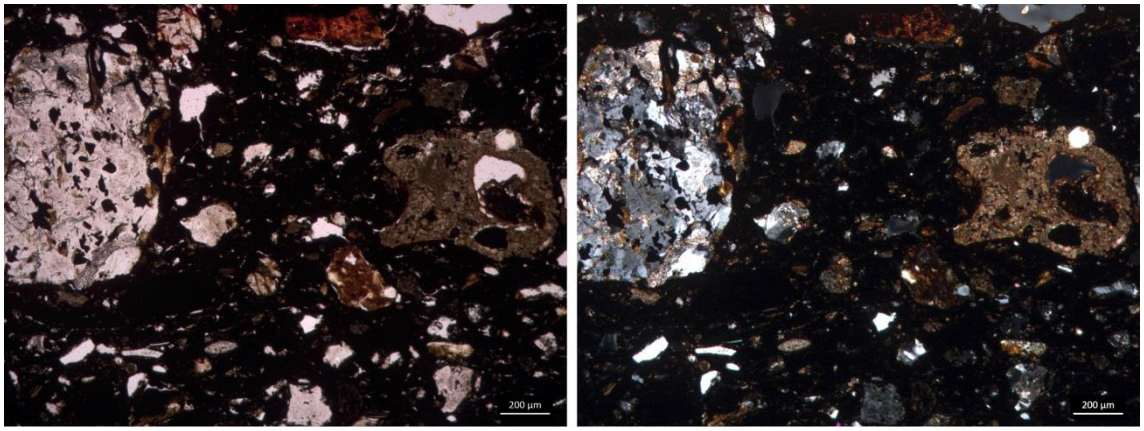


Figure 87. Subgroup 'Graphite C2' containing micrite fragments (middle of the right edge of the photomicrograph) (S124, PPL and XP)

Low graphite subgroup ('Graphite D')

Subgroup 'Graphite D' includes five samples (S13, S49, S53, S54 and S62) that contain less graphite (30–50%) than the other subgroups of graphite-containing ceramics (> 50%). They have brighter matrix than the other subgroups and the optical activity of the matrix is also higher ranging from slightly active to highly active.

The most abundant inclusions are graphite flakes and graphite gneiss fragments followed by quartz and potassium feldspar (plagioclase occurs only in S13 and S54). The biotite content varies up to 30% and less than 2% of muscovite is present in the matrix (except S49, where no biotite or muscovite can be identified). Rutile occurs in three samples (S13, S49 and S54) and garnet in two samples (S54 and S62). The thin sections of this subgroup are special because they contain sedimentary rock fragments in a notable amount (5–30%). S13 and S62 have chert fragments (S13 contains only one grain; *Figure 88*), S49 and S54 include argillaceous rock fragments (siltstone/claystone; *Figure 89*). In S53 many argillaceous inclusions occur, which are rounded, equant and inclusion-poor with neutral density and sharp to merging boundaries and

they are surrounded by thin pores. The identification of these inclusions is not obvious as the surrounding pores suggest argillaceous rock fragments, but they are very similar to the matrix, have rounded boundaries and sometimes sharp to merging boundaries which refer to clay pellets.

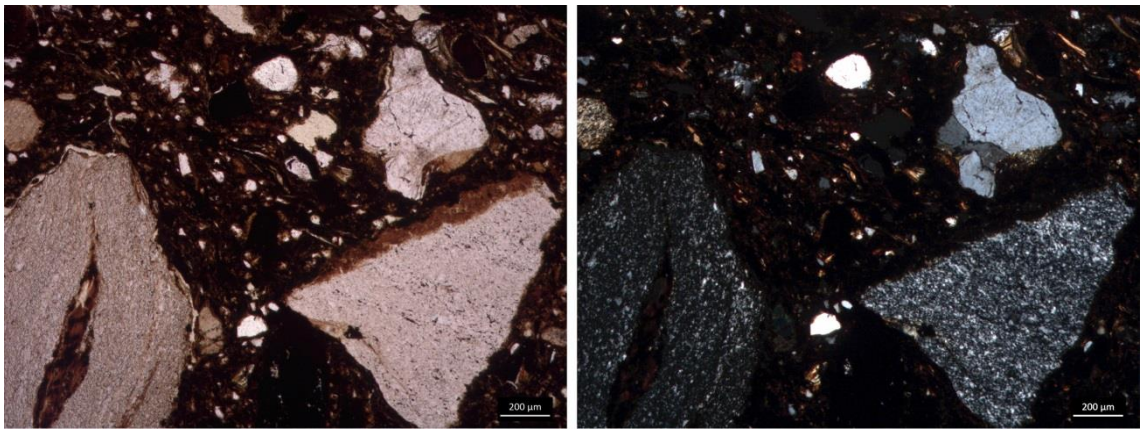


Figure 88. Chert fragments in S62 (lower half of the photomicrograph) (PPL and XP)

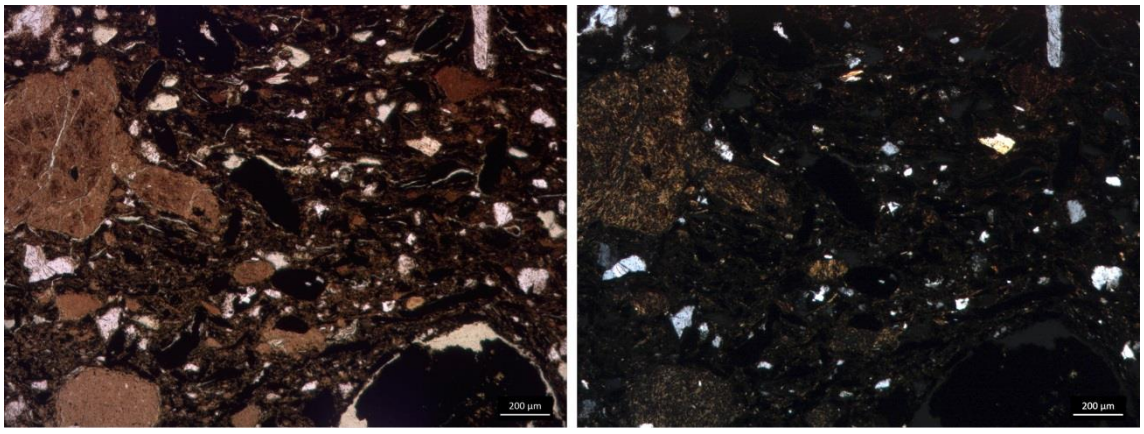


Figure 89. Argillaceous rock fragments in S54 (e.g. top left-hand quarter of the picture) (PPL and XP)

4.2.3 Summary

The 135 thin sections are divided into graphite-free and graphite-rich samples. Graphite-free ceramics are grouped into four main petrographic groups with different mineralogical compositions (Granitoid, Amphibole, Diorite and Carbonate groups) and several subgroups based on microstructure and composition. Five individual samples differ significantly from the rest of the graphite-free samples. The graphite-rich Graphite group comprises three subgroups containing different graphitic rocks (graphite gneiss, graphitic mica schist and graphitic carbonate rock) and a subgroup containing a smaller amount of graphite (30–50%) than the three other subgroups (> 50%).

4.3 Scanning electron microscopy

Scanning electron microscopy was performed on 49 samples chosen from each petrographic group and subgroup (*Table 19*). The same sample set was analysed by SEM as by chemical analysis (ICP-OES, see Section 4.4) and X-ray diffraction (XRD, see Section 4.5). Therefore, sample selection was also determined by the amount of sample left after thin sectioning so that there would be enough material for all three methods. At least two samples were investigated in each subgroup, however, in few cases ('Graphite B1', 'Graphite C1' and 'Graphite C2') it was not possible because of the unavailability of (sufficient amount of) potsherds.

Table 19. Samples investigated by SEM, ICP-OES and XRD with their petrographic groups

Granitoid group	**A1**: S10, S70, S88, S98 **A2**: S52, S65, S78 **A3**: S40, S51 **B1**: S12, S83	**B2**: S9, S93 **B3**: S45, S46 **C**: S1, S87 **D**: S5, S21
Amphibole group	S8, S61, S90	
Diorite group	**A**: S11, S75	**B**: S67, S97
Carbonate group	**A**: S57, S58	**B**: S89
Individual sample	S15	
Graphite group	**A1**: S102, S103, S110 **A2**: S100, S104 **A3**: S32, S36, S86, S107 **A4**: S31, S128 **A5**: S35, S108, S109	**B**: S130 **C1**: S132 **C2**: S129 **D**: S13, S54

SEM was used for the examination of vitrification structure with SE detector and for chemical analysis of the matrix and minerals with EDS (for methodology see Section 3.4.3). The results of these analyses are detailed below.

4.3.1 Results of vitrification analysis

Vitrification analysis was carried out on 25 samples chosen from different petrographic groups.[58] The analysed samples include S1, S8, S9, S10, S11, S12, S13, S15, S21, S31, S36, S40, S57, S65, S75, S89, S90, S97, S98, S102, S104, S107, S129, S130 and S132. In addition, another potsherd of S10 was examined to determine whether there was any difference between different parts of the same vessel.

[58] Vitrification analysis was performed on a reduced sample number of the set of 49 samples chosen for SEM, ICP-OES and XRD analyses because of the similarity of results.

The SE images of the 25 samples show great similarity (Appendix D.1). Almost all of them have unvitrified microstructure with distinguishable clay platelets (e.g. *Figure 90*). This structure is consistent with the first category defined by Maniatis and Tite (1981), referred to as the 'no vitrification' stage. This stage can be connected to firing temperatures under 800 °C in oxidising atmosphere and under 750 °C in reducing atmosphere (Maniatis and Tite 1981, 68: Table 1).

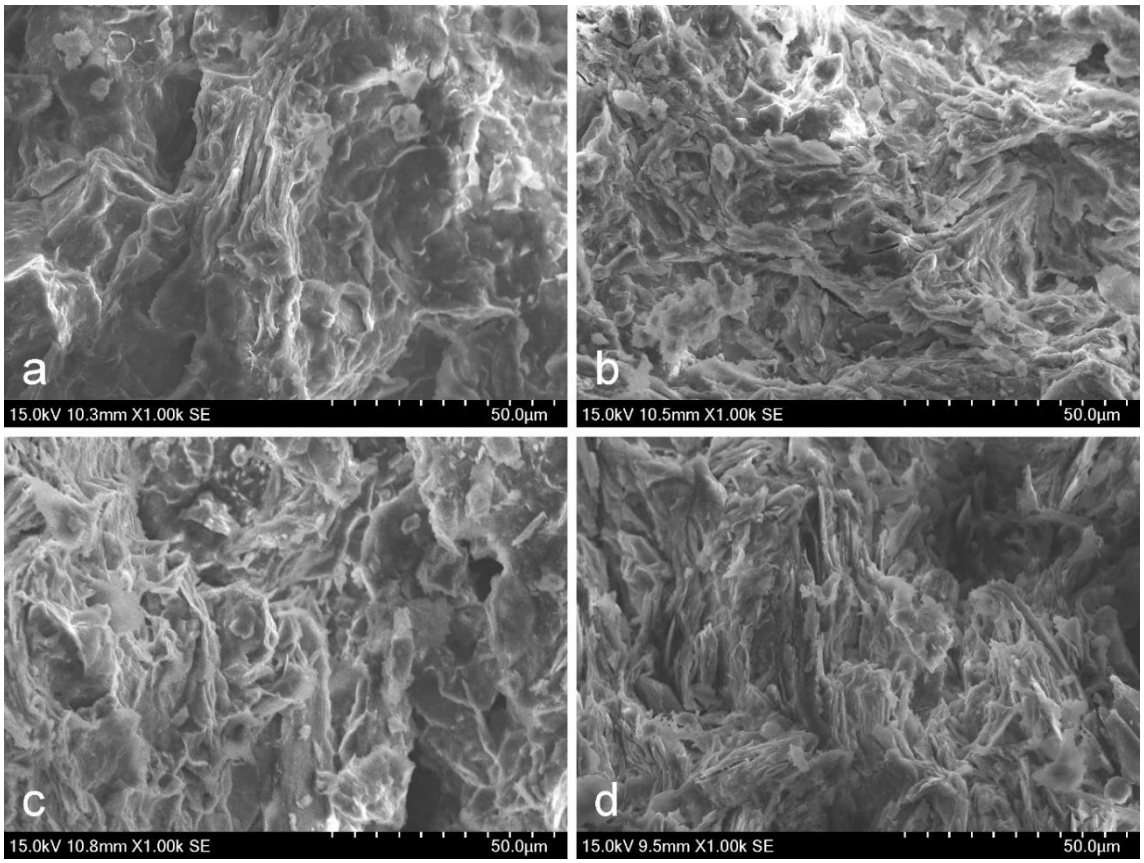


Figure 90. Examples for unvitrified microstructure (a. S8, b. S10, c. S97, d. S130)

The two sherds of S10 are identical under SEM, they show the same microstructure with no vitrification (see S10-1 and S10-2 in Appendix D.1).

There is one sherd that somewhat differs from the rest of the samples. S90 of the Amphibole group (*Figure 91*) seems to be slightly vitrified and thus is comparable to the examples of the 'initial vitrification' stage of Maniatis and Tite (1981). The assigned temperature ranges to this stage are 800–850 °C (oxidising atmosphere) and 750–800 °C (reducing atmosphere; Maniatis and Tite 1981, 68: Table 1). However, the other sample analysed from this group (S8) shows the same unvitrified structure as most of the sherds do (*Figure 90a*).

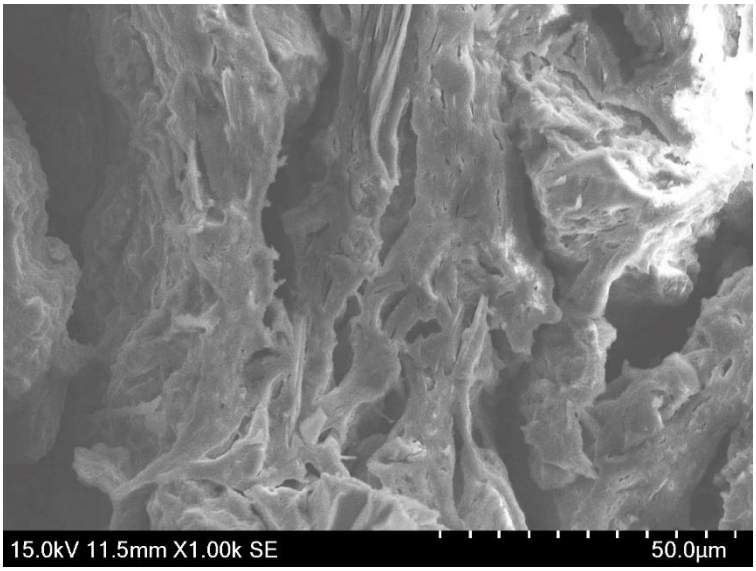


Figure 91. Initial vitrification structure of S90

4.3.2 Results of chemical analysis by SEM-EDS

In the following sections, the results of SEM-EDS analysis are detailed including that of the matrix, various minerals and the surface layer of S113. This section and the following parts of the thesis contain graphs in which the samples are presented with symbols indicating their main petrographic groups. The symbols of the petrographic groups are presented in *Figure 92* below. The chemical data of the matrix and minerals forming the basis of the graphs of the SEM-EDS subchapter are included in Appendix D.2.

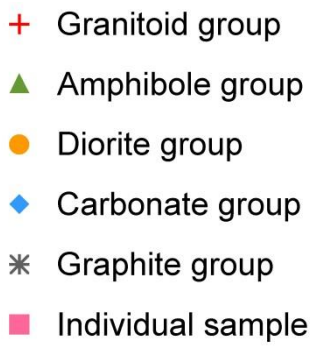


Figure 92. Legend for the graphs and diagrams used throughout the thesis

Matrix analysis

Matrix analysis was carried out on all 49 samples by SEM-EDS presented in *Table 19*. At least three matrix points were measured of each sample. The average of these values is plotted on several diagrams below, which are used to differentiate between different clays in archaeometric literature.

The two ternary graphs below (*Figures 93* and *94*) show overlapping petrographic groups which suggest that the clays of the investigated samples are chemically similar.

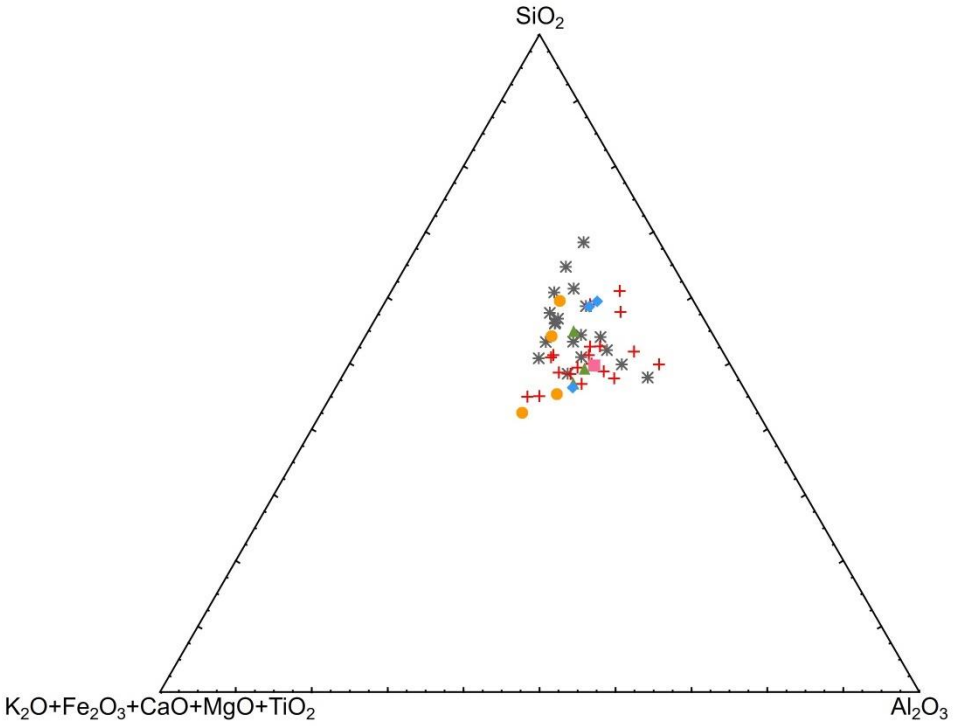


Figure 93. Matrix compositions plotted on the ternary diagram of SiO_2, Al_2O_3 and fluxes (K_2O, Fe_2O_3, CaO, MgO, TiO_2) following Maniatis and Tite (1978, 485: Fig. 1)

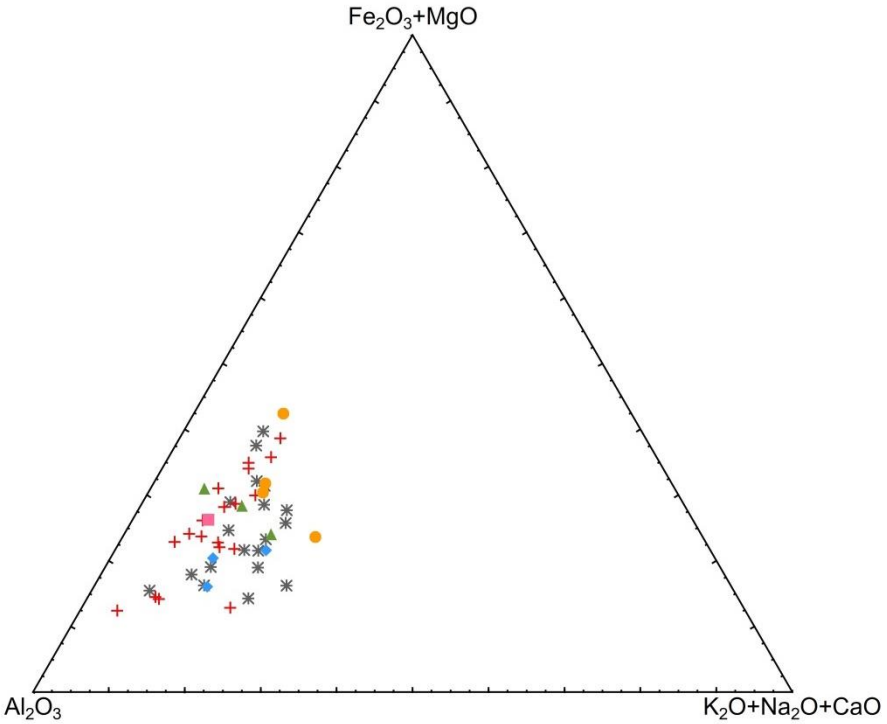


Figure 94. Matrix compositions plotted on the ternary diagram of Fe_2O_3+MgO, Al_2O_3 and K_2O+Na_2O+CaO following Philpotts and Wilson (1994, 615: Fig. 8)

The composition of the matrix is largely determined by the clay minerals present such as kaolinite, illite and different smectite species. The identification of the clay type may be possible through the calculation of atom percentages of main elements as suggested by Tite et al. (1982, 112: Fig. 5). As shown by *Figure 95*, there are some samples that are consistent with the composition of smectites and illites, but most of them seem to contain different clay minerals. The ratio of silicon and aluminium also have importance in defining clay types according to Velde and Druc (1999, 249). Based on Si/Al ratio, the clays are most likely illite clays or have a composition between illite and kaolinite and few samples might be made up of kaolinite and a smectite type called montmorillonite (*Figure 96*).

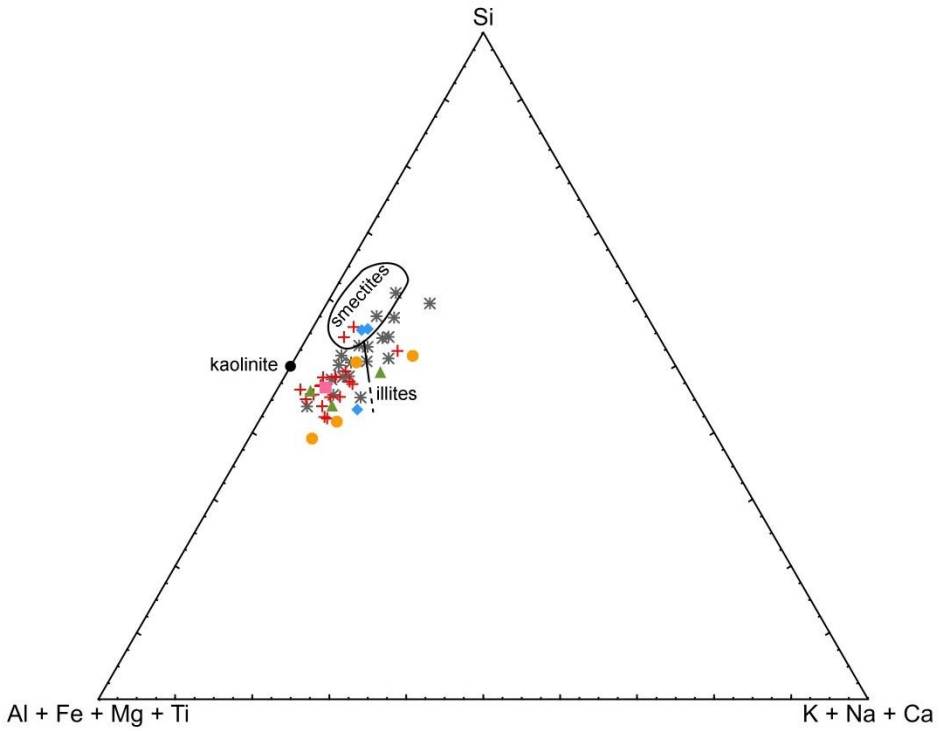


Figure 95. Matrix compositions plotted on the ternary diagram of Si, Al+Fe+Mg+Ti and K+Na+Ca with the position of the three main types of clay minerals (smectites, illites and kaolinite) following Tite et al. (1982, 112: Fig. 5)[59]

The matrices of 48 (out of 49) samples are non-calcareous as they contain less than 6 wt% of CaO. Only one sample, S89 of the Carbonate group has a slightly calcareous matrix with a CaO content just above 6 wt%. This sample slightly stands out from the other samples in *Figure 97* because of its higher CaO content.

[59] The authors defined the circle of smectites based on smectite analyses and the point/line for kaolinite/illite, respectively, are based on the theoretical formula of these clay minerals Tite et al. (1982, 112: Fig. 5).

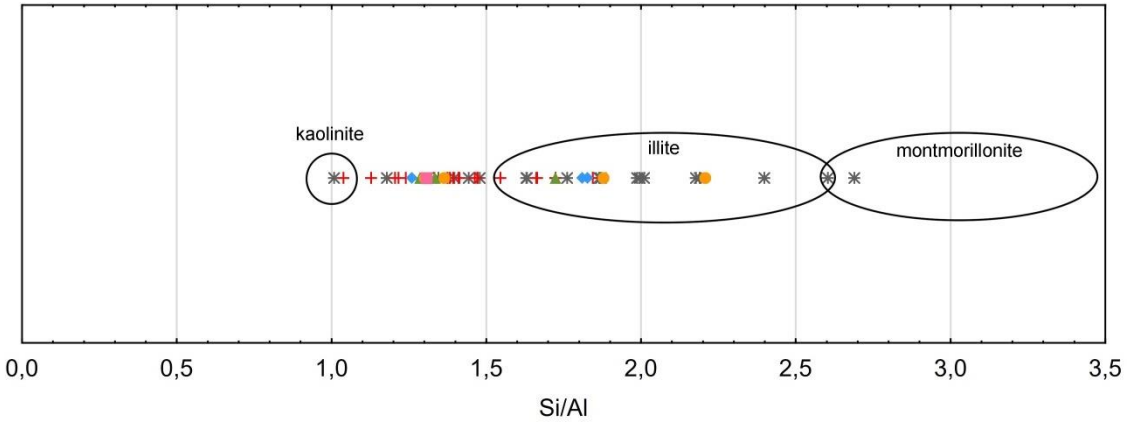


Figure 96. Si/Al ratios of the matrices. The fields of kaolinite, illite and montmorillonite are based on the values published by Velde and Druc (1999, 249)

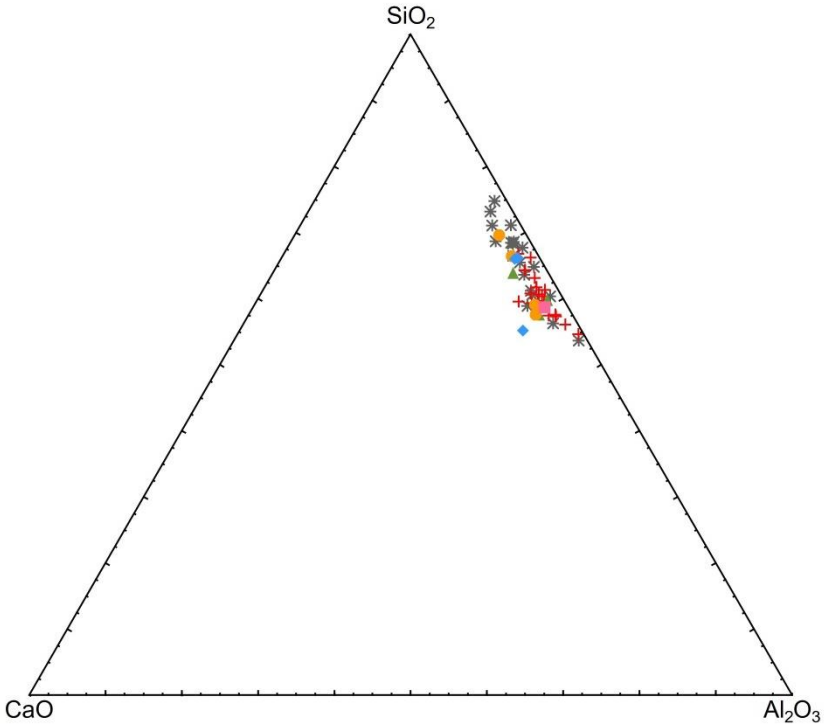


Figure 97. Matrix compositions plotted on the ternary diagram of SiO_2, CaO and Al_2O_3 following Artioli (2010, 233)

Mineral analyses

Feldspars and heavy minerals of all 49 samples were investigated by SEM-EDS. In addition, some other minerals that are typical or distinctive for their petrographic groups were also analysed in certain samples. Each mineral was measured at one spot/area, thus each point of the diagrams below belongs to a different grain (although not necessarily to a different sample, see figure captions).

In most of the cases, uncovered thin sections were available thus the composition of certain grains chosen by petrography could be determined. In the case of samples with covered thin sections however, flat surfaces of sherds were used, thus grain selection could not be carried out by petrography. Therefore SEM-EDS data of the samples should be seen as it carries some randomness since not all mineral grains could be measured in a sample.

Feldspars

Both main types of feldspar, alkali feldspar (including potassium feldspar) and plagioclase are present in the samples as shown in *Figure 98*. This ternary plot depicts three feldspars of different composition, the calcium-rich anorthite, the sodium-rich albite and the potassium-rich orthoclase, in which system the majority of feldspars can be placed (Deer et al. 1992, 393). Different names are used for the specification of the composition of plagioclase including albite, oligoclase, andesine, labradorite, bytownite and anorthite corresponding to 0–10%, 10–30%, 30–50%, 50–70%, 70–90% and 90–100% of anorthite content, respectively (*Figure 98*). The measured plagioclase feldspars of the samples have 0–40% of anorthite content with an outlier labradorite. Most of the alkali feldspars in the samples are potassium-rich having 70–100% of orthoclase.

The samples of the Granitoid group contain potassium feldspars with 70–100% orthoclase content and plagioclase feldspars belonging to the albite–andesine range. Subgroup A1, A2 and B3 also contain alkali feldspars with higher albite content (30–90%) in addition to potassium feldspars falling into the 'usual' range (Ab < 30%).

The Amphibole group contains plagioclase feldspar falling into the oligoclase–andesine range. The composition of only one potassium feldspar was recorded since most of the feldspars identified as potassium feldspar by petrography turned out to be plagioclase when analysed with SEM-EDS. This suggests that there might be more plagioclase in the samples than it was previously thought, but they do not exhibit the characteristic optical properties (lamellar twinning) based on which plagioclase and potassium feldspar is distinguished by polarising microscopy.

The Diorite group have oligoclase and andesine as plagioclase. Small compositional differences can be observed between the two subgroups in terms of alkali feldspars. Many of the alkali feldspars measured in 'Diorite A' are relatively potassium-poor (10–60% of orthoclase) while in 'Diorite B' they are potassium-rich (80–90% of orthoclase).

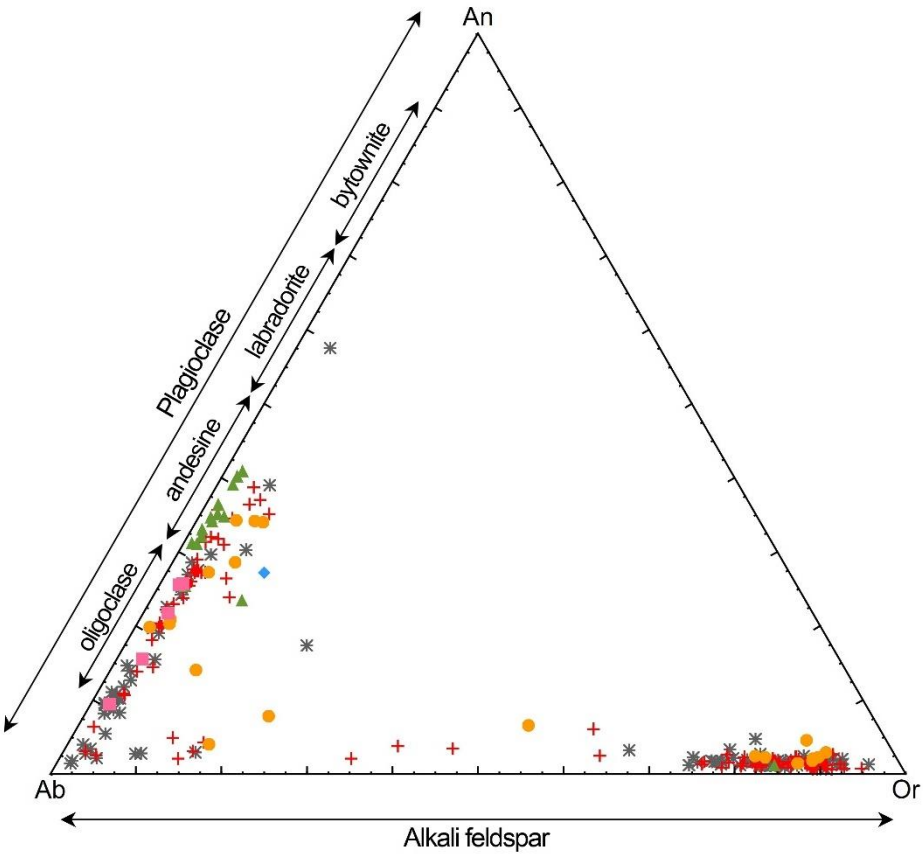


Figure 98. Feldspar compositions plotted on the ternary diagram of anorthite (An, $CaAlSi_2O_8$), albite (Ab, $NaAlSi_3O_8$) and orthoclase (Or, $KAlSi_3O_8$). (The diagram includes the data of 226 feldspar grains from 47 samples.)

The samples of the Carbonate group contain very few feldspars, only one could be measured, which has about 30% of anorthite content.

The individual sample, S15 contains only plagioclase (oligoclase) based on the measured feldspar grains. However, both potassium feldspar and plagioclase were recorded in the sample by petrography. The disagreement between the results of the two methods might have the same reason (lack of lamellar twinning) as mentioned above in the case of the Amphibole group.

Both potassium feldspar and plagioclase can be detected in the Graphite group. The composition of plagioclase feldspars in the subgroups fall into the albite–oligoclase range and in addition, 'Graphite A3' and 'Graphite D' also contain andesine grains. One sample (S128) in 'Graphite A4' contain labradorite, which is clearly separated from the other feldspars in *Figure 98*.

Heavy minerals

Heavy minerals are present in each sample as accessory minerals. The most common are zircon, rutile and titanite (sphene). Iron-rich phases are particularly abundant and titanium+iron-rich, calcium+phosphorus-rich and phosphorus+rare earth element-rich phases also occur frequently.

The zircon grains of the samples have similar compositions although slight differences can be identified when focusing on aluminium and iron content as shown in *Figure 99*. In this graph, some zircon grains of subgroups 'Granitoid A2', 'Granitoid D', 'Diorite A' and 'Diorite B' are 'isolated' from the rest because of their higher aluminium content (7–10 wt%, Appendix D.2). However, the aluminium content of the zircon is not group specific as other grains of these subgroups have 'usual' composition (< 5 wt% of Al_2O_3).

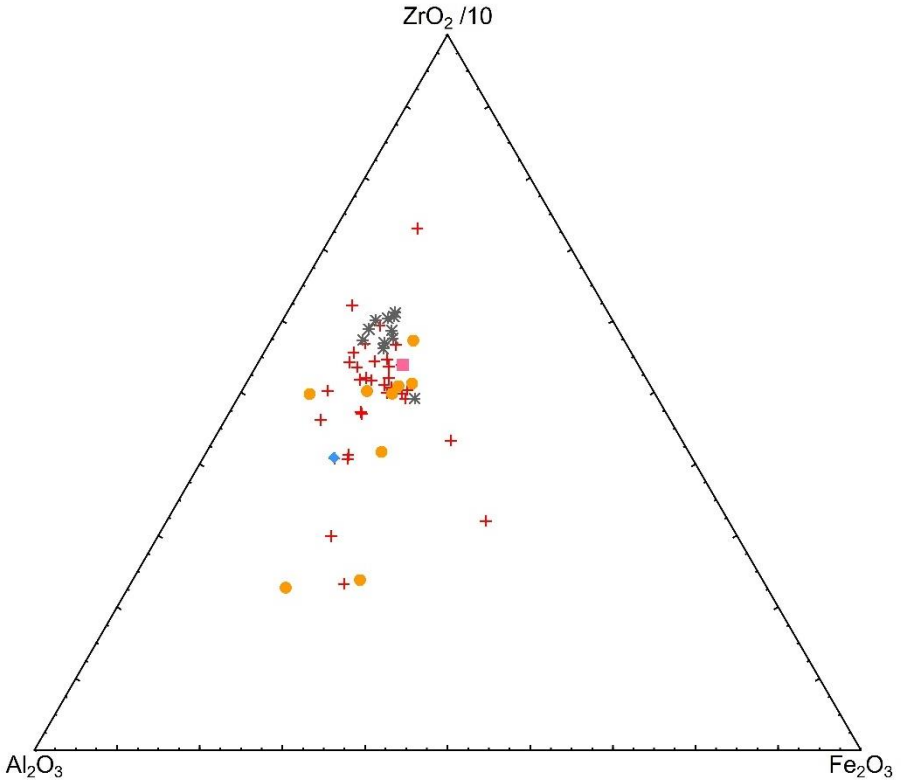


Figure 99. Zircon compositions plotted on the ternary diagram of ZrO_2, Al_2O_3 and Fe_2O_3. The values of ZrO_2 are divided by 10 for a better presentation of the data. (The diagram includes the data of 55 zircon grains from 30 samples.)

The composition of the rutile grains also differs slightly in terms of aluminium content (*Figure 100*). Rutile grains of the Granitoid group are usually richer in aluminium than the majority of those in the Graphite group. Five grains from four samples (S31, S54, S86 and S102) of the Graphite group contain niobium as a special constituent (Appendix D.2).

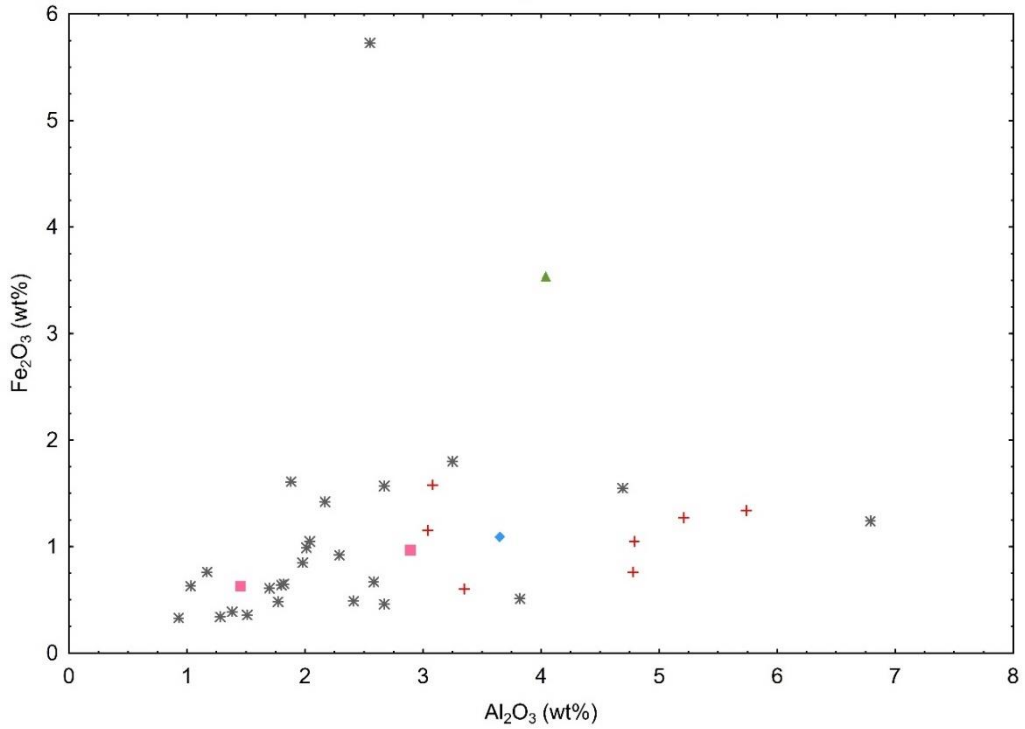


Figure 100. Al_2O_3 and Fe_2O_3 content of rutile grains. (The diagram includes the data of 36 rutile grains from 21 samples.)

Some titanite grains were also analysed and proved to be very similar in terms of composition (*Figure 101*).

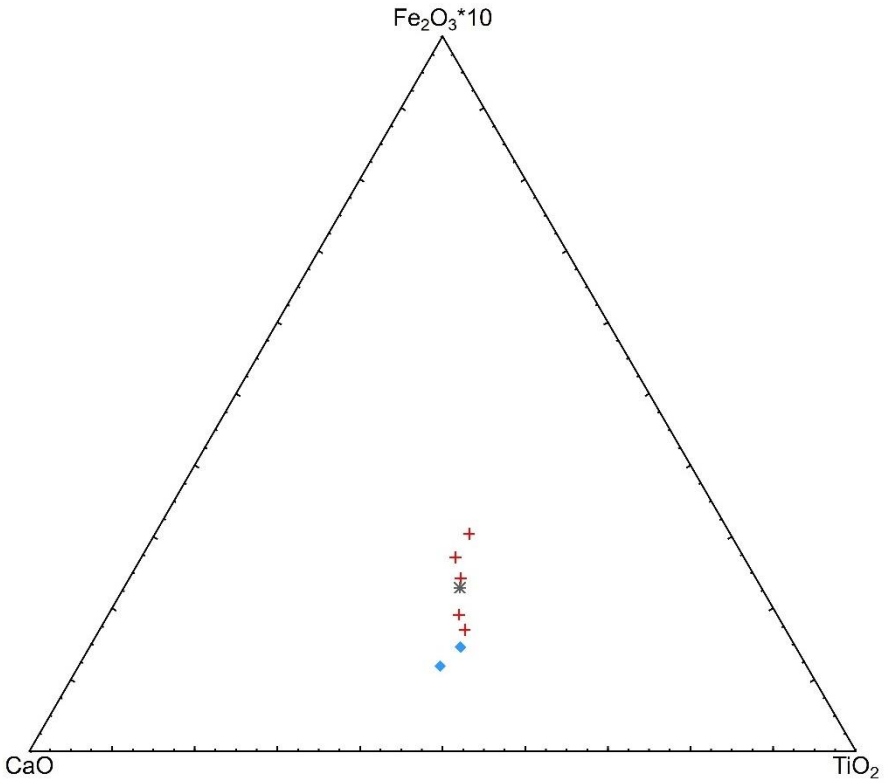


Figure 101. Titanite compositions plotted on the ternary diagram of Fe_2O_3, CaO and TiO_2. Fe_2O_3 values are multiplied by 10. (The diagram includes the data of 8 titanite grains from 6 samples.)

All petrographic groups contain samples with iron-rich phases which include Fe_2O_3, SiO_2 and Al_2O_3 as main components. They show a wide range of compositions from those of very high iron content to those which are rather rich in silica and alumina (*Figure 102*). No characteristic composition range can be linked to any petrographic groups or subgroups. Iron hydroxide nodules are common features of soils (Stoops 2003). It is likely that these iron-rich phases are natural inhomogeneities in the clay some of which were also recorded by petrography as limonitic nodules (Section 4.2.1).

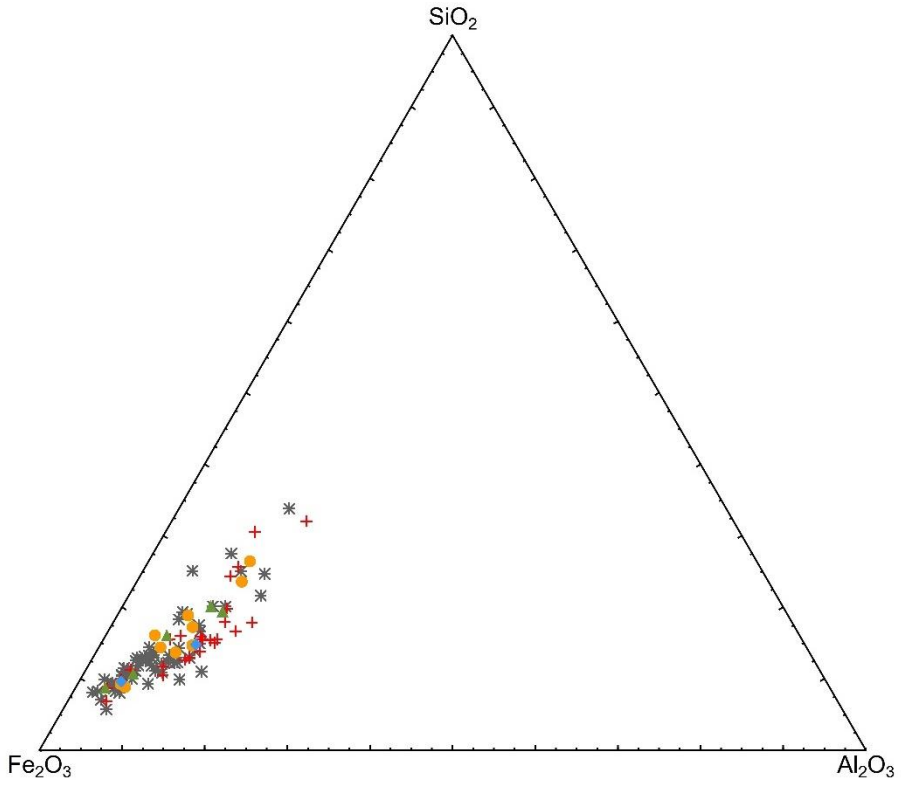


Figure 102. Compositions of iron-rich phases plotted on the ternary diagram of SiO_2, Fe_2O_3 and Al_2O_3. (The diagram includes the data of 103 iron-rich phases from 31 samples.)

Other minerals

Amphibole

Amphibole grains were analysed from the Amphibole and Diorite groups as one of their main components. The samples of the Amphibole group contain amphiboles usually with less CaO content and higher Na_2O content than the amphiboles of the Diorite group (*Figure 103*).

Two main types of amphiboles were identified in these groups by polarising microscopy: green or greenish-brown amphibole in both Amphibole and Diorite groups and colourless amphibole in subgroup 'Diorite A'. These two types are clearly seen in *Figure 104* showing the difference in iron content as it is mostly the iron content which determines the colour of the amphibole

crystals. The lower group on this graph containing less Fe_2O_3 (< 5 wt%) represents colourless amphiboles and the rest of the amphiboles located on the upper part of the graph with a higher iron content represent greenish/brownish amphiboles.

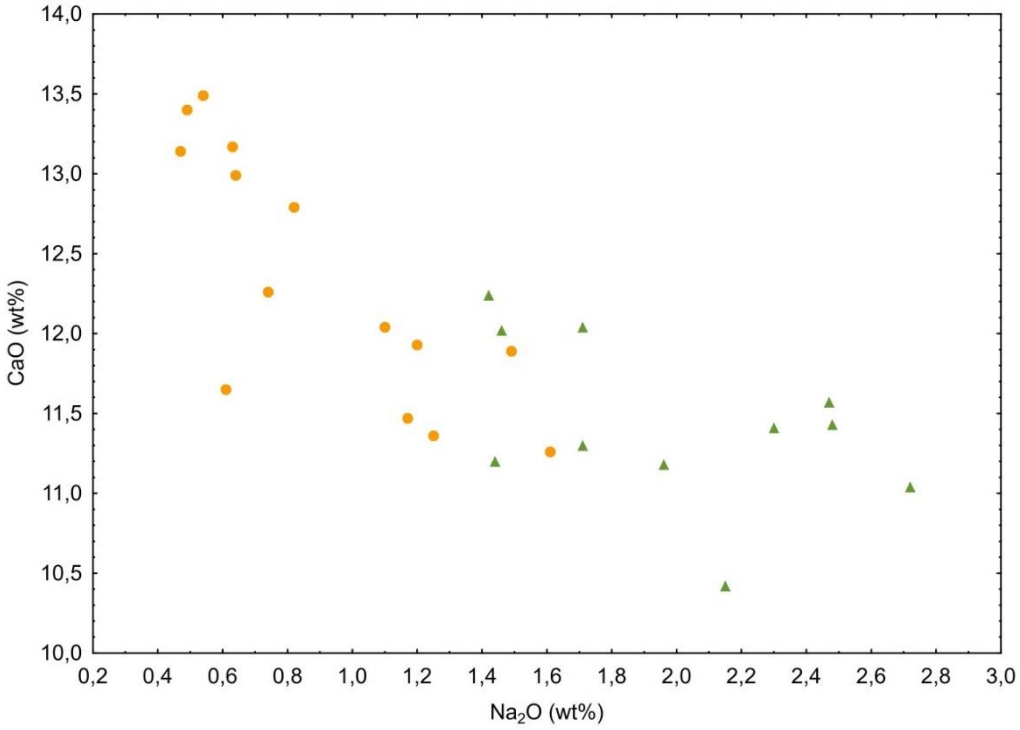


Figure 103. Na_2O and CaO content of amphibole grains of the Amphibole and Diorite groups. (The diagram includes the data of 25 amphibole grains from 7 samples.)

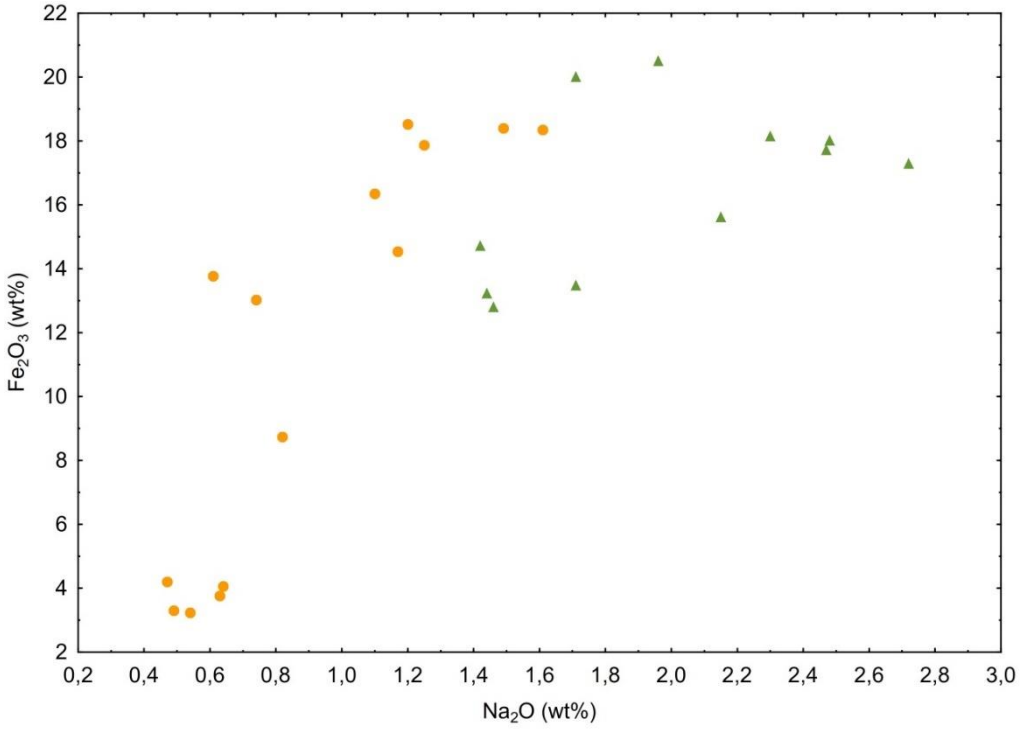


Figure 104. Na_2O and Fe_2O_3 content of amphibole grains of the Amphibole and Diorite groups. (The diagram includes the data of 25 amphibole grains from 7 samples.)

A clear distinction can be observed between the two petrographic groups when plotting aluminium percentages against magnesium percentages of amphibole grains (*Figure 105*). The crystals of the Amphibole group have higher aluminium content and lower magnesium content while those of the Diorite group have lower aluminium content and higher magnesium content. Colourless amphiboles of subgroup 'Diorite A' are plotted together on this graph as well: they can be found as a small group with low aluminium (< 2 wt%) and high magnesium (> 23 wt%) content in the bottom right corner. There are four grains of the Amphibole group (from S8 and S90) which are slightly separated from the rest of this group because of their higher (> 13 wt%) MgO content. The MgO however, does not seem to have distinguishing role in this case as S8 contains both amphiboles with higher and lower magnesium content.

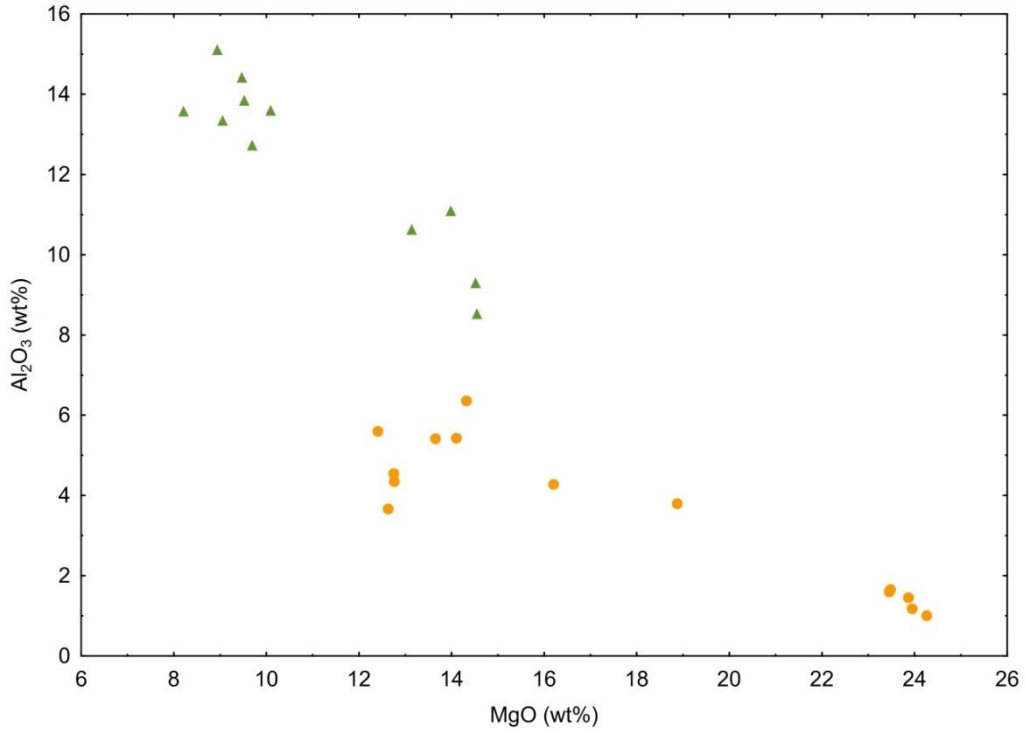


Figure 105. MgO and Al_2O_3 content of amphibole grains of the Amphibole and Diorite groups. (The diagram includes the data of 25 amphibole grains from 7 samples.)

Pyroxene

Pyroxene is one of the main constituents of the Carbonate group and subgroup 'Diorite B'. As *Figure 106* shows, all pyroxenes measured from these two groups belong to the quad pyroxenes (Ca-Mg-Fe pyroxenes) based on the Q-J diagram for pyroxene nomenclature created by Morimoto et al. (1988) (*Figure 107*).

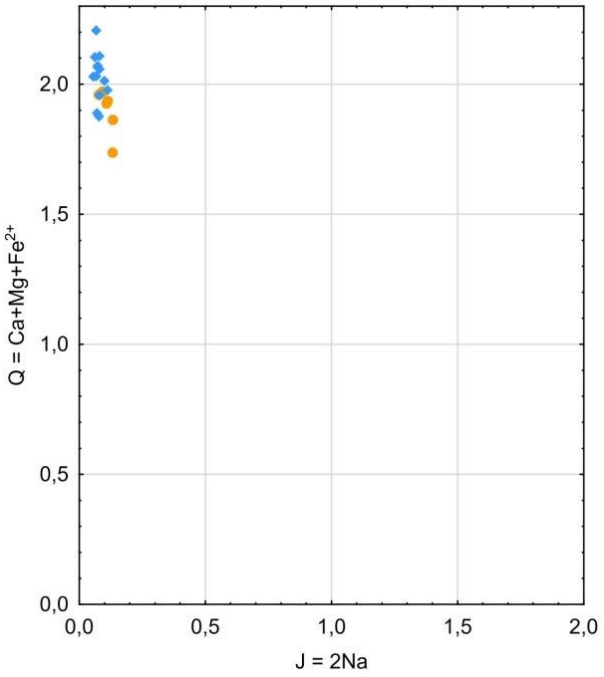


Figure 106. Q-J diagram of pyroxenes of the Carbonate group and subgroup 'Diorite B' following Morimoto et al. (1988, 1127: Fig. 2). (The diagram includes the data of 19 pyroxene grains from 5 samples.)

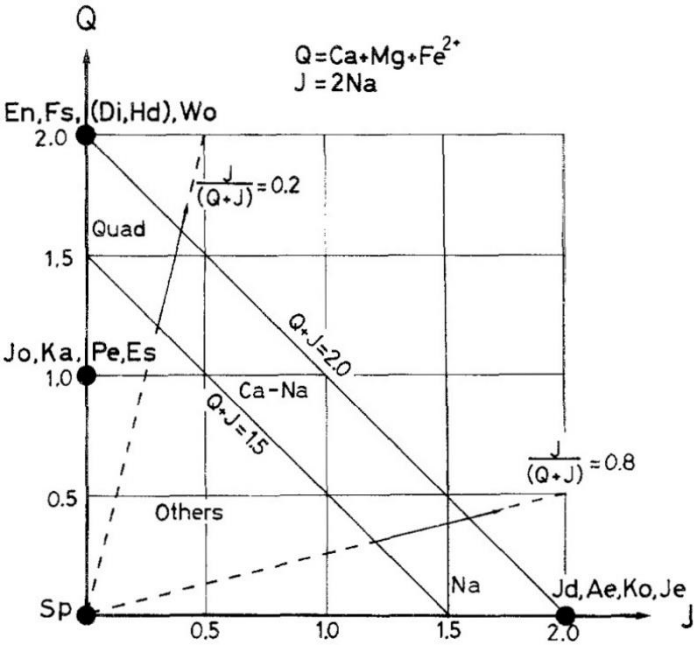


Figure 107. Q-J diagram for pyroxenes with the 13 endmembers (Morimoto et al. 1988, 1127: Fig. 2)[60]

[60] Abbreviation of pyroxenes: En = enstatite, Fs = ferrosilite, Di = diopside, Hd = hedenbergite, Wo = wollastonite, Jo = johannsenite, Ka = kanoite, Pe = petedunnite, Es = esseneite, Sp = spodumene, Jd = jadeite, Ae = aegirine, Ko = kosmochlor, Je = jervisite.

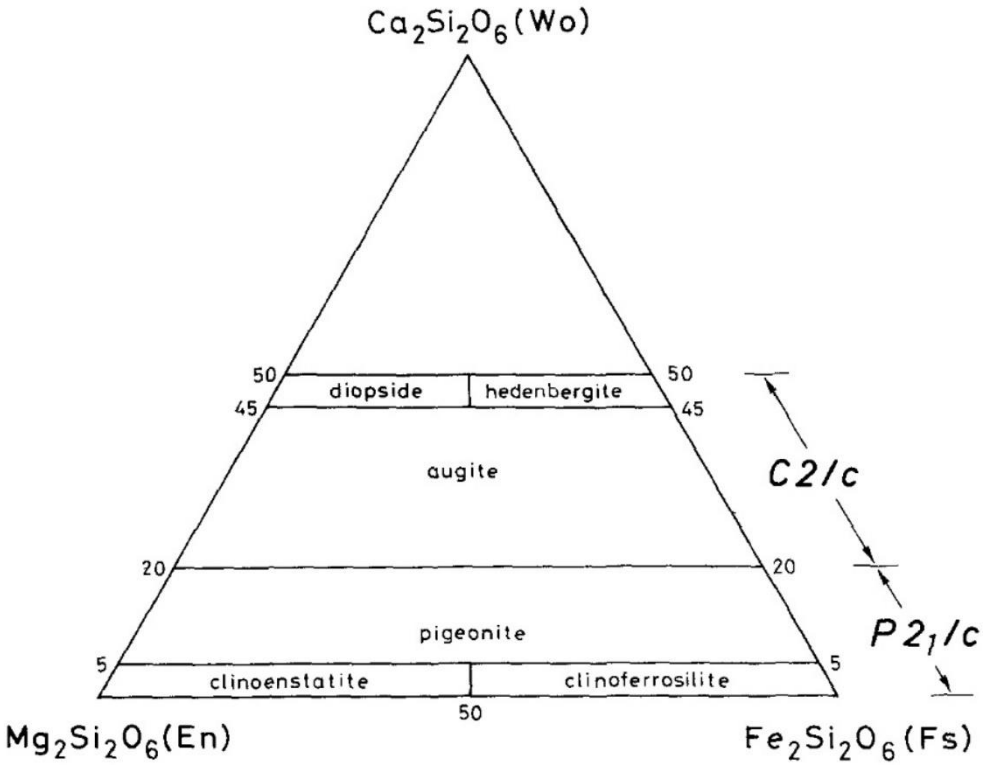


Figure 108. Nomenclature of Ca-Mg-Fe clinopyroxenes by Morimoto et al. (1988, 1129: Fig 4)

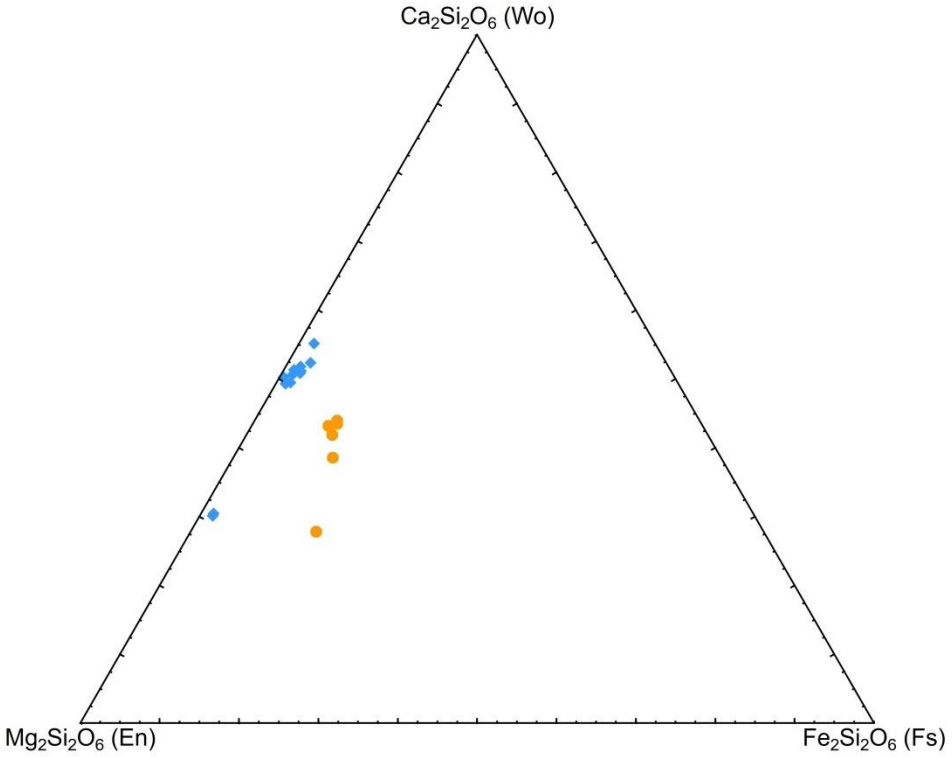


Figure 109. Pyroxene compositions of the Carbonate group and subgroup 'Diorite B' plotted on the ternary diagram of wollastonite (Wo, $Ca_2Si_2O_6$), enstatite (En, $Mg_2Si_2O_6$) and ferrosilite (Fs, $Fe_2Si_2O_6$) following Morimoto et al. (1988, 1128, 1129: Fig. 4). (The diagram includes the data of 19 pyroxene grains from 5 samples.)

Within the group of quad pyroxenes, further distinction of pyroxenes is possible using the ternary diagram of three pyroxenes of different composition including the calcium-rich wollastonite, the magnesium-rich enstatite and the iron-rich ferrosilite (*Figure 108*). Based on this graph, pyroxenes of subgroup 'Diorite B' represent augite crystals (*Figure 109*). Both augite and diopside is present in the Carbonate group.[61]

Mica

Almost all samples contain biotite and muscovite flakes based on petrography. Especially those were measured by SEM, which are significant constituents of their subgroups such as biotite of the biotite-rich subgroup and muscovite of the muscovite-rich subgroup of the Granitoid group ('Granitoid C' and 'Granitoid D', respectively). Some other flakes from other subgroups were also analysed for comparison in order to examine how similar/different the mica compositions are. The ternary diagram in *Figure 110* shows the chemical data of mica flakes of the investigated samples: the lower group of measurements represents muscovite poor in iron while the upper group corresponds to iron-rich biotite. The composition data is very similar within 'Granitoid C' and 'Granitoid D' and do not show significant differences from other mica measurements of other petrographic groups.

A slight difference is exhibited in the titanium content of biotite: flakes of the Granitoid-group are usually more titanium-rich than those of the other groups as shown in the upper part of *Figure 111*.

Garnet

Garnet is a common accessory mineral in the samples from Lower Austria. Especially subgroup 'Graphite A3' is abundant in garnet, but other samples also contain garnet grains such as some samples of subgroup 'Graphite D' and S15 as an individual sample. Based on SEM-EDS analysis, the samples of the subgroups of the Graphite group contain spessartine and almandine (*Figure 112*). The almandine-component slightly exceeds the pyrope-component in the garnet grains of S15, thus these crystals may be termed as almandines.

[61] Some pyroxenes contain more than 50% of $Ca_2Si_2O_6$. These are pyroxenes of unusual composition according to Morimoto et al. (1988, 1128: Footnote 10).

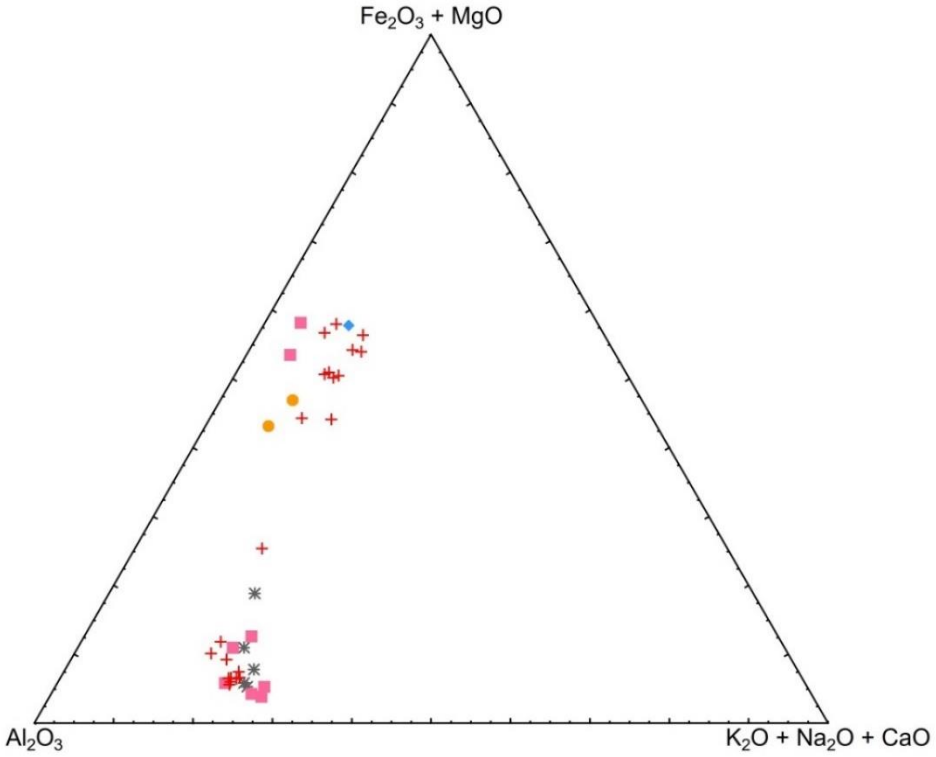


Figure 110. Mica compositions plotted on the ternary diagram of Fe_2O_3+MgO, Al_2O_3 and K_2O+Na_2O+CaO following Shriner and Dorais (1999, 40: Fig. 7). The upper group of measurements represents biotite, the lower group of measurements represents muscovite. (The diagram includes the data of 38 mica flakes from 13 samples.)

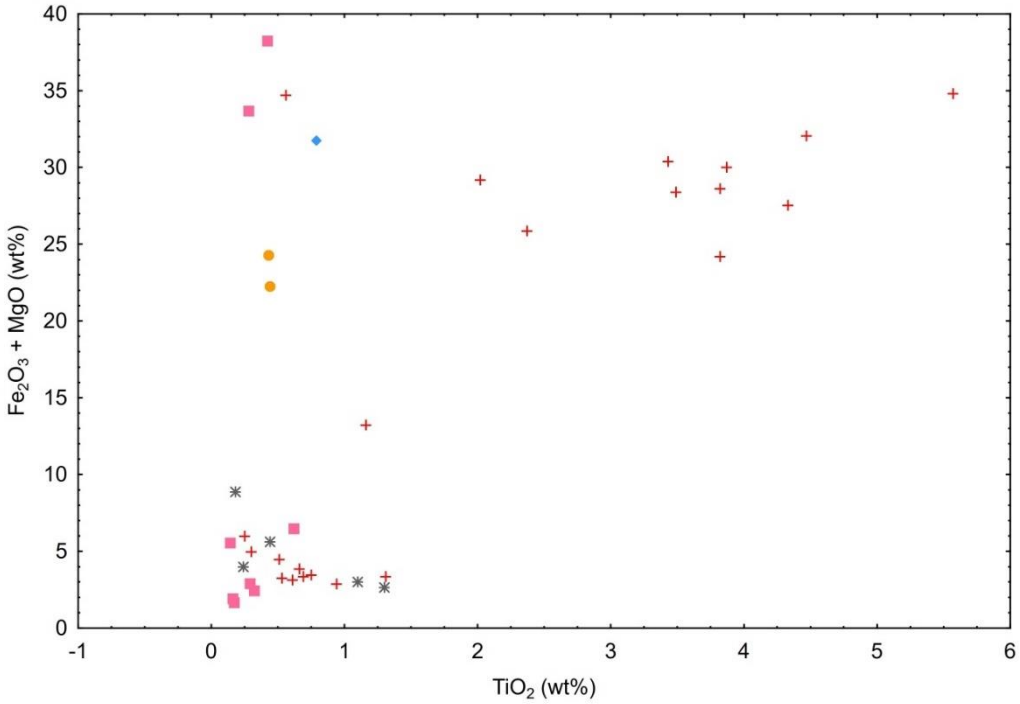


Figure 111. Fe_2O_3+MgO and TiO_2 content of mica flakes. The upper group of measurements represent biotite, the lower group of measurements represent muscovite. (The diagram includes the data of 38 mica flakes from 13 samples.)

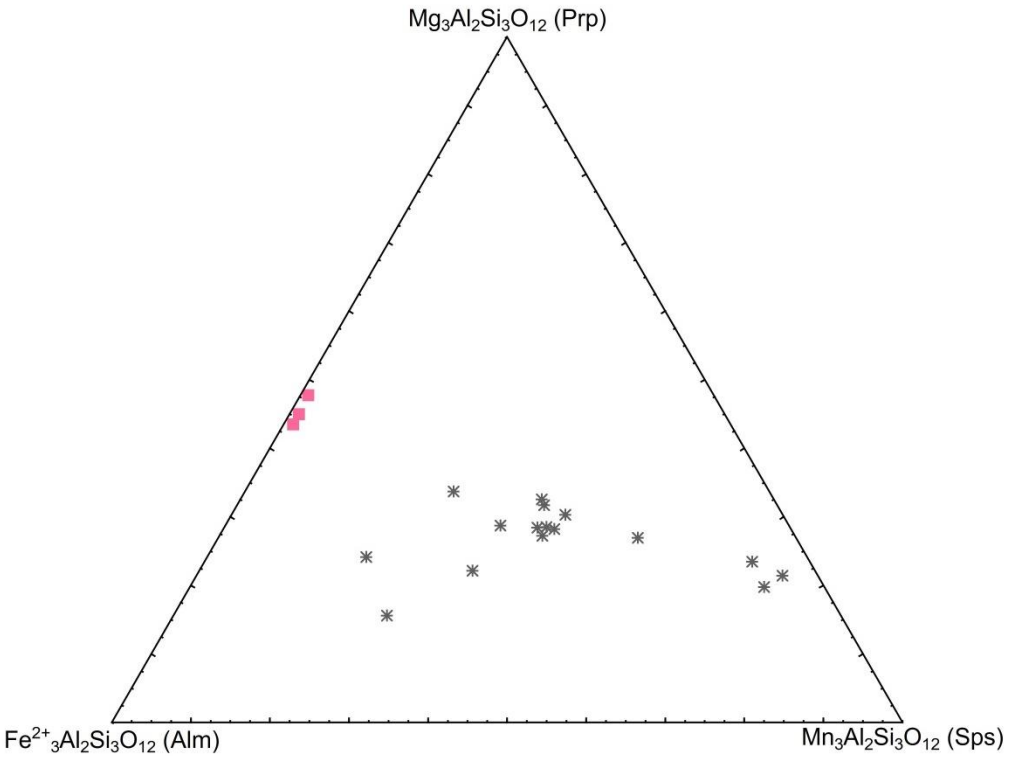


Figure 112. Garnet compositions of the Graphite group and S15 plotted on the ternary diagram of pyrope (Prp, $Mg_3Al_2Si_3O_{12}$), almandine (Alm, $Fe^{2+}{}_3Al_2Si_3O_{12}$) and spessartine (Sps, $Mn_3Al_2Si_3O_{12}$). (The diagram includes the data of 19 garnet grains from 5 samples.)

Calcite

The results of SEM-EDS analysis shows that the calcite/dolomite grains in the Carbonate group and the carbonate-containing subgroup of the Graphite group ('Graphite C') contain 80–100 wt% of CaO (excluding carbon) and thus can be identified as calcite (Appendix D.2).

Surface layer of S113

A layer of weathered glaze or surface deposition was observed on the inner side of S113 by petrography (*Figure 82*). This layer is clearly distinguished from the ceramic body in the BSE image as well (*Figure 113*). It is mainly of calcium and phosphorus as it was proved by SEM-EDS analysis while the main components of the clay matrix are aluminium and silicon (Appendix D.2). Based on composition, the layer is probably the result of post-burial deposition or the past use of the vessel.[62]

[62] Both phosphorus and calcium are common components of post-burial alterations (Freestone et al. 1994; Buxeda i Garrigós 1999; Maritan 2020). The possibility of the surface layer being a weathered glaze is not probable based on compositional considerations and the fact that no part of the original

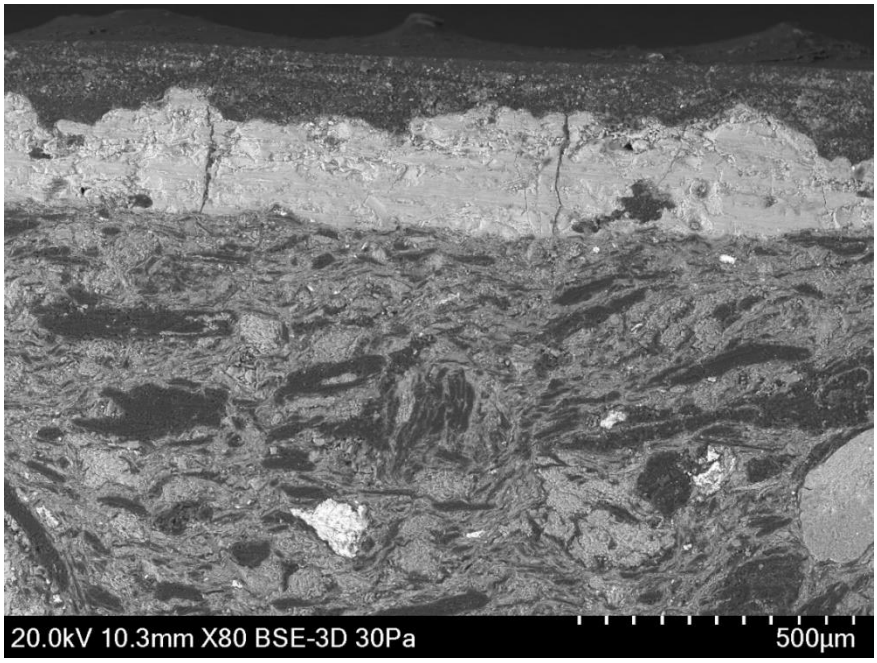


Figure 113. Surface layer on the inner side of S113

4.3.3 Summary

The microstructure of the investigated samples shows similarity without any signs of vitrification (except S90). The chemical analysis (SEM-EDS) of the matrix also resulted in similar compositions with calcium oxide contents below 6 wt% (except S89). Both potassium feldspar and plagioclase are present in the samples revealing slight differences between certain petrographic subgroups. Heavy minerals show compositional variations (although these are not group-specific) and the abundant presence of iron-rich nodules are remarkable. The analysis of different other minerals specifies and complements petrographic data and shows that many times petrographic groups can be distinguished by SEM-EDS as well.

unaltered glaze is visible (about glazes and their weathering see Pradell and Molera 2020). Here, I would like to thank Dr Judit Molera for giving her opinion about this surface layer (October 2020).

4.4 Inductively coupled plasma optical emission spectrometry (ICP-OES)

ICP-OES analysis was carried out on 49 samples (*Table 19*). To have a comparison between two different samples of the same specimen, one sample of this set, S10, was analysed twice leading to 50 measurements in total. The specification of the ICP-OES instrument and the methodology are detailed in Section 3.5.3.

This subchapter is divided into two main parts. Firstly, the raw data are analysed by elements and the relationships between element concentrations are illustrated by binary and ternary diagrams. This is followed by statistical analysis including cluster analysis and principal component analysis (PCA).

4.4.1 Raw data analysis

Normalisation of data, loss on ignition, limit of quantification

The results of the ICP-OES analysis of the samples can be found in Appendix E.1. This data table includes compositional data normalised to 100%. Normalisation was needed as each sample had different value for loss on ignition (LOI), which signifies the percentage of material burnt out from the sample during sample preparation (e.g. graphite in the case of graphite-containing ceramics). LOI is presented in the last column of the table.

The following 9 major and 16 trace elements were measured: Al, Ca, Fe, K, Mg, Na, P, Si, Ti, As, Ba, Cr, Cu, Mn, Ni, Pb, Rb, Sb, Sc, Sn, Sr, V, Y, Zn, Zr. The major elements are expressed in weight percent (wt%) as oxides and the trace elements in parts per million (ppm). Among these elements, the concentration of As and Sb was consistently below the limit of quantification (LOQ), therefore they are not included in the data table. Some of the other elements (e.g. Pb, Sn, Zn) have values falling below the LOQ in multiple samples. In these cases, a '<' symbol and the LOQ value is given meaning that the actual value is below the LOQ. The LOQ of an element is different in each sample partly because of normalisation and partly because the samples were analysed in two batches resulting in different LOQ for Batch 1 and Batch 2.

Analysis by elements

In this section, a preliminary analysis of the chemical composition of the samples is given including the tabular inspection of the data. Each element is discussed separately and

illustrated by a box plot, except for those trace elements (Mn, Pb, Sn, Zn), which have values below the limit of quantification.[63] Minimum values, maximum values, means and standard deviations by elements for all samples and for petrographic groups are shown in *Table 20*.

Before examining the concentrations of the major and trace elements one by one, it is reasonable to compare the outcome of the analysis of two samples from the same potsherd (S10-1 and S10-2). As shown by the table in Appendix E.1, the two measurements of S10 resulted in very similar values, except for one element. The concentration of copper differs extremely in S10-1 and S10-2, which might be the result of the relatively poor data quality detected for this trace element (see Section 3.5.3).

Major elements

The concentrations of the major elements in the samples are broadly similar with few unusual values as shown by *Figure 114* and discussed below.

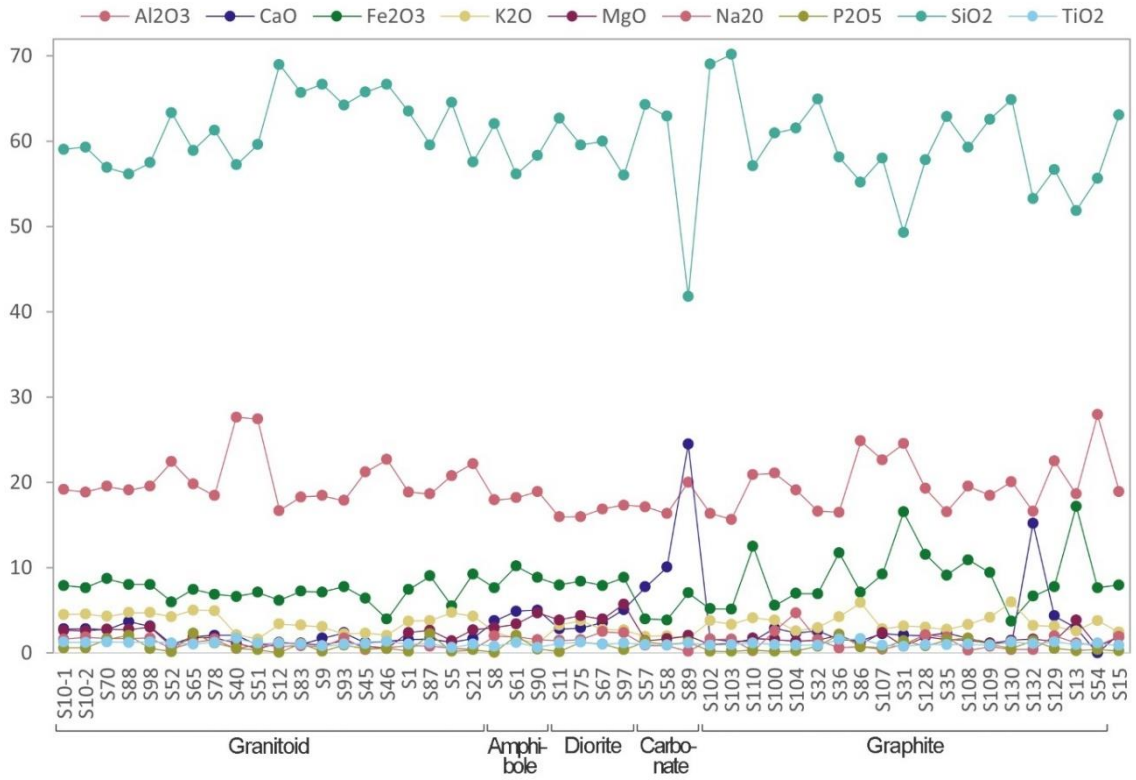


Figure 114. Concentration of major element oxides (wt%) in the samples by petrographic groups. The last sample (S15) is an outlier based on petrography.

[63] In these box plots, the boxes indicate the central 50% of the data (25%–75%), the lines in the boxes mark the medians and whiskers represent the non-outlier range. Circles plotted outside of the whiskers are outliers.

Table 20. Minimum values, maximum values, means and standard deviations of the compositional data of all samples and the different petrographic groups. Major elements are expressed in weight percentages as oxides and trace elements are expressed in ppm.

All samples		Al_2O_3	CaO	Fe_2O_3	K_2O	MgO	Na_20	P_2O_5	SiO_2	TiO_2	Ba	Cr	Cu	Mn	Ni	Pb	Rb	Sc	Sn	Sr	V	Y	Zn	Zr
	Min	15.68	0.98	3.75	1.17	0.51	0.20	0.08	41.78	0.63	330	69	19	157	14	38	56	14	28	86	98	14	64	38
	Max	27.93	24.48	17.22	5.99	5.75	4.71	2.31	70.18	1.75	3993	340	608	10212	233	77	319	32	63	1082	466	84	292	514
	Mean	19.59	3.31	7.97	3.38	2.03	1.28	0.83	60.17	1.11	1018	147	102	1422	72	51	144	20	44	265	189	38	152	228
	SD	3.00	3.96	2.65	1.11	1.15	0.82	0.64	5.17	0.22	644	62	109	2311	46	15	53	4	18	194	92	15	73	115
Petrographic groups		Al_2O_3	CaO	Fe_2O_3	K_2O	MgO	Na_20	P_2O_5	SiO_2	TiO_2	Ba	Cr	Cu	Mn	Ni	Pb	Rb	Sc	Sn	Sr	V	Y	Zn	Zr
Granitoid group	Min	16.69	0.98	3.98	1.62	0.51	0.43	0.08	56.17	0.63	362	69	20	157	26	38	78	14	28	86	98	25	64	138
	Max	27.64	3.68	9.28	5.02	3.04	1.87	2.31	68.99	1.75	1867	212	239	866	117	77	319	26	63	548	194	70	284	514
	Mean	20.39	1.93	7.23	3.70	1.76	1.07	0.83	61.62	1.16	1135	142	83	505	60	51	170	20	44	256	131	36	152	320
	SD	2.90	0.78	1.24	1.11	0.86	0.53	0.71	3.93	0.22	425	49	80	218	26	15	56	3	18	146	25	11	66	107
Amphibole group	Min	17.96	3.78	7.64	1.17	2.99	1.59	0.10	56.13	0.68	362	93	36	361	36		56	18		238	153	14		75
	Max	18.95	5.04	10.18	2.50	4.72	1.99	2.06	62.02	1.24	906	113	216	921	58		95	29		359	260	18		133
	Mean	18.37	4.58	8.89	1.76	3.70	1.84	0.88	58.84	0.91	677	101	96	610	50		78	24		299	190	16		94
	SD	0.52	0.69	1.27	0.68	0.90	0.22	1.04	2.97	0.29	282	11	104	285	12		20	5		61	60	2		34
Diorite group	Min	15.95	2.82	7.92	2.69	3.89	1.49	0.17	56.02	1.03	517	286	45	666	65	38	101	18		265	121	21	113	155
	Max	17.34	5.11	8.86	3.78	5.75	2.50	1.28	62.68	1.28	3993	340	202	787	149	67	151	21		1082	162	41	292	334
	Mean	16.55	3.61	8.29	3.14	4.50	1.99	0.72	59.56	1.16	2031	302	87	728	107	52	120	20		636	141	31	203	239
	SD	0.68	1.05	0.44	0.50	0.86	0.53	0.53	2.74	0.11	1694	26	77	51	35	20	22	1		397	17	10	127	78
Carbonate group	Min	16.36	7.76	3.87	1.74	1.43	0.20	1.01	41.78	0.94	494	97	19		43		72	15		297	100	32	101	149
	Max	20.01	24.48	7.05	2.02	2.05	0.89	1.34	64.27	1.21	699	111	209		44		122	17		615	120	37	235	231
	Mean	17.84	14.10	4.97	1.91	1.72	0.66	1.21	56.32	1.04	623	103	82		44		98	16		420	107	34	168	194
	SD	1.92	9.06	1.80	0.15	0.31	0.40	0.17	12.61	0.14	113	8	109		1		25	1		171	11	3	95	42
Graphite group	Min	15.68	1.18	3.75	2.61	0.77	0.25	0.20	49.30	0.80	330	97	22	441	14		68	15		89	148	20	81	38
	Max	27.93	15.21	17.22	5.99	3.88	4.71	2.19	70.18	1.66	1820	263	608	10212	233		230	32		378	466	84	287	280
	Mean	19.90	2.82	9.01	3.64	1.58	1.32	0.81	59.44	1.09	811	135	133	2684	87		142	21		174	274	45	139	158
	SD	3.39	3.19	3.68	0.97	0.69	1.07	0.60	5.50	0.23	338	40	142	3254	62		45	5		70	94	17	80	67

Aluminium oxide (*Figure 115*)

Al_2O_3 is between 16 wt% and 28 wt% in the samples. The values within subgroups of the Granitoid, Amphibole, Diorite and Carbonate groups are usually very close to each other, the maximum difference being around 1 wt%. In contrast, the Graphite group shows a higher diversity as the maximum difference can reach 9 wt% in some subgroups.

Calcium oxide (*Figure 116*)

The concentration of CaO ranges from 1 wt% to 24 wt% throughout the entire assemblage. The Granitoid and Graphite groups contain CaO below 4 wt%, except for subgroup 'Graphite C' with its larger amount of CaO (15 wt% and 4 wt%) as a result of the presence of carbonate rock fragments in the samples. The Amphibole group contains 4–5 wt% of CaO; this slightly higher concentration than that of the Granitoid and Graphite groups might be explained by the presence of calcium-rich feldspar (plagioclase) and calcium amphibole (hornblende) as shown by the SEM and XRD results. The CaO values are around 3 wt% in subgroup 'Diorite A' while they are around 4–5 wt% in subgroup 'Diorite B'; the higher values in the latter are possibly because of the presence of calcium-rich pyroxene (augite). As expected, the Carbonate group is clearly separated from the rest of the samples with 8–24 wt% of CaO content.

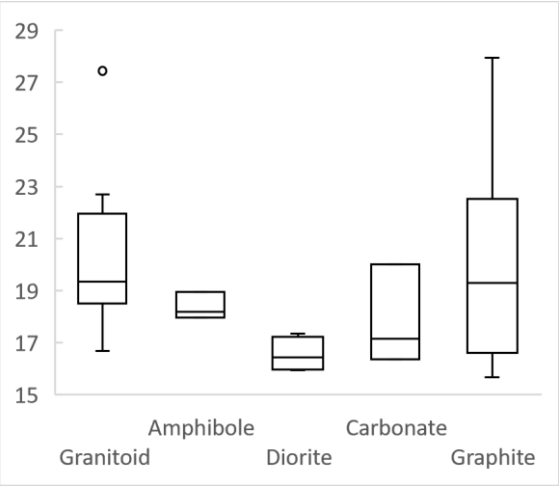


Figure 115. Box plot of Al_2O_3 (wt%) by petrographic groups

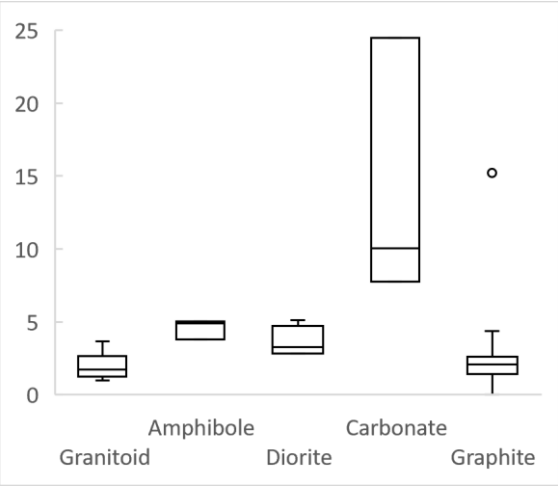


Figure 116. Box plot of CaO (wt%) by petrographic groups

Iron oxide (*Figure 117*)

The Fe_2O_3 content of the samples is between 4 wt% and 17 wt%. The difference between the values within the subgroups is usually no more than 3 wt%, except the subgroups of the Graphite group, which are quite diverse in terms of concentration of Fe_2O_3.

Potassium oxide (*Figure 118*)

The amount of K_2O ranges between 1 wt% and 6 wt%, usually being around 3–5 wt%. The Amphibole and Carbonate groups have a smaller concentration of K_2O (1–2.5 wt%) probably because of the lack of abundant potassium feldspar.

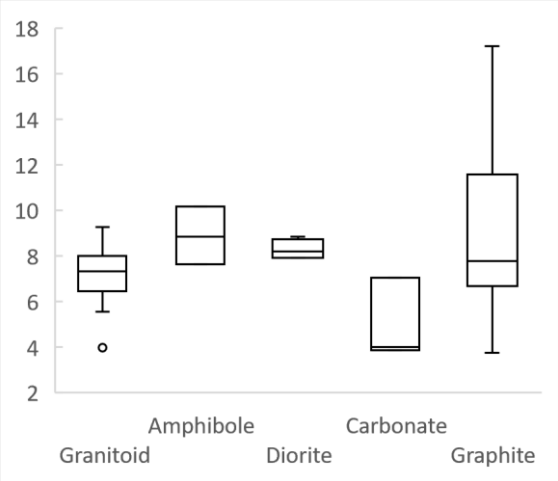


Figure 117. Box plot of Fe_2O_3 (wt%) by petrographic groups

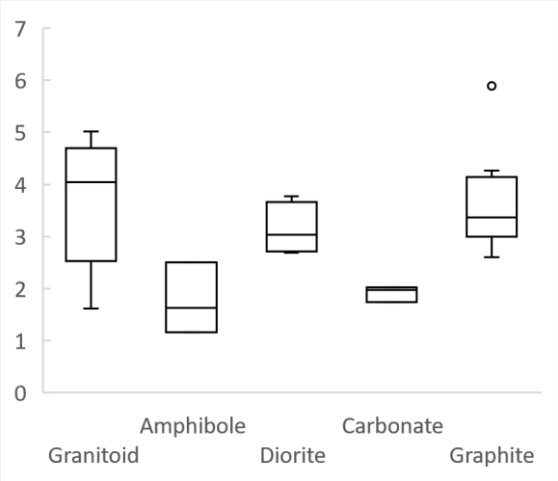


Figure 118. Box plot of K_2O (wt%) by petrographic groups

Magnesium oxide (*Figure 119*)

MgO concentrations range between 0.5 wt% and 6 wt%. The Granitoid, Carbonate and Graphite groups have less than 3 wt% of MgO. The Amphibole and Diorite groups, however, contain 3–6 wt% of MgO possibly due to the abundant amphibole and/or pyroxene grains present in the samples.

Sodium oxide (*Figure 120*)

The concentration of Na_2O ranges from 0.2 wt% to 4.7 wt% in the samples, usually below or around 2 wt%. Subgroup 'Diorite B' and some samples of the Graphite group have a higher Na_2O content (2.4–4.7 wt%) than the average.

Phosphorus pentoxide (*Figure 121*)

P_2O_5 is present with values below 2.3 wt%. The concentration of phosphorus can be the subject of post-depositional changes causing enrichment of this element in the ceramics. The porous structure of the ceramics can easily adsorb phosphorus when interacting with phosphorus-containing soil solutions originating from fertilisers or dissolved bones (Freestone et al. 1994; Buxeda i Garrigós 1999, 308; Maritan 2020, 11). Because of its mobility, P_2O_5 is not considered in further analysis.

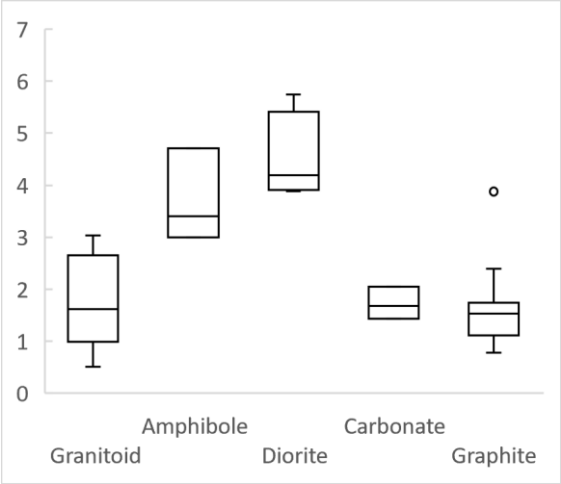


Figure 119. Box plot of MgO (wt%) by petrographic groups

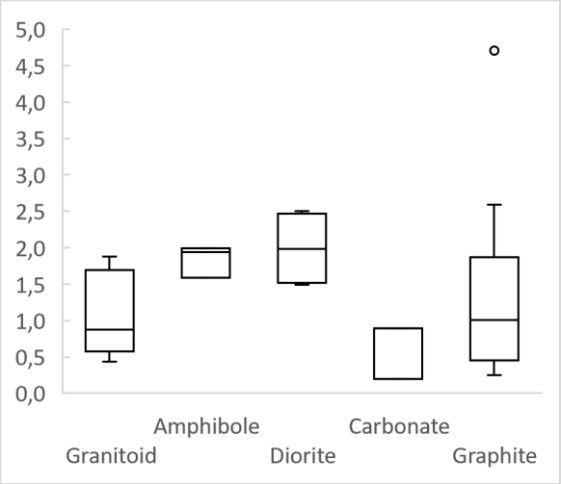


Figure 120. Box plot of Na_2O (wt%) by petrographic groups

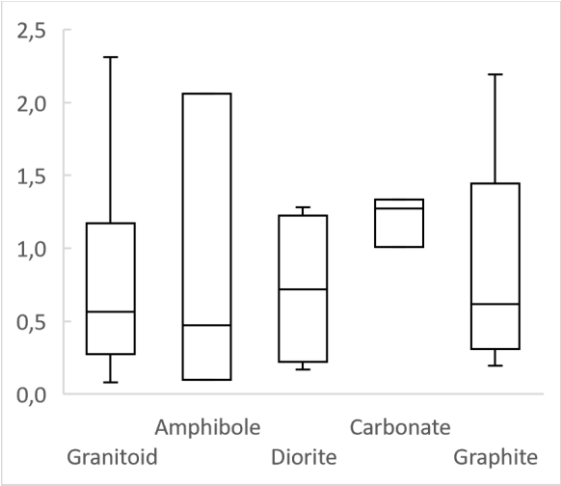


Figure 121. Box plot of P_2O_5 (wt%) by petrographic groups

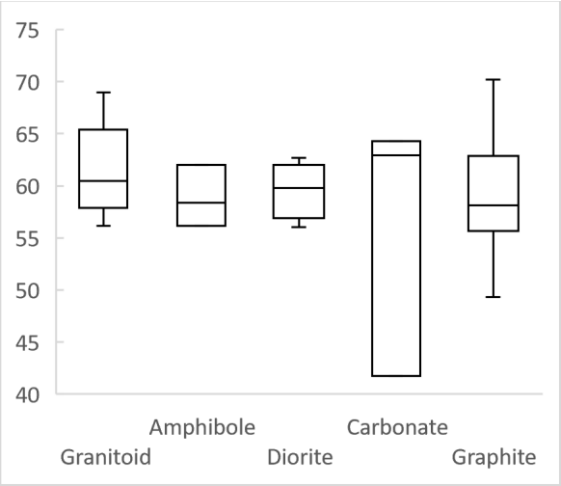


Figure 122. Box plot of SiO_2 (wt%) by petrographic groups

Silica (*Figure 122*)

SiO_2 makes up the largest part of the samples ranging between 42 wt% and 70 wt%. Within the Granitoid group, the quartz-rich 'Granitoid B' has the highest values (64–69 wt%) as expected. Subgroup 'Carbonate A' has also high percentage of SiO2 (63 wt% and 64 wt%) due to the abundant fine-grained monocrystalline quartz present in the matrix in contrast with subgroup 'Carbonate B' (42 wt% of SiO_2) where only few of these small grains can be found. The concentration of SiO_2 in the Amphibole and Diorite groups is in the middle-range (56–63 wt%). The values in the Graphite group are quite diverse (49–70 wt%) showing relatively low percentages (49–58 wt%) in subgroups 'Graphite A4', 'Graphite C' and Graphite D.

Titanium dioxide (*Figure 123*)

TiO_2 values ranges from 0.63 wt% to 1.75 wt%, the usual range being between 0.9 wt% and 1.3 wt%. There are some lower values in the Granitoid, Amphibole and Graphite groups and higher values in the Granitoid and Graphite groups depending on the amount of rutile and titanite present.

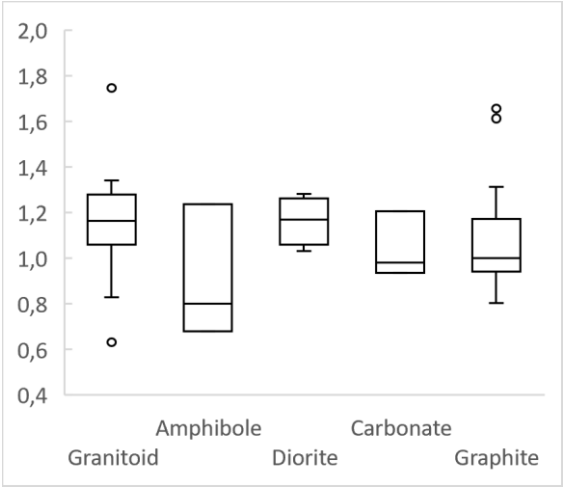


Figure 123. Box plot of TiO_2 (wt%) by petrographic groups

Trace elements

In the case of trace elements, the differences between the samples are more obvious due to the extreme diversity of concentrations that is present in several cases. The diagram of the trace elements gives a general overview of how the data is spread out (*Figure 124*).

Barium (*Figure 125*)

The presence of Ba is significant in the samples with values usually between 330 ppm and 2000 ppm. The highest concentration values are in subgroup 'Diorite A' (2893 ppm and 3993 ppm) while subgroup 'Diorite B' represents the lower end of the range (517 ppm and 719 ppm). Feldspar composition might be behind this huge difference as feldspars can contain significant amount of Ba (Deer, Howie & Zussman 1992, 412, 455–456). Similarly, there is variation in the amount of Ba in the Granitoid group with the lowest amount (below 700 ppm) of Ba in subgroups 'Granitoid A3' and 'Granitoid B3'. These subgroups are the most inclusion-poor among the subgroups of the Granitoid group and therefore contain less feldspar, which might be the reason why their Ba level is lower compared to other Granitoid subgroups. As for the

other groups, Ba values are normally under 1000 ppm with few exceptions in the Graphite group.

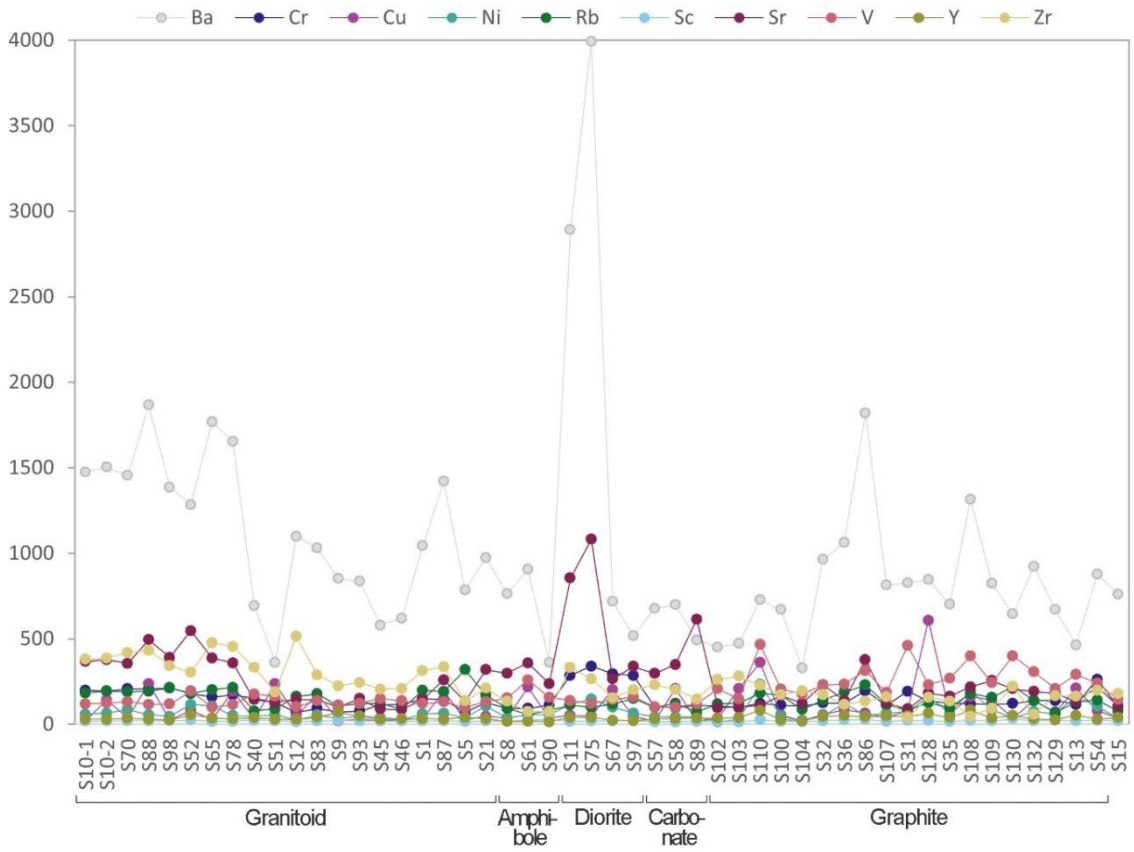


Figure 124. Concentration of trace elements (ppm) in the samples by petrographic groups. The last sample (S15) is an outlier based on petrography. Those trace elements which have values below the limit of quantification (Mn, Pb, Sn, Zn) are not presented in this diagram.

Chromium (*Figure 126*)

The concentration of Cr is between 69 ppm and 340 ppm, and is between 100 and 200 ppm in most of the samples. Subgroups 'Granitoid B1' and 'Granitoid B2' have consistently low values ranging between 70–93 ppm. The Diorite group has the highest values being around 300 ppm (and one sample in the Graphite group measuring 263 ppm of Cr). One possibility is that Cr originates from amphibole and/or pyroxene crystals (which are abundant in the Diorite group) as Cr can be the constituent of these minerals (Deer, Howie & Zussman 1992, 145, 149, 225). On the other hand, chromium is a main constituent of chromite, and although none of the other methods detected this mineral in the samples, its sporadic presence cannot be ruled out.

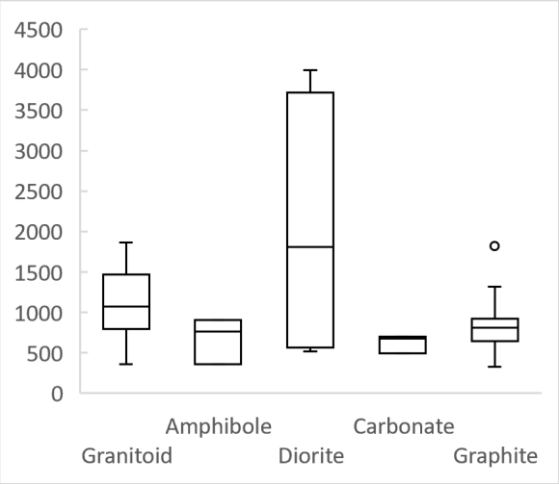


Figure 125. Box plot of Ba (ppm) by petrographic groups

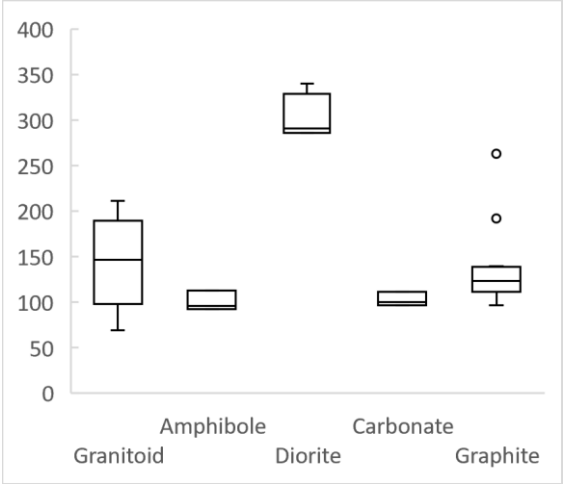


Figure 126. Box plot of Cr (ppm) by petrographic groups

Copper (*Figure 127*)

The Cu content of the samples covers a wide range between 19 to 608 ppm. The two measurements of S10 resulted in 22 ppm and 142 ppm, which suggest that either the concentration of Cu can be very different within a potsherd or more likely that data quality for Cu is poor as precision and accuracy calculations showed (see Section 3.5.3). For this reason, Cu was excluded from further analysis.

Manganese[64]

The concentration of Mn is extremely diverse ranging from below the limit of quantification to 10212 ppm. All groups, except for the Graphite group, contain Mn below 1000 ppm. The Graphite group, however, has several samples with Mn above this level; especially subgroup 'Graphite A3' and one sample from 'Graphite D' have very high values falling between 3800 and 10200 ppm. These samples contain Mn-rich garnets based on the SEM results which is most probably the reason for this high concentration.

Nickel (*Figure 128*)

The amount of Ni varies between 14 ppm and 233 ppm in the samples. Groups can contain both low and high values and group-specific pattern cannot be recognised regarding Ni concentration.

[64] As concentration of Mn in some samples falls below the LOQ, box plot is not provided for Mn.

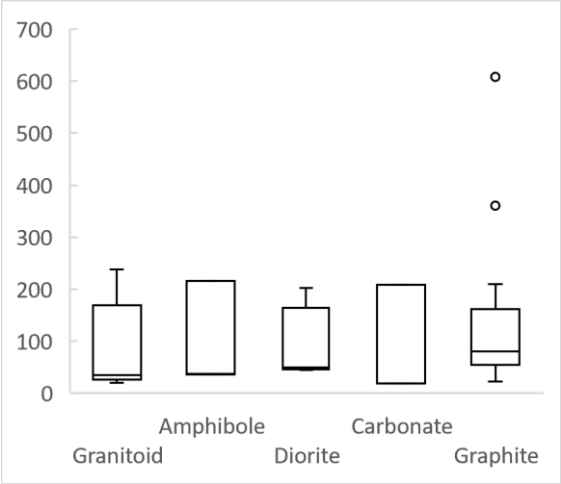


Figure 127. Box plot of Cu (ppm) by petrographic groups

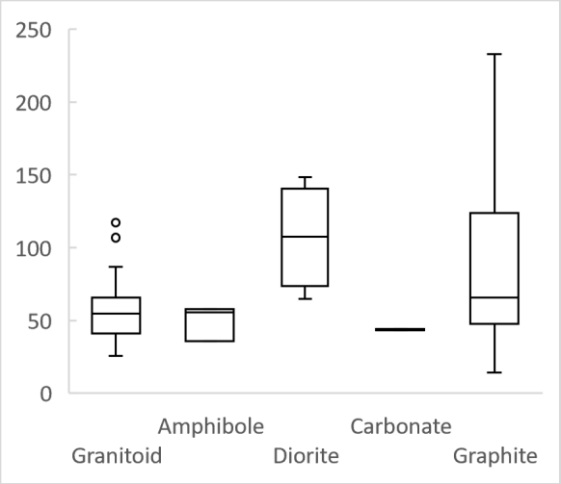


Figure 128. Box plot of Ni (ppm) by petrographic groups

Lead[65]

Pb values are normally under the limit of quantification. It was detected in 12 samples only with values between 38 ppm and 77 ppm.

Rubidium (*Figure 129*)

Rb is present with 56–319 ppm in the samples with a usual concentration between 50 ppm and 200 ppm. Relatively low values (< 100 ppm) are connected to subgroup 'Granitoid A3', 'Graphite C2', the Amphibole group, the Carbonate group and the individual sample.

Scandium (*Figure 130*)

Sc values are quite consistent ranging between 14 ppm and 32 ppm without any significant differences between groups and subgroups.

Tin[66]

Sn values are provided only for three samples as the amount of this element was below the limit of quantification in the rest of the samples.

[65] As concentration of Pb in most of the samples falls below the LOQ, box plot is not provided for Pb.
[66] As concentration of Sn in most of the samples falls below the LOQ, box plot is not provided for Sn.

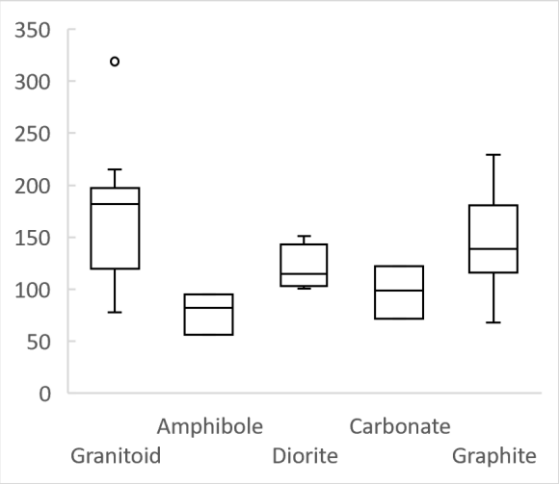


Figure 129. Box plot of Rb (ppm) by petrographic groups

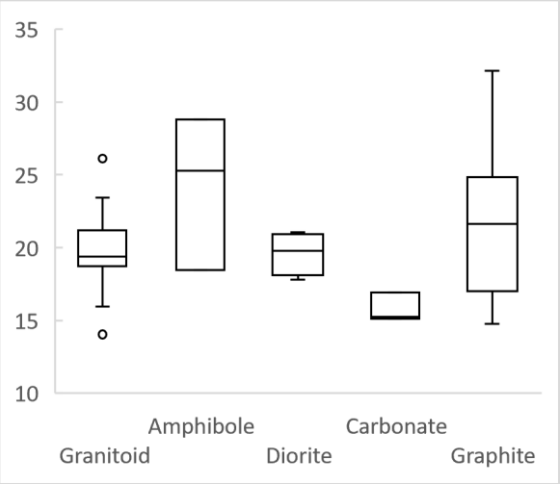


Figure 130. Box plot of Sc (ppm) by petrographic groups

Strontium (*Figure 131*)

The samples contain 86 ppm to 1082 ppm of Sr. There is a difference between subgroups 'Granitoid A1' and 'Granitoid A2' and the rest of the subgroups of the Granitoid group as the former subgroups have a higher amount of Sr (356–548 ppm) than the rest of the Granitoid subgroups (86–319 ppm, but usually below 150 ppm). There is a clear distinction between the two subgroups of the Diorite group, subgroup 'Diorite A' having higher values (856 ppm, 1082 ppm) and subgroup 'Diorite B' having smaller amount of Sr (339 ppm, 265 ppm). Similarly, subgroups 'Carbonate A' and 'Carbonate B' can be separated based on Sr composition ('Carbonate A': 297 ppm, 350 ppm; 'Carbonate B': 615 ppm).

Vanadium (*Figure 132*)

Values of V range between 98 ppm and 466 ppm. The concentration is below 200 ppm in the Granitoid, Amphibole, Diorite and Carbonate groups (apart form one sample). Samples of the Graphite group have the highest amount of V (usually above 200 ppm).

Yttrium (*Figure 133*)

The concentration of Y varies between 14 ppm and 84 ppm. The Amphibole group is distinctive with its low values falling below 20 ppm. The values within the Carbonate group and within the subgroups of the Diorite group are quite similar (Carbonate group: 32–37 ppm; 'Diorite A': 39 ppm, 41 ppm; 'Diorite B': 21 ppm, 24 ppm). There are more 'homogeneous' subgroups in the Granitoid group ('Granitoid A1: 25–31 ppm; 'Granitoid B3': 28 ppm, 31 ppm; 'Granitoid C': 30

ppm, 34 ppm) and in the Graphite group ('Graphite A2': 20 ppm, 27 ppm; 'Graphite A3': 45–51 ppm) as well in terms of Y content, however, the values are quite different in other subgroups of these groups.

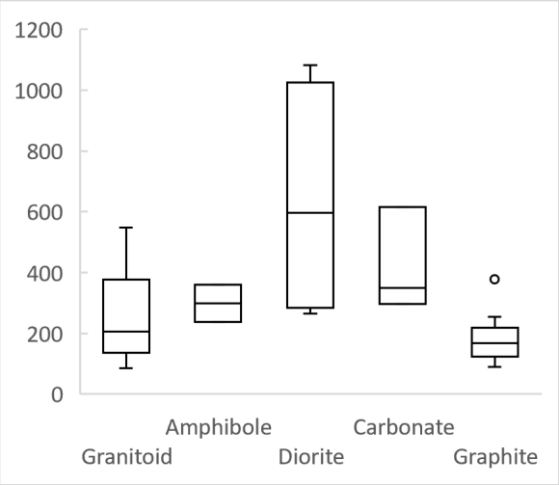


Figure 131. Box plot of Sr (ppm) by petrographic groups

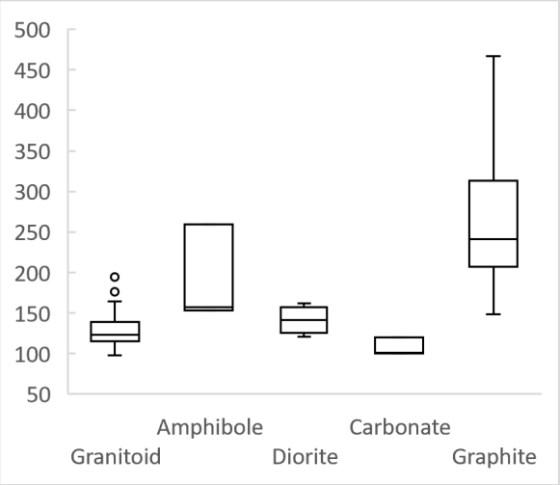


Figure 132. Box plot of V (ppm) by petrographic groups

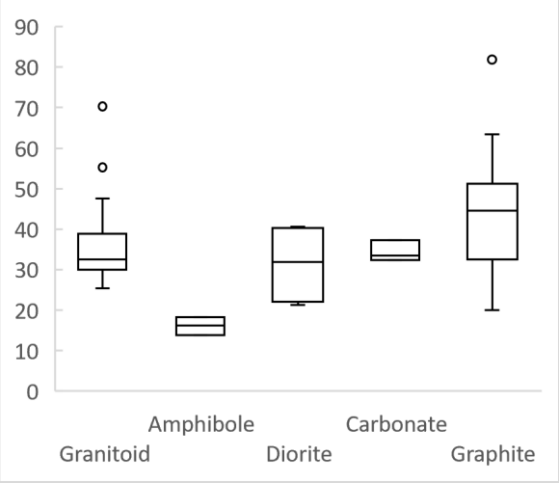


Figure 133. Box plot of Y (ppm) by petrographic groups

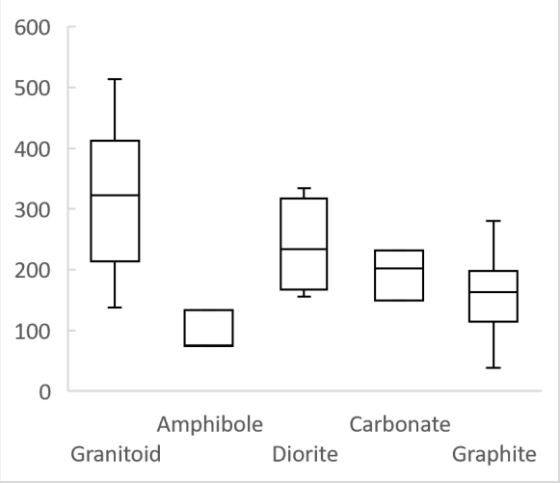


Figure 134. Box plot of Zr (ppm) by petrographic groups

Zink[67]

The amount of Zn is below the limit of quantification in 15 measurements. The rest of the samples contain Zn up to 292 ppm.

[67] As concentration of Zn in many samples falls below the LOQ, box plot is not provided for Zn.

Zirconium (*Figure 134*)

Zr is present between 38 ppm and 514 ppm in the samples. As expected, the Granitoid group has high levels of Zr (usually above 200 ppm) as the mineral zircon, consisting partly of zirconium, is common in granites and granitoids (Deer, Howie & Zussman 1992, 25). The Amphibole group has relatively small amount of Zr (75–133 ppm), while the Diorite and Carbonate groups are in the middle range (149–334 ppm). The Graphite group contains less than 200 ppm of Zr except subgroups 'Graphite A1' and 'Graphite B'.

Comparison of elements

Trivariate and bivariate plots are now presented including those elements which commonly substitute each other. The petrographic groups are indicated with the usual symbols shown by *Figure 92* (on page 188).

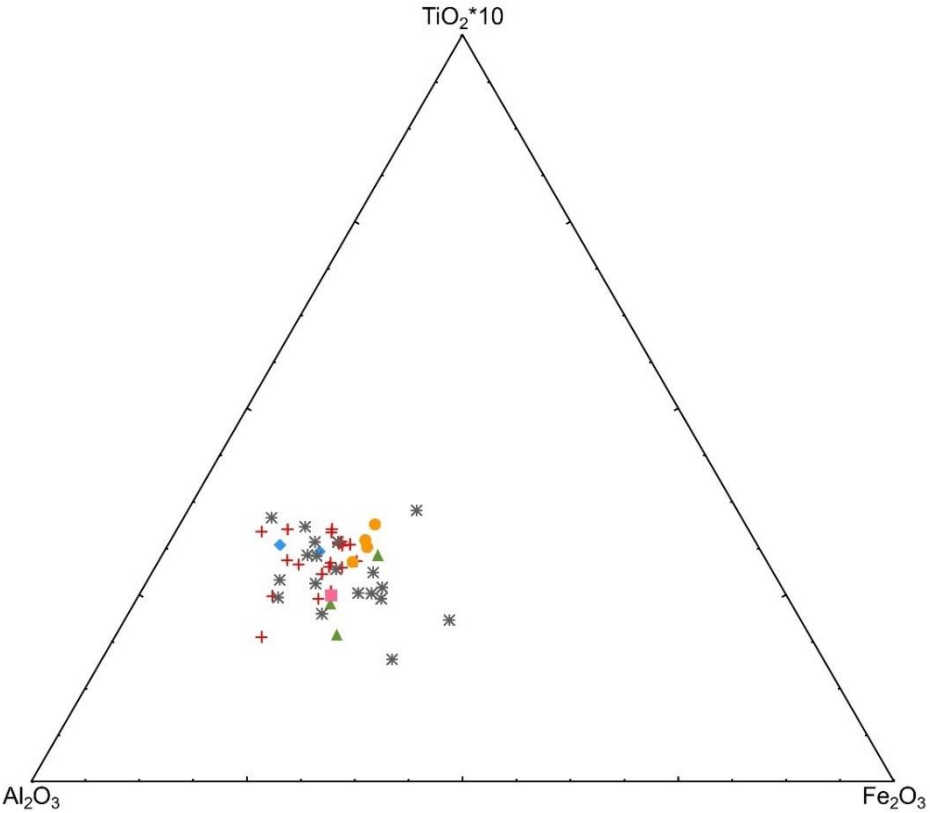


Figure 135. Ternary diagram of Al_2O_3, Fe_2O_3 and TiO_2. The values of TiO_2 are multiplied by 10 for a better presentation of the data.

The ternary plot of aluminium oxide, iron oxide and titanium oxide (*Figure 135*) shows that the proportion of these oxides is quite homogeneous in the different petrographic groups with some outliers from the Graphite group (S13, S31, S36) and one outlier from the Granitoid

group (S5). The individual sample (S15), however, is not distinguished as an outlier by this graph.

The plots in the ternary diagram of aluminium oxide, potassium oxide and sodium oxide (*Figure 136*) are more scattered. Most of the samples of the Granitoid group are grouped together, but there are some samples to the left separated from them that are less rich in potassium (S40, S45, S46, S51, S93). The samples of the Amphibole group are more potassium-poor and more sodium-rich than most of the other samples. The two subgroups of both the Diorite and Carbonate groups are clearly distinguished. The Graphite group can be separated into two groups, a smaller group having more potassium and less sodium/aluminium (S36, S86, S108, S109, S110, S130, S132) and a larger group having less potassium and more sodium/aluminium (S13, S31, S32, S35, S54, S100, S102, S103, S107, S128, S129), but they do not correspond to any of the petrographic subgroups. There is one potassium-rich sample of the Graphite group which is plotted far away from the rest of the samples (S104).

Transition metals can also substitute each other such as iron, titanium and manganese. The graph of these elements (*Figure 137*) shows that the Granitoid and Graphite groups are separated (although with some overlap): the Graphite group being the more manganese-rich and the Granitoid group containing less manganese. The samples having the highest manganese content belong in subgroup 'Graphite A3' and subgroup 'Graphite D' and contain manganese-rich garnets as mentioned above. The samples of the Amphibole group are quite scattered in contrast with the samples of the Diorite group, which appear very close to each other. Only one sample of the Carbonate group is present on the diagram (S58) as the manganese content of the other two samples are below the limit of quantification.

In the trivariate plot of alkali metals: potassium, sodium and rubidium (*Figure 138*), the samples of the Granitoid group are fairly close to each other, except some samples which are more sodium-rich (S51, S93), potassium-rich (S21, S52) or rubidium-rich (S5) and thus slightly separated from the rest of the group. The Graphite group is divided into two smaller groups (one of which is richer in Rb and K_2O while the other one is richer in Na_2O), which do not correspond to the petrographic groups, and a sodium-rich outlier (S104). The two subgroups of both the Diorite and Carbonate groups are quite evident from the graph.

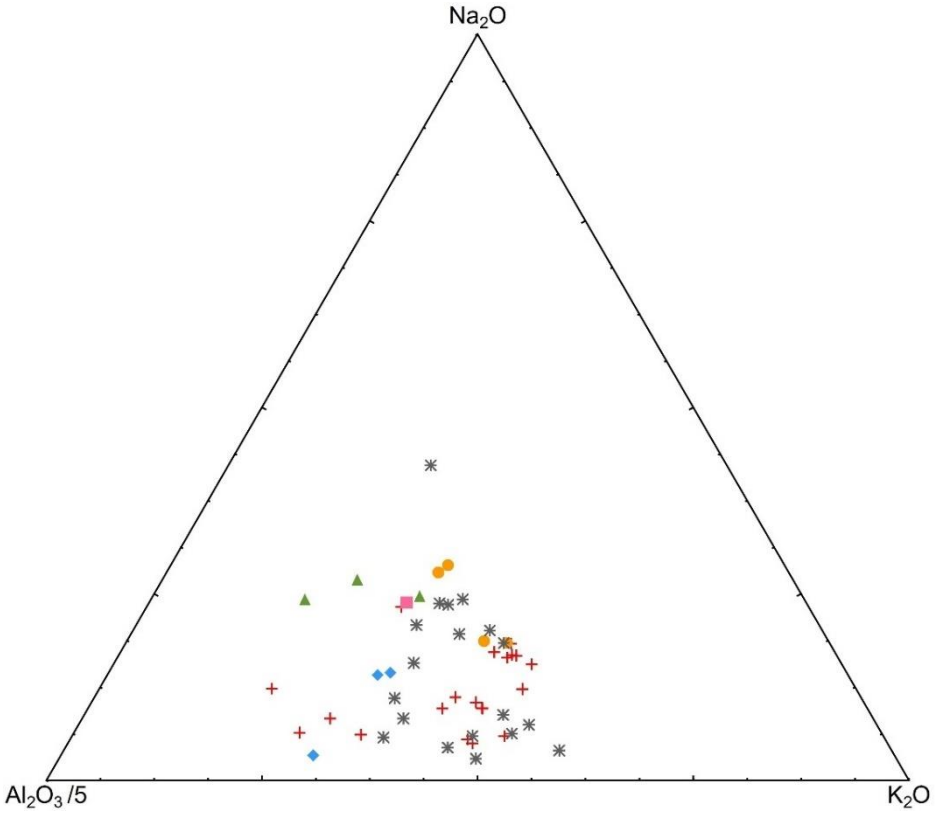


Figure 136. Ternary diagram of Al_2O_3, K_2O and Na_2O (Al_2O_3 values are divided by 5)

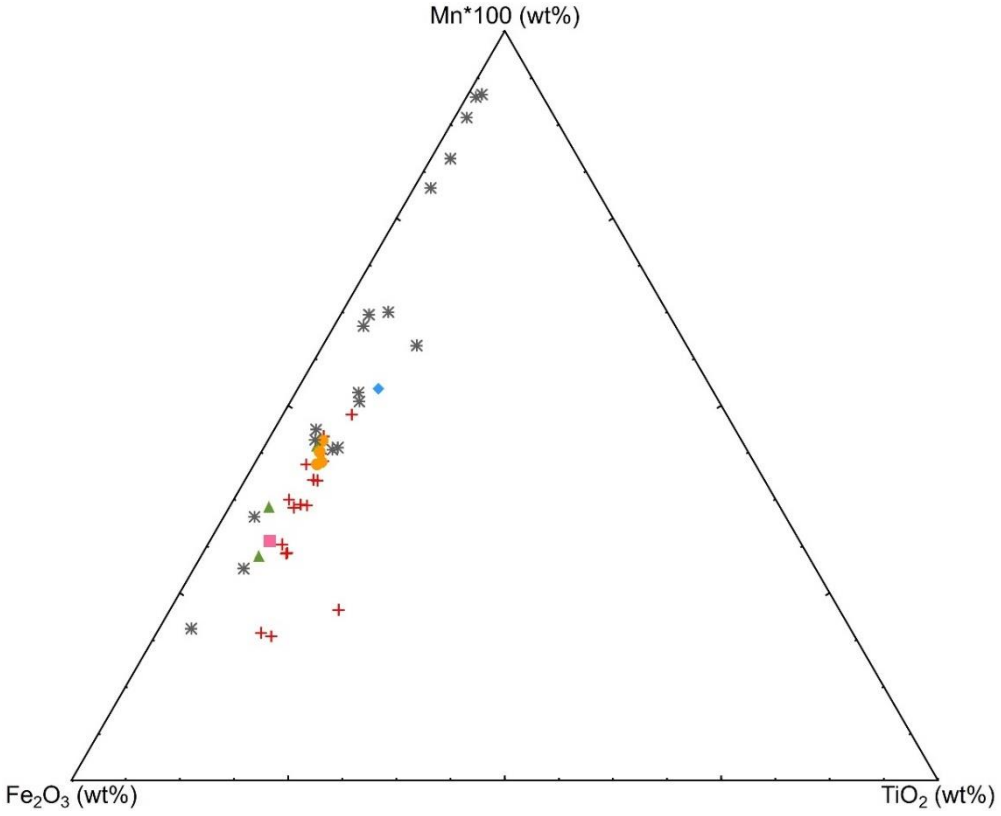


Figure 137. Ternary diagram of Fe_2O_3, TiO_2 and Mn (Mn values are multiplied by 100). Only those samples are presented on this graph which contain Mn above the limit of quantification.

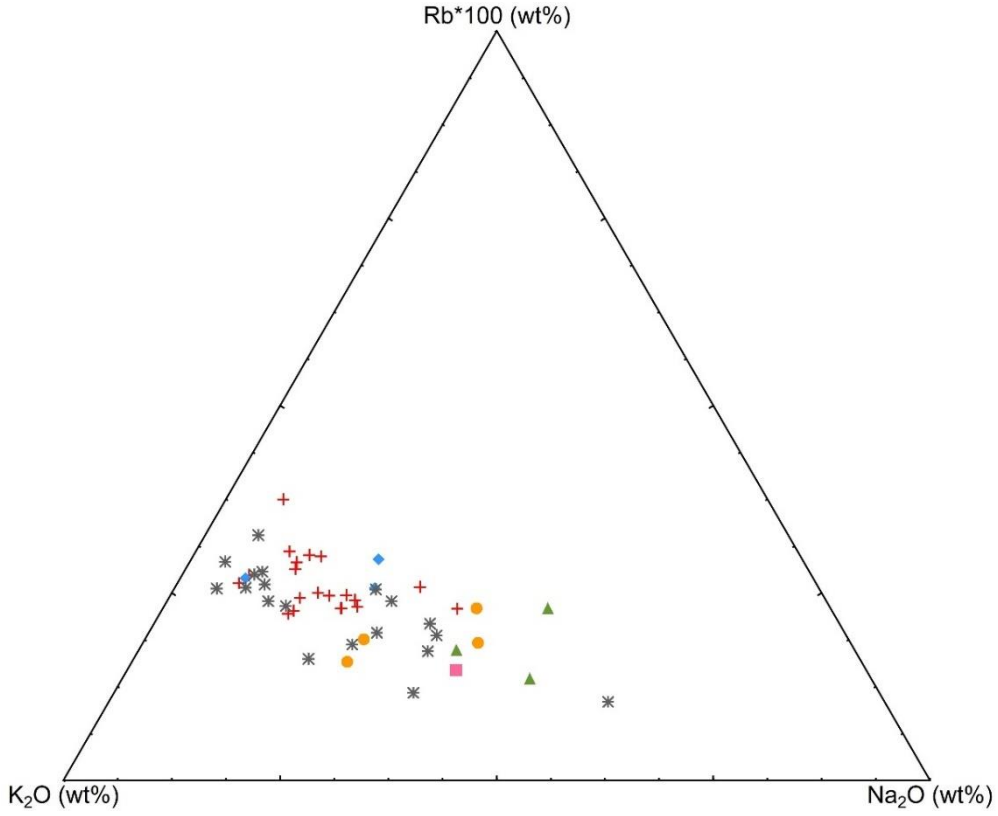


Figure 138. Ternary diagram of K_2O, Na_2O and Rb (Rb values are multiplied by 100)

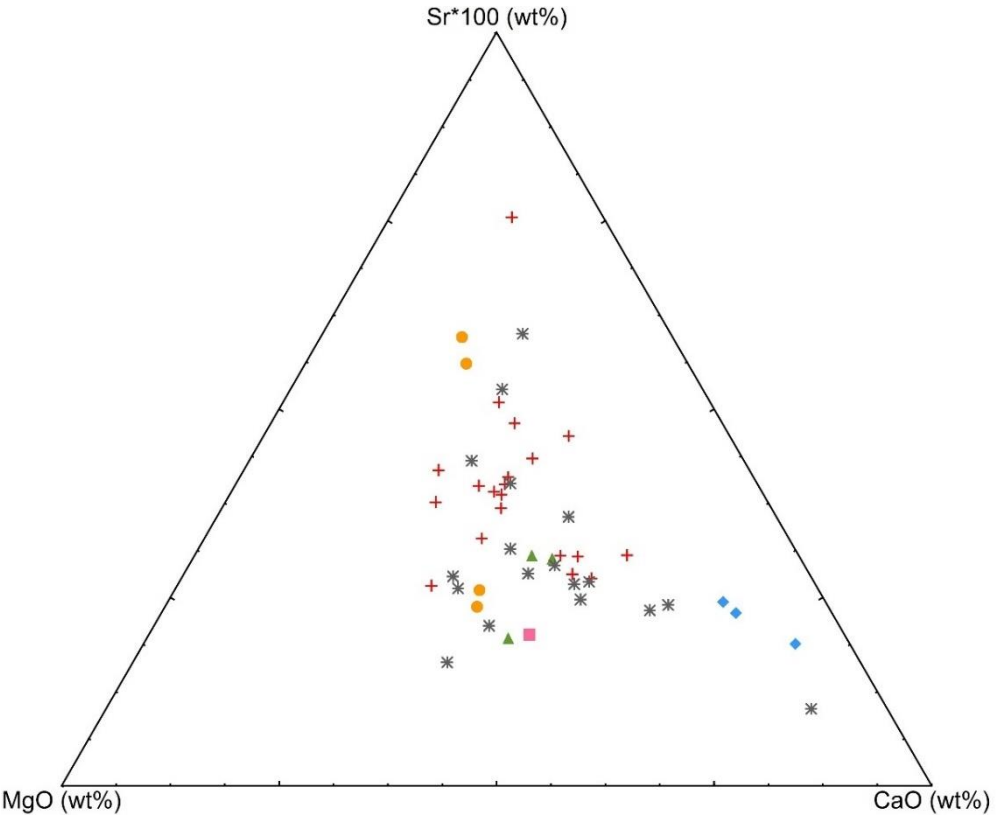


Figure 139. Ternary diagram of MgO, CaO and Sr (Sr values are multiplied by 100). S54 is not present in the graph as its CaO content is below the limit of quantification.

The ternary graph of alkaline earth metals including magnesium, calcium and strontium (*Figure 139*), shows the separation of six samples in its calcium-rich corner. Five of them belonging to the Carbonate group (S57, S58, S89) and 'Graphite C' (S129, S132) are expected to appear in this part of the graph because of the carbonate rock fragments present in these samples. Additionally, there is another graphite-containing sample (S31) with a much smaller amount of calcium oxide, which is located very close to these five samples based on the proportion of the three elements in question. The rest of the samples form a blend of the Granitoid, Graphite, Amphibole and Diorite groups; although it is clear that the two subgroups of the Diorite group have different strontium levels. One sample of the Granitoid group (S52) is an outlier in this graph due to its high strontium content.

The scatterplot below (*Figure 140*) shows a weak correlation between the amount of barium and strontium in the samples. Those samples which have higher values of barium usually have higher values of strontium as well. This correlation might be connected to the amount of feldspars or certain feldspar types present in the samples as feldspars can contain both of these elements (Deer, Howie & Zussman 1992, 412). The samples of the Granitoid group confirm this idea as the samples containing more than 300 ppm strontium and more than 1200 ppm barium are all from the feldspar-rich subgroups of the Granitoid-group ('Granitoid A1' and 'Granitoid A2') in contrast with the samples containing strontium and barium below these values, which belong to the quartz, biotite, and muscovite-rich subgroups (and the inclusion-poor 'Granitoid A3'). This biplot also clearly separates subgroup 'Diorite A' from the rest of the samples with its extreme high concentration of strontium and barium.

Elements chromium, zirconium and vanadium together are quite distinctive for some petrographic groups as shown by *Figure 141*. The Granitoid and Graphite groups can be separated based on their zirconium and vanadium content. The Diorite group stands apart from the rest of the samples due to the higher levels of chromium of its samples. However, the Amphibole and Carbonate groups are not separated in this graph, but mixed with the Graphite and Granitoid groups, respectively. The individual sample (S15) has similar proportions of the elements in question as the other samples.

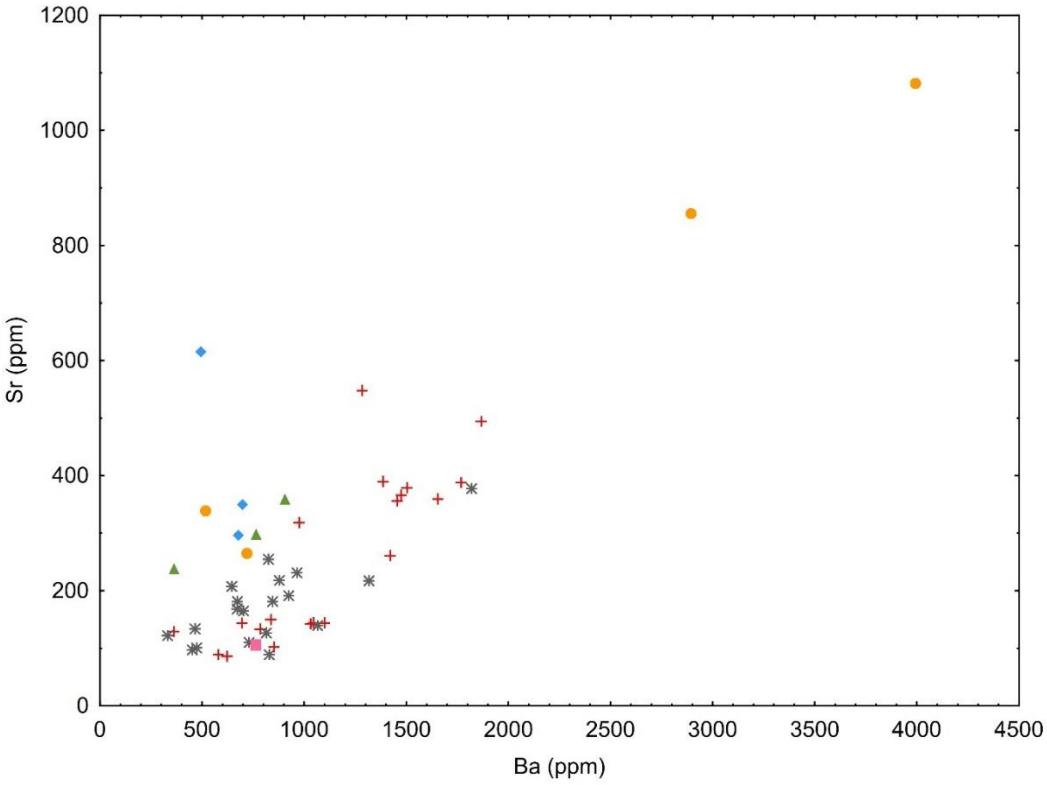


Figure 140. Scatterplot of Ba and Sr showing slight correlation

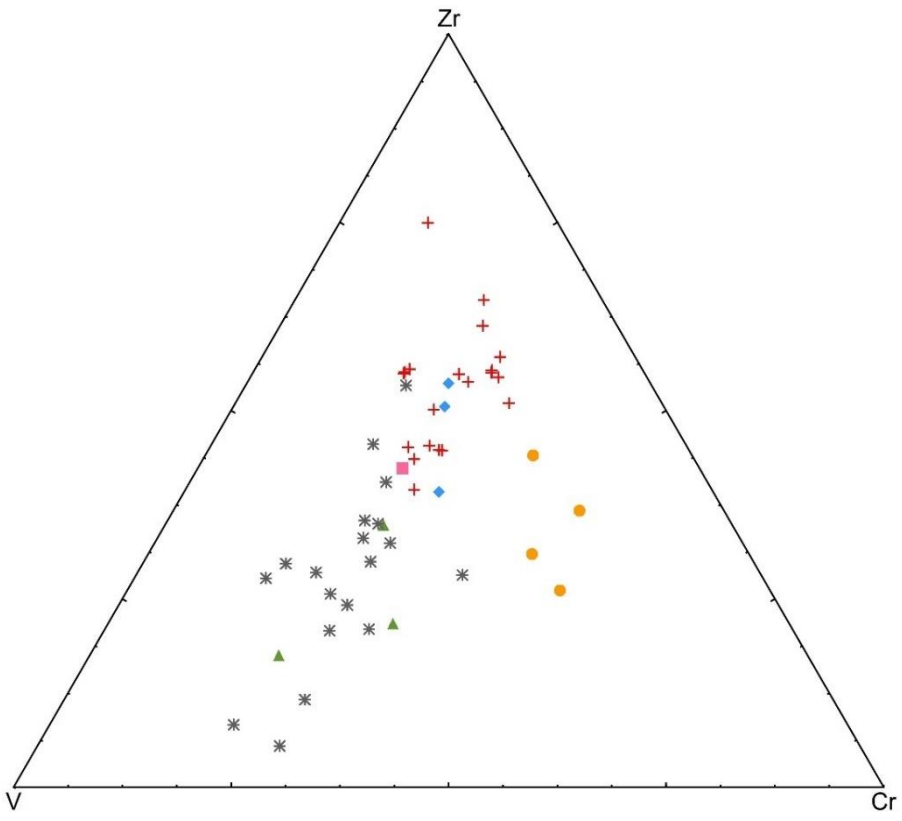


Figure 141. Ternary diagram of V, Cr and Zr

4.4.2 Statistical analysis

The chemical data of the 49 samples were subjected to statistical analyses. Principal component analysis (PCA) and cluster analysis were carried out on a reduced data set including 17 elements (Al, Ca, Fe, K, Mg, Na, Si, Ti, Ba, Cr, Ni, Rb, Sc, Sr, V, Y, Zr). Among major elements, phosphorus was excluded because its unreliability to characterise the original (pre-burial) composition of the ceramic samples as mentioned above (Freestone et al. 1994; Buxeda i Garrigós 1999, 308; Maritan 2020, 11). One sample (S54) has lower values of CaO than the limit of quantification and because it is the only sample with a major element value 'missing', a decision was made to keep this sample in the statistical analysis and change its CaO value to 0.001 wt%. Trace elements with values below the limit of quantification (Mn, Pb, Sn, Zn) were not included in the statistical analysis. Additionally, copper was excluded because of its high variability in the two measurements of S10 as explained above.

For PCA and cluster analysis the software Statistica was used (version 13.3). The results of the analyses are detailed below.

PCA

PCA was carried out on the whole (reduced) data set and also separately on major elements as well as trace elements. The standardisation of data was included in the analysis as a 'built-in' feature of the PCA software (Statistica). In this section, biplots are presented, along with their variable (element) plots. Related statistics such as the eigenvalues of the correlation matrix, the graphs of the new variables (principal components) showing their percentage of the total variance as well as the variable contributions to the principal components can be found in Appendix E.2.

Starting with all (both major and trace) elements, PCA resulted in three more or less distinguishable groups when plotting the first two principal components (*Figure 142*). There are some graphite-containing samples in the right bottom graph quarter, which are slightly separated from the rest because of their higher Al_2O_3, Fe_2O_3, Ni, Sc, V and Y content as it can be deducted from *Figure 143*. They are the members of several subgroups of the Graphite group. There is another group of samples just above the middle of the diagram, rich in MgO, Na_2O, Ba, Sr and Zr, and consisting of samples from the Granitoid group (all samples in subgroups 'Granitoid A1', 'Granitoid A2', 'Granitoid C', and one sample from 'Granitoid D') and the Diorite group ('Diorite B'). The rest of the samples in the left half of the scatterplot represent a mixed 'cloud' of samples originating from many petrographic groups (Granitoid, Amphibole, Carbonate, Graphite groups) and the individual sample is also located here. The

two samples of subgroup ‘Diorite A’ are located in the upper right corner due to their high Ba and Sr levels.

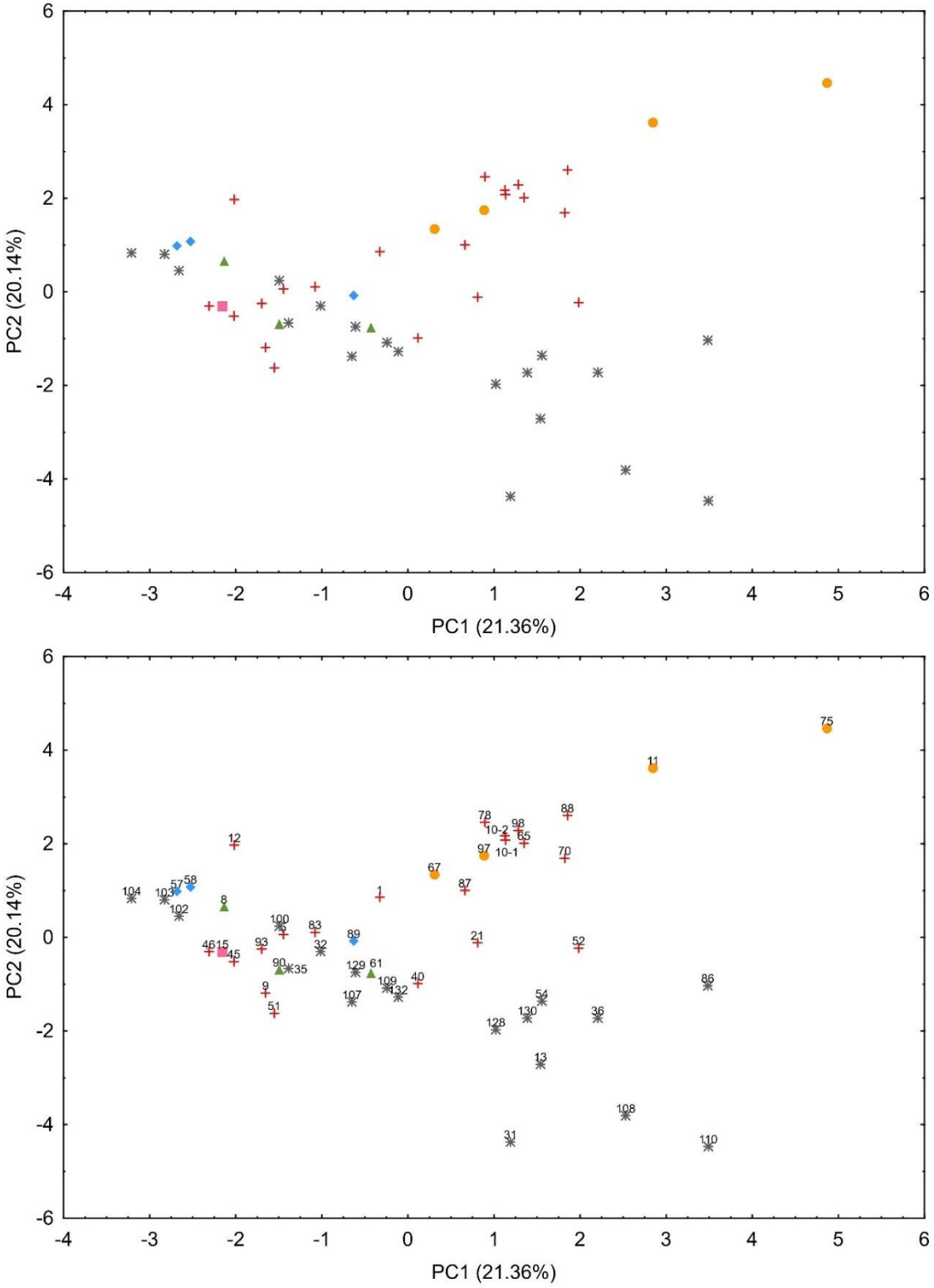


Figure 142. Scatterplot of the first two principal components (PC1 and PC2) based on all (major and trace) elements without sample numbers (upper graph) and with sample numbers (lower graph)

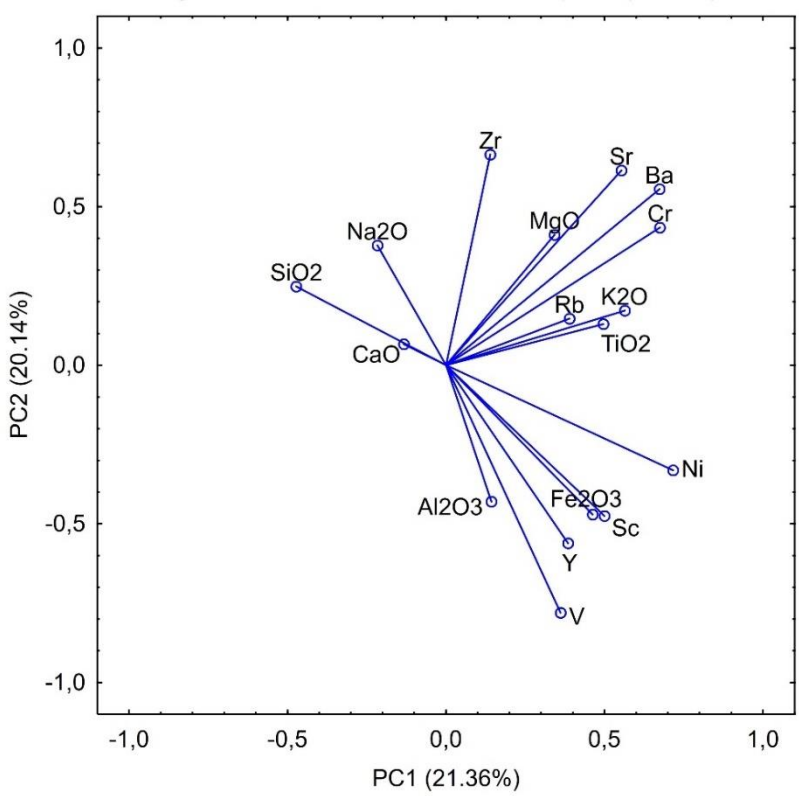


Figure 143. Projection of the variables for PC1 and PC2 based on all (major and trace) elements

Examining further the principal components, the binary diagram below (*Figure 144*) plots the first and the third principal components of the same analysis. In this graph, the Granitoid group clearly occupies the lower half of the graph, meaning that the presence of the oxides and elements projected on the lower half of the graph of the variables (*Figure 145*; Al_2O_3, K_2O, SiO_2, TiO_2, Ba, Rb, Sc, Y, Zr) is significant in these samples. Regarding the internal connections of the Granitoid group, PCA is able to distinguish between some petrographic subgroups, such as 'Granitoid A1', 'Granitoid A2' and 'Granitoid B3'. Furthermore, the samples of the different subgroups of the Diorite and Carbonate groups are plotted together. The slightly scattered samples of the Amphibole group are in the upper left corner of the biplot showing that their CaO and Na_2O contents are notable. The samples of the Graphite group are scattered all over the graph and petrographic subgroups are not plotted together. However, some sample pairs of the same petrographic subgroups are located relatively close to each other such as S102 and S103, S129 and S132 as well as S31 and S128.

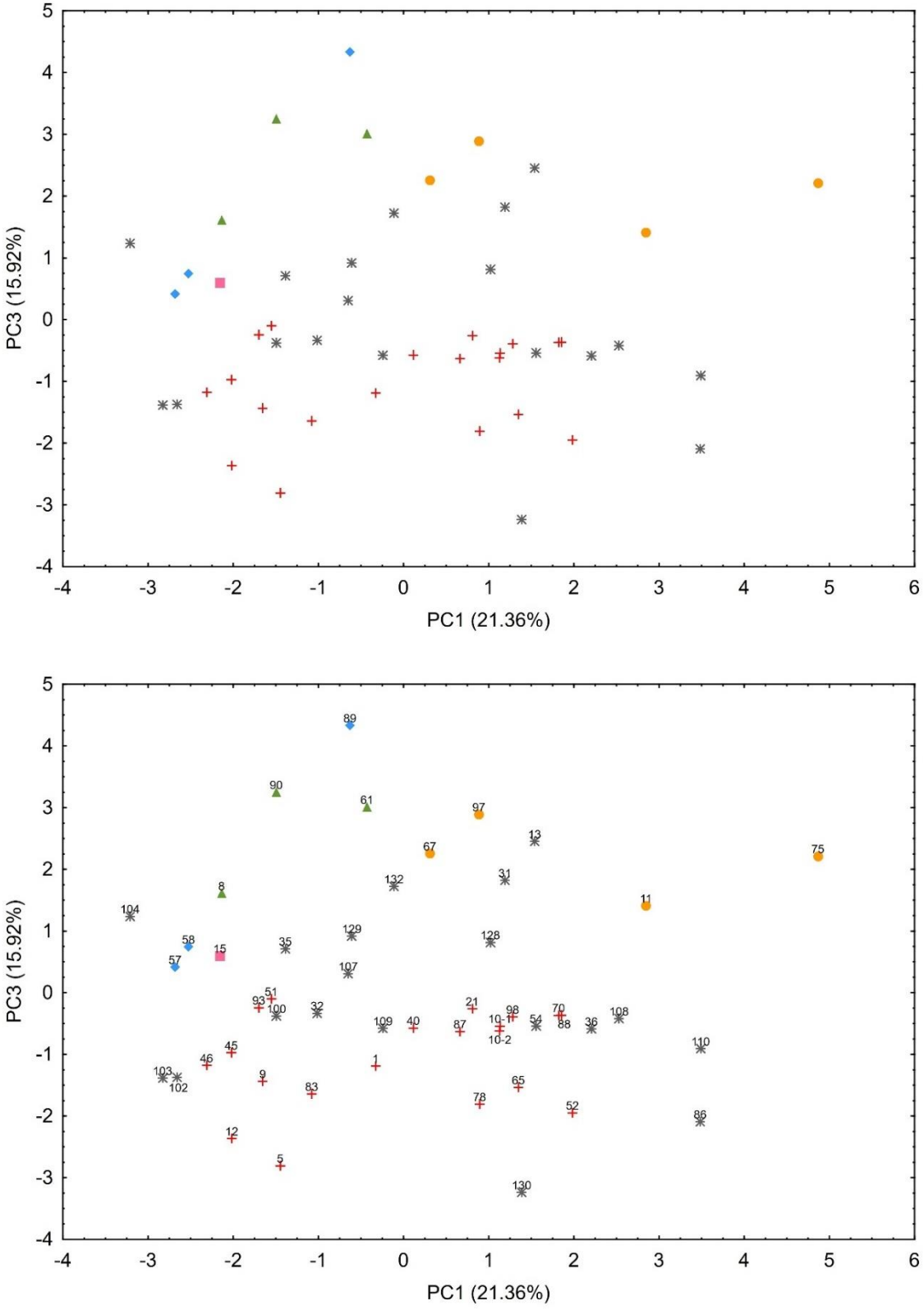


Figure 144. Scatterplot of the first and third principal components (PC1 and PC3) based on all (major and trace) elements without sample numbers (upper graph) and with sample numbers (lower graph)

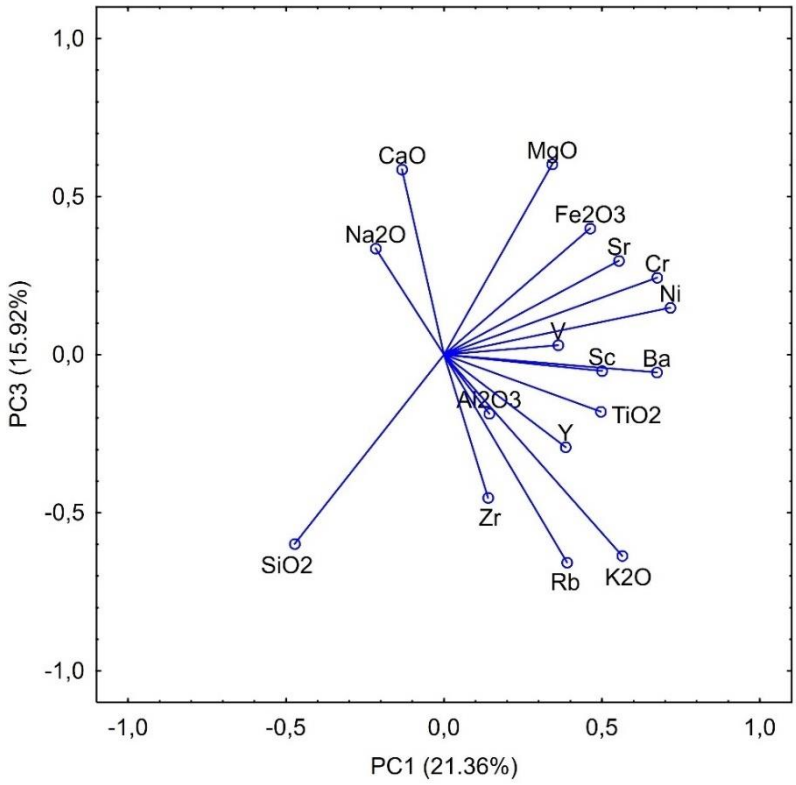


Figure 145. Projection of the variables for PC1 and PC3 based on all (major and trace) elements

In the plot created by the PCA of the major elements (*Figure 146*), several small groups may be recognised. These groups do not overlap with the petrographic groups, but there are some samples which are close to each other by both petrography and the PCA of chemical data such as the members of subgroups 'Granitoid A1', 'Granitoid A3', 'Granitoid B1', 'Granitoid B3', 'Carbonate A' and S102 and S103 from subgroup 'Graphite A1'. The Diorite and the Amphibole groups can also be separated from the rest of the samples although these two groups are not separated from each other. They are in the upper left quarter of the PCA graph and defined by their similar Na_2O and MgO content (*Figure 147*).

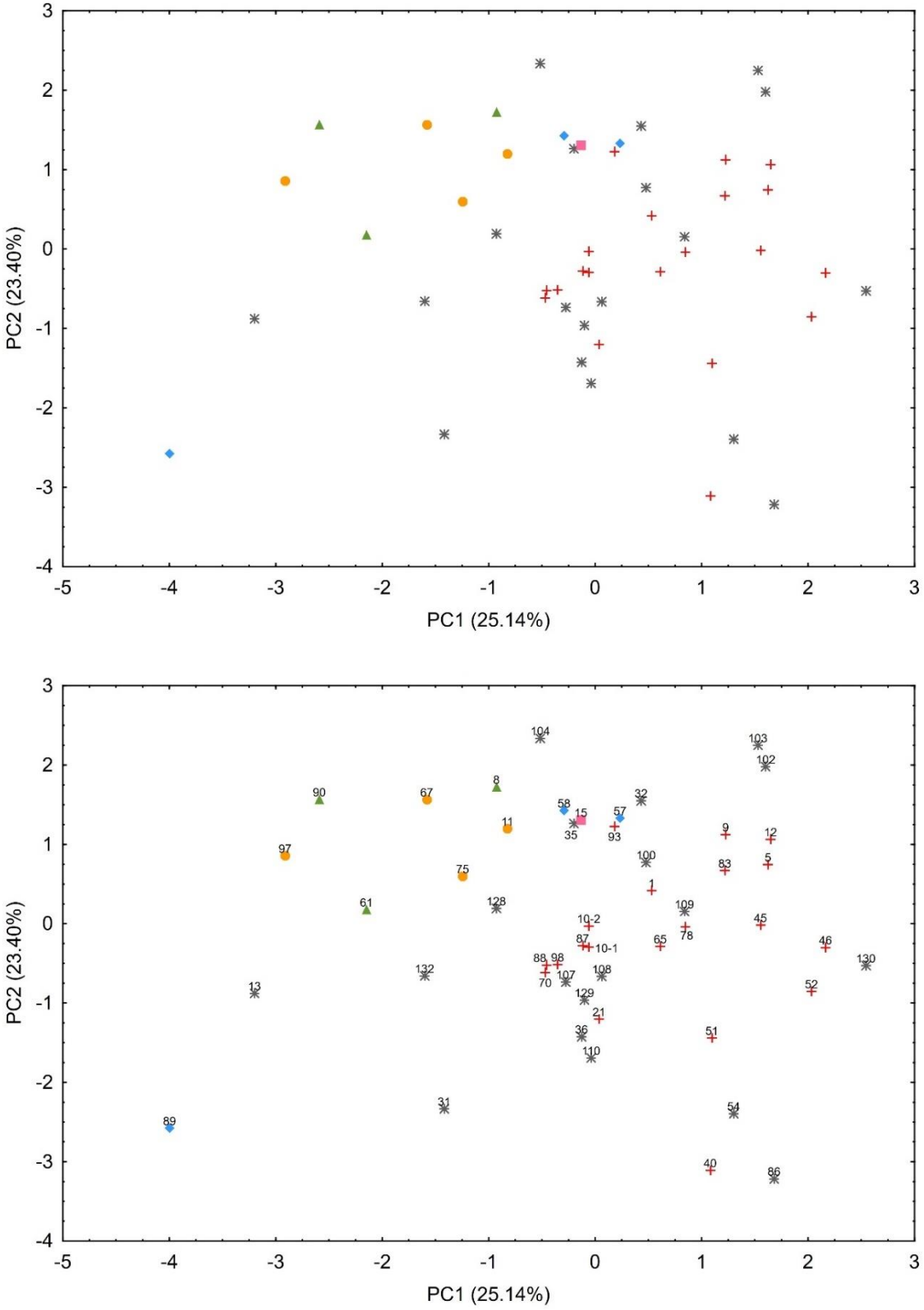


Figure 146. Scatterplot of the first two principal components (PC1 and PC2) based on the major elements without sample numbers (upper graph) and with sample numbers (lower graph)

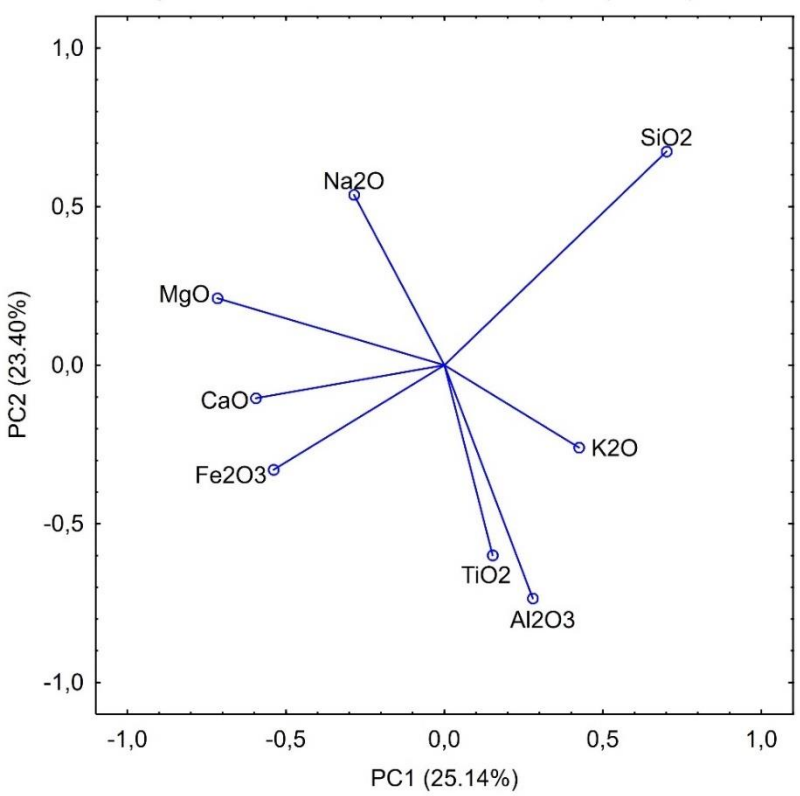


Figure 147. Projection of the variables for PC1 and PC2 based on the major elements

When choosing the trace elements as variables, the PCA results in another arrangement of the samples in the graph (*Figure 148*). Although the samples of the Graphite and Granitoid groups are mixed at certain parts of the scatterplot, trends can be recognised in their distribution. The Graphite group occupies the left-hand side of the graph, while the Granitoid group dominates the upper part of the graph. There is a small Zr-rich (*Figure 149*) group consisting of Granitoid samples above the centre of the graph, which includes subgroup 'Granitoid A1' and 'Granitoid A2' (except one sample, S52, from the latter subgroup). The samples of 'Granitoid A3' as well as 'Granitoid C' are also located close to each other. As for the Graphite group, the petrographic subgroups are mixed on the PCA graph; only S102 and S103 can be highlighted as they are plotted close to each other and they are the members of the same subgroup ('Graphite A1'). The samples of the Amphibole group are quite scattered. In contrast, all three samples of the Carbonate group are located very close to each other, which cannot be seen in the other PCA graphs (of all elements and major elements). The Diorite group is divided into two groups on the graph, which correspond to the two petrographic subgroups. The comparison of the plot of the samples and that of the variables (*Figure 149*) indicates that many of the samples are relatively poor in trace elements as they are located far from the vectors of the trace elements, on the opposite side of the graph.

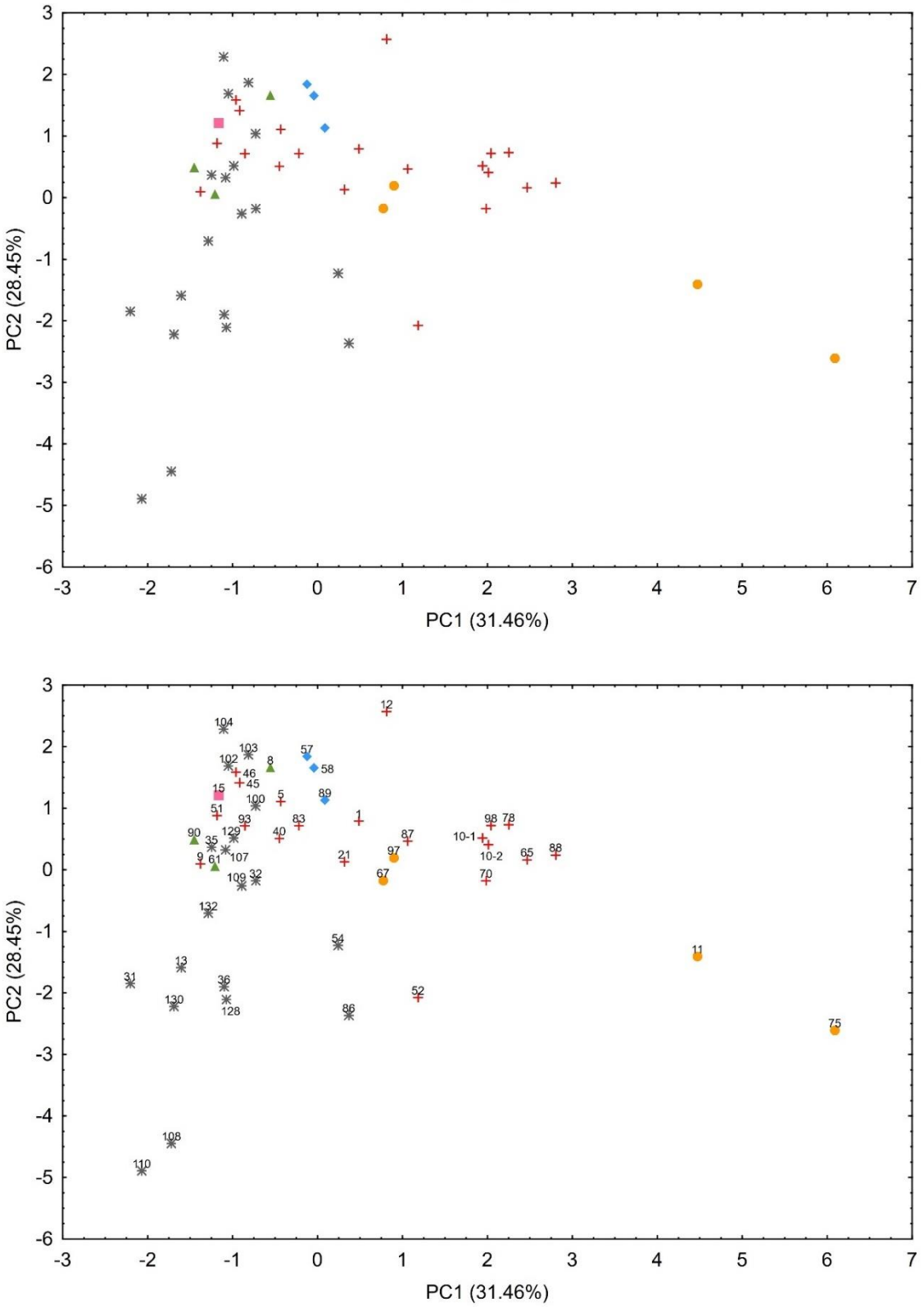


Figure 148. Scatterplot of the first two principal components (PC1 and PC2) based on the trace elements without sample numbers (upper graph) and with sample numbers (lower graph)

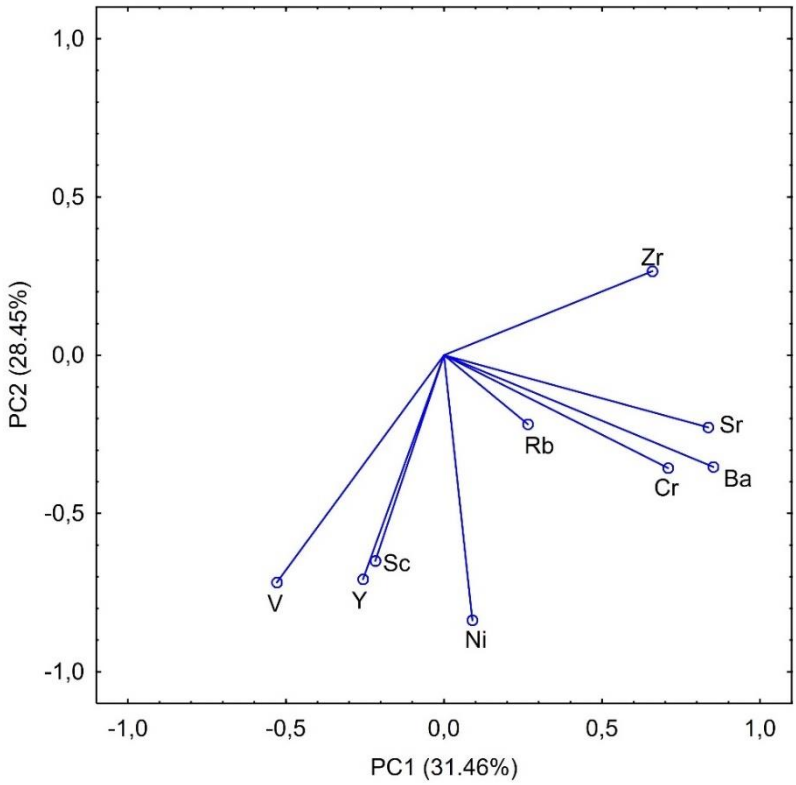


Figure 149. Projection of the variables for PC1 and PC2 based on the trace elements

Cluster analysis

Cluster analysis was carried out on standardised values using different methods (Ward's method, complete linkage, weighted pair-group average, unweighted pair-group average, single linkage). The results are presented by selected dendrograms below. As cluster analysis failed to differentiate between the two basic types of pottery, the graphite-containing and graphite-free samples, it was carried out separately on these two sample groups. Analyses were run using the chemical data of all elements as well as the major and trace elements separately.

Graphite-free pottery

Examining both major and trace element concentrations of the graphite-free pottery, the dendrogram below (*Figure 150;* using complete linkage) shows a mixture of samples of different petrographic groups. However, there is a clear separation of subgroups in most of the cases even though the subgroups of a main group are not closely connected. To give an example, cluster analysis recognises the similarity between the samples in subgroup 'Diorite A' and in subgroup 'Diorite B', but these two subgroups are not clustered together clearly as the

Diorite group. The same is true for the Carbonate and Granitoid groups, where subgroups are usually recognised, but not connected at a higher level (main petrographic groups).

The next dendrogram of all elements (*Figure 151*) was created using Ward's method and shows the same characteristics as the previous dendrogram: the samples within subgroups are usually of the same cluster, but the subgroups of a main group are not closely connected. What is evident from both dendrograms in terms of the largest group, the Granitoid group, is that subgroup 'Granitoid A1', 'Granitoid B3' and 'Granitoid C' are clearly separated and form three clusters in both graphs. Furthermore, the individual sample (S15) does not appear as an outlier in any of the dendrograms.

The dendrogram of the major elements (*Figure 152*) exhibits four groups and an outlier if cut at linkage distance 3.25. The group on the right-hand side of the dendrogram (including samples from S5 to S10-1) consists only of the samples of the Granitoid group. Furthermore, the subgroups of the Diorite group are clustered together in this dendrogram. However, the Amphibole and Carbonate groups are still divided and there are three samples (S40, S51, S93) of the Granitoid group that are separated from the rest of the group.

Figure 153 shows the result of the cluster analysis based on the trace elements. If the dendrogram is cut at linkage distance 7, four groups are distinguished. The first of these groups (S67 to S90) contains samples from the Diorite and Amphibole groups. The next cluster (S89 to S40) is quite mixed as it includes samples from all groups except the Diorite group. The following cluster is of two samples (S11, S75) of the Diorite group and the last cluster (S5 to S10-1) incorporates only samples of the Granitoid group.

Graphite-containing pottery

The cluster analysis of the graphite-containing pottery (Graphite group) does not reflect the petrographic grouping as it resulted in clusters containing samples from different petrographic subgroups. The reason for this mixed arrangement of samples might be the heterogeneity of the Graphite group as also indicated by petrography. The dendrogram of all elements (*Figure 154*) and the trace elements (*Figure 155*) are very similar and displays the same two big clusters. The cluster occupying the left half of both dendrograms (including samples from S130 to S110) contains all investigated samples from 'Graphite A4' and 'Graphite D', while the cluster on the right-hand side includes all investigated samples from 'Graphite A2' and 'Graphite C'. There are subgroups, however, members of which are present in both big clusters including 'Graphite A1', 'Graphite A3' and 'Graphite A5'.

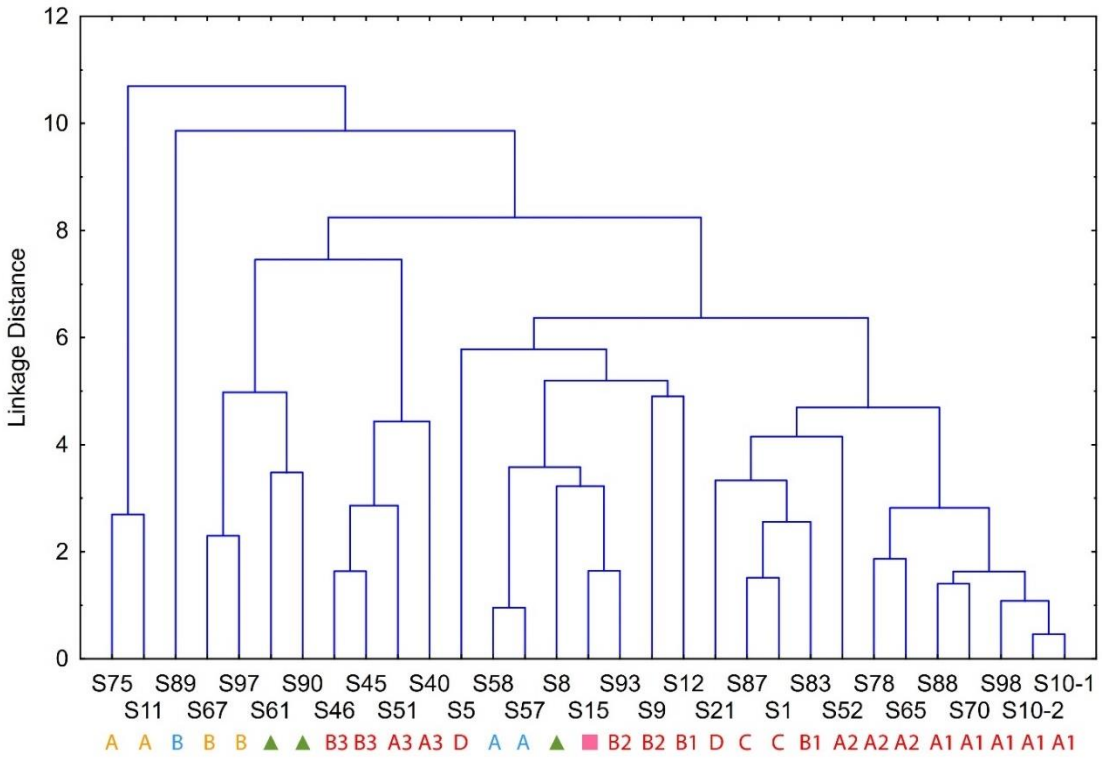


Figure 150. Cluster analysis of all 17 elements of graphite-free pottery using complete linkage and Euclidean distances. Petrographic groups/subgroups are indicated below the sample numbers: Granitoid group = red subgroups, Amphibole group = green triangles, Diorite group = yellow subgroups, Carbonate group = blue subgroups, and S15 as an individual sample = pink square.

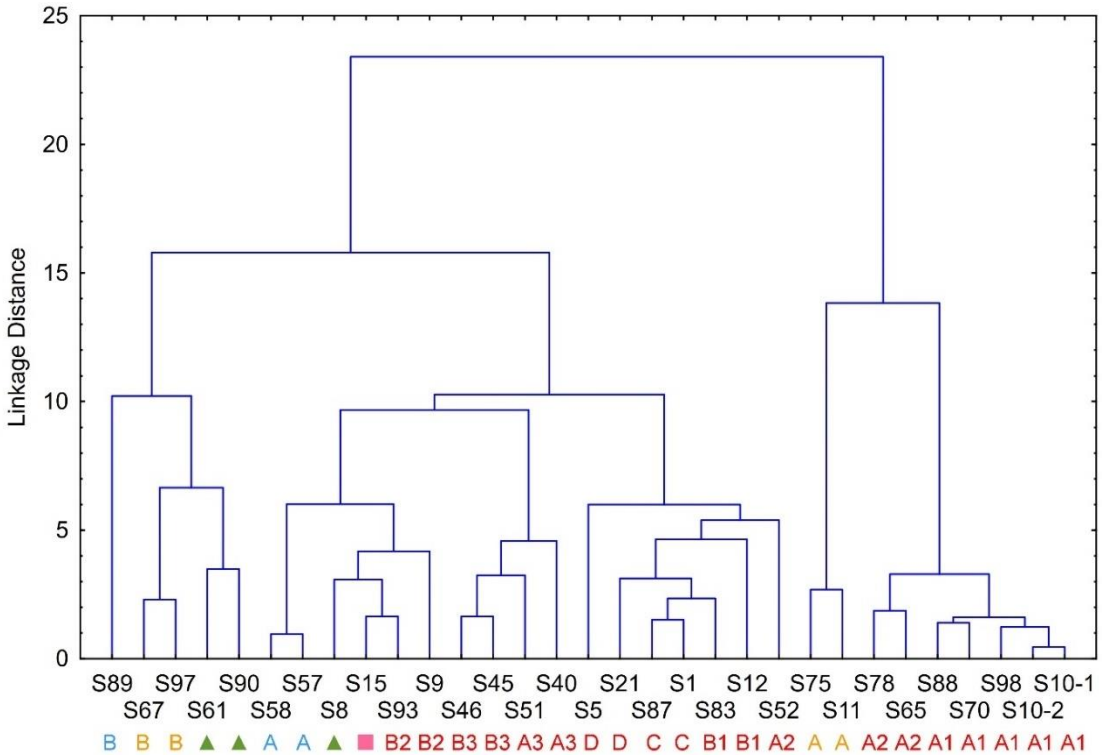


Figure 151. Cluster analysis of all 17 elements of graphite-free pottery using Ward's method and Euclidean distances. Petrographic groups/subgroups are indicated below the sample numbers as explained in the caption of Figure 150.

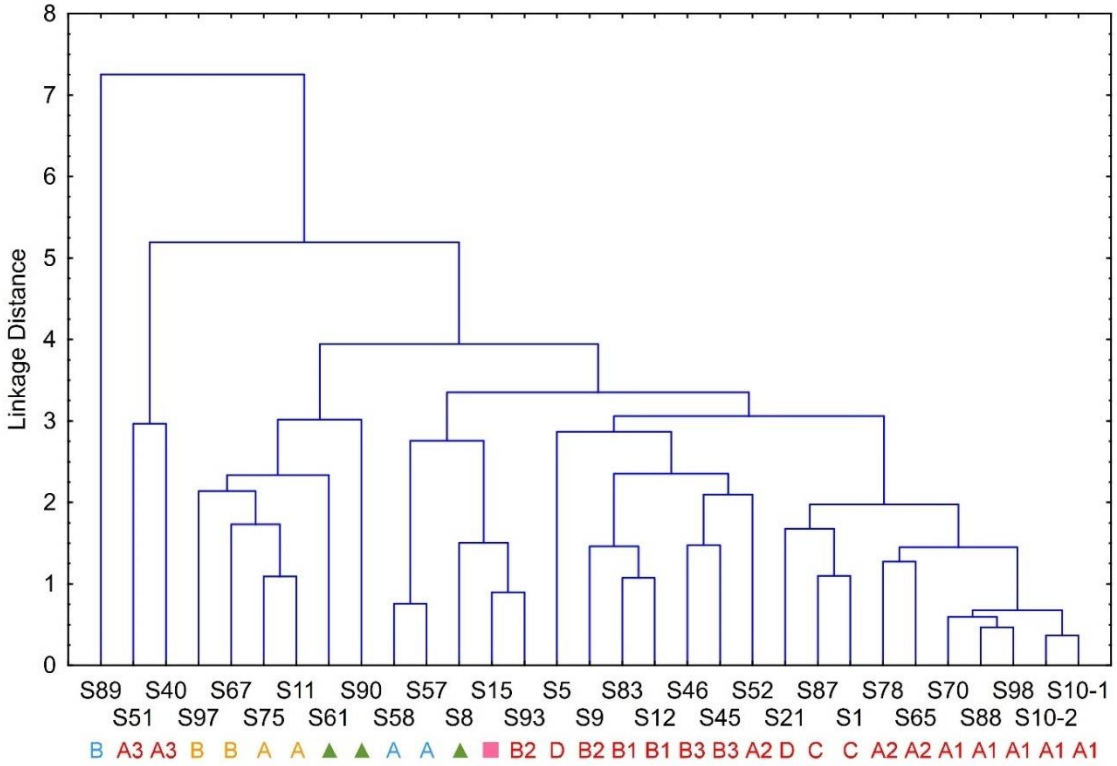


Figure 152. Cluster analysis of the major elements of graphite-free pottery using weighted pair-group average and Euclidean distances. Petrographic groups/subgroups are indicated below the sample numbers as explained in the caption of Figure 150.

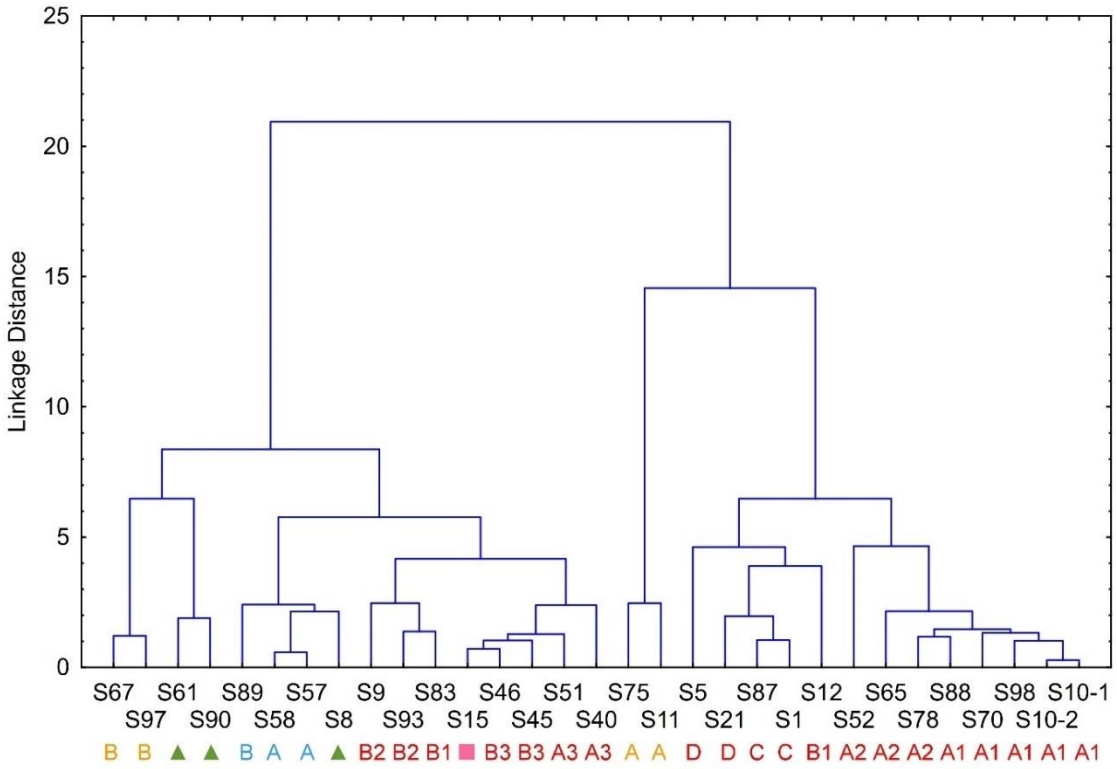


Figure 153. Cluster analysis of the trace elements of graphite-free pottery using Ward's method and Euclidean distances. Petrographic groups/subgroups are indicated below the sample numbers as explained in the caption of Figure 150.

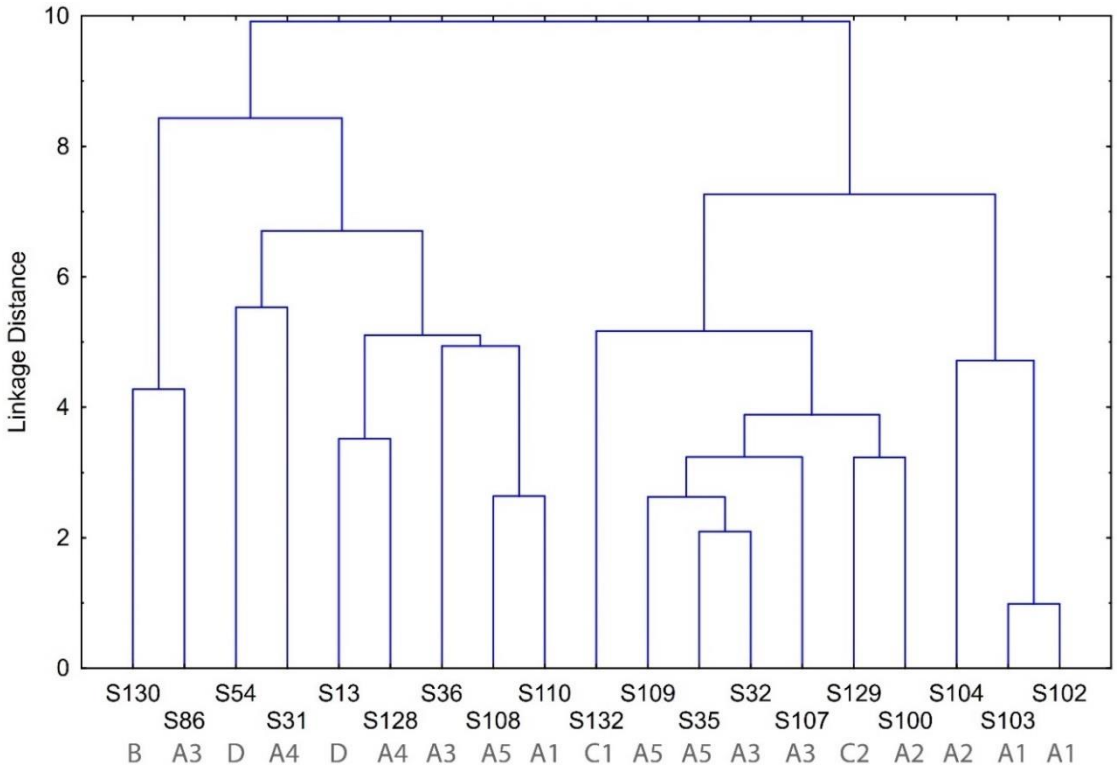


Figure 154. Cluster analysis of all 17 elements of graphite-containing pottery using complete linkage and Euclidean distances. Subgroups within the Graphite group are indicated below the sample numbers.

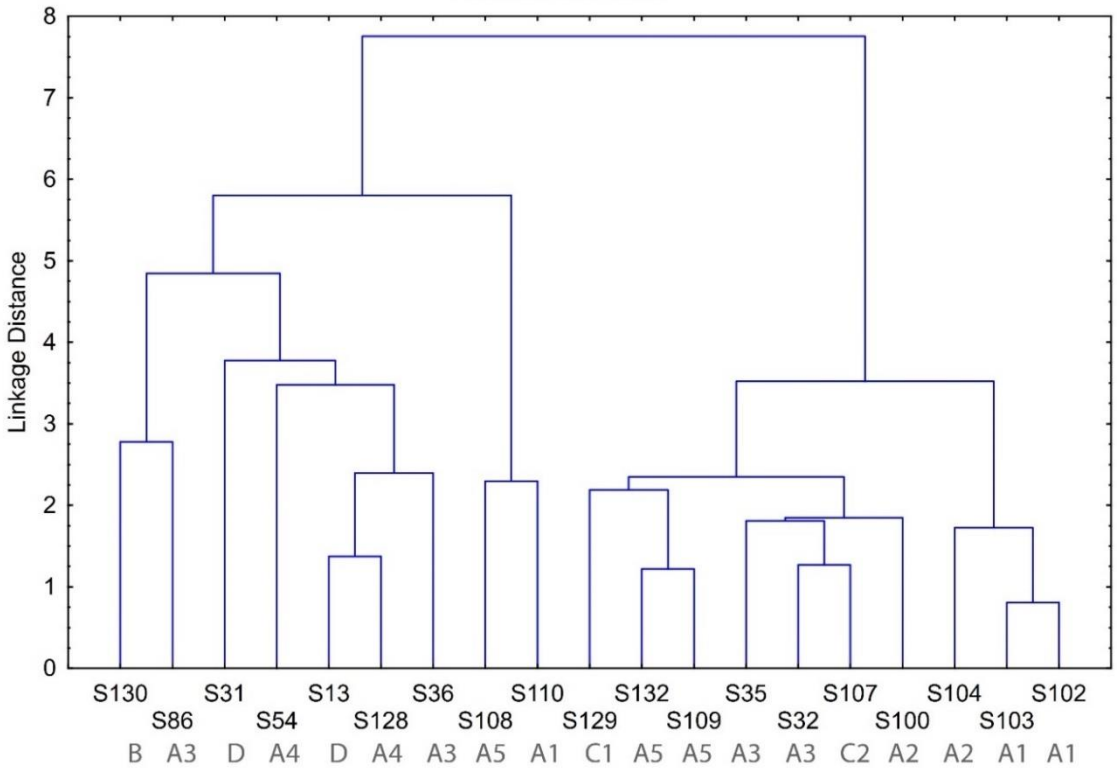


Figure 155. Cluster analysis of the trace elements of graphite-containing pottery using complete linkage and Euclidean distances. Subgroups within the Graphite group are indicated below the sample numbers.

4.4.3 Summary

The chemical analysis provided further pieces of information about the relationship of the samples from Lower Austria. The preliminary analysis of raw data shows that certain petrographic subgroups can be distinguished based on the differences in concentration of certain elements. The PCA of the samples is able to confirm some petrographic connections and subgroups and shows certain trends in the chemical composition of the main groups. The cluster analysis gives mixed results, however, some of the subgroups can be recognised and it also proves close connections between certain samples.

The analysis of the ICP-OES data reveals that subgroup 'Granitoid A1' is chemically more uniform than it was suggested by the petrographic results as its samples are plotted and clustered together in almost every case. The separation of the subgroups of the Diorite and Carbonate groups is also well-presented by the ICP-OES results. The analysis shows that the individual sample is not significantly different from the rest of the samples in terms of chemistry as it is not differentiated as an outlier by any of the graphs and dendrograms.

4.5 X-ray diffraction

The same set of 49 samples were subjected to XRD analysis, which was analysed by SEM and ICP-OES (*Table 19*). One sample (S10) was run twice resulting in a total of 50 measurements. The results of the phase identification are described below by petrographic groups. The diffractogram of each measurement can be found in Appendix F.

4.5.1 Graphite-free ceramics

Granitoid group

The diffractograms of the samples in the Granitoid group show remarkable similarity (*Figure 156*). Quartz, potassium feldspar and plagioclase were detected by XRD in all samples (*Table 21*). Additionally, most (possibly all) samples contain illite as the clay mineral. Mica minerals such as muscovite and biotite were identified by petrography in all samples, however, they do not usually appear in the diffractograms. This may be because of the small amount present, which falls below the detection limit of the XRD instrument, or might be because their peaks (especially those of muscovite) overlap with those of illite (Arnold 1972, 94). Overlapping is the result of the compositional similarity between illite and the micas, as illite (and clay in general) is the product of weathering of rock-forming minerals including micas (Velde and Druc 1999, 40, 59).[68] Amphibole was also detected by XRD in many samples, the structure of which is consistent with that of hornblende (magnesiohornblende).

The petrographic subgroups of the Granitoid group can also be recognised in the diffractograms based on differences in phase composition and the intensity (height) of certain peaks, with the latter being proportional to the amount of the phases present.

In the feldspar-rich subgroup 'Granitoid A', the potassium feldspar phases are consistent with orthoclase and the plagioclase phases are consistent with albite (and labradorite in some cases) based on the XRD results. In addition, samples also contain hornblende (except S52). Samples of subgroup 'Granitoid A1' include both albite and labradorite as plagioclase feldspars, and feldspar peaks in general are quite intensive in the diffractograms. In addition to

[68] S10 is a good example of the difficulty of separating muscovite and illite peaks and the limitations of the Search-Match computer programs. The two analyses of this sample produced two almost identical diffractograms. The software identified muscovite based on the first diffractogram, however it identified illite based on the second (*Table 21*). This also points out the necessity of checking the identification of the Search-Match programs.

illite, two samples of this subgroup (S10, S98) also contain vermiculite as clay mineral. The diffractograms of 'Granitoid A2' show lower feldspar content than those of 'Granitoid A1' and they do not include labradorite. Among the 'Granitoid A' subgroups, feldspar peaks (especially those of the orthoclase) are the least intensive in 'Granitoid A3', which incorporate probably both albite and labradorite. A form of titanium oxide (rutile?, anatase?) is also present in 'Granitoid A3'.

Table 21. Mineral phases in the Granitoid group detected by XRD. Abbreviations as follows based on Siivola and Schmid 2007. Ab = albite, Bt = biotite, Cal = calcite, Hbl = hornblende, Ill = illite, Lab = labradorite, Mc = microcline, Ms = muscovite, Or = orthoclase, Phl = phlogopite, Ttn = titanite, Vrm = vermiculite.

Subgroup	Sample	Quartz	Potassium feldspar	Plagioclase	Clay mineral	Mica	Other
Granitoid A1	**S10 (1)**	✓	Or	Ab, Lab		Ms	Hbl
	S10 (2)	✓	Or	Ab, Lab	Ill		Hbl
	S70	✓	Or	Ab, Lab	Ill	Bt	Hbl
	S88	✓	Or	Ab, Lab	Ill		Hbl
	S98	✓	Or	Ab, Lab	Ill, Vrm	Bt	Hbl, Ttn
Granitoid A2	**S52**	✓	Or	Ab	Ill	Ms	
	S65	✓	Or	Ab	Ill		Hbl
	S78	✓	Or	Ab	Ill		Hbl
Granitoid A3	**S40**	✓	Or	Ab, Lab(?)	Ill		Hbl, Ti oxide
	S51	✓	Or	Ab, Lab(?)	Ill		Hbl, Ti oxide
Granitoid B1	**S12**	✓	Or	Ab	Ill	Bt	
	S83	✓	Or	Ab	Ill	Bt (Phl), Ms	Ti oxide
Granitoid B2	**S9**	✓	Or	Ab	Ill		Cal
	S93	✓	Or	Ab, Lab	Ill	Bt, Ms	
Granitoid B3	**S45**	✓	Or	Ab	Ill	Bt, Ms	Ttn, Ti oxide
	S46	✓	Or	Ab	Ill		Ttn, Ti oxide
Granitoid C	**S1**	✓	Mc, Or	Ab, Lab(?)	Ill	Bt, Ms	Hbl
	S87	✓	Mc, Or	Ab, Lab(?)	Ill	Bt	Hbl
Granitoid D	**S5**	✓	Mc	Ab		Bt, Ms	
	S21	✓	Mc, Or	Ab	Ill	Ms	

In the samples of the quartz-rich subgroup 'Granitoid B', the closest matches to the feldspar phases are orthoclase and albite, which exhibit considerably fewer intensive peaks than the feldspar-rich 'Granitoid A'. Mica minerals were detected in each sample except S46. Subgroups 'Granitoid B1' and 'Granitoid B2' cannot be distinguished based on the diffractograms. S93 is distinctive among the samples of these subgroups as it contains another feldspar phase that is structurally consistent with labradorite and its biotite content is much higher than the other three samples. S9 also differs slightly from the other samples because of its calcite content.[69] The samples of 'Granitoid B3' contain both titanite and titanium oxide, which make this subgroup different from 'Granitoid B1' and 'Granitoid B2'.

Subgroups 'Granitoid C' and 'Granitoid D' are similar in terms of potassium feldspar content as both subgroups include phases structurally matching microcline and orthoclase (except S5, which possibly contains only microcline). Albite, possibly labradorite, biotite and hornblende were detectable in both samples of the biotite-rich 'Granitoid C'. Plagioclase in 'Granitoid D' includes probably albite and the muscovite content is quite apparent from the diffractograms in this muscovite-rich subgroup.

Amphibole group

The samples of the amphibole group are rich in quartz, plagioclase (labradorite) and hornblende (magnesiohornblende; *Table 22, Figure 157*). Some potassium feldspar (orthoclase) was also detected in two samples (S8, S61). There is no evidence of the presence of illite or other clay minerals in the diffractograms. Biotite (phlogopite) is identified in one sample (S8) only.

Diorite group

All samples of the Diorite group contain quartz, orthoclase, albite and hornblende (*Table 22, Figure 157*). However, the diffractograms show some compositional differences between the two subgroups. Samples of 'Diorite A' contain illite and the XRD results indicate the presence of another type of amphibole in addition to hornblende, called tremolite. In subgroup 'Diorite B', a pyroxene phase that is consistent with augite and biotite occur, and no illite can be identified (although S97 contains some vermiculite) in contrast to 'Diorite A'.

[69] The difference is not obvious from *Figure 156* as the calcite peaks of S9 are very small.

Carbonate group

The samples of the Carbonate group are rich in quartz and calcite (*Table 22, Figure 157*). They also contain illite, muscovite and pyroxene (diopside). In the samples of subgroup 'Carbonate A', feldspar phases matching orthoclase and albite were also detected. The one sample analysed from 'Carbonate B' (S89) has extremely intense calcite peaks, has no feldspar peaks and contains amphibole (tremolite) in addition to the above-mentioned phases that are common is both subgroups (quartz, calcite, illite, muscovite and diopside).

Table 22. Mineral phases in the Amphibole, Diorite and Carbonate groups and the individual sample detected by XRD. Abbreviations as follows based on Siivola and Schmid 2007. Ab = albite, Alm = almandine, Ann = annite, Aug = augite, Bt = biotite, Cal = calcite, Di = diopside, Hbl = hornblende, Ill = illite, Lab = labradorite, Ms = muscovite, Or = orthoclase, Phl = phlogopite, Rt = rutile, Tr = tremolite, Vrm = vermiculite.

Group		Sample	Quartz	Potassium feldspar	Plagioclase	Clay mineral	Mica	Amphibole	Pyroxene	Other
Amphibole		**S8**	✓	Or	Lab		Bt (Phl)	Hbl		
		S61	✓	Or	Lab			Hbl		
		S90	✓		Lab			Hbl		
Diorite	**A**	**S11**	✓	Or	Ab	Ill	Ms	Hbl, Tr		
		S75	✓	Or	Ab	Ill		Hbl, Tr		
	B	**S67**	✓	Or	Ab		Bt (Ann)	Hbl	Aug	
		S97	✓	Or	Ab	Vrm	Bt	Hbl	Aug	
Carbonate	**A**	**S57**	✓	Or	Ab	Ill	Ms		Di	Cal
		S58	✓	Or	Ab	Ill	Ms		Di	Cal
	B	**S89**	✓			Ill	Ms(?)	Tr	Di	Cal
Individual sample		**S15**	✓	Or	Ab		Ms(?)		Di(?)	Alm, Rt

Individual sample

The main phases in S15 include quartz, two types of feldspar (albite, orthoclase) and garnet (that is structurally consistent with almandine). It also contains rutile, and possibly muscovite and diopside based on its diffractogram (*Table 22, Figure 157*).

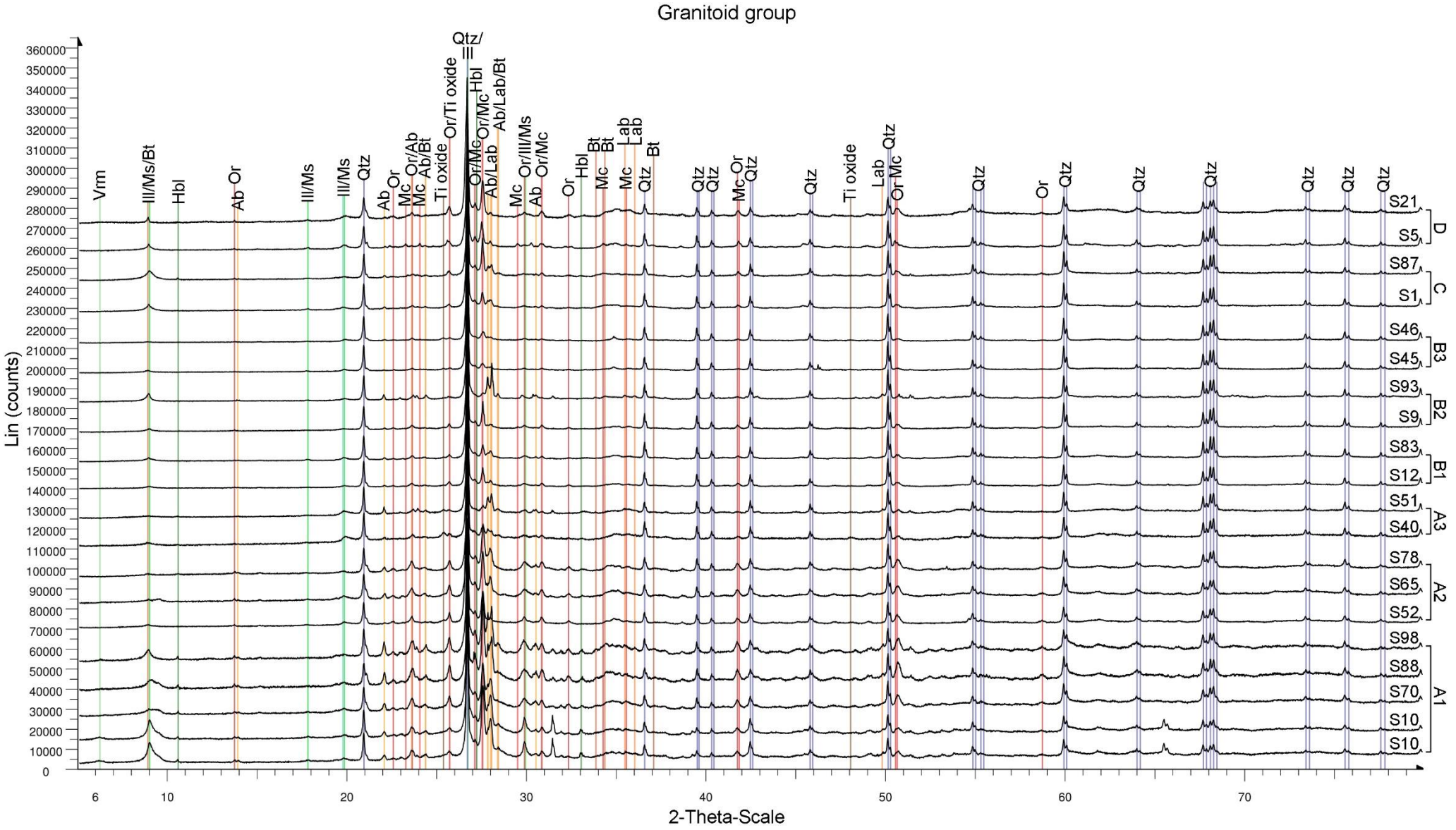


Figure 156. Diffractograms of the samples of the Granitoid group (data are normalised) with the indication of the most significant peaks of important phases. Abbreviations of phases as follows based on Siivola and Schmid 2007. Ab = albite, Bt = biotite, Hbl = hornblende, Ill = illite, Lab = labradorite, Mc = microcline, Ms = muscovite, Or = orthoclase, Qtz = quartz, Vrm = vermiculite.

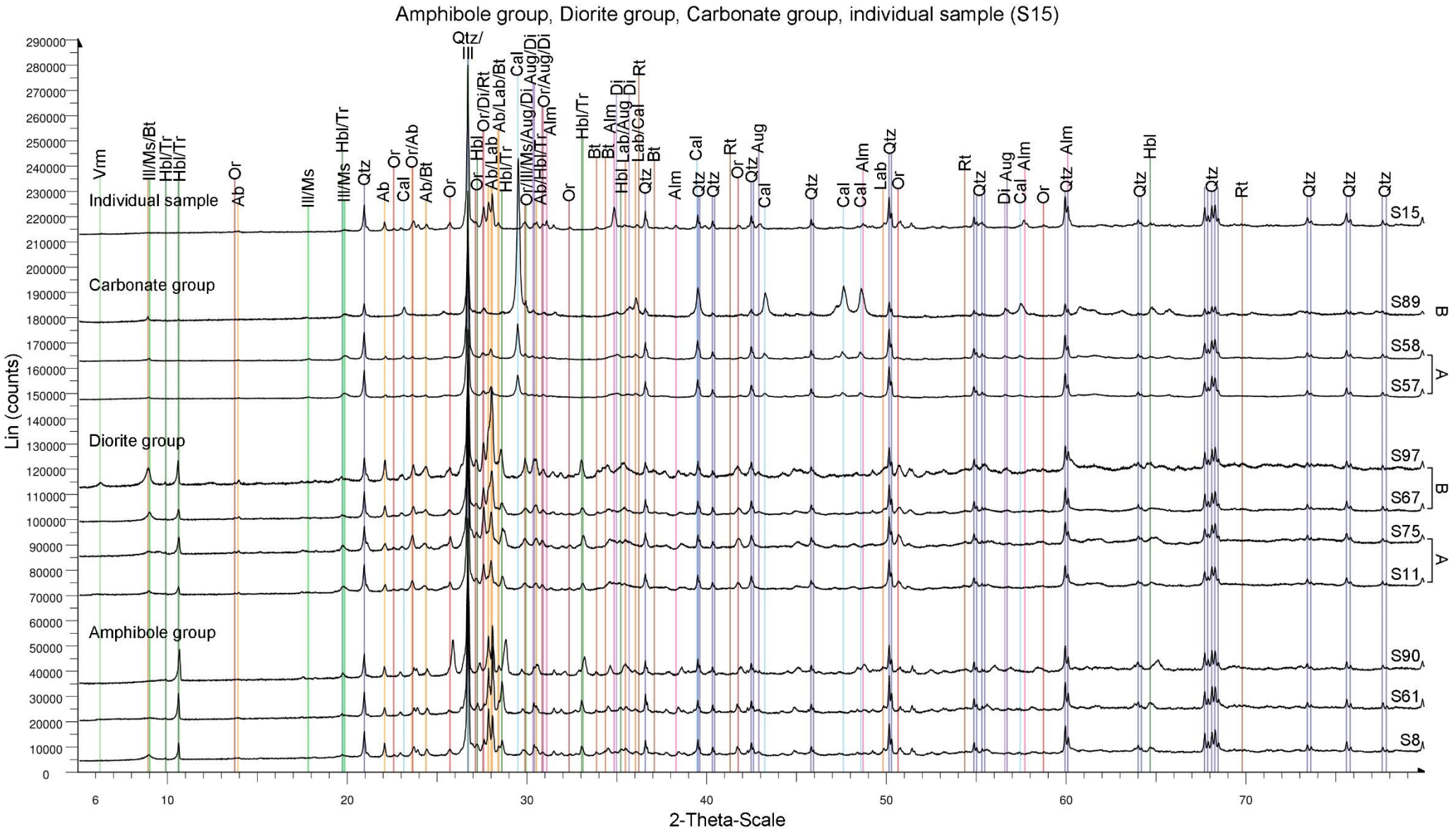


Figure 157. Diffractograms of the samples of the Amphibole, Diorite and Carbonate groups and the individual sample (data are normalised) with the indication of the most significant peaks of important phases. Abbreviations of phases as follows based on Siivola and Schmid 2007. Ab = albite, Alm = almandine, Aug = augite, Bt = biotite, Cal = calcite, Di = diopside, Hbl = hornblende, Ill = illite, Lab = labradorite, Ms = muscovite, Or = orthoclase, Qtz = quartz, Rt = rutile, Tr = tremolite, Vrm = vermiculite.

4.5.2 Graphite-containing ceramics

It is apparent from the XRD results that the diversity of the compositions in the Graphite group is much higher than in the graphite-free ceramics. There are only three phases, which can be found in all samples; these are quartz, graphite and orthoclase (*Table 23, Figure 158*). In addition, almost all samples contain albite and many samples contain rutile as well as illite/muscovite.

Table 23. Mineral phases in the Graphite group detected by XRD. Abbreviations as follows based on Siivola and Schmid 2007. Ab = albite, Alm = almandine, An = anorthite, Ann = annite, Ant = anatase, Bt = biotite, Grs = grossular, Hbl = hornblende, Hem = hematite, Ill = illite, Kln = kaolinite, Ms = muscovite, Or = orthoclase, Phl = phlogopite, Prp = pyrope, Rt = rutile, Sil = sillimanite, Tr = tremolite, Ttn = titanite, Vrm = vermiculite.

Subgroup	Sample	Quartz	Graphite	Potassium feldspar	Plagioclase	Clay mineral	Mica	Ti oxide	Other
Graphite A1	S102	✓	✓	Or	Ab	Ill		Rt	Sil
	S103	✓	✓	Or	Ab			Rt	Sil
	S110	✓	✓	Or		Ill/Ms		Rt	Sil
Graphite A2	S100	✓	✓	Or	Ab		Ms		
	S104	✓	✓	Or	Ab, An	Ill		Rt	
Graphite A3	S32	✓	✓	Or	Ab	Ill			Hbl(?), Alm
	S36	✓	✓	Or	Ab		Ms	Rt	Prp
	S86	✓	✓	Or	Ab	Ill/Ms			Alm
	S107	✓	✓	Or	Ab	Ill	Bt (Ann), Ms	Rt	Prp
Graphite A4	S31	✓	✓	Or	Ab				Sil
	S128	✓	✓	Or	Ab	Ill/Ms		Rt	
Graphite A5	S35	✓	✓	Or	Ab	Ill/Ms		Rt	
	S108	✓	✓	Or	Ab	Ill	Ms		
	S109	✓	✓	Or	Ab	Ill	Ms	Rt	Sil
Graphite B	S130	✓	✓	Or	Ab	Ill	Bt (Phl), Ms	Rt	
Graphite C1	S132	✓	✓	Or		Kln	Ms	Ant	$CaCO_3$
Graphite C2	S129	✓	✓	Or	Ab	Ill	Bt	Rt	$CaCO_3$
Graphite D	S13	✓	✓	Or	Ab	Vrm	Ms		Hbl/Tr, Ttn, Hem
	S54	✓	✓	Or	Ab		Ms	Rt	Grs

Subgroup ‘Graphite A’ consists of five smaller subgroups as demonstrated by petrographic analysis. The XRD results show that two of these are quite distinctive: the sillimanite gneiss-containing ‘Graphite A1’ and the garnet-rich ‘Graphite A3’ thanks to their sillimanite and garnet content, respectively. The compositions of the other three subgroups are relatively similar as the subgroups were based on structural considerations (‘Graphite A2’), or the distinguishing minerals are present in a small amount, which is invisible for the XRD (‘Graphite A4’), or they had relatively simple mineralogical composition with no special minerals (‘Graphite A5’). XRD revealed the presence of sillimanite in another two samples (S31, S109) than those of the sillimanite gneiss-containing ‘Graphite A1’.

One sample (S130) was analysed from the mica schist-containing subgroup ‘Graphite B’. This sample includes illite, muscovite, biotite (phlogopite), albite and rutile in addition to the above-mentioned three common phases present in all graphite-containing ceramics (quartz, graphite and orthoclase).

Subgroup ‘Graphite C’ is distinctive among the samples of the Graphite group because its samples contain calcium carbonate. Besides the three common phases, clay minerals, micas and titanium oxide were also detected in both samples. S132 of ‘Graphite C1’ includes kaolinite as clay mineral, muscovite as mica and anatase as titanium oxide. The diffractogram of S129 of ‘Graphite C2’ shows the presence of illite, biotite and rutile as well as albite. It is worth to note, that S132 is the only one among all the samples analysed by XRD where kaolinite was detected.

The samples of the low-graphite-containing ‘Graphite D’ include albite and muscovite in addition to the three common phases. Peaks of amphibole (hornblende or tremolite), titanite, hematite and vermiculite also appear in the diffractogram of S13. The other sample analysed from subgroup ‘Graphite D’ (S54) contains garnet (that is structurally consistent with grossular) and rutile.

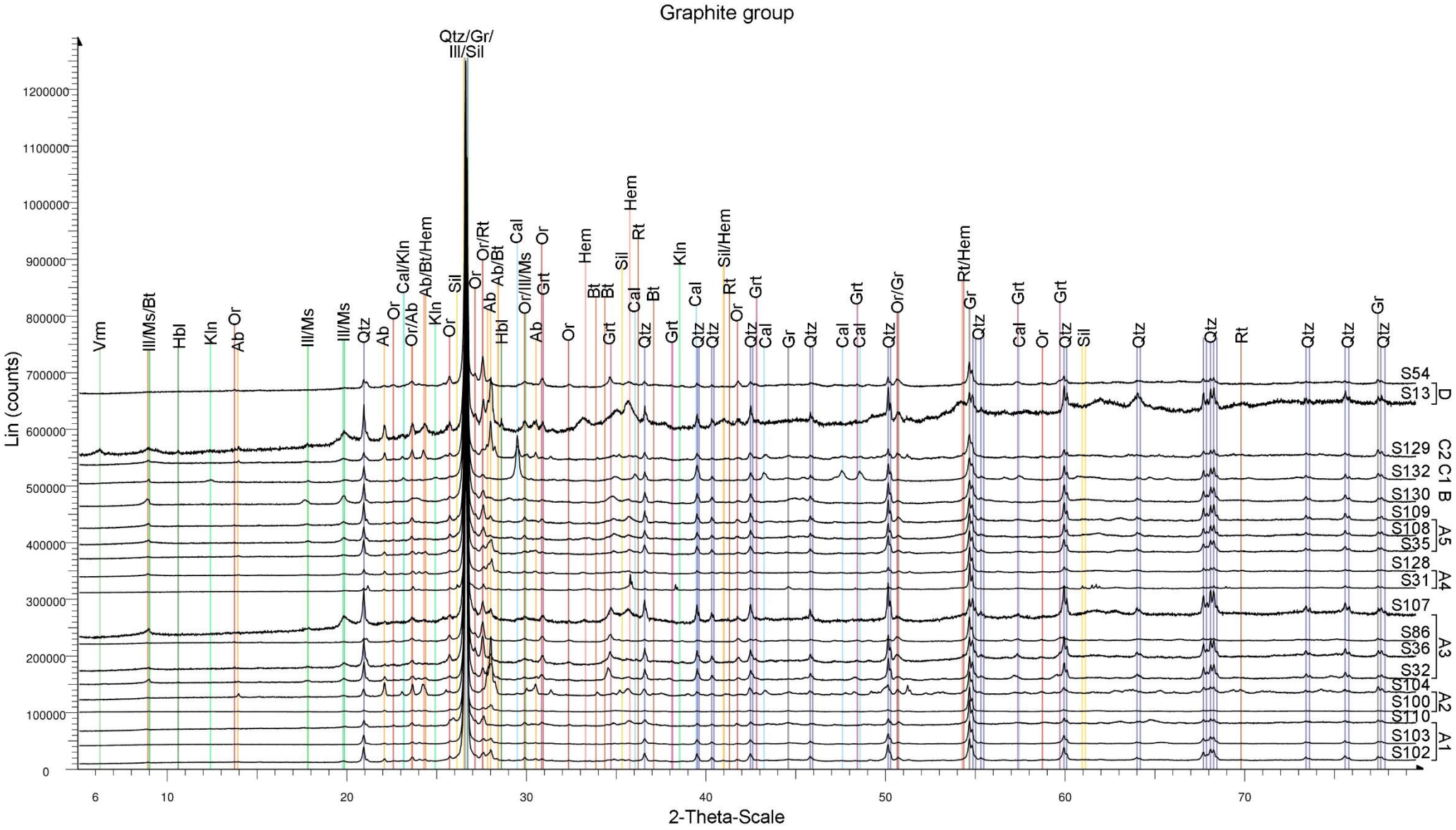


Figure 158. Diffractograms of the samples of the Graphite group (data are normalised) with the indication of the most significant peaks of important phases. Abbreviations of phases as follows based on Siivola and Schmid 2007. Ab = albite, Bt = biotite, Cal = calcite, Gr = graphite, Grt = garnet, Hbl = hornblende, Hem = hematite, Ill = illite, Kln = kaolinite, Ms = muscovite, Or = orthoclase, Qtz = quartz, Rt = rutile, Sil = sillimanite, Vrm = vermiculite.

4.5.3 Mineral phases and firing temperature

Besides phase identification and grouping, XRD is widely used in archaeological science to estimate firing temperatures (see Section 3.6.2). The samples (except S89) are of non-calcareous clays based on the SEM-EDS results, and it is known from the literature that non-calcareous clays usually exhibit fewer mineralogical changes occurred during firing than calcareous clays (Section 3.6.2).

However, some conclusions can be drawn about the firing temperature of the investigated samples based on the presence of certain mineral phases. Many samples contain illite (or muscovite) including the Granitoid and Carbonate groups, subgroup 'Diorite A', and probably the whole of the Graphite group, which suggest that the maximum firing temperature did not reach 800–950 °C during their firing (*Table 9*). Samples of the Carbonate group and subgroup 'Graphite C' might have a lower maximum temperature than this being at 700–900 °C because they also include calcite/calcium carbonate. S132 of 'Graphite C1' contains kaolinite, which may even lower the maximum firing temperature of this sample, around 500–600 °C based on the literature (*Table 9*).[70]

There is not enough information from XRD analysis to assign maximum firing temperatures to the Amphibole group, subgroup 'Diorite B' and the individual sample (S15).

Hematite and diopside as secondary phases are also used as a basis of temperature estimation, and although both are present in some samples from Lower Austria, these phases have a primary origin or their secondary formation is not proven, so they cannot be used for this purpose. No formation of mullite or other high temperature phases was detected in any of the samples, which would indicate high (> 900/1000 °C) firing temperatures.

4.5.4 Summary

XRD analysis provided further information about the mineralogy of the samples, which confirms and complements the petrographic results. All main petrographic groups and many of the petrographic subgroups can be distinguished based on their diffractograms. In many cases,

[70] This temperature range might seem a bit low to fire ceramics, but experiments show that it is possible to have 500–600 °C as maximum firing temperature at certain locations when firing in a bonfire (Thér et al. 2019, 1166: Table 4). At the same time, it is useful to keep in mind that post-depositional changes can also cause the crystallisation of clay minerals in the ceramics (Maritan 2020, 8–9).

XRD specifies the mineral identification of thin section analysis and reveals new phases difficult to identify in thin section petrography such as clay minerals and other phases with small grain size. However, it is also seen that the detection of phases present in low abundance and the detection of micas (especially biotite[71]) is not always possible with XRD analysis.

Results of the XRD analysis allow assigning maximum firing temperature ranges to the samples based on the presence of certain phases. They indicate that most of the samples were fired under 800–950 °C.

[71] Notable amounts of biotite were identified in the Amphibole and Graphite groups and in subgroup 'Diorite A' by thin section analysis, however, the diffractograms can confirm this only in few cases.

5 DISCUSSION

The different methods used for the analysis of the ceramics from the Erlauf Valley and Lower Austria resulted in valuable data, which help understand and characterise ceramic raw materials and different aspects of pottery production. This chapter starts with a general overview about the groups in the ceramic material under investigation and their chronological positions. Then, the data of the different analyses are interpreted in terms of raw material sources and the distribution of the ceramics is outlined. Next, the *chaîne opératoire* approach is used to analyse the various steps involved in ceramic production from raw material preparation to firing. This is followed by a section examining the organisational aspects of pottery production, which also includes suggestions about whether local, regional or supra-regional production is probable in the case of the studied ceramics. Technological choices in pottery making, continuity, change and innovation are assessed in the next subchapter and compared with political or social changes happening during the late Roman and early medieval periods. Finally, the vessels under investigation are compared to other ceramics from the wider region.

5.1 Ceramic groups and chronology

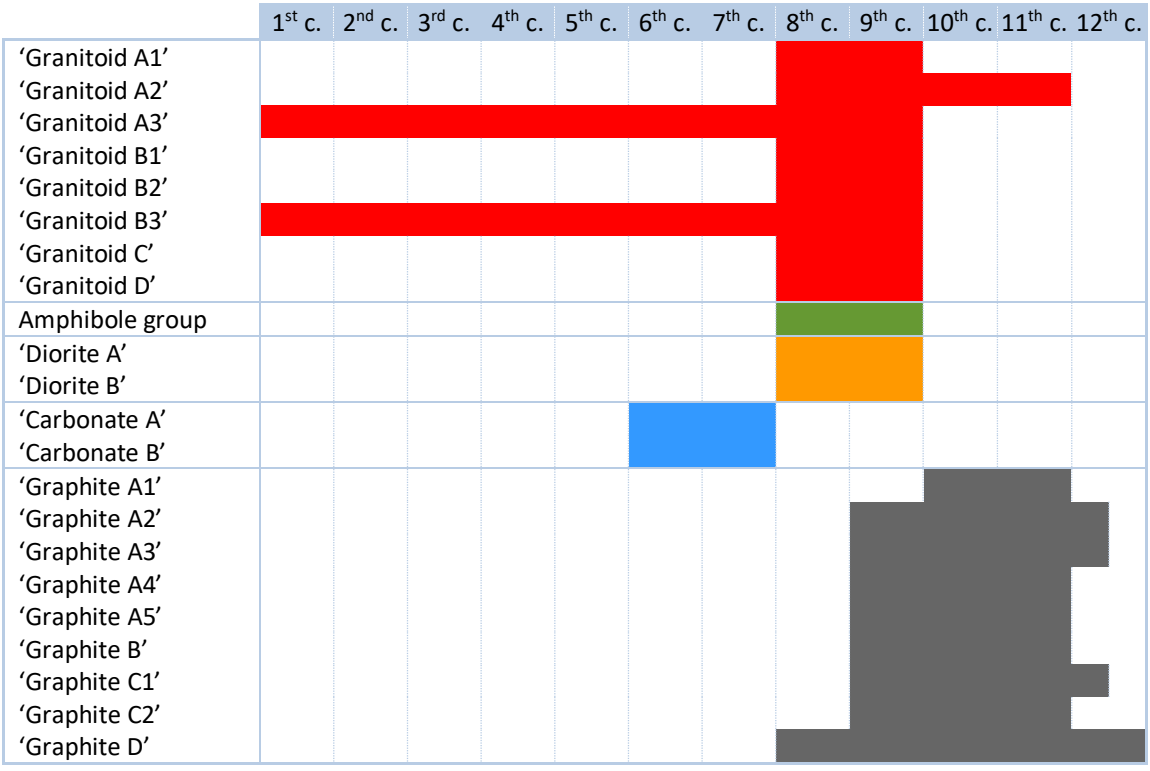
Two main types of pottery can be distinguished in the studied ceramic assemblage: graphite-free and graphite-containing ceramics. The distinction is clearly visible macroscopically as graphite-free sherds exhibit reddish-brownish shades (due to mixed, mainly oxidising firing atmosphere), while graphite-containing sherds have a dark greyish colour and shiny surface (due to reducing firing atmosphere and their graphite-content). Some graphite-containing ceramics that include a lower amount of graphite ('Graphite D') exhibit similar characteristics to graphite-free ware as they were fired in a mainly oxidising atmosphere and have a reddish-brownish colour. The two main types of pottery investigated in this thesis cover different periods: the graphite-free ware is dated to the 1st to 9th centuries AD and originates from the Erlauf Valley, while graphite-containing pottery is dated to the 9th to 12th centuries AD and originates from the Erlauf Valley and other parts of Lower Austria as well as Vienna.

Both macroscopic analysis and thin section analysis allowed the establishment of groups within the studied graphite-free and graphite-containing ceramics (Sections 4.1.1 and 4.2). The macroscopic and microscopic groups, however, overlap only partly. Macroscopic analysis of the samples resulted in a rough grouping, which was modified by thin section petrography. The

other methods used for the analysis of the samples from Lower Austria (SEM, ICP-OES and XRD) confirmed the results of the petrographic grouping. Therefore, petrographic groups will be the basis of interpretation throughout the whole discussion chapter.

The following chronological overview of the different petrographic groups and subgroups dated between the 1st to the 12th centuries AD is summarised by *Table 24*, and a more detailed summary is given by *Table 25* including site names and sample numbers as well. The samples were dated based on their macroscopic characteristics in the case of sherds from surface collection and based on their archaeological contexts in the case of ceramics from excavations (Section 3.1).

Table 24. An overview of the chronology of the petrographic groups and subgroups



The Granitoid group is the largest group in the investigated ceramic material and appears from the Roman/late Roman period (1st–5th centuries) to the 8th–9th centuries at several sites in the Erlauf Valley (three sherds might be dated up to the 11th century). Some of its samples can be placed chronologically to the Roman/late Roman period, and these samples all belong to the inclusion-poor (< 20%) subgroups 'Granitoid A3' and 'Granitoid B3'. The majority of the Granitoid samples originate from the 8th–9th centuries, including all samples from subgroups 'Granitoid A1', 'Granitoid B1', 'Granitoid B2', 'Granitoid C' and 'Granitoid D' and most samples from 'Granitoid A2'. Three samples of 'Granitoid A2' (S39, S50, S52) containing distinctive

amount of graphite (5–15%) compared to the other samples of this subgroup (containing < 2% of graphite/opaque mineral) may originate from a slightly later period (9th–11th centuries).

Samples of the Amphibole group can be dated to the 8th–9th centuries. Those of the Diorite group also originate from the 8th–9th centuries. The Carbonate group is slightly earlier and is dated to the 6th–7th centuries.

The graphite-containing ceramics (Graphite group) are dated from the 9th century onwards. The samples of the sillimanite gneiss-bearing 'Graphite A1' originate from the 10th–11th centuries. The other four subgroups of 'Graphite A' can be positioned chronologically within a longer period between the 9th and 11th/mid-12th centuries. The dating of the mica schist-containing two samples of 'Graphite B' falls between the 9th and 11th centuries. Those graphite-containing samples which also include carbonate rock fragments ('Graphite C') originate from the 9th–11th/mid-12th centuries. Within the low graphite-containing ceramics of 'Graphite D', one of the five samples (S13) originates from the 8th/9th centuries, two samples (S49 and S62) are dated to the 9th–11th centuries, and there are two samples (S53 and S54) which might be slightly 'younger' (10th–12th centuries) based on their macroscopic appearance (reddish surface; Felgenhauer-Schmiedt 1998, 203).

The overview of the dating and petrographic groups of the samples presented above shows that four chronological groups can be differentiated within the investigated ceramic material. These groups cover the periods between the 1st–5th, 6th–7th, 8th–9th and the 9th–12th centuries and are used in the following subchapters to enhance the clarity of interpretation and ease the comparison between raw material sources, technologies and other topics discussed below. Concerning the two main ceramic types, graphite-free ceramics can be connected to the first three periods (1st–9th centuries), while graphite-containing ceramics originate from the end of the chronological spectrum of the studied pottery assemblage (9th–12th centuries).

The first period (1st–5th centuries) includes 11 pieces of ceramics, which belong to the petrographic subgroups 'Granitoid A3' and 'Granitoid B3', and one individual sample (S48) is also dated to this period. There are three samples (S38, S46 and S51), which cannot be dated more precisely than the 1st–9th centuries based on their macroscopic features (*Table 25*). From their microscopic characteristics (small amount of granitoid inclusions in a relatively pure matrix, see Section 4.2.1), they clearly belong to 'Granitoid A3' and 'Granitoid B3', and as the rest of the samples in these subgroups are dated between the 1st and 5th centuries (1st–6th

centuries in the case of S47), this suggests a dating to the Roman/late Roman period for the above-mentioned three samples as well.

From the 6th–7th centuries, only four samples were examined (S57, S58, S59 and S89), all of which are the members of the Carbonate group.

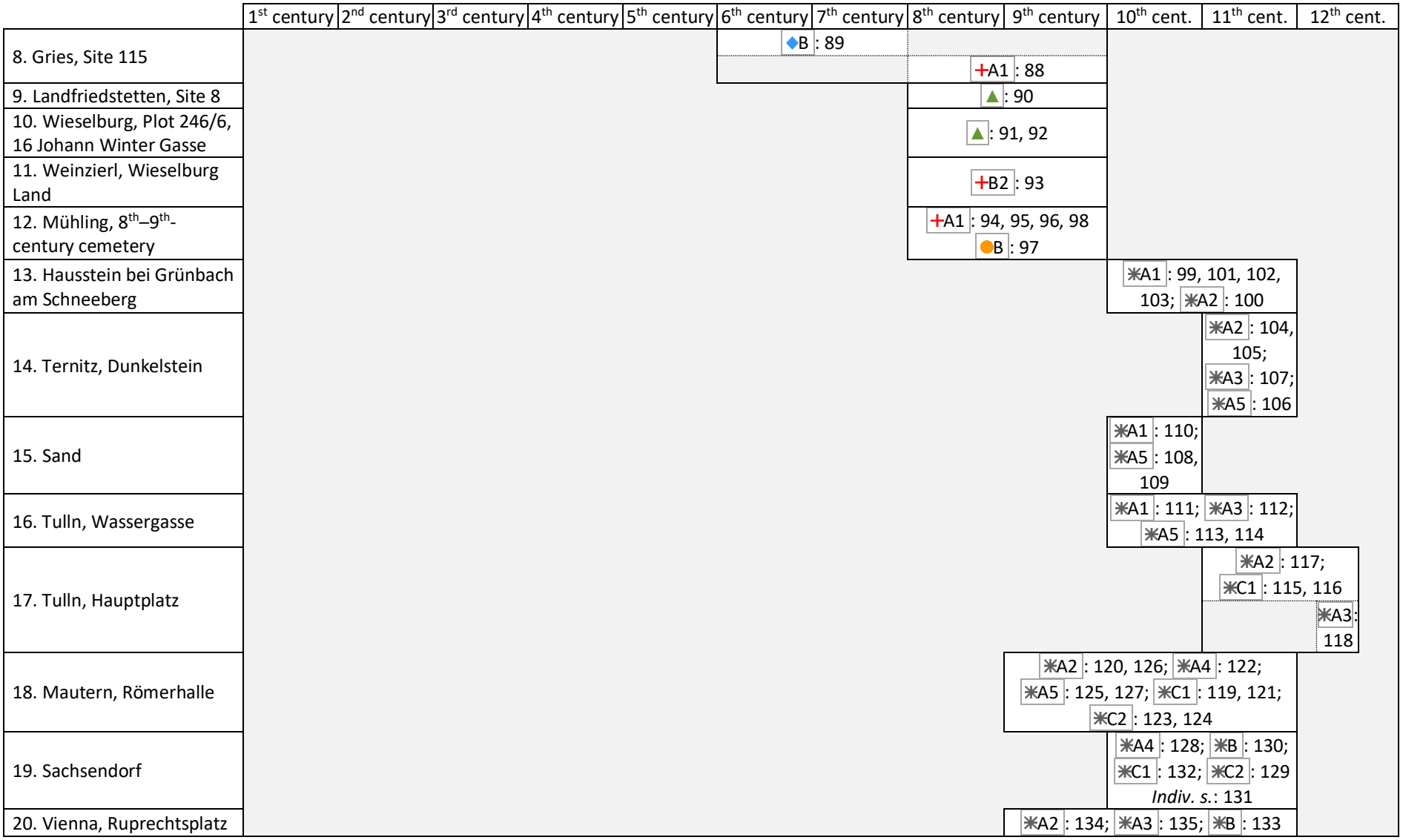
The bulk of the investigated ceramic material is dated to the 8th–9th centuries and the 9th–12th centuries. Ceramics from the 8th–9th centuries include 69 graphite-free samples from the Erlauf Valley belonging to the Granitoid group (subgroups 'Granitoid A1', 'Granitoid A2', 'Granitoid B1', 'Granitoid B2', 'Granitoid C' and 'Granitoid D'), Amphibole group and Diorite group as well as three individual samples (S15, S17 and S23).

The last chronological group (9th–12th centuries) includes all graphite-containing ceramics (Graphite group, 51 samples[72]) originating from the Erlauf Valley and from other parts of Lower Austria as well as from Vienna.

[72] These 51 samples include the following: 50 samples termed as graphite-containing by macroscopic and thin section analysis and S131. S131 is identified as an individual sample containing a very small amount of graphite based on ceramic petrography (Appendix C). Macroscopic analysis, however, shows that the proportion of graphite in the potsherd is much higher than it is observed in its thin section and the sample in fact belongs to the graphite-containing samples.

Table 25. Table summarising the site, dating and petrographic group of the samples. Subgroups are indicated with the symbol of the main petrographic group (Figure 92) and the group code of the subgroup; e.g. +A1 *= 'Granitoid A1',* ◆B *= 'Carbonate B'. Individual samples are abbreviated as 'Indiv. s.'*

	1st century	2nd century	3rd century	4th century	5th century	6th century	7th century	8th century	9th century	10th cent.	11th cent.	12th cent.
1. Purgstall, 8th–9th-century cemetery								+A1: 3, 4, 6, 10, 18, 19, 25, 30; +B1: 12, 20; +B2: 7, 9, 14, 26; +C: 1, 22; +D: 5, 21; ▲: 2, 8, 28, 29; ●A: 11, 16, 24, 27; ✳D: 13; *Indiv. s.*: 15, 17, 23				
2. Wieselburg, Kirchenberg										✳A3: 32, 34, 36; ✳A4: 31; ✳A5: 33, 35		
3. Purgstall, Site 10												
		+A3: 37, 40, 41, 42, 43; +B3: 45										
			+B3: 47									
			Indiv. s.: 48									
					+A3: 38; +B3: 46							
								+A1: 44				
									+A2: 39, 50			
									✳D: 49			
4. Purgstall, Site 26												
					+A3: 51							
									+A2: 52			
										✳D: 53, 54		
5. Purgstall, Site 47												
						◆A: 57, 58; ◆B: 59						
								▲: 55, 56, 60, 61				
6. Zehnbach, Site 16												
								▲: 63				
									✳D: 62			
7. Hochrieß, site 39												
								+A1: 64, 70, 71, 73, 74, 76, 77; +A2: 65, 66, 68, 69, 72, 78, 79, 81; +B1: 80, 82, 83; +C: 87; ●A: 75; ●B: 67				
										✳A3: 84, 85, 86		


1st century
2nd century
3rd century
4th century
5th century
6th century
7th century
8th century
9th century
10th cent.
11th cent.
12th cent.
8. Gries, Site 115
B : 89
A1 : 88
9. Landfriedstetten, Site 8
: 90
10. Wieselburg, Plot 246/6, 16 Johann Winter Gasse
: 91, 92
11. Weinzierl, Wieselburg Land
B2 : 93
12. Mühling, 8th–9th-century cemetery
A1 : 94, 95, 96, 98
B : 97
13. Hausstein bei Grünbach am Schneeberg
A1 : 99, 101, 102, 103; A2 : 100
14. Ternitz, Dunkelstein
A2 : 104, 105; A3 : 107; A5 : 106
15. Sand
A1 : 110; A5 : 108, 109
16. Tulln, Wassergasse
A1 : 111; A3 : 112; A5 : 113, 114
17. Tulln, Hauptplatz
A2 : 117; C1 : 115, 116
A3 : 118
18. Mautern, Römerhalle
A2 : 120, 126; A4 : 122; A5 : 125, 127; C1 : 119, 121; C2 : 123, 124
19. Sachsendorf
A4 : 128; B : 130; C1 : 132; C2 : 129
Indiv. s.: 131
20. Vienna, Ruprechtsplatz
A2 : 134; A3 : 135; B : 133

5.2 Provenance of the ceramics

One of the main questions of pottery research is where the ceramics under investigation originate from geologically. In addition to the identification of potential raw materials used for ceramic making, further interpretations such the separation of local or imported goods and theories about the locations of unknown production sites can be made based on geological information. In this section, an attempt is made to identify possible sources of the inclusions present in the ceramics based on the mineralogical data provided by thin section petrography, SEM and XRD and the literature detailing the geology of Lower Austria.

Ceramics from the 1st to 5th centuries

Similarly to the rest of the Granitoid group, the two 1st–5th-century subgroups, 'Granitoid A3' and 'Granitoid B3', contain fragments and minerals of granitoid rocks (Section 4.2.1). The closest occurrence of granitoid rocks is in the Bohemian Massif north of the Erlauf Valley with some outcrops south of the Danube.

Based on the ratio of the two feldspar types, potassium feldspar and plagioclase, the rock-fragments of the Granitoid group are consistent with granites.[73] The Weinsberg Granite comprising of potassium feldspar (microcline), plagioclase (oligoclase-andesine), quartz and biotite (Matura 2006c, 33) seems to be a good match to the inclusions seen in the thin sections of the Granitoid group. The potassium feldspar of the Weinsberg Granite is typically coarse-grained with grain-sizes up to 10 cm (Matura 2006c, 33). Many thin sections also contain relatively large potassium feldspar grains up to few mm sizes. Based on the cloudy appearance (initial alteration) of the feldspar grains, the inclusions were probably derived from weathered rocks.

The largest occurrence of the Weinsberg Granite is *c.* 15 km west/northwest of the Erlauf Valley as shown in *Figure 159* (No. 1). It has a smaller outcrop in the north-eastern part of the Valley near Zelking.

[73] No lineation or gneiss structure in the rock fragments can be observed in any of the Granitoid group samples under microscope. It must be noted, however, that the recognition of any kinds of lineation is rarely possible at this level of magnification, as it is normally identified macroscopically. Therefore, the option of the granitoid inclusions being gneiss fragments in the samples cannot be ruled out entirely.

The mineralogical composition of S48, the individual sample belonging to this chronological group, is consistent with that of the samples of the Granitoid group (Section 4.2.1). It is the vitreous matrix, which makes S48 an individual sample and which is probably the result of secondary burning. The minerals (quartz, feldspar, biotite and zircon) and rock fragments show typical granitoid composition and may be originated from the Weinsberg Granite similarly to subgroups 'Granitoid A3' and 'Granitoid B3' (*Figure 159*: 1).

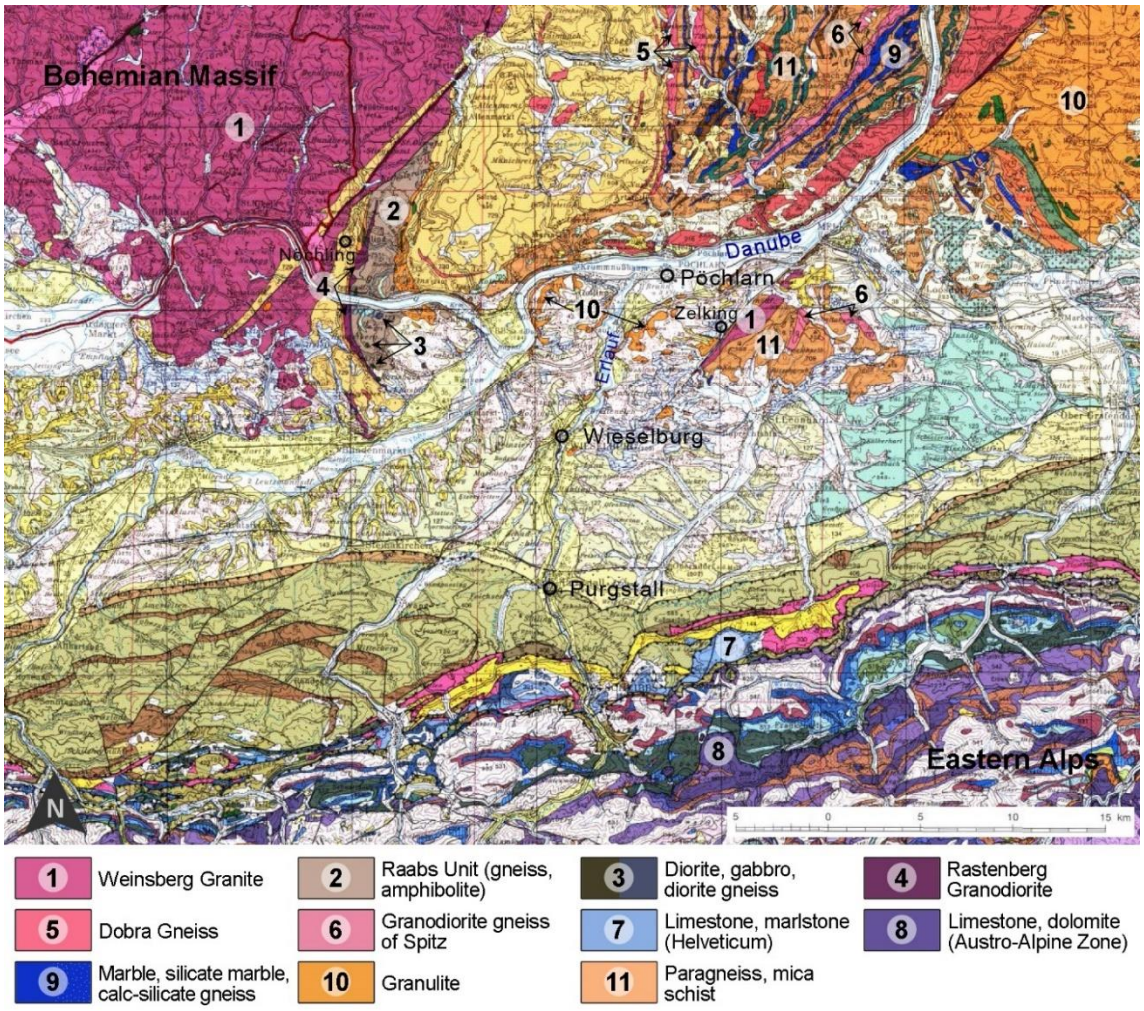


Figure 159. Geological map of the Erlauf Valley and its vicinity with potential sources of the inclusions of graphite-free ceramic samples (modified detail of the geological map compiled by the Geologische Bundesanstalt (2002))

Ceramics from the 6th to 7th centuries

The samples of the Carbonate group include rock fragments consisting primarily of calcite and accessory minerals such as diopside, muscovite, graphite/opaque mineral, biotite and tremolite (Section 4.2.1).

The largest occurrence of carbonate rocks in the vicinity of the Erlauf Valley is in the Eastern Alps. Limestone is a common rock type here present in the Helveticum (Grestein Klippen Zone) and in the Austro-Alpine Zone, just to name the closest locations (within 10 km) to the Valley (*Figure 159*: 7, 8).

However, there are also carbonate rocks in the Bohemian Massif: the Drosendorf Unit consisting mainly of paragneiss and mica schist includes several other rock types such as medium to coarse grained marble, which may extend over several kilometres (*Figure 159*: 9). In addition to calcite, graphite, quartz, feldspar, diopside, tremolite and biotite (phlogopite) are commonly present in the marble of the Drosendorf Unit (Matura 2006c, 30).

The rock fragments of the Carbonate group could have an origin in both the Eastern Alps and the Bohemian Massif. However, the presence of diopside, biotite, tremolite and at least one graphite flake in a rock fragment in S58[74] suggest the marble of the Drosendorf Unit as the source.

Ceramics from the 8th to 9th centuries

Granitoid subgroups: 'Granitoid A1', 'Granitoid A2', 'Granitoid B1', 'Granitoid B2', 'Granitoid C' and 'Granitoid D'

The subgroups of the Granitoid group are essentially the same in terms of composition with varying proportion of the main minerals (feldspar, quartz, biotite, muscovite; Section 4.2.1). Therefore, it is likely that all members of the Granitoid group point at the same source and the differences in proportion are the result of the natural variability of the raw material or the result of sampling (thin section making). This source might again have been the Weinsberg granite (*Figure 159*: 1) as explained above in the case of the two 'early' Granitoid subgroups ('Granitoid A3' and 'Granitoid B3'). The cloudy appearance and alteration of feldspars suggest that the inclusions of the Granitoid subgroups were exposed to weathering.

Amphibole group

The samples of the Amphibole group include granitoid fragments and abundant amphibole crystals sometimes occurring in the granitoid fragments as well (Section 4.2.1). These granitoid

[74] S58 and S59 contain several grains of graphite/opaque mineral and there is one grain with calcite and diopside in S58, which has a clear 'flake' shape and therefore it was identified as graphite.

fragments are probably gneiss fragments, but it is also possible that some of the amphibole grains originate from weathered amphibolite.[75] The initial alteration of feldspars suggest that the rock fragments and minerals came from weathered surface deposits. Two samples, S91 and S92, have an important role in identifying the potential origin of the inclusions, since diorite fragments are also present in these samples in addition to gneiss fragments.

There is one location in the vicinity of the Erlauf Valley where granitoid gneiss, amphibolite and diorite occur together. This is a relatively small area in the Bohemian Massif west to the mouth of the Rivel Erlauf, east of Nöchling (*Figure 159*: 2). Here a part of the Raabs Unit is exposed consisting of a mixture of hornblende-biotite-plagioclase gneiss and amphibolite (Matura 2006c, 31). This unit also includes lenses of diorite, diorite gneiss and gabbro (*Figure 159*: 3). Another rock type borders the western edge of the Raabs Unit, the Rastenberg Granodiorite, which includes rock bodies of monzonitic to dioritic composition (*Figure 159*: 4; Matura 2006c, 33).[76]

There are two other possible raw material sources for the Amphibole group in the Bohemian Massif. These are the Dobra Gneiss, which is a gneiss with granitic to granodioritic composition and with layers of amphibolite, and the granodiorite gneiss of Spitz, which includes lenticular bodies of amphibolite (*Figure 159*: 5, 6; Matura 2006c, 30). However, since a close association of granitoid gneiss, amphibolite and diorite is suggested by S91 and S92, and diorite is not recorded in the vicinity of the Dobra gneiss and Spitz gneiss, the above-mentioned Raabs Unit and Rastenberg Granodiorite near Nöchling seem more likely to be the raw material sources of the Amphibole group.

Diorite group

Both subgroups of the Diorite group contain diorite fragments with zoned feldspars. The main difference between the rock fragments of the two subgroups is represented by the presence of colourless amphibole aggregates (‘Diorite A’) and augite (‘Diorite B’) as part of the diorite fragments (Section 4.2.1).

The origin of the diorite fragments is possibly in the outcrops of the Raabs Unit and the Rastenberg Granodiorite near Nöchling (*Figure 159*: 4). As mentioned above, both the Raabs

[75] Rudolf Dell’mour, personal communication (by email), October 2019.
[76] The Raabs Unit and the Rastenberg Granodiorite were named after their more extensive occurrences in the northern part of Lower Austria near Raabs and Rastenberg, respectively.

Unit and the Rastenberg Granodiorite contain blocks of diorite, which can locally reach dimensions up to kilometre size in the case of the Rastenberg Granodiorite (Matura 2006c, 33). The samples of the two subgroups might be made of raw materials from different parts (possibly different lenses of diorite) of the same source.

Individual samples

S15 contains abundant quartz grains, rock fragments with granitoid composition (quartz, feldspar, plagioclase, garnet, rutile, muscovite/sillimanite, biotite and graphite/opaque mineral) and some grains of kyanite (Section 4.2.1). The association of quartz, feldspar, garnet, rutile and kyanite is present in the Erlauf Valley near Pöchlarn as granulite[77] of the Bohemian Massif (*Figure 159*: 10; Matura 2006c, 32–33). However, the identification of the rock fragments as granulite is uncertain because of the presence of muscovite – unless muscovite has secondary origin (e.g. kyanite altered to muscovite). In any case, it is probable that the source of the inclusions of S15 is somewhere in the Bohemian Massif as also suggested by the chemical similarity of this sample to the above-mentioned groups (particularly the Granitoid and Amphibole groups) based on the ICP-OES results (Section 4.4).

The composition of S17 is consistent with the composition of the quartz-rich subgroup 'Granitoid B' except for the presence of few calcite grains (Section 4.2.1).[78] The granitoid fragments are probably from the Weinsberg Granite as explained above (*Figure 159*: 1). The calcite possibly originates from a different source than the granitoid fragments. It might have a similar origin to the rock fragments of the Carbonate group, in the Drosendorf Unit of the Bohemian Massif (*Figure 159*: 9).

The non-plastic components of S23, including a very large amount of biotite, some grains of feldspar and quartz and a few grains of hornblende, can derive from multiple locations of the Bohemian Massif (Section 4.2.1). The Dobra Gneiss, for example, is a close match to the samples' composition as it includes layers of biotite-hornblende schist and biotite schist (*Figure 159*: 5; Matura 2006c, 30). Also, there are mixed gneisses and mica schists belonging to the Drosendorf Unit and the Gföhl Unit east of the Dobra gneiss, comprising mainly of biotite,

[77] E.g. Lasselsberger quarry (Melk District): https://www.mindat.org/loc-306014.html, accessed on 24/11/2020.
[78] These grains, referred as calcite/dolomite in Section 4.2.1, were identified as calcite by SEM-EDS.

plagioclase and quartz; in addition, garnet and sillimanite can also be present (*Figure 159*: 11; Matura 2006c, 30).

Ceramics from the 9th to 12th centuries

The grain-size of the graphite and the accompanying rock fragments in the thin sections of the Graphite group help narrowing down its place of origin. There are two main groups of graphite sources in Lower Austria, the Drosendorf Unit in the Bohemian Massif and the Veitsch Nappe in the Eastern Alps (Section 2.3.4). The graphite of the Bohemian Massif is coarse-grained occurring with various high-grade metamorphic rocks, while that of the Eastern Alps is fine-grained occurring with phyllites and quartzites. All investigated ceramic samples contain coarse-grained graphite in the form of flakes and nodules, which, together with their associated rock fragments, suggest the Drosendorf Unit as the source of graphite.

The upper part of the Drosendorf Unit, referred to as the Variegated Group, comprises several rock types that are host rocks of the graphite including paragneiss, quartzite, amphibolite and calc-silicate-marble (Weber and Götzinger 1997; Heinrich 2006, 298: Tabelle 22). The graphite occurring in paragneiss or marble may accumulate into graphite schist in places (Matura 2006c, 30).

Most of the graphite-containing samples include graphite gneiss fragments; these samples make up subgroup 'Graphite A'. Besides the gneiss fragments (consisting usually of graphite, quartz, feldspar, biotite, muscovite and rutile), the samples may also contain a significant amount of (green, colourless or brown) amphibole, scapolite, rutile, sillimanite, garnet, kyanite and pyroxene (Section 4.2.2). This composition is similar to that of the paragneiss of the Drosendorf Unit (*Figure 160*: 1), which is mainly of biotite, plagioclase and quartz accompanied by garnet and sillimanite as accessory minerals (Matura 2006c, 30). Gneisses of the Drosendorf Unit may be enriched in graphite, and these graphite gneisses include graphite, feldspar and quartz, may include kyanite, mica (phengite) as well as tourmaline, rutile, apatite and calcite as accessories (Schrauder et al. 1993, 178). The inclusions of different subgroups named after the presence of certain minerals ('Graphite A1', 'Graphite A3', 'Graphite A4') may be from sillimanite[79], garnet[80] and kyanite-rich[81] areas of the Drosendorf Unit.

[79] E.g. near Bengelbach (Krems-Land District): https://www.mindat.org/loc-251839.html, Paudorf (Krems-Land District): https://www.mindat.org/loc-73298.html, Hafnerbach (Sankt Pölten-Land District):

The two samples of subgroup 'Graphite B' contain graphitic mica schist fragments, which are built up mainly of graphite, mica (biotite, muscovite) and quartz, and feldspar and rutile grains are also present in the matrix (Section 4.2.2). In addition to paragneiss, mica schist is another common rock type of the Drosendorf Unit (*Figure 160*: 1; Matura 2006c, 30), which might be the source of the graphitic mica schist fragments in subgroup 'Graphite B'.

The samples of subgroup 'Graphite C' include carbonate rock fragments. The rock fragments of 'Graphite C1' contain coarse-grained calcite crystals, feldspar, quartz, mica, scapolite and epidote/zoisite/clinozoisite (Section 4.2.2). Garnet can also occur in the matrix (S119, S121) as accessory mineral. The rock fragments can be identified as graphite marble and can probably be connected to the Drosendorf Unit. The marble of this Unit is medium to coarse grained and contains graphite, calcite, quartz, feldspar, diopside, tremolite, biotite (phlogopite), and sometimes scapolite, zoisite and chlorite (Schrauder et al. 1993, 178; Matura 2006c, 30). It forms elongated zones within the Drosendorf Unit often extending over several kilometres (*Figure 160*: 2).[82]

As for the other subgroup of 'Graphite C' ('Graphite C2'), which contains graphite gneiss (graphite, quartz, feldspar, biotite, occasionally rutile and scapolite) and rock fragments built up of microcrystalline calcite (micrite; Section 4.2.2), the location of the raw material source is not obvious. It might be identified in the Drosendorf Unit, which is also rich in fine to coarse-grained calc-silicate gneiss consisting mainly of calcite, quartz, feldspar, diopside, garnet, sometimes hornblende, scapolite, zoisite and chlorite (*Figure 160*: 3; Schrauder et al. 1993, 178; Matura 2006c, 30). It is possible that the inclusions of 'Graphite C2' originate from a border area where graphite gneiss and carbonate rocks meet.

---

https://www.mindat.org/loc-246288.html, Drosendorf (Horn District): https://www.mindat.org/loc-257190.html; accessed on 30/11/2020

[80] E.g. in the Krems-Land District, near Bengelbach: https://www.mindat.org/loc-251839.html, Spitz: https://www.mindat.org/loc-231264.html, Paudorf: https://www.mindat.org/loc-73298.html; accessed on 30/11/2020

[81] E.g. in the Horn District, near Röhrenbach: https://www.mindat.org/loc-246291.html, Irnfritz-Messern: https://www.mindat.org/loc-257662.html, Wollmersdorf: https://www.mindat.org/loc-57613.html; accessed on 30/11/2020

[82] Marble quarries (active or abandoned) can be found e.g. at Amstall (Krems-Land District): https://www.mindat.org/loc-221394.html, Loja (Melk District): https://www.mindat.org/loc-57110.html, Kochholz (Melk District): https://www.mindat.org/loc-155680.html, Häusling (Melk District): https://www.mindat.org/loc-303771.html; accessed on 30/11/2020

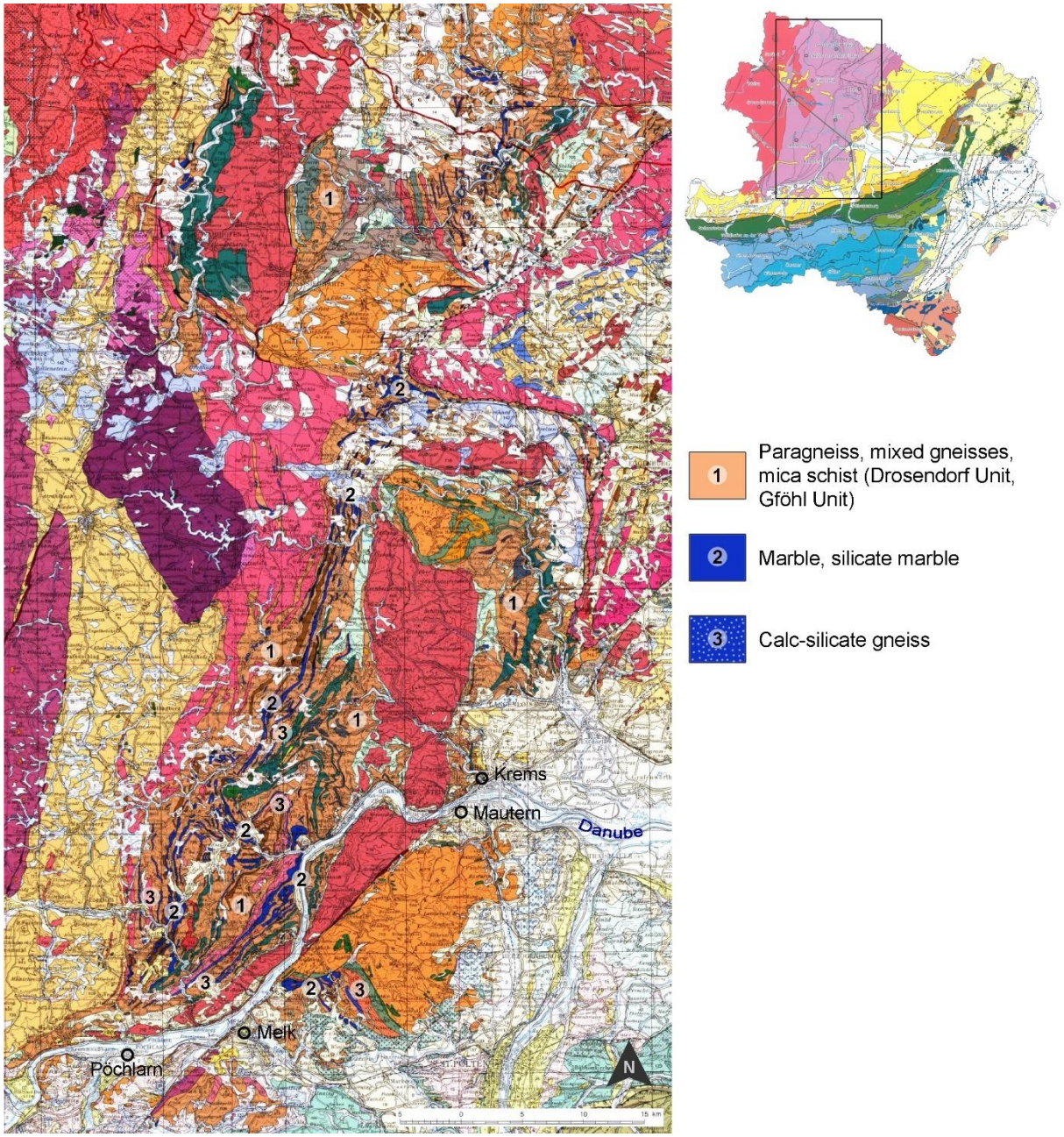


Figure 160. Potential sources of the inclusions of graphite-containing ceramic samples in the Bohemian Massif (modified detail of the geological map compiled by the Geologische Bundesanstalt (2002))

The fourth subgroup of the graphite-containing ceramics ('Graphite D') differs from the others because it contains less graphite (Section 4.2.2). Nevertheless, similarly to 'Graphite A', these samples also include graphite gneiss and minerals such as rutile and garnet, which could have an origin in the Drosendorf Unit as explained above (*Figure 160*: 1). Other rock fragments can also be found in samples of subgroup 'Graphite D' such as chert and argillaceous rocks. The identification of the provenance of these fragments is uncertain.

Finally, there is one distinctive graphite-containing sample, which does not belong to any of the groups.[83] S131 contains fragments of kyanite-rich mica schist, which include quartz, muscovite, biotite, kyanite, graphite, potassium feldspar and rutile. In addition, plagioclase and scapolite are also present in the matrix (Section 4.2.1). The inclusions may have an origin in the mica schist of the Drosendorf Unit (*Figure 160*: 1), which is enriched in kyanite locally such as near Plank am Kamp or Stockern.[84]

Clay deposits

The analytical techniques revealed that the analysed samples were made of non-calcareous (except S89) and mostly illite-rich clay (Sections 4.3.2, 4.5.1 and 4.5.2). The origin of the clay, however, can hardly be identified with certainty without analysing raw clays and comparing the results to the samples' composition.

Nevertheless, there are some petrographic groups where it is likely that the clay and the inclusions are from the same source. In these cases, an inclusion-rich clay, a 'ready mix' was used without adding temper to the paste. There are several places in the Bohemian Massif where residual clay deposits are exposed originating from weathering rocks of the Massif (Dell'mour 2001, 93–99; Heinrich 2006, 274, 296). Such material is recognisable in the Granitoid and Amphibole groups based on the weathered state of feldspars and the angularity of the grains, which latter suggests *in situ* weathering of the clay (primary/residual clay) in contrast to long transportation (secondary/sedimentary clay), which would result in rounded grains (Quinn 2013, 120–122).

For the other petrographic groups, however, it is not clear whether the clay and the inclusions have the same origin. In the case of those ceramics, which show the characteristics of tempering (see Section 5.4.1), separate raw material sources for the clay and the temper are likely. It is possible that the clay used for making these vessels was obtained locally, as the Erlauf Valley and its vicinity are rich in potential clay sources (including deposits at Klein-Pöchlarn, Krummnußbaum, Wieselburg and at several locations west of the Erlauf and in the Bohemian Massif) and clayey soils are also very frequent (Section 2.3.3).

[83] See footnote 72 on page 252.
[84] Plank am Kamp (Krems-Land District): https://www.mindat.org/loc-155486.html, Stockern (Horn District): https://www.mindat.org/loc-57502.html; accessed on 30/11/2020

As for the graphite-containing ceramics, the clay could have been obtained from around the Bohemian Massif, where graphite-containing residual clays are frequent (Scharrer-Liška 2007, 15), or from other parts of Lower Austria rich in clay deposits (Section 2.3.3).

Summary

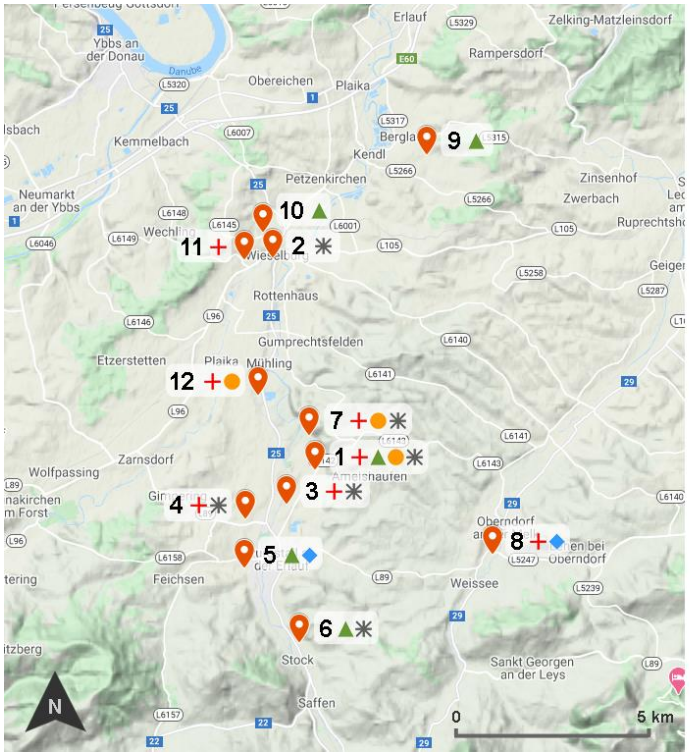
Interestingly, all samples point to the Bohemian Massif as the potential place of origin of the inclusions regardless of their petrographic groups or dating. (In the case of the Carbonate group, the inclusions could also originate from the Eastern Alps.) Different rock types of the Bohemian Massif can be recognised in the different petrographic groups: it is likely that the inclusions are derived from the Weinsberg Granite in the Granitoid group, from the Raabs Unit in the Amphibole group, from the Raabs Unit and the Rastenberg Granodiorite in the Diorite group and from the Drosendorf Unit in the Carbonate and Graphite groups. It has to be kept in mind, however, that these identifications are based on geological data (maps and literature) and the analysis of raw materials would be beneficial to confirm these suggestions.

5.3 Distribution of the ceramics

The pottery sherds investigated in this thesis originate from 20 archaeological sites. Graphite-free ceramics were collected from sites in the Erlauf Valley, while graphite-containing ceramics were found in the Valley, other Lower Austrian sites and Vienna (*Table 25)*.

Ceramics from the 1st to 5th centuries

Six of the seven samples of 'Granitoid A3' originate from Purgstall, Site 10, located east of the Erlauf, and one sample (S51) from Purgstall, Site 26, located west of the River. The three sherds of 'Granitoid B3' and individual sample S48 were also found at Purgstall, Site 10. The distribution of the Roman/late Roman ceramics studied in this thesis thus can be connected to the southern part of the Valley and to both banks of the Erlauf (*Figure 161*).



1. Purgstall, 8th–9th-century cemetery
   +A1, +B1, +B2, +C, +D, ▲, ●A, ✳D
2. Wieselburg, Kirchenberg
   ✳A3, ✳A4, ✳A5
3. Purgstall, site 10
   +A1, +A2, +A3, +B3, ✳D
4. Purgstall, site 26
   +A2, +A3, ✳D
5. Purgstall, site 47
   ◆A, ◆B, ▲
6. Zehnbach, site 16
   ▲, ✳D
7. Hochrieß, site 39
   +A1, +A2, +B1, +C, ●A, ●B, ✳A3
8. Gries, site 115
   ◆B, +A1
9. Landfriedstetten, site 8
   ▲
10. Wieselburg, plot 246/6, 16 Johann Winter Gasse
    ▲
11. Weinzierl, Wieselburg Land
    +B2
12. Mühling, 8th–9th-century cemetery
    +A1, ●B

Figure 161. Archaeological sites in the Erlauf Valley with the indication of the petrographic groups and subgroups of the ceramics investigated in this thesis (Base map: Google Maps). The usual symbols are used for the petrographic groups as shown in Figure 92 (page 188). Individual samples were found at archaeological sites numbered 1 and 3 on this map.

Ceramics from the 6th to 7th centuries

The samples of the Carbonate group were collected at the southern part of the Erlauf Valley as well. One sample of 'Carbonate B' (S89) originates from Gries, Site 115, which is located east of

the Erlauf and relatively far from it (ca. 15 km). The other three samples (both from 'Carbonate A' and 'Carbonate B') are from the other side of the River, from Purgstall, Site 47 (*Figure 161*).

Ceramics from the 8th to 9th centuries

Granitoid subgroups: 'Granitoid A1', 'Granitoid A2', 'Granitoid B1', 'Granitoid B2', 'Granitoid C' and 'Granitoid D'

Most of the 8th–9th century Granitoid subgroups contain samples from two or more different sites of the Erlauf Valley. Subgroup 'Granitoid A1' is the largest of them including 21 ceramics from five archaeological sites, which are located in the middle part of the Valley (Purgstall, 8th–9th-century cemetery; Purgstall, Site 10; Hochrieß, Site 39; and Mühling, 8th–9th-century cemetery), or further east of it (Gries, Site 115). The 11 samples of 'Granitoid A2' were collected from three sites (Purgstall, Site 10; Purgstall, Site 26; and Hochrieß, Site 39) in the southern/middle section of the Valley as well. The five ceramic sherds belonging to subgroup 'Granitoid B1' are from two neighbouring sites on the eastern side of the Erlauf (Purgstall, 8th–9th-century cemetery and Hochrieß, Site 39), while those five belonging to 'Granitoid B2' are from two sites located farther away from each other (Purgstall, 8th–9th-century cemetery and Weinzierl, Wieselburg Land) in the southern and northern part of the Valley. Subgroup 'Granitoid C' contains three samples from the above-mentioned neighbouring sites (Purgstall, 8th–9th-century cemetery and Hochrieß, Site 39), and finally, the two samples of 'Granitoid D' originate from one site (Purgstall, 8th–9th-century cemetery). The distribution of the Granitoid group samples thus practically cover the whole area of the Erlauf Valley (*Figure 161*).

Amphibole group

The Amphibole group contains 12 samples, which were collected from five sites located in the southern part (Purgstall, 8th–9th-century cemetery; Purgstall, Site 47; and Zehnbach, Site 16) and in the northern part of the Valley (Landfriedstetten, Site 8 and Wieselburg, Plot 246/6; *Figure 161*).

Diorite group

The seven samples of the Diorite group were found in the middle area of the Erlauf Valley: in two cemeteries (8th–9th-century cemeteries of Purgstall and Mühling) and a settlement near Hochrieß (Site 39). The samples (n=4) from Purgstall belong to subgroup 'Diorite A', that from

Mühling belong to subgroup ‘Diorite B’, while the Hochrieß samples (n=2) are from both subgroups of the Diorite group (*Figure 161*).

Ceramics from the 9th to 12th centuries

The 51 graphite-containing ceramics investigated in this thesis are relatively heterogeneous and originate from 14 archaeological sites. Six of these sites are located in the Erlauf Valley and eight sites are situated in other parts of Lower Austria and Vienna.



Figure 162. Archaeological sites and subgroups of graphite-containing ceramics from outside of the Erlauf Valley (Base map: Google Maps). The boundaries of Lower Austria and Vienna are marked with a red outline. One individual sample originates from Sachsendorf.

The graphite gneiss-containing pottery sherds are connected to various locations. The six samples of subgroup ‘Graphite A1’ were found at three sites located relatively far from each other in the southern (Hausstein), middle (Tulln, Wassergasse) and northern (Sand) part of Lower Austria. Seven samples belong to subgroup ‘Graphite A2’, which were collected from five scattered sites (Hausstein; Ternitz; Tulln, Hauptplatz; Mautern; and Vienna). Ceramics from subgroup ‘Graphite A3’ (n=10) originate from the Erlauf Valley (Wieselburg, Kirchenberg and Hochrieß, Site 39) as well as from other Lower Austrian sites south of the Danube (Ternitz; Tulln, Wassergasse and Tulln, Hauptplatz) and Vienna. The three samples of subgroup ‘Graphite A4’ are from three different sites, including Wieselburg, Kirchenberg in the Erlauf

Valley and two other sites (Mautern and Sachsendorf) along the Danube. Finally, subgroup 'Graphite A5' with its nine samples originates from one site in the Erlauf Valley (Wieselburg, Kirchenberg) and four other Lower Austrian locations (Ternitz; Sand; Tulln-Wassergasse; and Mautern; *Figure 162*).

The mica schist-containing two samples of 'Graphite B' were recovered during excavations at the castle of Sachsendorf and in Vienna. The sites of those eight graphite-containing samples that also include carbonate rock fragments ('Graphite C') are located in the middle (Tulln, Hauptplatz – 'C1', and Mautern – 'C1', 'C2') and northern (Sachsendorf – 'C1', 'C2') part of Lower Austria.

There is no graphite-containing subgroup which can be linked to a single site, there is one however, which contains samples from the Erlauf Valley only. This is the last subgroup of the Graphite group, the low (30–50%) graphite-containing 'Graphite D'. The five samples of this subgroup were found at four different sites in the Valley near Purgstall (Purgstall 8th–9th-century cemetery; Purgstall, Site 10; Purgstall, Site 26; and Zehnbach, Site 16).

Summary

To sum up, all ceramics from the 1st–5th and 6th–7th centuries were found at the southern part of the Erlauf Valley. Based on the investigated assemblage, the 8th–9th-century sherds from the Granitoid and Amphibole groups have similar distributions covering the whole area of the Valley. The Diorite group is limited to the middle area of the Valley as far as the studied ceramic material is concerned. These distribution patterns, however, are likely influenced by the number of archaeological sites and samples included in the analysis. It is important to note that much more ceramics were analysed from the 8th–9th centuries (69 samples) than from the previous periods (1st–5th centuries: 11 samples, 6th–7th centuries: four samples).

There is no indication of how far ceramics originating from the Erlauf Valley occurred beyond the Valley, whether their distribution was restricted or extended outside of it, as no other pottery has been analysed from the vicinity of the Valley to which the studied pottery sherds could be compared (see also Section 5.7). Nevertheless, as potential raw material sources are located close to the sites where these ceramics were found (Section 5.2), it seems likely that they represent local products with a limited distribution (Section 5.5).

In the case of the graphite-containing ceramics, almost all of the subgroups (except for 'Graphite D') show relatively wide distributions with sherds originating from different and often distant archaeological sites in Lower Austria. The heterogeneity of these subgroups compared to the graphite-free subgroups, however, must be emphasised. Subgroup 'Graphite D' with its samples originating solely from the Erlauf Valley seems local, but the investigations of more ceramics from other surrounding regions would be needed to outline the distribution of these low graphite-containing ceramics more reliably.

Studies of graphite-containing pottery from other regions have proved that this type of pottery was widespread especially in the later periods of the Middle Ages (see Section 5.7). It seems that the distribution of the earliest graphite-containing ceramics in the 9th century was limited to the vicinity of the graphite deposits including Lower and Upper Austria and the southern part of Czechia (Scharrer-Liška 2007, 30, 67). From the 10th/11th centuries, however, this pottery type became more widespread, and eventually appeared in the area of today's Hungary, Slovakia, Poland and even made their way up to the Baltic Sea (Kühtreiber 2006, 134; Scharrer-Liška 2007, 68–70; Merva 2016; 521–522).

5.4 From clay to ceramics: pottery production technologies

In this section, the different stages of the production sequence of the studied pottery are analysed using the *chaîne opératoire* approach in order to reconstruct the manufacturing process (Section 2.5.1). This investigation opens an avenue to study the organisation of pottery production as well as to highlight technological choices made during ceramic making, technological traditions and changes in Lower Austria through the comparison of technologies over space and time (Sections 5.5 and 5.6).

The main elements of the pottery production *chaîne opératoire* studied here are summarised by *Table 26* below along with the analysis methods, which were used to collect information about these steps of ceramic manufacture. In the case of the assemblage under investigation, analytical techniques were especially useful when interpreting raw material procurement, preparation and firing, while macroscopic analysis was the main source of information regarding fashioning, finishing, surface treatment and decoration.

Table 26. Methods used for the interpretation of the different steps of the ceramic chaîne opératoire in this thesis

Element of the *chaîne opératoire*	**Analysed by which method**
Raw material procurement and preparation	Thin section analysis
Fashioning and finishing	Macroscopic analysis, thin section analysis
Surface treatment and decoration	Macroscopic analysis, thin section analysis, SEM
Firing	Macroscopic analysis, thin section analysis, SEM, XRD

5.4.1 Raw material procurement and preparation

Scientific analysis methods can provide few pieces of information about the procurement of raw materials (with regards to the actual activity of collecting raw materials), which is the first link in the operational chain of ceramic making. The raw materials can, however, be studied by these methods and their potential source can be localised as shown in Section 5.2.

There are several aspects of raw material preparation which can be considered here including tempering, clay mixing, sieving/levigation and kneading/homogenising the paste. These are all common paste preparation techniques of archaeological ceramics, which can be inferred mostly from microstructural characteristics (Section 3.3.1). There are of course actions, which leave no traces in the ceramics such as drying, hydrating or pounding of the clay (Roux 2017, 103).

Ceramics from the 1st to 5th centuries

It is likely that tempering and the modification of the natural clay were carried out in the case of subgroups 'Granitoid A3' and 'Granitoid B3'. Samples of both subgroups are made of a relatively pure clay and contain few inclusions (15–20%), which are mostly coarse-grained. This fine fraction-poor clay might suggest the 'cleaning' of clay by sieving or levigation and adding a coarse-grained temper to it.

Two of the seven samples in 'Granitoid A3' (S41 and S42) contain inclusion-free clay nodules, which can also support that tempering or clay mixing were carried out. In these samples, the inclusion-poor clay pellets might represent relicts of the initial pure clay that was subsequently tempered, or they can also represent an inclusion-free clay 1 which was mixed with clay 2 containing some inclusions. Colour streaks in another two samples of 'Granitoid A3' (S38 and S51) might also be signs of clay mixing, however, these can naturally occur in clay sources as well (Szakmány and Nagy 2017, 252).

In the case of 'Granitoid B3', tempering can also be inferred from the roundness of inclusions: they consist of sub-angular to rounded grains, which is different from the very angular to sub-angular grains present in the 8th–9th-century Granitoid subgroups ('Granitoid A1', 'Granitoid A2', 'Granitoid B1', 'Granitoid B2') made probably of residual clays (see below). Besides, one sample of 'Granitoid B3' (S47) also contains pure clay nodules, which could be the remains of the initial untempered clay.

Bimodal grain-size distribution and difference in the quality of the coarse and fine fraction are exhibited in S48 (individual sample), which suggest tempering. The fine fraction is made up of fine, mostly monocrystalline quartz grains, while the coarse fraction includes granitoid fragments and minerals. The careful preparation of the clay prior to tempering by sieving or levigation is possible in this case as well.

Ceramics from the 6th to 7th centuries

The microstructure of the samples of the Carbonate group shows clear indication of tempering.

In the samples of subgroup 'Carbonate A', the coarse and fine fraction clearly differ not only in size (strongly bimodal grain-size distribution, Section 4.2.1) but they are also of different types of minerals and rock fragments. The fine fraction of these samples is of small quartz grains,

while the coarse fraction consists of carbonate rock fragments. It is hard to imagine that this mineralogical composition and grain size difference were achieved by any other way than tempering. It is also possible that the clay was treated before tempering, which could include the sieving or settling out of the large inclusions.

In the case of subgroup 'Carbonate B', a pure clay was tempered with large carbonate rock fragments. Here, the scarce presence (5–15%) of the fine fraction suggests the preparation of the clay (sieving/levigation) before tempering.

Clay pellets are present in all samples of the Carbonate group, which manifest that natural inhomogeneities of the clay were not fully disintegrated during the homogenisation process even in this carefully prepared pottery type.

Ceramics from the 8th to 9th centuries

Granitoid subgroups: 'Granitoid A1', 'Granitoid A2', 'Granitoid B1', 'Granitoid B2', 'Granitoid C' and 'Granitoid D'

The 8th–9th-century samples of the Granitoid group were probably not tempered, but made of residual clay formed above the granite rocks of the Bohemian Massif based on the weathered state of feldspars as mentioned in Section 5.2. Although bimodal grain-size distribution was observed in the samples, which could suggest tempering, bimodality can also be natural (Szakmány and Nagy 2017, 251). Angularity of grains and poor/very poor sorting are common characteristics of residual clays (Quinn 2013, 120). Even with the use of a residual clay, which needed no tempering, it is likely that other preparation techniques were used such as kneading, homogenising the paste and sorting out of large inclusions, roots, etc.

Examining the microstructure of the feldspar-rich 'Granitoid A1' and 'Granitoid A2', it is apparent that the samples of 'Granitoid A2' are more alike than those of the other subgroup because of the presence of abundant small grains of the fine fraction. Particularly the samples free of graphite flakes are uniform (S65, S66, S68, S69, S72, S78, S79 and S81).[85] The similarity of these samples may be due to them being made of the same part of the clay source, and it is

[85] The other three members of subgroup 'Granitoid A2' (S39, S50 and S52) contain a small amount of graphite flakes (5–15% of inclusions), but except for this feature, they are very similar to the rest of the subgroup. They are not handled as graphite-containing ceramics as their graphite-content is much less than that of those samples, which are termed graphite-containing in this thesis (> 30% of inclusions).

also possible that they represent a batch made at the same time by the same hands, which might be supported by the fact that they are all from one archaeological site, Hochrieß, Site 39.

Many samples of the Granitoid subgroups in question (S3–S6, S9, S10, S18, S25, S26, S30, S39, S50, S65, S66, S68, S69, S73, S78, S79, S83, S93 and S95) contain clay pellets which were probably natural parts of the clay based on their similarity to the matrix.

Amphibole group

Samples of the Amphibole group are probably of residual clays of the Bohemian Massif as it is suggested by the weathered feldspars present in the rock fragments and the matrix. Similarly to the Granitoid subgroups, the angularity of grains and very poor sorting support the use of a residual clay rich in inclusions. At the same time, it has to be noted that the samples show bimodal grain-size distribution, which is often a sign of anthropogenic intervention.

Diorite group

The two subgroups of the Diorite group show different microstructure. Subgroup 'Diorite A' includes a fine and coarse fraction very different in composition. The fine fraction is mainly of monocrystalline quartz while the coarse fraction is of diorite fragments. This difference of the inclusions in size and quality is most likely because of tempering. Possibly a fine-grained quartz-rich clay was tempered with diorite rock fragments. It is also possible that preparation was needed to have only small quartz grains in the clay and the large grains were eliminated through sieving or levigation. Another option is that a pure clay was tempered with two different materials: fine-grained quartz and crushed diorite fragments. Tempering, however, was most likely part of the preparation process in any case.

In the case of the other subgroup of the Diorite group, 'Diorite B', it is not clear whether the ceramics were tempered or an inclusion-rich clay was used. Bimodal grain-size distribution could refer to tempering, but the coarse and the fine fraction consist of the same minerals and rock fragments, thus the addition of materials to the clay seems unlikely in these samples.

Individual samples

None of the individual samples originating from the 8th–9th centuries (S15, S17 and S23) show obvious traces of refinement of the clay or tempering. The granitoid fragments and the few

calcite grains in S17, however, are likely from different raw material sources, which suggest that the calcite grains were, either deliberately or accidentally, added to the paste.

Ceramics from the 9th to 12th centuries

One of the main questions regarding the manufacturing technology of the graphite-containing pottery is tempering. In most of the samples, it is not obvious whether the graphite and graphitic rock fragments were added to the clay or a graphite-rich clay was used. This residual clay originating from weathered graphite-rich rocks of the Drosendorf Unit (Section 5.2) is available on the surface of the Bohemian Massif at present day (Scharrer-Liška 2007, 15).

Tempering can be identified based on different characteristics of the ceramics in thin sections (Whitbread 1995, 393; Quinn 2013, 159–168). One of them is the unusually high ratio of inclusions to the clay matrix. The ration of inclusions can be seen as 'normal' (ranging between 15% to 40%) in the case of the studied graphite-containing ceramics. High angularity of grains might be another marker of tempering. The investigation of the angularity of graphite grains might be misleading, as graphite could easily become rounded during kneading because of its soft nature even if it was added to the clay as temper. Other mineral grains occurring with graphite, however, are very angular to sub-angular in the samples and thus may signal tempering.

Tempering can also be inferred from bimodal grain-size distribution, which is present in the studied samples. This kind of distribution, however, also occurs in some natural clay sources as mentioned earlier in the case of the 8th–9th-century ceramics. The use of a graphite-containing residual clay could be suggested by the weathered state of feldspars and poor sorting of the grains, but a graphite-containing detritus with similar characteristics could also be found in the area of the Massif and used as a temper.

The composition of the thin sections can also be informative in terms of tempering as special types of grains (e.g. grog, slag, shell, bone) or grains with different geological origins might indicate the addition of temper materials. The latter might be the case with subgroup 'Graphite D'. Based on the diversity of the inclusions present in these samples (graphitic rock fragments and sedimentary rock fragments), it seems likely that the inclusions are at least from two sources. The sedimentary rock fragments could originate from the same source as the clay or from a different source. In any case, samples of 'Graphite D' were most likely tempered.

Another sign of tempering could be the uneven distribution of the inclusions caused by incomplete mixing and kneading. Similar distribution pattern could be achieved when another clay was added to the paste. In the case of three samples (S107, S112 and S118) of subgroup 'Graphite A3', there is a possibility of clay mixing because of the large number of clay pellets present. At the same time, the potentially natural occurrence of these pellets in the clay cannot be discarded either, which could be suggested by the similar composition of the pellets to that of the matrix (both include graphite flakes) as well as their shape (elongated/distorted) and boundaries (angular to sub-rounded or diffuse).

All in all, traces for raw material preparation present in the graphite-containing ceramics are controversial. Nevertheless, tempering is likely in a couple of cases ('Graphite D'), which might be extended to the other graphite-containing samples as well. Tempering could happen either through the addition of crushed graphitic rock or graphitic residual clay to the paste. The weathered feldspars in many samples would suggest the latter option. However, analyses of raw materials would be needed to confirm these hypotheses regarding tempering and the use of graphitic clay as temper.

5.4.2 Shaping: fashioning and finishing

There are multiple ways to achieve the desired form of a vessel by hand forming, moulding or using a wheel (Section 3.2.1). Various techniques were frequently combined, which can mask each other's traces and make complicated the recognition of all techniques involved in the making of a vessel. However, it is possible to identify some of the techniques by the thorough observation of the traces of the forming method, which is carried out mainly by macroscopic analysis and less frequently by thin section petrography.

In terms of shaping, the samples from the four periods seem quite uniform. As explained in Section 4.1.2, most likely all samples were parts of pots (jars). This vessel shape was developed/finished using rotation as marked by the rotation marks (fine thin lines) running across the surface of the sherds, but the use of the potter's wheel can be excluded because of the lack of the typical traces of wheel-throwing. Taking all traces into consideration (uneven wall thickness, rotation marks, occasional presence of bottom marks), the vessels under investigation from each period were probably made by hand forming (e.g. building up of the vessel from coils) and finished by slow wheel turning (Section 4.1.3). The moderate alignment of the elongated grains and voids in most of the thin sections could also support the use of a

turntable (Section 4.2). This device could have been similar to the turntable depicted on a wall painting from the 13th century in the Gurk Cathedral (*Figure 163*).



Figure 163. Depiction of a potter and his turntable from the 13th century (Fresco from the 'Bischofskapelle' in the west gallery of the Gurk Cathedral, Carinthia, Austria)[86]

5.4.3 Surface treatment and decoration

After completing the forming process and giving the vessels their final shape, the vessel surface can be modified by surface treatments such as burnishing, polishing or the application of coatings (Section 3.2.1). There are no signs of surface treatments in the studied ceramics by macroscopy and no preferred orientation of inclusions referring to polishing/burnishing or the presence of a separate layer (slip/glaze) at the surface of the sherds can be identified in thin section.

There is, however, one sample which has to be mentioned here, S113 of the Graphite group, where a well-distinguished layer is exhibited on the inner side of the vessel (Section 4.2.2). SEM-EDS analysis showed that it has a calcium and phosphorous-rich composition, which

[86] https://www.ooegeschichte.at/fileadmin/_processed_/5/8/csm_handtoepferscheibe_gurk1_2f77e59310.jpg (accessed on 16/02/2021)

elements are typical subjects of post-burial alterations suggesting the deposition of this layer in the soil (Section 4.3.2). At the same time, this layer is not present on the outer side of the potsherd which would suggest that it might be a weathered glaze[87] or it might have been deposited during the use of the vessel (Rice 1987, 255). However, it is also possible that different soil conditions were present near the inner and outer side of the sherd.

As for decorations, the studied ceramic material exhibits different techniques and motives summarised below by chronological groups (for images of the different decoration elements see *Figure 33* in Section 3.2.2).

Ceramics from the 1st to 5th centuries

Some of the ceramic sherds belonging to 'Granitoid A3' show incised decorations including parallel lines and parallel wavy lines. S47 ('Granitoid B3') and S48 (individual sample) exhibit a fraction of two line bands crossing each other.

Ceramics from the 6th to 7th centuries

The potsherds of the Carbonate group are decorated with incised parallel lines or parallel wavy lines.

Ceramics from the 8th to 9th centuries

The 8th–9th-century ceramics are often decorated with incised (parallel) wavy lines and incised (parallel) lines, which are present in almost all petrographic groups and subgroups (Granitoid subgroups, Amphibole group, 'Diorite B' and individual samples). These decoration elements usually make up several rows on the body of the vessels and are frequently combined as shown by the pots with full profile (see *Figures 50–53*). In one case, comb-impressed dots are also used as decoration (S22 of subgroup 'Granitoid C').

Incised decoration can also occur on the inner side of vessel rims, which is represented by two ceramic fragments (S73 and S77) from subgroup 'Granitoid A1', where parallel wavy lines are incised on the inner side of the rims.

[87] However, the layer being weathered glaze seems unlikely, see footnote 62 on page 203.

There is one subgroup, 'Diorite A', where none of the samples are decorated. In the case of four (out of five) samples (S11, S16, S24, S27), it is certain that the vessels had no decoration at all as the remaining parts allowed a full reconstruction of the pots.

Ceramics from the 9th to 12th centuries

In the Graphite group, the most common decoration elements are incised (parallel) wavy lines. Furthermore, a raised band (some samples of 'Graphite A1', 'Graphite A2' and 'Graphite A3') and comb-impressed dots (some samples of 'Graphite A1', 'Graphite A5' and 'Graphite B') are also frequent. The arrangement of the comb-impressed dots is different for the Graphite group samples and the Granitoid group sample mentioned above.[88]

5.4.4 Firing

Different characteristics of pottery can refer to the firing atmosphere and maximum temperature achieved. The temperature and atmosphere at the same time is dependent on the way how the firing was carried out and the construction that was used to fire the vessels.

Atmosphere conditions

The colour of the ceramics, among others, can provide information about the firing atmosphere. The reddish-brownish colour of the graphite-free ceramics from the 1st to the 9th century suggests that these vessels were fired mostly in an oxidising atmosphere (Section 3.2.1; Dell'mour 1989, 30; Orton and Hughes 2013, 88).[89] Many of these sherds (from all subgroups) show differences in their surface and cross-section colour (Section 4.1.1); the latter are also exhibited in the thin sections (Section 4.2.1). Colour differences are often the result of a mixed atmosphere during firing, which refer to the change of oxidising and reducing conditions over time (sherd fracture with colour stripes) or space (changes in surface colour; Rye 1981, 116: Fig. 104, 120). When only the surface regions of the ceramics are affected, these differences can also be the result of changing conditions during cooling or the reheating of the vessel during use (cooking, baking; Rye 1981, 116–118).

[88] The comb-impressed dots are arranged in two rows on the shoulder of S22 while they are arranged in short parallel diagonal lines or in a herringbone pattern on the graphite-containing ceramics.
[89] Reddish-brownish colour also suggest that these samples are of iron-containing clays (Rice 1987, 335), which was confirmed by SEM-EDS (Appendix D.2).

As for the graphite-containing ceramics from the 9th to 12th centuries, they all (except samples of subgroup 'Graphite D') have dark grey colour which is partly because of the abundant presence of graphite and partly because of reducing conditions during firing (Dell'mour 1989, 30; Orton and Hughes 2013, 88). Occasionally, surface colour changes to a greyish-brown shade also occur in patches, which might be the result of vessel use (direct contact with fire). Samples of subgroup 'Graphite D' are different from the rest of the Graphite group as they have reddish-brownish shades and similarly to the graphite-free ceramics, they were fired in oxidising or mixed atmosphere.

Maximum temperature

The ceramics have similar hardness of the Mohs' scale (2–3; Section 4.1.1), which might be a sign of similar firing temperatures, but it has to be kept in mind that hardness can be affected by other factors as well (Orton and Hughes 2013, 158; Whitbread 2017, 204).

The optical activity of the matrix in thin section can also be an indicator of firing temperatures (Section 3.3.1). The graphite-free ceramics, the individual samples and samples of subgroup 'Graphite D' usually exhibit different levels of optical activity within one sample, the typical optical activity being moderate-high (Sections 4.2.1 and 4.2.2). This suggest that the maximum firing temperature did not go much beyond 800–850 °C as ceramics gradually loose their optical activity beyond this temperature range (Section 3.3.1; Rice 1987, 431; Quinn 2013, 191).

The investigation of the optical activity was more difficult in the Graphite group because of the dark matrix resulting after reduced firing as well as the opaque graphite particles. The graphite-containing samples usually show inactive or very slightly active optical activity, except subgroup 'Graphite D' (as mentioned above) and subgroup 'Graphite A5' with slight to moderate optical activity (Section 4.2.2). Low optical activity of the matrix could indicate higher firing temperatures than 800–850 °C, but the dark/black matrix can also mask the 'real' level of optical activity.

There are, however, also other methods for the estimation of firing temperatures of which SEM and XRD were used in this thesis (see Sections 4.3.1 and 4.5.3). The estimated maximum temperatures are summarised in *Table 27* for each petrographic subgroup. It has to be noted that *Table 27* is based on the investigation of 49 samples only as there was no possibility to analyse all 135 samples by SEM and XRD. Nevertheless, the results of ceramic petrography

(optical activity of matrix) confirm that the samples were fired at similar temperatures, thus the extension of the firing temperature estimation of the few analysed samples to all members of a given subgroup seems reasonable.

Ceramics from the 1st to 5th centuries

The SEM analysis identified no vitrification in the investigated samples from 'Granitoid A3' and 'Granitoid B3', which suggest that their estimated firing temperatures fall below *c.* 800 °C. A similar maximum temperature falling below 800–950 °C can be estimated based on the presence of illite in the XRD data.

Ceramics from the 6th to 7th centuries

The unvitrified matrix of the samples of the Carbonate group refer to a maximum firing temperature below *c.* 800 °C, but here it is also important to take into consideration the presence of the calcite grains and their shape. Calcite starts decomposing at *c.* 700 °C and its decomposition is finished at *c.* 900 °C (*Table 9*; Rice 1987, 98; Szakmány and Nagy 2017, 258–259). Calcite grains in three thin sections (S57, S58, S89) have angular boundaries and no signs of decomposition are visible, which suggest that the maximum firing temperature for these samples was below or around 700 °C. The calcite crystals in one sample (S59), however, are slightly decomposed along the edges, which might be because of a higher temperature possibly between 700 °C and 750 °C.

Table 27. Estimated maximum firing temperatures of the samples by petrographic subgroups based on the results of SEM, XRD and thin section analysis

Granitoid	A1	< ~800 °C	B1	< ~800 °C
	A2	< ~800 °C	B2	< ~800 °C
	A3	< ~800 °C	B3	< ~800 °C
	C	< ~800 °C	D	< ~800 °C
Amphibole		< ~800 °C (S8); 800–850 °C (S90)		
Diorite	A	< ~800 °C	B	< ~800 °C
Carbonate	A	< ~700 °C	B	700–750 °C (S59); < ~700 °C (S89)
Graphite	A1	< ~750 °C	B	< ~750 °C
	A2	< ~750 °C	C1	< ~700 °C
	A3	< ~750 °C	C2	< ~700 °C
	A4	< ~750 °C	D	< ~800 °C
	A5	< ~750 °C		
Individual sample	S15	< ~800 °C		

Ceramics from the 8th to 9th centuries

The 8th–9th-century samples investigated from the Granitoid group ('Granitoid A1', 'Granitoid A2', 'Granitoid B1', 'Granitoid B2', 'Granitoid C' and 'Granitoid D') have no vitrification thus their estimated maximum firing temperatures fall below *c.* 800 °C. XRD analysis suggested a similar estimation based on the presence of illite the maximum temperature being below 800–950 °C.

Vitrification analysis by SEM provided information about the firing temperatures of samples of the Amphibole group. The maximum firing temperature can be estimated below *c.* 800 °C for one analysed sample (S8) because it is unvitrified and between 800 and 850 °C for the other analysed sample (S90) because it is slightly vitrified.

Samples of the two subgroups of the Diorite group could also be fired at under *c.* 800 °C based on their unvitrified microstructure, which was also confirmed for 'Diorite A' by the XRD results (<800–950 °C).

The maximum firing temperature of the analysed individual sample (S15) can be estimated below 800 °C based on its unvitrified matrix.

Ceramics from the 9th to 12th centuries

The vitrification analysis showed that the microstructure of the samples of the Graphite group is not vitrified, based on which the maximum firing temperature can be estimated below *c.* 750 °C for reduced samples (subgroups 'Graphite A', 'Graphite B' and 'Graphite C') and below *c.* 800 °C for oxidised samples (subgroup 'Graphite D'). XRD analysis led to similar estimations based on the presence of illite (<800–950 °C). Subgroup 'Graphite C' is special in the Graphite group as it contains carbonate-rock fragments. The calcite grains in subgroup 'Graphite C1' and the micritic rock fragments in 'Graphite C2' are angular, which suggest a maximum firing temperature below or around 700 °C.

Firing construction

There are two basic techniques for ceramic firing: open firing and kiln firing. During open firing, the vessels to be fired and the fuel are placed together (Rye 1981, 96). Ceramics are usually fired for a relatively short time at relatively low temperatures (600–850 °C; Rye 1981, 98; Rice 1987, 153–158). The rate of firing can be adjusted to some extent by choosing an appropriate

fuel type, however, the firing atmosphere can hardly be controlled (Rye 1981, 98; Rice 1987, 157). There are several variations of open firing: ceramics can be placed on the ground, on stones, in a pit, etc. (Rye 1981, 98).

When pottery is fired in a kiln, the fuel and the vessels are separated (Rye 1981, 96). In a kiln, high temperatures can be achieved (1000–1300 °C) and both the rate and atmosphere of the firing can be controlled (Rye 1981, 98). Kilns have a range of types which are variations of the two basic types: updraft kilns and downdraft kilns (Rye 1981, 98–104; Rice 1987, 158–163).

The samples give no information about the firing structure. Both oxidised and reduced wares can be produced by open or kiln firing. The change of oxidising and reducing conditions is typical for open firing, thus it is possible that the graphite-free ceramics (1st–9th centuries) and samples of 'Graphite D' (9th–12th centuries) were fired with this technique based on their frequent colour differences in cross-section, but there is no evidence, which could confirm this. Grey fractures of graphite-containing ceramics ('Graphite A', 'Graphite B' and 'Graphite C', 9th–12th centuries) usually show no changes of atmosphere during firing (although differences in surface colour can occur), which suggests a controlled environment. Often it could be challenging to maintain reducing conditions even in kilns (Mayes 1962), not to mention open firings. This might indicate the use of a kiln for the firing of the graphite-containing ceramics.

Some examples show that kilns were present and used in the study area at the start and end of the study period. Two late antique pottery kilns were found in Ternitz and Mautern, Lower Austria (Friesinger and Kerchler 1981). An 11th-century kiln was excavated in Auhof (Upper Austria), which was probably functioning as a pottery kiln (Kloiber and Pertlwieser 1967, 84–88; Scharrer-Liška 2007, 104–110). There are several examples of pottery kilns from the late medieval period (13th–15th centuries) in Lower Austria, e.g. Amstetten (Scharrer 1994) and St. Pölten (Scharrer-Liška 2009). It is possible, however that pit firing was used simultaneously with kiln firing, traces of which are less easily detectable by archaeology.

5.4.5 Summary

The earliest samples of the assemblage originating from the Roman/late Roman period belong to subgroups 'Granitoid A3' and 'Granitoid B3'. Samples of both subgroups were likely tempered and possibly another technique (sieving, levigation) was used during preparation of the paste to remove large grains from the clay. The investigated sherds of these subgroups were parts of pots, which were made by slow wheel turning. The sherds had incised decoration

('Granitoid A3') or no decoration ('Granitoid A3', 'Granitoid B3'). They were fired in a mixed, but mainly oxidising atmosphere at or below *c.* 800 °C.

The presence of the carbonate rock fragments in the matrix is the result of tempering in both subgroups of the Carbonate group (6th–7th centuries). It is possible that sieving or levigation was carried out before tempering. Slow wheel turning was used as the forming method of these pots, which were decorated with incised lines and wavy lines. They were fired in a mostly oxidising atmosphere, but the colour of the sherds shows changes of conditions (both fracture and surface). The maximum firing temperature can be estimated at 700–750 °C based on the calcite crystals present in the samples.

The majority of the 8th–9th-century samples of the Granitoid group were likely made from the residual clay of the Bohemian Massif without tempering ('Granitoid A1', 'Granitoid A2', 'Granitoid B1', 'Granitoid B2', 'Granitoid C' and 'Granitoid D'). The forming method of all pots belonging to the Granitoid group was slow wheel turning. They were commonly decorated with incised (parallel) lines and wavy lines. They were fired under mixed conditions, but in a mainly oxidising atmosphere at or below *c.* 800 °C.

The pots belonging to the Amphibole group were probably made from residual clays of the Bohemian Massif as well. These slow wheel-turned vessels were decorated with incised decoration and analytical results suggest that they were fired in an oxidising atmosphere (often with changing conditions) at or below 800–850 °C.

As for the Diorite group, the samples of 'Diorite A' were probably tempered while tempering cannot be confirmed or excluded in the case of 'Diorite B'. The pots of both subgroups were made on the slow wheel. The vessels of 'Diorite A' were not decorated; those of 'Diorite B' could have incised decoration. The firing atmosphere was mixed, but mainly oxidising conditions were present. The firing temperature was probably below *c.* 800 °C for both subgroups.

The graphite-containing samples can be dated from the 9th century up to the 12th century. Although it is not obvious from most of the samples, it is likely that they were tempered as some samples indicate it (subgroup 'Graphite D'), which could have happened by the addition of graphitic clay to the paste as suggested by some sherds (S107, S112 and S118). All graphite-containing samples were made by slow wheel turning. Incised lines and wavy lines are present on graphite-containing pots as well and typical decoration elements for these ceramics are the

raised band and comb-impressed dots. The vessels, except those of 'Graphite D', were fired under reducing conditions and at or below *c.* 750 °C ('Graphite A' and 'Graphite B'); the maximum firing temperature for samples of subgroup 'Graphite C' can be estimated below 700 °C based on the presence of carbonate rock fragments. Samples of 'Graphite D' are similar to the graphite-free samples in terms of firing atmosphere (oxidising/mixed) and temperature (< ~800 °C).

5.5 Organisation of pottery production

This subchapter discusses questions related to the organisation of pottery production including what scale, level of control, standardisation and specialisation possibly characterised the production units that made the studied ceramics and what these units could look like in terms of mode of production. Furthermore, topics concerning the possible number and location of the producing units are explored.

The Lower Austrian region is lacking direct historical or archaeological sources about early medieval pottery production and its organisational structure. The thorough investigation of the ceramic material, however, can give ideas about some aspects of the organisation of pottery production. As only indirect information is available in this topic, it has to be emphasised that the following statements are hypothetical.

Ceramics from the 1st to 5th centuries

The earliest ceramics belonging to subgroups 'Granitoid A3' and 'Granitoid B3' show relative homogeneity within the subgroups compared to ceramics from later periods. Homogeneity is detectable particularly in 'Granitoid A3' where more samples are available ('Granitoid A3': seven samples; 'Granitoid B3': three samples). The careful preparation of the raw materials (sieving/levigation, tempering) is apparent and consistent in both subgroups. Based on this low variation in microstructure and composition, some level of standardisation may be hypothesised along with a scale that could exceed household production.

There is no indication of whether any control was exercised over production of these ceramics. However, they represent utilitarian pots possibly with no considerable value, used likely for cooking and storing, which make unlikely that their production was monitored. It is not possible to identify whether these ceramics were made by specialised units or non-specialists as the low sample number and rough dating does not allow this. Wider pottery spectra of shorter periods would be needed to evaluate specialisation, e.g. whether few vessel types were produced in large numbers or not. The skill level and consistency involved in making these ceramics, however, could point to some degree of specialisation.

Among the described production modes, taking into account the above information as well as the forming and firing characteristics (slow wheel turning, mixed firing atmosphere), production units of 'Granitoid A3' and 'Granitoid B3' resemble the most 'household industries'

or ‘individual workshops’ identified by Peacock (1982, 8–9) being probably closer to the definition of ‘individual workshops’.

Ceramics from the 6th to 7th centuries

Four samples were investigated from the 6th–7th centuries that are divided into two subgroups (‘Carbonate A’ and ‘Carbonate B’). Therefore, it is not realistic to estimate the scale of production in this case. The similarity of the two samples of ‘Carbonate A1’ in composition and microstructure, however, could be an indicator of a highly standardised production if it was certain that these two samples would originate from different vessels and there would be more samples with the same characteristics.

Using carbonate rock fragments as temper is a sign of high skill level and great technological knowledge of the producer as calcite can cause spalling and cracking of the pot if care is not taken to ensure appropriate firing temperature and conditions (Rice 1987, 98; Hoard et al. 1995). Prior to tempering, the removal of large grains is assumed in the samples of the Carbonate group based on their microstructure contributing to the proficiency of production. This skilfulness could indicate some level of specialisation, but this alone is not enough to determine a specialised production.

The nature of these ceramics (utilitarian, cooking/storing pots, low value), similarly to those from the Roman/late Roman period, give no reason to assume control over production.

The homogeneity of the samples as well as the effort involved in the preparation of raw materials and firing could point to similar organisations as Peacock’s (1982, 9) ‘individual workshops’. At the same time, these pots are characterised by slow wheel turning and changing firing atmosphere, which, however, are features associated with ‘household industries’ (Peacock 1982, 8).

Ceramics from the 8th to 9th centuries

Granitoid subgroups: ‘Granitoid A1’, ‘Granitoid A2’, ‘Granitoid B1’, ‘Granitoid B2’, ‘Granitoid C’ and ‘Granitoid D’

The largest of the 8th–9th-century subgroups of the Granitoid group is ‘Granitoid A1’ with 21 samples. It is more or less homogeneous, which is possibly the characteristic of the raw material as tempering or modification of the clay are not detected and the use of a residual

clay can be hypothesised. This variability and using the clay in its natural form may suggest the lack of endeavour to achieve standardised production, which is shown by the varying pot shapes and sizes as well as decorations. Based on this large sample number among the randomly chosen sherds from the Erlauf Valley ('Granitoid A1' makes up *c*. 20% of the ceramics from the Valley) and the presence of this subgroup at multiple archaeological sites (*Figure 161*), it is possible that the production of these samples surpassed small scale. Nevertheless, it could still happen in households with a higher output rate.

Subgroup 'Granitoid A2' is very similar to 'Granitoid A1' but seems more homogeneous. Although further subgroups were not separated in 'Granitoid A2', three samples (S39, S50, S52) slightly stand out because they contain some graphite flakes (5–15% of inclusions), but in any other characteristics they are very similar to the other eight samples of this subgroup. The uniformity of these eight samples is remarkable. Based on the similarity of 'Granitoid A2' to 'Granitoid A1', it is possible that all of these ceramics were made by the same production unit and the graphite-free samples of 'Granitoid A2' were the products of the same batch, as mentioned earlier (Section 5.4.1).

Both subgroup 'Granitoid B1' and subgroup 'Granitoid B2' contain five samples. Similarly to 'Granitoid A1', these samples are characterised by relative homogeneity and made probably of the same residual clay. The only difference compared to 'Granitoid A1' is the quartz abundance over feldspars and the presence of a better-sorted inclusion range in 'Granitoid B1', both of which may be due to the natural variability of the raw material source. Therefore, it is possible that samples of 'Granitoid B1' and 'Granitoid B2' were made by the same household/workshop as those of 'Granitoid A1'. At the same time, the existence of a separate production unit producing 'Granitoid B1' and 'Granitoid B2' ware cannot be ruled out.

The number of samples in the rest of the subgroups of the Granitoid group ('Granitoid C' and 'Granitoid D') is three or less, which makes it difficult to deduce reliable information about the scale or standardisation of production.

The relative heterogeneity and relatively low skill level observed in the Granitoid subgroups compared to pottery from the previous periods suggest that specialisation was less likely present in the production of these ceramics. Specialised production might arise in the case of ceramics from graves as several vessels of the Granitoid subgroups were found in cemeteries. However, as those ceramics that were excavated in graves are not different from those

originating from settlements, a workshop providing vessels only for graves is not realistic. It is much more likely that vessels of everyday use were put in the burials.

Being utilitarian objects with no high-value or uniqueness, control over production was less likely in the case of the Granitoid group samples. Based on their technology (slow wheel turning, mixed firing atmosphere), the production units of these ceramics might be likened to Peacock's 'household industry', and the potential larger output of the units manufacturing vessels of 'Granitoid A1' and 'Granitoid A2' might also suggest some similarities with the category of 'individual workshops' (Peacock 1982, 8–9).

Amphibole group

The Amphibole group is characterised by some level of homogeneity regarding both the composition and microstructure of its 12 samples. The vessels were probably not tempered, but a residual clay was used from a different location of the Bohemian Massif than the clay used for making the ceramics in the Granitoid group.[90] Standardisation is not exhibited, neither in microscopic nor in macroscopic features of the vessels.

The samples are from several archaeological sites, which are located relatively far from each other covering the full area of the investigated part of the Erlauf Valley (*Figure 161*). Based on their relatively wide distribution and their relative homogeneity, the samples of the Amphibole group probably indicate a production surpassing small-scale.

The production of these ceramics was probably not controlled by elite or other groups/individuals because of the reasons mentioned in the case of the other ceramic groups. Signs of specialised production (e.g. great skill involved, a multitude of few vessel types) cannot be observed either.

Similarly to the above-mentioned Granitoid samples, the production of these samples may have happened in units that are comparable to Peacock's 'household industry' (slow wheel turning, mixed firing atmosphere), which could have similar features to 'individual workshops' (scale of production).

[90] As mentioned above (Section 5.2), there are two samples (S91 and S92) that are slightly different in composition as besides the 'usual' rock fragments of the Amphibole group they also contain 'unusual' inclusions. This might indicate that the raw materials of these samples were collected from the border of two different types of rock, which are alternating in the source area.

Diorite group

Samples of subgroup 'Diorite A' show great homogeneity and were made from well-prepared, probably tempered clay. The similarity of the pots' composition and microstructure as well as the lack of decoration on their surface suggest a certain level of standardisation. At the same time, the size and shape of the vessels are slightly different. As this subgroup contains only five samples, there is no solid basis to make conclusions about the scale of production. The skill and consistency involved in raw material preparation may suggest some degree of specialisation of production.

The samples of 'Diorite A' may point to a production form resembling 'household industry' based on their technology (slow wheel turning, mixed firing atmosphere) and also resembling 'individual workshop' based on their homogeneity, being possibly closer to the definition of 'individual workshop' (Peacock 1982, 8–9).

Subgroup 'Diorite B' contains only two samples, and therefore there is not enough information to assess the organisation of production in this case.

There is no reason to hypothesise a centralised control over ceramic production in the case of the Diorite group, similarly to the previously discussed ceramic groups.

Ceramics from the 9th to 12th centuries

Turning to the 51 graphite-containing ceramics collected from the Erlauf Valley and other parts of Lower Austria, heterogeneity is exhibited within the different subgroups. The possibility that the samples may originate from different periods within the 9th–11th (in few cases up to 12th) centuries and that they are from multiple often distant sites (6 sites in the Erlauf Valley, 12 sites from other parts of Lower Austria; *Figures 161* and *162*) can contribute to this heterogeneity. Furthermore, it also reflects the variability of the host rocks with which graphite can occur in the Drosendorf Unit of the Bohemian Massif (Section 5.2).

The large number and heterogeneity of the subgroups could indicate the existence of multiple production sites. The scale of production cannot be estimated because of the small number of samples compared to the large number of sites and the long period to which the samples are dated. There are no signs of standardisation in the investigated graphite-containing ceramics.

Because of the distinctiveness of graphite-containing ceramics and the spatial limitedness of graphite deposits, the question emerges whether this type of pottery was made in specialised production units or not. Although the skill level that is needed to produce graphite-containing ware is probably similar to that needed for manufacturing other graphite-free pottery, it is likely that the graphite changed the properties of the paste to some extent. It could be that a different treatment of the raw materials was needed when preparing the paste, and graphite could also impact the forming characteristics. Firing was different as it happened in a reducing atmosphere in contrast to the mixed atmosphere of the graphite-free pottery, which needed the acquisition of different knowledge and practices. Thus, because they likely needed a different treatment and skill set compared to other graphite-free ceramics during the preparation, forming and firing process, it is possible that there were units specialised in graphite-containing pottery production.

Graphite-containing ceramics may have represented a higher-value than the average graphite-free ceramics as graphite sources are restricted to certain areas. It is also possible that their manufacture was monitored or more likely that control was exercised over their distribution. Other studies investigating graphite-containing pottery raise the possibility that manorial organisation played an important role in the production and distribution of 9th–12th-century graphite-containing ceramics (Felgenhauer-Schmiedt 1998, 204; Scharrer-Liška 2007, 150). The manufacture of ceramics may have been carried out in manors located close to the graphite deposits for their own needs and they also supplied their estates, which could be widely scattered (Felgenhauer-Schmiedt 1998, 204; Scharrer-Liška 2007, 150). At the same time, they may have produced pottery for trade/exchange as well. It is also possible that they exercised control over graphite mining, but it could have been difficult to ban people from surface deposits exposed in the Massif.

As for the mode of production, based on the forming method (slow wheel turning) and its heterogeneity, the graphite-containing ware may be connected to 'household industry'-like production units, but their distribution over a relatively large area compared to their limited source area in the Bohemian Massif indicates a more organised form of production such as 'individual workshops' or even 'nucleated workshops' (Peacock 1982, 8–9). The lack of direct evidence for production organisation must, however, be emphasised.

Number of production units

The above considerations, especially the number and homogeneity/heterogeneity of ceramic groups can also provide information about the number of production units. The ceramics of the investigated material dated within the 1st–5th-century ('Granitoid A3' and 'Granitoid B3') could be made by one or two workshops/households. Those from the 6th–7th centuries ('Carbonate A' and 'Carbonate B') may be connected to one or two production units as well. The rest of the graphite-free ceramics dated to the 8th–9th centuries (rest of the Granitoid group, Amphibole group, 'Diorite A' and 'Diorite B') show the technological and compositional signature of at least four-five households/workshops.

The graphite-containing ceramics from the 9th–12th centuries were probably made at multiple contemporary and consecutive production sites. An estimate cannot be given because of the heterogeneity of the subgroups, but it is possible that the number of workshops/households producing the analysed graphite-containing vessels were in the range of 10–20.

Local, regional, supra-regional production?

Now that production organisation has been investigated and the number of producing units has been estimated, the question arises regarding where these households or workshops were located and how big the consumption areas of their products were. There are no clear answers to these questions as the production sites of the studied samples have not been found and excavated yet. An estimation, however, can be given based on the geological origin of the raw materials used for pottery manufacture. Three categories are differentiated in this section to characterise how far ceramics travelled from their potential location of production including 'local' (0–5 km), 'regional' (5–20 km) and 'supra-regional' (20–100 km) production.

It would seem practical to establish workshops close to the source of the raw materials and such a setup is often confirmed by archaeological and ethnographic research (Rice 1987, 177; Quinn 2013, 119). Dean Arnold (1985, 38–52; 2006, 5–7), for example, found that the preferred distance to travel on foot for clay and temper was within 7 km, and often (40–50% of cases) less than 1 km based on his own and other researchers' work examining communities from different parts of the world. A subsequent study (Heidke et al. 2007, 146–149) reviewing ethnographic literature resulted in similar values, the usual distance of the clay source being less than 5 km and frequently around 3 km from the production site on foot. Ethnographic data show that raw material procurement was carried out in a range less than 9 km and

usually *c.* 3 km in the Andes (Druc 2013, 493, 502). The exploitation of more distant sources is also manageable when applying a cart or a pack animal (Arnold 1985, 37–38; Heidke et al. 2007, 149).

At the same time, it must be remembered that the distance to raw material sources is not only influenced by proximity and availability but can also be affected by cultural or political reasons, social connections or tradition (Arnold 2011, 86; Druc 2013, 491–492). Also, the accessibility of other resources than clay, temper or an inclusion-rich residual clay needed for ceramic making, such as fuel and water might have affected the location of the production sites as well.

Ceramics from the 1st to 9th centuries

The ceramics belonging to the Roman/late Roman period ('Granitoid A3', 'Granitoid B3' and S48), the 6th–7th centuries (Carbonate group) and the 8th–9th centuries (the rest of the subgroups of the Granitoid group, the Amphibole group, Diorite group, S15, S17 and S23) were found in the Erlauf Valley. They all have a local character as the raw materials are available in the vicinity of the sites where the ceramics were found. Although the petrographic analysis pointed out the Bohemian Massif as the potential source of the raw materials, it does not mean that the production sites were necessarily located in the area of the Massif. This geological unit continues below the Erlauf Valley and it is also likely that clays from the erosion of the rocks of the Massif extend just below the soil layer, especially in the northern part of the Valley (north of Wieselburg), where the Massif is very close to the surface (Section 2.3.2, *Figure 21*). Therefore, the production sites of the vessels originating from the Erlauf Valley could be located in either the Bohemian Massif or the Erlauf Valley.

The farthest site (Zehnbach, Site 16) from the outcrops of the Bohemian Massif, where ceramics with raw materials from the Massif are studied, is *c.* 20 km. This distance is considered the upper limit of what is defined as 'regional' (5–20 km) in this thesis. However, it seems very likely that raw material sources were available closer to the sites than this originating from the weathering bedrock (Bohemian Massif) as mentioned above, and most of the vessels from the Erlauf Valley can be termed as 'local' products (< 5 km).

There is no information available about how the ceramics travelled to their site where they were unearthed in the Erlauf Valley in the 1st–9th centuries; whether the producers or consumers travelled to sell/buy/exchange the products or whether there was an intermediate place (market) or person (middleman) involved in the exchange process (Rice 1987, 192–195).

Generally utilitarian pottery (such as pots in this case) are not transported far from their place of production because of their fragile nature and the cost of transportation (Rice 1987, 200). In this Valley, however, the distances are rather small, thus each of the above-mentioned scenarios is possible. It seems logical to consider exchange as the basis of movement of goods for these mostly locally produced vessels, although the presence of small-distance trade cannot be ruled out entirely.

Ceramics from the 9th to 12th centuries

The petrographic analysis suggests that non-plastic inclusions of the ceramics of the Graphite group originate from the Bohemian Massif. It is possible that the production units were located close to the graphite sources (Drosendorf Unit in the Bohemian Massif, see Section 5.2), especially if graphitic clay was used to make or temper the vessels.

The distribution of the Graphite group samples covers a relatively large area; the farthest site (Ternitz) is *c.* 100 km away from the Drosendorf Unit (*Figure 162*). Based on the distance between the archaeological sites with graphite-containing pottery and the production units possibly located near the Drosendorf Unit, the production goes beyond the scale of 'local' (< 5 km) and 'regional' (5–20 km) – except maybe for graphite-containing ceramics found in the Erlauf Valley or other sites located close to the graphite deposits (including Mautern, Sachsendorf and Sand) – and these ceramics may be defined as 'supra-regional' products.

It was already mentioned that graphite-containing ceramics achieved a wide distribution in Central Europe and beyond (Section 5.3). The samples originating from archaeological sites near the Danube investigated in this thesis as well as the distribution of other graphite-containing ceramics indicate that river transport had an important part in spreading this type of ware (Scharrer-Liška 2007, 72). At the same time, it is also possible that the graphite was transported as temper instead of the ceramic products, and the vessels were made locally (Felgenhauer-Schmiedt 1998, 203). There are examples of both the finished products and raw materials being the subject of trade/exchange (Poláček 1998, 155; Kühtreiber 2006, 134; Scharrer-Liška 2007, 71).

It is not clear whether graphite-containing vessels changed hands through trade or exchange networks. The fact that they were widely spread and reached distant locations as well as the presence of trade in the case of other goods (e.g. salt, food, cattle; Scharrer-Liška 2007, 12–13) suggest the involvement of trade networks in the distribution of this ware. Historical and

archaeological sources are also silent about whether the pots or their contents (if any) were the subject of interest to the consumers (Scharrer-Liška 2007, 72). The beneficial characteristics of graphite-containing pots (see Section 5.6.1 below), which permitted a longer usage time than other ceramics, suggest that they were valuable on their own as vessels.

With the exception of subgroup 'Graphite D', none of the other Graphite subgroups are limited to certain areas in Lower Austria as the ceramics of the same subgroup occur at several, often relatively distant sites (*Figure 162*). This would indicate that the consumption areas of the different production units were similarly large, at least no significant differences in distribution can be identified based on the investigated samples.

Ceramics of 'Graphite D' differ in many ways from the other Graphite subgroups, the main difference being the lower graphite content of the 'Graphite D' samples. Their distribution is also different and limited to the Erlauf Valley based on the investigated ceramic material. Therefore, they may have been the local/regional products of workshops/households in the Erlauf Valley or in its vicinity.

Summary

The studied ceramics were investigated from different perspectives in order to gain information about the organisation of pottery production. The scale of production cannot be reliably identified in many cases (Carbonate group, Diorite group and Graphite group), but there are cases where a larger-scale production may be hypothesised carried out potentially by households (8th–9th-century samples of the Granitoid group) or workshops (subgroup 'Granitoid A3'). Some petrographic groups show some level of standardisation (subgroups 'Granitoid A3' and 'Granitoid B3', Carbonate group and subgroup 'Diorite A'), while others seem to represent non-standardised production (8th–9th-century samples of the Granitoid group, Amphibole group and Graphite group).

The production of graphite-free ceramics was possibly uncontrolled, while graphite-containing ceramics raise the possibility of control over production and/or distribution. Specialisation of production is not likely in some cases (8th–9th-century samples of the Granitoid group and Amphibole group), it cannot be evaluated in others (subgroups 'Granitoid A3' and 'Granitoid B3', Carbonate group and Diorite group), while it seems to be an option concerning graphite-containing ceramics. If modes of production are compared to those defined by Peacock, they can be likened to production modes between 'household industry' and 'individual workshops',

some groups being closer to household industry (8th–9th-century subgroups of the Granitoid group and Amphibole group) while the others resembling more individual workshops (subgroups 'Granitoid A3' and 'Granitoid B3', Carbonate group, subgroup 'Diorite A' and Graphite group).

As for the number of the production units, it is possible that the samples dated within the 1st–5th centuries and the samples within the 6th–7th centuries were made by one or two units, those from the 8th–9th centuries by at least four-five units and the samples of the Graphite group by several units (10–20?).

The 1st–9th-century vessels originating from the Erlauf Valley and those belonging to subgroup 'Graphite D' were probably made locally/regionally in the Valley or its close vicinity. Most of the graphite-containing ceramics from Lower Austria and Vienna might have been supra-regional products.

5.6 Technological continuity and change in pottery production and socio-political processes in early medieval Lower Austria

The production technologies of the different ceramic groups have been analysed and some elements of the manufacturing process could be reconstructed building on the results of the multi-analytical approach used in this thesis (Section 5.4). Now it is time to compare these technologies over space and time, and investigate whether continuity and changes can be detected in pottery production in Lower Austria. Furthermore, the question of how technological changes are linked with historical events and processes in the study region and period is also addressed.

5.6.1 Technological choices, tradition and innovation in pottery production

Technological choices are detectable through the examination of the different steps of the *chaîne opératoire*. The comparison of these steps can shed light on how similar or different technological choices were within a period or region. Repeated conscious or unconscious choices lead to the formation of technological traditions, while different choices induce technological change and may result in the emergence of innovations (Section 2.5.1). The ceramics from Lower Austria are examined from these perspectives in this section both diachronically and synchronically.

Continuity and change in pottery production technologies in Lower Austria

In the following sections, the ceramic groups are compared diachronically to explore whether any changes can be detected in raw material use and processing, forming and decorative techniques as well as firing between the 1st and 12th centuries. Special emphasis is placed on the appearance of graphite in pottery pastes in the 8th/9th centuries and the potential reasons of using this raw material for vessel making.

Raw materials

1st to 9th century ceramics

Investigating the raw material selection in the Erlauf Valley, the inclusions of the ceramics of all periods are consistent with different rock types of the Bohemian Massif. (The carbonate rock fragments of the four 6th–7th-century samples could also have an origin in the Eastern Alps.) The repeated exploitation of raw materials in the northern part and north of the Erlauf Valley

might suggest a continuity in resource use or the rediscovering of raw material sources. It is best illustrated by the Granitoid group, samples of which are of the same raw materials (as far as the inclusions are concerned), and some of them originate from the Roman/late Roman period (1st–5th centuries), while the rest of them is dated to the 8th–9th centuries. It would be interesting to know the reasons behind these technological choices, which led to the use of the same granite fragments (or residual clay) in the two periods in this particular case, or generally why people selected raw materials over several centuries that can be connected to one geological unit, the Bohemian Massif, which is largely outside of the area where the studied potsherds were found.

At the present stage of research, there is no clear indication why the raw materials of the Bohemian Massif were this popular, but some aspects may help understand the reasons behind this consistent technological choice. The Massif provided suitable raw materials for ceramic making, which were probably easily available as surface deposits based on the weathered state of minerals in most of the samples. The closeness of the raw materials of the Massif either as outcrops or as bedrock in the northern part of the Erlauf Valley (see Section 5.5 above) could also increase the preference of these sources. Additionally, the presence of residual clays originating from eroded rocks of the Massif could determine raw material choice. These residual clays likely needed no tempering or preparation (as it can be hypothesised in the case of several 8th–9th-century samples of the Granitoid group and Amphibole group) and this way ceramic making could be easier.

Examining the question from another perspective, it is interesting to consider why people used vessels made from the raw materials of the Bohemian Massif when more local clayey deposits were also available based on the soil map of Austria.[91] As suggested in Section 5.5, the rocks of the Massif are very close to the surface in the northern part of the Erlauf Valley, thus it is quite possible that these raw materials were obtainable closer than the more distant outcrops of the Massif. If, however, the raw materials originate from the outcrops, it might be that the local clays/loams were too calcareous to be suitable for ceramic making without special care. The soil map could support this possibility as calcareous soils were recorded from several locations in the vicinity of the archaeological sites of the samples. It must be noted, however, that non-calcareous clayey soils are also present at each site based on the soil map, which also indicates

[91] https://bodenkarte.at/ (accessed on 02/03/2021)

that the soil compositions are rather variable in the Erlauf Valley. At the same time, this variability could also be associated with unpredictability by the past communities of practice and thus could be another cause of avoiding these deposits. In addition to practical reasons, political factors and landowners could also have an effect on the preference/availability of raw materials of the Bohemian Massif by encouraging or denying access to natural resources.

Another potential source area of raw materials could be the Eastern Alps. However, carbonate-rich rocks, such as those of the Eastern Alps in the vicinity of the Erlauf Valley, need more attention throughout the technological process when used as temper; especially firing adjustments are critical to prevent lime spalling. This might be one of the reasons why the raw materials available in the Eastern Alps were less frequently used based on the investigated ceramic material. At the same time, carbonate rocks are used as temper in 6th and 7th century samples (Carbonate group), which along with other carbonate-containing early medieval ceramics in Lower Austria (see Section 5.7) suggest rather a chronological distribution and thus a different technology and tradition of the communities of practice of these centuries from those of the 8th–9th-centuries.

Graphite-containing ceramics and innovation

In the case of the graphite-containing samples from the 9th to 12th centuries found in the Erlauf Valley and other parts of Lower Austria, the consistent and deliberate choice of this special graphite-rich raw material of the Bohemian Massif can be followed throughout these centuries. While graphite-containing ceramics seem similar in external attributes, they are rather heterogeneous in mineralogical composition, which show that a range of different deposits were used within the Massif.

The use of the graphite as pottery raw material can be seen as an innovation in the early Middle Ages. Graphite-containing ware, however, is not without antecedents in Central Europe. Graphite-containing and graphite-coated ceramics were already produced in prehistoric times, in the Neolithic and later in the Hallstatt and La Tène periods (Dostál 1998, 67; Trebsche 2011, 454). In the Middle Ages, their existence can be proven from the 9th century in Lower Austria, but there are also traces which might permit the dating of their earliest examples to the 8th century (Scharrer-Liška 2007, 19). Graphite-containing ceramics thus reappear following a large chronological gap (of about eight centuries) after their Iron Age use, which makes it very unlikely to suppose the continuity of technological knowledge

between the two periods and makes graphite a unique and novel choice of raw material in the early Middle Ages.

The questions of why people started using graphite in the 8th/9th centuries in ceramic making, what motives led to the rediscovery of this raw material are most interesting. Although there are not enough sources (either historical or archaeological) yet to understand fully the reasons behind this technological innovation, some factors may be mentioned that probably contributed to the spreading of this type of ware.

One of the most probable reasons for producing graphite-containing pottery is the ability of graphite to advantageously change the physical-chemical properties of the vessels. It has been suggested that graphite-containing ceramics have a better resistance to temperature changes and mechanical stress, thermal conductivity, refractoriness, impermeability to liquids and resistance to chemical abrasion than pottery without graphite (Duma and Ravasz 1976; Martinón-Torres and Rehren 2005, 142; Scharrer-Liška 2007, 20; Kreiter et al. 2013, 173). It is not clear how early these properties were recognised and whether they had any importance when making the first graphite-containing pots, but it is certain that they were recognised eventually, which is proven by the popularity of its late medieval version (so-called Eisentonware) and crucibles of graphite-containing clay (Felgenhauer-Schmiedt 1998, 203; Scharrer-Liška 2007, 20, 70). These vessels might have been produced as ordinary cooking or storage vessels at the beginning and it is likely that the reason for producing this type of ware had shifted towards the practicality of graphite within these ceramics over time (Scharrer-Liška 2007, 20).

Another reason that might have induced the production and spreading of graphite-containing ceramics is connected to special functions. It is possible that they were made as containers for the transportation, storage or production of specific type of food or substances. For example, it was suggested that graphite-containing ceramics were used for the production of paints, acids and alkalis, boiling poisons or salt transportation and storage (Kolenda 1998, 27 with further references). However, these are only guesses at the moment, as scientific research of residues would be needed to have a better understanding of the role of these vessels.

The appearance of graphite-containing ceramics might have had an aesthetic reason as well. Graphite-rich vessels looked very different from graphite-free ware exhibiting a shiny grey surface which could have induced symbolism and the special treatment of these vessels (see

also Kreiter et al. 2013, 176). It could also be that potters wanted to reach a similar appearance to the potentially more 'precious' metal vessels. (This possibility was raised for example in the case of Late Bronze Age graphite-coated ceramics: Kreiter et al. 2014, 130.) Although there is nothing known about the graphite-containing pottery's association with prestige items or its potential symbolic meaning, it could have been exhibited as a wealth or identity marker especially when imported further from its source area and seen as a curiosity (e.g. in Hungary; Holl 1963, 343). It seems that this option was unlikely in the vicinity of the graphite deposits as graphite-containing ceramics originate from many different contexts (including rural, urban and castle) and they do not appear to be linked to higher status or wealthy social groups (Scharrer-Liška 2007, 74–75). Thus, in this case, no signs so far refer to the possibility that the appearance of this innovation had been influenced by social factors or intentions to reproduce social hierarchy (Schiffer 2011, 43–54).

There might have been other, rather atypical reasons that could contribute to the rediscovery of the graphite-containing pottery. It seems possible that the suitability of graphitic clay for ceramic making or the suitability of the graphite as a temper were forgotten after the Iron Age and graphite or graphitic clay were not considered as potential pottery raw materials in the early Middle Ages. It might have been that people in the 8th/9th centuries discovered sherds of graphite-containing ceramics from previous archaeological ages (e.g. during ploughing), and this led to experimenting with graphitic raw materials and the production of the first medieval graphite-containing vessels.

It is also interesting, that graphite-containing ceramics could reach such a popularity against some of its properties that could be considered as drawbacks. Vessels that are rich in graphite can stain the hand which is due to the relatively soft nature of the graphite (see also Scharrer-Liška 2007, 20). Firstly, this could give a feeling of dirtiness; the popularity of these ceramics, however, shows that people did not bother touching and using these vessels. Of course these things were probably not perceived by people in the past in the same way as they are now, when ideas about cleanliness and hygiene were different. Secondly and more importantly, a small amount of graphite could have been mixed into the food or liquids that were stored in these vessels, not to mention the heating or boiling of food in these pots (see also Kreiter et al. 2013, 176). From this perspective, it would seem reasonable that when these ceramics could be associated with food and drinks, they were more likely used for storing than heating. This could also be supported by the possibility that if these vessels were repeatedly used over

oxidising fire, their graphite-content could gradually burn out, which may cause the disintegration of the pot (Martinón-Torres and Rehren 2006, 520; Kreiter et al. 2013, 175–176). In any case, it seems that these constraints were not enough to hold back the popularity and spreading of graphite-containing ware.

As mentioned earlier, graphite-containing ceramics appeared in the vicinity of graphite deposits first, and gradually they became widespread in Central Europe (Section 5.3; Scharrer-Liška 2007, 68–70). Two processes may be distinguished here which contributed to the spreading of this ware: the first is when finished products travel, which is a topic of trade/exchange mechanisms. The second process, however, includes the transportation of raw materials to a production unit located farther from the graphite deposits as it was observed at some archaeological sites (Section 5.5; Scharrer-Liška 2007, 71). The movement of raw materials implied the diffusion of knowledge and technologies as well, thus this process is related to innovation. It is possible that the adoption of this technology did not cause much difficulty to pottery producing communities of practice as most part of the production process was similar to what they were used to follow during manufacturing graphite-free vessels (e.g. same forming technology: slow wheel turning, similar decoration techniques such as incised wavy lines). At the same time, techniques had to be adjusted to this new type of material and previously not used methods had to be introduced (e.g. reducing firing atmosphere). All in all, pottery workshops that previously had not been producing graphite-containing ware had a firm basis to adopt this innovation, and this compatibility of the technology of graphite-containing ceramics with pre-existing practices likely enhanced the diffusion and adoption of this innovation (Lemonnier 1993, 12–16; Bernbeck and Burmeister 2017).

Raw material processing

The preparation of the raw materials of the ceramics exhibits some differences throughout the centuries.

All samples analysed from the 1st–5th and 6th–7th centuries are of carefully prepared, tempered clay. The 6th–7th-century samples containing calcite suggest a high level of technological knowledge and skills because, if treated carelessly, carbonate rock fragments can cause the cracking of pots as mentioned above.

With the exception of one subgroup ('Diorite A'), the 8th–9th-century samples were probably not tempered but made of an inclusion-rich residual clay, which suggest that the practice of tempering might have been occasional in the 8th–9th centuries in the Erlauf Valley.

The difference of the raw material preparation techniques between the two chronological groups of the Granitoid group (1st–5th and 8th–9th centuries) raises an interesting question. The producers of the Roman/late Roman period chose to temper their ceramics, yet the 8th–9th-century samples showed that vessels can be made from the same raw materials without tempering. There are no clear answers to the question of why they chose the seemingly harder way. They might have not found the residual clay sources, or there might have been a more complex reason of this choice originating from tradition or the 'right way' of vessel making (Sillar and Tite 2000, 10). At the same time, it is also interesting how people in the 8th–9th centuries found these raw material sources, whether there were any precedents or it was only a matter of experimenting with raw materials. In any case, 1st–7th-century ceramics show a more sophisticated technological knowledge about raw material preparation than those from the 8th–9th centuries based on the investigated material.

In the case of the graphite-containing samples, some signs (e.g. subgroup 'Graphite D') indicate that tempering was present in the 9th–12th centuries as well and suggest that graphite itself or a graphite-rich residual clay was added as temper to a graphite-free clay.

Vessel forming and decoration

As for the forming techniques, the traces on potsherds of all investigated periods indicate the use of the slow wheel. Slow wheel turning was thus continuously present in the Erlauf Valley throughout the centuries.

Continuity in the application of the same decoration elements is also detectable between the 1st and 9th centuries in the Erlauf Valley, which is shown by parallel wavy lines and parallel lines incised in the wall of vessels of each period. With the appearance of the new pottery type, the graphite-containing ceramics, new decoration elements also appeared such as the raised band, and, at the same time, traditional choices of decoration motifs are also present on these pots.

Firing

As for firing, significant differences in maximum firing temperatures and firing atmosphere are hardly detectable among the ceramics from the 1st–9th centuries. Their colour changes refer to

a mixed, mainly oxidising atmosphere and maximum temperatures below *c.* 800 °C. In the case of the Carbonate group samples of the 6th–7th centuries, the maximum firing temperature might have not exceeded 700/750 °C.

The graphite-containing samples of the 9th–12th centuries, except 'Graphite D', were fired under reducing conditions, probably below *c.* 750 °C. It is therefore apparent, that the production of this special type of ware required the use of specific firing techniques. At the same time, there were also vessels with a lower graphite content ('Graphite D'), which were fired as the graphite-free ware (mixed atmosphere, < *c.* 800 °C).

Practices in pottery production in the 8th–9th centuries

Now that a diachronic comparison of the different chronological groups has been outlined, it is worth considering the possibilities for synchronic comparison of ceramics from the same period. The 8th–9th-century ceramics of the studied assemblage provide a basis for this, as they are numerous and limited to a relatively short period and a relatively small area (Erlauf Valley). The three 8th–9th-century ceramic groups (8th–9th-century Granitoid subgroups, Amphibole group and Diorite group) and 8th–9th-century individual samples show the use of at least five different raw materials (Section 5.2), all of which can be linked to the rocks of the Bohemian Massif and two of which might have been adjacent (providing raw materials for the Amphibole and Diorite groups). The preparation, forming, decorating and firing techniques seem quite similar in the different groups, which suggest that communities of practice that produced 8th–9th-century ceramics shared similar traditions and technological knowledge about ceramic making.

One subgroup, 'Diorite A', however, slightly stands out from the rest and is special in many ways. It might be the only group, which is of tempered clay in the 8th–9th centuries. Furthermore, it is interesting that none of the vessels of this group are decorated. Thus 'Diorite A' is clearly separated from the other petrographic groups of the 8th–9th-century by both microscopic and macroscopic features. While the 'invisible' (microscopic) differences might have been the result of subconscious decisions originating from custom or tradition (where to collect raw materials, tempering the clay), the choice of not decorating their vessels, which is a visible mark, might express that the producer(s) wanted to differentiate themselves from other communities of practice since it is obvious from the investigated material that the application of rich decoration was common in the 8th–9th centuries. At the same time, they also

used similar forming and firing techniques to those used for making the other 8th–9th-century ceramics, which indicate that they had technological knowledge in common with other pottery producers.

5.6.2 Changing pottery technology – changing society?

Technologies, as they are embedded in society, characterise communities that they are parts of. Technological changes thus often induce social changes and *vice versa* (Section 2.5.1). In this section, the historical context of pottery technology is explored in early medieval Lower Austria and the topic of whether there is any correlation between socio-political and technological changes is assessed in this ever-changing borderland.

Starting with the late Roman period, Roman structures had likely been existing south of the Danube until the end of the 5th century, when Noricum, the province covering the southern/south-western part of present-day Lower Austria, was abandoned by Odoacer (Section 2.1.2). The late antique society of Noricum was mainly agrarian including at least an upper class (*honestiores*) and a lower class (*humiliores*; Wickham 2005, 259; Eichert 2016, 200). It probably consisted of different population groups such as Roman people, Romanised descendants of indigenous Celtic tribes, and 'barbarian' groups that settled into Roman territory (Scherrer 2015, 47; Stuppner 2015, 124).

Regarding late antique ceramic technology, wheel-thrown and slow wheel-turned vessels both occurred within the borders of the Empire (e.g. Herold 2014) and the potters' wheel was also taken up by Germanic groups living outside of the *limes* on Roman influence (Adler 1977a, 53–54). Based on the results of this thesis, the ceramic material dated to this period is characterised by the careful preparation of the raw materials and expertise. It shows that past potters had a clear idea about how to manipulate raw materials, how to achieve a relatively pure clay and what temper should be added and in what amount. This suggests that communities of practice had a great knowledge about material properties and the right ways of doing vessels, and they had the tools and methods (sieve, levigation) to achieve proficiency in pottery making. It is interesting, however, that this proficiency is 'invisible' as communities of practice in the Erlauf Valley producing the studied ceramics did not adopt the potter's wheel, which could enhance the visual qualities of the vessels even more. It is less likely that they were uninformed about the existence of the potters' wheel since it was adopted beyond

Roman borders. Rather, this might suggest an adherence to local traditions, roots of which might have predated Roman expansion.

It is interesting here, that Roman/late Roman ceramics investigated in this thesis potentially originate from workshops located in the Bohemian Massif (Section 5.5), as this geological unit was situated outside of the Roman *limes*. This, along with historical evidence of trade and exchange with the *barbaricum* (Section 2.5.2), could indicate that although the *limes* represented a static political and military border, economic boundaries were porous and fluid.

After the abandonment of Noricum in 488, the next couple of years were characterised by the gradual decline of the Roman rule (Section 2.1.2). Political structures slowly collapsed, and the area of the former province became 'no man's land' for a while. Different Germanic population groups appeared mainly north but also south of the Danube, whose traces of stay can be followed for a short time only as most of them migrated to other areas (Sections 2.1.3 and 2.2.2). It is likely that the majority of the Roman period population living south of the Danube remained in place (Breibert 2005, 420, 425; Eichert 2016, 200). At the same time, there are some indications of some members of the late antique elite, whose subsistence depended on Roman laws, taxes, state administration and organisation, leaving their homeland and migrating to Italy, (Eugippius 44; Eichert 2016, 199–200).

It seems that the level of technological expertise, the level of skill and knowledge involved in pottery making remained unchanged. The investigated 6th–7th-century samples clearly show proficiency in 'producing' a very clear clay free of large inclusions as well as proficiency in tempering. The fact that calcite temper was used proves a high level of expertise because of the difficulties that its unstable nature causes during firing (Section 5.5). At the same time, difference can be detected in the type of temper used compared to the Roman period. The investigation included, however, only a small number of ceramics from the two periods, and other examples show that calcite temper was also present in the late Roman period (see Section 5.7 below).

Overall, no significant change can be traced in pottery technology before and after the collapse of the Roman rule in the area of Lower Austria based on the studied samples. Continuity is exhibited in preparation methods, forming techniques, decoration, and firing characteristics of the sherds. It seems that communities of practice had a similar level of technological

knowledge, skills and toolkit in both periods. The presence of the carbonate temper seems novel in the Erlauf Valley, but this can easily be the result of sampling.

By the 7th century, the territory of Lower Austria likely became the north-western borderland of the Avar Khaganate, while the territories west of it (and west of the River Enns) were likely under Bavarian control. As historical and archaeological evidence are scarce (Sections 2.1.4 and 2.2.3), little is known about the population living in the Erlauf Valley and Lower Austria in the 7th and 8th centuries. The immigration of Slavic groups from the south-east can be hypothesised in the 7th century (or maybe earlier, see Section 2.1.4). The continuity of the existing population including late antique and Germanic groups is also likely (Section 2.2.3). The possibility of whether political changes in the 7th century bring change in pottery technology as well or not, cannot be evaluated, because there are no samples that can be dated to the 7th century only.

There are many pieces of ceramics among the studied samples, however, that can be dated to the 8th–9th centuries. Technological continuity is exhibited compared to the 6th–7th centuries in resource use, forming techniques, decorative motifs and firing techniques. At the same time, most of them show a clear difference compared to the previous periods in terms of paste preparation. However, this difference is only perceivable through scientific techniques (thin section analysis), it is not evident from macroscopic characteristics. It seems that less care is taken to achieve a fine pure clay and add temper to it (an exception is probably subgroup 'Diorite A') as residual clays are used practically in the state as they were found. Members of these communities of practice realised that the residual clay of the Bohemian Massif can be used for vessel making without tempering and it was certainly an easier way of pottery production, although other preparation techniques such as kneading, sorting out large inclusions, could not be omitted from the production process. This way of pottery preparation might indicate a lower technological level than that of the previous centuries.

Whether this change was connected to the appearance of Slavic groups or it was the result of an internal development, it cannot be decided. If these ceramics originate from the 9th century, their appearance could also be parallel to the Carolingian expansion. But most likely the emergence of these 8th–9th-century untempered vessels can be seen as an internal development as all the other methods used during manufacture (forming techniques, decoration, mixed firing atmosphere) are consistent with those of the previous periods.

The early 9th century brought change in the history of Lower Austria as with the defeat of the Avars by Charlemagne, Carolingian expansion had begun, which included probably the Erlauf Valley and other Lower Austrian territories south of the Danube (Section 2.1.5). With the establishment of the Avar March between the Enns and Pannonia, this region (the Bavarian Eastland) became a borderland of Bavaria and the Carolingian Empire. As in other parts of the Empire, society was likely organised based on feudal principles in the territory of Lower Austria as well (Wolfram 1999, 296). Manorialism gradually developed by the 10th century, which, besides agricultural activities, possibly included the organisation of craft making and trade/exchange until the late 12th century (Sandgruber 1995, 24; Adam 1996, 179; Scharrer-Liška 2007, 10–13). Historical evidence suggests that the Austrian Danube region might have had an important role in trading salt, food and cattle as well as slaves to Bavaria and the Carolingian Empire (Mitterauer 1969, 115; Scharrer-Liška 2007, 12–13), which highlights one of the frequent benefits of borderlands: the possibility of exploitation of resources (Parker 2006, 83).

Borderlands often provided stages for innovations because of the multiple influences (cultural, political, economic, etc.) present in these areas (Mullin 2011a, 6; Rice 2015, 52–54). This is exactly the case in the late 8th/9th centuries in this eastern borderland of the Carolingian Empire, when there was a significant change in pottery practices as a new vessel type appeared: the graphite-containing ceramics. Some of them look very similar to graphite-free pottery (subgroup 'Graphite D', containing few graphite grains), but many of them represent a totally new vessel type with shiny dark grey colour (other subgroups of the Graphite group, containing abundant graphite). It could be possible that political processes induced the development of this innovation, such as the Carolingian expansion. Frankish influence, together with other influences, can also be studied in graves in Lower Austria, which could be conveyed by members of the elite, military as well as Christian missionaries arriving in the area (Sections 2.2.3 and 2.1.6). However, although graphite deposits are also found in south-eastern Germany, for now, it is unlikely that Charlemagne's campaigns would bring this technology into the territory of Lower Austria, as Lower Austria seems to be the core area of these ceramics and their spreading in the opposite direction is indicated by the published finds (Scharrer-Liška 2007, 19, 67, 70).

As mentioned, it is possible that centralised control was exercised over graphite-containing pottery production and/or distribution (Section 5.5). One of such power centres overlooking

pottery production could have been the fortified settlement of Thunau am Kamp, as it was situated in the Bohemian Massif near the graphite deposits. It might have been the centre of Joseph, a Slavic prince mentioned in the historical sources in the 9th–10th century (Sections 2.1.5 and 2.2.3). Clear evidence of ceramic manufacture, however, has not been excavated here apart from few raw graphite pieces, which could potentially suggest pottery production (Dell'mour 2001, 72, 90). Based on the heterogeneity of the graphite-containing ceramics, it is possible that if production/distribution was controlled, it was controlled by not one, but several manorial centres of the elite located at different parts of the Bohemian Massif near the graphite deposits (Section 5.5; Felgenhauer-Schmiedt 1998, 204; Scharrer-Liška 2007, 150).

From the beginning of the 10th century until 955 the territory of Lower Austria came under Hungarian rule, but it is probable that the existing settlement system and population largely remained the same except for the most south-eastern part of the territory (Section 2.5.2). After 955, the border was finally fixed around the River Leitha (south-eastern edge of Lower Austria) between Bavaria (as part of the East Frankish Kingdom) and the Hungarians, and soon the Austrian March was established belonging to the Dutchy of Bavaria (Section 2.1.8). With the rule of the Babenberg family from the last quarter of the 10th century, this area started to be consolidated, which is shown by the foundation of new settlements and monasteries (Section 2.1.8). This period of stability is also reflected in the spreading of graphite-containing pottery.

The distribution of graphite-containing ceramics in the 9th–12th centuries shows that this type of pottery was somehow special: it had the ability to cross borders. It seems that the earliest (8th/9th centuries) graphite-containing ceramics were made close to the graphite deposits in the Bavarian Eastland and territories located north of it (Felgenhauer-Schmiedt 1998, 203). They soon (from the mid-9th century, or potentially earlier) appeared slightly farther from the graphite deposits in Moravian territories, which could indicate economic connections between the Bavarian Eastland and the Moravians (Dostál 1998, 84; Scharrer-Liška 2007, 30). Graphite-containing pottery was also present in Hungarian territories from the 9th or 10th centuries (Merva 2016, 535) and in Bohemia from the 10th century at the latest (Scharrer-Liška 2007, 31), which all prove that this type of ware did not stop at the borders of the Bavarian Eastland and those of the subsequent Austrian March. Graphite-containing ceramics from Silesia (present day easternmost Czechia and south-westernmost Poland) from the turn of the 12th and 13th century indicate that not only trade/exchange connections existed between the territories

with graphite deposits and those located further from deposits, but raw materials and technological knowledge had also been transferred and mixed with local traditions (Kolenda 1998, 21–25). The fact that these vessels became this popular in a short time is very likely linked to the reasons of their appearance (Section 5.6.1). People in the past could realise that they were better than their local vessels regarding some practical aspects (longer use life because of better thermal shock resistance, less permeability to liquids), which could also be supplemented by aesthetic or symbolic factors (expression of identity, wealth?).

While graphite-containing ceramics were crossing borders, graphite-free ceramics studied in this thesis were likely restricted to the Erlauf Valley. It is not surprising as it was probably not worth transporting ceramics much further when other clay sources were available at different parts of Lower Austria, from which similar quality pottery could be produced (see Section 5.7 below). As people living in other regions could obtain similar utilitarian ceramics closer, there would have been no market for Erlauf Valley ware much further than the Valley itself. Not only local ware did not cross borders, but there is no indication in the investigated material that imported goods were used by people living in the Valley. Graphite-containing ceramics, however, are present in the Valley, some of which might indicate regional economic connections. Those that contain fewer grains of graphite and resemble other utilitarian ceramics fired in a mixed/oxidising atmosphere of the Valley (subgroup 'Graphite D') were probably made locally (Section 5.5). Those, however, that are different in appearance (shiny grey surface) due to their abundant graphite-content and reducing firing atmosphere might have been transported from potentially specialised workshops sitting farther in the Bohemian Massif. Although it would be an exaggeration to term these ceramics as imported goods because of the relative closeness of the Erlauf Valley to graphite deposits of the Bohemian Massif, but still, they could be more than 'local' and could originate from neighbouring regions of the Erlauf Valley. The use of mainly locally produced ware and the lack of 'exotic' pottery could be true for other microregions of Lower Austria as shown by some studies discussed in the next subchapter (Section 5.7).

5.6.3 Summary

The investigation of patterns of technological continuity and change and their comparison with socio-historical events and processes during the late Roman period and the early Middle Ages resulted in interesting conclusions. On the one hand, the choice of the same raw materials (1st–5th and 8th–9th-century ceramics of the Granitoid group) and the general preference of

deposits from the Bohemian Massif as well as similar vessel forming, decoration and firing techniques could indicate technological and economic continuity. This, however, cannot be firmly stated because of the small number of the studied samples and their wide dating. Nevertheless, it is clear that communities of practice of each period inherited techniques from the previous periods, which they could keep, change or develop.

On the other hand, some elements of the pottery producing process show changes throughout the centuries. Various types of Bohemian Massif materials are present in the studied ceramics suggesting the use of various raw material sources, which indicate that ceramic manufacturing communities had their own idea about what deposits should be used. Different technological choices were made regarding raw material preparation as well. The samples from the 1st–7th centuries are consistently tempered, while the majority of the ceramics of the 8th–9th centuries are made of untempered inclusion-rich residual clays. The innovation of graphite-containing ceramics brought novelty in many ways in the 8th/9th centuries with the use of a new raw material, decoration elements and firing technique.

The comparison of techniques clearly shows the presence of different communities of practice within the 8th and 9th centuries, which used different raw material sources, paste preparation and vessel decoration techniques. At the same time, they had a shared knowledge about pottery manufacturing as forming methods and firing techniques suggest.

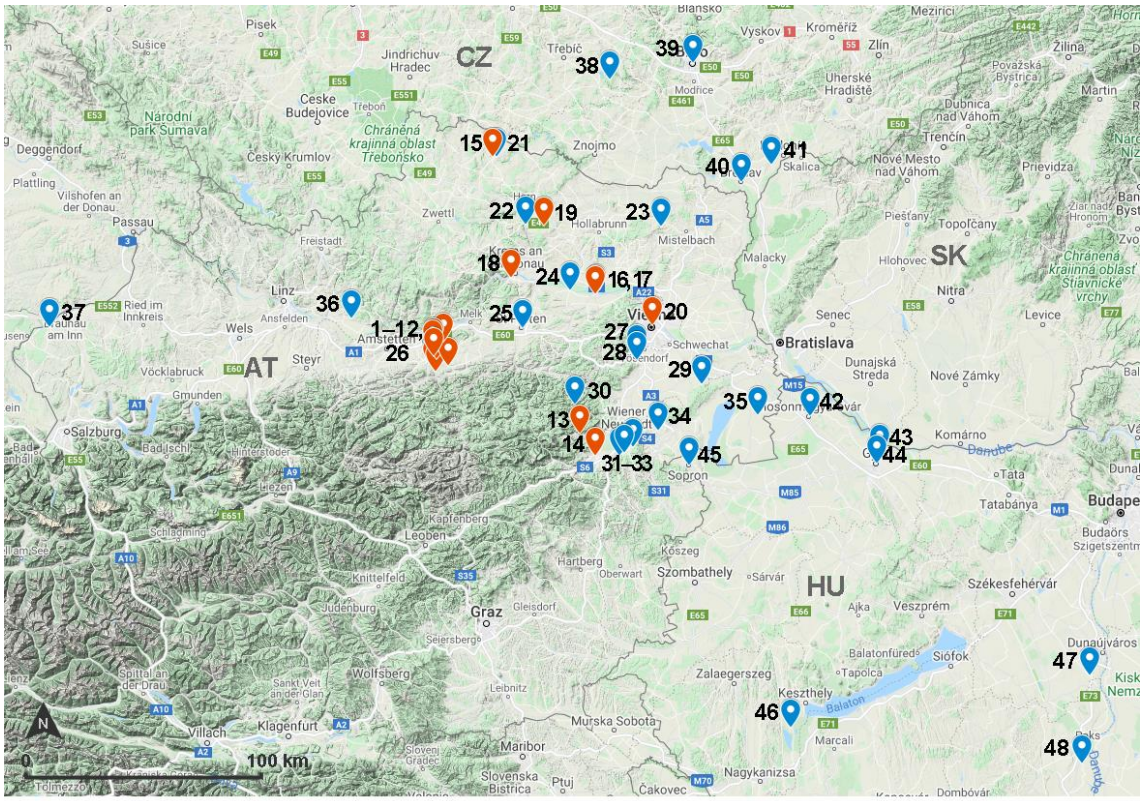
The placement of the trends in pottery production into historical context shows that changes in political systems may or may not coincide with changes in pottery technology. It seems that against the great changes after the decline of the Western Roman Empire, which probably included some degree of emigration from the study area, the level of skilfulness and technological knowledge did not decrease in the 6th–7th centuries.

At the same time, change can be registered in raw material preparation in the 8th–9th centuries, while other techniques remain similar to the previous centuries. Also, graphite-containing pottery appears at this time, whose border-crossing nature could be an indication of stable economic relationships between early medieval political entities (between the study area as part of the Bavarian Eastland, later Austrian March and Moravians, Bohemians, Hungarians). These changes could be linked to changes of population (Slavic immigration), political spheres (being an Avar borderland and later a Carolingian-Bavarian borderland), or can be seen as an internal development, but it must be emphasised that there is not enough

historical and archaeological evidence yet, which could indisputably support any of these hypotheses.

5.7 Comparison of the studied ceramics with other ceramics from Lower Austria and the Central European region

Following the discussion of different aspects of ceramic technology and production within the studied ceramic assemblage, now it is time to take a broader view and examine how similar/different the investigated ceramic material is compared to other vessels of the region. The comparison will be carried out in three chronological groups: Roman/late Roman ceramics (1st–5th centuries), early medieval ceramics (6th–9th centuries) and graphite-containing ceramics (9th–12th centuries). At the end of this section, the chemical composition of the studied ceramics is discussed in comparison with other contemporary ceramics from Central Europe. The archaeological sites mentioned in the text are presented in *Figure 164*.



Investigated sites
1–12. Sites in the Erlauf Valley
13. Hausstein near Grünbach am Schneeberg
14. Ternitz, Dunkelstein
15. Sand
16. Tulln, Wassergasse
17. Tulln, Hauptplatz
18. Mautern, Römerhalle
19. Sachsendorf
20. Vienna, Ruprechtsplatz

Comparison sites
21. Castle Raabs
22. Thunau am Kamp
23. Michelstetten
24. Zwentendorf
25. St. Pölten
26. Purgstall-Schauboden
27. Brunn am Gebirge
28. Mödling
29. Sommerein
30. Muggendorf
31. Frohsdorf
32. Erlach
33. Pitten
34. Zillingtal
35. Halbturn
36. Auhof
37. Ratzlburg
38. Kramolín-Burgwall
39. Brno-Líšeň
40. Břeclav-Pohansko
41. Mikulčice
42. Moson-Királydomb
43. Bácsa-Szent Vid Hill
44. Győr-Káptalandomb
45. Sopron
46. Zalavár
47. Daruszentmiklós
48. Dunaszentgyörgy

Figure 164. The location of the sites in Lower Austria studied in this thesis (orange markers, 1–20) and the sites included in the comparison (blue markers, 21–48) (Base map: Google Maps)

Roman and late antique pottery (1st–5th centuries)

The studied ceramic material from the 1st–5th centuries has similar characteristics to other Roman and late antique ceramics published from Halbturn (Herold 2014) and Michelstetten (Herold 2016). The use of local raw materials and the preparation of the paste by tempering are likely in all three cases (Sections 5.2 and 5.4.1; Herold 2014, 671; Herold 2016, 279–283). While the Michelstetten samples are hand modelled and the majority of the Halbturn samples are wheel-thrown, there are some samples from Halbturn (Group 6), which were made on the slow wheel just as those from the Erlauf Valley (Section 5.4.2; Herold 2014, 665, 669; Herold 2016, 277). This group of the Halbturn ceramics has other similarities with the Erlauf Valley samples including their firing characteristics (mixed atmosphere) and the relatively small amount of temper added to the paste (*c.* 20% in Halbturn samples, 15–20% in Erlauf Valley samples; Sections 4.2.1 and 5.4.4; Herold 2014, 669, 685).

The pottery samples from the two comparison sites were associated with different categories of Peacock regarding the organisation of production. These include 'household production' (late antique samples from Michelstetten), 'household industry' (4th–5th-century slow wheel-turned ceramics from Halbturn (Group 6)), 'individual workshop' and 'nucleated workshop' (2nd–3rd-century and 4th–5th-century wheel-thrown ceramics from Halbturn; Herold 2014, 674; Herold 2016, 285). The Erlauf Valley samples, which could be products of similar units as 'household industries' or 'individual workshops' (Section 5.5), are not different from other sites in this respect.

Early medieval pottery (6th–9th centuries)

The 6th–7th century samples from the Erlauf Valley (Carbonate group) are special and represent high quality because of the use of calcite temper. Other early medieval examples of carbonate-tempered ceramics are known from Michelstetten (Herold 2016, 279–281), Brunn am Gebirge (Herold 2002a, 164; Sauer 2002, 179), Mödling (Herold 2002a, 165), Pitten and Sommerein (Herold 2009a, 349; Herold 2015a, 336: Tab. 1). Tempering with carbonate rocks was also present in the late Roman period in the area of present-day Lower Austria as shown by a sample from Pirotorto/Zwentendorf containing large calcite grains (Dell'mour 1989, 29: Abb. 13/1) and some samples from Michelstetten containing microcrystalline carbonates (Herold 2016, 279–281). This similarity might raise the idea of this type of tempering being a tradition surviving from the late Roman period into the 6th–7th centuries.

An interesting question is what archaeological sites in Lower Austria show about the transition between the late Roman period and early Middle Ages, whether the two periods exhibit different ceramic technologies or whether technological continuity is tangible. In the case of a settlement near Michelstetten, which was located north of the Roman Empire, different technological traits were pointed out between the late antique and early medieval ceramic finds regarding the preparation of the raw materials and firing techniques (Herold 2016, 285). A change is also perceptible between the 1st–5th-century and 6th–7th-century samples from the Erlauf Valley, but this is exhibited only by the use of different temper, otherwise preparation techniques (levigation/sieving and tempering), forming method, decoration and firing, and the level of technological knowledge in general were similar in the two periods (Section 5.6).

Practices of ceramic making in the 8th–9th-century Erlauf Valley are consistent with contemporary trends in raw material use, technology and production organisation as shown by analyses of ceramics from other sites in the region. As it was demonstrated in Section 5.2, the studied ceramics are very likely of local raw materials which was also the case in the majority of the pottery from Michelstetten (Herold 2016, 285), Brunn am Gebirge (Sauer 2002) and Zillingtal (Herold and Petschick 2003, 41; Herold 2010a, 40, 91, 94). At some sites (Thunau am Kamp (Dell'mour 2001, 99–107) and Brunn am Gebirge (Sauer 2002, 179)) a small amount of non-local ware was also identified.

Regarding raw material preparation, thin section analysis suggests that the majority of the studied 8th–9th-century samples (Granitoid and Amphibole group) was produced using residual clay without the addition of temper (Section 5.4.1). Ceramic analyses from the fortified hilltop settlement of Thunau am Kamp, located in the area of the Bohemian Massif, resulted in similar observations. There are three ceramic types here (Type B, C and D), which are particularly similar to the above-mentioned Erlauf Valley samples because they are all of residual clays from the surface of the Massif (Dell'mour 2001, 93–99, 104). Similarities are represented even in mineralogical composition between the Amphibole group of the Erlauf Valley and two samples from Thunau am Kamp (B3145 and B3171) as they all contain weathered fragments of amphibole-rich rocks (Dell'mour 2001, 102, 103: Bild 4). At the same time, some Erlauf Valley samples ('Diorite A') were probably tempered, and tempering was suggested in the case of ceramics from Michelstetten (Herold 2016, 285), Brunn am Gebirge (Herold 2002a, 164), Zillingtal (Herold 2010a, 91; Herold 2011b, 200), Frohsdorf, Pitten and Erlach (Herold 2015a, 336: Tab. 1).

As for the forming technique, the Erlauf Valley samples were made on the slow wheel (Section 5.4.2). This technique was commonly used for the making of ceramics found at other sites in the region such as Michelstetten (Herold 2016, 277), Brunn am Gebirge (Herold 2002a, 164), sites in the valley of the River Leitha (Herold 2009b, 113–118) and Zillingtal (Herold 2011b, 194). In addition, hand formed ceramics were also frequent in the early Middle Ages at the above-mentioned sites.

The decoration of the early medieval vessels is dominated by incised (parallel) lines and wavy lines in the Erlauf Valley (Section 5.4.3) as well as at other sites including Brunn am Gebirge (Herold 2002a, 164), Zillingtal (Herold 2011b, 196–197), Frohsdorf, Pitten and Erlach (Herold 2015a, 340).

The firing atmosphere of the vessels from the Erlauf Valley was mixed based on their inhomogeneous colour and they were fired at below 800 °C as suggested by vitrification and XRD analyses (Section 5.4.4). Similar observations were made about the colour of pots at other sites as well, based on which open/pit firing was assumed for ceramics from Thunau am Kamp (Dell'mour 2001, 71, 104) and Zillingtal (Herold 2011b, 200). Regarding maximum firing temperatures, 550–750 °C and slightly higher than 600 °C were suggested for ceramics from Thunau am Kamp (Dell'mour 2001, 71) and Zillingtal (Herold and Petschick 2003, 39; Herold 2010a, 94), respectively.

As discussed in Section 5.5, the results of the different methods could indicate that the studied ceramics were made in production units similar to 'household industry' and 'individual workshop' defined by Peacock (1982, 8–9). Slow wheel-turned vessels from Michelstetten (Herold 2016, 285) and Zillingtal (Herold 2010, 97–99) were also likened to a production form between these two organisation models.

There is a distinctive type of pottery in the 9th century, the so-called polished yellow pottery, which has been investigated by several archaeometric methods (Herold 2008a; Herold 2010b). The polished yellow pottery was found in power centres such as Thunau am Kamp (Lower Austria), Mikulčice (Czechia), Břeclav-Pohansko (Czechia) and Zalavár (Hungary) and represented the highest quality ceramics of its time. Although the forming method of this pottery type and that of the studied vessels is the same (slow wheel turning), the two groups are hardly comparable because of their different quality (fine-grained polished yellow pottery; coarse-grained Erlauf Valley vessels), form (polished yellow pottery: usually flasks; Erlauf Valley

ceramics: jars) and function (polished yellow pottery: probably drink serving/storing – Erlauf Valley ceramics: probably cooking/storing).

Graphite-containing pottery (9th–12th centuries)

Moving on to the graphite-containing pottery from the 9th–12th centuries, it can generally be stated that this type of pottery is quite heterogenous regarding inclusions not just in the case of the investigated vessels but other ceramics from the region as well (e.g. the analysis of seven samples from St. Pölten suggested seven different raw material sources, the analysis of 17 samples from Muggendorf suggested 13 different raw material sources; Sauer 2007, 94–95).[92] Although the variable mineralogical compositions reflect the use of numerous different raw material sources, some similarities are present between the studied graphite-containing samples and other samples from the region.

Most of the studied ceramics (subgroups 'Graphite A' and 'Graphite D') contain gneiss fragments as the host rock of graphite (Section 4.2.2). In samples from Thunau am Kamp (Dell'mour 2001, 82) and north-western Hungary (Bácsa-Szent Vid domb, Győr-Káptalandomb, Sopron and Moson-Királydomb; Szakmány and Bendő 2016, 544–546, 549–551, 556, 558) graphite also occurs with gneiss. Graphite-containing sillimanite gneiss fragments are present in ceramics from Hausstein, Sand and Tulln, Wassergasse ('Graphite A1', Section 4.2.2) as well as from Győr-Káptalandomb and Moson-Királydomb in north-western Hungary (Szakmány and Bendő 2016, 544–546, 556). Another group of graphite-containing samples under study includes graphite marble (subgroup 'Graphite C1', Section 4.2.2). This rock type is also present in ceramics from Thunau am Kamp (sample B 3329, Dell'mour 2001, 82), Castle Raabs (Sauer n.d.), St. Pölten, Muggendorf, Auhof (Sauer 2007, 83, 87–89, 91–93) and Győr-Káptalandomb (Szakmány and Bendő 2016, 547). These similarities exhibited in the rock fragments and heavy minerals, however, are not surprising as the raw materials of the studied vessels and the mentioned parallels are very likely from the same, graphite-containing unit (Variegated Group) of the Bohemian Massif (Section 5.2; Dell'mour 2001, 82, 87; Sauer n.d.; Sauer 2007, 94–95; Szakmány and Bendő 2016, 558–559).

[92] It is possible that the dating of the samples from St. Pölten and Muggendorf overlaps only partly with that of the graphite-containing ceramics studied in this thesis. The samples analysed by scientific techniques were chosen from large assemblages dated to the 10th–13th centuries in the case of St. Pölten and to the 11th–13/14th centuries in the case of Muggendorf (Scharrer-Liška 2007, 134, 148). A closer dating of the ceramics analysed by Sauer (2007) is not given in the publication.

The most common accessory minerals in the investigated samples are rutile, amphibole, garnet, sillimanite and kyanite (Section 4.2.2). These minerals were also detected in samples from the above-mentioned sites (Dell'mour 2001, 82; Sauer n.d.; Sauer 2007, 83–94; Szakmány and Bendő 2016, 544–558).[93] Nevertheless, some differences are also present between the inclusions of the ceramics investigated in this thesis and those of other graphite-containing vessels. For example, pyroxene (diopside) and tourmaline are not very frequent in the studied samples in contrast with the other sites. Scapolite is a common accessory mineral in several thin sections analysed in this thesis (Section 4.2.2), but not mentioned in the literature analysing ceramics from other sites in the region.

There are two graphite-containing ceramics from the Iron Age found at Purgstall-Schauboden (Sauer 1994, 244), which are mentioned here because their site is very close (1–2 km) to some Erlauf Valley sites where early medieval graphite-containing ceramics were found.[94] One of the Iron Age samples (SCHB1) contains graphite gneiss fragments similarly to the Erlauf Valley samples and, although the Iron Age sample have a larger variety of accessory minerals than the Erlauf Valley samples, amphibole, garnet and rutile are common in the ceramics of both periods. The other sample (SCHB2) is rich in graphite marble and diopside and comparable thus to the above-mentioned graphite marble-containing ceramics.

The identification of tempering or the use of a residual clay causes difficulty in the case of the studied graphite-containing vessels, although tempering might be hypothesised based on the characteristics of some samples (Section 5.4.1). Tempering was also suggested for graphite-containing samples from Thunau am Kamp (Dell'mour 2001, 82–83, 88) and north-western Hungary (Szakmány and Bendő 2016, 544–558). The inclusions, however, were described as natural components of the clay in vessels from St. Pölten, Muggendorf, Auhof and Ratzlburg (Sauer 2007, 83–94).

The studied vessels were made on the slow wheel based on macroscopic traces (Section 5.4.2). Slow wheel turning was also applied for the making of ceramics from Thunau am Kamp

[93] Similarities are also exhibited sometimes in mineral composition: niobium-rich rutile was detected in some samples from the Erlauf Valley (S31, S54 and S86) and from Hausstein (S102; see Appendix D.2) as well as in a sample from north-western Hungary (Győr-Káptalandomb; Szakmány and Bendő 2016, 546–547).

[94] These sites are Purgstall, Site 26 on the same, western bank of the Erlauf as Purgstall-Schauboden, and sites on the eastern bank of the river: Purgstall, 8th–9th-century cemetery, Purgstall, Site 10 and Hochrieß, Site 39.

(Dell'mour 2001, 82) and, besides hand forming, this technique is commonly observed at other early medieval ceramics of graphite-containing clay from Lower Austria (Felgenhauer-Schmiedt 1998, 201–203; Scharrer-Liška 2007, 35–36).

The decoration of the investigated ceramics and other vessels of the region are similar including incised (parallel) wavy lines, incised (parallel) lines, comb-impressed dots and raised band (Section 5.4.3; Felgenhauer-Schmiedt 1992, 65–66; Felgenhauer-Schmiedt 1998, 201–203; Dell'mour 2001, 79; Scharrer-Liška 2007, 36).

The maximum firing temperatures for the studied pieces of graphite-containing pottery are estimated at 700–800 °C or below based on the analyses carried out in this thesis and relevant literature (Section 5.4.4). Similar or slightly higher firing temperatures falling between 700 °C and 900 °C were indicated by experimental archaeology and thin section analysis of graphite-containing samples from Thunau am Kamp (Dell'mour 2001, 91, 104). Another study, however, suggests an extremely low temperature for the firing of the graphite-containing ceramics estimating it in the range of 360 ± 100 °C (Gregerová and Kristová 1995). It was hypothesised at Thunau am Kamp that the graphite-containing ware was fired in kilns (Dell'mour 2001, 104), which could be suggested by the fact that reducing atmosphere is more easily achievable and maintainable in kilns than in open or pit fires. It is quite possible, however, that open/pit firing was also used especially in the case of the earliest graphite-containing vessels based on the lack of pottery kiln finds (Scharrer-Liška 2007, 26).

The production of the graphite-containing ceramics under investigation might have happened in similar organisation forms as 'household industries' or 'individual workshops' described by Peacock (1982, 8–9; Section 5.5). It is possible that these production units were working for larger economic/social structures. It was mentioned earlier in Section 5.5 that Austrian researchers suggested that manorial organisation may have had a controlling role in the production and distribution of these ceramics (Felgenhauer-Schmiedt 1998, 204; Scharrer-Liška 2007, 150). The level of specialisation in graphite-containing pottery production has not been discussed in detail in publications, but it has been suggested that a high level of specialisation is not probable until the beginnings of urbanisation in the late Middle Ages (13th century; Scharrer-Liška 2007, 5, 112).

Comparison of chemical compositions

Statistical analysis of the ICP-OES results shows that the studied samples have similar chemical composition (Section 4.4.2). Petrographic groups are not always clearly replicated from the PCA scatterplots and dendrograms. This indicates that the elemental compositions of the used raw materials are similar in the different petrographic groups. One of the reasons of this similarity might be the same place of origin (Bohemian Massif) of the inclusions as suggested by the mineralogy of the samples (Section 5.2).

Seeing this similarity, the question arises how different the investigated ceramics are from samples from other regions. To answer this question, the chemical data of the studied ceramics and other early medieval samples from western Hungary and south-eastern Czechia were compared by principal component analysis. The samples from Hungary were found at Zalavár, Dunaszentgyörgy and Daruszentmiklós and the majority of the samples from Czechia were found at Mikulčice and few samples are from Břeclav, Brno and Kramolín (*Figure 164*).

As the focus is on the comparison of early medieval ceramics, only the data of the 6th–12th-century ceramics investigated in this thesis were used and the Roman/late Roman samples from the Erlauf Valley were left out from the analysis. In addition to the early medieval samples, some graphite-containing samples from the La Tène period from Hungary were also included in the comparison as the source of the graphite present in the Late Iron Age and early medieval samples was very likely in the Bohemian Massif (Havancsák et al. 2009, 12; Section 5.2) regardless of the time difference (*Table 28*).

It is important to note that the data are produced by different chemical techniques: the samples from Lower Austria were analysed by ICP-OES while the samples from Czechia and Hungary were analysed by X-ray fluorescence (XRF). Only those elements were taken into account which are present in all datasets including Al, Ca, Fe, K, Mg, Si and Ti among major elements and Ba, Ni, Rb, Sr and Zr among trace elements.

The results of the comparison are presented on three scatterplots based on all (major and trace) elements, the major elements and the trace elements (*Figures 165–170*; see also Appendix E.2). The scatterplots show that the samples from the same sites are close to each other, and at the same time, there are also areas of the plots where the sites overlap.

Table 28. Details of the ceramics from Hungary and Czechia included in the comparison

Archaeological site	Symbol in PCA graphs	Ceramic type	Number of samples included in comparison	Dating of ceramics	Publications
Zalavár	○	Graphite-free pottery (polished yellow pottery)	50	9th century AD	Herold 2010b
Dunaszentgyörgy	◇	Graphite-containing ceramics	17	Late Iron Age (3rd century BC)	Havancsák et al. 2009
Dunaszentgyörgy	△	Graphite-free pottery	29	Middle and Late Avar period (AD *c.* 670 – beginning of 9th century)	Kreiter et al. 2017, Archaeology database of the Hungarian National Museum[95]
Daruszentmiklós	□	Graphite-free pottery	11	Avar period (AD 630/640 – beginning of 8th century)	Kondé et al. 2018, Archaeology database of the Hungarian National Museum [96]
Mikulčice	▲	Graphite-free (58) and graphite-containing (3) pottery	61	8th–10th centuries AD	Dvorská et al. 1998
Břeclav-Pohansko	◆	Graphite-free pottery	2	9th century AD	Dvorská et al. 1998
Brno-Líšeň	●	Graphite-free pottery	2	8th–11th centuries AD	Dvorská et al. 1998
Kramolín-Burgwall	■	Graphite-free pottery	2	9th–10th centuries AD	Dvorská et al. 1998

The best PCA graph to illustrate the differences between the Lower Austrian and the other Central European sites is surprisingly not the trace element plot as it would have been expected, but the all element plot or the major element plot. In the graph based on the analysis of all elements (*Figure 165*), the samples from Lower Austria are located mostly in the lower left part of the field, while the samples from Hungary are mostly in its upper right part. This shows that the ceramics form Lower Austria are richer in Al_2O_3, K_2O, TiO_2, Ba, Rb and Zr than those from Hungary (*Figure 166*). The samples from Czechia are located between the Lower Austrian and Hungarian samples.

[95] https://archeodatabase.hnm.hu/hu/node/1617 (accessed on 04/01/2020)
[96] https://archeodatabase.hnm.hu/hu/node/76903 (accessed on 04/01/2020)

In the PCA analysis plot of the major elements (*Figure 167*), the ceramic assemblage from Lower Austria is relatively well-distinguished from the other samples occupying the right half of the graph and indicating a more K_2O, TiO_2, Al_2O_3 and Fe_2O_3-rich composition than the other Central European samples (*Figure 168*). The ceramics from Hungarian sites are neighbouring the Lower Austrian ceramics to the left (and are also partly mixed with them) and the majority of the samples from Czechia appear in the upper left corner showing higher silica. This scatterplot also points out internal differences of the Lower Austrian samples and shows that the Granitoid and Graphite groups (similar Al_2O_3, K_2O and TiO_2 content) and the Diorite and Amphibole groups (similar Fe_2O_3 and MgO content) are close to each other in terms of major elemental composition.

In the trace element plot, the Austrian samples are quite scattered and overlap with other ceramic groups from Czechia and Hungary (*Figure 169*). Nevertheless, in contrast to the above-mentioned compositional similarity between the Granitoid and Graphite groups, the trace elements clearly separate these two groups here, the Granitoid group being more Zr and Rb rich and the Graphite group being more Ni and Sr rich (*Figure 170*).

Summary

This subchapter has shown that the ceramic assemblage analysed in this thesis and other vessels from the same period have many similar characteristics. They indicate that the same technological toolkit and level of knowledge were present in the Erlauf Valley as at other areas of Lower Austria. The comparison revealed the heterogeneity of the graphite-containing pottery regarding mineralogical composition, which reflects the variability of the graphite-rich raw materials, but also the numerous production units that used different deposits for vessel making.

The comparison between the samples investigated in this thesis and samples from Czechia and Hungary shows that the ceramic material from Lower Austria can be differentiated from other regions of Central Europe. It also suggests that the composition of the Lower Austrian samples is specific for their region and confirms the similar origin of the raw materials used for making these ceramics, which is also indicated by the petrographic results. A more detailed picture of chemical groups could be achieved by analysing more ceramics from Lower Austria. Nevertheless, the data presented in this thesis will clearly contribute to the establishment of reference groups for 1st–12th-century pottery in the Lower Austrian region.

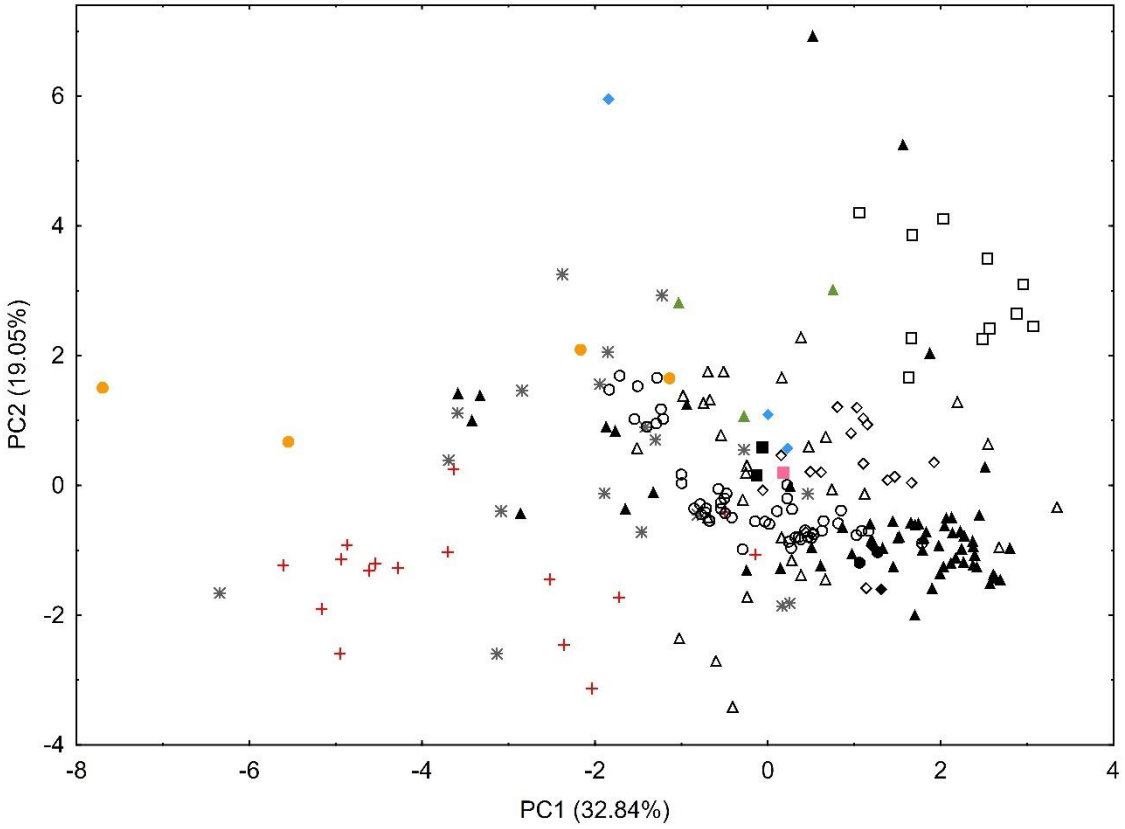


Figure 165. Comparison of the chemical compositions of the samples from Lower Austria with samples from Hungary and Czechia. The scatterplot shows the result of PCA (including PC1 and PC2) of the major and trace elements measured by ICP-OES in the samples from Lower Austria and by XRF in the samples from Hungary and Czechia. The Lower Austria samples are marked by the usual symbols in colour (see Figure 92 on page 188) and the other samples are marked by black filled an unfilled shapes as shown in Table 28.

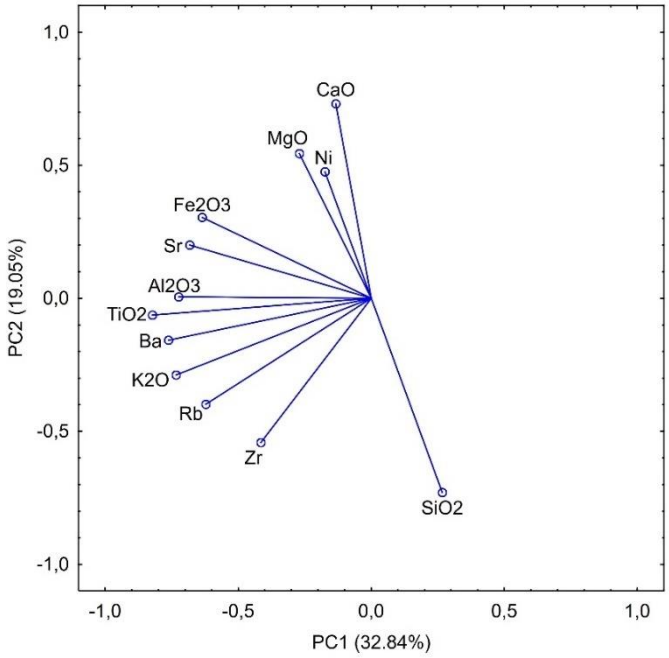


Figure 166. Projection of the variables for Figure 165

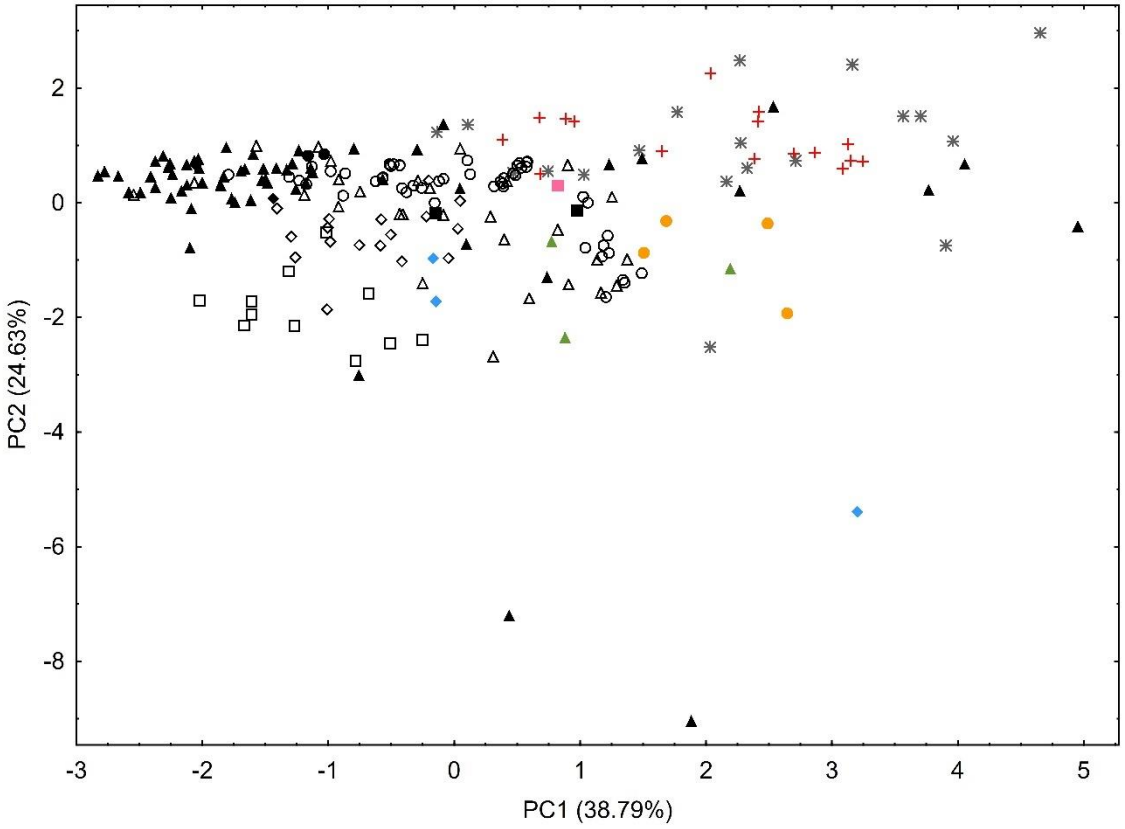


Figure 167. Comparison of the chemical compositions of the samples from Lower Austria with samples from Hungary and Czechia. The scatterplot shows the result of PCA (including PC1 and PC2) of the major elements. For legend, see caption of Figure 165.

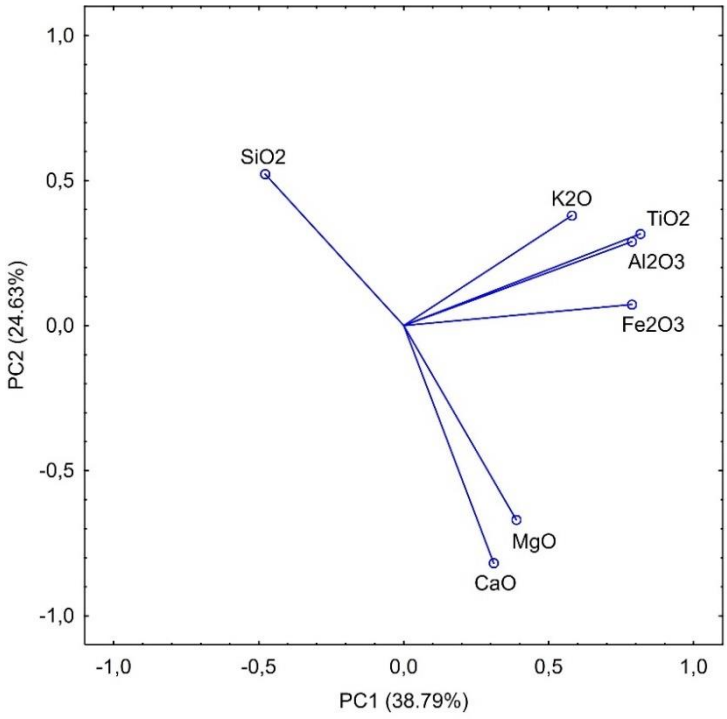


Figure 168. Projection of the variables for Figure 167

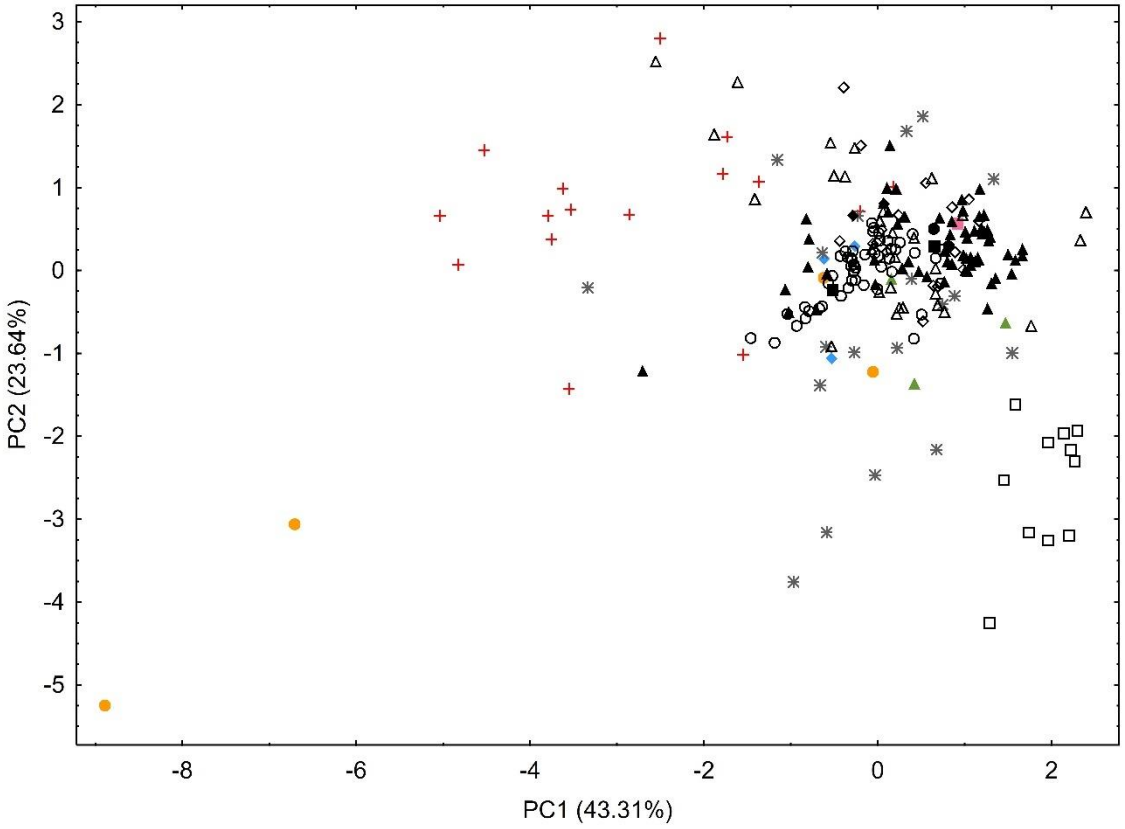


Figure 169. Comparison of the chemical compositions of the samples from Lower Austria with samples from Hungary and Czechia. The scatterplot shows the result of PCA (including PC1 and PC2) of the trace elements. For legend, see caption of Figure 165.

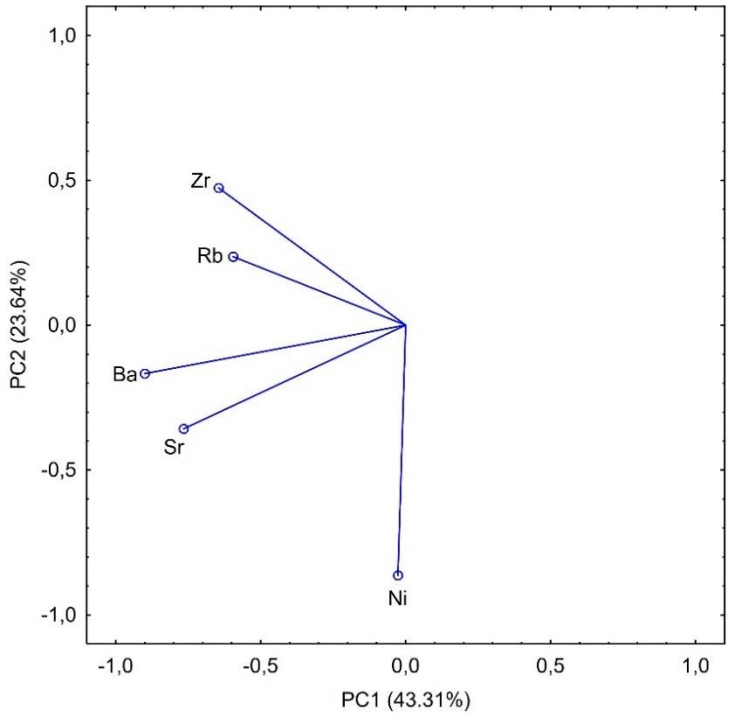


Figure 170. Projection of the variables for Figure 169

6 CONCLUSIONS

Through the scientific analysis of ceramics, this thesis has provided information about early medieval pottery production and raw material sources in the Erlauf Valley and Lower Austria. In addition to the characterisation and reconstruction of the production technology and origin of the studied vessels, the results have given an insight into the organisational aspects of pottery production, different pottery making practices over space and time as well as how technological and historical changes can be connected.

Within the studied assemblage of 135 samples, two main types of pottery were investigated: graphite-free ceramics and graphite-containing ceramics. Graphite-free ceramics, originating from the Erlauf Valley, were dated to the 1st–9th centuries, while graphite-containing ceramics, originating from the Erlauf Valley and other sites of Lower Austria and Vienna, were dated to the 9th–12th centuries.

The main outcomes of this thesis are summarised below.

Analyses carried out in this thesis characterised the composition and microstructure of the raw materials used for ceramic making, based on which petrographic groups could be distinguished. These included four main groups and many subgroups of graphite-free ceramics (Granitoid group, Amphibole group, Carbonate group and Diorite group) as well as several subgroups of graphite-containing ceramics (Graphite group). This grouping was different from the macroscopic categorisation to some extent as scientific methods made it possible to differentiate between ceramics of similar macroscopic features.

Within the investigated ceramic material, four chronological groups were distinguished, which were dated to the 1st–5th centuries (subgroups ‘Granitoid A3’ and ‘Granitoid B3’ of the Granitoid group), 6th–7th centuries (Carbonate group), 8th–9th centuries (rest of the Granitoid group, Amphibole group and Diorite group) and 9th–12th centuries (Graphite group).

The rock fragments and minerals present in the clay permitted an identification of potential raw material sources. The inclusions of the studied ceramics from all chronological groups were consistent with different and usually weathered rock types of the Bohemian Massif, which is largely located north of the Danube and the Erlauf Valley, but is relatively close to the surface and has outcrops south of the Danube as well. The four samples of the Carbonate

group could also be associated with rocks of the Eastern Alps located south of the Valley based on their calcite-rich inclusion spectra.

The distributions of the graphite-free pottery groups could outline past consumption areas, which were limited to the southern (sherds from 1st–5th and 6th–7th centuries) or middle (Diorite group from the 8th–9th centuries) area of the Erlauf Valley or were present Valley-wide (8th–9th-century sherds of the Granitoid and Amphibole groups), but it must be emphasised that these patterns could be influenced by sample number and selection as well. Ceramics belonging to subgroups of the heterogenous Graphite group may have had similarly wide distributions in the area of Lower Austria, except for the low graphite-containing subgroup ('Graphite D') which may have been restricted to the territory of the Erlauf Valley.

The analysis results contributed to the reconstruction of the different stages of ceramic making technology including raw material preparation, fashioning, finishing, surface treatment, decoration and firing. Among raw material preparation techniques, the evaluation of whether tempering was part of the preparation process was a central question. Within the studied assemblage there were examples both for the addition of temper (ceramics from the 1st–5th and 6th–7th centuries, subgroup 'Diorite A' from the 8th–9th centuries and possibly the Graphite group) and the use of a residual clay that naturally contained inclusions (8th–9th-century samples of the Granitoid group and Amphibole group).

The forming process (fashioning and finishing) included the use of a turntable in the case of ceramic pots from the whole duration of the studied period based on macroscopic traces. Another common characteristic of the ceramics is that they lack clear traces of surface treatment. Incised (parallel) lines and wavy lines were widely used in each petrographic group and slight differences in the decoration of the investigated graphite-containing and other vessels were pointed out.

Firing, as the last step of the manufacturing process, took place in a mixed atmosphere in the case of graphite-free ceramics and the graphite-containing subgroup 'Graphite D', and in a reducing atmosphere in the case of the rest of the graphite-containing samples. The maximum temperatures could be in the range of 800 °C for the ceramics of the Granitoid, Amphibole and Diorite groups and subgroup 'Graphite D', 750 °C for most of the graphite-containing samples, and 700–750 °C for the Carbonate group and subgroup 'Graphite C' based on the vitrification stage of the clay and the temperature-sensitive phases present in the ceramics.

The consideration of all above-mentioned pieces of information together helped draw conclusions about the organisation of pottery production. In some cases, the scale of production potentially exceeded small-scale (Roman/late Roman samples of 'Granitoid A3' and 8th–9th-century samples of the Granitoid group), but in many cases scale could not be estimated due to the small sample number. Some level of standardisation characterised a smaller part of the assemblage (1st–7th-century samples and subgroup 'Diorite A'), while the rest of the samples showed no signs of standardised production. Specialisation and centralised control were not likely present in the case of the manufacture of graphite-free vessels, however, they both could potentially characterise graphite-containing pottery production. Among the modes of production described by Peacock (1982, 6–11), production units of the studied ceramics could be likened to 'household industries' and 'individual workshops' exhibiting features of both categories.

It was possible to get a rough estimation about the number of these households/workshops: each of the main petrographic groups of graphite-free ceramics may be associated with one or two production units (six to nine units altogether: one or two operating within the 1st–5th centuries, one or two in the 6th–7th centuries and about four/five in the 8th–9th centuries) and the graphite-containing vessels may be associated with a large number of production units (10–20?). Although, the production sites of the investigated pieces of pottery have not been found, it is likely that they were located close to the raw material sources. Based on the distance of these sources and the sites where the ceramics were found, local or regional products (<20 km, Erlauf Valley samples) and supra-regional products (20–100 km, majority of the graphite-containing samples) could be outlined.

Technological choices of the pottery producers, made consciously or unconsciously during the manufacturing process, were also examined. In the case of ceramics from the Erlauf Valley, raw material selection was clearly dominated by materials of the Bohemian Massif, and some of the reasons for this might have been the availability of residual clays in the Massif and the unsuitability or unreliability of the local clays and loams. Graphite-containing pottery of the early Middle Ages can be considered as an innovation, and, although the motivation behind the production of this ware is not clear, the fact that graphite enhances the physical properties of the vessels likely played an important a role in choosing graphite-containing raw materials besides potential aesthetic and symbolic reasons.

Through the comparison of pottery from different periods, recurring or continuously present traditions were detected in the Erlauf Valley regarding some elements of the operational sequence such as vessel forming (slow wheel turning), decoration (incised parallel lines and wavy lines) and firing (mixed firing, firing temperatures below 700–800 °C). At the same time, newly introduced techniques could also be highlighted in terms of using tempered or residual clay; the investigated ceramics suggest that tempering was preferred in the 1st–5th and 6th–7th centuries, while most of the ceramics of the 8th–9th centuries are made of naturally inclusion-rich clays. This difference, together with the challenging carbonate temper of the 6th–7th centuries, reflects a higher level of technological knowledge in the 1st–7th centuries than in the 8th–9th centuries in the Erlauf Valley. In addition to suggesting continuity to some extent (forming technique), graphite-containing ceramics are good examples of breaking up with previous practices from many perspectives including the use of a new raw material, the application of new types of decorations and firing in a reducing atmosphere.

A comparison of contemporary ceramics from the 8th–9th centuries studied in this thesis indicated that the techniques used in pottery making were largely similar in the Erlauf Valley. However, individual ways of ceramic production, suggesting the presence of different communities of practice, could also be detected as shown by subgroup 'Diorite A', samples of which were probably tempered and not decorated in contrast with other 8th–9th-century ceramics.

The investigated ceramic assemblage ranging from the 1st to the 12th centuries allowed the comparison between changes in pottery technology and changes in political and societal structures. The techniques and level of proficiency in 6th–7th-century vessel manufacturing remained similar to the previous period in the Erlauf Valley based on the studied ceramics against the radical political, social and cultural changes induced by the collapse of the Western Roman Empire. It could be possible that technological and historical changes were interrelated in the 8th and 9th century when the use of residual clays (without tempering) was detected for the first time in graphite-free vessels and the appearance of graphite-containing pottery took place.

The studied ceramics fit into the picture of 1st–12th century pottery drawn by other ceramic analyses from Lower Austria and the Central European region. The vessels from the Erlauf Valley were made by practices that were widely used in their time and indicate the same technological level as other pieces of pots from the wider region. The graphite-containing

ceramics studied here and in other publications, although they look similar and were made by similar techniques, reinforce compositional heterogeneity and mirror the variability of the raw material sources used by different production units. Statistical analysis of chemical data showed that the ceramics from Lower Austria are similar in terms of chemical composition, but they can be differentiated from those originating from other regions of Central Europe.

This PhD project also allowed drawing conclusions about the applicability of the methods involved in the analysis of this specific ceramic assemblage. It showed that macroscopic analysis is essential to have information about the ceramic fabric as well as forming, decorating and firing techniques. Among scientific methods, thin section analysis was extremely useful in providing data about geological origin, raw material preparation and firing. It was also the best and most reliable technique to differentiate between fabrics and establish groups within the investigated material, which formed the basis of sample selection for further analyses. The dating of some samples found by field-walking could also be narrowed down based on their similar petrographic characteristics to other ceramics with a more precise dating. SEM analysis resulted in less abundant but equally important results confirming and completing the petrographic data (SEM-EDS) and giving information about firing temperatures (vitrification analysis).

Although chemical analysis (ICP-OES) showed the limitations of this method regarding the recognition of the petrographically distinguished groups in this special case (coarse-grained ceramic material) and at this stage of ceramic archaeometry in Lower Austria (lack of chemical data of archaeological ceramics to compare), it provided valuable data for a future database. In addition, it was able to identify and thus verify some of the connections detected by ceramic petrography. The benefits of XRD analysis were exhibited in the identification of fine-grained phases unknown for the other methods, which completed the firing temperature estimations by SEM. By analysing another part of the sample than its thin section, XRD analysis also confirmed and completed the petrographic results.

The novelty of this thesis lies in the analysis of a previously uninvestigated assemblage, which contributed with new data to the reconstruction of early medieval pottery technologies in Lower Austria. The archaeometric investigation of 1st–12th-century ceramics from the Erlauf Valley carried out in this thesis is a pioneer work as no publications about scientific analysis of ceramics are available from this microregion. It is also one of the few studies involving graphite-free pottery analysis by multiple materials science techniques in Lower Austria.

Early medieval graphite-containing ceramics were widespread and are thus investigated by many studies, which concern mainly macroscopic characteristics and typology of these vessels. With the inclusion of four analytical methods besides macroscopic examination, this thesis provides currently the most comprehensive scientific analysis of graphite-containing ceramics from Lower Austria.

Other studies involving ceramic archaeometry might find useful this thesis even if their subject cannot be connected to Lower Austria or its adjacent regions. This thesis provides an insight into the applicability of the different scientific methods used for the analysis of a relatively coarse-grained ceramic material, which can be considered when analysing similar assemblages from other areas or periods. It is also an example study of what information can be gained when analysing locally produced utilitarian ware in a microregion similar to the Erlauf Valley. Ceramics from field walking are often considered less valuable than those found at excavations. This thesis, in which half of the analysed samples originate from surface collection, however, showed that a large amount of valuable data can be gained from their analysis and interpretations can be made about their origin and production technology.

The results of this thesis also open avenues for future research. Analysis of clay samples from the Erlauf Valley as well as the analysis of residual clays and rocks from the Bohemian Massif would be beneficial to confirm and refine the potential raw material sources suggested by this thesis based on geological literature. Some analyses on raw materials of the Bohemian Massif originating from the vicinity of Thunau am Kamp (*c.* 70 km northeast of the Erlauf Valley sites) were carried out by Dell'mour (2001, 71, 108–109), but it would be useful to investigate and compare raw materials closer to the sites studied in this thesis. Sampling and analysis of different graphite deposits in the Drosendorf Unit as well as archaeometric analysis of large series of ceramics containing graphite could facilitate a more exact localisation of the raw material sources and interpretation of the technology (e.g. raw material preparation techniques) of graphite-containing pottery.

REFERENCES

Historical sources and source collections

Annales Bertiniani	*Annales Bertiniani*. Edited by Waitz, G. (Monumenta Germaniae Historica, Scriptores Rerum Germanicarum 5.) Hannoverae: Impensis Bibliopolii Hahniani, 1883.
Annales regni Francorum	*Annales regni Francorum inde ab a. 741 usque ad a. 829, qui dicuntur annales Laurissenses maiores et Einhardi*. Edited by Kurze, F. (Monumenta Germaniae Historica, Scriptores Rerum Germanicarum 6.) Hannoverae: Impensis Bibliopolii Hahniani, 1895.
Conversio	Conversio Bagoariorum et Carantanorum. Critical edition by Lošek, F. *Die Conversio Bagoariorum et Carantanorum und der Brief des Erzbischofs Theotmar von Salzburg*. (Monumenta Germaniae Historica, Studien und texte 15.) Hannover: Hahnsche Buchhandlung, 1997.
Eugippius	Eugippius. Vita Severini. Edited by Mommsen, T. *Eugippii vita Severini*. (Monumenta Germaniae Historica, Scriptores Rerum Germanicarum 26.) Berolini: Apud Weidmannos, 1898.
Fredegar	Fredegar. Chronicae. Edited by Krusch, B. *Fredegarii et aliorum chronica. Vitae sanctorum.* (Monumenta Germaniae Historica, Scriptores Rerum Merovingicarum 2.) Hannoverae: Impensis Bibliopolii Hahniani, 1888, 18–139.
NÖUB I.	*Niederösterreichisches Urkundenbuch I, 777 bis 1076*. Edited by Weltin, M. and Zehetmayer, R. (Publikationen des Instituts für Österreichische Geschichtsforschung, 8. Reihe) St. Pölten: Niederösterreichisches Institut für Landeskunde, 2008.
MGH Capit. 1.	*Monumenta Germaniae Historica, Capitularia regum Francorum 1*. Edited by Boretius, A. Hannoverae: Impensis Bibliopolii Hahniani, 1883.
MGH Conc. 2.1.	*Monumenta Germaniae Historica, Concilia 2.1. Concilia aevi Karolini 1*. Edited by Werminghoff, A. Hannoverae et Lipsiae: Impensis Bibliopolii Hahniani, 1906.
MGH Dipl. Kar. 1.	*Monumenta Germaniae Historica, Diplomata Karolinorum 1*. Edited by Societas Aperiendis Fontibus. Hannoverae: Impensis Bibliopolii Hahniani, 1906.
MGH Dipl. reg. Germ. 1.	*Monumenta Germaniae Historica, Diplomata regum Germaniae ex stirpe Karolinorum 1. Ludowici Germanici, Karlomanni, Ludowici Iunioris diplomata*. Edited by Kehr, P. Berolini: Apud Weidmannos, 1934.

MGH Dipl. reg. imp. Germ. 2.2.	*Monumenta Germaniae Historica, Diplomata regum et imperatorum Germaniae 2.2. Ottonis III. diplomata*. Edited by Societas Aperiendis Fontibus. Hannoverae: Impensis Bibliopolii Hahniani, 1893.
Trad. Hoch. Freising I.	*Die Traditionen des Hochstifts Freising I (744–926)*. Edited by Bitterauf, T. (Quellen und Erörterungen zur bayerischen und deutschen Geschichte, Neue Folge 4.) München: M. Rieger'sche Universitäts-Buchhandlung, 1905.

Bibliography

Abzalov, M. 2008. Quality control of assay data: A review of procedures for measuring and monitoring precision and accuracy. *Exploration and Mining Geology* 17, 131–144.

Adam, H. 1996. *Das Zollwesen im Fränkischen Reich und das spätkarolingische Wirtschaftsleben. Ein Überblick über Zoll, Handel und Verkehr im 9. Jahrhundert.* (Vierteljahrschrift für Sozial- und Wirtschaftsgeschichte, Beihefte 126.) Stuttgart: Franz Steiner Verlag.

Adams, A. E. and MacKenzie, W. S. 1998. *Carbonate sediments and rocks under the microscope*. London: Manson Publishing.

Adams, A. E., MacKenzie, W. S. and Guilford, C. 1984. *Atlas of sedimentary rocks under the microscope*. Essex: Longman.

Adler, H. 1977a. Materielle Kultur der Germanen während der Römischen Kaiserzeit. In: Windl, H. (ed.) *Germanen, Awaren, Slawen in Niederösterreich. Das erste Jahrtausend nach Christus. Gestaltung der Ausstellung*. Wien: Amt der Niederösterreichischen Landesregierung, 50–61.

Adler, H. 1977b. Die Langobarden in Niederösterreich. In: Windl, H. (ed.) *Germanen, Awaren, Slawen in Niederösterreich. Das erste Jahrtausend nach Christus. Gestaltung der Ausstellung*. Wien: Amt der Niederösterreichischen Landesregierung, 73–82.

Adlington, L. W. 2017. The Corning archaeological reference glasses: New values for “old” compositions. *Papers from the Institute of Archaeology* 27 (1): Art. 2, 1–8. http://doi.org/10.5334/pia-515

Aitchison, J. 1986. *The statistical analysis of compositional data*. London and New York: Chapman and Hall.

Albero Santacreu, D. and Cau Ontiveros, M. Á. 2017. Technological choices in hand-made indigenous pottery from Western Mallorca (Balearic Islands, Spain) (C.1200–75 BC): An archaeometric approach. *Archaeometry* 59 (4), 642–666.

Alföldy, G. 1974. *Noricum. The provinces of the Roman Empire*. Translated by Birley, A. London and Boston: Routledge & Kegan Paul.

Allaby, M. 2013. *A dictionary of geology and earth sciences.* (Fourth edition.) Oxford: Oxford University Press.

Amicone, S., Mathur, A. R., Pavitra, R. D., Mirković-Marić, N., Pantović, I. and Kuzmanović-Cvetković, J. 2020. Beneath the surface: Exploring variability in pottery paste recipes within

Vinča culture. *Quaternary International* 560–561, 86–101.

Arnold, D. E. 1972. Mineralogical analyses of ceramic materials from Quinua, Department of Ayacucho, Peru. *Archaeometry* 14 (1), 93–102.

Arnold, D. E. 1985. *Ceramic theory and cultural process*. Cambridge: Cambridge University Press.

Arnold, D. E. 2000. Does the standardization of ceramic pastes really mean specialization? *Journal of Archaeological Method and Theory* 7 (4), 333–375.

Arnold, D. E. 2006. The threshold model for ceramic resources: a refinement. In: Gheorghiu, D. (ed.) *Ceramic studies. Papers on the social and cultural significance of ceramics in Europe and Eurasia from Prehistoric to Historic times*. (BAR International Series 1553.) Oxford: Archaeopress, 3–9.

Arnold, D. E. 2008. *Social change and the evolution of ceramic production and distribution in a Maya community*. Boulder: University Press of Colorado.

Arnold, D. E. 2011. Classics review: Ceramic theory and cultural process after 25 years. *Ethnoarchaeology* 3 (1), 63–98.

Arnold, J. E. and Munns, A. 1994. Independent or attached specialization: the organization of shell bead production in California. *Journal of Field Archaeology* 21, 473–489.

Arnold, P. J. 1991. Dimensional standardization and production scale in Mesoamerican ceramics. *Latin American Antiquity* 2 (4), 363–370.

Arthur, P. 2007. Form, function and technology in pottery production from Late Antiquity to the Early Middle Ages. In: Lavan, L., Zanini, E. and Sarantis, A. (eds) *Technology in transition: A.D. 300–650.* Leiden and Boston: Brill, 159–186.

Artioli, G. 2010. *Scientific methods and cultural heritage. An introduction to the application of materials science to archaeometry and conservation science*. Oxford: Oxford University Press.

Aspöck, E. 2001. Merowingerzeitliche Grabfunde aus Fischlham-Hafeld. Reste eines Baierischen Reihengräberfeldes. *Jahrbuch des Oberösterreichischen Musealvereines* 146 (1), 235–266.

Aspöck, E. 2003. Graböffnungen im Frühmittelalter und das Fallbeispiel der langobardenzeitlichen Gräber von Brunn am Gebirge, Flur Wolfholz, Niederösterreich. *Archaeologia Austriaca* 87, 225–264.

Aspöck, E. 2011. Past 'disturbances' of graves as a source: Taphonomy and interpretation of reopened early medieval inhumation graves at Brunn Am Gebirge (Austria) and Winnall II (England). *Oxford Journal of Archaeology* 30 (3), 299–324.

Bakay, K. 1999. Hungary (Chapter 21). In: Reuter, T. (ed.) *The new Cambridge medieval history. Volume III c. 900–c. 1024*. Cambridge: Cambridge University Press, 536–552.

Baldi, J. and Roux, V. 2016. The innovation of the potter's wheel: A comparative perspective between Mesopotamia and the southern Levant. *Levant* 48, 236–253.

Baxter, M. J. 1994. *Exploratory multivariate analysis in archaeology*. Edinburgh: Edinburgh University Press.

Baxter, M. J. 2003. *Statistics in archaeology*. London: Arnold.

Baxter, M. J. and Buck, C. E. 2000. Data handling and statistical analysis. In: Ciliberto, E. and Spoto, G. (eds) *Modern analytical methods in art and archaeology*. (Chemical Analysis Series, Vol. 155.) New York – Chichester – Weinheim – Brisbane – Singapore – Toronto: John Wiley & Sons, 681–746.

Beller, S. 2006. *A concise history of Austria*. Cambridge: Cambridge University Press.

Benesch, E. 2003. Pfarrkirche, Wieselburg. In: Aichinger-Rosenberger, P., Benesch, E., Bleicher, K., Grün, S., Holzschuh-Hofer, R., Huber, W., Karner, H., Packpfeifer, K., Piuk, A., Russwurm-Biró, G., Rychlik, O., Szendey, A. and Wanek F. P. (eds) *Niederösterreich. Südlich der Donau*. (Dehio-Handbuch. Die Kunstdenkmäler Österreich. Teil 2, M bis Z.) Horn/Wien: Verlag Berger, 2684–2687.

Berger, J.-P. 2008. North Alpine Foreland Basin: Western part. In: McCann., T. (ed.) *The geology of Central Europe. Volume 2: Mesozoic and Cenozoic*. London: The Geological Society, 1054–1056.

Blackman, M., Stein, G. and Vandiver, P. 1993. The standardization hypothesis and ceramic mass production: Technological, compositional, and metric indexes of craft specialization at Tell Leilan, Syria. *American Antiquity* 58 (1), 60–80.

Bóna, I., Cseh, J., Nagy, M., Tomka, P. and Tóth, Á. 1993. *Hunok – Gepidák – Langobardok. Történeti régészeti tézisek és címszavak*. [Huns – Gepids – Langobards. Historical-archaeological theses and keywords.] Szeged.

Boozer, A. 2018. The Archaeology of Imperial Borderlands: A View from Roman Egypt and Sudan. In: Düring, B. and Stek, T. (eds) *The archaeology of imperial landscapes: A comparative study of empires in the ancient Near East and Mediterranean World*. Cambridge: Cambridge University Press, 206–239.

Borgers, B., Quinn, P., Degryse, P., De Bie, M. and Welkenhuysen, K. 2019. Roman pottery production in Civitas Tungrorum, central Belgium, during the first–third centuries CE. *Archaeometry* 62 (2), 267–284.

Boumans, P. W. J. M. 1987a. Introduction to atomic emission spectrometry. In: Boumans, P. W. J. M. (ed.) *Inductively coupled plasma emission spectroscopy. Part 1. Methodology, instrumentation and performance*. (Chemical Analysis Series, Vol. 90.) New York – Chichester – Brisbane – Toronto – Singapore: John Wiley & Sons, 1–44.

Boumans, P. W. J. M. 1987b. Inductively coupled plasmas. In: Boumans, P. W. J. M. (ed.) *Inductively coupled plasma emission spectroscopy. Part 1. Methodology, instrumentation and performance*. (Chemical Analysis Series, Vol. 90.) New York – Chichester – Brisbane – Toronto – Singapore: John Wiley & Sons, 69–99.

Boumans, P. W. J. M. 1987c. Basic concepts and characteristics of ICP-AES. In: Boumans, P. W. J. M. (ed.) *Inductively coupled plasma emission spectroscopy. Part 1. Methodology, instrumentation and performance*. (Chemical Analysis Series, Vol. 90.) New York – Chichester – Brisbane – Toronto – Singapore: John Wiley & Sons, 100–257.

Bourdieu, P. 1977. *Outline of a theory of practice*. Cambridge: Cambridge University Press.

Braekmans, D. and Degryse, P. 2017. Petrography. Optical microscopy. In: Hunt, A. M. W. (ed.)

The Oxford handbook of archaeological ceramic analysis. Oxford: Oxford University Press, 234–265.

Braekmans, D., Neyt, B., Degryse, P., Poblome, J. and Waelkens, M. 2012. Electron microprobe analysis of Classical and Hellenistic pottery from Düzen Tepe and Sagalassos (southwest Turkey). In: Scott, R. B, Braekmans, D., Carremans, M. and Degryse, P. (eds) *Proceedings of the 39th International Symposium for Archaeometry*. Leuven: Leuven University Press, 186–192.

Bray, T. L. and Minc, L. 2020. Imperial Inca-style pottery from Ecuador: Insights into provenance and production using INAA and ceramic petrography. *Journal of Archaeological Science: Reports* 34, 102628.

Breibert, W. 2005. Das karolingerzeitliche Hügelgräberfeld von Wimm, MG Maria Taferl, VB Melk, Niederösterreich. Untersuchungen zur Problematik frühmittelalterlicher Bestattungssitten im niederösterreichischen Donauraum. *Arheološki vestnik* 56, 391–433.

Brill, R. H. 1999. *Chemical analyses of early glasses. Volume 2, Tables of analyses*. Corning, New York: The Corning Museum of Glass.

Broekaert, J. A. C. and Boumans, P. W. J. M. 1987. Sample introduction techniques in ICP-AES. In: Boumans, P. W. J. M. (ed.) *Inductively coupled plasma emission spectroscopy. Part 1. Methodology, instrumentation and performance*. (Chemical Analysis Series, Vol. 90.) New York – Chichester – Brisbane – Toronto – Singapore: John Wiley & Sons, 296–357.

Brumfiel, E. M. and Earle, T. K. 1987. Specialization, exchange and complex societies: An introduction. In: Brumfiel, E. M. and Earle, T. K. (eds) *Specialization, Exchange and complex societies. New directions in archaeology*. Cambridge: Cambridge University Press, 1–9.

Bubert, H. and Hagenah, W.-D. 1987. Detection and measurement. In: Boumans, P. W. J. M. (ed.) *Inductively coupled plasma emission spectroscopy. Part 1. Methodology, instrumentation and performance*. (Chemical Analysis Series, Vol. 90.) New York – Chichester – Brisbane – Toronto – Singapore: John Wiley & Sons, 536–565.

Burke, C., Zavadil, M. and Kordatzaki, G. 2020. The chaîne opératoire of pottery traditions at Pheneos, Peloponnese, mainland Greece. *Journal of Archaeological Science: Reports* 35, 102660.

Burlot, J., Waksman, S. Y., Bellot-Gurlet, L. and Simsek Franci, G. 2020. The glaze production technology of an early Ottoman pottery (mid-14th(?)-16th century): The case of 'Miletus Ware'. *Journal of Archaeological Science: Reports* 29, 102073.

Burmeister, S. and Bernbeck, R. (eds) 2017. *The interplay of people and technologies: Archaeological case studies on innovations. (Berlin Studies of the Ancient World 43.)* Berlin: Edition Topoi.

Buxeda i Garrigós, J. 1999. Alteration and contamination of archaeological ceramics: The perturbation problem. *Journal of Archaeological Science* 26, 295–313.

Byrant, G. F. 1970. Two experimental Romano-British kiln firings at Barton-on-Humber, Lincolnshire. *Journal of the Scunthorpe Museum Society* 3, 1–16.

Byrant, G. F. 1971. *Experimental Romano-British kiln firings at Barton-on-Humber, Lincolnshire*. (Occasional Paper No. 1.) Barton-on-Humber: Workers' Educational Association, Barton-on-Humber Branch.

Callaghan, M. G., Pierce, D. E., Kovacevich, Brigitte and Glascock, M. D. 2017. Chemical paste characterization of Late Middle Preclassic-period ceramics from Holtun, Guatemala and its implications for production and exchange. *Journal of Archaeological Science: Reports* 12, 334–345.

Calvo Peña, S., Bosch Argilagós, J., Gómez Bach, A. and Molist Montaña, M. 2021. USE of imaging and chemical techniques to observe technological features of the Venus de Gavà. *Journal of Archaeological Science: Reports* 40, 103237.

Campbell, R. 2021. On borders as an archaeological/historical problem. In: d'Alfonso, L. and Rubinson, K. S. (eds) *Borders in archaeology: Anatolia and the South Caucasus ca. 3500-500 BCE (Volume 58)*. Leuven – Paris – Bristol, CT.: Peeters, 37–47.

Casale, S., van Dessel, K., Hoogland, M. L. P., Degryse, P. and Hofman, C. L. 2022. Technological persistence in ceramic production in the southeastern Hispaniola. The case study of El Cabo (600–1502 CE). *Journal of Anthropological Archaeology* 65, 101387.

Caso, G., Tanasi, D., Glascock, M. D. and Tykot, R. H. 2022. A landmark for local communities. Compositional analysis of the early Iron Age sanctuary at Polizzello Mountain (Sicily, Italy). *Journal of Archaeological Science: Reports* 41, 103311.

Catherine Lara, C. and Iliopoulos, I. 2020. Ceramic technology, ethnic identification and multiethnic contacts: The archaeological example of the Cuyes river valley (Southeastern Ecuadorian highlands). *Journal of Archaeological Science: Reports* 33, 102557.

Charalambidou, X., Kiriatzi, E., Müller, N. S., Müller Celka, S., Verdan, S., Huber, S., Gex, K., Ackermann, G., Palaczyk, M. and Maillard, P. 2018. Eretrian ceramic production through time: Geometric to Hellenistic periods. *Journal of Archaeological Science: Reports* 21, 983–994.

Clark, G. 2007. Specialisation, standardisation and Lapita ceramics. In: Bedford, S., Sand, C. and Connaughton, S. P. (eds) *Oceanic explorations: Lapita and Western Pacific settlement*. (Terra Australis 26.) Canberra: ANU Press, 289–299.

Clark, J. E. and Parry, W. J. 1990. Craft specialization and cultural complexity. *Research in Economic Anthropology* 12, 289–346.

Cohen, A. S., Galaty, M. L. and Fisher, C. T. 2018. Petrographic analysis of ceramics and clay from Angamuco, Michoacán. *Journal of Archaeological Science: Reports* 19, 155–165.

Cootes, K. V. E. and Quinn, P. S. 2018. Prehistoric settlement, mobility and societal structure in the Peak District National Park: New evidence from ceramic compositional analysis. *Archaeometry* 60 (4), 678– 694.

Costin, C. L. 1991. Craft specialization: Issues in defining, documenting, and explaining the organization of production. In: Schiffer, M. B. (ed.) *Archaeological Method and Theory. Volume 3*. Tucson: University of Arizona Press, 1–56.

Costin, C. L. 1998. Introduction: Craft and social identity. In: Costin, C. L. and Wright, R. P. (eds) *Craft and social identity*. (Archaeological Papers of the American Anthropological Association, Vol. 8, issue 1.) Washington, DC: American Anthropological Association, 3– 16.

Costin, C. L. 2005. The study of craft production. In: Maschner, H. D. G. and Chippindale, C. (eds) *Handbook of archaeological methods*. Lanham: AltaMira Press, 1032–1105.

Costin, C. L. and Hagstrum, M. B. 1995. Standardization, labor investment, skill, and the organization of ceramic production in late Prehispanic Highland Peru. *American Antiquity* 60 (4), 619–639.

Cresswell, R. 1976. Techniques et culture. Les bases d'un programme de travail. *Techniques et Culture (ancienne série)* 1, 7–59.

Cresswell, R. 2010. Techniques et culture. Les bases d'un programme de travail. *Techniques & Culture* 54-55 (1), 23–45.

Cullity, B. D. and Stock, S. R. 2014. *Elements of X-ray diffraction*. (Third edition.) Harlow: Pearson.

Cultrone, G., Rodriguez-Navarro, C., Sebastian, E., Cazalla, O. and de la Torre, M. J. 2001. Carbonate and silicate phase reactions during ceramic firing. *European Journal of Mineralogy* 13, 621–634.

Cultrone, G., Sebastián, E. and de la Torre, M. J. 2005. Mineralogical and physical behaviour of solid bricks with additives. *Construction and Building Materials* 19, 39–48.

Curewitz, D. C. and Foit, F. F. 2018. Shards in sherds: Identifying production locations and exchange patterns using electron microprobe analysis of volcanic ash temper in northern Rio Grande Biscuit ware. *Journal of Archaeological Science: Reports* 18, 487–498.

Curta, F. 2001. *The making of the Slavs. History and archaeology of the Lower Danube Region, c.500–700*. (Cambridge Studies in Medieval Life and Thought. Fourth Series.) Cambridge: Cambridge University Press.

Cusick, J. G. 2015. Introduction. In: Cusick, J. G. (ed.) *Studies in culture contact: Interaction, culture change, and archaeology*. Carbondale, Illinois: Southern Illinois University Press, 1–20.

d'Alfonso, L. and Rubinson, K. S. 2021. Borders and archaeology. In: d'Alfonso, L. and Rubinson, K. S. (eds) *Borders in archaeology: Anatolia and the South Caucasus ca. 3500-500 BCE (Volume 58)*. Leuven – Paris – Bristol, CT.: Peeters, 3–35.

Daghmehchi, M., Rathossi, C., Omrani, H. Emami, M. and Rahbar, M. 2018. Mineralogical and thermal analyses of the Hellenistic ceramics from Laodicea Temple, Iran. *Applied Clay Science* 162, 146–154.

Daim, F. 1977. Das 7. und 8. Jh. in Niederösterreich. In: Windl, H. (ed.) *Germanen, Awaren, Slawen in Niederösterreich. Das erste Jahrtausend nach Christus. Gestaltung der Ausstellung*. Wien: Amt der Niederösterreichischen Landesregierung, 88–94.

Daim, F. 2003. Avars and Avar archaeology. An introduction. In: Goetz, H.-W., Jarnut, J. and Pohl, W. (eds) *Regna and gentes. The relationship between late antique and early medieval peoples and kingdoms in the transformation of the Roman world*. Leiden and Boston: Brill, 463–570.

Day, P. M. and Kilikoglou, V. 2001. Analysis of ceramics from the kiln. *Hesperia Supplements* 30, 111–133.

Day, P. M., Relaki, M. and Faber, E. W. 2006. Pottery making and social reproduction in Bronze Age Mesara, Crete. In: Warner, J. L., Wiener, M. H., Polonsky, J. and Hayes E. (eds) *Pottery and society: The impact of recent studies in Minoan pottery. Gold Medal Colloquium in Honor of*

Philip P. Betancourt at the 104th Annual Meeting of the Archaeological Institute of America, New Orleans, Louisiana, 5 January 2003. Boston: Archaeological Institute of America, 22–72.

de Galan, L. and van der Plas, P. S. C. 1987. Low-gas-flow torches for ICP spectrometry. In: Montaser, A. and Golightly, D. W. (eds) *Inductively coupled plasmas in analytical atomic spectrometry*. New York: VCH, 527–562.

de Groot, B. and Bloxam, A. 2022. Radiocarbon approaches for mapping technological change: The spread of the potter's wheel in the Iberian Peninsula, 1000–0 BCE. *Journal of Archaeological Science: Reports* 41, 103288.

de Groot, B., Thissen, L., Özbal, R. and Gerritsen, F. 2017. Clay preparation and function of the first ceramics in north-west Anatolia: A case study from Neolithic Barcın Höyük. *Journal of Archaeological Science: Reports* 16, 542–552.

Deer, W. A., Howie, R. A. and Zussman, J. 1992. *An introduction to the rock forming minerals*. Harlow: Longman.

Dell'mour, R. W. 1989. Keramikanalyse mit dem Polarisationsmikroskop. Methodik – Interpretation – Beispiele. *Archaeologia Austriaca* 73, 17–34.

Dell'mour, R. W. 2001. Mikroskopische Untersuchungen an frühmittelalterlicher Keramik von Thunau am Kamp, NÖ. Lokalware – Importe – Rohstoffherkunft. *Anzeiger der philosophisch-historischen Klasse der Österreichischen Akademie der Wissenshcaften* 136, 69–109.

Denk, L. 1975. Weinzierl. *Fundberichte aus Österreich* 14, 181.

Denk, S. 1962. *Das Erlaufgebiet in ur- und frühgeschichtlicher Zeit*. (Forschungen zur Landeskunde von Niederösterreich, Band 13.) Wien: Verein für Landeskunde von Niederösterreich und Wien.

D'Ercole, G., Garcea, E. A. A., Eramo, G. and Muntoni, I. M. 2017. Variability and continuity of ceramic manufacturing of prehistoric pottery from Upper Nubia, Sudan: An ethnographic comparison. *Journal of Archaeological Science: Reports* 16, 553–563.

Di Prado, V., Píccoli, C., Silva, C., Morosi, M., Politis, G., Bonomo, M. and Barboza, C. 2020. Communities of practice in pre-Hispanic Middle and Lower Paraná (Northeastern Argentina). Ceramic petrography contributions. *Journal of Archaeological Science: Reports* 34, 102563.

Dietler, M., and Herbich, I. 1998. Habitus, techniques, style: An integrated approach to the social understanding of material culture and boundaries. In: Stark, M. (ed.), *The archaeology of social boundaries*. Washington, DC: Smithsonian Institution Press, 232–263.

Dill, H. G., Sachsenhofer, R. F., Grecula, P., Sasvári, T., Palinkaš, L. A., Borojević-Soštarić S., Strmić-Palinkaš S., Prochaska, W., Garuti, G., Zaccarini, F., Arbouille, D. and Schulz H.-M. 2008. Fossil fuels, ore and industrial minerals. In: McCann., T. (ed.) *The geology of Central Europe. Volume 2: Mesozoic and Cenozoic*. London: The Geological Society, 1341–1449.

Dondi, M., Ercolani, G., Guarini, G., Marsigli, M. and Venturi, I. 1999. Evoluzione della microstruttura durante la cottura rapida di impasti per piastrelle porose. *Ceramurgia* 25, 301–314.

Donner, N. R., Casale, S., Braekmans, D. and Geurds, A. 2019. Ceramic comales at the Barillas site (cal 1255–1390 CE), central Nicaragua: Defining a local technical tradition of griddle

manufacture. *Journal of Archaeological Science: Reports* 24, 829–842.

Dostál, B. 1998. Über die Anfänge der slawischen Graphittonkeramik in Mähren. In: Poláček, L. (ed.) *Slawische Keramik in Mitteleuropa vom 8. bis zum 11. Jahrhundert. Terminologie und Beschreibung*. (Internationale Tagungen in Mikulčice II.) Brno: Archeologický ústav Akademie věd České republiky, 67–86.

Dow, M. M. 1985. Agricultural intensification and craft specialization: A nonrecursive model. *Ethnology* 24 (2), 137–152.

Druc, I. 2013. What is local? Looking at ceramic production in the Peruvian highlands and beyond. *Journal of Anthropological Research* 69, 485–513.

Druc, I. C., Inokuchi, K. and Dussubieux, L. 2017. LA-ICP-MS and petrography to assess ceramic interaction networks and production patterns in Kuntur Wasi, Peru. *Journal of Archaeological Science: Reports* 12, 151–160.

Druc, I., Giersz, M., Kałaska, M., Siuda, R., Syczewski, M., Pimentel Nita, R., Chyla, J. M. and Makowski, K. 2020. Offerings for Wari Ancestors: Strategies of ceramic production and distribution at Castillo de Huarmey, Peru. *Journal of Archaeological Science: Reports* 30, 102229.

Druc, I., Underhill, A., Wang, F., Luan, F. and Lu, Q. 2018. A preliminary assessment of the organization of ceramic production at Liangchengzhen, Rizhao, Shandong: Perspectives from petrography. *Journal of Archaeological Science: Reports* 18, 222–238.

Duistermaat, K. 2017. The organization of pottery production. Toward a relational approach. In: Hunt, A. M. W. (ed.) *The Oxford handbook of archaeological ceramic analysis*. Oxford: Oxford University Press, 114–147.

Duma, G. and Ravasz, C. 1976. Graphithaltige Gefäße aus Österreichs Mittelalter. *Archaeologia Austriaca* 59/60, 225–242.

Duminuco, P., Messiga, B., Riccardi, M. P. 1998. Firing process of natural clays. Some microtextures and related phase compositions. *Thermochimica Acta* 321, 185–190.

Dunne, J., Chapman, A., Blinkhorn, P. and Evershed, R. P. 2020. Fit for purpose? Organic residue analysis and vessel specialisation: The perfectly utilitarian medieval pottery assemblage from West Cotton, Raunds. *Journal of Archaeological Science* 120, 105178.

Dvorská, J. and Poláček, L. 1995. Mineralogisch-petrographische Charakteristik der Mikulčicer Keramik. In: Poláček, L. (ed.) *Slawische Keramik in Mitteleuropa vom 8. bis zum 11. Jahrhundert. Terminologie und Beschreibung*. (Internationale Tagungen in Mikulčice II.) Brno: Archeologický ústav Akademie věd České republiky, 196–202.

Dvorská, J., Poláček, L. and Schneider, G. 1998. Chemische Analysen der Keramik von Mikulčice (Bez. Hodonín, Tschechien). In: Poláček, L. (ed.) *Slawische Keramik in Mitteleuropa vom 8. bis zum 11. Jahrhundert. Terminologie und Beschreibung*. (Internationale Tagungen in Mikulčice II.) Brno: Archeologický ústav Akademie věd České republiky, 295–312.

Earle, T. 1981. Comment on P. Rice, Evolution of specialized pottery production: a trial model. *Current Anthropology* 22, 230–231.

Echenique, E., Avila, F. and Nielsen, A. E. 2021. Potting practices and social integration in the

southern Andes during the late intermediate period: The case of Yavi-Chicha pottery. *Journal of Anthropological Archaeology* 61, 101244.

Eckert, S. L., Schleher, K. L. and James, W. D. 2015. Communities of identity, communities of practice: Understanding Santa Fe black-on-white pottery in the Española Basin of new Mexico. *Journal of Archaeological Science* 63, 1–12.

Egerton, R. F. 2005. *Physical principles of electron microscopy. An introduction to TEM, SEM, and AEM*. New York: Springer.

Eichert, S. 2013. Zur Absolutchronologie des Ostalpenraums im Frühmittelalter unter besonderer Berücksichtigung 14C-datierter Grabinventare. *Bericht der Bayerischen Bodendenkmalpflege* 54, 419–427.

Eichert, S. 2016. Wandel durch Migration – Der Ostalpenraum im Frühmittelalter als Fallstudie. In: Geisler, H. (Hrsg.) *Wandel durch Migration? 26. internationales Symposium, „Grundprobleme der frühgeschichtlichen Entwicklung im mittleren Donauraum", Straubing 2014.* (Arbeiten zur Archäologie Süddeutschlands 29.) Büchenbach: Dr. Faustus, 197–212.

El Ouahabi, M., Daoudi, L., Hatert, F. and Fagel, N. 2015. Modified mineral phases during clay ceramic firing. *Clays and Clay Minerals* 63, 404–413.

Erb-Satullo, N. L. 2019. The innovation and adoption of iron in the ancient Near East. *Journal of Archaeological Research* 27, 557–607.

Erb-Satullo, N. L. 2020. Archaeomaterials, innovation, and technological change. *Advances in Archaeomaterials* 1, 36–50.

Erb-Satullo, N. L. 2021. Technological rejection in regions of early gold innovation revealed by geospatial analysis. *Scientific Reports* 11, 20255.

Erb-Satullo, N. L., Gilmour, B. J. J. and Khakhutaishvili, N. 2017. Copper production landscapes of the South Caucasus. *Journal of Anthropological Archaeology* 47, 109–126.

Ermrich, M. and Opper, D. 2013. *XRD for the analyst. Getting acquainted with the principles*. Almelo: PANalytical B. V.

Espinosa, A., Druc, I., Millaire, J.-F., Prieto, G. and Arrelucea, L. 2021. Cultural filiations between the Virú communities, Early Intermediate Period, northern coast of Peru: Recent contributions from ceramic technology. *Journal of Archaeological Science: Reports* 40, 103232.

Falabella, F., Sanhueza, l., Correa, I., Glascock, M. D., Ferguson, T. J. and Fonseca, E. 2013. Studying technological practices at a local level: neutron activation and petrographic analyses of early ceramic period pottery in Central Chile. *Archaeometry* 55, 33–53.

Felgenhauer-Schmiedt, S. 1992. Früh- bis hochmittelalterliche Funde aus Wien I., Ruprechtsplatz und Sterngasse. *Beiträge zur Mittelalterarchäologie in Österreich* 8, 61–84.

Felgenhauer-Schmiedt, S. 1998. Graphittonkeramik des Früh- und Hochmittelalters in Niederösterreich. In: Poláček, L. (ed.) *Frühmittelalterliche Graphittonkeramik in Mitteleuropa. Naturwissenschaftliche Keramikuntersuchungen*. (Internationale Tagungen in Mikulčice IV.) Brno: Archeologický ústav Akademie věd České republiky, 199–212.

Felgenhauer-Schmiedt, S. 2008. Die Burganlage „Sand“ bei Raabs an der Thaya – ein Zentrum ohne Hinterland? In: Poláček, L. (ed.) *Das wirtschafliche Hinterland der frühmittelalterlichen Zentren*. (Internationale Tagungen in Mikulčice VI.) Brno: Archeologický ústav Akademie věd České republiky, 327–336.

Feuer, B. 2016. *Boundaries, borders, and frontiers in archaeology*. Jefferson, NC: McFarland & Company, Inc., Publishers.

Fischer, T. 2015. Bauten und Truppen des römischen Grenzheeres in Österreich. In: Gassner, V. and Pülz, A. (eds) *Der römische Limes in Österreich. Führer zu den archäologischen Denkmälern*. Wien: Österreichische Akademie der Wissenschaften, 26–46.

Flad, R. and Hruby, Z. 2007. “Specialized” production in archaeological contexts: Rethinking specialization, the social value of products, and the practice of production. *Archaeological Papers of the American Anthropological Association* 17, 1–19.

Flemming, R. L. 2007. Micro X-ray diffraction (μXRD): a versatile technique for characterization of Earth and planetary materials. *Canadian Journal of Earth Sciences* 44, 1333–1346.

Floyd, C. R. 1995. An assessment of Minoan slips from Pseira, Crete, using scanning electron microscopy. In: Vandiver, P. B., Druzik, J. R., Galvan Madrid, J. L., Freestone, I. C. and Wheeler, G. S. (eds) *Materials issues in art and archaeology I*. (Materials Research Society Symposium Proceedings 352.) Pittsburgh: Materials Research Society, 663–672.

Fodor, I. 1996. A Kárpátokon túli lelőhelyek. [Archaeological sites beyond the Carpathians.] In: István, F. (ed.) *Őseinket felhozád... A honfoglaló magyarság. Kiállítási katalógus*. Budapest: Nemzeti Múzeum, 437–439.

Fragnoli, P. 2018. Pottery production in pastoral communities: Archaeometric analysis on the LC3-EBA1 Handmade Burnished Ware from Arslantepe (in the Anatolian Upper Euphrates). *Journal of Archaeological Science*: Reports 18, 318–332.

Fragnoli, P. and Palmieri, M. 2017. Petrographic and geochemical investigations on the pottery production from Arslantepe-Malatya (Eastern Anatolia) from the fourth to the second millennium BCE: Technological continuity, innovation and cultural change. *Archaeometry* 59 (4), 612–641.

Frahm, E. 2018. Ceramic studies using portable XRF: from experimental tempered ceramics to imports and imitations at Tell Mozan, Syria. *Journal of Archaeological Science* 90, 12–38.

Freestone, I. C. 1982. Applications and potential of electron probe micro-analysis in technological and provenance investigations of ancient ceramics. *Archaeometry* 24 (2), 99–116.

Freestone, I. C., Middleton, A. P. and Meeks, N. D. 1994. Significance of phosphate in ceramic bodies: discussion of paper by Bollong et al. *Journal of Archaeological Science* 21, 425–426.

Fried, J. 1995. The Frankish kingdoms, 817–911: The East and Middle kingdoms (Chapter 5). In: McKitterick, R. (ed.) *The new Cambridge medieval history. Volume II c. 700–c. 900*. Cambridge: Cambridge University Press, 142–168.

Frieman, C. J. 2021. *An archaeology of innovation: Approaching social and technological change in human society*. Manchester: Manchester University Press.

Friesinger, H. 1971–1974. *Studien zur Archäologie der Slawen in Niederösterreich*. (Mitteilungen der Prähistorischen Kommission der Österreichischen Akademie der Wissenschaften, Band: 15–16.) Wien: Verlag der Österreichischen Akademie der Wissenschaften.

Friesinger, H. 1977. Die archäologischen Funde der ersten zwei Drittel des 5. Jh.s in Niederösterreich. In: Windl, H. (ed.) *Germanen, Awaren, Slawen in Niederösterreich. Das erste Jahrtausend nach Christus. Gestaltung der Ausstellung*. Wien: Amt der Niederösterreichischen Landesregierung, 62–65.

Friesinger, H. and Friesinger, I. 1977. Niederösterreich im 9. und 10. Jh. In: Windl, H. (ed.) *Germanen, Awaren, Slawen in Niederösterreich. Das erste Jahrtausend nach Christus. Gestaltung der Ausstellung*. Wien: Amt der Niederösterreichischen Landesregierung, 103–112.

Friesinger, H. and Kerchler, H. 1981. Töpferöfen der Völkerwanderungszeit in Niederösterreich. Ein Betrag zur völkerwanderungszeitlichen Keramik (2. Hälfte 4. –6. Jahrhundert n. Chr.) in Niederösterreich, Oberösterreich und dem Burgenland. *Archaeologia Austriaca* 65, 193–266.

Friesinger, H. and Vacha, B. 1988. *Römer – Germanen – Slawen in Österreich, Bayern und Mähren. Eine Spurensuche*. Stuttgart: Konrad Theiss Verlag.

Froitzheim, N. and Schuster, R. 2008. The Alps In: McCann., T. (ed.) *The geology of Central Europe. Volume 2: Mesozoic and Cenozoic*. London: The Geological Society, 1141–1181.

Fusek, G. and Spišiak, J. 2005. Vrcholnostredoveká grafitová keramika z Nitry-Šindolky. Archeológia a mineralógia. (Hochmittelalterliche Graphitkeramik von Nitra-Šindolka. Archäologie und Mineralogie.) *Slovenská archeológia* 53, 265–336.

Gaisbauer, I. 2019. Die mittelaterliche Keramik der Ausgrabungen Ruprechtsplatz / Sterngasse / Judengasse im Überblick und Vergleich. In: Felgenhauer-Schmiedt, S. (ed.) *Von Vindobona zu Wienna – Archäologisch-historische Untersuchungen zu den Anfängen Wiens*. (Beiträge zur Mittelalterarchäologie in Österreich, Beiheft 11.) Wien: Österreichische Gesellschaft für Mittelalterarchäologie, 105–134.

Gandon, E., Roux V. and Coyle, T. 2014. Copying errors of potters from three cultures: Predictable directions for a so-called random phenomenon. *Journal of Anthropological Archaeology* 33, 99–107.

Gassner, V. and Pülz, A. (eds) 2015. *Der römische Limes in Österreich. Führer zu den archäologischen Denkmälern*. Wien: Österreichische Akademie der Wissenschaften.

Gell, A. 1998. *Art and agency*. Oxford: Clarendon.

Geologische Bundesanstalt (ed.) 2002. *Geologische Karte von Niederösterreich, 1 : 200 000*. Wien: Geologische Bundesanstalt.

Gerberding, R. 2005. The later Roman Empire (Chapter 1). In: Fouracre, P. (ed.) *The new Cambridge medieval history. Volume I c.500–c.700*. Cambridge: Cambridge University Press, 13–34.

Giesler, J. 1980. Zur Archäologie des Ostalpenraumes vom 8. bis zum 11. Jahrhundert. *Archäologisches Korrespondenzblatt* 10, 85–98.

Gilstrap, W. D., Day, P. M. and Kilikoglou, V. 2016. Pottery production at two neighbouring

centres in the Late Bronze Age Saronic Gulf: historical contingency and craft organisation. *Journal of Archaeological Science: Reports* 7, 499–509.

González-García, F., Romero-Acosta, V., García-Ramos, G. and González-Rodríguez, M. 1990. Firing transformations of mixtures of clays containing illite, kaolinite and calcium carbonate used by ornamental tile industries. *Applied Clay Science* 5, 361–375.

Goodhew, P. J., Humphreys, J. and Beanland, R. 2001. *Electron microscopy and analysis*. London and New York: Taylor & Francis, 2001.

Gosden, C. 2005. What do objects want? *Journal of Archaeological Method and Theory* 12 (3), 193–211.

Gosselain, O. P. 1998. Social and technical identity in a clay crystal ball. In: Stark, M. T. (ed.) *The archaeology of social boundaries*. Washington, DC: Smithsonian Institution Press, 78–106.

Gosselain, O. P. 2000. Materializing identities: an African perspective. *Journal of Archaeological Method and Theory* 7 (3), 187–217.

Gosselain, O. P. 2008. Mother Bella was not a Bella: inherited and transformed traditions in Southwestern Niger. In: Stark, M. T., Bowser, B. J. and Horne, L. (eds) *Cultural transmission and material culture: breaking down boundaries*. Tucson: The University of Arizona Press, 150–177.

Gosselain, O. P. 2011. Technology. In: Instoll, T. (ed.) *The Oxford handbook of the archaeology of ritual and religion*. Oxford: Oxford University Press, 243–260.

Gosselain, O. P. 2018. Pottery chaînes opératoires as historical documents. In: Spear, T. (ed.) *Oxford research encyclopedia of African history*. https://oxfordre.com/view/10.1093/acrefore/9780190277734.001.0001/acrefore-9780190277734-e-208, accessed on 2 February 2022. (No page numbers of the printed book are indicated in the electronic copy.)

Grave, P., Kealhofer, L., Hnila, P., Marsh, B., Aslan, C., Thumm-Doğrayan, D. and Rigter, W. 2013. Cultural dynamics and ceramic resource use at Late Bronze Age/Early Iron Age Troy, northwestern Turkey. *Journal of Archaeological Science* 40 (4), 1760–1777.

Greenfield, S. 1987. Common radio frequency generators, torches, and sample introduction systems. In: Montaser, A. and Golightly, D. W. (eds) *Inductively coupled plasmas in analytical atomic spectrometry*. New York: VCH, 123–161.

Gregerová, M. and Kristová, L. 1995. Probleme der Interpretation der differenz-thermischen Analysen der Graphittonkeramik. In: Poláček, L. (ed.) *Slawische Keramik in Mitteleuropa vom 8. bis zum 11. Jahrhundert. Terminologie und Beschreibung*. (Internationale Tagungen in Mikulčice II.) Brno: Archeologický ústav Akademie věd České republiky, 213–221.

Gregerová, M. and Procházka, R. 1998. Erste Ergebnisse naturwissenschaftlicher Untersuchungen an Graphittonkeramik aus Brno (Brünn). In: Poláček, L. (ed.) *Frühmittelalterliche Graphittonkeramik in Mitteleuropa. Naturwissenschaftliche Keramikuntersuchungen*. (Internationale Tagungen in Mikulčice IV.) Brno: Archeologický ústav Akademie věd České republiky, 275–278.

Gustavsson, A. G. T. 1987. Liquid sample introduction into plasmas. In: Montaser, A. and Golightly, D. W. (eds) *Inductively coupled plasmas in analytical atomic spectrometry*. New York: VCH, 399–430.

Halsall, G. 2005. The Barbarian invasions (Chapter 2). In: Fouracre, P. (ed.) *The new Cambridge medieval history. Volume I c.500–c.700*. Cambridge: Cambridge University Press, 35–55.

Hameter, W. 2015. Die historische Entwicklung des österreichischen Limes. In: Gassner, V. and Pülz, A. (eds) *Der römische Limes in Österreich. Führer zu den archäologischen Denkmälern*. Wien: Österreichische Akademie der Wissenschaften, 21–25.

Hammer, V. M. F. 2002. Röntgendiffraktionsanalyse (Anhang). In: Herold, H. Die Keramik der awarischen Siedlungsreste von Brunn am Gebirge, Flur Wolfholz, Bezirk Mödling, Niederösterreich. *Archaeologia Austriaca* 86, 161–181, 181.

Harreither, R. 2015. Enns – Lauriacum. Legionslager – vicus – „Zivilstadt" – *canabae legionis*. In: Gassner, V. and Pülz, A. (eds) *Der römische Limes in Österreich. Führer zu den archäologischen Denkmälern*. Wien: Österreichische Akademie der Wissenschaften, 163–178.

Harzhauser, M. and Roetzel, R. 2008. North Alpine Foreland Basin: Eastern part. In: McCann., T. (ed.) *The geology of Central Europe. Volume 2: Mesozoic and Cenozoic*. London: The Geological Society, 1056–1058.

Harzhauser, M., Kováč, M. and Roetzel, R. 2008. Vienna Basin and its satellite basins. In: McCann., T. (ed.) *The geology of Central Europe. Volume 2*: Mesozoic and Cenozoic. London: The Geological Society, 1060–1063.

Hasaki, E. 2012. Craft apprenticeship in ancient Greece: reaching beyond the masters. In: Wendrich, W. (ed.) *Archaeology and apprenticeship: body knowledge, identity, and communities of practice*. Tucson: University of Arizona Press, 171–202.

Havancsák, I., Bajnóczi, B., Tóth, M., Kreiter, A. and Szöllősi, S. 2009. Kelta grafitos kerámia: elmélet és gyakorlat dunaszentgyörgyi kerámiák ásványtani, petrográfiai és geokémiai vizsgálatának tükrében. (Celtic graphitic pottery: theory and practice in the light of mineralogical, petrographic and geochemical study of ceramics from Dunaszentgyörgy (S-Hungary).) *Archeometriai Műhely* 2009, 39–51.

Heidke, J. M. 2009. Multi-village specialized craft production and distribution of Hokoham Sedentary Period pottery, Tucson, Arizona. In: Quinn, P. S. (ed.) *Interpreting silent artefacts: Petrographic approaches to archaeological ceramics*. Oxford: Archaeopress, 227–244.

Heidke, J. M., Leary, S. C., Herr, S. A. and Elson, M. D. 2007. Alameda Brown Ware and San Francisco Mountain Gray Ware technology and economics. In: Van Keuren, S., Elson, M. D. and Herr, S. A. (eds) *Sunset Crater archaeology: The history of a volcanic landscape. Ceramic technology, distribution, and use*. (Anthropological Papers No. 32.) Tucson: Center for Desert Archaeology, 145–183.

Heimann, R. B. and Maggetti, M. 2014. *Ancient and historical ceramics: Materials, technology, art, and culinary traditions*. Stuttgart: Schweizerbart Science Publishers.

Hein, A. and Stilborg, O. 2019. Ceramic production in prehistoric northwest China: Preliminary findings of new analyses of old material from the Museum of Far Eastern Antiquities, Stockholm. *Journal of Archaeological Science*: Reports 23, 104–115.

Hein, A., Day, P. M., Cau Ontiveros, M. A. and Kilikoglou, V. 2004. Red clays from Central and Eastern Crete: geochemical and mineralogical properties in view of provenance studies on ancient ceramics. *Applied Clay Science* 24, 245–255.

Hein, A., Day, P. M., Quinn, P. S. and Kilikoglou, V. 2004. The geochemical diversity of Neogene clay deposits in Crete and its implications for provenance studies of Minoan pottery. *Archaeometry* 46 (3), 357–384.

Hein, A., Tsolakidou, A. and Mommsen, H. 2002. Mycenaean pottery from the Argolid and Achaia – A mineralogical approach where chemistry leaves unanswered questions. *Archaeometry* 44 (2), 177–186.

Heinrich, M. 2006. Rohstoffe und Bergbau. In: Wessely, G. (ed.) *Niederösterreich. Geologie der österreichischen Bundesländer*. Wien: Geologische Bundesanstalt, 265–298.

Herbich, I. and Dietler, M. 2008. The long arm of the mother-in-law: learning, postmarital resocialization of women, and material culture style. In: Stark, M. T., Bowser, B. J. and Horne, L. (eds) *Cultural transmission and material culture: breaking down boundaries*. Tucson: The University of Arizona Press, 223–244.

Herold, H. 2002a. Die Keramik der awarischen Siedlungsreste von Brunn am Gebirge, Flur Wolfholz, Bezirk Mödling, Niederösterreich. *Archaeologia Austriaca* 86, 161–181.

Herold, H. 2002b. Die awarenzeitliche Keramik von Zillingtal im Burgenland (Österreich) – eine archäologische und naturwissenschaftliche Analyse. *Bodendenkmalpflege in Mecklenburg-Vorpommern* 50, 281–292.

Herold, H. 2004. Archaeological and Scientific Analysis of Early Medieval Ceramics in Austria – A Case Study: Zillingtal (Burgenland, Eastern Austria). In: Schüssler, U. and Pernicka, E. (eds), *Archäometrie und Denkmalpflege 2004. Jahrestagung in den Reiss-Engelhorn Museen*. Mannheim, 156–158.

Herold, H. 2007. Die Besiedlung Niederösterreichs im Frühmittelalter. In: Zehetmayer, R. (ed.) *Schicksalsjahr 907. Die Schlacht bei Pressburg und das frühmittelalterliche Niederösterreich. Katalog zur Ausstellung des Niederösterreichischen Landesarchivs, 3. Juli bis 28. Oktober 2007 in der Kulturfabrik Hainburg*. St. Pölten: Niederösterreichisches Institut für Landeskunde, 77–91.

Herold, H. 2008a. Frühmittelalterliche Prunkkeramik aus Mikulčice, Mähren – archäometrische Analysen und ihre Interpretation. In: Poláček, L. (ed.) *Das wirtschaftliche Hinterland der frühmittelalterlichen Zentren.* (Internationale Tagungen in Mikulčice VI.) Brno: Archeologický ústav Akademie věd České republiky, 299–311.

Herold, H. 2008b. Archäometrische Analysen latènezeitlicher Keramik von Schwarzenbach-Burg. *VIAVIAS* 2, 24–30.

Herold, H. 2009a. Archäometrische Untersuchungen frühmittelalterlicher Keramik aus Frohsdorf, Pitten und Erlach (NÖ). In: Heinrich-Tamáska, O., Krohn, N. and Ristow, S. (eds) *Dunkle Jahrhunderte in Mitteleuropa?* (Studien zu Spätantike und Frühmittelalter, Band 1.) Hamburg: Verlag Dr. Kovač, 335–350.

Herold, H. 2009b. Materielle Kultur – technologische Traditionen – Identität. Untersuchungen zur Archäologie des Frühmittelalters in Niederösterreich. *ZAM. Zeitschrift für Archäologie des Mittelalters* 37, 111–134.

Herold, H. 2010a. *Zillingtal, Burgenland – Die awarenzeitliche Siedlung und die Keramikfunde des Gräberfeldes*. (Monographien des Römisch-Germanischen Zentralmuseums, Band 80, 1–2.) Mainz: Verlag des Römisch-Germanischen Zentralmuseums.

Herold, H. 2010b. The ceramic 'tableware' of the Carolingian Period in Zalavár, South West Hungary. *Antaeus*. *Communicationes ex Instituto Archaeologico Academiae Scientiarum Hungaricae* 31–32, 155–172.

Herold, H. 2011a. The fortified hilltop site of Gars-Thunau and the settlements of the 9th and 10th centuries AD in Lower Austria. In: Macháček, J. and Ungerman, Š. (eds) *Frühgeschichtliche Zentralorte in Mitteleuropa. Internationale Konferenz und Kolleg der Alexander von Humboldt-Stiftung zum 50. Jahrestag des Beginns archäologischer Ausgrabungen in Pohansko bei Břeclav, 5.–9.10.2009, Břeclav, Tschechische Republik*. Bonn: Verlag Dr. Rudolf Habelt GmbH, 519–528.

Herold, H. 2011b. Archäologische und archäometrische Analysen der awarenzeitlichen Keramik von Zillingtal (Burgeland, Österreich). In: Kolozsi, B. and Szilágyi, K. A. (eds) *Sötét idők falvai* (Villages of the Dark Ages). Debrecen, 193–208.

Herold, H. 2013. The Avar period settlement and the ceramic finds from the cemetery in Zillingtal, Burgenland, eastern Austria. In: Theune, C., Scharrer-Liška, G., Huber, E. H. and Kühtreiber, T. (eds) *Stadt – Land – Burg. Festschrift für Sabine Felgenhauer-Schmiedt zum 70. Geburtstag*. Rahden/Westfalen: Verlag Marie Leidorf, 131–138.

Herold, H. 2014. Archäometrische Analysen spätantiker keramik aus Halbturn. In: Doneus, N. (ed.) *Das kaiserzeitliche Gräberfeld von Halbturn, Burgenland. Teil 2: Intention, Abfall oder Zufall – naturwissenschaftliche Untersuchungen*. (Monographien des Römisch-Germanischen Zentralmuseums, Band 122, 2.) Mainz: Verlag des Römisch-Germanischen Zentralmuseums, 665–690.

Herold, H. 2015a. Technological traditions in early medieval eastern Austria. In: Heinrich-Tamáska, O., Herold, H., Straub, P. and Vida, T. (eds) *„Castellum, civitas, urbs". Zentren und Eliten im frühmittelalterlichen Ostmitteleuropa / Centres and elites in early medieval east-central Europe*. Budapest – Leipzig – Keszthely – Rahden/Westfalen: Verlag Marie Leidorf, 329–344.

Herold, H. 2015b. Frühmittelalterliche Funde aus dem Gebiet des Leitha-Flusses, Niederösterreich – Archäologische und archäometrische Untersuchungen. In: Doneus, M. and Griebl, M. (eds) *Die Leitha – Facetten einer Landschaft*. (Archäologie Österreichs Spezial 3.) Wien: Österreichische Gesellschaft für Ur- und Frühgeschichte, 63–73.

Herold, H. 2016. Spätantike und Frühmittelalter – eine technologische Kontinuität? Analysen zu Funden aus Michelstetten (Niederösterreich). In: *Beatus homo qui invenit sapientiam. Ünnepi kötet Tomka Péter 75. születésnapjára*. Győr: Lekri Group Kft., 277–309.

Herold, H. and Petschick, R. 2003. Herkunftsbestimmung frühmittelalterlicher Keramik und Rekonstruktion ihrer Brenntemperatur mittels Kombination von Röntgendiffraktionsanalyse, Tonprobennahme und Brennversuchen. *Berliner Beiträge zur Archäometrie* 20, 31–47.

Hinterwallner, M. and Schmid, S. 2015. Pöchlarn – Arelape. Auxiliarkastell. In: Gassner, V. and Pülz, A. (eds) *Der römische Limes in Österreich. Führer zu den archäologischen Denkmälern*. Wien: Österreichische Akademie der Wissenschaften, 194–198.

Hoard, R. J., O'Brien, M. J., Khorasgany, M. G. and Gopalaratnam, V. S. 1995. A materials-science approach to understanding limestone-tempered pottery from the midwestern United States. *Journal of archaeological science* 22, 823–832.

Hodder, I. 2012. *Entangled: An archaeology of the relationships between humans and things*. Oxford: Wiley-Blackwell.

Holl, I. 1956. Adatok a középkori magyar fazekasság munkamódszereihez. (Beiträge zu den Arbeitsmethoden der Ungarischen Töpferei des Mittelalters.) *Budapest Régiségei* 17, 177–196.

Holl, I. 1963. Középkori cserépedények a budai várpalotából (XIII–XV. század). (Mittelalterliche Keramik aus dem Burgpalast von Buda (13.–15. Jahrhundert).) *Budapest Régiségei* 20, 335–394.

Höllrigl, J. 1930. Árpádkori keramikánk. [Pottery of the Arpadian age.] *Archaeológiai Értesítő* 44, 142–169.

Holzer, H. 1964. Niederösterreichische Graphitlagerstätten. Exkursion II/3. *Mitteilungen der Geologischen Gesellschaft in Wien* 57, 163–168.

Hönig, J. and Schedl, A. 1984. Ausgewählte Tonvorkommen der niederösterreichischen Molassezone zwischen Enns und Erlauf. *Archiv für Lagerstättenforschung der Geologischen Bundesanstalt* 5, 45–48.

Ingold, T. 2013. *Making. Anthropology, archaeology, art and architecture*. Abingdon and New York: Routledge.

Janoschek, W. R. and Matura, A. 1980. Outline of the geology of Austria. In: Geologische Bundesanstalt (ed.) *Austria. Outline of the geology of Austria and selected excursions*. (Abhandlungen der Geologischen Bundesanstalt 34.) Vienna: Geologische Bundesanstalt, 7–101.

Jeitler, M. and Schön, D. 2019. St. Ruprecht in Wien. In: Felgenhauer-Schmiedt, S. (ed.) *Von Vindobona zu Wienna – Archäologisch-historische Untersuchungen zu den Anfängen Wiens*. (Beiträge zur Mittelalterarchäologie in Österreich, Beiheft 11.) Wien: Österreichische Gesellschaft für Mittelalterarchäologie, 135–155.

Jenkins, R. and Snyder, R. L. 1996. *Introduction to X-ray powder diffractometry*. (Chemical Analysis Series, Vol. 138.) New York – Chichester – Brisbane – Toronto – Singapore: John Wiley & Sons.

Jordan, J. M., Hoggarth, J. A. and Awe, J. J. 2020. Pottery, practice, and place: A communities of practice approach to commoner interaction in the Late to Terminal Classic Belize River Valley. *Journal of Anthropological Archaeology* 58, 101148.

Jordán, M. M., Boix, A., Sanfeliu, T. and de la Fuente, C. 1999. Firing transformations of cretaceous clays used in the manufacturing of ceramic tiles. *Applied Clay Science* 14, 225–234.

Jordán, M. M., Martín-Martín, J. D., Sanfeliu, T., Gómez-Gras, D. and de la Fuente, C. 2009. Mineralogy and firing transformations of Permo–Triassic clays used in the manufacturing of ceramic tile bodies. *Applied Clay Science* 44, 173–177.

Kamp, K. A. 2001. Prehistoric children working and playing: a Southwestern case study in learning ceramics. *Journal of Anthropological Research*, 57 (4), 427–450.

Kappel, I. 1969. *Die Graphittonkeramik von Manching*. (Ausgrabungen in Manching, Band 2.) Wiesbaden: F. Steiner.

Kelly-Buccellati, M. 2012. Apprenticeship and learning from the ancestors: the case of ancient Urkesh. In: Wendrich, W. (ed.) *Archaeology and apprenticeship: body knowledge, identity, and communities of practice*. Tucson: University of Arizona Press, 203–223.

Kilikoglou, V. 1994. Scanning electron microscopy. In: Wilson, D. E. and Day, P. M. Ceramic regionalism in prepalatial Central Crete: the Mesara imports at EM I to EM IIA Knossos. *Annals of the British School at Athens* 89, 1–87, 70–75.

Kloiber, Ä. and Pertlwieser, M. 1967. Die Ausgrabungen 1966 auf der „Berglitzl" in Gusen und auf dem „Hausberg" in Auhof bei Perg, Oberösterreich. *Jahrbuch des Oberösterreichischen Musealvereines* 112 (1), 75–90.

Kobyliński, Z. 2005. The Slavs (Chapter 19). In: Fouracre, P. (ed.) *The new Cambridge medieval history. Volume I c.500–c.700*. Cambridge: Cambridge University Press, 524–544.

Kolenda, J. 1998. Forschungsprobleme bei der frühmittelalterlichen Graphitkeramik in Schlesien. In: Poláček, L. (ed.) *Slawische Keramik in Mitteleuropa vom 8. bis zum 11. Jahrhundert. Terminologie und Beschreibung*. (Internationale Tagungen in Mikulčice II.) Brno: Archeologický ústav Akademie věd České republiky, 20–31.

Kondé, Z., Kreiter, A., Bajnóczi, B., Tóth, M. and Viktorik, O. 2018. The organization of ceramic production: A comparative analysis of typology and petrography at the Avar Age settlement of Daruszentmiklós (Hungary). In: Rácz, Z., Koncz, I. and Gulyás, B. (eds) *„Hadak útján". A népvándorláskor fiatal kutatóinak XXVI. konferenciája. Gazdaság – kereskedelem – kézművesség*. (26th Conference of Young Scholars on the Migration Period. Economy – trade – craftsmanship.) Budapest: ELTE, 177–231.

Kostonas, A. 2014. Standardization, variation, and the study of ceramics in the Mediterranean and beyond. In: Kostonas, A. (ed.) *Understanding standardization and variation in Mediterranean ceramics: mid 2nd to late 1st millennium BC*. Leuven – Paris – Walpole, MA: Peeters, 7–23.

Kreiter, A., Bartus-Szöllősi, S., Bajnóczi, B., Havancsák, I. A., Tóth, M. and Szakmány, G. 2013. Ceramic technology and the materiality of Celtic graphitic pottery. In: Alberti, M. E. and Sabatini, S. (eds) *Exchange networks and local transformations: Interaction and local change in Europe and the Mediterranean from the Bronze Age to the Iron Age*. Oxford: Oxbow Books, 169–180.

Kreiter, A., Czifra, S., Bendő, Z. Egri Imre, Jánosné, Pánczél, P. and Váczi, G. 2014. Shine like metal: an experimental approach to understand prehistoric graphite coated pottery technology. *Journal of Archaeological Science* 52, 129–142.

Kreiter, A., May, Z., Pető, Á. Tóth, M., Bajnóczi, B., Máté, L., Viktorik, O., Szabó, L., Sklánitz, A., Mészáros Kis, Z., Gődény, M., Cseri, Z. and Raczky, P. 2021. Bucrania revisited: Exploring the chaîne opératoire of bucranium figurines of the Körös culture from the 6th millennium. *Journal of Archaeological Science: Reports* 37, 102982.

Kreiter, A., Skriba, P., Bajnóczi, B., Tóth, M., Viktorik, O. and Pánczél, P. 2017. A dunaszentgyörgyi avar temető kerámiái az archeometria tükrében. (The ceramic assemblage of the Avar cemetery at Dunaszentgyörgy (Tolna County, Hungary) in the light of archaeometry.)

In: Türk A., Balogh, C. and Major, B. (eds) *Hadak útján XXIV. A népvándorláskor fiatal kutatóinak XXIV. konferenciája. Esztergom, 2014. november 4–6. 2. kötet*. (Conference of Young Scholars on the Migration Period. November 4–6, 2014, Esztergom. Volume 2). Budapest–Esztergom: PPKE BTK Régészeti Tanszék – Magyar Tudományos Akadémia, Bölcsészettudományi Kutatóközpont, Magyar Őstörténeti Témacsoport, 21–102.

Kremer, G. 2015. Nekropolen im Limesgebiet. In: Gassner, V. and Pülz, A. (eds) *Der römische Limes in Österreich. Führer zu den archäologischen Denkmälern*. Wien: Österreichische Akademie der Wissenschaften, 86–94.

Krenn, M. 1991. Vorbericht zu den Untersuchungen in der Burganlage von Sachsendorf, Niederösterreich. In: Böhme, H. W. (ed.) *Burgen der Salierzeit. Teil 2. In den südlichen Landschaften des Reiches*. (Monographien des Römisch-Germanischen Zentralmuseums, Band 26.) Jan Thorbecke Verlag Sigmaringen, 351–376.

Krenn, M. and Krenn-Leeb, A. 1993. Sachsendorf – ein Beitrag zum derzeitigen Forschungsstand der mittelalterlichen Burganlage. *Archäologie Österreichs* 4/2, 51–60.

Krenn, M., Hinterwallner, M. and Schön, D. 2005. KG Mautern, SG Mautern an der Donau, VB Krems. *Fundberichte aus Österreich* 44, 26–27.

Kroner, U., Mansy, J.-L., Mazur, S., Aleksandrowski, P., Hann, H. P., Huckriede, H., Lacquement, F., Lamarche, J., Ledru, P., Pharaoh, T. C., Zedler, H., Zeh, A. and Zulauf, G. 2008. Variscan tectonics. In: McCann, T. (ed.) *The geology of Central Europe. Volume 1: Precambrian and Palaeozoic*. London: The Geological Society, 599–664.

Kroon, E. J., Huisman, D. J., Bourgeois, Q. P. J., Braekmans, D. J. G. and Fokkens, H. 2019. The introduction of Corded Ware Culture at a local level: An exploratory study of cultural change during the Late Neolithic of the Dutch West Coast through ceramic technology. *Journal of Archaeological Science: Reports* 26, 101873.

Kühtreiber, K. 2006. *Burg Dunkelstein. Ergebnisse der archäologischen Untersuchungen eines hochmittelalterlichen Adelssitzes im südöstlichen Niederösterreich*. Unpublished thesis, University of Vienna.

Kühtreiber, K. 2006. Die Hochmittelalterliche Keramik im südöstlichen Niederösterreich. Ihre Entwicklung, ihre Formen und die Beziehungen zu den benachbarten Keramikregionen. *Beiträge zur Mittelalterarchäologie in Österreich* 22, 93–148.

Kühtreiber, K. and Obenaus, M. 2017. *Burgen des 9. bis zur Mitte des 11. Jahrhunderts in Niederösterreich – eine Bestandsaufnahme*. (Monographien des Römisch-Germanischen Zentralmuseums, Band 132.) Mainz: Verlag des Römisch-Germanischen Zentralmuseums.

Ladenbauer-Orel, H. 1972. Wieselburg an der Erlauf, das östlichste Imperium des hl. Wolfgang. *Jahrbuch des Oberösterreichischen Musealvereines* 117a, 26–62.

Laita, E. and Bauluz, B. 2018. Mineral and textural transformations in aluminium-rich clays during ceramic firing. *Applied Clay Science* 152, 284–294.

Latour, B. 1988. *The pasteurization of France*. Cambridge, Mass: Harvard University Press.

Latour, B. 2005. *Reassembling the social: An introduction to Actor-Network-Theory*. Oxford: Oxford University Press.

Law, J. 1992. *Notes on the Theory of the Actor Network: Ordering, strategy and heterogeneity*. Lancaster: Centre for Science Studies, Lancaster University.

Lechtman, H. 1977. Style in technology – some early thoughts. In: Lechtman, H. and Merrill, R. (eds) *Material culture: styles, organization, and dynamics of technology*. New York: West Publishing, 3–20.

Lemonnier, P. (ed.) 1993. *Technological choices. Transformation in material cultures since the Neolithic*. London and New York: Routledge.

Lemonnier, P. 1976. La Description des chaînes opératoires: contribution à l'analyse des systèmes techniques. *Techniques et Culture (ancienne série)* 1, 100–151.

Lemonnier, P. 1986. The study of material culture today: toward an anthropology of technical systems. *Journal of Anthropological Archaeology* 5, 147–186.

Lemonnier, P. 1992. *Elements for an anthropology of technology. (Anthropological papers 88.)* Ann Arbor: Museum of Anthropology, University of Michigan.

Lemonnier, P. 1993. Introduction. In: Lemonnier, P. (ed.) *Technological choices. Transformation in material cultures since the Neolithic*. London and New York: Routledge, 1–35.

Lemonnier, P. 2012. Technology. In: Thieberger, N. (ed.) *The Oxford handbook of linguistic fieldwork*. Oxford: Oxford University Press, 298–316.

Leroi-Gourhan, A. 1964. *Le geste et la parole. Technique et langage*. Paris: Albin Michel. (Translation: Leroi-Gourhan, A. 1993. *Gesture and speech*, translated by Bostock Berger, A. Cambridge, Mass. and London: MIT Press.)

Lewis, M. P., Quinn, P. S. and Carter, R. 2020. Uruk expansion or integrated development? A petrographic and geochemical perspective from Gurga Chiya, Iraqi Kurdistan. *Journal of Archaeological Science: Reports* 33, 102516.

Lewis, M., and Arntz, M. 2020. The chaîne opératoire: past, present and future. *Archaeological Review from Cambridge* 35 (1), 6–16.

Li, T., Li, P., Song, H., Xie, Z., Fan, W. and Lü, Q.-Q. 2022. Pottery production at the Miaodigou site in central China: Archaeological and archaeometric evidence. *Journal of Archaeological Science: Reports* 41, 103301.

Li, T., Yao, S., He, L., Yu, X. and Shan, S. 2021. Compositional study of household ceramic assemblages from a Late Neolithic (5300–4500 cal BP) earthen walled-town in the middle Yangtze River valley of China. *Journal of Archaeological Science: Reports* 39, 103159.

Lightfoot, K. G. and Martinez, A. 1995. Frontiers and boundaries in archaeological perspective. *Annual Review of Anthropology* 24, 471–492.

Linnemann, U., Romer, R. R., Pin, C., Aleksandrowski, P., Buła, Z., Geisler, T., Kachlik, V., Krzemińska, E., Mazur, S., Motuza, G., Murphy, J. B., Nance, R. D., Pisarevsky, S. A., Schulz, B., Ulrich, J., Wiszniewska, J., Żaba, J. and Zeh, A. 2008. Bohemian Massif. In: McCann, T. (ed.) *The geology of Central Europe. Volume 1: Precambrian and Palaeozoic*. London: The Geological Society, 60–63.

Livingstone Smith, A. 2000. Processing clay for pottery in northern Cameroon: Social and technical requirements. *Archaeometry* 42 (1), 21–42.

MacKenzie, W. S. and Guilford, C. 1980. *Atlas of rock-forming minerals in thin section*. Essex: Longman.

MacKenzie, W. S., Donaldson, C. H. and Guilford, C. 1982. *Atlas of igneous rocks and their textures*. Essex: Longman.

Mączyńska, A. 2021. Regularised pottery production in Lower Egypt in the second half of 4th millennium BCE. *Journal of Archaeological Science: Reports* 39, 103157.

Maggetti, M. 1981. Composition of Roman pottery from Lousonna (Switzerland). In: Hughes, M. J. (ed.) *Scientific studies in ancient ceramics*. (British Museum Occasional Paper No. 19.) London: British Museum, 33–49.

Maggetti, M. 1982. Phase analysis and its significance for technology and origin. In Olin, J. S. and Franklin, A. D. (eds) *Archaeological Ceramics*. Washington D.C.: Smithsonian Institute Press, 121–133.

Maggetti, M. 1986. Majolika aus Mexiko – ein Archaometrisches Fallbeispiel. *Fortschritte der Mineralogie* 64:1, 87–103.

Maggetti, M. 1994. Mineralogical and petrographical methods for the study of ancient pottery. In: Burragato, F., Grubessi, O. and Lazzarini, L. (eds) *1st European workshop on archaeological ceramics*. Dipartimento di Scienza della Terra, Università degli studi di Roma "La Sapienza", 23–35.

Maggetti, M., Westley, H. and Olin, J. S. 1994. Provenance and technical studies of Mexican majolica using elemental and phase analysis. In: Lambert, J. B. (ed.) *Archaeological chemistry—III.* (Advances in Chemistry Series, Vol. 205.) Washington, D.C.: American Chemical Society, 151–191.

Mahias, M-C. 1993. Pottery techniques in India: technical variants and social choice, In: Lemonnier, P. (ed.) *Technological choices. Transformation in material cultures since the Neolithic.* London and New York: Routledge, 157–180.

Maniatis, Y. and Tite, M. S. 1978. Ceramic technology in the Aegean world during the Bronze Age. In: Doumas, C. (ed.) *Thera and the Aegean World*. London: The Thera Foundation, 483–492.

Maniatis, Y. and Tite, M. S. 1981. Technological examination of Neolithic–Bronze Age pottery from central and southeast Europe and from the Near East. *Journal of Archaeological Science* 8, 59–76.

Marghussian, A. K., Coningham, R. A. E. and Fazeli, H. 2017. Investigation of Neolithic pottery from Ebrahimabad in the central plateau of Iran, utilising chemical–mineralogical and microstructural analyses. *Journal of Archaeological Science: Reports* 16, 604–615.

Maritan, L. 2019. Archaeo-ceramic 2.0: investigating ancient ceramics using modern technological approaches. *Archaeological and Anthropological Sciences* 11, 5085–5093.

Maritan, L. 2020. Ceramic abandonment. How to recognise post-depositional transformations. *Archaeological and Anthropological Sciences* 12, Article 199. https://link.springer.com/article/

10.1007/s12520-020-01141-y

Maritan, L., Nodari, L., Mazzoli, C., Milano, A. and Russo, U. 2006. Influence of firing conditions on ceramic products: Experimental study on clay rich in organic matter. *Applied Clay Science* 31, 1– 15.

Martineau, R., Walter-Simonnet, A.-V., Grobéty, B. and Buatier, M. 2007. Clay resources and technical choices for neolithic pottery (Chalain, Jura, France): Chemical, mineralogical and grain-size analyses. *Archaeometry* 49, 23–52.

Martinón-Torres, M. 2002. Chaîne opératoire: the concept and its applications within the study of technology. *Gallaecia* 21, 29–43.

Martinón-Torres, M. and Rehren, T. 2005. Ceramic materials in fire assay practices: a case study of 16th-century laboratory equipment'. In Prudencio, M. I., Dias, M. I. and Waerenborgh, J. C. (eds) *Understanding people through their pottery. Proceedings of the 7th European Meeting on Ancient Ceramics (EMAC '03), Lisbon 2003*. Lisbon: Instituto Português de Arqueologia, 139–149.

Martinón-Torres, M. and Rehren, T. 2006. The 'mystery' of the post-medieval triangular crucibles reconsidered – a global perspective. In: Pérez-Arantegui, J. (ed.) *Proceedings of the 34th International Symposium on Archaeometry, Zaragoza, 3–7 May 2004*. Zaragoza: Institución Fernando el Católico, CSIC, 515–524.

Martinón-Torres, M., Li, X. J., Bevan, A., Xia, Y., Zhao, K., Rehren, T. 2014. Forty thousand arms for a single emperor: from chemical data to the labor organization behind the bronze arrows of the terracotta army. *Journal of Archaeological Method and Theory* 21, 534–562.

Massart, D. L. and Kaufman, L. 1983. *The interpretation of analytical chemical data by the use of cluster analysis*. New York – Chichester – Brisbane – Toronto – Singapore: John Wiley & Sons.

Matthew, A. J., Woods, A. J. and Oliver, C. 1991. Spots before the eyes: new comparison charts for visual percentage estimation in archaeological material. In: Middleton, A. and Freestone, I. (eds) *Recent developments in ceramic petrology*. (British Museum Occasional Paper No. 81.) London: British Museum Research Laboratory, 211–263.

Matura, A. 2006a. Grauwackenzone. In: Wessely, G. (ed.) *Niederösterreich. Geologie der österreichischen Bundesländer*. Wien: Geologische Bundesanstalt, 167–171.

Matura, A. 2006b. Kristallin-Einheiten der Zentralalpen. In: Wessely, G. (ed.) *Niederösterreich. Geologie der österreichischen Bundesländer*. Wien: Geologische Bundesanstalt, 173–181.

Matura, A. 2006c. Böhmische Masse. In: Wessely, G. (ed.) *Niederösterreich. Geologie der österreichischen Bundesländer*. Wien: Geologische Bundesanstalt, 25–39.

Mayes, P. 1961. The firing of a pottery kiln of a Romano-British type at Boston, Lincs. *Archaeometry* 4 (1), 4–18.

Mayes, P. 1962. The firing of a second pottery kiln of Romano-British type at Boston, Lincolnshire. *Archaeometry* 5 (1), 80–86.

Mazur, S. and Kroner, U. 2008. Moldanubian Zone (sensu stricto). In: McCann (ed.) *The geology of Central Europe. Volume 1: Precambrian and Palaeozoic*. London: The Geological Society, 611–613.

McGovern, P. E. 1989. Ancient ceramic technology and stylistic change: Contrasting studies from southwest and southeast Asia. In: Henderson, J. (ed.) *Scientific analysis in archaeology and its interpretation*. Oxford: Oxford University, 63–81.

Mentesana, R., Day, P. M., Kilikoglou, V. and Todaro, S. 2016. United in our differences: The production and consumption of pottery at EM IB Phaistos, Crete. *Journal of Archaeological Science: Reports* 7, 489–498.

Menzl, F. 1988. Genese und Alter der Kaolinlagerstätte Krumnußbaum an der Donau (Niederösterreich). *Archiv für Lagerstättenforschung der Geologischen Bundesanstalt* 9, 67–72.

Merva, S. 2016. "Rejtélyes bélyegű cserépedények". Adatok a kisalföldi kora középkori grafitos kerámia régészeti és archaeometriai kutatásához. ("Clay vessels with mysterious marks". Archaeological and archaeometric research on early medieval graphitic pottery from the Hungarian Little Plain.) In: Kovács, L. and Révész, L. (eds) *Népek és kultúrák a Kárpát-medencében. Tanulmányok Mesterházy Károly tiszteletére*. Budapest – Debrecen – Szeged: Magyar Nemzeti Múzeum – Déri Múzeum – MTA BTK Régészeti Intézet – Szegedi Tudományegyetem, 521 – 541.

Middleton, A. P. 1987. Technological investigation of the coatings on some 'haematite-coated' pottery from southern England. *Archaeometry* 29 (2), 250–261.

Middleton, A. P., Freestone, I. C. and Leese, M. N. 1985. Textural analysis of ceramic thin sections: Evaluation of grain sampling procedures. *Archaeometry* 27 (1), 64–74.

Minar, C. J. 2001. Motor Skills and the learning process: the conservation of cordage final twist direction in communities of practice. *Journal of Anthropological Research* 57 (4), 381–405.

Minar, C. J. and Crown, P. L. 2001. Learning and craft production: an introduction. *Journal of Anthropological Research* 57 (4), 369–380.

Miras, A., Galán, E., González, I., Romero-Baena, A. and Martín, D. 2018. Mineralogical evolution of ceramic clays during heating. An ex/in situ X-ray diffraction method comparison study. *Applied Clay Science* 161, 176–183.

Mitterauer, M. 1969. *Zollfreiheit und Marktbereich. Studien zur mittelalterlichen Wirtschaftsverfassung am Beispiel einer niederösterreichischen Altsiedellandschaft.* (Forschungen zur Landeskunde von Niederösterreich 19.) Wien: Verein für Landeskunde.

Moorhead, J. 2005. Ostrogothic Italy and the Lombard invasions (Chapter 6). In: Fouracre, P. (ed.) *The new Cambridge medieval history. Volume I c. 500–c. 700*. Cambridge: Cambridge University Press, 140–161.

Morimoto, N., Fabries, J., Ferguson, A. K., Ginzburg, I. V., Ross, M., Seifert, F. A., Zussman, J., Aoki, K. and Gottardi, G. 1988. Nomenclature of pyroxenes. *American Mineralogist* 73, 1123–1133.

Muller, J. 1984. Mississippian specialization and salt. *American Antiquity* 49 (3), 489–507.

Müller-Mertens, E. 1999. The Ottonians as kings and emperors (Chapter 9). In: Reuter, T. (ed.) *The new Cambridge medieval history. Volume III c. 900–c. 1024*. Cambridge: Cambridge University Press, 233–266.

Mullin 2011a. Border crossings: The archaeology of borders and borderlands. An introduction. In: Mullin, D. (ed.) *Places in between: The archaeology of social, cultural and geographical borders and borderlands*. Oxford: Oxbow Books, 1–12.

Mullin 2011b. Towards an archaeology of borders and borderlands. In: Mullin, D. (ed.) *Places in between: The archaeology of social, cultural and geographical borders and borderlands*. Oxford: Oxbow Books, 99–104.

Munsell Color Company, 2004. *The Munsell Book of Color. Glossy Collection.* Munsell Color Company.

Nam, S., Walsh, R. and Lee, G.-A. 2020. Innovation, imitation, and identity: Mayeon Black ware and social complexity in Southwestern Korea. *Archaeological Research in Asia* 23, 100197.

Naum, M. 2012. Difficult middles, hybridity and ambivalence of a medieval frontier: the cultural landscape of Lolland and Falster (Denmark). *Journal of Medieval History* 38 (1), 56–75.

Nesse, W. D. 1991. *Introduction to optical mineralogy*. (Second edition.) New York and Oxford: Oxford University Press.

Newman, A. C. D. (ed.) 1987. *Chemistry of clays and clay minerals*. (Mineralogical Society Monograph 6.) Harlow: Longman Scientific & Technical, 1987.

Niziolek, L. C. 2013. Earthenware production and distribution in the prehispanic Philippine polity of Tanjay: results from laser ablation-inductively coupled plasma-mass spectrometry (LA-ICP-MS). *Journal of Archaeological Science* 40 (6), 2824–2839.

Nodari, L., Marcuz, E., Maritan, L., Mazzoli, C. and Russo, U. 2007. Hematite nucleation and growth in the firing of carbonate-rich clay for pottery production. *Journal of the European Ceramic Society* 27, 4665–4673.

O'Brien, M. J. and Bentley, R. A. 2011. Stimulated variation and cascades: Two processes in the evolution of complex technological systems. *Journal of Archaeological Method and Theory* 18, 309–337.

Obenaus, M. 2014. Niederösterreich an der Wende vom 10. zum 11. Jahrhundert – Eine archäologische Bilanz. In: Zehetmayer, R. (ed.) *Die Babenbergermark um die Jahrtausendwende. Zum Millenium des heiligen Koloman. Die Vorträge des 32. Symposiums des Niederösterreichischen Instituts für Landeskunde, Stockerau, 2. Bis 4. Juli 2012*. St. Pölten: Niederösterreichisches Institut für Landeskunde, 165–194.

Olesik, J. W. 1987. Spectrometers. In: Boumans, P. W. J. M. (ed.) *Inductively coupled plasma emission spectroscopy. Part 1. Methodology, instrumentation and performance*. (Chemical Analysis Series, Vol. 90.) New York – Chichester – Brisbane – Toronto – Singapore: John Wiley & Sons, 466–535.

Olsen, S. L. 1988. Introduction: Applications of scanning electron microscopy to archaeology. In: Olsen, S. L. (ed.): *Scanning electron microscopy in archaeology*. (BAR International Series 452.) Oxford: B.A.R., 3–7.

Orton, C. and Hughes, M. 2013. *Pottery in archaeology*. (Second edition.) New York: Cambridge University Press.

Orts, M. J., Escardino, A., Amorós, J. L. and Negre, F. 1993. Microstructural changes during the firing of stoneware floor tiles. *Applied Clay Science* 8, 193–205.

Otruba, G. 1987. Überblick der Entwicklung des niederösterreichischen Bergbaus von seinen Anfängen bis zur Gegenwart. In: Kusternig, A. (ed.) *Bergbau in Niederösterreich. Vorträge und Diskussionen des sechsten Symposions des Niederösterreichischen Instituts Für Landeskunde. Pitten, 1.-3. Juli 1985*. Wien: Selbstverlag des NÖ Instituts für Landeskunde, 61–307.

Parker, B. J. 2002. At the edge of empire: Conceptualizing Assyria's Anatolian frontier ca. 700 B.C. *Journal of Anthropological Archaeology* 21 (3), 371–395.

Parker, B. J. 2003. Archaeological manifestations of empire: Assyria's imprint on southeastern Anatolia. *American Journal of Archaeology*, 107 (4), 525–557.

Parker, B. J. 2006. Toward an understanding of borderland processes. *American Antiquity* 71 (1), 77–100.

Peacock, D. P. S. 1970. The scientific analysis of ancient ceramics: A review. *World Archaeology* 1 (3), 375–389.

Peacock, D. P. S. 1982. *Pottery in the Roman world: An ethnoarchaeological approach*. London and New York: Longman.

Peterson, S. E. and Betancourt, P. P. 2009. *Thin-section petrography of ceramic materials*. Philadelphia, Pennsylvania: INSTAP Academic Press.

Pfaffenberger, B. 1992. Social anthropology of technology. *Annual Review of Anthropology* 21, 491–516.

Philpotts, A. R. and Wilson, N. 1994. Application of petrofabric and phase equilibra analysis to the study of a potsherd. *Journal of Archaeological Science* 21, 607–618.

Poblome, J., Degryse, P., Viaene, W., Ottenburgs, R., Waelkens, M., Degeest, R. and Naud, J. 2002. The concept of a pottery production centre. An archaeometrical contribution from ancient Sagalassos. *Journal of Archaeological Science* 29 (8), 873–882.

Pohl, W. 2018. *The Avars. A steppe empire in Central Europe, 567–822*. Ithaca and London: Cornell University Press.

Poláček, L. 1998. Graphittonkeramik aus Mikulčice. In: Poláček, L. (ed.) *Frühmittelalterliche Graphittonkeramik in Mitteleuropa. Naturwissenschaftliche Keramikuntersuchungen*. (Internationale Tagungen in Mikulčice IV.) Brno: Archeologický ústav Akademie věd České republiky, 127–197.

Pool, C. A. and Bey, G. J., III 2007. Conceptual issues in Mesoamerican pottery economics. In: Pool, C. A. and Bey, G. J., III (eds) *Pottery economics in Mesoamerica*. Tucson: University of Arizona Press, 1–38.

Pradell, T. and Molera, J. 2020. Ceramic technology. How to characterise ceramic glazes. *Archaeological and Anthropological Sciences* 12, Article 189. https://link.springer.com/article/10.1007/s12520-020-01136-9

Quinn, P. S. 2008. The occurrence and research potential of microfossils in inorganic archaeological materials. *Geoarchaeology: An International Journal* 23 (2), 275–291.

Quinn, P. S. 2013. *Ceramic petrography. The interpretation of archaeological pottery & related artefacts in thin section*. Oxford: Archaeopress.

Quinn, P. S. and Benzonelli, A. 2018. XRD and materials analysis. In: López Varela, S. L. (ed.) *The encyclopedia of archaeological sciences.* New York: John Wiley & Sons. Online version: https://onlinelibrary.wiley.com/doi/abs/10.1002/9781119188230.saseas0619

Quinn, P. S. and Burton, M. 2009. Ceramic petrography and the reconstruction of hunter-gatherer craft technology in Late Prehistoric Southern California. In: Quinn, P. S. (ed.) *Interpreting silent artefacts: Petrographic approaches to cultural materials*. Oxford: Archaeopress, 267–295.

Quinn, P. S. and Burton, M. M. 2016. Ceramic distribution, migration and cultural interaction among late prehistoric (ca. 1300–200 B.P.) hunter-gatherers in the San Diego region, Southern California. *Journal of Archaeological Science: Reports* 5, 285–295.

Quinn, P. S. and Day, P. M. 2007. Ceramic micropalaeontology: the analysis of microfossils in ancient ceramics. *Journal of Micropalaeontology* 26 (2), 159–168.

Quinn, P., Yang, Y., Xia, Y., Li, X., Ma, S., Zhang, S. and Wilke, D. 2021. Geochemical evidence for the manufacture, logistics and supply-chain management of Emperor Qin Shihuang's Terracotta Army, China. *Archaeometry* 63, 40–52.

Quinn, P., Zhang, S., Xia, Y. and Li, X. 2017. Building the Terracotta Army: ceramic craft technology and organisation of production at Qin Shihuang's mausoleum complex. *Antiquity* 91 (358), 966–979.

Rasser, M. W. 2008. The European Plate: Overview. In: McCann, T. (ed.) *The geology of Central Europe. Volume 2: Mesozoic and Cenozoic*. London: The Geological Society, 1035–1036.

Rausch, A. 1992. KG Gries, MG Oberndorf an der Melk, VB Scheibbs (ÖK 54, W 195 mm, S 132 mm). *Fundberichte aus Österreich* 31, 492.

Rausch, A. 1993. KG Gries, MG Oberndorf an der Melk, VB Scheibbs. *Fundberichte aus Österreich* 32, 740–742.

Reed, S. J. B. 2005. *Electron microprobe analysis and scanning electron microscopy in geology*. Cambridge: Cambridge University Press.

Riccardi, M. P., Messiga, B. and Duminuco, P. 1999. An approach to the dynamics of clay firing. *Applied Clay Science* 15, 393–409.

Rice, P. 1981. Evolution of specialized pottery production: a trial model. *Current Anthropology* 22 (3), 219–240.

Rice, P. 1991. Specialization, standardization, and diversity: A retrospective. In: Bishop, R. and Lange, F.W. (eds) *The ceramic legacy of Anna O. Shepard*. Niwot: University of Colorado Press, 257–279.

Rice, P. M. 1987. *Pottery analysis. A sourcebook*. Chicago and London: The University of Chicago Press.

Rice, P. M. 2015. Contexts of contact and change: Peripheries, frontiers, and boundaries. In: Cusick, J. G. (ed.) *Studies in culture contact: Interaction, culture change, and archaeology*. Carbondale, Illinois: Southern Illinois University Press, 44–66.

Rice, P. M. and Rice, D. S. 2005. The final frontier of the Maya: Central Petén, Guatemala, 1450–1700 CE. In: Rodseth, L. and Parker., B. J. (eds) *Untaming the frontier in anthropology, archaeology and history*. Tucson: University of Arizona Press, 147–173.

Rodriguez-Navarro, C., Cultrone, G., Sanchez-Navas, A. and Sebastian, E. 2003. TEM study of mullite growth after muscovite breakdown. *American Mineralogist* 88, 713–724.

Rodseth, L. 2005. The fragmentary frontier: Expansion and ethnogenesis in the Himalayas. In: Rodseth, L. and Parker., B. J. (eds) *Untaming the frontier in anthropology, archaeology and history*. Tucson: University of Arizona Press, 83–109.

Rodseth, L. and Parker., B. J. 2005. Theoretical considerations in the study of frontiers. In: Rodseth, L. and Parker., B. J. (eds) *Untaming the frontier in anthropology, archaeology and history*. Tucson: University of Arizona Press, 3–21.

Rogers, E. M. 1983. *Diffusion of innovations*. (Third edition.) New York: The Free Press.

Ross, J., Fowler, K. D., Shai, I., Greenfield, H. J. and Maeir, A. M. 2018. A scanning method for the identification of pottery forming techniques at the mesoscopic scale: A pilot study in the manufacture of Early Bronze Age III holemouth jars and platters from Tell es-Safi/Gath. *Journal of Archaeological Science: Reports* 18, 551–561.

Roux, V. 2003. Ceramic standardization and intensity of production: Quantifying degrees of specialization. *American Antiquity* 68, 768–782.

Roux, V. 2015. Cultural transmission, migration and plain wheelmade pottery in the MB II Southern Levant. In: Glatz, C. (ed.) *Plain pottery traditions of the Eastern Mediterranean and Near East. Production, use, and social significance*. Walnut Creek: Left Coast Press, 69–90.

Roux, V. 2017. Ceramic manufacture: The *chaîne opératoire* approach. In: Hunt, A. M. W. (ed.) *The Oxford handbook of archaeological ceramic analysis*. Oxford: Oxford University Press, 101–113.

Roux, V. 2019. *Ceramics and society. A technological approach to archaeological assemblages*. Springer, Cham.

Rye, O. S. 1981. *Pottery technology. Principles and reconstruction*. Washington, D.C.: Taraxacum.

Sahlén, D. 2013. Selected with care? – the technology of crucibles in late prehistoric Scotland. A petrographic and chemical assessment. *Journal of Archaeological Science* 40 (12), 4207–4221.

Saliari, K. and Felgenhauer-Schmiedt, S. 2017. Skin, leather, and fur may have disappeared, but bones remain… The case study of the 10th century AD fortified settlement Sand in Lower Austria. *Annalen des Naturhistorischen Museums in Wien*, Serie A, 119, 95–114.

Sanders, A. 2015. Fingerprints, sex, state, and the organization of the Tell Leilan ceramic industry. *Journal of Archaeological Science Volume* 57, 223–238.

Sandgruber, R. 1995. *Ökonomie und Politik. Österreichische Wirtschaftsgeschichte vom Mittelalter bis zur Gegenwart.* Wien: Ueberreuter.

Sanjurjo-Sánchez, J., Montero Fenollós, J.-L., Prudêncio, M. I., Barrientos, V., Marques, R. and Dias, M. I. 2016. Geochemical study of beveled rim bowls from the Middle Syrian Euphrates sites. *Journal of Archaeological Science*: Reports 7, 808–818.

Sassaman, K. E. and Rudolphi, W. 2001. Communities of practice in the early pottery traditions of the American Southeast. *Journal of Anthropological Research*, 57 (4), 407–425.

Sauer, F. (n.d.): *Das karolingerzeitliche Gräberfeld von Purgstall*. (Leaflet.) Purgstall an der Erlauf: Bundesdenkmalamt.

Sauer, F. and Czubak, J. 1997. Hochrieβ. *Fundberichte aus Österreich* 36, 19–20.

Sauer, R. 1994. Vorbericht über archäometrische Untersuchungen von latènzeitlichen Graphittonkeramikproben. *Linzer Archäologische Forschungen* 22, 231–245.

Sauer, R. 2002. Petrographische Dünnschliffanalyse und Schwermineralanalyse (Anhang). In: Herold, H. Die Keramik der awarischen Siedlungsreste von Brunn am Gebirge, Flur Wolfholz, Bezirk Mödling, Niederösterreich. *Archaeologia Austriaca* 86, 161–181, 179–180.

Sauer, R. 2007. Ergebnisse mineralogisch-petrografischer Analysen an ausgewählten Keramikproben aus Muggendorf, Auhof, Ratzlburg und St. Pölten. In: Scharrer-Liška, G. 2007. *Die hochmittelalterliche Grafitkeramik in Mitteleuropa und ihr Beitrag zur Wirtschaftsgeschichte*. (Monographien des Römisch-Germanischen Zentralmuseums, Band 68.) Mainz: Verlag des Römisch-Germanischen Zentralmuseums, 81–102.

Sauer, R. n.d. *Ergebnisse mineralogisch-petrographischer Analysen an ausgewählten Keramikproben aus Sand, Raabs, Hard und Kleinhard*. Unpublished manuscript.

Scharrer, G. 1994. Ein Töpferofen aus Amstetten, Nö. *Beiträge zur Mittelalterarchäologie in Österreich* 10, 131–150.

Scharrer-Liška, G. 2007. *Die hochmittelalterliche Grafitkeramik in Mitteleuropa und ihr Beitrag zur Wirtschaftsgeschichte*. (Monographien des Römisch-Germanischen Zentralmuseums, Band 68.) Mainz: Verlag des Römisch-Germanischen Zentralmuseums.

Scharrer-Liška, G. 2009. … Darnach brenn ich sie in dem Feutver... Die spätmittelalterlichen Hafner in St. Pölten – Das Handwerk und seine Produkte. In: Diözesanmuseum St. Pölten (ed.) *Sant Ypoelten. Stift und Stadt im Mittelalter: Katalogbuch zur Sonderausstellung des Diözesanmuseums St. Pölten in Kooperation mit dem Österreichischen Archäologischen Institut, 5. Mai bis 31. Oktober 2009*. St. Pölten: Diözesanarchiv St. Pölten, 183–188.

Scherrer, P. 2015. Ziviles Leben am Limes. In: Gassner, V. and Pülz, A. (eds) *Der römische Limes in Österreich. Führer zu den archäologischen Denkmälern*. Wien: Österreichische Akademie der Wissenschaften, 47–67.

Schiffer, M. B. 1975. Behavioral chain analysis: activities, organization, and the use of space. In: *Chapters in the Prehistory of Eastern Arizona, IV. Fieldiana. Anthropology 65*. Chicago: Field Museum of Natural History, 103–119.

Schiffer, M. B. 2011. *Studying technological change: a behavioral approach*. Salt Lake City: University of Utah Press.

Schiffer, M. B. and Skibo, M. 1997. The explanation of artifact variability. *American Antiquity* 62 (1), 27–50.

Schlanger, N. 2005. The chaîne opératoire. In: Renfrew, C. and Bahn, P. (eds) *Archaeology: The key concepts.* London and New York: Routledge Key Guides, 25–31.

Scholz, U. M. 2015. *Die Grabung Tulln Hauptplatz: Untersuchungen zu Markt und Raum in der mittelalterlichen Stadt*. Unpublished thesis, University of Vienna.

Schön, D., Gaisbauer, I. and Langendorf, A. 2019. Die Ausgrabung nach dem Abbruch der beiden Häuser Ruprechtsplatz 4 und 5 im Jahr 1970. In: Felgenhauer-Schmiedt, S. (ed.) *Von Vindobona zu Wienna – Archäologisch-historische Untersuchungen zu den Anfängen Wiens*. (Beiträge zur Mittelalterarchäologie in Österreich, Beiheft 11.) Wien: Österreichische Gesellschaft für Mittelalterarchäologie, 36–57.

Schrauder, M., Beran, A., Hoernes, S. and Richter, W. 1993. Constraints on the origin and genesis of graphite-bearing rocks from the Variegated Sequence of the Bohemian Massif (Austria). *Mineralogy and Petrology* 49, 175–188.

Shelley, D. 1985. *Optical mineralogy*. (Second edition.) Amsterdam, Oxford and New York: Elsevier.

Shennan, S. J. 2000. Population, culture history, and the dynamics of culture change. *Current Anthropology* 4, 811–835.

Shepard, J. 1995. Slavs and Bulgars (Chapter 9). In: McKitterick, R. (ed.) *The new Cambridge medieval history. Volume II c. 700–c. 900*. Cambridge: Cambridge University Press, 228–248.

Shortland, A. J. 2004. Hopeful monsters? Invention and innovation in the archaeological record. In: Bourriau, J. and Phillips, J. (eds) *Invention and innovation: the social context of technological change. Volume 2.* Egypt, the Aegean and the Near East, 1650–1150 BC. Oxford: Oxbow books, 1–11.

Shortland, A. J., Kirk, S., Eremin, K., Degryse, P. and Walton, M. 2018. The analysis of late Bronze Age glass from Nuzi and the question of the origin of glass-making. *Archaeometry* 60, 764–783.

Shriner, C. and Dorais, M. J. 1999. A comparative electron microprobe study of Lerna III and IV ceramics and local clay-rich sediments. *Archaeometry* 41 (1), 25–49.

Siivola, J. and Schmid, R. 2007. *List of mineral abbreviations. Recommendations by the IUGS Subcommission on the Systematics of Metamorphic Rocks*. Web version 01.02.07. http://www.bgs.ac.uk/scmr/docs/papers/paper_12.pdf

Sillar, B. 2000. Dung by preference: the choice of fuel as an example of how Andean pottery production is embedded within wider technical, social, and economic practices." *Archaeometry* 42 (1), 43–60.

Sillar, B. and Tite, M. S. 2000. The challenge of 'technological choices' for materials science approaches in archaeology. *Archaeometry* 42 (1), 2–20.

Sinopoli, C. M. 1988. The organisation of craft production at Vijayanagara, South India. *American Anthropologist* 90 (3), 580–597.

Skibo, J. M. and Schiffer, M. B. 2008. *People and things. A behavioral approach to material culture*. New York: Springer.

Smith, J. M. H. 1995. Fines imperii: the marches (Chapter 6). In: McKitterick, R. (ed.) *The new Cambridge medieval history. Volume II c. 700–c. 900*. Cambridge: Cambridge University Press, 169–189.

Sørensen, M. L. S. 1989. Ignoring innovation – denying change: The role of iron and the impact of external influences on the transformation of Scandinavian societies 800–500 BC. In: van der Leeuw, S. E. and Torrence, R. (eds) *What's new? A closer look at the process of innovation*. London: Unwin Hyman, 182–202.

Sorresso, D. C. and Quinn, P. S. 2020. Re-examining shell-tempered Chickasaw pottery in post-contact Mississippi, USA. *Journal of Archaeological Science: Reports* 32, 102415.

Spišiak, J. 2007. Petrografia, mineralógia a geochémia úlomkov grafitovej keramiky z Beluše. (Petrographie, Mineralogie und Geochemie der Bruchstücke von Graphitkeramik aus Beluša.) *Slovenská archeológia* 55, 123–26.

St. John, A. and Ferris, N. 2019. Unravelling identities on archaeological borderlands: Late Woodland Western Basin and Ontario Iroquoian Traditions in the Lower Great Lakes region. *The Canadian Geographer / Le Géographe canadien* 63, 43–56.

Stadler, P., Friesinger, H., Kutschera, W., Priller, A., Steier, P. and Wild, E. M. 2003. Ein Beitrag zur Absolutchronologie der Langobarden und ein Versuch zur Datierung der Beraubung langobardischer Gräber. *Archaeologia Austriaca* 87, 265–278.

Stanley, C. R. and Lawie, D. 2007. Average relative error in geochemical determinations: Clarification, calculation, and a plea for consistency. *Exploration and Mining Geology* 16, 265–274.

Stark, M. T. 1991. Ceramic production and community specialization: A Kalinga ethnoarchaeological study. *World Archaeology* 23 (1), 64–78.

Stark, M. T. 1998. Technical choices and social boundaries in material culture patterning: an introduction. In: Stark, M. T. (ed.) *The archaeology of social boundaries. (Smithsonian series in archaeological inquiry.)* Washington, WA and London: Smithsonian Institution Press, 1–11.

Stockhammer, P. W. and Athanassov, B. 2018. Conceptualising contact zones and contact spaces: An archaeological perspective. In: Gimatzidis, S., Pieniążek, M. and Mangaloğlu-Votruba, S. (eds) *Archaeology across Frontiers and borderlands: Fragmentation and connectivity in the North Agean and the Central Balkans from the Bronze Age to the Iron Age*. Austrian Academy of Sciences Press, 93–112.

Stoner, W. D., Pool, C. A., Neff, H. and Glascock, M. D. 2008. Exchange of Coarse Orange pottery in the Middle Classic Tuxtla Mountains, Southern Veracruz, Mexico. *Journal of Archaeological Science* 35 (5), 1412–1426.

Stoops, G. 2003. *Guidelines for analysis and description of soil and regolith thin sections*. Madison, Wisconsin: Soil Science Society of America.

Strasheim, A. 1987. Instrumentation for optical emission spectrometry. In: Montaser, A. and Golightly, D. W. (eds) *Inductively coupled plasmas in analytical atomic spectrometry*. New York: VCH, 69–121.

Strzelczyk, J. 1999. Bohemia and Poland: two examples of successful western Slavonic state-formation (Chapter 20). In: Reuter, T. (ed.) *The new Cambridge medieval history. Volume III c. 900–c. 1024*. Cambridge: Cambridge University Press, 514–535.

Stuppner, A. 2015. Römer und Germanen am norisch-pannonischen Limes. In: Gassner, V. and Pülz, A. (eds) *Der römische Limes in Österreich. Führer zu den archäologischen Denkmälern*. Wien: Österreichische Akademie der Wissenschaften, 110–126.

Suhr, N. H. and Ingamells, C. O. 1966. Solution technique for analysis of silicates. *Analytical Chemistry* 38 (6), 730–734.

Szakmány, G. 2013. Kerámiák archeometriai vizsgálata – kőzettani és geokémiai módszerek. (Archeometric analysis of pottery: petrographic and geochemical methods.) In: Révész, L. and Wolf, M. (eds) *A honfoglalás kor kutatásának legújabb eredményei. Tanulmányok Kovács László 70. születésnapjára*. Szeged: Szegedi Tudományegyetem Régészeti Tanszék, 735–754.

Szakmány, G. and Bendő, Z. 2016. Kora középkori kisalföldi grafitos kerámiák petrográfiai és SEM-EDX vizsgálati eredményei. (Results of petrographical and SEM-EDX analyses on early medieval graphitic pottery from the Little Hungarian Plain.) In: Kovács, L. and Révész, L. (eds) *Népek és kultúrák a Kárpát-medencében. Tanulmányok Mesterházy Károly tiszteletére*. Budapest – Debrecen – Szeged: Magyar Nemzeti Múzeum – Déri Múzeum – MTA BTK Régészeti Intézet – Szegedi Tudományegyetem, 542–561.

Szakmány, G. and Nagy, A. 2017. Kerámiák petrográfiai mikroszkópos vizsgálata: megfigyelések és értelmezés. (Ceramics under the petrographic microscope: observations and interpretation.) In: Ridovics, A., Bajnóczi, B., Dági, M. and Lővei, P. (eds) *Interdiszciplinaritás. Archeometriai, régészeti és művészettörténeti tanulmányok*. Budapest: Magyar Nemzeti Múzeum – Szépművészeti Múzeum, 249–261.

Szameit, E. 1991. Anmerkungen zur Chronologie des 8.–9. Jahrhunderts im Ostalpenraum. *Zalai Múzeum* 3, 73–79.

Szameit, E. 2000. Zum archäologischen Bild der frühen Slawen in Österreich. Mit Fragen zur ethnischen Bestimmung karolingerzeitlichen Gräberfelder im Ostalpenraum. In: Bratož, R. (ed.): *Slowenien und die Nachbarländer zwischen Antike und karolingischer Epoche. Anfänge der slowenischen Ethnogenese. Band I*. Ljubljana, 507–547.

Szőke, B. M. 2004. A határ fogalmának változásai a korai középkorban. (Adatok a Kerka-vidék kora középkori településtörténetéhez.) (Changes in the concept of border in Early Medieval Period. Some data to the settlement history of the Kerka region.) *Zalai Múzeum* 13, 177–192.

Szőke, B. M. 2021. *Die Karolingerzeit in Pannonien*. (Monographien des Römisch-Germanischen Zentralmuseums, Band 145.) Mainz: Verlag des Römisch-Germanischen Zentralmuseums.

Tatje, T. A. and Naroll, R. 1973. Two measures of societal complexity: An empirical cross cultural comparison. In: Naroll, R. and Cohen, R. (eds) *A handbook of method in cultural anthropology*. New York: Columbia University Press, 766–833.

Thér, R. and Mangel, T. 2021. Two trajectories of the development of pottery forming methods in central Europe in the Iron Age: The contribution of analysis of the orientation of components of a ceramic body. *Journal of Archaeological Science: Reports* 35, 102717.

Thér, R., Kallistová, A., Svoboda, Z., Květina, P., Lisá, L., Burgert, P. and Bajer, A. 2019. How was neolithic pottery fired? An exploration of the effects of firing dynamics on ceramic products. *Journal of Archaeological Method and Theory* 26, 1143–1175.

Thér, R., Mangel, T. and Gregor, M. 2017. Potter's wheel in the Iron Age in central Europe: Process or product innovation? *Journal of Archaeological Method and Theory* 24, 1256–1299.

Thompson, M. 1987. Analytical performance of inductively coupled plasma-atomic emission spectrometry. In: Montaser, A. and Golightly, D. W. (eds) *Inductively coupled plasmas in analytical atomic spectrometry*. New York: VCH, 163–199.

Thompson, M. and Walsh, J. N. 2003. *A handbook of inductively coupled plasma atomic emission spectrometry*. Woking: Viridian Publishing.

Thornton, C. P. and Rehren, T. 2009. A truly refractory crucible from fourth millennium Tepe Hissar, Northeast Iran. *Journal of Archaeological Science* 36 (12), 2700–2712.

Tilley, C., Keane, W., Küchler, S., Rowlands, M. and Spyer, P. (eds) 2006. *Handbook of material culture*. London: Sage.

Tite M., Herringer S. N., Shortland A., Matin M., Pradell T. and Alcock S. E. 2018. Production technology of Nabataean painted pottery compared with that of Roman terra sigillata. *Journal of Archaeological Science: Reports* 21, 1073–1078.

Tite, M. S. 1992. The impact of electron microscopy on ceramic studies. *Proceedings of the British Academy* 77, 111–131.

Tite, M. S. 1999. Pottery production, distribution, and consumption. The contribution of the physical sciences. *Journal of Archaeological Method and Theory* 6, 181–233.

Tite, M. S. 2009. The production technology of Italian maiolica: a reassessment. *Journal of Archaeological Science* 36 (10), 2065–2080.

Tite, M. S. and Maniatis, Y. 1975. Examination of ancient pottery using the scanning electron microscope. *Nature* 257, 122–123.

Tite, M. S., Freestone, I. C., Meeks, N. D. and Bimson, M. 1982. The use of scanning electron microscopy in the technological examination of ancient ceramics. In: Olin, J. S. and Franklin, A. D. (eds) *Archaeological ceramics*. Washington, D.C.: Smithsonian Institution Press, 109–120.

Tite, M. S., Kilikoglou, V., and Vekinis, V. 2001. Strength, toughness and thermal shock resistance of ancient ceramics, and their influence on technological choice (Review article). *Archaeometry* 43 (3), 301–324.

Trebsche, P. 2011. Eisenzeitliche Graphittonkeramik im mittleren Donauraum. In: Schmotz, K. (Hrsg.) *Vorträge des 29. Niederbayerischen Archäologentages*. Rahden/Westf.: Verlag Marie Leidorf GmbH, 449–481.

Trindade, M. J., Dias, M. I., Coroado, J. and Rocha, F. 2009. Mineralogical transformations of calcareous rich clays with firing: A comparative study between calcite and dolomite rich clays from Algarve, Portugal. *Applied Clay Science* 42, 345–355.

Tsolakidou, A. and Kilikoglou, V. 2002. Comparative analysis of ancient ceramics by neutron activation analysis, inductively coupled plasma–optical-emission spectrometry, inductively

coupled plasma–mass spectrometry, and X-ray fluorescence. *Analytical and Bioanalytical Chemistry* 374, 566–572.

Tsolakidou, A., Buxeda i Garrigós, J. and Kilikoglou, V. 2002. Assessment of dissolution techniques for the analysis of ceramic samples by plasma spectrometry. *Analytica Chimica Acta* 474, 177–188.

Underhill, A. P. 2003. Investigating variation in organization of ceramic production: An ethnoarchaeological study in Guizhou, China. *Journal of Archaeological Method and Theory* 10, 203–275.

van der Leeuw, S. 1977. Towards a study of the economics of pottery making. In: van Beek, B. L., Brandt, R. W. and Groenman-Van Waateringe, W. (eds) *Ex Horreo*. Amsterdam: University of Amsterdam, 68–76.

van der Leeuw, S. 1993. Giving the potter a choice. Conceptual aspects of pottery techniques. In: Lemonnier, P. (ed.) *Technological choices. Transformation in material cultures since the Neolithic*. London and New York: Routledge, 238–288.

Vaughn, K. J. and Neff, H. 2004. Tracing the clay source of Nasca polychrome pottery: results from a preliminary raw material survey. *Journal of Archaeological Science* 31 (11), 1577–1586.

Velde, B. and Druc, I. C. 1999. *Archaeological Ceramic Materials. Origin and Utilization*. Berlin: Springer.

Viani, A., Cultrone, G., Sotiriadis, K., Ševčík, R. and Šašek, P. 2018. The use of mineralogical indicators for the assessment of firing temperature in fired-clay bodies. *Applied Clay Science* 163, 108–118.

Vicenzi, E. P., Eggins, S., Logan, A. and Wysoczanski, R. 2002. Microbeam characterization of Corning archeological reference glasses: New additions to the Smithsonian Microbeam Standard Collection. *Journal of Research of the National Institute of Standards and Technology* 107 (6), 719–727.

Vocelka, K. 2010. *Österreichische Geschichte*. (3. Auflage) München: Verlag C. H. Beck.

Wagner, B., Nowak, A., Bulska, E., Hametner, K. and Günther, D. 2012. Critical assessment of the elemental composition of Corning archeological reference glasses by LA-ICP-MS. *Analytical and Bioanalytical Chemistry* 402 (4), 1667–1677.

Walton S. J. 2003. The analysis of archaeological materials by ICP-AES. In: Thompson, M. and Walsh, J. N. *A handbook of inductively coupled plasma atomic emission spectrometry*. Woking: Viridian Publishing, 232–237.

Wang, L.-Y. and Marwick, B. 2020. Standardization of ceramic shape: A case study of Iron Age pottery from northeastern Taiwan. *Journal of Archaeological Science: Reports* 33, 102554.

Warren, B. E. 1969. *X-ray diffraction*. Reading, Massachusetts – Menlo Park, California – London – Amsterdam – Don Mills, Ontario – Sydney: Addison-Wesley Publishing Company.

Watson, O. 2014. Revisiting Samarra: the rise of Islamic glazed pottery. In: Gonnella, J., Abdellatif, R. and Struth, S. (eds) *Beiträge zur Islamischen Kunst und Archäologie. Band 4.* Wiesbaden: Dr. Ludwig Reichert Verlag, 123–142.

Weber, L. (ed.) 1997a. Verzeichnis der bearbeiteten Rohstoffvorkommen, nach ÖK-Blättern geordnet (Beilage). In: Weber, L. (ed.) *Handbuch der Lagerstätten der Erze, Industrieminerale und Energierohstoffe Österreichs*. (Archiv für Lagerstätten Forschung, Band 19.) Wien: Geologische Bundesanstalt.

Weber, L. 1987. Die geologischen Grundlagen des Grafitbergbaues in Niederösterreich. In: Kusternig, A. (ed.) *Bergbau in Niederösterreich. Vorträge und Diskussionen des sechsten Symposions des Niederösterreichischen Instituts für Landeskunde. Pitten, 1.-3. Juli 1985*. (Studien und Forschungen aus dem Niederösterreichischen Institut für Landeskunde, Band 10.) Wien: NÖ Instituts für Landeskunde, 369–387.

Weber, L. 1997b. Kaolinbezirk Mühl- und Waldviertel. In: Weber, L. (ed.) *Handbuch der Lagerstätten der Erze, Industrieminerale und Energierohstoffe Österreichs*. (Archiv für Lagerstätten Forschung, Band 19.) Wien: Geologische Bundesanstalt, 235.

Weber, L. 1997c. Graphitbezirk Veitscher Decke. In: Weber, L. (ed.) *Handbuch der Lagerstätten der Erze, Industrieminerale und Energierohstoffe Österreichs*. (Archiv für Lagerstätten Forschung, Band 19.) Wien: Geologische Bundesanstalt, 341.

Weber, L. and Götzinger M. A. 1997. Graphitbezirk Bunte Serie. In: Weber, L. (ed.) *Handbuch der Lagerstätten der Erze, Industrieminerale und Energierohstoffe Österreichs*. (Archiv für Lagerstätten Forschung, Band 19.) Wien: Geologische Bundesanstalt, 231.

Wells, P. S. 2015. Culture contact, identity, and change in the European provinces of the Roman Empire. In: Cusick, J. G. (ed.) *Studies in culture contact: Interaction, culture change, and archaeology*. Carbondale, Illinois: Southern Illinois University Press, 316–334.

Wendrich, W. 2012a. Archaeology and apprenticeship: body knowledge, identity, and communities of practice. In: Wendrich, W. (ed.) *Archaeology and apprenticeship: body knowledge, identity, and communities of practice*. Tucson: University of Arizona Press, 1–19.

Wendrich, W. 2012b. Recognizing knowledge transfer in the archaeological record. In: Wendrich, W. (ed.) *Archaeology and apprenticeship: body knowledge, identity, and communities of practice*. Tucson: University of Arizona Press, 255–262.

Wenger, E. 1998. *Communities of practice: learning, meaning, and identity*. Cambridge and New York: Cambridge University Press.

Wenger, E. 2000. Communities of practice and social learning systems. *Organization* 7, 225–246.

Wessely, G. 2006a. Kalkalpen. In: Wessely, G. (ed.) *Niederösterreich. Geologie der österreichischen Bundesländer*. Wien: Geologische Bundesanstalt, 105–166.

Wessely, G. 2006b. Geologie Niederösterreichs in Kurzfassung. In: Wessely, G. (ed.) *Niederösterreich. Geologie der österreichischen Bundesländer*. Wien: Geologische Bundesanstalt, 11–13.

Wessely, G. 2006c. Geologisch geprägte Landschaften - Eine Einstimmung. In: Wessely, G. (ed.) *Niederösterreich. Geologie der österreichischen Bundesländer*. Wien: Geologische Bundesanstalt, 15–21.

Wessely, G. 2006d. Wiener Becken. In: Wessely, G. (ed.) *Niederösterreich. Geologie der österreichischen Bundesländer*. Wien: Geologische Bundesanstalt, 189–226.

Wessely, G. 2006e. Molassezone. In: Wessely, G. (ed.) *Niederösterreich. Geologie der österreichischen Bundesländer*. Wien: Geologische Bundesanstalt, 41–67.

Wessely, G. 2006f. Alpen und Karpaten. In: Wessely, G. (ed.) *Niederösterreich. Geologie der österreichischen Bundesländer*. Wien: Geologische Bundesanstalt, 77–83.

Wessely, G. 2006g. Flyschzone und Klippenzonen. In: Wessely, G. (ed.) *Niederösterreich. Geologie der österreichischen Bundesländer*. Wien: Geologische Bundesanstalt, 85–103.

Whitbread, I. K. 1986. The characterisation of argillaceous inclusions in ceramic thin sections. *Archaeometry* 28 (1), 79–88.

Whitbread, I. K. 1989. A proposal for the systematic description of thin sections towards the study of ancient ceramic techonogy. In: Maniatis, Y. (ed.) *Archaeometry. Proceedings of the 25th International Symposium*. Amsterdam, Oxford, New York and Tokyo: Elsevier, 127–138.

Whitbread, I. K. 1995. *Greek transport amphorae. A petrological and archaeological study*. Athens: British School at Athens.

Whitbread, I. K. 1996. Detection and interpretation of preferred orientaion in ceramic thin sections. In: Higgins, T., Main, P. and Lang, J. (eds) *Imaging the past. Electronic imaging and computer graphics in museums and archaeology*. (British Museum Occasional Paper No. 114.) London: British Museum Research Laboratory, 173–181.

Whitbread, I. K. 2001. Ceramic petrology, clay geochemistry and ceramic production – from the technology to the mind of the potter. In: Brothwell, D. R. and Pollard, A. M. (eds) *Handbook of archaeological sciences*. London: Wiley, 449–459.

Whitbread, I. K. 2017. Fabric description of archaeological ceramics. In: Hunt, A. M. W. (ed.) *The Oxford handbook of archaeological ceramic analysis*. Oxford: Oxford University Press, 200–216.

Wiese, F. and Čech, S. 2008. Waschberg-Ždánice Zone and autochthonous equivalents. In: McCann, T. (ed.) *The geology of Central Europe. Volume 2: Mesozoic and Cenozoic*. London: The Geological Society, 964.

Wilkinson, I. P., Quinn, P. S., Williams, M., Taylor, J. and Whitbread, I. K. 2017. Ceramic micropalaeontology. In: Hunt, A. M. W. (ed.) *The Oxford handbook of archaeological ceramic analysis*. Oxford: Oxford University Press, 266–287.

Winckler, K. 2012. Die Alpen als Grenze und Grenzen in den Alpen. *Archaeologia Austriaca* 96, 147–161.

Winter, H. 1997. *Awarische Grab- und Streufunde aus Ostösterreich. Ein Beitrag zur Siedlungsgeschichte*. (Monographien zur Frühgeschichte und Mittelalterarchäologie 4.) Innsbruck: Universitätsverlag Wagner.

Wolfram, H. 1995. *Grenzen und Räume. Geschichte Österreichs vor seiner Entstehung. Österreichische Geschichte 378–907*. Wien: Ueberreuter.

Wolfram, H. 1999. Bavaria in the tenth and early eleventh centuries (Chapter 11). In: Reuter, T. (ed.) *The new Cambridge medieval history. Volume III c. 900–c. 1024*. Cambridge: Cambridge University Press, 293–309.

Wright, H. T. 2016. The Uruk expansion and beyond: archaeometric and social perspectives on exchange in the IVth millennium BCE. *Journal of Archaeological Science: Reports* 7, 900–904.

Yardley, B. W. D., MacKenzie, W. S. and Guilford, C. 1990. *Atlas of metamorphic rocks and their textures*. Essex: Longman.

Young, R. A. (ed.) 1993. *The Rietveld method*. (IUCr Monographs on Crystallography, Vol. 5.) New York: Oxford University Press.

Young, S. M. M. and Pollard, A. M. 2000. Atomic spectroscopy and spectrometry. In: Ciliberto, E. and Spoto, G. (eds) *Modern analytical methods in art and archaeology*. (Chemical Analysis Series, Vol. 155.) New York – Chichester – Weinheim – Brisbane – Singapore – Toronto: John Wiley & Sons, 21–53.

Zehetmayer, R. (ed.) 2007a. *Schicksalsjahr 907. Die Schlacht bei Pressburg und das frühmittelalterliche Niederösterreich. Katalog zur Ausstellung des Niederösterreichischen Landesarchivs, 3. Juli bis 28. Oktober 2007 in der Kulturfabrik Hainburg*. St. Pölten: Niederösterreichisches Institut für Landeskunde.

Zehetmayer, R. 2007b. Zur Geschichte des niederösterreichischen Raums im 9. und in der ersten Hälfte des 10. Jahrhunderts. In: Zehetmayer, R. (ed.) *Schicksalsjahr 907. Die Schlacht bei Pressburg und das frühmittelalterliche Niederösterreich. Katalog zur Ausstellung des Niederösterreichischen Landesarchivs, 3. Juli bis 28. Oktober 2007 in der Kulturfabrik Hainburg*. St. Pölten: Niederösterreichisches Institut für Landeskunde, 17–30.

Zeller, B. 2007. Baiern, das Ostfränkische Reich und die Ungarn zwischen der Niederlage bei Pressburg und dem Sieg auf dem Lechfeld bei Augsburg 907–955. In: Zehetmayer, R. (ed.) *Schicksalsjahr 907. Die Schlacht bei Pressburg und das frühmittelalterliche Niederösterreich. Katalog zur Ausstellung des Niederösterreichischen Landesarchivs, 3. Juli bis 28. Oktober 2007 in der Kulturfabrik Hainburg*. St. Pölten: Niederösterreichisches Institut für Landeskunde, 45–56.

Zimmermann, U. 2012. Tulln. *Fundberichte aus Österreich* 51, 235–236.

Živković, J., Bikić, V., Carvajal López, J. C. and Georgakopoulou, M. 2021. Ceramic production on the Middle Danube frontier: Belgrade in the 14th and 15th centuries. *Journal of Archaeological Science: Reports* 36, 102809.

Zöllner, E. 1970. *Geschichte Österreichs. Von den Anfängen bis zur Gegenwart*. (4. Auflage) Wien: Verlag für Geschichte und Politik.

APPENDICES

Appendix A Archaeological data of the investigated pottery sherds

	Site name	Type of site	Find collection	Find context	Find / inventory number; former sample / probe number	Dating (century AD)
S1	Purgstall, 8th-9th-century cemetery	Cemetery	Excavation	Grave 37	Find Nr. 29; Probe 1	8–9
S2	Purgstall, 8th-9th-century cemetery	Cemetery	Excavation	Grave 82	Find Nr. 84; Probe 2	8–9
S3	Purgstall, 8th-9th-century cemetery	Cemetery	Excavation	Grave 60	Find Nr. 319; Probe 3	8–9
S4	Purgstall, 8th-9th-century cemetery	Cemetery	Excavation	Grave 1	Find Nr. 523; Probe 4	8–9
S5	Purgstall, 8th-9th-century cemetery	Cemetery	Excavation	Grave 3	Find Nr. 248; Probe 5	8–9
S6	Purgstall, 8th-9th-century cemetery	Cemetery	Excavation	Grave 57	Find Nr. 313; Probe 6	8–9
S7	Purgstall, 8th-9th-century cemetery	Cemetery	Excavation	Grave 50	Find Nr. 93; Probe 7	8–9
S8	Purgstall, 8th-9th-century cemetery	Cemetery	Excavation	Grave 65	Find Nr. 321; Probe 8	8–9
S9	Purgstall, 8th-9th-century cemetery	Cemetery	Excavation	Grave 101	Find Nr. 702; Probe 9	8–9
S10	Purgstall, 8th-9th-century cemetery	Cemetery	Excavation	Grave 287	Find Nr. 456; Probe 10	8–9
S11	Purgstall, 8th-9th-century cemetery	Cemetery	Excavation	Grave 181	Find Nr. 738 (Vessel 1, smaller vessel); Probe 11	8–9
S12	Purgstall, 8th-9th-century cemetery	Cemetery	Excavation	Grave 181	Find Nr. 738 (Vessel 2, larger vessel); Probe 12	8–9
S13	Purgstall, 8th-9th-century cemetery	Cemetery	Excavation	Grave 133	Find Nr. 423; Probe 13	8–9
S14	Purgstall, 8th-9th-century cemetery	Cemetery	Excavation	Grave 182	Find Nr. 101; Probe 14	8–9
S15	Purgstall, 8th-9th-century cemetery	Cemetery	Excavation	Grave 161	Find Nr. 600; Probe 15	8–9
S16	Purgstall, 8th-9th-century cemetery	Cemetery	Excavation	Grave 180	Find Nr. 782; Probe 16	8–9
S17	Purgstall, 8th-9th-century cemetery	Cemetery	Excavation	Grave 106	Find Nr. 96; Probe 17	8–9
S18	Purgstall, 8th-9th-century cemetery	Cemetery	Excavation	Grave 151	Find Nr. 127; Probe 18	8–9
S19	Purgstall, 8th-9th-century cemetery	Cemetery	Excavation	Grave 102	Find Nr. 363; Probe 19	8–9
S20	Purgstall, 8th-9th-century cemetery	Cemetery	Excavation	Grave 154	Find Nr. 215; Probe 20	8–9
S21	Purgstall, 8th-9th-century cemetery	Cemetery	Excavation	Grave 55	Find Nr. 311; Probe 21	8–9
S22	Purgstall, 8th-9th-century cemetery	Cemetery	Excavation	Grave 257	Find Nr. 626; Probe 22	8–9
S23	Purgstall, 8th-9th-century cemetery	Cemetery	Excavation	Grave 98	Find Nr. 50; Probe 23	8–9
S24	Purgstall, 8th-9th-century cemetery	Cemetery	Excavation	Grave 293	Find Nr. 525; Probe 24	8–9
S25	Purgstall, 8th-9th-century cemetery	Cemetery	Excavation	Grave 244	Find Nr. 655; Probe 25	8–9
S26	Purgstall, 8th-9th-century cemetery	Cemetery	Excavation	Grave 254	Find Nr. 663; Probe 26	8–9
S27	Purgstall, 8th-9th-century cemetery	Cemetery	Excavation	Grave 171	Find Nr. 256; Probe 27	8–9
S28	Purgstall, 8th-9th-century cemetery	Cemetery	Excavation	Grave 152	Find Nr. 133; Probe 28	8–9
S29	Purgstall, 8th-9th-century cemetery	Cemetery	Excavation	Grave 222	Find Nr. 772; Probe 29	8–9

	Site name	Type of site	Find collection	Find context	Find / inventory number; former sample / probe number	Dating (century AD)
S30	Purgstall, 8th-9th-century cemetery	Cemetery	Excavation	Grave 288	Find Nr. 552; Probe 30	8–9
S31	Wieselburg, Kirchenberg	Settlement	Surface collection			10–11
S32	Wieselburg, Kirchenberg	Settlement	Surface collection			10–11
S33	Wieselburg, Kirchenberg	Settlement	Surface collection			10–11
S34	Wieselburg, Kirchenberg	Settlement	Surface collection			10–11
S35	Wieselburg, Kirchenberg	Settlement	Surface collection			10–11
S36	Wieselburg, Kirchenberg	Settlement	Surface collection			10–11
S37	Purgstall, Site 10, Plot 731, 732, 735, 737/1, 737/2, 752/1, 752/4	Settlement	Surface collection			1–5
S38	Purgstall, Site 10, Plot 731, 732, 735, 737/1, 737/2, 752/1, 752/4	Settlement	Surface collection			1–9
S39	Purgstall, Site 10, Plot 731, 732, 735, 737/1, 737/2, 752/1, 752/4	Settlement	Surface collection			9–11
S40	Purgstall, Site 10, Plot 731, 732, 735, 737/1, 737/2, 752/1, 752/4	Settlement	Surface collection			1–5
S41	Purgstall, Site 10, Plot 731, 732, 735, 737/1, 737/2, 752/1, 752/4	Settlement	Surface collection			1–5
S42	Purgstall, Site 10, Plot 731, 732, 735, 737/1, 737/2, 752/1, 752/4	Settlement	Surface collection			1–5
S43	Purgstall, Site 10, Plot 731, 732, 735, 737/1, 737/2, 752/1, 752/4	Settlement	Surface collection			1–5
S44	Purgstall, Site 10, Plot 731, 732, 735, 737/1, 737/2, 752/1, 752/4	Settlement	Surface collection			8–9
S45	Purgstall, Site 10, Plot 731, 732, 735, 737/1, 737/2, 752/1, 752/4	Settlement	Surface collection			1–5
S46	Purgstall, Site 10, Plot 731, 732, 735, 737/1, 737/2, 752/1, 752/4	Settlement	Surface collection			1–9
S47	Purgstall, Site 10, Plot 731, 732, 735, 737/1, 737/2, 752/1, 752/4	Settlement	Surface collection			1–6
S48	Purgstall, Site 10, Plot 731, 732, 735, 737/1, 737/2, 752/1, 752/4	Settlement	Surface collection			1–6
S49	Purgstall, Site 10, Plot 731, 732, 735, 737/1, 737/2, 752/1, 752/4	Settlement	Surface collection			9–11
S50	Purgstall, Site 10, Plot 731, 732, 735, 737/1, 737/2, 752/1, 752/4	Settlement	Surface collection			9–11
S51	Purgstall, Site 26, Plot 107	Settlement	Surface collection			1–9
S52	Purgstall, Site 26, Plot 107	Settlement	Surface collection			9–11
S53	Purgstall, Site 26, Plot 107	Settlement	Surface collection			10–12
S54	Purgstall, Site 26, Plot 107	Settlement	Surface collection			10–12
S55	Purgstall, Site 47, Plot 304/1, 313	Settlement	Surface collection			8–9
S56	Purgstall, Site 47, Plot 304/1, 313	Settlement	Surface collection			8–9
S57	Purgstall, Site 47, Plot 304/1, 313	Settlement	Surface collection			6–7
S58	Purgstall, Site 47, Plot 304/1, 313	Settlement	Surface collection			6–7
S59	Purgstall, Site 47, Plot 304/1, 313	Settlement	Surface collection			6–7
S60	Purgstall, Site 47, Plot 304/1	Settlement	Surface collection		Sample 9	8–9
S61	Purgstall, Site 47, Plot 304/1	Settlement	Surface collection		Sample 10	8–9
S62	Zehnbach, Site 16, Plot 220/3	Settlement	Surface collection			9–11
S63	Zehnbach, Site 16, Plot 220/3	Settlement	Surface collection			8–9
S64	Hochrieß, Site 39, Plot 281, 285/1, 290	Settlement	Surface collection			8–9
S65	Hochrieß, Site 39, Plot 281, 285/1, 290	Settlement	Surface collection			8–9

	Site name	Type of site	Find collection	Find context	Find / inventory number; former sample / probe number	Dating (century AD)
S66	Hochrieß, Site 39, Plot 281, 285/1, 290	Settlement	Surface collection			8–9
S67	Hochrieß, Site 39, Plot 281, 285/1, 290	Settlement	Surface collection			8–9
S68	Hochrieß, Site 39, Plot 281, 285/1, 290	Settlement	Surface collection			8–9
S69	Hochrieß, Site 39, Plot 281, 285/1, 290	Settlement	Surface collection			8–9
S70	Hochrieß, Site 39, Plot 281, 285/1, 290	Settlement	Surface collection			8–9
S71	Hochrieß, Site 39, Plot 281, 285/1, 290	Settlement	Surface collection			8–9
S72	Hochrieß, Site 39, Plot 281, 285/1, 290	Settlement	Surface collection			8–9
S73	Hochrieß, Site 39, Plot 281, 285/1, 290	Settlement	Surface collection			8–9
S74	Hochrieß, Site 39, Plot 281, 285/1, 290	Settlement	Surface collection			8–9
S75	Hochrieß, Site 39, Plot 281, 285/1, 290	Settlement	Surface collection			8–9
S76	Hochrieß, Site 39, Plot 281, 285/1, 290	Settlement	Surface collection			8–9
S77	Hochrieß, Site 39, Plot 281, 285/1, 290	Settlement	Surface collection			8–9
S78	Hochrieß, Site 39, Plot 281, 285/1, 290	Settlement	Surface collection			8–9
S79	Hochrieß, Site 39, Plot 281, 285/1, 290	Settlement	Surface collection			8–9
S80	Hochrieß, Site 39, Plot 281, 285/1, 290	Settlement	Surface collection			8–9
S81	Hochrieß, Site 39, Plot 281, 285/1, 290	Settlement	Surface collection			8–9
S82	Hochrieß, Site 39, Plot 281, 285/1, 290	Settlement	Surface collection			8–9
S83	Hochrieß, Site 39, Plot 281, 285/1, 290	Settlement	Surface collection			8–9
S84	Hochrieß, Site 39, Plot 281, 285/1, 290	Settlement	Surface collection			9–11
S85	Hochrieß, Site 39, Plot 281, 285/1, 290	Settlement	Surface collection			9–11
S86	Hochrieß, Site 39, Plot 281, 285/1, 290	Settlement	Surface collection			9–11
S87	Hochrieß, Site 39, Plot 281, 285/1, 290	Settlement	Surface collection		Sample 12	8–9
S88	Gries, Site 115, Plot 210, 213, 225, 1149	Settlement	Surface collection			8–9
S89	Gries, Site 115, Plot 210, 213, 225, 1150	Settlement	Surface collection			6–7
S90	Landfriedstetten, Site 8, Plot 211/217/220/228	Settlement	Surface collection		Sample 11	8–9
S91	Wieselburg, Plot 246/6, Johann Winter Gasse 16	Settlement	Surface collection		Inv. Nr. 100; Sample 1	8–9
S92	Wieselburg, Plot 246/6, Johann Winter Gasse 16	Settlement	Surface collection		Inv. Nr. 100; Sample 2	8–9
S93	Weinzierl, Wieselburg Land	Undefined	Surface collection		Inv. Nr. 286; Sample 3	8–9
S94	Mühling, 8th-9th-century cemetery	Cemetery	Excavation	Grave 31	Inv. Nr. 232; Sample 4	8–9
S95	Mühling, 8th-9th-century cemetery	Cemetery	Excavation	Grave 3	Inv. Nr. 255; Sample 5	8–9
S96	Mühling, 8th-9th-century cemetery	Cemetery	Excavation	Grave 4	Inv. Nr. 258; Sample 6	8–9
S97	Mühling, 8th-9th-century cemetery	Cemetery	Excavation	Grave 32	Inv. Nr. 234; Sample 7	8–9
S98	Mühling, 8th-9th-century cemetery	Cemetery	Excavation	Grave 19	Inv. Nr. 204; Sample 8	8–9
S99	Hausstein near Grünbach am Schneeberg	Settlement	Surface collection		Find Nr. 2004/1	10–11
S100	Hausstein near Grünbach am Schneeberg	Settlement	Surface collection		Find Nr. 2004/2	10–11
S101	Hausstein near Grünbach am Schneeberg	Settlement	Surface collection		Find Nr. 2004/3	10–11

	Site name	Type of site	Find collection	Find context	Find / inventory number; former sample / probe number	Dating (century AD)
S102	Hausstein near Grünbach am Schneeberg	Settlement	Surface collection		Find Nr. 2004/4	10–11
S103	Hausstein near Grünbach am Schneeberg	Settlement	Surface collection			10–11
S104	Ternitz, Dunkelstein	Settlement	Excavation		Find Nr. 988	11 (2nd half)
S105	Ternitz, Dunkelstein	Settlement	Excavation		Find Nr. 1004	11 (2nd half)
S106	Ternitz, Dunkelstein	Settlement	Excavation		Find Nr. 1311	11 (2nd half)
S107	Ternitz, Dunkelstein	Settlement	Excavation		Find Nr. 1361	11 (2nd half)
S108	Sand near Oberpfaffendorf	Settlement	Excavation		Find Nr. 42/94	10
S109	Sand near Oberpfaffendorf	Settlement	Excavation		Find Nr. 86/98	10
S110	Sand near Oberpfaffendorf	Settlement	Excavation		Find Nr. 105, 114/96	10
S111	Tulln, Wassergasse	Settlement	Excavation		Find Nr. 299/2	10–11
S112	Tulln, Wassergasse	Settlement	Excavation		Find Nr. 362/1	10–11
S113	Tulln, Wassergasse	Settlement	Excavation		Find Nr. 381/2	10–11
S114	Tulln, Wassergasse	Settlement	Excavation		Find Nr. 381/4	10–11
S115	Tulln, Hauptplatz	Settlement	Excavation		Find Nr. 725/1	11–mid-12
S116	Tulln, Hauptplatz	Settlement	Excavation		Find Nr. 725/2	11–mid-12
S117	Tulln, Hauptplatz	Settlement	Excavation		Find Nr. 741/1	11–mid-12
S118	Tulln, Hauptplatz	Settlement	Excavation		Find Nr. 1105/1	Mid-12
S119	Mautern, Römerhalle	Settlement	Excavation		Find Nr. 102/3	9–11
S120	Mautern, Römerhalle	Settlement	Excavation		Find Nr. 115/1	9–11
S121	Mautern, Römerhalle	Settlement	Excavation		Find Nr. 164/3	9–11
S122	Mautern, Römerhalle	Settlement	Excavation		Find Nr. 164/5	9–11
S123	Mautern, Römerhalle	Settlement	Excavation		Find Nr. 164/6	9–11
S124	Mautern, Römerhalle	Settlement	Excavation		Find Nr. 164/8	9–11
S125	Mautern, Römerhalle	Settlement	Excavation		Find Nr. 164/10	9–11
S126	Mautern, Römerhalle	Settlement	Excavation		Find Nr. 164/11	9–11
S127	Mautern, Römerhalle	Settlement	Excavation		Find Nr. 164/12	9–11
S128	Sachsendorf	Settlement	Excavation		Find Nr. 746	10–11
S129	Sachsendorf	Settlement	Excavation		Find Nr. 1674	10–11
S130	Sachsendorf	Settlement	Excavation		Find Nr. 1696	10–11
S131	Sachsendorf	Settlement	Excavation		Find Nr. 2535	10–11
S132	Sachsendorf	Settlement	Excavation		Find Nr. 5203	10–11
S133	Vienna, Ruprechtsplatz	Settlement	Excavation		MV 60.201/42	9–11
S134	Vienna, Ruprechtsplatz	Settlement	Excavation		MV 60.201/51	9–11
S135	Vienna, Ruprechtsplatz	Settlement	Excavation		MV 60.201/73	9–11

Appendix B Macroscopic analysis data of the ceramics

	Fabric	Vessel part	Form	Forming technique	Decoration	Comments
S1	Gold mica B	Body	Pot	Slow wheel turning	Vessel: incised parallel wavy lines	Rim diameter: 14 cm; base diameter: 10.5 cm; Impression of the turntable/turntable cover on the bottom of the vessel
S2	Feldspar + quartz B	Body	Pot	Slow wheel turning	Vessel: combination of incised parallel wavy lines and incised parallel lines	Rim diameter: 13.5 cm; base diameter: 9 cm
S3	Gold mica A	Body	Pot	Slow wheel turning	Vessel: combination of incised parallel wavy lines and incised parallel lines	Rim diameter: 21.5 cm; base diameter: 10 cm
S4	Gold mica B	Body	Pot	Slow wheel turning	Vessel: combination of incised parallel wavy lines and incised parallel lines	Rim diameter: 12 cm; base diameter: 8.5 cm
S5	White mica	Body	Pot	Slow wheel turning	Vessel: incised wavy lines (not parallel)	Rim diameter: 17 cm; base diameter: 11 cm
S6	Gold mica A	Body	Pot	Slow wheel turning	Vessel: incised parallel wavy lines	Rim diameter: 15.5 cm; base diameter: 9.5 cm
S7	Feldspar + quartz B	Body	Pot	Slow wheel turning	Vessel: incised parallel wavy lines	Rim diameter: 12 cm; base diameter: 8 cm
S8	Gold mica A	Body	Pot	Slow wheel turning	Vessel: combination of incised parallel wavy lines and incised parallel lines	Rim diameter: 18.5 cm; base diameter: 10 cm
S9	Feldspar + quartz A	Body	Pot	Slow wheel turning	Vessel: combination of incised parallel wavy lines and incised parallel lines	Rim diameter: 17 cm; base diameter: 10.5 cm
S10	Gold mica A	Body	Pot	Slow wheel turning	Vessel: combination of incised parallel wavy lines and incised parallel lines	Rim diameter: 16 cm; base diameter: 9.5 cm
S11	Gold mica B	Body	Pot	Slow wheel turning	Vessel: no decoration	Rim diameter: 10 cm; base diameter: 7 cm
S12	Feldspar + quartz A	Shoulder	Pot	Slow wheel turning	Large sherds: incised parallel wavy lines	Rim diameter: 17 cm
S13	Graphite B	Body	Pot	Slow wheel turning	Vessel: combination of incised parallel wavy lines and incised parallel lines	Rim diameter: 21.5 cm; base diameter: 12.5 cm
S14	Gold mica B	Body	Pot	Slow wheel turning	Vessel: incised parallel wavy lines	Rim diameter: 19 cm; base diameter: 13.5 cm
S15	Feldspar + quartz A	Body	Pot	Slow wheel turning	Vessel: combination of incised parallel wavy lines and incised parallel lines	Rim diameter: 13 cm; base diameter: 8 cm
S16	Feldspar + quartz B	Body	Pot	Slow wheel turning	Vessel: no decoration	Rim diameter: 14.5 cm; base diameter: 7.5 cm
S17	Feldspar + quartz B	Body	Pot	Slow wheel turning	Vessel: combination of incised wavy lines (not parallel) and incised parallel lines	Rim diameter: 11 cm; base diameter: 7.5 cm
S18	Feldspar + quartz A	Body	Pot	Slow wheel turning	Vessel: combination of incised parallel wavy lines and incised parallel lines	Rim diameter: 21 cm; base diameter: 13.5 cm
S19	Feldspar + quartz A	Body	Pot	Slow wheel turning	Vessel: combination of incised parallel wavy lines and incised parallel lines	Rim diameter: 11.5 cm; base diameter: 6.5 cm; Impression of the turntable/turntable cover on the bottom of the vessel
S20	Feldspar + quartz A	Body	Pot	Slow wheel turning	Vessel: incised parallel wavy lines	Rim diameter: 21.5 cm; base diameter: 12 cm

	Fabric	Vessel part	Form	Forming technique	Decoration	Comments
S21	Graphite B	Body	Pot	Slow wheel turning	Vessel: incised parallel wavy lines	Rim diameter: 8.5 cm; base diameter: 6 cm
S22	Gold mica B	Body	Pot	Slow wheel turning	Vessel: combination of comb-impressed dots and incised wavy lines	Rim diameter: 13 cm; base diameter: 9.5 cm; Impression of the turntable/turntable cover on the bottom of the vessel
S23	Gold mica B	Body	Pot	Slow wheel turning	Vessel: combination of incised wavy lines and incised parallel lines	Rim diameter: 17 cm; base diameter: 13.5 cm
S24	Feldspar + quartz B	Body	Pot	Slow wheel turning	Vessel: no decoration	Rim diameter: 9.5 cm; base diameter: 6 cm
S25	Gold mica A	Body	Pot	Slow wheel turning	Vessel: combination of incised parallel wavy lines and incised parallel lines	Rim diameter: 15.5 cm; base diameter: 13.5 cm
S26	Gold mica A	Body	Pot	Slow wheel turning	Vessel: combination of incised parallel wavy lines and incised parallel lines	Rim diameter: 16 cm; base diameter: 11.5 cm
S27	Gold mica B	Body	Pot	Slow wheel turning	Vessel: no decoration	Rim diameter: 14 cm; base diameter: 9 cm
S28	Gold mica B	Body	Pot	Slow wheel turning	Vessel: incised wavy lines (not parallel)	Rim diameter: 18.5 cm; base diameter: 12.5 cm
S29	Gold mica B	Body	Pot	Slow wheel turning	Vessel: incised lines (not parallel)	Rim diameter: 12 cm; base diameter: 9 cm
S30	Gold mica B	Body	Pot	Slow wheel turning	Vessel: combination of incised parallel wavy lines and incised parallel lines	Rim diameter: 17.5 cm; base diameter: 10.5 cm; Impression of the turntable/turntable cover on the bottom of the vessel
S31	Graphite A	Rim	?	Slow wheel turning		
S32	Graphite A	Body	Pot?	Slow wheel turning	Incised line and incised wavy line	
S33	Graphite A	Body	?	Slow wheel turning		
S34	Graphite A	Body	?	Slow wheel turning		
S35	Graphite A	Base	?	Slow wheel turning		
S36	Graphite A	Base	?	Slow wheel turning		
S37	Gold mica A	Body	Pot?	Slow wheel turning	Incised parallel lines	
S38	Gold mica B	Rim	Pot	Slow wheel turning		
S39	Gold mica B	Body	?	Slow wheel turning	Incised vertical parallel lines	
S40	Gold mica B	Body	Pot?	Slow wheel turning	Incised parallel lines	
S41	Gold mica B	Body	Pot?	Slow wheel turning		
S42	Gold mica B	Body	?	Slow wheel turning		
S43	Gold mica B	Body	Pot?	Slow wheel turning	Combination of incised parallel wavy lines and an incised line	
S44	Gold mica B	Body	Pot?	Slow wheel turning	Incised parallel wavy lines	
S45	Feldspar + quartz A	Body	?	Slow wheel turning		
S46	Feldspar + quartz B	Rim	Pot	Slow wheel turning		
S47	Feldspar + quartz B	Body	?	Slow wheel turning	Incised parallel lines - two line-band crossing each other	

	Fabric	Vessel part	Form	Forming technique	Decoration	Comments
S48	Feldspar + quartz B	Body	?	Slow wheel turning	Incised parallel lines - two line-band crossing each other	
S49	Graphite B	Body	?	Slow wheel turning		
S50	Graphite B	Body	?	Slow wheel turning		
S51	Feldspar + quartz A	Rim	Pot	Slow wheel turning		It might contain grog
S52	Graphite B	Rim	Pot	Slow wheel turning		
S53	Graphite B	Body	?	Slow wheel turning		
S54	Graphite B	Body	?	Slow wheel turning		
S55	Gold mica B	Body	Pot?	Slow wheel turning	Incised parallel lines	
S56	Gold mica B	Body	?	Slow wheel turning		
S57	Carbonate rock A	Shoulder	Pot?	Slow wheel turning	Incised parallel lines	
S58	Carbonate rock A	Body	Pot?	Slow wheel turning	Incised parallel lines	
S59	Carbonate rock A	Body	Pot?	Slow wheel turning	Incised parallel wavy lines	
S60	Gold mica B	Body	Pot?	Slow wheel turning	Incised parallel lines	
S61	Gold mica B	Body	?	Slow wheel turning		
S62	Graphite B	Body	?	Between slow wheel turning and wheel throwing		Grooves and ridges - probably the result of the forming technique
S63	Gold mica B	Shoulder	?	Slow wheel turning	Incised parallel wavy lines	
S64	Gold mica A	Shoulder	Pot?	Slow wheel turning	Incised parallel wavy lines	
S65	Gold mica A	Shoulder	Pot?	Slow wheel turning	Incised parallel wavy lines	
S66	Gold mica A	Shoulder	Pot?	Slow wheel turning	Incised parallel lines	
S67	Gold mica A	Body	Pot?	Slow wheel turning	Incised parallel lines	
S68	Gold mica A	Body	Pot?	Slow wheel turning	Incised parallel wavy lines	
S69	Gold mica A	Body	?	Slow wheel turning		
S70	Gold mica A	Body	Pot?	Slow wheel turning	Incised parallel lines	
S71	Gold mica A	Body	?	Slow wheel turning	?	
S72	Gold mica A	Body	?	Slow wheel turning	Incised parallel lines	
S73	Gold mica B	Rim	Pot	Slow wheel turning	Incised parallel wavy lines (inner surface)	
S74	Gold mica B	Body	Pot?	Slow wheel turning	Incised parallel wavy lines?	
S75	Gold mica B	Body	?	Slow wheel turning		
S76	Gold mica B	Body	Pot?	Slow wheel turning	Incised parallel wavy lines	
S77	Feldspar + quartz A	Rim	Pot?	Slow wheel turning	Incised parallel wavy lines (inner surface)	
S78	Feldspar + quartz A	Shoulder	?	Slow wheel turning	Incised wavy line	
S79	Feldspar + quartz A	Body	Pot?	Slow wheel turning	Incised parallel wavy lines	
S80	Feldspar + quartz A	Body	?	Slow wheel turning	Fingernail marks?	

	Fabric	Vessel part	Form	Forming technique	Decoration	Comments
S81	Feldspar + quartz A	Body	Pot?	Slow wheel turning	Incised parallel wavy lines	
S82	Feldspar + quartz B	Shoulder	Pot?	Slow wheel turning	Incised parallel wavy lines	
S83	Feldspar + quartz B	Body	Pot?	Slow wheel turning	Incised parallel lines	
S84	Graphite A	Shoulder	?	Slow wheel turning	Incised parallel lines? / traces of slow wheel turning just below the neck?	
S85	Graphite A	Body	?	Slow wheel turning		
S86	Graphite A	Body	?	Slow wheel turning	Combination of a raised band and incised parallel wavy lines	
S87	Gold mica B	Body	Pot?	Slow wheel turning	Incised parallel wavy lines	
S88	Gold mica A	Body	?	Slow wheel turning		
S89	Carbonate rock B	Body	?	Slow wheel turning		
S90	Gold mica B	Body	Pot?	Slow wheel turning	Combination of incised parallel lines and incised parallel wavy lines	
S91	Gold mica A	Body	Pot?	Slow wheel turning	Incised parallel wavy lines	
S92	Gold mica A	Body	Pot?	Slow wheel turning	Incised parallel wavy lines	
S93	Gold mica A	Body	Pot	Slow wheel turning	Vessel: incised wavy lines (not parallel)	
S94	Gold mica A	Body	Pot	Slow wheel turning	Vessel: incised wavy lines (not parallel)	Rim diameter: 14 cm; base diameter: 11 cm
S95	Gold mica A	Body	Pot	Slow wheel turning	Large sherds: incised parallel wavy lines	Rim diameter: 22.5 cm
S96	Gold mica A	Body	Pot	Slow wheel turning	Incised parallel wavy lines	
S97	Gold mica A	Body	?	Slow wheel turning		
S98	Gold mica A	Body	Pot	Slow wheel turning	Vessel: incised parallel wavy lines	Rim diameter: 15.5 cm; base diameter: 11.5 cm
S99	Graphite A	Body	?	Slow wheel turning	Raised band	
S100	Graphite A	Body	?	Slow wheel turning	Incised wavy line	
S101	Graphite A	Body	?	Slow wheel turning		
S102	Graphite A	Body	?	Slow wheel turning		
S103	Graphite A	Body	?	Slow wheel turning		
S104	Graphite A	Rim	Pot	Slow wheel turning		Rim diameter: 17 cm
S105	Graphite A	Body	?	Between slow wheel turning and wheel throwing		Fine parallel lines on the exterior can be the result of wheel turning/throwing
S106	Graphite A	Body	?	Slow wheel turning		
S107	Graphite A	Shoulder	?	Slow wheel turning		
S108	Graphite A	Body	Pot	Slow wheel turning	Large sherds: comb-impressed dots	Rim diameter: 16 cm
S109	Graphite A	Body	?	Slow wheel turning	Incised wavy line	
S110	Graphite A	Body	Pot	Slow wheel turning	Large sherds: combination of incised parallel wavy lines, comb-impressed dots and a raised	Rim diameter: 31 cm

	Fabric	Vessel part	Form	Forming technique	Decoration	Comments
					band	
S111	Graphite A	Rim	Pot	Slow wheel turning	Incised parallel wavy lines	Rim diameter: 20 cm
S112	Graphite A	Rim	Pot	Slow wheel turning	Incised wavy lines (not parallel)	Rim diameter: 14 cm
S113	Graphite A	Body	Pot	Slow wheel turning	Incised parallel wavy lines	Brownish and white deposition? layers on the inner surface
S114	Graphite A	Body	?	Slow wheel turning		
S115	Graphite A	Rim	Pot	Slow wheel turning		Rim diameter: 18 cm
S116	Graphite A	Neck	Pot	Slow wheel turning	Incised parallel wavy lines	
S117	Graphite A	Body	?	Slow wheel turning	Raised band	
S118	Graphite A	Rim	Pot	Slow wheel turning		Rim diameter: 20 cm
S119	Graphite A	Body	Pot?	Slow wheel turning	Incised parallel wavy lines	
S120	Graphite A	Rim	Pot	Slow wheel turning	Incised parallel wavy lines	Rim diameter: 15 cm
S121	Graphite A	Body	Pot	Slow wheel turning	Large sherds: impressed dots	Rim diameter: 18 cm
S122	Graphite A	Shoulder	Pot?	Slow wheel turning	Incised parallel wavy lines	
S123	Graphite A	Shoulder	Pot?	Slow wheel turning	Incised parallel wavy lines	
S124	Graphite A	Shoulder	Pot?	Slow wheel turning	Incised wavy line	
S125	Graphite A	Shoulder	Pot?	Slow wheel turning	Comb-impressed dots	
S126	Graphite A	Body	?	Slow wheel turning	Incised wavy lines (not parallel)	
S127	Graphite A	Body	Pot?	Slow wheel turning	Incised wavy lines (not parallel)	
S128	Graphite A	Body	?	Slow wheel turning	Combination of incised parallel wavy lines and incised line	
S129	Graphite A	Shoulder	?	Slow wheel turning	Incised wavy lines (not parallel)	
S130	Graphite B	Body	?	Slow wheel turning	Combination of comb-impressed dots and incised parallel wavy lines	
S131	Graphite B	Rim	Pot	Slow wheel turning	Incised wavy lines (not parallel)	
S132	Graphite A	Rim	Pot	Slow wheel turning	Combination of incised short, inclined lines and parallel wavy lines	
S133	Graphite A	Body	Pot	Slow wheel turning	Incised parallel wavy lines	
S134	Graphite A	Body	Pot	Slow wheel turning	Incised wavy lines (not parallel)	
S135	Graphite A	Body	Pot	Slow wheel turning	Combination of incised parallel wavy lines and a raised band	

Appendix C Thin section analysis data of the ceramics

C.1 Petrographic description

List of mineral abbreviations used in the descriptions (following Siivola and Schmid 2007)

Am	amphibole
Bt	biotite
Cal	calcite
Cb	carbonate
Chl	chlorite
Cpx	clinopyroxene
Czo	clinozoisite
Di	diopside
Dol	dolomite
Ep	epidote
Fsp	feldspar
Gr	graphite
Grt	garnet
Kfs	potassium feldspar
Ky	kyanite
Mc	microcline
Ms	muscovite
Op	opaque mineral
Opx	orthopyroxene
Or	orthoclase
Pl	plagioclase
Px	pyroxene
Qtz	quartz
Rt	rutile
Scp	scapolite
Sil	sillimanite
Ttn	titanite (sphene)
Tur	tourmaline
Zo	zoisite
Zrn	zircon

S1 – Granitoid group (Granitoid C)

Microstructure and voids

The ratio of inclusions, matrix and voids in the sample is 30:60:10. The sample can be considered as homogeneous apart from slight differences in the colour of the matrix. Elongated grains and voids are oriented moderately-strongly parallel to the walls of the ceramic sherd. The size of the voids ranges between 100 µm and 1000 µm, including mainly meso- and macroplanar voids and mesovughs.

Matrix

The sample has a non-calcareous matrix. The colour of the matrix is dark reddish-brown with light reddish-brown margins in plane polarised light. It shows the same shades in crossed polarisers and is optically slightly active to moderately active.

Inclusions

The sample has bimodal grain-size distribution and the grains are very poorly sorted. The modal grain size ranges from 10 µm to 500 µm in the fine fraction (~50% of inclusions) and 750 µm to 4700 µm in the coarse fraction (~50% of inclusions); the maximum grain size is 4700 µm. The sample contains more elongated than equant grains with very angular to angular boundaries.

The following inclusions were identified in the sample. *Frequent*: **granitoid** fragments (including Qtz, Kfs, Pl, Bt, Ms – Kfs seems to have Mc structure), **Bt** (some oxidised); *Common*: **Qtz** (mono- and polycrystalline, undulose extinction, sutured boundaries); *Few*: **Kfs** (perthitic), **pseudomorph** consisting of Ms/Bt/Sil? After an Al-rich mineral, such as andalusite, cordierite – pseudomorphs occur together with granitoid fragments; *Very few*: **Pl**, **Ms**; *Rare*: **Gr/Op**; *Very rare*: **rock fragment** consisting of Qtz and green Am, **colourless Am**.

S2 – Amphibole group

Microstructure and voids

The ratio of inclusions, matrix and voids in the sample is 45:48:7. The sample can be considered as homogeneous apart from slight differences in alignment and the colour of the matrix. Elongated grains and voids are oriented moderately parallel to the walls of the ceramic sherd. The size of the voids ranges between 50 µm and 1750 µm, including mainly mesovughs and mesoplanar voids.

Matrix

The sample has a non-calcareous matrix. The colour of the matrix is black with a light reddish-brown margin on one side in plane polarised light. It shows the same shades in crossed polarisers and is optically inactive to moderately active.

Inclusions

The sample has bimodal grain-size distribution and the grains are very poorly sorted. The modal grain size ranges from 10 µm to 400 µm in the fine fraction (~70% of inclusions) and 800 µm to 2750 µm in the coarse fraction (~30% of inclusions); the maximum grain size is 2750 µm. The sample contains more elongated than equant grains with very angular to angular boundaries.

The following inclusions were identified in the sample. *Dominant*: **rock fragments** including Qtz, Pl, Kfs, green Am and Bt (many feldspar grains in rock fragments and individual feldspar grains have yellowish alteration along the edges and cleavage lines); *Common*: **green Am**, **Bt**, **Qtz** (mono- and

polycrystalline, undulose extinction, sutured boundaries); *Few*: **Pl** (some sericitic, antiperthitic), **Kfs** (cloudy); *Rare*: **Grt**; *Very rare*: **Op/Gr**.

S3 – Granitoid group (Granitoid A1)

Microstructure and voids

The ratio of inclusions, matrix and voids in the sample is 30:60:10. The sample can be considered as homogeneous apart from slight differences in alignment and the colour of the matrix. Elongated grains and voids are oriented moderately parallel to the walls of the ceramic sherd. The size of the voids ranges between 50 µm and 1300 µm, including mainly meso- and macroplanar voids and mesovughs.

Matrix

The sample has a non-calcareous matrix. The colour of the matrix changes from dark reddish-brown to light reddish-brown in plane polarised light. It shows the same shades in crossed polarisers and is optically moderately active to highly active.

Inclusions

The sample has bimodal grain-size distribution and the grains are very poorly sorted. The modal grain size ranges from 10 µm to 250 µm in the fine fraction (~30% of inclusions) and 400 µm to 2850 µm in the coarse fraction (~70% of inclusions); the maximum grain size is 2850 µm. The sample contains more elongated than equant grains with very angular to sub-angular boundaries.

The following inclusions were identified in the sample. *Frequent*: **granitoid** fragments (including Kfs, Qtz, Pl, Bt, once Gr/Op); *Common*: **Kfs** (some sericitic, perthitic), **Qtz** (mono- and polycrystalline, undulose extinction, sutured boundaries), **Bt**; *Few*: **Pl** (some sericitic); *Very few*: **clay pellets** (very dark reddish-brown in PPL and XP, optically very slightly active, elongated, rounded, max. size: 1500 µm, high optical density, diffuse boundaries, concordant orientation, similar composition to matrix); *Very rare*: **Ms**.

S4 – Granitoid group (Granitoid A1)

Microstructure and voids

The ratio of inclusions, matrix and voids in the sample is 30:60:10. The sample can be considered as homogeneous apart from slight differences in alignment and the colour of the matrix. Elongated grains and voids are oriented moderately parallel to the walls of the ceramic sherd. The size of the voids ranges between 50 µm and 1200 µm, including mainly mesoplanar voids and mesovughs.

Matrix

The sample has a non-calcareous matrix. The colour of the matrix is dark reddish-brown with light reddish-brown margins in plane polarised light. It shows the same shades in crossed polarisers and is optically moderately active to highly active.

Inclusions

The sample has bimodal grain-size distribution and the grains are very poorly sorted. The modal grain size ranges from 10 µm to 200 µm in the fine fraction (~50% of inclusions) and 400 µm to 3350 µm in the coarse fraction (~50% of inclusions); the maximum grain size is 3350 µm. The sample contains more elongated than equant grains with very angular to sub-angular boundaries.

The following inclusions were identified in the sample. *Frequent*: **granitoid** fragments (including Kfs, Qtz, Pl, Bt, green Am); *Common*: **Kfs** (some sericitic, perthitic), **Qtz** (mono- and polycrystalline, undulose extinction, sutured boundaries), **Bt** (some oxidised); *Few*: **Pl** (sericitic); *Rare*: **green Am**, **Ms**, **clay pellets** (very dark reddish-brown in PPL and XP, optically slightly active, elongated, well-rounded, max. size: 850 µm, high optical density, diffuse boundaries, concordant orientation, similar composition to matrix); *Very rare*: **Gr**.

S5 – Granitoid group (Granitoid D)

Microstructure and voids

The ratio of inclusions, matrix and voids in the sample is 20:70:10. The sample can be considered as homogeneous apart from slight differences in the colour of the matrix. Elongated grains and voids are oriented strongly parallel to the walls of the ceramic sherd. The size of the voids ranges between 150 µm and 1850 µm, including mainly meso- and macroplanar voids and meso- and macrovughs.

Matrix

The sample has a non-calcareous matrix. The colour of the matrix is dark reddish-brown with a light reddish-brown margin on one side in plane polarised light. It shows the same shades in crossed polarisers and is optically slightly active to very highly active.

Inclusions

The sample has bimodal grain-size distribution and the grains are poorly sorted. The modal grain size ranges from 10 µm to 100 µm in the fine fraction (~20% of inclusions) and 300 µm to 2000 µm in the coarse fraction (~80% of inclusions); the maximum grain size is 2000 µm. The sample contains more elongated than equant grains with very angular boundaries.

The following inclusions were identified in the sample. *Dominant*: **granitoid** fragments (including Kfs (Mc), Qtz, Ms, Bt); *Frequent*: **Qtz** (mono- and polycrystalline, undulose extinction, sutured boundaries); *Common*: **Kfs (Mc)**, **Ms** (relatively large flakes); *Few*: **Bt**; *Very few*: **clay pellets** (dark reddish-brown in PPL and XP, optically moderately active, elongated, well-rounded, max. size: 700 µm, high optical density, diffuse boundaries, concordant orientation, similar composition to matrix); *Rare*: **Gr/Op**.

S6 – Granitoid group (Granitoid A1)

Microstructure and voids

The ratio of inclusions, matrix and voids in the sample is 30:63:7. The sample can be considered as homogeneous apart from slight differences in alignment and the colour of the matrix. Elongated grains and voids are oriented weakly/moderately parallel to the walls of the ceramic sherd. The size of the voids ranges between 100 µm and 1600 µm, including mainly mesoplanar voids and meso- and macrovughs.

Matrix

The sample has a non-calcareous matrix. The colour of the matrix changes from black to light reddish-brown in plane polarised light. It shows the same shades in crossed polarisers and is optically inactive to moderately active.

Inclusions

The sample has bimodal grain-size distribution and the grains are very poorly sorted. The modal grain size ranges from 10 µm to 200 µm in the fine fraction (~30% of inclusions) and 450 µm to 4850 µm in the coarse fraction (~70% of inclusions); the maximum grain size is 4850 µm. The sample contains more elongated than equant grains with very angular to sub-angular boundaries.

The following inclusions were identified in the sample. *Dominant*: **granitoid** fragments (including Kfs, Qtz, Pl, Bt, green Am); *Common*: **Kfs** (some sericitic, perthitic, altered), **Qtz** (mono- and polycrystalline, undulose extinction, sutured boundaries), **Bt** (some oxidised); *Few*: **Pl** (altered); *Very few*: **green Am**; *Rare*: **Gr**, **Ms**; *Very rare*: **clay pellet** (very dark reddish-brown in PPL and XP, optically very slightly active, elongated, well-rounded, max. size: 250 µm, high optical density, diffuse boundaries, concordant orientation, similar composition to matrix).

S7 – Granitoid group (Granitoid B2)

Microstructure and voids

The ratio of inclusions, matrix and voids in the sample is 30:63:7. The sample can be considered as homogeneous apart from slight differences in alignment and the colour of the matrix. Elongated grains and voids are oriented moderately-strongly parallel to the walls of the ceramic sherd. The size of the voids ranges between 100 µm and 2250 µm, including mainly meso- and macroplanar voids and meso- and macrovughs.

Matrix

The sample has a non-calcareous matrix. The colour of the matrix is dark reddish-brown with a light reddish-brown margin on one side in plane polarised light. It shows the same shades in crossed polarisers and is optically slightly active to moderately active.

Inclusions

The sample has bimodal grain-size distribution and the grains are very poorly sorted. The modal grain size ranges from 10 µm to 300 µm in the fine fraction (~40% of inclusions) and 500 µm to 3150 µm in the coarse fraction (~60% of inclusions); the maximum grain size is 3150 µm. The sample contains more elongated than equant grains with very angular to sub-angular boundaries.

The following inclusions were identified in the sample. *Common*: **granitoid** fragments (including Qtz, Kfs, Pl, Bt, Ms), **Qtz** (mono- and polycrystalline, undulose extinction, sutured boundaries), **Bt**; *Few*: **Pl** (some sericitic), **Kfs** (some sericitic, cloudy); *Rare*: **Ms**, **Gr/Op** (once with Kfs and Qtz).

S8 – Amphibole group

Microstructure and voids

The ratio of inclusions, matrix and voids in the sample is 40:50:10. The sample can be considered as homogeneous apart from slight differences in alignment and the colour of the matrix. Elongated grains and voids are oriented moderately parallel to the walls of the ceramic sherd. The size of the voids ranges between 100 µm and 1700 µm, including mainly mesoplanar voids and meso- and macrovughs.

Matrix

The sample has a non-calcareous matrix. The colour of the matrix is light reddish-brown with a dark reddish-brown margin on one side in plane polarised light. It shows the same shades in crossed polarisers and is optically highly active to moderately active.

Inclusions

The sample has bimodal grain-size distribution and the grains are very poorly sorted. The modal grain size ranges from 10 µm to 150 µm in the fine fraction (~50% of inclusions) and 300 µm to 2600 µm in the coarse fraction (~50% of inclusions); the maximum grain size is 2600 µm. The sample contains more elongated than equant grains with very angular to angular boundaries.

The following inclusions were identified in the sample. *Dominant*: **rock fragments** including Qtz, Pl, Kfs, Bt, green Am and Gr/Op (many feldspar grains in rock fragments and individual feldspar grains have yellowish alteration along the edges and cleavage lines); *Common*: **Pl** (sericitic, altered to clay mineral), **Qtz** (mono- and polycrystalline, undulose extinction, sutured boundaries); *Few*: **green Am**, **Bt**, **Kfs** (some sericitic); *Rare*: **Gr/Op**; Very rare: **Ms**, **Zrn**.

S9 – Granitoid group (Granitoid B2)

Microstructure and voids

The ratio of inclusions, matrix and voids in the sample is 25:65:10. The sample can be considered as homogeneous apart from slight differences in alignment and the colour of the matrix and one big clay nodule (see below). Elongated grains and voids

are oriented moderately parallel to the walls of the ceramic sherd. The size of the voids ranges between 100 µm and 2000 µm, including mainly meso- and macroplanar voids and meso- and macrovughs. Some voids are partly filled with secondary Cb.

Matrix

The sample has a non-calcareous matrix. The colour of the matrix changes from black to light reddish-brown in plane polarised light. It shows the same shades in crossed polarisers and is optically slightly active to moderately active.

Inclusions

The sample has bimodal grain-size distribution and the grains are very poorly sorted. The modal grain size ranges from 10 µm to 300 µm in the fine fraction (~30% of inclusions) and 550 µm to 2500 µm in the coarse fraction (~70% of inclusions); the maximum grain size is 2500 µm. The sample contains more elongated than equant grains with very angular to angular boundaries.

The following inclusions were identified in the sample. *Dominant*: **Qtz** (mono- and polycrystalline, undulose extinction, sutured boundaries); *Common*: **granitoid** fragments (including Qtz, Bt, Kfs, Pl, Ms); *Few*: **Kfs** (some sericitic), **loess**, **Pl** (some sericitic, altered); *Very few*: **Bt**; *Rare*: **Gr/Op** (once with Qtz), **Ms**, **clay pellet** (greenish-brown in PPL, light reddish-brown in XP, optically moderately active, equant, rounded, max. size: 3800 µm, neutral optical density, diffuse boundaries, concordant orientation, similar composition to matrix); *Very rare*: **Ky?**.

S10 – Granitoid group (Granitoid A1)

Microstructure and voids

The ratio of inclusions, matrix and voids in the sample is 30:60:10. The sample can be considered as homogeneous apart from slight differences in alignment and the colour of the matrix. Elongated grains and voids are oriented moderately parallel to the walls of the ceramic sherd. The size of the voids ranges between 50 µm and 1900 µm, including mainly mesoplanar voids and meso- and macrovughs.

Matrix

The sample has a non-calcareous matrix. The colour of the matrix is light reddish-brown with a black margin on one side in plane polarised light. It shows the same shades in crossed polarisers and is optically slightly active to highly active.

Inclusions

The sample has bimodal grain-size distribution and the grains are very poorly sorted. The modal grain size ranges from 10 µm to 150 µm in the fine fraction (~40% of inclusions) and 400 µm to 3600 µm in the coarse fraction (~60% of inclusions); the maximum grain size is 3600 µm. The sample contains more elongated than equant grains with very angular to angular boundaries.

The following inclusions were identified in the sample. *Dominant*: **granitoid** fragments (including Pl, Kfs, Qtz, Bt); *Common*: **Kfs** (sericitic, perthitic), **Bt** (some oxidised); *Few*: **Qtz** (monocrystalline > polycrystalline, undulose extinction, sutured boundaries), **Pl** (sericitic); *Very few*: **clay pellets** (dark reddish-brown in PPL and XP, optically slightly active, elongated, well-rounded, max. size: 650 µm, high optical density, sharp to merging boundaries, concordant orientation, similar composition to matrix); *Rare*: **rock fragment** consisting of green Am and Bt, **Gr/Op** (once with Kfs), **Ms**, **clay pellet** (light reddish-brown in PPL, dark reddish-brown in XP, optically slightly active, elongated, sub-rounded, max. size: 1650 µm, neutral optical density, sharp to merging boundaries, concordant orientation, similar composition to matrix); *Very rare*: **Zrn**.

S11 – Diorite group (Diorite A)

Microstructure and voids

The ratio of inclusions, matrix and voids in the sample is 40:55:5. The sample can be considered as homogeneous apart from slight differences in alignment and the colour of the matrix. Elongated grains and voids are oriented moderately parallel to the walls of the ceramic sherd. The size of the voids ranges between 100 µm and 850 µm, including mainly mesoplanar voids and mesovughs.

Matrix

The sample has a non-calcareous matrix. The colour of the matrix is dark reddish-brown with light reddish-brown margins in plane polarised light. It shows the same shades in crossed polarisers and is optically moderately active.

Inclusions

The sample has bimodal grain-size distribution and the grains are very poorly sorted. The modal grain size ranges from 10 µm to 100 µm in the fine fraction (~60% of inclusions) and 300 µm to 2950 µm in the coarse fraction (~40% of inclusions); the maximum grain size is 2950 µm. The sample contains equant and elongated grains in about the same amount with very angular to angular boundaries.

The following inclusions were identified in the sample. *Frequent*: **rock fragments** (diorite/monzonite) including Fsp (sericitic core and unaltered outer zone), Bt, Qtz, greenish-brown Am and Gr, **Qtz** (monocrystalline > polycrystalline, undulose extinction, fine-grained (<100 µm), makes up most of the fine fraction); *Common*: **colourless Am aggregates** with Px and Bt; *Few*: **Bt**; *Very few*: **Ms**; *Rare*: **colourless Am**, **clay pellets** (dark reddish-brown in PPL and XP, optically slightly active, elongated, rounded, max. size: 1650 µm, high optical density, sharp to merging boundaries, concordant orientation, similar composition to matrix); *Very rare*: **greenish-brown Am**.

S12 – Granitoid group (Granitoid B1)

Microstructure and voids

The ratio of inclusions, matrix and voids in the sample is 25:65:10. The sample can be considered as homogeneous apart from slight differences in the colour of the matrix. Elongated grains and voids are oriented moderately-strongly parallel to the walls of the ceramic sherd. The size of the voids ranges between 100 µm and 650 µm, including mainly meso- and macroplanar voids and mesovughs.

Matrix

The sample has a non-calcareous matrix. The colour of the matrix is dark reddish-brown with light reddish-brown margins in plane polarised light. It shows the same shades in crossed polarisers and is optically moderately active to highly active.

Inclusions

The sample has bimodal grain-size distribution and the grains are poorly sorted. The modal grain size ranges from 10 µm to 300 µm in the fine fraction (~55% of inclusions) and 700 µm to 3450 µm in the coarse fraction (~45% of inclusions); the maximum grain size is 3450 µm. The sample contains more elongated than equant grains with very angular to angular boundaries.

The following inclusions were identified in the sample. *Frequent*: **Qtz** (monocrystalline > polycrystalline, undulose extinction, sutured boundaries), **granitoid** fragments (including Qtz, Kfs, Pl, Bt); *Few*: **Kfs** (some sericitic, reddish-brown); *Very few*: **Pl**, **Bt**; *Rare*: **Gr/Op** (with Qtz), **Ms**; *Very rare*: **Tur**.

S13 – Graphite group (Graphite D)

Microstructure and voids

The ratio of inclusions, matrix and voids in the sample is 30:60:10. The sample can be considered as homogeneous. Elongated grains and voids are oriented moderately parallel to the walls of the ceramic sherd. The size of the voids ranges between 150 µm and 1100 µm, including mainly mesoplanar voids and mesovughs.

Matrix

The sample has a non-calcareous matrix. The colour of the matrix is dark reddish-brown in plane polarised light. It shows the same shade in crossed polarisers and is optically slightly active to moderately active.

Inclusions

The sample has bimodal grain-size distribution and the grains are very poorly sorted. The modal grain size ranges from 10 µm to 400 µm in the fine fraction (~80% of inclusions) and 650 µm to 1850 µm in the coarse fraction (~20% of inclusions); the maximum grain size is 1850 µm. The sample contains elongated and equant grains in about the same amount with very angular to sub-angular boundaries.

The following inclusions were identified in the sample. *Common*: **Gr flakes** (some with inclusions of Rt) and **Gr gneiss** fragments consisting of Qtz, Kfs, Bt, Gr, green Am and Pl, **Qtz** (mono- and polycrystalline, undulose extinction, sutured boundaries); *Few*: **Kfs** (some sericitic), **Bt** (some oxidised), **Pl**, **rock fragments** containing Ms (sericite), Bt, colourless Am and Ttn?, **colourless Am** (some altered); *Rare*: **Ms**; *Very rare*: **chert** fragment.

S14 – Granitoid group (Granitoid B2)

Microstructure and voids

The ratio of inclusions, matrix and voids in the sample is 30:60:10. The sample can be considered as homogeneous apart from slight differences in alignment and the colour of the matrix. Elongated grains and voids are oriented moderately-strongly parallel to the walls of the ceramic sherd. The size of the voids ranges between 150 µm and 2100 µm, including mainly meso- and macroplanar voids, mesovughs and macrochannels.

Matrix

The sample has a non-calcareous matrix. The colour of the matrix changes from dark reddish-brown to light reddish-brown in plane polarised light. It shows the same shades in crossed polarisers and is optically highly active.

Inclusions

The sample has bimodal grain-size distribution and the grains are very poorly sorted. The modal grain size ranges from 10 µm to 200 µm in the fine fraction (~40% of inclusions) and 500 µm to 4250 µm in the coarse fraction (~60% of inclusions); the maximum grain size is 4250 µm. The sample contains more elongated than equant grains with very angular to angular boundaries.

The following inclusions were identified in the sample. *Dominant*: **granitoid** fragments (including Qtz, Kfs, Pl, Bt, Ms); *Frequent*: **Qtz** (mono- and polycrystalline, undulose extinction, sutured boundaries); *Common*: **Kfs** (some sericitic); *Few*: **Pl** (some sericitic), **Bt** (some faded); *Very few*: **Gr** (with Qtz, Rt, Ms?); *Rare*: **Ms**, **green Am**, **colourless Am**, **clay pellets (?)** (dark reddish-brown in PPL and XP, optically slightly active, equant, sub-rounded, max. size: 2000 µm, high optical density, sharp boundaries, discordant orientation, distinctive composition from that of the matrix).

S15 – Individual sample

Microstructure and voids

The ratio of inclusions, matrix and voids in the sample is 50:40:10. The sample can be considered as homogeneous apart from slight differences in alignment and the colour of the matrix. Elongated grains and voids are oriented weakly parallel to the walls of the ceramic sherd. The size of the voids

ranges between 100 µm and 1650 µm, including mainly meso- and macrovughs and mesoplanar voids.

Matrix

The sample has a non-calcareous matrix. The colour of the matrix is light reddish-brown with dark reddish-brown patches in the core in plane polarised light. It shows the same shades in crossed polarisers and is optically moderately active.

Inclusions

The sample has bimodal grain-size distribution and the grains are poorly sorted. The modal grain size ranges from 10 µm to 150 µm in the fine fraction (~60% of inclusions) and 400 µm to 3800 µm in the coarse fraction (~40% of inclusions); the maximum grain size is 3800 µm. The sample contains more equant than elongated grains with very angular to sub-rounded boundaries.

The following inclusions were identified in the sample. *Predominant*: **Qtz** (mono- and polycrystalline, undulose extinction, both straight boundaries (triple junctions) and sutured boundaries); *Few*: **granitoid** fragments containing Qtz, Kfs, Pl, Grt, Rt, Ms/Sil, Bt, Gr/Op, **Grt** (well-rounded grains), **Pl**; *Very few*: **Kfs**, **Bt**; *Rare*: **Ky** (once with Gr/Op and Qtz, once with Grt), **Gr/Op**, **Rt**, **clay pellet** (very dark reddish-brown in PPL, almost black in XP, optically very slightly active, distorted, rounded, max. size: 1100 µm, neutral optical density, diffuse boundaries, concordant orientation, different composition from that of the matrix); *Very rare*: **Ms**.

S16 – Diorite group (Diorite A)

Microstructure and voids

The ratio of inclusions, matrix and voids in the sample is 35:58:7. The sample can be considered as homogeneous apart from slight differences in alignment and the colour of the matrix. Elongated grains and voids are oriented moderately parallel to the walls of the ceramic sherd. The size of the voids ranges between 100 µm and 1600 µm, including mainly mesoplanar voids and mesovughs.

Matrix

The sample has a non-calcareous matrix. The colour of the matrix changes from black to light reddish-brown in plane polarised light. It shows the same shades in crossed polarisers and is optically very slightly active to highly active.

Inclusions

The sample has bimodal grain-size distribution and the grains are very poorly sorted. The modal grain size ranges from 10 µm to 100 µm in the fine fraction (~60% of inclusions) and 350 µm to 1900 µm in the coarse fraction (~40% of inclusions); the maximum grain size is 1900 µm. The sample contains equant and elongated grains in about the same amount with very angular to angular boundaries.

The following inclusions were identified in the sample. *Frequent*: **rock fragments** (diorite/monzonite) including Fsp (sericitic core and unaltered outer zone), Bt, Qtz and greenish-brown Am, **Qtz** (monocrystalline > polycrystalline, undulose extinction, fine-grained (<100 µm), makes up most of the fine fraction); *Common*: **colourless Am aggregates** with Px and Bt; *Few*: **Bt**; *Very few*: **Gr/Op** (with Qtz), **clay pellets** (very dark reddish-brown in PPL, black in XP, optically inactive, elongated>equant, well-rounded, max. size: 600 µm, high optical density, clear boundaries, concordant orientation, similar composition to matrix); *Rare*: **colourless Am**, **Ms**.

S17 – Individual sample

Microstructure and voids

The ratio of inclusions, matrix and voids in the sample is 30:55:15. The sample can be considered as homogeneous apart from slight differences in alignment and the colour of the matrix. Elongated grains and voids are oriented moderately-strongly parallel to the walls of the ceramic sherd. The size of the voids ranges between 150 µm and 1000 µm, including mainly meso- and macroplanar voids and mesovughs.

Matrix

The sample has a non-calcareous matrix. The colour of the matrix changes from very dark reddish-brown to light reddish-brown in plane polarised light. It shows the same shades in crossed polarisers and is optically slightly active to highly active.

Inclusions

The sample has bimodal grain-size distribution and the grains are very poorly sorted. The modal grain size ranges from 10 µm to 250 µm in the fine fraction (~55% of inclusions) and 500 µm to 3300 µm in the coarse fraction (~45% of inclusions); the maximum grain size is 3300 µm. The sample contains more elongated than equant grains with very angular to angular boundaries.

The following inclusions were identified in the sample. *Dominant*: **granitoid** fragments (including Qtz, Kfs, Pl, Bt); *Frequent*: **Qtz** (mono- and polycrystalline, undulose extinction, sutured boundaries); *Few*: **Kfs**, **Bt**, **Pl**; *Very few*: **green Am**, **Cal/Dol** (once with Cpx) *Rare*: **Gr/Op**.

S18 – Granitoid group (Granitoid A1)

Microstructure and voids

The ratio of inclusions, matrix and voids in the sample is 25:65:10. The sample is slightly homogeneous as it contains clay nodules and has differences in alignment and the colour of the matrix. Elongated grains and voids are oriented weakly/moderately parallel to the walls of the ceramic sherd. The size of the voids ranges between 100 µm and 2050 µm,

including mainly mesoplanar voids and meso- and macrovughs.

Matrix

The sample has a non-calcareous matrix. The colour of the matrix is dark reddish-brown with light reddish-brown margins in plane polarised light. It shows the same shades in crossed polarisers and is optically moderately active.

Inclusions

The sample has bimodal grain-size distribution and the grains are very poorly sorted. The modal grain size ranges from 10 µm to 200 µm in the fine fraction (~35% of inclusions) and 500 µm to 2700 µm in the coarse fraction (~65% of inclusions); the maximum grain size is 2700 µm. The sample contains more elongated than equant grains with very angular to angular boundaries.

The following inclusions were identified in the sample. *Frequent*: **granitoid** fragments (including Kfs, Qtz, Pl, Bt), **Kfs** (some sericitic, perthitic, altered); *Common*: **Qtz** (mono- and polycrystalline, undulose extinction, sutured boundaries), **Bt**, **Pl** (some sericitic, altered); *Few*: **clay nodules** (light and darker reddish-brown in PPL and yellowish-brown in XP, optically very slightly active, equant>elongated, sub-rounded, max. size: 2500 µm, neutral optical density, sharp>sharp to merging boundaries, concordant orientation, similar composition to matrix but having very few inclusions); *Rare*: **clay pellets** (very dark reddish-brown in PPL and XP, optically very slightly active/inactive, equant, rounded, max. size: 1400 µm, high optical density, sharp boundaries, concordant orientation, similar composition to matrix), **Gr** (with Qtz/Fsp), **Ms**.

S19 – Granitoid group (Granitoid A1)

Microstructure and voids

The ratio of inclusions, matrix and voids in the sample is 25:68:7. The sample can be considered as homogeneous apart from slight differences in alignment and the colour of the matrix. Elongated grains and voids are oriented moderately parallel to the walls of the ceramic sherd. The size of the voids ranges between 50 µm and 1150 µm, including mainly mesoplanar voids and mesovughs.

Matrix

The sample has a non-calcareous matrix. The colour of the matrix is very dark reddish-brown with a dark reddish-brown margin on one side in plane polarised light. It shows the same shades in crossed polarisers and is optically slightly active to moderately active.

Inclusions

The sample has bimodal grain-size distribution and the grains are very poorly sorted. The modal grain size ranges from 10 µm to 200 µm in the fine fraction (~35% of inclusions) and 500 µm to 3450 µm in the coarse fraction (~65% of inclusions); the maximum grain size is 3450 µm. The sample contains more elongated than equant grains with very angular to angular boundaries.

The following inclusions were identified in the sample. *Frequent*: **granitoid** fragments (including Kfs, Pl, Qtz, Bt), **Kfs** (some perthitic, sericitic, altered); *Common*: **Qtz** (monocrystalline > polycrystalline, undulose extinction, sutured boundaries), **Bt**; *Few*: **Pl** (some sericitic, cloudy); *Rare*: **Ms**; *Very rare*: **green Am**, **Gr** (with Qtz).

S20 – Granitoid group (Granitoid B1)

Microstructure and voids

The ratio of inclusions, matrix and voids in the sample is 25:65:10. The sample can be considered as homogeneous apart from slight differences in alignment and the colour of the matrix. Elongated grains and voids are oriented moderately-strongly parallel to the walls of the ceramic sherd. The size of the voids ranges between 150 µm and 1300 µm, including mainly meso- and macroplanar voids and mesovughs.

Matrix

The sample has a non-calcareous matrix. The colour of the matrix changes from dark reddish-brown to light reddish-brown in plane polarised light. It shows the same shades in crossed polarisers and is optically moderately active to highly active.

Inclusions

The sample has bimodal grain-size distribution and the grains are poorly sorted. The modal grain size ranges from 10 µm to 350 µm in the fine fraction (~60% of inclusions) and 550 µm to 2200 µm in the coarse fraction (~40% of inclusions); the maximum grain size is 2200 µm. The sample contains more elongated than equant grains with very angular to angular boundaries.

The following inclusions were identified in the sample. *Dominant*: **Qtz** (monocrystalline > polycrystalline, undulose extinction, sutured boundaries); *Common*: **granitoid** fragments (including Qtz, Kfs, Pl, Bt, Ms); *Few*: **Kfs** (some sericitic, reddish-brown), **Pl** (some sericitic); *Very few*: **Gr**; *Rare*: **Bt**, **Ms**.

S21 – Granitoid group (Granitoid D)

Microstructure and voids

The ratio of inclusions, matrix and voids in the sample is 20:73:7. The sample can be considered as homogeneous apart from slight differences in alignment and the colour of the matrix. Elongated grains and voids are oriented weakly-moderately parallel to the walls of the ceramic sherd. The size of the voids ranges between 50 µm and 1650 µm, including mainly meso- and macroplanar voids and mesovughs.

Matrix

The sample has a non-calcareous matrix. The colour of the matrix changes from dark reddish-brown/black to light reddish-brown in plane polarised light. It shows the same shades in crossed polarisers and is optically inactive to moderately active.

Inclusions

The sample has bimodal grain-size distribution and the grains are very poorly sorted. The modal grain size ranges from 10 µm to 200 µm in the fine fraction (~40% of inclusions) and 400 µm to 5200 µm in the coarse fraction (~60% of inclusions); the maximum grain size is 5200 µm. The sample contains more elongated than equant grains with very angular to sub-angular boundaries.

The following inclusions were identified in the sample. *Common*: **granitoid** fragments (including Kfs, Qtz, Bt, Ms), **Kfs** (some show Mc structure, some sericitic), **Qtz** (monocrystalline > polycrystalline, undulose extinction, sutured boundaries); *Few*: **Ms**, **Gr** (with Qtz and Rt); *Very few*: **Bt**; *Very rare*: **green Am**, **rock fragment** containing fine-grained Bt, Op and Qtz.

S22 – Granitoid group (Granitoid C)

Microstructure and voids

The ratio of inclusions, matrix and voids in the sample is 35:55:10. The sample can be considered as homogeneous apart from slight differences in alignment and the colour of the matrix. Elongated grains and voids are oriented moderately parallel to the walls of the ceramic sherd. The size of the voids ranges between 100 µm and 1000 µm, including mainly mesoplanar voids and mesovughs.

Matrix

The sample has a non-calcareous matrix. The colour of the matrix changes from black to light reddish-brown in plane polarised light. It shows the same shades in crossed polarisers and is optically inactive to highly active.

Inclusions

The sample has bimodal grain-size distribution and the grains are poorly sorted. The modal grain size ranges from 10 µm to 500 µm in the fine fraction (~60% of inclusions) and 900 µm to 2700 µm in the coarse fraction (~40% of inclusions); the maximum grain size is 2700 µm. The sample contains more elongated than equant grains with very angular to angular boundaries.

The following inclusions were identified in the sample. *Frequent*: **Bt** (started altering to Sil); *Common*: **granitoid** fragments (including Kfs (Mc, Or), Qtz, Bt, Ms, Pl), **Qtz** (mono- and polycrystalline, undulose extinction, both straight (triple junctions) and sutured boundaries); *Few*: **Kfs** (**Or, Mc** – some Or are perthitic), **Pl**; *Very few*: **rock fragments** containing sericite and Bt; *Rare*: **Ms**, **green Am**; *Very rare*: **Zrn**.

S23 – Individual sample

Microstructure and voids

The ratio of inclusions, matrix and voids in the sample is 75:20:5. The sample can be considered as homogeneous apart from slight differences in the colour of the matrix. Elongated grains and voids are oriented strongly parallel to the walls of the ceramic sherd. The size of the voids ranges between 100 µm and 500 µm, including mainly mesovughs and mesoplanar voids.

Matrix

The sample has a non-calcareous matrix. The colour of the matrix changes from dark reddish-brown to light reddish-brown in plane polarised light. It shows the same shades in crossed polarisers and is optically moderately active to very highly active.

Inclusions

The sample has bimodal grain-size distribution and the grains are poorly sorted. The modal grain size ranges from 10 µm to 200 µm in the fine fraction (~80% of inclusions) and 700 µm to 2200 µm in the coarse fraction (~20% of inclusions); the maximum grain size is 2200 µm. The sample contains more elongated than equant grains with angular to sub-angular boundaries.

The following inclusions were identified in the sample. *Dominant*: **Bt** (some oxidised); *Common*: **Pl**, **Kfs** (some sericitic), **Qtz** (mono- and polycrystalline, undulose extinction, sutured boundaries); *Very few*: **green Am**, *Rare*: **rock fragments** including green Am, Kfs and Qtz, **clay pellets** (very dark brown/black in PPL and XP, optically very slightly active, equant, well-rounded, max. size: 550 µm, high optical density, sharp to merging boundaries, discordant orientation, similar composition to matrix), **Gr/Op** (once with Kfs); *Very rare*: **Ms**.

S24 – Diorite group (Diorite A)

Microstructure and voids

The ratio of inclusions, matrix and voids in the sample is 40:55:5. The sample can be considered as homogeneous apart from slight differences in alignment and the colour of the matrix. Elongated grains and voids are oriented moderately parallel to the walls of the ceramic sherd. The size of the voids ranges between 100 µm and 360 µm, including mainly mesoplanar voids and mesovughs.

Matrix

The sample has a non-calcareous matrix. The colour of the matrix is light reddish-brown with a dark/very dark reddish-brown core in plane polarised light. It shows the same shades in crossed polarisers and is optically slightly active to moderately active.

Inclusions

The sample has bimodal grain-size distribution and the grains are very poorly sorted. The modal grain size ranges from 10 µm to 100 µm in the fine fraction

(~60% of inclusions) and 400 µm to 2700 µm in the coarse fraction (~40% of inclusions); the maximum grain size is 2700 µm. The sample contains equant and elongated grains in about the same amount with very angular to angular boundaries.
The following inclusions were identified in the sample. *Frequent*: **rock fragments** (diorite/monzonite) including Fsp (sericitic core and unaltered outer zone), Bt, greenish-brown Am, Qtz, colourless Am (in aggregates, occasionally with Px) and Gr, **Qtz** (monocrystalline > polycrystalline, undulose extinction, fine-grained (<100 µm), makes up most of the fine fraction); *Few*: **Bt**; *Very few*: **Fsp** (sericitic); *Rare*: **colourless Am**, **Ms**; *Very rare*: **clay pellet** (dark reddish-brown in PPL and XP, optically moderately active, elongated, sub-rounded, max. size: 300 µm, high optical density, diffuse boundaries, concordant orientation, similar composition to matrix).

S25 – Granitoid group (Granitoid A1)

Microstructure and voids
The ratio of inclusions, matrix and voids in the sample is 30:63:7. The sample can be considered as homogeneous apart from slight differences in alignment and the colour of the matrix. Elongated grains and voids are oriented weakly/moderately parallel to the walls of the ceramic sherd. The size of the voids ranges between 100 µm and 1100 µm, including mainly meso- and macroplanar voids, mesochannels and mesovughs.
Matrix
The sample has a non-calcareous matrix. The colour of the matrix is light reddish-brown in plane polarised light. It shows the same shade in crossed polarisers and is optically highly active.
Inclusions
The sample has bimodal grain-size distribution and the grains are very poorly sorted. The modal grain size ranges from 10 µm to 150 µm in the fine fraction (~50% of inclusions) and 600 µm to 4200 µm in the coarse fraction (~50% of inclusions); the maximum grain size is 4200 µm. The sample contains more elongated than equant grains with angular to sub-angular boundaries.
The following inclusions were identified in the sample. *Common*: **granitoid** fragments (including Kfs, Pl, Qtz, Bt), **Bt** (some in aggregates, some oxidised, some contain Zrn), **Kfs** (some sericitic), **Pl** (sericitic); *Few*: **Qtz** (monocrystalline > polycrystalline, undulose extinction, straight boundaries referring to triple junctions); *Rare*: **Gr/Op** (with Pl and Qtz), **clay pellets** (dark reddish-brown in PPL and XP, optically moderately active, elongated, rounded, max. size: 450 µm, high optical density, diffuse boundaries, discordant orientation, similar composition to matrix); *Very rare*: **Ms**.

S26 – Granitoid group (Granitoid B2)

Microstructure and voids
The ratio of inclusions, matrix and voids in the sample is 25:68:7. The sample can be considered as homogeneous apart from slight differences in alignment and the colour of the matrix. Elongated grains and voids are oriented weakly-moderately parallel to the walls of the ceramic sherd. The size of the voids ranges between 100 µm and 1600 µm, including mainly mesoplanar voids and meso- and macrovughs.
Matrix
The sample has a non-calcareous matrix. The colour of the matrix changes from black to light reddish-brown in plane polarised light. It shows the same shades in crossed polarisers and is optically very slightly active to highly active.
Inclusions
The sample has bimodal grain-size distribution and the grains are very poorly sorted. The modal grain size ranges from 10 µm to 150 µm in the fine fraction (~30% of inclusions) and 500 µm to 2400 µm in the coarse fraction (~70% of inclusions); the maximum grain size is 2400 µm. The sample contains more elongated than equant grains with very angular to angular boundaries.
The following inclusions were identified in the sample. *Dominant*: **granitoid** fragments (including Qtz, Kfs, Bt, Gr, Ms); *Common*: **Qtz** (mono- and polycrystalline, undulose extinction, sutured boundaries), **Bt**; *Few*: **Kfs** (some sericitic, perthitic), **Pl**, **Gr**; *Rare*: **Ms**, **clay pellet** (very dark reddish-brown in PPL and XP, optically very slightly active, equant, rounded, max. size: 300 µm, high optical density, diffuse boundaries, concordant orientation, similar composition to matrix but containing no inclusion).

S27 – Diorite group (Diorite A)

Microstructure and voids
The ratio of inclusions, matrix and voids in the sample is 35:60:5. The sample can be considered as slightly heterogeneous because there is one big clay nodule in the thin section and there are slight differences in alignment and the colour of the matrix. Elongated grains and voids are oriented weakly-moderately parallel to the walls of the ceramic sherd. The size of the voids ranges between 100 µm and 600 µm, including mainly mesoplanar voids and mesovughs.
Matrix
The sample has a non-calcareous matrix. The colour of the matrix is light reddish-brown with a black/very dark reddish-brown margin on one side in plane polarised light. It shows the same shades in crossed polarisers and is optically very slightly active to very highly active.
Inclusions

The sample has bimodal grain-size distribution and the grains are very poorly sorted. The modal grain size ranges from 10 µm to 100 µm in the fine fraction (~50% of inclusions) and 500 µm to 2100 µm in the coarse fraction (~50% of inclusions); the maximum grain size is 2100 µm. The sample contains equant and elongated grains in about the same amount with very angular to angular boundaries.

The following inclusions were identified in the sample. *Dominant*: **rock fragments** (diorite/monzonite) including Fsp (sericitic core and unaltered outer zone), Bt, greenish-brown Am, colourless Am (in aggregates, occasionally with Px), Qtz and Gr; *Common*: **Qtz** (monocrystalline > polycrystalline, undulose extinction, fine-grained (<100 µm), makes up most of the fine fraction); *Few*: **Bt**; *Very few*: **Fsp** (sericitic), **clay pellets** (very dark reddish-brown in PPL and XP, optically slightly/very slightly active, equant>distorted, well-rounded, max. size: 500 µm, high optical density, sharp to merging boundaries, concordant orientation, similar composition to matrix), **Gr**, **colourless Am**; *Very rare*: **Grt**, **Ms**.

S28 – Amphibole group

Microstructure and voids

The ratio of inclusions, matrix and voids in the sample is 30:63:7. The sample can be considered as homogeneous apart from slight differences in alignment and the colour of the matrix. Elongated grains and voids are oriented moderately parallel to the walls of the ceramic sherd. The size of the voids ranges between 100 µm and 700 µm, including mainly mesoplanar voids and mesovughs.

Matrix

The sample has a non-calcareous matrix. The colour of the matrix changes from black to light reddish-brown in plane polarised light. It shows the same shades in crossed polarisers and is optically inactive to moderately active.

Inclusions

The sample has bimodal grain-size distribution and the grains are very poorly sorted. The modal grain size ranges from 10 µm to 200 µm in the fine fraction (~50% of inclusions) and 500 µm to 2600 µm in the coarse fraction (~50% of inclusions); the maximum grain size is 2600 µm. The sample contains more elongated than equant grains with very angular to angular boundaries.

The following inclusions were identified in the sample. *Frequent*: **rock fragments** including Qtz, Kfs, Bt, Pl, Ms, green Am and Grt (foliation can be observed in some grains – gneiss?); *Common*: **Qtz** (mono- and polycrystalline, undulose extinction, sutured boundaries), **green Am**; *Few*: **Kfs** (sericitic), **Pl**, **Bt**; *Very few*: colourless Am; *Rare*: **Gr** (once with Bt); *Very rare*: **Ms**.

S29 – Amphibole group

Microstructure and voids

The ratio of inclusions, matrix and voids in the sample is 30:60:10. The sample can be considered as homogeneous apart from slight differences in alignment and the colour of the matrix. Elongated grains and voids are oriented moderately parallel to the walls of the ceramic sherd. The size of the voids ranges between 100 µm and 1100 µm, including mainly mesoplanar voids and meso- and macrovughs.

Matrix

The sample has a non-calcareous matrix. The colour of the matrix changes from dark reddish-brown to light reddish-brown in plane polarised light. It shows the same shades in crossed polarisers and is optically moderately active to highly active.

Inclusions

The sample has bimodal grain-size distribution and the grains are very poorly sorted. The modal grain size ranges from 10 µm to 200 µm in the fine fraction (~55% of inclusions) and 500 µm to 2750 µm in the coarse fraction (~45% of inclusions); the maximum grain size is 2750 µm. The sample contains elongated and equant grains in about the same amount with very angular to -angular boundaries.

The following inclusions were identified in the sample. *Frequent*: **rock fragments** including Pl, Qtz, green Am Bt, Gr (some green Am are altered to Chl); *Common*: **Qtz** (mono- and polycrystalline, undulose extinction, sutured boundaries), **Pl**, **Bt**; *Few*: **green Am** (some altered to Chl); *Very few*: **rock fragments** containing Pl, Chl (Bt altered to Chl), Kfs, green Am (started altering to Chl), Bt and Gr/Op; *Rare*: **Kfs**, **clay pellets** (very dark brown in PPL and XP, optically very slightly active, equant, rounded, max. size: 650 µm, high optical density, sharp to merging boundaries, concordant orientation, similar composition to matrix), **Gr/Op**, **Ms**.

S30 – Granitoid group (Granitoid A1)

Microstructure and voids

The ratio of inclusions, matrix and voids in the sample is 30:60:10. The sample can be considered as homogeneous apart from slight differences in alignment and the colour of the matrix. Elongated grains and voids are oriented weakly parallel to the walls of the ceramic sherd. The size of the voids ranges between 100 µm and 1150 µm, including mainly meso- and macroplanar voids and mesovughs.

Matrix

The sample has a non-calcareous matrix. The colour of the matrix changes from very dark reddish-brown to light reddish-brown in plane polarised light. It shows the same shades in crossed polarisers and is optically very slightly active to highly active.

Inclusions

The sample has bimodal grain-size distribution and the grains are very poorly sorted. The modal grain size ranges from 10 µm to 150 µm in the fine fraction (~35% of inclusions) and 500 µm to 3600 µm in the coarse fraction (~65% of inclusions); the maximum grain size is 3600 µm. The sample contains more elongated than equant grains with very angular to angular boundaries.

The following inclusions were identified in the sample. *Frequent*: **granitoid** fragments (including Kfs, Pl, Qtz, Bt, brownish-green Am, Gr); *Common*: **Kfs** (sericitic, cloudy); *Few*: **Bt**, **Qtz** (monocrystalline > polycrystalline, undulose extinction, both straight boundaries referring to triple junctions and sutured boundaries); *Very few*: **Pl**, **clay pellets** (very dark reddish-brown in PPL and XP, optically very slightly active/inactive, elongated>equant, rounded, max. size: 1100 µm, high optical density, clear/diffuse boundaries, concordant orientation, similar composition to matrix); *Rare*: **Gr/Op**, one big grain of a **rock fragment** consisting of saussuritic Fsp, Ms, Bt, Qtz, Gr/Op; *Very rare*: **brownish-green Am, Ms**.

S31 – Graphite group (Graphite A4)

Microstructure and voids

The ratio of inclusions, matrix and voids in the sample is 35:56:8. The sample can be considered as homogeneous. Elongated grains and voids are oriented moderately parallel to the walls of the ceramic sherd. The size of the voids ranges between 100 µm and 1150 µm, including mainly meso- and macrovughs and mesoplanar voids.

Matrix

The sample has a non-calcareous matrix. The colour of the matrix is black in plane polarised light and in crossed polarisers and is optically inactive.

Inclusions

The sample has bimodal grain-size distribution and the grains are very poorly sorted. The modal grain size ranges from 10 µm to 200 µm in the fine fraction (~60% of inclusions) and 500 µm to 2600 µm in the coarse fraction (~40% of inclusions); the maximum grain size is 2600 µm. The sample contains equant and elongated grains in about the same amount with very angular to angular boundaries.

The following inclusions were identified in the sample. *Predominant*: **Gr flakes and Gr gneiss** fragments consisting of Gr, Qtz, Rt, Kfs, Pl, Bt and Ms; *Few*: **Qtz** (monocrystalline > polycrystalline, undulose extinction, sutured boundaries), **Ky**, **Kfs** (some cloudy); *Very few*: **Rt**, **Ms**.

S32 – Graphite group (Graphite A3)

Microstructure and voids

The ratio of inclusions, matrix and voids in the sample is 35:58:7. The sample can be considered as homogeneous apart from slight differences in alignment and the colour of the matrix. Elongated grains and voids are oriented moderately parallel to the walls of the ceramic sherd. The size of the voids ranges between 100 µm and 1200 µm, including mainly meso- and macrovughs. Some voids are Cb-filled.

Matrix

The sample has a non-calcareous matrix. The colour of the matrix changes from light yellowish-greyish-brown to very dark reddish-brown in plane polarised light. It shows the same shades in crossed polarisers and is optically highly active to very slightly active.

Inclusions

The sample has bimodal grain-size distribution and the grains are very poorly sorted. The modal grain size ranges from 10 µm to 300 µm in the fine fraction (~80% of inclusions) and 550 µm to 1800 µm in the coarse fraction (~20% of inclusions); the maximum grain size is 1800 µm. The sample contains more equant than elongated grains with angular to sub-angular boundaries.

The following inclusions were identified in the sample. *Dominant*: **Gr flakes and Gr gneiss** fragments consisting of Gr, Qtz, Kfs, Pl and Bt; *Common*: **Qtz** (monocrystalline > polycrystalline, undulose extinction, sutured boundaries, fine-grained, makes up most of the fine fraction); *Few*: **Grt** (with inclusions of Gr/Op, Qtz and Bt), **Pl**, **Kfs**, **Ms** (fine-grained, <100 µm); *Very few*: **clay pellets** (dark reddish-brown in PPL, very dark reddish-brown in XP, optically slightly active, elongated, rounded, max. size: 800 µm, high optical density, diffuse boundaries, concordant orientation, similar composition to matrix); *Rare*: **secondary Cb** (in voids); *Very rare*: **Bt** (some started altering to Sil, Chl).

S33 – Graphite group (Graphite A5)

Microstructure and voids

The ratio of inclusions, matrix and voids in the sample is 35:58:7. The sample can be considered as homogeneous apart from slight differences in the colour of the matrix. Elongated grains and voids are oriented moderately parallel to the walls of the ceramic sherd. The size of the voids ranges between 100 µm and 1000 µm, including mainly mesovughs.

Matrix

The sample has a non-calcareous matrix. The colour of the matrix is very light yellowish-greyish-brown with dark yellowish-greyish-brown patches in plane polarised light. It shows the same shades in crossed polarisers and is optically very highly active to moderately active.

Inclusions

The sample has bimodal grain-size distribution and the grains are very poorly sorted. The modal grain size ranges from 10 µm to 500 µm in the fine fraction (~60% of inclusions) and 700 µm to 2900 µm in the

coarse fraction (~40% of inclusions); the maximum grain size is 2900 µm. The sample contains more elongated than equant grains with angular to sub-angular boundaries.
The following inclusions were identified in the sample. *Dominant*: **Gr flakes and Gr gneiss** fragments consisting of Gr, Kfs, Pl, Qtz and Rt; *Common*: **Kfs**, **Qtz** (monocrystalline > polycrystalline, undulose extinction, sutured boundaries); *Few*: **Pl**, **Ms** (mainly fine-grained, <100 µm); *Very few*: **clay pellets** (dark reddish-brown in PPL, very dark reddish-brown in XP, optically slightly active, elongated, rounded, max. size: 550 µm, high optical density, diffuse boundaries, concordant orientation, similar composition to matrix); *Rare*: **Rt**, **Sil(?)**; *Very rare*: **rock fragment** including Qtz, Bt and Ms, **Bt**.

S34 – Graphite group (Graphite A3)

Microstructure and voids
The ratio of inclusions, matrix and voids in the sample is 30:62:8. The sample can be considered as homogeneous apart from slight differences in the colour of the matrix. Elongated grains and voids are oriented moderately parallel to the walls of the ceramic sherd. The size of the voids ranges between 100 µm and 1250 µm, including mainly mesovughs and mesoplanar voids.
Matrix
The sample has a non-calcareous matrix. The colour of the matrix changes from light reddish-brown to very dark reddish-brown in plane polarised light. It changes from light yellowish-greyish-brown to very dark reddish-brown in crossed polarisers and is optically highly active to slightly active.
Inclusions
The sample has bimodal grain-size distribution and the grains are poorly sorted. The modal grain size ranges from 10 µm to 100 µm in the fine fraction (~45% of inclusions) and 300 µm to 2050 µm in the coarse fraction (~55% of inclusions); the maximum grain size is 2050 µm. The sample contains more elongated than equant grains with angular to sub-angular boundaries.
The following inclusions were identified in the sample. *Dominant*: **Gr flakes and Gr gneiss** fragments consisting of Gr, Qtz, Ms and Rt; *Common*: **Qtz** (monocrystalline > polycrystalline, undulose extinction, sutured boundaries); *Few*: **Grt** (with inclusions of Qtz and Bt), **Bt** (some started altering to Sil), **Pl**, **Kfs**; *Rare*: **brown Am**, **Ms**; *Very rare*: **Rt**.

S35 – Graphite group (Graphite A5)

Microstructure and voids
The ratio of inclusions, matrix and voids in the sample is 35:55:10. The sample can be considered as homogeneous. Elongated grains and voids are oriented moderately parallel to the walls of the ceramic sherd. The size of the voids ranges between 50 µm and 700 µm, including mainly mesovughs and mesoplanar voids. Some voids are filled with secondary Cb.
Matrix
The sample has a non-calcareous matrix. The colour of the matrix is very light yellowish-greyish-brown in plane polarised light. It is very dark grey in crossed polarisers and is optically slightly active.
Inclusions
The sample has bimodal grain-size distribution and the grains are very poorly sorted. The modal grain size ranges from 10 µm to 200 µm in the fine fraction (~50% of inclusions) and 500 µm to 2350 µm in the coarse fraction (~50% of inclusions); the maximum grain size is 2350 µm. The sample contains more elongated than equant grains with angular to sub-angular boundaries.
The following inclusions were identified in the sample. *Dominant*: **Gr flakes and Gr gneiss** fragments consisting of Gr, Kfs, Qtz, Pl, Bt, Scp and Rt; *Common*: **Qtz** (monocrystalline > polycrystalline, undulose extinction, sutured boundaries); *Few*: **Kfs**, **Scp** (with pale yellow pleochroism); *Very few*: **clay pellets** (dark/very dark reddish-brown in PPL, very dark reddish-brown/black in XP, optically very slightly active/inactive, distorted, sub-angular, max. size: 1200 µm, high optical density, diffuse boundaries, concordant orientation, similar composition to matrix); *Rare*: **chert** fragments, **Bt** (almost faded), **Ms**, **Rt**, **secondary Cb** (in voids).

S36 – Graphite group (Graphite A3)

Microstructure and voids
The ratio of inclusions, matrix and voids in the sample is 30:65:5. The sample can be considered as homogeneous apart from slight differences in alignment. Elongated grains and voids are oriented moderately parallel to the walls of the ceramic sherd. The size of the voids ranges between 50 µm and 700 µm, including mainly mesovughs. Few voids are filled with a brownish (PPL and XP) material.
Matrix
The sample has a non-calcareous matrix. The colour of the matrix is very dark reddish-brown/black in plane polarised light. It shows the same shades in crossed polarisers and is optically very slightly active to inactive.
Inclusions
The sample has bimodal grain-size distribution and the grains are very poorly sorted. The modal grain size ranges from 10 µm to 300 µm in the fine fraction (~65% of inclusions) and 500 µm to 1850 µm in the coarse fraction (~35% of inclusions); the maximum grain size is 1850 µm. The sample contains equant and elongated grains in about the same amount with very angular to angular boundaries.

The following inclusions were identified in the sample. *Dominant*: **Gr flakes and Gr gneiss** fragments consisting of Kfs, Gr, Qtz and Rt; *Common*: **Qtz** (monocrystalline > polycrystalline, undulose extinction, sutured boundaries); *Few*: **Kfs** (some cloudy), **Grt**; *Very few*: **Rt**, **Pl**; *Rare*: **clay pellets** (light reddish-brown in PPL and XP, optically moderately active, equant, rounded, max. size: 350 µm, neutral optical density, clear boundaries, concordant orientation, similar composition to matrix), **Ms**.

S37 – Granitoid group (Granitoid A3)

Microstructure and voids

The ratio of inclusions, matrix and voids in the sample is 15:75:10. The sample can be considered as homogeneous apart from slight differences in alignment and the colour of the matrix. Elongated grains and voids are oriented weakly-moderately parallel to the walls of the ceramic sherd. The size of the voids ranges between 50 µm and 1500 µm, including mainly meso- and macroplanar voids and mesovughs.

Matrix

The sample has a non-calcareous matrix. The colour of the matrix is very light reddish-brown in plane polarised light. It is very light yellowish-greyish brown in crossed polarisers and is optically very highly active.

Inclusions

The sample has bimodal grain-size distribution and the grains are very poorly sorted. The modal grain size ranges from 10 µm to 400 µm in the fine fraction (~35% of inclusions) and 1500 µm to 2000 µm in the coarse fraction (~65% of inclusions); the maximum grain size is 2000 µm. The sample contains elongated and equant grains in about the same amount with angular to sub-angular boundaries.

The following inclusions were identified in the sample. *Frequent*: **granitoid** fragments (including Pl, Kfs, Qtz, Bt, green Am (?), Gr (?)); *Common*: **Qtz** (monocrystalline > polycrystalline, undulose extinction, sutured boundaries), **Kfs** (some sericitic); *Few*: **Bt**; **Pl** (some sericitic), **ARF (?)** (light/dark reddish-brown in PPL, dark/very dark reddish-brown in XP, optically moderately/slightly active, elongated, sub-angular-sub-rounded, max. size: 600 µm, high optical density, sharp to merging boundaries, concordant orientation, similar composition to matrix); *Very rare*: **green Am (?)**.

S38 – Granitoid group (Granitoid A3)

Microstructure and voids

The ratio of inclusions, matrix and voids in the sample is 20:70:10. The sample can be considered as homogeneous apart from slight differences in alignment and the colour of the matrix. Fine clay stripes with different colour than the matrix also occur which might be the result of clay mixing. Elongated grains and voids are oriented moderately parallel to the walls of the ceramic sherd. The size of the voids ranges between 25 µm and 1850 µm, including mainly meso- and macroplanar voids and mesovughs.

Matrix

The sample has a non-calcareous matrix. The colour of the matrix changes from dark reddish-brown to light reddish-brown in plane polarised light. It shows the same shades in crossed polarisers and is optically moderately active to very highly active. The matrix exhibits fine darker stripes at some places (clay mixing?).

Inclusions

The sample has bimodal grain-size distribution and the grains are very poorly sorted. The modal grain size ranges from 10 µm to 200 µm in the fine fraction (~35% of inclusions) and 500 µm to 3800 µm in the coarse fraction (~65% of inclusions); the maximum grain size is 3800 µm. The sample contains elongated and equant grains in about the same amount with angular to sub-angular boundaries.

The following inclusions were identified in the sample. *Frequent*: **granitoid** fragments (including Kfs, Qtz, Pl, Bt, green Am); *Common*: **Kfs** (perthitic, sericitic, perthitic), **Bt**, **Qtz** (mono- and polycrystalline, undulose extinction, sutured boundaries); *Few*: **clay pellets/grog?** (very dark reddish-brown/black in PPL and XP, optically very slightly active/inactive, elongated > equant, rounded, 2600 µm, high optical density, clear boundaries, discordant orientation, similar composition to matrix); *Very few*: **green Am**, **Gr**; *Rare*: **Pl**.

S39 – Granitoid group (Granitoid A2)

Microstructure and voids

The ratio of inclusions, matrix and voids in the sample is 35:58:7. The sample can be considered as homogeneous apart from slight differences in alignment and the colour of the matrix. Elongated grains and voids are oriented moderately parallel to the walls of the ceramic sherd. The size of the voids ranges between 100 µm and 900 µm, including mainly meso- and macrovughs and mesoplanar voids.

Matrix

The sample has a non-calcareous matrix. The colour of the matrix is light reddish-brown with dark reddish-brown margins in plane polarised light. It shows the same shades in crossed polarisers and is optically highly active to moderately active.

Inclusions

The sample has bimodal grain-size distribution and the grains are very poorly sorted. The modal grain size ranges from 10 µm to 200 µm in the fine fraction (~60% of inclusions) and 600 µm to 2800 µm in the coarse fraction (~40% of inclusions); the maximum

grain size is 2800 µm. About two thirds of the grains making up the fine fraction are less than 50 µm. The fine fraction is mainly of fine-grained Qtz. The sample contains more equant than elongated grains with angular to sub-angular boundaries.
The following inclusions were identified in the sample. *Frequent*: **granitoid** fragments (including Qtz, Kfs, Gr, Bt, Ms), **Qtz** (monocrystalline > polycrystalline, undulose extinction, sutured boundaries); *Common*: **Bt**; *Few*: **Kfs** (some sericitic), **Pl**, **Gr** (some with inclusions of Qtz, Bt); Very few: **clay pellets** (dark reddish-brown in PPL and very dark reddish-brown in XP, optically very slightly active, equant, rounded, max. size: 750 µm, high optical density, diffuse boundaries, concordant orientation, similar composition to matrix), **schist/gneiss** fragments (including Bt, Qtz and Ms); *Rare*: **Ms** (fine-grained, <100 µm), **Ep/Zo/Czo(?)**.

S40 – Granitoid group (Granitoid A3)

Microstructure and voids
The ratio of inclusions, matrix and voids in the sample is 15:78:7. The sample can be considered as homogeneous apart from slight differences in alignment and the colour of the matrix. Elongated grains and voids are oriented weakly parallel to the walls of the ceramic sherd. The size of the voids ranges between 25 µm and 2250 µm, including mainly mesovughs and meso- and macroplanar voids.
Matrix
The sample has a non-calcareous matrix. The colour of the matrix is very light reddish-brown with dark reddish-brown margins in plane polarised light. It is very light yellowish-grey with dark reddish-brown margins in crossed polarisers and is optically very highly active to moderately active.
Inclusions
The sample has bimodal grain-size distribution and the grains are very poorly sorted. The modal grain size ranges from 10 µm to 200 µm in the fine fraction (~30% of inclusions) and 800 µm to 6350 µm in the coarse fraction (~70% of inclusions); the maximum grain size is 6350 µm. The sample contains elongated and equant grains in about the same amount with angular to rounded boundaries.
The following inclusions were identified in the sample. *Common*: **ARF?** (light/dark reddish-brown in PPL and dark reddish-brown in XP, optically moderately active, elongated, well-rounded, max. size: 2350 µm, neutral optical density, sharp to merging boundaries, discordant orientation, similar composition to matrix); **granitoid** fragments (including Kfs, Pl, Qtz, Bt); *Few*: **ARF/grog?** (very dark reddish-brown in PPL and XP, optically very slightly active, elongated, sub-angular/rounded, 6350 µm, high optical density, sharp boundaries, discordant orientation, similar composition to matrix), **Qtz** (monocrystalline > polycrystalline, undulose extinction, sutured boundaries), **Bt**; *Very few*: **Kfs**, **Pl**; *Rare*: **green Am**; *Very rare*: **clay pellet** (very light reddish-brown in PPL, dark yellowish-brown in XP, optically moderately active, elongated, rounded, max. size: 1450 µm, neutral optical density, diffuse boundaries, concordant orientation, similar composition to matrix – this clay pellet seems to be an inclusion-poor concentration of the matrix), **rock fragment** containing Qtz, Gr/Op and Bt.

S41 – Granitoid group (Granitoid A3)

Microstructure and voids
The ratio of inclusions, matrix and voids in the sample is 20:73:7. The sample can be considered as slightly heterogeneous because concentrations of pure clay are present in the matrix. Elongated grains and voids are oriented moderately parallel to the walls of the ceramic sherd. The size of the voids ranges between 25 µm and 3100 µm, including mainly macroplanar voids and mesovughs.
Matrix
The sample has a non-calcareous matrix. The colour of the matrix is light reddish-brown in plane polarised light. It is light yellowish-greyish-brown in crossed polarisers and is optically highly active.
Inclusions
The sample has bimodal grain-size distribution and the grains are very poorly sorted. The modal grain size ranges from 10 µm to 250 µm in the fine fraction (~25% of inclusions) and 550 µm to 5050 µm in the coarse fraction (~75% of inclusions); the maximum grain size is 5050 µm. The sample contains more elongated than equant grains with angular to sub-angular boundaries.
The following inclusions were identified in the sample. *Dominant*: **granitoid** fragments (including Kfs, Pl, Qtz, Bt, green Am, Zo?, Ti?); *Common*: **Bt**; *Few*: **Kfs** (some perthitic, sericitic, saussuritic), **Pl** (some sericitic, saussuritic), **Qtz** (monocrystalline > polycrystalline, undulose extinction, sutured boundaries); *Very few*: **green Am**; *Rare*: **Gr**; *Very rare*: **Zrn**.

S42 – Granitoid group (Granitoid A3)

Microstructure and voids
The ratio of inclusions, matrix and voids in the sample is 15:80:5. The sample can be considered as slightly heterogeneous because concentrations of pure clay are present in the matrix. Elongated grains and voids are oriented moderately parallel to the walls of the ceramic sherd. The size of the voids ranges between 25 µm and 1250 µm, including mainly mesoplanar voids and mesovughs.
Matrix
The sample has a non-calcareous matrix. The colour of the matrix is very light reddish-brown with dark

reddish-brown margins in plane polarised light. It is very light yellowish-grey with dark reddish-brown margins in crossed polarisers and is optically very highly active to moderately active.

Inclusions

The sample has bimodal grain-size distribution and the grains are very poorly sorted. The modal grain size ranges from 10 µm to 250 µm in the fine fraction (~35% of inclusions) and 500 µm to 1750 µm in the coarse fraction (~65% of inclusions); the maximum grain size is 1750 µm. The sample contains elongated and equant grains in about the same amount with angular to sub-angular boundaries.

The following inclusions were identified in the sample. *Frequent*: **granitoid** fragments (including Pl, Kfs, Bt, green-brown Am, Gr/Op); *Common*: **Qtz** (monocrystalline > polycrystalline, undulose extinction, sutured boundaries), **Bt**; *Few*: **Kfs** (some sericitic, saussuritic), **Pl**; *Rare*: **green-brown Am**, **Gr**, **clay pellets** (orange in PPL, light yellowish-brown in XP, optically moderately active, equant, rounded, max. size: 600 µm, high optical density, diffuse boundaries, concordant orientation, similar composition to matrix), **Ms** (fine-grained, < 100 µm); *Very rare*: **clay pellet/grog?** (dark reddish-brown in PPL, very dark reddish-brown in XP, optically very slightly active, elongated, sub-angular, 1750 µm, high optical density, sharp boundaries, concordant orientation, similar composition to matrix), **Ttn**.

S43 – Granitoid group (Granitoid A3)

Microstructure and voids

The ratio of inclusions, matrix and voids in the sample is 20:75:5. The sample can be considered as homogeneous apart from slight differences in the colour of the matrix. Elongated grains and voids are oriented moderately parallel to the walls of the ceramic sherd. The size of the voids ranges between 25 µm and 950 µm, including mainly meso- and macroplanar voids and mesovughs.

Matrix

The sample has a non-calcareous matrix. The colour of the matrix is very light reddish-brown with a dark reddish-brown margin on one side in plane polarised light. It is very light yellowish-greyish-brown with a light reddish-brown margin on one side in crossed polarisers and is optically very highly active to moderately active.

Inclusions

The sample has bimodal grain-size distribution and the grains are very poorly sorted. The modal grain size ranges from 10 µm to 350 µm in the fine fraction (~25% of inclusions) and 700 µm to 2600 µm in the coarse fraction (~75% of inclusions); the maximum grain size is 2600 µm. The sample contains elongated and equant grains in about the same amount with angular to sub-angular boundaries.

The following inclusions were identified in the sample. *Dominant*: **granitoid** fragments (including Pl, Kfs, Qtz, Bt, green-brown Am); *Common*: **Qtz** (mono- and polycrystalline, undulose extinction, sutured boundaries); *Few*: **Bt**, **Kfs** (some saussuritic), **Pl**; *Very few*: **clay pellets/limonitic nodules** (dark reddish-brown in PPL, very dark reddish-brown in XP, optically slightly active, elongated, sub-rounded, max. size: 800 µm, high optical density, clear boundaries, concordant orientation, similar composition to matrix), **green-brown Am**; *Rare*: **Gr**, **Ms** (fine-grained, < 100 µm); *Very rare*: **rock fragment** including green-brown Am, Bt, Kfs and Qtz, **Ep?**.

S44 – Granitoid group (Granitoid A1)

Microstructure and voids

The ratio of inclusions, matrix and voids in the sample is 35:60:5. The sample can be considered as homogeneous apart from slight differences in the colour of the matrix. Elongated grains and voids are oriented moderately parallel to the walls of the ceramic sherd. The size of the voids ranges between 25 µm and 1750 µm, including mainly mesoplanar voids and mesochannels.

Matrix

The sample has a non-calcareous matrix. The colour of the matrix is light reddish-brown with a dark reddish-brown margin on one side and a dark reddish-brown strip along a linear pore-chain oriented parallel to the walls of the sample in plane polarised light. It shows the same shades in crossed polarisers and is optically highly active to moderately active.

Inclusions

The sample has bimodal grain-size distribution and the grains are very poorly sorted. The modal grain size ranges from 10 µm to 200 µm in the fine fraction (~60% of inclusions) and 800 µm to 3400 µm in the coarse fraction (~40% of inclusions); the maximum grain size is 3400 µm. The sample contains more equant than elongated grains with angular to sub-angular boundaries.

The following inclusions were identified in the sample. *Frequent*: **granitoid** fragments (including Pl, Kfs, Qtz, Bt, green Am), **Qtz** (mono- and polycrystalline, undulose extinction, sutured boundaries); *Common*: **ARF/grog?** (very dark reddish-brown/black in PPL and XP, optically very slightly active/inactive, elongated, sub-angular, max. size: 2250 µm, high optical density, sharp/sharp to merging boundaries, concordant orientation, similar composition to matrix); *Few*: **Bt**, **Kfs** (some perthitic, sericitic), **Pl**; *Rare*: **Ms** (fine grained, <100 µm); *Very rare*: **green Am**.

S45 – Granitoid group (Granitoid B3)

Microstructure and voids

The ratio of inclusions, matrix and voids in the sample is 20:72:8. The sample can be considered as homogeneous apart from slight differences in the colour of the matrix. Elongated grains and voids are oriented moderately parallel to the walls of the ceramic sherd. The size of the voids ranges between 100 µm and 3000 µm, including mainly mesoplanar voids and meso- and macrovughs.

Matrix

The sample has a non-calcareous matrix. The colour of the matrix is light reddish-brown with dark reddish-brown core and a black margin on one side in plane polarised light. It shows the same shades in crossed polarisers and is optically highly active to inactive.

Inclusions

The sample has bimodal grain-size distribution and the grains are very poorly sorted. The modal grain size ranges from 10 µm to 250 µm in the fine fraction (~65% of inclusions) and 600 µm to 2000 µm in the coarse fraction (~35% of inclusions); the maximum grain size is 2000 µm. The sample contains more equant than elongated grains with sub-angular to well-rounded boundaries.

The following inclusions were identified in the sample. *Dominant*: **granitoid** fragments (including Qtz, Kfs, Bt, Pl); *Common*: **Qtz** (mono- and polycrystalline, undulose extinction, sutured boundaries); *Few*: **Kfs** (some sericitic), **clay pellets/limonitic nodules** (very dark reddish-brown in PPL and XP, optically inactive, equant, rounded, max. size: 550 µm, high optical density, sharp to merging boundaries, concordant orientation, similar composition to matrix); *Very few*: **Grt**, **Tur**, **Bt**, **Ky/Opx**; *Rare*: **Gr/Op**; **Ms** (fine-grained, < 100 µm); *Very rare*: **Sil?** (pseudomorph of Sil after a tabular mineral), **Ttn/Rt?**.

S46 – Granitoid group (Granitoid B3)

Microstructure and voids

The ratio of inclusions, matrix and voids in the sample is 20:65:15. The sample can be considered as homogeneous apart from slight differences in alignment and the colour of the matrix. Elongated grains and voids are oriented moderately parallel to the walls of the ceramic sherd. The size of the voids ranges between 100 µm and 3900 µm, including mainly macroplanar voids and mesovughs.

Matrix

The sample has a non-calcareous matrix. The colour of the matrix is dark reddish-brown with light reddish-brown margins in plane polarised light. It shows the same shades in crossed polarisers and is optically very slightly active to moderately active.

Inclusions

The sample has bimodal grain-size distribution and the grains are poorly sorted. The modal grain size ranges from 10 µm to 300 µm in the fine fraction (~80% of inclusions) and 600 µm to 1450 µm in the coarse fraction (~20% of inclusions); the maximum grain size is 1450 µm. The sample contains more equant than elongated grains with sub-angular to sub-rounded boundaries.

The following inclusions were identified in the sample. *Frequent*: **granitoid** fragments (including Qtz, Kfs), **Qtz** (mono- and polycrystalline, undulose extinction, sutured boundaries); *Very few*: **Kfs** (some cloudy), **Grt**; *Rare*: **Ky/Opx**, **Pl**, **Ms** (mostly fine-grained, <100µm); **clay pellet** (light reddish-brown in PPL, very dark reddish-brown in XP, optically very slightly active, elongated, sub-rounded, max. size: 450 µm, neutral optical density, sharp to merging boundaries, concordant orientation, similar composition to matrix), **Rt**.

S47 – Granitoid group (Granitoid B3)

Microstructure and voids

The ratio of inclusions, matrix and voids in the sample is 20:75:5. The sample can be considered as slightly heterogeneous because concentrations of pure clay are present in the matrix. Elongated grains and voids are oriented moderately parallel to the walls of the ceramic sherd. The size of the voids ranges between 100 µm and 1900 µm, including mainly meso- and macroplanar voids.

Matrix

The sample has a non-calcareous matrix. The colour of the matrix is light reddish-brown with a black margin on one side in plane polarised light. It shows the same shades in crossed polarisers and is optically moderately highly active to inactive.

Inclusions

The sample has bimodal grain-size distribution and the grains are very poorly sorted. The modal grain size ranges from 10 µm to 200 µm in the fine fraction (~75% of inclusions) and 600 µm to 2950 µm in the coarse fraction (~25% of inclusions); the maximum grain size is 2950 µm. The sample contains more equant than elongated grains with angular to rounded boundaries.

The following inclusions were identified in the sample. *Frequent*: **granitoid** fragments (including Qtz, Kfs, Pl, Ttn, Grt, Rt?), **Qtz** (mono- and polycrystalline, mainly undulose extinction and sutured boundaries, but there are grains with straight extinction and straight boundaries); *Few*: **Bt**, **Grt**, **Pl**, **Kfs**; *Rare*: **sedimentary rock fragment (?)** including Qtz, altered Kfs, Op, Pl, Bt and Ms, **chert?** fragments, **siltstone?** fragments, **Gr/Op**, **Ms** (fine-grained, <100 µm); *Very rare*: **fine-grained sedimentary rock fragment (?)** including Qtz, altered Fsp, Bt and Op.

S48 – Individual sample

Microstructure and voids

The ratio of inclusions, matrix and voids in the sample is 45:45:10. The sample can be considered as homogeneous. Elongated grains and voids are oriented weakly parallel to the walls of the ceramic sherd. The size of the voids ranges between 100 µm and 1200 µm, including mainly meso- and macrovughs.

Matrix

The sample has a non-calcareous matrix. The colour of the matrix is very light yellowish-greyish-brown in plane polarised light. It is very dark grey in crossed polarisers and is optically inactive. The matrix seems quite vitrified, glassy, which is probably the result of secondary burning.

Inclusions

The sample has bimodal grain-size distribution and the grains are very poorly sorted. The modal grain size ranges from 10 µm to 100 µm in the fine fraction (~70% of inclusions) and 400 µm to 2600 µm in the coarse fraction (~30% of inclusions); the maximum grain size is 2600 µm. The sample contains more equant than elongated grains with sub-angular boundaries.

The following inclusions were identified in the sample. *Frequent*: **Qtz** (monocrystalline > polycrystalline, mostly fine-grained (<100 µm), larger grains have undulose extinction and sutured boundaries, Qtz makes up most of the fine fraction), **granitoid** fragments (including Pl, Kfs, Qtz, Bt, Zrn); *Common*: **Bt** (some altered to a brownish-grey mineral (Ttn?)); *Few*: **Kfs** (some sericitic), **Pl**; *Rare*: **Zrn**, **Ms**.

S49 – Graphite group (Graphite D)

Microstructure and voids

The ratio of inclusions, matrix and voids in the sample is 30:63:7. The sample can be considered as homogeneous apart from slight differences in alignment and the colour of the matrix. Elongated grains and voids are oriented moderately parallel to the walls of the ceramic sherd. The size of the voids ranges between 50 µm and 1350 µm, including mainly mesovughs and meso- and macroplanar voids.

Matrix

The sample has a non-calcareous matrix. The colour of the matrix changes from light reddish-brown to dark reddish-brown in plane polarised light. It changes from dark reddish-brown to very dark reddish-brown in crossed polarisers and is optically slightly active to inactive.

Inclusions

The sample has bimodal grain-size distribution and the grains are very poorly sorted. The modal grain size ranges from 10 µm to 400 µm in the fine fraction (~60% of inclusions) and 800 µm to 2500 µm in the coarse fraction (~40% of inclusions); the maximum grain size is 2500 µm. The sample contains elongated and equant grains in about the same amount with angular to sub-rounded boundaries.

The following inclusions were identified in the sample. *Frequent*: **Gr flakes and Gr gneiss** fragments consisting of Gr, Qtz, Kfs, and mica (colourless in PPL); *Common*: **Qtz** (mono- and polycrystalline, undulose extinction, sutured boundaries); *Few*: **ARF (siltstone?)** (light/dark reddish-brown in PPL, dark/very dark reddish-brown in XP, optically very slightly to moderately active, elongated, sub-rounded, max. size: 2150 µm, neutral optical density, sharp to merging boundaries, concordant orientation, similar composition to matrix but having very few or no inclusions), **Kfs** (some cloudy), **mica** (colourless in PPL); *Rare*: **Rt**.

S50 – Granitoid group (Granitoid A2)

Microstructure and voids

The ratio of inclusions, matrix and voids in the sample is 35:60:5. The sample can be considered as homogeneous apart from slight differences in alignment and the colour of the matrix. Elongated grains and voids are oriented moderately parallel to the walls of the ceramic sherd. The size of the voids ranges between 100 µm and 1250 µm, including mainly mesovughs, mesoplanar voids and meso- and macrochannels.

Matrix

The sample has a non-calcareous matrix. The colour of the matrix is light reddish-brown with dark reddish-brown margins in plane polarised light. It shows the same shades in crossed polarisers and is optically moderately active to slightly active.

Inclusions

The sample has bimodal grain-size distribution and the grains are very poorly sorted. The modal grain size ranges from 10 µm to 150 µm in the fine fraction (~55% of inclusions) and 500 µm to 1700 µm in the coarse fraction (~45% of inclusions); the maximum grain size is 1700 µm. About two thirds of the grains making up the fine fraction are less than 50 µm. The fine fraction is mainly of fine-grained Qtz. The sample contains more elongated than equant grains with angular to sub-rounded boundaries.

The following inclusions were identified in the sample. *Frequent*: **Qtz** (monocrystalline > polycrystalline, undulose extinction, sutured boundaries); *Common*: **Bt** (flakes and aggregates of Bt), **Kfs** (some cloudy, sericitic); *Few*: **Gr**; Very few: **granitoid** fragments (including Qtz, Kfs), **clay pellets** (very dark reddish-brown/black in PPL and XP, optically very slightly active/inactive, equant, rounded, max. size: 500 µm, high optical density, diffuse boundaries, concordant orientation, similar composition to matrix); *Rare*: **graphitic rock** fragments (including Gr, Qtz, Fsp) **Pl**, **Ms** (fine-grained, <100 µm); *Very rare*: **green Am?**.

S51 – Granitoid group (Granitoid A3)

Microstructure and voids

The ratio of inclusions, matrix and voids in the sample is 20:70:10. The sample can be considered as homogeneous apart from slight differences in alignment and the colour of the matrix. Elongated grains and voids are oriented moderately-strongly parallel to the walls of the ceramic sherd. The size of the voids ranges between 50 µm and 2000 µm, including mainly macrochannels and macroplanar voids.

Matrix

The sample has a non-calcareous matrix. The colour of the matrix is very light reddish-brown with dark reddish-brown fine stripes in the core in plane polarised light. It is very light reddish-brown or yellowish-greyish brown with dark reddish-brown fine stripes in the core in crossed polarisers and is optically highly active to slightly active. The fine stripes in the matrix might be the result of clay mixing or firing.

Inclusions

The sample has bimodal grain-size distribution and the grains are very poorly sorted. The modal grain size ranges from 10 µm to 150 µm in the fine fraction (~20% of inclusions) and 400 µm to 2850 µm in the coarse fraction (~80% of inclusions); the maximum grain size is 2850 µm. The sample contains more elongated than equant grains with sub-angular to sub-rounded boundaries.

The following inclusions were identified in the sample. *Frequent*: **granitoid** fragments (including Kfs, Qtz, Pl, green Am, Gr/Op); *Common*: **Qtz** (mono- and polycrystalline, undulose extinction, sutured boundaries); *Few*: **Kfs** (cloudy, perthitic), **green Am**, **grog?** (dark/very dark reddish-brown in PPL and XP, optically very slightly active/inactive, elongated, rounded/well-rounded, max. size: 1600 µm, high optical density, sharp boundaries, discordant orientation, distinctive composition from that of the matrix – some have abundant inclusions in contrast to the matrix); *Very few*: **Pl**, **clay pellets/limonitic nodules** (light/dark reddish-brown in PPL and XP, optically moderately-slightly active, elongated, rounded/well-rounded, max. size: 1500 µm, neutral optical density, clear boundaries, concordant orientation, similar composition to matrix but having very few or no inclusions), **Gr/Op** (hard to distinguish from clay pellet/ARF); *Rare*: **Bt**, **Ms** (fine-grained, <100 µm); *Very rare*: **Opx?**, **Grt/glass**.

S52 – Granitoid group (Granitoid A2)

Microstructure and voids

The ratio of inclusions, matrix and voids in the sample is 35:60:5. The sample can be considered as homogeneous apart from slight differences in alignment and the colour of the matrix. Elongated grains and voids are oriented moderately parallel to the walls of the ceramic sherd. The size of the voids ranges between 100 µm and 850 µm, including mainly mesovughs, mesoplanar voids and meso- and macrochannels.

Matrix

The sample has a non-calcareous matrix. The colour of the matrix is light reddish-brown with dark reddish-brown patches in plane polarised light. It shows the same shades in crossed polarisers and is optically highly active to slightly active.

Inclusions

The sample has bimodal grain-size distribution and the grains are very poorly sorted. The modal grain size ranges from 10 µm to 200 µm in the fine fraction (~60% of inclusions) and 450 µm to 3250 µm in the coarse fraction (~40% of inclusions); the maximum grain size is 3250 µm. About two thirds of the grains making up the fine fraction are less than 50 µm. The fine fraction is mainly of fine-grained Qtz. The sample contains more equant than elongated grains with angular to rounded boundaries.

The following inclusions were identified in the sample. *Frequent*: **Kfs** (cloudy, few perthitic), **Qtz** (monocrystalline > polycrystalline, undulose extinction, sutured boundaries); *Few*: **Gr** (some with Kfs); Very few: **granitoid** fragments (including Kfs, Qtz); *Rare*: **Ms** (fine-grained, <100 µm), **Bt**.

S53 – Graphite group (Graphite D)

Microstructure and voids

The ratio of inclusions, matrix and voids in the sample is 35:60:5. The sample can be considered as homogeneous apart from slight differences in the colour of the matrix. Elongated grains and voids are oriented moderately parallel to the walls of the ceramic sherd. The size of the voids ranges between 50 µm and 1200 µm, including mainly meso- and macrovughs and mesoplanar voids.

Matrix

The sample has a non-calcareous matrix. The colour of the matrix is dark reddish-brown with a light reddish-brown margin on one side in plane polarised light. It shows the same shades in crossed polarisers and is optically slightly active to highly active.

Inclusions

The sample has bimodal grain-size distribution and the grains are poorly sorted. The modal grain size ranges from 10 µm to 300 µm in the fine fraction (~70% of inclusions) and 500 µm to 2500 µm in the coarse fraction (~30% of inclusions); the maximum grain size is 2500 µm. The sample contains elongated and equant grains in about the same amount with angular to sub-angular boundaries.

The following inclusions were identified in the sample. *Frequent*: **Gr flakes and Gr gneiss** fragments consisting of Gr, Qtz, Kfs and Bt; *Common*: **Qtz**

(mono- and polycrystalline, undulose extinction, sutured boundaries); *Few*: **Kfs** (some sericitic, cloudy), **clay pellets/ARF?** (light/dark reddish-brown in PPL, very dark reddish-brown/black in XP, optically very slightly active to inactive, equant, rounded, max. size: 450 µm, neutral optical density, sharp to merging boundaries, concordant orientation, similar composition to matrix but having no inclusions – they are surrounded by thin pores); *Rare*: **Zo?**, **Sil?**, **Ms**; *Very rare*: **Bt**.

S54 – Graphite group (Graphite D)

Microstructure and voids

The ratio of inclusions, matrix and voids in the sample is 30:65:5. The sample can be considered as homogeneous apart from slight differences in the colour of the matrix. Elongated grains and voids are oriented moderately parallel to the walls of the ceramic sherd. The size of the voids ranges between 100 µm and 1350 µm, including mainly mesoplanar voids and meso- and macrovughs.

Matrix

The sample has a non-calcareous matrix. The colour of the matrix is light yellowish-greyish-brown with light/dark reddish-brown margins in plane polarised light. It is very dark yellowish-greyish-brown with light reddish-brown margins in crossed polarisers and is optically slightly active to moderately active.

Inclusions

The sample has bimodal grain-size distribution and the grains are poorly sorted. The modal grain size ranges from 10 µm to 350 µm in the fine fraction (~60% of inclusions) and 600 µm to 2500 µm in the coarse fraction (~40% of inclusions); the maximum grain size is 2500 µm. The sample contains more elongated than equant grains with angular to rounded boundaries.

The following inclusions were identified in the sample. *Frequent*: **Gr flakes and Gr gneiss** fragments consisting of Gr, Qtz, Kfs, Grt and Rt; *Common*: **ARF (siltstone?)** (light reddish-brown in PPL and XP, optically moderately active, elongated>equant, rounded, max. size: 1200 µm, neutral optical density, sharp to merging boundaries, concordant orientation, similar composition to matrix but having very few or no inclusions), **Qtz** (mono- and polycrystalline, undulose extinction, sutured boundaries); *Few*: **Kfs** (some sericitic); *Very few*: **Grt** (some altered which produce interference colour); *Rare*: **Rt**, **Ms** (fine-grained, <100 µm), **Bt**; *Very rare*: **Tur**.

S55 – Amphibole group

Microstructure and voids

The ratio of inclusions, matrix and voids in the sample is 35:60:5. The sample can be considered as homogeneous apart from slight differences in the colour of the matrix. Elongated grains and voids are oriented moderately parallel to the walls of the ceramic sherd. The size of the voids ranges between 50 µm and 500 µm, including mainly mesovughs and mesoplanar voids.

Matrix

The sample has a non-calcareous matrix. The colour of the matrix changes from light reddish-brown to very dark reddish-brown in plane polarised light. It shows the same shades in crossed polarisers and is optically highly active to very slightly active.

Inclusions

The sample has bimodal grain-size distribution and the grains are poorly sorted. The modal grain size ranges from 10 µm to 350 µm in the fine fraction (~60% of inclusions) and 500 µm to 3200 µm in the coarse fraction (~40% of inclusions); the maximum grain size is 3200 µm. The sample contains more elongated than equant grains with angular to sub-angular boundaries.

The following inclusions were identified in the sample. *Frequent*: **rock fragments** including Qtz, Kfs, Pl, green Am and Bt (many feldspar grains in rock fragments and individual feldspar grains have yellowish alteration along the edges and cleavage lines), **green Am**; *Few*: **Qtz** (mono- and polycrystalline, undulose extinction, sutured boundaries), **Pl**, **Bt**; *Very few*: **Kfs** (some sericitic, cloudy).

S56 – Amphibole group

Microstructure and voids

The ratio of inclusions, matrix and voids in the sample is 30:65:5. The sample can be considered as homogeneous apart from slight differences in the colour of the matrix. Elongated grains and voids are oriented moderately parallel to the walls of the ceramic sherd. The size of the voids ranges between 50 µm and 1400 µm, including mainly mesoplanar voids and mesovughs.

Matrix

The sample has a non-calcareous matrix. The colour of the matrix is light reddish-brown with a black margin on one side in plane polarised light. It shows the same shades in crossed polarisers and is optically highly active to very slightly active.

Inclusions

The sample has bimodal grain-size distribution and the grains are moderately sorted. The modal grain size ranges from 10 µm to 250 µm in the fine fraction (~70% of inclusions) and 600 µm to 1500 µm in the coarse fraction (~30% of inclusions); the maximum grain size is 1500 µm. The sample contains more elongated than equant grains with angular to sub-angular boundaries.

The following inclusions were identified in the sample. *Frequent*: **rock fragments** including Qtz, Kfs, Pl and Bt (many feldspar grains in rock fragments and

individual feldspar grains have yellowish alteration along the edges and cleavage lines), **Qtz** (mono- and polycrystalline, undulose extinction, sutured boundaries); *Common*: **Kfs**, **Pl**; *Few*: **Bt**, **green Am**; **clay pellets** (very dark reddish-brown in PPL and XP, optically very slightly active, elongated, sub-rounded, max. size: 350 µm, high optical density, sharp to merging boundaries, concordant orientation, similar composition to matrix but having few or no inclusions), **Gr/Op**, **Zo?**; *Very rare*: **Ms**.

S57 – Carbonate group (Carbonate A)

Microstructure and voids

The ratio of inclusions, matrix and voids in the sample is 45:51:4. The sample can be considered as homogeneous apart from slight differences in alignment and the colour of the matrix. Elongated grains and voids are oriented moderately parallel to the walls of the ceramic sherd. The size of the voids ranges between 50 µm and 800 µm, including mainly mesovughs. Some of the voids are Cb-filled.

Matrix

The sample has a non-calcareous matrix. The colour of the matrix is light reddish-brown with a very dark reddish-brown margin on one side in plane polarised light. It shows the same shades in crossed polarisers and is optically highly active to very slightly active.

Inclusions

The sample has bimodal grain-size distribution and the grains are very poorly sorted. The modal grain size ranges from 10 µm to 100 µm in the fine fraction (~60% of inclusions) and 500 µm to 2400 µm in the coarse fraction (~40% of inclusions); the maximum grain size is 2400 µm. The sample contains elongated and equant grains in about the same amount with very angular to sub-angular boundaries.

The following inclusions were identified in the sample. *Frequent*: **Cal/Dol grains and Cb rock fragments** consisting mainly of Cal/Dol and Cpx (Di) and additionally of Ms and faded Bt; *Common*: **Qtz** (monocrystalline > polycrystalline, mostly fine-grained (<100 µm), larger grains have undulose extinction and sutured boundaries, Qtz makes up most of the fine fraction); *Few*: **Ms** (mostly fine-grained, <100 µm), **Kfs** (fine-grained, <100 µm), **clay pellets** (very dark reddish-brown in PPL and XP, optically very slightly active/inactive, elongated> equant, sub-rounded, max. size: 700 µm, high optical density, sharp to merging boundaries, discordant orientation, similar composition to matrix); *Very few*: **Cpx (Di)**, **Pl** (fine-grained, <100 µm); *Very rare*: **Bt**.

S58 – Carbonate group (Carbonate A)

Microstructure and voids

The ratio of inclusions, matrix and voids in the sample is 45:50:5. The sample can be considered as homogeneous apart from slight differences in the colour of the matrix. Elongated grains and voids are oriented moderately parallel to the walls of the ceramic sherd. The size of the voids ranges between 50 µm and 1450 µm, including mainly mesovughs and mesochannels.

Matrix

The sample has a non-calcareous matrix. The colour of the matrix is light reddish-brown with a dark reddish-brown margin on one side in plane polarised light. It shows the same shades in crossed polarisers and is optically highly active to slightly active.

Inclusions

The sample has bimodal grain-size distribution and the grains are very poorly sorted. The modal grain size ranges from 10 µm to 100 µm in the fine fraction (~50% of inclusions) and 400 µm to 3500 µm in the coarse fraction (~50% of inclusions); the maximum grain size is 3500 µm. The sample contains elongated and equant grains in about the same amount with very angular to sub-angular boundaries.

The following inclusions were identified in the sample. *Frequent*: **Cal/Dol grains and Cb rock fragments** consisting mainly of Cal/Dol and Cpx (Di) and additionally of Gr and faded Bt; *Common*: **Qtz** (monocrystalline > polycrystalline, mostly fine-grained (<100 µm), larger grains have undulose extinction and sutured boundaries, Qtz makes up most of the fine fraction); *Few*: **Ms** (mostly fine-grained, <100 µm), **Kfs** (fine-grained, <100 µm), **clay pellets** (dark/very dark reddish-brown in PPL and XP, optically moderately active/inactive, elongated> equant, sub-rounded, max. size: 1150 µm, high optical density, sharp to merging boundaries, concordant orientation, similar composition to matrix); *Very few*: **Pl** (fine-grained, <100 µm); *Rare*: **Cpx (Di)**.

S59 – Carbonate group (Carbonate B)

Microstructure and voids

The ratio of inclusions, matrix and voids in the sample is 15:82:3. The sample can be considered as homogeneous apart from slight differences in the colour of the matrix. Elongated grains and voids are oriented moderately parallel to the walls of the ceramic sherd. The size of the voids ranges between 100 µm and 2000 µm, including mainly mesovughs.

Matrix

The sample has a non-calcareous matrix. The colour of the matrix is light reddish-brown with dark reddish-brown patches and a dark reddish-brown margin on one side in plane polarised light. It is light yellowish-greyish-brown with dark reddish-brown patches and a dark reddish-brown margin on one side in crossed polarisers and is optically moderately active to slightly active.

Inclusions

The sample has bimodal grain-size distribution and the grains are very poorly sorted. The modal grain size ranges from 10 µm to 100 µm in the fine fraction (~5% of inclusions) and 350 µm to 2400 µm in the coarse fraction (~95% of inclusions); the maximum grain size is 2400 µm. The sample contains more equant than elongated grains with sub-angular to sub-rounded boundaries.

The following inclusions were identified in the sample. *Predominant*: **Cal/Dol grains and Cb rock fragments** consisting mainly of Cal/Dol and Cpx (Di) and additionally of Ms and Gr/Op – Cal/Dol grains have started decomposing; *Few*: **Cpx (Di)**, **clay pellets?** (light yellowish-brown in PPL, dark greyish-brown in XP, optically slightly active, equant, well-rounded, max. size: 500 µm, neutral optical density, sharp to merging boundaries, discordant orientation, different composition from that of matrix – matrix has very few Qtz inclusions, while these pellets have abundant Qtz (and Fsp?) inclusions), **Qtz** (monocrystalline, fine-grained (<100 µm), larger grains have undulose extinction and sutured boundaries); *Very few*: **Ms**.

S60 – Amphibole group

Microstructure and voids

The ratio of inclusions, matrix and voids in the sample is 35:60:5. The sample can be considered as homogeneous apart from slight differences in the colour of the matrix. Elongated grains and voids are oriented moderately parallel to the walls of the ceramic sherd. The size of the voids ranges between 100 µm and 900 µm, including mainly mesovughs and mesoplanar voids.

Matrix

The sample has a non-calcareous matrix. The colour of the matrix is light reddish-brown with a dark reddish-brown margin on one side in plane polarised light. It shows the same shades in crossed polarisers and is optically highly active to slightly active.

Inclusions

The sample has bimodal grain-size distribution and the grains are very poorly sorted. The modal grain size ranges from 10 µm to 350 µm in the fine fraction (~60% of inclusions) and 650 µm to 2700 µm in the coarse fraction (~40% of inclusions); the maximum grain size is 2700 µm. The sample contains more elongated than equant grains with angular to sub-angular boundaries.

The following inclusions were identified in the sample. *Frequent*: **rock fragments** including Kfs, Qtz, Pl, Bt, green Am and Gr (many feldspar grains in rock fragments and individual feldspar grains have yellowish alteration along the edges and cleavage lines), **green Am**; *Common*: **Kfs**, **Bt**; *Few*: **Qtz** (mono- and polycrystalline, undulose extinction, sutured boundaries), **Pl**; *Rare*: **Gr/Op**; *Very rare*: **Grt**, **Zrn**.

S61 – Amphibole group

Microstructure and voids

The ratio of inclusions, matrix and voids in the sample is 30:63:7. The sample can be considered as homogeneous apart from slight differences in the colour of the matrix. Elongated grains and voids are oriented moderately parallel to the walls of the ceramic sherd. The size of the voids ranges between 100 µm and 1200 µm, including mainly meso- and macrovughs.

Matrix

The sample has a non-calcareous matrix. The colour of the matrix is black/ very dark reddish-brown with a light reddish-brown margin on one side in plane polarised light. It shows the same shades in crossed polarisers and is optically inactive to highly active.

Inclusions

The sample has bimodal grain-size distribution and the grains are very poorly sorted. The modal grain size ranges from 10 µm to 250 µm in the fine fraction (~70% of inclusions) and 500 µm to 3250 µm in the coarse fraction (~30% of inclusions); the maximum grain size is 3250 µm. The sample contains elongated and equant grains in about the same amount with angular to sub-angular boundaries.

The following inclusions were identified in the sample. *Frequent*: **rock fragments** including Qtz, Pl, Kfs, Bt and green Am (many feldspar grains in rock fragments and individual feldspar grains have yellowish alteration along the edges and cleavage lines); *Common*: **green Am**, **Bt**, **Qtz** (mono- and polycrystalline, undulose extinction, sutured boundaries), some oxidised), **Pl**; *Few*: **Kfs** (some sericitic, cloudy); *Rare*: **Gr/Op**; *Very rare*: **clay pellet** (dark reddish-brown with black margins in PPL and XP, optically slightly active/inactive, elongated, sub-rounded, max. size: 1400 µm, high optical density, clear boundaries, discordant orientation, similar composition to matrix).

S62 – Graphite group (Graphite D)

Microstructure and voids

The ratio of inclusions, matrix and voids in the sample is 30:65:5. The sample can be considered as homogeneous apart from slight differences in alignment and the colour of the matrix. Elongated grains and voids are oriented moderately parallel to the walls of the ceramic sherd. The size of the voids ranges between 50 µm and 1100 µm, including mainly meso- and macrovughs and mesoplanar voids.

Matrix

The sample has a non-calcareous matrix. The colour of the matrix changes from dark reddish-brown to light reddish-brown in plane polarised light. It shows the same shades in crossed polarisers and is optically slightly active to highly active.

Inclusions

The sample has bimodal grain-size distribution and the grains are very poorly sorted. The modal grain size ranges from 10 µm to 250 µm in the fine fraction (~55% of inclusions) and 600 µm to 2550 µm in the coarse fraction (~45% of inclusions); the maximum grain size is 2550 µm. The sample contains more elongated than equant grains with angular to sub-angular boundaries.

The following inclusions were identified in the sample. *Frequent*: **Gr flakes and Gr gneiss** fragments consisting of Gr, Qtz, Kfs, Bt, Grt, Rt and Ep/Zo/Czo; *Common*: **Qtz** (mono- and polycrystalline, undulose extinction, sutured boundaries), **Kfs** (some cloudy), **Bt**; *Few*: **chert** fragments; *Very few*: **Pl**, **pseudomorphs** (Sil/Ms?); *Rare*: **Grt**, **Ms** (fine-grained, <100 µm); *Very rare*: **clay pellet** (light reddish-brown in PPL and XP, optically moderately active, elongated, rounded, max. size: 1500 µm, neutral optical density, diffuse boundaries, discordant orientation, similar composition to matrix).

S63 – Amphibole group

Microstructure and voids

The ratio of inclusions, matrix and voids in the sample is 30:62:8. The sample can be considered as homogeneous apart from slight differences in the colour of the matrix. Elongated grains and voids are oriented strongly parallel to the walls of the ceramic sherd. The size of the voids ranges between 100 µm and 1350 µm, including mainly mesovughs and mesoplanar voids.

Matrix

The sample has a non-calcareous matrix. The colour of the matrix changes from very dark reddish-brown to dark reddish-brown in plane polarised light. It shows the same shades in crossed polarisers and is optically very slightly active to highly active.

Inclusions

The sample has bimodal grain-size distribution and the grains are very poorly sorted. The modal grain size ranges from 10 µm to 300 µm in the fine fraction (~65% of inclusions) and 500 µm to 4000 µm in the coarse fraction (~35% of inclusions); the maximum grain size is 4000 µm. The sample contains more elongated than equant grains with angular to sub-angular boundaries.

The following inclusions were identified in the sample. *Frequent*: **rock fragments** including Qtz, Pl, Kfs, Bt and green Am (many feldspar grains in rock fragments and individual feldspar grains have yellowish alteration along the edges and cleavage lines); *Common*: **Qtz** (mono- and polycrystalline, undulose extinction, sutured boundaries), **Pl**, **Bt**, **green Am**; *Few*: **Kfs**; *Rare*: **Gr** (with inclusions of cloudy Fsp), **graphitic rock fragments/clay pellets?** (dark reddish-brown in PPL and XP, optically slightly active, elongated, sub-angular, max. size: 1400 µm, high optical density, sharp to merging boundaries, concordant orientation, similar composition to matrix, they have Gr and Qtz inclusions), **Ms** (fine-grained, <100 µm).

S64 – Granitoid group (Granitoid A1)

Microstructure and voids

The ratio of inclusions, matrix and voids in the sample is 30:60:10. The sample can be considered as homogeneous apart from slight differences in alignment and the colour of the matrix. Elongated grains and voids are oriented moderately parallel to the walls of the ceramic sherd. The size of the voids ranges between 25 µm and 1550 µm, including mainly mesoplanar voids and meso- and macrovughs.

Matrix

The sample has a non-calcareous matrix. The colour of the matrix is black/very dark reddish-brown with a light reddish-brown margin on one side in plane polarised light. It shows the same shades in crossed polarisers and is optically inactive to highly active.

Inclusions

The sample has bimodal grain-size distribution and the grains are very poorly sorted. The modal grain size ranges from 10 µm to 200 µm in the fine fraction (~50% of inclusions) and 400 µm to 2650 µm in the coarse fraction (~50% of inclusions); the maximum grain size is 2650 µm. The sample contains more elongated than equant grains with angular to sub-angular boundaries.

The following inclusions were identified in the sample. *Common*: **Kfs** (usually cloudy, perthitic, saussuritic), **granitoid** fragments (including Kfs, Pl, Qtz, Bt), **Bt**; *Few*: **Pl** (usually sericitic, cloudy), **Qtz** (mono- and polycrystalline, undulose extinction, sutured boundaries); *Rare*: **Ms** (fine-grained, <100 µm) **green Am**.

S65 – Granitoid group (Granitoid A2)

Microstructure and voids

The ratio of inclusions, matrix and voids in the sample is 30:60:10. The sample can be considered as homogeneous apart from slight differences in alignment and the colour of the matrix. Elongated grains and voids are oriented moderately parallel to the walls of the ceramic sherd. The size of the voids ranges between 50 µm and 1800 µm, including mainly mesoplanar voids and mesovughs.

Matrix

The sample has a non-calcareous matrix. The colour of the matrix is light reddish-brown with a very light reddish-brown core in plane polarised light. It shows the same shades in crossed polarisers and is optically highly active.

Inclusions

The sample has bimodal grain-size distribution and the grains are very poorly sorted. The modal grain

size ranges from 10 µm to 200 µm in the fine fraction (~50% of inclusions) and 500 µm to 3350 µm in the coarse fraction (~50% of inclusions); the maximum grain size is 3350 µm. About two thirds of the grains making up the fine fraction are less than 50 µm. The sample contains elongated and equant grains in about the same amount with angular to sub-angular boundaries.

The following inclusions were identified in the sample. *Frequent*: **Kfs** (perthitic, sericitic), **granitoid** fragments (including Kfs, Pl, Qtz, Bt, Op); *Common*: **Qtz** (mono- and polycrystalline, undulose extinction, sutured boundaries); *Few*: **Bt**, **Pl** (some sericitic, cloudy); *Rare*: **Gr/Op**, **Ms** (fine-grained, <100 µm), **clay pellets** (dark reddish-brown/black in PPL and XP, optically slightly active/inactive, equant, rounded, max. size: 500 µm, neutral optical density, diffuse boundaries, concordant orientation, similar composition to matrix); *Very rare*: **green Am**.

S66 – Granitoid group (Granitoid A2)

Microstructure and voids

The ratio of inclusions, matrix and voids in the sample is 30:60:10. The sample can be considered as homogeneous apart from slight differences in alignment and the colour of the matrix. Elongated grains and voids are oriented moderately parallel to the walls of the ceramic sherd. The size of the voids ranges between 100 µm and 1350 µm, including mainly meso- and macrovughs and mesoplanar voids.

Matrix

The sample has a non-calcareous matrix. The colour of the matrix is light reddish-brown with dark reddish-brown patches in plane polarised light. It shows the same shades in crossed polarisers and is optically highly active to moderately active.

Inclusions

The sample has bimodal grain-size distribution and the grains are very poorly sorted. The modal grain size ranges from 10 µm to 200 µm in the fine fraction (~45% of inclusions) and 500 µm to 3650 µm in the coarse fraction (~55% of inclusions); the maximum grain size is 3650 µm. About two thirds of the grains making up the fine fraction are less than 50 µm. The sample contains more elongated than equant grains with angular to sub-angular boundaries.

The following inclusions were identified in the sample. *Frequent*: **granitoid** fragments (including Kfs, Pl, Qtz, Bt, Ms); *Common*: **Bt**, **Kfs** (perthitic, sericitic, saussuritic), **Qtz** (mono- and polycrystalline, undulose extinction, sutured boundaries), **Pl** (some sericitic, cloudy); *Very few*: **clay pellets** (very dark reddish-brown in PPL and XP, optically slightly active/inactive, elongated, sub-rounded, max. size: 750 µm, high optical density, sharp to merging boundaries, concordant orientation, similar composition to matrix); *Rare*: **Ms** (fine-grained, <100 µm), **Zrn** (many relatively large grains, 60–130 µm), **Gr/Op**, **green Am**.

S67 – Diorite group (Diorite B)

Microstructure and voids

The ratio of inclusions, matrix and voids in the sample is 30:60:10. The sample can be considered as homogeneous apart from slight differences in alignment and the colour of the matrix. Elongated grains and voids are oriented moderately parallel to the walls of the ceramic sherd. The size of the voids ranges between 100 µm and 1550 µm, including mainly meso- and macrovughs and mesoplanar voids.

Matrix

The sample has a non-calcareous matrix. The colour of the matrix is light reddish-brown with a dark reddish-brown margin on one side in plane polarised light. It shows the same shades in crossed polarisers and is optically moderately active to slightly active.

Inclusions

The sample has bimodal grain-size distribution and the grains are very poorly sorted. The modal grain size ranges from 10 µm to 250 µm in the fine fraction (~45% of inclusions) and 500 µm to 2400 µm in the coarse fraction (~55% of inclusions); the maximum grain size is 2400 µm. The sample contains more elongated than equant grains with angular to sub-angular boundaries.

The following inclusions were identified in the sample. *Dominant*: **rock fragments** (diorite/monzonite) including Fsp (Kfs and Pl, sericitic and cloudy, Pl usually has a sericitic core and unaltered outer zone, some Kfs have saussuritic alteration), Qtz, green Am, Cpx, Bt, Ms and Gr – in some rock fragments the oriented intergrowth of Qtz and Fsp is observed (micrographic texture); *Few*: **Bt**, **Kfs** (some sericitic, cloudy, saussuritic), **Qtz** (mono- and polycrystalline, undulose extinction, sutured boundaries), **Pl** (some have a sericitic core and an unaltered outer zone); *Very few*: **Grt**, **Cpx**, **green Am**; *Rare*: **clay pellets** (very dark reddish-brown in PPL and XP, optically slightly active, elongated, rounded, max. size: 300 µm, high optical density, diffuse boundaries, concordant orientation, similar composition to matrix), **Gr**, **Ms**; *Very rare*: **Rt**.

S68 – Granitoid group (Granitoid A2)

Microstructure and voids

The ratio of inclusions, matrix and voids in the sample is 30:63:7. The sample can be considered as homogeneous apart from slight differences in alignment and the colour of the matrix. Elongated grains and voids are oriented moderately parallel to the walls of the ceramic sherd. The size of the voids ranges between 100 µm and 1050 µm, including mainly mesovughs and mesoplanar voids.

Matrix

The sample has a non-calcareous matrix. The colour of the matrix is dark reddish-brown with light reddish-brown margins in plane polarised light. It shows the same shades in crossed polarisers and is optically moderately active to very highly active.

Inclusions

The sample has bimodal grain-size distribution and the grains are very poorly sorted. The modal grain size ranges from 10 µm to 150 µm in the fine fraction (~55% of inclusions) and 500 µm to 2350 µm in the coarse fraction (~45% of inclusions); the maximum grain size is 2350 µm. About two thirds of the grains making up the fine fraction are less than 50 µm. The sample contains elongated and equant grains in about the same amount with angular to sub-angular boundaries.

The following inclusions were identified in the sample. *Common*: **Kfs** (perthitic, sericitic), **Qtz** (mono- and polycrystalline, undulose extinction, sutured boundaries); *Few*: **Bt**, **Pl**, **granitoid** fragments (including Kfs, Pl, Bt); *Very few*: **clay pellets** (dark/very dark reddish-brown in PPL and XP, optically moderately/slightly active, equant>elongated, rounded, max. size: 800 µm, high optical density, diffuse boundaries, concordant orientation, similar composition to matrix); *Rare*: **Op/Gr**, **Ms** (fine-grained, <100 µm), **Zrn**.

S69 – Granitoid group (Granitoid A2)

Microstructure and voids

The ratio of inclusions, matrix and voids in the sample is 30:65:5. The sample can be considered as homogeneous apart from slight differences in alignment and the colour of the matrix. Elongated grains and voids are oriented moderately parallel to the walls of the ceramic sherd. The size of the voids ranges between 100 µm and 2500 µm, including mainly meso- and macrovughs and mesoplanar voids.

Matrix

The sample has a non-calcareous matrix. The colour of the matrix is very light yellowish-greyish-brown with light reddish-brown margins in plane polarised light. It is light yellowish-greyish-brown with light reddish-brown margins in crossed polarisers and is optically moderately active to highly active.

Inclusions

The sample has bimodal grain-size distribution and the grains are very poorly sorted. The modal grain size ranges from 10 µm to 150 µm in the fine fraction (~50% of inclusions) and 400 µm to 2600 µm in the coarse fraction (~50% of inclusions); the maximum grain size is 2600 µm. About two thirds of the grains making up the fine fraction are less than 50 µm. The sample contains more elongated than equant grains with angular to sub-angular boundaries.

The following inclusions were identified in the sample. *Frequent*: **granitoid** fragments (including Kfs, Pl, Qtz, Bt, Zo/Czo, green Am – Zo/Czo might originate from alteration of Fsp); *Common*: **Kfs** (cloudy, perthitic), **Qtz** (mono- and polycrystalline, undulose extinction, sutured boundaries); *Few*: **Bt**, **Pl**; *Very few*: **green Am**, **clay pellets** (dark reddish-brown or light greyish-brown with black margin in PPL, dark reddish-brown or dark greyish-brown with black margin in XP, optically moderately active to slightly active, elongated>equant, sub-rounded/well-rounded, max. size: 1650 µm, high/neutral optical density, sharp to merging boundaries, concordant orientation, similar composition to matrix); *Rare*: **Gr** (once with granitoid fragment), **Ms** (fine-grained, <100 µm), **Zrn?**.

S70 – Granitoid group (Granitoid A1)

Microstructure and voids

The ratio of inclusions, matrix and voids in the sample is 30:63:7. The sample can be considered as homogeneous apart from slight differences in the colour of the matrix. Elongated grains and voids are oriented moderately parallel to the walls of the ceramic sherd. The size of the voids ranges between 100 µm and 2000 µm, including mainly mesoplanar voids and meso- and macrovughs.

Matrix

The sample has a non-calcareous matrix. The colour of the matrix changes from very dark reddish-brown to light reddish-brown in plane polarised light. It shows the same shades in crossed polarisers and is optically inactive to highly active.

Inclusions

The sample has bimodal grain-size distribution and the grains are very poorly sorted. The modal grain size ranges from 10 µm to 300 µm in the fine fraction (~60% of inclusions) and 750 µm to 2600 µm in the coarse fraction (~40% of inclusions); the maximum grain size is 2600 µm. The sample contains more elongated than equant grains with angular to sub-angular boundaries.

The following inclusions were identified in the sample. *Frequent*: **granitoid** fragments (including Kfs, Pl, Qtz, Bt, green Am); *Common*: **Bt**, **Kfs** (usually cloudy, perthitic), **Qtz** (mono- and polycrystalline, undulose extinction, sutured boundaries); *Very few*: **green Am**, **Pl** (some cloudy); *Rare*: **Ms** (fine-grained, <100 µm), **Gr** (once with granitoid fragment); *Very rare*: **Zrn(?)**.

S71 – Granitoid group (Granitoid A1)

Microstructure and voids

The ratio of inclusions, matrix and voids in the sample is 25:68:7. The sample can be considered as homogeneous apart from slight differences in the colour of the matrix. Elongated grains and voids are oriented moderately parallel to the walls of the ceramic sherd. The size of the voids ranges between

100 µm and 1000 µm, including mainly mesoplanar voids and mesovughs.

Matrix

The sample has a non-calcareous matrix. The colour of the matrix changes from light reddish-brown to dark reddish-brown in plane polarised light. It shows the same shades in crossed polarisers and is optically highly active to inactive.

Inclusions

The sample has bimodal grain-size distribution and the grains are very poorly sorted. The modal grain size ranges from 10 µm to 250 µm in the fine fraction (~35% of inclusions) and 500 µm to 1850 µm in the coarse fraction (~65% of inclusions); the maximum grain size is 1850 µm. The sample contains more elongated than equant grains with angular to sub-angular boundaries.

The following inclusions were identified in the sample. *Frequent*: **granitoid** fragments (including Kfs, Pl, Qtz, Bt), **Kfs** (perthitic); *Common*: **Qtz** (monocrystalline > polycrystalline, undulose extinction, sutured boundaries); *Few*: **Bt**; *Very few*: **Pl** (some cloudy); *Rare*: **Ms** (fine-grained, <100 µm), **Op/Gr**; *Very rare*: **green Am**, **Zrn**.

S72 – Granitoid group (Granitoid A2)

Microstructure and voids

The ratio of inclusions, matrix and voids in the sample is 30:65:5. The sample can be considered as homogeneous apart from slight differences in alignment and the colour of the matrix. Elongated grains and voids are oriented weakly/moderately parallel to the walls of the ceramic sherd. The size of the voids ranges between 100 µm and 650 µm, including mainly mesovughs and mesoplanar voids.

Matrix

The sample has a non-calcareous matrix. The colour of the matrix is light reddish-brown with a dark reddish-brown core in plane polarised light. It shows the same shades in crossed polarisers and is optically moderately active.

Inclusions

The sample has bimodal grain-size distribution and the grains are very poorly sorted. The modal grain size ranges from 10 µm to 250 µm in the fine fraction (~50% of inclusions) and 500 µm to 2500 µm in the coarse fraction (~50% of inclusions); the maximum grain size is 2500 µm. About two thirds of the grains making up the fine fraction are less than 50 µm. The sample contains more elongated than equant grains with angular to sub-angular boundaries.

The following inclusions were identified in the sample. *Frequent*: **Kfs** (cloudy, sericitic, perthitic), **Qtz** (mono- and polycrystalline, undulose extinction, sutured boundaries); *Common*: **Bt**, **Pl** (sericitic); *Very few*: **granitoid** fragments (including Kfs, Qtz); *Rare*: **green Am**, **Ms** (fine-grained, <100 µm), **Gr/Op**; *Very rare*: **Zrn**.

S73 – Granitoid group (Granitoid A1)

Microstructure and voids

The ratio of inclusions, matrix and voids in the sample is 30:65:5. The sample can be considered as homogeneous apart from slight differences in alignment and the colour of the matrix. Elongated grains and voids are oriented moderately parallel to the walls of the ceramic sherd. The size of the voids ranges between 100 µm and 1250 µm, including mainly meso- and macrovughs and mesoplanar voids.

Matrix

The sample has a non-calcareous matrix. The colour of the matrix is dark reddish-brown with light reddish-brown patches in plane polarised light. It shows the same shades in crossed polarisers and is optically slightly active to highly active.

Inclusions

The sample has bimodal grain-size distribution and the grains are very poorly sorted. The modal grain size ranges from 10 µm to 250 µm in the fine fraction (~35% of inclusions) and 400 µm to 2550 µm in the coarse fraction (~65% of inclusions); the maximum grain size is 2250 µm. The sample contains more elongated than equant grains with angular to sub-angular boundaries.

The following inclusions were identified in the sample. *Common*: **granitoid** fragments (including Kfs, Pl, Qtz, Bt) **Kfs** (perthitic, sericitic), **Bt**; *Few*: **Qtz** (mono- and polycrystalline, undulose extinction, sutured boundaries), **Pl** (sericitic); *Very rare*: **clay pellet** (dark reddish-brown in PPL and XP, optically slightly active, equant, rounded, max. size: 550 µm, high optical density, sharp to merging boundaries, concordant orientation, similar composition to matrix), **green Am**, **Ms**.

S74 – Granitoid group (Granitoid A1)

Microstructure and voids

The ratio of inclusions, matrix and voids in the sample is 30:63:7. The sample can be considered as homogeneous. Elongated grains and voids are oriented moderately parallel to the walls of the ceramic sherd. The size of the voids ranges between 50 µm and 750 µm, including mainly mesovughs, mesoplanar voids and mesochannels.

Matrix

The sample has a non-calcareous matrix. The colour of the matrix is dark reddish-brown in plane polarised light. It shows the same shade in crossed polarisers and is optically slightly active.

Inclusions

The sample has bimodal grain-size distribution and the grains are very poorly sorted. The modal grain size ranges from 10 µm to 250 µm in the fine fraction

(~60% of inclusions) and 500 µm to 2200 µm in the coarse fraction (~40% of inclusions); the maximum grain size is 2200 µm. The sample contains more elongated than equant grains with angular to sub-angular boundaries.
The following inclusions were identified in the sample. *Common*: **granitoid** fragments (including Kfs, Pl, Qtz, Bt), **Qtz** (mono- and polycrystalline, undulose extinction, sutured boundaries); *Few*: **Bt**, **Kfs** (perthitic, sericitic), **Pl** (cloudy, sericitic); *Very few*: **green Am** (aggregates, once with sericitic Fsp suggesting that Am aggregates were the part of the granitoid fragments); *Rare*: **Ms** (fine-grained, <100 µm).

S75 – Diorite group (Diorite A)

Microstructure and voids
The ratio of inclusions, matrix and voids in the sample is 35:60:5. The sample can be considered as homogeneous apart from slight differences in alignment and the colour of the matrix. Elongated grains and voids are oriented moderately parallel to the walls of the ceramic sherd. The size of the voids ranges between 100 µm and 1250 µm, including mainly mesovughs and mesoplanar voids.
Matrix
The sample has a non-calcareous matrix. The colour of the matrix changes from very light reddish-brown to light reddish-brown in plane polarised light. It changes from light yellowish-greyish-brown to light reddish-brown in crossed polarisers and is optically moderately active to highly active.
Inclusions
The sample has bimodal grain-size distribution and the grains are very poorly sorted. The modal grain size ranges from 10 µm to 100 µm in the fine fraction (~35% of inclusions) and 300 µm to 1850 µm in the coarse fraction (~50% of inclusions); the maximum grain size is 1850 µm. The sample contains elongated and equant grains in about the same amount with angular to sub-angular boundaries.
The following inclusions were identified in the sample. *Dominant*: **rock fragments** (diorite/monzonite) including Fsp (sericitic core and unaltered outer zone), greenish-brown Am, Bt, Qtz, colourless Am (in aggregates, occasionally with Px) and Gr/Op; *Common*: **Qtz** (monocrystalline > polycrystalline, undulose extinction, fine-grained (<100 µm), makes up most of the fine fraction); *Few*: **Bt**, **Fsp**; *Very few*: **colourless Am**, **clay pellets** (very dark reddish-brown in PPL and XP, optically very slightly active, elongated>equant, sub-rounded, max. size: 450 µm, high optical density, sharp to merging boundaries, concordant orientation, similar composition to matrix); *Rare*: **Gr/Op** (with inclusions of Qtz/Fsp), **greenish-brown Am**; *Very rare*: **Ms** (fine-grained, <100 µm).

S76 – Granitoid group (Granitoid A1)

Microstructure and voids
The ratio of inclusions, matrix and voids in the sample is 25:65:10. The sample can be considered as homogeneous apart from slight differences in alignment and the colour of the matrix. Elongated grains and voids are oriented moderately parallel to the walls of the ceramic sherd. The size of the voids ranges between 50 µm and 1200 µm, including mainly mesovughs and mesoplanar voids.
Matrix
The sample has a non-calcareous matrix. The colour of the matrix is light reddish-brown with a dark reddish-brown margin on one side in plane polarised light. It shows the same shades in crossed polarisers and is optically moderately active.
Inclusions
The sample has bimodal grain-size distribution and the grains are very poorly sorted. The modal grain size ranges from 10 µm to 350 µm in the fine fraction (~50% of inclusions) and 700 µm to 4300 µm in the coarse fraction (~50% of inclusions); the maximum grain size is 4300 µm. The sample contains elongated and equant grains in about the same amount with angular to sub-angular boundaries.
The following inclusions were identified in the sample. *Frequent*: **granitoid** fragments (including Kfs, Qtz, Pl, Bt), **Qtz** (mono- and polycrystalline, undulose extinction, sutured boundaries); *Common*: **Bt**, **Kfs** (perthitic, sericitic); *Rare*: **Gr/Op**, **Pl** (sericitic), **Ms** (fine-grained, <100 µm).

S77 – Granitoid group (Granitoid A1)

Microstructure and voids
The ratio of inclusions, matrix and voids in the sample is 25:70:5. The sample can be considered as homogeneous apart from slight differences in alignment. Elongated grains and voids are oriented moderately parallel to the walls of the ceramic sherd. The size of the voids ranges between 50 µm and 1050 µm, including mainly meso- and macrovughs and mesoplanar voids.
Matrix
The sample has a non-calcareous matrix. The colour of the matrix is light reddish-brown in plane polarised light. It shows the same shade in crossed polarisers and is optically moderately active.
Inclusions
The sample has bimodal grain-size distribution and the grains are very poorly sorted. The modal grain size ranges from 10 µm to 300 µm in the fine fraction (~45% of inclusions) and 500 µm to 2600 µm in the coarse fraction (~55% of inclusions); the maximum grain size is 2600 µm. The sample contains more equant than elongated grains with angular to sub-angular boundaries. Many particles of the coarse

fraction are equant and between 500 µm and 600 µm.
The following inclusions were identified in the sample. *Frequent*: **granitoid** fragments (including Kfs, Pl, Qtz, Bt); *Common*: **Kfs** (perthitic, sericitic), **Qtz** (monocrystalline > and polycrystalline, undulose extinction, sutured boundaries); *Few*: **Bt**; *Very few*: **Pl** (sericitic, cloudy); *Rare*: **greenish-brown Am**, **Gr**, **Ms** (fine-grained, <100 µm).

S78 – Granitoid group (Granitoid A2)

Microstructure and voids
The ratio of inclusions, matrix and voids in the sample is 30:63:7. The sample can be considered as homogeneous apart from slight differences in alignment and the colour of the matrix. Elongated grains and voids are oriented moderately parallel to the walls of the ceramic sherd. The size of the voids ranges between 25 µm and 2000 µm, including mainly mesoplanar voids and meso- and macrovughs.
Matrix
The sample has a non-calcareous matrix. The colour of the matrix is very dark reddish-brown with a dark reddish-brown margin on one side in plane polarised light. It shows the same shades in crossed polarisers and is optically slightly active to moderately active.
Inclusions
The sample has bimodal grain-size distribution and the grains are very poorly sorted. The modal grain size ranges from 10 µm to 200 µm in the fine fraction (~50% of inclusions) and 500 µm to 2250 µm in the coarse fraction (~50% of inclusions); the maximum grain size is 2250 µm. About two thirds of the grains making up the fine fraction are less than 50 µm. The sample contains more equant than elongated grains with angular to sub-angular boundaries.
The following inclusions were identified in the sample. *Frequent*: **granitoid** fragments (including Pl, Qtz, Kfs, Bt); *Common*: **Qtz** (mono- and polycrystalline, undulose extinction, sutured boundaries); *Few*: **clay pellets** (very dark reddish-brown in PPL and XP, optically very slightly active, equant, rounded, max. size: 900 µm, high optical density, sharp to merging boundaries, discordant orientation, similar composition to matrix); *Very few*: **Kfs** (perthitic, cloudy), **Pl** (cloudy), **Bt**; *Rare*: **Ms** (fine-grained, <100 µm), **green Am**; *Very rare*: **rock fragment** containing Zo/Czo, Ms, Fsp? and Op (Zo/Czo might be from alteration of Fsp).

S79 – Granitoid group (Granitoid A2)

Microstructure and voids
The ratio of inclusions, matrix and voids in the sample is 30:63:7. The sample can be considered as homogeneous apart from slight differences in alignment and the colour of the matrix. Elongated grains and voids are oriented moderately parallel to the walls of the ceramic sherd. The size of the voids ranges between 25 µm and 1000 µm, including mainly mesoplanar voids and meso- and macrovughs.
Matrix
The sample has a non-calcareous matrix. The colour of the matrix changes from very dark reddish-brown to dark reddish-brown in plane polarised light. It shows the same shades in crossed polarisers and is optically slightly active to moderately active.
Inclusions
The sample has bimodal grain-size distribution and the grains are very poorly sorted. The modal grain size ranges from 10 µm to 200 µm in the fine fraction (~45% of inclusions) and 400 µm to 2500 µm in the coarse fraction (~55% of inclusions); the maximum grain size is 2500 µm. About two thirds of the grains making up the fine fraction are less than 50 µm and consist of Qtz and Fsp. The sample contains elongated and equant grains in about the same amount with angular to sub-angular boundaries.
The following inclusions were identified in the sample. *Frequent*: **Kfs** (perthitic, sericitic, cloudy), **granitoid** fragments (including Kfs, Pl, Qtz); *Common*: **Qtz** (mono- and polycrystalline, undulose extinction, sutured boundaries); *Few*: **clay pellets** (very dark reddish-brown in PPL and XP, optically very slightly active, equant, sub-rounded, max. size: 2000 µm, high optical density, sharp to merging boundaries, discordant orientation, similar composition to matrix); *Very few*: **Pl** (sericitic, cloudy), **Bt**; *Rare*: **green Am**, **Ms** (fine-grained, <100 µm), *Very rare*: **rock fragment** including Gr/Op and Kfs.

S80 – Granitoid group (Granitoid B1)

Microstructure and voids
The ratio of inclusions, matrix and voids in the sample is 25:70:5. The sample can be considered as homogeneous apart from slight differences in the colour of the matrix. Elongated grains and voids are oriented moderately parallel to the walls of the ceramic sherd. The size of the voids ranges between 100 µm and 1300 µm, including mainly meso- and macrovughs and mesoplanar voids.
Matrix
The sample has a non-calcareous matrix. The colour of the matrix changes from very dark reddish-brown to light reddish-brown in plane polarised light. It shows the same shades in crossed polarisers and is optically very slightly active to moderately active.
Inclusions
The sample has bimodal grain-size distribution and the grains are moderately sorted. The modal grain size ranges from 10 µm to 200 µm in the fine fraction (~40% of inclusions) and 400 µm to 3100 µm in the coarse fraction (~60% of inclusions); the maximum grain size is 3100 µm. The sample contains more

elongated than equant grains with angular to sub-angular boundaries.
The following inclusions were identified in the sample. *Dominant*: **Qtz** (mono- and polycrystalline, undulose extinction, sutured boundaries); *Common*: **granitoid** fragments (including Kfs, Pl, Qtz); *Very few*: **Kfs**, **Pl** (some sericitic); *Rare*: **Gr/Op** (with Qtz), **Ms** (fine-grained, <100 µm).

S81 – Granitoid group (Granitoid A2)

Microstructure and voids
The ratio of inclusions, matrix and voids in the sample is 30:63:7. The sample can be considered as homogeneous apart from slight differences in alignment and the colour of the matrix. Elongated grains and voids are oriented moderately parallel to the walls of the ceramic sherd. The size of the voids ranges between 50 µm and 1600 µm, including mainly meso- and macrovughs and mesoplanar voids.
Matrix
The sample has a non-calcareous matrix. The colour of the matrix is light reddish-brown with a slightly darker core in plane polarised light. It shows the same shades in crossed polarisers and is optically highly active to moderately active.
Inclusions
The sample has bimodal grain-size distribution and the grains are very poorly sorted. The modal grain size ranges from 10 µm to 200 µm in the fine fraction (~50% of inclusions) and 500 µm to 2500 µm in the coarse fraction (~50% of inclusions); the maximum grain size is 2500 µm. About two thirds of the grains making up the fine fraction are less than 50 µm. The sample contains elongated and equant grains in about the same amount with very angular to angular boundaries.
The following inclusions were identified in the sample. *Common*: **Kfs** (perthitic, some sericitic), **granitoid** fragments (including Kfs, Pl, Qtz), **Qtz** (mono- and polycrystalline, undulose extinction, sutured boundaries); *Few*: **Bt**, **Pl** (some sericitic); *Rare*: **Op/Gr**, **Ms** (fine-grained, <100 µm), **Zrn**.

S82 – Granitoid group (Granitoid B1)

Microstructure and voids
The ratio of inclusions, matrix and voids in the sample is 25:65:10. The sample can be considered as homogeneous. Elongated grains and voids are oriented moderately parallel to the walls of the ceramic sherd. The size of the voids ranges between 100 µm and 1600 µm, including mainly meso- and macrovughs and mesoplanar voids. Some voids are filled with a yellowish material (both in PPL and XP).
Matrix
The sample has a non-calcareous matrix. The colour of the matrix is very dark reddish-brown in plane polarised light. It shows the same shade in crossed polarisers and is optically very slightly active.
Inclusions
The sample has bimodal grain-size distribution and the grains are poorly sorted. The modal grain size ranges from 10 µm to 200 µm in the fine fraction (~40% of inclusions) and 400 µm to 2250 µm in the coarse fraction (~60% of inclusions); the maximum grain size is 2250 µm. The sample contains more elongated than equant grains with very angular to sub-rounded boundaries.
The following inclusions were identified in the sample. *Dominant*: **Qtz** (mono- and polycrystalline, undulose extinction, sutured boundaries); *Few*: **granitoid** fragments (including Kfs, Qtz, Bt, Ms), **Kfs** (cloudy); *Very few*: **Pl**, **Bt**; *Rare*: **Ms** (fine-grained, <100 µm); *Very rare*: **Ep?**.

S83 – Granitoid group (Granitoid B1)

Microstructure and voids
The ratio of inclusions, matrix and voids in the sample is 25:65:10. The sample can be considered as homogeneous apart from slight differences in the colour of the matrix. Elongated grains and voids are oriented moderately parallel to the walls of the ceramic sherd. The size of the voids ranges between 100 µm and 1700 µm, including mainly meso- and macrovughs and mesoplanar voids.
Matrix
The sample has a non-calcareous matrix. The colour of the matrix is light reddish-brown with a dark reddish-brown margin on one side in plane polarised light. It shows the same shades in crossed polarisers and is optically moderately active to slightly active.
Inclusions
The sample has bimodal grain-size distribution and the grains are moderately sorted. The modal grain size ranges from 10 µm to 200 µm in the fine fraction (~50% of inclusions) and 400 µm to 1200 µm in the coarse fraction (~50% of inclusions); the maximum grain size is 1200 µm. The sample contains elongated and equant grains in about the same amount with very angular to sub-angular boundaries.
The following inclusions were identified in the sample. *Frequent*: **Qtz** (mono- and polycrystalline, undulose extinction, sutured boundaries); *Few*: **granitoid fragments** (including Qtz, Kfs, Bt, Pl), **Kfs**, **Pl**; *Very few*: **Bt**; *Rare*: **Gr/Op**, **rock fragment** containing Qtz and Ms, **Ms**; *Very rare*: **pseudomorph** consisting probably of Ms and Bt, **clay pellet** (very dark reddish-brown in PPL and XP, optically very slightly active, elongated, sub-angular, max. size: 850 µm, high optical density, diffuse boundaries, concordant orientation, similar composition to matrix), **Rt?**, **Zrn?**.

S84 – Graphite group (Graphite A3)

Microstructure and voids

The ratio of inclusions, matrix and voids in the sample is 30:65:5. The sample can be considered as homogeneous apart from slight differences in alignment. Elongated grains and voids are oriented weakly-moderately parallel to the walls of the ceramic sherd. The size of the voids ranges between 50 µm and 1550 µm, including mainly mesovughs and mesoplanar voids.

Matrix

The sample has a non-calcareous matrix. The colour of the matrix is black in plane polarised light and in crossed polarisers and is optically inactive.

Inclusions

The sample has bimodal grain-size distribution and the grains are very poorly sorted. The modal grain size ranges from 10 µm to 150 µm in the fine fraction (~60% of inclusions) and 400 µm to 3500 µm in the coarse fraction (~40% of inclusions); the maximum grain size is 3500 µm. The sample contains more equant than elongated grains with very angular to sub-angular boundaries.

The following inclusions were identified in the sample. *Dominant*: **Gr flakes and Gr gneiss** fragments consisting of Gr, Qtz, Kfs, Rt and Grt; *Common*: **Qtz** (monocrystalline > polycrystalline, undulose extinction, sutured boundaries); *Few*: **Kfs** (cloudy), **Grt**; *Very few*: **Bt**; *Rare*: **Rt**, **Ms**; *Very rare*: **rock fragment** containing green Am, Kfs, Qtz and Bt, **rock fragment** containing Ms and Qtz, **green Am**.

S85 – Graphite group (Graphite A3)

Microstructure and voids

The ratio of inclusions, matrix and voids in the sample is 30:60:10. The sample can be considered as homogeneous apart from slight differences in the colour of the matrix. Elongated grains and voids are oriented moderately parallel to the walls of the ceramic sherd. The size of the voids ranges between 50 µm and 1050 µm, including mainly meso- and macrovughs and mesoplanar voids.

Matrix

The sample has a non-calcareous matrix. The colour of the matrix is very dark reddish-brown a dark reddish-brown margin on one side in plane polarised light. It shows the same shades in crossed polarisers and is optically inactive to moderately active.

Inclusions

The sample has bimodal grain-size distribution and the grains are very poorly sorted. The modal grain size ranges from 10 µm to 300 µm in the fine fraction (~60% of inclusions) and 500 µm to 3200 µm in the coarse fraction (~40% of inclusions); the maximum grain size is 3200 µm. The sample contains more equant than elongated grains with very angular to sub-angular boundaries.

The following inclusions were identified in the sample. *Dominant*: **Gr flakes and Gr gneiss** fragments consisting of Gr, Kfs, Qtz, and Bt; *Common*: **Qtz** (monocrystalline > polycrystalline, undulose extinction, sutured boundaries); *Few*: **Grt**, **Kfs**; *Rare*: **green Am**, **Bt** (some started altering to Sil), **Ms**.

S86 – Graphite group (Graphite A3)

Microstructure and voids

The ratio of inclusions, matrix and voids in the sample is 35:58:7. The sample can be considered as homogeneous apart from slight differences in alignment. Elongated grains and voids are oriented weakly-moderately parallel to the walls of the ceramic sherd. The size of the voids ranges between 50 µm and 1000 µm, including mainly mesovughs and mesoplanar voids.

Matrix

The sample has a non-calcareous matrix. The colour of the matrix is black in plane polarised light and in crossed polarisers and is optically inactive.

Inclusions

The sample has bimodal grain-size distribution and the grains are very poorly sorted. The modal grain size ranges from 10 µm to 200 µm in the fine fraction (~50% of inclusions) and 400 µm to 2300 µm in the coarse fraction (~50% of inclusions); the maximum grain size is 2300 µm. The sample contains more equant than elongated grains with very angular to angular boundaries.

The following inclusions were identified in the sample. *Dominant*: **Gr flakes and Gr gneiss** fragments consisting of Kfs, Gr, Qtz, Bt and Grt; *Common*: **Kfs** (cloudy), **Qtz** (mono- and polycrystalline, undulose extinction, sutured boundaries); *Few*: **Grt**; *Very few*: **green Am**; *Rare*: **Bt**, **Ms** (fine-grained, <100 µm); *Very rare*: **rock fragment** consisting of green Am, Kfs and Qtz.

S87 – Granitoid group (Granitoid C)

Microstructure and voids

The ratio of inclusions, matrix and voids in the sample is 30:63:7. The sample can be considered as homogeneous apart from slight differences in alignment and the colour of the matrix. Elongated grains and voids are oriented moderately parallel to the walls of the ceramic sherd. The size of the voids ranges between 50 µm and 1000 µm, including mainly mesovughs and mesoplanar voids.

Matrix

The sample has a non-calcareous matrix. The colour of the matrix is very dark reddish-brown/black with light reddish-brown margins in plane polarised light. It shows the same shades in crossed polarisers and is optically very slightly active to highly active.

Inclusions

The sample has bimodal grain-size distribution and the grains are very poorly sorted. The modal grain size ranges from 10 µm to 200 µm in the fine fraction

(~55% of inclusions) and 400 µm to 3000 µm in the coarse fraction (~45% of inclusions); the maximum grain size is 3000 µm. The sample contains more elongated than equant grains with very angular to angular boundaries.
The following inclusions were identified in the sample. *Frequent*: **granitoid** fragments (including Kfs (Mc), Qtz, Bt, Pl), **Bt**; *Common*: **Qtz** (mono- and polycrystalline, undulose extinction, sutured boundaries); *Few*: **Kfs (Mc)**, **Pl**; *Very few*: **green Am**; *Rare*: **Ms** (mainly fine-grained, <100 µm).

S88 – Granitoid group (Granitoid A1)

Microstructure and voids
The ratio of inclusions, matrix and voids in the sample is 30:63:7. The sample can be considered as homogeneous apart from slight differences in the colour of the matrix. Elongated grains and voids are oriented moderately parallel to the walls of the ceramic sherd. The size of the voids ranges between 100 µm and 1750 µm, including mainly meso- and macrovughs and mesoplanar voids.
Matrix
The sample has a non-calcareous matrix. The colour of the matrix changes from very light reddish-brown to dark reddish-brown in plane polarised light. It shows the same shades in crossed polarisers and is optically slightly active to very highly active.
Inclusions
The sample has bimodal grain-size distribution and the grains are very poorly sorted. The modal grain size ranges from 10 µm to 250 µm in the fine fraction (~40% of inclusions) and 400 µm to 2800 µm in the coarse fraction (~60% of inclusions); the maximum grain size is 2800 µm. The sample contains more elongated than equant grains with very angular to sub-angular boundaries.
The following inclusions were identified in the sample. *Frequent*: **granitoid** fragments (including Kfs, Pl, Bt, green Am, Qtz, Zrn); *Common*: **Bt** (some started altering to Sil), **Kfs** (perthitic, sericitic); *Few*: **Qtz** (monocrystalline > polycrystalline, undulose extinction, sutured boundaries); *Very few*: **green Am**, **Pl**; *Rare*: **Gr**; *Very rare*: **Ms**, **Zrn**.

S89 – Carbonate group (Carbonate B)

Microstructure and voids
The ratio of inclusions, matrix and voids in the sample is 20:73:7. The sample can be considered as homogeneous apart from slight differences in alignment and the colour of the matrix. Elongated grains and voids are oriented moderately parallel to the walls of the ceramic sherd. The size of the voids ranges between 50 µm and 1400 µm, including mainly macroplanar voids, macrochannels and mesovughs. Some voids are filled with a brownish (PPL and XP) material.
Matrix
The sample has a non-calcareous matrix. The colour of the matrix is black with a light reddish-brown margin on one side in plane polarised light. It shows the same shades in crossed polarisers and is optically inactive to moderately active.
Inclusions
The sample has bimodal grain-size distribution and the grains are very poorly sorted. The modal grain size ranges from 10 µm to 150 µm in the fine fraction (~15% of inclusions) and 400 µm to 2150 µm in the coarse fraction (~85% of inclusions); the maximum grain size is 2150 µm. The sample contains more elongated than equant grains with very angular to sub-angular boundaries.
The following inclusions were identified in the sample. *Predominant*: **Cal/Dol grains and Cb rock fragments** consisting mainly of Cal/Dol and Cpx (Di) and additionally of colourless Am and Ms; *Few*: **Qtz** (monocrystalline, fine-grained (<100 µm), larger grains have undulose extinction, Qtz makes up most of the fine fraction), **Cpx (Di)**; *Very few*: **Ms** (coarse-grained, >250 µm); *Rare*: **clay pellets/ARF?** (black in PPL and XP, optically inactive, elongated, sub-angular/sub-rounded, max. size: 1800 µm, high optical density, sharp boundaries, discordant orientation, different composition from that of the matrix – matrix has more inclusions, these pellets have few Qtz inclusions); *Very rare*: **clay pellet** (pure clay nodule, very light reddish-brown in PPL, very light yellowish-greyish-brown in XP, optically highly active, distorted, sub-rounded, max. size: 2250 µm, neutral optical density, sharp to merging boundaries, discordant orientation, similar composition to matrix), **colourless Am**.

S90 – Amphibole group

Microstructure and voids
The ratio of inclusions, matrix and voids in the sample is 35:55:10. The sample can be considered as homogeneous apart from slight differences in alignment and the colour of the matrix. Elongated grains and voids are oriented moderately parallel to the walls of the ceramic sherd. The size of the voids ranges between 50 µm and 1200 µm, including mainly meso- and macrovughs and mesoplanar voids.
Matrix
The sample has a non-calcareous matrix. The colour of the matrix is dark reddish-brown with light reddish-brown margins in plane polarised light. It shows the same shades in crossed polarisers and is optically slightly active to highly active.
Inclusions
The sample has bimodal grain-size distribution and the grains are very poorly sorted. The modal grain size ranges from 10 µm to 300 µm in the fine fraction (~55% of inclusions) and 500 µm to 3200 µm in the

coarse fraction (~45% of inclusions); the maximum grain size is 3200 µm. The sample contains more elongated than equant grains with angular to sub-angular boundaries.
The following inclusions were identified in the sample. *Frequent*: **Pl**, **rock fragments** including Pl, green Am and Qtz (many feldspar grains in rock fragments and individual feldspar grains have yellowish alteration along the edges and cleavage lines); *Common*: **green Am**, **Bt** (started altering to Sil); *Few*: **Qtz** (monocrystalline > polycrystalline, undulose extinction, sutured boundaries); *Rare*: **Gr/Op**; *Very rare*: **rock fragment** with alignment containing Qtz and Bt, **clay pellet** (very dark reddish-brown in PPL and XP, optically very slightly active, equant, rounded, max. size: 350 µm, high optical density, sharp to merging boundaries, discordant orientation, similar composition to matrix).

S91 – Amphibole group

Microstructure and voids

The ratio of inclusions, matrix and voids in the sample is 35:55:10. The sample can be considered as homogeneous apart from slight differences in alignment and the colour of the matrix. Elongated grains and voids are oriented moderately parallel to the walls of the ceramic sherd. The size of the voids ranges between 50 µm and 1350 µm, including mainly meso- and macrovughs and mesoplanar voids.

Matrix

The sample has a non-calcareous matrix. The colour of the matrix is light reddish-brown with a dark reddish-brown margin on one side in plane polarised light. It shows the same shades in crossed polarisers and is optically moderately active to slightly active.

Inclusions

The sample has bimodal grain-size distribution and the grains are very poorly sorted. The modal grain size ranges from 10 µm to 300 µm in the fine fraction (~55% of inclusions) and 500 µm to 5000 µm in the coarse fraction (~45% of inclusions); the maximum grain size is 5000 µm. The sample contains more elongated than equant grains with angular to sub-angular boundaries.
The following inclusions were identified in the sample. *Common*: **rock fragments** including Qtz, Pl, Kfs and Bt (many feldspar grains in rock fragments and individual feldspar grains have yellowish alteration along the edges and cleavage lines), **rock fragments** (diorite/monzonite) including Fsp (sericitic core and unaltered outer zone), greenish-brown Am, Bt, Qtz and colourless Am aggregates, **green Am**, **Bt**; *Few*: **Pl**, **Qtz** (monocrystalline > polycrystalline, undulose extinction, sutured boundaries), **colourless Am** (individual crystals and crystal aggregates); *Very few*: **Kfs**; *Rare*: **Gr** (once with Fsp/Qtz), **greenish-brown Am**, **Ms** (fine-grained, <100 µm); *Very rare*: **clay pellet** (very dark reddish-brown in PPL and XP, optically very slightly active, elongated, sub-rounded, max. size: 500 µm, high optical density, sharp to merging boundaries, concordant orientation, similar composition to matrix), **Zrn**.

S92 – Amphibole group

Microstructure and voids

The ratio of inclusions, matrix and voids in the sample is 35:55:10. The sample can be considered as homogeneous apart from slight differences in the colour of the matrix. Elongated grains and voids are oriented moderately-strongly parallel to the walls of the ceramic sherd. The size of the voids ranges between 50 µm and 900 µm, including mainly mesovughs and mesoplanar voids.

Matrix

The sample has a non-calcareous matrix. The colour of the matrix is light reddish-brown with dark reddish-brown patches in plane polarised light. It shows the same shades in crossed polarisers and is optically moderately active.

Inclusions

The sample has bimodal grain-size distribution and the grains are very poorly sorted. The modal grain size ranges from 10 µm to 200 µm in the fine fraction (~55% of inclusions) and 400 µm to 2400 µm in the coarse fraction (~45% of inclusions); the maximum grain size is 2400 µm. The sample contains more elongated than equant grains with angular to sub-rounded boundaries.
The following inclusions were identified in the sample. *Frequent*: **rock fragments** including Qtz, Pl, Kfs, green Am and Bt (many feldspar grains in rock fragments and individual feldspar grains have yellowish alteration along the edges and cleavage lines); *Common*: **rock fragments** (diorite/monzonite) including Fsp (sericitic core and unaltered outer zone), greenish-brown Am, Bt, Qtz and Gr, **green Am**, **Bt**; *Few*: **Pl**, **Qtz** (mono- and polycrystalline, undulose extinction, sutured boundaries); *Very few*: **Kfs**, **colourless Am** (individual crystals and crystal aggregates); *Rare*: **Gr**, **Ms** (fine-grained, <100 µm); *Very rare*: **greenish-brown Am**.

S93 – Granitoid group (Granitoid B2)

Microstructure and voids

The ratio of inclusions, matrix and voids in the sample is 30:60:10. The sample can be considered as homogeneous. Elongated grains and voids are oriented moderately parallel to the walls of the ceramic sherd. The size of the voids ranges between 50 µm and 700 µm, including mainly mesovughs and mesoplanar voids.

Matrix

The sample has a non-calcareous matrix. The colour of the matrix is light reddish-brown in plane polarised

light. It shows the same shade in crossed polarisers and is optically moderately active to highly active.

Inclusions

The sample has bimodal grain-size distribution and the grains are very poorly sorted. The modal grain size ranges from 10 µm to 300 µm in the fine fraction (~40% of inclusions) and 500 µm to 2250 µm in the coarse fraction (~60% of inclusions); the maximum grain size is 2250 µm. The sample contains more elongated than equant grains with very angular to angular boundaries.

The following inclusions were identified in the sample. *Frequent*: **Qtz** (mono- and polycrystalline, undulose extinction, sutured boundaries); *Common*: **Pl** (some sericitic), **Kfs** (some sericitic); *Few*: **granitoid** fragments (including Qtz, Kfs, Pl, Gr, Bt, Rt?), **Bt**; *Very few*: **Gr/Op** (with Qtz, Fsp, Grt), **clay pellets** (dark reddish-brown in PPL and XP, optically slightly active, elongated>equant, well-rounded, max. size: 950 µm, high optical density, clear boundaries, concordant orientation, similar composition to matrix but with few inclusions); *Rare*: **Grt**, **Ms**, *Very rare*: **Tur?**, **Zrn**.

S94 – Granitoid group (Granitoid A1)

Microstructure and voids

The ratio of inclusions, matrix and voids in the sample is 25:68:7. The sample can be considered as homogeneous apart from slight differences in alignment and the colour of the matrix. Elongated grains and voids are oriented moderately parallel to the walls of the ceramic sherd. The size of the voids ranges between 50 µm and 2000 µm, including mainly mesovughs and mesoplanar voids.

Matrix

The sample has a non-calcareous matrix. The colour of the matrix is light reddish-brown with a very dark reddish-brown margin on one side in plane polarised light. It shows the same shades in crossed polarisers and is optically moderately active to very slightly active.

Inclusions

The sample has bimodal grain-size distribution and the grains are very poorly sorted. The modal grain size ranges from 10 µm to 150 µm in the fine fraction (~30% of inclusions) and 300 µm to 3000 µm in the coarse fraction (~70% of inclusions); the maximum grain size is 3000 µm. The sample contains more equant than elongated grains with angular to sub-angular boundaries.

The following inclusions were identified in the sample. *Frequent*: **granitoid** fragments (including Kfs, Pl, Qtz, Bt); *Common*: **Bt**; **Kfs** (perthitic, sericitic, saussuritic), **Qtz** (monocrystalline > polycrystalline, undulose extinction, sutured boundaries); *Few*: **Pl** (some altered); *Rare*: **Gr/Op**, **Ms** (fine-grained, <100 µm), **Zrn**.

S95 – Granitoid group (Granitoid A1)

Microstructure and voids

The ratio of inclusions, matrix and voids in the sample is 25:65:10. The sample can be considered as homogeneous apart from slight differences in alignment. Elongated grains and voids are oriented weakly parallel to the walls of the ceramic sherd. The size of the voids ranges between 50 µm and 1500 µm, including mainly meso- and macrovughs and mesoplanar voids.

Matrix

The sample has a non-calcareous matrix. The colour of the matrix is light reddish-brown in plane polarised light. It shows the same shade in crossed polarisers and is optically moderately active.

Inclusions

The sample has bimodal grain-size distribution and the grains are very poorly sorted. The modal grain size ranges from 10 µm to 150 µm in the fine fraction (~30% of inclusions) and 300 µm to 3350 µm in the coarse fraction (~70% of inclusions); the maximum grain size is 3350 µm. The sample contains more equant than elongated grains with angular to sub-angular boundaries.

The following inclusions were identified in the sample. *Frequent*: **granitoid** fragments (including Qtz, Pl, Kfs, Bt, green Am); *Common*: **Bt**, **Qtz** (mono- and polycrystalline, undulose extinction, sutured boundaries), **Kfs** (perthitic, sericitic, saussuritic); *Few*: **Pl** (some sericitic); *Very few*: **clay pellets** (dark reddish-brown in PPL and XP, optically slightly active, elongated, rounded, max. size: 1500 µm, neutral optical density, diffuse boundaries, concordant orientation, similar composition to matrix); *Rare*: **Ms** (mainly fine-grained, <100 µm), **Gr/Op**; *Very rare*: **green Am**, **Zrn**.

S96 – Granitoid group (Granitoid A1)

Microstructure and voids

The ratio of inclusions, matrix and voids in the sample is 25:70:5. The sample can be considered as homogeneous apart from slight differences in the colour of the matrix. Elongated grains and voids are oriented moderately/strongly parallel to the walls of the ceramic sherd. The size of the voids ranges between 100 µm and 1250 µm, including mainly meso- and macroplanar voids and mesovughs.

Matrix

The sample has a non-calcareous matrix. The colour of the matrix changes from light reddish-brown to very dark reddish-brown in plane polarised light. It shows the same shades in crossed polarisers and is optically highly active to slightly active.

Inclusions

The sample has bimodal grain-size distribution and the grains are very poorly sorted. The modal grain size ranges from 10 µm to 100 µm in the fine fraction

(~30% of inclusions) and 300 µm to 3250 µm in the coarse fraction (~70% of inclusions); the maximum grain size is 3250 µm. The sample contains more elongated than equant grains with angular to sub-angular boundaries.
The following inclusions were identified in the sample. *Frequent*: **granitoid** fragments (including Kfs, Pl, Qtz, Bt, green Am), **Kfs** (some perthitic, sericitic); *Common*: **Bt**, **Qtz** (mono- and polycrystalline, undulose extinction, sutured boundaries); *Few*: **Pl** (some sericitic, cloudy); *Rare*: **Gr**, **clay pellets/limonitic nodules?** (dark reddish-brown in PPL and XP, optically slightly active, elongated, rounded, max. size: 600 µm, high optical density, clear/diffuse boundaries, concordant orientation, similar composition to matrix but containing almost no inclusions), **Ms** (fine-grained, <100); *Very rare*: **green Am**, **Rt(?)**, **Zrn(?)**.

S97 – Diorite group (Diorite B)

Microstructure and voids
The ratio of inclusions, matrix and voids in the sample is 30:63:7. The sample can be considered as homogeneous apart from slight differences in alignment and the colour of the matrix. Elongated grains and voids are oriented moderately parallel to the walls of the ceramic sherd. The size of the voids ranges between 100 µm and 3600 µm, including mainly meso- and macrovughs and mesoplanar voids.
Matrix
The sample has a non-calcareous matrix. The colour of the matrix changes from light reddish-brown to very dark reddish-brown/black in plane polarised light. It shows the same shades in crossed polarisers and is optically highly active to inactive.
Inclusions
The sample has bimodal grain-size distribution and the grains are very poorly sorted. The modal grain size ranges from 10 µm to 300 µm in the fine fraction (~30% of inclusions) and 700 µm to 2350 µm in the coarse fraction (~70% of inclusions); the maximum grain size is 2350 µm. The sample contains more elongated than equant grains with angular to sub-angular boundaries.
The following inclusions were identified in the sample. *Dominant*: **rock fragments** (diorite/monzonite) including Fsp (Kfs and Pl, cloudy, sericitic, saussuritic, some have a sericitic core and unaltered outer zone), Qtz, green Am, Bt, Cpx and Gr – in some rock fragments the oriented intergrowth of Qtz and Fsp is observed (micrographic texture); *Very few*: **Cpx**, **Qtz** (mono- and polycrystalline, undulose extinction, sutured boundaries), **green Am**; *Rare*: **Kfs**, **Pl**, **Gr**, **Ms**.

S98 – Granitoid group (Granitoid A1)

Microstructure and voids
The ratio of inclusions, matrix and voids in the sample is 25:68:7. The sample can be considered as homogeneous apart from slight differences in alignment and the colour of the matrix. Elongated grains and voids are oriented moderately parallel to the walls of the ceramic sherd. The size of the voids ranges between 25 µm and 2100 µm, including mainly meso- and macrovughs and mesoplanar voids.
Matrix
The sample has a non-calcareous matrix. The colour of the matrix changes from light reddish-brown to very dark reddish-brown in plane polarised light. It shows the same shades in crossed polarisers and is optically highly active to very slightly active.
Inclusions
The sample has bimodal grain-size distribution and the grains are very poorly sorted. The modal grain size ranges from 10 µm to 400 µm in the fine fraction (~45% of inclusions) and 600 µm to 5200 µm in the coarse fraction (~55% of inclusions); the maximum grain size is 5200 µm. The sample contains more elongated than equant grains with angular to sub-angular boundaries.
The following inclusions were identified in the sample. *Frequent*: **granitoid** fragments (including Pl, Kfs, Qtz, Bt, green Am, Ms); *Common*: **Kfs** (some sericitic, perthitic), **Pl** (altered), **Bt**, **Qtz** (mono- and polycrystalline, undulose extinction, sutured boundaries); *Rare*: **green Am**, **Ms** (fine-grained, <100 µm); *Very rare*: **rock fragment** consisting of Ms and Bt, **Gr/Op**.

S99 – Graphite group (Graphite A1)

Microstructure and voids
The ratio of inclusions, matrix and voids in the sample is 35:58:7. The sample can be considered as homogeneous apart from slight differences in alignment. Elongated grains and voids are oriented moderately parallel to the walls of the ceramic sherd. The size of the voids ranges between 100 µm and 1650 µm, including mainly meso- and macrovughs.
Matrix
The sample has a non-calcareous matrix. The colour of the matrix is very dark reddish-brown in plane polarised light. It shows the same shade in crossed polarisers and is optically very slightly active.
Inclusions
The sample has bimodal grain-size distribution and the grains are very poorly sorted. The modal grain size ranges from 10 µm to 200 µm in the fine fraction (~65% of inclusions) and 400 µm to 1800 µm in the coarse fraction (~35% of inclusions); the maximum grain size is 1800 µm. The sample contains more elongated than equant grains with very angular to angular boundaries.
The following inclusions were identified in the sample. *Dominant*: **Gr flakes and Gr gneiss** fragments

consisting of Gr, Qtz, Kfs, Pl, Bt and Ms; *Frequent*: **Qtz** (mono- and polycrystalline, undulose extinction, sutured boundaries); *Few*: **Kfs**; *Very few*: **Sil** (originating probably from Sil gneiss), **Pl**; *Rare*: **Bt** (some faded), **Ms** (fine-grained, <100 µm); *Very rare*: **Scp**.

S100 – Graphite group (Graphite A2)

Microstructure and voids

The ratio of inclusions, matrix and voids in the sample is 30:55:15. The sample can be considered as homogeneous apart from slight differences in alignment. Elongated grains and voids are oriented moderately parallel to the walls of the ceramic sherd. The size of the voids ranges between 100 µm and 3300 µm, including mainly meso- and macroplanar voids, mesochannels and mesovughs.

Matrix

The sample has a non-calcareous matrix. The colour of the matrix is very dark reddish-brown in plane polarised light. It shows the same shade in crossed polarisers and is optically very slightly active.

Inclusions

The sample has bimodal grain-size distribution and the grains are very poorly sorted. The modal grain size ranges from 10 µm to 200 µm in the fine fraction (~60% of inclusions) and 400 µm to 3050 µm in the coarse fraction (~40% of inclusions); the maximum grain size is 3050 µm. The sample contains more elongated than equant grains with angular to sub-angular boundaries.

The following inclusions were identified in the sample. *Predominant*: **Gr flakes and Gr gneiss** fragments consisting of Gr, Qtz, Kfs, Pl, Rt, Bt and Ms (triple junctions of Qtz and Fsp grains occur); *Common*: **Qtz** (mono- and polycrystalline, undulose extinction, both straight boundaries (triple junctions) and sutured boundaries); *Very few*: **Kfs**, **Pl**; *Rare*: **Scp**, **Rt**, **Ms**.

S101 – Graphite group (Graphite A1)

Microstructure and voids

The ratio of inclusions, matrix and voids in the sample is 30:60:10. The sample can be considered as homogeneous apart from slight differences in alignment and the colour of the matrix. Elongated grains and voids are oriented moderately parallel to the walls of the ceramic sherd. The size of the voids ranges between 50 µm and 1200 µm, including mainly mesovughs, mesoplanar voids and mesochannels.

Matrix

The sample has a non-calcareous matrix. The colour of the matrix is light reddish-brown with a very light reddish-brown core in plane polarised light. It is light reddish-brown with a light yellowish-greyish-brown core in crossed polarisers and is optically moderately active.

Inclusions

The sample has bimodal grain-size distribution and the grains are very poorly sorted. The modal grain size ranges from 10 µm to 250 µm in the fine fraction (~60% of inclusions) and 600 µm to 2650 µm in the coarse fraction (~40% of inclusions); the maximum grain size is 2650 µm. The sample contains more elongated than equant grains with angular to sub-angular boundaries.

The following inclusions were identified in the sample. *Dominant*: **Gr flakes and Gr gneiss** fragments consisting of Gr, Qtz, Kfs, Rt, Pl and Ms; *Common*: **Kfs**, **Qtz** (monocrystalline > polycrystalline, undulose extinction, sutured boundaries); *Few*: **clay pellets** (dark reddish-brown in PPL and XP, optically moderately/slightly active, equant, well-rounded, max. size: 2100 µm, neutral/high optical density, sharp to merging boundaries, concordant orientation, similar composition to matrix), **Sil gneiss** fragments including Sil, Gr and Qtz/Kfs; *Very few*: **Bt**, **Ms**; *Rare*: **Rt**; *Very rare*: **Scp**.

S102 – Graphite group (Graphite A1)

Microstructure and voids

The ratio of inclusions, matrix and voids in the sample is 35:58:7. The sample can be considered as homogeneous apart from slight differences in alignment. Elongated grains and voids are oriented moderately parallel to the walls of the ceramic sherd. The size of the voids ranges between 100 µm and 1150 µm, including mainly meso- and macrovughs.

Matrix

The sample has a non-calcareous matrix. The colour of the matrix is dark reddish-brown in plane polarised light. It is very dark reddish-brown in crossed polarisers and is optically very slightly active to inactive.

Inclusions

The sample has bimodal grain-size distribution and the grains are very poorly sorted. The modal grain size ranges from 10 µm to 400 µm in the fine fraction (~55% of inclusions) and 600 µm to 2200 µm in the coarse fraction (~45% of inclusions); the maximum grain size is 2200 µm. The sample contains more elongated than equant grains with angular to sub-angular boundaries.

The following inclusions were identified in the sample. *Dominant*: **Gr flakes and Gr gneiss** fragments consisting of Gr, Qtz, Kfs, Pl, Scp and Ms; *Frequent*: **Qtz** (mono- and polycrystalline, undulose extinction, sutured boundaries); *Few*: **Kfs**, **Sil gneiss** fragments including Sil and Gr; *Very few*: **Pl**; *Rare*: **Ms**, **Bt**, **Scp**, **chert** fragments, **Rt**; *Very rare*: **clay pellet** (very dark reddish-brown in PPL and XP, optically very slightly active, equant, well-rounded, max. size: 500 µm,

neutral optical density, sharp boundaries, concordant orientation, similar composition to matrix), **organic inclusion?** (plant remain?).

S103 – Graphite group (Graphite A1)

Microstructure and voids

The ratio of inclusions, matrix and voids in the sample is 35:60:5. The sample can be considered as homogeneous. Elongated grains and voids are oriented moderately-strongly parallel to the walls of the ceramic sherd. The size of the voids ranges between 50 µm and 1000 µm, including mainly meso- and macrovughs.

Matrix

The sample has a non-calcareous matrix. The colour of the matrix is dark reddish-brown/black in plane polarised light. It is very dark reddish-brown/black in crossed polarisers and is optically very slightly active to inactive.

Inclusions

The sample has bimodal grain-size distribution and the grains are very poorly sorted. The modal grain size ranges from 10 µm to 200 µm in the fine fraction (~55% of inclusions) and 400 µm to 2400 µm in the coarse fraction (~45% of inclusions); the maximum grain size is 2400 µm. The sample contains more elongated than equant grains with very angular to sub-angular boundaries.

The following inclusions were identified in the sample. *Dominant*: **Gr flakes and Gr gneiss** fragments consisting of Gr, Kfs, Pl, Qtz and Scp; *Common*: **Qtz** (mono- and polycrystalline, undulose extinction, sutured boundaries); *Few*: **Kfs**; *Very few*: **Sil** (originating probably from Sil gneiss); *Rare*: **Ms**, **Bt**, **Rt**; *Very rare*: **clay pellet** (light reddish-brown in PPL, very dark yellowish-greyish-brown in XP, optically very slightly active, elongated, sub-rounded, max. size: 500 µm, high optical density, clear boundaries, concordant orientation, similar composition to matrix).

S104 – Graphite group (Graphite A2)

Microstructure and voids

The ratio of inclusions, matrix and voids in the sample is 35:55:10. The sample can be considered as homogeneous. Elongated grains and voids are oriented moderately parallel to the walls of the ceramic sherd. The size of the voids ranges between 100 µm and 1360 µm, including mainly meso- and macrovughs, mesochannels and mesoplanar voids.

Matrix

The sample has a non-calcareous matrix. The colour of the matrix is very dark reddish-brown/black in plane polarised light. It shows the same shades in crossed polarisers and is optically very slightly active to inactive.

Inclusions

The sample has bimodal grain-size distribution and the grains are very poorly sorted. The modal grain size ranges from 10 µm to 400 µm in the fine fraction (~50% of inclusions) and 750 µm to 2500 µm in the coarse fraction (~50% of inclusions); the maximum grain size is 2500 µm. The sample contains more elongated than equant grains with very angular to sub-angular boundaries.

The following inclusions were identified in the sample. *Predominant*: **Gr flakes and Gr gneiss** fragments consisting of Gr, Qtz, Kfs, Pl, Scp and Rt (triple junctions of Qtz and Fsp grains occur); *Common*: **Qtz** (mono- and polycrystalline, undulose extinction, both straight boundaries (triple junctions) and sutured boundaries); *Few*: **Kfs**, **Pl**; *Very few*: **Scp**; *Rare*: **Bt**, **Rt**.

S105 – Graphite group (Graphite A2)

Microstructure and voids

The ratio of inclusions, matrix and voids in the sample is 35:55:10. The sample can be considered as homogeneous apart from slight differences in alignment. Elongated grains and voids are oriented moderately parallel to the walls of the ceramic sherd. The size of the voids ranges between 50 µm and 1300 µm, including mainly meso- and macrovughs and mesochannels. Some voids are filled with secondary Cb.

Matrix

The sample has a non-calcareous matrix. The colour of the matrix is very dark reddish-brown/black in plane polarised light. It shows the same shades in crossed polarisers and is optically very slightly active to inactive.

Inclusions

The sample has bimodal grain-size distribution and the grains are very poorly sorted. The modal grain size ranges from 10 µm to 500 µm in the fine fraction (~55% of inclusions) and 750 µm to 2000 µm in the coarse fraction (~45% of inclusions); the maximum grain size is 2000 µm. The sample contains more equant than elongated grains with angular to sub-angular boundaries.

The following inclusions were identified in the sample. *Predominant*: **Gr flakes and Gr gneiss** fragments consisting of Gr, Qtz, Kfs, Pl, Scp, Rt and Bt (triple junctions of Qtz and Fsp grains occur); *Common*: **Qtz** (mono- and polycrystalline, undulose extinction, both straight boundaries (triple junctions) and sutured boundaries); *Few*: **Kfs**, **Pl**, **Scp**; *Very few*: **secondary Cb** (in voids); *Rare*: **Rt**, **Ms** (fine-grained, <100 µm), **Bt**; *Very rare*: **clay pellet** (very dark reddish-brown in PPL and XP, optically very slightly active, elongated, angular, max. size: 4250 µm, neutral optical density, diffuse boundaries, concordant orientation, similar composition to matrix).

S106 – Graphite group (Graphite A5)

Microstructure and voids

The ratio of inclusions, matrix and voids in the sample is 30:60:10. The sample can be considered as homogeneous apart from slight differences in alignment. Elongated grains and voids are oriented moderately parallel to the walls of the ceramic sherd. The size of the voids ranges between 50 µm and 2350 µm, including mainly meso- and macrovughs meso- and macroplanar voids and mesochannels.

Matrix

The sample has a non-calcareous matrix. The colour of the matrix is dark reddish-brown in plane polarised light. It shows the same shade in crossed polarisers and is optically slightly active.

Inclusions

The sample has bimodal grain-size distribution and the grains are very poorly sorted. The modal grain size ranges from 10 µm to 350 µm in the fine fraction (~50% of inclusions) and 500 µm to 3000 µm in the coarse fraction (~50% of inclusions); the maximum grain size is 3000 µm. The sample contains more elongated than equant grains with very angular to angular boundaries.

The following inclusions were identified in the sample. *Dominant*: **Gr flakes and Gr gneiss** fragments consisting of Gr, Qtz, Kfs, Rt and Ms; *Common*: **Qtz** (mono- and polycrystalline, undulose extinction, sutured boundaries); *Few*: **Kfs**, **Pl**, **green Am**; *Very few*: **Ms**, **Bt**, **Rt**; *Rare*: **clay pellets** (dark/very dark reddish-brown in PPL and XP, optically slightly/very slightly active, elongated, sub-angular, max. size: 950 µm, high optical density, sharp to merging boundaries, concordant orientation, similar composition to matrix), **rock fragments** containing Sil and Kfs; *Very rare*: fine-grained **rock fragment** containing Qtz, Bt and Op.

S107 – Graphite group (Graphite A3)

Microstructure and voids

The ratio of inclusions, matrix and voids in the sample is 30:60:10. The sample can be considered as moderately heterogeneous because of the presence of a large amount of clay pellets (clay mixing?). Elongated grains and voids are oriented moderately parallel to the walls of the ceramic sherd. The size of the voids ranges between 50 µm and 1600 µm, including mainly mesoplanar voids, mesovughs and mesochannels. One of the voids is filled with some secondary Cb.

Matrix

The sample has a non-calcareous matrix. The colour of the matrix is dark reddish-brown with a black margin on one side in plane polarised light. It shows the same shades in crossed polarisers and is optically slightly active to inactive.

Inclusions

The sample has bimodal grain-size distribution and the grains are very poorly sorted. The modal grain size ranges from 10 µm to 500 µm in the fine fraction (~80% of inclusions) and 750 µm to 1300 µm in the coarse fraction (~20% of inclusions); the maximum grain size is 1300 µm. The sample contains elongated and equant grains in about the same amount with angular to sub-angular boundaries.

The following inclusions were identified in the sample. *Frequent*: **Qtz** (mono- and polycrystalline, undulose extinction, sutured boundaries), **Gr flakes and Gr gneiss** fragments consisting of Gr, Qtz, Bt, Rt and Kfs; *Common*: **clay pellets** (light/dark greyish-yellowish-brown in PPL, dark greyish-yellowish-brown in XP, optically very slightly active, elongated/distorted, angular to sub-rounded, max. size: 2000 µm, neutral optical density, diffuse boundaries, concordant orientation, similar composition to matrix); *Few*: **mica schist** fragments consisting of Qtz, Ms and Bt; *Very few*: **Grt**, **Bt**; *Rare*: **Ms**, **green Am**, **Opx**, **Pl**; *Very rare*: **secondary Cb** (in a void).

S108 – Graphite group (Graphite A5)

Microstructure and voids

The ratio of inclusions, matrix and voids in the sample is 30:65:5. The sample can be considered as homogeneous apart from slight differences in alignment. Elongated grains and voids are oriented moderately parallel to the walls of the ceramic sherd. The size of the voids ranges between 50 µm and 950 µm, including mainly mesovughs and mesochannels. Some voids are filled with a colourless material (inactive in XP).

Matrix

The sample has a non-calcareous matrix. The colour of the matrix is dark reddish-brown in plane polarised light. It shows the same shade in crossed polarisers and is optically moderately active.

Inclusions

The sample has bimodal grain-size distribution and the grains are moderately sorted. The modal grain size ranges from 10 µm to 350 µm in the fine fraction (~75% of inclusions) and 450 µm to 2400 µm in the coarse fraction (~25% of inclusions); the maximum grain size is 2400 µm. The sample contains elongated and equant grains in about the same amount with angular to sub-angular boundaries.

The following inclusions were identified in the sample. *Dominant*: **Gr flakes and Gr gneiss** fragments consisting of Gr, Qtz, Ms and Rt; *Frequent*: **Qtz** (mono- and polycrystalline, undulose extinction, sutured boundaries); *Few*: **rock fragments** containing Qtz, Bt, Ms and Op/Gr, **Kfs**; *Very few*: **Bt**, **Rt**; *Rare*: **Scp**, **Cpx?**, void-filling colourless material (inactive in XP).

S109 – Graphite group (Graphite A5)

Microstructure and voids

The ratio of inclusions, matrix and voids in the sample is 35:60:5. The sample can be considered as homogeneous apart from slight differences in alignment and the colour of the matrix. Elongated grains and voids are oriented moderately parallel to the walls of the ceramic sherd. The size of the voids ranges between 50 µm and 1050 µm, including mainly mesovughs and mesochannels.

Matrix

The sample has a non-calcareous matrix. The colour of the matrix is dark reddish-brown with a black margin on one side in plane polarised light. It is dark yellowish-greyish-brown with a black margin on one side in crossed polarisers and is optically moderately active to inactive.

Inclusions

The sample has bimodal grain-size distribution and the grains are very poorly sorted. The modal grain size ranges from 10 µm to 350 µm in the fine fraction (~70% of inclusions) and 500 µm to 2650 µm in the coarse fraction (~30% of inclusions); the maximum grain size is 2650 µm. The sample contains more equant than elongated grains with very angular to angular boundaries.

The following inclusions were identified in the sample. *Dominant*: **Gr flakes and Gr gneiss** fragments consisting of Gr, Qtz, Kfs, Bt, Ms, Rt and Scp; *Frequent*: **Qtz** (mono- and polycrystalline, undulose extinction, sutured boundaries); *Few*: **Kfs**; *Very few*: **Scp**, **Pl**, **Bt**; *Rare*: **Ms**, **Opx**, **Rt**; *Very rare*: **clay pellet** (dark reddish-brown in PPL, very dark reddish-brown in XP, optically very slightly active, elongated, sub-rounded, max. size: 600 µm, neutral optical density, diffuse boundaries, concordant orientation, similar composition to matrix).

S110 – Graphite group (Graphite A1)

Microstructure and voids

The ratio of inclusions, matrix and voids in the sample is 35:60:5. The sample can be considered as homogeneous apart from slight differences in alignment and the colour of the matrix. Elongated grains and voids are oriented moderately parallel to the walls of the ceramic sherd. The size of the voids ranges between 50 µm and 1300 µm, including mainly meso- and macrovughs. Some voids are filled with a colourless material (inactive in XP), some voids are Cb-filled.

Matrix

The sample has a non-calcareous matrix. The colour of the matrix is very dark reddish-brown with black margins in plane polarised light. It shows the same shades in crossed polarisers and is optically very slightly active to inactive.

Inclusions

The sample has bimodal grain-size distribution and the grains are poorly sorted. The modal grain size ranges from 10 µm to 300 µm in the fine fraction (~70% of inclusions) and 500 µm to 1200 µm in the coarse fraction (~30% of inclusions); the maximum grain size is 1200 µm. The sample contains more elongated than equant grains with angular to sub-angular boundaries.

The following inclusions were identified in the sample. *Dominant*: **Gr flakes and Gr gneiss** fragments consisting of Gr, Kfs, mica and Scp (triple junctions of Qtz and Fsp grains occur); *Frequent*: **Qtz** (mono- and polycrystalline, undulose extinction, sutured boundaries); *Few*: **Kfs**; *Very few*: **Sil gneiss** including Sil and Gr, **Scp**; *Rare*: void-filling colourless material (inactive in XP), **Rt**, **Ms**, **secondary Cb** in voids.

S111 – Graphite group (Graphite A1)

Microstructure and voids

The ratio of inclusions, matrix and voids in the sample is 30:63:7. The sample can be considered as homogeneous apart from slight differences in alignment and the colour of the matrix. Elongated grains and voids are oriented moderately parallel to the walls of the ceramic sherd. The size of the voids ranges between 50 µm and 2000 µm, including mainly mesoplanar voids and meso- and macrovughs. Some voids contain secondary Cb along their edges.

Matrix

The sample has a non-calcareous matrix. The colour of the matrix is very dark reddish-brown with dark reddish-brown margins in plane polarised light. It shows the same shades in crossed polarisers and is optically inactive to slightly active.

Inclusions

The sample has bimodal grain-size distribution and the grains are very poorly sorted. The modal grain size ranges from 10 µm to 300 µm in the fine fraction (~50% of inclusions) and 500 µm to 4200 µm in the coarse fraction (~50% of inclusions); the maximum grain size is 4200 µm. The sample contains more elongated than equant grains with angular to sub-angular boundaries.

The following inclusions were identified in the sample. *Dominant*: **Gr flakes and Gr gneiss** fragments consisting of Gr, Qtz, Kfs, Pl, Rt and Bt; *Common*: **Kfs** (some cloudy); *Few*: **Qtz** (mono- and polycrystalline, undulose extinction, sutured boundaries), **Bt**; *Very few*: **colourless Am**; *Rare*: **Sil** (originating probably from Sil gneiss), **secondary Cb** (in voids), **Ms**, **Scp**, **Pl**; *Very rare*: **Rt**.

S112 – Graphite group (Graphite A3)

Microstructure and voids

The ratio of inclusions, matrix and voids in the sample is 30:60:10. The sample can be considered as moderately heterogeneous because of the presence

of a large amount of clay pellets (clay mixing?). Elongated grains and voids are oriented moderately parallel to the walls of the ceramic sherd. The size of the voids ranges between 50 µm and 1000 µm, including mainly mesoplanar voids and mesovughs. Many inclusions in the sample are surrounded by voids. Some voids are filled with secondary Cb.

Matrix

The sample has a non-calcareous matrix. The colour of the matrix is dark reddish-brown with light reddish-brown margins in plane polarised light. It shows the same shades in crossed polarisers and is optically slightly active to highly active.

Inclusions

The sample has bimodal grain-size distribution and the grains are very poorly sorted. The modal grain size ranges from 10 µm to 250 µm in the fine fraction (~70% of inclusions) and 650 µm to 2250 µm in the coarse fraction (~30% of inclusions); the maximum grain size is 2250 µm. The sample contains elongated and equant grains in about the same amount with very angular to sub-angular boundaries.

The following inclusions were identified in the sample. *Dominant*: **Gr flakes and Gr gneiss** fragments consisting of Gr, Qtz, Kfs, Pl, Bt and Grt; *Common*: **Qtz** (mono- and polycrystalline, undulose extinction, sutured boundaries), **clay pellets** (light greyish-yellowish-brown in PPL and XP, optically moderately active, elongated/distorted, angular to sub-rounded, max. size: 500 µm, neutral optical density, diffuse boundaries, concordant orientation, similar composition to matrix); *Few*: **Kfs**; *Very few*: **Grt**, **Ms**, **Bt**; *Rare*: **Sil**, **green Am**, **secondary Cb** (in voids), **organic inclusions** (plant remains: fitolite), **Pl**, **Scp**; *Very rare*: **Rt**.

S113 – Graphite group (Graphite A5)

Microstructure and voids

The ratio of inclusions, matrix and voids in the sample is 30:60:10. The sample can be considered as homogeneous apart from slight differences in alignment and the colour of the matrix. Elongated grains and voids are oriented moderately parallel to the walls of the ceramic sherd. The size of the voids ranges between 50 µm and 1500 µm, including mainly mesovughs and meso- and macrochannels.

Matrix

The sample has a non-calcareous matrix. The colour of the matrix is very dark reddish-brown in plane polarised light. It is dark yellowish-greyish-brown in crossed polarisers and is optically moderately active.

Inclusions

The sample has bimodal grain-size distribution and the grains are very poorly sorted. The modal grain size ranges from 10 µm to 250 µm in the fine fraction (~65% of inclusions) and 500 µm to 2100 µm in the coarse fraction (~35% of inclusions); the maximum grain size is 2100 µm. The sample contains elongated and equant grains in about the same amount with angular to sub-angular boundaries.

The following inclusions were identified in the sample. *Dominant*: **Gr flakes and Gr gneiss** fragments consisting of Gr, Kfs, Qtz, Bt and Pl; *Frequent*: **Qtz** (monocrystalline > polycrystalline, undulose extinction, sutured boundaries); *Few*: **Kfs**; *Very few*: **Bt** (altered); *Rare*: **Pl**, **Ms**, **organic inclusion** (plant remains); *Very rare*: **Grt**.

On the inner side of this rim fragment there is a light yellow (PPL) layer, which is optically inactive in XP. It is not continuous along the ceramic wall. It might be an eroded glaze or a layer deposited in the soil. There is another layer on top of this light yellow layer consisting of Cal/Dol crystals, Qtz and Ms in a Cb-rich matrix (dark yellowish-greyish-brown in PPL, very dark grey in XP, optically very slightly active). This upper layer might be a deposition of food or the result of post-burial alterations.

S114 – Graphite group (Graphite A5)

Microstructure and voids

The ratio of inclusions, matrix and voids in the sample is 30:62:8. The sample can be considered as homogeneous. Elongated grains and voids are oriented moderately-strongly parallel to the walls of the ceramic sherd. The size of the voids ranges between 50 µm and 1450 µm, including mainly meso- and macrovughs. Some voids contain secondary Cb along their edges.

Matrix

The sample has a non-calcareous matrix. The colour of the matrix is very dark reddish-brown in plane polarised light. It is dark yellowish-greyish-brown in crossed polarisers and is optically slightly active.

Inclusions

The sample has bimodal grain-size distribution and the grains are very poorly sorted. The modal grain size ranges from 10 µm to 300 µm in the fine fraction (~60% of inclusions) and 500 µm to 4200 µm in the coarse fraction (~40% of inclusions); the maximum grain size is 4200 µm. The sample contains elongated and equant grains in about the same amount with very angular to angular boundaries.

The following inclusions were identified in the sample. *Dominant*: **Gr flakes and Gr gneiss** fragments consisting of Gr, Kfs, Qtz, Bt and Pl; *Frequent*: **Qtz** (monocrystalline > polycrystalline, undulose extinction, sutured boundaries); *Few*: **Kfs**; *Very few*: **Bt** (altered); *Rare*: **Pl**, **secondary Cb** (in voids), **Ms**; *Very rare*: **clay pellet** (very dark reddish-brown in PPL and XP, optically very slightly active, elongated, sub-angular, max. size: 3000 µm, high optical density, clear boundaries, concordant orientation, similar composition to matrix).

S115 – Graphite group (Graphite C1)

Microstructure and voids

The ratio of inclusions, matrix and voids in the sample is 30:65:5. The sample can be considered as homogeneous apart from slight differences in alignment. Elongated grains and voids are oriented moderately parallel to the walls of the ceramic sherd. The size of the voids ranges between 50 µm and 1300 µm, including mainly meso- and macrovughs, meso- and macrochannels and mesoplanar voids. Many voids are filled with secondary Cb.

Matrix

The sample has a non-calcareous matrix. The colour of the matrix is very dark reddish-brown/black in plane polarised light. It shows the same shades in crossed polarisers and is optically very slightly active to inactive.

Inclusions

The sample has bimodal grain-size distribution and the grains are very poorly sorted. The modal grain size ranges from 10 µm to 300 µm in the fine fraction (~65% of inclusions) and 500 µm to 2800 µm in the coarse fraction (~35% of inclusions); the maximum grain size is 2800 µm. The sample contains more elongated than equant grains with very angular to sub-angular boundaries.

The following inclusions were identified in the sample. *Dominant*: **Gr flakes**, **Gr marble** fragments (consisting of Gr and coarse-grained Cal) and **graphite gneiss** fragments (consisting of Gr, Kfs, Qtz, Pl); *Few*: **Qtz** (monocrystalline > polycrystalline, undulose extinction, sutured boundaries), **Bt** (some started altering to Sil), **secondary Cb** (in voids); *Very few*: **Kfs**; *Rare*: **Scp**, **rock fragments** including Ms and Bt, **Ms**.

S116 – Graphite group (Graphite C1)

Microstructure and voids

The ratio of inclusions, matrix and voids in the sample is 25:65:10. The sample can be considered as homogeneous apart from slight differences in alignment and the colour of the matrix. Elongated grains and voids are oriented moderately parallel to the walls of the ceramic sherd. The size of the voids ranges between 50 µm and 760 µm, including mainly meso- and macrovughs, mesochannels and mesoplanar voids. Many voids contain secondary Cb along their edges.

Matrix

The sample has a non-calcareous matrix. The colour of the matrix changes from very dark reddish-brown to light reddish-brown in plane polarised light. It changes from very dark reddish-brown to light yellowish-greyish-brown in crossed polarisers and is optically very slightly active to highly active.

Inclusions

The sample has bimodal grain-size distribution and the grains are moderately sorted. The modal grain size ranges from 10 µm to 600 µm in the fine fraction (~45% of inclusions) and 1000 µm to 2150 µm in the coarse fraction (~55% of inclusions); the maximum grain size is 2150 µm. The sample contains more elongated than equant grains with angular to sub-rounded boundaries.

The following inclusions were identified in the sample. *Dominant*: **Gr flakes**, **Gr marble** fragments (consisting of Gr and coarse-grained Cal) and **graphite gneiss** fragments (consisting of Gr, Qtz, Pl, Scp, Bt, Ms); *Few*: **clay pellets** (light reddish-brown in PPL and XP, optically very moderately to highly active, equant, sub-rounded, max. size: 1150 µm, neutral optical density, sharp to merging boundaries, concordant orientation, similar composition to matrix but having very few or no inclusions – pure clay nodules?), **Qtz** (mono- and polycrystalline, undulose extinction, sutured boundaries), **Cal**, **Scp** (with pale yellow pleochroism); *Very few*: **secondary Cb** (in voids), **Bt** (some faded, some oxidised), **Ms**, **Pl**, **Kfs**; *Rare*: **Cpx(?)**.

S117 – Graphite group (Graphite A2)

Microstructure and voids

The ratio of inclusions, matrix and voids in the sample is 30:62:8. The sample can be considered as homogeneous apart from slight differences in alignment and the colour of the matrix. Elongated grains and voids are oriented moderately parallel to the walls of the ceramic sherd. The size of the voids ranges between 50 µm and 1450 µm, including mainly mesovughs and mesoplanar voids. Some voids contain secondary Cb along their edges.

Matrix

The sample has a non-calcareous matrix. The colour of the matrix is very dark reddish-brown with dark reddish-brown margins in plane polarised light. It shows the same shades in crossed polarisers and is optically inactive to moderately active.

Inclusions

The sample has bimodal grain-size distribution and the grains are very poorly sorted. The modal grain size ranges from 10 µm to 400 µm in the fine fraction (~55% of inclusions) and 750 µm to 4700 µm in the coarse fraction (~45% of inclusions); the maximum grain size is 4700 µm. The sample contains more elongated than equant grains with very angular to sub-angular boundaries.

The following inclusions were identified in the sample. *Dominant*: **Gr flakes and Gr gneiss** fragments consisting of Gr, Kfs, and Bt (triple junctions of Qtz and Fsp grains occur); *Common*: **Kfs** (some cloudy); *Few*: **Bt** (some faded, some started altering to Sil), **Qtz** (mono- and polycrystalline, undulose extinction, both straight boundaries (triple junctions) and sutured boundaries), **colourless Am** (once with Qtz/Fsp);

Rare: **rock fragments** consisting of Ms and Bt, **secondary Cb** (in voids), **Ms/faded Bt**; *Very rare*: **Grt?**. At some places, the ceramic wall is covered by a Cb-rich deposition layer.

S118 – Graphite group (Graphite A3)

Microstructure and voids

The ratio of inclusions, matrix and voids in the sample is 25:60:15. The sample can be considered as moderately heterogeneous because of the presence of a large amount of clay pellets (clay mixing?). Elongated grains and voids are oriented moderately parallel to the walls of the ceramic sherd. The size of the voids ranges between 50 µm and 1850 µm, including mainly meso- and macroplanar voids and meso- and macrochannels.

Matrix

The sample has a non-calcareous matrix. The colour of the matrix changes from very dark reddish-brown to dark reddish-brown in plane polarised light. It shows the same shades in crossed polarisers and is optically inactive to slightly active.

Inclusions

The sample has bimodal grain-size distribution and the grains are very poorly sorted. The modal grain size ranges from 10 µm to 350 µm in the fine fraction (~55% of inclusions) and 550 µm to 3000 µm in the coarse fraction (~45% of inclusions); the maximum grain size is 3000 µm. The sample contains more elongated than equant grains with very angular to sub-angular boundaries.

The following inclusions were identified in the sample. *Dominant*: **Gr flakes and Gr gneiss** fragments consisting of Gr, Qtz, Bt and Grt; *Common*: **Qtz** (monocrystalline > polycrystalline, undulose extinction, sutured boundaries), **Kfs** (some sericitic); *Few*: **clay pellets** (light yellowish-greyish-brown in PPL, dark yellowish-greyish-brown in XP, optically very slightly active, elongated, angular to sub-rounded, max. size: 2850, neutral optical density, diffuse boundaries, concordant orientation, similar composition to matrix), **clay pellets** (light/dark reddish-brown in PPL and XP, optically slightly to moderately active, elongated, sub-angular, max. size: 2900 µm, neutral optical density, sharp to merging boundaries, concordant orientation, similar composition to matrix but having very few or no inclusions – pure clay nodules?); *Very few*: **Grt**, **Bt** (some altered to Sil); *Rare*: **Ms** (mainly fine-grained, <100 µm), **green Am** (with Qtz), **Scp**.

S119 – Graphite group (Graphite C1)

Microstructure and voids

The ratio of inclusions, matrix and voids in the sample is 40:53:7. The sample can be considered as homogeneous apart from slight differences in alignment. Elongated grains and voids are oriented moderately parallel to the walls of the ceramic sherd. The size of the voids ranges between 50 µm and 2500 µm, including mainly mesoplanar voids, meso- and macrovughs and mesochannels.

Matrix

The sample has a non-calcareous matrix. The colour of the matrix is very dark reddish-brown in plane polarised light. It shows the same shade in crossed polarisers and is optically very slightly active.

Inclusions

The sample has bimodal grain-size distribution and the grains are very poorly sorted. The modal grain size ranges from 10 µm to 500 µm in the fine fraction (~65% of inclusions) and 700 µm to 3200 µm in the coarse fraction (~35% of inclusions); the maximum grain size is 3200 µm. The sample contains more elongated than equant grains with very angular to angular boundaries.

The following inclusions were identified in the sample. *Dominant*: **Gr flakes**, **graphite gneiss** fragments (consisting of Qtz, Gr, Kfs, Pl, Ep/Zo/Czo, green Am, Ttn) and **Gr marble** fragments (consisting of Gr, coarse-grained Cal and Pl); *Few*: **Qtz** (mono- and polycrystalline, undulose extinction, sutured boundaries), **Kfs** (some sericitic, cloudy), **Bt**; *Very few*: **green Am**, **colourless Am**, **Pl** (some sericitic, altered to reddish-brown mineral), **Ep/Zo/Czo**; *Rare*: **Ms**; *Very rare*: **Grt**, **Cal**.

S120 – Graphite group (Graphite A2)

Microstructure and voids

The ratio of inclusions, matrix and voids in the sample is 15:80:5. The sample can be considered as homogeneous. Elongated grains and voids are oriented moderately parallel to the walls of the ceramic sherd. The size of the voids ranges between 50 µm and 2400 µm, including mainly meso- and macrochannels and meso- and macrovughs.

Matrix

The sample has a non-calcareous matrix. The colour of the matrix is black in plane polarised light and in crossed polarisers and is optically inactive.

Inclusions

The sample has bimodal grain-size distribution and the grains are very poorly sorted. The modal grain size ranges from 10 µm to 300 µm in the fine fraction (~70% of inclusions) and 600 µm to 3800 µm in the coarse fraction (~30% of inclusions); the maximum grain size is 3800 µm. The sample contains more elongated than equant grains with very angular to angular boundaries.

The following inclusions were identified in the sample. *Predominant*: **Gr flakes and Gr gneiss** fragments consisting of Gr, Qtz, Kfs and Rt (triple junctions of Qtz and Fsp grains occur)*; *Few*: **Qtz** (monocrystalline > polycrystalline, undulose extinction, both straight boundaries (triple junctions)

and sutured boundaries); *Very few*: **Kfs**; *Rare*: **Bt**, **organic inclusions** (plant remains), **green Am?**, **colourless Am/Cpx?**.
*Gr flakes an Gr gneiss fragments are hardly distinguishable from the matrix because of the dark colour of the matrix.

S121 – Graphite group (Graphite C1)

Microstructure and voids
The ratio of inclusions, matrix and voids in the sample is 40:53:7. The sample can be considered as homogeneous apart from slight differences in alignment and the colour of the matrix. Elongated grains and voids are oriented moderately parallel to the walls of the ceramic sherd. The size of the voids ranges between 50 µm and 1850 µm, including mainly meso- and macrovughs, mesochannels and mesoplanar voids. Some voids contain secondary Cb along their edges.
Matrix
The sample has a non-calcareous matrix. The colour of the matrix is very dark reddish-brown with a dark reddish-brown margin on one side in plane polarised light. It shows the same shades in crossed polarisers and is optically very slightly active to moderately active.
Inclusions
The sample has bimodal grain-size distribution and the grains are very poorly sorted. The modal grain size ranges from 10 µm to 400 µm in the fine fraction (~50% of inclusions) and 500 µm to 3850 µm in the coarse fraction (~50% of inclusions); the maximum grain size is 3850 µm. The sample contains more elongated than equant grains with angular to sub-rounded boundaries.
The following inclusions were identified in the sample. *Dominant*: **Gr flakes**, **Gr marble** fragments (consisting of coarse-grained Cal and Gr) and **graphite gneiss** fragments (consisting of Bt, Gr, Kfs); *Common*: **Bt** (flakes and aggregates, some aggregates contain Ep/Zo/Czo, some Bt started altering to Sil); *Few*: **Qtz** (monocrystalline > polycrystalline, undulose extinction, sutured boundaries); *Very few*: **rock fragments** containing Bt and Ms, **Ep/Zo/Czo**, **Pl**, **Kfs**; *Rare*: **Ms**, **secondary Cb** (in voids); *Very rare*: **Grt**.

S122 – Graphite group (Graphite A4)

Microstructure and voids
The ratio of inclusions, matrix and voids in the sample is 25:68:7 The sample can be considered as homogeneous apart from slight differences in alignment. Elongated grains and voids are oriented moderately parallel to the walls of the ceramic sherd. The size of the voids ranges between 100 µm and 840 µm, including mainly meso- and macroplanar voids, meso- and macrochannels and meso- and macrovughs.
Matrix
The sample has a non-calcareous matrix. The colour of the matrix is very dark reddish-brown/black in plane polarised light. It shows the same shades in crossed polarisers and is optically very slightly active.
Inclusions
The sample has bimodal grain-size distribution and the grains are very poorly sorted. The modal grain size ranges from 10 µm to 350 µm in the fine fraction (~50% of inclusions) and 500 µm to 2560 µm in the coarse fraction (~50% of inclusions); the maximum grain size is 2560 µm. The sample contains more elongated than equant grains with angular to sub-angular boundaries.
The following inclusions were identified in the sample. *Dominant*: **Gr flakes*** (with inclusions of Rt, Qtz, Kfs and Pl) **and Gr gneiss** fragments consisting of Qtz, Kfs and Bt; *Common*: **Qtz** (mono- and polycrystalline, undulose extinction, sutured boundaries); *Few*: **Kfs**, **Ky** (occur with Gr and Ms, most of them started altering to a brownish mineral), **Bt**; *Very few*: **Scp**; *Rare*: **Ms**, **colourless Am**, **Rt**, **Pl**.
*Gr flakes are hardly distinguishable from the matrix because of the dark colour of the matrix.

S123 – Graphite group (Graphite C2)

Microstructure and voids
The ratio of inclusions, matrix and voids in the sample is 25:65:10. The sample can be considered as homogeneous apart from slight differences in alignment. Elongated grains and voids are oriented moderately parallel to the walls of the ceramic sherd. The size of the voids ranges between 50 µm and 1440 µm, including mainly mesochannels, meso- and macrovughs and mesoplanar voids. One void is filled with secondary Cb.
Matrix
The sample has a non-calcareous matrix. The colour of the matrix is very dark reddish-brown/black in plane polarised light. It shows the same shades in crossed polarisers and is optically very slightly active.
Inclusions
The sample has bimodal grain-size distribution and the grains are very poorly sorted. The modal grain size ranges from 10 µm to 200 µm in the fine fraction (~50% of inclusions) and 400 µm to 3300 µm in the coarse fraction (~50% of inclusions); the maximum grain size is 3300 µm. The sample contains more elongated than equant grains with very angular to sub-angular boundaries.
The following inclusions were identified in the sample. *Dominant*: **Gr flakes and graphite gneiss** fragments consisting of Gr, Qtz, Kfs, Bt, Rt, Scp and Ep/Zo/Czo; *Few*: **Qtz** (mono- and polycrystalline, undulose extinction, sutured boundaries), **Bt** (some faded); *Very few*: **Kfs**, **pseudomorphs?** (after Ky?),

Scp; *Rare*: **micrite** fragments (only two fragments, one with Bt), **Ms**, **Rt**; **secondary Cb** (in void).

S124 – Graphite group (Graphite C2)

Microstructure and voids

The ratio of inclusions, matrix and voids in the sample is 30:65:5. The sample can be considered as homogeneous apart from slight differences in alignment. Elongated grains and voids are oriented moderately parallel to the walls of the ceramic sherd. The size of the voids ranges between 50 µm and 640 µm, including mainly meso- and macrovughs and mesoplanar voids. Many voids are filled with secondary Cb.

Matrix

The sample has a non-calcareous matrix. The colour of the matrix is very dark reddish-brown/black in plane polarised light. It shows the same shades in crossed polarisers and is optically slightly active.

Inclusions

The sample has bimodal grain-size distribution and the grains are very poorly sorted. The modal grain size ranges from 10 µm to 350 µm in the fine fraction (~55% of inclusions) and 600 µm to 3400 µm in the coarse fraction (~45% of inclusions); the maximum grain size is 3400 µm. The sample contains more elongated than equant grains with angular to sub-rounded boundaries.

The following inclusions were identified in the sample. *Dominant*: **Gr flakes and graphite gneiss** fragments consisting of Kfs, Qtz, Gr, Bt and Pl; *Frequent*: **micrite** fragments (some have inclusions of Qtz and Gr/Op); *Few*: **Qtz** (mono- and polycrystalline, undulose extinction, sutured boundaries), **Bt** (some started altering to Sil), **secondary Cb** (in voids); *Very few*: **Pl**, **Kfs** (usually cloudy), **green Am** (once with Gr and Qtz); *Rare*: **Ms**.

S125 – Graphite group (Graphite A5)

Microstructure and voids

The ratio of inclusions, matrix and voids in the sample is 25:68:7. The sample can be considered as homogeneous apart from slight differences in alignment. Elongated grains and voids are oriented moderately parallel to the walls of the ceramic sherd. The size of the voids ranges between 50 µm and 640 µm, including mainly mesovughs and mesochannels.

Matrix

The sample has a non-calcareous matrix. The colour of the matrix is black in plane polarised light and in crossed polarisers and is optically inactive.

Inclusions

The sample has bimodal grain-size distribution and the grains are very poorly sorted. The modal grain size ranges from 10 µm to 300 µm in the fine fraction (~60% of inclusions) and 500 µm to 2750 µm in the coarse fraction (~40% of inclusions); the maximum grain size is 2750 µm. The sample contains more elongated than equant grains with angular to sub-angular boundaries.

The following inclusions were identified in the sample. *Dominant*: **Gr flakes and Gr gneiss** fragments consisting of Kfs, Gr, Qtz, Pl and Bt*; *Common*: **Fsp** (both Kfs>Pl, many of them have a reddish-brown alteration/high iron content); *Few*: **Qtz** (mono- and polycrystalline, undulose extinction, sutured boundaries), **green Am** (once with Kfs), **Bt** (some started altering to Sil); *Rare*: **Ms**.

*Gr flakes an Gr gneiss fragments are hardly distinguishable from the matrix because of the dark colour of the matrix.

S126 – Graphite group (Graphite A2)

Microstructure and voids

The ratio of inclusions, matrix and voids in the sample is 25:70:5. The sample can be considered as homogeneous apart from slight differences in alignment and the colour of the matrix. Elongated grains and voids are oriented moderately parallel to the walls of the ceramic sherd. The size of the voids ranges between 50 µm and 400 µm, including mainly mesovughs and mesochannels. Some voids are filled with secondary Cb.

Matrix

The sample has a non-calcareous matrix. The colour of the matrix changes from black to very dark reddish-brown in plane polarised light. It shows the same shades in crossed polarisers and is optically inactive to very slightly active.

Inclusions

The sample has bimodal grain-size distribution and the grains are very poorly sorted. The modal grain size ranges from 10 µm to 200 µm in the fine fraction (~50% of inclusions) and 400 µm to 3600 µm in the coarse fraction (~50% of inclusions); the maximum grain size is 3600 µm. The sample contains more equant than elongated grains with very angular to angular boundaries.

The following inclusions were identified in the sample. *Dominant*: **Gr flakes and Gr gneiss** fragments consisting of Gr, Qtz, Kfs, Rt and Bt (triple junctions of Qtz and Fsp grains occur)*; *Common*: **Qtz** (mono- and polycrystalline, undulose extinction, both straight boundaries (triple junctions) and sutured boundaries); *Very few*: **Kfs**, **Bt**; *Rare*: **Scp**, **Grt**, **secondary Cb** (in voids); *Very rare*: **chert** fragment, **green Am**, **Rt**.

*Gr flakes an Gr gneiss fragments are hardly distinguishable from the matrix because of the dark colour of the matrix.

S127 – Graphite group (Graphite A5)

Microstructure and voids

The ratio of inclusions, matrix and voids in the sample is 35:55:10. The sample can be considered as homogeneous apart from slight differences in alignment. Elongated grains and voids are oriented moderately parallel to the walls of the ceramic sherd. The size of the voids ranges between 50 µm and 1300 µm, including mainly meso- and macrovughs and mesoplanar voids.

Matrix

The sample has a non-calcareous matrix. The colour of the matrix is very dark reddish-brown in plane polarised light. It shows the same shade in crossed polarisers and is optically slightly active.

Inclusions

The sample has bimodal grain-size distribution and the grains are very poorly sorted. The modal grain size ranges from 10 µm to 150 µm in the fine fraction (~65% of inclusions) and 450 µm to 3450 µm in the coarse fraction (~35% of inclusions); the maximum grain size is 3450 µm. The sample contains more equant than elongated grains with very angular to angular boundaries.

The following inclusions were identified in the sample. *Dominant*: **Gr flakes and Gr gneiss** fragments consisting of Qtz, Gr, Bt and Rt; *Frequent*: **Qtz** (mono- and polycrystalline, undulose extinction, sutured boundaries); *Very few*: **Bt**, **Scp**, **Kfs**.

S128 – Graphite group (Graphite A4)

Microstructure and voids

The ratio of inclusions, matrix and voids in the sample is 25:67:8. The sample can be considered as homogeneous. Elongated grains and voids are oriented moderately parallel to the walls of the ceramic sherd. The size of the voids ranges between 100 µm and 1400 µm, including mainly meso- and macrovughs, meso- and macroplanar voids and meso- and macrochannels.

Matrix

The sample has a non-calcareous matrix. The colour of the matrix is very dark reddish-brown in plane polarised light. It shows the same shade in crossed polarisers and is optically slightly active.

Inclusions

The sample has bimodal grain-size distribution and the grains are very poorly sorted. The modal grain size ranges from 10 µm to 500 µm in the fine fraction (~45% of inclusions) and 800 µm to 3650 µm in the coarse fraction (~55% of inclusions); the maximum grain size is 3650 µm. The sample contains more elongated than equant grains with angular to sub-angular boundaries.

The following inclusions were identified in the sample. *Dominant*: **Gr flakes and Gr gneiss** fragments consisting of Gr, Kfs, Pl, Ky, Ms and Sil (triple junctions of Qtz and Fsp grains occur); *Common*: **Kfs**, **Pl**; *Few*: **Qtz** (mono- and polycrystalline, undulose extinction, both straight boundaries (triple junctions) and sutured boundaries); *Very few*: **Ky** (most of them started altering to a brownish alteration product, some are totally altered); *Rare*: **Ms**, **Rt**; *Very rare*: **Sil**, **green Am**.

S129 – Graphite group (Graphite C2)

Microstructure and voids

The ratio of inclusions, matrix and voids in the sample is 25:68:7. The sample can be considered as homogeneous. Elongated grains and voids are oriented moderately parallel to the walls of the ceramic sherd. The size of the voids ranges between 50 µm and 2000 µm, including mainly meso- and macrovughs, meso- and macrochannels and meso- and macroplanar voids. Many voids are filled with secondary Cb.

Matrix

The sample has a non-calcareous matrix. The colour of the matrix is very dark reddish-brown/black in plane polarised light. It shows the same shades in crossed polarisers and is optically very slightly active to inactive.

Inclusions

The sample has bimodal grain-size distribution and the grains are very poorly sorted. The modal grain size ranges from 10 µm to 200 µm in the fine fraction (~60% of inclusions) and 500 µm to 1700 µm in the coarse fraction (~40% of inclusions); the maximum grain size is 1700 µm. The sample contains more elongated than equant grains with angular to sub-angular boundaries.

The following inclusions were identified in the sample. *Dominant*: **Gr flakes and graphite gneiss** fragments consisting of Gr, Qtz, Kfs, Pl, Bt, Rt and Scp (triple junctions of Qtz and Fsp grains occur); *Common*: **Qtz** (mono- and polycrystalline, undulose extinction, both straight boundaries (triple junctions) and sutured boundaries), **micrite** fragments (some have inclusions of Qtz and Op); *Few*: **Kfs**, **secondary Cb** (in voids); *Very few*: **Pl**, **Bt**; *Rare*: **Scp**, **Ms**; *Very rare*: **green Am**.

Calcareous depositions are present on both the inner and outer wall of the sherd as well as on the fractures (post-burial alteration?, restoration material (filler)?).

S130 – Graphite group (Graphite B)

Microstructure and voids

The ratio of inclusions, matrix and voids in the sample is 30:60:10. The sample can be considered as homogeneous apart from slight differences in the colour of the matrix. Elongated grains and voids are oriented moderately parallel to the walls of the ceramic sherd. The size of the voids ranges between 50 µm and 1250 µm, including mainly meso- and macrovughs and mesoplanar voids.

Matrix

The sample has a non-calcareous matrix. The colour of the matrix is dark yellowish-greyish-brown with light reddish-brown margins in plane polarised light. It is dark yellowish-greyish-brown with light yellowish-greyish-brown margins in crossed polarisers and is optically slightly active to moderately active.

Inclusions

The sample has bimodal grain-size distribution and the grains are very poorly sorted. The modal grain size ranges from 10 µm to 300 µm in the fine fraction (~55% of inclusions) and 500 µm to 4250 µm in the coarse fraction (~45% of inclusions); the maximum grain size is 4250 µm. The sample contains equant and elongated grains in about the same amount with angular to sub-angular boundaries.

The following inclusions were identified in the sample. *Dominant*: **Gr flakes and graphitic mica schist** fragments consisting of Gr, Qtz, Bt, Ms and Rt; *Common*: **Qtz** (mono- and polycrystalline, undulose extinction, sutured boundaries); *Few*: **Kfs**, **Bt**, **Ms**; *Rare*: **Pl**, **Rt**.

S131 – Individual sample

Microstructure and voids

The ratio of inclusions, matrix and voids in the sample is 30:63:7. The sample can be considered as homogeneous. Elongated grains and voids are oriented moderately parallel to the walls of the ceramic sherd. The size of the voids ranges between 100 µm and 2000 µm, including mainly meso- and macroplanar voids, meso- and macrochannels and mesovughs.

Matrix

The sample has a non-calcareous matrix. The colour of the matrix is light reddish-brown in plane polarised light. It shows the same shade in crossed polarisers and is optically highly active.

Inclusions

The sample has bimodal grain-size distribution and the grains are very poorly sorted. The modal grain size ranges from 10 µm to 500 µm in the fine fraction (~55% of inclusions) and 750 µm to 2600 µm in the coarse fraction (~45% of inclusions); the maximum grain size is 2600 µm. The sample contains more elongated than equant grains with angular to sub-angular boundaries.

The following inclusions were identified in the sample. *Dominant*: **Ky-bearing mica schist** fragments consisting of Qtz, Ms, Bt, Ky, Gr, Kfs and Rt; *Common*: **Ms**, **Qtz** (mono- and polycrystalline, undulose extinction, sutured boundaries); *Few*: **Ky**; *Very few*: **Bt** (some oxidised), **Gr***; *Rare*: **Kfs**, **Pl**, **Scp**; *Very rare*: **clay pellet** (light reddish-brown in PPL and XP, optically moderately active, elongated, sub-angular, max. size: 650 µm, high optical density, clear boundaries, discordant orientation, similar composition to matrix but having no inclusions), **organic inclusion** (plant remain), **green Am?**.

*The analysed thin section of the sample contains some Gr grains, however, this low amount is not representative for the potsherd based on the macroscopic analysis, which clearly identifies this piece of ceramics as a graphite-containing sample.

S132 – Graphite group (Graphite C1)

Microstructure and voids

The ratio of inclusions, matrix and voids in the sample is 30:60:10. The sample can be considered as homogeneous. Elongated grains and voids are oriented moderately parallel to the walls of the ceramic sherd. The size of the voids ranges between 50 µm and 2000 µm, including mainly meso- and macrovughs and mesoplanar voids.

Matrix

The sample has a non-calcareous matrix. The colour of the matrix is very dark reddish-brown/black in plane polarised light. It is dark yellowish-greyish-brown in crossed polarisers and is optically very slightly active.

Inclusions

The sample has bimodal grain-size distribution and the grains are very poorly sorted. The modal grain size ranges from 10 µm to 500 µm in the fine fraction (~40% of inclusions) and 700 µm to 4000 µm in the coarse fraction (~60% of inclusions); the maximum grain size is 4000 µm. The sample contains more elongated than equant grains with angular to sub-rounded boundaries.

The following inclusions were identified in the sample. *Dominant*: **Gr flakes** (with inclusions of Rt, Scp and Bt), **Gr marble** fragments (consisting of coarse-grained Cal, Gr, Kfs and Scp) and **graphite gneiss** fragments (consisting of Qtz, Gr and Bt); *Common*: **Qtz** (monocrystalline > polycrystalline, undulose extinction, sutured boundaries), **Cal**; *Few*: **Scp**, **Bt** (usually almost faded); *Very few*: **Kfs**, **Ms**; *Rare*: **organic inclusions** (plant remains), **Rt**.

S133 – Graphite group (Graphite B)

Microstructure and voids

The ratio of inclusions, matrix and voids in the sample is 35:55:10. The sample can be considered as homogeneous apart from slight differences in alignment and the colour of the matrix. Elongated grains and voids are oriented moderately parallel to the walls of the ceramic sherd. The size of the voids ranges between 100 µm and 1200 µm, including mainly mesovughs and mesochannels. Some voids are filled with Cb, some voids contain a brownish-yellowish (PPL) material.

Matrix

The sample has a non-calcareous matrix. The colour of the matrix changes from very dark reddish-brown

to black in plane polarised light. It shows the same shades in crossed polarisers and is optically very slightly active to inactive.

Inclusions

The sample has bimodal grain-size distribution and the grains are very poorly sorted. The modal grain size ranges from 10 µm to 400 µm in the fine fraction (~55% of inclusions) and 700 µm to 2050 µm in the coarse fraction (~45% of inclusions); the maximum grain size is 2050 µm. The sample contains more elongated than equant grains with very angular to angular boundaries.

The following inclusions were identified in the sample. *Dominant*: **Gr flakes and graphitic mica schist** fragments consisting of Gr, Ms, Bt, Qtz and Kfs; *Few*: **Kfs**; *Very few*: **Qtz** (mono- and polycrystalline, undulose extinction, sutured boundaries), **Ms**, **Bt** (almost faded); *Rare*: **Scp** (with pale yellow pleochroism), **Rt** (relatively large grains), **Cpx**, **secondary Cb** (in voids), **green Am**.

S134 – Graphite group (Graphite A2)

Microstructure and voids

The ratio of inclusions, matrix and voids in the sample is 35:60:5. The sample can be considered as homogeneous apart from slight differences in the colour of the matrix. Elongated grains and voids are oriented moderately parallel to the walls of the ceramic sherd. The size of the voids ranges between 50 µm and 1300 µm, including mainly meso- and macrovughs. Some voids are filled with secondary Cb and some voids are partly filled with a brownish-yellowish (PPL) mineral.

Matrix

The sample has a non-calcareous matrix. The colour of the matrix changes from very dark reddish-brown to black in plane polarised light. It shows the same shades in crossed polarisers and is optically very slightly active to inactive.

Inclusions

The sample has bimodal grain-size distribution and the grains are very poorly sorted. The modal grain size ranges from 10 µm to 400 µm in the fine fraction (~55% of inclusions) and 800 µm to 2400 µm in the coarse fraction (~45% of inclusions); the maximum grain size is 2400 µm. The sample contains more elongated than equant grains with very angular to sub-angular boundaries.

The following inclusions were identified in the sample. *Dominant*: **Gr flakes and Gr gneiss** fragments consisting of Qtz, Kfs, Gr, Bt and Rt (triple junctions of Qtz and Fsp grains occur); *Common*: **Qtz** (mono- and polycrystalline, undulose extinction, both straight boundaries (triple junctions) and sutured boundaries); *Few*: **Kfs** (usually cloudy); *Very few*: **Bt** (some faded); *Rare*: **Scp**, **Ms**, **Ky?**, **green Am**, **secondary Cb** (in voids); *Very rare*: **Rt**, **Pl**.

S135 – Graphite group (Graphite A3)

Microstructure and voids

The ratio of inclusions, matrix and voids in the sample is 35:55:10. The sample can be considered as homogeneous apart from slight differences in alignment. Elongated grains and voids are oriented moderately parallel to the walls of the ceramic sherd. The size of the voids ranges between 100 µm and 1000 µm, including mainly meso- and macrovughs and mesochannels.

Matrix

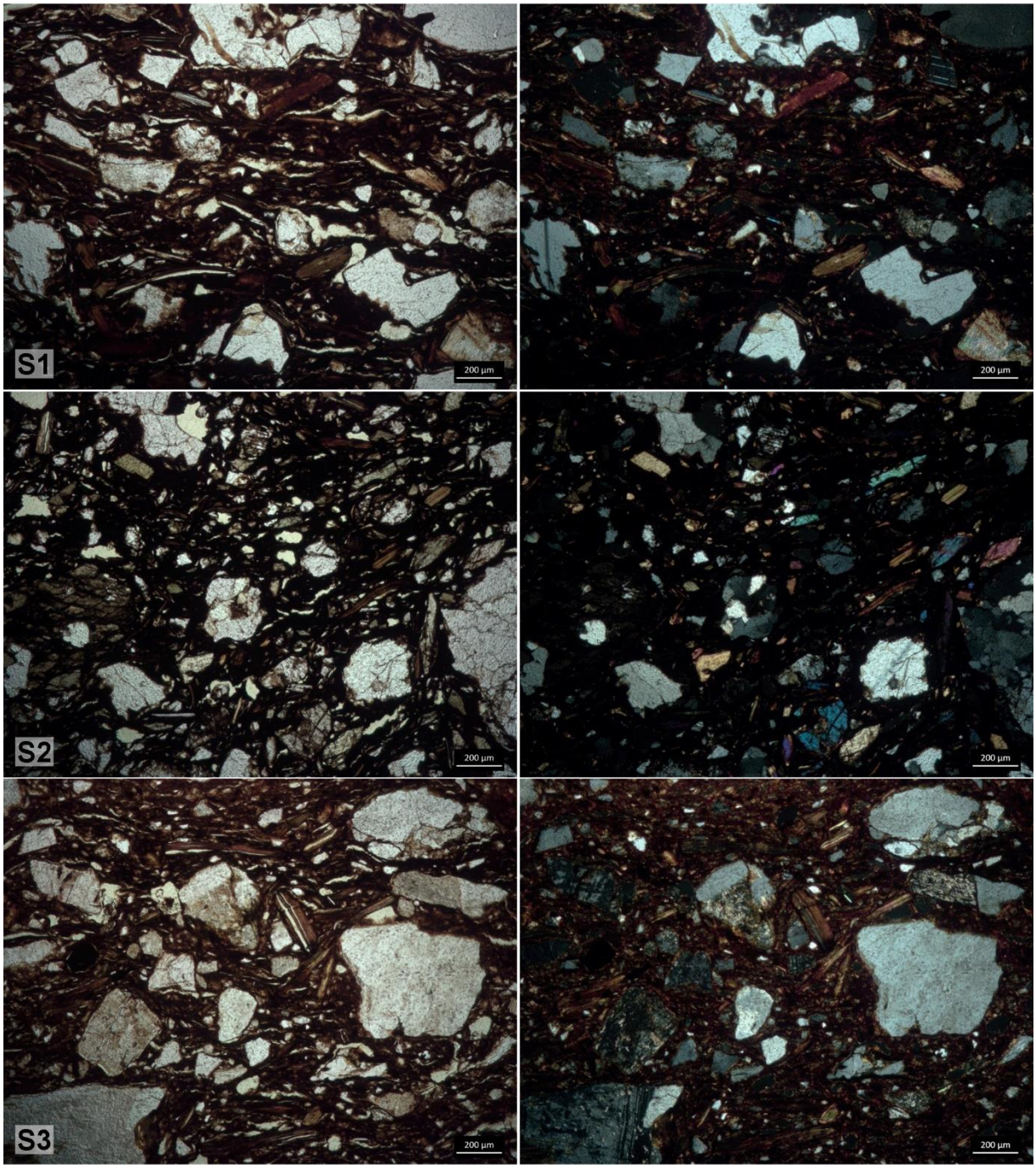
The sample has a non-calcareous matrix. The colour of the matrix is very dark reddish-brown/black in plane polarised light. It shows the same shades in crossed polarisers and is optically very slightly active to inactive.

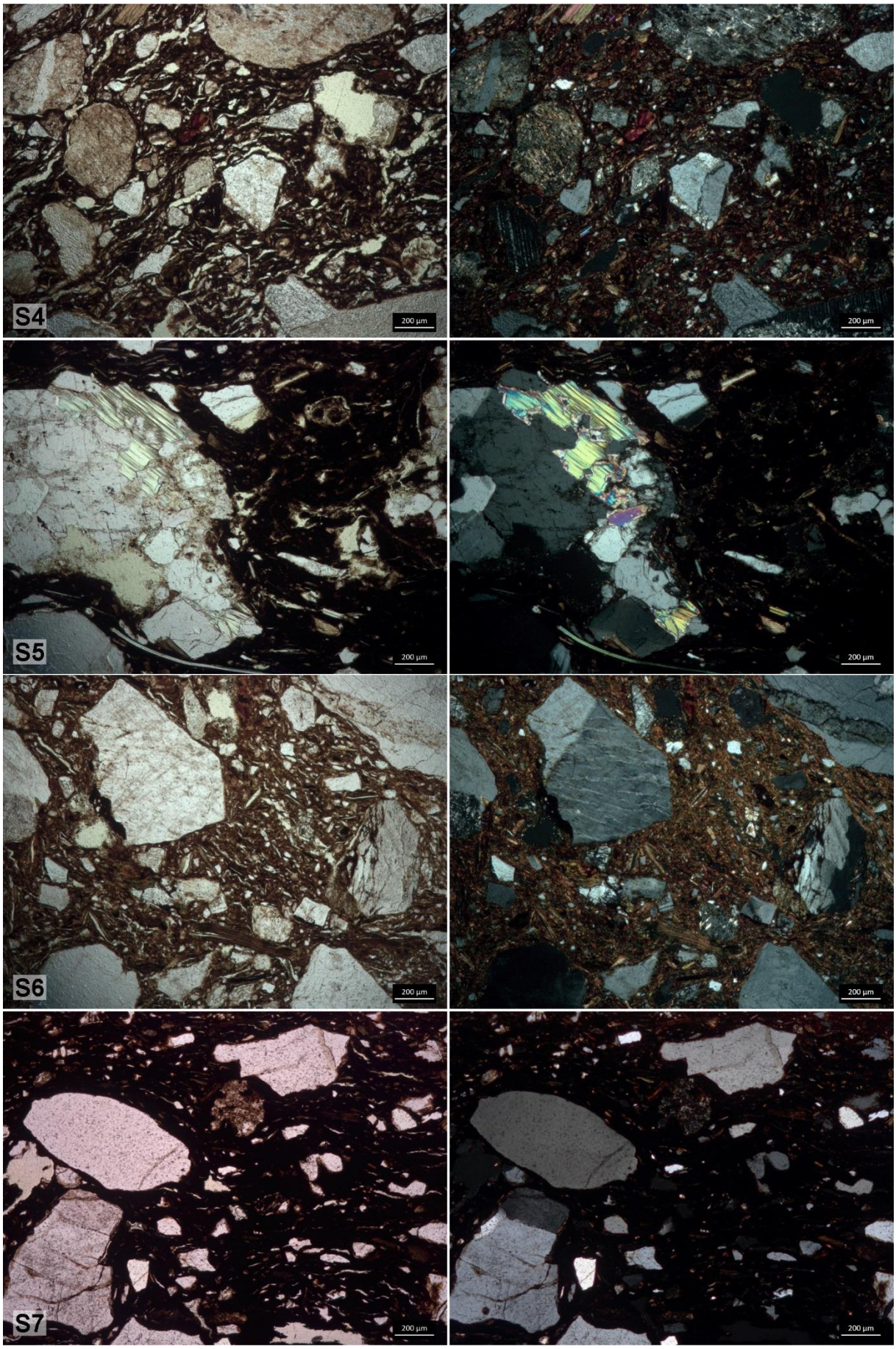
Inclusions

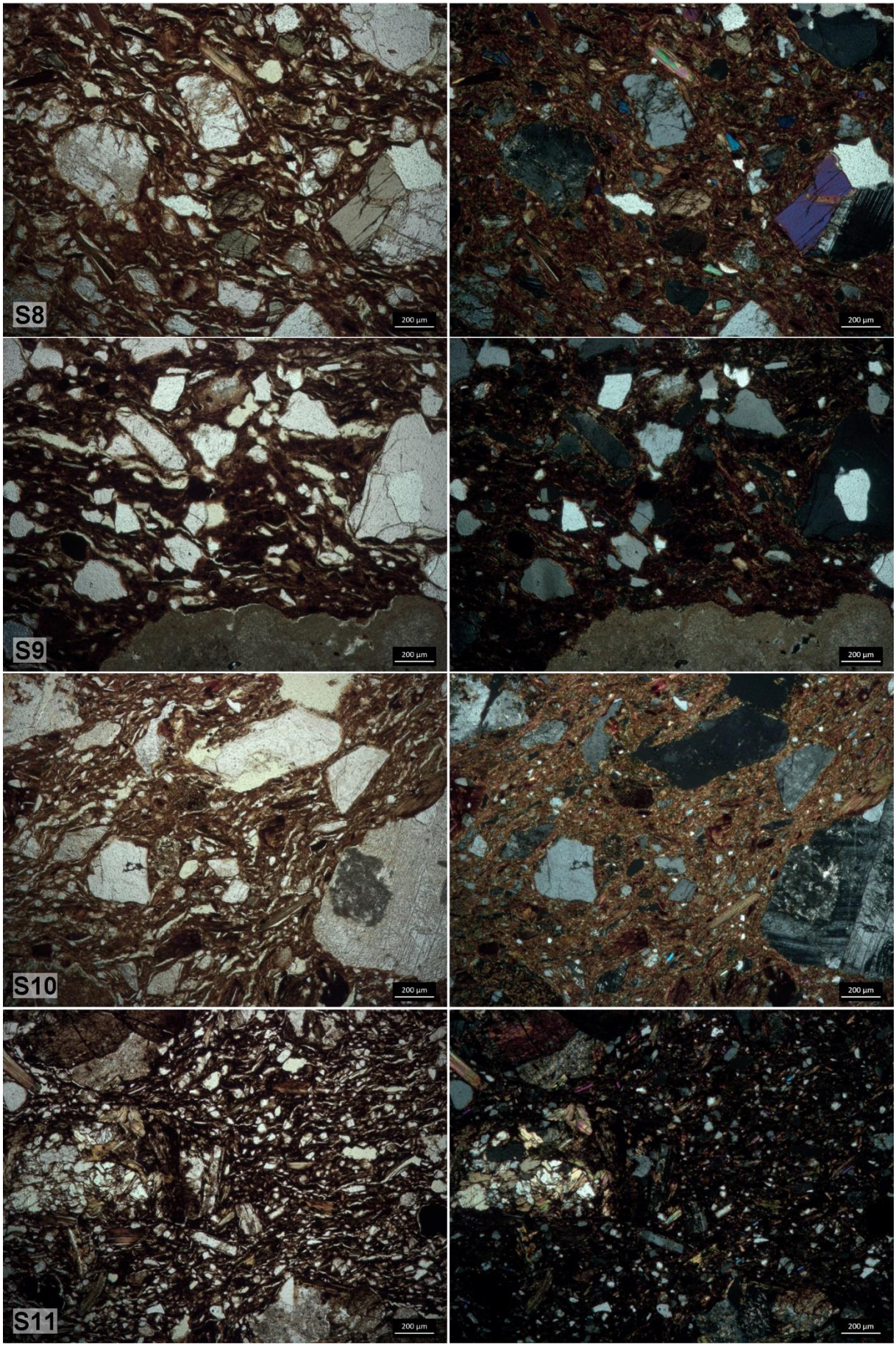
The sample has bimodal grain-size distribution and the grains are very poorly sorted. The modal grain size ranges from 10 µm to 200 µm in the fine fraction (~60% of inclusions) and 500 µm to 1500 µm in the coarse fraction (~40% of inclusions); the maximum grain size is 1500 µm. The sample contains more elongated than equant grains with very angular to rounded boundaries.

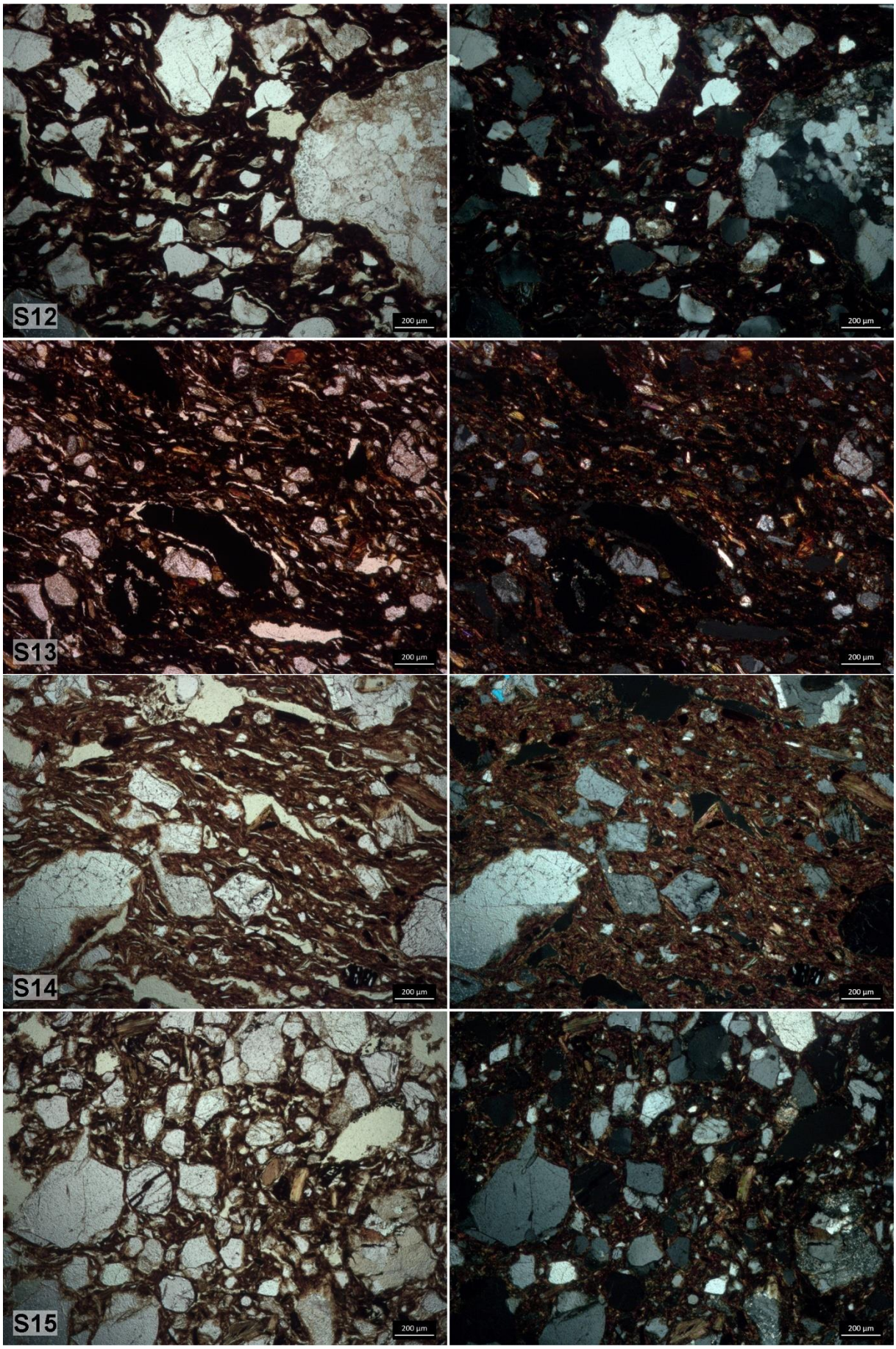
The following inclusions were identified in the sample. *Dominant*: **Gr flakes and Gr gneiss** fragments consisting of Gr, Kfs and Qtz; *Common*: **Kfs**, **Qtz** (mono- and polycrystalline, undulose extinction, sutured boundaries); *Few*: **Grt**; *Very few*: **Bt**; *Rare*: **clay pellets** (light reddish-brown in PPL and XP, optically moderately active, equant, sub-rounded, max. size: 600 µm, neutral optical density, sharp boundaries, concordant orientation, similar composition to matrix but having no inclusions), **green Am**, **Ms**, **Cpx?**, **Scp**; *Very rare*: **clay pellet** (very dark reddish-brown in PPL and XP, optically very slightly active, equant, rounded, max. size: 400 µm, neutral optical density, sharp boundaries, concordant orientation, similar composition to matrix but having no inclusions), **secondary Cb** (deposited on the fracture of the sherd).

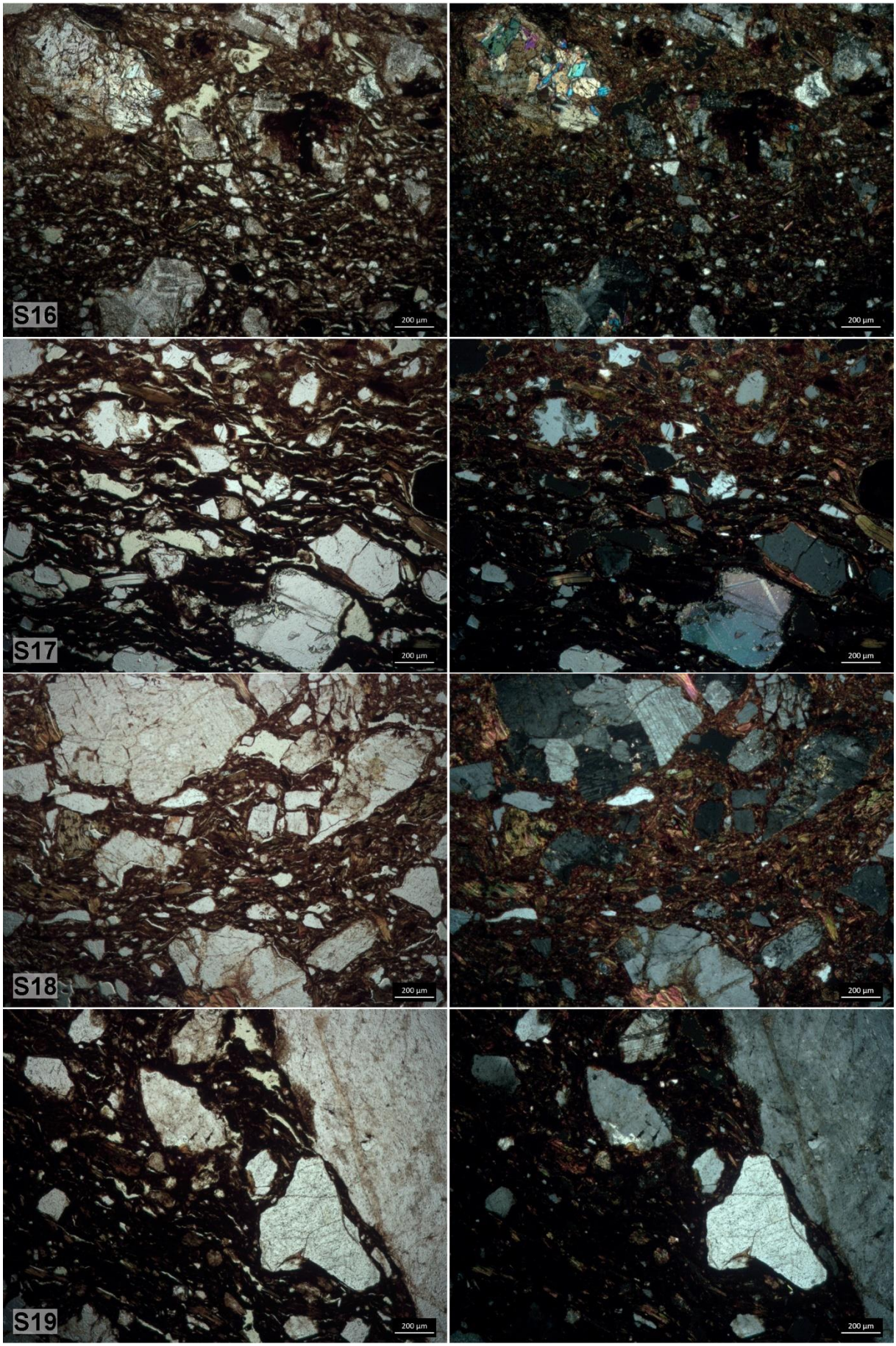
C.2 Photomicrographs

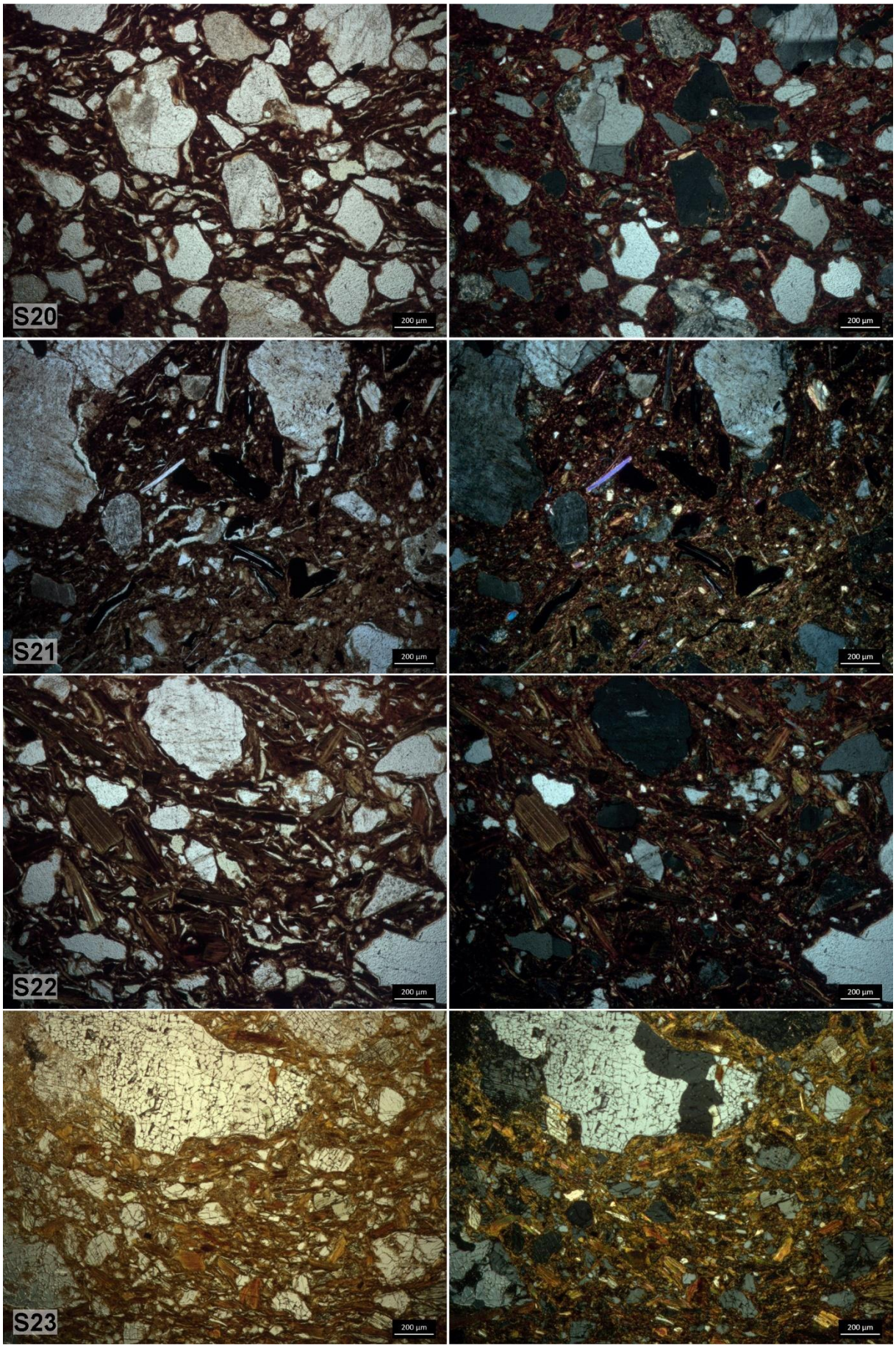


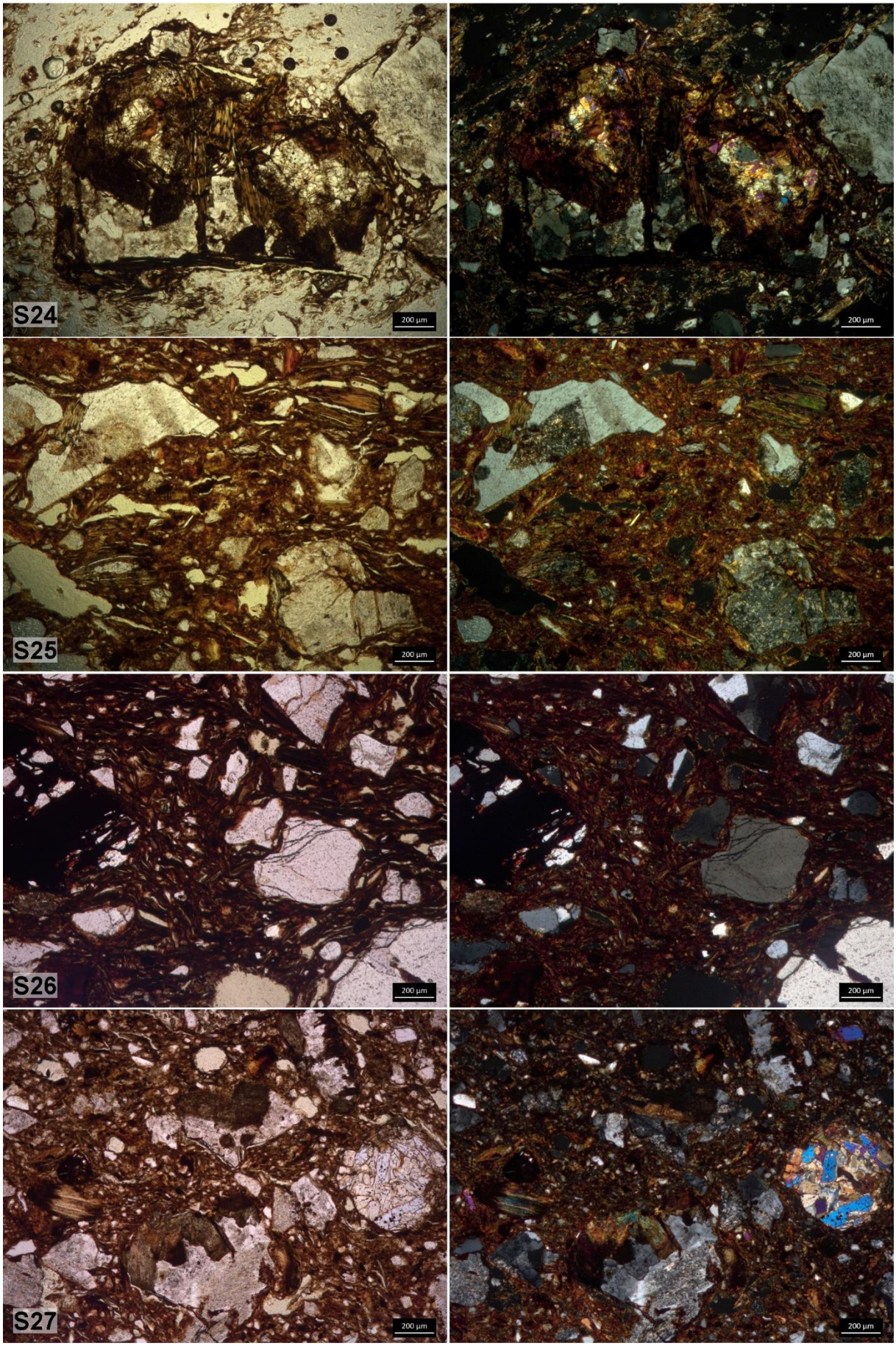

S4
200 µm
200 µm
S5
200 µm
200 µm
S6
200 µm
200 µm
S7
200 µm
200 µm

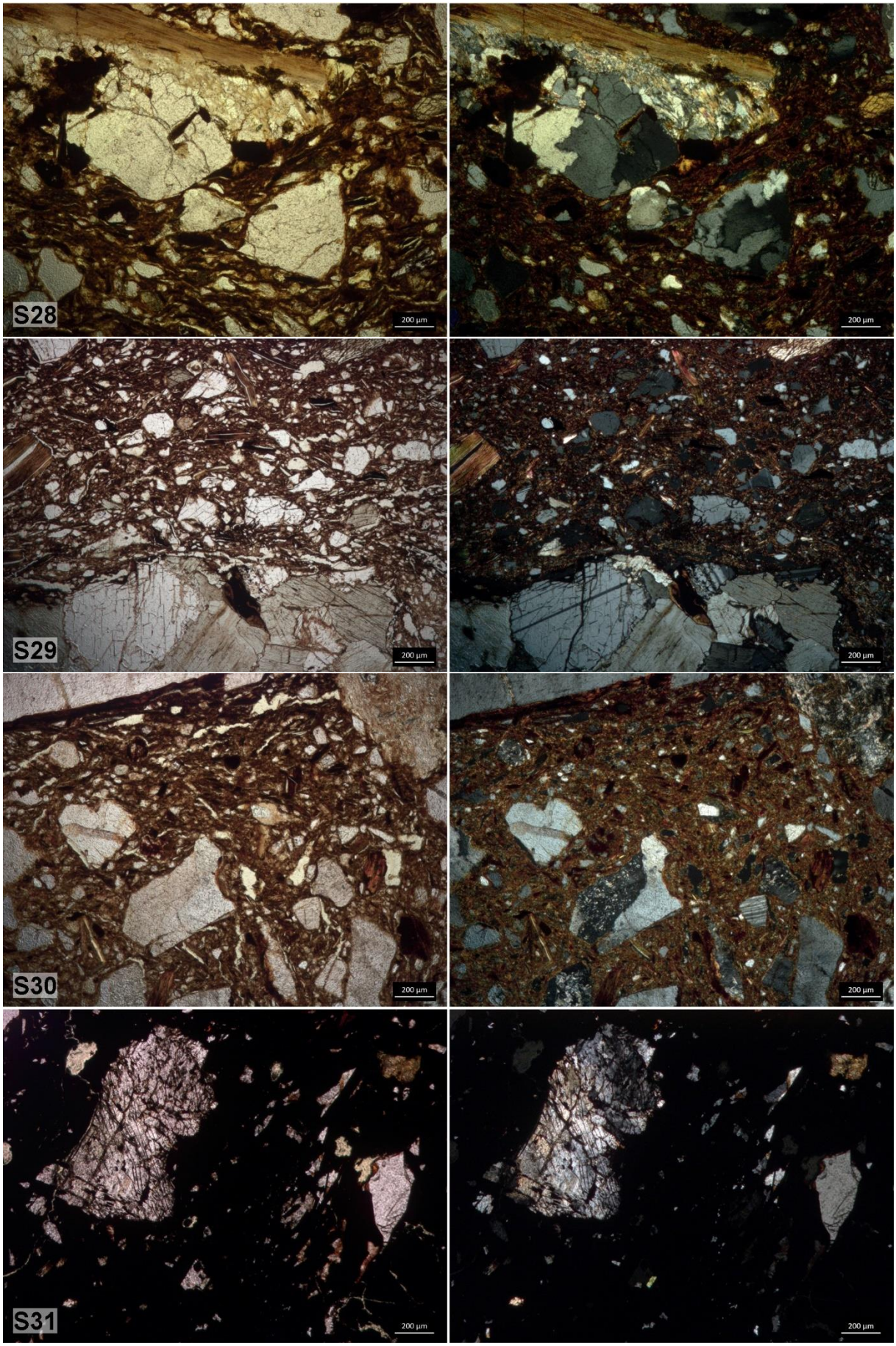

S8
200 µm
200 µm
S9
200 µm
200 µm
S10
200 µm
200 µm
S11
200 µm
200 µm

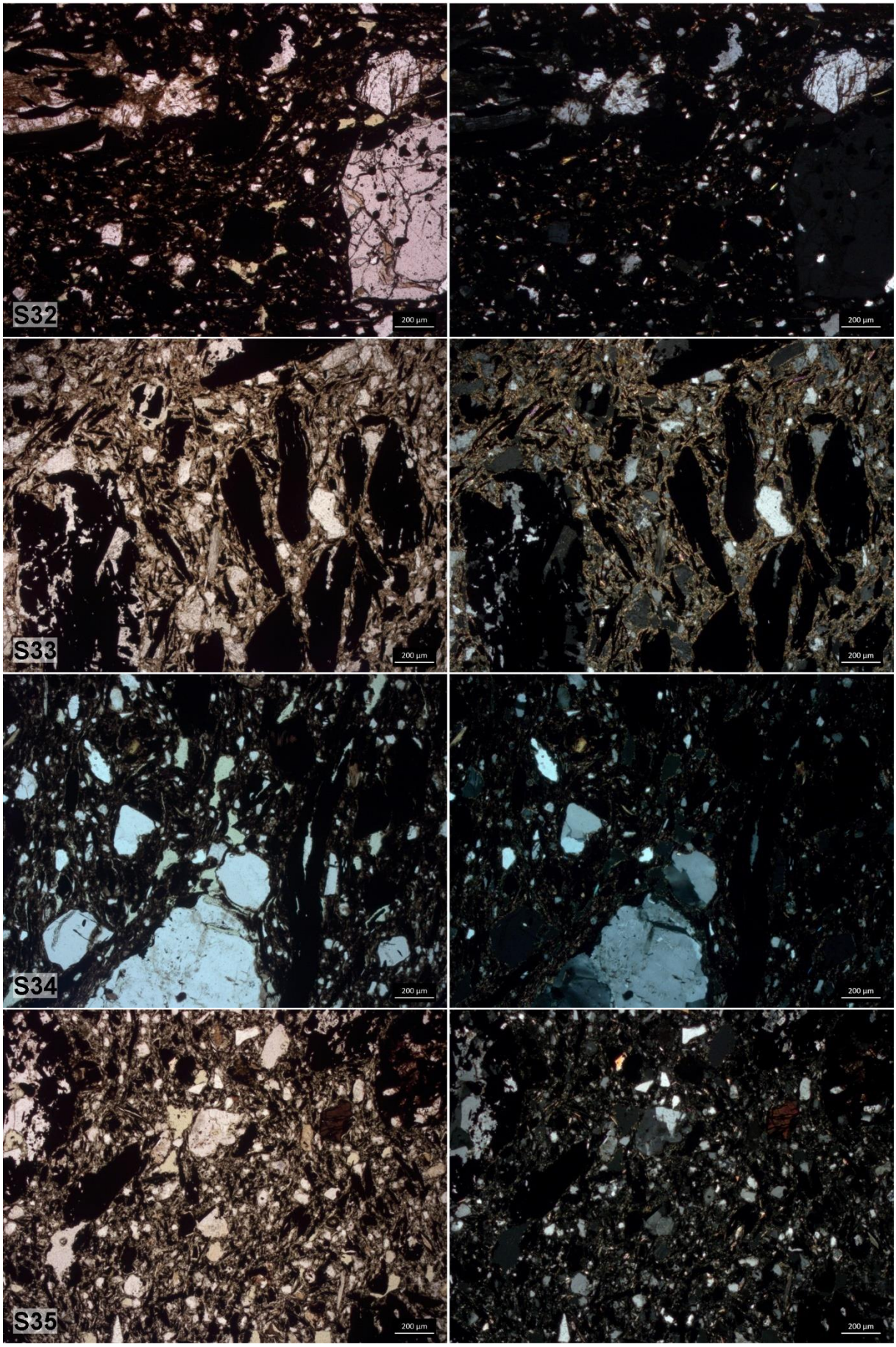

S12
200 µm
200 µm
S13
200 µm
200 µm
S14
200 µm
200 µm
S15
200 µm
200 µm

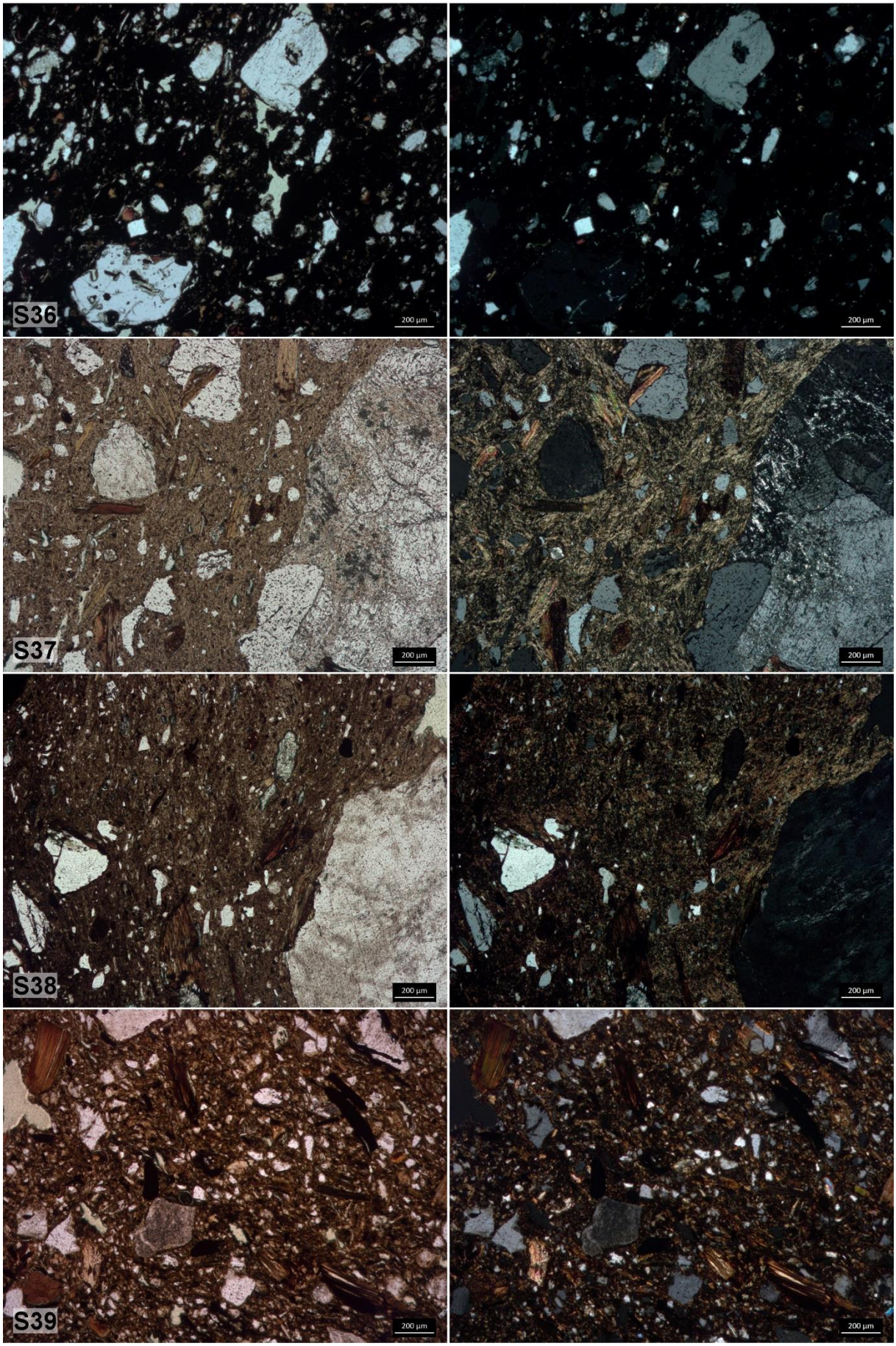

S16
200 µm
200 µm
S17
200 µm
200 µm
S18
200 µm
200 µm
S19
200 µm
200 µm

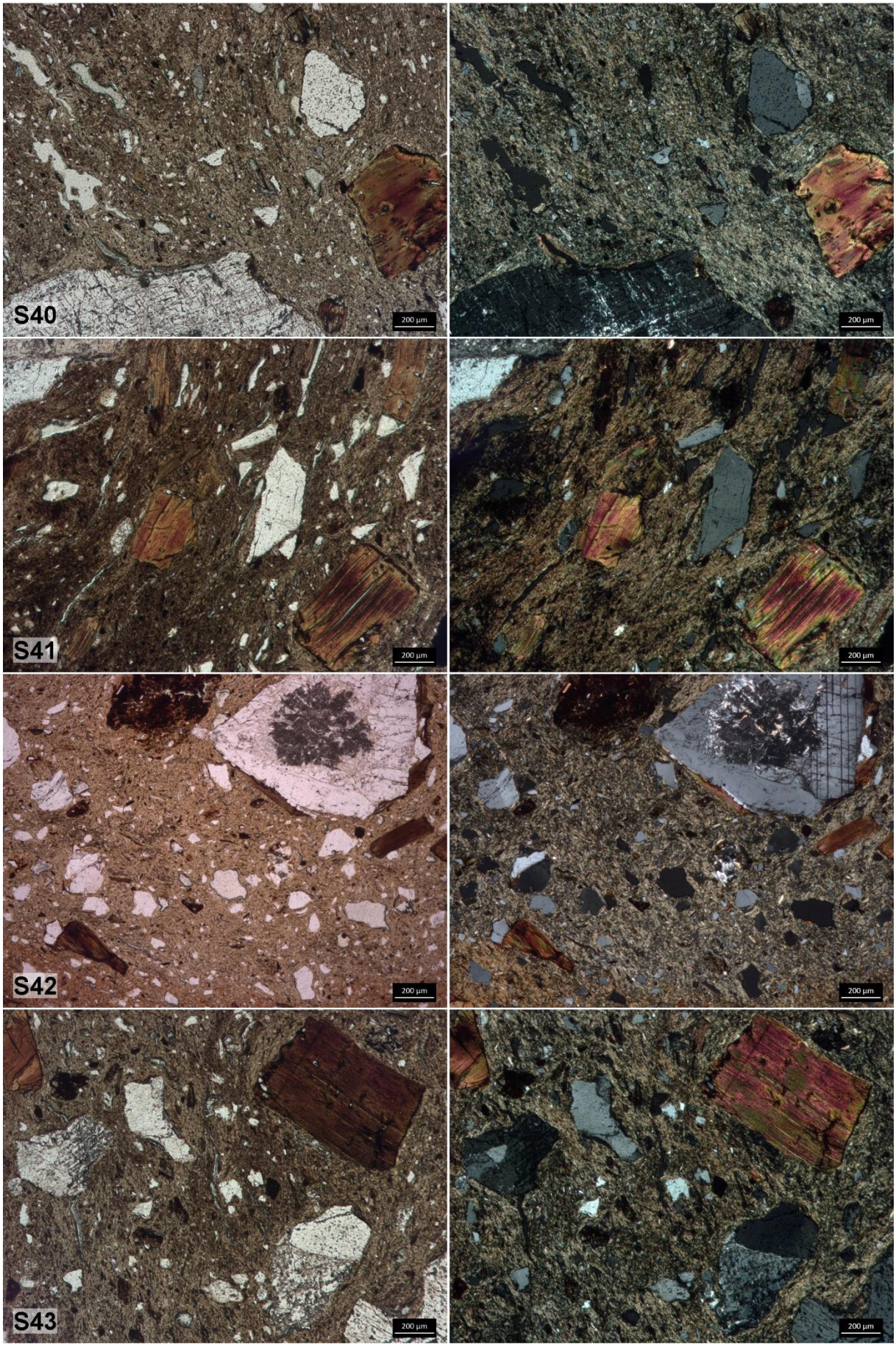

S20
200 µm
200 µm
S21
200 µm
200 µm
S22
200 µm
200 µm
S23
200 µm
200 µm

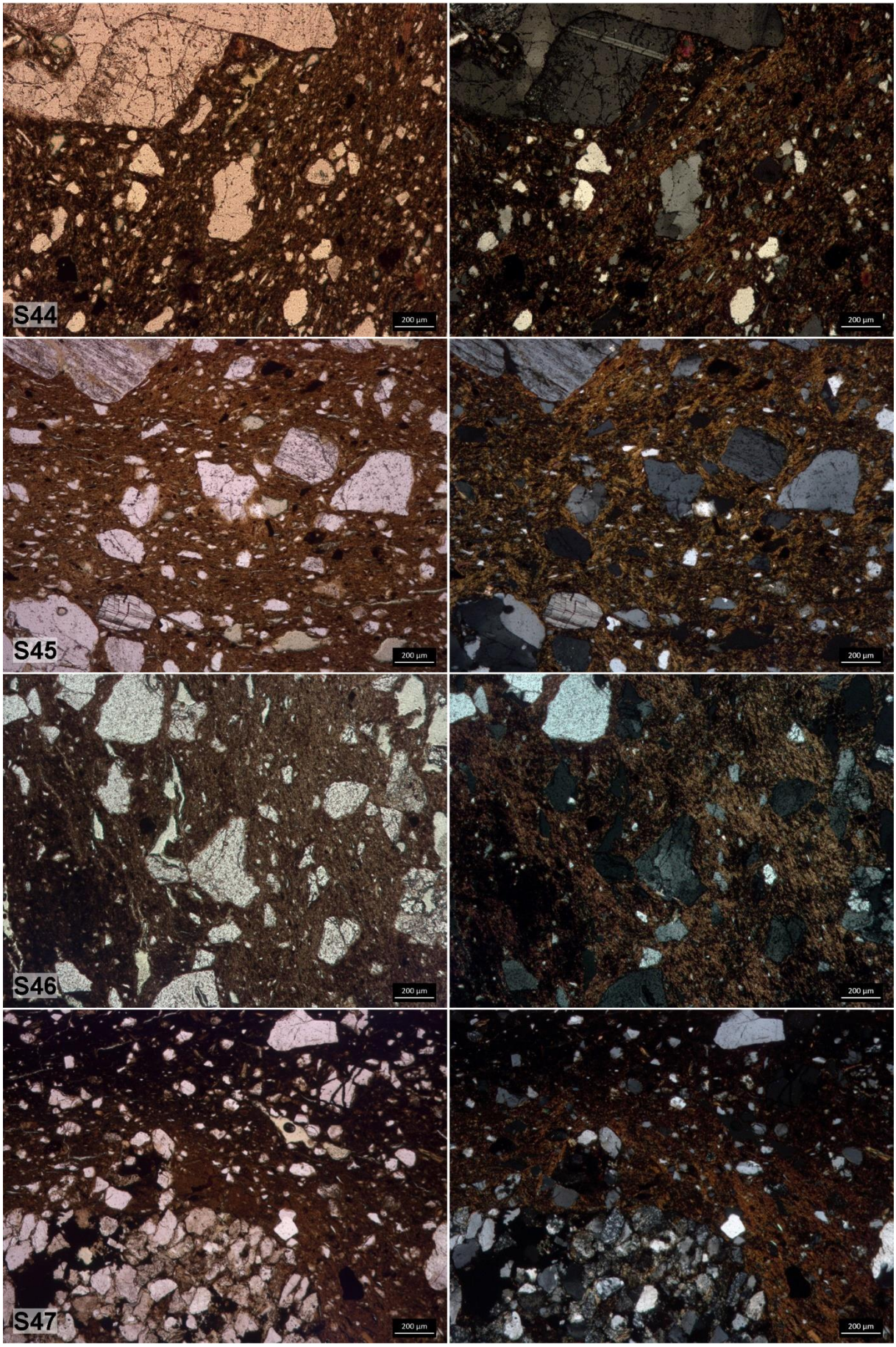

S24
200 µm
200 µm
S25
200 µm
200 µm
S26
200 µm
200 µm
S27
200 µm
200 µm

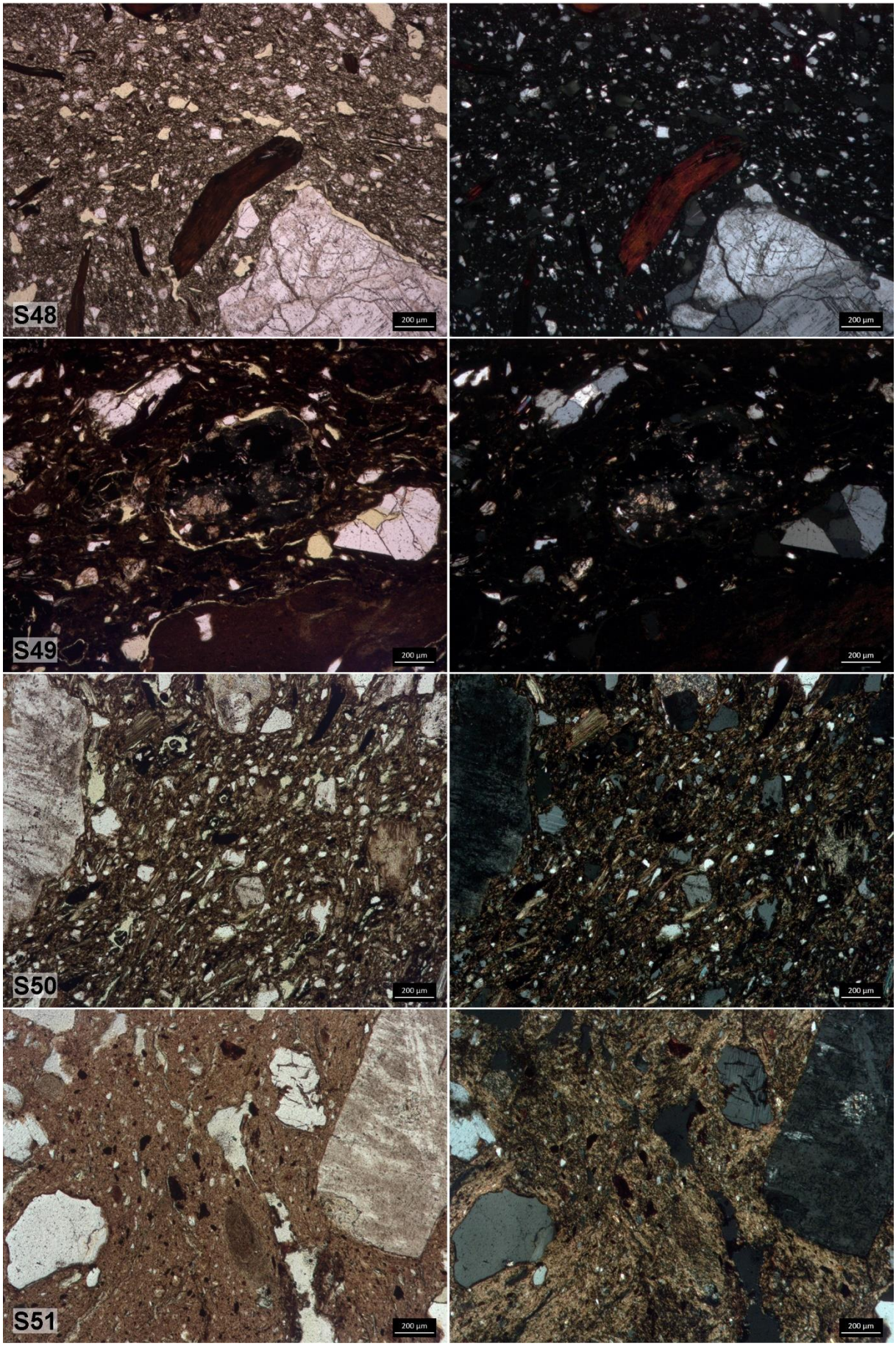

S28
200 µm
200 µm
S29
200 µm
200 µm
S30
200 µm
200 µm
S31
200 µm
200 µm

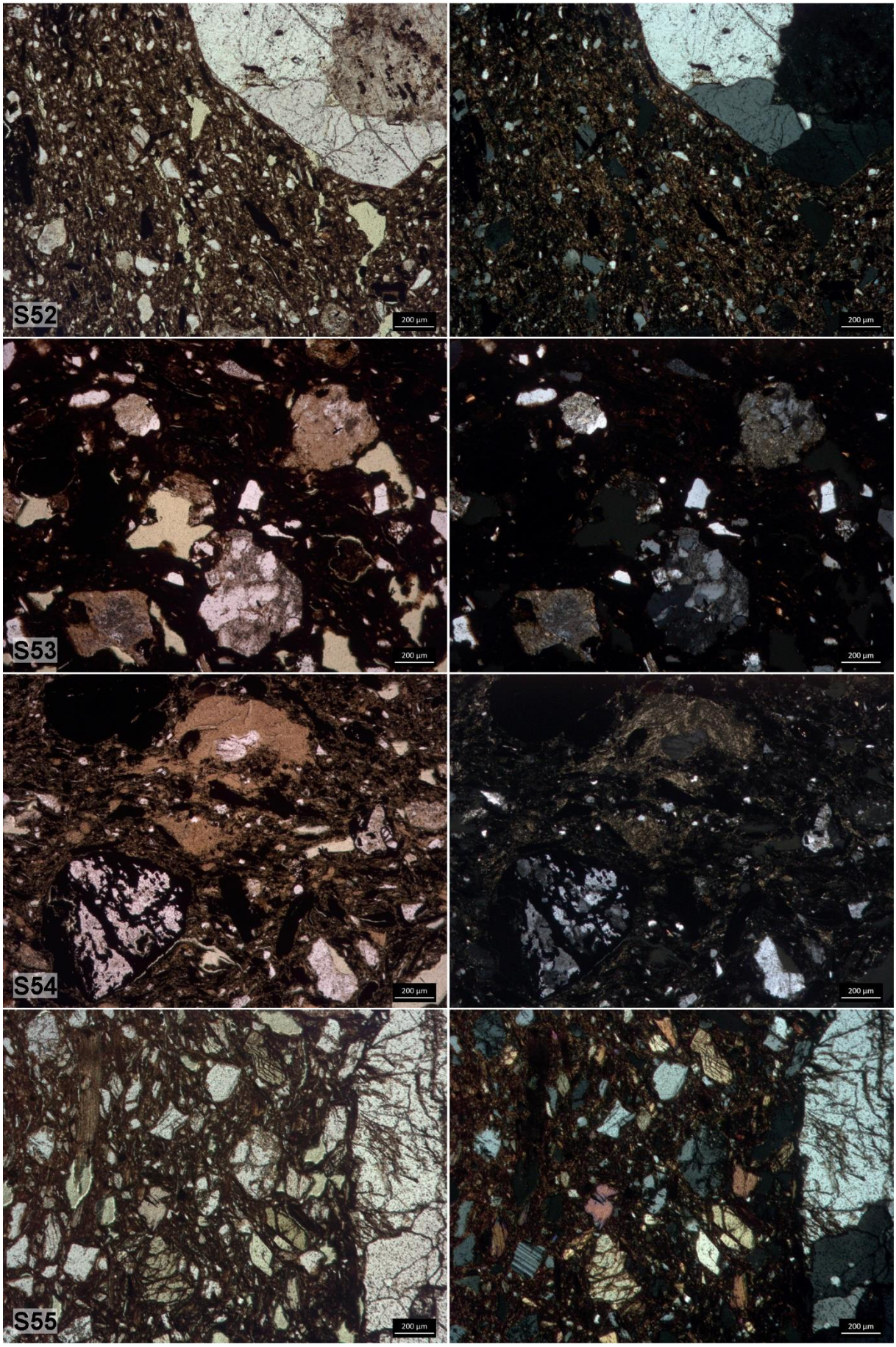

S32
200 µm
200 µm
S33
200 µm
200 µm
S34
200 µm
200 µm
S35
200 µm
200 µm

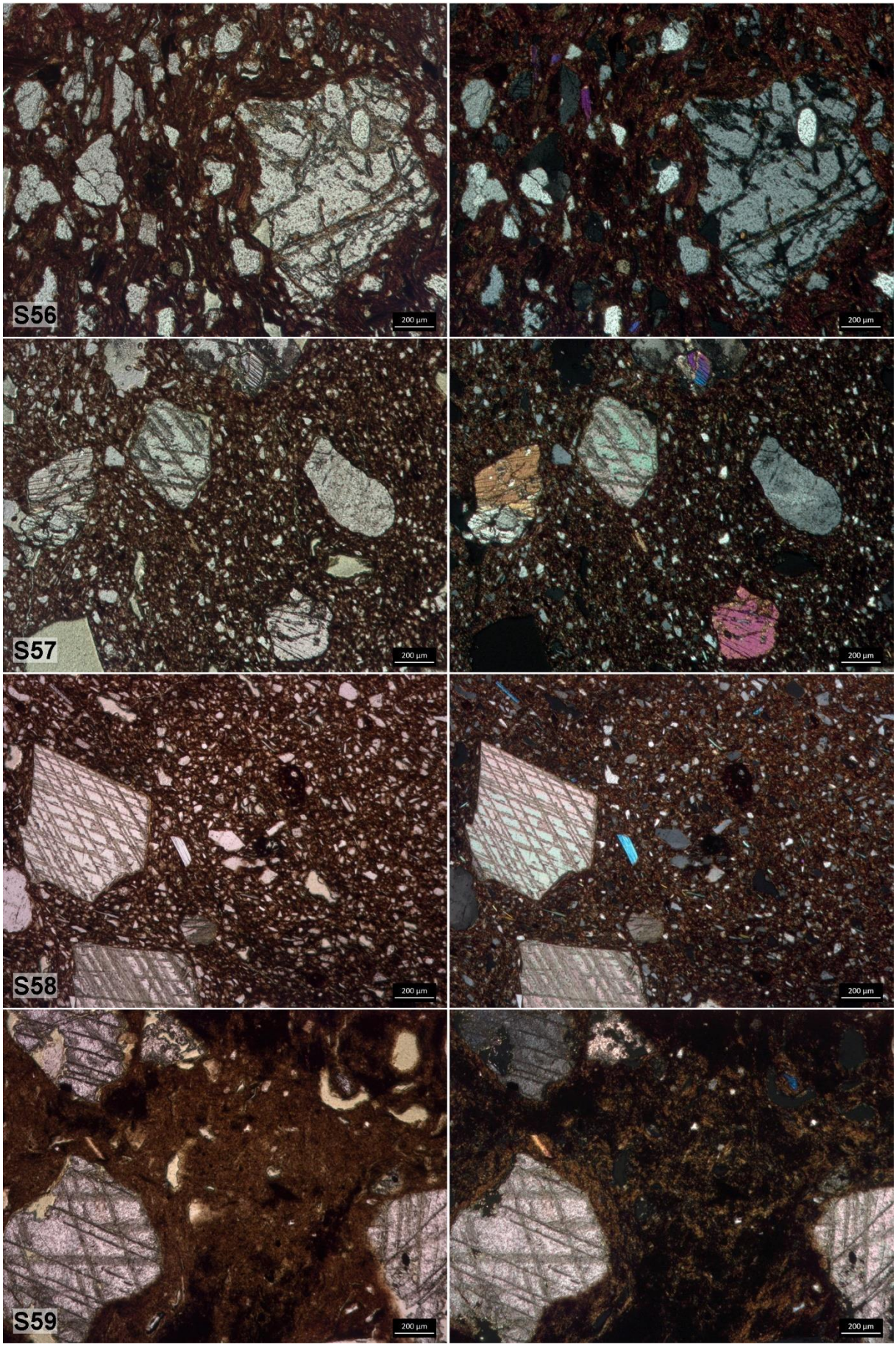

S36
200 µm
200 µm
S37
200 µm
200 µm
S38
200 µm
200 µm
S39
200 µm
200 µm

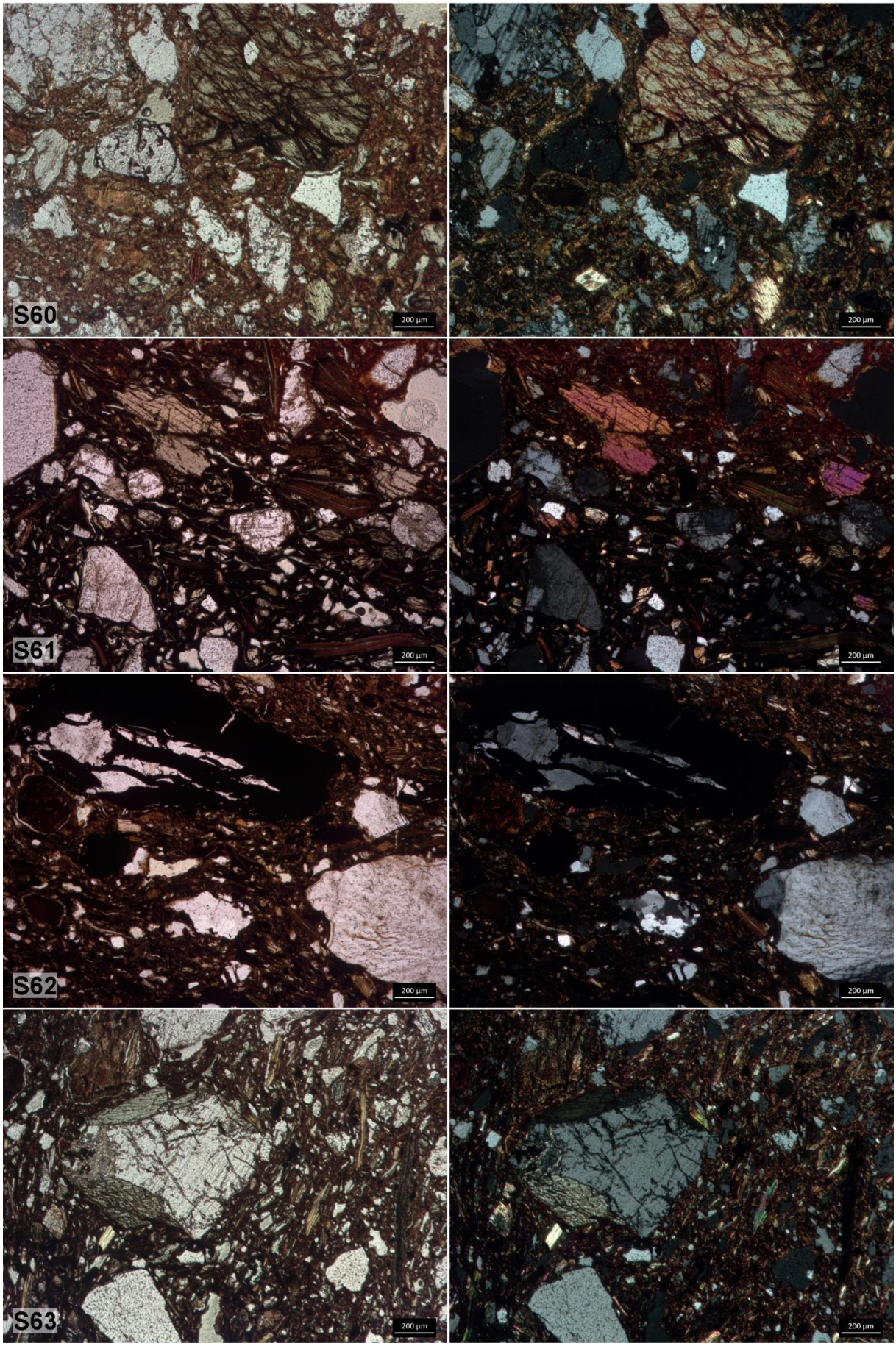

S40
200 µm
200 µm
S41
200 µm
200 µm
S42
200 µm
200 µm
S43
200 µm
200 µm

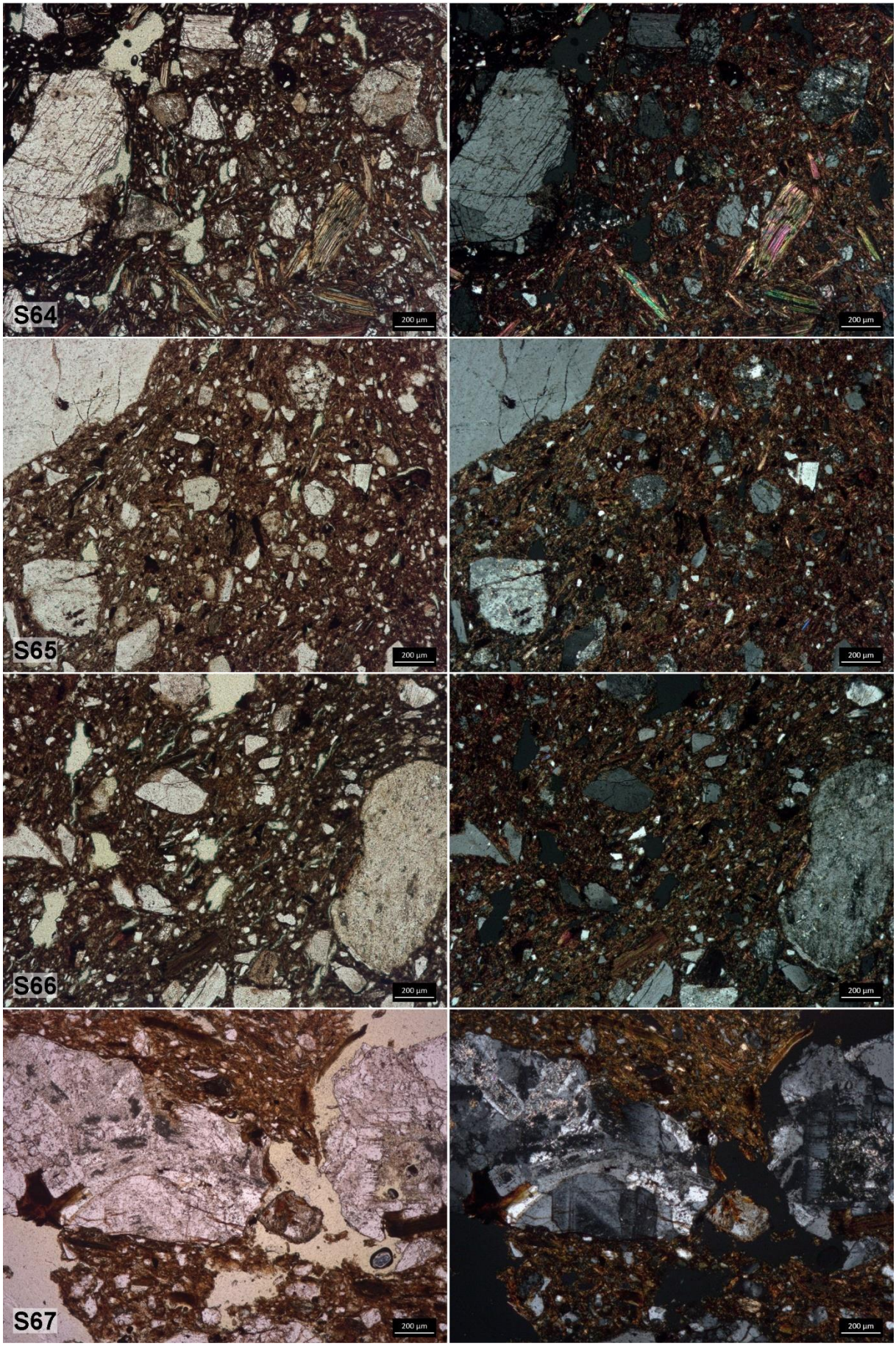

S44
200 µm
200 µm
S45
200 µm
200 µm
S46
200 µm
200 µm
S47
200 µm
200 µm

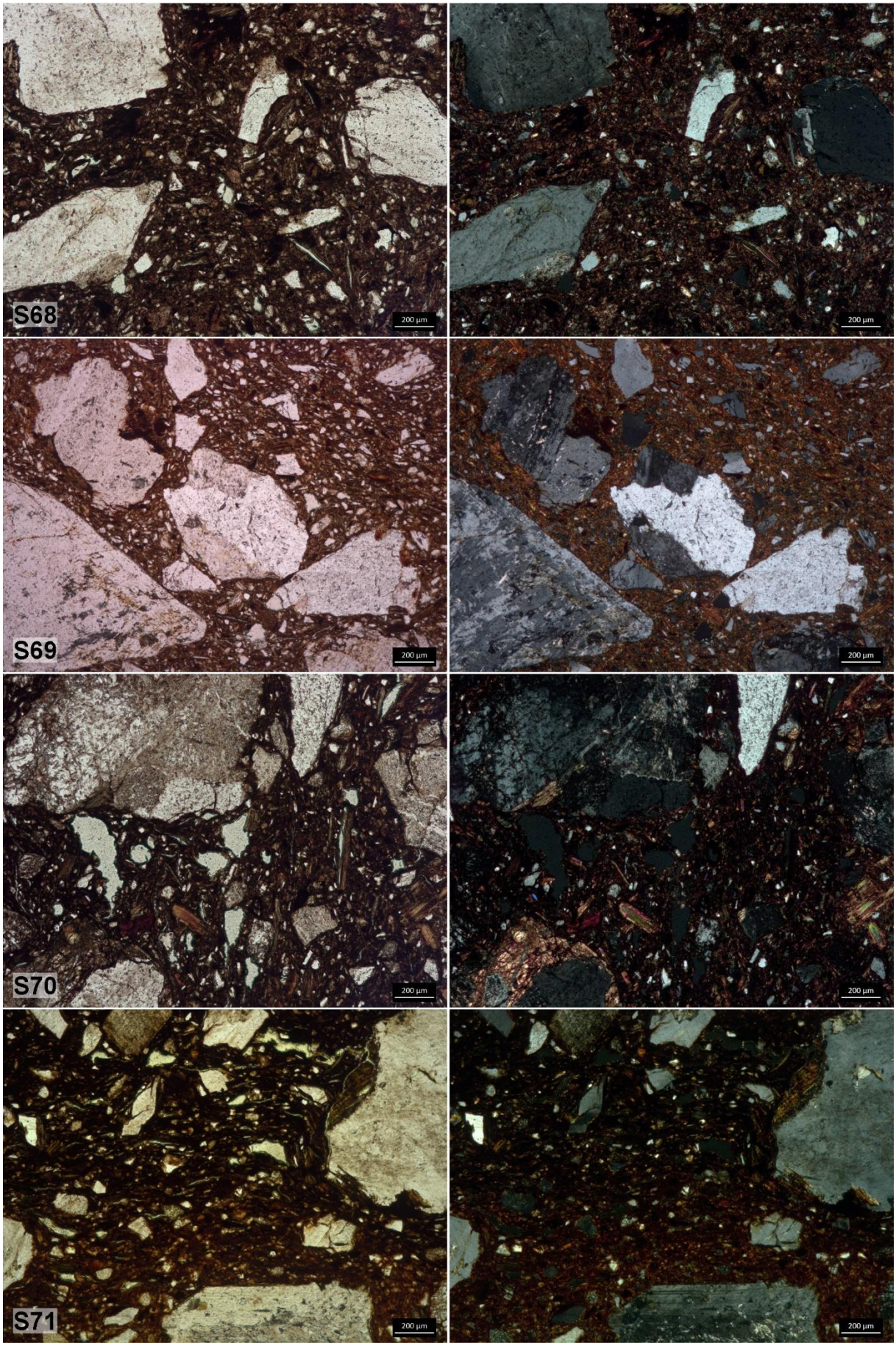

S48
200 µm
200 µm
S49
200 µm
200 µm
S50
200 µm
200 µm
S51
200 µm
200 µm

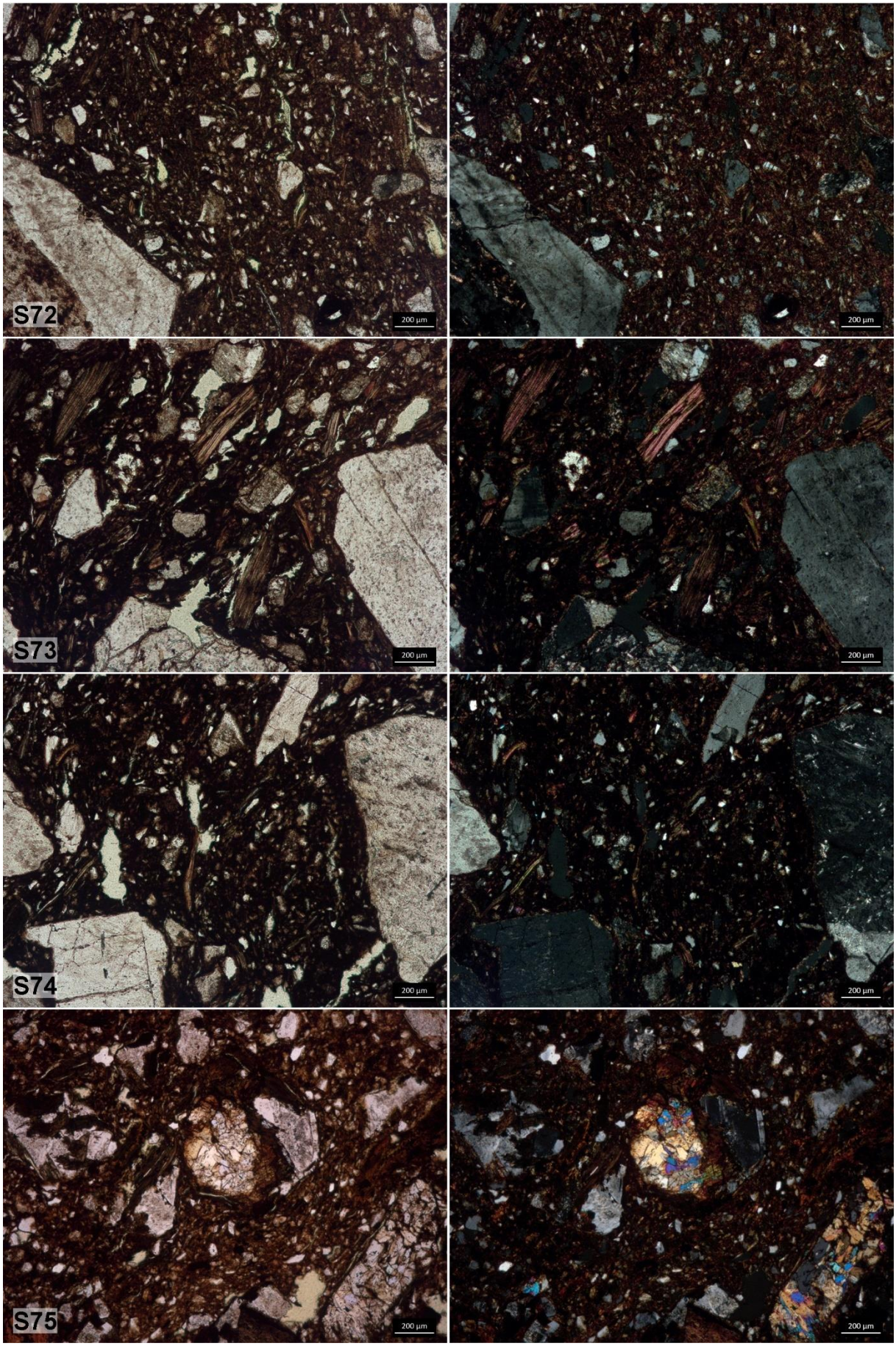

S52
200 µm
200 µm
S53
200 µm
200 µm
S54
200 µm
200 µm
S55
200 µm
200 µm

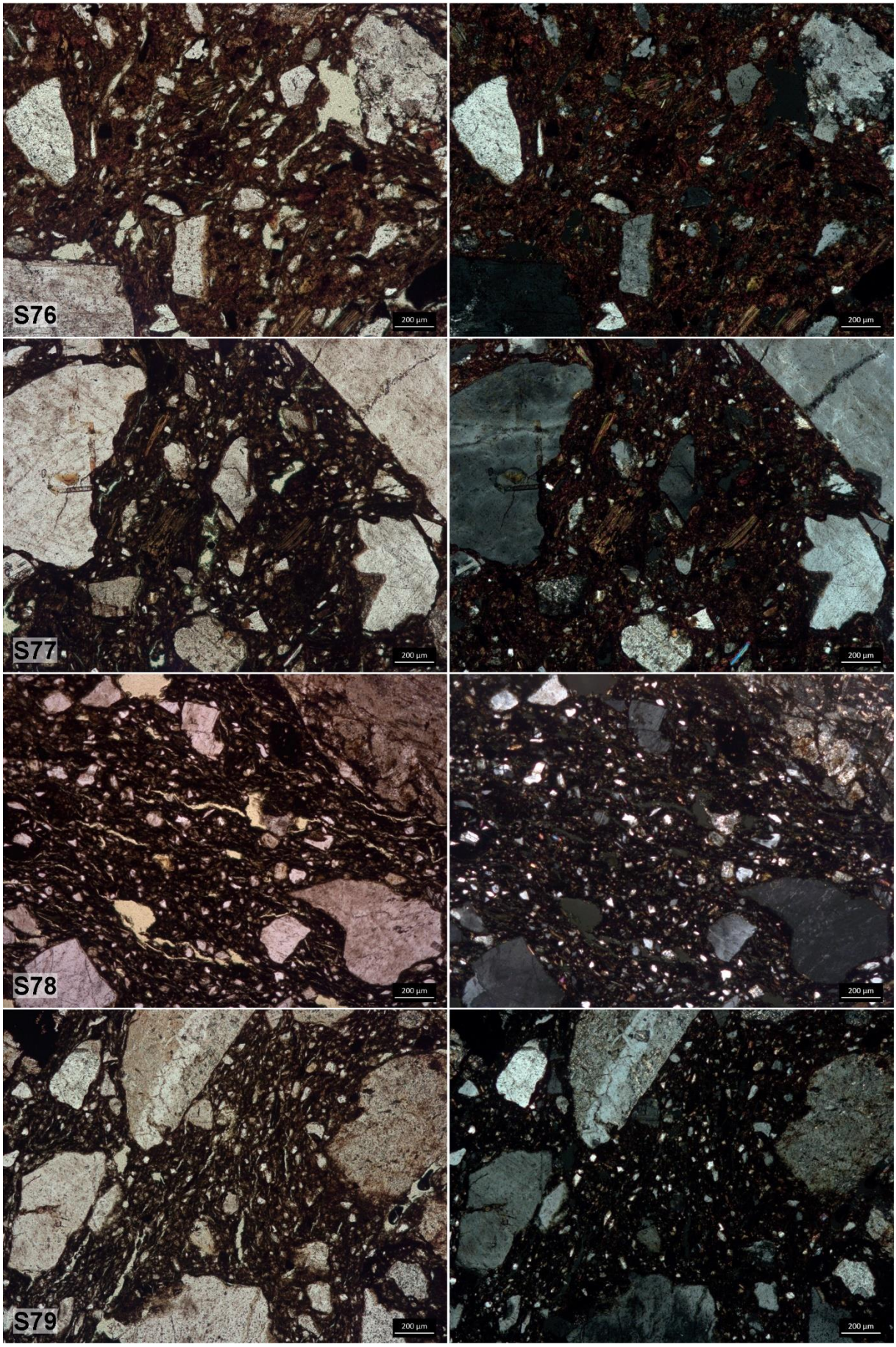

S56
200 µm
200 µm
S57
200 µm
200 µm
S58
200 µm
200 µm
S59
200 µm
200 µm

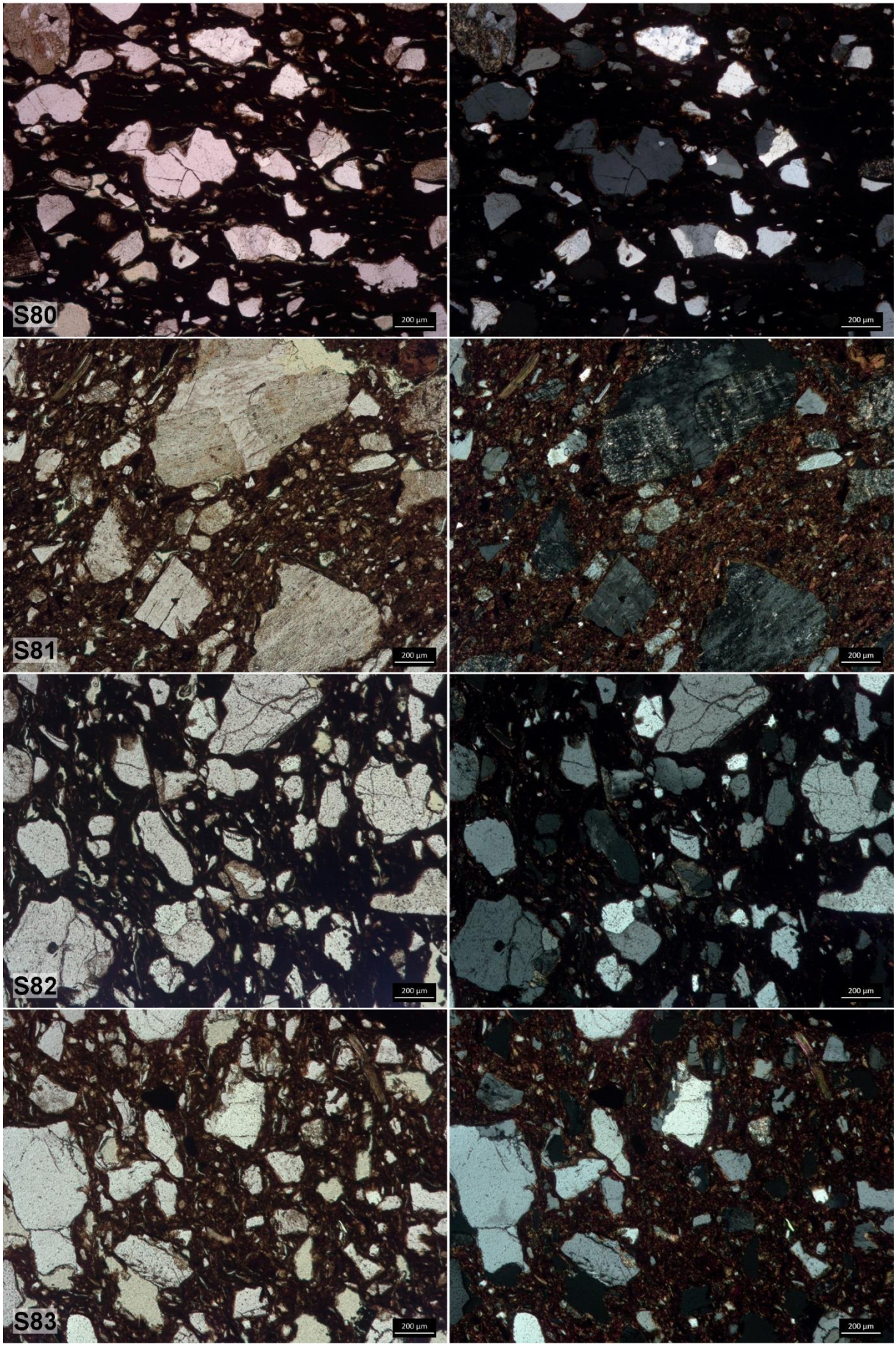

S60
200 µm
200 µm
S61
200 µm
200 µm
S62
200 µm
200 µm
S63
200 µm
200 µm

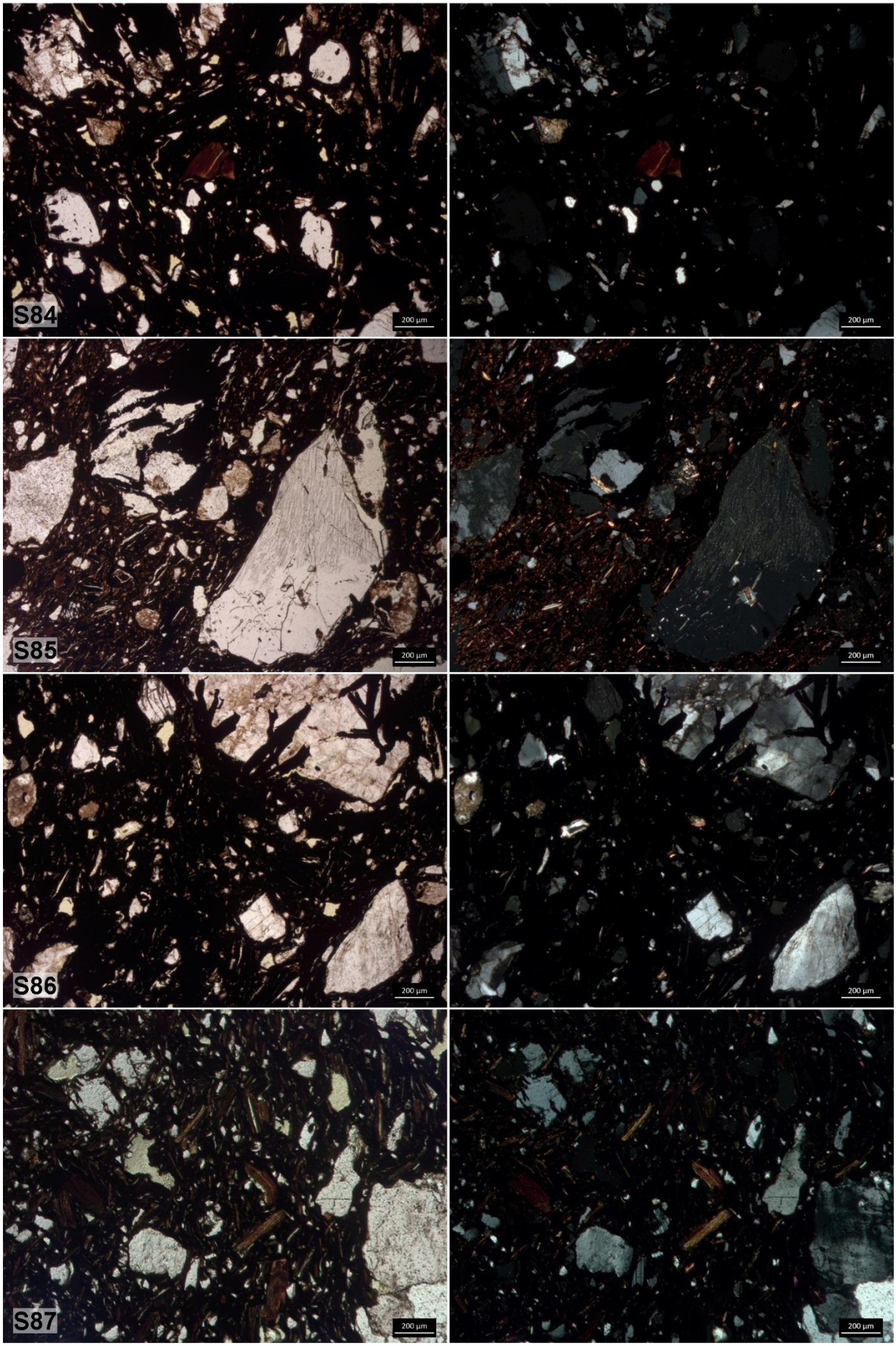

S64
200 µm
200 µm
S65
200 µm
200 µm
S66
200 µm
200 µm
S67
200 µm
200 µm

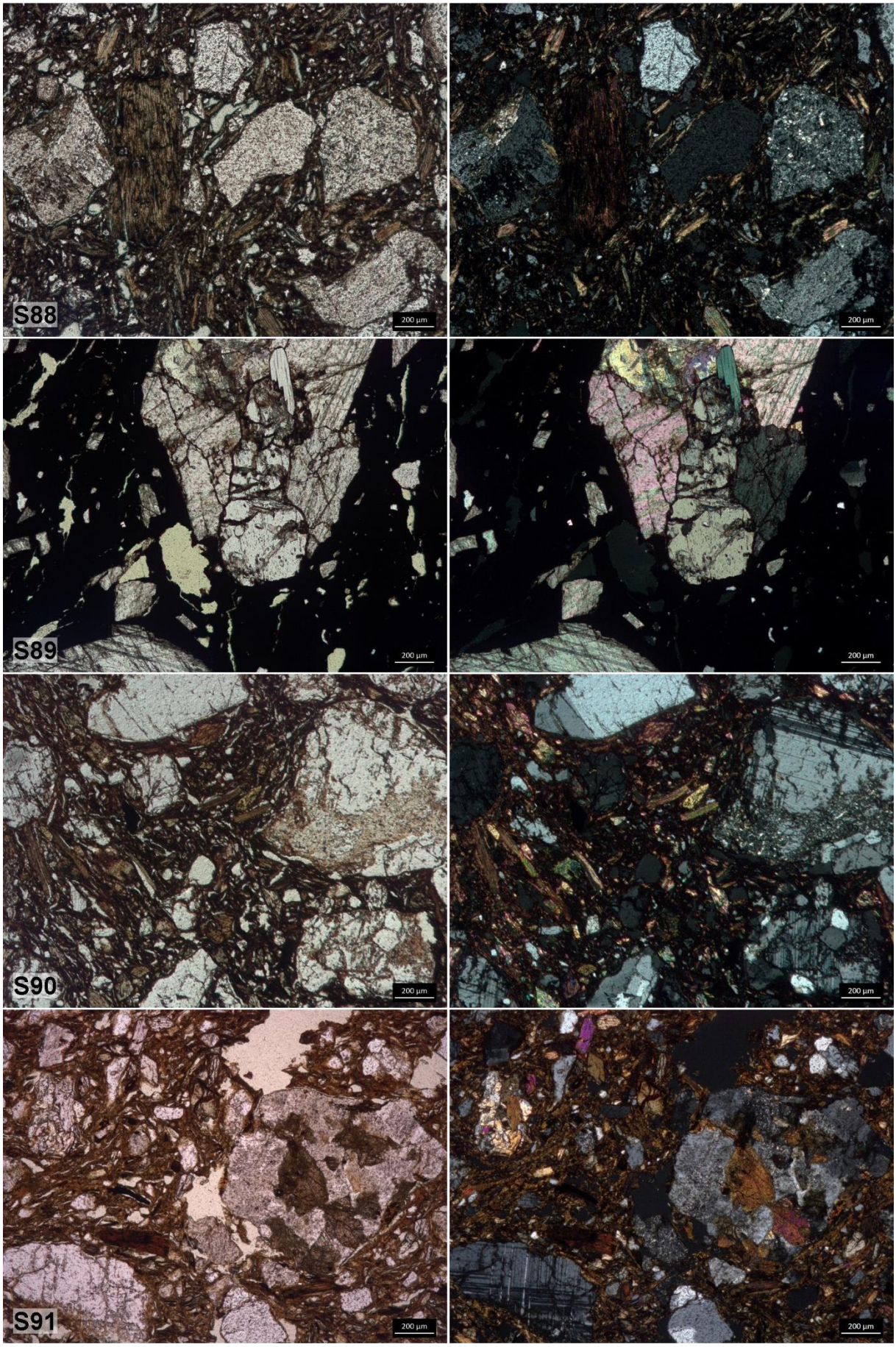

S68
200 µm
200 µm
S69
200 µm
200 µm
S70
200 µm
200 µm
S71
200 µm
200 µm

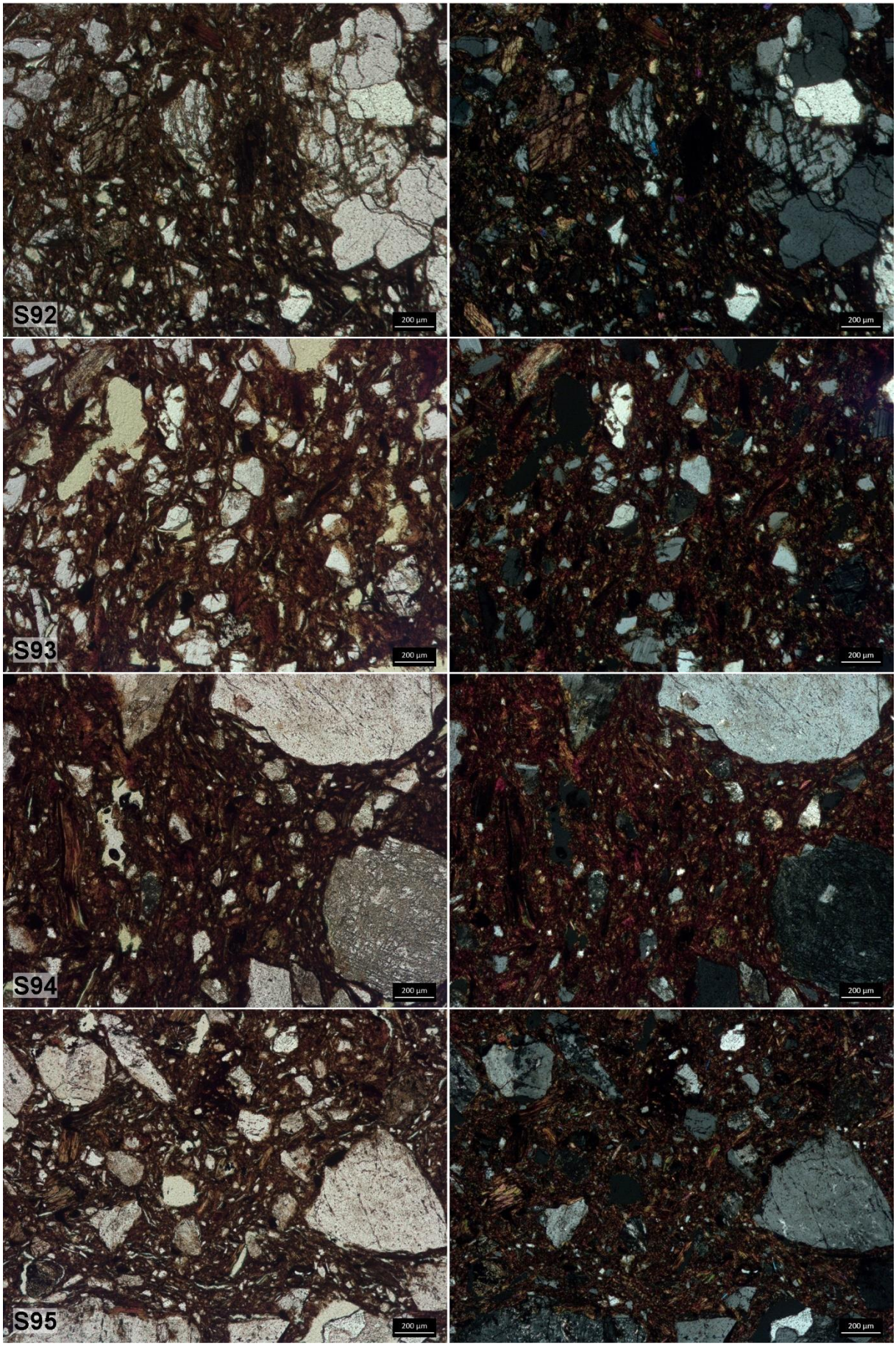

S72
200 µm
200 µm
S73
200 µm
200 µm
S74
200 µm
200 µm
S75
200 µm
200 µm

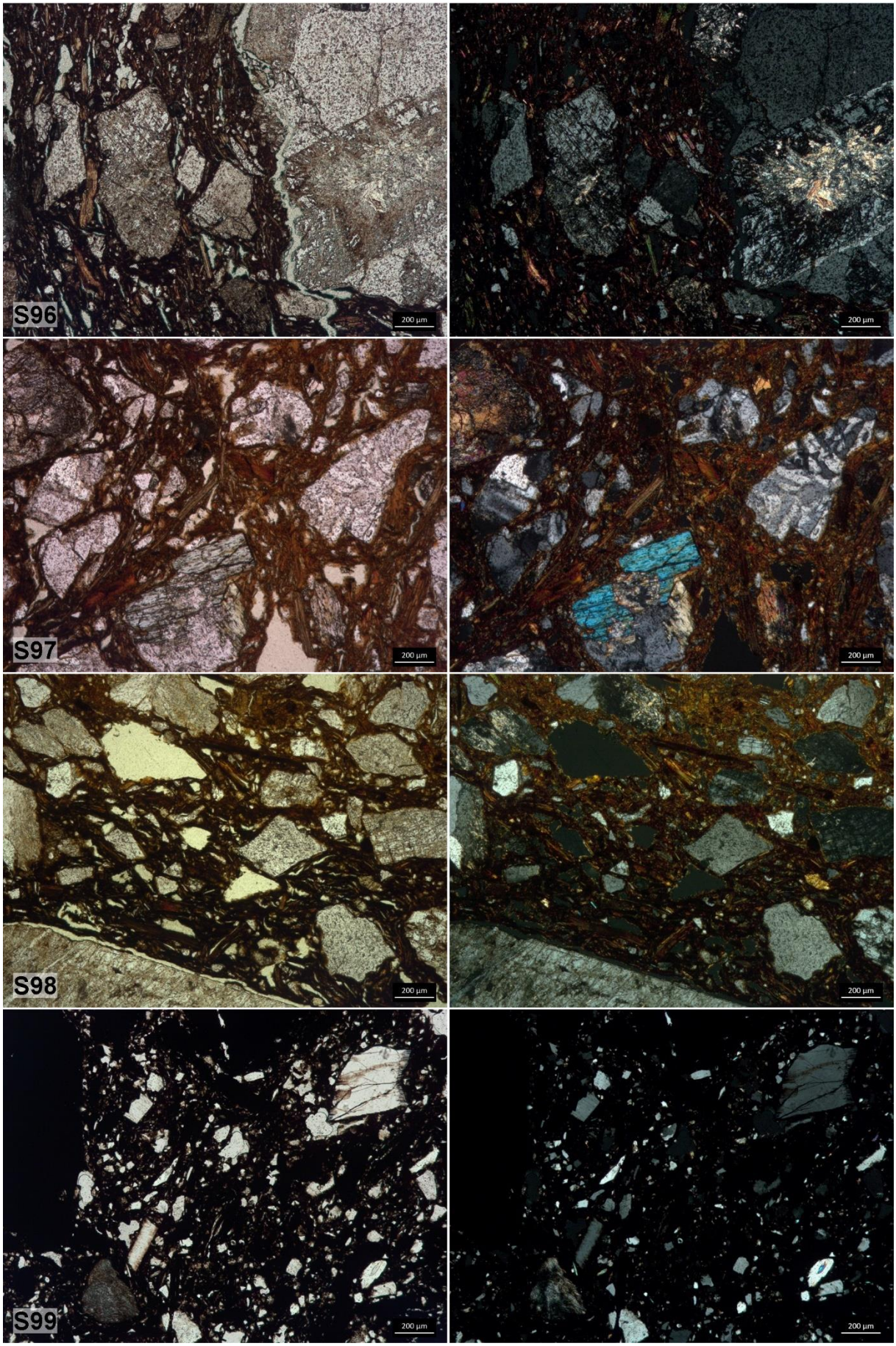

S76
200 µm
200 µm
S77
200 µm
200 µm
S78
200 µm
200 µm
S79
200 µm
200 µm

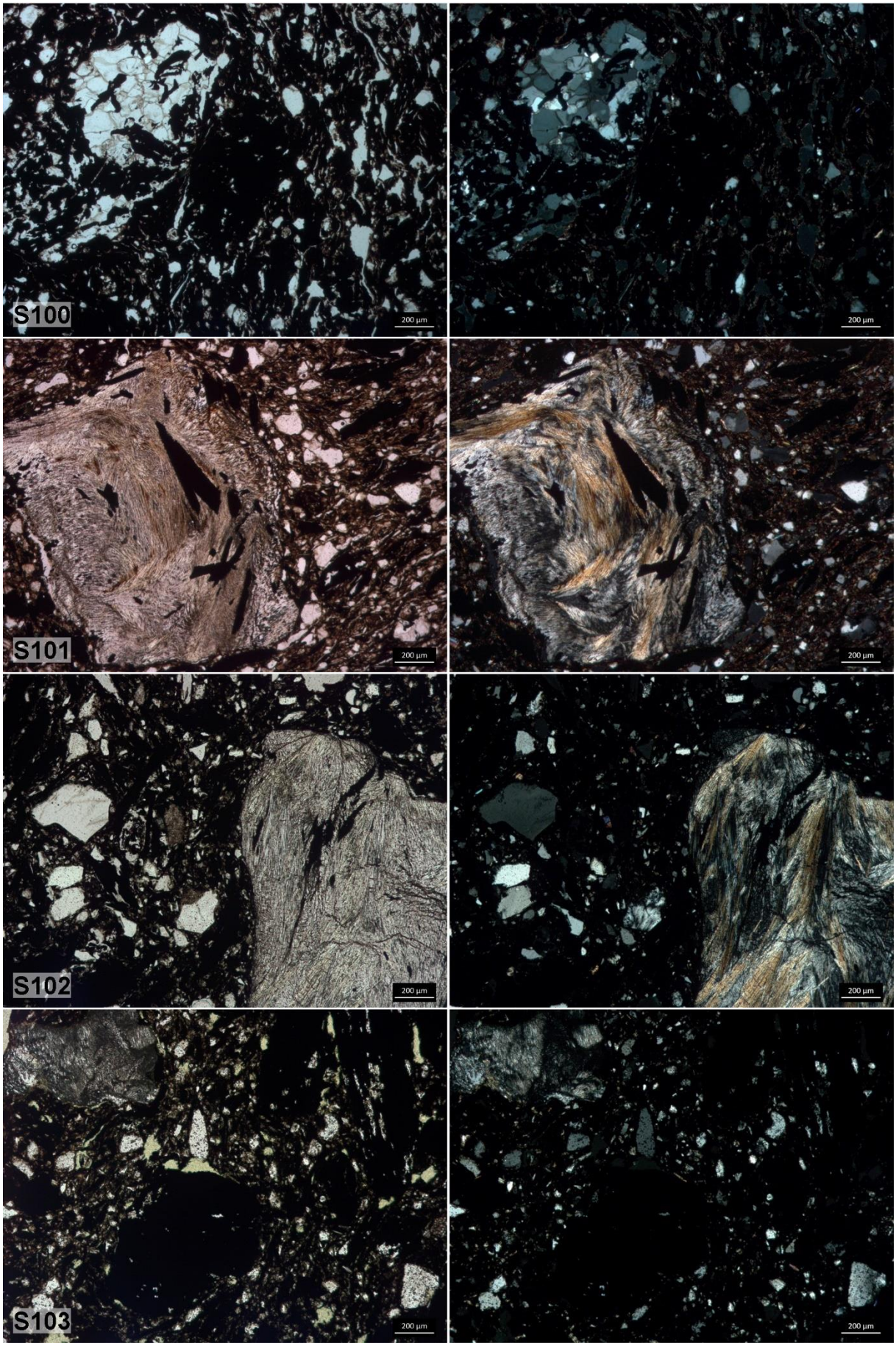

S80
200 µm
200 µm
S81
200 µm
200 µm
S82
200 µm
200 µm
S83
200 µm
200 µm

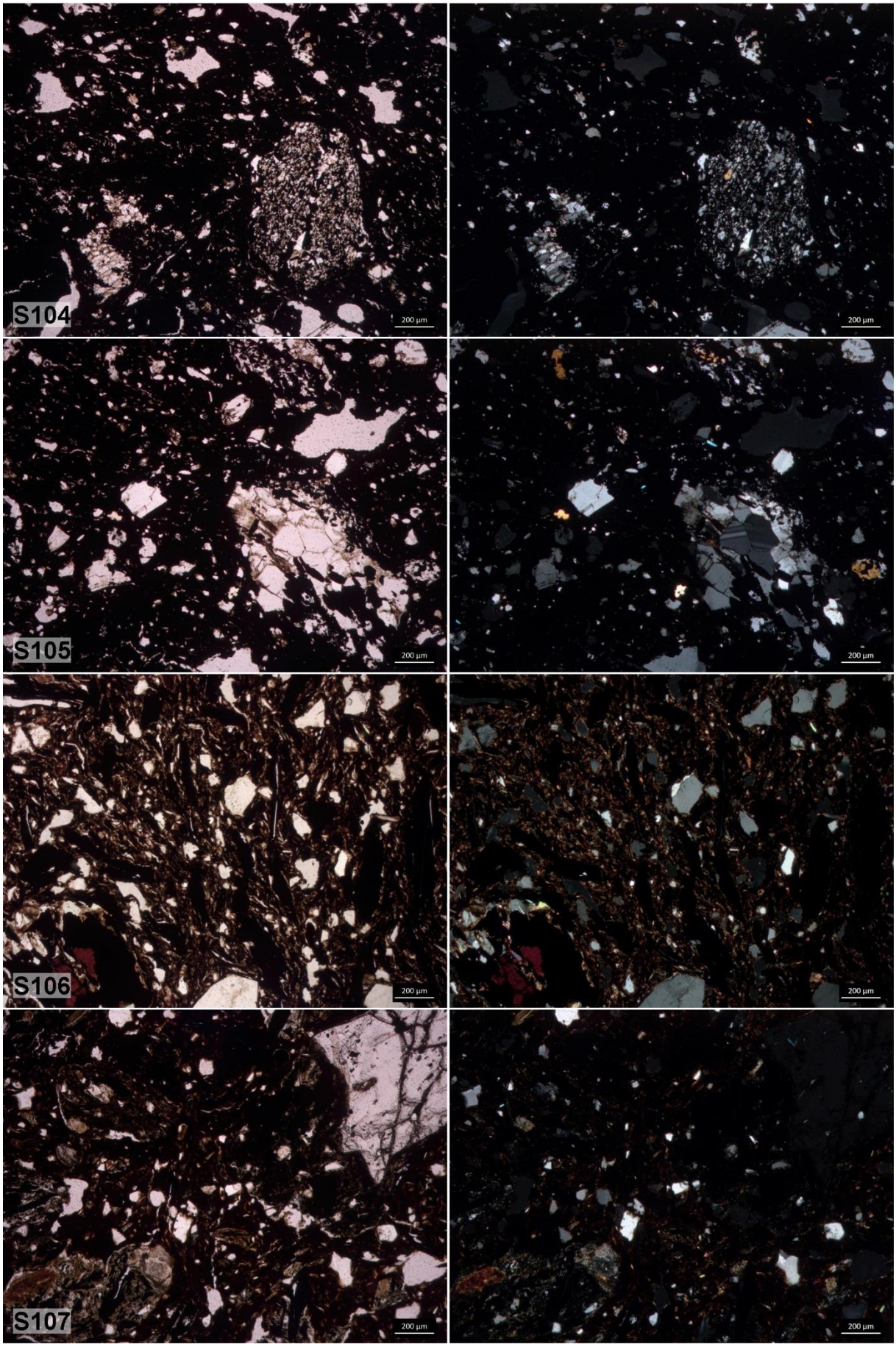

S84
200 µm
200 µm
S85
200 µm
200 µm
S86
200 µm
200 µm
S87
200 µm
200 µm

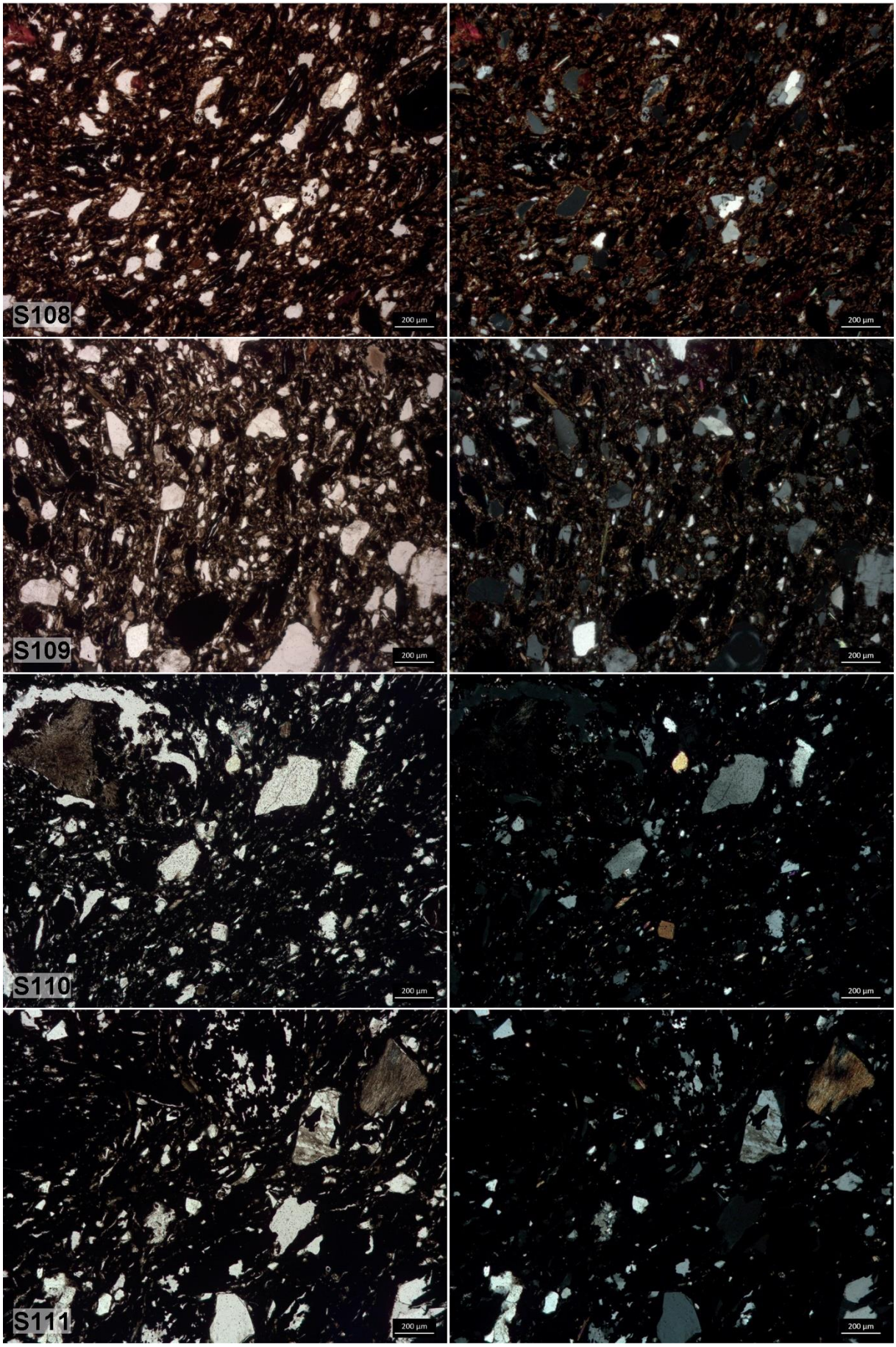

S88
200 µm
200 µm
S89
200 µm
200 µm
S90
200 µm
200 µm
S91
200 µm
200 µm

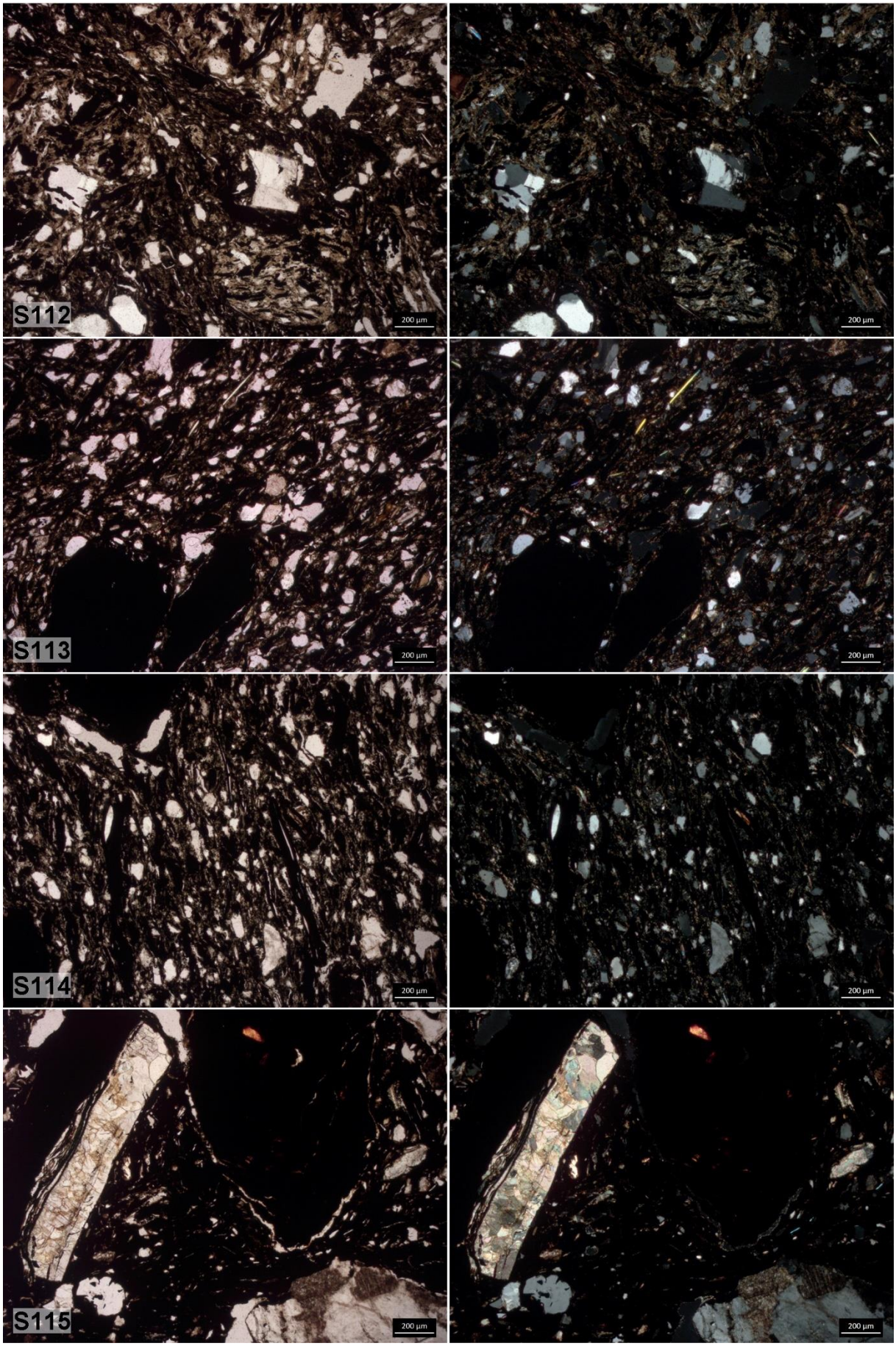

S92
200 µm
200 µm
S93
200 µm
200 µm
S94
200 µm
200 µm
S95
200 µm
200 µm

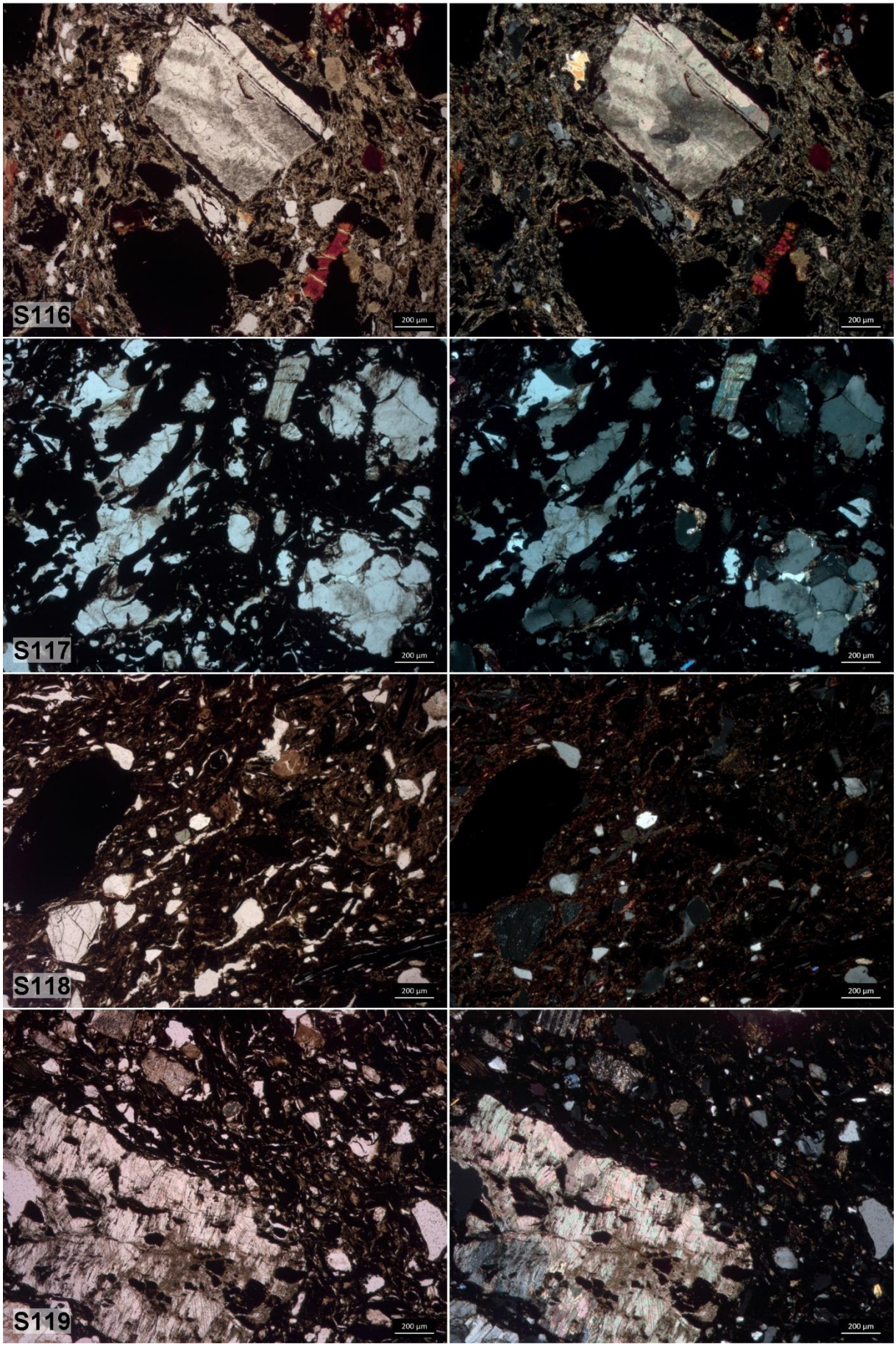

S96
200 µm
200 µm
S97
200 µm
200 µm
S98
200 µm
200 µm
S99
200 µm
200 µm

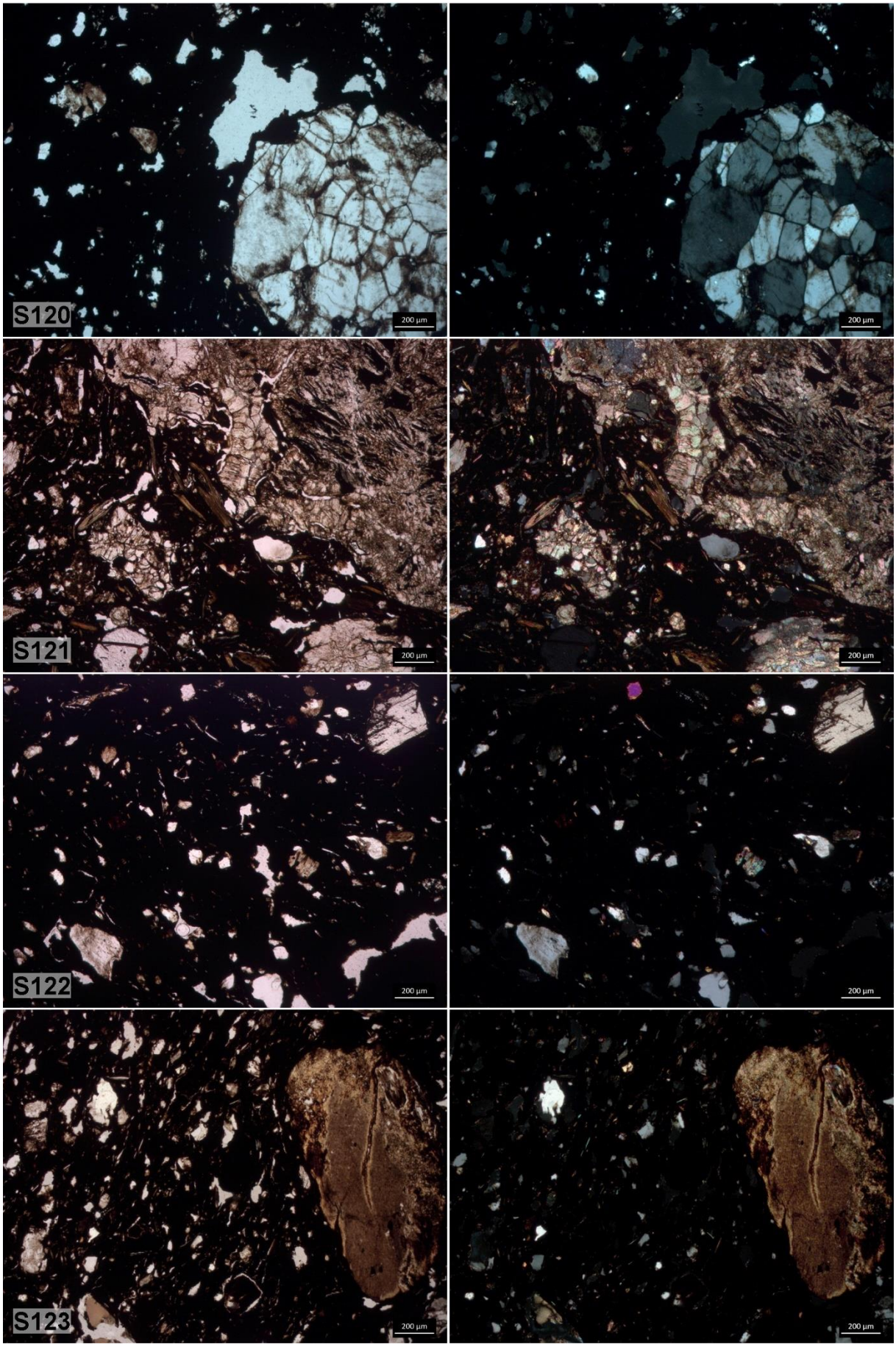

S100
200 µm
200 µm
S101
200 µm
200 µm
S102
200 µm
200 µm
S103
200 µm
200 µm

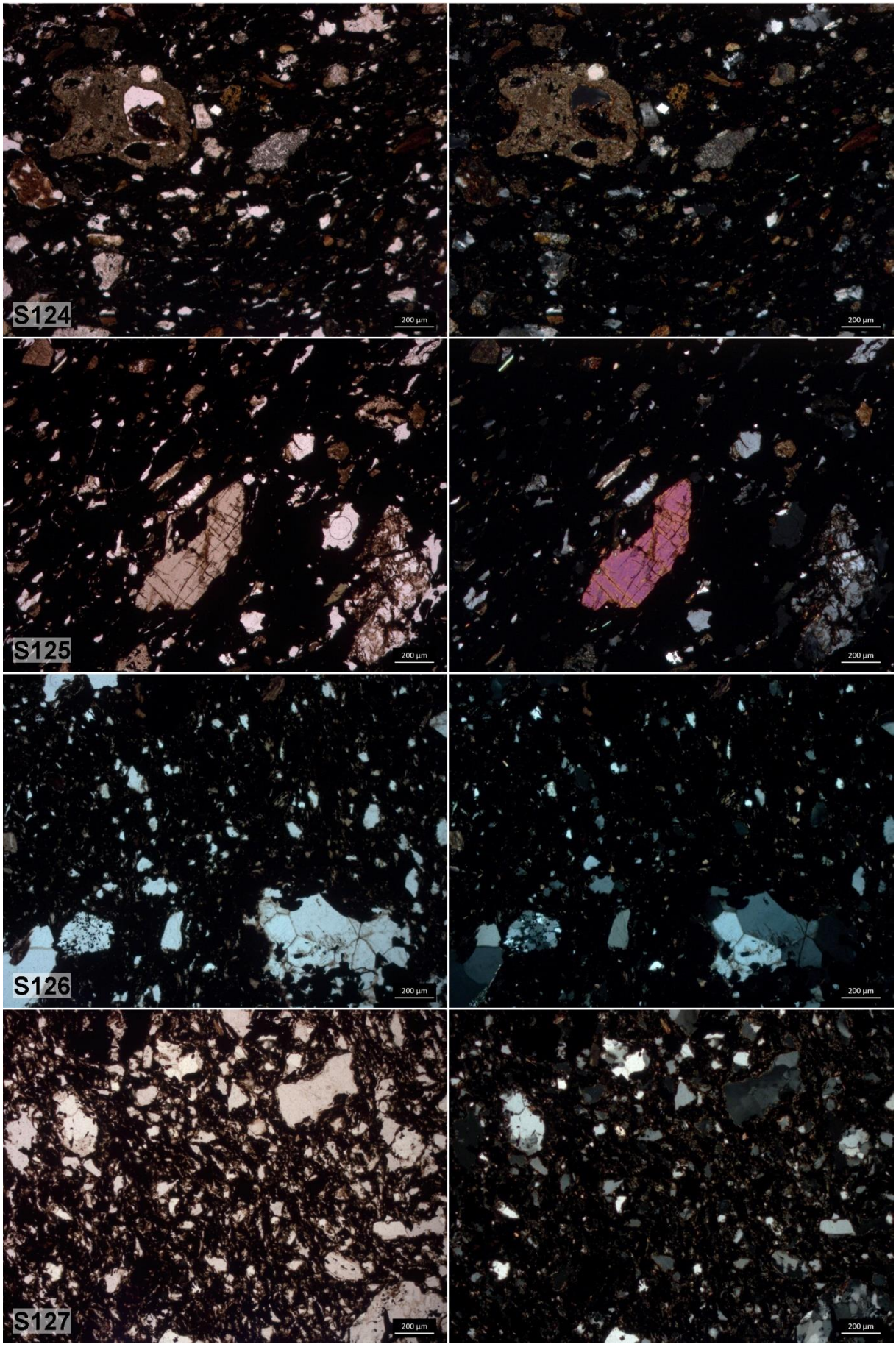

S104
200 µm
200 µm
S105
200 µm
200 µm
S106
200 µm
200 µm
S107
200 µm
200 µm

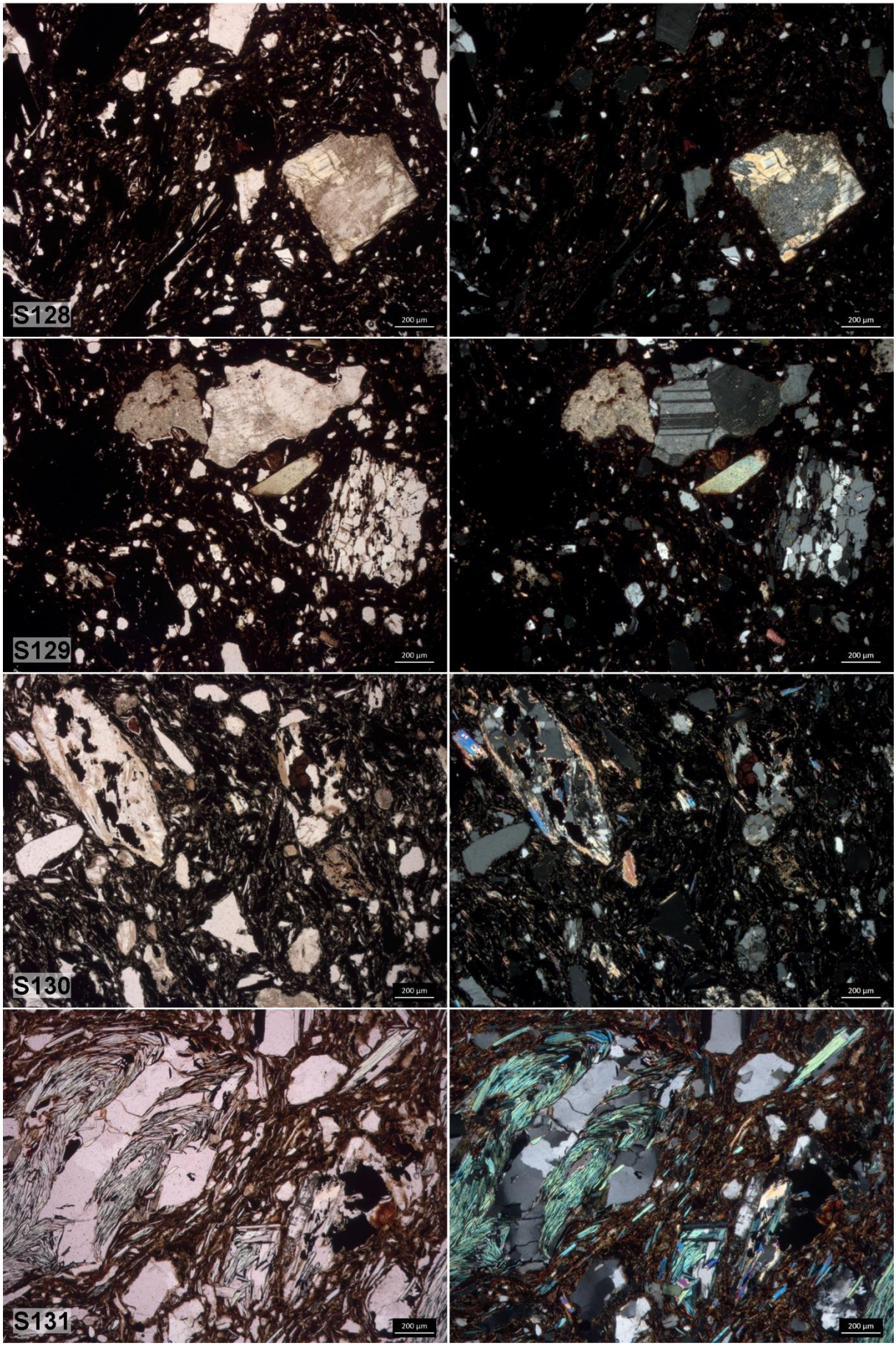

S108
200 µm
200 µm
S109
200 µm
200 µm
S110
200 µm
200 µm
S111
200 µm
200 µm

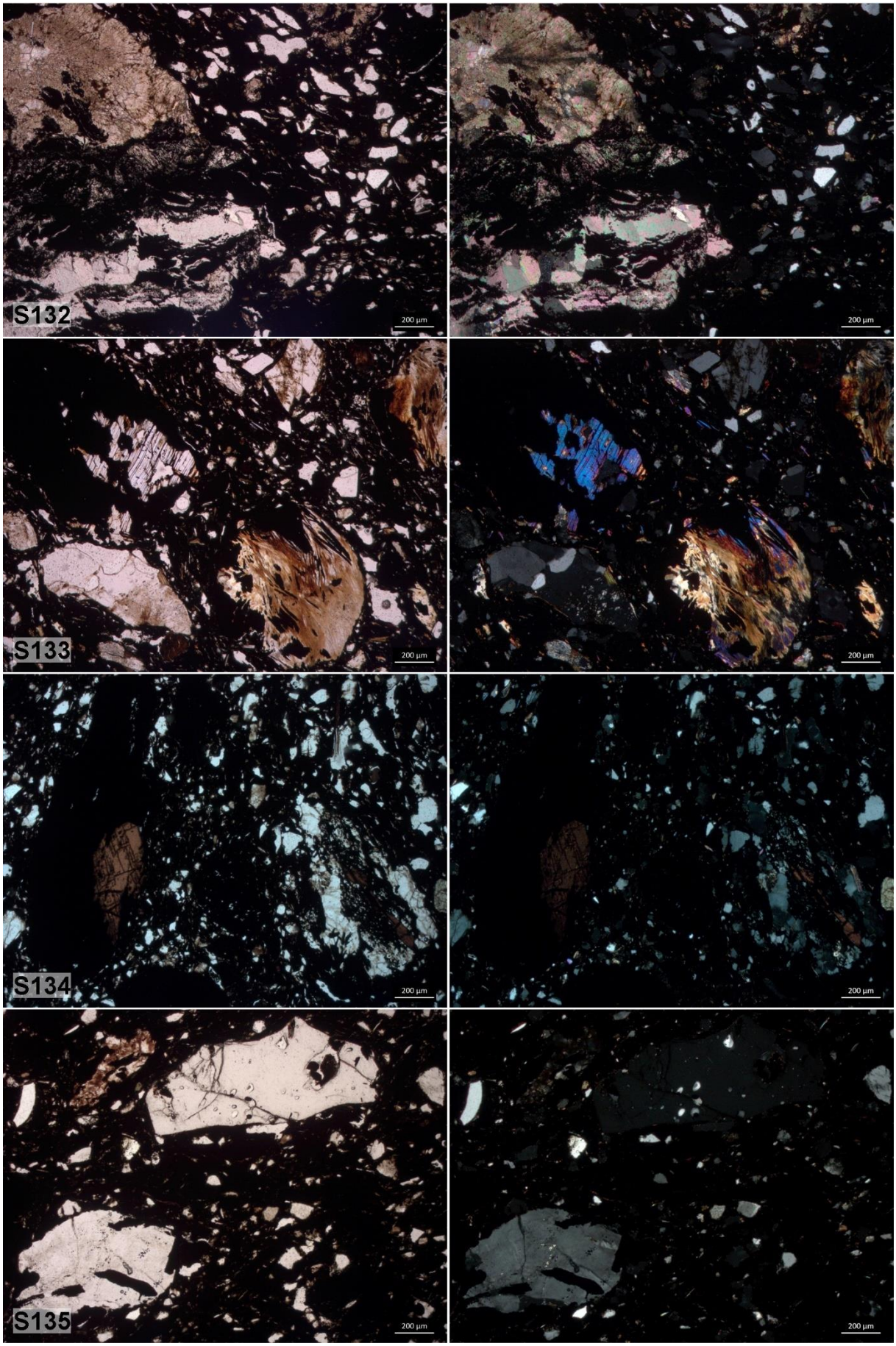

S112
200 µm
200 µm
S113
200 µm
200 µm
S114
200 µm
200 µm
S115
200 µm
200 µm


S116
200 µm
200 µm
S117
200 µm
200 µm
S118
200 µm
200 µm
S119
200 µm
200 µm


S120
200 µm
200 µm
S121
200 µm
200 µm
S122
200 µm
200 µm
S123
200 µm
200 µm

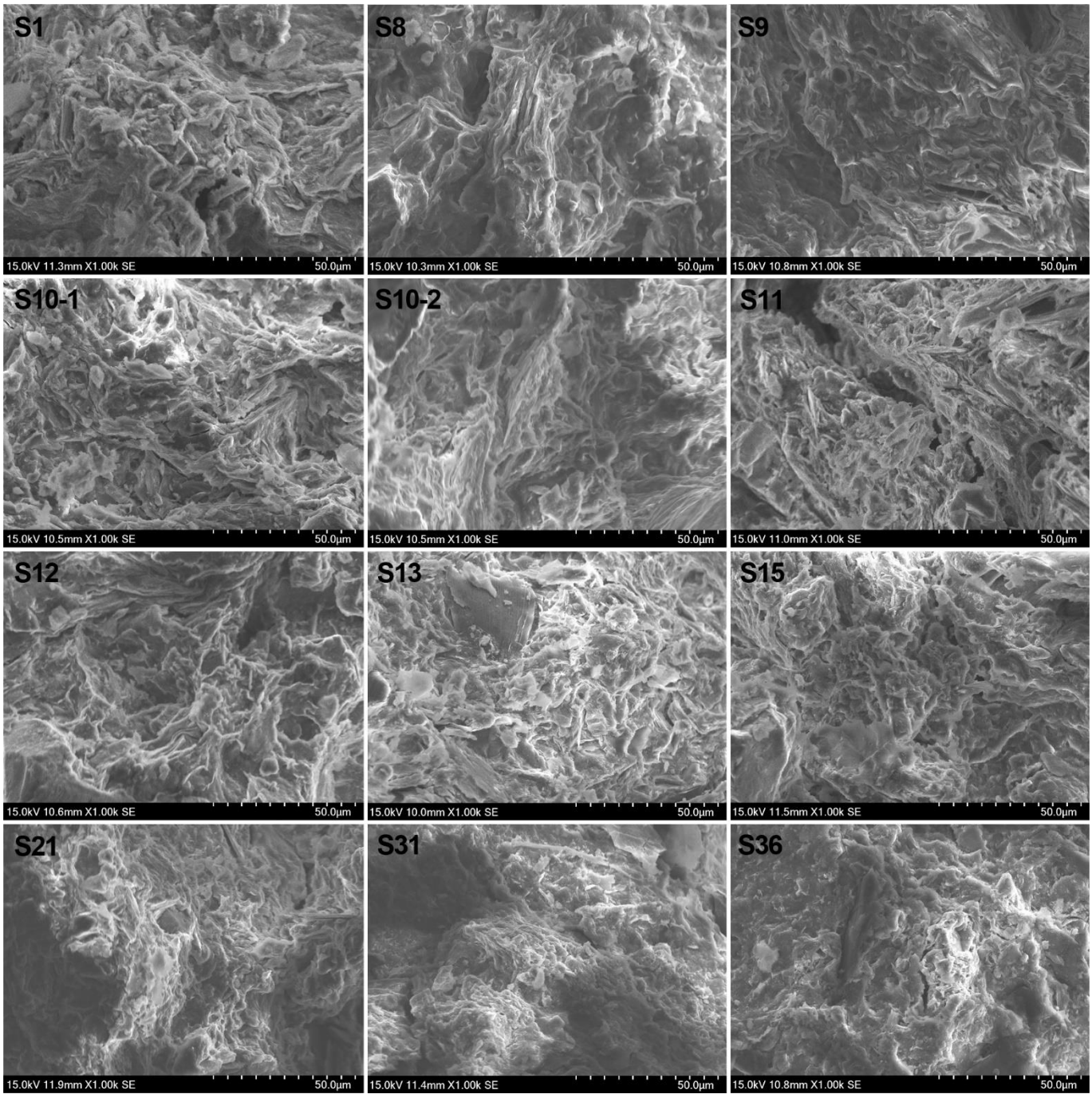

S124
200 µm
200 µm
S125
200 µm
200 µm
S126
200 µm
200 µm
S127
200 µm
200 µm

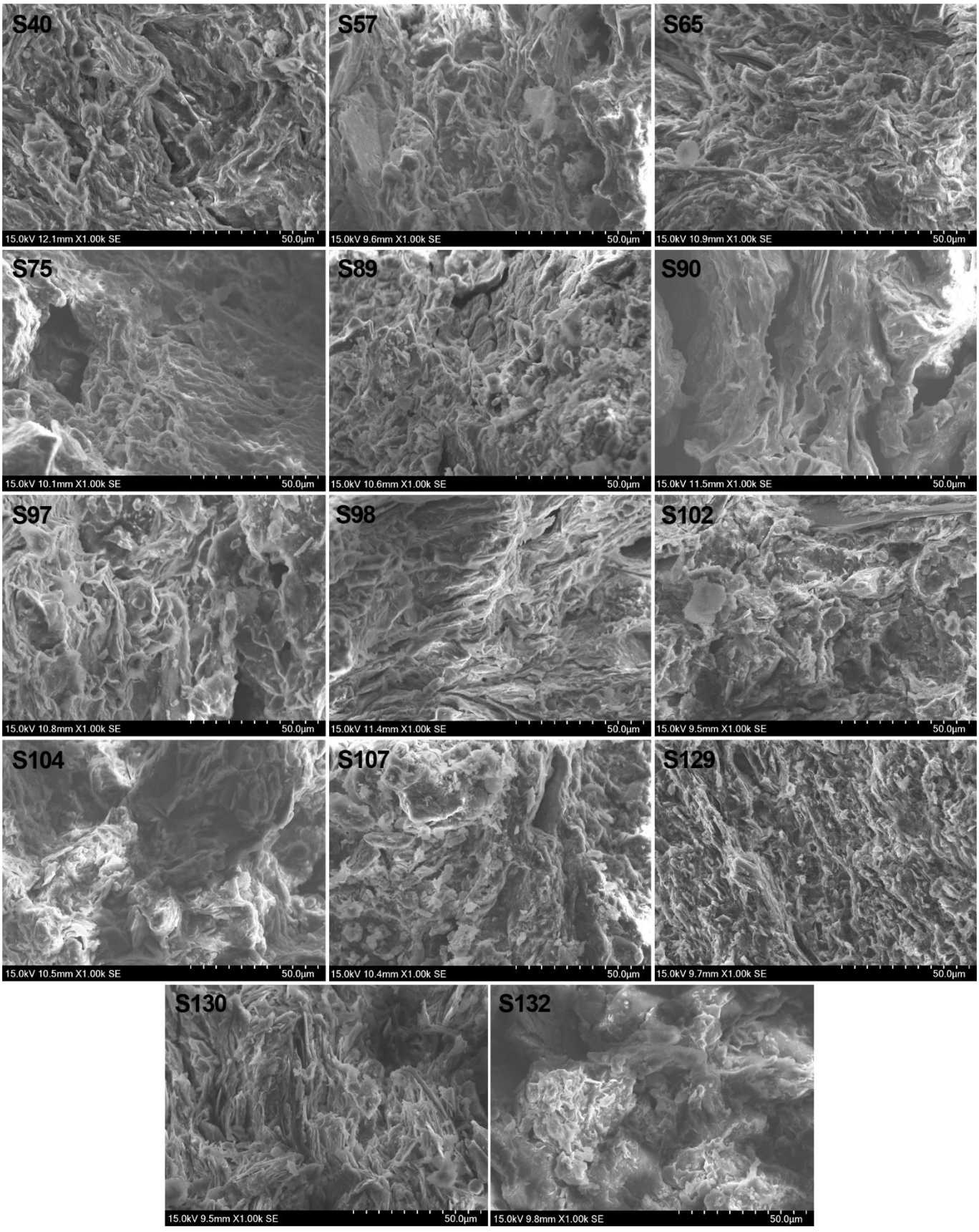

S128
200 µm
200 µm
S129
200 µm
200 µm
S130
200 µm
200 µm
S131
200 µm
200 µm


S132
200 µm
200 µm
S133
200 µm
200 µm
S134
200 µm
200 µm
S135
200 µm
200 µm

Appendix D SEM analysis data of the ceramics

D.1 Secondary electron images of the vitrification structure of the sherds at a magnification of 1000x




S40
15.0kV 12.1mm X1.00k SE
50.0µm
S57
15.0kV 9.6mm X1.00k SE
50.0µm
S65
15.0kV 10.9mm X1.00k SE
50.0µm
S75
15.0kV 10.1mm X1.00k SE
50.0µm
S89
15.0kV 10.6mm X1.00k SE
50.0µm
S90
15.0kV 11.5mm X1.00k SE
50.0µm
S97
15.0kV 10.8mm X1.00k SE
50.0µm
S98
15.0kV 11.4mm X1.00k SE
50.0µm
S102
15.0kV 9.5mm X1.00k SE
50.0µm
S104
15.0kV 10.5mm X1.00k SE
50.0µm
S107
15.0kV 10.4mm X1.00k SE
50.0µm
S129
15.0kV 9.7mm X1.00k SE
50.0µm
S130
15.0kV 9.5mm X1.00k SE
50.0µm
S132
15.0kV 9.8mm X1.00k SE
50.0µm

D.2 Compositional data of the matrix and minerals by SEM-EDS

Matrix

Data of each sample represent the average of three (or more) spot measurements of the matrix.

	Petrographic group	Na_2O (wt%)	MgO (wt%)	Al_2O_3 (wt%)	SiO_2 (wt%)	K_2O (wt%)	CaO (wt%)	TiO_2 (wt%)	MnO (wt%)	Fe_2O_3 (wt%)	P_2O_5 (wt%)	SUM (wt%)
S10	Granitoid A1	1.10	4.17	27.81	47.94	2.97	3.06	1.89	0.29	10.78	0.00	100
S70	Granitoid A1	1.02	4.10	25.85	50.69	1.97	2.22	1.47	0.11	12.58	0.00	100
S88	Granitoid A1	0.72	6.31	25.31	43.91	1.79	4.47	1.88	0.20	14.04	1.37	100.01
S98	Granitoid A1	1.00	5.80	27.08	44.46	2.84	3.33	1.91	0.32	13.27	0.00	99.99
S52	Granitoid A2	5.65	0.96	28.31	57.51	1.54	0.99	0.50	0.10	4.42	0.00	100
S65	Granitoid A2	1.25	2.70	30.01	49.95	3.88	2.36	0.76	0.35	7.76	1.00	99.99
S78	Granitoid A2	0.77	3.96	25.46	49.84	2.29	2.24	2.16	0.16	11.91	1.20	99.99
S40	Granitoid A3	0.65	1.24	36.15	51.33	1.49	2.05	1.20	0.31	5.60	0.00	100
S51	Granitoid A3	0.39	0.85	40.56	49.62	1.37	0.64	1.22	0.12	5.23	0.00	100.00
S12	Granitoid B1	0.57	2.93	31.54	49.50	1.57	2.38	1.32	0.34	9.84	0.00	100
S83	Granitoid B1	2.78	2.09	30.72	51.07	1.98	1.44	0.98	0.14	8.80	0.00	100.00
S9	Granitoid B2	0.82	1.68	26.85	58.35	1.23	2.15	0.68	0.26	7.98	0.00	100
S93	Granitoid B2	0.88	2.93	31.54	46.06	2.33	2.54	1.16	0.12	11.71	0.72	100.00
S45	Granitoid B3	0.41	1.90	35.73	47.47	1.84	1.44	1.26	0.15	9.80	0.00	99.99
S46	Granitoid B3	0.62	1.06	31.51	57.38	1.34	1.96	1.20	0.13	4.80	0.00	99.99
S1	Granitoid C	0.86	3.79	29.55	47.87	2.49	2.81	1.84	0.21	10.58	0.00	100
S87	Granitoid C	0.44	3.01	32.89	47.14	1.89	1.83	1.11	0.11	8.75	2.83	100.00
S5	Granitoid D	0.49	2.74	30.16	52.24	3.63	2.23	0.79	0.13	7.60	0.00	100
S21	Granitoid D	0.49	2.84	30.04	48.96	1.84	2.12	0.70	0.34	12.67	0.00	100.00
S8	Amphibole	3.64	2.68	25.95	52.72	1.41	3.81	1.09	0.34	8.34	0.00	100
S61	Amphibole	0.79	2.89	29.55	44.77	2.58	3.39	0.74	0.08	11.51	3.71	100
S90	Amphibole	0.69	4.00	30.97	48.70	1.05	1.79	0.94	0.35	11.50	0.00	100.00
S11	Diorite A	1.25	4.45	24.06	53.29	2.54	2.82	1.36	0.37	9.86	0.00	100
S75	Diorite A	5.01	3.77	21.63	56.26	2.85	2.90	0.90	0.44	6.24	0.00	100
S67	Diorite B	1.97	4.21	27.94	42.83	2.14	3.60	2.38	0.14	11.37	3.43	100
S97	Diorite B	1.28	9.11	26.06	41.88	2.46	2.94	1.07	0.21	15.02	0.00	100.01
S57	Carbonate A	0.60	1.82	26.67	57.43	1.96	2.89	0.74	0.13	6.41	1.34	100
S58	Carbonate A	0.83	1.73	27.54	58.73	2.62	2.51	1.03	0.14	4.68	0.21	100.00
S89	Carbonate B	0.70	1.69	30.32	45.02	3.32	6.29	1.04	0.26	9.50	1.85	100
S102	Graphite A1	0.79	1.69	30.70	53.49	2.41	3.16	0.50	0.21	7.05	0.00	100
S103	Graphite A1	5.42	1.44	20.39	64.62	1.98	1.41	0.40	0.10	4.22	0.00	99.99
S110	Graphite A1	0.69	2.12	28.02	53.82	5.85	1.20	0.30	0.21	7.75	0.00	99.96
S100	Graphite A2	0.73	3.58	21.33	60.29	2.31	3.19	1.02	0.15	7.43	0.00	100
S104	Graphite A2	3.39	2.99	23.13	54.77	3.28	2.09	2.07	0.21	8.07	0.00	100.01
S32	Graphite A3	1.00	1.99	20.66	63.40	3.03	2.52	0.88	0.17	5.48	0.86	100
S36	Graphite A3	1.53	2.22	23.06	54.22	3.08	1.73	0.81	0.37	11.26	1.73	100
S86	Graphite A3	0.72	1.18	32.53	51.58	4.72	1.31	1.33	0.17	6.45	0.00	100.00
S107	Graphite A3	0.45	4.31	27.55	52.96	2.13	2.74	0.57	0.22	9.07	0.00	100.01
S31	Graphite A4	1.73	1.46	35.18	48.86	1.46	2.79	0.76	0.25	7.53	0.00	100
S128	Graphite A4	0.97	3.00	23.53	55.09	2.86	1.96	0.96	0.19	10.89	0.00	99.44
S35	Graphite A5	0.82	3.27	21.71	55.69	3.59	3.65	0.49	0.10	8.13	2.55	100.00
S108	Graphite A5	0.31	2.75	23.75	52.36	1.94	2.62	0.45	0.18	14.46	1.17	99.99
S109	Graphite A5	0.98	1.70	23.50	60.62	5.69	1.10	0.53	0.24	5.62	0.00	99.99
S130	Graphite B	0.61	2.21	26.49	58.22	6.85	1.26	0.47	0.25	3.65	0.00	100
S132	Graphite C1	1.07	2.01	28.76	47.34	4.20	4.21	1.58	0.36	9.59	0.88	100
S129	Graphite C2	0.49	1.70	29.64	50.42	2.75	3.18	1.08	0.62	10.11	0.00	100
S13	Graphite D	0.86	5.51	24.20	50.22	1.96	2.25	0.96	0.25	13.78	0.00	100
S54	Graphite D	1.11	1.62	39.77	47.24	1.83	0.99	0.90	0.15	6.38	0.00	100.00
S15	Individual sample	0.89	2.05	31.91	49.15	1.45	2.61	0.54	0.30	11.11	0.00	100

Feldspar

	Petrographic group	Identification	Na_2O (wt%)	MgO (wt%)	Al_2O_3 (wt%)	SiO_2 (wt%)	K_2O (wt%)	CaO (wt%)	TiO_2 (wt%)	MnO (wt%)	Fe_2O_3 (wt%)	P_2O_5 (wt%)	BaO (wt%)	Cl_2O (wt%)	OsO (wt%)	SUM (wt%)	Ab mol%	An mol%	Or mol%
S10	Granitoid A1	Plagioclase (andesine)	8.76	0.45	26.5	55.1	0.49	7.52	0.42	0.25	0.5					99.99	66.17	31.39	2.44
S70	Granitoid A1	Plagioclase (oligoclase)	9.09	0.58	25.33	56.51	0.81	6.5	0.25	0.14	0.8					100.01	68.79	27.18	4.03
S70	Granitoid A1	Alkali feldspar	6.5	0.47	20.64	61.86	8.74	0.79	0.25	0.1	0.65					100	51.23	3.44	45.32
S70	Granitoid A1	Potassium feldspar (orthoclase)	1.91	0.3	20.17	62.03	14.29	0.36	0.44	0.12	0.37					99.99	16.59	1.73	81.68
S70	Granitoid A1	Potassium feldspar (orthoclase)	1.26	0.39	19.76	62.12	15.29	0.31	0.23	0.09	0.56					100.01	10.97	1.49	87.54
S70	Granitoid A1	Potassium feldspar (orthoclase)	1.31	0.5	19.98	61.6	14.95	0.41	0.37	0.13	0.77					100.02	11.52	1.99	86.49
S70	Granitoid A1	Plagioclase (andesine)	7.07	0.56	28.41	52.99	1.13	8.32	0.22	0.16	0.55	0.59				100	56.97	37.04	5.99
S88	Granitoid A1	Potassium feldspar (orthoclase)	1.67	0.29	20.04	61.85	14.75	0.38	0.57	0.11	0.35					100.01	14.42	1.81	83.77
S88	Granitoid A1	Potassium feldspar (orthoclase)	1.4	0.32	19.84	61.89	15.05	0.33	0.35	0.08	0.73					99.99	12.19	1.59	86.22
S88	Granitoid A1	Potassium feldspar (orthoclase)	1.32	0.47	20.09	61.38	14.77	0.47	0.57	0.09	0.83					99.99	11.68	2.30	86.02
S88	Granitoid A1	Alkali feldspar (anorthoclase)	10.77	0.44	23.38	61.21	2.33	1.15	0.22	0.08	0.43					100.01	83.24	4.91	11.85
S88	Granitoid A1	Plagioclase (andesine)	7.77	0.51	27.19	54.2	0.77	7.9	0.25	0.14	1.27					100	61.46	34.53	4.01
S88	Granitoid A1	Plagioclase (andesine)	7.53	0.85	26.89	53.01	0.99	8.48	0.55	0.2	1.5					100	58.52	36.42	5.06
S88	Granitoid A1	Alkali feldspar	7.41	0.43	20.54	62.3	7.58	0.88	0.26	0.08	0.53					100.01	57.52	3.77	38.71
S98	Granitoid A1	Potassium feldspar (orthoclase)	1.7	0.51	20.01	60.87	14.89	0.45	0.48	0.35	0.75					100.01	14.47	2.12	83.41
S98	Granitoid A1	Potassium feldspar (orthoclase)	1	0.41	19.76	61.65	15.13	0.36	0.8	0.25	0.63					99.99	8.97	1.78	89.25
S98	Granitoid A1	Plagioclase (andesine)	7.29	0.64	26.94	53.72	1.56	8.15	0.44	0.37	0.9					100.01	56.86	35.13	8.01
S98	Granitoid A1	Plagioclase (andesine)	8.24	0.36	26.89	54.57	0.34	8.49	0.3	0.32	0.49					100	62.64	35.66	1.70
S52	Granitoid A2	Potassium feldspar (orthoclase)	0.54	0.15	19.88	62.56	16.17	0.15	0.26	0.06	0.23					100	4.80	0.74	94.47
S52	Granitoid A2	Potassium feldspar (orthoclase)	0.75	0.23	20.3	61.98	15.37	0.15	0.52	0.13	0.57					100	6.85	0.76	92.39
S52	Granitoid A2	Potassium feldspar (orthoclase)	1.66	0.29	20.04	62.2	14.77	0.24	0.42	0.1	0.29					100.01	14.42	1.15	84.43
S52	Granitoid A2	Potassium feldspar (orthoclase)	1.43	0.29	20.18	62.29	14.73	0.27	0.27	0.1	0.43					99.99	12.69	1.32	85.99
S52	Granitoid A2	Potassium feldspar (orthoclase)	1.12	0.29	20.18	62.48	14.9	0.2	0.29	0.09	0.44					99.99	10.15	1.00	88.85
S65	Granitoid A2	Potassium feldspar (orthoclase)	2.02	0.61	19.99	61.06	13.86	0.48	0.78	0.35	0.86					100.01	17.71	2.33	79.96
S65	Granitoid A2	Potassium feldspar (orthoclase)	2.23	0.59	19.92	61.44	13.47	0.55	0.7	0.39	0.73					100.02	19.57	2.67	77.77
S65	Granitoid A2	Alkali feldspar (anorthoclase)	11.26	0.42	20.99	62.71	2.83	0.51	0.33	0.34	0.61					100	84.01	2.10	13.89
S78	Granitoid A2	Potassium feldspar (orthoclase)	1.27	1.01	19.96	60.82	14.15	0.46	0.51	0.11	1.72					100.01	11.72	2.35	85.93
S78	Granitoid A2	Potassium feldspar (orthoclase)	0.98	0.43	20.09	61.71	14.92	0.31	0.46	0.14	0.97					100.01	8.94	1.56	89.50
S78	Granitoid A2	Potassium feldspar (orthoclase)	1.4	0.34	19.75	62.16	14.65	0.34	0.57	0.09	0.7					100	12.47	1.67	85.86
S78	Granitoid A2	Alkali feldspar (anorthoclase)	11.08	0.35	21.09	62.36	3.32	1.08	0.21	0.1	0.41					100	79.94	4.31	15.76
S78	Granitoid A2	Plagioclase (albite)	12.28	0.32	21.58	63.49	0.38	1.54	0.08	0	0.33					100	91.77	6.36	1.87
S78	Granitoid A2	Alkali feldspar	8.36	0.39	20.49	62.6	6.8	0.5	0.22	0.08	0.55					99.99	63.77	2.11	34.13
S78	Granitoid A2	Plagioclase (oligoclase)	12.14	0.45	19.57	59.3	1.09	3.94	0.22	0.13	0.71	2.46				100.01	80.75	14.48	4.77

	Petrographic group	Identification	Na_2O (wt%)	MgO (wt%)	Al_2O_3 (wt%)	SiO_2 (wt%)	K_2O (wt%)	CaO (wt%)	TiO_2 (wt%)	MnO (wt%)	Fe_2O_3 (wt%)	P_2O_5 (wt%)	BaO (wt%)	Cl_2O (wt%)	OsO (wt%)	SUM (wt%)	Ab mol%	An mol%	Or mol%
S40	Granitoid A3	Potassium feldspar (orthoclase)	2.59	0.35	20.41	61.56	13.1	0.35	0.8	0.41	0.44					100.01	22.71	1.70	75.59
S40	Granitoid A3	Plagioclase (andesine)	7.48	0.51	27.62	52.84	0.88	9.22	0.35	0.44	0.66					100	56.87	38.73	4.40
S51	Granitoid A3	Potassium feldspar (orthoclase)	1.21	0.26	20.07	62.04	15.49	0.13	0.33	0.13	0.33					99.99	10.55	0.63	88.83
S51	Granitoid A3	Potassium feldspar (orthoclase)	2.08	0.22	19.53	63.72	13.56	0.21	0.2	0.1	0.38					100	18.71	1.04	80.25
S51	Granitoid A3	Potassium feldspar (orthoclase)	2.12	0.36	20.15	62.04	14.11	0.3	0.28	0.11	0.53					100	18.32	1.43	80.24
S51	Granitoid A3	Plagioclase (oligoclase)	9.86	0.35	25.23	57.77	0.48	5.25	0.18	0.13	0.76					100.01	75.40	22.19	2.41
S51	Granitoid A3	Plagioclase (oligoclase)	9.11	0.41	26.43	56.08	0.58	6.58	0.23	0.12	0.45					99.99	69.40	27.70	2.91
S51	Granitoid A3	Potassium feldspar (orthoclase)	2.43	0.34	20.33	62.1	13.68	0.18	0.57	0.09	0.28					100	21.08	0.86	78.06
S51	Granitoid A3	Plagioclase (oligoclase)	9.58	0.41	25.56	56.9	0.61	6.31	0.2	0.14	0.31					100.02	71.13	25.89	2.98
S51	Granitoid A3	Plagioclase (oligoclase)	11.81	0.27	22.65	61.66	0.65	2.71	0.1	0.03	0.13					100.01	85.98	10.90	3.11
S51	Granitoid A3	Plagioclase (oligoclase)	9.87	0.42	25.76	57.03	0.59	5.54	0.23	0.13	0.44					100.01	74.10	22.98	2.91
S12	Granitoid B1	Potassium feldspar (orthoclase)	2.27	0.45	20.43	61.44	13.61	0.32	0.55	0.26	0.67					100	19.91	1.55	78.54
S12	Granitoid B1	Plagioclase (oligoclase)	9.92	0.4	24.04	58.88	0.5	4.75	0.45	0.3	0.77					100.01	77.06	20.39	2.56
S83	Granitoid B1	Plagioclase (albite)	12.33	0.4	21.57	62.72	0.5	0.73	0.19	0.13	1.43					100	94.39	3.09	2.52
S83	Granitoid B1	Potassium feldspar (orthoclase)	1.2	0.3	20.12	62.22	15.03	0.16	0.31	0.08	0.59					100.01	10.74	0.79	88.47
S83	Granitoid B1	Potassium feldspar (orthoclase)	1.79	0.31	21.82	61.4	12.98	0.18	0.37	0.1	1.04					99.99	17.16	0.95	81.88
S83	Granitoid B1	Potassium feldspar (orthoclase)	1.63	0.31	20.01	62.25	14.55	0.18	0.54	0.09	0.44					100	14.42	0.88	84.70
S83	Granitoid B1	Potassium feldspar (orthoclase)	0.72	0.4	22.28	60.72	14.39	0.26	0.36	0.11	0.75					99.99	6.97	1.39	91.64
S83	Granitoid B1	Potassium feldspar (orthoclase)	1.84	0.29	20.2	62.43	14.06	0.2	0.25	0.07	0.66					100	16.43	0.99	82.59
S83	Granitoid B1	Potassium feldspar (orthoclase)	0.94	0.4	20.02	62.19	14.84	0.24	0.56	0.09	0.72					100	8.67	1.22	90.10
S83	Granitoid B1	Plagioclase (oligoclase)	11.23	0.41	23.26	60.16	0.66	3.39	0.19	0.1	0.59					99.99	82.95	13.84	3.21
S83	Granitoid B1	Plagioclase (oligoclase)	11.04	0.42	23.41	61.43	0.65	2.47	0.09	0	0.49					100	86.03	10.64	3.33
S9	Granitoid B2	Potassium feldspar (orthoclase)	1.21	0.4	19.68	62.16	14.74	0.24	0.54	0.35	0.69					100.01	10.96	1.20	87.84
S9	Granitoid B2	Plagioclase (albite)	12.73	0.37	21.07	63.36	0.84	0.63	0.25	0.3	0.45					100	93.39	2.55	4.05
S93	Granitoid B2	Plagioclase (oligoclase)	8.54	0.55	25.81	56.74	0.84	6.16	0.23	0.12	1.01					100	68.34	27.24	4.42
S93	Granitoid B2	Plagioclase (andesine)	7.26	0.44	26.79	56.31	0.82	6.34	0.21	0.12	1.71					100	64.23	31.00	4.77
S93	Granitoid B2	Plagioclase (oligoclase)	8.39	0.42	24.73	57.98	1.42	6.06	0.2	0.11	0.7					100.01	66.20	26.42	7.37
S93	Granitoid B2	Potassium feldspar (orthoclase)	1.56	0.46	20.16	61.98	14.34	0.34	0.23	0.14	0.8					100.01	13.95	1.68	84.37
S93	Granitoid B2	Plagioclase (oligoclase)	9.16	0.54	25.67	56.23	0.67	6.59	0.26	0.14	0.75					100.01	69.17	27.50	3.33
S93	Granitoid B2	Plagioclase (oligoclase)	9.29	0.45	24.79	57.69	0.69	6.03	0.24	0.12	0.71					100.01	71.05	25.48	3.47
S93	Granitoid B2	Plagioclase (oligoclase)	9.17	0.46	25.55	56.49	0.72	6.59	0.26	0.15	0.62					100.01	69.02	27.41	3.57
S93	Granitoid B2	Plagioclase (oligoclase)	9.33	0.4	25.58	57.51	0.57	6.19	0.09	0	0.32					99.99	71.08	26.06	2.86
S93	Granitoid B2	Plagioclase (oligoclase)	9.29	0.43	24.94	57.43	0.68	6.2	0.22	0.13	0.69					100.01	70.57	26.03	3.40
S93	Granitoid B2	Potassium feldspar (orthoclase)	0.76	0.24	19.16	63.76	14.52	0.51	0.41	0.11	0.53					100	7.17	2.66	90.17
S45	Granitoid B3	Potassium feldspar (orthoclase)	1.47	0.25	20.33	62.08	14.81	0.17	0.24	0.1	0.56					100.01	13.00	0.83	86.17

	Petrographic group	Identification	Na_2O (wt%)	MgO (wt%)	Al_2O_3 (wt%)	SiO_2 (wt%)	K_2O (wt%)	CaO (wt%)	TiO_2 (wt%)	MnO (wt%)	Fe_2O_3 (wt%)	P_2O_5 (wt%)	BaO (wt%)	Cl_2O (wt%)	OsO (wt%)	SUM (wt%)	Ab mol%	An mol%	Or mol%
S45	Granitoid B3	Plagioclase (oligoclase)	10.36	0.33	24.21	58.94	0.62	4.86	0.16	0.16	0.37					100.01	77.01	19.96	3.03
S45	Granitoid B3	Alkali feldspar (anorthoclase)	8.68	0.83	26.78	58.89	2.44	0.6	0.2	0.13	1.45					100	81.76	3.12	15.12
S45	Granitoid B3	Plagioclase (oligoclase)	8.69	0.46	25.23	57.3	1.77	5.59	0.21	0.21	0.54					100	67.14	23.87	9.00
S45	Granitoid B3	Alkali feldspar	3.55	0.42	22.37	60.59	9.85	0.46	0.25	0.08	2.42					99.99	34.52	2.47	63.01
S46	Granitoid B3	Plagioclase (oligoclase)	10.7	0.43	24.64	58.69	0.58	4.44	0.15	0.12	0.24					99.99	79.05	18.13	2.82
S46	Granitoid B3	Plagioclase (oligoclase)	10.09	0.31	24.63	59.1	0.55	4.68	0.21	0.12	0.31					100	77.39	19.84	2.78
S46	Granitoid B3	Plagioclase (oligoclase)	8.68	0.36	26.36	57.17	0.52	6.67	0.08	0.01	0.16					100.01	68.30	29.00	2.69
S46	Granitoid B3	Potassium feldspar (orthoclase)	1.92	0.32	20.36	62.29	14.16	0.26	0.27	0.11	0.31					100	16.87	1.26	81.87
S46	Granitoid B3	Potassium feldspar (orthoclase)	0.97	0.31	20.33	62.46	14.85	0.23	0.38	0.09	0.37					99.99	8.93	1.17	89.90
S46	Granitoid B3	Alkali feldspar	3.75	0.57	22.09	59.35	10.31	1.24	0.31	0.14	2.25					100.01	33.43	6.11	60.46
S46	Granitoid B3	Plagioclase (oligoclase)	9.29	0.41	25.75	56.84	0.61	6.07	0.25	0.13	0.65					100	71.21	25.71	3.08
S1	Granitoid C	Potassium feldspar	1.6	0.49	20.04	61.89	14.39	0.26	0.51	0.24	0.57					99.99	14.27	1.28	84.45
S1	Granitoid C	Plagioclase (oligoclase)	9.61	0.68	25.33	56.21	0.74	5.7	0.38	0.3	1.07					100.02	72.55	23.78	3.68
S87	Granitoid C	Potassium feldspar	1.99	0.35	19.93	62.06	14.78	0.3	0.29	0.09	0.23					100.02	16.75	1.40	81.85
S87	Granitoid C	Potassium feldspar	2.77	0.44	19.93	62.1	13.71	0.28	0.29	0.11	0.37					100	23.19	1.30	75.51
S87	Granitoid C	Potassium feldspar	1.89	0.37	19.97	62.34	14.66	0.25	0.29	0.06	0.17					100	16.19	1.18	82.63
S87	Granitoid C	Plagioclase (andesine)	8.59	0.66	26.57	54.42	0.55	7.63	0.32	0.2	1.06					100	65.23	32.02	2.75
S87	Granitoid C	Plagioclase (oligoclase)	9.21	0.74	25.93	55.48	0.65	6.51	0.27	0.14	1.06					99.99	69.59	27.18	3.23
S87	Granitoid C	Plagioclase (andesine)	7.55	0.83	27.17	54.04	0.66	6.72	0.3	0.08	2.65					100	64.54	31.75	3.71
S21	Granitoid D	Potassium feldspar (orthoclase)	1.47	0.58	20.02	61.78	14.67	0.3	0.3	0.35	0.53					100	13.02	1.47	85.51
S5	Granitoid D	Potassium feldspar (microcline)	1.22	0.32	20.25	62.04	15.41	0.18	0.29	0.1	0.19					100	10.65	0.87	88.48
S5	Granitoid D	Potassium feldspar (microcline)	1	0.29	19.86	62.63	15.55	0.15	0.2	0.07	0.25					100	8.84	0.73	90.43
S5	Granitoid D	Potassium feldspar (microcline)	1.22	0.41	20.39	61.76	15.3	0.18	0.21	0.14	0.4					100.01	10.72	0.87	88.41
S5	Granitoid D	Potassium feldspar (microcline)	0.94	0.25	20.15	62.42	15.65	0.13	0.08	0.1	0.28					100	8.31	0.64	91.05
S5	Granitoid D	Potassium feldspar (microcline)	1.15	0.38	20.36	61.93	15.48	0.13	0.17	0.14	0.26					100	10.08	0.63	89.29
S5	Granitoid D	Potassium feldspar (microcline)	1.07	0.38	20.06	62.21	15.42	0.21	0.24	0.09	0.32					100	9.44	1.02	89.53
S61	Amphibole	Plagioclase (oligoclase)	9.65	0.34	25.14	57.9	0.46	6.18	0.1	0	0.23					100	72.19	25.55	2.26
S61	Amphibole	Plagioclase (andesine)	7.84	0.51	28.1	52.97	0.36	9.38	0.18	0.12	0.55					100.01	59.12	39.09	1.79
S61	Amphibole	Plagioclase (andesine)	8.91	0.47	25.88	56.13	0.32	7.44	0.17	0.13	0.55					100	67.34	31.07	1.59
S61	Amphibole	Plagioclase (andesine)	8.37	0.49	26.64	55.18	0.28	8.23	0.21	0.13	0.47					100	63.88	34.71	1.41
S61	Amphibole	Plagioclase (andesine)	8.47	0.46	25.4	56.93	0.31	7.44	0.22	0.15	0.62					100	66.25	32.16	1.60
S61	Amphibole	Plagioclase (andesine)	9.12	0.38	26.47	55.56	0.19	7.59	0.14	0.13	0.42					100	67.86	31.21	0.93
S61	Amphibole	Plagioclase (andesine)	8.49	0.4	25.88	56.93	0.24	7.73	0.08	0.01	0.23					99.99	65.71	33.06	1.22
S8	Amphibole	Potassium feldspar (orthoclase)	1.68	0.38	20.06	61.82	14.55	0.25	0.52	0.3	0.44					100	14.75	1.21	84.04
S8	Amphibole	Plagioclase (andesine)	7.06	0.52	27.64	52.65	0.37	9.16	0.32	0.3	1.98					100	57.10	40.94	1.97

	Petrographic group	Identification	Na_2O (wt%)	MgO (wt%)	Al_2O_3 (wt%)	SiO_2 (wt%)	K_2O (wt%)	CaO (wt%)	TiO_2 (wt%)	MnO (wt%)	Fe_2O_3 (wt%)	P_2O_5 (wt%)	BaO (wt%)	Cl_2O (wt%)	OsO (wt%)	SUM (wt%)	Ab mol%	An mol%	Or mol%
S8	Amphibole	Plagioclase (oligoclase)	8.31	0.78	24.76	56.66	2.04	5.37	0.46	0.4	1.22					100	65.85	23.51	10.64
S8	Amphibole	Plagioclase (oligoclase)	9.12	0.49	24.91	57.4	0.53	5.91	0.33	0.31	1					100	71.62	25.65	2.74
S8	Amphibole	Plagioclase (oligoclase)	9.46	0.41	25.18	57.26	0.6	6.1	0.25	0.33	0.4					99.99	71.53	25.49	2.98
S8	Amphibole	Plagioclase (andesine)	7.59	0.53	27.67	53.14	0.34	9.52	0.3	0.23	0.69					100.01	58.05	40.24	1.71
S90	Amphibole	Plagioclase (andesine)	8.43	0.47	26.78	54.7	0.36	8.14	0.3	0.37	0.46					100.01	64.03	34.17	1.80
S90	Amphibole	Plagioclase (andesine)	8.26	0.67	27.13	53.35	0.28	8.77	0.35	0.38	0.8					99.99	62.15	36.46	1.39
S90	Amphibole	Plagioclase (andesine)	8.23	0.79	26.7	54.72	0.39	8.32	0.27	0.24	0.34					100	62.90	35.14	1.96
S90	Amphibole	Plagioclase (andesine)	7.77	0.64	26.87	54.22	0.55	7.86	0.41	0.42	1.25					99.99	62.28	34.82	2.90
S11	Diorite A	Alkali feldspar	4.26	1.15	26.02	56.01	8.33	1.24	1.19	0.29	1.5					99.99	40.86	6.57	52.57
S11	Diorite A	Plagioclase (oligoclase)	9.65	1	22.34	59.39	1.93	3.23	0.46	0.25	1.75					100	75.96	14.05	9.99
S11	Diorite A	Alkali feldspar (anorthoclase)	8.59	0.51	24.69	58.57	3.99	1.73	0.68	0.22	1.02					100	70.58	7.85	21.57
S11	Diorite A	Alkali feldspar (anorthoclase)	10.02	0.62	22.76	60.84	3.17	0.92	0.63	0.35	0.69					100	79.44	4.03	16.53
S75	Diorite A	Potassium feldspar (orthoclase)	0.84	0.76	19.78	61.35	14.52	0.57	1.08	0.28	0.81					99.99	7.84	2.94	89.21
S75	Diorite A	Potassium feldspar (orthoclase)	0.99	0.98	19.84	60.2	13.9	0.88	1.77	0.44	1.01					100.01	9.32	4.58	86.10
S67	Diorite B	Plagioclase (oligoclase)	9.11	0.49	25.23	56.76	0.99	6.62	0.22	0.13	0.46					100.01	67.89	27.26	4.85
S67	Diorite B	Plagioclase (andesine)	8.02	0.47	25.97	54.91	1.4	8.4	0.15	0.12	0.56					100	59.04	34.17	6.78
S67	Diorite B	Plagioclase (oligoclase)	10.26	0.51	23.98	58.64	0.74	5.14	0.19	0.13	0.41					100	75.51	20.90	3.58
S67	Diorite B	Potassium feldspar (orthoclase)	1.14	0.32	19.6	62.66	15.23	0.37	0.24	0.09	0.36					100.01	10.03	1.80	88.17
S67	Diorite B	Potassium feldspar (orthoclase)	1.72	0.25	19.75	62.06	14.07	0.46	1.09	0.11	0.49					100	15.31	2.26	82.42
S67	Diorite B	Potassium feldspar (orthoclase)	1.92	0.26	19.49	62.55	14.43	0.51	0.46	0.1	0.29					100.01	16.42	2.41	81.17
S67	Diorite B	Potassium feldspar (orthoclase)	1.38	0.29	19.54	62.69	15.21	0.31	0.14	0.12	0.33					100.01	11.94	1.48	86.58
S67	Diorite B	Plagioclase (andesine)	7.53	0.61	25.93	54.59	0.86	7.64	0.31	0.18	1.73	0.61				99.99	61.13	34.27	4.59
S67	Diorite B	Plagioclase (andesine)	7.58	0.49	25.94	55.3	1.31	6.12	0.21	0.09	2.34	0.62				100	64.11	28.60	7.29
S67	Diorite B	Plagioclase (andesine)	7.32	0.59	27.1	54.37	1.5	7.76	0.23	0.16	0.95					99.98	58.12	34.05	7.84
S97	Diorite B	Potassium feldspar (orthoclase)	1.35	0.4	19.08	63.15	14.99	0.3	0.23	0.19	0.31					100	11.86	1.46	86.68
S97	Diorite B	Plagioclase (oligoclase)	10.34	0.46	23.52	58.94	0.78	5.01	0.2	0.24	0.5					99.99	75.91	20.32	3.77
S97	Diorite B	Plagioclase (oligoclase)	10.83	0.82	24.1	57.78	0.35	4.95	0.15	0.08	0.94					100	78.50	19.83	1.67
S97	Diorite B	Potassium feldspar (orthoclase)	0.98	0.51	18.47	64.09	14.61	0.45	0.27	0.13	0.48					99.99	9.04	2.29	88.67
S97	Diorite B	Potassium feldspar (orthoclase)	1.07	0.49	18.59	64	14.54	0.41	0.28	0.21	0.41					100	9.85	2.09	88.06
S57	Carbonate A	Plagioclase (oligoclase)	8.11	3.08	26.14	51.97	2.29	6.5	0.35	0.24	0.35					99.03	61.40	27.19	11.41
S102	Graphite A1	Plagioclase (oligoclase)	11.64	0.36	23.51	60.06	0.34	3.69	0.16	0.08	0.18					100.02	83.72	14.67	1.61
S102	Graphite A1	Potassium feldspar (orthoclase)	2.78	0.54	20.33	61.71	13.19	0.48	0.3	0.25	0.41					99.99	23.71	2.26	74.02
S102	Graphite A1	Plagioclase (oligoclase)	11.75	0.4	23.52	59.46	0.49	3.55	0.23	0.25	0.35					100	83.72	13.98	2.30
S102	Graphite A1	Potassium feldspar (orthoclase)	2.55	0.47	20.18	61.95	13.58	0.38	0.29	0.19	0.4					99.99	21.80	1.80	76.40
S102	Graphite A1	Potassium feldspar (orthoclase)	2.16	0.36	20.16	62.45	13.99	0.26	0.2	0.14	0.27					99.99	18.77	1.25	79.98

	Petrographic group	Identification	Na_2O (wt%)	MgO (wt%)	Al_2O_3 (wt%)	SiO_2 (wt%)	K_2O (wt%)	CaO (wt%)	TiO_2 (wt%)	MnO (wt%)	Fe_2O_3 (wt%)	P_2O_5 (wt%)	BaO (wt%)	Cl_2O (wt%)	OsO (wt%)	SUM (wt%)	Ab mol%	An mol%	Or mol%
S102	Graphite A1	Potassium feldspar (orthoclase)	2.72	0.36	20.17	62.44	13.12	0.33	0.33	0.15	0.39					100.01	23.58	1.58	74.84
S102	Graphite A1	Plagioclase (albite)	11.95	0.39	21.84	62.12	0.62	2.12	0.21	0.18	0.56					99.99	88.33	8.66	3.02
S103	Graphite A1	Potassium feldspar (orthoclase)	2.93	0.35	20.22	62.25	13.32	0.26	0.18	0.13	0.37					100.01	24.75	1.21	74.03
S103	Graphite A1	Potassium feldspar (orthoclase)	2.5	0.42	20.03	62.18	13.81	0.35	0.21	0.16	0.32					99.98	21.22	1.64	77.13
S103	Graphite A1	Potassium feldspar (orthoclase)	2.55	0.47	20.21	61.92	13.83	0.36	0.22	0.13	0.31					100	21.52	1.68	76.80
S103	Graphite A1	Plagioclase (oligoclase)	11.32	0.44	23.01	59.22	0.96	3.96	0.19	0.17	0.31			0.44		100.02	80.06	15.48	4.47
S110	Graphite A1	Potassium feldspar (orthoclase)	1.87	0.35	19.96	62.21	14.46	0.25	0.19	0.07	0.65					100.01	16.23	1.20	82.57
S110	Graphite A1	Potassium feldspar (orthoclase)	1.6	0.46	20.12	61.73	14.74	0.31	0.2	0.11	0.73					100	13.95	1.49	84.56
S100	Graphite A2	Plagioclase (oligoclase)	9.1	0.47	25.25	57.05	0.7	6.58	0.2	0.14	0.51					100	68.96	27.55	3.49
S100	Graphite A2	Potassium feldspar (orthoclase)	1.87	0.32	19.94	62.31	14.77	0.24	0.26	0.08	0.22					100.01	15.96	1.13	82.91
S100	Graphite A2	Plagioclase (albite)	12.55	0.44	22.63	61.71	0.77	1.36	0.11	0.09	0.35					100.01	90.89	5.44	3.67
S100	Graphite A2	Plagioclase (oligoclase)	10.22	0.35	24.85	58.27	0.49	5.56	0.11	0.02	0.13					100	75.07	22.57	2.37
S100	Graphite A2	Plagioclase (oligoclase)	9.63	0.49	25.26	57.07	0.64	5.82	0.19	0.12	0.78					100	72.58	24.24	3.17
S104	Graphite A2	Plagioclase (oligoclase)	12.31	0.34	22.23	61.08	0.59	2.61	0.25	0.19	0.41					100.01	87.06	10.20	2.75
S104	Graphite A2	Plagioclase (oligoclase)	11.04	0.49	20.49	63.44	0.53	2.75	0.21	0.18	0.85					99.98	85.53	11.77	2.70
S104	Graphite A2	Plagioclase (albite)	11.86	0.3	21.68	62.19	0.47	2.61	0.16	0.16	0.57					100	87.13	10.60	2.27
S104	Graphite A2	Plagioclase (albite)	12.3	0.41	22.03	61.44	0.84	2.1	0.25	0.15	0.48					100	87.77	8.28	3.94
S104	Graphite A2	Plagioclase (albite)	12.6	0.43	22.16	61.59	0.34	2.47	0.15	0.09	0.16					99.99	88.80	9.62	1.58
S104	Graphite A2	Plagioclase (albite)	12.49	0.31	22.26	61.39	0.35	2.38	0.17	0.26	0.37					99.98	88.99	9.37	1.64
S104	Graphite A2	Plagioclase (albite)	12.62	0.41	22.13	61.35	0.49	2.36	0.14	0.22	0.28					100	88.58	9.15	2.26
S104	Graphite A2	Plagioclase (albite)	12.59	0.46	22.23	60.64	0.5	2.46	0.33	0.24	0.54					99.99	88.18	9.52	2.30
S104	Graphite A2	Plagioclase (albite)	12.46	0.32	22.38	61.38	0.38	2.38	0.18	0.12	0.39					99.99	88.84	9.38	1.78
S107	Graphite A3	Potassium feldspar (orthoclase)	1.53	0.56	20.55	61.35	14.18	0.33	0.28	0.21	1.02					100.01	13.86	1.65	84.49
S107	Graphite A3	Potassium feldspar (orthoclase)	1.2	0.47	20.37	60.89	14.78	0.49	0.36	0.2	1.23					99.99	10.72	2.42	86.86
S107	Graphite A3	Plagioclase (oligoclase)	7.3	0.77	26.29	55.32	1.38	6.46	0.38	0.28	1.83					100.01	61.98	30.31	7.71
S107	Graphite A3	Potassium feldspar (orthoclase)	1.11	0.47	20.25	61.87	14.55	0.4	0.35	0.21	0.78					99.99	10.18	2.03	87.79
S32	Graphite A3	Potassium feldspar (orthoclase)	1.7	0.27	19.93	62.55	14.41	0.34	0.26	0.13	0.41					100	14.95	1.65	83.39
S32	Graphite A3	Plagioclase (oligoclase)	9.64	0.48	24.78	57.44	0.6	6.04	0.18	0.14	0.7					100	72.09	24.96	2.95
S32	Graphite A3	Plagioclase (oligoclase)	9.65	0.42	25.11	57.51	0.54	6.13	0.13	0.11	0.4					100	72.05	25.29	2.65
S32	Graphite A3	Alkali feldspar (anorthoclase)	8.16	0.48	23.13	58.99	4.31	4.18	0.26	0.13	0.35					99.99	61.33	17.36	21.31
S32	Graphite A3	Plagioclase (andesine)	7.8	0.55	23.74	59.33	0.7	6.31	0.25	0.12	1.2					100	66.40	29.68	3.92
S32	Graphite A3	Plagioclase (oligoclase)	9.29	0.42	25.74	56.42	0.46	6.94	0.15	0.12	0.45					99.99	69.19	28.56	2.25
S36	Graphite A3	Potassium feldspar (orthoclase)	1.09	0.54	19.91	61.48	15.21	0.4	0.45	0.27	0.65					100	9.63	1.95	88.42
S36	Graphite A3	Potassium feldspar (orthoclase)	0.78	0.43	20.07	63.06	14.39	0.23	0.18	0.16	0.71					100.01	7.52	1.23	91.26
S36	Graphite A3	Plagioclase (albite)	13.21	0.55	21.04	62.45	0.63	0.87	0.26	0.26	0.73					100	93.65	3.41	2.94

	Petrographic group	Identification	Na_2O (wt%)	MgO (wt%)	Al_2O_3 (wt%)	SiO_2 (wt%)	K_2O (wt%)	CaO (wt%)	TiO_2 (wt%)	MnO (wt%)	Fe_2O_3 (wt%)	P_2O_5 (wt%)	BaO (wt%)	Cl_2O (wt%)	OsO (wt%)	SUM (wt%)	Ab mol%	An mol%	Or mol%
S36	Graphite A3	Potassium feldspar (orthoclase)	0.77	0.31	19.73	61.93	15.65	0.25	0.27	0.24	0.85					100	6.87	1.23	91.89
S36	Graphite A3	Potassium feldspar (orthoclase)	0.81	0.6	20.13	61.45	15.1	0.42	0.26	0.24	0.99					100	7.38	2.11	90.51
S86	Graphite A3	Potassium feldspar (orthoclase)	1.08	0.26	20.61	60.67	14.59	0.21	0.15	0.07	0.27		2.09			100	10.00	1.07	88.92
S86	Graphite A3	Potassium feldspar (orthoclase)	1.69	0.44	20.43	61.67	14.61	0.31	0.26	0.11	0.48					100	14.73	1.49	83.78
S86	Graphite A3	Potassium feldspar (orthoclase)	1.45	0.38	20.26	61.76	14.79	0.33	0.36	0.13	0.54					100	12.76	1.60	85.63
S128	Graphite A4	Potassium feldspar (orthoclase)	1.88	0.51	20.16	62.01	14.19	0.23	0.2	0.07	0.75					100	16.57	1.12	82.31
S128	Graphite A4	Potassium feldspar (orthoclase)	0.46	0	18.88	61.09	18.14	0.3	0.25	0.11	0.77					100	3.66	1.32	95.02
S128	Graphite A4	Potassium feldspar (orthoclase)	2.01	0.3	20.18	62.03	13.98	0.4	0.19	0.1	0.82					100.01	17.59	1.93	80.48
S128	Graphite A4	Potassium feldspar (orthoclase)	2.38	0.52	20.15	61.76	13.57	0.38	0.29	0.11	0.85					100.01	20.66	1.82	77.51
S128	Graphite A4	Plagioclase (labradorite)	4.32	0.32	27.86	53.22	0.67	11.67	0.12	0.13	1.69					100	38.54	57.53	3.93
S31	Graphite A4	Potassium feldspar (orthoclase)	2.11	0.31	19.81	59.99	13.19	0.67	0.2	0.19	3.53					100	18.91	3.32	77.77
S31	Graphite A4	Potassium feldspar (orthoclase)	2.16	0.38	20.66	61.24	13.53	0.44	0.29	0.22	1.09					100.01	19.11	2.15	78.74
S31	Graphite A4	Potassium feldspar (orthoclase)	1.67	0.22	20.38	61.71	13.88	0.22	0.21	0.16	1.55					100	15.29	1.11	83.60
S31	Graphite A4	Potassium feldspar (orthoclase)	1.6	0.24	19.41	60.24	14.63	0.38	0.32	0.26	2.93					100.01	13.99	1.84	84.17
S31	Graphite A4	Potassium feldspar (orthoclase)	2.4	0.41	20.35	61.7	13.53	0.27	0.18	0.22	0.94					100	20.96	1.30	77.74
S108	Graphite A5	Plagioclase (albite)	14.27	1.07	20.12	62.05	0.36	0.39	0.1	0.07	1.56					99.99	96.93	1.46	1.61
S109	Graphite A5	Potassium feldspar (orthoclase)	1.57	0.23	19.93	62.38	14.89	0.19	0.24	0.11	0.46					100	13.69	0.92	85.40
S109	Graphite A5	Potassium feldspar (orthoclase)	1.01	0.35	19.92	62.31	15.38	0.14	0.25	0.09	0.55					100	9.01	0.69	90.30
S109	Graphite A5	Plagioclase (albite)	13.3	0.44	20.81	63.3	0.58	0.69	0.17	0.11	0.6					100	94.58	2.71	2.71
S109	Graphite A5	Plagioclase (albite)	13.76	0.42	20.59	63.71	0.36	0.47	0.1	0.09	0.5					100	96.52	1.82	1.66
S35	Graphite A5	Potassium feldspar (orthoclase)	1.96	0.31	19.99	62.41	14.08	0.33	0.21	0.1	0.6					99.99	17.18	1.60	81.22
S35	Graphite A5	Potassium feldspar (orthoclase)	1.87	0.3	19.92	62.52	14.27	0.24	0.16	0.15	0.58					100.01	16.42	1.16	82.42
S35	Graphite A5	Potassium feldspar (orthoclase)	0.85	0.4	19.01	62.68	14.85	0.4	0.22	0.12	1.46					99.99	7.84	2.04	90.12
S35	Graphite A5	Plagioclase (albite)	12.99	0.36	20.95	63.36	0.38	1	0.14	0.08	0.73					99.99	94.18	4.01	1.81
S35	Graphite A5	Plagioclase (oligoclase)	10.59	0.52	24.17	58.57	0.44	4.84	0.23	0.16	0.49					100.01	78.13	19.73	2.14
S35	Graphite A5	Plagioclase (albite)	12.23	0.45	21.07	59.59	0.45	2.03	0.15	0.07	3.96					100	89.61	8.22	2.17
S130	Graphite B	Potassium feldspar (orthoclase)	1.68	0.74	20.01	61.47	13.45	0.95	0.41	0.2	1.08					99.99	15.20	4.75	80.05
S132	Graphite C1	Potassium feldspar (orthoclase)	4.24	0.46	19.33	59.22	13.86	0.81	0.33	0.18	0.7				0.89	100.02	30.71	3.24	66.05
S129	Graphite C2	Alkali feldspar (anorthoclase)	11.29	0.47	20.39	62.33	3.25	0.74	0.26	0.23	1.04					100	81.59	2.96	15.45
S129	Graphite C2	Plagioclase (albite)	11.49	0.38	22.42	61.71	0.6	2.45	0.17	0.12	0.67					100.01	86.79	10.23	2.98
S129	Graphite C2	Potassium feldspar (orthoclase)	1.78	0.32	20.41	61.26	14.14	0.56	0.48	0.18	0.87					100	15.62	2.72	81.66
S129	Graphite C2	Plagioclase (oligoclase)	10.5	0.42	23.51	58.69	0.65	4.65	0.39	0.36	0.84					100.01	77.79	19.04	3.17
S129	Graphite C2	Plagioclase (albite)	12.51	0.43	21.84	61.13	0.52	2.34	0.2	0.23	0.81					100.01	88.44	9.14	2.42
S129	Graphite C2	Plagioclase (oligoclase)	10.28	0.29	22.42	61.93	0.56	2.81	0.32	0.23	1.16					100	84.25	12.73	3.02
S13	Graphite D	Potassium feldspar (orthoclase)	2.36	0.53	19.7	62.02	13.41	0.36	0.43	0.27	0.92					100	20.73	1.75	77.52

	Petrographic group	Identification	Na_2O (wt%)	MgO (wt%)	Al_2O_3 (wt%)	SiO_2 (wt%)	K_2O (wt%)	CaO (wt%)	TiO_2 (wt%)	MnO (wt%)	Fe_2O_3 (wt%)	P_2O_5 (wt%)	BaO (wt%)	Cl_2O (wt%)	OsO (wt%)	SUM (wt%)	Ab mol%	An mol%	Or mol%
S13	Graphite D	Plagioclase (oligoclase)	9.26	0.54	25.5	56.21	0.52	6.4	0.25	0.14	1.19					100.01	70.48	26.92	2.60
S13	Graphite D	Plagioclase (andesine)	6.88	0.82	28.46	51.81	1.17	8.85	0.3	0.24	1.48					100.01	54.86	39.00	6.14
S13	Graphite D	Potassium feldspar (orthoclase)	0.68	0.55	20.29	61.9	14.83	0.4	0.3	0.13	0.92					100	6.38	2.07	91.55
S13	Graphite D	Potassium feldspar (orthoclase)	1.36	0.58	20.03	61.47	14.17	0.37	0.44	0.13	1.45					100	12.49	1.88	85.63
S13	Graphite D	Plagioclase (oligoclase)	12	0.42	22.4	60.3	0.34	2.75	0.16	0.13	1.5					100	87.31	11.06	1.63
S13	Graphite D	Plagioclase (oligoclase)	10.26	0.71	21.31	56.75	0.42	2.33	0.18	0.1	7.93					99.99	86.77	10.89	2.34
S54	Graphite D	Plagioclase (oligoclase)	1.56	0.35	20.81	61.49	14.48	0.25	0.37	0.17	0.52					100	13.90	1.23	84.87
S54	Graphite D	Potassium feldspar (orthoclase)	0.73	0.36	20.69	61.58	15.3	0.28	0.29	0.14	0.62					99.99	6.67	1.41	91.92
S54	Graphite D	Potassium feldspar (orthoclase)	1.04	0.31	20.28	62.09	15.34	0.27	0.18	0.07	0.42					100	9.22	1.32	89.46
S54	Graphite D	Potassium feldspar (orthoclase)	1.34	0.36	20.64	61.92	14.59	0.24	0.28	0.12	0.52					100.01	12.10	1.20	86.70
S54	Graphite D	Plagioclase (albite)	11.26	0.56	23.85	60.77	1.65	0.63	0.16	0.17	0.94					99.99	88.71	2.74	8.55
S54	Graphite D	Plagioclase (albite)	11.42	0.48	23.25	61.24	1.81	0.66	0.14	0.11	0.89					100	88.01	2.81	9.18
S54	Graphite D	Plagioclase (albite)	12.79	0.44	21.44	62.9	0.89	0.54	0.2	0.12	0.67					99.99	93.54	2.18	4.28
S15	Individual sample	Plagioclase (oligoclase)	9.29	0.41	24.78	57.75	0.51	6.04	0.2	0.2	0.82					100	71.66	25.75	2.59
S15	Individual sample	Plagioclase (oligoclase)	9.5	0.35	25.23	57.37	0.45	6.1	0.22	0.2	0.58					100	72.15	25.60	2.25
S15	Individual sample	Plagioclase (oligoclase)	9.83	0.28	24.48	58.63	0.56	5.14	0.22	0.19	0.67					100	75.39	21.78	2.83
S15	Individual sample	Plagioclase (oligoclase)	10.78	0.53	23.58	58.97	0.59	3.72	0.3	0.25	1.28					100	81.52	15.55	2.94
S15	Individual sample	Plagioclase (albite)	11.46	0.44	22.39	61.37	0.42	2.23	0.22	0.25	1.21					99.99	88.37	9.50	2.13

Zircon

	Petrographic group	Na_2O (wt%)	MgO (wt%)	Al_2O_3 (wt%)	SiO_2 (wt%)	K_2O (wt%)	CaO (wt%)	TiO_2 (wt%)	MnO (wt%)	Fe_2O_3 (wt%)	ZrO_2 (wt%)	SUM (wt%)
S10	Granitoid A1	0.8	0.73	2.65	37.57	0.56	0.11	0.69	0.68	1.12	55.09	100
S10	Granitoid A1	0.45	0.73	3.37	37.43	0.39	0.37	0.68	0.87	3.47	52.24	100
S10	Granitoid A1	1.01	0.91	3.42	38.3	0.65	0.19	0.39	0.49	1.86	52.79	100.01
S10	Granitoid A1	1.11	0.92	3.26	38.29	0.45	0.13	0.63	0.58	2.16	52.46	99.99
S70	Granitoid A1	0.83	0.86	3.14	38.58	0.42	0.27	0.38	0.12	2.11	53.30	100.01
S70	Granitoid A1	0.67	0.80	2.95	39.62	0.27	0.14	0.19	0.06	1.51	53.78	99.99
S88	Granitoid A1	0.24	0.21	1.29	42.26	0.10	0.12	0.13	0.19	0.74	54.71	99.99
S88	Granitoid A1	1.01	0.41	2.64	39.94	0.68	0.41	0.20	0.14	0.64	53.92	99.99
S88	Granitoid A1	0.78	0.96	2.89	37.54	0.42	0.48	0.52	0.23	1.77	54.41	100
S88	Granitoid A1	0.42	0.72	2.73	37.64	0.40	0.45	0.44	0.26	1.51	55.43	100
S98	Granitoid A1	0.76	1.01	3.25	38.41	0.30	0.28	0.45	0.46	2.07	53.01	100
S52	Granitoid A2	0.65	0.60	4.21	38.71	0.46	0.14	0.24	0.08	1.11	53.80	100
S52	Granitoid A2	0.61	0.71	7.68	38.94	1.05	0.26	0.51	0.22	3.27	46.76	100.01
S52	Granitoid A2	0.62	0.71	5.24	39.10	0.51	0.20	0.21	0.09	2.20	51.12	100
S65	Granitoid A2	0.53	0.48	3.47	38.68	0.32	0.14	0.57	0.42	1.55	53.83	99.99
S65	Granitoid A2	1.78	1.21	4.37	36.73	0.42	0.79	0.54	0.65	5.76	47.75	100
S65	Granitoid A2	0.54	0.79	3.32	38.20	0.37	0.22	0.62	0.61	1.88	53.44	99.99
S65	Granitoid A2	0.74	0.76	4.09	38.66	0.39	0.23	0.63	0.55	1.79	52.16	100
S78	Granitoid A2	0.80	0.68	3.08	38.03	0.45	0.39	0.32	0.08	1.64	54.53	100
S78	Granitoid A2	0.55	0.64	3.21	39.00	0.53	0.28	0.31	0.11	1.74	53.62	99.99
S78	Granitoid A2	0.54	0.52	3.04	38.75	0.67	0.12	0.34	0.16	1.11	54.74	99.99
S51	Granitoid A3	0.39	0.35	4.93	38.12	0.34	0.05	0.34	0.25	1.35	53.86	99.98
S12	Granitoid B1	0.54	0.65	3.40	39.57	0.92	0.09	0.51	0.61	1.42	52.29	100
S83	Granitoid B1	0.43	0.43	3.18	39.24	0.25	0.05	0.28	0.18	1.40	54.56	100
S83	Granitoid B1	0.33	0.42	3.49	38.90	0.50	0.02	0.33	0.12	1.25	54.64	100
S9	Granitoid B2	0.43	0.49	4.03	40.54	0.29	0.10	0.41	0.31	1.73	51.68	100.01
S9	Granitoid B2	0.99	1.04	3.54	38.78	0.37	0.18	0.57	0.34	1.37	52.83	100.01
S45	Granitoid B3	0.40	0.27	3.49	39.26	0.47	0.03	0.25	0.23	1.11	54.50	100.01
S45	Granitoid B3	0.33	0.44	5.76	35.86	0.32	0.43	0.28	0.21	2.11	54.27	100.01
S1	Granitoid C	0.76	1.15	5.04	38.57	0.74	0.25	0.70	0.34	2.11	50.33	99.99
S87	Granitoid C	0.25	0.58	3.43	38.19	0.59	0.16	0.35	0.18	1.79	54.50	100.02
S5	Granitoid D	0.60	0.65	3.32	38.41	0.45	0.15	0.26	0.11	1.07	54.97	99.99
S21	Granitoid D	0.34	0.78	10.25	33.65	0.51	1.69	0.40	0.36	5.19	46.85	100.02
S11	Diorite A	0.58	0.98	3.62	38.73	0.41	0.43	0.58	0.64	1.58	52.45	100
S11	Diorite A	0.79	1.05	3.09	39.84	0.37	0.23	0.65	0.54	1.88	51.55	99.99
S11	Diorite A	0.23	0.84	2.92	39.96	0.48	0.24	0.57	0.55	2.04	52.16	99.99
S75	Diorite A	0.25	0.68	2.41	39.72	0.26	0.23	0.37	0.44	1.62	54.01	99.99
S75	Diorite A	0.87	1.12	3.31	39.25	0.47	0.15	0.62	0.45	1.91	51.86	100.01
S75	Diorite A	0.49	0.84	4.78	34.98	0.69	0.86	0.49	0.50	2.72	53.65	100
S75	Diorite A	0.70	1.54	8.78	37.93	0.83	1.07	0.71	0.66	4.95	42.84	100.01
S97	Diorite B	0.39	0.17	3.95	44.20	2.67	0.30	0.15	0.30	0.79	47.06	99.98
S97	Diorite B	1.14	2.39	10.55	37.33	0.91	2.08	0.75	0.24	3.45	41.17	100.01
S89	Carbonate B	0.47	0.82	5.53	34.68	0.38	3.03	0.55	0.30	2.02	52.23	100.01
S102	Graphite A1	1.00	0.85	2.82	39.03	0.36	0.48	0.48	0.35	1.34	53.29	100
S102	Graphite A1	0.69	0.55	2.27	39.95	0.32	0.20	0.46	0.50	1.15	53.90	99.99
S102	Graphite A1	0.02	0.19	2.68	41.25	0.66	1.00	0.40	0.34	1.27	52.19	100
S104	Graphite A2	1.10	0.80	2.76	39.08	0.37	0.12	0.66	0.17	1.01	53.92	99.99
S32	Graphite A3	0.33	0.60	2.57	39.27	0.38	0.19	0.22	0.16	1.30	54.98	100
S36	Graphite A3	0.46	0.48	3.08	38.51	0.46	0.67	2.19	0.48	2.24	51.44	100.01
S35	Graphite A5	0.56	0.42	2.38	39.22	0.35	0.29	0.27	0.17	1.20	55.13	99.99
S109	Graphite A5	0.34	0.54	3.05	38.51	0.37	0.14	0.32	0.23	1.07	55.43	100
S132	Graphite C1	1.19	0.65	2.50	37.17	0.27	0.72	0.22	0.28	1.16	55.85	100.01

	Petrographic group	Na_2O (wt%)	MgO (wt%)	Al_2O_3 (wt%)	SiO_2 (wt%)	K_2O (wt%)	CaO (wt%)	TiO_2 (wt%)	MnO (wt%)	Fe_2O_3 (wt%)	ZrO_2 (wt%)	SUM (wt%)
S132	Graphite C1	0.24	0.33	2.64	37.87	0.21	2.03	0.35	0.33	1.38	54.61	99.99
S54	Graphite D	0.31	0.29	2.78	36.30	0.21	0.39	0.20	0.18	1.09	58.27	100.02
S15	Individual sample	0.55	0.50	2.80	40.44	0.26	0.18	0.28	0.34	1.73	52.92	100

Rutile

	Petrographic group	Na_2O (wt%)	MgO (wt%)	Al_2O_3 (wt%)	SiO_2 (wt%)	K_2O (wt%)	CaO (wt%)	TiO_2 (wt%)	MnO (wt%)	Fe_2O_3 (wt%)	Nb_2O_5 (wt%)	N_2O_5 (wt%)	Au_2O_3 (wt%)	SUM (wt%)
S40	Granitoid A3	0.90	0.39	5.74	8.17	0.47	0.43	82.22	0.34	1.34				100.00
S51	Granitoid A3	0.94	0.22	4.79	5.91	0.44	0.19	86.41	0.06	1.05				100.01
S51	Granitoid A3	0.96	0.26	4.78	6.08	0.25	0.17	76.14	0.07	0.76		10.53		100.00
S9	Granitoid B2	0.87	0.36	3.08	6.69	0.25	0.40	86.55	0.22	1.58				100.00
S45	Granitoid B3	1.03	0.50	3.04	5.58	0.27	0.23	76.74	0.11	1.15		11.34		99.99
S46	Granitoid B3	0.94	0.26	5.21	8.16	0.23	0.38	83.51	0.03	1.27				99.99
S46	Granitoid B3	0.99	0.12	3.35	7.34	1.04	0.21	86.30	0.06	0.60				100.01
S90	Amphibole	1.10	0.99	4.04	10.52	0.27	0.72	78.54	0.28	3.54				100.00
S58	Carbonate A	1.03	0.39	3.65	10.21	0.45	0.49	82.15	0.02	1.09			0.52	100.00
S102	Graphite A1	1.05	0.39	2.55	8.27	0.34	0.50	78.56	0.20	5.73	2.41			100.00
S103	Graphite A1	0.85	0.17	0.93	2.35	0.15	0.15	83.04	0.10	0.33		11.93		100.00
S103	Graphite A1	0.99	0.23	1.70	6.38	0.27	0.24	89.48	0.10	0.61				100.00
S100	Graphite A2	1.30	0.34	1.38	3.09	0.18	0.19	93.01	0.11	0.39				99.99
S100	Graphite A2	0.80	0.18	1.28	2.84	0.28	0.21	82.68	0.09	0.34		11.30		100.00
S100	Graphite A2	0.84	0.22	1.80	3.86	0.27	0.31	91.97	0.07	0.64				99.98
S100	Graphite A2	1.20	0.33	2.58	5.06	0.33	0.45	89.29	0.09	0.67				100.00
S104	Graphite A2	1.10	0.22	1.82	4.84	0.23	0.33	90.64	0.16	0.65				99.99
S36	Graphite A3	0.75	0.41	1.88	4.35	0.30	0.31	90.21	0.18	1.61				100.00
S36	Graphite A3	1.03	0.40	2.41	7.05	0.96	0.21	87.30	0.15	0.49				100.00
S36	Graphite A3	0.74	0.37	2.17	5.49	0.54	0.34	88.72	0.21	1.42				100.00
S86	Graphite A3	0.13	0.00	1.03	1.94	0.15	0.13	95.95	0.04	0.63				100.00
S86	Graphite A3	0.92	0.22	1.77	3.33	0.50	0.24	91.71	0.11	0.48	0.73			100.01
S86	Graphite A3	0.86	0.22	2.67	4.87	0.79	0.24	88.96	0.10	0.46	0.84			100.01
S31	Graphite A4	0.66	0.14	1.17	3.23	0.53	0.19	82.76	0.10	0.76	10.46			100.00
S31	Graphite A4	0.87	0.20	2.67	3.49	0.23	0.27	90.58	0.10	1.57				99.98
S109	Graphite A5	0.72	0.21	4.69	8.98	0.47	1.71	81.62	0.06	1.55				100.01
S109	Graphite A5	0.58	0.16	2.01	4.68	0.28	0.19	91.04	0.06	0.99				99.99
S130	Graphite B	1.26	1.13	6.79	12.40	1.22	0.37	75.50	0.08	1.24				99.99
S130	Graphite B	0.76	0.16	1.51	7.80	0.48	0.26	88.47	0.20	0.36				100.00
S132	Graphite C1	0.80	0.69	3.82	4.71	0.24	2.14	86.98	0.12	0.51				100.01
S132	Graphite C1	0.39	0.11	2.29	4.59	0.43	1.45	89.57	0.24	0.92				99.99
S129	Graphite C2	1.18	0.52	3.25	5.16	0.34	0.87	86.68	0.21	1.80				100.01
S13	Graphite D	0.99	0.63	2.04	3.97	0.22	0.29	81.13	0.11	1.05		9.57		100.00
S54	Graphite D	0.21	0.00	1.98	3.21	0.05	0.01	92.87	0.37	0.85	0.45			100.00
S15	Individual sample	0.71	0.23	1.45	6.21	0.25	0.19	80.34	0.14	0.63		9.84		99.99
S15	Individual sample	1.30	0.45	2.89	6.38	0.33	0.42	87.02	0.23	0.97				99.99

Titanite

	Petrographic group	Na_2O (wt%)	MgO (wt%)	Al_2O_3 (wt%)	SiO_2 (wt%)	K_2O (wt%)	CaO (wt%)	TiO_2 (wt%)	MnO (wt%)	Fe_2O_3 (wt%)	SUM (wt%)
S98	Granitoid A1	0.97	0.77	4.4	32.26	0.5	26.4	31.75	0.39	2.54	99.98
S98	Granitoid A1	1.21	0.85	5.48	33.42	0.63	26.74	29.13	0.45	2.08	99.99
S78	Granitoid A2	1.11	0.48	4.23	33.48	0.33	27.99	30.83	0.15	1.39	99.99
S45	Granitoid B3	0.81	0.38	5.19	33.78	0.4	27.24	30.97	0.04	1.19	100
S1	Granitoid C	0.83	0.68	6.39	35.8	0.7	25.34	28.4	0.16	1.71	100.01
S57	Carbonate A	0.77	0.71	7.44	36.89	0.17	26.82	26.45	0.03	0.72	100
S57	Carbonate A	1.08	0.91	5.44	35.82	0.34	26.24	29.07	0.17	0.94	100.01
S13	Graphite D	1.01	0.87	4.41	33.51	0.26	27.4	30.49	0.34	1.72	100.01

Iron-rich phases

	Petrographic groups	Na_2O (wt%)	MgO (wt%)	Al_2O_3 (wt%)	SiO_2 (wt%)	K_2O (wt%)	CaO (wt%)	TiO_2 (wt%)	MnO (wt%)	Fe_2O_3 (wt%)	P_2O_5 (wt%)	Cl_2O (wt%)	SO_3 (wt%)	SUM (wt%)
S10	Granitoid A1	1.97	0.87	4.61	9.23	0.46	0.49	2.74	0.23	79.39				99.99
S70	Granitoid A1	1.49	1.18	3.64	8.30	0.32	0.81	0.31	0.15	83.24	0.57			100.01
S98	Granitoid A1	1.45	1.67	9.96	22.12	0.59	2.74	1.15	0.43	58.77	1.12			100.00
S40	Granitoid A3	1.49	0.99	12.10	18.87	0.46	0.93	0.71	0.40	64.05				100.00
S51	Granitoid A3	1.20	0.67	11.18	12.45	0.51	0.38	0.84	0.38	72.39				100.00
S83	Granitoid B1	1.28	1.44	10.57	24.14	0.95	0.94	0.53	0.29	59.46	0.39			99.99
S9	Granitoid B2	1.11	0.97	11.36	14.69	0.43	1.36	1.04	0.41	68.62				99.99
S9	Granitoid B2	1.16	1.13	10.86	15.00	0.50	1.41	0.60	0.49	68.23	0.61			99.99
S93	Granitoid B2	1.53	0.62	5.13	10.78	0.33	0.69	0.34	0.98	79.61				100.01
S45	Granitoid B3	1.63	2.33	15.47	16.55	0.27	0.99	1.39	0.20	60.39	0.78			100.00
S1	Granitoid C	1.26	1.02	7.57	14.63	0.73	1.03	0.17	0.15	72.11	1.33			100.00
S1	Granitoid C	1.50	1.30	8.34	14.70	1.42	1.19	0.41	0.35	68.72	1.57	0.50		100.00
S1	Granitoid C	1.25	1.65	14.05	27.65	0.88	2.27	3.21	0.41	44.54	3.57	0.53		100.01
S1	Granitoid C	1.01	1.19	11.36	12.50	1.16	1.65	1.57	0.66	66.81	2.10			100.01
S87	Granitoid C	1.26	0.86	4.05	6.00	0.47	0.30	9.87	0.11	77.07				99.99
S5	Granitoid D	1.24	1.17	12.91	14.59	0.60	1.04	0.29	0.18	66.55	1.43			100.00
S5	Granitoid D	2.04	1.73	14.24	15.41	0.48	1.23	0.30	0.17	62.78	1.63			100.01
S5	Granitoid D	0.89	0.54	12.55	16.76	1.27	1.98	0.43	0.27	63.98	1.32			99.99
S21	Granitoid D	0.80	1.42	9.25	10.00	0.54	0.65	0.38	0.73	76.21				99.98
S21	Granitoid D	0.80	1.01	12.94	14.18	0.62	1.32	0.44	0.47	67.33	0.89			100.00
S21	Granitoid D	2.09	2.23	8.12	10.59	1.12	1.09	0.81	1.04	71.21	1.13	0.58		100.01
S21	Granitoid D	1.04	1.13	11.31	13.43	0.71	1.75	5.75	0.71	62.63	1.56			100.02
S21	Granitoid D	1.44	0.98	10.58	11.85	0.85	1.05	0.36	0.34	71.28	1.27			100.00
S21	Granitoid D	1.26	1.52	9.90	28.05	1.35	1.72	1.08	0.44	53.88	0.27	0.55		100.02
S8	Amphibole	1.51	1.28	10.06	19.02	0.77	1.26	0.49	0.36	65.25				100.00
S8	Amphibole	1.55	1.42	6.92	15.17	0.51	1.14	0.77	0.51	72.00				99.99
S8	Amphibole	1.23	1.67	11.58	18.14	0.48	1.40	1.56	0.37	63.58				100.01
S90	Amphibole	1.41	1.52	5.67	10.13	0.31	0.77	0.86	0.42	78.90				99.99
S90	Amphibole	1.53	1.50	3.36	8.25	0.25	1.03	0.32	0.46	82.65	0.65			100.00
S11	Diorite A	2.04	2.05	8.99	15.65	0.47	1.86	0.64	0.63	66.19	1.47			99.99
S11	Diorite A	1.16	6.24	10.80	23.31	0.82	1.91	0.60	0.31	54.06	0.79			100.00
S11	Diorite A	1.92	1.60	7.81	17.28	0.44	1.71	1.58	0.12	66.44	1.11			100.01

	Petrographic groups	Na_2O (wt%)	MgO (wt%)	Al_2O_3 (wt%)	SiO_2 (wt%)	K_2O (wt%)	CaO (wt%)	TiO_2 (wt%)	MnO (wt%)	Fe_2O_3 (wt%)	P_2O_5 (wt%)	Cl_2O (wt%)	SO_3 (wt%)	SUM (wt%)
S11	Diorite A	2.12	1.78	5.44	14.77	0.60	1.41	0.62	0.49	71.54	1.24			100.01
S75	Diorite A	1.48	1.72	6.81	13.18	0.57	1.21	0.48	0.48	71.62	2.43			99.98
S75	Diorite A	1.51	1.21	4.81	8.68	0.50	0.83	0.41	0.57	79.84	1.65			100.01
S75	Diorite A	1.74	1.63	8.84	12.57	0.46	0.85	0.93	0.53	70.30	2.15			100.00
S75	Diorite A	1.60	2.08	11.31	21.06	0.79	1.36	1.38	0.47	56.87	3.08			100.00
S75	Diorite A	1.15	1.10	5.49	8.20	0.38	1.02	0.46	0.72	78.95	2.52			99.99
S75	Diorite A	1.23	1.90	10.19	13.46	0.50	1.12	0.60	0.13	67.98	2.90			100.01
S89	Carbonate B	1.78	1.31	4.79	8.99	0.22	2.15	0.27	0.53	79.96				100.00
S89	Carbonate B	1.43	1.88	10.71	13.61	0.42	2.87	0.49	0.53	68.06				100.00
S110	Graphite A1	1.78	0.98	4.66	7.71	0.36	1.12	0.37	0.41	80.48	2.14			100.01
S110	Graphite A1	1.44	0.83	2.76	7.81	0.35	1.10	0.31	0.26	83.95	1.19			100.00
S110	Graphite A1	1.05	0.39	2.26	7.73	0.52	0.89	0.43	0.89	85.09	0.75			100.00
S110	Graphite A1	1.70	0.96	4.85	8.43	0.41	1.10	0.34	0.34	79.14	2.71			99.98
S110	Graphite A1	1.75	2.22	5.54	23.27	0.62	1.73	0.22	0.28	63.91	0.45			99.99
S104	Graphite A2	1.87	1.27	6.99	16.57	0.84	2.14	0.89	0.31	66.99	0.75		1.37	99.99
S104	Graphite A2	1.58	0.45	2.78	9.50	0.36	0.61	0.33	0.33	83.68			0.38	100.00
S104	Graphite A2	1.37	1.14	4.46	9.94	0.41	1.08	0.43	0.34	79.98	0.49		0.37	100.01
S104	Graphite A2	2.14	1.45	6.14	12.21	0.67	1.71	0.23	0.27	74.08			1.11	100.01
S104	Graphite A2	2.05	1.25	6.87	17.44	1.23	2.77	0.67	0.28	65.73	0.74		0.97	100.00
S104	Graphite A2	2.81	1.97	7.57	17.34	0.76	1.27	0.42	0.18	66.10			1.59	100.01
S107	Graphite A3	1.15	1.46	5.35	10.55	0.41	1.23	0.39	0.33	78.17	0.98			100.02
S107	Graphite A3	1.44	1.14	5.29	7.56	0.38	1.32	0.35	0.26	80.92	1.34			100.00
S107	Graphite A3	1.36	1.60	7.24	11.17	0.49	0.78	0.62	0.32	76.14	0.28			100.00
S107	Graphite A3	1.52	1.37	4.37	4.77	0.32	0.46	11.93	0.65	74.61				100.00
S107	Graphite A3	1.19	1.93	10.56	11.58	0.31	2.02	1.87	0.78	67.84	1.93			100.01
S32	Graphite A3	1.45	0.72	5.72	11.31	0.59	0.64	0.58	0.30	78.23	0.45			99.99
S32	Graphite A3	1.74	0.91	5.78	13.67	0.58	0.70	0.29	0.21	75.46	0.26		0.41	100.01
S31	Graphite A4	1.04	0.72	7.75	10.14	1.01	2.39	0.40	0.33	73.63	2.06		0.54	100.01
S31	Graphite A4	1.50	0.92	9.86	16.42	0.64	1.46	0.94	0.43	67.34	0.26		0.23	100.00
S31	Graphite A4	1.65	1.05	8.09	11.95	0.72	4.02	0.35	0.27	69.80	1.83		0.28	100.01
S31	Graphite A4	1.96	0.91	8.08	11.14	0.83	0.85	0.38	0.35	73.11	1.62	0.27	0.50	100.00
S31	Graphite A4	1.84	1.02	5.65	10.36	0.52	1.12	0.25	0.27	77.47	1.49			99.99
S31	Graphite A4	1.93	0.71	9.52	11.42	0.65	0.89	0.12	0.31	72.37	1.97	0.09		99.98
S31	Graphite A4	1.52	1.08	10.98	13.01	0.44	1.88	0.36	0.46	69.12	1.14			99.99
S31	Graphite A4	1.58	1.30	12.92	10.07	0.42	2.91	0.42	0.41	68.60	1.39			100.02
S31	Graphite A4	1.46	1.06	11.13	9.25	0.42	1.93	0.36	0.36	72.81	1.22			100.00
S31	Graphite A4	1.52	0.80	7.87	8.65	0.32	2.53	0.46	0.43	76.33	1.10			100.01
S128	Graphite A4	1.99	1.19	4.72	8.05	0.69	1.09	0.24	0.17	75.17	1.07		5.62	100.00
S128	Graphite A4	1.36	0.64	4.44	9.74	0.77	0.83	0.34	0.18	79.43			2.27	100.00
S128	Graphite A4	1.53	0.74	3.25	7.72	1.27	1.22	0.49	0.24	71.77	0.69		11.08	100.00
S35	Graphite A5	1.24	1.30	10.04	18.50	0.33	2.25	0.18	0.06	63.36	2.73			99.99
S35	Graphite A5	1.08	0.60	8.52	24.88	0.31	2.76	0.25	0.18	56.97	3.42		1.03	100.00
S35	Graphite A5	1.06	0.71	10.45	22.07	0.52	3.01	0.27	0.17	55.70	6.04			100.00
S35	Graphite A5	1.49	1.86	9.37	14.03	0.54	5.27	0.50	0.44	60.68	5.81			99.99
S35	Graphite A5	1.29	1.66	11.09	17.97	0.71	3.38	0.40	0.28	60.15	3.07			100.00
S35	Graphite A5	1.02	0.84	13.10	21.67	0.40	4.60	0.51	0.18	53.06	4.62			100.00
S108	Graphite A5	0.86	0.57	5.62	9.11	0.60	1.90	0.58	0.64	76.24	3.88			100.00

	Petrographic groups	Na_2O (wt%)	MgO (wt%)	Al_2O_3 (wt%)	SiO_2 (wt%)	K_2O (wt%)	CaO (wt%)	TiO_2 (wt%)	MnO (wt%)	Fe_2O_3 (wt%)	P_2O_5 (wt%)	Cl_2O (wt%)	SO_3 (wt%)	SUM (wt%)
S108	Graphite A5	1.47	0.94	8.10	11.94	0.39	1.39	9.39	0.30	63.41	2.67			100.00
S109	Graphite A5	1.55	1.81	8.76	10.19	0.81	0.42	0.40	0.53	74.66	0.86			99.99
S109	Graphite A5	1.47	0.71	4.41	8.12	0.34	0.66	0.59	0.20	81.59	1.91			100.00
S109	Graphite A5	1.41	0.59	4.34	8.32	0.31	0.53	0.48	0.17	82.14	1.72			100.01
S109	Graphite A5	1.42	0.79	4.91	9.88	0.38	0.71	0.53	0.27	79.31	1.79			99.99
S109	Graphite A5	1.42	0.89	3.85	8.77	0.43	0.78	1.75	0.24	80.81	1.06			100.00
S130	Graphite B	0.46	1.46	12.40	31.53	1.53	2.24	0.75	0.34	49.29				100.00
S132	Graphite C1	1.18	0.78	3.56	6.53	0.47	2.29	0.52	0.79	82.28	1.60			100.00
S129	Graphite C2	1.02	0.75	14.95	20.31	0.61	2.25	1.16	0.41	58.53				99.99
S129	Graphite C2	1.40	0.94	9.49	11.13	0.54	2.34	1.26	0.66	69.92	2.31			99.99
S13	Graphite D	1.48	1.23	5.11	12.29	0.54	0.77	0.41	0.38	77.79				100.00
S13	Graphite D	2.07	1.18	4.68	10.75	0.26	0.77	0.30	0.34	79.00	0.65			100.00
S13	Graphite D	1.31	1.15	5.10	11.94	0.45	0.86	0.33	0.44	77.95	0.47			100.00
S13	Graphite D	1.50	1.43	5.63	12.17	0.50	0.79	0.91	0.35	76.72				100.00
S13	Graphite D	1.96	1.29	4.27	10.95	0.32	0.66	0.18	0.19	79.87	0.32			100.01
S13	Graphite D	1.18	1.18	5.91	12.52	0.36	0.78	0.43	0.43	77.07	0.13			99.99
S13	Graphite D	1.52	1.33	6.75	12.39	0.43	0.82	0.34	0.31	76.10				99.99
S13	Graphite D	1.05	1.38	11.23	14.12	0.31	1.25	0.89	0.21	68.99	0.59			100.02
S13	Graphite D	1.39	1.26	6.83	12.73	0.47	0.83	0.26	0.42	75.80				99.99
S13	Graphite D	1.38	1.24	8.72	11.48	0.36	1.32	0.74	0.80	72.85	1.12			100.01
S13	Graphite D	1.31	0.79	4.85	10.38	0.30	0.70	0.24	0.55	80.88				100.00
S13	Graphite D	1.59	0.58	6.18	11.65	0.63	1.07	1.25	0.64	75.93	0.47			99.99
S13	Graphite D	1.49	0.78	6.65	13.11	0.27	0.87	0.33	0.42	76.08				100.00
S13	Graphite D	1.77	1.32	5.86	12.33	0.43	0.93	0.55	0.32	75.94	0.54			99.99

Amphibole

	Petrographic groups	Na_2O (wt%)	MgO (wt%)	Al_2O_3 (wt%)	SiO_2 (wt%)	K_2O (wt%)	CaO (wt%)	TiO_2 (wt%)	MnO (wt%)	Fe_2O_3 (wt%)	SUM (wt%)
S8	Amphibole	1.96	8.21	13.58	41.39	1.03	11.18	1.52	0.60	20.52	99.99
S8	Amphibole	1.44	14.52	9.30	47.96	0.80	11.20	0.92	0.61	13.24	99.99
S61	Amphibole	2.30	8.94	15.11	41.34	1.19	11.41	1.33	0.23	18.16	100.01
S61	Amphibole	2.72	10.09	13.60	42.59	0.85	11.04	1.47	0.35	17.30	100.01
S61	Amphibole	1.71	9.05	13.35	41.62	0.91	11.30	1.68	0.36	20.02	100.00
S61	Amphibole	2.47	9.52	13.85	41.90	0.98	11.57	1.64	0.34	17.73	100.00
S61	Amphibole	2.48	9.47	14.42	40.91	1.12	11.43	1.81	0.35	18.03	100.02
S61	Amphibole	2.15	9.69	12.73	47.26	0.52	10.42	1.27	0.34	15.63	100.01
S90	Amphibole	1.42	13.14	10.63	45.83	0.73	12.24	0.77	0.51	14.73	100.00
S90	Amphibole	1.46	14.55	8.53	48.75	0.58	12.02	0.73	0.58	12.81	100.01
S90	Amphibole	1.71	13.98	11.10	45.71	0.72	12.04	0.66	0.58	13.49	99.99
S11	Diorite A	0.82	18.87	3.80	53.61	0.30	12.79	0.53	0.53	8.74	99.99
S11	Diorite A	0.74	16.20	4.28	52.31	0.30	12.26	0.42	0.44	13.03	99.98
S11	Diorite A	0.47	23.45	1.60	55.94	0.33	13.14	0.37	0.50	4.20	100.00
S11	Diorite A	0.64	23.48	1.66	56.10	0.33	12.99	0.26	0.48	4.06	100.00
S11	Diorite A	0.63	23.87	1.46	56.21	0.27	13.17	0.38	0.25	3.76	100.00
S75	Diorite A	0.61	14.10	5.43	52.76	0.61	11.65	0.63	0.44	13.77	100.00
S75	Diorite A	0.49	24.26	1.01	56.71	0.18	13.40	0.30	0.35	3.30	100.00
S75	Diorite A	0.54	23.95	1.18	56.54	0.23	13.49	0.36	0.47	3.23	99.99
S67	Diorite B	1.10	13.65	5.42	50.32	0.37	12.04	0.51	0.23	16.35	99.99

	Petrographic groups	Na_2O (wt%)	MgO (wt%)	Al_2O_3 (wt%)	SiO_2 (wt%)	K_2O (wt%)	CaO (wt%)	TiO_2 (wt%)	MnO (wt%)	Fe_2O_3 (wt%)	SUM (wt%)
S67	Diorite B	1.17	14.32	6.36	51.03	0.38	11.47	0.43	0.30	14.54	100.00
S67	Diorite B	1.25	12.75	4.55	50.68	0.55	11.36	0.32	0.67	17.87	100.00
S97	Diorite B	1.20	12.63	3.67	50.86	0.38	11.93	0.33	0.48	18.52	100.00
S97	Diorite B	1.61	12.41	5.60	49.27	0.42	11.26	0.57	0.51	18.35	100.00
S97	Diorite B	1.49	12.76	4.35	49.54	0.41	11.89	0.71	0.46	18.40	100.01

Pyroxene

	Petrographic groups	Na_2O (wt%)	MgO (wt%)	Al_2O_3 (wt%)	SiO_2 (wt%)	K_2O (wt%)	CaO (wt%)	TiO_2 (wt%)	MnO (wt%)	Fe_2O_3 (wt%)	P_2O_5 (wt%)	SUM (wt%)	Wo (mol%)	En (mol%)	Fs (mol%)
S67	Diorite B	0.63	16.93	2.91	50.11	0.12	21.57	0.61	0.25	6.87		100.00	47.28	37.11	15.61
S67	Diorite B	0.92	16.70	4.19	50.29	0.19	18.32	0.59	0.32	8.47		99.99	41.82	38.12	20.06
S97	Diorite B	0.78	16.69	3.37	49.90	0.17	20.55	0.72	0.29	7.54		100.01	45.60	37.03	17.37
S97	Diorite B	0.74	15.98	4.23	48.97	0.16	21.40	0.98	0.35	7.20		100.01	47.63	35.57	16.80
S97	Diorite B	0.53	16.32	3.72	49.11	0.23	21.51	0.78	0.33	7.48		100.01	47.13	35.76	17.11
S97	Diorite B	0.93	18.26	4.40	52.27	0.35	12.53	0.77	0.35	10.14		100.00	30.35	44.23	25.41
S57	Carbonate A	0.51	17.72	1.41	51.31	0.14	26.68	0.17	0.36	1.71		100.01	57.41	38.13	4.45
S57	Carbonate A	0.51	17.45	1.53	51.27	0.20	27.11	0.27	0.27	1.39		100.00	58.65	37.75	3.59
S57	Carbonate A	0.47	18.49	1.24	52.68	0.19	25.62	0.18	0.25	0.90		100.02	56.61	40.85	2.54
S57	Carbonate A	0.57	17.84	2.07	53.46	0.20	25.35	0.14	0.00	0.37		100.00	58.20	40.96	0.85
S58	Carbonate A	0.43	18.22	0.95	51.59	0.14	27.43	0.15	0.14	0.95		100.00	58.69	38.98	2.33
S58	Carbonate A	0.46	17.01	1.26	48.90	0.12	30.37	0.20	0.20	1.48		100.00	61.90	34.67	3.42
S58	Carbonate A	0.56	17.14	1.14	50.83	0.11	27.84	0.09	0.14	2.15		100.00	58.90	36.26	4.84
S89	Carbonate B	0.70	18.01	1.97	51.76	0.24	25.39	0.35	0.31	1.27		100.00	56.45	40.04	3.51
S89	Carbonate B	0.51	24.60	1.52	56.28	0.23	15.10	0.27	0.30	1.18		99.99	36.67	59.74	3.59
S89	Carbonate B	0.57	24.32	2.05	55.93	0.30	15.16	0.26	0.27	1.13		99.99	37.08	59.49	3.42
S89	Carbonate B	0.56	18.02	1.70	51.44	0.16	26.52	0.25	0.24	1.10		99.99	57.80	39.28	2.92
S89	Carbonate B	0.78	16.85	3.51	49.83	0.33	25.68	0.48	0.36	1.62	0.56	100.00	57.69	37.86	4.45
S89	Carbonate B	0.39	17.40	3.06	50.39	0.22	26.36	0.42	0.36	1.39		99.99	57.92	38.23	3.85

Mica

	Petrographic group	Identification	Na_2O (wt%)	MgO (wt%)	Al_2O_3 (wt%)	SiO_2 (wt%)	K_2O (wt%)	CaO (wt%)	TiO_2 (wt%)	MnO (wt%)	Fe_2O_3 (wt%)	P_2O_5 (wt%)	N_2O_5 (wt%)	SUM (wt%)
S70	Granitoid A1	Biotite	1.47	8.46	19.82	33.41	1.19	2.79	5.57	0.18	26.35	0.76		100.00
S70	Granitoid A1	Biotite	1.34	12.13	20.45	40.21	2.74	2.84	4.33	0.21	15.41	0.34		100.00
S70	Granitoid A1	Biotite	1.64	12.42	21.33	39.98	2.90	1.75	3.49	0.16	15.98	0.36		100.01
S70	Granitoid A1	Biotite	1.44	9.32	20.68	38.88	2.77	3.21	3.82	0.26	19.30	0.32		100.00
S70	Granitoid A1	Biotite	1.73	7.80	22.21	38.41	3.17	3.52	3.82	2.46	16.39	0.48		99.99
S88	Granitoid A1	Biotite	1.19	12.21	17.30	38.15	4.17	2.16	4.47	0.31	19.84	0.21		100.01
S88	Granitoid A1	Biotite	1.09	12.20	18.38	40.18	4.65	1.54	3.43	0.15	18.18	0.20		100.00
S88	Granitoid A1	Biotite	0.85	12.32	17.71	39.94	5.43	1.64	3.87	0.27	17.68	0.29		100.00
S83	Granitoid B1	Muscovite	0.44	1.88	34.57	50.80	8.68	0.39	0.51	0.12	2.60			99.99
S83	Granitoid B1	Muscovite	0.21	2.06	35.81	48.98	8.23	0.47	0.25	0.08	3.93			100.02
S83	Granitoid B1	Muscovite or faded biotite	0.31	3.52	30.55	46.68	7.48	0.54	1.16	0.06	9.70			100.00
S1	Granitoid C	Biotite	0.85	8.70	25.78	38.84	4.33	1.57	2.37	0.39	17.16			99.99
S1	Granitoid C	Muscovite	0.27	2.08	35.69	50.37	7.56	0.62	0.30	0.20	2.90		9.84	99.99
S1	Granitoid C	Muscovite	1.16	1.47	37.73	47.02	9.93	0.25	0.61	0.16	1.67			100.00
S1	Granitoid C	Muscovite	1.04	1.31	37.27	47.54	9.89	0.25	0.94	0.19	1.56			99.99
S1	Granitoid C	Muscovite	0.93	1.43	36.62	47.58	9.66	0.35	1.31	0.20	1.92			100.00

	Petrographic group	Identification	Na_2O (wt%)	MgO (wt%)	Al_2O_3 (wt%)	SiO_2 (wt%)	K_2O (wt%)	CaO (wt%)	TiO_2 (wt%)	MnO (wt%)	Fe_2O_3 (wt%)	P_2O_5 (wt%)	N_2O_5 (wt%)	SUM (wt%)
S87	Granitoid C	Biotite	1.20	11.62	21.49	37.92	2.80	1.03	0.56	0.30	23.08			100.00
S87	Granitoid C	Biotite	0.50	10.37	21.42	39.86	5.20	0.97	2.02	0.29	18.81	0.56		100.00
S5	Granitoid D	Muscovite	0.57	1.06	35.92	49.67	9.57	0.39	0.53	0.11	2.19			100.01
S5	Granitoid D	Muscovite	0.84	1.24	36.48	47.49	10.38	0.18	0.66	0.11	2.61			99.99
S5	Granitoid D	Muscovite	1.06	1.28	37.09	46.82	10.48	0.27	0.75	0.08	2.18			100.01
S5	Granitoid D	Muscovite	1.44	1.33	37.22	46.98	9.87	0.29	0.69	0.15	2.03			100.00
S11	Diorite A	Biotite	1.02	12.44	25.24	47.56	0.69	2.37	0.44	0.44	9.81			100.01
S11	Diorite A	Biotite	1.33	13.56	22.79	47.59	0.69	2.67	0.43	0.21	10.72			99.99
S57	Carbonate A	Biotite	1.44	29.19	17.31	44.09	0.71	3.75	0.79	0.17	2.55			100.00
S109	Graphite A5	Muscovite	0.39	3.91	29.57	52.46	7.72	0.52	0.18	0.27	4.97			99.99
S109	Graphite A5	Muscovite	0.83	2.09	36.09	47.73	10.91	0.24	1.10	0.10	0.91			100.00
S130	Graphite B	Muscovite	0.27	1.79	35.28	48.56	11.30	0.52	1.30	0.11	0.86			99.99
S132	Graphite C1	Muscovite	0.91	2.32	34.88	48.13	8.18	1.62	0.44	0.21	3.31			100.00
S13	Graphite D	Muscovite	1.22	1.90	35.01	48.43	10.14	0.79	0.24	0.17	2.09			99.99
S15	Individual sample	Biotite	1.09	11.21	24.57	33.59	0.56	1.25	0.42	0.27	27.03			99.99
S15	Individual sample	Biotite	0.65	10.64	25.81	36.62	1.91	0.86	0.28	0.19	23.04			100.00
S15	Individual sample	Muscovite	1.38	1.30	36.16	50.06	8.55	0.49	0.29	0.15	1.61			99.99
S15	Individual sample	Muscovite	1.56	2.58	34.01	47.95	8.77	0.43	0.62	0.18	3.90			100.00
S15	Individual sample	Muscovite	0.84	2.04	35.16	49.23	8.74	0.27	0.14	0.07	3.51			100.00
S15	Individual sample	Muscovite	5.50	0.93	31.51	53.43	5.93	0.67	0.32	0.20	1.51			100.00
S15	Individual sample	Muscovite	5.13	0.79	31.83	54.51	5.46	0.78	0.16	0.20	1.14			100.00
S15	Individual sample	Muscovite	6.30	0.62	30.15	56.27	4.62	0.63	0.17	0.19	1.05			100.00

Garnet

	Petrographic group	Identification	Na_2O (wt%)	MgO (wt%)	Al_2O_3 (wt%)	SiO_2 (wt%)	K_2O (wt%)	CaO (wt%)	TiO_2 (wt%)	MnO (wt%)	Fe_2O_3 (wt%)	SUM (wt%)
S32	Graphite A3	Almandine	0.64	4.29	21.99	37.07	0.13	5.08	0.17	11.77	18.86	100.00
S32	Graphite A3	Almandine	0.94	2.41	22.15	39.07	0.27	7.67	0.19	7.34	19.96	100.00
S32	Graphite A3	Almandine	0.56	4.18	21.78	36.77	0.11	8.61	0.17	6.12	21.70	100.00
S36	Graphite A3	Spessartine	0.73	4.82	22.38	39.36	0.27	3.65	0.43	25.00	3.37	100.01
S36	Graphite A3	Spessartine	0.63	3.87	22.77	40.02	0.28	3.65	0.37	25.04	3.36	99.99
S36	Graphite A3	Spessartine	0.46	4.84	22.11	36.54	0.10	3.81	0.40	29.46	2.28	100.00
S36	Graphite A3	Spessartine	0.52	6.91	23.07	38.56	0.28	2.17	0.23	14.24	14.02	100.00
S36	Graphite A3	Spessartine	0.50	6.37	22.55	38.26	0.41	3.15	0.21	15.59	12.97	100.01
S86	Graphite A3	Almandine?	0.78	6.30	22.35	36.45	0.34	2.06	0.35	13.41	17.96	100.00
S86	Graphite A3	Spessartine	0.55	5.75	23.32	37.62	0.24	2.79	0.18	19.93	9.61	99.99
S86	Graphite A3	Almandine	0.80	6.63	23.28	38.53	0.58	3.26	0.13	9.13	17.66	100.00
S54	Graphite D	Spessartine	0.68	6.20	22.83	37.15	0.17	1.83	0.16	16.18	14.81	100.01
S54	Graphite D	Spessartine	0.88	5.81	23.83	38.88	0.35	1.43	0.14	14.59	14.10	100.01
S54	Graphite D	Spessartine	0.68	6.43	24.27	38.92	0.21	2.06	0.12	13.85	13.45	99.99
S54	Graphite D	Spessartine	0.73	6.26	22.81	36.79	0.21	1.43	0.64	15.32	15.81	100.00
S54	Graphite D	Spessartine	0.75	5.91	23.01	37.16	0.17	1.51	0.35	15.58	15.58	100.02
S15	Individual sample	Almandine	0.45	9.13	21.66	37.65	0.13	4.22	0.27	0.41	26.08	100.00

	Petrographic group	Identification	Na_2O (wt%)	MgO (wt%)	Al_2O_3 (wt%)	SiO_2 (wt%)	K_2O (wt%)	CaO (wt%)	TiO_2 (wt%)	MnO (wt%)	Fe_2O_3 (wt%)	SUM (wt%)
S15	Individual sample	Almandine	0.51	10.12	22.63	38.16	0.16	3.46	0.21	0.34	24.42	100.01
S15	Individual sample	Almandine	0.76	9.20	22.69	37.62	0.28	4.06	0.23	0.41	24.75	100.00

Calcite

Carbon was excluded from the measurements.

	Petrographic groups	Na_2O (wt%)	MgO (wt%)	Al_2O_3 (wt%)	SiO_2 (wt%)	K_2O (wt%)	CaO (wt%)	TiO_2 (wt%)	MnO (wt%)	Fe_2O_3 (wt%)	SUM (wt%)
S57	Carbonate A	1.16	1.13	1.22	3.47	0.19	91.49	0.36	0.33	0.64	99.99
S57	Carbonate A	1.01	0.89	1.58	3.74	0.18	91.15	0.31	0.48	0.66	100.00
S57	Carbonate A	1.23	0.81	2.21	5.84	0.20	87.74	0.56	0.41	1.01	100.01
S57	Carbonate A	1.20	1.54	1.87	5.50	0.13	88.32	0.42	0.36	0.65	99.99
S58	Carbonate A	0.97	0.69	0.95	2.81	0.08	93.32	0.38	0.29	0.51	100.00
S58	Carbonate A	0.95	1.18	1.00	3.42	0.09	92.26	0.38	0.20	0.52	100.00
S58	Carbonate A	1.13	0.81	2.01	5.16	0.15	89.20	0.50	0.26	0.77	99.99
S89	Carbonate B	0.68	1.51	1.98	3.37	0.22	90.41	0.46	0.36	1.01	100.00
S89	Carbonate B	0.73	1.25	1.61	2.61	0.27	91.55	0.56	0.41	1.01	100.00
S89	Carbonate B	0.64	1.10	2.43	3.51	0.32	89.50	0.55	0.44	1.51	100.00
S89	Carbonate B	0.64	2.79	1.23	5.86	0.24	87.55	0.53	0.42	0.75	100.01
S132	Graphite C1	0.59	0.58	1.07	2.41	0.25	93.50	0.49	0.38	0.72	99.99
S132	Graphite C1	0.54	0.74	2.78	7.76	0.85	84.13	0.43	0.40	2.39	100.02
S132	Graphite C1	0.60	1.37	3.39	5.77	0.56	85.36	0.51	0.51	1.93	100.00

Surface layer and matrix of S113

		Na_2O (wt%)	MgO (wt%)	Al_2O_3 (wt%)	SiO_2 (wt%)	K_2O (wt%)	CaO (wt%)	TiO_2 (wt%)	MnO (wt%)	Fe_2O_3 (wt%)	P_2O_5 (wt%)	SUM (wt%)
S113	Deposition	1.40	2.88	1.26	2.56	0.28	48.38	0.20	0.13	0.85	42.07	100.01
S113	Deposition	1.47	2.15	1.37	2.65	0.38	49.28	0.23	0.12	0.54	41.22	99.41
S113	Deposition	0.33	0.61	0.53	1.90	0.21	56.94	0.16	0.14	0.47	38.72	100.01
S113	Deposition	1.64	1.87	1.11	2.20	0.21	50.52	0.25	0.11	0.57	41.05	99.53
S113	Matrix	0.97	3.38	24.08	52.99	3.62	2.96	3.10	0.16	7.45	1.28	99.99
S113	Matrix	2.07	2.24	24.33	56.42	3.06	3.05	0.85	0.08	6.66	1.25	100.01
S113	Matrix	0.00	1.71	25.51	61.40	2.73	2.35	0.00	0.00	5.32	0.98	100.00
S113	Matrix	0.88	3.61	26.95	53.99	6.95	1.27	0.55	0.13	5.14	0.51	99.98

Appendix E ICP-OES analysis data of the ceramics

E.1 Chemical composition of the samples by ICP-OES

	Petrographic group	Batch	Al_2O_3	CaO	Fe_2O_3	K_2O	MgO	Na_2O	P_2O_5	SiO_2	TiO_2	Ba	Cr	Cu	Mn	Ni	Pb	Rb	Sc	Sn	Sr	V	Y	Zn	Zr	LOI
			wt%	wt%	wt%	wt%	wt%	wt%	wt%	wt%	wt%	ppm	ppm	ppm	ppm	ppm	ppm	ppm	ppm	ppm	ppm	ppm	ppm	ppm	ppm	ppm	
S10-1	Granitoid A1	Batch1	19.15	2.83	7.92	4.51	2.66	1.65	0.60	59.04	1.28	1475	199	22	533	59	70	184	19	< 34	366	119	30	< 187	379	6.88%
S10-2	Granitoid A1	Batch2	18.89	2.85	7.68	4.57	2.61	1.87	0.61	59.30	1.24	1503	193	142	596	65	39	194	19	< 30	379	124	30	113	388	7.38%
S70	Granitoid A1	Batch2	19.55	2.75	8.71	4.29	2.81	1.70	1.61	56.90	1.31	1455	207	36	671	87	39	190	21	< 30	356	132	35	153	420	8.98%
S88	Granitoid A1	Batch2	19.11	3.68	8.03	4.74	2.75	1.72	2.10	56.17	1.25	1867	207	238	690	56	48	193	20	28	494	117	31	133	432	5.97%
S98	Granitoid A1	Batch1	19.59	3.15	8.04	4.75	3.04	1.75	0.56	57.48	1.30	1386	212	25	408	46	< 55	214	19	< 34	390	119	25	204	344	7.00%
S52	Granitoid A2	Batch2	22.42	1.02	6.00	4.27	0.76	0.51	0.15	63.33	1.20	1284	179	82	171	117	46	180	26	< 31	548	194	55	266	303	11.45%
S65	Granitoid A2	Batch1	19.81	1.89	7.47	5.02	1.85	1.25	2.31	58.93	1.05	1767	160	28	660	107	< 55	202	18	< 34	388	101	37	< 183	478	6.06%
S78	Granitoid A2	Batch2	18.46	2.09	6.90	4.98	1.78	1.60	1.20	61.31	1.27	1655	172	193	778	51	42	215	18	< 28	359	115	32	105	454	4.00%
S40	Granitoid A3	Batch1	27.64	2.09	6.64	2.14	1.20	0.53	0.57	57.21	1.75	694	153	32	< 303	47	< 58	78	23	63	144	176	38	219	331	9.72%
S51	Granitoid A3	Batch2	27.44	0.98	7.13	1.62	0.51	1.00	0.38	59.61	1.14	362	126	239	359	55	74	91	22	< 31	129	165	30	88	190	11.12%
S12	Granitoid B1	Batch1	16.69	1.26	6.19	3.41	1.22	0.73	0.08	68.99	1.17	1100	70	47	< 304	26	< 58	163	14	40	144	102	29	217	514	9.36%
S83	Granitoid B1	Batch2	18.31	1.00	7.25	3.26	1.15	0.87	1.11	65.71	1.06	1030	93	179	484	55	44	176	19	< 29	142	139	41	111	289	7.73%
S9	Granitoid B2	Batch1	18.46	1.74	7.13	3.08	0.94	0.72	0.21	66.68	0.83	852	71	20	< 294	33	< 56	109	23	< 34	102	112	70	< 187	225	7.77%
S93	Granitoid B2	Batch2	17.90	2.38	7.80	2.24	1.45	1.76	0.95	64.26	1.03	836	77	28	506	47	< 30	119	21	< 29	150	123	48	107	244	6.32%
S45	Granitoid B3	Batch2	21.22	1.23	6.41	2.34	0.80	0.43	0.52	65.75	1.13	579	114	20	185	39	< 31	122	19	< 30	89	151	28	96	205	7.92%
S46	Granitoid B3	Batch2	22.68	1.39	3.98	2.07	0.55	0.60	0.54	66.66	1.34	621	116	26	157	27	< 31	89	19	< 30	86	137	31	64	210	8.89%
S1	Granitoid C	Batch1	18.87	1.59	7.44	3.74	2.40	0.88	0.24	63.50	1.06	1046	148	35	390	61	< 57	199	19	< 35	144	122	34	< 190	314	8.11%
S87	Granitoid C	Batch2	18.66	1.68	9.03	3.82	2.65	0.81	2.26	59.55	1.16	1420	145	194	866	66	38	190	21	< 29	261	131	30	128	335	7.40%
S5	Granitoid D	Batch2	20.81	1.29	5.56	4.75	1.43	0.56	0.21	64.53	0.63	785	69	28	371	39	40	319	16	< 30	133	98	39	138	138	8.83%
S21	Granitoid D	Batch1	22.20	1.70	9.28	4.33	2.71	0.46	0.39	57.53	1.08	974	126	45	755	107	77	171	19	< 37	319	133	33	284	210	14.29%
S8	Amphibole	Batch1	17.96	3.78	7.64	2.50	2.99	1.99	0.10	62.02	0.80	764	96	37	361	36	< 54	95	18	< 33	299	153	16	< 181	133	5.14%
S61	Amphibole	Batch2	18.19	4.92	10.18	1.63	3.40	1.94	2.06	56.13	1.24	906	93	216	921	58	< 31	56	25	< 30	359	260	18	120	75	8.00%
S90	Amphibole	Batch1	18.95	5.04	8.84	1.17	4.72	1.59	0.47	58.36	0.68	362	113	36	547	56	< 53	82	29	< 32	238	157	14	< 177	75	2.52%

	Petrographic group	Batch	Al_2O_3	CaO	Fe_2O_3	K_2O	MgO	Na_20	P_2O_5	SiO_2	TiO_2	Ba	Cr	Cu	Mn	Ni	Pb	Rb	Sc	Sn	Sr	V	Y	Zn	Zr	LOI
			wt%	wt%	wt%	wt%	wt%	wt%	wt%	wt%	wt%	ppm	ppm	ppm	ppm	ppm	ppm	ppm	ppm	ppm	ppm	ppm	ppm	ppm	ppm	ppm	
S11	Diorite A	Batch1	15.95	2.82	7.98	3.30	3.89	1.49	0.17	62.68	1.14	2893	286	52	666	116	67	111	18	< 35	856	138	41	< 191	334	8.45%
S75	Diorite A	Batch1	16.00	2.94	8.43	3.78	4.40	1.58	1.28	59.58	1.28	3993	340	48	718	149	< 54	101	19	< 34	1082	121	39	292	267	5.25%
S67	Diorite B	Batch2	16.89	3.58	7.92	2.78	3.98	2.50	1.06	59.97	1.03	719	296	202	743	100	38	119	20	< 29	265	143	24	113	155	3.40%
S97	Diorite B	Batch1	17.34	5.11	8.86	2.69	5.75	2.38	0.38	56.02	1.20	517	286	45	787	65	< 55	151	21	< 34	339	162	21	< 185	201	6.69%
S57	Carbonate A	Batch1	17.15	7.76	4.01	1.97	1.43	0.89	1.34	64.27	0.98	677	100	19	< 313	44	< 59	99	15	< 37	297	100	32	235	231	13.06%
S58	Carbonate A	Batch2	16.36	10.07	3.87	2.02	1.68	0.89	1.01	62.92	0.94	699	97	209	526	43	< 34	122	15	< 33	350	101	33	101	202	13.64%
S89	Carbonate B	Batch1	20.01	24.48	7.05	1.74	2.05	0.20	1.27	41.78	1.21	494	111	19	< 353	44	< 67	72	17	< 41	615	120	37	< 224	149	23.29%
S102	Graphite A1	Batch1	16.37	1.65	5.20	3.80	1.00	1.60	0.23	69.01	0.94	451	107	33	491	14	< 77	120	16	< 47	97	207	36	< 258	262	32.51%
S103	Graphite A1	Batch2	15.68	1.41	5.16	3.37	1.15	1.64	0.20	70.18	0.98	473	97	208	628	26	< 45	123	15	< 44	101	148	39	85	280	37.37%
S110	Graphite A1	Batch2	20.92	1.37	12.49	4.14	1.74	0.25	0.34	57.10	1.17	730	123	361	2105	233	< 39	181	26	< 37	110	466	82	119	227	25.54%
S100	Graphite A2	Batch2	21.07	2.92	5.57	3.84	1.61	2.59	0.20	60.96	0.98	670	111	55	704	48	< 50	170	17	< 48	169	206	27	81	174	42.58%
S104	Graphite A2	Batch1	19.12	2.33	6.99	2.61	1.38	4.71	0.25	61.51	0.94	330	109	22	< 388	22	< 74	86	15	< 45	122	178	20	< 246	195	29.29%
S32	Graphite A3	Batch2	16.65	2.62	6.95	2.99	1.54	1.54	0.81	64.92	0.94	964	125	55	8179	48	< 36	142	21	< 34	231	229	46	110	175	20.15%
S36	Graphite A3	Batch1	16.51	1.56	11.76	4.27	2.07	0.61	2.19	58.13	1.61	1065	124	87	10212	124	< 72	189	26	< 44	140	235	51	287	115	27.10%
S86	Graphite A3	Batch2	24.87	1.45	7.12	5.89	1.07	0.73	0.74	55.20	1.66	1820	196	66	9501	49	< 44	230	29	< 42	378	313	45	87	135	34.78%
S107	Graphite A3	Batch1	22.66	2.29	9.22	2.83	2.39	0.45	0.62	58.03	0.93	813	111	41	3827	65	< 63	116	18	< 39	127	185	48	< 210	160	17.23%
S31	Graphite A4	Batch1	24.56	2.13	16.53	3.16	0.79	1.00	1.44	49.30	0.80	828	192	80	441	71	< 82	81	22	< 51	89	460	48	282	38	36.53%
S128	Graphite A4	Batch2	19.31	2.06	11.57	3.06	1.89	2.16	0.84	57.80	1.00	845	137	608	496	163	< 41	125	22	< 39	181	232	63	109	158	30.78%
S35	Graphite A5	Batch2	16.55	2.37	9.15	2.76	1.62	1.87	1.53	62.89	1.00	704	124	62	846	66	< 38	97	16	< 37	165	268	39	105	135	26.20%
S108	Graphite A5	Batch2	19.54	1.70	10.93	3.38	1.54	0.34	1.76	59.31	1.03	1317	119	162	1963	196	< 40	181	23	< 39	218	398	84	119	47	29.26%
S109	Graphite A5	Batch2	18.49	1.18	9.43	4.21	1.12	0.76	1.01	62.57	0.94	824	118	143	912	85	< 37	156	19	< 36	255	242	36	81	95	24.02%
S130	Graphite B	Batch1	20.09	1.23	3.75	5.99	1.51	0.42	0.53	64.90	1.30	644	122	37	698	38	< 69	221	32	< 42	208	400	51	< 230	220	23.75%
S132	Graphite C1	Batch1	16.61	15.21	6.68	3.24	1.64	0.42	1.45	53.30	1.10	924	139	139	1298	75	< 89	139	22	< 55	191	307	32	< 298	59	41.09%
S129	Graphite C2	Batch1	22.52	4.36	7.79	3.13	1.38	2.01	0.56	56.68	1.31	673	139	70	720	60	< 78	68	22	< 48	182	209	27	< 261	167	33.61%
S13	Graphite D	Batch1	18.65	2.95	17.22	2.61	3.88	1.19	0.31	51.89	0.99	465	117	210	988	164	< 63	130	20	< 39	134	290	52	262	163	15.87%
S54	Graphite D	Batch2	27.93	< 1.13	7.67	3.82	0.77	0.85	0.42	55.65	1.17	877	263	82	4299	105	< 39	142	25	< 38	218	241	30	84	198	22.79%
S15	Individual sample	Batch1	18.94	2.30	7.97	2.44	1.91	1.95	0.27	63.10	0.90	761	99	34	417	34	< 55	76	20	< 34	106	144	38	231	179	6.30%

E.2 Statistical analysis (PCA) of chemical data

PCA of all elements

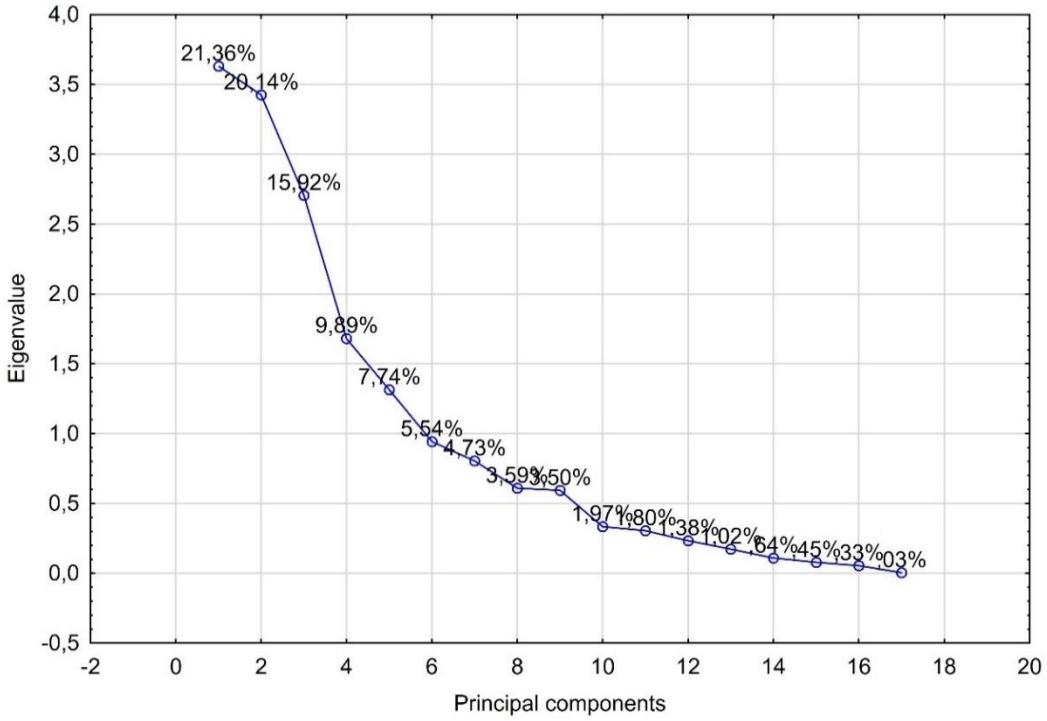
Variable contributions based on all elements

Variable	PC 1	PC 2	PC 3	PC 4	PC 5	PC 6	PC 7	PC 8	PC 9
Al_2O_3	0.005614	0.053890	0.012861	0.237330	0.079463	0.016305	0.125542	0.115888	0.065964
CaO	0.004836	0.001286	0.126777	0.076077	0.291404	0.075964	0.001865	0.000176	0.051753
Fe_2O_3	0.059016	0.064565	0.058875	0.076988	0.025906	0.003883	0.166258	0.031246	0.000112
K_2O	0.087536	0.008682	0.149638	0.001829	0.000851	0.162060	0.001737	0.034719	0.047302
MgO	0.032301	0.049375	0.133936	0.038872	0.017810	0.051336	0.019307	0.104418	0.160386
Na_2O	0.012849	0.041562	0.041807	0.044959	0.275931	0.008515	0.001500	0.008254	0.275936
SiO_2	0.061372	0.018016	0.132260	0.086159	0.003634	0.104399	0.107820	0.001943	0.010811
TiO_2	0.067732	0.004907	0.011895	0.212319	0.008023	0.023138	0.005744	0.286169	0.124014
Ba	0.125034	0.090075	0.001171	0.006463	0.015167	0.076946	0.001998	0.052720	0.000603
Cr	0.125257	0.054983	0.022033	0.006191	0.058706	0.010507	0.001172	0.070040	0.000309
Ni	0.141354	0.031936	0.008144	0.081043	0.010643	0.030843	0.028934	0.007334	0.002451
Rb	0.041670	0.006291	0.159599	0.010192	0.006532	0.322851	0.001863	0.001191	0.027677
Sc	0.068799	0.065873	0.000967	0.042986	0.039883	0.000669	0.307342	0.044270	0.061758
Sr	0.084376	0.110182	0.032539	0.004118	0.054648	0.030836	0.021702	0.071286	0.000532
V	0.035978	0.177689	0.000338	0.005556	0.005869	0.004204	0.058963	0.019924	0.136310
Y	0.040899	0.091959	0.031560	0.067020	0.105474	0.069105	0.000373	0.003955	0.026775
Zr	0.005377	0.128729	0.075600	0.001899	0.000055	0.008439	0.147880	0.146466	0.007308

Variable	PC 10	PC 11	PC 12	PC 13	PC 14	PC 15	PC 16	PC 17
Al_2O_3	0.034939	0.014147	0.007627	0.003919	0.102451	0.000861	0.007691	0.115508
CaO	0.037287	0.000296	0.013945	0.000027	0.012245	0.012499	0.010356	0.283207
Fe_2O_3	0.192453	0.021670	0.001299	0.023575	0.035390	0.006307	0.091842	0.140614
K_2O	0.011611	0.003310	0.004294	0.000317	0.000702	0.363817	0.106087	0.015511
MgO	0.002523	0.003434	0.001891	0.001268	0.304623	0.002630	0.068696	0.007194
Na_2O	0.119517	0.090435	0.052582	0.000492	0.000582	0.014092	0.000332	0.010656
SiO_2	0.000014	0.037407	0.000209	0.005321	0.001301	0.001337	0.014823	0.413172
TiO_2	0.019228	0.071116	0.132783	0.010184	0.014126	0.001059	0.005322	0.002243
Ba	0.145805	0.051062	0.021838	0.001538	0.003923	0.213979	0.186531	0.005147
Cr	0.042932	0.244086	0.149066	0.145408	0.057492	0.001235	0.010381	0.000202
Ni	0.175180	0.059860	0.082678	0.239500	0.066483	0.004497	0.028713	0.000406
Rb	0.018113	0.007617	0.064039	0.004131	0.000628	0.205176	0.121729	0.000700
Sc	0.020277	0.199477	0.018225	0.000458	0.124933	0.002184	0.000624	0.001276
Sr	0.000125	0.057162	0.009781	0.054607	0.045387	0.080235	0.340544	0.001940
V	0.035077	0.037432	0.132135	0.138239	0.134509	0.072420	0.004957	0.000400
Y	0.117772	0.045416	0.002679	0.298866	0.094965	0.001627	0.000004	0.001550
Zr	0.027147	0.056073	0.304928	0.072149	0.000260	0.016045	0.001369	0.000275

Eigenvalues of the correlation matrix based on all elements

No. of PC	Eigenvalue	% Total variance	Cumulative eigenvalue	Cumulative %
1	3.631095	21.35938	3.63109	21.3594
2	3.424272	20.14277	7.05537	41.5022
3	2.705841	15.91671	9.76121	57.4189
4	1.681570	9.89159	11.44278	67.3105
5	1.315118	7.73599	12.75789	75.0464
6	0.942366	5.54333	13.70026	80.5898
7	0.803943	4.72907	14.50420	85.3188
8	0.609672	3.58630	15.11388	88.9051
9	0.594192	3.49525	15.70807	92.4004
10	0.334241	1.96613	16.04231	94.3665
11	0.305847	1.79910	16.34816	96.1656
12	0.233866	1.37568	16.58202	97.5413
13	0.173158	1.01857	16.75518	98.5599
14	0.108301	0.63706	16.86348	99.1969
15	0.076880	0.45224	16.94036	99.6492
16	0.055353	0.32561	16.99571	99.9748
17	0.004285	0.02521	17.00000	100.0000



Eigenvalues and principal components with their percentages of the total variance based on all elements

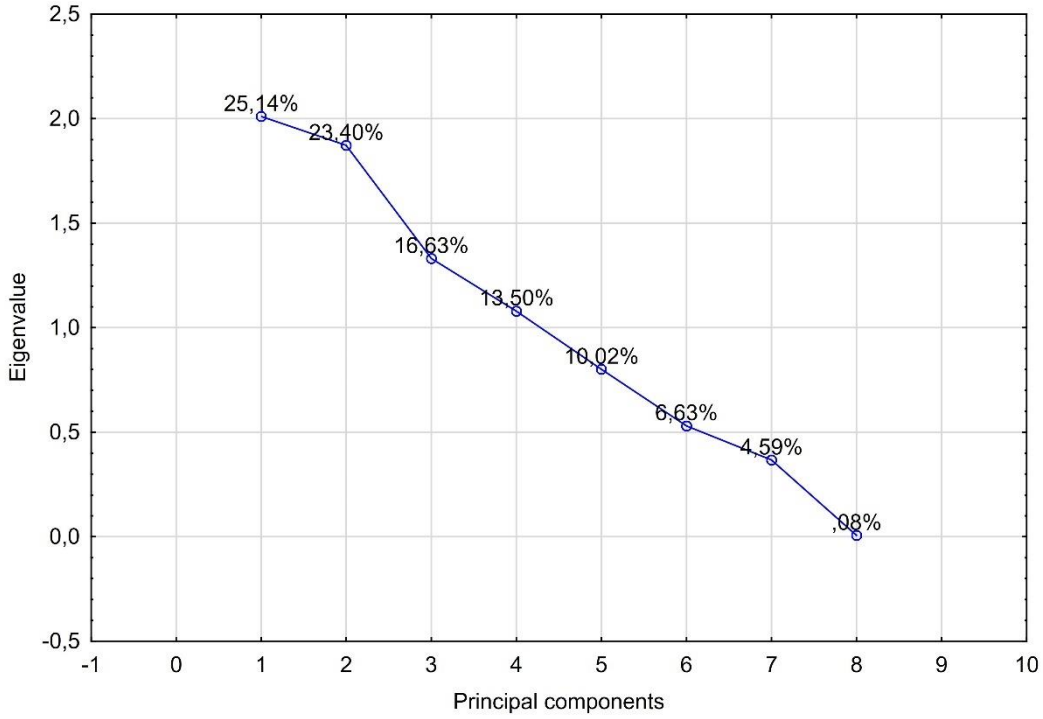
PCA of major elements

Variable contributions based on the major elements

Variable	PC 1	PC 2	PC 3	PC 4	PC 5	PC 6	PC 7	PC 8
Al_2O_3	0.038691	0.288659	0.003421	0.140631	0.174206	0.006415	0.221685	0.126292
CaO	0.176205	0.005730	0.348564	0.111604	0.005042	0.078642	0.008484	0.265729
Fe_2O_3	0.144228	0.057928	0.183605	0.202152	0.081621	0.007900	0.186062	0.136504
K_2O	0.089763	0.036027	0.225377	0.169367	0.112826	0.325573	0.015816	0.025252
MgO	0.255050	0.023827	0.117575	0.070254	0.000780	0.123180	0.392086	0.017248
Na_2O	0.040500	0.154007	0.099550	0.000000	0.495595	0.162904	0.037953	0.009491
SiO_2	0.244084	0.242297	0.000103	0.000118	0.003752	0.092860	0.001064	0.415723
TiO_2	0.011479	0.191525	0.021804	0.305875	0.126178	0.202527	0.136850	0.003762

Eigenvalues of the correlation matrix based on the major elements

No. of PC	Eigenvalue	% Total variance	Cumulative eigenvalue	Cumulative %
1	2.010884	25.13605	2.010884	25.1360
2	1.872306	23.40383	3.883190	48.5399
3	1.330767	16.63458	5.213957	65.1745
4	1.080108	13.50135	6.294065	78.6758
5	0.801621	10.02026	7.095686	88.6961
6	0.530675	6.63344	7.626361	95.3295
7	0.367433	4.59291	7.993794	99.9224
8	0.006206	0.07757	8.000000	100.0000



Eigenvalues and principal components with their percentages of the total variance based on the major elements

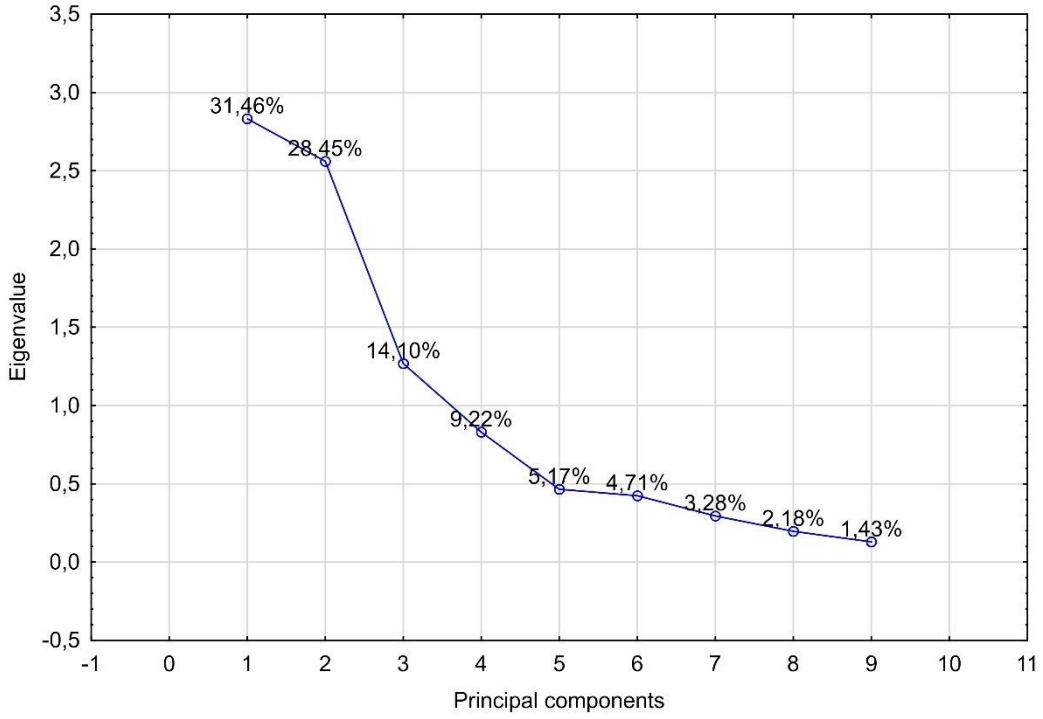
PCA of trace elements

Variable contributions based on the trace elements

Variable	PC 1	PC 2	PC 3	PC 4	PC 5	PC 6	PC 7	PC 8	PC 9
Ba	0.256222	0.048630	0.000098	0.010844	0.027055	0.095290	0.091196	0.005750	0.464915
Cr	0.177276	0.049573	0.097272	0.056454	0.130545	0.187900	0.015619	0.281032	0.004330
Ni	0.002839	0.273450	0.001098	0.130113	0.072002	0.084400	0.290712	0.127967	0.017419
Rb	0.024859	0.018571	0.480557	0.163703	0.188803	0.107601	0.006306	0.000530	0.009071
Sc	0.016577	0.164755	0.011521	0.431682	0.284935	0.000945	0.083808	0.000091	0.005685
Sr	0.246974	0.020349	0.076799	0.009569	0.020784	0.166620	0.006112	0.041204	0.411589
V	0.098734	0.201380	0.007024	0.010161	0.031279	0.005341	0.462384	0.155807	0.027889
Y	0.023153	0.195721	0.123147	0.187141	0.110032	0.003101	0.013245	0.310097	0.034363
Zr	0.153364	0.027572	0.202483	0.000334	0.134566	0.348802	0.030618	0.077522	0.024740

Eigenvalues of the correlation matrix based on the trace elements

No. of PC	Eigenvalue	% Total variance	Cumulative eigenvalue	Cumulative %
1	2.831778	31.46420	2.831778	31.4642
2	2.560412	28.44903	5.392191	59.9132
3	1.268636	14.09596	6.660827	74.0092
4	0.829892	9.22102	7.490718	83.2302
5	0.464931	5.16590	7.955649	88.3961
6	0.424127	4.71252	8.379776	93.1086
7	0.295030	3.27811	8.674806	96.3867
8	0.196633	2.18481	8.871439	98.5715
9	0.128561	1.42846	9.000000	100.0000



Eigenvalues and principal components with their percentages of the total variance based on the trace elements

Comparison of the samples from Lower Austria and samples from Hungary (Zalavár, Dunaszentgyörgy and Daruszentmiklós) and Czechia (Mikulčice, Břeclav, Brno and Kramolín)

PCA of all elements

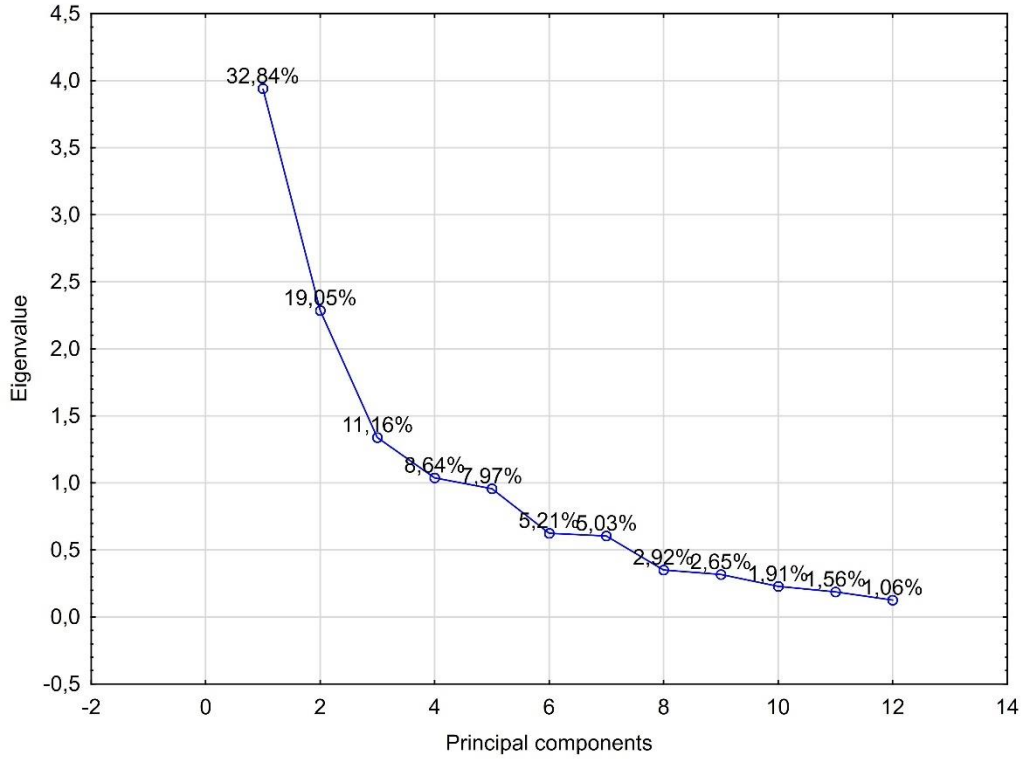
Variable contributions based on all elements

Variable	PC 1	PC 2	PC 3	PC 4	PC 5	PC 6
Al_2O_3	-0.723614	0.005347	0.187554	0.100486	0.440062	0.007453
CaO	-0.133484	0.731086	-0.502497	0.127352	0.042938	0.130171
Fe_2O_3	-0.635449	0.304434	0.405201	-0.089520	0.357032	-0.109969
K_2O	-0.733943	-0.287775	0.072855	0.421399	-0.264636	0.044957
MgO	-0.270189	0.543894	-0.495078	0.327246	0.028180	-0.079464
SiO_2	0.266731	-0.729977	-0.262627	0.003628	0.161413	-0.441617
TiO_2	-0.822717	-0.063350	0.046790	-0.175384	0.348917	0.049802
Ba	-0.762454	-0.157906	-0.194299	-0.305536	-0.282983	-0.266675
Ni	-0.173726	0.475560	0.600813	-0.089006	-0.492662	-0.099944
Rb	-0.621829	-0.397717	0.024504	0.578750	-0.181988	-0.003448
Sr	-0.682555	0.200014	-0.355265	-0.389844	-0.210766	-0.174554
Zr	-0.414710	-0.541754	-0.201009	-0.315021	-0.120709	0.527590

Variable	PC 7	PC 8	PC 9	PC 10	PC 11	PC 12
Al_2O_3	0.273748	-0.371151	-0.099135	-0.035707	-0.112405	-0.030659
CaO	0.192216	0.093158	0.240147	-0.217730	-0.090361	-0.036296
Fe_2O_3	-0.300322	0.215428	-0.084891	-0.162776	0.076697	-0.124785
K_2O	0.130647	0.168723	0.047584	0.182487	-0.090396	-0.185207
MgO	-0.463153	-0.167341	-0.083882	0.149147	-0.008613	0.002795
SiO_2	-0.132368	-0.103704	0.247948	-0.078741	-0.015899	-0.098569
TiO_2	-0.039237	0.105193	0.297596	0.189631	0.020551	0.156209
Ba	-0.043140	0.103464	-0.159380	-0.083729	-0.236248	0.103142
Ni	-0.134665	-0.216603	0.234940	-0.029308	-0.030249	-0.006122
Rb	-0.007088	-0.016836	-0.004206	-0.194241	0.168433	0.141478
Sr	0.242565	-0.077741	-0.042969	0.049596	0.257890	-0.073041
Zr	-0.268984	-0.123720	0.036921	-0.089334	-0.007693	-0.069938

Eigenvalues of the correlation matrix based on all elements

No. of PC	Eigenvalue	% Total variance	Cumulative eigenvalue	Cumulative %
1	3.940968	32.84140	3.94097	32.8414
2	2.285483	19.04569	6.22645	51.8871
3	1.339386	11.16155	7.56584	63.0486
4	1.037212	8.64343	8.60305	71.6921
5	0.956502	7.97085	9.55955	79.6629
6	0.624872	5.20726	10.18442	84.8702
7	0.603955	5.03295	10.78838	89.9031
8	0.350387	2.91989	11.13876	92.8230
9	0.317873	2.64894	11.45664	95.4720
10	0.228923	1.90769	11.68556	97.3797
11	0.187268	1.56056	11.87283	98.9402
12	0.127173	1.05977	12.00000	100.0000



Eigenvalues and principal components with their percentages of the total variance based on all elements

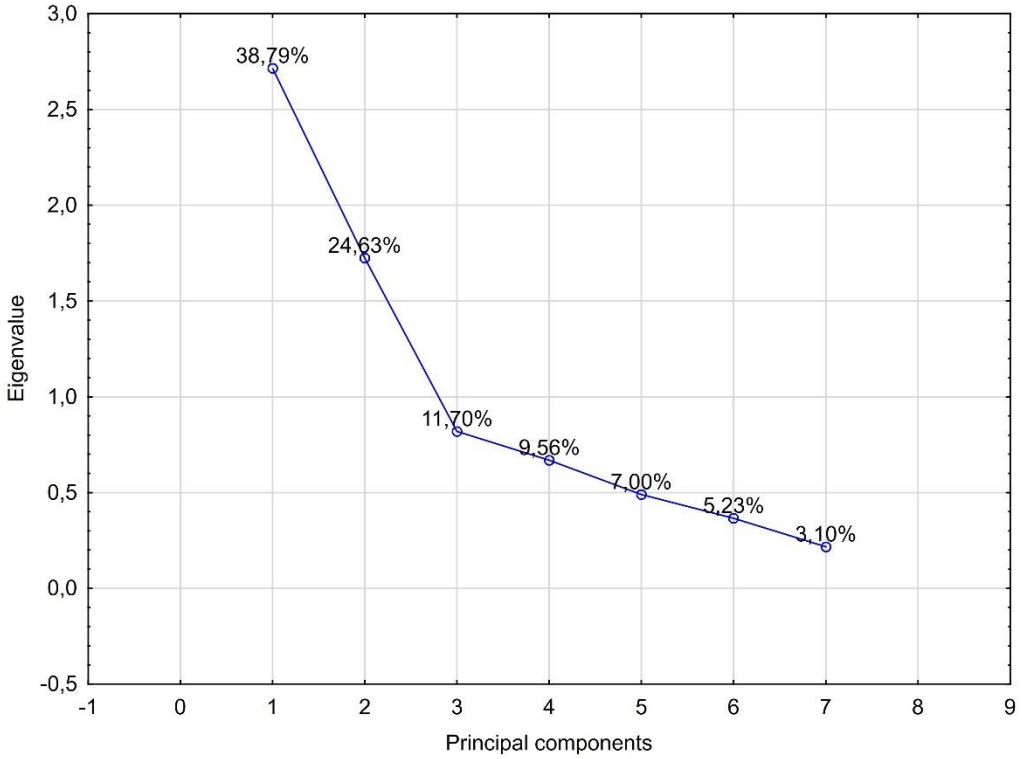
PCA of major elements

Variable contributions based on the major elements

Variable	PC 1	PC 2	PC 3	PC 4	PC 5	PC 6	PC7
Al_2O_3	0.786480	0.289864	0.009060	-0.057462	0.352351	0.411651	-0.020892
CaO	0.310235	-0.817764	-0.157958	0.041859	0.363961	-0.201814	-0.187396
Fe_2O_3	0.786571	0.073100	0.355416	-0.311436	-0.295105	-0.073032	-0.245417
K_2O	0.579512	0.379676	-0.420085	0.542956	-0.178736	-0.056109	-0.116808
MgO	0.387814	-0.669513	-0.454469	-0.227252	-0.302985	0.191568	0.121115
SiO_2	-0.478488	0.522842	-0.526792	-0.429661	0.081366	-0.048573	-0.163059
TiO_2	0.816262	0.316102	-0.085819	-0.189808	0.125088	-0.329207	0.257644

Eigenvalues of the correlation matrix based on the major elements

No. of PC	Eigenvalue	% Total variance	Cumulative eigenvalue	Cumulative %
1	2.714957	38.78510	2.714957	38.7851
2	1.723789	24.62555	4.438746	63.4107
3	0.819241	11.70345	5.257987	75.1141
4	0.669127	9.55895	5.927114	84.6731
5	0.489719	6.99599	6.416833	91.6690
6	0.366102	5.23003	6.782935	96.8991
7	0.217065	3.10093	7.000000	100.0000



Eigenvalues and principal components with their percentages of the total variance based on the major elements

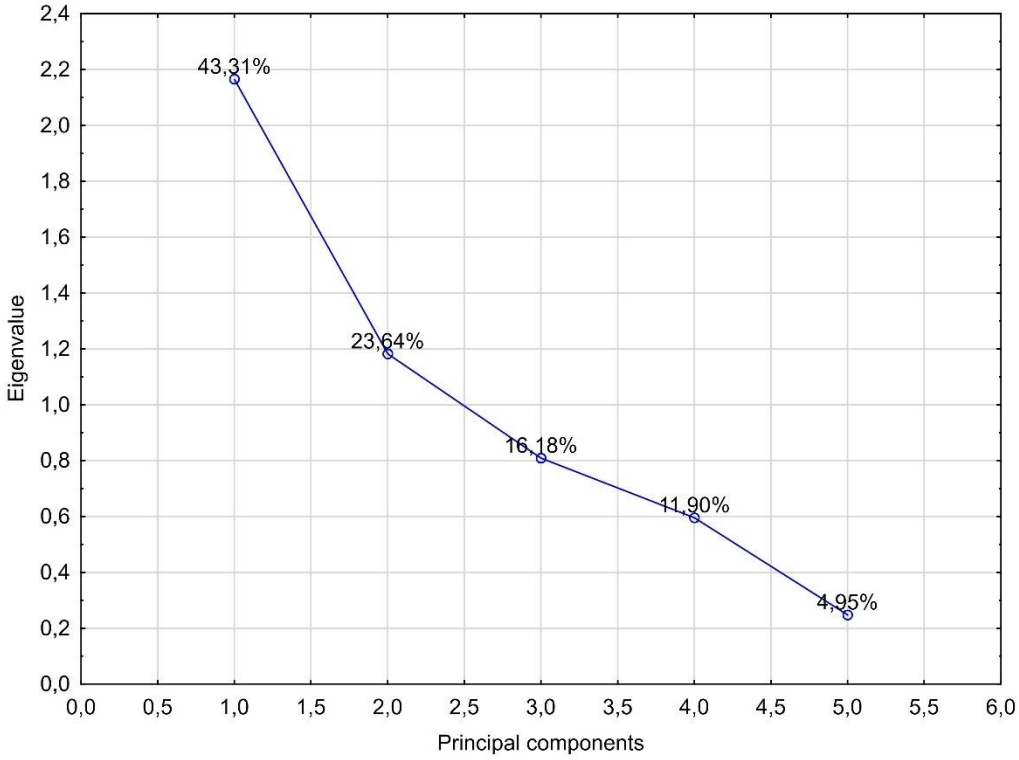
PCA of trace elements

Variable contributions based on the trace elements

Variable	PC 1	PC 2	PC 3	PC 4	PC 5
Ba	-0.899510	-0.166919	0.117740	-0.083360	-0.377106
Ni	-0.026931	-0.863528	-0.361874	0.349590	0.020691
Rb	-0.595017	0.236433	-0.711011	-0.273829	0.097651
Sr	-0.765192	-0.357286	0.396876	-0.200770	0.298342
Zr	-0.645223	0.474428	0.035978	0.592242	0.080996

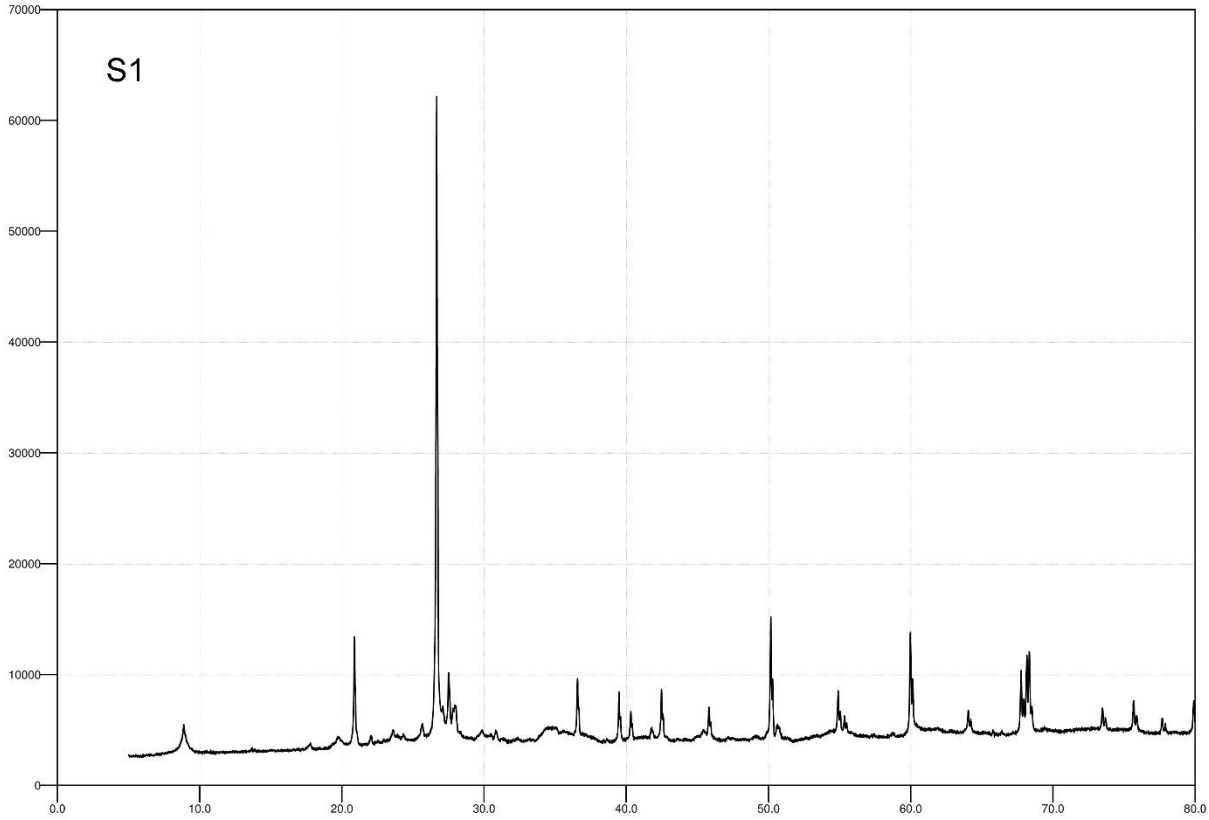
Eigenvalues of correlation matrix based on the trace elements

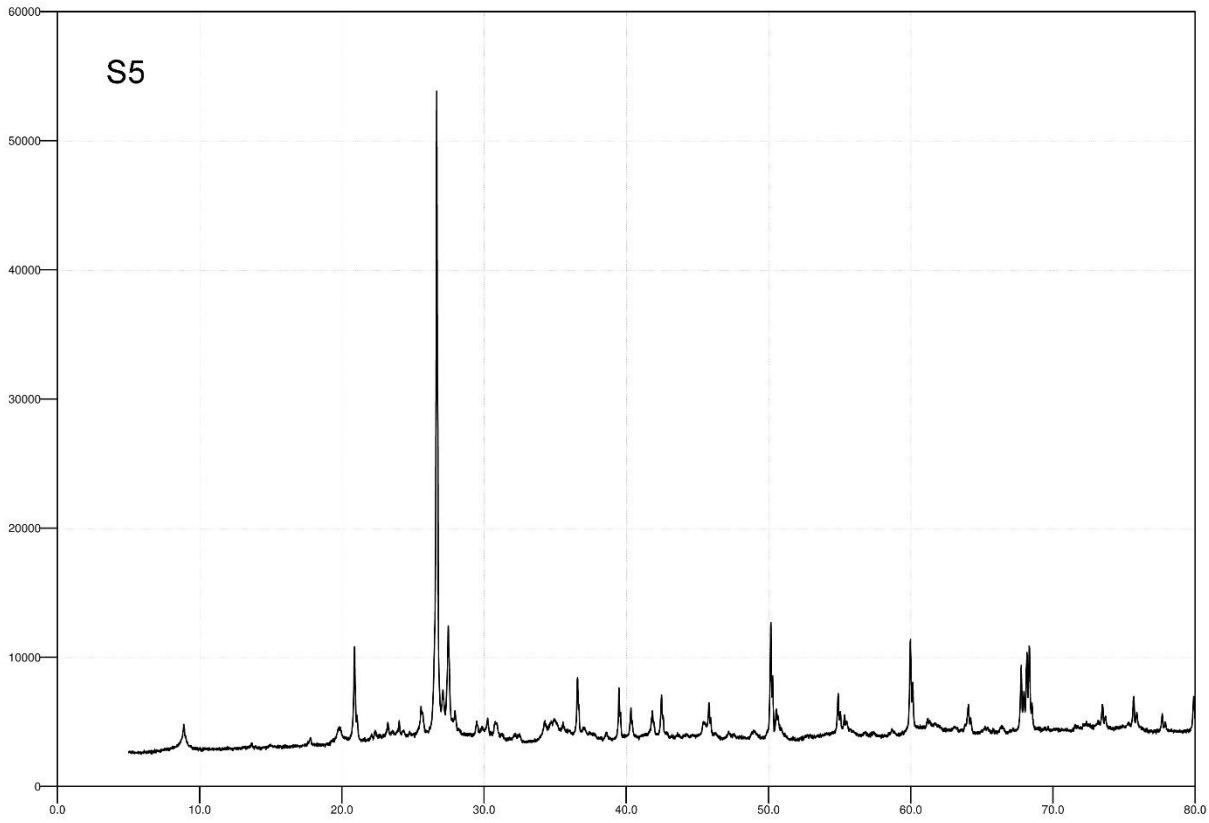
No. of PC	Eigenvalue	% Total variance	Cumulative eigenvalue	Cumulative %
1	2.165719	43.31439	2.165719	43.3144
2	1.182178	23.64356	3.347897	66.9579
3	0.809158	16.18316	4.157055	83.1411
4	0.595203	11.90407	4.752259	95.0452
5	0.247741	4.95482	5.000000	100.0000

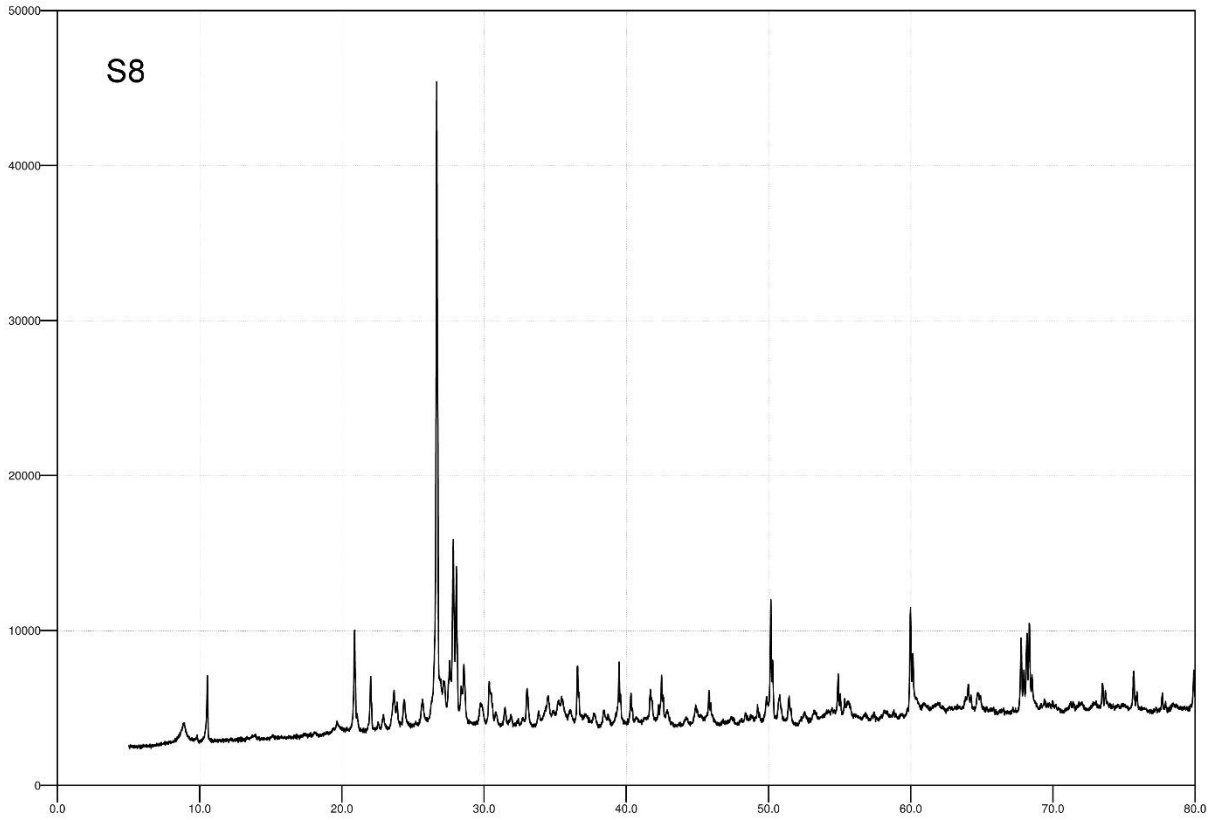


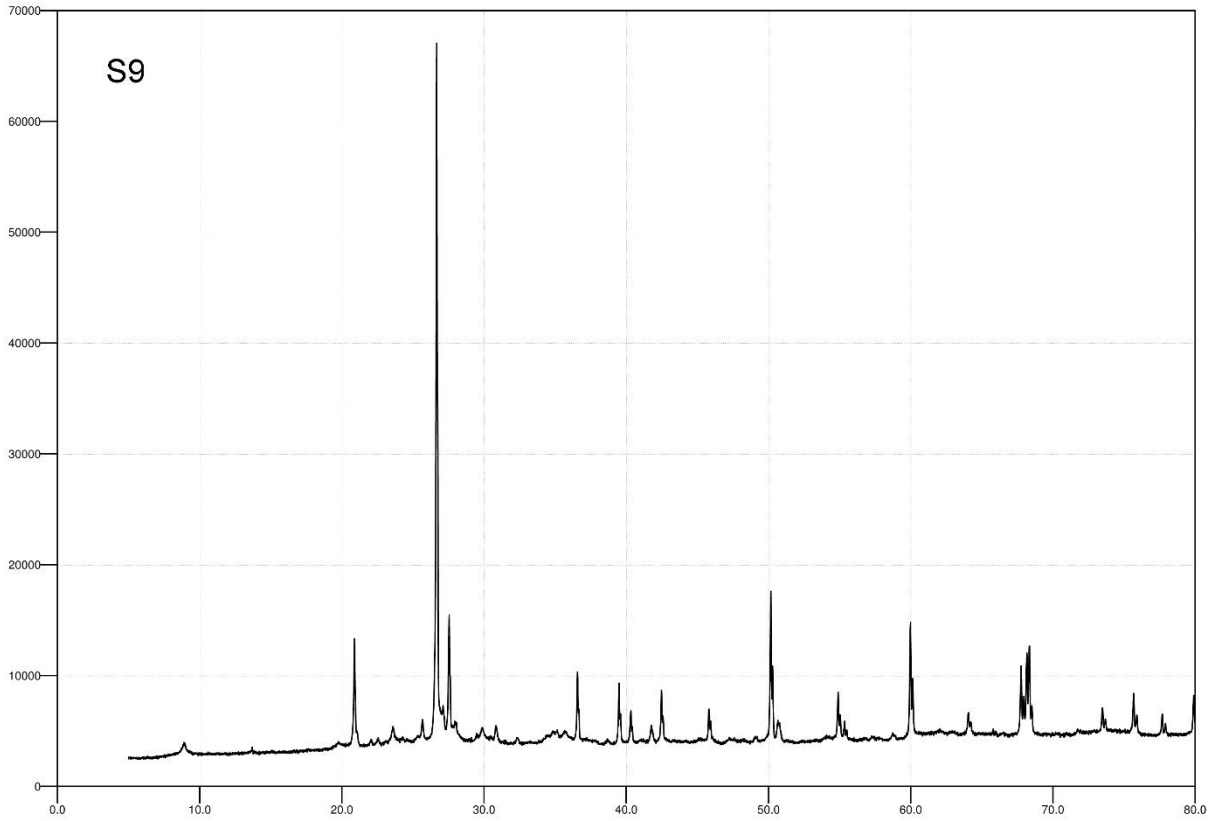
Eigenvalues and principal components with their percentages of the total variance based on the trace elements

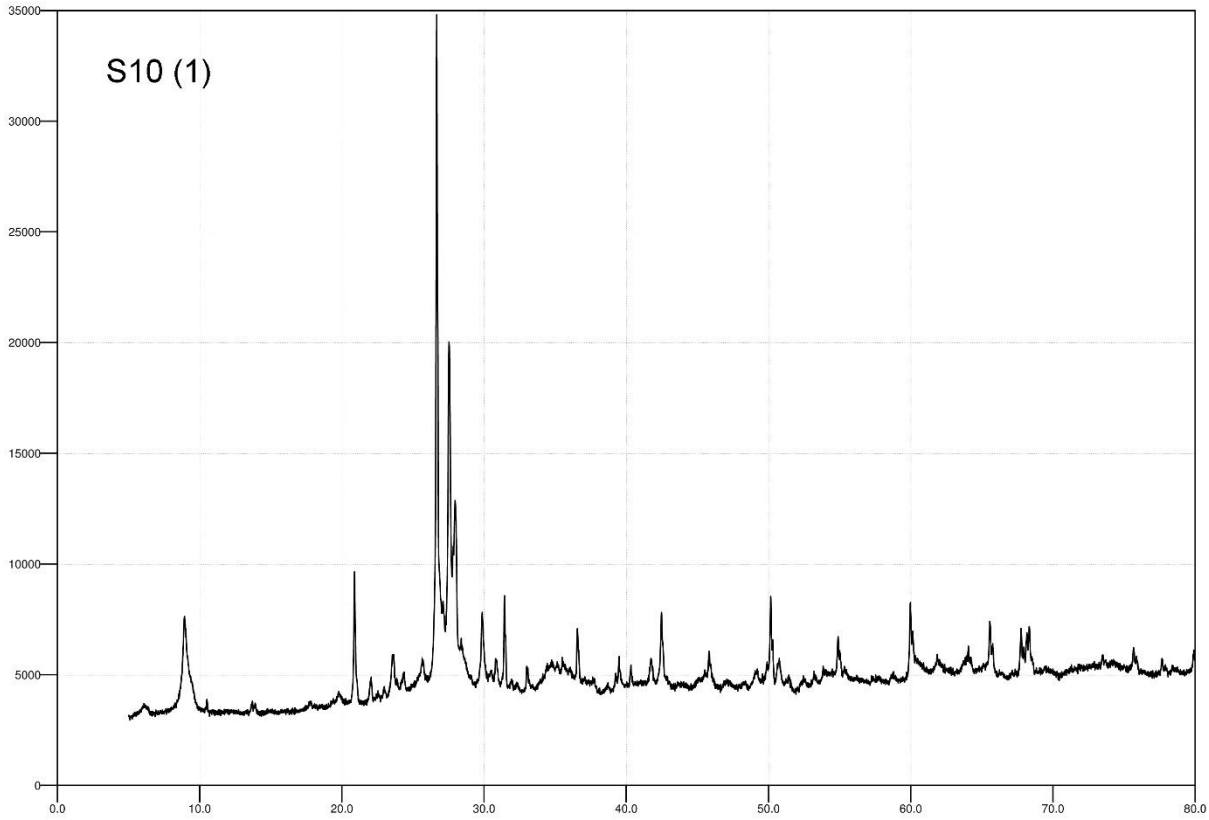
Appendix F Diffractograms of the ceramics analysed by XRD

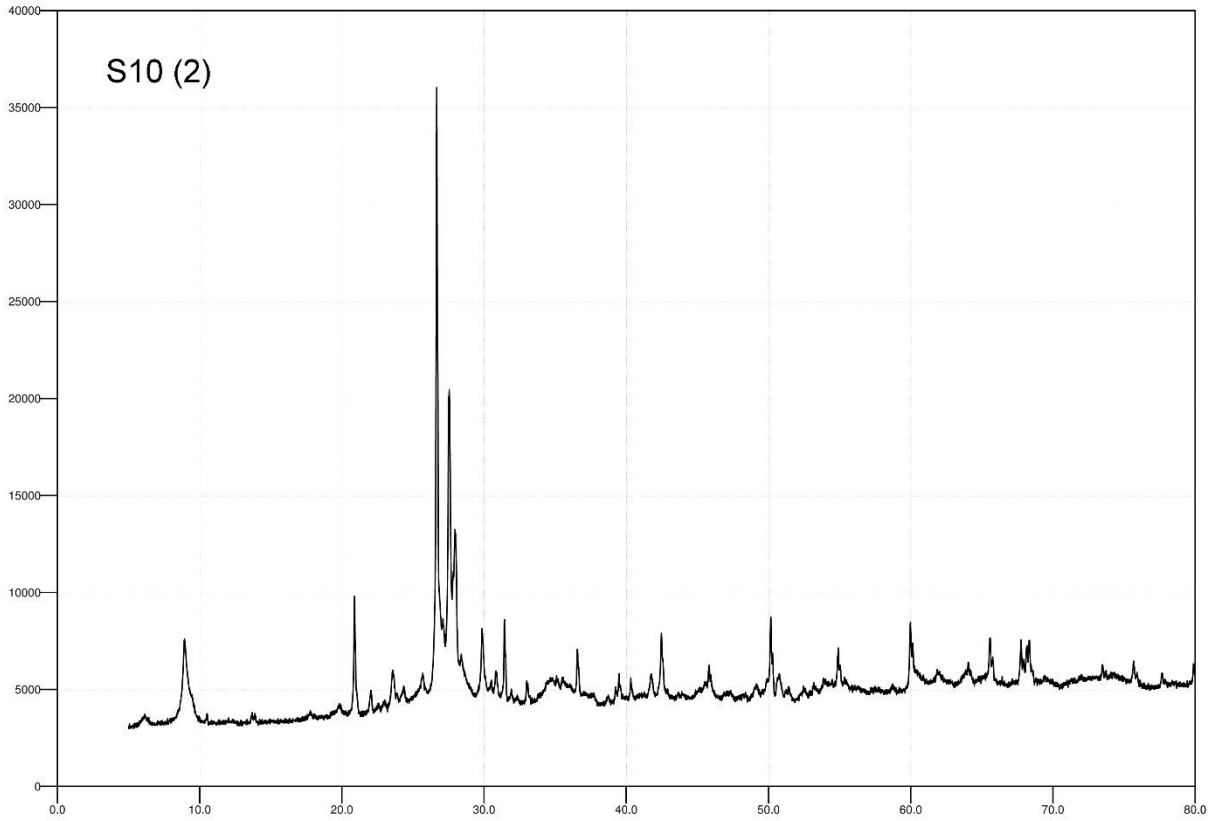


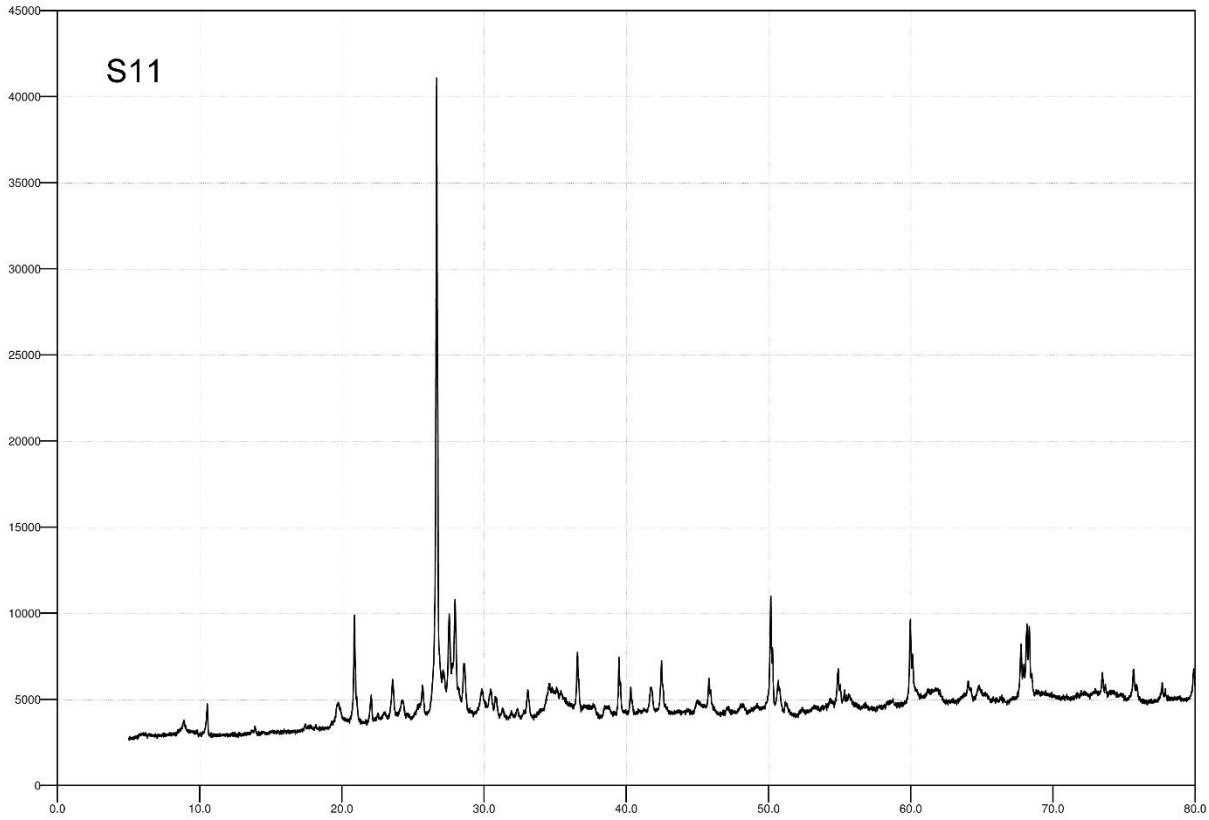


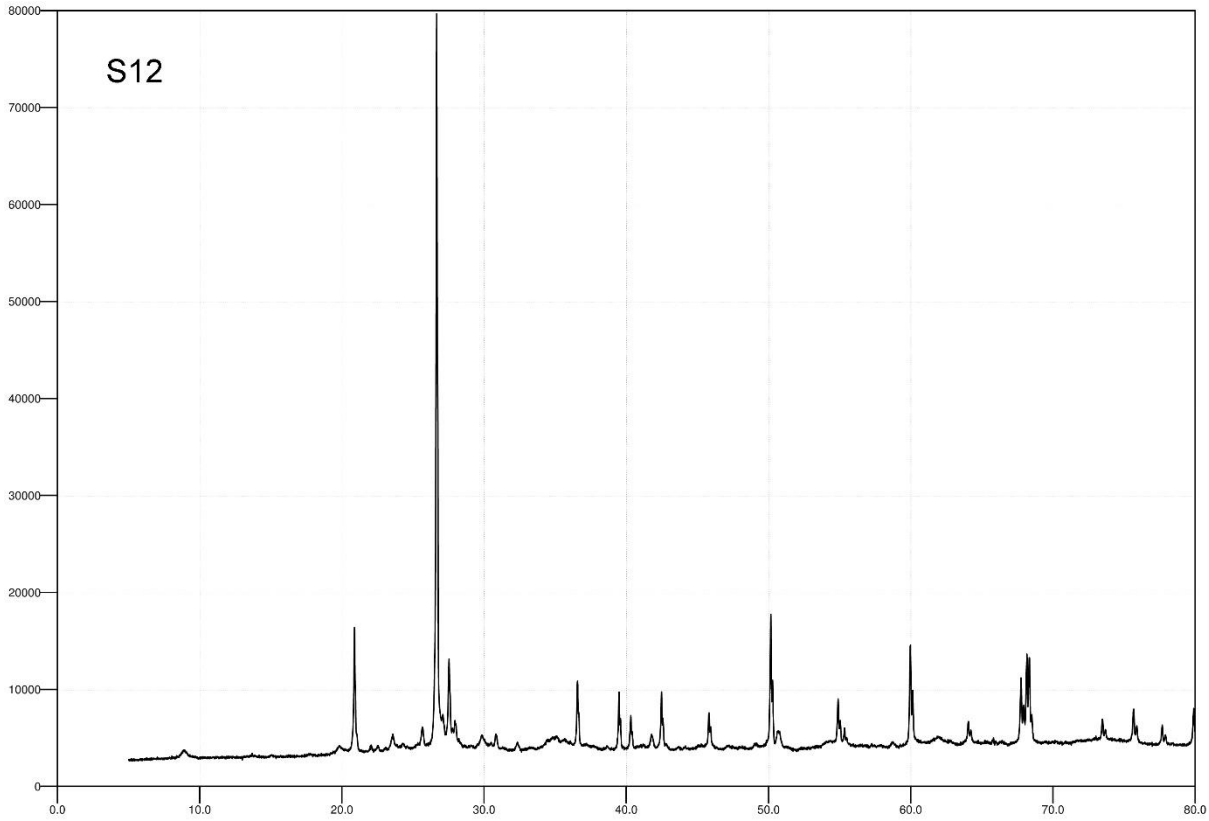

S8
50000
40000
30000
20000
10000
0
0.0
10.0
20.0
30.0
40.0
50.0
60.0
70.0
80.0

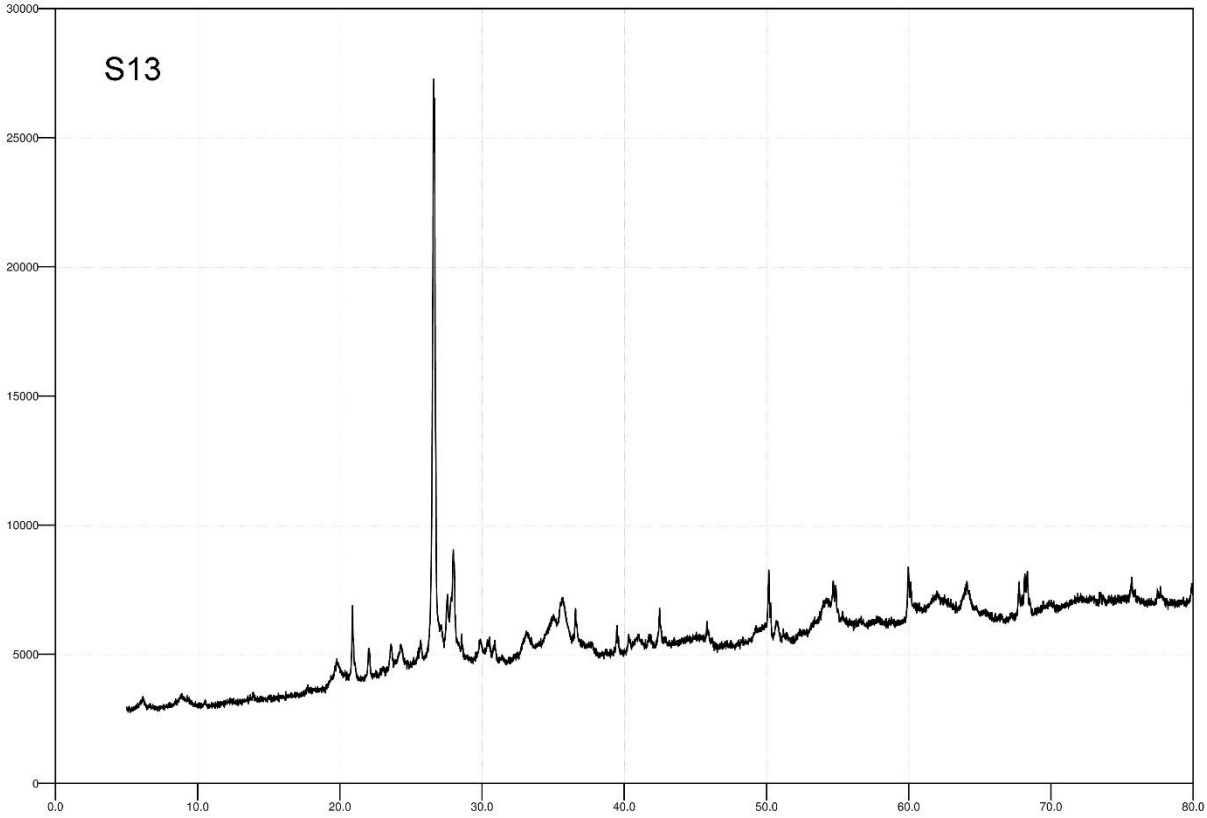

S9
70000
60000
50000
40000
30000
20000
10000
0
0.0
10.0
20.0
30.0
40.0
50.0
60.0
70.0
80.0

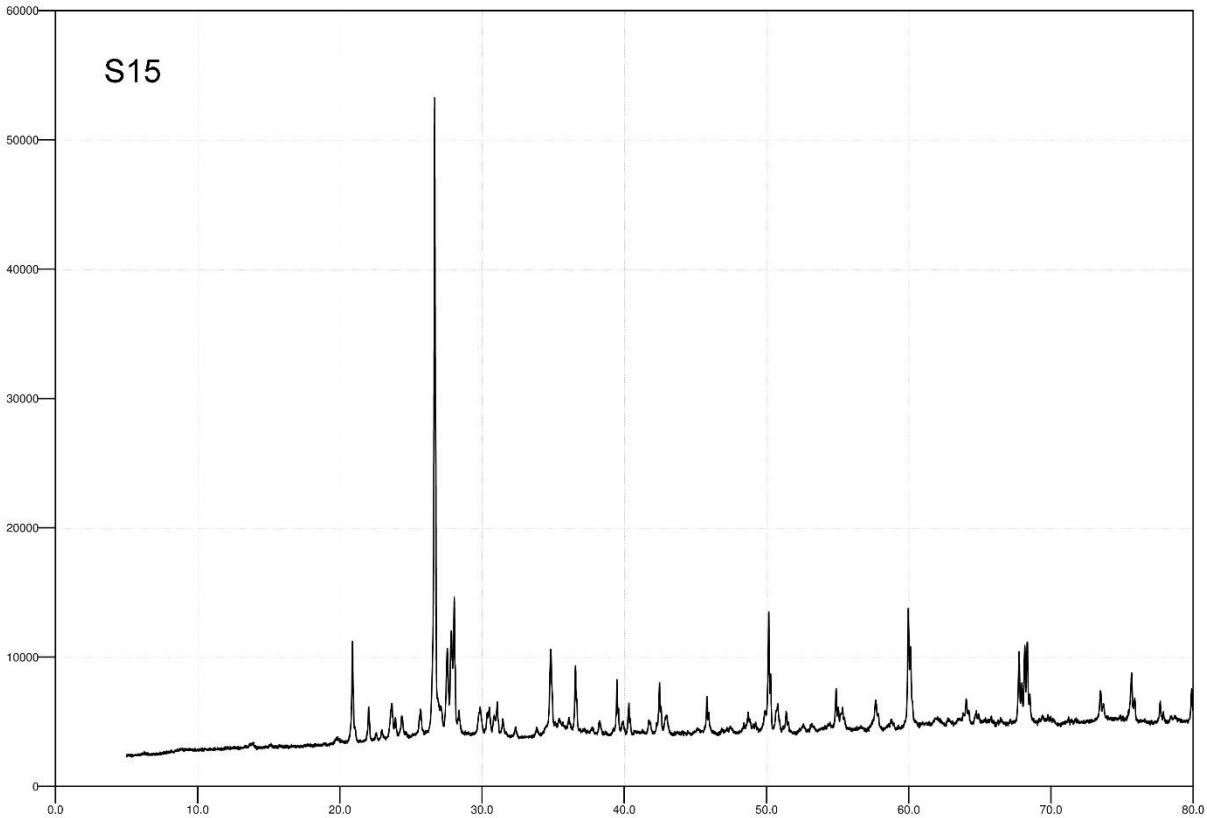

S10 (1)
35000
30000
25000
20000
15000
10000
5000
0
0.0
10.0
20.0
30.0
40.0
50.0
60.0
70.0
80.0

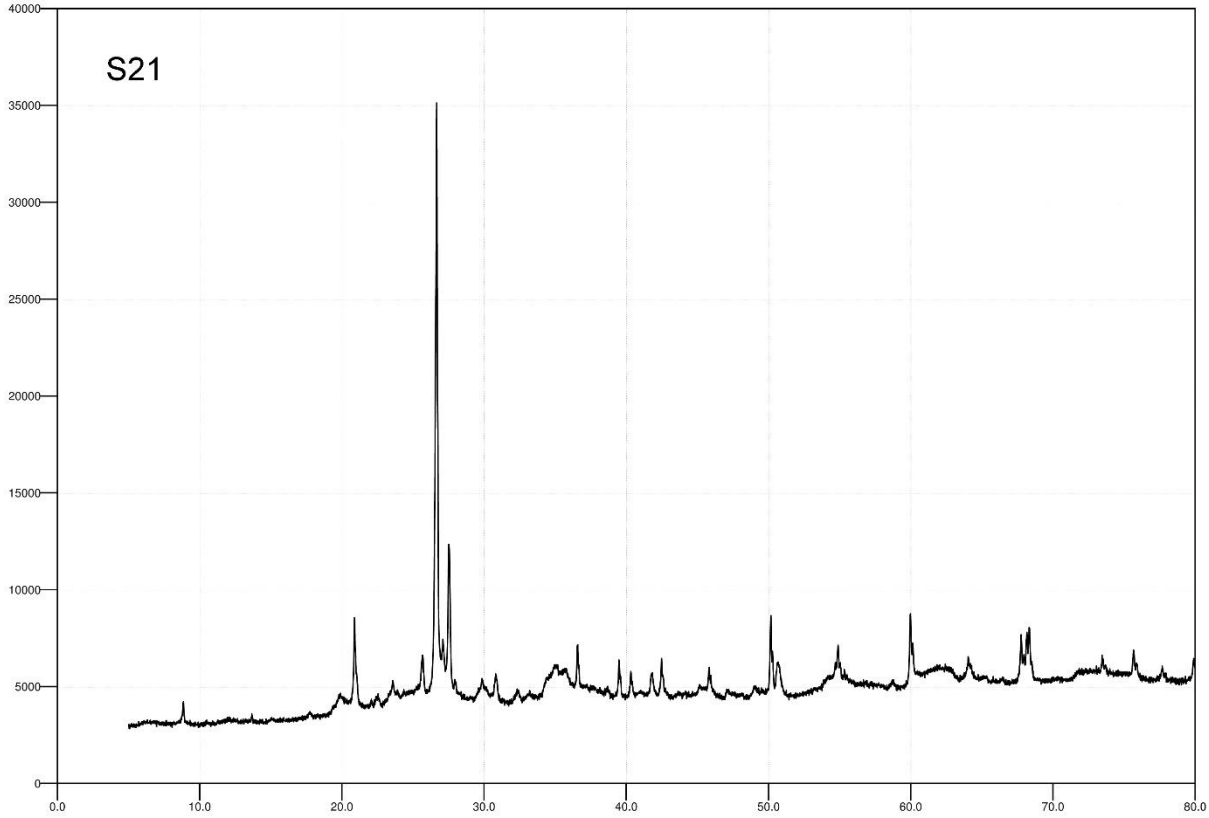

S10 (2)
40000
35000
30000
25000
20000
15000
10000
5000
0
0.0
10.0
20.0
30.0
40.0
50.0
60.0
70.0
80.0

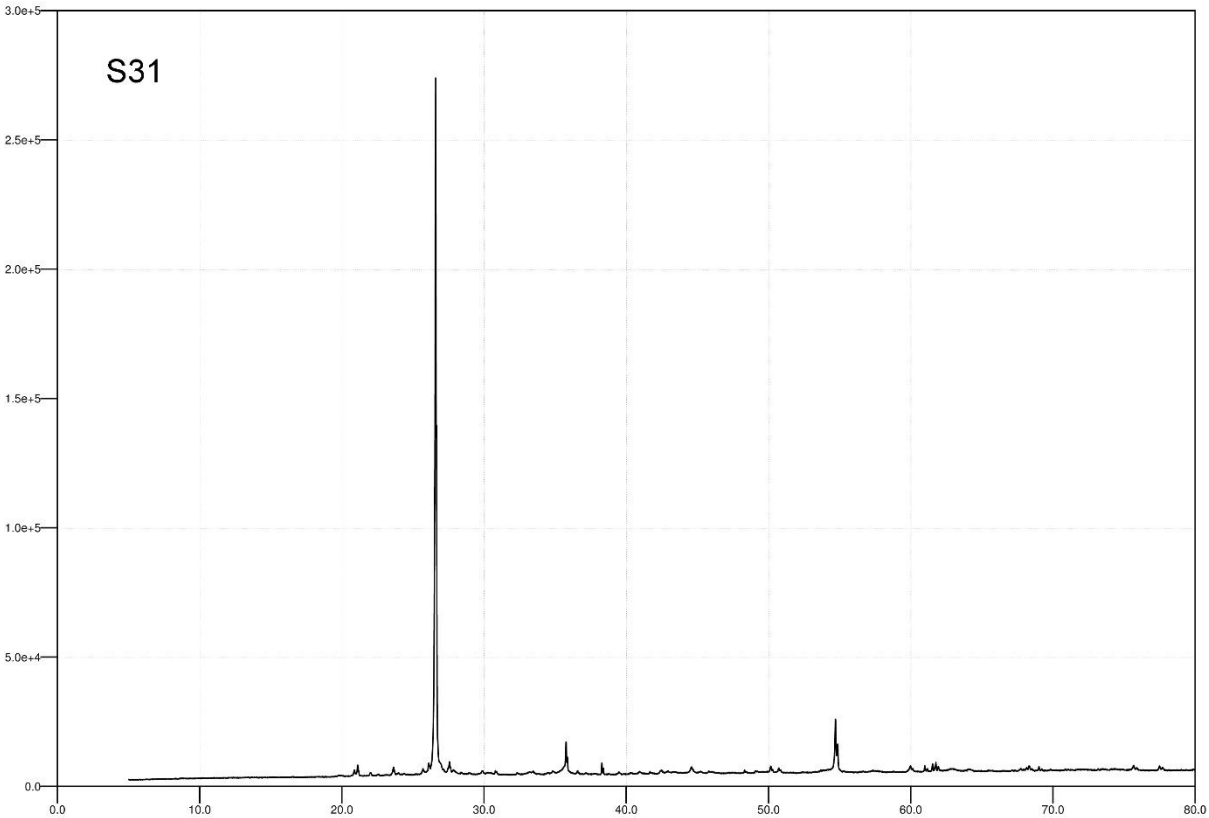

S11
45000
40000
35000
30000
25000
20000
15000
10000
5000
0
0.0
10.0
20.0
30.0
40.0
50.0
60.0
70.0
80.0

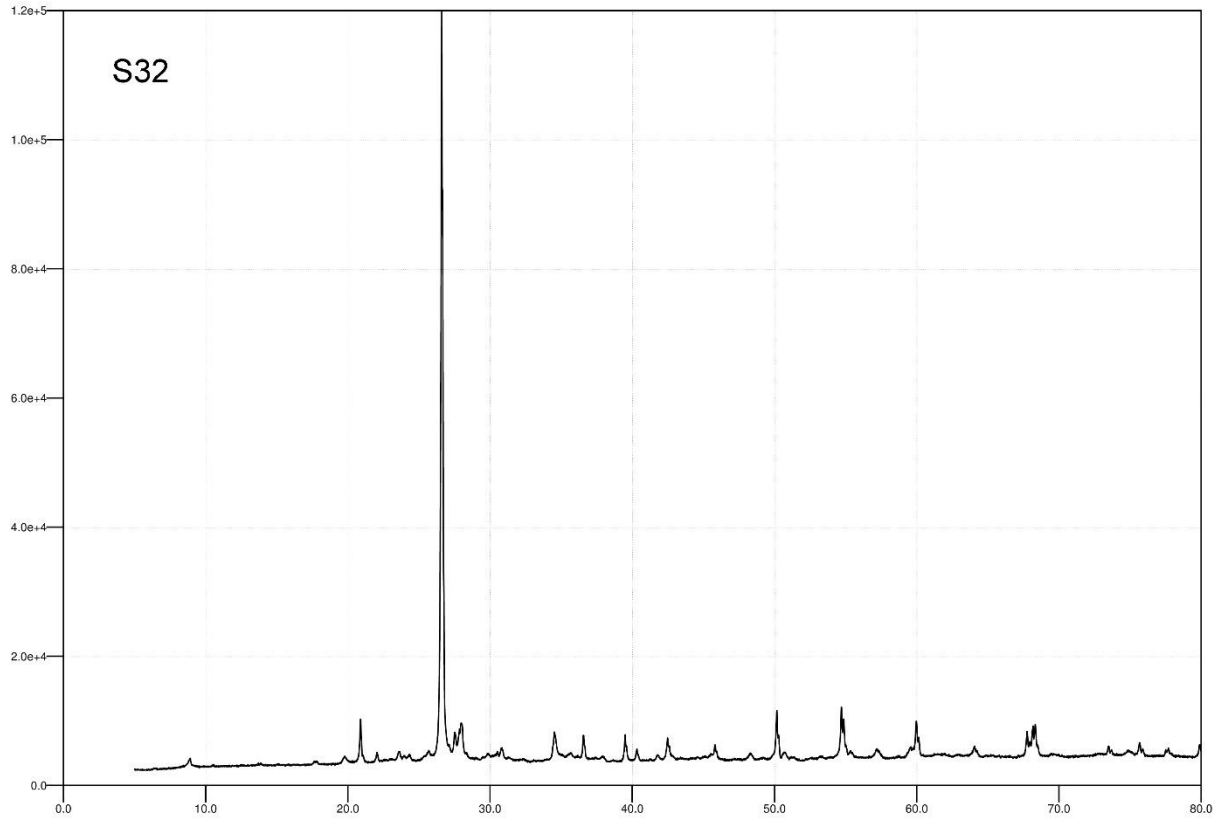

S12
80000
70000
60000
50000
40000
30000
20000
10000
0
0.0
10.0
20.0
30.0
40.0
50.0
60.0
70.0
80.0

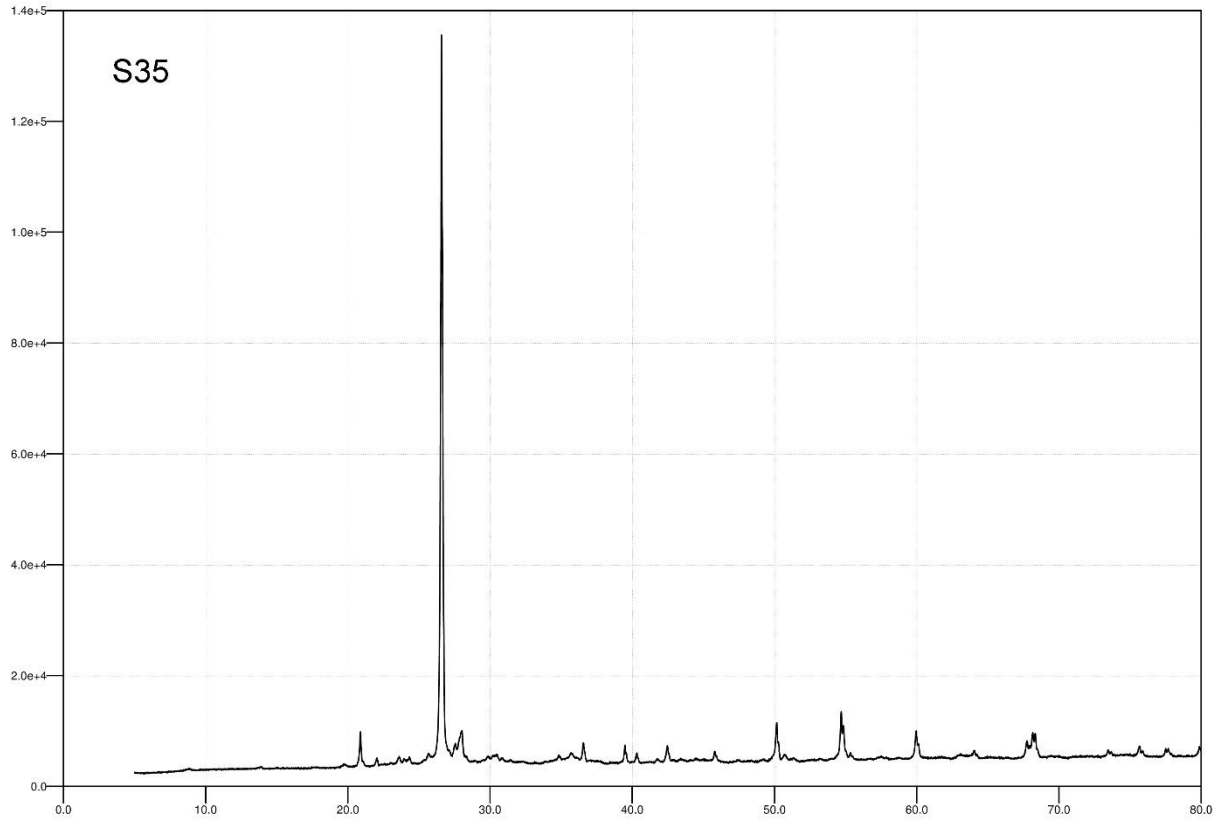

S13
30000
25000
20000
15000
10000
5000
0
0.0
10.0
20.0
30.0
40.0
50.0
60.0
70.0
80.0

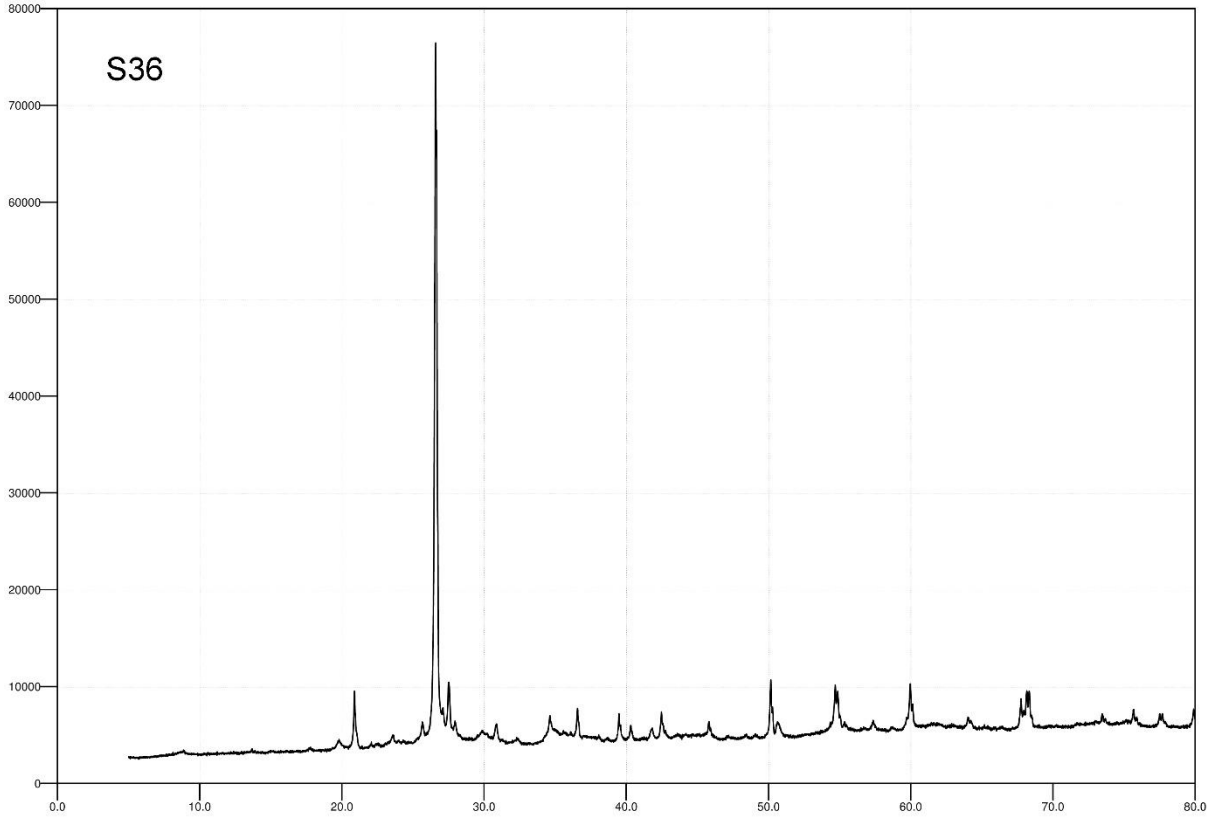

S15
60000
50000
40000
30000
20000
10000
0
0.0
10.0
20.0
30.0
40.0
50.0
60.0
70.0
80.0

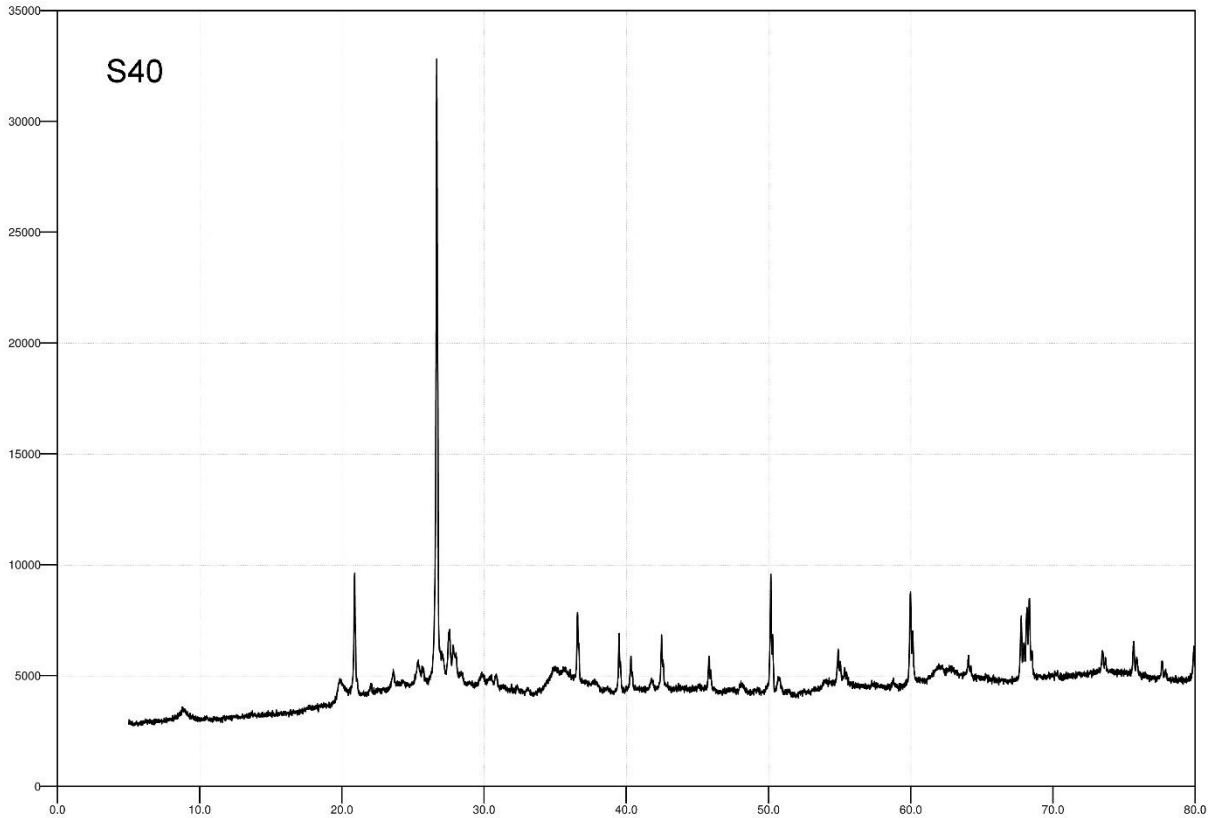

S21
40000
35000
30000
25000
20000
15000
10000
5000
0
0.0
10.0
20.0
30.0
40.0
50.0
60.0
70.0
80.0

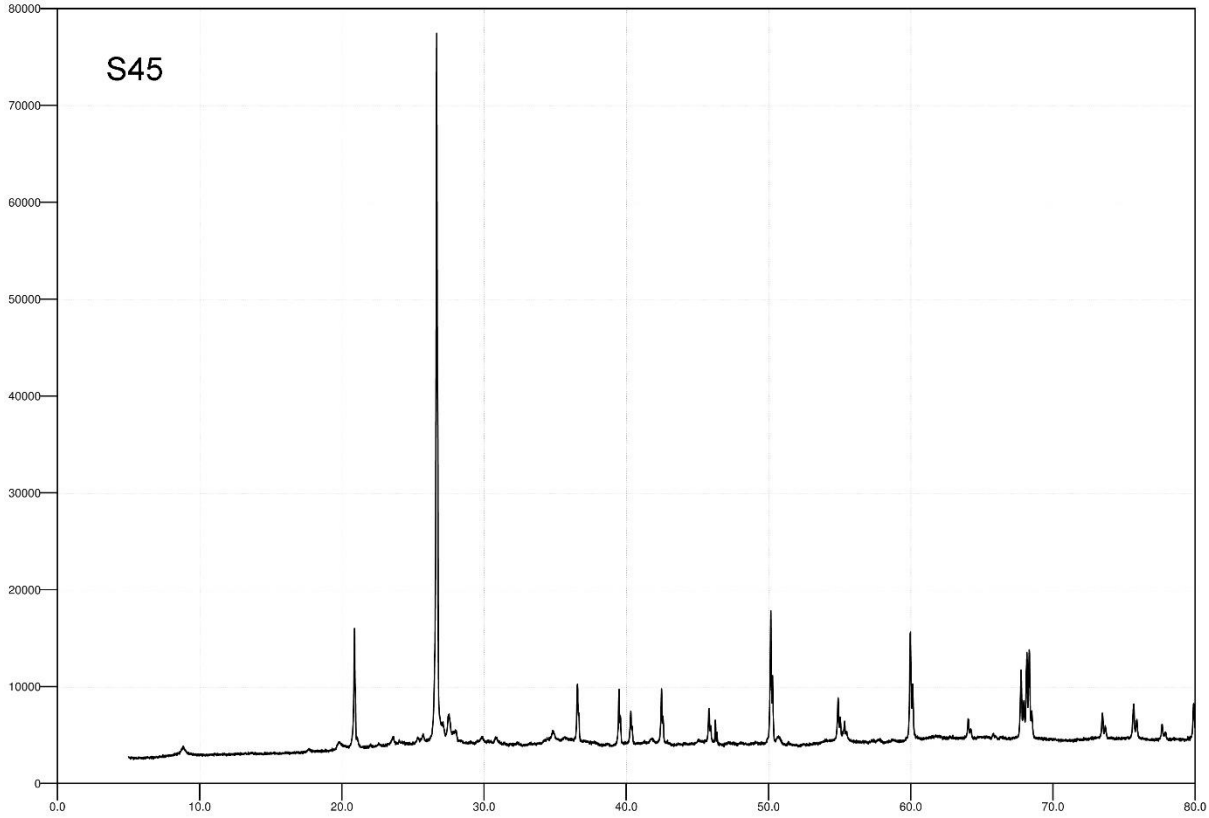

S31
3.0e+5
2.5e+5
2.0e+5
1.5e+5
1.0e+5
5.0e+4
0.0
0.0
10.0
20.0
30.0
40.0
50.0
60.0
70.0
80.0

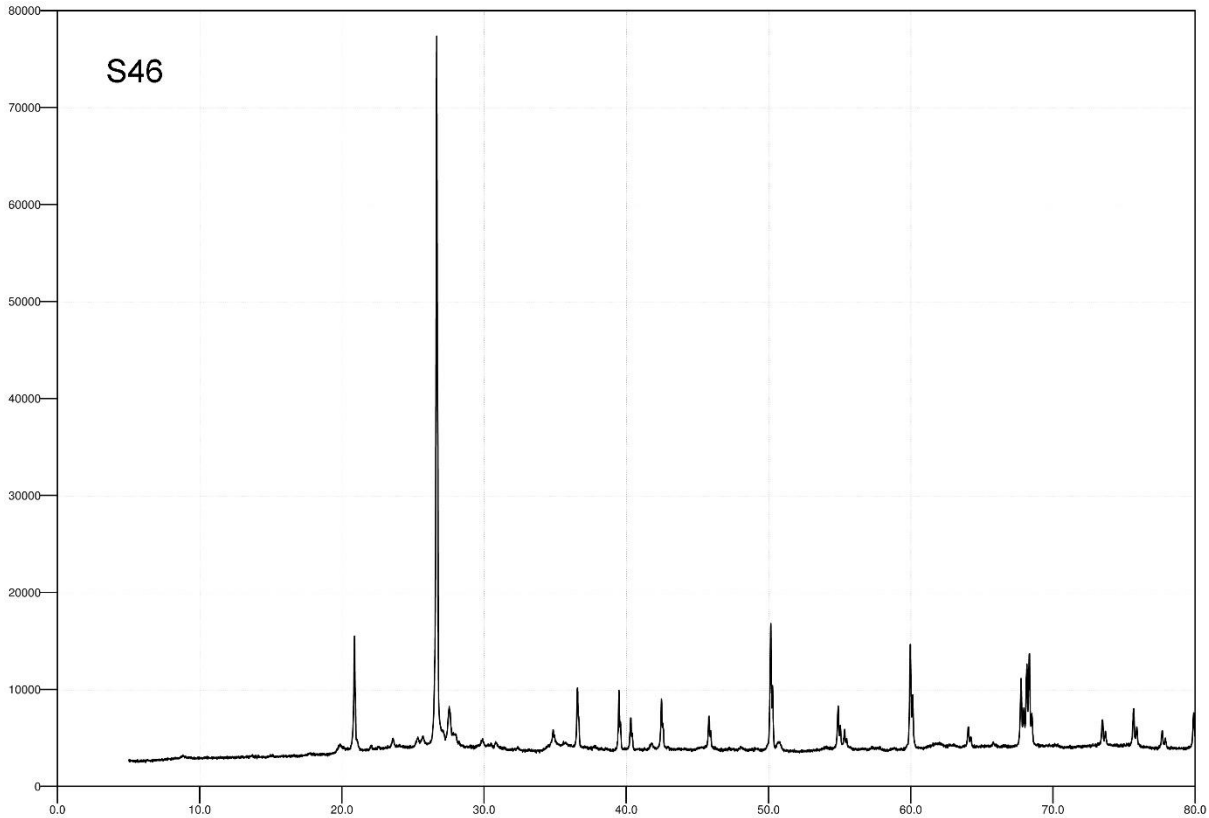

S32
1.2e+5
1.0e+5
8.0e+4
6.0e+4
4.0e+4
2.0e+4
0.0
0.0
10.0
20.0
30.0
40.0
50.0
60.0
70.0
80.0

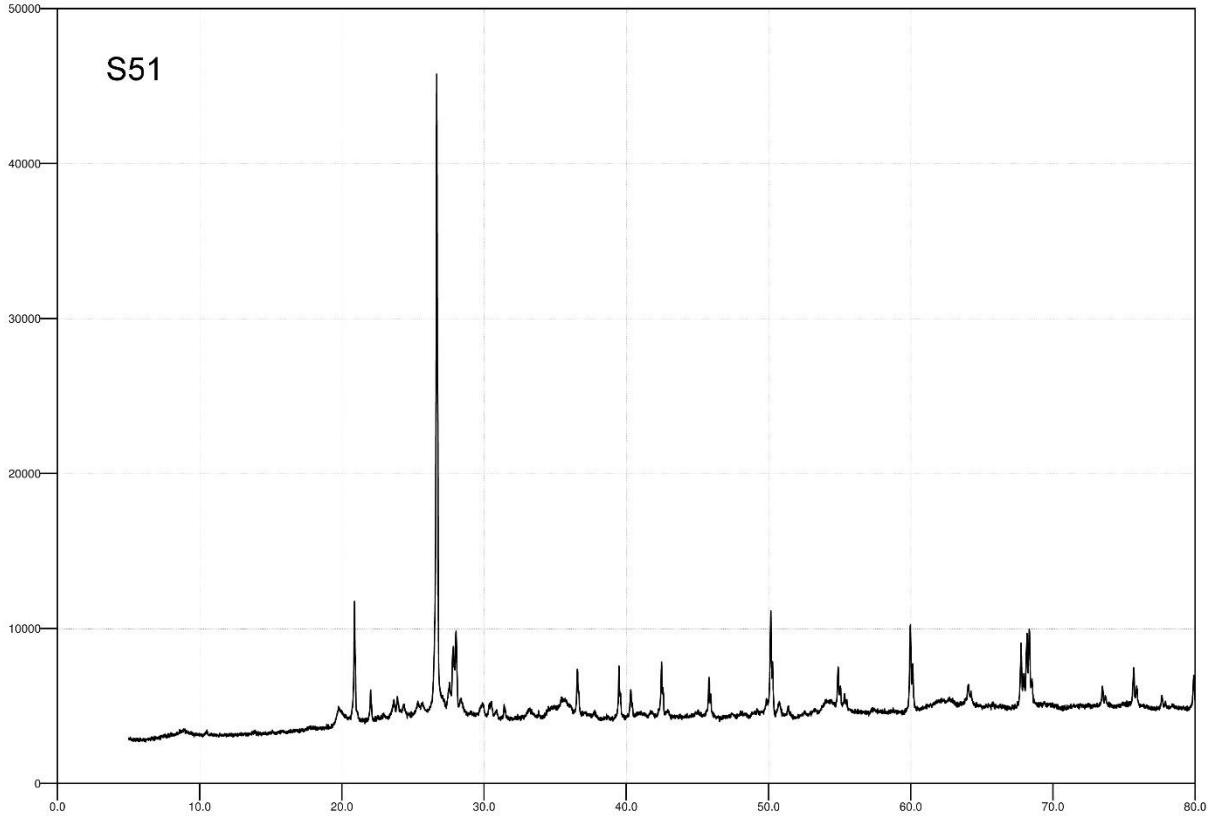

S35
1.4e+5
1.2e+5
1.0e+5
8.0e+4
6.0e+4
4.0e+4
2.0e+4
0.0
0.0
10.0
20.0
30.0
40.0
50.0
60.0
70.0
80.0

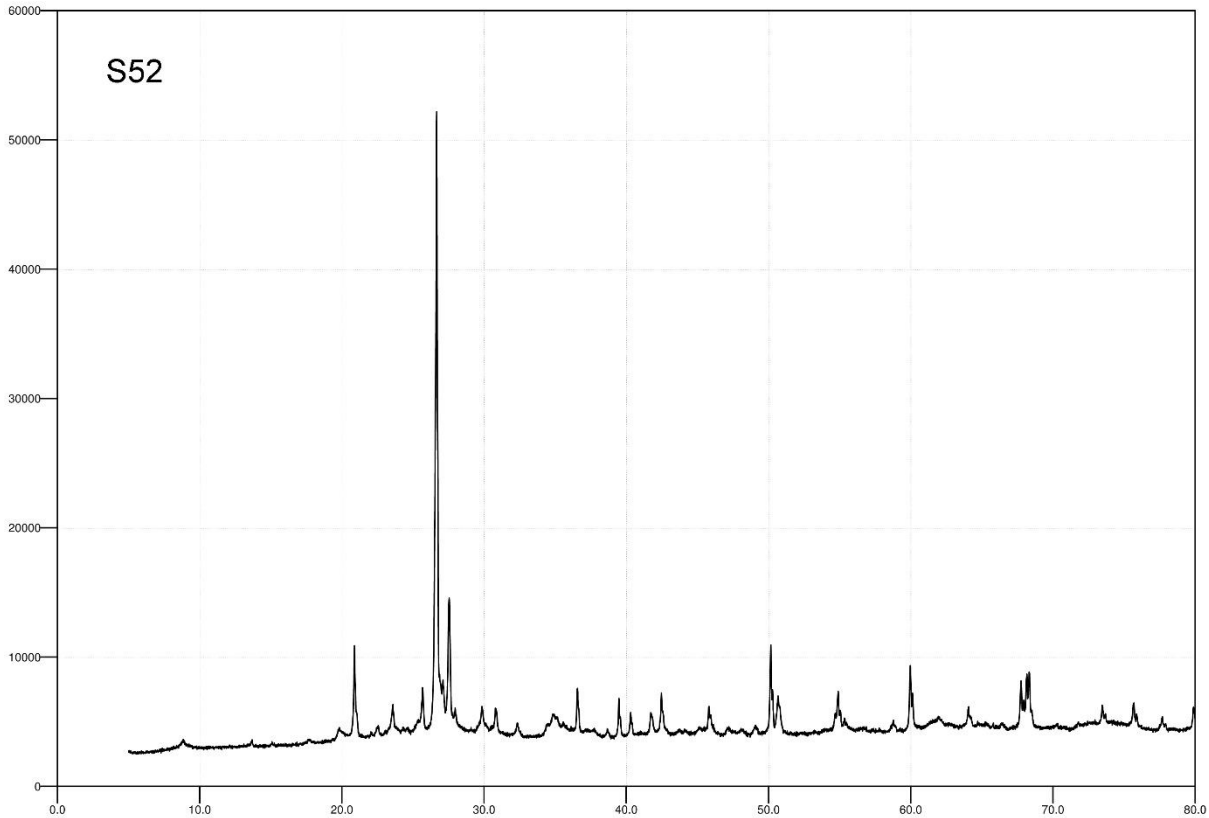

S36
80000
70000
60000
50000
40000
30000
20000
10000
0
0.0
10.0
20.0
30.0
40.0
50.0
60.0
70.0
80.0

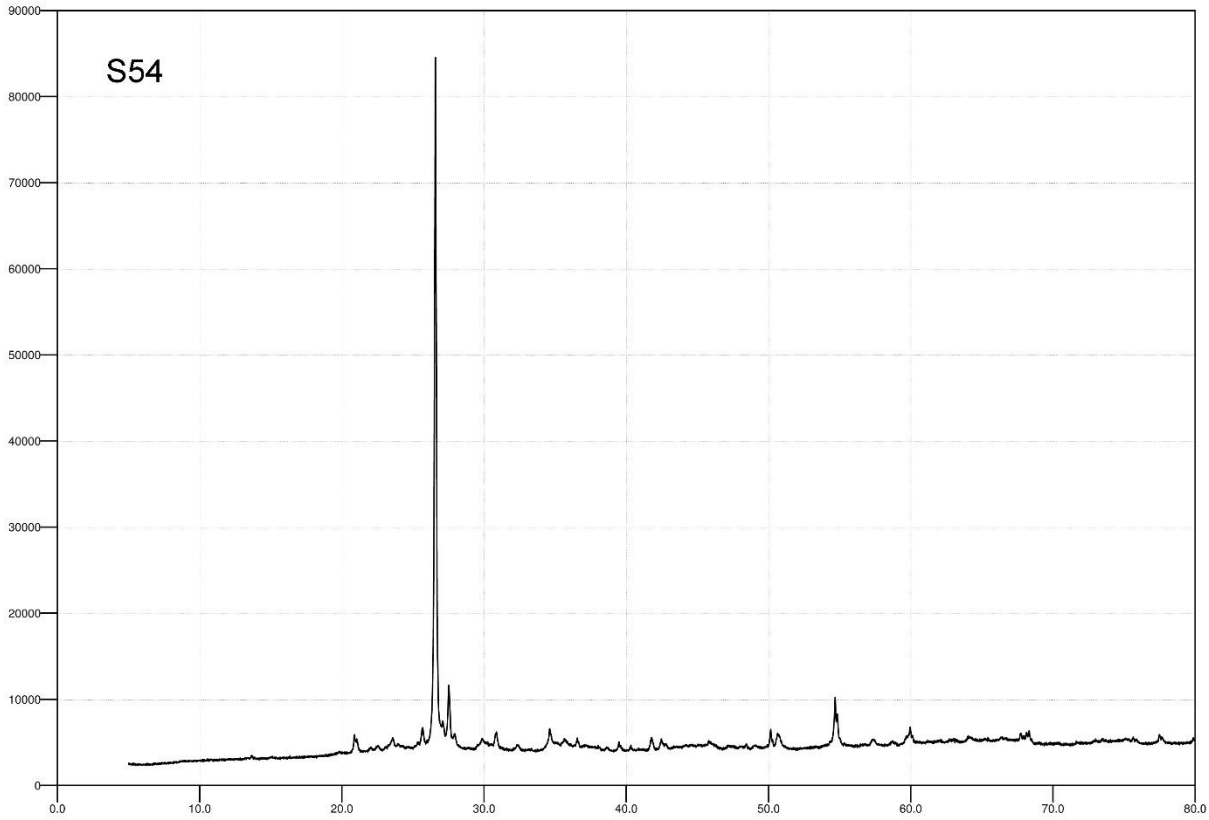

S40
35000
30000
25000
20000
15000
10000
5000
0
0.0
10.0
20.0
30.0
40.0
50.0
60.0
70.0
80.0

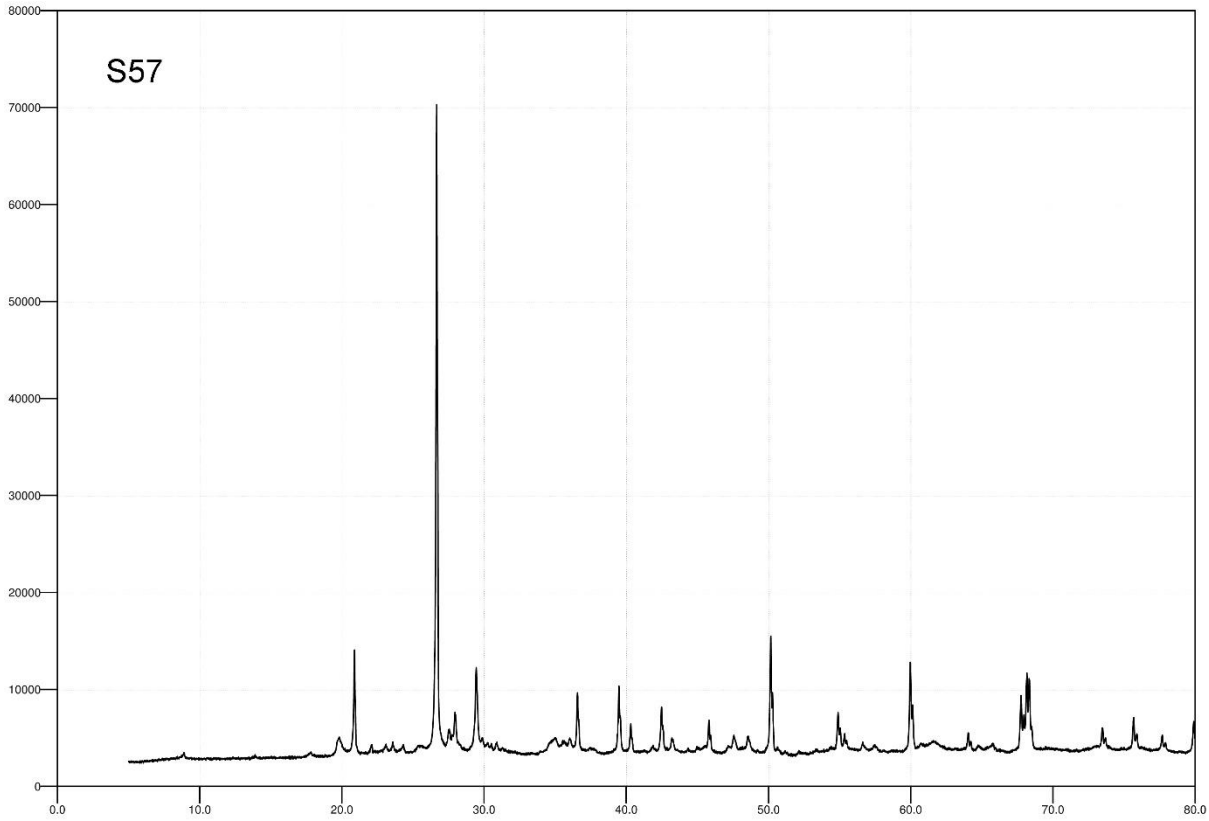

S45
80000
70000
60000
50000
40000
30000
20000
10000
0
0.0
10.0
20.0
30.0
40.0
50.0
60.0
70.0
80.0

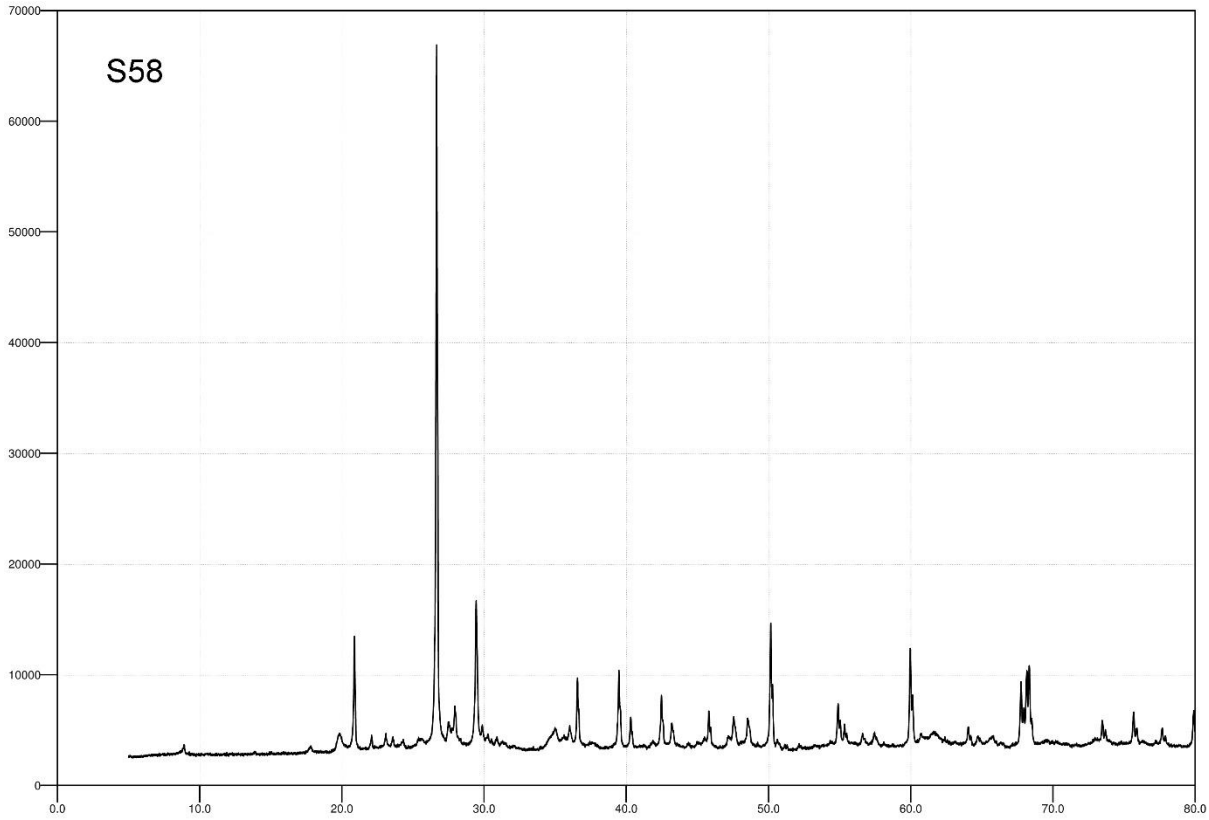

S46
80000
70000
60000
50000
40000
30000
20000
10000
0
0.0
10.0
20.0
30.0
40.0
50.0
60.0
70.0
80.0

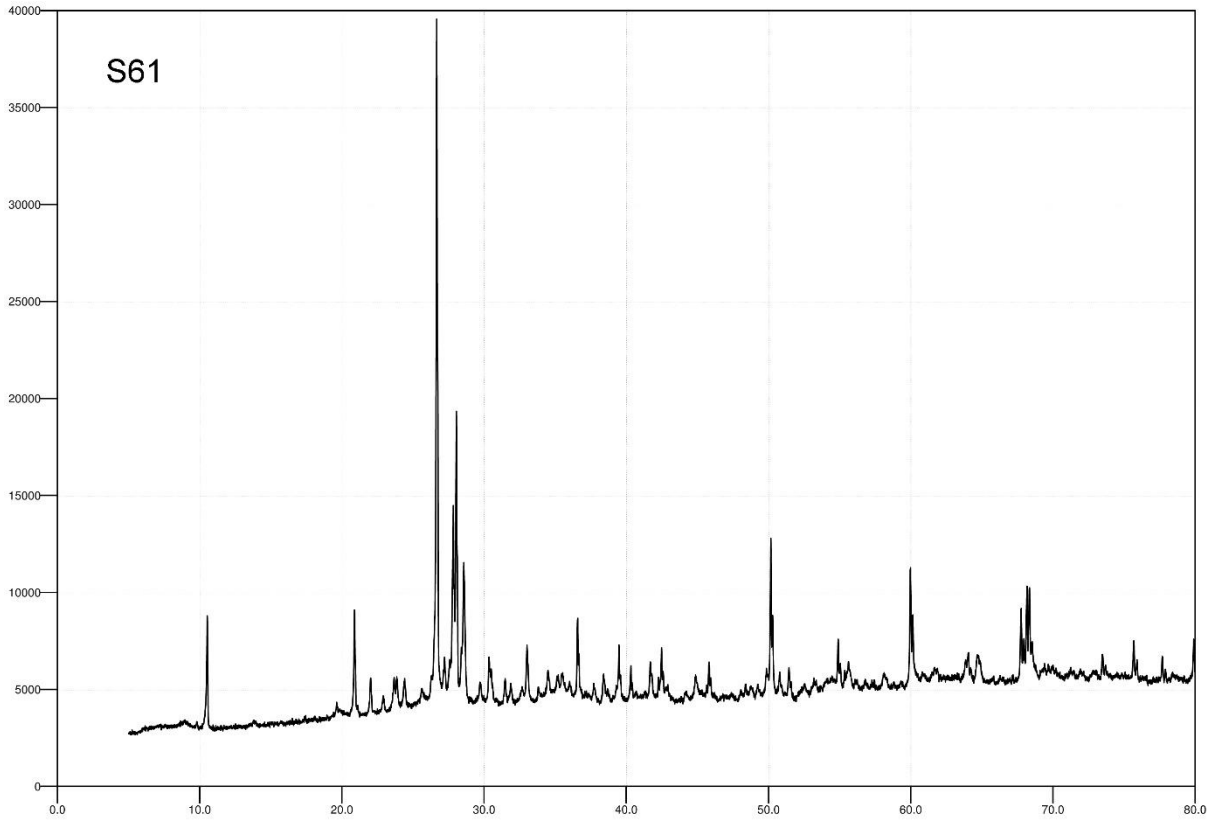

S51
50000
40000
30000
20000
10000
0
0.0
10.0
20.0
30.0
40.0
50.0
60.0
70.0
80.0

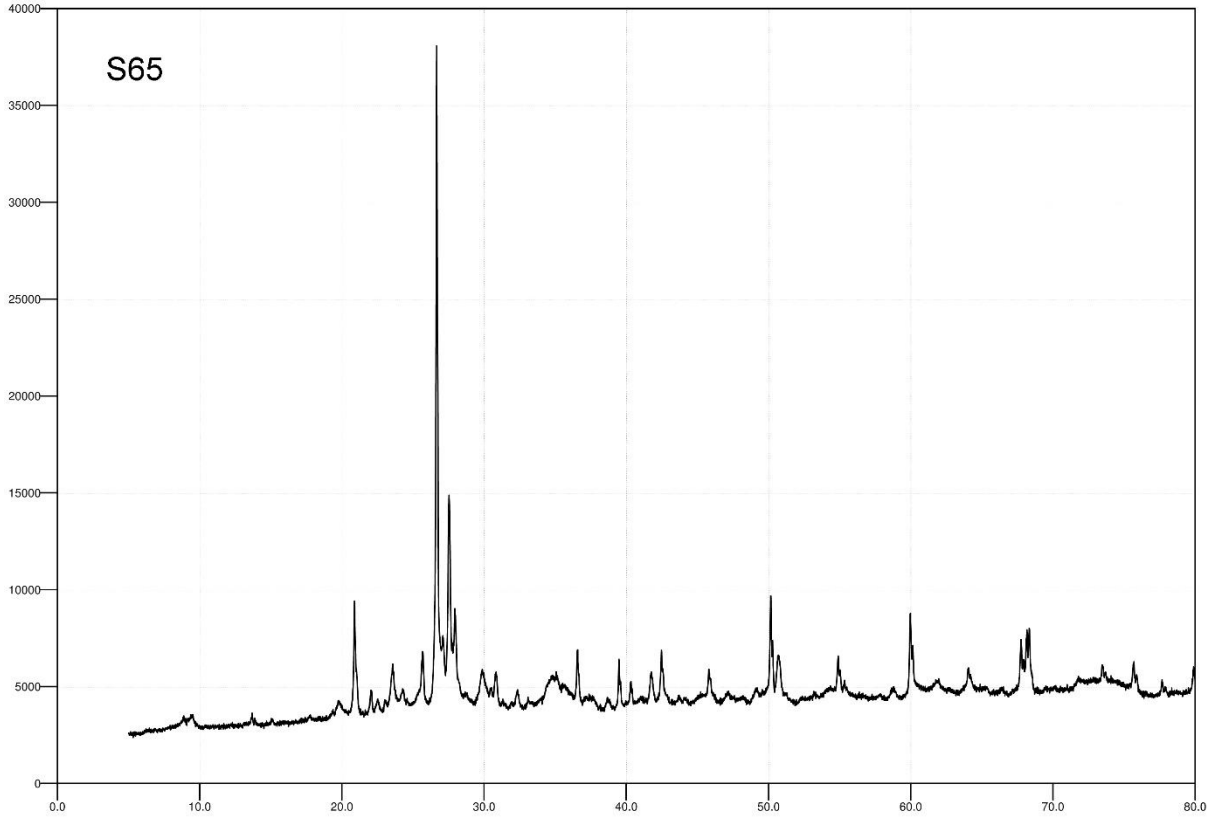

S52
60000
50000
40000
30000
20000
10000
0
0.0
10.0
20.0
30.0
40.0
50.0
60.0
70.0
80.0

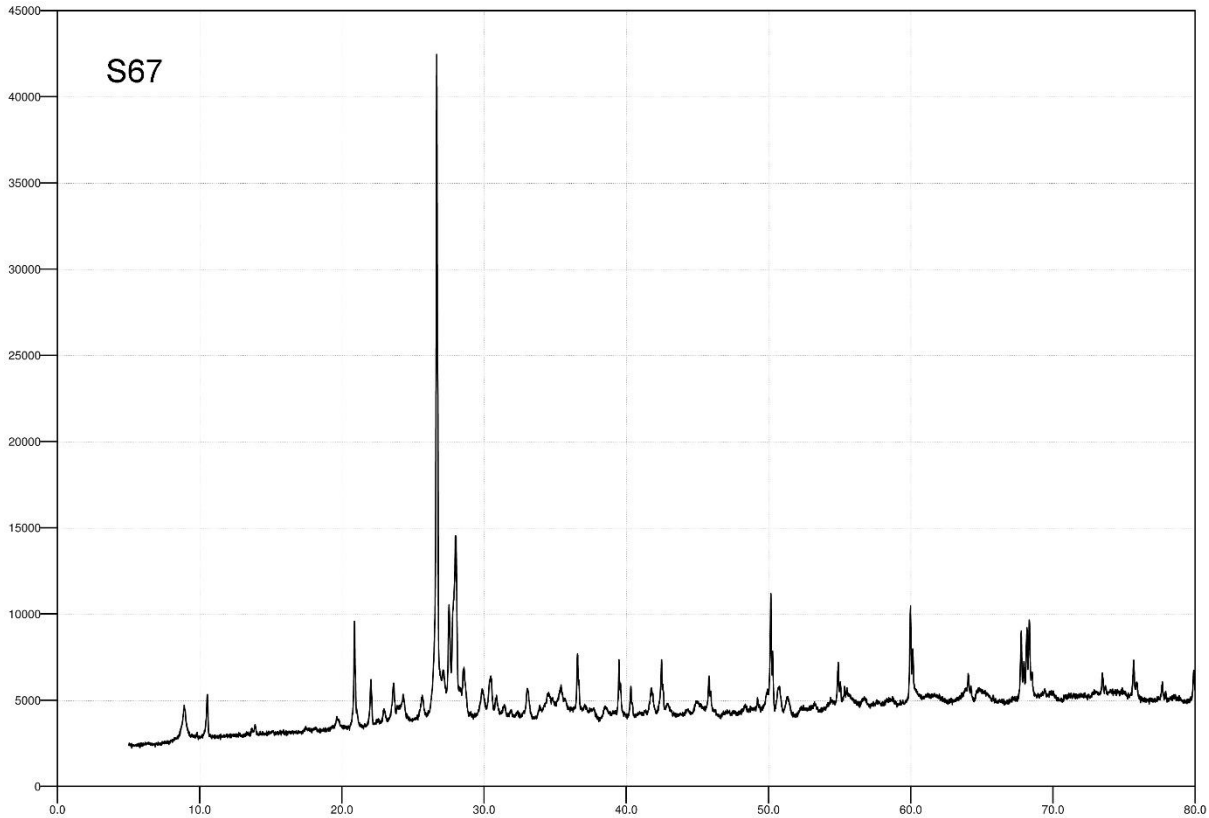

S54
90000
80000
70000
60000
50000
40000
30000
20000
10000
0
0.0
10.0
20.0
30.0
40.0
50.0
60.0
70.0
80.0

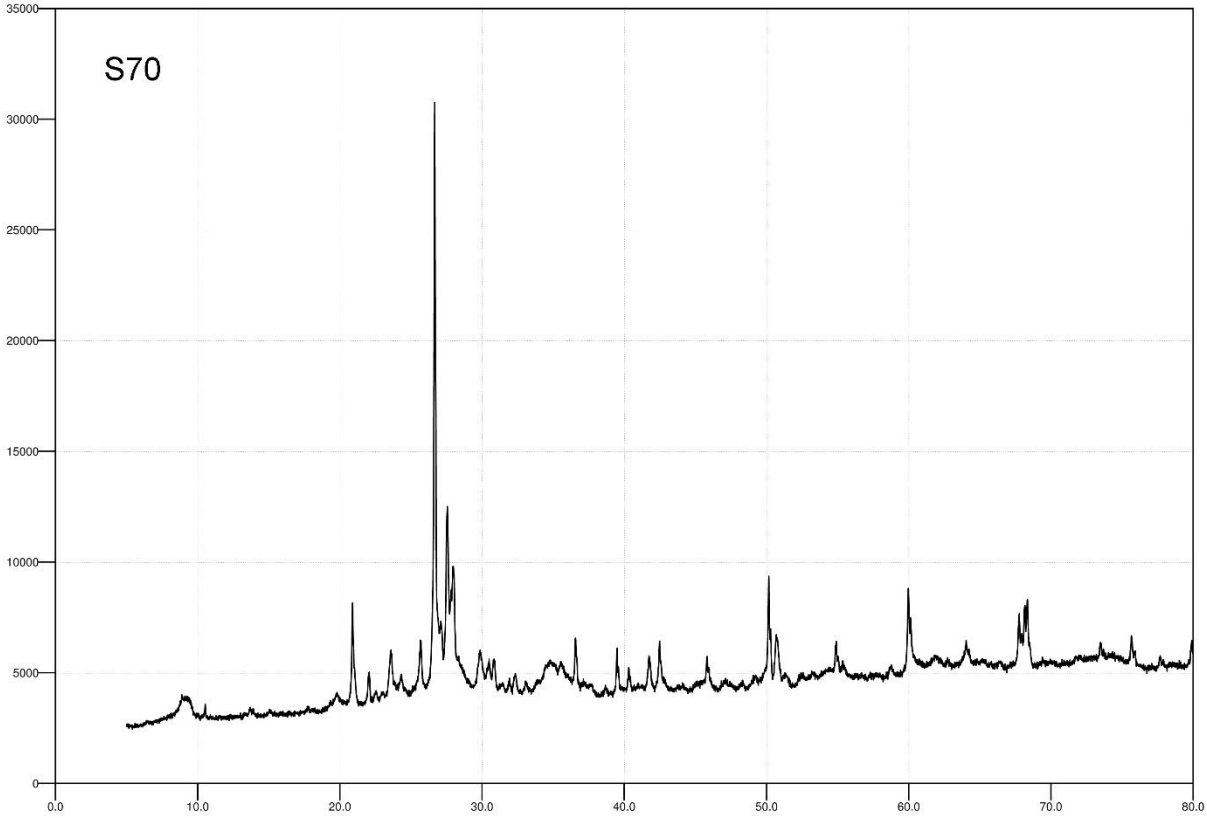

S57
80000
70000
60000
50000
40000
30000
20000
10000
0
0.0
10.0
20.0
30.0
40.0
50.0
60.0
70.0
80.0

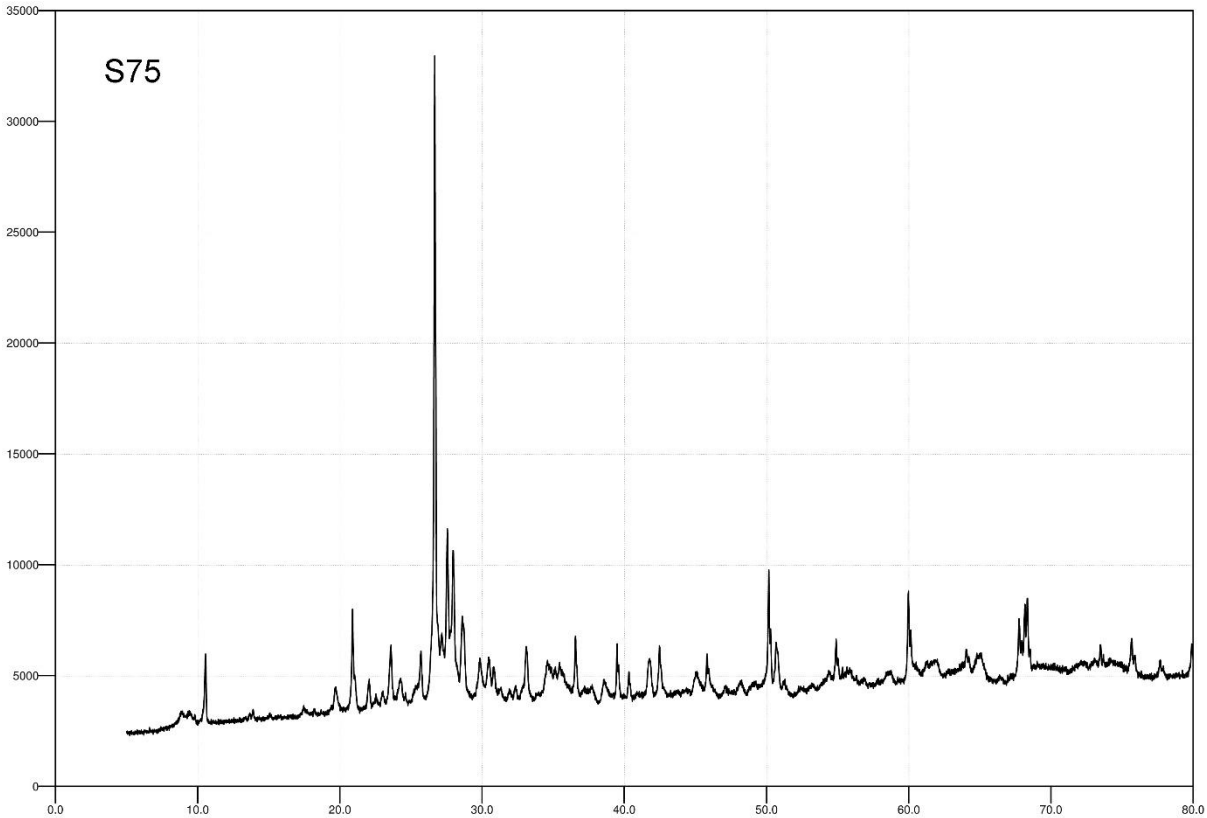

S58
70000
60000
50000
40000
30000
20000
10000
0
0.0
10.0
20.0
30.0
40.0
50.0
60.0
70.0
80.0

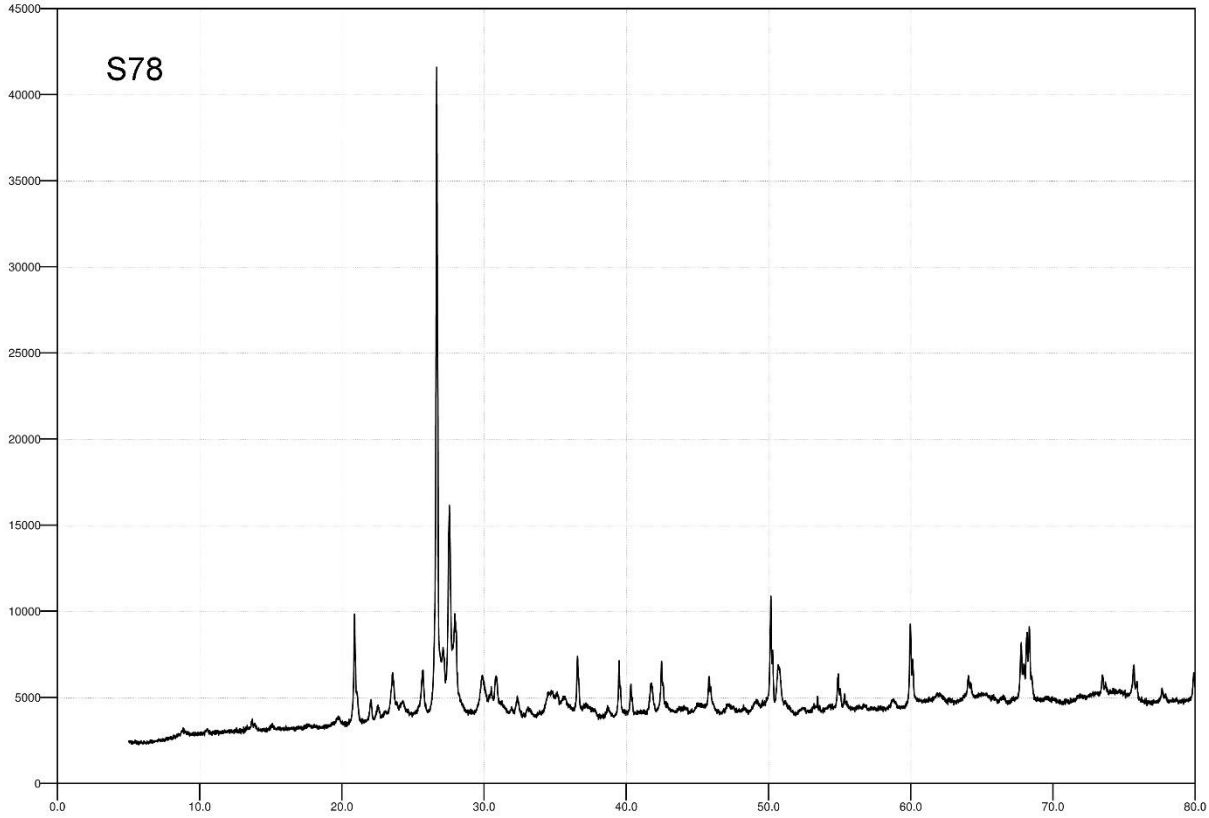

S61
40000
35000
30000
25000
20000
15000
10000
5000
0
0.0
10.0
20.0
30.0
40.0
50.0
60.0
70.0
80.0

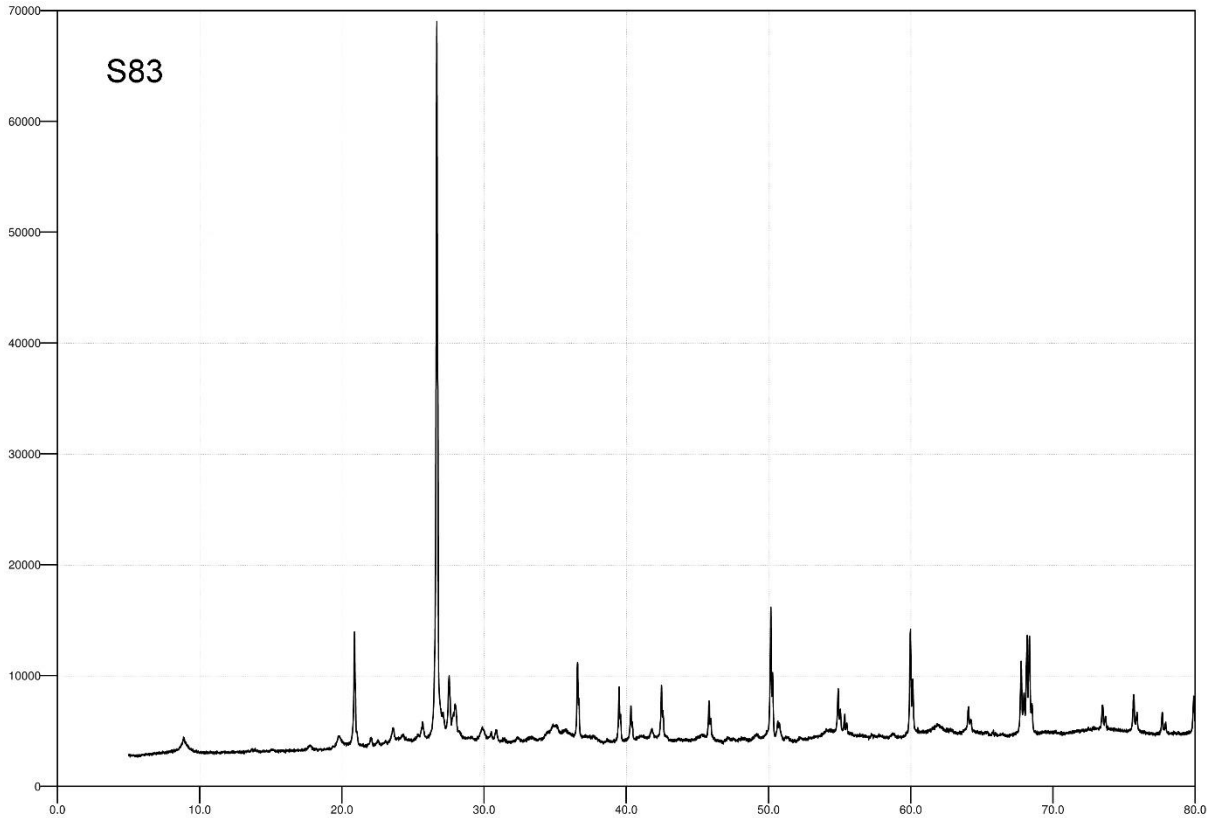

S65
40000
35000
30000
25000
20000
15000
10000
5000
0
0.0
10.0
20.0
30.0
40.0
50.0
60.0
70.0
80.0

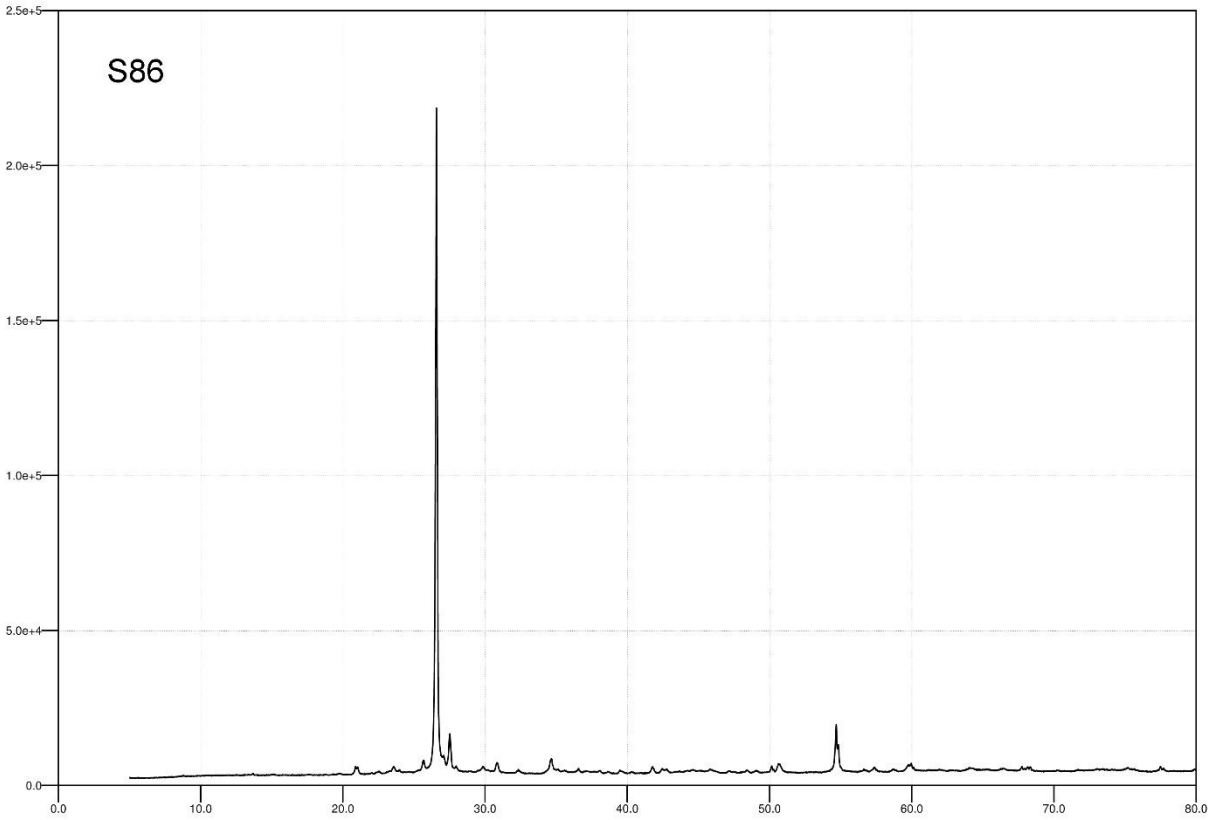

S67
45000
40000
35000
30000
25000
20000
15000
10000
5000
0
0.0
10.0
20.0
30.0
40.0
50.0
60.0
70.0
80.0

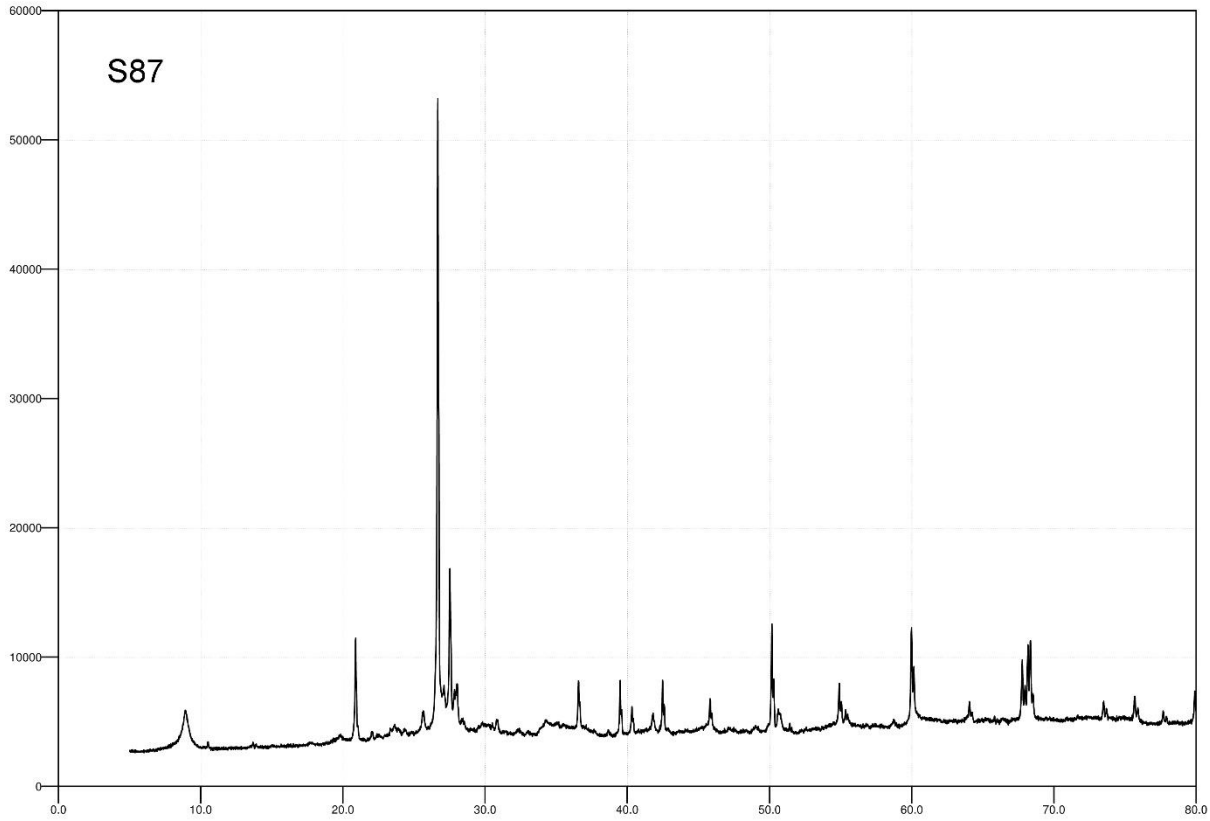

S70
35000
30000
25000
20000
15000
10000
5000
0
0.0
10.0
20.0
30.0
40.0
50.0
60.0
70.0
80.0

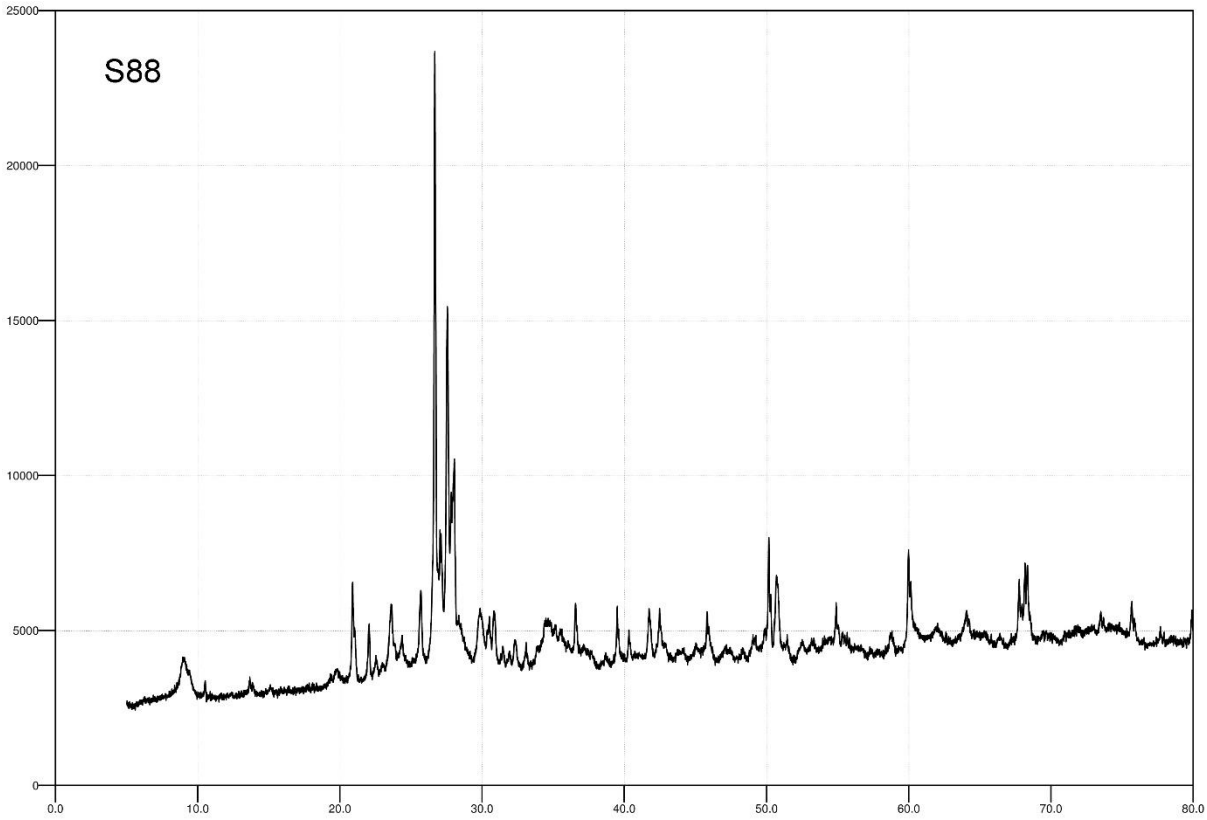

S75
35000
30000
25000
20000
15000
10000
5000
0
0.0
10.0
20.0
30.0
40.0
50.0
60.0
70.0
80.0

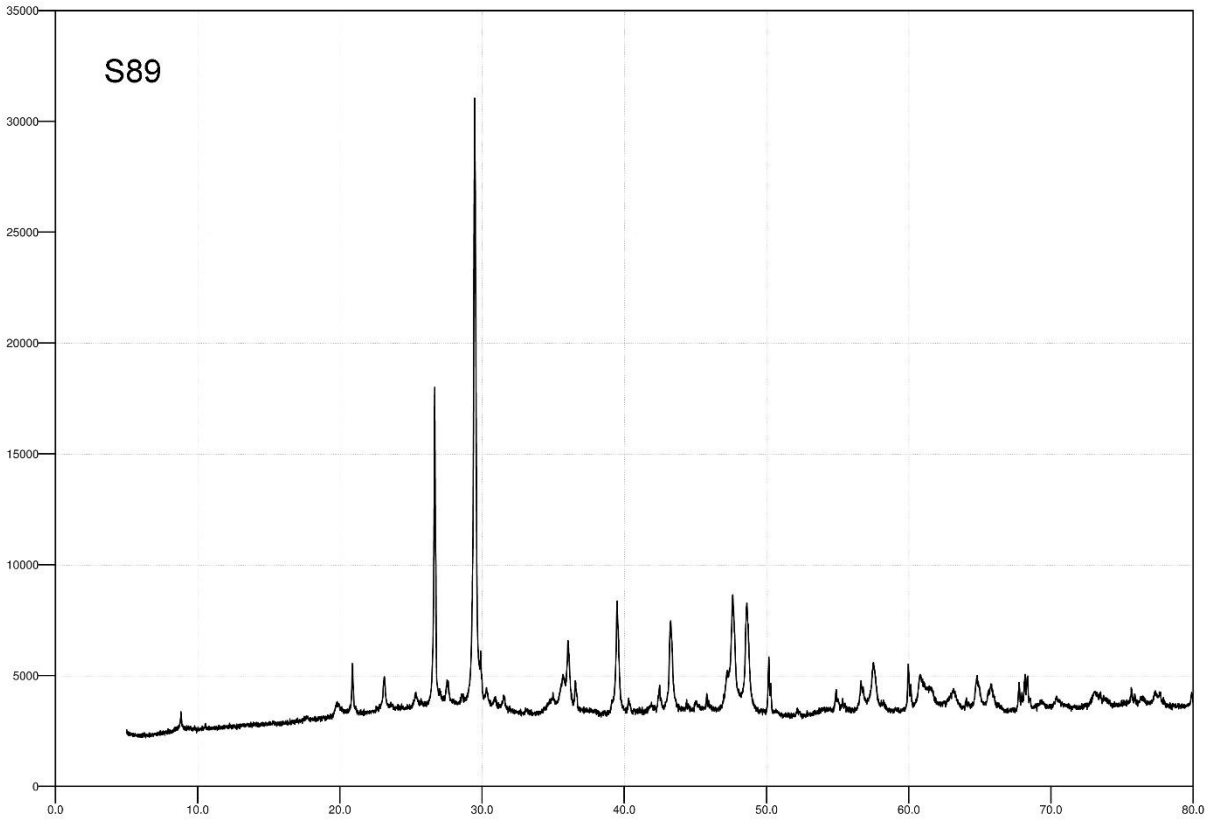

S78
45000
40000
35000
30000
25000
20000
15000
10000
5000
0
0.0
10.0
20.0
30.0
40.0
50.0
60.0
70.0
80.0

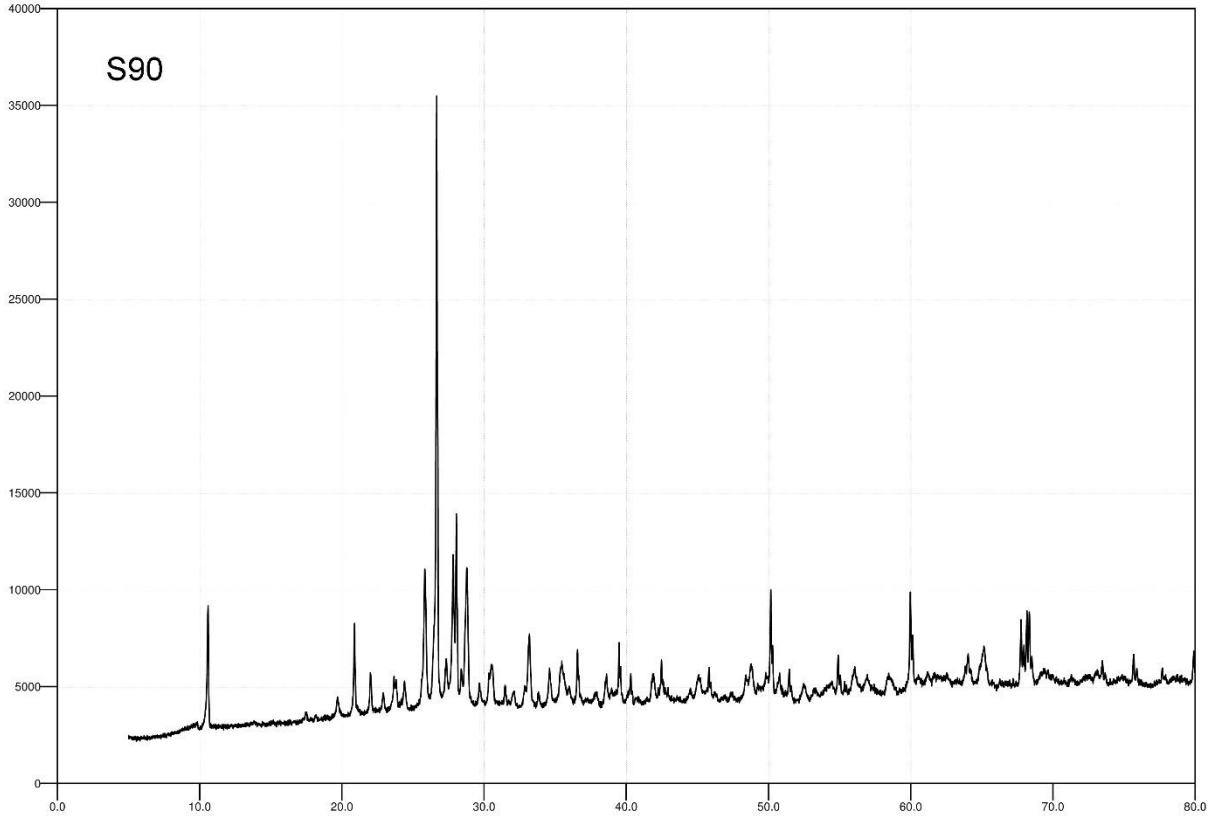

S83
70000
60000
50000
40000
30000
20000
10000
0
0.0
10.0
20.0
30.0
40.0
50.0
60.0
70.0
80.0

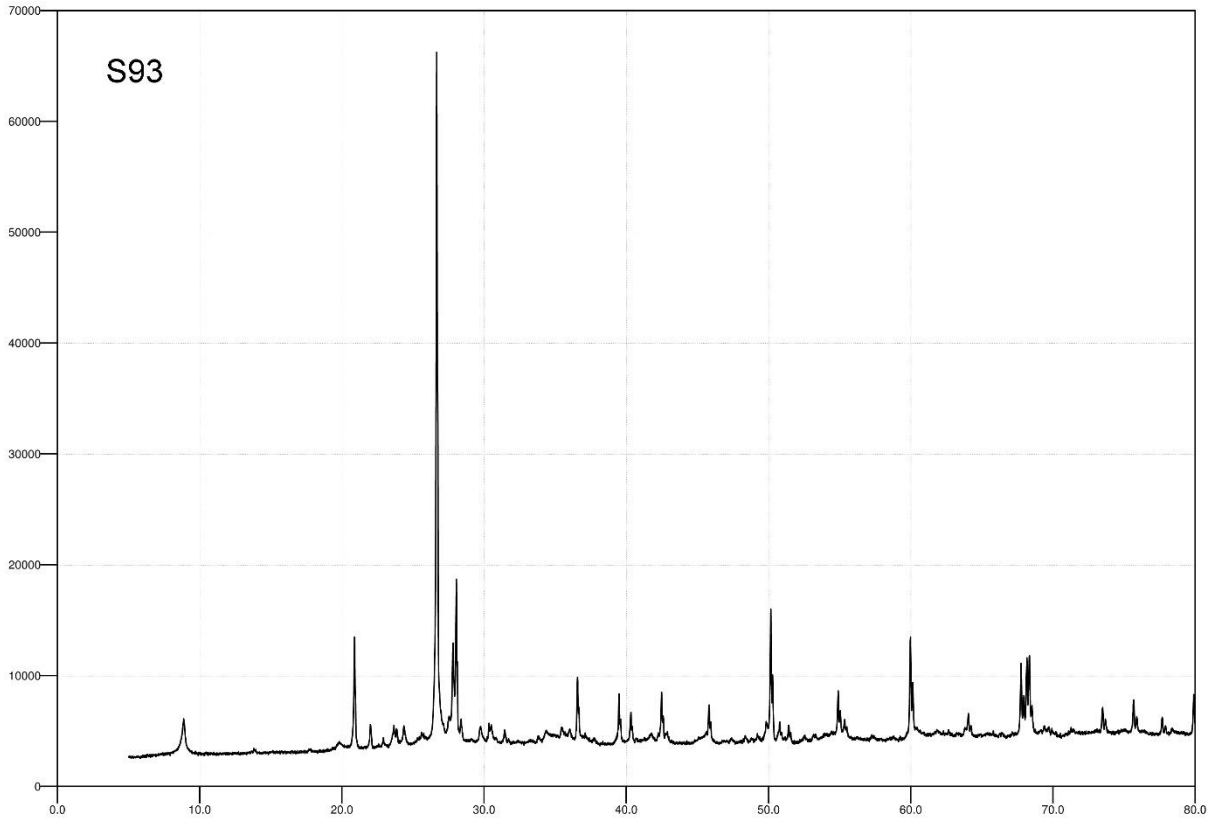

S86
2.5e+5
2.0e+5
1.5e+5
1.0e+5
5.0e+4
0.0
0.0
10.0
20.0
30.0
40.0
50.0
60.0
70.0
80.0

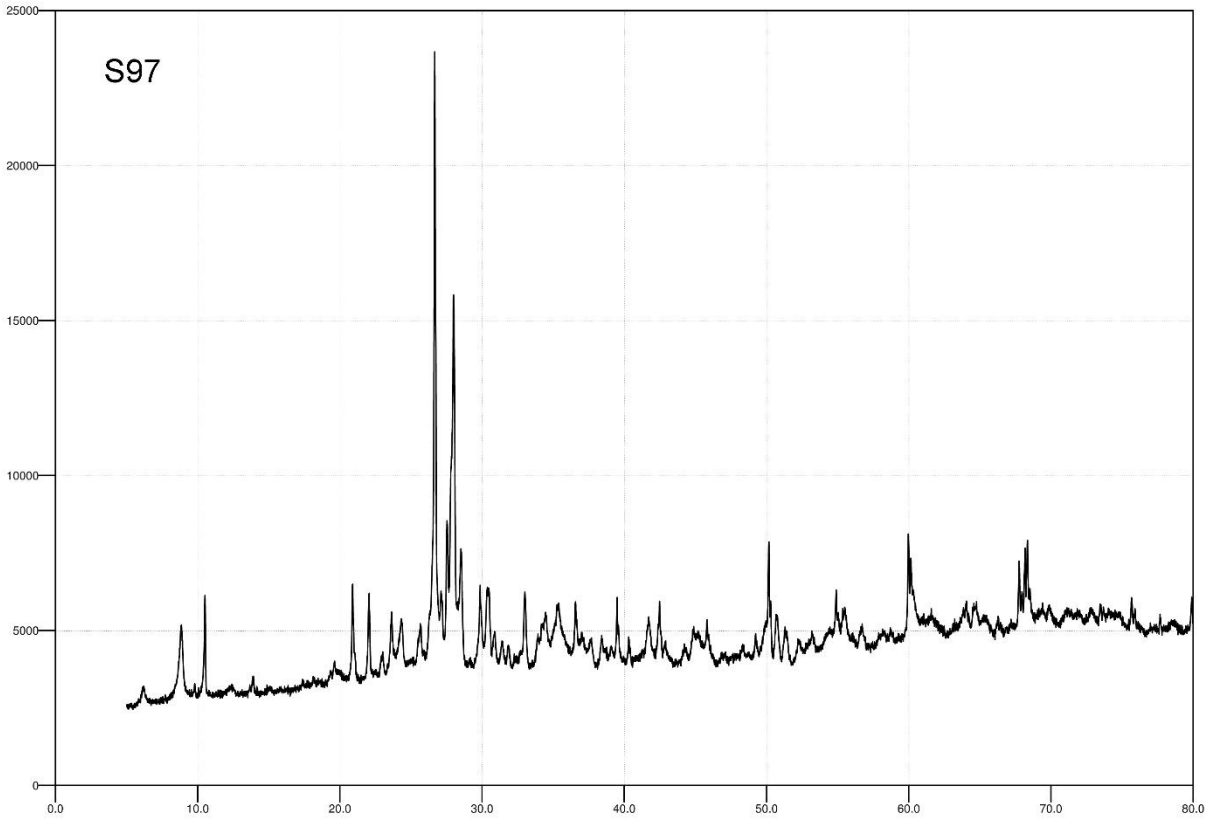

S87
60000
50000
40000
30000
20000
10000
0
0.0
10.0
20.0
30.0
40.0
50.0
60.0
70.0
80.0

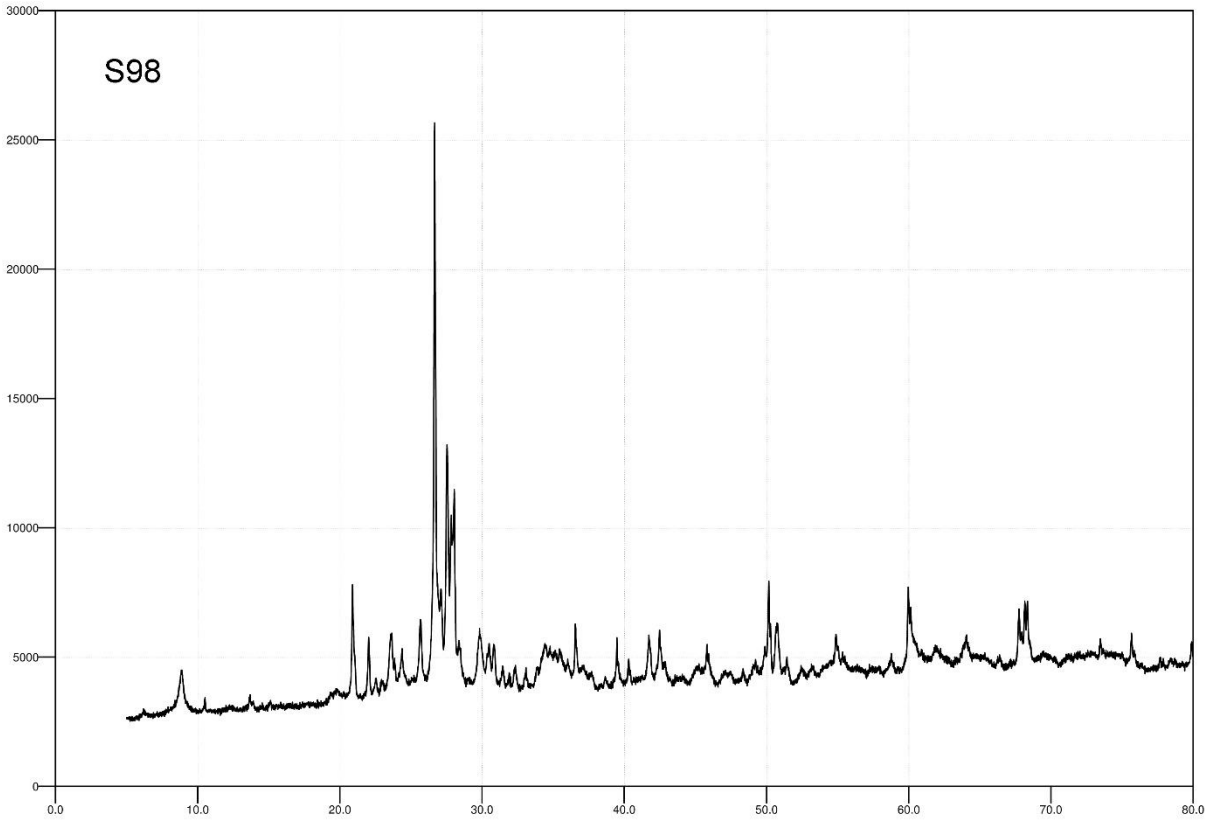

S88
25000
20000
15000
10000
5000
0
0.0
10.0
20.0
30.0
40.0
50.0
60.0
70.0
80.0

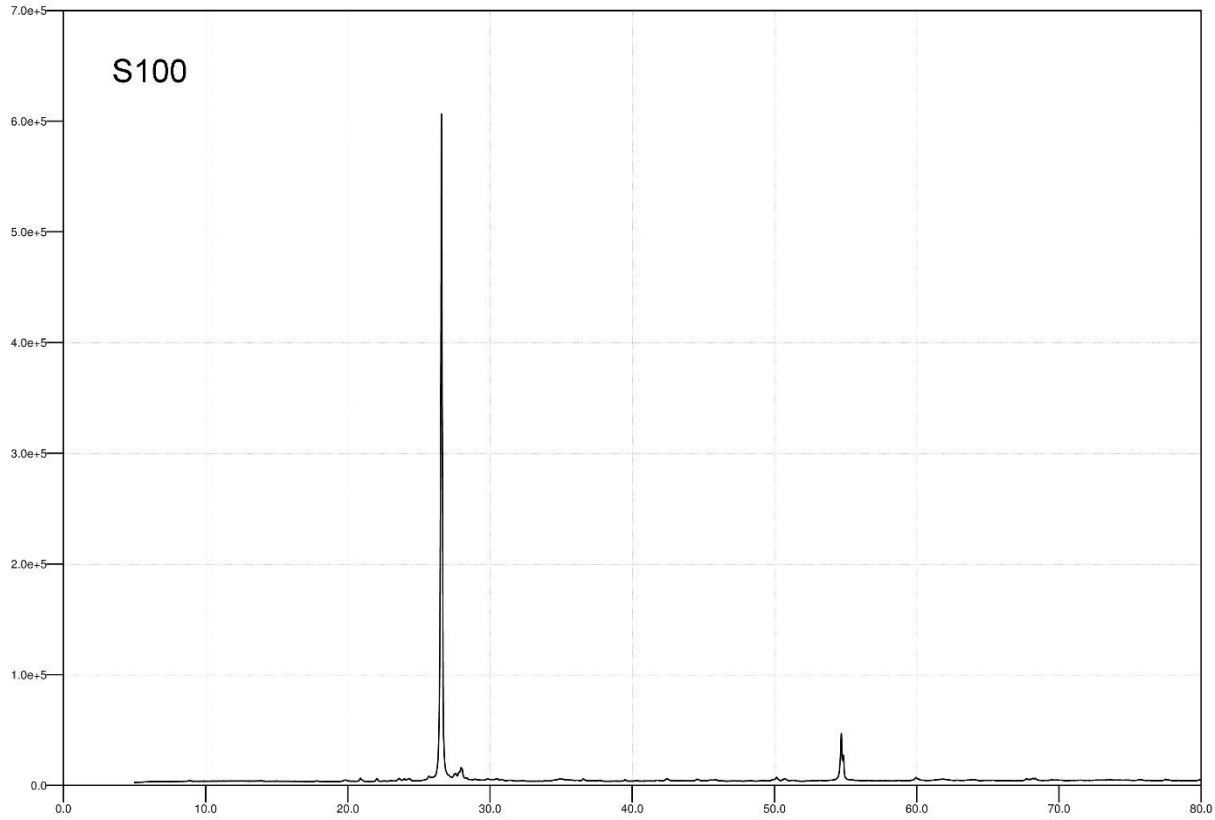

S89
35000
30000
25000
20000
15000
10000
5000
0
0.0
10.0
20.0
30.0
40.0
50.0
60.0
70.0
80.0

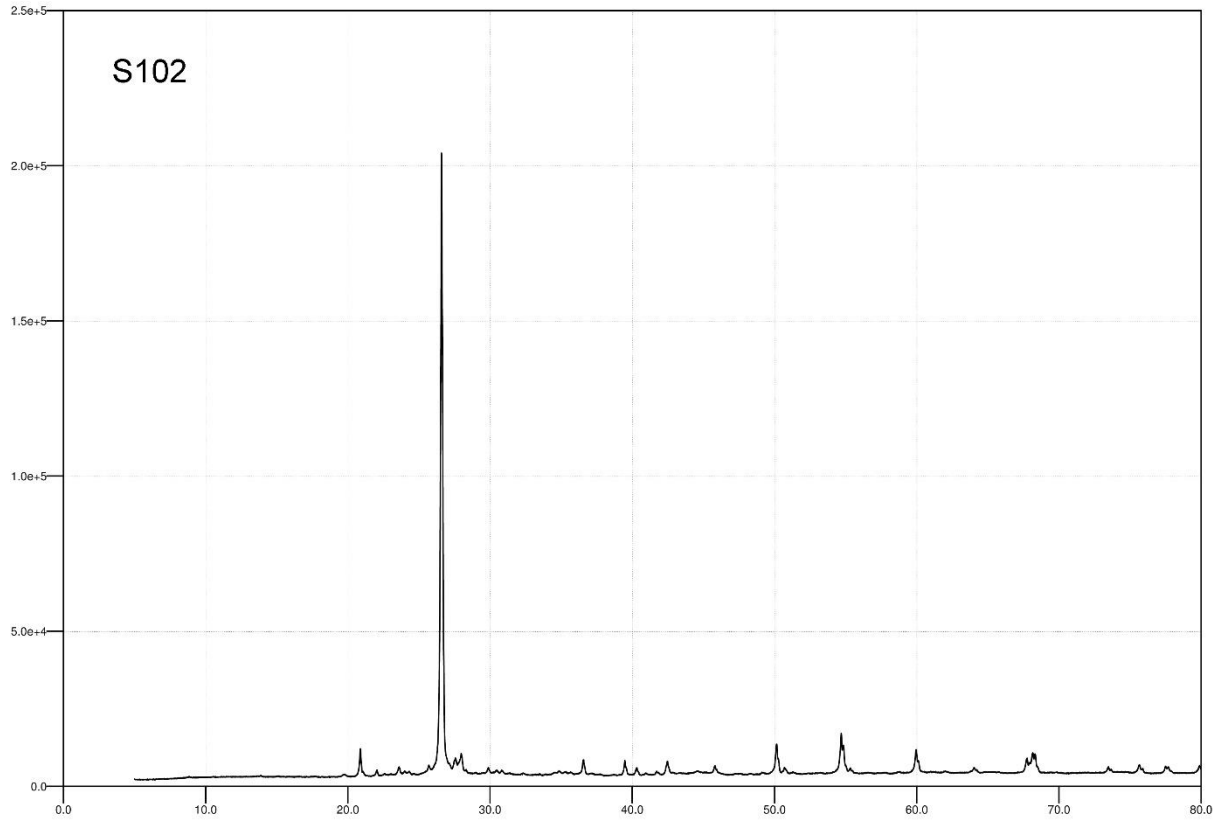

S90
40000
35000
30000
25000
20000
15000
10000
5000
0
0.0
10.0
20.0
30.0
40.0
50.0
60.0
70.0
80.0

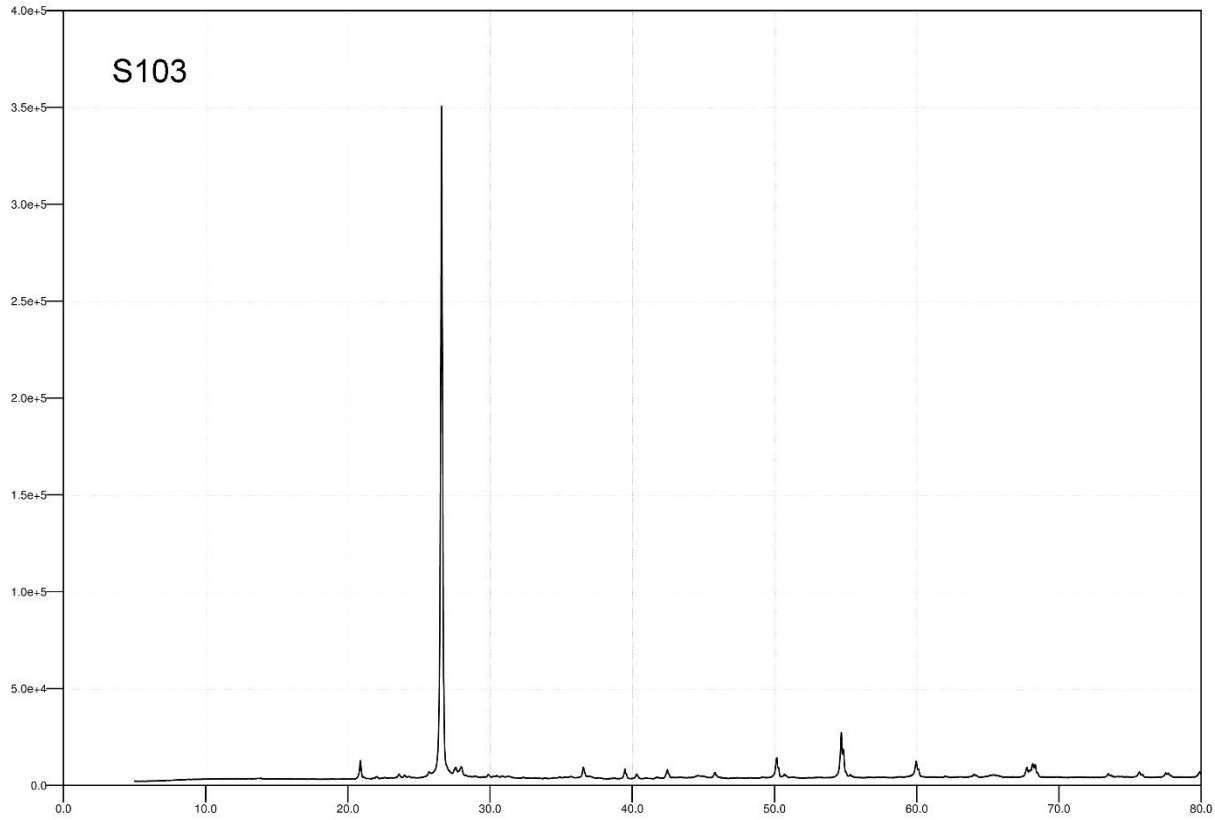

S93
70000
60000
50000
40000
30000
20000
10000
0
0.0
10.0
20.0
30.0
40.0
50.0
60.0
70.0
80.0

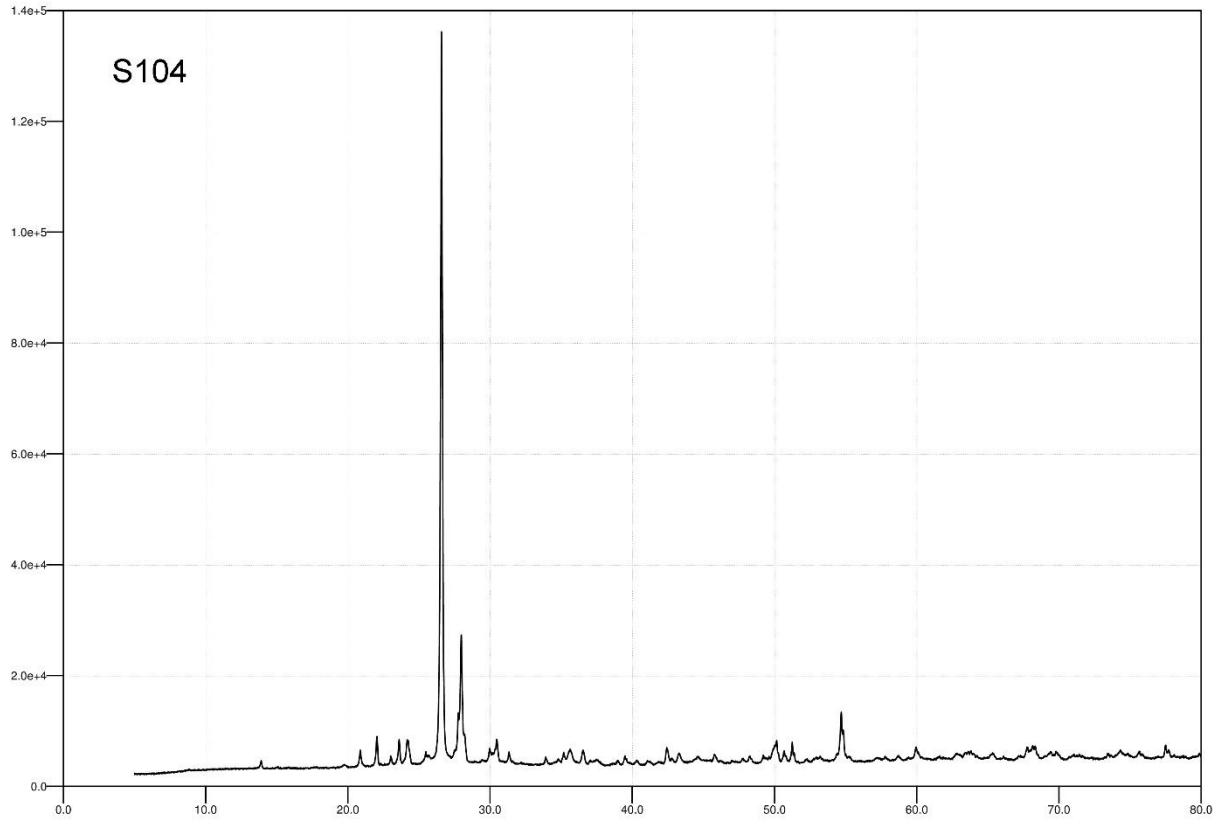

S97
25000
20000
15000
10000
5000
0
0.0
10.0
20.0
30.0
40.0
50.0
60.0
70.0
80.0

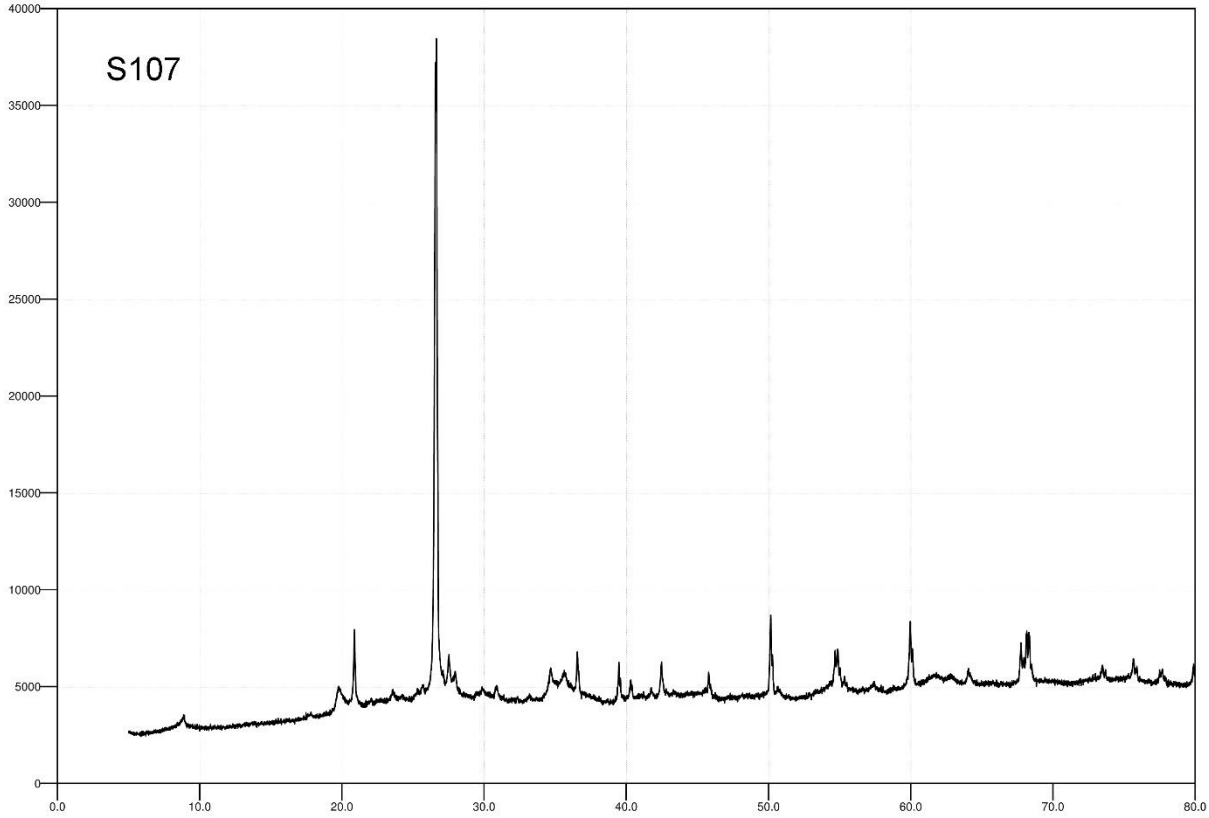

S98
30000
25000
20000
15000
10000
5000
0
0.0
10.0
20.0
30.0
40.0
50.0
60.0
70.0
80.0

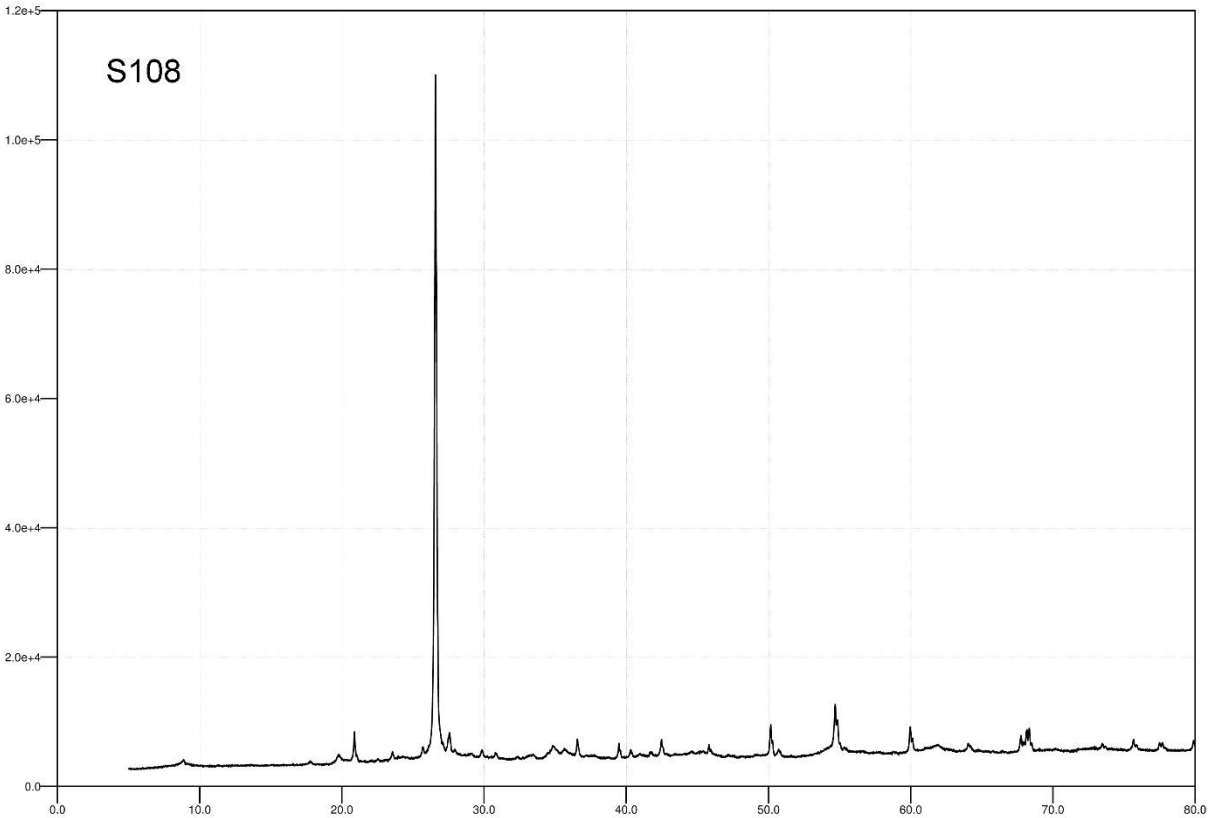

S100
7.0e+5
6.0e+5
5.0e+5
4.0e+5
3.0e+5
2.0e+5
1.0e+5
0.0
0.0
10.0
20.0
30.0
40.0
50.0
60.0
70.0
80.0

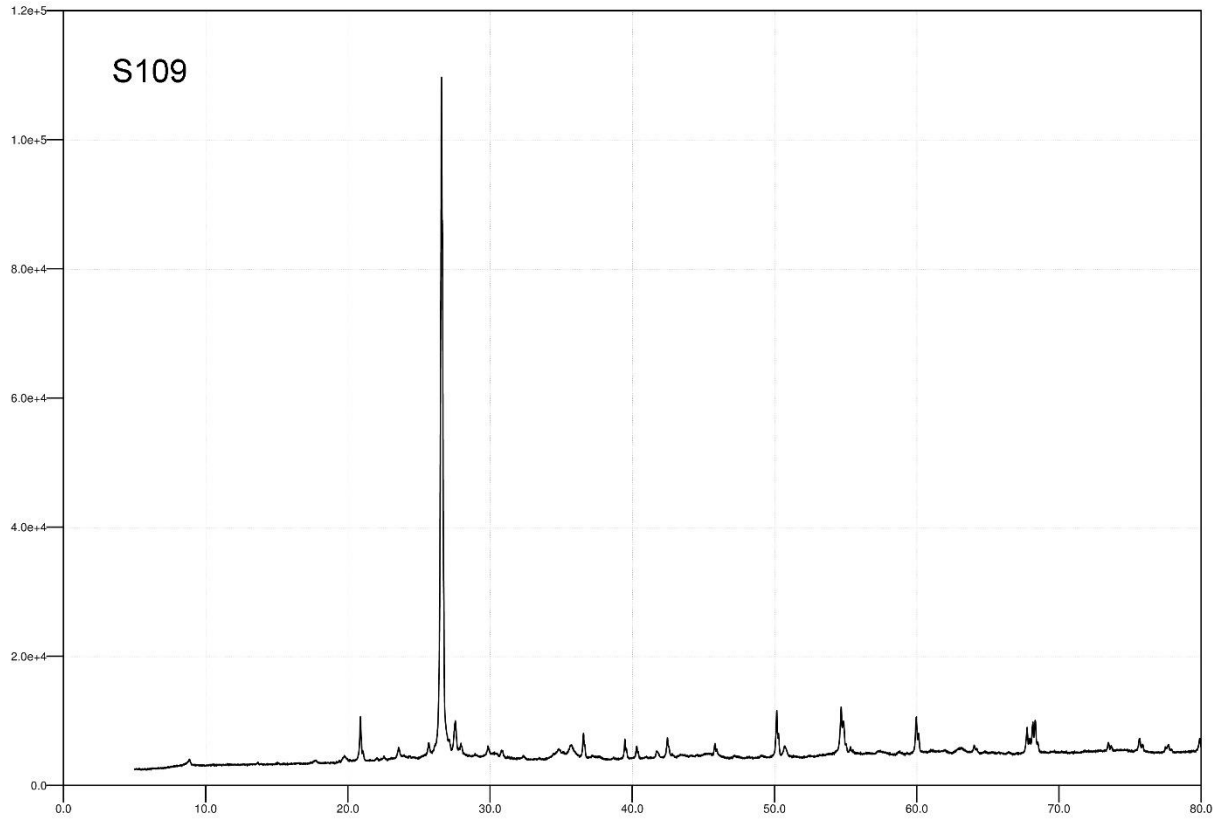

S102
2.5e+5
2.0e+5
1.5e+5
1.0e+5
5.0e+4
0.0
0.0
10.0
20.0
30.0
40.0
50.0
60.0
70.0
80.0

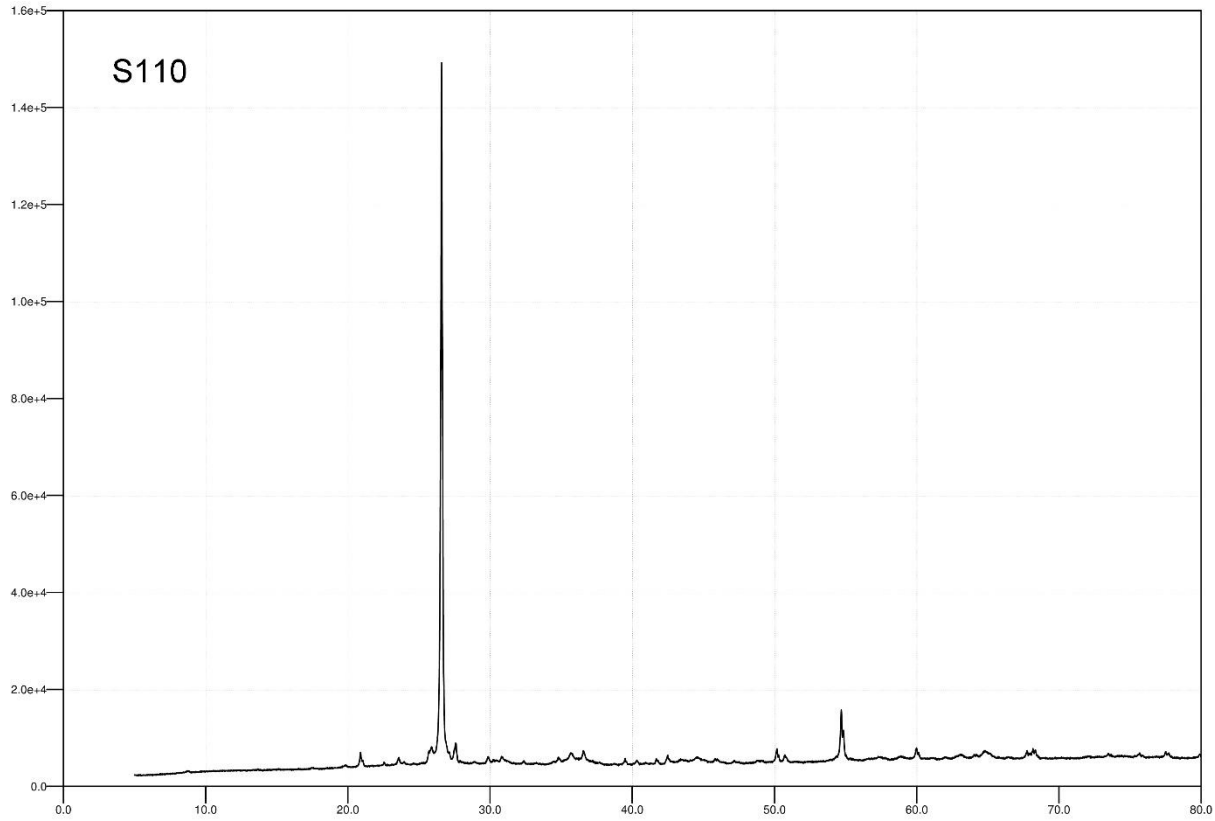

S103
4.0e+5
3.5e+5
3.0e+5
2.5e+5
2.0e+5
1.5e+5
1.0e+5
5.0e+4
0.0
0.0
10.0
20.0
30.0
40.0
50.0
60.0
70.0
80.0

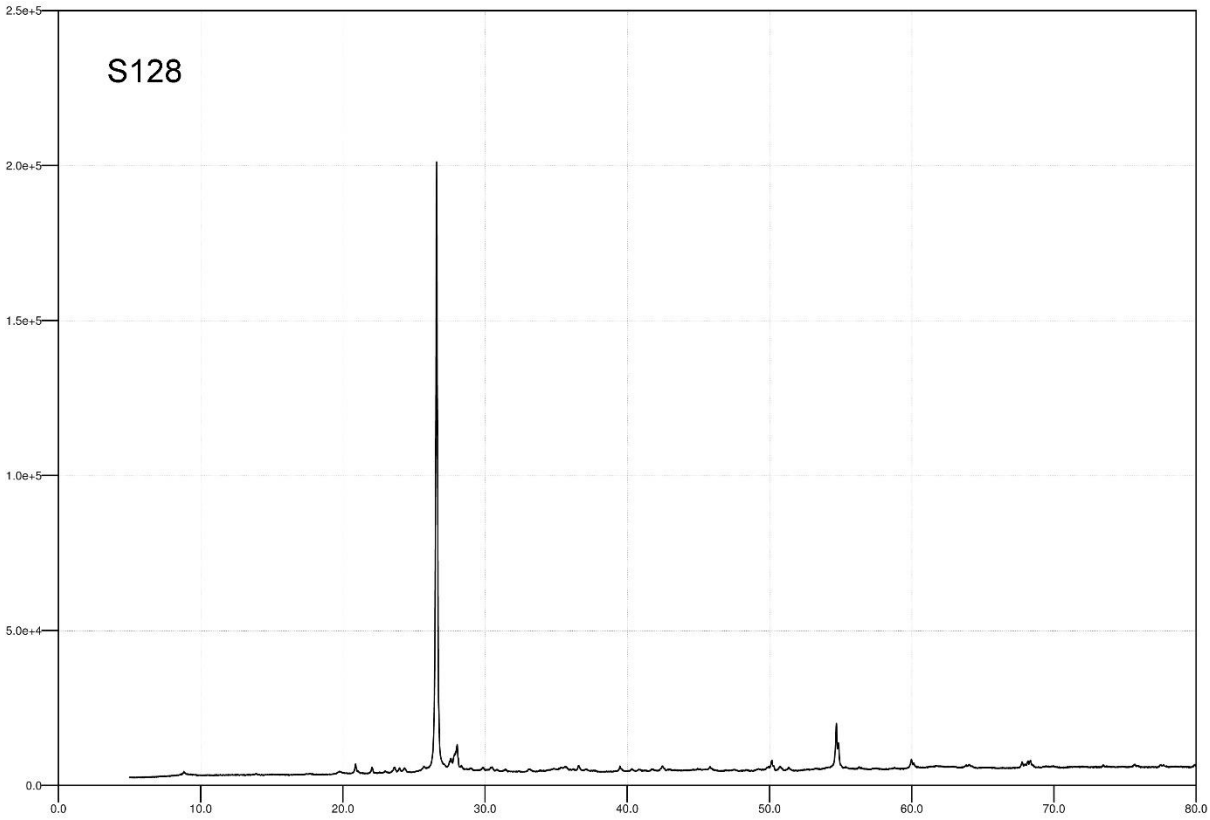

S104
1.4e+5
1.2e+5
1.0e+5
8.0e+4
6.0e+4
4.0e+4
2.0e+4
0.0
0.0
10.0
20.0
30.0
40.0
50.0
60.0
70.0
80.0

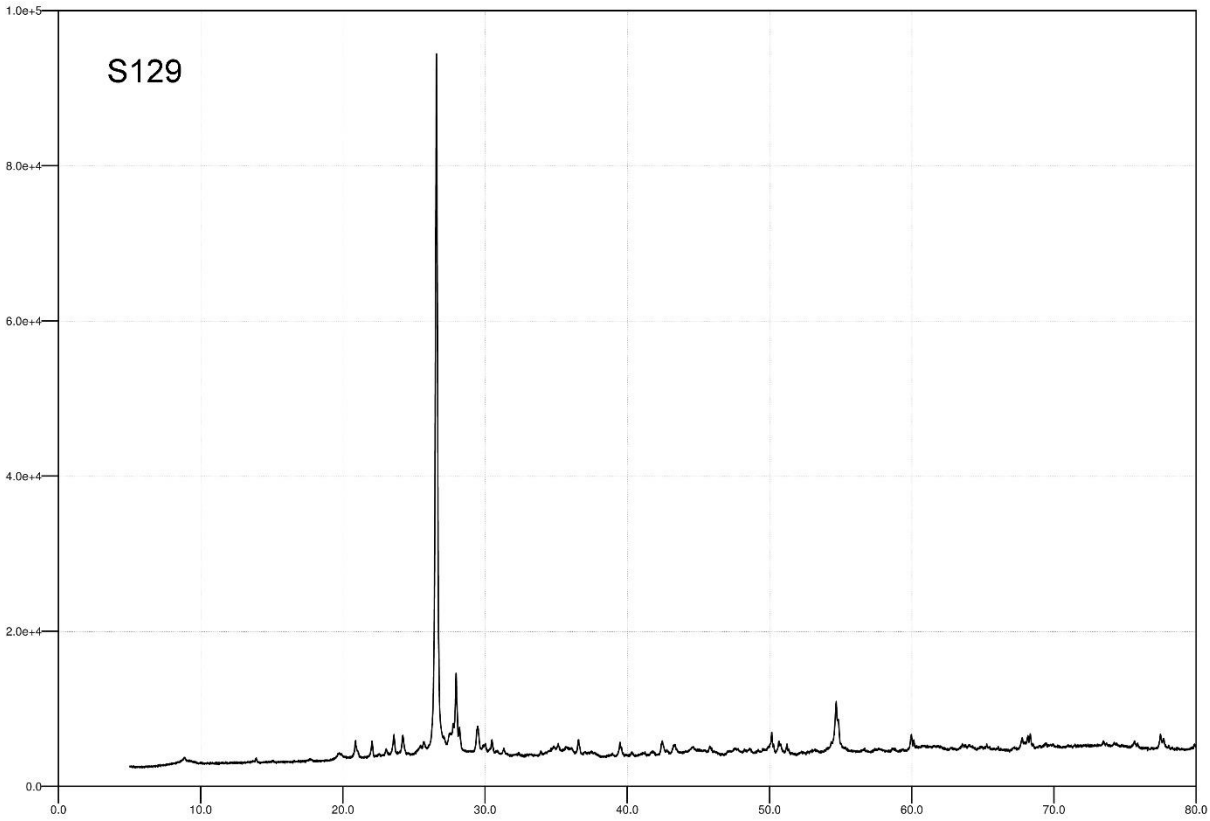

S107
40000
35000
30000
25000
20000
15000
10000
5000
0
0.0
10.0
20.0
30.0
40.0
50.0
60.0
70.0
80.0

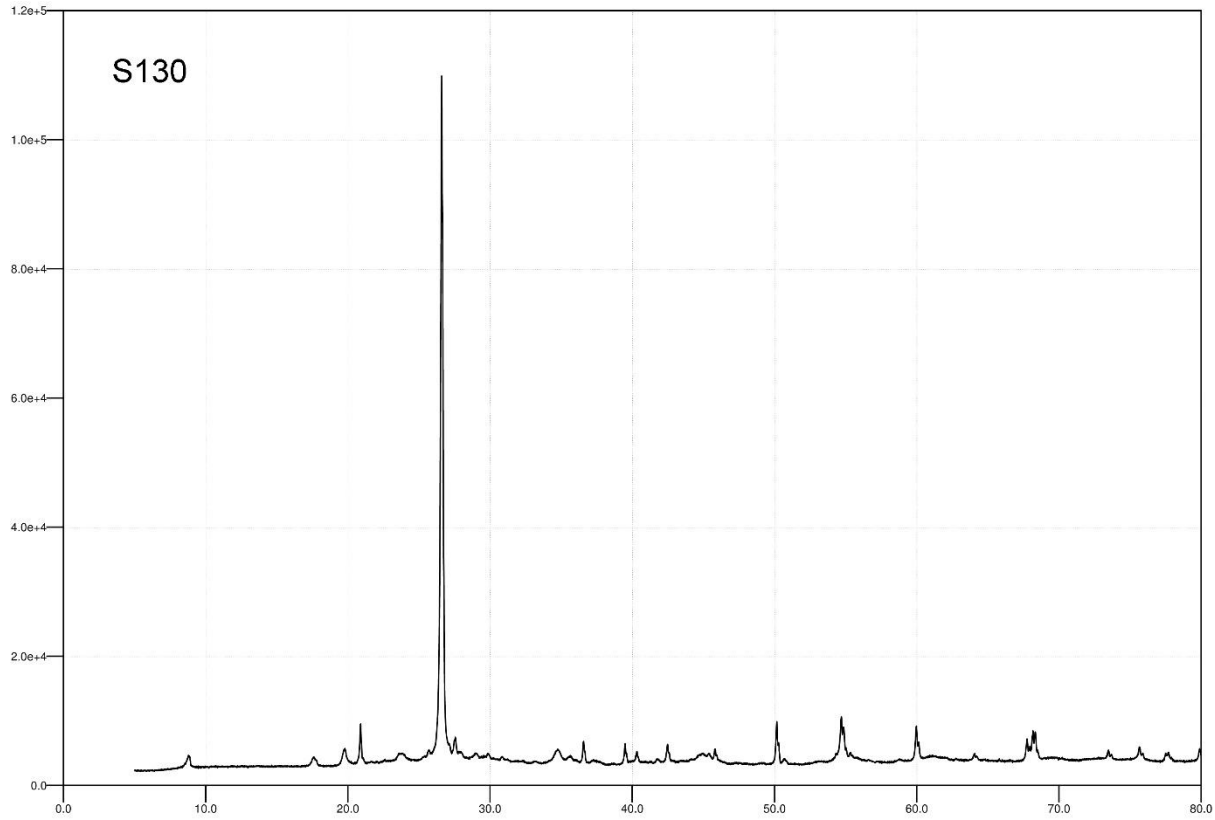

S108
1.2e+5
1.0e+5
8.0e+4
6.0e+4
4.0e+4
2.0e+4
0.0
0.0
10.0
20.0
30.0
40.0
50.0
60.0
70.0
80.0

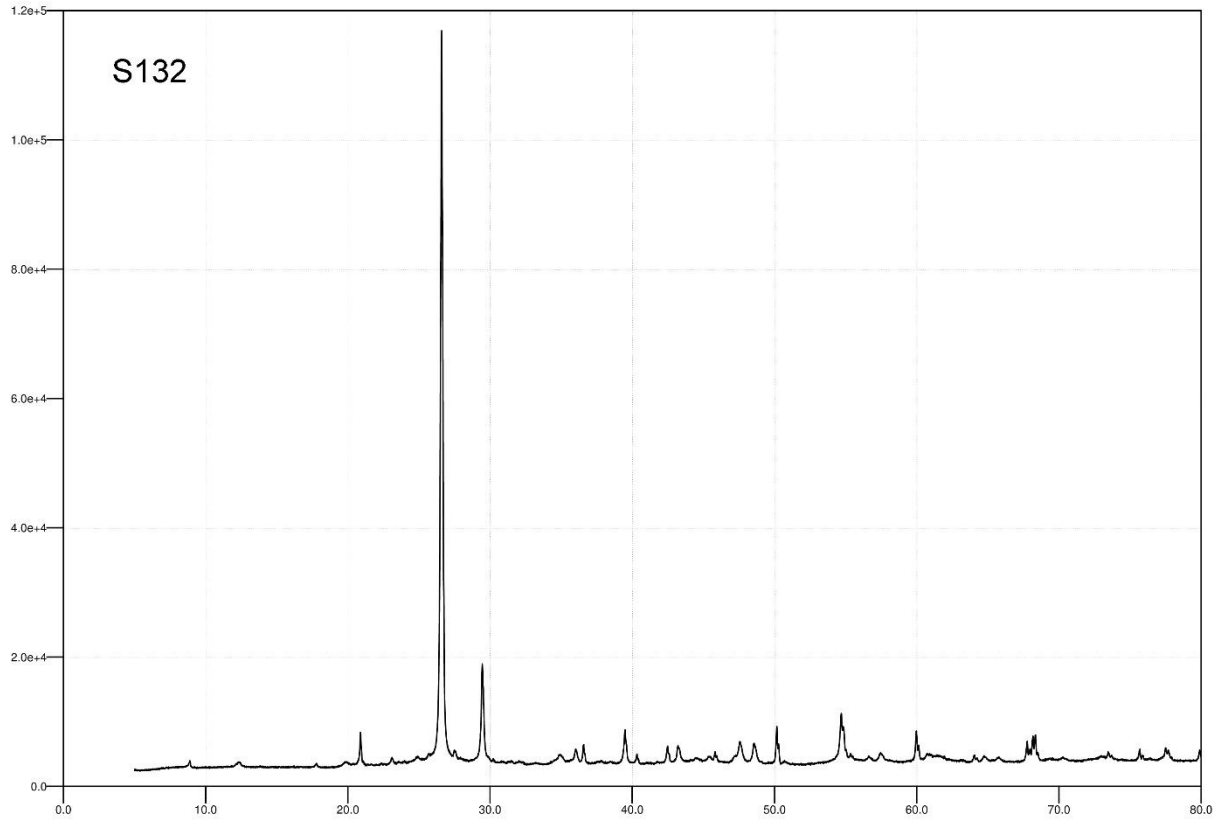

S109
1.2e+5
1.0e+5
8.0e+4
6.0e+4
4.0e+4
2.0e+4
0.0
0.0
10.0
20.0
30.0
40.0
50.0
60.0
70.0
80.0


S110
1.6e+5
1.4e+5
1.2e+5
1.0e+5
8.0e+4
6.0e+4
4.0e+4
2.0e+4
0.0
0.0
10.0
20.0
30.0
40.0
50.0
60.0
70.0
80.0


S128
2.5e+5
2.0e+5
1.5e+5
1.0e+5
5.0e+4
0.0
0.0
10.0
20.0
30.0
40.0
50.0
60.0
70.0
80.0


S129
1.0e+5
8.0e+4
6.0e+4
4.0e+4
2.0e+4
0.0
0.0
10.0
20.0
30.0
40.0
50.0
60.0
70.0
80.0


S130
1.2e+5
1.0e+5
8.0e+4
6.0e+4
4.0e+4
2.0e+4
0.0
0.0
10.0
20.0
30.0
40.0
50.0
60.0
70.0
80.0


S132
1.2e+5
1.0e+5
8.0e+4
6.0e+4
4.0e+4
2.0e+4
0.0
0.0
10.0
20.0
30.0
40.0
50.0
60.0
70.0
80.0